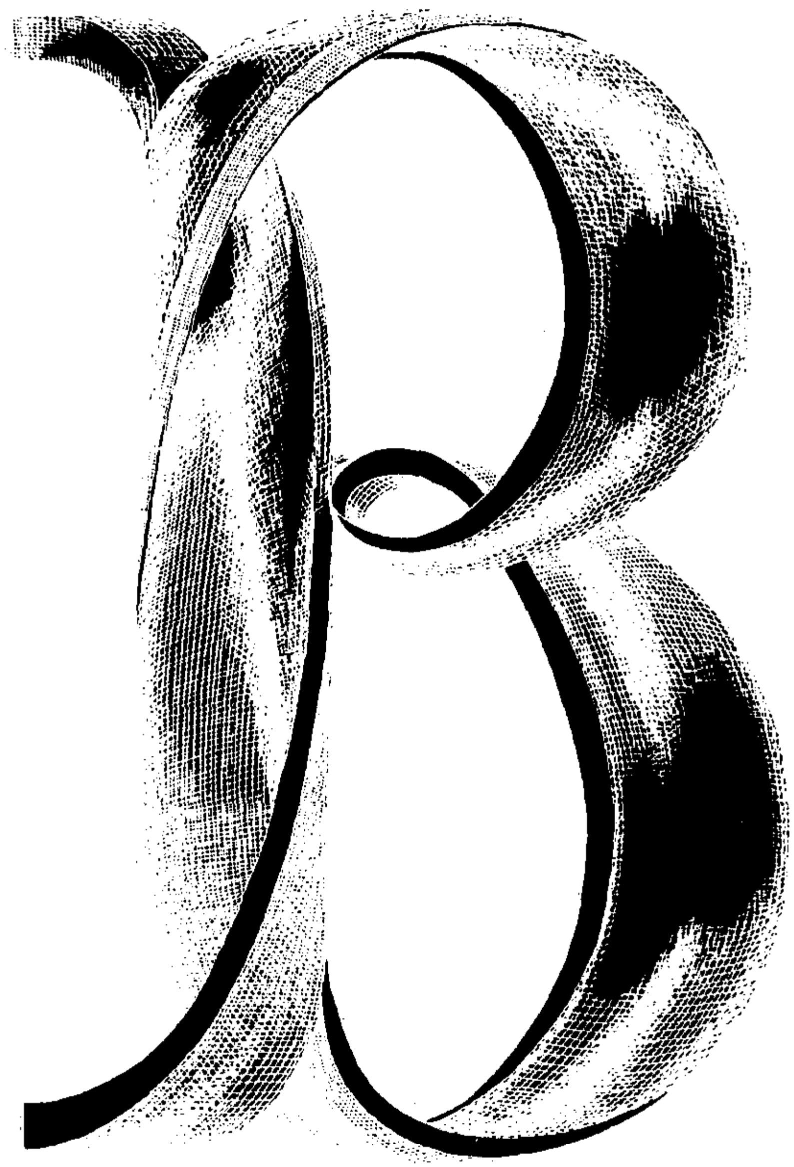

Proceedings of the Workshop on B Physics at Hadron Accelerators

Snowmass, Colorado
June 21 - July 2, 1993

Editors:
Patricia McBride, SSCL
C. Shekhar Mishra, Fermilab

Sponsored by
Fermi National Accelerator Laboratory
Superconducting Super Collider Laboratory

SSCL-SR-1225
Fermilab-Conf-93/267

Proceedings of the

Workshop on B Physics at Hadron Accelerators

Snowmass, Colorado

June 21–July 2, 1993

SSCL-SR-1225
Fermilab-CONF-93/267

Proceedings of the
Workshop on B Physics at Hadron Accelerators

Snowmass, Colorado

July 21–July 2, 1993

Editors

Patricia McBride, SSCL
C. Shekhar Mishra, Fermilab

Sponsored by

Fermi National Accelerator Laboratory • Superconducting Super Collider Laboratory

FOREWORD

This "Workshop on B Physics at Hadron Accelerators," held at Snowmass in the summer of 1993, is to be viewed both as the culmination and end of a series of meetings held at and sponsored by Fermilab and the SSC Laboratory in the preceding twelve months. The workshop brought together over 200 participants, theorists, experimentalists, and accelerator scientists of varied backgrounds. The purpose of the Snowmass Workshop was to explore opportunities and to compare capabilities for the study of B physics and CP violation in colliding beam experiments with central and forward rapidity coverage at Fermilab, LHC, and SSC, as well as fixed target experiments with internal targets at HERA and LHC and external targets at Fermilab, LHC, and SSC. It is hoped that these studies will lay the foundation for future proposals for new detector facilities or major upgrades of existing ones, by defining the physics objectives, setting the performance goals, and studying the layouts and technology choices for the detector subsystems, and examining background conditions. It was anticipated that Fermilab and the SSC Laboratory would call for Letters of Intent for such experiments in the near future. Such a call has been made by Fermilab.

During the workshop, participants attended plenary sessions and daily seminars. Most of the time was reserved for work in smaller groups. These groups were organized to maximize the interaction of the participants. There were two sets of working groups which met in parallel. In the mornings, three groups examined various methods of measuring one of the three angles α, β, and γ, of the unitarity triangle. A fourth group studied the wide range of other physics topics that can be studied in B experiments. In the afternoons, five groups examined detector subsystems for tracking and vertexing, photon and electron detection, muon detection, particle identification, and electronics and data acquisition. A sixth group focused on issues related to the interface between the detector and the accelerator, and a seventh group discussed various theoretical topics related to heavy flavor particles.

During the deliberations of the working groups, many ideas and studies were presented, including reports on ongoing analysis of data recorded recently. Assumptions were challenged; methods and results were examined. In particular, for the measurements of the three unitarity angles, comparisons of the analysis and the projected performance were made. For these comparisons, a real attempt was made to use common assumptions for cross sections and branching ratios, and to apply common levels of realism in the evaluation of the detection efficiencies, subsystem performance and data acquisition rates. The experience gained in recent fixed target and collider experiments was extremely valuable in this effort. A large number of B decay modes were considered both from the theoretical and experimental points of view, the background processes were analyzed, and their demands on the detector capabilities were examined. Detection efficiency, trigger, and flavor tagging signals were studied and compared in various detectors and beam configurations at different energies.

These proceedings are to serve as a record of the workshop activities and discussions and could form a basis for the development of a coherent long-term program, capable of measuring CP violating affects in many different decay modes and addressing many other critical questions accessible via the production and decay of B hadrons. The proceedings contain most of the plenary talks, describing the principal physics issues and reporting results on charm and beauty decays from existing experiments at CESR, LEP, and the Tevatron. In addition, the proceedings contain summaries and individual contributions from the eleven working groups.

The proceedings of this workshop underline the fact that hadron accelerators have a very large potential to study CP violation and other difficult questions in the B system. The enormous production rates in high energy beams allow for a large variety of event selection schemes by multi-level triggers, both in hardware and software. Promising schemes have been proposed and will be further developed and tested in the next few years.

Near the end of the Workshop, the United States House of Representatives voted to terminate the funding for the construction of the SSC. Since then, both Houses of Congress have agreed to cancel the SSC project and close the SSC Laboratory. This action has an immeasurable impact on the future of high energy physics and fundamental research in general, in this country and abroad. Dedicated B experiments at the highest energies are among the many exciting scientific opportunities that are lost. Nevertheless, these proceedings will serve as a valuable guide to the potential of hadron accelerators for the understanding of the origin of CP violation in particular and beauty physics in general. The projections presented here are to be compared with the capabilities of present and future high luminosity e^+e^- storage rings operating at the $\Upsilon(4s)$ resonance. The Fermilab Collider remains a viable opportunity for reaching many of the goals examined here. The proposed LHC project at CERN can benefit from many of the insights recorded here, as can the fixed target experiments planned for 1 TeV proton beams at Fermilab and HERA.

We would like take this opportunity to thank the members of the Organizing Committee, the working group convenors, the speakers, the editors of the proceedings, and the members of our dedicated workshop staff. They all worked hard to make this workshop possible and they, along with the enthusiastic participants, deserve credit for the very fruitful results generated in the thin air and natural beauty of the Colorado Rockies. We would also like to thank Patricia Ehresmann, Valerie Kelly and the staff of the Technical Information and Publication Services at the Superconducting Super Collider Laboratory for their efforts in putting together this document.

Regrettably, this was the last in a long and successful series of Snowmass workshops related to SSC physics!

Vera Lüth and Jeffrey Appel

ORGANIZING COMMITTEE

J. Appel	Fermi National Accelerator Laboratory
S. Conetti	University of Virginia
I. Dunietz	Fermi National Accelerator Laboratory
P. Hale	Superconducting Super Collider Laboratory
P. Karchin	Yale University
R. Lipton	Fermi National Accelerator Laboratory
N. Lockyer	University of Pennsylvania
V. Lüth	Superconducting Super Collider Laboratory
P. McBride	Superconducting Super Collider Laboratory
C.S. Mishra	Fermi National Accelerator Laboratory
C.M. Sazama	Fermi National Accelerator Laboratory
J. Skarha	Johns Hopkins University
S. Wojcicki	Stanford University/Superconducting Super Collider Laboratory

EDITORIAL BOARD

Measurement of Angle α

A. Jawahery
University of Maryland

Measurement of Angle β

V. Sharma
CERN

Measurement of Angle γ

P. Sphicas
Massachusetts Institute of Technology

Other B Physics

A. Zieminski
Indiana University

Theory of Heavy Flavors

B. Grinstein
Superconducting Super Collider Laboratory

Charged Particle Tracking and Vertexing

A. Weidemann
University of Tennessee

e and γ Detection

E.C. Dukes
University of Virginia

Muon Detection

M.C. Cummings
Fermi National Accelerator Laboratory

Hadron ID

K. Nelson
University of Virginia

Electronics, DAQ and Computing

S. Conetti
University of Virginia

J. Slaughter
Fermi National Accelerator Laboratory

Machine Detector Interface

V. Bharadwaj
Fermi National Accelerator Laboratory

CONVENORS

Measurement of Angle α

A. Jawahery
University of Maryland

K.B. Luk
Lawrence Berkeley Laboratory

D. London
University of Montreal

Measurement of Angle β

F. DeJongh
Fermi National Accelerator Laboratory

V. Sharma
University of Wisconsin

Measurement of Angle γ

R. Aleksan
CEN Saclay

B. Kayser
National Science Foundation

P. Sphicas
Massachusetts Institute of Technology

Other B Physics

S. Wojcicki
Stanford Linear Accelerator Center/
Superconducting Super Collider Laboratory

A. Zieminski
University of Indiana

Y. Nir
Weizmann Institute of Science

Theory of Heavy Flavors

B. Grinstein
Superconducting Super Collider Laboratory

J. Smith
State University of New York at Stony Brook

Charged Particle Tracking and Vertexing

R. Johnson
University of California–Santa Cruz

M. Purohit
Princeton University

A. Weidemann
University of Tennessee

e and γ Detection

E.C. Dukes
University of Virginia/
Superconducting Super Collider Laboratory

H. Paar
University of California–San Diego

Muon Detection

D. Hedin
North Illinois University

N. Stanton
Ohio State University

Hadron ID

K. Nelson
University of Virginia

M. Sheaff
University of Wisconsin–Madison

Electronics, DAQ, and Computing

J. Dorenbosch
Superconducting Super Collider Laboratory

S. Geer
Fermi National Accelerator Laboratory

Machine Detector Interface

V. Bharadwaj
Fermi National Accelerator Laboratory

S. White
Brookhaven National Laboratory

TABLE OF CONTENTS

Plenary Session

CP Violation in the Standard Mode' The *B* Meson System ... 1
M. Gronau

B Decays in the Standard Model and Beyond ... 11
D. London

Heavy-Flavor Production ... 19
J. Smith and W. K. Tung

B Decay—Measurements and Predictions ... 29
H. Yamamoto

Design Choices and Issues for Collider Experiments ... 45
J. Spalding

Design Choices and Issues in Fixed-Target *B* Experiments ... 53
L. Camilleri

Recent Results on *B* Physics with CDF ... 63
J. A. Mueller

B Physics at the D0 Detector ... 73
M. C. Cummings

Extracting CKM Parameters from *B* Decays ... 83
I. Dunietz

B Mesons Semileptonic Decays from $\Upsilon(4S)$ Resonance Data ... 97
M. Artuso

Light-Quark, Heavy-Quark Systems: An Update ... 109
B. Grinstein

B Physics at LEP ... 121
R. V. Kowalewski

B-Physics in Hadron Colliders ... 127
C. T. Hill

Secondary Particle Background Levels and Effects on Detectors at Future Hadron Colliders ... 139
T. Pal

Physics Opportunities at Asymmetric e^+e^- Collider at Υ ... 151
Y. Sakai

Charm and Beauty Measurements at Fermilab Fixed Target ... 163
C. S. Mishra

Beauty and the Beast: What Lattice QCD can do for B Physics ... 175
A. S. Kronfeld

New Physics Effects on CP Violation in B Decays ... 185
Y. Nir

Measurement of Angle α

Summary Report of the Working Group on: Measurement of the Angle α ... 199
A. Jawahery, D. London, and K. B. Luk

Fixed Target B Experiments and the Angle Alpha using $B^0 \to \pi\pi$ and $B^0 \to a_1\pi$ ... 209
A. P. McManus, B. Cox, E. C. Dukes, and T. Lawry

Report of the α Subgroup on Forward Collider Experiments ... 213
S. Kwan and K. B. Luk

Central Collider Experiments: A Feasibility Study of Measuring the Angle α with CDF ... 217
J. D. Lewis, J. Mueller, J. Spalding, and P. Wilson

D0 Upgrade: Feasibility Study of Measuring Alpha by $B^o \to \pi^+\pi^-$ ... 221
C. S. Mishra and R. Lipton

A $B^0 \to \pi^+\pi^-$ Trigger for CDF ... 227
G. Punzi, S. Donati, and G. Gagliardi

Study of Combinatorical Background in the Decay $B_d^0 \to \pi^+\pi^-$ From p-p Interactions at $\sqrt{s} = 40$ TeV ... 229
O. Long, F. Azfar, and J. Heinrich

Background to $B_d \to \pi^+\pi^-$ From Secondary Interactions in a Silicon Microvertex Detector at the SFT ... 231
T. J. Lawry, E. C. Dukes, and A. P. McManus

Vertex Resolution in Experiment 791 ... 233
K. Gounder

Reconstruction of $B_d^0 \to \pi^+\pi^-$ Decays in the Atlas Experiment at LHC ... 237
S. Gadomski, P. Eerola, N. Ellis, and D. Froidevaux

Measurement of Angle β

Beta Group Summary ... 243
F. DeJongh

Comparing the Physics Reach of Detectors in Measuring CP Violating Angle β ... 247
W. Toki and J. F. Hassard

Probing Beta ... 251
B. Kayser

A Fixed Target B Experiment at the HERA Proton Ring ... 255
T. Lohse

Measuring the Angle β in $B_d \to D^*\bar{D}^*$ Decays at the SFT ... 259
T. J. Lawry, S. Conetti, and G. Corti

Measurement of CP-Violation with the GEM Detector ... 263
H. Yamamoto

Prospects for Measuring CP Violation in SDC Using $B_d^0 \to \psi K_S^0$ ... 267
D. P. Coupal

Reconstruction of $B_d^0 \to J/\psi K_S^0$ Decays in the Atlas Experiment at LHC ... 271
P. Eerola, N. Ellis, D. Froidevaux, and S. Weinzierl

Measurement of $\sin(2\beta)$ with the CMS Detector at LHC ... 275
N. Neumeister

K^o Finding Efficiencies in Increasing Luminosities ... 279
J. F. Hassard and S. Margetides

A Novel Track Finding Technique for $pp \to b\bar{b}$ Events ... 281
J. F. Hassard and S. Margetides

Measurement of Ratio of Branching Ratios
$BR(B^+ \to J/\psi K^+)/BR(B^0 \to J/\psi K^0)$ 285
J. Gonzalez-A

Measurement of Angle γ

Measurement of the Angle Gamma 291
R. Aleksan, B. Kayser, and P. Sphicas

In Pursuit of Gamma 299
R. Aleksan, B. Kayser, and D. London

Measuring γ with the Decays $B_s^0 \to D_s K$ and $B_u \to D^0 K$ with the CDF Detector at the Tevatron 309
E. Blucher, J. Cunningham, J. Kroll, F. D. Snider, and P. Sphicas

Measurement of the Angle Gamma with a Forward Collider Detector 313
P. Karchin, C. Kennedy, R. Harr, L. Garren, P. Avery, and D. Cords

The Measurement of the Angle Gamma in the SFT: an SSC Fixed Target B Experiment 319
B. Cox, G. Corti, K. Nelson, and A. Erwin

The Prospect for Determining the Angle γ in the Decay $B_d^0 \to \psi\rho^0$ at the SSC 323
F. Bird

Other B Physics

Hadro- and Photo-Production

An Overview of the δ Working Group 331
A. Zieminski

B-Quark Production at Hadron Colliders 333
S. Riemersma and R. Meng

Bottom Quark Cross Sections at Collider and Fixed-Target Energies at the SSC and LHC 339
E. L. Berger and R. Meng

Quarkonia Production, b-Quark Production and $b\bar{b}$ Correlation Studies with CDF 343
V. Papadimitriou

B Production at D0 351
B. C. Choudhary for the D0 Collaboration

B_s Mixing

Report of the Mixing Sub-Group of the δ Working Group (Other B Physics) 357
D. J. Ritchie, J. E. Skarha, and A. Zieminski

Prospects for Measuring B_s Mixing at CDF 361
J. E. Skarha and A. B. Wicklund

Methodology for Comparison of B-Mixing Experiments 367
T. H. Burnett

Observability of Mixing in Partially Reconstructed B_d and B_s at the SFT 371
T. J. Lawry, S. Conetti, G. Corti, B. Cox, E. C. Dukes, A. P. McManus, K. Nelson, and I. Tzamouranis

Prospects for $B_S^0\overline{B_S^0}$ Oscillation Measurement at LEP 373
X. Lou

$B - \overline{B}$ Mixing in SLD 377
C. Baltay for the SLD Collaboration

Measurement of $B^\circ - \bar{B}^\circ$ Mixing Using Dimuons at D0 383
K. Johns

B Decays

Semileptonic and Leptonic Decays of B Hadrons 389
K. Kinoshita, J. Amundson, C. Dib, G. W. S. Hou, V. Jain, A. Kronfeld, P. Lebrun, R. J. Oakes, and J. Taron

An Overview of B Rare Decays 395
Y. Nir for the δ B Rare Decays Subgroup

A Study of Some Rare Self-Tagging B Decays 405
A. J. Schwartz

CP Violation Outside the Standard Model Phenomenology for Pedestrians 411
H. J. Lipkin

The Search for Flavor Changing Neutral Currents in Rare B Decays 417
D. B. Cline

Simulation Study of $B \to X_s\gamma$ 427
D. Cline, J. Park, J. Rhoades, and M. Atac

Other Spectroscopy

Heavy Flavor Spectroscopy 435
J. Rosen, J. Marques, and L. Spiegel

B_c 439
C. Quigg

B^{**} Properties 443
C. Quigg

Theory of Heavy Flavors

New Phases in CP Violating B Decay Asymmetries from Mixing to Singlet Down Quarks 449
D. Silverman and W.-S. Choong

Chiral Lagrangians, Soft-Meson Limits and Effective Lagrangians 451
R. J. Oakes

PCAC Relation for $D^* \to D$ Axial Form Factors 453
C. O. Dib and J. Taron

Probing the $WW\gamma$ Vertex in Radiative b-Quark Decays 455
U. Baur

Parton Model (Mössbauer) Sum Rules for $b \to c$ Decays 457
H. J. Lipkin

B Meson Decay Constants 459
R. J. Oakes

Charged Particle Tracking and Vertexing

Tracking and Vertexing for B Physics at Hadron Accelerators 463
R. Johnson, M. Purohit, and A. W. Weidemann

SDC Tracking Capabilities for B Physics 475
D. P. Coupal

Comparison of Forward Collider Vertex Detectors for B Physics at Hadron Accelerators 479
R. F. Harr, P. E. Karchin, and C. J. Kennedy

Tracking Considerations for Fixed Target B Experiments at SSC and LHC 485
A. P. McManus, S. Conetti, G. Corti, B. Cox, E. C. Dukes, T. Lawry, K. Nelson, and I. Tzamouranis

On the Configuration of an Active Target for a Fixed-Target B Experiment at SSC Energies 489
E. C. Dukes

A Realistic Study on a Forward Geometry Collider Spectrometer: Performance of a Typical Fixed Target Spectrometer at the Tevatron Collider 497
P. Lebrun

e and γ Detection

Summary of the Electron ID Group 505
E. C. Dukes

Improvement in the CDF L2 Electron Trigger Using the Central Shower Max Detector 511
K. L. Byrum

Electron Identification in the D0 Detector 515
N. Denisenko for the D0 Collaboration

Identifying B-Jets with Electrons 519
A. Peryshkin for the D0 Collaboration

Electromagnetic Shower Spectroscopy in a High Rate Hadronic Interaction Environment; Fermilab Experiment E760 Performance 523
J. L. Marques and J. Rosen

Muon Detection

Summary Muon Detection Working Group 531
N. R. Stanton

Muon Identification and Triggering at D0 537
M. C. Cummings, D. Hedin, and K. Johns

The CDF Muon System 543
T. J. LeCompte and V. Papadimitriou

Hadron ID

Summary of the Hadron ID Group 551
K. Nelson, M. Sheaff, R. Aleksan, T. Alexopoulos, M. Artuso, B. Cox, F. DeJongh, J. Giomataris, V. Jain, C. Kennedy, B. Kephart, K. Kinoshita, S. Kwan, J. Lewis, X. Lou, Y. Mukhin, P. Schuler, and H. Yamamoto

Comparison of Particle Identification Methods 557
S. Kwan

Use of Transition Radiation Detectors (TRD's) for B Tagging/Triggering in Future Collider or Fixed Target Experiments 561
M. Sheaff

Fast Ring Imaging Detectors for Forward B Collider Experiments 569
M. Artuso and Y. Mukhin

Hadron Identification in a Fixed Target Experiment at the SSC 575
K. S. Nelson and B. Cox

Experience with dE/dx at CDF 583
J. D. Lewis

Electronics, DAQ and Computing

Electronics, Trigger, Data Acquisition, and Computing Working Group on Future B Physics Experiments 587
S. Geer

Comparison of Trigger and Data Acquisition Parameters for Future B Physics Experiments 589
S. Conetti and S. Geer

Triggering at the SFT 595
S. Conettti, M. Arenton, G. Corti, B. Cox, C. Dukes, T. Lawry, I. Tzamouranis, and A. Erwin

Cobex Trigger and Data Acquisition Parameters 599
E. P. Hartouni

Part 2 of the Summary for the Electronics, DAQ, and Computing Working Group: Technological Developments 603
A. J. Slaughter

Report of the Subgroup on Deadtimeless Front-end Electronics 605
P. F. Shepard

An Impact-Parameter Optical Discriminator for B Decays 607
Y. Giomataris and S. Loucatos

The P_t Selection of B Events with the Optical Discriminator 611
Y. Giomataris and J. Derré

A Multiplicity Jump Trigger Using Silicon Planes 615
T. Alexopoulos and A. R. Erwin

Impact Parameter Trigger and Vertex Detector for Forward Collider 617
W. Selove

Real-Time Tracking with a 3D-Flow Processor Array 625
D. Crosetto

Data Driven Processor "Vertex Trigger" for B Experiments 629
E. P. Hartouni

Report of the Trigger Processor Subgroup 633
M. Johnson

Machine Detector Interface

Summary of the Machine Detector Interface Working Group 637
S. White and V. Bharadwaj

Fixed and Internal Target Options: Parameters and Impact 639
C. T. Murphy

Test of an Internal Wire Target at the HERA Proton Ring 641
T. Lohse

Extraction from TeV-Range Accelerators Using Bent Crystal Channeling 645
R. A. Carrigan, Jr., G. Jackson, C. T. Murphy, and B. Newberger

Synopsis of a Design of a Crystal Extraction Facility in the SSC East Utility Straight 649
E. C. Dukes, C. T. Murphy, and B. Parker

Design of the SSC Medium-Beta Interaction Regions 653
Y. M. Nosochkov

Summary of the Snowmass Working Group on Machine-Detector Interface 657
V. Bharadwaj, P. Colestock, J. Cooper, G. Goderre, and J. Holt

Asymmetric Collider 663
V. Bharadwaj, P. Colestock, G. Goderre, D. Johnson, P. Martin, J. Holt, and D. Kaplan

Experimental Modification of SSC Interaction Region 667
D. E. Johnson

Radiation Environment and Shielding at the SSC 669
M. V. Diwan

Fixed-Target Particle Fluxes and Radiation Levels at SSC Energies 673
E. C. Dukes

Longitudinal Wakefield Focusing: An Unconventional Approach to Reduce the Bunch Length in Tevatron 677
A. Gerasimov

Obtaining Slow Beam Spills at the SSC Collider 681
D. Ritson

Ultra Thin Beam Pipes for Internal Target B Experiments 685
H. Jöstlein

Point-Like Internal Targets for B Experiments 687
H. Jöstlein

Other Contributed Papers

Measurements of the $B^0\bar{B}^0$ CP Asymmetry 691
V. Lüth

Dilution Measurements for CP Violation in B Decay 695
A. Fridman

Flavor Identification of Neutral B Mesons Using Correlated Pions 701
M. Gronau and J. L. Rosner

Comparison of Forward and Central Collider Detectors for Beauty Physics 707
C. J. Kennedy, R. F. Harr, and P. E. Karchin

The SFT a Super Fixed Target Beauty Experiment at the SSC 713
B. Cox, T. Alexopoulos, M. Arenton, S. Conetti, G. Corti, C. Dukes, A. Erwin, V. Golovatyuk, T. Lawry A. McManus, C. T. Murphy, K. Nelson, L. Spiegel, and I. Tzamouranis

Conference Program 727

Photographs 731

List of Attendees 745

Author Index 753

Plenary Session

CP VIOLATION IN THE STANDARD MODEL: THE B MESON SYSTEM

Michael Gronau
Department of Physics, Technion - Israel Institute of Technology
32000 Haifa, Israel

1. INTRODUCTION

We review various phenomena of CP violation in B decays within the standard model. Section 2 describes the mechanism of CP violation in the Standard Model, which is based on a complex phase in the Cabibbo-Kobayashi-Maskawa quark mixing matrix. Three different manifestations of CP breakdown in the B system are studied in Sections 3, 4, 5. These include CP asymmetries in direct decays of charged B mesons, CP nonconservation in $B^0-\overline{B}^0$ mixing and CP violation which occurs when mixed neutral B mesons decay to states which are common decay products of B^0 and $\overline{B}^0$. We show how to use measured CP asymmetries to determine angles of the CKM unitarity triangle, which are fundamental parameters of the Standard Model. Complications due to penguin amplitudes and due to possible color suppression of certain decay amplitudes are discussed. Section 6 presents a method which uses correlated pions to identify the flavor of neutral B mesons in order to measure CP asymmetries. We conclude in Section 7.

This review is not supposed to be complete. Rather, it represents our own view about the most promising ways of testing the CKM mechanism of CP violation in B decays. A more complete list of references may be found in previous reviews.[1]

2. CP VIOLATION IN THE STANDARD MODEL

2.1 The CKM Matrix

In the standard model the $SU(3)_C \times SU(2)_L \times U(1)_Y$ gauge group is spontaneously broken by the vacuum expectation value of a single scalar Higgs doublet. CP violation occurs in the interactions of the three families of left-handed quarks with the charged gauge boson:

$$-\mathcal{L} = (\,\overline{u}\quad \overline{c}\quad \overline{t}\,)\begin{pmatrix} m_u & & \\ & m_c & \\ & & m_t \end{pmatrix}\begin{pmatrix} u \\ c \\ t \end{pmatrix} + (\,\overline{d}\quad \overline{s}\quad \overline{b}\,)\begin{pmatrix} m_d & & \\ & m_s & \\ & & m_b \end{pmatrix}\begin{pmatrix} d \\ s \\ b \end{pmatrix}$$

$$+\frac{g}{\sqrt{2}}(\,\overline{u}\quad \overline{c}\quad \overline{t}\,)_L\,\gamma^\mu V\begin{pmatrix} d \\ s \\ b \end{pmatrix}_L W^+_\mu + \ldots \qquad (1)$$

CP violation requires a complex (rather than real) Cabibbo-Kobayashi-Maskawa [2] (CKM) mixing matrix V. The quark mass terms exhibit a symmetry under phase redefinitions of the six quark fields. This freedom leaves a single phase in V. The unitary matrix V, which can be defined in terms of this phase (γ) and three Euler-like mixing angles, is approximated for most practical purposes by the following form:

$$V \approx \begin{pmatrix} 1 & |V_{us}| & |V_{ub}|e^{-i\gamma} \\ -|V_{us}| & 1 & |V_{cb}| \\ |V_{us}V_{cb}| - |V_{ub}|e^{i\gamma} & -|V_{cb}| & 1 \end{pmatrix} . \tag{2}$$

The measured values of the three mixing angles ($\sin\theta_{12} \equiv |V_{us}|$, $\sin\theta_{23} \equiv |V_{cb}|$, $\sin\theta_{13} \equiv |V_{ub}|$) have a hierarchial structure in generation space,[3]

$$|V_{us}| = 0.220 \pm 0.002\,(\lambda)\;, \quad |V_{cb}| = 0.040 \pm 0.007\,(\mathcal{O}(\lambda^2))\;, \quad |V_{ub}| = 0.003 \pm 0.001\,(\mathcal{O}(\lambda^3))\;, \tag{3}$$

often characterized [4] by powers of a parameter λ. This structure was used with unitarity to obtain the approximate expressions of the three t quark couplings in V. It is amusing to note that the yet unmeasured value of $|V_{tb}|$ obtained from unitarity is the most accurately known parameter of the mixing matrix.

Unitarity of V can be represented geometrically in terms of triangles, such as the one depicted in Fig.1 representing the relation

$$V_{ud}V^*_{ub} + V_{cd}V^*_{cb} + V_{td}V^*_{tb} = 0\;. \tag{4}$$

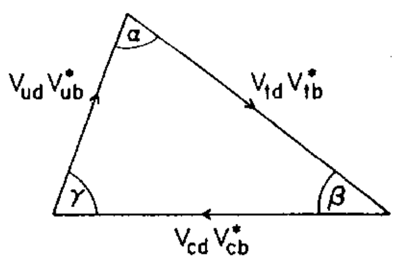

Figure 1: The CKM unitarity triangle.

The three angles of the unitarity triangle, α, β and γ (which appears as a phase in (2)), are rather badly known at present. Current constraints from direct measurements and from the observed $B^0 - \overline{B}^0$ mixing and CP violation in K decays, which depend on uncertainties in K- and B-meson hadronic parameters, can be approximately summarized by the following ranges:[5]

$$5^0 \le \alpha \le 160^0, \quad 5^0 \le \beta \le 45^0, \quad 10^{\le}\gamma \le 170^0\;. \tag{5}$$

As we will show, CP asymmetries in B decays are directly related to these angles in a manner which is free of hadronic uncertainties, and can provide a more precise determination for some of these fundamental parameters.

2.2 CP Violation in B vs. K Decays

One advantage of using the B system compared to the neutral K system is simply illustrated in Fig. 2, which compares the unitarity triangles of these two cases. For B^0_d all the three sides of the triangle have comparable lengths ($\mathcal{O}(\lambda^3)$), while in the K meson triangle, which essentially collapses to a line, two sides are much longer (λ) and the third one is extremely tiny ($\mathcal{O}(\lambda^5)$). Unitarity implies that the two triangles have equal areas.

Figure 2: Unitarity triangles of B^0_d (a) and K^0 (b).

Therefore, CP asymmetries in B decays, represented, for instance, by the angle γ, are much larger than the asymmetries expected in K decays, which are given by the angle θ. In physical terms, this follows from the fact that the difference between particle and antiparticle decay rates for both K and B mesons involves the same universal CKM factor, given by the area of either triangle. That is, when two CKM amplitudes interfere in K and B decays the particle-antiparticle decay-rate-difference contains in both cases a common factor $\mathrm{Im}(V_{ud}V^*_{us}V_{cs}V^*_{cd}) = \mathrm{Im}(V_{ud}V^*_{ub}V_{cb}V^*_{cd})$. On the other hand, the CKM factors which determine the decay rates themselves are much larger for K decays than for B decays.

The experimental and theoretical situation of CP violation in K decays is nicely summarized in ref. 6. In brief, the overall magnitude of the very precisely measured parameter ϵ_K, which measures CP violation in $K^0 - \overline{K}^0$ mixing, can be accounted for in the Standard Model. However, the theoretical calculation involves large uncertainties in the CKM parameters, in the t quark mass and in the hadronic "bag" parameter B_K, which gives the box-diagram $K^0 - \overline{K}^0$ matrix element. These uncertainties lead to the large range of allowed values of $\sin\gamma$ (Eq.(5)) to which ϵ_K is propoprtional. The theoretical situation with respect to CP violation in $K \to 2\pi$ decay, where the 30 year experimental search for a nonzero value of ϵ'/ϵ is still going on, is worse. The effect of the QCD penguin amplitude is to yield values of ϵ'/ϵ around 10^{-3} with about an order of magnitude uncertainty. The contributions of additional electroweak penguin amplitudes which tend to cancel this term can lead to much smaller values. Values as small as 10^{-4} or even smaller cannot be excluded. These calculations involve uncertaities in a few hadronic matrix elements. The advantage of certain CP asymmetries in B decays, to which we now turn, is that they are both very large and free of such uncertainties, and can potenially provide future tests of the mechanism of CP violation in the Standard Model.

3. CP VIOLATION IN CHARGED B DECAYS

3.1 A Theoretical Difficulty

The simplest manifestations of CP violation are different partial decay widths for a particle and its antiparticle into corresponding decay modes. Consider a general decay $B^+ \to f$ and its charge-conjugate process $B^- \to \overline{f}$. In order that these two proceses have different rates, two amplitudes (A_1, A_2) must contribute, with different CKM phases $(\phi_1 \neq \phi_2)$ and different final state interaction phases $(\delta_1 \neq \delta_2)$:

$$
\begin{aligned}
A(B^+ \to f) &= |A_1|e^{i\phi_1}e^{i\delta_1} + |A_2|e^{i\phi_2}e^{i\delta_2} , \\
\overline{A}(B^- \to \overline{f}) &= |A_1|e^{-i\phi_1}e^{i\delta_1} + |A_2|e^{-i\phi_2}e^{i\delta_2} , \\
|A|^2 - |\overline{A}|^2 &= 2|A_1A_2|\sin(\phi_1 - \phi_2)\sin(\delta_1 - \delta_2) . \qquad (6)
\end{aligned}
$$

The theoretical difficulty of relating an asymmetry in charged B decays to a pure CKM phase follows from having two unknowns in the problem: The ratio of amplitudes, $|A_2/A_1|$, and the final state phase difference, $\delta_2 - \delta_1$. Both quantities involve quite large theorertical uncertainties.

This is demonstrated in Fig. 3, which describes the two amplitudes A_1 and A_2 for $B^+ \to K^+\pi^0$, given by the "penguin" (a) and "tree" (b) diagrams, respectively. In this case

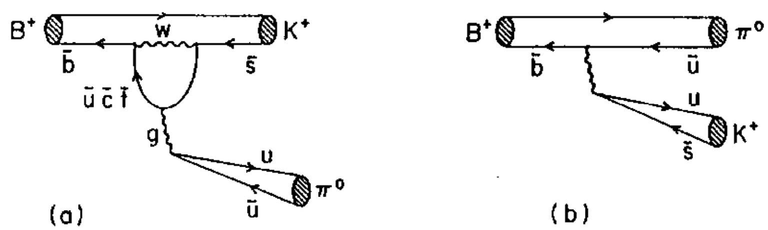

Figure 3: Penguin (a) and tree (b) diagrams in $B^+ \to K^+\pi^0$.

$\phi_1 = 0$, $\phi_2 = \gamma$. A few calculations of the asymmetry in this process were made,[7] based on estimates of the tree-to-penguin ratio of amplitudes and of the strong phase difference. They all involve large theoretical uncertainties. To demonstrate the difficulty, note that the strong phase includes a phase due to the absorptive part of the physical $c\bar{c}$ quark pair in the penguin diagram, arising for instance from the rescattering process $B \to \overline{D}D_s \to K\pi$.

3.2 A Way to Measure γ

The decays $B^\pm \to D_1^0(D_2^0)K^\pm$ and a few other processes of this type provide a unique case,[8] in which one can measure separately the magnitudes of the two contributing amplitudes, and thereby determine the CKM phase γ. $D_1^0(D_2^0) = (D^0 + (-)\overline{D}^0)/\sqrt{2}$ is a CP-even (odd) state, which is identified by its CP-even (odd) decay products. For instance, the states $K_S\pi^0$, $K_S\rho^0$, $K_S\omega$, $K_S\phi$ identify a D_2^0, while $\pi^+\pi^-$, K^+K^- represent a D_1^0. The decay amplitudes of the above two charge-conjugate processes can be written (say for D_1^0) in the form

$$
\begin{aligned}
\sqrt{2}A(B^+ \to D_1^0K^+) &= |A_1|\exp(i\gamma)\exp(i\delta_1) + |A_2|\exp(i\delta_2) , \\
\sqrt{2}A(B^- \to D_1^0K^-) &= |A_1|\exp(-i\gamma)\exp(i\delta_1) + |A_2|\exp(i\delta_2).
\end{aligned} \qquad (7)
$$

A_1 and A_2 are the two weak amplitudes, shown in Fig. 4(b) and 4(a), respectively. Their CKM factors $V_{ub}^*V_{cs}$ and $V_{cb}^*V_{us}$ are of comparable magnitudes. Their weak phases are γ and zero in the standard convention of Fig. 1. Since A_1 leads to final states with isospin 0 and 1, whereas A_2 can only lead to isospin 1 states, one generally expects [9] $\delta_1 \neq \delta_2$.

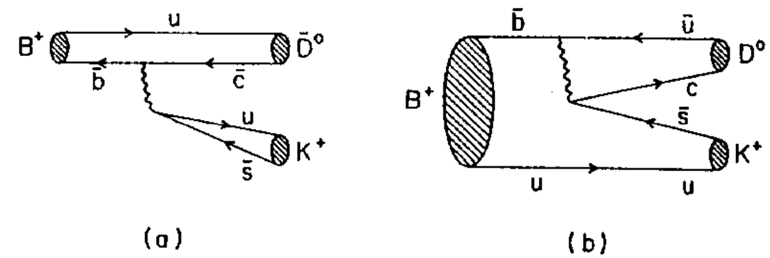

Figure 4: Two diagrams decribing $B^+ \to \overline{D}^0K^+$ (a) and $B^+ \to D^0K^+$ (b).

As shown in Fig. 4, the two amplitudes on the right-hand-sides of the first of Eqs. (7) are the amplitudes of $B^+ \to D^0K^+$ and $B^+ \to \overline{D}^0K^+$, respectively. Similarly, the two terms in the second equation describe the amplitudes of $B^- \to \overline{D}^0K^-$ and $B^- \to D^0K^-$, respectively. The flavor states D^0 and $\overline{D}^0$ are identified by the charge of the decay lepton or kaon. Thus we find:

$$
\begin{aligned}
\sqrt{2}A(B^+ \to D_1^0K^+) &= A(B^+ \to D^0K^+) + A(B^+ \to \overline{D}^0K^+), \\
\sqrt{2}A(B^- \to D_1^0K^-) &= A(B^- \to \overline{D}^0K^-) + A(B^- \to D^0K^-).
\end{aligned} \qquad (8)
$$

Eqs. (8) can be described by two triangles in the complex plane as shown in Fig. 5.

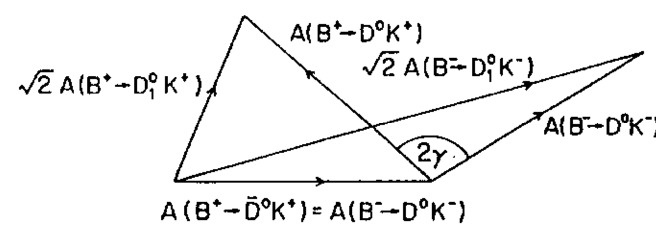

Figure 5: Triangles describing Eqs.(8).

The two triangles represent the complex B^+ and B^- decay amplitudes. Note that

$$
\begin{aligned}
&A(B^+ \to \overline{D}^0K^+) = A(B^- \to D^0K^-) , \\
&A(B^+ \to D^0K^+) = \exp(2i\gamma)A(B^- \to \overline{D}^0K^-), \\
&|A(B^+ \to D_1^0K^+)| \neq |A(B^- \to D_1^0K^-)| .
\end{aligned} \qquad (9)
$$

This implies that CP is conserved in $B^\pm \to D^0(\overline{D}^0)K^\pm$ but is violated in $B^\pm \to D_1^0K^\pm$. In the last of Eqs.(9) we assumed $\gamma \neq 0$, $\delta_1 \neq \delta_2$. The asymmetry in the rates of $B^\pm \to D_1^0K^\pm$

depends on γ and $\delta_2 - \delta_1$; clearly

$$|A(B^+ \to D_1^0 K^+)|^2 - |A(B^- \to D_1^0 K^-)|^2 = 2|A(B^+ \to \overline{D}^0 K^+)||A(B^+ \to D^0 K^+)| \sin(\delta_2 - \delta_1) \sin\gamma. \tag{10}$$

The procedure for obtaining γ is straightforward. Measurements of the rates of the above six proccesses, two pairs of which are equal, determine the lengths of all six sides of the two triangles. When the two triangles are formed, 2γ is the angle between $A(B^+ \to D^0 K^+)$ and $A(B^- \to \overline{D}^0 K^-)$. This determines the magnitude of γ (even if $\delta_1 = \delta_2$) within a two-fold ambiguity related to a possible interchange of γ and $\delta_1 - \delta_2$. This ambiguity may be resolved by carrying out this analysis for other decay processes of the type $B^\pm \to D^0(\overline{D}^0, D^0_{1(2)})X^\pm$, where $X^\pm$ is any other state with the flavor quantum number of a $K^\pm$.

The feasibility of observing a CP asymmetry in $B^+ \to D^0_{1(2)}K^+$ depends on the branching ratios of the three related decays, and on the values of the weak and strong phases. An estimate, $BR(B^+ \to \overline{D}^0 K^+) \approx 2 \times 10^{-4}$, is obtained from the corresponding Cabibbo-allowed rate [10] of $B^+ \to \overline{D}^0 \pi^+$. The number of $B^+ \to D^0_{1(2)}K^+$ events is suppressed by a 5 – 10% efficiency for detecting a neutral D meson through its CP decay modes. The worst factor may be the unknown branching ratio of $B^+ \to D^0 K^+$. This process, in which the two quarks of the $c\bar{s}$ current enter two different meson states, is usually assumed to be "color-suppressed". Color suppression has already been varified in $B \to D\pi$, for which two processes are shown in Fig.6. Here one has [10] $BR(B_d^0 \to D^-\pi^+) = (2.2 \pm 0.5) \times 10^{-3}$ for the

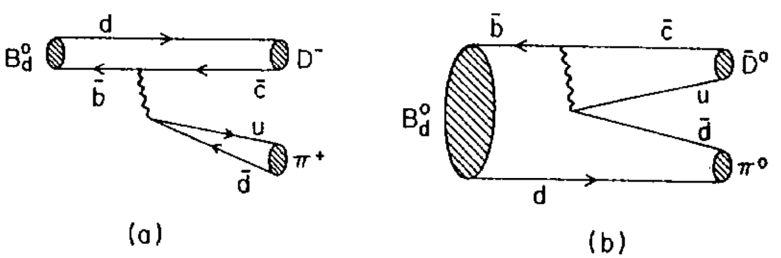

Figure 6: Color-allowed (a) and color-suppressed (b) $B \to D\pi$ decays.

color-allowed decay, whereas for the color-suppressed mode one has the limit $BR(B_d^0 \to \overline{D}^0\pi^0) < 3.5 \times 10^{-4}$. *If the same suppression factor applies also to* $B^+ \to D^0 K^+$, then the branching ratio of this process is at the level of a few times 10^{-5} or smaller.

Using the value $BR(B^+ \to D^0 K^+) = 5 \times 10^{-6}$, the feasibility for observing a CP asymmetry in $B^+ \to D^0_{1(2)}K^+$ was recently studied [11] as function of γ and $\delta_2 - \delta_1$, for a (symmetric) $e^+e^- \to \Upsilon(4S)$ B-factory with an integrated luminosity of $20 fb^{-1}$. It was found that even with the above small branching ratio the discovery region covers a significant part of the $(\gamma, \delta_2 - \delta_1)$ plane. For small final state phase differences the experiment is sensitive mainly to values of γ around 90^0. Large values of $\delta_2 - \delta_1$ allow measurement of γ in the range $50^0 \leq \gamma \leq 130^0$. Note that the branching ratio of $B^+ \to D^0 K^+$ may be considerably larger than 5×10^{-6} which would lead to a wider discovery region.

Present experiments are reaching the level of being able to observe the first Cabibbo suppressed decays $B \to DK$. The question of color-suppression in these decays needs to be studied. At this point, the assumption of a universal color-suppression factor should be taken with a great deal of caution. For instance, the dynamics may be different in $B^+ \to D^0 K^+$ (Fig. 4(b)), which involves a heavy-to-light quark transition, and in $B_d^0 \to \overline{D}^0\pi^0$ (Fig.6(b)), which is a heavy-to-heavy quark transition. Factorization, which is one assumption needed to calculate two-body decay rates, can only be argued for in heavy-to-heavy transitions.[12]

4. CP VIOLAION IN $B^0 - \overline{B}^0$ MIXING

The flavor states B^0 and $\overline{B}^0$ mix through the weak interactions to form the "Light" and "Heavy" mass-eigenstates B_L and B_H:

$$|B_L\rangle = p|B^0\rangle + q|\overline{B}^0\rangle\ ,$$

$$|B_H\rangle = p|B^0\rangle - q|\overline{B}^0\rangle\ . \tag{11}$$

The Hamiltonian eigenvalue equation (using CPT)

$$\begin{pmatrix} M - \frac{i}{2}\Gamma & M_{12} - \frac{i}{2}\Gamma_{12} \\ M_{12}^* - \frac{i}{2}\Gamma_{12}^* & M - \frac{i}{2}\Gamma \end{pmatrix} \begin{pmatrix} p \\ \pm q \end{pmatrix} = (m_{L,H} - \frac{i}{2}\Gamma_{L,H}) \begin{pmatrix} p \\ \pm q \end{pmatrix} \tag{12}$$

has the following solution for the mixing parameter $q/p \equiv (1 - \epsilon_B)/(1 + \epsilon_B)$:

$$\frac{q}{p} = \sqrt{\frac{M_{12}^* - \frac{i}{2}\Gamma_{12}^*}{M_{12} - \frac{i}{2}\Gamma_{12}}}\ . \tag{13}$$

Since q/p has a phase freedom under redefinition of the phases of the flavor states B^0, $\overline{B}^0$ ($|B^0\rangle \to e^{i\xi}|B^0\rangle$, $|\overline{B}^0\rangle \to e^{-i\xi}|\overline{B}^0\rangle \Rightarrow (q/p) \to e^{2i\xi}(q/p)$), $|q/p| = 1$ means CP conservation in $B^0 - \overline{B}^0$ mixing, and the deviation of $|q/p|$ from one measures CP violation in the mixing. Now, in the B system one has $|\Gamma_{12}| \ll |M_{12}|$. Γ_{12} is given by the absorptive part of the box diagram, Fig.7(a), arising from decay channels which are common to B^0 and $\overline{B}^0$. On the other hand, M_{12} is the dispersive part of the diagram, Fig.7(b), governed by the t quark mass. Crudely speaking $|\Gamma_{12}/M_{12}| \sim m_b^2/m_t^2$. Thus CP violation in $B^0 - \overline{B}^0$ mixing is expected to be very small in the Standard Model,[13] $|q/p| - 1 \sim \mathcal{O}(10^{-3})$. This is about the level of violation measured in the neutral K meson system.

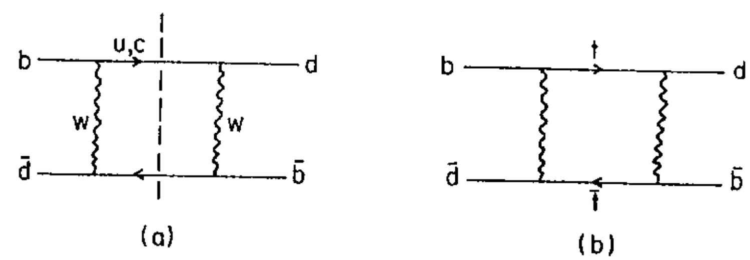

Figure 7: Box diagrams of Γ_{12} (a) and M_{12} (b).

CP violation in $B^0 - \overline{B}^0$ mixing is expected to show up as a charge asymmetry in semileptonic decays to "wrong charge" leptons, namely leptons to which only a mixed neutral B can decay:

$$A_{SL} = \frac{\Gamma(\overline{B}^0(t) \to \ell^+\nu X) - \Gamma(B^0(t) \to \ell^-\overline{\nu}X)}{\Gamma(\overline{B}^0(t) \to \ell^+\nu X) + \Gamma(B^0(t) \to \ell^-\overline{\nu}X)} . \tag{14}$$

$B^0(t)$ $(\overline{B}^0(t))$ is a time-evolving state, which was a pure B^0 $(\overline{B}^0)$ state at $t = 0$. The asymmetry can be easily shown to be time-independent:

$$A_{SL} = \frac{1 - |q/p|^4}{1 + |q/p|^4} \approx 4\mathrm{Re}\epsilon_B . \tag{15}$$

A recent 90% c.l. experimental upper limit from CLEO,[14] $|\mathrm{Re}\epsilon_B| < 45 \times 10^{-3}$, is almost two orders of magnitude above the Standard Model prediction. It will be extremely difficult to observe an asymmetry at this tiny level. Also, since the calculation of $|q/p| - 1$ involves hadronic uncertainties, this asymmetry would not provide a useful quantitative test of the CKM mechanism. A large asymmetry would rule out the model.

Let us note in passing that while CP violation in the $B^0 - \overline{B}^0$ *mixing* is expected to be at the level of the one observed in $K^0 - \overline{K}^0$ mixing, the asymmetries expected in neutral B *decays* are much larger than those of K decays. Thus, when discussing neutral B decay asymmetries in the following section we will take $|q/p| = 1$ which is a very good approximation. In this approximation

$$\frac{q}{p} \approx \sqrt{\frac{M_{12}^*}{M_{12}}} \equiv e^{-2i\phi_M} = \begin{cases} e^{-2i\beta} & \text{for } B_d^0 , \\ 1 & \text{for } B_s^0 , \end{cases} \tag{16}$$

where the last relation is obtained in the quite standard phase convention used in Fig.1. We will also assume $\Gamma_L = \Gamma_H$, which is a good approximation, in particular for B_d^0 where it is expected to hold within better than 1% accuracy.

5. CP VIOLATION IN DECAYS OF MIXED $B^0 - \overline{B}^0$

5.1 Time-dependent Asymmetries in the General Case

Consider the time-evolution of a state which is identified at time $t = 0$ as a B^0:

$$t = 0 : \quad |B^0\rangle = \frac{e^{-i\phi_M}}{\sqrt{2}}(|B_L\rangle + |B_H\rangle) . \tag{17}$$

The time-evolutions of the states $B_{L,H}$ are given simply by their masses and by their equal decay width Γ: $|B_{L,H}(t=0)\rangle \to |B_{L,H}(t)\rangle = \exp[-i(m_{L,H} - \frac{i}{2}\Gamma)t]|B_{L,H}(t=0)\rangle$. Thus, in proper time t the B^0 oscillates into a mixture of B^0 and $\overline{B}^0$:

$$t : \quad |B^0(t)\rangle = e^{-i\overline{m}t}e^{-\frac{\Gamma}{2}t}[\cos(\frac{\Delta mt}{2})|B^0\rangle + ie^{-2i\phi_M}\sin(\frac{\Delta mt}{2})|\overline{B}^0\rangle] , \tag{18}$$

where $\overline{m} \equiv (m_H + m_L)/2$, $\Delta m \equiv m_H - m_L$. Now, assume that both B^0 and $\overline{B}^0$ can decay to a common state f, with amplitudes A and $\overline{A}$, respectively. The time-dependent decay rate to f of an initial B^0 and the corresponding rate for an initial $\overline{B}^0$ are then given by

$$\Gamma(B^0(t) \to f) = e^{-\Gamma t}|A|^2[\cos^2(\frac{\Delta mt}{2}) + |\overline{A}/A|^2\sin^2(\frac{\Delta mt}{2}) - \mathrm{Im}(e^{-2i\phi_M}\overline{A}/A)\sin(\Delta mt)] ,$$

$$\Gamma(\overline{B}^0(t) \to f) = e^{-\Gamma t}|A|^2[|\overline{A}/A|^2\cos^2(\frac{\Delta mt}{2}) + \sin^2(\frac{\Delta mt}{2}) + \mathrm{Im}(e^{-2i\phi_M}\overline{A}/A)\sin(\Delta mt)] . \tag{19}$$

In the special case that f is an eigenstate of CP, $CP|f\rangle = \pm|f\rangle$, CP violation is manifest when $\Gamma(t) \equiv \Gamma(B^0(t) \to f) \neq \Gamma(\overline{B}^0(t) \to f) \equiv \overline{\Gamma}(t)$. In general the CP asymmetry is then given by:[15]

$$Asym.(t) \equiv \frac{\Gamma(t) - \overline{\Gamma}(t)}{\Gamma(t) + \overline{\Gamma}(t)} = \frac{(1 - |\overline{A}/A|^2)\cos(\Delta mt) - 2\mathrm{Im}(e^{-2i\phi_M}\overline{A}/A)\sin(\Delta mt)}{1 + |\overline{A}/A|^2} . \tag{20}$$

The two terms in the numerator represent different sources of CP violation. The first term follows from CP violation in the direct decay of a neutral B meson, whereas the second term is induced by $B^0 - \overline{B}^0$ mixing.

5.2 Deacys to CP Eigenstates Dominated by a Single CKM Phase

Let us first consider the case of no direct CP violation, $|\overline{A}| = |A|$, in which a single weak amplitude (or rather a single weak phase) dominates the decay.[16] This is the case of a maximal interference term in Eqs.(19). Denoting the weak and strong phases by ϕ_D and δ, respectively, we have $A = |A|\exp(i\phi_D)\exp(i\delta)$, $\overline{A} = \pm|\overline{A}|\exp(-i\phi_D)\exp(i\delta)$, and the asymmetry is given simply by

$$Asym.(t) = \pm\sin 2(\phi_M + \phi_D)\sin(\Delta mt) . \tag{21}$$

The sign is given by $CP(f)$. The time-integrated asymmetry is

$$Asym. = \pm(\frac{\Delta m/\Gamma}{1 + (\Delta m/\Gamma)^2})\sin 2(\phi_M + \phi_D) . \tag{22}$$

That is, in this case *the CP asymmetry measures a CKM phase with no hadronic uncertainty.*

The best example is the well-known and much studied [17] case of $B_d^0 \to \psi K_S$, for which a branching ratio of $(5.6 \pm 0.9) \times 10^{-4}$ may be obtained by isospin from the measured [10] value of $BR(B^- \to \psi K^-)$. In this case $\phi_M = \beta$, $\phi_D = \arg(V_{cb}^*V_{cs}) = 0$, $CP(\psi K_S) = -1$. Another case is $B_d^0 \to \pi^+\pi^-$, for which only a combined branching ratio $BR(B_d^0 \to \pi^+\pi^- + K^+\pi^-) = (2.3 \pm 0.8) \times 10^{-5}$ exists at present, with $\phi_D = \arg(V_{ub}^*V_{ud}) = \gamma$, $CP(\pi^+\pi^-) = 1$. Consequently one has in these two cases

$$Asym.(B_d^0 \to \psi K_S; t) = -\sin 2\beta\sin(\Delta mt) ,$$

$$Asym.(B_d^0 \to \pi^+\pi^-; t) = -\sin 2\alpha\sin(\Delta mt) . \tag{23}$$

In the case of decay to two pions the asymmetry obtains, however, corrections from a second (penguin) CKM phase. This problem will be studied below.

5.3 Deacys to Non-CP Eigenstates

Angles of the unitarity triangle can also be determined from neutral B decays to states f which are not eigenstates of CP.[18] This is feasible when both a B^0 and a $\overline{B}^0$ can decay to a final state which appears in only one partial wave, provided that a single CKM phase dominates each of the corresponding decay amplitudes.

The time-dependent rates for states which were B^0 or $\overline{B}^0$ at $t=0$ and decay at time t to a state f or its charge-conjugate $\overline{f}$ are given by:[19]

$$\Gamma_f(t) = e^{-\Gamma t}[|A|^2\cos^2(\frac{\Delta mt}{2}) + |\overline{A}|^2\sin^2(\frac{\Delta mt}{2}) + |A\overline{A}|\sin(\Delta\delta + \Delta\phi_D + 2\phi_M)\sin(\Delta mt)]\ ,$$

$$\overline{\Gamma}_f(t) = e^{-\Gamma t}[|\overline{A}|^2\cos^2(\frac{\Delta mt}{2}) + |A|^2\sin^2(\frac{\Delta mt}{2}) - |A\overline{A}|\sin(\Delta\delta + \Delta\phi_D + 2\phi_M)\sin(\Delta mt)]\ ,$$

$$\Gamma_{\overline{f}}(t) = e^{-\Gamma t}[|\overline{A}|^2\cos^2(\frac{\Delta mt}{2}) + |A|^2\sin^2(\frac{\Delta mt}{2}) - |A\overline{A}|\sin(\Delta\delta - \Delta\phi_D - 2\phi_M)\sin(\Delta mt)]\ ,$$

$$\overline{\Gamma}_{\overline{f}}(t) = e^{-\Gamma t}[|A|^2\cos^2(\frac{\Delta mt}{2}) + |\overline{A}|^2\sin^2(\frac{\Delta mt}{2}) + |A\overline{A}|\sin(\Delta\delta - \Delta\phi_D - 2\phi_M)\sin(\Delta mt)]\ . \quad (24)$$

Here $\Delta\delta$, $(\Delta\phi_D)$ is the differences between the strong (weak) phases of A and $\overline{A}$. The four rates depend on four unknown quantities, $|A|$, $|\overline{A}|$, $\sin(\Delta\delta + \Delta\phi_D + 2\phi_M)$, $\sin(\Delta\delta - \Delta\phi_D - 2\phi_M)$. Measurement of the rates allows a determination of the weak CKM phase $\Delta\phi_D + 2\phi_M$ apart from a two-fold ambiguity.[18]

There are two interesting examples to which this method may be applied. In the first case, $B_d^0 \to \rho^+\pi^-$, one must neglect a second contribution of a penguin amplitude, a problem which will be addressed in the following subsection. Assuming for a moment that tree diagrams, shown in Figs. 8(a), 8(b), dominate A and $\overline{A}$, one can measure in this manner the angle α, since in this case $\Delta\phi_D + 2\phi_M = 2(\gamma+\beta) = 2(\pi-\alpha)$. A decay, which may be used to measure γ, is $B_s^0 \to D_s^+K^-$, in which the single amplitude which contributes is shown in Figs.9(a), 9(b) for A and $\overline{A}$. Here $\Delta\phi_D + 2\phi_M = \gamma$.

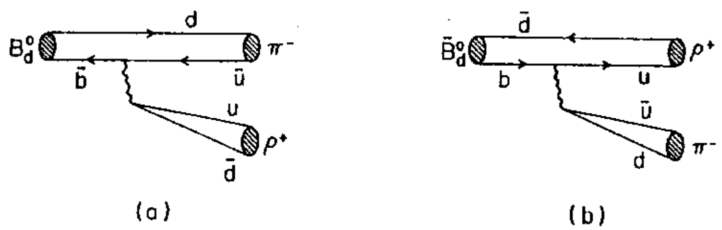

Figure 8: Diagrams of $B_d^0 \to \rho^+\pi^-$ (a) and $\overline{B}_d^0 \to \rho^+\pi^-$ (b).

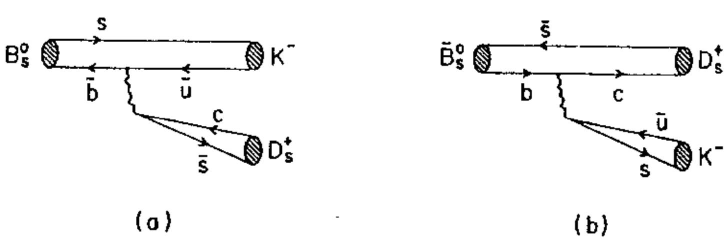

Figure 9: Diagrams of $B_s^0 \to D_s^+K^-$ (a) and $\overline{B}_s^0 \to D_s^+K^-$ (b).

5.4 Corrections from Penguin Amplitudes

A crucial question is, of course, how good is the assumption of a single dominant CKM phase, which is needed for a hadronic-free determination of an angle of the unitarity triangle. An experimental way to answer this question is to look for an extra $\cos(\Delta mt)$ term in the time-dependent asymmetry of Eq.(20) which describes CP violation in the direct decay of B^0. There is, however, the danger that this term will be unobservably small, just because final state interaction phase differences happen to be small. The effect of a second amplitude on the coefficient of $\sin(\Delta mt)$, which is proportional to the cosine of this phase-difference, may still be large.

In a large variety of decay processes there exists a second amplitude due to "penguin" diagrams[20] in addition to the usual "tree" diagram. In general, the new contribution becomes more disturbing when the process becomes more CKM-suppressed. Thus, in the case of $B_d^0 \to K_S\pi^0$, for which the two diagrams are similar to those shown in Fig.3, the penguin diagram may, in fact, dominate. The penguin-to-tree ratio of amplitudes is proportinal to the ratio of the corresponding CKM factors and to a QCD fator $(\alpha_s(m_b^2)/12\pi)\ln(m_t^2/m_b^2)$. This ratio may be estimated for a given process. A few examples of final states in B_d^0 decays, characterizing different levels of CKM suppression, are:[15]

$$\frac{\text{Penguin}}{\text{Tree}} = \begin{cases} 10^{-3} & \psi K_S\ , \\ 0.05 & D^+D^-\ (D^{*+}D^-)\ , \\ 0.20 & \pi^+\pi^-\ (\rho^+\pi^-)\ , \\ \mathcal{O}(1) & K_S\pi^0\ . \end{cases} \quad (25)$$

These numbers represent quite crude estimates, since there exists no reliable method to calculate hadronic matrix elements of penguin operators. One way to obtain information about these matrix elements would be to measure pure penguin processes, such as $B_d^0 \to \phi K_S$.

We see from Eqs.(25) that the decay $B_d^0 \to \psi K_S$ remains a pure case, within less than 1%, also in the presence of penguin contributions. On the other hand, penguin effects on the CP asymmetry of $B_d^0 \to \pi^+\pi^-$ may be substantial. This is demonstrated in Fig.10, taken from Ref. 21, which shows the coefficient of the $\sin(\Delta mt)$ term in this asymmetry as function of the angle α for a zero final state interaction phase difference. The range of values comes from taking the ratio (Penguin/Tree) to be between 0.04 and 0.20. An asymmetry as large as 0.4 can possibly be measured even when $\sin(2\alpha) = 0$.

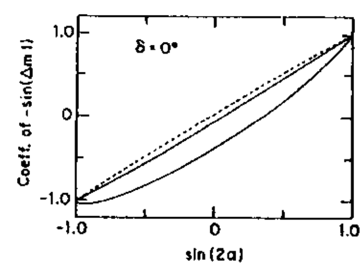

Figure 10: Asymmetry in $B_d^0 \to \pi^+\pi^-$ as function of α .

5.5 Removing Penguin Corrections in $B_d^0 \to \pi^+\pi^-$

It is possible to disentangle the penguin contribution in $B_d^0 \to \pi^+\pi^-$ from the tree-dominating asymmetry by measuring also the rates of $B^+ \to \pi^+\pi^0$ and $B_d^0 \to \pi^0\pi^0$. The method [22] is based on the observation that the two weak operators contributing to the three isospin-related processes have different isospin properties. Whereas the tree operator is a mixture of $\Delta I = 1/2$ and $\Delta I = 3/2$, the penguin operator is pure $\Delta I = 1/2$. Denoting the physical amplitudes of $B \to \pi^+\pi^-, \pi^0\pi^0, \pi^+\pi^0$ by the charges of the two corresponding pions, one finds from an isospin decomposition

$$\frac{1}{\sqrt{2}}A^{+-} = A_2 - A_0\ , \quad A^{00} = 2A_2 + A_0\ , \quad A^{+0} = 3A_2\ , \tag{26}$$

where A_0 and A_2 are the amplitudes for a B_d^0 or a B^+ to decay into a $\pi\pi$ state with $I = 0$ and $I = 2$, respectively. This yields the complex triangle relation

$$\frac{1}{\sqrt{2}}A^{+-} + A^{00} = A^{+0}\ . \tag{27}$$

There is a similar triangle relation for the charge-conjugated processes:

$$\frac{1}{\sqrt{2}}\overline{A}^{+-} + \overline{A}^{00} = \overline{A}^{-0}\ . \tag{28}$$

Here, $\overline{A}^{+-}$, $\overline{A}^{00}$, and $\overline{A}^{-0}$ are the amplitudes for the processes $\overline{B}_d^0 \to \pi^+\pi^-$, $\overline{B}_d^0 \to \pi^0\pi^0$, and $B^- \to \pi^-\pi^0$, respectively. The $\overline{A}$ amplitudes are obtained from the A amplitudes by simply changing the sign of the CKM phases (the strong phases remain the same).

The crucial point in the analysis is that the pure "tree" amplitude A_2 has a well-defined weak phase, which is given by the angle γ of the unitarity triangle:

$$A_2 = |A_2|e^{i\delta_2}e^{i\gamma}\ , \quad \overline{A}_2 = |A_2|e^{i\delta_2}e^{-i\gamma}\ . \tag{29}$$

where δ_2 is the $I = 2$ final-state-interaction phase. It is convenient to define $\tilde{A} = \exp(2i\gamma)\overline{A}$ so that $\tilde{A}_2 = A_2$ and $\tilde{A}^{-0} = A^{+0}$. The two complex triangles representing Eqs. (27)(28) (where $\overline{A}$ is replaced by $\tilde{A}$) are shown in Fig.11. They have a common base (CP is conserved in $B^+ \to \pi^+\pi^0$); however the length of their corresponding sides are different. That is, CP is violated in $B_d^0 \to \pi^+\pi^-$ and in $B_d^0 \to \pi^0\pi^0$.

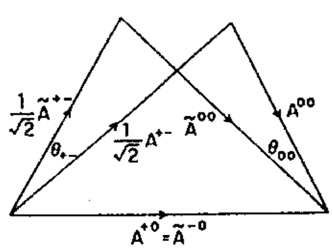

Figure 11: Isospin triangles of $B \to \pi\pi$.

The six sides of the two triangles are measured by the decay rates of $B^\pm$ and by the time-integrated rates of B_d^0 ($\overline{B}_d^0$). This determines the two triangles within a two-fold ambiguity; each triangle may be turned up-side-down. The coefficient of the $\sin(\Delta mt)$ term in the time-dependent decay rate of $B_d^0 \to \pi^+\pi^-$ measures the quantity

$$\mathrm{Im}\,(e^{-2i(\beta+\gamma)}\frac{\tilde{A}^{+-}}{A^{+-}}) = \frac{|\tilde{A}^{+-}|}{|A^{+-}|}\sin(2\alpha + \theta_{+-}). \tag{30}$$

θ_{+-}, which vanishes in the absence of the penguin correction, is obtained from Fig.11. This determines the angle α.

The feasibilty of applying this method in asymmetric e^+e^- B-Factories [23] depends not only on the small branching ratio of $B_d^0 \to \pi^+\pi^-$, but also on the presumably smaller decay rate into neutral pions. Measurement of a much smaller rate for neutral pions would confirm color-suppression of the tree diagram in this process.

Similar isospin analyses may be carried out for other decays in which penguin amplitudes are involved.[24] In general, the precision of determining a CKM phase becomes worse when a larger number of amplitudes must be related. Also a few ambiguities show up in this case. In the above-discussed case of $B_d^0 \to \rho\pi$ (and $B^+ \to \rho\pi$) five physical decay amplitudes appear. In this case the ambiguity can be resolved if a full Dalitz plot analysis can be made for the three pion final states.[25]

6. FLAVOR-TAGGING OF NEUTRAL B MESONS

6.1 The Conventional Method

In order to measure CP asymmetries in neutral B decays one must identify the flavor of the decaying meson at some reference time ($t = 0$ in Eq.(21)). In a $e^+e^- \to \Upsilon(4S)$ B-factory this is achieved [17] by observing a lepton (or a cascade charged kaon from $B \to D \to K$) from the decay of the other neutral B. Since at any time after production the two neutral B mesons form a *coherent* $C(B^0\overline{B}^0) = -1$ EPR pair, the charge of the lepton serves to "tag" the opposite flavor of the other B at the time of semileptonic decay. Furthermore, the CP asymmetry is odd in the time-difference of the two decays, and consequently asymmetric storage rings are required for an asymmetry measurement.

The conventional method of determining the flavor of neutral B mesons in high energy e^+e^- or in hadronic collisions [26] is to use as a "tag" the lepton from a semileptonic decay of an associated b-meson or b-baryon. The flavor is misidentified part of the time as a result of $B^0 - \overline{B}^0$ mixing. The probability of misidentification and its effect on diluting the measured CP asymmetry can only be crudely estimated. Since the B^0 and $\overline{B}^0$ are usually produced with many other particles, it is commonly assumed that they are in an *incoherent* mixture.

6.2 Flavor-Tagging by Correlated Pions

Recently an alternative method of flavor identification was suggested [27], which uses a correlation of the decaying neutral B with charged pions produced nearby in phase space.

We have also presented a way of testing experimentally for arbitrary coherence properties of the B^0, $\overline{B}^0$ mixture state [28]. This general tagging procedure can determine weak phases from measured asymmetries, independent of any theoretical assumption about properties of the initially produced state. We will briefy describe the idea of this method and the manner in which it can be applied.

There are two arguments for an expected correlation between the flavor of a neutral B and the charge of a pion which makes a low mass $B-\pi$ system. The first argument is based on the existence of positive-parity "B^{**}" resonances, with $J^P = 0^+, 1^+, 2^+$ and masses below about 5.8 GeV/c^2. Using Heavy Quark Symmetry, this mass value is obtained from the corresponding observed "D^{**}" masses (2420, 2460 GeV/c^2). The B^{**} resonances decay to $B\pi$ and/or $B^*\pi$ mesons in $I = 1/2$ states. That is, a π^+ will accompany a B^0_d and not a $\overline{B}^0_d$. The production of D^{**} is about 20% of all D mesons produced in the e^+e^- continuum and in charm- photoproduction.[29] Similar relative rates may be assumed for B^{**} production.

The second argument is that in b-quark fragmentation the leading pion carries information about the flavor of the neutral B (B^*), as illustrated in Fig.12. This effect was calculated for LEP energies [30], and an asymmetry $[N(B^0\pi^+)-N(B^0\pi^-)]/[N(B^0\pi^+)+N(B^0\pi^-)] = 0.27$ was found at and slightly above a $B\pi$ mass of 5.8 GeV/c^2. Adding B^{**} production at a level of 20% may lead to asymmetries as large as 40% or so. The asymmetries may be less pronounced at the Tevatron, where the b and $\bar{b}$ jets are not as strongly separated. An important experimental question is, of course, how to maximize this correlation using different kinematical constraints on the $B-\pi$ system, such as the range of invariant mass or the relative angle/transverse momentum/rapidity of the two particles.

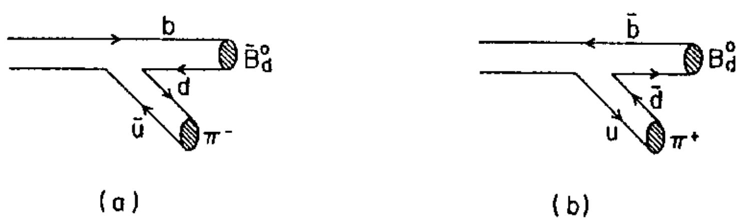

Figure 12: Fragmentation of $b(\bar{b})$ into $\overline{B}^0_d(B^0_d)$ with production of a charged pion.

Let us denote $N(B^0\pi^+) = P_1$ and $N(B^0\pi^-) = P_2$, for low-mass $B-\pi$ combinations, so that one expects $P_1 > P_2$. We will consider charge-symmetric production processes, such as in e^+e^- and $\bar{p}p$ collisions, in which $N(B^0\pi^+) = N(\overline{B}^0\pi^-)$, $N(B^0\pi^-) = N(\overline{B}^0\pi^+)$. Let us imagine that a neutral B decays to a state of identifiable flavor, for instance $B^0 \to \psi K^{*0}$ where the flavor of the neutral K^* is identified by $K^{*0} \to K^+\pi^-$. Denoting the relative numbers of "right-sign" combinations ($B^0\pi^+$ or $\overline{B}^0\pi^-$) by R and the numbers of "wrong-sign" combinations ($B^0\pi^-$ or $\overline{B}^0\pi^+$) by W, these time-dependent numbers are obtained from Eq.(18) as functions of proper decay time:

$$R(t) = e^{-\Gamma t}[P_1\cos^2(\frac{\Delta m t}{2}) + P_2\sin^2(\frac{\Delta m t}{2})] ,$$

$$W(t) = e^{-\Gamma t}[P_1\sin^2(\frac{\Delta m t}{2}) + P_2\cos^2(\frac{\Delta m t}{2})] . \tag{31}$$

In obtaining Eqs.(31) we assumed that the produced B^0 and $\overline{B}^0$ are always incoherent with respect to one another. The time-dependent asymmetry is

$$\frac{R(t)-W(t)}{R(t)+W(t)} = \frac{P_1-P_2}{P_1+P_2}\cos(\Delta m t) . \tag{32}$$

The corresponding time-integrated asymmetry is

$$\frac{\int[R(t)-W(t)]dt}{\int[R(t)+W(t)]dt} = \frac{P_1-P_2}{P_1+P_2}\frac{1}{1+(\Delta m/\Gamma)^2} . \tag{33}$$

The tagging dilution factor $(P_1-P_2)/(P_1+P_2)$, which measures the $B-\pi$ correlation, may be determined from Eqs.(32) (33). Statistically, the time-dependent asymmetry may be more powerful than the time-integrated one. Also, to gain statistics, one may add up in the numerator and denominator of the asymmetry a few specific-flavor decay modes, such as ψK^{*0}, $D^{*-}\pi^+$, etc.

Let us note in passing that Eqs.(31)-(33) hold also for the conventional method of flavor tagging, which uses the semileptonic decay of the b-hadron produced in association with the neutral B. In this case P_1 and P_2 are the probabilities of right and wrong flavor tagging.

6.3 CP Asymmetries with Correlated Pions

In neutral B decays to a CP eigenstate, such as $B^0_d \to \psi K_S$, one now considers $B-\pi$ combinations in the same low mass range as in the specific flavor decays. An asymmetry is defined in terms of the charge of the pion produced along with the neutral B:

$$Asym.(\psi K_S, \pi; t) \equiv \frac{N(\psi K_S, \pi^+; t) - N(\psi K_S, \pi^-; t)}{N(\psi K_S, \pi^+; t) + N(\psi K_S, \pi^-; t)} . \tag{34}$$

Using Eq.(18) one finds

$$Asym.(\psi K_S, \pi; t) = -(\frac{P_1-P_2}{P_1+P_2})\sin 2\beta \sin(\Delta m t) , \tag{35}$$

and an integrated asymmetry

$$Asym.(\psi K_S, \pi) = -(\frac{P_1-P_2}{P_1+P_2})(\frac{(\Delta m/\Gamma)}{1+(\Delta m/\Gamma)^2})\sin 2\beta . \tag{36}$$

These asymmetries and the correlation factor $(P_1-P_2)/P_1+P_2)$ determined from Eqs.(32)

(33) can then be used to find $\sin 2\beta$. Again, we should point out that Eqs.(35)(36) hold also in case of tagging with leptons from decays of the associated b-hadron; however here the asymmetry in Eq.(34) is defined in terms of $\ell^{\pm}$ instead of $\pi^{\pm}$.

6.4 The Question of Coherence

The tagging asymmetries of Eqs.(32)(33) and the CP asymmetries of Eqs.(35)(36) were obtained under the assumption that the produced B^0 and $\overline{B}^0$ are incoherent with respect to one another. Although this is quite plausible, since the two mesons are usually separated in rapidity by many intermediate hadrons, this assumption should be tested. In a recent study [28] we have shown how to use the above two kinds of asymmetries both to completely specify the coherence properties of the produced $B^0/\overline{B}^0$ state and to determine a weak CKM phase. In brief, one uses a density matrix in a "quasispin" space of B^0 and $\overline{B}^0$ to describe a general neutral B state. One then finds instead of Eqs.(32) and (35) the following asymmetries:

$$\frac{R(t) - W(t)}{R(t) + W(t)} = Q'_{\perp} \cos(\Delta m t + \varphi) \;, \tag{37}$$

$$Asym.(\psi K_S, \pi; t) = -(\frac{Q'_{\perp}}{1 - Q'_3 \cos 2\beta}) \sin 2\beta \sin(\Delta m t + \varphi) \;. \tag{38}$$

The three parameters $Q'_{\perp}$, Q'_3 and φ describe an arbitrary coherent, partially coherent, or incoherent combination of neutral B^0 and $\overline{B}^0$. Incoherent production, with relative probabilities P_1, P_2 for B^0, $\overline{B}^0$, is described by $Q'_{\perp} = (P_1 - P_2)/(P_1 + P_2)$, $Q'_3 = 0$, $\varphi = 0$. Coherence ($\varphi \neq 0$ and/or $Q'_3 \neq 0$) is characterized by a phase shift in Eqs.(37)(38), and by a change in normalization of the CP-eigenstate production rate. $Q'_{\perp}$ and φ can be measured by Eq.(37). The CP asymmetry of Eq.(38) can then be used to determine both Q'_3 and β. For the former one needs to normalize the production rate of the CP eigenstate ψK_S by the production rate of a corresponding flavor state, such as ψK^+.[28]

7. CONCLUSION

We have shown how expected large CP asymmetries in B decays can determine CKM phases in manners which are free of hadronic uncertainties. With other (CP conserving) measurements, this may eventually serve to overconstrain the CKM matrix. A determination of the three angles of the unitarity triangle is based theoretically on different types of asymmetries and is expected to involve different levels of experimental difficulty. The most promising measurement seems at present to be that of the angle β in $B^0_d \to \psi K_S$. This is the simplest case of CP violation in decays of mixed $B^0\overline{B}^0$, which essentially involves no corrections from CP nonconservation in direct decay. In the asymmetry of $B^0_d \to \pi^+\pi^-$ ($\rho^{\pm}\pi^{\mp}$), which measures the angle α , one will have to disentangle direct decay CP violation from the measured asymmetry. This requires a good detector for neutral pions. A time-independent determination of γ from direct decay CP violation in $B^{\pm} \to D^0_{1,2}K^{\pm}$ may be feasible if $BR(B^+ \to D^0 K^+)$ is not too strongly color-suppressed.

Finally, we presented a new idea of tagging neutral B mesons, based on their correlation with nearby pions. This may be a very promising possibility if one can establish experimentally a strong correlation. The number of B mesons in modes such as ψK and ψK^* reconstructed by CDF [31] and LEP collaborations [32] is sufficiently large that these correlations are already under investigation.[33] A first time-dependent measurement of $B^0 - \overline{B}^0$ oscillations was recently made by the ALEPH Collaboration.[34] In view of the sizable number of reconstructed B's and the expected progress in high resolution vertex detectors, it seems that the first time-dependent studies searching for CP violation may be made not too far in the future.

8. ACKNOWLEDGEMENTS

It is a pleasure to thank David London, Jonathan Rosner and Daniel Wyler for very enjoyable collaborations. I wish to thank numerous friends and other participants at this meeting for useful discussions. This work was supported in part by the United States - Israel Binational Science Foundation under Research Grant Agreement 90-00483/2 and by the Fund for Promotion of Research at the Technion.

9. REFERENCES

1. I.I. Bigi, V.A. Khoze, N.G. Uraltsev and A.I. Sanda, in *CP Violation*, ed. C. Jarlskog (World Scientific, Singapore, 1989), p. 175; Y. Nir and H. Quinn, *Ann. Rev. Nucl. Part. Sci.* **42** (1992) 211.
2. N. Cabibbo, *Phys. Rev. Lett.* **10** (1963) 531; M. Kobayashi and T. Maskawa, *Prog. Theor. Phys.* **49** (1973) 652.
3. D. Besson, Invited talk presented at *the XVI International Symposium on Lepton and Photon Interactions*, Cornell University, August 10-15, 1993.
4. L. Wolfenstein, *Phys. Rev. Lett.* **51** (1983) 1945.
5. See, e.g., Y. Nir and H. Quinn, Ref.1 and references therein.
6. B. Winstein and L. Wolfenstein, to appear in *Rev. Mod. Phys.* **65**, October 1993.
7. L.L. Chau and H. Y. Cheng, *Phys. Rev. Lett.* **59** (1987) 958; N. Deshpande and J. Trampetic, *Phys. Rev.* **D41** (1990) 2926; J.M. Gerard and W.S. Hou, *Phys. Rev.* **D43** (1991) 2909; H. Simma, G. Eilam and D. Wyler, *Nucl. Phys.* **B352** (1991) 367.
8. M. Gronau and D. Wyler, *Phys. Lett.* **B265** (1991) 172. See also M. Gronau and D. London, *Phys. Lett.* **B253** (1991) 483; I. Dunietz, *Phys. Lett* **B270** (1991) 75.
9. I.I. Bigi and A.I. Sanda, *Phys. Lett.* **B211** (1988) 213.
10. S.L Stone, Invited talk presented at *the Fifth International Symposium on Heavy Flavor Physics*, Montreal, Canada, July 6-10, 1993.
11. S. Stone, in *Beauty 93, Proceedings of the First International Workshop on B Physics at Hadron Machines*, Liblice Castle, Melnik, Czech Republic, Jan. 18-22, 1993; edited by P.E. Schlein, *Nucl. Instrum. Meth.* **333** (1993) 15.
12. M.J. Dugan and B. Grinstein, *Phys. Lett.* **B255** (1991) 583.
13. I. I. Bigi, et al., Ref. 1.

14. CLEO Collaboration, J. Bartelt *et al.*, *Phys. Rev. Lett.* **71** (1993) 1680.
15. M. Gronau, *Phys. Rev. Lett.* **63** (1989) 1451.
16. A.B. Carter and A.I. Sanda, *Phys. Rev. Lett.* **45** (1980) 952; *Phys. Rev.* **D23** (1981) 1567; I.I. Bigi and A.I. Sanda, *Nucl. Phys.* **B193** (1981) 85; **B281** (1987) 41; I. Dunietz and J.L. Rosner, *Phys. Rev.* **D34** (1986) 1404.
17. *The Physics Program of a High-Luminosity Asymmetric B-Factory at SLAC*, ed. D. Hitlin, SLAC-PUB-353 (1989) and SLAC-PUB-373 (1991); *Physics Rationale for a B-Factory*, K. Lingel *et al.*, CLNS 91-1043 (1991); *Physics and Detector at KEK Asymmetric B Factory*, K. Abe *et al.*, KEK Report 92-3 (1992).
18. R. Aleksan, I. Dunietz, B. Kayser and F. Le Diberder, *Nucl. Phys.* **B361** (1991) 141; R. Aleksan, I. Dunietz and B. Kayser, *Zeit. Phys.* **C54** (1992) 653.
19. M. Gronau, *Phys. Lett.* **B233** (1989) 479.
20. M. Gronau, Ref.15; D. London and R.D. Peccei, *Phys. Lett.* **B223** (1989) 257; B. Grinstein, *Phys. Lett.* **B229** (1989) 280.
21. M. Gronau, *Phys. Lett.* **B300** (1993) 163.
22. M. Gronau and D. London, *Phys. Rev. Lett.* **65** (1990) 3381.
23. R. Aleksan, A. Gaidot and G. Vasseur, in *B Factories, The State of the Art in Accelerators, Detectors and Physics*, ed. D. Hitlin, SLAC-400 (1992), p. 588.
24. H.J. Lipkin, Y. Nir, H.R. Quinn and A.E. Snyder, *Phys. Rev.* **D44** (1991) 1454; M. Gronau, *Phys. Lett.* **B265** (1991) 389.
25. A.E. Snyder and H.R. Quinn, *Phys. Rev.* **D48** (1993) 2139.
26. See e.g. *B Physics at Hadron Accelerators, Proceedings of a workshop at Fermilab*, Nov., 1992, ed. J.A. Appel (Fermilab, Batavia, Il, 1992); *Beauty 93*, Ref. 11; M. Chaichian and A. Fridman, *Phys. Lett.* **B298** (1993) 218.
27. M. Gronau, A. Nippe and J.L. Rosner, *Phys. Rev.* **D47** (1993) 1988; M. Gronau and J.L. Rosner, TECHNION-PH-93-32, EFI 93-41 (September 1993), to be published in *Phys. Rev.* **D**.
28. M. Gronau and J.L. Rosner, EFI 93-43, TECHNION-PH-93-31 (August 1993), submitted to *Phys. Rev. Lett.*
29. ARGUS Collaboration, H. Albrecht *et al.*, *Phys. Lett.* **B221** (1989) 422; **B232** (1989) 398; Fermilab E691 Collabortion, J.C. Anjos *et al.*, *Phys. Rev. Lett.* **62** (1989) 1717; CLEO Collaboration, P. Avery *et al.*, *Phys. Rev.* **D41** (1990) 774; *Phys. Lett.* **B303** (1993) 377; Fermilab E687 Collaboration, P.L. Frabetti *et al.*, FERMILAB-Pub-93/249-E (1993).
30. G. Gustafson and J. Hakkinen, work in preparation. I thank G. Gustafson for informing me about these results prior to their publication.
31. CDF Collaboration, F. Abe *et al.*, *Phys. Rev. Lett.* **68** (1992) 3403; Fermilab-Pubs-93-(091, 141, 145, 158)-E, submitted to *Phys. Rev. Lett.*
32. ALEPH Collaboration, , D.Buskulic *et al.*, *Phys. Lett.* **B307** (1993) 194; OPAL Collaboration, P.D. Acton *et al.*, *Phys. Lett.* **B307** (1993) 247.
33. T. LeCompte, V. Sharma and A. Yagil, private communications.
34. ALEPH Collaboration, D. Buskulic *et al.*, *Phys. Lett.* **B313** (1993) 498.

B DECAYS IN THE STANDARD MODEL A.ND BEYOND

DAVID LONDON
Laboratoire de physique nucléaire, Université de Montréal
C.P. 6128, succ. A, Montréal, Québec, CANADA, H3C 3J7.

1. INTRODUCTION

When Vera Lüth asked me to give a talk on B decays in and beyond the standard model (SM), I readily accepted. However, when I sat down and made a list of the topics I would have to cover, I quickly realized that I had bitten off more than I could chew. My list consisted of the following subjects:

- Semileptonic B decays: these are typically described in one of two ways. Either one picks a specific model,[1] or one uses the Heavy Quark Effective Theory (HQET);[2]
- Hadronic B decays: such decays are usually described by the BSW model;[3]
- Right-handed B decays:[4] the suggestion here is that B decays are mediated not by the ordinary W, but rather by a right-handed W_R;
- Rare B decays: included are the flavour-changing neutral-current decays $b \to s\gamma$, $b \to s\ell^+\ell^-$, $b \to s\nu\bar{\nu}$, $b \to sg$, $b \to sq\bar{q}$, and $B^0 \to \ell^+\ell^-$, as well as hadronic penguins ($B \to K\pi$, etc.), and $B^0 \to \gamma\gamma$;
- the decay $B_u^+ \to \ell^+\nu$;
- Exotic B states such as B_c's and Λ_b's;
- B-$\overline{B}$ mixing – x_d and x_s;
- T Violation (triple products),

and I'm sure I've overlooked some other possibilities. Given the length of this list, I realized that I would have to limit myself to a subset of the above topics. I therefore decided to discuss only right-handed B decays, certain rare B decays, B_c decays, B_s^0-$\overline{B_s^0}$ mixing, and T violation. Some of the other subjects, such as HQET and B baryons, are discussed elsewhere in these proceedings.[5]

2. RIGHT-HANDED B DECAYS

Gronau and Wakaizumi[4] (GW) have suggested that B decays might in fact be mediated by a right-handed W_R, instead of the SM left-handed W. This possibility is predicated on two facts. First, the chirality of B decays has not yet been measured. And second, the mass of the W_R could still be relatively small:[6]

$$M_R^g \equiv \left(\frac{g_L}{g_R}\right) M_R > 300 \text{ GeV} , \tag{1}$$

where M_R is the mass of the W_R, and g_L and g_R are the left and right couplings, respectively.

With this in mind, GW have proposed a model in which the SM W doesn't couple to B's at all. They interpret the long B lifetime as being due to the heaviness of the W_R, *not* to the smallness of V_{cb}. That is,

$$\beta_g \equiv \left(\frac{g_R^2}{g_L^2}\right)\left(\frac{M_L^2}{M_R^2}\right) \sim |V_{cb}| = 0.044 \pm 0.006. \tag{2}$$

Phenomenologically, β_g is bounded to be < 0.07.

In order for this model to be viable, the form of the right-handed CKM matrix V^R must take into account a large number of phenomenological constraints involving B's – the B lifetime, $b \to u$ transitions, 2-body B decays, Cabibbo-suppressed B decays, B_d^0-$\overline{B_d^0}$ mixing – as well as the K_L-K_S mass difference, Δm_K. The forms suggested by GW for both the left- and right-handed CKM matrix, consistent with the above data, are

$$V^L = \begin{pmatrix} \cos\theta_c & \sin\theta_c & 0 \\ -\sin\theta_c & \cos\theta_c & 0 \\ 0 & 0 & 1 \end{pmatrix} , \quad V^R = \begin{pmatrix} c^2 & -cs & s \\ s(1-c)/\sqrt{2} & (c+s^2)\sqrt{2} & c/\sqrt{2} \\ -s(1-c)/\sqrt{2} & -(c-s^2)\sqrt{2} & c/\sqrt{2} \end{pmatrix}, \tag{3}$$

in which θ_c is the Cabibbo angle, and $s \equiv \sin\theta^R$, $c \equiv \cos\theta^R$. The magnitude of s is determined from $|V_{ub}/V_{cb}|$, i.e.

$$s = 0.08 \pm 0.02 \; . \tag{4}$$

With this choice of left- and right-handed CKM matrices, all known data can be explained with

$$M_R^g = 300\text{–}600 \text{ GeV}. \tag{5}$$

In fact, strictly speaking, this is not completely true – additional assumptions are necessary. For example, this model demands the existence of a right-handed neutrino with a mass $m(\nu_R) < m_b - m_c$. Furthermore, if the ν_R is very light, muon decay experiments require either that M_R^g be in the upper part of the range of Eq. 5, or that the ν_R be unstable. In addition, from direct searches for right-handed W's at hadron colliders, the limit $M_R > 520$ GeV is obtained for $g_R = g_L$. Thus, if one wants a value for M_R^g in the lower part of the range of Eq. 5, it is necessary that g_R be larger than g_L. Nevertheless, despite these caveats, the model is interesting in the sense that it points out certain aspects of B decays which must be examined in order to fully test the SM.

One possibly bothersome aspect of the GW solution (Eq. 3), pointed out by Hou and Wyler[7] (HW), is that V_{cd}^R is unnaturally small ($= 0.0003$). One way to avoid this is to parametrize the right-handed CKM matrix using two angles θ_{12} and θ_{13}. HW propose[7]

$$V^R = \begin{pmatrix} 1 & 0 & 0 \\ 0 & 1/\sqrt{2} & 1/\sqrt{2} \\ 0 & -1/\sqrt{2} & 1/\sqrt{2} \end{pmatrix} \begin{pmatrix} c_{13} & 0 & s_{13} \\ 0 & 1 & 0 \\ -s_{13} & 0 & c_{13} \end{pmatrix} \begin{pmatrix} c_{12} & -s_{12} & 0 \\ s_{12} & c_{12} & 0 \\ 0 & 0 & 1 \end{pmatrix}, \tag{6}$$

and take $s_{12} \simeq 0.098$, $s_{13} \simeq 0.085$, in which case $V_{cd}^R = s_{12} - c_{12}s_{13} \simeq 0.01$. I will refer to this as solution (I).

HW also point out that even if the $b \to c$ transitions are dominated by right-handed currents, $b \to u$ decays might still be mediated mainly via left-handed currents. They thus arrive at solution (II):

$$V^L \simeq \begin{pmatrix} 1 & \lambda & \delta \\ -\lambda & 1 & \delta \\ -\delta & -\delta & 1 \end{pmatrix} , \quad V^R \simeq \begin{pmatrix} 1 & -\varepsilon & \varepsilon \\ \varepsilon & 1/\sqrt{2} & 1/\sqrt{2} \\ -\varepsilon & -1/\sqrt{2} & 1/\sqrt{2} \end{pmatrix}, \tag{7}$$

with $\lambda = \sin\theta_c$, $\delta \sim 0.05$ and $\varepsilon < 0.01$.

Now, the question is, how can one rule out these models? One of the advantages of a hadron collider, as compared to an asymmetric e^+e^- collider operating at the $\Upsilon(4s)$ resonance, is that one can search directly for new physics. It is more likely that physics beyond the standard model – supersymmetry, extra Higgses, technicolour, etc. – will be first found via direct searches than by looking for indirect signals in B physics. As such, the most straightforward way to rule out models of right-handed B decays is simply to look for, and fail to find, a light W_R.

Another possibility[7] is to look at certain B decays which are suppressed in these models relative to the SM. For example,

$$\begin{aligned} \frac{BR(b \to c\bar{c}d)}{BR(b \to c\bar{c}s)} &= \lambda^2 \simeq 0.05, && \text{(SM)}, \\ &= O(10^{-7}), && \text{(GW)}, \\ &\lesssim O(10^{-4}), && \text{(I,II)}. \end{aligned} \tag{8}$$

In this case, if right-handed currents were responsible for B decays, the ratio of the decay rates of $B \to D^{(*)}D_s^{-(*)}$ and $B \to D^{(*)}D^{-(*)}$ would differ from that of the SM. Similarly,

$$\begin{aligned} \frac{BR(b \to c\bar{u}s)}{BR(b \to c\bar{u}d)} &= \lambda^2 \simeq 0.05, && \text{(SM)}, \\ &\simeq 0.008, && \text{(GW,I)}, \\ &\simeq \varepsilon^2 \lesssim O(10^{-4}), && \text{(II)}. \end{aligned} \tag{9}$$

Here one should compare, for example, $\overline{B} \to D^{(*)}\rho$ and $\overline{B} \to D^{(*)}K^*$.

Finally, there is the possibility of measuring the chirality of B decays. The lepton forward-backward decay asymmetry A_{fb} in the decay $\overline{B} \to D^*\ell^-\overline{\nu}_\ell$ is sensitive to the chirality of the $b \to c$ coupling.[8] However, not being parity-violating, A_{fb} also depends on the chirality of the lepton current, and therefore cannot distinguish models of right-handed B decays from the standard model. On the other hand, experiments at LEP *can* make such a distinction. One looks[9] at the reaction $e^+e^- \to Z^0 \to \Lambda_b X$, in which the Λ_b is highly polarized, its spin carried essentially entirely by the b-quark. The electron energy spectrum in $\Lambda_b \to$ *charm* semileptonic decays is then quite sensitive to the $V \pm A$ nature of the $b \to c$ coupling. In this way it might be possible to rule out models of right-handed B decays at LEP.

3. RARE B DECAYS

3.1 $b \to s\gamma$ (and $b \to d\gamma$)

The flavour-changing decay $b \to s\gamma$ occurs first at one loop, and is dominated at lowest order by the t-quark contribution:

$$\mathcal{M}(b \to s\gamma) = \frac{G_F}{\sqrt{2}} \frac{e}{4\pi^2} \lambda_t F_2(x_t) q^\mu \epsilon^\nu \bar{s} \sigma_{\mu\nu} \left(m_b(1+\gamma_5) + m_s(1-\gamma_5) \right) b \ , \tag{10}$$

in which $\lambda_t \equiv V_{tb}V_{ts}^*$, $x_t = m_t^2/M_W^2$, and

$$F_2(x) = \frac{x}{24(x-1)^4} \left[6x(3x-2)\log x - (x-1)(8x^2+5x-7) \right] . \tag{11}$$

However, this process receives important QCD contributions,[10] as shown in Fig. 1. For example, for $m_t = 150$ GeV, we find

$$\begin{aligned} BR(b \to s\gamma) &= 1.4 \times 10^{-4} \quad \text{(no QCD corrections)}, \\ &= 4.2 \times 10^{-4} \quad \text{(including QCD corrections)}. \end{aligned} \tag{12}$$

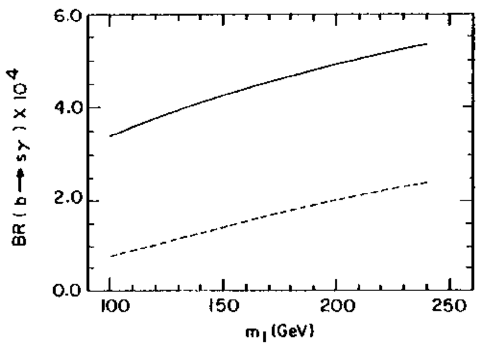

Figure 1: Branching ratio for $b \to s\gamma$ in the SM with (solid line) and without (dashed line) QCD corrections (from Ref. 11 (reproduced by permission)).

The rate for $b \to d\gamma$ is obtained from that for $b \to s\gamma$ (Eq. 10) by replacing the s-quark variables by d-quark variables. Thus, to lowest order,

$$\frac{BR(b \to d\gamma)}{BR(b \to s\gamma)} = \left| \frac{V_{td}}{V_{ts}} \right|^2 . \tag{13}$$

However, there are additional corrections due to the breaking of $SU(3)_{flavour}$. Estimating these, and taking into account the uncertainty in the magnitude of V_{td}, one finds[11]

$$\begin{aligned} BR(b \to s\gamma) &= 3\text{-}5 \times 10^{-4} \ , \\ BR(b \to d\gamma) &= 0.5\text{-}3 \times 10^{-5} \ . \end{aligned} \tag{14}$$

Although the inclusive decay rate for $b \to s\gamma$ can be calculated with good precision, it is well-known that exclusive decays are poorly understood theoretically:

$$R_B \equiv \frac{BR(B \to K^*\gamma)}{BR(b \to s\gamma)} = 4\text{-}40 \ \%. \tag{15}$$

CLEO has measured both inclusive and exclusive flavour-changing decays:[12]

$$\begin{aligned} BR(b \to s\gamma) &< 8.4 \times 10^{-4} \quad (1991), \\ &< 5.4 \times 10^{-4} \quad (1993), \\ BR(B \to K^*\gamma) &= (4.5 \pm 1.5 \pm 0.9) \times 10^{-5} \quad (1993). \end{aligned} \tag{16}$$

These measurements have important consequences for models of new physics.

First consider models with two Higgs doublets (2HDM). In general, such models will lead to flavour-changing neutral currents. This then requires that the Higgs bosons be very heavy, rendering their effects in B physics unobservable. There are two ways to avoid this, distinguished by the couplings of the fermions and the Higgses. One possibility (model I) is that one Higgs doublet, ϕ_2, gives mass to all fermions, while the other doublet, ϕ_1, decouples. In the other case (model II), one doublet, ϕ_2, couples to all u-type quarks, while the second Higgs doublet, ϕ_1, gives mass to d-type quarks. It is model II which appears in supersymmetric and axion models.

In either of these 2HDM there are new contributions to the decay $b \to s\gamma$, found by replacing the $W^\pm$ in the loop by a charged Higgs, $H^\pm$. In these models, both Higgs doublets acquire vacuum expectation values, denoted v_1 and v_2. We define $\tan\beta \equiv v_2/v_1$, which is apriori completely free. The transition amplitude is then proportional to

$$A_W\left(\frac{m_t^2}{M_W^2}\right) + \lambda A_H^1\left(\frac{m_t^2}{M_{H^\pm}^2}\right) + \frac{1}{\tan^2\beta} A_H^2\left(\frac{m_t^2}{M_{H^\pm}^2}\right) , \tag{17}$$

where A_W and $A_H^{1,2}$ represent the SM and charged-Higgs contributions to the amplitude, respectively. In model I, $\lambda = -1/\tan^2\beta$, while $\lambda = +1$ in model II.

From this we see that in model I, there is an enhancement to the rate for $b \to s\gamma$ only for small values of $\tan\beta$. In model II, the rate is also enhanced for small $\tan\beta$. More importantly, due to the A_H^1 term, the rate is *always* larger than that of the SM. This leads to a lower bound on the mass of the charged Higgs in this model,[13,14] independent of the value of m_t. In Fig. 2, taken from Ref. 13, the constraints on models I and II are shown for $m_t = 150$ GeV, using the 1991 CLEO bound (Eq. 16).

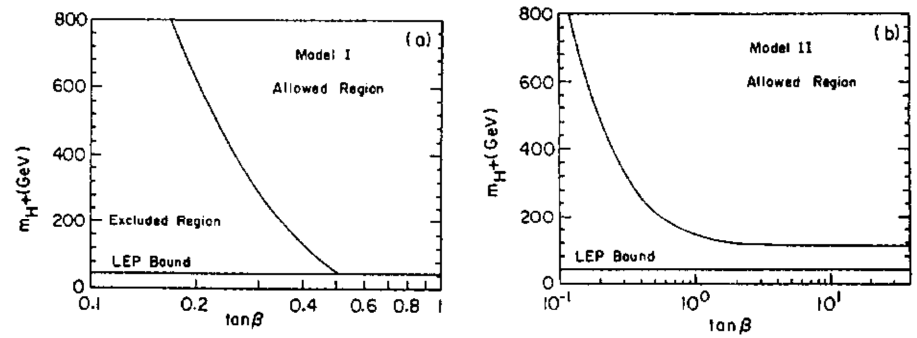

Figure 2: Excluded regions in the $M_{H^\pm}$-$\tan\beta$ plane for models I and II, for $m_t = 150$ GeV, (from Ref. 13 (reproduced by permission)).

For model I, we see that there is no $\tan\beta$-independent lower limit on $M_{H^\pm}$ coming from the bound on $b \to s\gamma$. However, in model II, we find that $M_{H^\pm} > 110$ GeV at large $\tan\beta$, with stronger bounds for smaller values of $\tan\beta$. For model II this lower limit has been updated[15] using the 1993 data on $b \to s\gamma$ (Eq. 16): $M_{H^\pm} > 320$ GeV (540 GeV) for $m_t = 120$ GeV (150 GeV). This new lower bound has several important consequences. First, the decay $t \to bH^+$ is no longer allowed. Second, if the two Higgs doublets are part of a supersymmetric theory, the difficult region for Higgs searches is now ruled out (see below, however). Finally, this eliminates most large effects in 2HDM in other rare B decays.

The implications of the limits on $BR(b \to s\gamma)$ are less clearcut for supersymmetric models. If the main new contributions to $b \to s\gamma$ came from the two Higgs doublets, then the constraints would be as described above. However, the situation is more complicated. First, electroweak radiative corrections to the charged-Higgs mass and to the charged Higgs-fermion-fermion vertex can be substantial.[16] These corrections tend to weaken the constraints on the charged-Higgs mass as a function of $\tan\beta$. More importantly, in the minimal supersymmetric standard model (MSSM), the contributions to $b \to s\gamma$ from other supersymmetric particles may not be negligible.[17] In this case there can be cancellations with the charged-Higgs contributions, possibly resulting in a branching ratio for $b \to s\gamma$ which is *smaller* than that of the SM. Thus, it is impossible to say anything concrete regarding the constraints on SUSY models due to $BR(b \to s\gamma)$.

Finally, left-right symmetric models are essentially unconstrained by the limits on $BR(b \to s\gamma)$ (Eq. 16). Models with right-handed B decays predict a rate for $b \to s\gamma$ which is down by a factor of 2 compared to the SM. And in models with manifest left-right symmetry, the W_R must be so heavy that its effects in $b \to s\gamma$ are negligible.

3.2 $b \to s\ell^+\ell^-$

In the SM, at the quark level, the decay $b \to s\ell^+\ell^-$ arises through penguin diagrams with a virtual γ or Z^0, as well as through box diagrams. In addition, in contrast to $b \to s\gamma$, $b \to s\ell^+\ell^-$ receives important long-distance contributions. These effects are dominated by the decays $B \to \Psi(\Psi')X \to \ell^+\ell^- X$, whose branching ratios have been measured by the ARGUS and CLEO collaborations[18] to be $O(10^{-3})$. The long-distance effects are then very important when the $\ell^+\ell^-$ pair has an invariant mass close to that of the Ψ or Ψ'. However, since the long-distance contribution is so much larger than the short-distance contribution, which is estimated to be $O(10^{-5})$ (see below), one has to worry about residual effects in the spectrum away from the Ψ and Ψ' resonances. In other words, the invariant dilepton mass spectrum is important in analysing $b \to s\ell^+\ell^-$.

The short-distance contributions have been calculated:[19,20,21]

$$\begin{aligned} BR(B \to X_s e^+e^-) &= 0.6\text{–}2.5 \times 10^{-5} , \\ BR(B \to X_s \mu^+\mu^-) &= 3.5\text{–}14.0 \times 10^{-6} , \end{aligned} \tag{18}$$

for 100 GeV $< m_t <$ 200 GeV. Note that the m_t-dependence is much more important here than in $b \to s\gamma$. Also note the the UA1 upper limit:[22]

$$BR(B \to \mu^+\mu^- X) < 5 \times 10^{-5} . \tag{19}$$

The short-distance contributions for the inclusive decays $b \to d\ell^+\ell^-$ have also been computed,[21] assuming $|V_{td}/V_{ts}| = 0.21$:

$$\begin{aligned} BR(B \to X_d e^+e^-) &= 2.6\text{–}10.0 \times 10^{-7} , \\ BR(B \to X_d \mu^+\mu^-) &= 1.5\text{–}6.0 \times 10^{-7} . \end{aligned} \tag{20}$$

Again, it must be remembered that the above cross sections are only the short-distance contributions. One can try to also include the long-distance effects, but there are large uncertainties. Nevertheless it is possible to isolate the short-distance contributions by looking at the forward-backward asymmetry in the decay. In Fig. 3 one sees the angular distribution of the decay, for three different values of m_t, in which θ is defined as the angle between the momentum of the B-meson and that of the ℓ^+ in the centre-of-mass frame of the dilepton pair, and $\hat{s}$ is the scaled dilepton invariant mass. This figure is taken from Ref. 23, to which I refer the reader for more details.

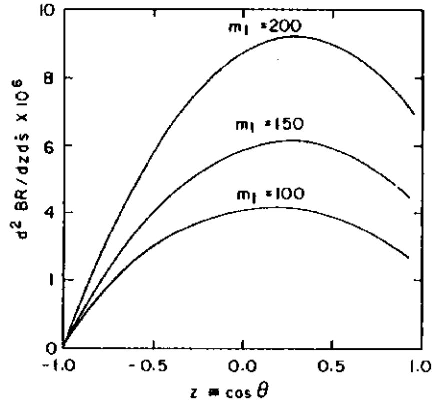

Figure 3: The angular distribution $d^2 BR/dz\, d\hat{s}$ in the decay $b \to s\ell^+\ell^-$, for $\hat{s} = 0.3$ (from Ref. 23 (reproduced by permission)).

As mentioned earlier, the constraints from $b \to s\gamma$ on two-Higgs-doublet models preclude large enhancements to $b \to s\ell^+\ell^-$. As to supersymmetric models, in Ref. 24, it is found that the rate for $b \to s\ell^+\ell^-$ can be greater than that of the SM by up to a factor of 2, when the electroweak symmetry is broken radiatively. On the other hand, this reference predates the recent CLEO bounds on $b \to s\gamma$, and I'm not sure how their inclusion would change the predictions of SUSY models for $b \to s\ell^+\ell^-$. The feeling seems to be that the CLEO data probably now precludes SUSY enhancements to $b \to s\ell^+\ell^-$, but this should be checked.[25]

Another type of new physics which could lead to an enhancement of the rate for $b \to s\ell^+\ell^-$ is extended technicolour. In fact, for certain models, specifically those which include a "techni-GIM" mechanism, the enhancement is too large.[26] In such models, barring delicate fine-tuned cancellations, the prediction for $BR(B \to \mu^+\mu^- X)$ is $O(10^{-4})$, which is in conflict with the UA1 bound (Eq. 19). These models therefore appear to be ruled out. On the other hand, extended technicolour models without a GIM mechanism are still allowed – they predict $BR(B \to \mu^+\mu^- X) = 1\text{–}3 \times 10^{-5}$, an enhancement of roughly a factor of 4 compared to the SM.

3.3 $b \to s\nu\bar{\nu}$

Although the decay $b \to s\nu\bar{\nu}$ has negligible QCD corrections, it is very sensitive to the value of m_t. In the SM, its branching ratio is calculated to be[19,21,27]

$$\sum_i BR(b \to s\bar{\nu}_i\nu_i) = 2.8\text{–}13.0 \times 10^{-5} \tag{21}$$

for 100 GeV $< m_t <$ 200 GeV.

This branching ratio is not expected to be significantly affected by the presence of new physics. In two-Higgs-doublet models, any possible effects are already ruled out by the $b \to s\gamma$ measurement, and the inclusion of supersymmetric particles[24] is not expected to lead to any enhancement.

3.4 $B_s^0 \to \mu^+\mu^- / \tau^+\tau^-$

In order to deduce the form of the operator leading to the decay $B_s^0 \to \ell^+\ell^-$, one notes the following points. First, the s-b matrix element is

$$\langle 0|\bar{s}\gamma^\mu\gamma_5 b|B\rangle = f_B P_B^\mu \ . \tag{22}$$

This is because the matrix element of $\bar{s}\gamma^\mu b$ vanishes due to considerations of parity (the B_s^0 is a pseudoscalar) and $\bar{s}\sigma^{\mu\nu}b$ won't work since there aren't enough Lorentz vectors to construct a scalar. Second, $P_B^\mu \bar{u}_\ell \gamma_\mu v_\ell = 0$, which means we need a helicity flip in the leptonic current. Thus, the operator describing the decay $B_s^0 \to \ell^+\ell^-$ is

$$\mathcal{O} \sim \bar{s}\gamma^\mu\gamma_5 b\,\bar{\ell}\gamma_\mu\gamma_5\ell \ . \tag{23}$$

The helicity flip means, of course, that the final answer will depend on the lepton mass.

The branching ratio for the decay $B_s^0 \to \mu^+\mu^-$ is given in Fig. 4 as a function of m_t,[27,28] for $f_{B_s} = 200$ MeV, $\tau_{B_s} = 1.49$ psec, and $|V_{ts}| = 0.042$. For $m_t = 150$ GeV, this gives

$$\begin{aligned} BR(B_s^0 \to \mu^+\mu^-) &= 2\times 10^{-9} \ , \\ BR(B_s^0 \to \tau^+\tau^-) &= 4\times 10^{-7} \ . \end{aligned} \tag{24}$$

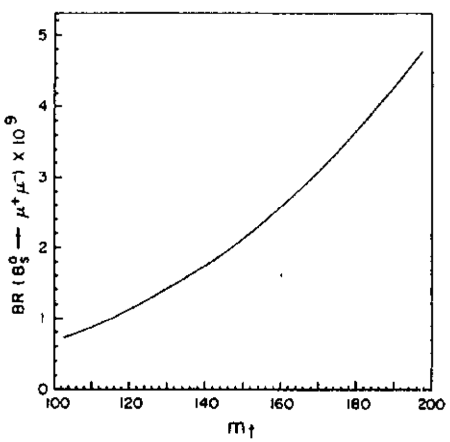

Figure 4: Standard model branching ratio for $B_s^0 \to \mu^+\mu^-$ as a function of m_t, assuming $f_{B_s} = 200$ MeV, $\tau_{B_s} = 1.49$ psec, and $|V_{ts}| = 0.042$.

In two-Higgs-doublet models, there can be an enhancement to the rate for $B_s^0 \to \mu^+\mu^-, \tau^+\tau^-$ by as much as one to two orders of magnitude.[29] Since this decay proceeds through the loop-induced exchange of a neutral Higgs scalar, the constraint on the $M_{H^\pm}$ from $b \to s\gamma$ is unimportant. In extended technicolour models without a GIM mechanism, the rate can also be an order of magnitude bigger than that of the SM.[30] (Recall that extended technicolour models with a GIM mechanism are already in conflict with date from $B \to \mu^+\mu^- X$.) Finally, light leptoquarks could also enhance the rate for $B_s^0 \to \mu^+\mu^-$.

3.5 $B_s \to \gamma\gamma$

All that I will say about this process[28,21] is that in the SM $BR(B_s \to \gamma\gamma) = 1.5\times 10^{-8}$ for $m_t = 150$ GeV and $f_{B_s} = 200$ MeV.

3.6 *Hadronic penguins*

The predictions for the exclusive rates of penguin-induced hadronic B decays are highly model dependent. However, it is important to measure the branching ratios of such decays for several reasons. First, this will give us some idea as to the importance of penguin contributions[31] in CP-violating hadronic B asymmetries. Also, we will be able to test different models of exclusive decays and hence gain some information regarding QCD effects in B decays.

Some examples of such penguin-induced decays[3,32] and their predicted branching ratios (taken from Ref. 32) are given in Table 1. These specific final states have been chosen since the signal consists only of charged particles, so that these processes might be observable at hadron colliders.

Mode	Branching Ratio
$B^+ \to K^0\pi^+$	1.06×10^{-5}
$K^+\phi$	1.12×10^{-5}
$K^{*0}\pi^+$	0.58×10^{-5}
$K^{*+}\phi$	3.12×10^{-5}
$B_d^0 \to K^{*0}\phi$	3.12×10^{-5}
$K^{*0}\rho^0$	0.62×10^{-5}

Table 1: Some exclusive penguin-induced hadronic B decays and their predicted branching ratios (from Ref. 32).

4. B_c PHYSICS

One particularly interesting piece of B physics which is likely to be studied at hadron colliders is the $B_c = (\bar{b}c)$ system (for further discussion regarding B_c physics, see Refs. 33 and 34). The mass of the B_c has been calculated,[34,35] using potential models, to be $\simeq 6.25$ GeV. Its production cross-section is about $\sigma(B_c)/\sigma(b\bar{b}) \sim 10^{-3}$. This leads to[36]

1.3×10^3	B_c's per year (10^7 sec.) at	LEP,
2.0×10^6		TeVatron,
1.1×10^7		LHC (fixed target),
1.1×10^{11}		LHC.

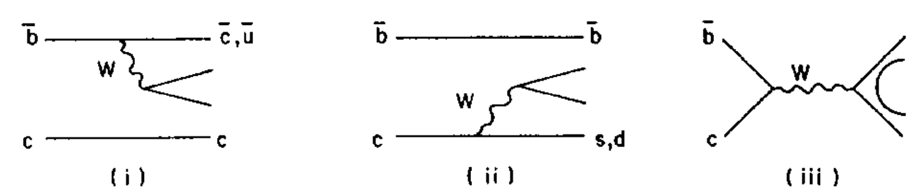

Figure 5: The three mechanisms for B_c decay: (i) c-spectator, (ii) b-spectator, (iii) annihilation.

The main reason that B_c mesons are so interesting is that there are three mechanisms for their decay, shown in Fig. 5. Examples of these different decays are:

$$\begin{aligned}
c\text{-spectator:}\quad & B_c^+ \to \Psi e^+ \nu_e \ , \\
& B_c^+ \to \eta_c e^+ \nu_e \ , \\
& B_c^+ \to \Psi \pi^+ \ , \\
& B_c^+ \to D^+ \overline{D^0} \ , \qquad (25) \\
b\text{-spectator:}\quad & B_c^+ \to B_s^{(*)} e^+ \nu_e \ , \\
& B_c^+ \to B^{(*)} e^+ \nu_e \ , \\
& B_c^+ \to B_s^{(*)} \rho^+ \ , \\
& B_c^+ \to B^{(*)+} \overline{K^0} \ , \qquad (26) \\
\text{annihilation:}\quad & B_c^+ \to \tau^+ \nu_\tau \ , \\
& B_c^+ \to D^{(*)+} K^0 \ . \qquad (27)
\end{aligned}$$

Note that, unlike B_u's, B_d's and B_s's, the annihilation decays of the B_c are expected to be important. There are a number of reasons for this. First, helicity suppression is ineffective if there are heavy particles (e.g. τ, D, ...) in the final state. Second, in the B_c system, such decays are unsuppressed by CKM factors. And finally, f_{B_c} is expected to be large.

The relative importance of these three different decay mechanisms have been estimated. Using quark and spectator models, and taking $\tau_{B_c} \simeq 5 \times 10^{-13}$ sec., the inclusive branching ratios for each of these three types of decay are predicted to be:[37]

$$\begin{aligned}
c\text{-spectator:}\quad & 37\%, \\
b\text{-spectator:}\quad & 45\%, \\
\text{annihilation:}\quad & 18\%. \qquad (28)
\end{aligned}$$

Assuming $\tau_{B_c} \simeq 9 \times 10^{-13}$ sec., QCD sum rules give:[38]

$$\begin{aligned}
c\text{-spectator:}\quad & 48\%, \\
b\text{-spectator:}\quad & 39\%, \\
\text{annihilation:}\quad & 13\%. \qquad (29)
\end{aligned}$$

For a more complete discussion of these relative inclusive branching ratios, see Ref. 34.

There are several particularly interesting decay modes of the B_c which involve a Ψ in the final state. The decay $B_c^+ \to \Psi\pi^+$ is likely to be the discovery mode. Its branching ratio is estimated to be 2×10^{-3} and it permits the full reconstruction of the B_c. The decay $B_c^+ \to \Psi\mu^+\nu_\mu$ has a large branching ratio (1-4×10^{-2}) and its signal is three leptons coming from the same vertex. In fact, $BR(B_c \to \Psi + X)$ is estimated to be (19-24)%, which means that the B_c probably can be seen at CDF.

Given a sufficiently large sample of B_c's, it is even possible to look for CP violation in the B_c system.[39] In order to have a non-zero CP-violating decay-rate asymmetry, it is necessary to choose a final state which can be reached via two different weak amplitudes. For example, the decay $B_c^+ \to D^0 K^+$ has two contributions with different CKM matrix elements – a c-spectator tree diagram and a $\bar{b} \to \bar{s}$ penguin diagram. Another example is the processes $B_c^\pm \to D^0 D_s^\pm$ and $B_c^\pm \to \overline{D^0} D_s^\pm$. By measuring these decay rates and the rate for $B_c^\pm \to D_{CP}^0 D_s^\pm$, where D_{CP}^0 is identified by its decay to a CP eigenstate, the angle γ of the unitarity triangle can in principle be extracted.[40] (Unfortunately, this particular example is probably experimentally unfeasible, due to the tiny product branching ratios.)

5. B_s^0-$\overline{B_s^0}$ MIXING

The measurement of B_s^0-$\overline{B_s^0}$ mixing[41] is important for a number of reasons:

- The mixing parameter $x_s \equiv (\Delta M)_{B_s}/\Gamma_{B_s}$ is expected to be large (> 3). If found to be small, this would be a smoking gun for new physics.
- x_s can be used in conjuction with x_d to get a handle on V_{td}:

$$\frac{x_d}{x_s} \sim \frac{f_{B_d}^2 B_{B_d}}{f_{B_s}^2 B_{B_s}} \left|\frac{V_{td}}{V_{ts}}\right|^2 . \qquad (30)$$

  The ratio of hadronic matrix elements is usually known better than each individual one. Thus, the measurement of x_s would enable us to extract $|V_{td}|$ with better precision.

- An accurate knowledge of x_s is needed to extract the CP-violating angle γ in B_s^0 decays.

In the SM, B_s^0-$\overline{B_s^0}$ mixing is dominated by t-quark exchange in the box diagram, leading to

$$x_s = \tau_{B_s} \frac{G_F^2}{6\pi^2} M_W^2 M_{B_s} \left(f_{B_s}^2 B_{B_s}\right) \eta_{B_s} y_t f_2(y_t) |V_{ts}^* V_{tb}|^2 \ , \qquad (31)$$

in which $y_t \equiv m_t^2/M_W^2$ and

$$f_2(x) = \frac{1}{4} + \frac{9}{4}\frac{1}{(1-x)} - \frac{3}{2}\frac{1}{(1-x)^2} - \frac{3}{2}\frac{x^2 \ln x}{(1-x)^3} . \qquad (32)$$

Taking

$$\begin{aligned}
|V_{ts}| = |V_{cb}| &= 0.042 \pm 0.005 \ , \\
\tau_{B_s} = \tau_B &= 1.49 \pm 0.04 \text{ psec} \ , \\
\eta_{B_s} = \eta_B &= 0.55 \ , \\
M_{B_s} &= 5.38 \text{ GeV} \ , \qquad (33)
\end{aligned}$$

this gives

$$x_s = (175 \pm 21) \frac{f_{B_s}^2 B_{B_s}}{(1 \text{ GeV})^2} y_t f_2(y_t). \qquad (34)$$

For 89 GeV $\leq m_t \leq$ 182 GeV, the function $y_t f_2(y_t)$ is in the range 0.88–2.72, and is equal to 2.03 for the "central" value of m_t, 150 GeV.

A consensus has not yet been reached regarding the value of $f_{B_s}^2 B_{B_s}$. Potential models and QCD sum rules tend to give smaller values, while lattice calculations give larger values. I will therefore consider two ranges for $f_{B_s}^2 B_{B_s}$:

$$\begin{aligned}
(I): &\quad f_{B_s}\sqrt{B_{B_s}} = 180 \pm 35 \text{ MeV}, \\
(II): &\quad f_{B_s}\sqrt{B_{B_s}} = 225 \pm 25 \text{ MeV}. \qquad (35)
\end{aligned}$$

These lead to the following "central" values for x_s (taking $m_t = 150$ GeV):

$$\begin{aligned}(I): \quad x_s &= 11.5, \\ (II): \quad x_s &= 18.0.\end{aligned} \tag{36}$$

The "1σ" lower limits on x_s are

$$\begin{aligned}(I): \quad & x_s > 3.3, \\ (II): \quad & x_s > 6.6.\end{aligned} \tag{37}$$

Clearly there is a large theoretical uncertainty regarding the hadronic matrix elements. For example, lattice estimates give[42]

$$\begin{aligned}f_{B_d} &= 188\text{–}246 \text{ MeV}, \\ f_{B_s} &= 204\text{–}241 \text{ MeV}.\end{aligned} \tag{38}$$

However, the error on the ratio of these two quantities is considerably smaller:[43]

$$\frac{f_{B_s}^2 B_{B_s}}{f_{B_d}^2 B_{B_d}} = 1.19 \pm 0.10 \ . \tag{39}$$

This is why a precise measurement of x_s can be used, along with x_d, to extract V_{td} (see Eq. 30).

It is possible to get smaller values of x_s if one invokes physics beyond the SM. Examples of such new physics are: a fourth generation,[44] non-minimal SUSY models,[45] fine-tuned left-right symmetric models[46] and models with Z-mediated flavour-changing neutral currents.[47] However, none of these is particularly compelling.

6. T VIOLATION

The last topic I wish to briefly discuss is T violation. By this I do not mean CP violation, which is discussed elsewhere,[18] but rather triple-product correlations. There are two examples of these which have been discussed in the literature, having to do with the decays $B \to V_1 V_2$ (V_1 and V_2 are spin-1 mesons) and $B \to D^* \ell \nu_\ell$. I won't go into very much detail regarding either of these decays, preferring instead to simply sketch out the salient features.

Consider first the decay[49]

$$B(p) \to V_1(k, \epsilon_1) V_2(q, \epsilon_2), \tag{40}$$

in which the particles are specified by their 4-momenta (p, k, q) and their polarizations (ϵ_1, ϵ_2). The most general decay amplitude can be written

$$\mathcal{M} = a\, \epsilon_1 \cdot \epsilon_2 + \frac{b}{m_1 m_2} (p \cdot \epsilon_1)(p \cdot \epsilon_2) + i \frac{c}{m_1 m_2} \epsilon^{\alpha\beta\gamma\delta} \epsilon_{1\alpha}\, \epsilon_{2\beta}\, k_\gamma\, p_\delta \ , \tag{41}$$

in which

$$\begin{aligned}a &= |a| e^{i(\delta_a + \phi_a)} \ , \\ b &= |b| e^{i(\delta_b + \phi_b)} \ , \\ c &= |c| e^{i(\delta_c + \phi_c)} \ ,\end{aligned} \tag{42}$$

where $\delta_{a,b,c}$ and $\phi_{a,b,c}$ are the strong phases and the weak phases, respectively. The corresponding amplitude for the decay of the antiparticle is

$$\overline{\mathcal{M}} = \bar{a}\, \epsilon_1 \cdot \epsilon_2 + \frac{\bar{b}}{m_1 m_2} (p \cdot \epsilon_1)(p \cdot \epsilon_2) - i \frac{\bar{c}}{m_1 m_2} \epsilon^{\alpha\beta\gamma\delta} \epsilon_{1\alpha}\, \epsilon_{2\beta}\, k_\gamma\, p_\delta \ , \tag{43}$$

in which $\bar{a}, \bar{b}, \bar{c}$ are identical to a, b, c (Eq. 42), except that the $\phi_{a,b,c}$ change sign.

Now, the asymmetry

$$A_B = \frac{N_{\text{events}}(\vec{k} \cdot \vec{\epsilon}_1 \times \vec{\epsilon}_2 > 0) - N_{\text{events}}(\vec{k} \cdot \vec{\epsilon}_1 \times \vec{\epsilon}_2 < 0)}{N_{TOT}} \tag{44}$$

can be written

$$A_B \sim \text{Im}(ac^*) \sim |ac| \sin(\delta + \phi), \tag{45}$$

where $\delta \equiv \delta_a - \delta_c$ and $\phi \equiv \phi_a - \phi_c$. If we imagine measuring a similar asymmetry $A_{\overline{B}}$ for the antiparticle decay, then we can obtain

$$\begin{aligned}A_B + A_{\overline{B}} &\sim |ac| \cos\delta \sin\phi \ , \\ A_B - A_{\overline{B}} &\sim |ac| \sin\delta \cos\phi \ .\end{aligned} \tag{46}$$

The useful thing about such asymmetries, particularly the sum $A_B + A_{\overline{B}}$, is that they are sensitive to the weak phases only, i.e. they do not vanish if $\delta = 0$. On the other hand, the question of how to relate phases at the meson level to phases at the quark level, and of how to calculate strong phases, introduces much theoretical uncertainty and model dependence.[50] Still, the signals would be interesting to look for. Some possible decay modes are: $\overline{B_d^0} \to \rho^{*+} K^{*-}$, $B^- \to \Psi K^{*-}$ and $\overline{B_s^0} \to \Psi\phi$.

Another interesting process is the decay $B \to D^* \ell \nu_\ell$, in which the D^* decays further to $D\pi$.[51] The triple product $\vec{p}_\ell \cdot (\vec{p}_{D^*} \times \vec{p}_D)$ is T-violating. There are a variety of asymmetries one can measure which depend on this triple product (I refer the reader to Ref. 51 for more details). Again, to go from the quark-level calculation to the meson-level measurement introduces hadronic uncertainties and model dependence. However, this triple product vanishes in the SM, so that this would be another way of looking for CP violation from new physics.

7. REFERENCES

1. G. Altarelli, M. Cabibbo, G. Corbo, L. Maiani and G. Martinelli, *Nucl. Phys.* **B208** (1982) 365; M. Wirbel, B. Stech and M. Bauer, *Zeit. Phys.* **C29** (1985) 637; J.G. Körner and G.A. Schuler, *Zeit. Phys.* **C38** (1988) 511; N. Isgur, D. Scora, B. Grinstein and M. Wise, *Phys. Rev.* **D39** (1989) 799.
2. N. Isgur and M.B. Wise, *Phys. Lett.* **232B** (1989) 113, **B237** (1990) 527.
3. M. Bauer, B. Stech and M. Wirbel, *Zeit. Phys.* **C34** (1987) 103;
4. M. Gronau and S. Wakaizumi, *Phys. Rev. Lett.* **68** (1992) 1814.
5. For a review of HQET, see B. Grinstein, these proceedings; for a discussion of B baryons, see B. Kayser, these proceedings.
6. P. Langacker and S.U. Sankar, *Phys. Rev.* **D40** (1989) 1569.
7. W.-S. Hou and D. Wyler, *Phys. Lett.* **292B** (1992) 364.

8. J.G. Körner and G.A. Schuler, *Phys. Lett.* **226B** (1989) 185; F.J. Gilman and R.L. Singleton, Jr., *Phys. Rev.* **D41** (1990) 142; M. Gronau and S. Wakaizumi, *Phys. Lett.* **280B** (1992) 79; S. Sanghera et. al. (CLEO Collaboration), *Phys. Rev.* **D47** (1993) 791.
9. J.F. Amundson, J.L. Rosner, M. Worah and M.B. Wise, *Phys. Rev.* **D47** (1993) 1260; Z. Hioki, *Phys. Lett.* **303B** (1993) 125.
10. S. Bertolini, F. Borzumati and A. Masiero, *Phys. Rev. Lett.* **59** (1987) 180; N.G. Deshpande et. al., *Phys. Rev. Lett.* **59** (1987) 183; B. Grinstein, R. Springer and M.B. Wise, *Phys. Lett.* **202B** (1988) 138, *Nucl. Phys.* **B339** (1990) 269; R. Grigjanis et. al., *Phys. Lett.* **213B** (1988) 355, **224** (1989) 209, **286** (1992) 413(E); G. Cella et. al., *Phys. Lett.* **248B** (1990) 181; A. Ali and C. Greub, *Zeit. Phys.* **C49** (1991) 431, *Phys. Lett.* **287B** (1992) 191; P. Cho and B. Grinstein, *Nucl. Phys.* **B365** (1991) 279; M. Misiak, *Nucl. Phys.* **B393** (1993) 23.
11. A. Ali, in *Proceedings of the 1991 ICTP, Trieste, Summer School in High Energy Physics and Cosmology* (World Scientific, Singapore, 1992), p. 153.
12. 1991: M. Battle et. al. (CLEO Collaboration), in *Proceedings of the Joint International Lepton-Photon Symposium & Europhysics Conference on High Energy Physics*, eds. S. Hegarty, K. Potter and E. Quercigh (World Scientific, Singapore, 1992), p. 869;
1993: E. Thorndike (CLEO Collaboration), talk given at the *1993 Meeting of the American Physical Society*, Washington, D.C., April, 1993; R. Ammar et. al. (CLEO Collaboration), *Phys. Rev. Lett.* **71** (1993) 674.
13. J.L. Hewett, *Phys. Rev. Lett.* **70** (1993) 1045.
14. V. Barger, M.S. Berger and R.J.N. Phillips, *Phys. Rev. Lett.* **70** (1993) 1368.
15. G. Bélanger, C.Q. Geng and P. Turcotte, UdeM-LPN-TH-93-148 (1993).
16. M.A. Díaz, *Phys. Rev.* **D48** (1993) 2152, *Phys. Lett.* **304B** (1993) 278.
17. N. Oshimo, *Nucl. Phys.* **B404** (1993) 20; T. Hayashi, M. Matsuda and M. Tanimoto, KU-01-93, AUE-01-93, EHU-01-93 (1993); R. Barbieri and G.F. Giudice, *Phys. Lett.* **309B** (1993) 86; J.L. Lopez, D. Nanopoulos and G.T. Park, *Phys. Rev.* **D48** (1993) 974; Y. Okada, *Phys. Lett.* **315B** (1993) 119; R. Garisto and J.N. Ng, TRI-PP-93-66 (1993); F. Borzumati, DESY 93-090 (1993).
18. Particle Data Group, *Phys. Rev.* **D45** (1992) Vol. 45, part II.
19. W.-S. Hou, R.S. Willey and A. Soni, *Phys. Rev. Lett.* **58** (1987) 1608.
20. N.G. Deshpande and J. Trampetic, *Phys. Rev. Lett.* **60** (1988) 2583; C.S. Lim, T. Morozumi and A.I. Sanda, *Phys. Lett.* **218B** (1989) 343; B. Grinstein, M.J. Savage and M.B. Wise, *Nucl. Phys.* **B319** (1989) 271; N.G. Deshpande, J. Trampetic and K. Panose, *Phys. Rev.* **D39** (1989) 1461; W. Jaus and D. Wyler, *Phys. Rev.* **D41** (1990) 3405.
21. A. Ali, C. Greub and T. Mannel, in *ECFA Workshop on a European B-Meson Factory*, eds. R. Aleksan and A. Ali (1993), p. 155.
22. C. Albajar et. al., UA1 Collaboration, *Phys. Lett.* **262B** (1991) 163.
23. A. Ali, T. Mannel and T. Morozumi, *Phys. Lett.* **273B** (1991) 505.
24. S. Bertolini, F. Borzumati and A. Masiero, in *B Decays*, ed. S. Stone (World Scientific, Singapore, 1992), p. 458, and references therein.
25. F. Borzumati, private communication.
26. B. Grinstein, Y. Nir and J.M. Soares, SSCL-Preprint-482, WIS-93/67/July-PH, CMU-HEP93-10; DOE-ER/40682-35 (1993).
27. A.J. Buras and G. Buchalla, *Nucl. Phys.* **B400** (1993) 225.
28. B.A. Campbell and P.J. O'Donnell, *Phys. Rev.* **D25** (1982) 1989.
29. M.J. Savage, *Phys. Lett.* **266B** (1991) 135; W. Skiba and J. Kalinowski, *Nucl. Phys.* **B404** (1993) 3.
30. L. Randall and R. Sundrum, *Phys. Lett.* **312B** (1993) 148.
31. D. London and R.D. Peccei, *Phys. Lett.* **223B** (1989) 257; M. Gronau, *Phys. Rev. Lett.* **63** (1989) 1451; B. Grinstein, *Phys. Lett.* **229B** (1989) 280.
32. N.G. Deshpande and J. Trampetic, *Phys. Rev.* **D41** (1990) 895.
33. C. Hill, these proceedings
34. C. Quigg, these proceedings.
35. A.K. Likhoded, S.R. Slabospitsky, M. Mangano, and G. Nardulli, BARI-TH/93-137 and references therein.
36. M. Lusignoli, M. Masetti and S. Petrarca, *Phys. Lett.* **266B** (1991) 142; C.-H. Chang, Y.-Q. Chen, *Phys. Lett.* **284B** (1992) 127, *Phys. Rev.* **D46** (1992) 3845; E. Braaten, K. Cheung and T.C. Yuan, NUHEP-TH-93-6, UCD-93-9 (1993).
37. V.V. Kiselev and A.V. Tkabladze, *Sov. J. Nucl. Phys.* **48** (1988) 536; M. Lusignoli and M. Masetti, *Zeit. Phys.* **C51** (1991) 549.
38. P. Colangelo, G. Nardulli and N. Paver, *Zeit. Phys.* **C57** (1993) 43.
39. M. Masetti, *Phys. Lett.* **286B** (1992) 160.
40. M. Gronau and D. Wyler, *Phys. Lett.* **253B** (1991) 483.
41. For a review of B_s^0-$\overline{B}_s^0$ mixing, see A. Ali and D. London, *J. Phys. G: Nucl. Part. Phys.* **19** (1993) 1069.
42. C. Alexandrou et. al., *Nucl. Phys.* **B374** (1992) 263.
43. A. Abada et. al., *Nucl. Phys.* **B376** (1992) 172.
44. D. London, *Phys. Lett.* **234B** (1990) 354.
45. I.I. Bigi and F. Gabbiani, *Nucl. Phys.* **B352** (1991) 309, and references therein.
46. D. London and D. Wyler, *Phys. Lett.* **232B** (1989) 503.
47. Y. Nir and D. Silverman, *Phys. Rev.* **D42** (1990) 1477; D. Silverman, *Phys. Rev.* **D45** (1992) 1800.
48. For a review of CP violation in the B system, see M. Gronau, these proceedings.
49. G. Valencia, *Phys. Rev.* **D39** (1989) 3339.
50. For an example of such a model analysis, see G. Kramer and W.F. Palmer, *Phys. Rev.* **D45** (1992) 193, *Phys. Lett.* **279B** (1992) 181, *Phys. Rev.* **D46** (1992) 2969, DESY 92-043 (1992); G. Kramer, T. Mannel and W.F. Palmer, *Zeit. Phys.* **C55** (1992) 497.
51. E. Golowich and G. Valencia, *Phys. Rev.* **D40** (1989) 112; J.G. Körner, K. Schilcher and Y.L. Wu, *Phys. Lett.* **242B** (1990) 119.

HEAVY-FLAVOR PRODUCTION

J. SMITH
Institute for Theoretical Physics,
SUNY at Stony Brook
NY 11794-3480

and

W. K. TUNG
Department of Physics and Astronomy,
Michigan State University,
East Lansing, MI 48824-1116

1. INTRODUCTION

This review combines material on heavy quark production presented at the Snowmass Workshop in the opening plenary session by the first author on established theory; and in the closing plenary session by the second author summarizing work and discussions by two working groups - the *heavy quark production subgroup* of the morning *delta group* and the afternoon *theory group*. This introductory section contains: (i) a general discussion on *heavy quarks* and energy scales; and (ii) an overview of the kinematic regions and the theoretical approaches to heavy quark calculation. Sec.2 consists of a brief summary of the experimental status, including the main successes and problems in the comparison between data and existing theoretical calculations. Sec.3 reviews the well-known calculations on photoproduction, leptoproduction and hadroproduction of heavy quarks. Sec.4 describes two current efforts to extend the region of validity of existing calculations, involving the resummation of relevant large logarithms inherent in fixed-order perturbative QCD calculations. Note that actual cross section values for individual experiments are not included in this article. They can be found in the contribution by Riemersma and Meng.

In order to provide the necessary background for describing the different approaches to heavy quark production calculations, we begin by some general remarks.

Energy Scales and Heavy Quarks: The term "heavy quark" depends on the energy scale. It is generally regarded that the up, down and strange quarks with masses m_u, m_d and m_s respectively are "light quarks" as their masses are below and/or comparable with the scale $\Lambda_{\rm QCD}$ in perturbative QCD. Therefore we only see experimental manifestations of their production via "jets". The "heavy" quarks are the charm, bottom and top quarks with masses m_c, m_b and m_t respectively. However in QCD this distinction should really depend on the energy scale in the process under consideration. At high energies where the total energy in the hadronic collision $\sqrt{s} \gg m_c$ then the effective mass of the charmed quark is zero and the charmed quark should be considered as a normal light quark in the hadron. Therefore it can be described by a parton density, and this parton can initiate a hard scattering. At even higher energies where $\sqrt{s} \gg m_b$ then the bottom quark should also be considered as a light quark. (Since the top quark has not been detected it is unclear how large the energy must be before it can be considered as a light quark.) This scale-dependent description of charm and bottom quarks has not so far been adopted in most theoretical calculations.

The mass parameters m_c and m_b need clarification since they are not directly measurable quantities. Originally the existence of heavy (confined) quarks was inferred from the discovery of colorless spin-1 vector meson states such as the J/ψ and Υ, which are produced copiously both in electron-positron and in hadronic collisions. These physical particles (let us call them heavy hadrons) are bound states of charmed and bottom quarks respectively and have well-defined masses and lifetimes. Within the context of QCD there must be quantities which we can designate as heavy quark masses with values approximately one-half those of the vector meson masses. Then $m_c \approx 1.5$ GeV/c^2 and $m_b \approx 4.75$ GeV/c^2 have a phenomenological significance. In perturbation theory, we can identify these masses as the renormalized masses of the basic QCD Lagrangian. When mass effects are important, for example just above the "threshold" for heavy quark antiquark production, we cannot ignore terms of order $m/\sqrt{s}$ in a partonic reaction.

The description of experimentally observed heavy hadron production and decay involve the following stages: (i) production of the heavy quark by the high energy collision; (ii) "fragmentation" of the heavy quark into a heavy meson or baryon (we only consider open heavy flavor hadrons, not "onium" states); and (iii) decay of the heavy flavor hadron into ordinary hadrons and leptons.

Heavy Quark Production: The production of a heavy quark is usually calculated in the parton model at a scale set approximately by the heavy quark mass, including higher order corrections if possible. As the heavy quark mass m is larger than Λ_{QCD}, there is an extra large energy scale compared to the usual light quark physics. It was proven by Collins, Soper and Sterman[1] that the production cross section factorizes into a partonic hard scattering cross section $\hat{\sigma}_{ij}(s, m^2, Q^2)$, which includes all short distance effects, multiplied by light quark parton densities $\phi_i(x, Q^2)$, which incorporate all long distance effects. The scale which separates these two regions is the mass factorization scale, which we denote by Q^2. Inherent in this factorization is the notion that the only quarks in the hadron are the light ones. (In view of the discussion in the first paragraph, this approach needs modification when $m \ll \sqrt{s}$, see below.) In hadronic collisions and in neutral current lepton-hadron processes, the heavy quark is produced in association with a heavy antiquark. This process is referred to in the literature as "flavor creation". In flavor-changing charged current neutrino interactions a single heavy quark can be produced from a light quark so there is no need for pair production [2].

Prior to the proof of this factorization theorem (valid for m not too small compared to $\sqrt{s}$), other production mechanisms were considered, one of them being "flavor excitation", where the heavy quark exists as a parton density in the hadron and is "excited" out of the hadron by the hard interaction. Since (as mentioned earlier) c and b quarks should be considered as *partons* at very high energies, this production mechanism does have a natural place in the complete QCD treatment of heavy quark production valid for a wide range of energies, especially when $m \ll Q < \sqrt{s}$. A consistent formulation of pQCD incorporating both flavor creation and flavor excitation will be described briefly in Sec.4 later. Within the QCD framework, there is a third kinematic region, $m \sim Q \ll \sqrt{s}$ (the so-called *small-x* region), which needs special attention as well. We shall describe recent developments on this topic also in section four. A schematic map of the various kinematic regions and the relevant underlying physics is shown in Fig.1. Finally, there are kinematical regions where factorization of short and long distance effects cannot be proven so other mechanisms may play a role [3].

Fragmentation and Decay: The heavy quarks referred to above carry color and do not have the proper quantum numbers to make colorless heavy hadrons. When they are produced in partonic collisions vacuum perturbations produce light quark-antiquark pairs over the time scale $\Delta E \Delta t \approx h$. The heavy quark then combines with a light quark to form a colorless physical hadron with well defined mass. Since this process involves long-distance physics, not calculable in perturbation theory, it is also factorized out as a phenomenological "fragmentation function" in the pQCD framework. This function is extracted by fitting other experimental data, usually from e^+e^- collisions. The heavy hadron finally decays into light on-mass-shell hadrons with branching ratios that can be measured experimentally. The decay process involves the transition of the heavy quark into a light quark according to weak or electromagnetic interactions. Decays of heavy quarks are extensively discussed in other sections of this proceedings.

2. STATUS OF EXPERIMENTS

Heavy flavor production has been experimentally studied at electron-positron, hadron-hadron and lepton-hadron facilities. Some general review articles are Refs.[4],[5]& [6]. In e^+e^- collisions the production of heavy flavors does not involve strong interactions in the initial state. The physics studied focus on decay properties and CP violation, hence lie outside the scope of this review. (However, these measurements do yield useful information on the fragmentation functions for heavy quarks into heavy flavor hadrons which are of considerable relevance to the interpretation of data in hadron collisions.)

Leptoproduction of charm has been observed in μN scattering (neutral current, or NC, interaction) experiments and νN scattering (charged current, or CC, interaction) experiments. The NC measurements[7] are too crude to yield quantitative information on the production mechanism so far. Both flavor-creation (virtual γ gluon fusion) and flavor-excitation (virtual γ charm parton scattering) have been invoked to interpret the data, with no conclusive evidence for either. Forthcoming data from HERA will be of vital importance in testing QCD predictions. Charged current data[8][9] are much more decisive. The conventional interpretation of these data was confined to the "leading order" QCD process – scattering of the exchanged W-boson off light quarks (d and s). Recently, it has been realized that the "next-to-leading order" (NLO) process of W-gluon fusion is of equal significance numerically and physically.[2] Thus the analysis of the most recent comprehensive data[9] has been carried to this order.[10] This process provides vital information on the basic QCD parameter m_c (1.61 ± 0.25 GeV) – the charm quark mass, and on the strange quark distribution inside the nucleon. (See Ref.[10] for details.) Charged current production of charm is also anticipated in ep collider (HERA) experiments.

The production of charmed mesons and baryons in hadron-hadron scattering at fixed target energies has been recently reviewed.[11] The second generation of charm production experiments have overcome many of the difficulties of the earlier experiments; and the recent high-statistics data from CERN and Fermilab are in good general agreement, in contrast to the conflicting results from the first generation days. The shape of the energy dependence of the total production cross-section agrees quite well with existing fixed-order QCD calculations. However the theoretical predictions on the overall normalization has very large uncertainties – first, the NLO contribution is of the same magnitude as the LO term; secondly, the results are strongly dependent on the choice of the (unknown) factorization (and renormalization) scale (usually denoted by μ or Q). Fig.2 shows the measured total cross-section with some specific choices of m_c and scale μ. Fig.3 shows the large scale dependence of the theory prediction. Note that the strong μ dependence persists in the NLO result. This is conclusive evidence that this scheme of perturbative calculation is not reliable, since, in general, the scale-dependence is expected to diminish with increased order of calculation. These problems are not unexpected. On one hand, at the charmed quark mass, α_s is large so small changes in the scale result in large changes in the theoretical cross section. On the other hand, since the mass m_c is much smaller than the typical energy scale, the charm quark should behave just like another parton - a fact not taken into account in the existing fixed-order calculations. We shall come back to this point in Sec.4.. Data are also available on the p_t and x_F inclusive distributions. For a discussion of these distributions we refer the reader to the above review article.

Photoproduction of charm is in a similar state as hadroproduction[12]. Due to the fact that real on-mass-shell photons fluctuate easily into virtual light mass quark-antiquark pairs, photoproduction consists of two components: the direct or *point like* component is similar to leptoproduction; and the hadronic or *resolved* component to hadroproduction. For the second component, we need to input the parton densities in the photon[13] as well as the parton densities in the proton[14]. These former quantities are not well known but the situation should be better clarified when data from HERA are analyzed. Electroproduction of charm (Cf. discussion in previous paragraphs on leptoproduction.) is probably a cleaner test of QCD but there will be many fewer events.

Hadroproduction of b-quarks has been observed at CERN and at Fermilab. The UA1 experiment produced the first inclusive differential spectrum in the transverse momentum of the b-quark [16]. This data were fitted rather well, both in shape and normalization, by the predictions from $O(\alpha_s^3)$ perturbative QCD (assuming only flavor creation), using the best available gluon and quark densities in the proton. At higher energies the same differential spectrum (actually in $p_T > p_{T\text{min}}$) has been presented by the CDF collaboration at the Fermilab Tevatron. In this case the data are generally a factor of two larger than the theoretical predictions and the points at small $p_{T\text{min}}$ are even higher. At this meeting we have seen the latest data analysis from the CDF group.[17] They have now discovered that there were more J/ψ decays from excited charmed states in the low p_T data. Therefore the data points at low $p_{T\text{min}}$ have come down so that the shape is more in line with the theory. We note that here, again, the theory predictions are fairly sensitive to the choice of the unknown factorization scale. See Fig.3. However, even allowing the scale to vary over a reasonable range, the rate is still uncomfortably large. Attempts have been made to fit this data using the $O(\alpha_s)$ corrections in[20] but by changing the gluon density in the proton (and stretching the choice of scale).[18] Another discussion of the discrepancy between theory and data is given in Ref.[19]. As mentioned earlier, systematic efforts to extend the validity of QCD predictions beyond the fixed-order calculations will be discussed in Sec.4.

3 REVIEW of FIXED-ORDER QCD CALCULATIONS

As explained above perturbative QCD calculations of the production cross sections for heavy quarks are only valid in specific regions in the energy scale. Near threshold, where the heavy quark mass m is not negligible with respect to the total energy in the partonic collision $\sqrt{s}$, fixed order calculations in α_s using the flavor-creation mechanism alone should generally be reliable. However, since the partonic collision energy is not fixed, even though the hadronic collision energy is set for a particular accelerator, the relevant scales are not constant. Therefore all quarks have to be subdivided into two classes at a typical scale, say the mass factorization scale Q^2, those with light masses m_L (where $m_L^2 \ll Q^2$), which can be produced in the final state, and those with heavy masses m_H (where $m_H^2 \gg Q^2$), which are too heavy to be produced in the final state. One can consider that the relevant scale is $Q^2 \approx m^2$, the mass of the heavy quark under study. The light mass quarks are then described by parton densities, $\phi_i(x, Q^2)$ which evolve in Q^2 as solutions of the QCD evolution equation [21].

The hadron-hadron production cross section is given by the convolution of parton-parton scattering cross-sections with distribution functions of the partons, as given by the *master formula* of the QCD parton model:

$$\sigma(S,m,Q^2) = \sum_{i,j} \int_{m^2/S}^{1} dx_1 \int_{m^2/x_1 S}^{1} dx_2\, \phi_i(x_1,Q^2)\, \phi_j(x_2,Q^2)\, \hat{\sigma}_{ij}(\hat{s},m,Q^2)\,, \tag{1}$$

where the parton distributions are labelled by $\phi_i(x, Q^2)$ for flavor i in the hadron and $\hat{s} = x_1 x_2 S$. The parton-parton scattering cross-section $\hat{\sigma}_{ij}(\hat{s}, m, Q^2)$ can be calculated in perturbative QCD. In lowest order the appropriate $\hat{\sigma}$ should be identified with one of simple cross sections given below. The carat is only significant in higher order when it means that we must take the finite part of the calculated parton-parton cross section in a specific renormalization and factorization scheme. Both $\phi_i(x, Q^2)$ and $\hat{\sigma}_{ij}(\hat{s}, m, Q^2)$ are scheme and scale dependent, but the calculated physical cross-section $\sigma(S, m, Q^2)$ should be insensitive to Q^2 if the choice of calculational scheme is appropriate for the process. (See Sec.1 and Sec.4 for discussions.)

3.1 *Leading Order Flavor Creation Cross-sections*

We will now write down the lowest order parton-level cross-sections for heavy quark production in the reactions $q + \bar{q} \to Q + \bar{Q}$ [22] $\gamma + g \to Q + \bar{Q}$ [23] and $g + g \to Q + \bar{Q}$ [24].

The differential and total cross sections for the reaction $q + \bar{q} \to Q + \bar{Q}$, where $q(\bar{q})$ are light (massless) quarks and $Q(\bar{Q})$ are heavy quarks with mass m, can be obtained from the well-known results for the QED reaction $e^+ + e^- \to \mu^+ + \mu^-$. Comparing the two Lagrangians one can easily show that the QCD results are

$$s^2 \frac{d^2\sigma}{dt_1 du_1} = \frac{4\pi\alpha_s^2(Q^2)}{3}\Big[\frac{t_1^2 + u_1^2}{s^2} + \frac{2m^2}{s}\Big]\delta(s + t_1 + u_1)\,, \tag{2}$$

and

$$\sigma(s, m^2) = \frac{8\pi\alpha_s^2(Q^2)}{27 s^2}(s + 2m^2)\beta\,. \tag{3}$$

We use the notation $t_1 = t - m^2$, $u_1 = u - m^2$ where s, t and u are the standard Mandelstam invariants, $\beta = (1 - 4m^2/s)^{1/2}$ and $\alpha_s = g^2/(4\pi)$. The results include a summation over final spins and colors and an average over initial spins and colors.

For photoproduction we need to consider the reaction $\gamma + g \to Q + \bar{Q}$, which has its QED counterpart in $\gamma + \gamma \to \mu^+ + \mu^-$. The differential cross section is

$$s^2 \frac{d^2\sigma}{dt_1 du_1} = \pi\alpha_{em}\alpha_s(Q^2)e_H^2 B_{QED}\delta(s + t_1 + u_1)\,, \tag{4}$$

where

$$B_{QED} = \frac{t_1}{u_1} + \frac{u_1}{t_1} + \frac{4m^2 s}{t_1 u_1}\Big(1 - \frac{m^2 s}{t_1 u_1}\Big), \tag{5}$$

is the same factor that appears in the QED result. The total cross section is

$$\sigma(s,m^2) = \frac{2\pi\alpha_{em}\alpha_s(Q^2)}{s} e_H^2 \Big\{\Big(1 + \frac{4m^2}{s} - \frac{8m^4}{s^2}\Big)\ln\Big(\frac{1+\beta}{1-\beta}\Big) - \Big(1 + \frac{4m^2}{s}\Big)\beta\Big\}. \tag{6}$$

For electroproduction we need the corresponding formulae for the transverse and longitudinal partonic cross sections in the reaction $\gamma^* + g \to Q + \bar{Q}$. These can be found in [25]-[28].

Finally for the reaction $g + g \to Q + \bar{Q}$ the color structure is more complicated and the differential scattering amplitude takes the form

$$s^2 \frac{d^2\sigma}{dt_1 du_1} = \frac{\pi\alpha_s^2(Q^2)}{16}\Big\{3\Big(1 - \frac{2t_1 u_1}{s^2}\Big) - \frac{1}{3}\Big\}\Big[\frac{t_1}{u_1} + \frac{u_1}{t_1} + \frac{4m^2 s}{t_1 u_1}\Big(1 - \frac{m^2 s}{t_1 u_1}\Big)\Big]\delta(s + t_1 + u_1), \tag{7}$$

again summed and averaged over initial polarizations and colors. The total cross section is

$$\sigma(s,m^2) = \frac{\pi\alpha_s^2(Q^2)}{3s}\Big\{\Big(1 + \frac{4m^2}{s} + \frac{m^4}{s^2}\Big)\ln\Big(\frac{1+\beta}{1-\beta}\Big) - \Big(7 + \frac{31m^2}{s}\Big)\frac{\beta}{4}\Big\}. \tag{8}$$

As mentioned before, the above results should be convoluted with the appropriate leading order parton densities to calculate hadronic cross sections and inclusive distributions in the Born approximation. Note that in lowest order the scale Q^2 only appears in the lowest order coupling constant (which we will discuss in more detail shortly) and in the parton densities. There is no real physical criterion for choosing any particular scale. Therefore one should not be surprised that there are rather large changes in the theoretical cross section when Q^2 is varied. One of the reasons why it is important to calculate the next order QCD corrections is to reduce this sensitivity to Q^2.

3.2 *Next-to-leading Order Calculations*

Now consider what happens when we calculate QCD corrections to the Born reactions given above. These corrections have been carried out for photoproduction [29],[30], electroproduction [31] and hadroproduction [32],[20] of heavy quarks through next order in α_s.

One has to calculate all diagrams containing loop corrections to the Born amplitude (in order to calculate the interference terms) and square the sum of all diagrams with emission of an additional parton. In this calculation several new features enter, which we will try to explain in as non-technical language as possible. The first problem is that there are several types of divergences in the diagrams, which are classified as ultraviolet (removed by renormalization), infrared (cancels when we sum over degenerate physical states) and collinear (absorbed into the definition of the light mass parton densities). The removal of these singularities is understood in principle but complex to carry out in practice. When the singularities are removed analytically, it is easiest to discuss the total cross section or the single particle inclusive heavy quark differential distributions in p_T or y.

Light Quark contributions: The classification of quarks into light and heavy has been mentioned earlier. The light mass quarks are absorbed into the definitions of parton densities at a certain scale Q^2. Another way of stating this is that during the calculation we find potentially dangerous terms in m_L, such as $\ln m_L^2/m^2$, which we rewrite as $\ln Q^2/m^2 + \ln m_L^2/Q^2$, and absorb the latter logarithms into the definitions of the light quark densities, which then satisfy the Altarelli-Parisi equations. The cross section still depends on the scale Q^2 via terms in $\ln Q^2/m^2$. The other scale, called the renormalization scale, enters via the running coupling constant $\alpha_s(Q^2)$, which is introduced to solve the renormalization group equation. These two scales are taken equal in all attempts to extract parton densities from experiment so we call them simply Q^2. Therefore the partonic cross sections are usually written in terms of so-called scaling ratios as

$$\hat{\sigma}_{i,j}(s,m^2,Q^2) = \frac{\alpha_s^2}{m^2}\Big[f_{i,j}^{(0)}(\eta) + 4\pi\alpha_S\Big\{f_{i,j}^{(1)}(\eta) + \bar{f}_{i,j}^{(1)}(\eta)\ln\frac{Q^2}{m^2}\Big\}\Big], \tag{9}$$

where the dimensionless functions $f_{i,j}^{(0)}(\eta), f_{i,j}^{(1)}(\eta)$ represent the Born contribution and the $O(\alpha_S)$ correction respectively. The function $\bar{f}_{i,j}^{(1)}(\eta)$ appears when the mass factorization scale Q^2 deviates from the square of the heavy flavor mass m^2. The scaling ratio η is denoted by

$$\eta = \frac{s}{4m^2} - 1 \quad , \tag{10}$$

although other ratios such as $4m^2/s$ are just as useful. In higher order QCD all these partonic cross sections as well as the parton densities are scheme dependent because they are only defined after a prescription is used to remove the collinear singularities.

Heavy Quark Decoupling: Now let us discuss the case of really heavy quarks, with $m_H \gg m$. At first sight one would neglect them since there is not enough energy to produce such quarks as physical particles. However this is not a correct procedure. Heavy quark loop corrections to the gluon propagator (like fermion loop corrections to the photon propagator in QCD) include a sum over all virtual quarks irrespective how heavy they are so we cannot ignore them. Fortunately there is a theorem due to Appelquist, Carrazone and Symanzik [33] which states that the higher order corrections due to the heavy quark loops can be absorbed into a redefinition of the measurable parameters of the theory (coupling constants and masses) so their effects are not observable. (In spontaneously broken theories such as the standard model of electroweak interactions, the particle masses are related to the coupling constants so the theorem is not valid. This is why accurate measurements of standard model parameters at the Z mass are sensitive to the top and Higgs masses.) In QCD the theorem is true and ***has to be implemented in a specific scheme*** if one wants the running coupling constant to be continuous across quark production thresholds. If this is not done then terms like $\ln(m_H^2/Q^2)$ appear in the perturbative expansion and they are large when $Q^2 \ll m_H^2$. Of course one can absorb them into a redefinition of the running coupling constant so it is discontinuous at the scale where $Q^2 = m_H^2$. Although there is nothing wrong with such a method it is simpler to remove all these large logarithms completely from the start. This is what is done when one follows the so-called Collins, Wilczek and Zee renormalization scheme [34], in which the heavy quarks are decoupled in the limit of small momentum flowing into heavy flavor loops. We will assume that this scheme is followed when we consider higher order corrections. Since the cross section is a renormalization group invariant we can limit ourselves to mass and coupling constant renormalization. Usually mass renormalization is performed in the on-mass-shell renormalization scheme and coupling constant renormalization follows the so-called $\overline{\text{MS}}$ scheme.

3.3 *Illustrative Results on Parton-level Cross sections*

In Fig.4 we show the contributions to the partonic functions $f^{(0)}_{g,g}(\eta)$, $f^{(1)}_{g,g}(\eta)$ and $\bar{f}^{(1)}_{g,g}(\eta)$ from the gluon-gluon scattering channel plotted versus η in the $\overline{\rm MS}$ scheme. The Born contribution $f^{(0)}_{g,g}(\eta)$ decreases at large and small η. However the higher order correction $f^{(1)}_{g,g}(\eta)$ is large in both these regions. The corrections at small η (near threshold) are partly due to the exchange of a "Coulomb" gluon between the heavy quark-antiquark pair. This has a QED counterpart which was discussed long ago by Schwinger [35]. However this correction is only important very close to threshold. The main contribution to the enhancement is due to an imperfect cancellation of soft and virtual $O(\alpha_s)$ corrections near threshold, which leaves behind some large logarithms.

There is also an enhancement in the cross section at large η which is due mainly to graphs where the incoming gluon splits into two i.e., these are the Feynman diagrams with massless t-channel exchanges. These are often referred to as the large corrections at small x where $x = m^2/s$.

We now examine the plot of $\bar{f}^{(1)}_{g,g}(\eta)$ the coefficient of the scale dependent logarithm $\ln(Q^2/m^2)$. This function changes sign an intermediate value of η. Since we do not know whether to choose a scale so that this logarithm is positive or negative we see that it can either enhance or suppress the contributions at large and/or small η. This is one reason that we still see large variations in the hadronic cross section at a different choice of the Q^2. There is of course a favorable situation where the variation is small, namely when the parton densities weight the central region heavily. However this only occurs at specific values of m for each experimental value of $\sqrt{s}$, which are often nowhere near the masses m_c, m_b or the estimated value of m_t. Clearly when m is small and the parton densities weight the large η region (high CM energies) then the prediction for the cross section is poor. Also when m is large and we are sensitive to the parton densities in the large x region (near threshold) then again we do not have a very accurate prediction of the cross section. These regions will be discussed shortly. We should remind the reader that these $f_{g,g}(\eta)$ functions are not physical quantities. Only after convolution with the corresponding $\overline{\rm MS}$ parton densities do we arrive at measurable cross sections.

3.4 *The QCD Running Coupling in the presence of Heavy Quark Masses:*

The above decomposition factors out the running coupling constant so it can be discussed separately. Our choice of which quark is "light" has a significant influence on α_s. Since the latter depends on n_f, the number of light quarks, it should change its numerical value when Q^2 crosses a heavy quark threshold. To maintain continuity of the running coupling constant across such thresholds, we have to change the value of $\Lambda = \Lambda_{\rm QCD}$. If we define the two-loop corrected α_s in the $\overline{\rm MS}$ scheme then

$$\alpha_s(Q^2, n_f) = \frac{1}{b_f \ln(Q^2/\Lambda^2)}\Big[1 - \frac{b'_f \ln\ln(Q^2/\Lambda^2)}{b_f \ln(Q^2/\Lambda^2)}\Big], \tag{11}$$

where b_f and b'_f are given by

$$b_f = \frac{33 - 2n_f}{12\pi} \quad , \quad b'_f = \frac{153 - 19n_f}{2\pi(33 - 2n_f)}, \tag{12}$$

is valid for top-quark production with $\Lambda = \Lambda_5$ and $n_f = 5$. For bottom and charm production we need α_s for four and three flavors with different Λ_4 and Λ_3 values respectively. So that there is continuity across the b and c thresholds we define following [36]

$$\begin{aligned} \alpha_{s,5}(Q^2) &= \alpha_s(Q^2,5) \\ \alpha_{s,4}^{-1}(Q^2) &= \alpha_s^{-1}(Q^2,4) + \alpha_s^{-1}(m_b^2,5) - \alpha_s^{-1}(m_b^2,4) \\ \alpha_{s,3}^{-1}(Q^2) &= \alpha_s^{-1}(Q^2,3) + \alpha_s^{-1}(m_c^2,4) + \alpha_s^{-1}(m_b^2,5) \\ &\quad -\alpha_s^{-1}(m_b^2,4) - \alpha_s^{-1}(m_c^2,3) \end{aligned} \tag{13}$$

so that

$$\begin{aligned} \alpha_s(Q^2) &= \alpha_{s,5}(Q^2)\theta(Q^2 - m_b^2) + \alpha_{s,4}(Q^2)\theta(m_b^2 - Q^2)\theta(Q^2 - m_c^2) \\ &\quad +\alpha_{s,3}(Q^2)\theta(Q^2 - m_c^2) \end{aligned} \tag{14}$$

This result is also often used in the calculation of the lowest order Born approximation even though one should only use the first term in Eq. (11) above, with yet another value of Λ.

3.5 *Limitations of Fixed-order Calculations*

We recall that these fixed $O(\alpha_s)$ correction calculations are only applicable in a kinematical region where the mass m and the other typical energy scales of the physical process, such as $\sqrt{s}$, p_t, etc. (generically called Q above), are roughly of the same magnitude and significantly larger than $\Lambda_{\rm QCD}$. Under such circumstances the scale parameter in the cross section is the heavy quark mass, so we need the running coupling constant at the scale m, and light-mass parton densities evaluated at the same scale. Single particle differential distributions are calculable when $p_t \approx m$ at a scale $Q^2 \approx p_t^2 + m^2$. Other distributions are available from Monte Carlo programs, which generally do not include the $O(\alpha_s)$ corrections [37]. Recently more effort has been put into the numerical cancellation of the singularities, since this allows one to calculate exclusive correlations [38] For charm and bottom quarks, the condition $Q \sim m$ is not well satisfied in current collider energies and beyond. Thus, as observed in the review of experimental status (Section 2), in spite of qualitative agreements, there are problems in comparison of these calculations with existing experimental results: in particular, the large scale dependence of theoretical results which diminishes the predictive power of the theory and the apparent disagreement of measured b-production cross-section at CDF with existing theory. Limitations on the range of applicability of fixed-order (say, n) calculations arise from terms of the form $[\alpha_s(Q)\ln(Q^2/m^2)]^n$ and $[\alpha_s(Q)\ln(s/Q^2)]^n$ which do not become small as n becomes large if either $Q^2/m^2 \gg 1$ or $s/Q^2 \gg 1$, hence vitiate the usefulness of the perturbation expansion. The truncated perturbative calculation then become a poor approximation, and it acquires large spurious scale-dependence. The following section gives a brief description of recent approaches to extend the region of applicability of QCD calculations of heavy quark production.

We close this section with a comment on the size of the next order corrections. For next-to-leading order heavy quark production, they are often large even in the region where fixed order calculation is supposed to be valid (typically, the ratio NLO/LO is of order 1), which brings up the question of whether the perturbation series is to be trusted at all. In our opinion this is not a real problem, since the origin of the large NLO correction is well-understood: the LO Feynman diagrams all give rise to cross-sections which vanish at asymptotic energies; only the next order contribution contains graphs with massless gluon exchanges in the t-channel which yield a constant cross-section which, of course dominates at high energies, even if down by one power of α_s. Further higher order contributions do not introduce similar large corrections, since no new qualitatively different mechanisms come in beyond the NLO. This type of phenomenon is well known in field theory. A dramatic (and familiar) example occurs in QED. The cross section for $e^+ + e^- \to \mu^+ + \mu^-$ in lowest order falls off as $\alpha_{\rm QED}^2 s^{-1}$ as the CM energy increases. In higher order the so-called two-photon process is allowed, for instance $e^+ + e^- \to e^+ + e^- + \mu^+ + \mu^-$, whose cross section grows logarithmically at large energies as $\alpha_{\rm QED}^4 m_\mu^{-2} \ln(S/m_\mu^2)\ln^2(S/m_e^2)$. The relevant Feynman diagrams now contain the t-channel exchange of massless particles. Since this process has completely different kinematics as compared to the Born reaction (the muons are produced at low p_t with a flat rapidity distribution) it should not be considered as a correction to it. The calculations of the true next order corrections to two-photon physics reactions generally find small effects, since the scale change is now correctly incorporated in the "Born" approximation. A similar phenomena is expected to occur in the production of heavy quarks in QCD.

4 BEYOND FIXED-ORDER CALCULATIONS - RECENT DEVELOPMENTS

Fig.1 in Sec.1 delineates the regions of phase space of applicability of the fixed-order calculations and its extensions. In the region where $Q^2/m^2 \gg 1$, the "heavy quark" (say, charm or bottom) behaves more or less like an ordinary *parton*, hence the calculational scheme must be adapted to reflect this fact. This will be discussed below in Sec.4.1. In the region where $s/Q^2 \gg 1$, the momentum fraction carried by the partons (typically, $x \sim O(Q/\sqrt{s})$) becomes very small, large logarithm factors $[\alpha_s(Q)\ln(s/Q^2)]^n$ must be *resummed* to all orders in n. This "small-x" region will be discussed in Sec.4.2.

4.1 Heavy quark partons and flavor excitation

To elucidate the basic physics, consider for example the production of a heavy quark-antiquark pair in deep inelastic electron scattering, $e + N \to Q + \bar{Q} + X$.[39] In addition to the energy scales s and m, the underlying process is characterized by another physical scale Q, the virtuality of the exchange photon. (Recall $s = W^2 = Q^2(1/x - 1)$, where x is the Bjorken scaling variable.) The leading order flavor creation process considered in fixed-order calculations is $\gamma^* + g \to Q + \bar{Q}$. For this reaction one can define analogous functions to the f's which appeared in Eq.(9) of the NLO calculation section, only they are now dependent on two ratios, namely $\eta = s/4m^2 - 1$ and $\xi = Q^2/m^2$. It is terms of the form $[\alpha_s(\mu)\ln\xi]^\beta$, $\beta = 1, 2$, which cause the results to be unreliable in the region $Q^2/m^2 \gg 1$. Here we encounter the same situation as ordinary light quark production in deep inelastic scattering at current fixed-target energies. The cure to this problem is well-known: we need to resum all logarithm factors of this form to all orders and this can be done "automatically" by use of the renormalization group equation (which is commonly called the Altarelli-Parisi equation in leading order). The net result is that, the "heavy quark" (denoted by Q and $\bar{Q}$) becomes one of the *partons* of the theory, and we must include the additional basic process $\gamma^* + Q(\bar{Q}) \to Q(\bar{Q})$ – *flavor excitation* – with the associated parton distribution function $\phi_N^Q(x, \mu)$ in the master formula! Since the $[\alpha_s(\mu)\ln\xi]^\beta$, $\beta = 1, 2$ terms are now included in this additional (finite) contribution, they must be removed from the original formulas for $\sigma(\gamma^* + g \to Q + \bar{Q})$ to avoid double-counting. This results in a subtracted hard cross-section to be inserted in the master formula. This subtraction involves a factorization scale μ which we can identify with the physical scale Q according to usual convention. (A good alternative choice is $\mu^2 = Q^2 + m^2$.)

The leading flavor excitation contribution $\gamma^* + Q(\bar{Q}) \to Q(\bar{Q})$ is formally of order α_s^0 — one order lower than that of flavor creation, $\gamma^* + g \to Q + \bar{Q}$, which begins at order α_s^1. Thus, at *very high energies* ($\mu(Q) \gg m$), $\gamma^* + Q(\bar{Q}) \to Q(\bar{Q})$ should be the dominant one, leading to *theoretical predictions substantially different from those of fixed-order flavor creation calculations.* In contrast, when $\mu(Q)$ is not too large compared to m, the contributions from the two mechanisms are numerically of the same order since the gluon distribution function ϕ_N^g is much larger than ϕ_N^Q, thus compensating for the extra power of α_s. (In fact, in this region $\phi_N^Q \sim \alpha_s \ln(\mu/m) \cdot P_g^Q \otimes \phi_N^g$ where P_g^Q is the splitting function of $g \to Q$.) Here, the flavor excitation contribution is rather unphysical (since the "parton" interpretation is not a good one when the mass is not negligible) and the QCD formalism corrects this by removing its contribution with the required "subtraction" of double-counting mentioned above. The end result is that, *flavor creation does emerge as the primary physical mechanism for producing heavy quarks when $\mu(Q) \sim m$.*

This brief discussion should make it clear that, in a properly formulated QCD framework, flavor creation and flavor excitation are complementary fundamental processes, each with their own natural region of dominance, but also must co-exist in some parts of phase space which mark the transition region. (See Fig.1) The ideas explained here applies to hadroproduction of heavy quarks as well. At the present, whereas fixed-order flavor creation calculations have been completed to NLO order, the generalized scheme to include flavor excitation is only beginning to be developed. First results[39] on leptoproduction, carried out to order α_s, is encouraging in that they show all the expected qualitative features discussed above, and yield the anticipated reduction in scale-dependence. Fig.5 shows results on the various contributions (flavor excitation, flavor creation, their overlap (i.e. subtraction)) to the structure function $F_2(x, Q)$ for charm production as a function of Q for a given x. Note how the subtraction interpolates between the flavor excitation (at low Q) and the flavor creation (at high Q) as the physics dictates. Fig.6 shows dependence on the choice of scale (μ) for the various terms. We see that the strong μ dependence of the individual terms is greatly reduced in the theoretically more complete combined result.

4.2 Small-x resummation – k_t Factorization

A similar problem occurs as the $\ln(1/x) \sim \ln(s/\mu^2)$variable gets large for not too large $\ln(\mu/m)$. Thus, for large CM energies when $\alpha_s \ln(1/x) \approx 1$, the fixed-order perturbation series again breaks down. Several groups have worked on this "small x" problem. and methods have to be developed to resum these large logarithms [40],[41],[42]. The basic tool for resumming leading $[\alpha_s \ln(1/x)]^n$ contributions to all orders in α_s was the Lipatov equation. This problem is extremely challenging theoretically. There is no simple physical picture which can be described in this short review. The three existing approaches differ considerably in technical detail. But they also share several general features which are worth mentioning. These are: (i) they all start with the Lipatov "hard pomeron" formalism, as already mentioned; (ii) they all involve using a *k_t-factorization formalism*, which employs a new type of gluon distribution involving off-shell gluons with definite transverse momentum $\varphi(x, k_t^2)$ which relates to the usual on-shell gluon distribution function $G(x, Q^2)$ qualitatively by $xG(x, Q^2) = \int^{Q^2} dk_t^2 \varphi(x, k_t^2)$; (iii) so far, they are limited to a theory of gluons (which dominate at small-x) only and to resummation of the "leading" contribution to small-x (i.e. no systematic extension to terms of the form $\alpha_s^n \ln^{n-1}(1/x)$ and lower is available).

Quantitative predictions from the efforts to include small-x resummation are still lacking. Estimates obtained by Refs.[40] & [41] suggest corrections to fixed-order flavor creation calculations are no more than 30-40% at current collider (both lepton-hadron and hadron-hadron) energies. However, Ref.[42] claims effects up to 100% or more for b-production at the Tevatron. At this workshop, considerable efforts were made to understand this result and to evaluate the potential for making quantitative predictions for cross-sections useful for the rest of the Workshop. These efforts were not fruitful. It appears the quoted results are very much dependent on the input gluon distribution function $\varphi(x, k_t^2)$ (which is not well determined) and that the numerical calculation of the hard cross-section and the convolution integral of the k_t-factorization formula are not yet fully under control. Much work is required to develop these individual new approaches and to reconcile the differences between them.

Also, it is important to clarify where the transition region between the "small-x" and the conventional physics takes place. In the absence of *a priori* theoretical prediction on the location of this transition, a phenomenological approach is to compare fixed order calculations hold with the alternative resummed results. Numerical studies focusing on this comparison completed so far[43] strongly suggest that distinctive small-x resummed results do not become important down to $x \sim 10^{-4}$. For practical applications, this type of comparison involves comparing data on the production of one specific heavy quark at different accelerators, or data on c, b and/or t production at the same machine.

4.3 Other Regions and considerations

Finally there is the region where both $\ln(1/x)$ and $\ln(\mu/m)$ are large. This is the multi-scale asymptotic region, where nothing much is known, either experimentally or theoretically. For completeness we should also warn the reader that the region where the quark is produced near threshold is also not theoretically clean. Then there are another set of large logarithms in the perturbation series which have to be resummed [44], see also Ref.[45]. These corrections are important for t-quark production at the Fermilab Tevatron [46].

5. ACKNOWLEDGEMENTS

We thank all members of the Heavy Quark Production work group, both theorists and experimentalists for fruitful discussions on all issues related to heavy flavor production in QCD. Professor Genya Levin, in particular, contributed a great deal in stimulating interest on the small-x problem. V. Papadimitriou and D. Zieminska contributed much to exploring the numerical study of the small-x approach.

The work in this paper was supported in part under the contracts NSF 92-11367 (J.S.) and PHY9396022 (W.K.T). Financial support was also provided by the Texas National Research Laboratory Commission (RGFY9240). J. Smith would like to thank NIKHEFH in Amsterdam for their hospitality while this paper was being completed.

6. REFERENCES

1. J. Collins, D. Soper and G. Sterman, *Nucl. Phys.* **B263**, 37 (1986).
2. M.A.G. Aivazis, F.I. Olness and W.K. Tung, *Phys. Rev. Letts.* **65**, 2339 (1990); J.J. van der Bij and G.J. van Oldenborgh, *Z. Phys.* **C51**, 477 (1991).
3. G. Ingelman, L. Jönsson and M. Nyborg, *Phys. Rev.* **D47**, 4872 (1993); S.J. Brodsky, P. Hoyer, A.H. Mueller and W-K. Tang, *Nucl. Phys.* **B369**, 519 (1992).
4. A. Ali in *Physics at LEP*, CERN Report 8602, eds. J. Ellis and R. Peccei, vol.2,p.81.
5. N. Ellis and A. Kernan, *Phys. Rep.* **C195**,24 (1990); R.K. Ellis and W.J. Stirling, FERMILAB-Conf-90/164-T.
6. J.P. Guillet, P. Nason and H. Plothow-Besch, in *Proceedings of the European Committee for Future Accelerators "Large Hadron Collider Workshop"*, CERN 90-10,eds G.Jarlskog and D.Rein, vol.2,p.116; G. Carboni *et al.*, *ibid* vol.2,p.199; E. Reya, P. Zerwas, W. Hollik, V. Khoze, R.J.N. Phillips, F. Berends, D. Rein and J. Zunft, *et al.*, *ibid* vol.2,p.295.
7. M. Arneodo, *et.al.*, *Z. Phys.* **C35** 1 (1987); J.J. Aubert, *et.al.*, *Nucl. Phys.* **B213**, 31 (1983); J.J. Aubert, *et.al.*, *Phys. Lett.* **94B**, 101 (1980).
8. H. Abramowicz, *et.al.*, *Phys. Rev. Lett.* **57**, 298 (1986); *Z. Phys.*, **C28**, 51 (1985).
9. CCFR Collaboration, *Phys. Rev. Lett.* **70**, 134 (1993).
10. A. Bazarko in Proceedings of 18th Rencontres de Moriond (1993), to be published.
11. J. Appel, *Ann. Rev. Nuci. Part. Sci.* **42**, 367 (1992).
12. M.S. Witherall, in *Proceedings of the 1987 International Symposium on Lepton and Photon Interactions*, Hamburg FRG, eds. W. Bartel and R. Rückl, North Holland, Amsterdam, 1988.
13. M. Drees and K. Grassie, *Z. Phys.* **C28**, 451 (1985); M. Drees and R. M. Godbole, *Phys. Rev.* **39**, 169 (1987); M. Glück, E. Reya and A. Vogt, *Phys. Rev* **D45**, 3986 (1992); *ibid* **D46**, 1973 (1992); P. Aurenche, P. Chiapetta, M. Fontannaz, J.Ph. Guillet and E. Pilon, *Nucl. Phys.* **B399**, 34 (1993); L.E. Gordon and J.K. Storrow, Z. Phys. C56, 307 (1992).
14. J. Botts, J.G. Morfín. J.F. Owens, J. Qiu, W.K. Tung, and H. Weerts, *Phys. Lett.* **B304** (1993) 159; A.D. Martin, W.J. Stirling and R.G. Roberts, *Phys.Letts* **B306**, 145 (1993); J. G. Morfín and W.K. Tung *Z. Phys.* **C52** 13 (1991).
15. J.J. Aubert *et al.*, *Phys. Lett.* **B110**, 73 (1982); *Nucl. Phys.* **B213**, 31 (1983).
16. UA1 Collaboration, C. Albajar *et al.*, *Phys. Lett.* **B213**, 4105 (1988); *Z. Phys.* **C48**, 1 (1990); Talk by S. McMahon (UA1 experiment) at the XXVth Rencontres de Moriond, Les Arcs, March 1990; UA1 Collaboration, C. Albajar *et al.*, *Phys. Lett.* **B256**, 121 (1991).
17. V. Papadimitriou, *private communication*; CDF Collaboration, F. Abe *et al.*, *Phys. Rev. Lett.* **68**, (1992) 3403; *ibid.*, *Phys. Rev. Lett.* **69**, (1992) 3704; CBF Collaboration, F. Abe *et al.*, FERMILAB-PUB-93/091-E (April 1993), submitted to *Phys. Rev. Lett.*; *ibid.*, FERMILAB-PUB-93/106-E (May 1993), submitted to *Phys. Rev. Lett.*; em ibid., FERMILAB-PUB-93/131-E (June 1993), submitted to *Phys. Rev.* **D**; *ibid.*, FERMILAB-PUB-93/145-E (June 1993), submitted to *Phys. Rev. Lett.*
18. E. Berger and R. Meng, *Proceedings of The Fermilab Meeting DPF '92*, eds. C.H. Albright, P.H. Kasper, R. Raja, and J. Yoh, World Scientific, (1993); E. Berger, R. Meng, and J.-W. Qiu, *Proceedings XXVI Int. Conf. on High Energy Physics* Dallas, 1992; E. Berger and R. Meng, *Phys. Rev.* **46**, 169 (1992); E. Berger, R. Meng, and W.K. Tung, Phys. Rev. **D46**, 1859 (1992).
19. M.L. Mangano, *Z. Phys.* **C58**, 861 (1993).
20. W. Beenakker, H. Kuijf, W.L. van Neerven and J. Smith, *Phys. Rev.* **D40**, 54 (1989); W. Beenakker, W.L. van Neerven, R. Meng, G.A. Schuler and J. Smith, *Nucl. Phys.* **B351**, 507 (1991).

21. G. Altarelli and G. Parisi, *Nucl. Phys.* **B126**, 298 (1977).

22. M. Glück, J.F. Owens and E. Reya, *Phys. Rev.* **D17**, 2324 (1978); B. L. Combridge, *Nucl. Phys.* **B151**,429 (1979); J. Babcock, D. Sivers and S. Wolfram, *Phys. Rev.***D18**, 162 (1978); K. Hagiwara and T. Yoshino, *Phys. Lett.* **B80**, 282 (1979); L.M. Jones and H. Wyld, *Phys. Rev.* **D17**, 782 (1978).

23. A. Ali, G. Ingelman, G. A. Schuler, F. Barreiro, M. A. Garcia, J. F. de Trocóniz, R. A. Eichler and Z. Kunszt, " Heavy Quark Physics at HERA", in *Proceedings of the DESY Workshop on HERA Physics*, DESY, Hamburg (1988), DESY 88-119; G.A. Schuler, *Nucl. Phys.*, **B299**, 21 (1988).

24. G. Matthiae, *Riv. Nuovo Cim.* **4**, 1 (1981).

25. E. Witten, *Nucl. Phys.* **B104**, 445 (1976); J. Babcock and D. Sivers, *Phys. Rev.* **D18**, 2301 (1978); M.A. Shifman, A.I. Vainstein and V.J. Zakharov, *Nucl. Phys.* **B136**, 157 (1978); M. Glück and E. Reya, *Phys. Letts.* **B83**, 98 (1979); J.V. Leveille and T. Weiler, *Nucl. Phys.* **B147**, 147 (1979).

26. M. Glück in *Proceedings of the HERA Workshop*, Hamburg. Oct. 1987 ed. R.D Peccei, vol 1, p.119; M. Glück, R.M. Godbole and E.Reya, *Z. Phys.* **C38**, 441 (1988).

27. R. K. Ellis and Z. Kunszt, *Nucl. Phys.* **B303**, 653 (1988).

28. A. Ali, F. Barreiro, J.F. de Trocóniz, G.A. Schuler and J.J van der Bij, in *Proceedings of the European Committee for Future Accelerators "Large Hadron Collider Workshop"* CERN 90-10, eds. G. Jarlskog and D. Rein, vol.2,p.917.

29. R. K. Ellis and P. Nason, *Nucl. Phys.* **B312**, 551 (1989).

30. J. Smith and W.L. van Neerven *Nucl. Phys.* **B374**, 36 (1992); S. Riemersma, J. Smith and W.L. van Neerven, *Phys. Letts.* **B282**, 171 (1992).

31. E. Laenen, S. Riemersma, J. Smith and W.L. van Neerven, *Phys. Letts.* **B291**; *Nucl. Phys.* **B392**, 162, 229 (1993).

32. P. Nason, S. Dawson and R.K. Ellis, *Nucl. Phys.* **B303**, 607 (1988); **B327**, 49 (1989); (E).**B335**, 260 (1990); S. Frixione *et.al.*, *Phys. Lett.* **B308**, 137 (1993) and CERN-TH.6921/93.

33. T. Appelquist and J. Carrazone, *Phys. Rev.* **D11**, 2856 (1975); *Nucl. Phys.* **B120**, 77 (1977); K. Symanzik, *Comm. Math. Phys.* **34**, 7 (1973).

34. J. Collins, F. Wilczek and A. Zee, *Phys. Rev.* **D18**, 242 (1978); J. Collins and W.K. Tung, *Nucl. Phys.* **B278**, 934 (1986).

35. J. Schwinger, *Particles Sources and Fields*, Vol.2 Addison Wesley, Reading, MA. (1973).

36. J.C. Collins and W.K. Tung, in Ref.[34]; G. Altarelli, M. Diemoz, G Martinelli, and P. Nason, *Nucl. Phys.* **B308**, 724 (1988).

37. G. Marchesini and B.R. Webber, *Nucl. Phys.* **B330**, 261 (1990); R. Meng, G. A. Schuler, J. Smith and W.L. van Neerven, *Nucl. Phys.* **B339**, 325 (1990); D. Kuebel, M. Pundurs, C-P. Yuan, E. Berger and F. Paige, *Phys. Rev.* **D43**, 767 (1991).

38. M.L. Mangano, P. Nason and G. Ridolphi, *Nucl. Phys.* **B373**, 295 (1992); M. L. Mangano and P. Nason, *Phys. Letts.* **B285**, 160 (1992).

39. M.G. Aivazis, F.I. Olness and W.K. Tung, SMU-HEP/92-04; and J.C. Collins, M.G. Aivazis, F.I. Olness and W.K. Tung, SMU-HEP/92-05.

40. S. Catani, M. Ciafaloni and F. Hauptmann, *Phys. Lett.* **B242**, 97 (1990); *Nucl. Phys.* **B366** (1991) 135; CERN-TH.6398/92, to be published in the *Proceedings of the Workshop on Physics at HERA*, Oct. 1991. eds. W. Buchmüller and G. Ingelman.

41. R.K. Ellis and D.A. Ross, *Nucl. Phys.* **B345**, 79 (1990); J.C. Collins and R.K. Ellis, *Nucl. Phys.* **B360**, 3 (1991).

42. E.M. Levin, M.G. Ryskin, Yu.M. Shabelskii, and A.G. Shuvaev, DESY-91-054; E.M. Levin, M.G. Ryskin, and Yu.M. Shabelskii, *Phys. Lett.* **B260** (1991) 429.

43. See contributions by B. Webber and by M. Krawczyk in *Proceedings of DESY Topical Meeting on the Small-x Behavior of Deep Inelastic Structure Functions in QCD*, Hamburg, 1990, Ed. A. Ali and J. Bartels, North Holland, *Nucl. Phys. B* (Proc. Suppl.) **18C** (1990).

44. E. Laenen, J. Smith and W.L. van Neerven, *Nucl. Phys.* **B369**,534 (1992); see also F.A. Berends, W.T. Giele and J.B. Tausk, *Phys. Rev.* **D47**, 2746 (1993).

45. O.J.P. Éboli, M.C. Gonzalez-Garcia, F. Halzen and S.F. Novaes, Phys. Rev. D47, 1889 (1993); M. Drees, M. Krämer, J. Zunft and P.M. Zerwas; *Phys. Letts.* **B306**, 371 (1993). V. Fadin, V. Khoze and T. Sjöstrand, *Z. Phys.* **C48**, 467 (1990).

46. F. Abe *et al.*, (CDF collaboration) *Phys. Rev. Letts.* **64**, 142, 147 (1990); P.K. Sinervo, Invited talk at the *Rencontres de Physique de la Vallee d'Aoste*, La Thuile, March (1990),UTPT-91-13; F. Abe *et al.*, (CDF collaboration) FermiLab-91-352-E; O. Li-Demarteau, Fermilab-Conf-93/223

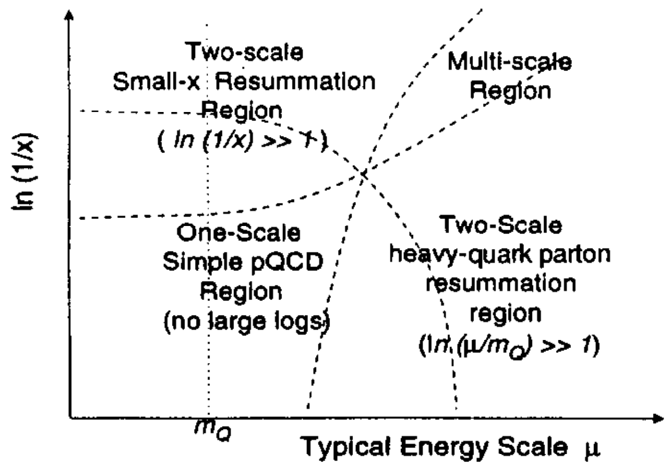

Figure 1: Kinematic map of regions in the (x, μ) plane where various distinct QCD formalisms are required.

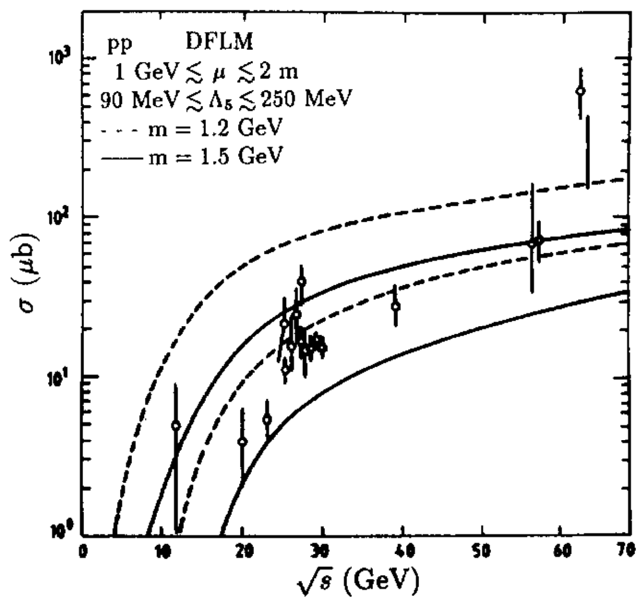

Figure 2: Energy dependence of the total cross-section for Charm Production. Note the theory lines are strongly dependent on the choice of the factorization scale and the charm quark mass.

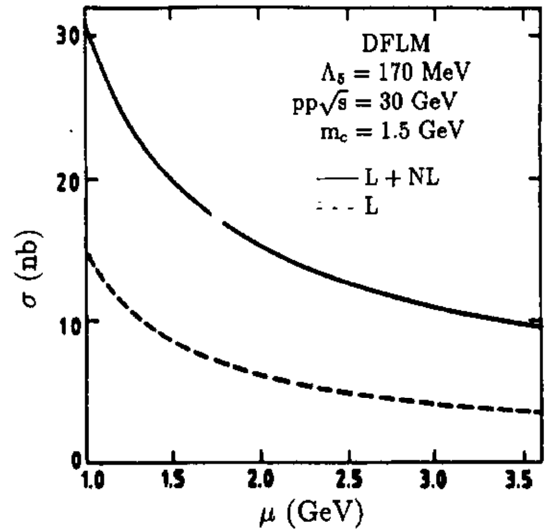

Figure 3: Dependence of Leading and Next-to-leading order fixed order QCD calculations of charm cross-section on the factorization scale. Note that the scale dependence is not reduced in the NLO case.

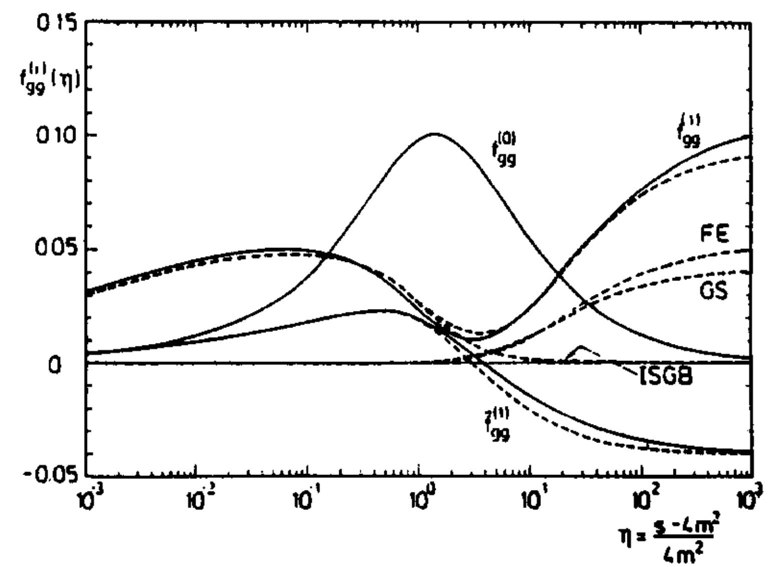

Figure 4: Contributions to the next-to-leading order formula for heavy quark production. The f's are defined in Eq.(9). The text refers to the solid lines. (The dashed lines represent approximations.)

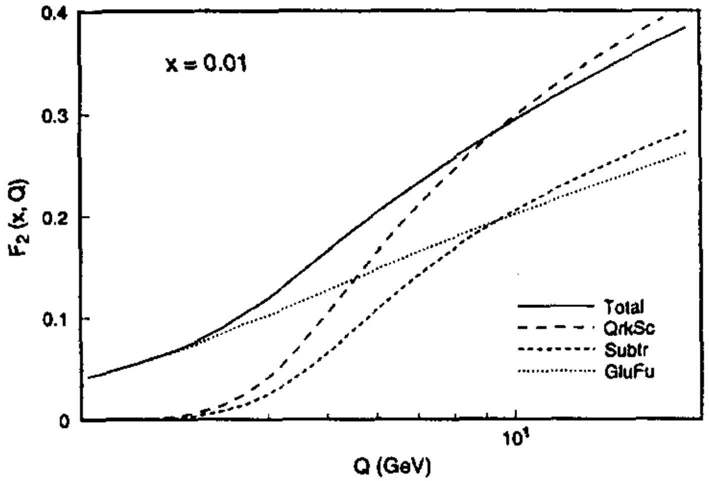

Figure 5: The structure function $F_2(x, Q)$ for neutral current leptoproduction of charm. Shown are the combined QCD prediction (Tot) along with the individual contributions from flavor excitation (QrkSc), flavor creation (Glufu), and the subtraction term (Subtr) which represents the overlap between the first two. Cf. Ref.[39]

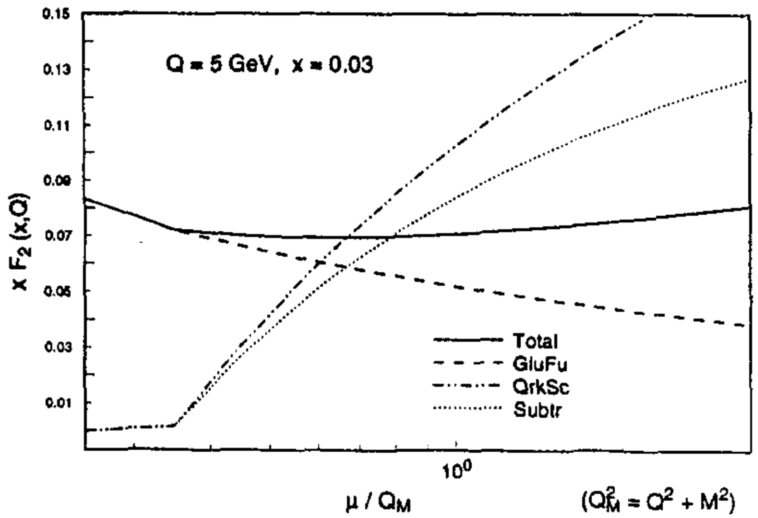

Figure 6: Scale dependence of the various contributions to the generalized QCD scheme. Note that the μ-dependence of the combined result, labelled "Tot", is much reduced from the individual terms.

B DECAYS—MEASUREMENTS AND PREDICTIONS

HITOSHI YAMAMOTO
Harvard University
42 Oxford St., Cambridge, MA 02138, USA

ABSTRACT

Hadronic decays of B mesons are reviewed. First, masses of B mesons and observed patterns together with physics behind them are discussed. Then the effective Hamiltonian responsible for major decays is presented and its practical applications is discussed in the context of factorization. Various tests of factorization are then studied. For rare decays, the focus is placed on $K\pi$, $\pi\pi$ final state and the penguin-mediated $X_s\gamma$. In general, the measurements are in excellent agreement with predictions of the standard model.

1. BASIC METHODS ON UPSILON-4S RESONANCE

Most of the data presented in the following are collected on the upsilon-4S resonance, and some basic experimental techniques are briefly described below.

The B meson pair production cross section on the upsilon-4S resonance is roughly 1 nb; namely, an integrated luminosity of 1 fb^{-1} would generate 1 million B meson pairs. The CLEO-II detector has logged about 1.2 fb^{-1} of data thus generating 1.2 million B meson pairs.

On the upsilon-4S resonance, light quark pairs ($u\bar{u}$, $d\bar{d}$, $s\bar{s}$, and $c\bar{c}$ - often referred to as the 'continuum') are also generated in addition to the B meson pairs. The cross section ratio of B meson pair to the continuum is roughly 1 to 2.5. The continuum is often a major background and in order to understand this component, data are taken right below the resonance (32 MeV below the peak) corresponding to about one half of the integrated luminosity taken on the resonance. When we want to plot a distribution of certain parameter for B meson pairs, we can subtract the distribution for the data taken off-resonance from that taken on-resonance (with a proper normalization). The distribution is then said to be 'continuum subtracted'.

At the upsilon-4S resonance, the B mesons are generated with definite energy and momentum given by

$$E_B = E_{\text{beam}} = 5.289\text{GeV}, \qquad P_B = 0.325\text{GeV/c}. \tag{1}$$

When reconstructing a decay $B \to f_1 + f_2 + \cdots f_n$, natural parameters to look at are thus the total energy and momentum of the decay products f_i $(i = 1, .., n)$:

$$E_{\rm tot} = \sum E_i, \qquad P_{\rm tot} = \sum \vec{P}_i \tag{2}$$

which should peak at $E_{\rm beam}$ and P_B respectively, where E_i and P_i are the energy and momentum of the i-th decay product. In practice, often used parameters are the 'energy difference' ΔE and the 'beam-constrained mass' M_B defined by

$$\Delta E = E_{\rm tot} - E_{\rm beam}, \qquad M_B = \sqrt{E^2_{\rm beam} - P^2_{\rm tot}}\,. \tag{3}$$

Since $E_{\rm beam}$ is a constant, measuring ΔE and M_B is equivalent to measuring $E_{\rm tot}$ and $P_{\rm tot}$. The mass reconstructed this way has a good resolution which varies from 2.5 to 3.3 MeV depending on decay mode and usually dominated by the spread of beam energy. The essence of this method in background rejection, however, is simply the conservation of energy and absolute momentum in a B meson decay. We will often be referring to M_B and ΔE in the rest of this article; the definitions are as defined above.

2. MASSES

2.1 B^- and $\overline{B}^0$

The masses of neutral and charged B mesons can be measured by fully reconstructing the major decay modes. Figure 1 shows the distribution of the beam-constrained mass M_B for B^- and $\overline{B}^0$ mesons after requiring that the energy difference ΔE is within 2.5σ of zero. The decay modes used are $B^- \to D^{*0}\pi^-, D^{*0}\rho-, D^0\pi^-, D^0\rho^-, \psi K^-$ for the charged B meson and $\overline{B}^0 \to D^{*+}\pi^-, D^{*+}\rho^-, D^+\pi^-, D+\rho^-, \psi K^{*0}$ for the neutral B meson. The D^* mesons are detected by the decays $D^{*0} \to D^0\pi^0, D^{*+} \to D^0\pi^+$ and D mesons are detected by $D^0 \to K^-\pi^+, D^+ \to K^-\pi^+\pi^+$. These modes are chosen since they are particularly clean. There are 362 signal events for B^- and 340 signal events for $\overline{B}^0$. With a correction due to initial state radiation of -1.1 ± 0.5 MeV, we obtain $M_{B^0} = 5280.3 \pm 0.2 \pm 2.0$ MeV and $M_{B^-} = 5279.9 \pm 0.2 \pm 2.0$ MeV . The first error is statistical and the second systematic. The systematic error is dominated by the uncertainty in the energy scale of the storage ring which cancels when we take the mass difference: $M_{B^0} - M_{B^-} = 0.44 \pm 0.25 \pm 0.19$ MeV; namely, the masses of B^- and $\overline{B}^0$ are consistent with being identical within several tenth of MeV. The results are summarized in Table 1 together with previous measurements.

It is interesting to compare this result with that for strange and charm mesons. There we have $M_{K^0} - M_{K^-} = 4.024 \pm 0.032$ MeV and $M_{D^+} - M_{D^0} = 4.77 \pm 0.27$ MeV[1] which seem to indicate that the meson mass is heavier when a heavy quark is combined with a d quark than with a u quark. The pattern, however, clearly does not repeat for B mesons. The current understanding for the isospin mass splitting is that there are effects due to the $u - d$ mass difference as well as QED effects[5] (i.e. due to the electric charge difference between u and d quarks). Both are of order a few MeV, and the two kinds of effects happen to cancel for the B meson case.[6] There seems to be no simple and intrinsic reason to give $M^0_B = M^+_B$.

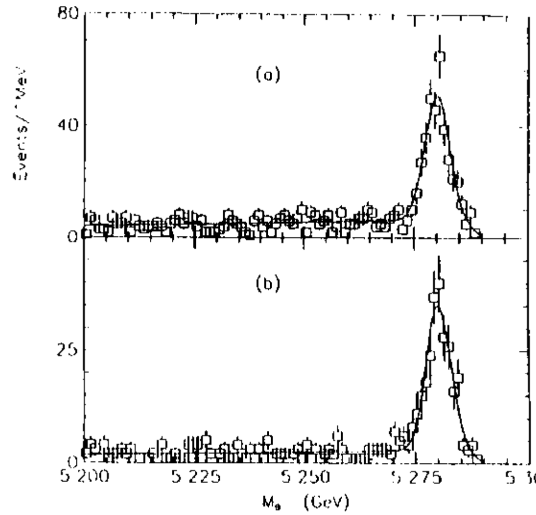

Figure 1. The beam-constrained mass for charged (a) and neutral (b) B mesons after ΔE is required to be consistent with zero. Particularly clean modes are selected and summed.

Table 1. Masses of neutral and charged B mesons.

(MeV)	CLEO 1.5[2]	ARGUS[3]	CLEO II[4]
M_{B^0}	$5278.0 \pm 0.4 \pm 2.0$	$5279.6 \pm 0.7 \pm 2.0$	$5280.3 \pm 0.2 \pm 2.0$
M_{B^-}	$5278.3 \pm 0.4 \pm 2.0$	$5280.5 \pm 1.0 \pm 2.0$	$5279.9 \pm 0.2 \pm 2.0$
$M_{B^0} - M_{B^-}$	$-0.4 \pm 0.6 \pm 0.5$	$-0.9 \pm 1.2 \pm 0.5$	$0.44 \pm 0.25 \pm 0.19$

2.2 Other Bottom Mesons

Bottom hadrons heavier than B^- and $\overline{B}^0$ are not produced on upsilon-4S resonance, and the results so far come from accelerators that operate at higher energies.

Figure 2 shows the decay $B_S \to \psi\phi, \phi \to K^+K^-$ observed by the CDF collaboration[7] in $p\overline{p}$ collisions at 1.8 TeV c.m. energy. There are 14 ± 4.7 events observed and fitting a gaussian to the peak, the B_S mass is determined to be $5383.3 \pm 4.5 \pm 5.0$ MeV. The ALEPH collaboration has also reported a result on B_S mass from two events $B_S \to \psi'\phi$ and $D^+_S\pi^-$. The mass measurement is dominated by the $\phi'\phi$ event and gives $5369 \pm 5.6 \pm 1.5$ MeV. These results are summarized in Table 2 together with a possible candidate event reported earlier by the OPAL collaboration and a recently reported result from DELPHI. The measurements by CDF and ALEPH are marginally consistent (2-sigma difference statistically); taking the weighted average, the mass difference between B_S and B^0 is 97 MeV. The value is strikingly similar to the charm case $M_{D^+_S} - M_{D^+} = 99.5 \pm 0.6$ MeV,[1] and also consistent with predictions of non-relativistic models: $M_{B_S} = 5345 - 5388$ MeV.[11]

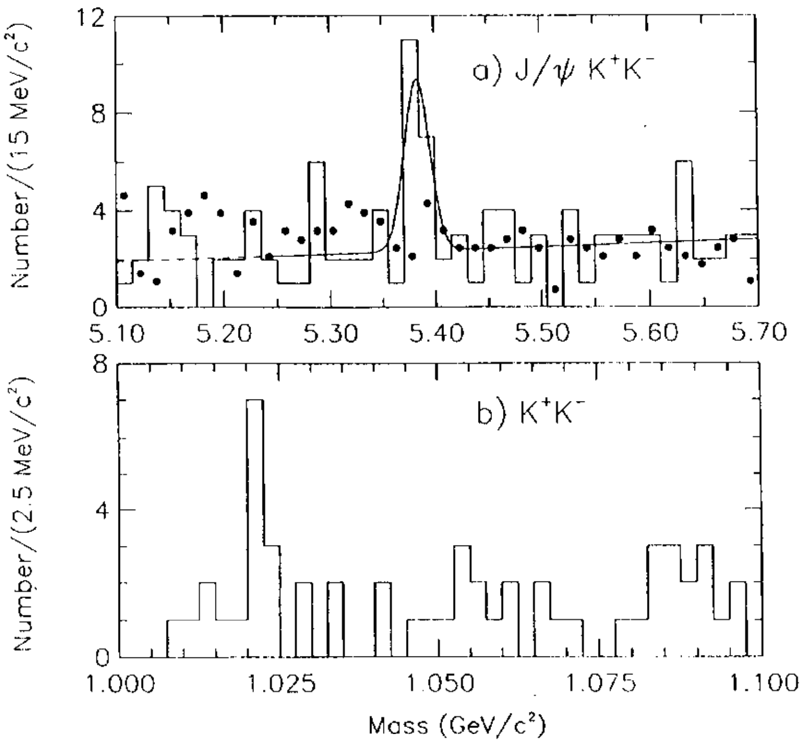

Figure 2. $B_S \to \psi\phi$ decay observed by the CDF collaboration. (a) Invariant mass of ψK^+K^- when the K^+K^- pair forms the ϕ mass (within ± 10 MeV). The dots are for a ϕ mass side band. (b) Invariant mass of K^+K^- when the ϕK^+K^- mass is in the B_S peak (within ± 20 MeV).

Table 2. Measurements of B_S meson mass. The $\psi^{(\prime)}$ and ϕ mesons are detected by $\psi^{(\prime)} \to l^+l^-$ and $\phi \to K^+K^-$ respectively, and D_s^+ mesons are detected in the modes $D_S^+ \to \phi\pi^+, K^*K$.

	Modes	Number of events	M_{B_S} (MeV)
ALEPH[8]	$\psi'\phi, D_S^+\pi^-$	2	$5368.6 \pm 5.6 \pm 1.5$
CDF[7]	$\psi\phi$	14 ± 4.7	$5383 \pm 4.5 \pm 5.0$
OPAL[9]	$\psi\phi$	(1 candidate)	5360 ± 70
DELPHI[10]	$D_S^+(\pi^- \mathrm{or} a_1^-), \psi\phi$	4	$5357 \pm 12 \pm 6$

The mass of $B^*(J^P = 1^-)$ has been measured by CUSP[12] and CLEO[13] by detecting the monochromatic photon in the transition $B^* \to B\gamma$. The numbers are[14]

$$M_{B^*} - M_B = \begin{array}{ll} 46.4 \pm 0.3 \pm 0.8 & \text{MeV (CLEO)} \\ 45.6 \pm 1.0 & \text{MeV (CUSP).} \end{array} \qquad \begin{array}{r}(4)\\(5)\end{array}$$

These measurements are in accordance with an intriguing observation on the hyperfine splitting

$$\Delta M \equiv M^2(1^-) - M^2(0^-) = \text{const} \approx 0.5\text{MeV}^2. \tag{6}$$

This holds well for (π, ρ), K, D, D_S and now for B. In non-relativistic models, such relation is realized when the potential between the constituent quarks is linearly increasing as a function of the distance between the quarks.[11,15] It is consistent with a naive picture that the two constituent quarks are connected by a flux tube with a constant tension. At short distance, the potential is expected to be Coulomb-like; this portion of the potential, however, is not expected to play a significant role.[16] Also, there is an electromagnetic hyperfine splitting which violates the relation 6, but its effect is also much smaller than the hyperfine splitting due to strong interaction.[17]

Apart from the theoretical importance, the above mass difference indicates that B^* cannot decay to $B\pi$. It has a practical implication that one cannot tag the sign of the bottom flavor by the decays such as $B^{*+} \to B^0\pi^+$ where the charge sign of the pion tells us if the neutral B meson is bottom or anti-bottom. Such flavor tagging would have made it easy to study the CP violating decay asymmetry in B^0 or $\overline{B}^0 \to \psi K_S, \pi^+\pi^-$ etc. particularly in hadron colliders. Now we have to hope that there may be a higher resonance that decays to $B\pi$ which is narrow and produced copiously.[18]

3. NON-SUPPRESSED DECAYS

3.1 *Effective Hamiltonian*

The interaction of interest for B meson decays comes from the charged current part of the Standard Model Lagrangian:[19]

$$\mathcal{L}_{CC} = \frac{g}{\sqrt{2}}(u, c, t)_L \gamma_\mu V \begin{pmatrix} d \\ s \\ b \end{pmatrix}_L W^\mu, \tag{7}$$

where g is the weak coupling constant, the subscript L for the quark field indicates left-handed component (e.g. $u_L = \frac{1}{2}(1 - \gamma_5)u$ etc.), and the matrix V is the Cabbibo-Kobayashi-Masukawa (CKM) matrix:

$$V \equiv \begin{pmatrix} V_{ud} & V_{us} & V_{ub} \\ V_{cd} & V_{cs} & V_{cb} \\ V_{td} & V_{ts} & V_{tb} \end{pmatrix} \tag{8}$$

The experimental value of the CKM matrix V is well represented by[20,21] (assuming unitarity of V)

$$V \sim \begin{pmatrix} 1 & \lambda & |V_{ub}|e^{i\alpha} \\ -\lambda & 1 & \lambda^2 \\ |V_{td}|e^{i\beta} & -\lambda^2 & 1 \end{pmatrix} \quad \text{where} \quad \begin{cases} \lambda \sim 0.22 \\ \alpha = \arg(V_{ub}) \\ \beta = \arg(V_{td}) \end{cases} \tag{9}$$

and the magnitude of V_{ub}, V_{td} is of order λ^3. Taking the first and third columns, the unitarity condition

$$V_{ud}^* V_{ub} + V_{cd}^* V_{cb} + V_{td}^* V_{tb} = 0 \tag{10}$$

becomes a triangle as below (called the unitary triangle).

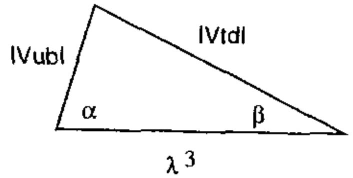

(11)

At energy scales well below the W mass, the propagation of W can be 'integrated out' and we obtain 4-fermion effective Hamiltonian[22] relevant to B decays given by

$$\mathcal{H}_{\text{eff}} = \frac{G_F}{\sqrt{2}} V^*_{ud} V_{cb} (C_1(\mu)\mathbf{O}_1 + C_2(\mu)\mathbf{O}_2) + \cdots \tag{12}$$

$$\mathbf{O}_1 = (\bar{d}u)(\bar{c}b), \qquad \mathbf{O}_2 = (\bar{c}u)(\bar{d}b) \tag{13}$$

where $G_F = g^2/(4\sqrt{2}M_W^2)$ is the Fermi coupling constant and the quark current $(\bar{q}'q)$ is a short hand for $\bar{q}'_\alpha \gamma_\mu (1-\gamma_5) q_\alpha$ which is a color-singlet $V-A$ current (α: color index). Any combination of replacements $c \to u, u \to c$ and $d \to s$ can be made to obtain other possible interactions as long as the replacements are consistently made including the indexes of the CKM matrix elements. The terms shown in (12) are part of an expansion of the effective hamiltonian (the operator product expansion[23]). It has an advantage that the calculable short-distance effects are separated into the coefficients of the operators (Wilson coefficients) while the long distance effects such as the state of valence quarks in mesons are absorbed into matrix elements of the operators.

Without QCD correction, we only have the first operator $\mathbf{O}_1$ which is shown diagramatically in Figure 3(a). With QCD correction, gluons flying between the quark lines can shuffle the color flows and generate an effective neutral current operator $\mathbf{O}_2$ shown in Figure 3(b). The Wilson coefficients $C_{1,2}$ can be calculated using the leading-logarithm approximation (LLA)[24]

$$C_1 = \frac{1}{2}(C_+ + C_-) \qquad C_2 = \frac{1}{2}(C_+ - C_-) \tag{14}$$

with

$$C_\pm = \left[\frac{\alpha_S(\mu^2)}{\alpha_S(M_W^2)}\right]^{\frac{d_\pm}{2b}} \tag{15}$$

where $d_- = -2d_+ = 8$, and α_S is the running coupling constant of strong interaction given by

$$\alpha_S(\mu^2) = \frac{4\pi}{b\log(\mu^2/\Lambda^2_{\text{QCD}})} \qquad \text{with} \quad b = 11 - \frac{2}{3}n_f \tag{16}$$

with n_f being the number of relevant flavors, and μ the typical mass scale of problems in question. Note that C_+ and C_- are related by $C_+^2 C_- = 1$. With $\mu = m_b = 5$ GeV, $n_f = 4$, and $\Lambda_{\text{QCD}} = 0.25$ GeV we have

$$C_1(m_b) = 1.11 \qquad C_2(m_b) = -0.26. \tag{17}$$

The next-to-leading logarithm approximation (NLLA) has been computed;[25] the result does not differ drastically from the LLA result quoted above. For the transition $b \to cs\bar{c}$, however, the momentum transfer associated with the light quarks are much smaller than the bottom mass scale and as a result the corresponding coefficients could be significantly different from (17). In fact, in one estimation using heavy quark effective theory (HQET),[31] the coefficients are about 30% larger for C_1 and almost twice as large for C_2:[32]

$$C_1 \sim 1.45 \qquad C_2 \sim -0.45 \qquad (\text{for } b \to cs\bar{c}). \tag{18}$$

There are also 4-fermion operators of the type shown in Figure 3(c) called Penguin operators.[26] The corresponding coefficients, however, are small and the Penguin operators are relevant only for highly suppressed decays such as $B \to K^*\gamma$ and $K\pi$, to which we will come back later.

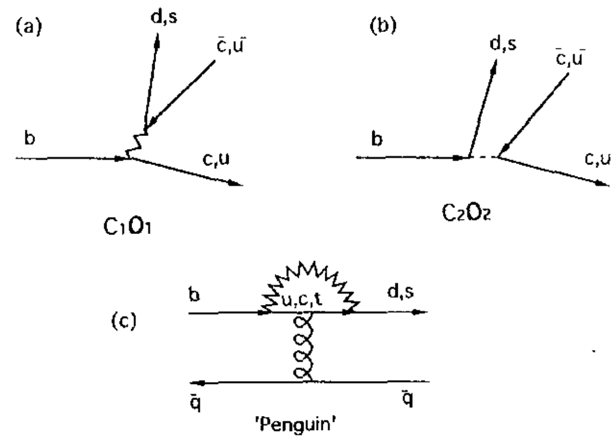

Figure 3. Four fermion operators of the effective Hamiltonian responsible for B meson decays.

3.2 *Two-body Decays and Factorization*

Compared to semileptonic decays, hadronic decays are harder to understand due to variety of short and long-distance strong interactions among the quarks involved. Two-body hadronic decays, however, are the simplest kind, and some framework of understanding - factorization - exists.[27] Also, it should be noted that two-body decays account for a substantial fraction of total hadronic decays of heavy mesons ($\sim$ 15% for bottom mesons and $\sim$ 75% for charm mesons when resonances are included[28]).

The idea of factorization for hadronic weak decay dates back at least to the early 60's when Schwinger showed that the $\Delta I = 3/2$ transition of $K \to \pi\pi$ can be estimated from the corresponding semileptonic rate.[29] The procedure, however, was not considered to be accurate; in fact, when Feynman reported calculations of $\Lambda \to p\pi$ and $K^+ \to \pi^+\pi^0$ using the idea of factorization,[30] he preceded the discussion by the following disclaimer: 'You may not wish to consider this line of flimsy reasoning; we are becoming very uncertain about this matter, nevertheless I shall present it.' There is, however, a good reason to believe that the factorization works well for certain B decays.

We take $\overline{B}^0 \to D^+\pi^-$ as an example. This can occur by the operator $\mathbf{O}_1$ as shown in Figure 4(a), where it is assumed that the $B \to D$ transition is caused by the current operator $(\bar{c}b)$ and that π^- is created by the current operator $(\bar{d}u)$. Assuming that the $B \to D$ transition and the π^- creation are independent, the amplitude can be written as

$$\langle D^+\pi^-|(\bar{d}u)(\bar{c}b)|\overline{B}^0\rangle = \langle \pi^-|(\bar{d}u)|0\rangle\langle D^+|(\bar{c}b)|\overline{B}^0\rangle \qquad (19)$$

which constitutes the essence of the factorization assumption.

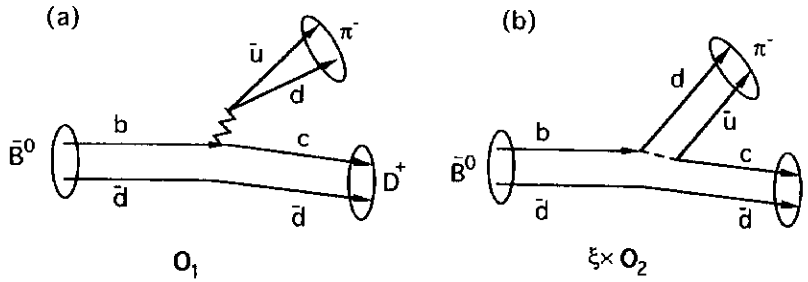

Figure 4. Decay $\overline{B}^0 \to D^+\pi^-$ by the operator $\mathbf{O}_1$ (a) and $\mathbf{O}_2$ (b). The latter is suppressed by a factor ξ.

It is instructive to visualize the situation intuitively. A B meson may be viewed as an analog of a hydrogen atom where the heavy bottom quark is at the center surrounded by a cloud made of light quark and gluon [Figure 5(a)]. Upon the decay of the b quark, the b quark disappears and c, $\bar{u}$, and d quarks appear. The c quark will combine with the original cloud that was around the b quark to form a D meson, and the $\bar{u}d$ pair will eventually turn into a pion. Here one can cast doubts on the factorization assumption on two points:

1. When the $\bar{u}d$ pair passes through the cloud, it may strongly interact with the cloud, in which case the formation of the D meson and the creation of the pion cannot be independent.
2. After the D meson and the pion are formed, they may re-scatter through final-state interaction (FSI); e.g. $D^+ + \pi^- \to D^0 + \pi^0$ etc.

For each of the above, Bjorken has argued that it does not pose serious problem for the factorization assumption.[33] First, the invariant mass of the $\bar{u}d$ pair is of order pion mass; thus, they are highly collinear and close together. Since the total color of the pair is zero, they form a small color dipole and the cloud cannot see them from some distance away. The pair is thus expected to pass through the cloud without much interaction. Second, the formation time of the pion in its own rest frame is of order 0.3 fm/c which is the time for light to propagate from the center of the pion to the edge. Since the pion is highly energetic ($\sim$ 2.5 GeV), by the time it is formed the distance between the D meson and the pion is already several fermis; thus, they cannot interact through FSI. A similar argument of 'color transparency' was also used for production of ρ and ψ in high energy scatterings.[34]

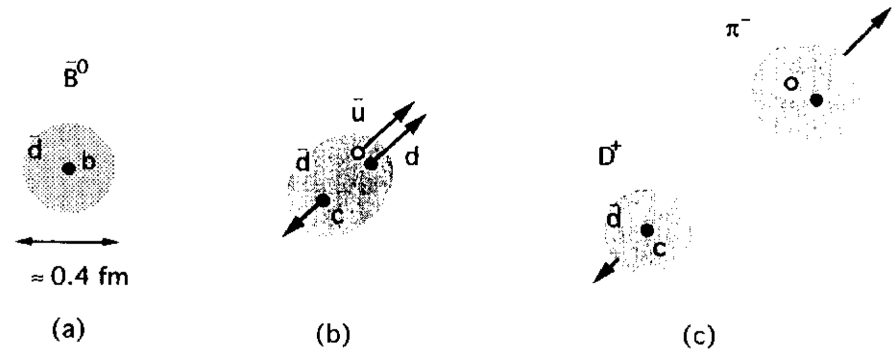

Figure 5. An intuitive picture of the decay $\overline{B}^0 \to D^+\pi^-$. Before the decay (a), immediately after the b quark decay (b), and right after the formation of final state mesons (c).

This line of argument has been put forward by Dugan and Grinstein in the framework of QCD and the heavy quark effective theory, and it has been shown that factorization holds in the limit of $M_{B,D} \to \infty$ while M_B/M_D is kept constant.[35] For decays which involve two charmed mesons such as $\overline{B}^0 \to D_S^- D^+$, the two mesons in the final state are partially overlapped at the formation time, and thus the factorization may not work well for these decays. Factorization is known to hold also for the large N_C limit where N_C is the number of colors.[36] Even though the correction to the limit is of order 1/3 which is quite large, the applicability of the $1/N_C$ argument is not restricted to the large velocity limit,[37] and thus complementary to the 'color transparency' argument.

The decay $\overline{B}^0 \to D^+\pi^-$ can also proceed by the operator $\mathbf{O}_2$ as shown in Figure 4(b). In this case, naively only the color singlet component of the $\bar{u}$ and d legs is expected to contribute. Applying Fierz transformations to color indexes as well as to gamma matrices,[38] $\mathbf{O}_2$ can be written as

$$\mathbf{O}_2 = \frac{1}{3}\mathbf{O}_1 + \frac{1}{2}(\bar{d}\lambda^i u)(\bar{c}\lambda_i b) \qquad (20)$$

where the second term is a color singlet operator formed by two color-octet currents with λ^i being the $SU(3)$ Gell-Mann matrices. Thus, $\mathbf{O}_2$ contains $\mathbf{O}_1$ within itself, and consequently $\mathbf{O}_1$ and $\mathbf{O}_2$ are *not* orthogonal.[37] The overall coefficient of $\mathbf{O}_1$ is then $C_1 + C_2/3$. For the decay $\overline{B}^0 \to D^0\pi^0$, the relevant operator is $\mathbf{O}_2$. There, the role of $\mathbf{O}_1$ and $\mathbf{O}_2$ are inverted with the overall coefficient of $\mathbf{O}_2$ being $C_2 + C_1/3$. In fact, we can write (12) in two ways

$$\begin{aligned} C_1\mathbf{O}_1 + C_2\mathbf{O}_2 &= (C_1 + \tfrac{C_2}{3})\mathbf{O}_1 + \tfrac{1}{2}(\bar{d}\lambda^i u)(\bar{c}\lambda_i b) \\ &= (C_2 + \tfrac{C_1}{3})\mathbf{O}_2 + \tfrac{1}{2}(\bar{d}\lambda^i b)(\bar{c}\lambda_i u). \end{aligned} \qquad (21)$$

Assuming factorization, the effective Hamiltonian may then be written in terms of 'factorized hadron operators'[39] as

$$\mathcal{H}_{\rm had} = \frac{G_F}{\sqrt{2}} V_{ud}^* V_{cb} [a_1(\bar{d}u)_{\rm had}(\bar{c}b)_{\rm had} + a_2(\bar{d}b)_{\rm had}(\bar{c}u)_{\rm had}] \qquad (22)$$

where the above arguments suggest

$$\begin{aligned} a_1 &= C_1 + \xi C_2 \\ a_2 &= C_2 + \xi C_1 \end{aligned} \qquad \text{with} \quad \xi = \frac{1}{3}, \qquad (23)$$

where the effect of $\mathbf{O}_2$ to the first term and that of $\mathbf{O}_1$ to the second term is parametrized by ξ (sometimes called 'color suppression factor'). The contribution of the octet current term in (20), however, may have a significant effect; in fact, an estimation using QCD sum rule indicates that its contribution may in effect lead to $\xi \sim 0$.[40] Also, an analysis of charm decays suggests ξ near zero.[28] It has thus been suggested that a_1, a_2 be taken as free parameters.[28]

Given the factorized Hamiltonian (22), one can then write down the amplitude for a decay. For example, if X^- is a meson made of valence quarks d and $\bar{u}$,

$$Amp(\overline{B}^0 \to D^+X^-) = \frac{G_F}{\sqrt{2}} V_{ud}^* V_{cb} a_1 \langle X^- | (\bar{u}d)^\mu_{\mathrm{had}} | 0 \rangle \langle D^+ | (\bar{c}b)_{\mathrm{had}\mu} | \overline{B}^0 \rangle \tag{24}$$

where we have from Lorentz invariance

$$\langle X^- | (\bar{u}d)^\mu_{\mathrm{had}} | 0 \rangle = -i f_X p^\mu \quad \text{(for } X\text{: pseudo scalar)} \tag{25}$$

$$\langle X^- | (\bar{u}d)^\mu_{\mathrm{had}} | 0 \rangle = f_X m_X \epsilon^\mu \quad \text{(for } X\text{: vector or axial vector)} \tag{26}$$

with f_X being a parameter of energy dimension (called the decay constant). The current matrix element is the same as that appearing in the corresponding semileptonic decay[41] evaluated at $q^2 = m_\pi^2$:

$$\langle D^+ | (\bar{c}b)_{\mathrm{had}\mu} | \overline{B}^0 \rangle = \left(P_B + P_D - \frac{m_B^2 - m_D^2}{q^2} q \right)_\mu F_1(q^2) + \frac{m_B^2 - m_D^2}{q^2} q_\mu F_0(q^2) \tag{27}$$

where F_0 and F_1 are longitudinal and transverse form factors respectively [one can easily verify that the coefficient of F_1 satisfies $(...)_\mu q^\mu = 0$]. For the case of pion emission, the transverse component exactly vanishes (by definition) and we have

$$Amp(\overline{B}^0 \to D^+\pi^-) = -i \frac{G_F}{\sqrt{2}} V_{ud}^* V_{cb} a_1 f_\pi (m_B^2 - m_D^2) F_0(m_\pi^2). \tag{28}$$

The form factors $F_{0,1}$ may be either obtained from semileptonic decays or calculated by models such as the relativistic harmonic oscillator model together with the pole dominance.[41] They are relatively slowly varying functions of order 1. In addition, the heavy quark effective theory allows us to relate all form factors for transitions between heavy mesons to a universal form factor.[42] Similar procedures are applied to other decay modes.

In general, we may distinguish three classes of decays when we consider two-body decays of heavy mesons mediated by operators of the types $\mathbf{O}_{1,2}$ in spectator mode (i.e. the light quark in the parent meson does not participate in the weak decay):[43]

Class 1 Only the first term in (22) contributes and the amplitude is proportional to a_1; e.g. $\overline{B}^0 \to D^+\pi^-$.

Class 2 Only the second term in (22) contributes and the amplitude is proportional to a_2; e.g. $\overline{B}^0 \to D^0\pi^0$. Sometimes called 'color-suppressed' decays.

Class 3 Both terms in (22) contribute and the amplitude contains both a_1 and a_2; e.g. $B^- \to D^0\pi^-$.

Some comments are in order. If both final-state particles are charged, then it is Class 1, if both are neutral, then it is Class 2, if one is neutral and the other is charged, then it depends. In $\overline{B}^0 \to D^+\pi^-$, the current $B \to D$ emits a π and thus the pion decay constant f_π is involved. In $\overline{B}^0 \to D^0\pi^0$, the current $B \to \pi$ emits a D meson and thus the D meson decay constant f_D is involved. In $B^- \to D^0\pi^-$, a class 1 amplitude and a class 2 amplitude interfere and thus both f_π and f_D are involved. Also, note that in $\overline{B}^0 \to D^0\pi^0$, the 'color transparency' argument does not apply since the color-singlet pair passing through the cloud is now $c\bar{u}$ pair which are moving quite slowly, and it may form a D meson before leaving the cloud. Thus, factorization may not be a good assumption in this case.

Heavy mesons may also decay through valence quark annihilation or W-exchange processes[44] as shown in Figure 6 which are also mediated by interactions of types $\mathbf{O}_{1,2}$. Such processes have been discussed in the context of the lifetime difference between D^+ and D^0, but thought to be helicity-suppressed,[45] and also suppressed by form factor effect when two-body decays are considered.[46] It was suggested, however, that the helicity suppression may be lifted when soft gluon effects are taken into account.[47] Even though annihilation/exchange processes are usually ignored in B decays, it has not been proven that they do not significantly contribute in all types of decays.

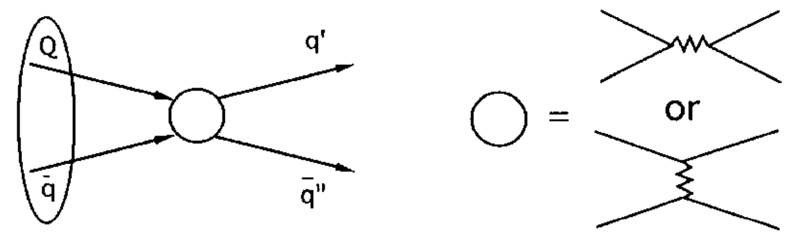

Figure 6. The annihilation and W-exchange processes.

3.3 *Experimental Test of Factorization*

The decays $B \to PP, PV$ have definite final spin state, where P is a pseudo scalar meson and V a vector meson, thus the decay rate is the only dynamical parameter that can be tested. On the other hand, the decays $B \to VV$ has three possible helicity amplitudes which can also be compared against prediction of factorization.

For the test of decay rates, we take $\overline{B}^0 \to D^{*+}X^-$ with X^- being π^-, ρ^-, or a_1^-. As described above, factorization allows us to estimate the decay rates of these modes from the q^2-dependent form factors of the corresponding semileptonic decay $\overline{B}^0 \to D^{*+}l^-\nu$. In other words, there is a simple relation between the differential decay rate of the semileptonic mode at $q^2 = m_X^2$ and the corresponding non-leptonic decay rate, which can be conveniently written as[33]

$$R \stackrel{\mathrm{def}}{\equiv} \frac{Br(\overline{B}^0 \to D^{*+}X^-)}{\frac{dBr}{dq^2}(\overline{B}^0 \to D^{*+}l^-\nu)\Big|_{q^2=m_X^2}} = 6\pi^2 f_X^2 |V_{ud}|^2 \tag{29}$$

where f_X is the decay constant of the meson X. No QCD correction is included in the expression on the right hand side.[49] If QCD correction is to be included, a reasonable choice would be to add $(C_1 + C_2/3)^2$ to the right hand side of (29). This is because, in (21), the contribution from the octet current has been shown to be suppressed in the decays in question as shown by Dugan and Grinstein.[35] However, $C_1 + C_2/3$ is unity to the first order due to the relation $C_+^2 C_1 = 1$; thus, we will proceed without QCD correction. The above formula is applicable for X being any spin-1 particle or any light spin-0 particle (assuming factorization, of course).[48] When the particle X is spin-0, it cannot replace all the helicity degrees of freedom of the D^* appearing in the semileptonic decay, and the formula is correct only in the limit of $m_X \ll m_B$. The correction for pion, however, is negligible ($\sim 0.5\%$). If X is spin-1, then no such restriction applies. If D^* is replaced by D, then a similar helicity projection factor should be included.

The procedure of the test is to measure the decay rate $B \to D^*X$ and the differential semileptonic rate $d\Gamma/dq^2$ to obtain the ratio R, and then compare it to the value expected from factorization: $6\pi^2 f_X^2 |V_{ub}|^2$. The q^2 distribution of the semileptonic decay $\overline{B} \to D^{*+} l^- \nu$ is shown in Figure 7, which is a combination of ARGUS[50] and CLEO[51] data. The shape is fit to three different models[41,52,53] to obtain the value at given q^2.

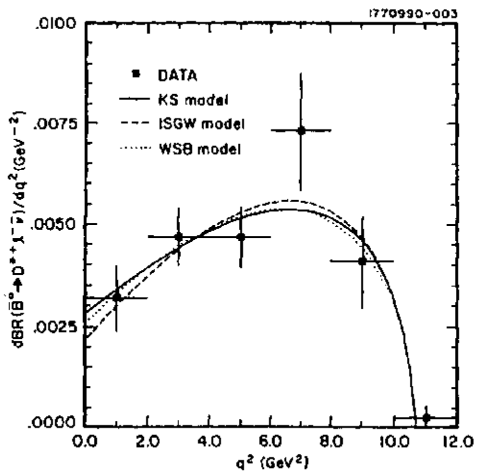

Figure 7. The distribution of the lepton-neutrino invariant mass (q^2) for the process $\overline{B} \to D^{*+} l^- \nu$ as measured by CLEO and ARGUS.

The decay constants can be obtained by the leptonic decay rate[54]

$$\Gamma(\pi^- \to \mu^- \overline{\nu}_\mu) = \frac{G_F^2 f_\pi^2}{8\pi} m_\pi m_\mu^2 \left(1 - \frac{m_\mu^2}{m_\pi^2}\right)^2 , \tag{30}$$

for pion which gives $f_\pi = 132$ MeV. From the tau decay rates

$$\Gamma(\tau^- \to V^- \overline{\nu}_\tau) = \frac{m_\tau^3}{16\pi} G_F^2 |V_{ud}|^2 f_V^2 \left(1 - \frac{m_V^2}{m_\tau^2}\right)^2 \left(1 + 2\frac{m_V^2}{m_\tau^2}\right) . \tag{31}$$

where V is a vector or axial vector, we get $f_\rho = 197 \pm 3$ MeV and $f_{a_1} = 178 \pm 28$ MeV. Including the effect of decay width of meson,[56] these go up to $f_\rho = 210 \pm 3$ MeV and $f_{a_1} = 201 \pm 32$ MeV. Using the isospin symmetry relation $f_{\rho^-} = f_{\rho^0}$, the decay constant of ρ can also be obtained from $\Gamma(\rho^0 \to e^+e^-)$ measured in $e^+e^- \to \rho^0$ by

$$\Gamma(V^0 \to e^+e^-) = \frac{4\pi\alpha^2}{3m_V} c_V f_V^2 \tag{32}$$

where $c_V = 1/2$ for ρ;[55] this gives $f_\rho = 216 \pm 5$ MeV which we will use.

Table 3 summarizes the result of the comparison. Note that in taking the ratio (29), uncertainty in D^* detection efficiency is canceled. This of course assumes that same D^* and D branching ratios are used for the measurements of $D^* l\nu$ mode and D^*X mode; a correction has been made to the values of Figure 7 using the new measurements from CLEO.[57,58] The agreement is quite good for π and ρ. For a_1, the measured R is about a factor of two larger than the expected value, but statistically it is only 1.5 sigma's. This could well be due to breakdown of factorization at a_1 mass of 1.26 GeV. The branching ratio of D^*a_1 is determined assuming that the $D^{*+}\pi^+\pi^-\pi^-$ final state with $1.0 < M_{3\pi} < 1.6$ GeV is dominated by a_1. Figure 8 shows the 3π invariant mass distribution for the decay mode $\overline{B}^0 \to D^{*+}\pi^+\pi^-\pi^-$. The a_1 peak is clearly seen, and amount of non a_1 contribution is quite small.

Table 3. Test of factorization. Branching fraction of $B \to D^*X$ is compared to the corresponding semileptonic decay evaluated at $q^2 = m_X^2$.

X	$Br(D^{*+}X^-)$ (%)$^{(a)}$	dBr/dq^2 (%/GeV²)	R(measured) (GeV²)	f_X (GeV)	$R = 6\pi^2 \lvert V_{ud}\rvert^2 f_X^2$ (GeV²)
π	0.265±0.036	0.23±0.05	1.15±0.30	0.132±0.0005	0.98±0.01
ρ	0.735±0.106	0.25±0.04	2.94±0.63	0.216±0.005	2.63±0.12
a_1	1.32 ±0.30$^{(b)}$	0.32±0.04	4.13±1.07	0.201±0.032	2.27±0.72

(a) The errors are statistical only.
(b) It is assumed that $D^{*+}a_1^-$ dominates $D^{*+}\pi^+\pi^-\pi^-$ mode where the 3π mass is between 1.0 and 1.6 GeV.

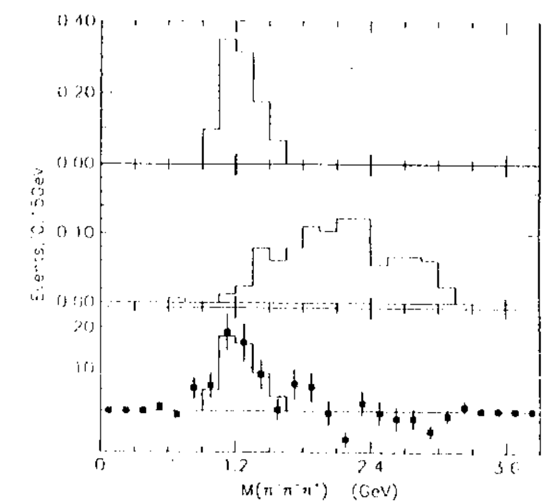

Figure 8. The 3π mass distribution in the decay $\overline{B}^0 \to D^{*+}\pi^+\pi^-\pi^-$. (a) Monte Carlo simulation for $\overline{B}^0 \to D^{*+}a_1^-, a_1^- \to \rho^0\pi^-$. (a) Monte Carlo simulation where $\rho^0\pi^-$ is uniform in phase space. (c) Data with B-mass side bands subtracted.

As stated earlier, for $B \to VV$ decays there are helicity degrees of freedom which cannot be uniquely determined by kinematics. The factorization assumption leads to specific prediction for helicity amplitudes which can then be tested experimentally. For example, once the matrix element is factorized as

$$Amp(B \to D^*\rho) \propto \langle\rho|(\overline{u}d)^{\mu}_{\rm had}|0\rangle\langle D^*|(\overline{c}b)_{{\rm had}_\mu}|\overline{B}\rangle, \tag{33}$$

then by Lorentz invariance the rho production part $\langle\rho|(\overline{u}d)^{\mu}_{\rm had}|0\rangle$ is proportional to the ρ polarization vector ϵ^μ [see (26)]. It then acts the same way as the polarization vector of W in semileptonic decay resulting in the same ρ polarization as that of the W in semileptonic decay at $q^2 = m_\rho^2$. If factorization is not valid, this argument cannot hold, and thus it serves as a good check of factorization.

The polarization of ρ can be measured by the distribution of $\rho^- \to \pi^0\pi^-$ polar decay angle θ_ρ in the ρ rest frame with respect to the D^* direction in the same frame. Longitudinal polarization (helicity = 0) would have $\cos^2\theta_\rho$ distribution while transverse polarization (helicity = ±1) would have $\sin^2\theta_\rho$ distribution. Or equivalently, one can measure the decay angle of D^* (θ_D) in the same way since the helicity of D^* is the same as that of ρ. In fact, the angular distribution can be written as

$$\frac{d\Gamma}{d\cos\theta_\rho d\cos\theta_D} \propto \frac{1-a_L}{4}\sin^2\theta_\rho\sin^2\theta_D + a_L\cos^2\theta_\rho\cos^2\theta_D \tag{34}$$

where a_L is the fraction of longitudinal polarization

$$a_L = \frac{|H_0|^2}{|H_+|^2 + |H_0|^2 + |H_-|^2} \tag{35}$$

with $H_{+,0,-}$ being the three helicity amplitudes. Figure 9 shows the distributions of θ_ρ and θ_D for data. A simultaneous fit to the two angles gives

$$a_L = 0.93 \pm 0.05 \pm 0.05 \qquad \text{(CLEO)} \tag{36}$$

where the first error is statistical and the second systematic which includes uncertainty in background subtraction and detection efficiencies. The experimental measurement of the polarization in the semileptonic decay is unfortunately not available at this point, and we have to compare the above measurement to absolute theoretical prediction which requires some assumption on form factors. One estimate using HQET[48] gives

$$a_L = 0.88 \qquad \text{(factorization + HQET)} \tag{37}$$

which is in agreement with the data.

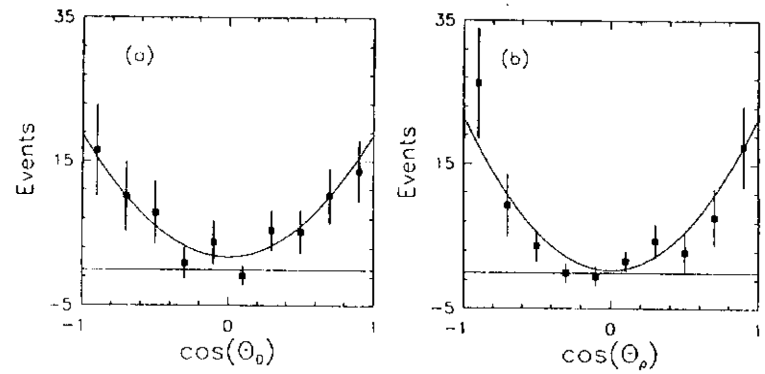

Figure 9. The angular distributions for ρ decay angle (a) and the D^* decay angle (b) in $\overline{B}^0 \to D^{*+}\rho^-$.

This helicity = 0 dominance can be intuitively understood as follows (see the figure below). When the $\overline{u}d$ pair is emitted, they are nearly collinear, and the helicities are left-handed for the d quark and right-handed for the $\overline{u}$ quark. Therefore the total helicity is zero which is transferred to the final ρ meson assuming that there is no final state interaction that changes the spin state. This feature is independent of specific choice of form factors, while it does assume factorization.

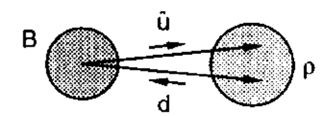

3.4 *Extraction of a_1 and a_2*

In this section, we will take the coefficients a_1 and a_2 as free parameters in the factorized effective Hamiltonian (22), and try to find their values by fitting to measured branching ratios. First, we will use $B \to D\pi$ and ψK decays to demonstrate the procedure, then a global fit to clean modes will be performed.

In order to extract a_1 and a_2, we need the form factors of $B \to D$ transition. This is quite well known; we will use the result of the fit to the universal form factor under the framework of HQET. The relevant value here is $F_0(q^2 = m_\pi^2) = 0.58$. For the $B \to \pi$ or K transition, there is no experimental data, and a model calculation is used where the overlap of B and the light meson wave functions is obtained by relativistic harmonic oscillator model and the q^2 dependence is given by pole dominance. The coefficients of $a_{1,2}$ below are taken from Reference 27.

Class-I (determination of a_1): The decay amplitude of $\overline{B}^0 \to D^+\pi^-$ (or for any two-body decay $B \to PP$) is given by

$$\Gamma = \frac{p}{8\pi M_B^2}|Amp|^2 \tag{38}$$

where p is the momentum in the B rest frame. Using the factorized amplitude (28) together with $V_{cb} = 0.045$, $V_{ud} = 0.975$, $G_F = 1.166\times10^{-5}$ (GeV^{-2}), $F_0(m_\pi^2) = 0.58$, and $\tau_B = 1.18$ ps, we get

$$Br(D^+\pi^-) = 0.264a_1^2 \quad (\%). \tag{39}$$

The measured branching ratio is $Br(D^+\pi^-) = 0.29 \pm 0.04\%$ from CLEO, where the error is statistical only. It then gives $a_1 = 1.1$.

Class-II (determination of a_2): In $\overline{B}^0 \to D^0\pi^0$, D meson is emitted and the transition is from B to π. Proceeding the same way as before, we get

$$Br(D^0\pi^0) = 0.201 \left(\frac{f_D(\mathrm{GeV})}{0.22}\right)^2 a_2^2 \quad (\%) \tag{40}$$

where the isospin factor 1/2 is included (π^0 is half $\overline{u}u$ and half $\overline{d}d$). Experimentally, only upper limit exists for this mode: a recent number from CLEO is $Br(D^0\pi^0) < 0.035\%(90\%C.L.)$, which corresponds to $|a_2| < 0.4$.

The decay $B^- \to \psi K^-$ is also a Cabbibo-favored Class-II decay. The transition is $B \to K$ and ψ is emitted. The decay constant of ψ can be obtained from its e^+e^- width: $f_\psi = 384 \pm 14MeV$. The expected branching ratio is

$$Br(\psi K^-) = 1.819a_2^2 \quad (\%) \tag{41}$$

where the large coefficient is primarily due to the large decay constant of ψ. The measurement $Br(\psi K^-) = 0.110 \pm 0.015$ (CLEO) gives $|a_2| = 0.26$. One point of caution is that a_2 in $b \to c\overline{c}s$ transition is likely to be different from a_2 in $b \to c\overline{u}d$ transition. In fact, the values of $C_{1,2}$ themselves are expected to be different as seen in (18). Nonetheless, they are often assumed to be the same and we will proceed with this assumption for now.

Class-III (determination of a_2/a_2): As stated earlier, for Class-II and Class-III decays, the factorization assumption is not well founded. However, if we assume the factorized Hamiltonian (22), we can obtain the sign as well as the absolute value of a_2/a_1 through the interference of the two types of diagrams shown in Figure 4. For example, the branching fraction of $B^- \to D^0\pi^-$ (normalized to $\overline{B}^0 \to D^+\pi^-$) is given by

$$\frac{Br(D^0\pi^-)}{Br(D^+\pi^-)} = \left[1 + 1.230\frac{a_2}{a_1}\left(\frac{f_D(MeV)}{220}\right)\right]^2. \tag{42}$$

The ratio measured by CLEO is $1.84 \pm 0.24 \pm 0.29$, and this leads to $a_2/a_1 = 0.29 \pm 0.11$. The positive sign is a direct consequence of $Br(D^0\pi^-) > Br(D^+\pi^-)$.

Tables 4 to 6 summarize measurements and expected branching ratios from the factorization model as calculated in Reference 27. The agreements are excellent in all cases.

In order to obtain more accurate value for a_1 we fit four Class-I modes, $\overline{B}^0 \to D^+\pi^-, D^+\rho^-, D^{*+}\pi^-$, and $D^{*+}\rho^-$. For a_2, we use the Class-II modes $\overline{B}^0 \to \psi K^0, \psi K^{*0}$ and $B^- \to \psi K^-, \psi K^{*-}$. The result is

$$|a_1| = 1.15 \pm 0.04 \pm 0.04 \pm 0.09, \qquad |a_2| = 0.26 \pm 0.01 \pm 0.01 \pm 0.02 \tag{43}$$

where the first error is statistical, the second and the third are systematic. The third error is due to the uncertainty in the ratio of production and that of lifetimes of charged vs neutral B mesons. The relevant quantity is $(f_+\tau_+)/(f_-\tau_-)$ where f_+, f_- are the production fractions and τ_+, τ_- are the lifetimes. This value is sometimes assumed to be unity. A measurement from $Br(B^- \to D^{*0}l\nu)/Br(\overline{B}^0 \to D^{*+}l\nu$[61] is

$$\frac{f_+\tau_+}{f_-\tau_-} = 1.2 \pm 0.20 \pm 0.10 \pm 0.16. \quad \text{(CLEO)}. \tag{44}$$

For determination of a_2/a_1, we use the following four ratios of branching fractions: $B(D^0\pi^-)/B(D^+\pi^-)$, $B(D^0\rho^-)/B(D^+\rho^-)$, $B(D^{*0}\pi^-)/B(D^{*+}\pi^-)$, and $B(D^{*0}\rho^-)/B(D^{*+}\rho^-)$ to obtain

$$\frac{a_2}{a_1} = 0.23 \pm 0.04 \pm 0.03 \pm 0.10 \tag{45}$$

where $(f_+\tau_+)/(f_-\tau_-) = 1.2$ is used and the last error is due to the uncertainty in this quantity. The absolute value of a_2/a_1 is consistent with the value obtained above which is $0.26/1.15 = 0.23$, and the negative sign seems to be excluded. From (23), we have

$$\frac{a_2}{a_1} = \frac{C_1 + \xi C_2}{C_2 + \xi C_1} \quad \to \quad \xi = \frac{a_2/a_1 - C_2/C_1}{1 - (C_2/C_1)(a_2/a_1)}. \tag{46}$$

Using $C_1 = 1.11$, $C_2 = -0.26$, the negative value $a_2/a_1 = -0.23$ corresponds to $\xi = 0.01$ and the positive value $a_2/a_1 = 0.23$ corresponds to $\xi = 0.44$. Thus, $\xi = 0$ as suggested by an analysis of charm decays[28] seems to be excluded in the B decays. However, one has to keep in mind that in the analysis above, the factorization was applied to questionable cases where emitted meson is heavy. Also, the factorization is not expected to hold well for charm decays, so the formulation using $a_{1,2}$ itself is in question in charm decays.

So far only Class-II modes observed are for $b \to c\overline{c}s$ only. As one can see from the table, however, the present sensitivity is close to the expected values for the $D^0\pi^0$ and related modes. It is likely that these modes will be observed soon.

Table 4. Class-I branching ratios.

$\overline{B}^0$	CLEO (%)	ARGUS (%)	Model (%)[27]	$a_1 = 1.15$
$D^+\pi^-$	$0.29 \pm 0.04 \pm 0.03 \pm 0.05^a$	$0.48 \pm 0.11 \pm 0.11^d$	$0.264a_1^2$	0.35
$D^+\rho^-$	$0.81 \pm 0.11 \pm 0.12 \pm 0.13^a$	$0.9 \pm 0.5 \pm 0.3^d$	$0.621a_1^2$	0.82
$D^{*+}\pi^-$	$0.26 \pm 0.03 \pm 0.03 \pm 0.01^a$	$0.28 \pm 0.09 \pm 0.06^d$	$0.254a_1^2$	0.34
$D^{*+}\rho^-$	$0.74 \pm 0.10 \pm 0.13 \pm 0.03^a$	$0.7 \pm 0.3 \pm 0.3^d$	$0.702a_1^2$	0.93
$D^{*+}a_1^{-e}$	$1.26 \pm 0.20 \pm 0.14 \pm 0.04^a$		$0.97a_1^2(f_{a1}/0.22)^2$	1.28
$D^{**+}_{(2460)}\pi^-$	$< 0.18^a$			
$D^+D_s^-$	1.2 ± 0.7^b	$1.7 \pm 1.3 \pm 0.6^c$	$1.213a_1^2(f_{Ds}/0.28)^2$	1.60
$D^+D_s^{*-}$		$2.7 \pm 1.7 \pm 0.9^c$	$0.859a_1^2(f_{Ds*}/0.28)^2$	1.14
$D^{*+}D_s^-$	2.4 ± 1.4^b	$1.4 \pm 1.0 \pm 0.3^c$	$0.824a_1^2(f_{Ds}/0.28)^2$	1.09
$D^{*+}D_s^{*-}$		$2.6 \pm 1.4 \pm 0.6^c$	$2.203a_1^2(f_{Ds*}/0.28)^2$	2.91
B^-				
$D^0D_s^-$	2.9 ± 1.3^b	$2.4 \pm 1.2 \pm 0.4^c$	$1.215a_1^2(f_{Ds}/0.28)^2$	1.61
$D^0D_s^{*-}$		$1.6 \pm 1.2 \pm 0.3^c$	$0.862a_1^2(f_{Ds*}/0.28)^2$	1.14
$D^{*0}D_s^-$		$1.3 \pm 0.9 \pm 0.2^c$	$0.828a_1^2(f_{Ds}/0.28)^2$	1.10
$D^{*0}D_s^{*-}$		$3.1 \pm 1.6 \pm 0.5^c$	$2.206a_1^2(f_{Ds*}/0.28)^2$	2.92

a. Preliminary result to be submitted to Phys. Rev. D. The first error is statistical, the second systematic, and the third error is due to uncertainties of D branching ratios.
b. Reference 59, $Br(D_s^+ \to \phi\pi^+) = 2\%$ is used.
c. Reference 60, $Br(D_s^+ \to \phi\pi^+) = 2.7\%$ is used.
d. Reference 3.
e. All events with 3π mass between 1.0 and 1.6 GeV (after background subtraction) are assumed to be a_1.

Table 5. Class-II branching ratios.

$\overline{B}^0$	CLEO (%)	ARGUS (%)	Model (%)[27]	$a_1 = 0.26$
$D^0\pi^0$	$< 0.035^a$		$0.201a_2^2(f_D/0.22)^2$	0.014
$D^0\rho^0$	$< 0.042^a$		$0.136a_2^2(f_D/0.22)^2$	0.009
$D^{*0}\pi^0$	$< 0.072^a$		$0.213a_2^2(f_{D^*}/0.22)^2$	0.014
$D^{*0}\rho^0$	$< 0.092^a$		$0.223a_2^2(f_{D^*}/0.22)^2$	0.015
$D^0\eta$	$< 0.075^a$			
$D^0\eta'$	$< 0.074^a$			
$D^0\omega$	$< 0.048^a$			
$D^{*0}\eta$	$< 0.086^a$			
$D^{*0}\eta'$	$< 0.36^a$			
$D^{*0}\omega$	$< 0.13^a$			
$\psi\overline{K}^0$	$0.075 \pm 0.024 \pm 0.008^a$	$0.08 \pm 0.06 \pm 0.02^b$	$1.817a_2^2$	0.123
$\psi\overline{K}^{*0}$	$0.169 \pm 0.031 \pm 0.018^a$	$0.11 \pm 0.05 \pm 0.02^b$	$2.927a_2^2$	0.198
$\psi'\overline{K}^0$	$< 0.08^a$	$< 0.28^b$	$1.065a_2^2$	0.072
$\psi'\overline{K}^{*0}$	$< 0.19^a$	$< 0.23^b$	$1.965a_2^2$	0.133
$\chi_{c1}\overline{K}^0$	$< 0.27^a$			
$\chi_{c1}\overline{K}^{*0}$	$< 0.21^a$			
B^-				
ψK^-	$0.110 \pm 0.015 \pm 0.009^a$	$0.07 \pm 0.03 \pm 0.01^b$	$1.819a_2^2$	0.123
ψK^{*-}	$0.178 \pm 0.051 \pm 0.023^a$	$0.16 \pm 0.11 \pm 0.03^b$	$2.932a_2^2$	0.198
$\psi' K^-$	$0.061 \pm 0.023 \pm 0.015^a$	$0.18 \pm 0.08 \pm 0.04^b$	$1.068a_2^2$	0.072
$\psi' K^{*-}$	$< 0.30^a$	$< 0.49^b$	$1.971a_2^2$	0.133
$\chi_{c1}K^-$	$0.097 \pm 0.040 \pm 0.009^a$			
$\chi_{c1}K^{*-}$	$< 0.21^a$			

a. Preliminary result to be submitted to Phys. Rev. D.
b. Reference 3. Modes involving a K_s are multiplied by two to obtain the branching ratios for $\overline{K}^0$.

Table 6. Class-III branching ratios.

B^-	CLEO (%)	ARGUS (%)	Model (%)[27]	$a_1 = 1.15$ $a_2 = 0.26$
$D^0\pi^-$	0.55 ± 0.04 $\pm 0.03 \pm 0.02^a$	$0.20 \pm 0.08 \pm 0.06^b$	$0.265(a_1 + 1.230a_2(f_D/0.22))^2$	0.57
$D^0\rho^-$	1.35 ± 0.12 $\pm 0.12 \pm 0.04^a$	$1.3 \pm 0.4 \pm 0.4^b$	$0.622(a_1 + 0.662a_2(f_D/0.22))^2$	1.09
$D^{*0}\pi^-$	0.49 ± 0.07 $\pm 0.06 \pm 0.03^a$	$0.40 \pm 0.14 \pm 0.12^b$	$0.255(a_1 + 1.292a_2(f_{D^*}/0.22))^2$	0.56
$D^{*0}\rho^-$	1.68 ± 0.21 $\pm 0.22 \pm 0.08^a$	$1.0 \pm 0.6 \pm 0.4^b$	$0.703[a_1^2 + 0.635a_2^2(f_{D^*}/0.22)^2$ $+1.487a_1a_2(f_{D^*}/0.22)]$	1.27
$D^{*0}a_1^{-c}$	1.88 ± 0.40 $\pm 0.30 \pm 0.10^a$			
$D^{**0}_{(2420)}\pi^-$	0.11 ± 0.05 $\pm 0.04 \pm 0.03^a$			
$D^{**0}_{(2460)}\pi^-$	$< 0.15^a$			
$D^{**0}_{(2420)}\rho^-$	$< 0.14^a$			
$D^{**0}_{(2460)}\rho^-$	$< 0.5^a$			

a. Preliminary result to be submitted to Phys. Rev. D. The first error is statistical, the second systematic, and the third error is due to uncertainties of D branching ratios.
b. Reference 3.
c. All events with 3π mass between 1.0 and 1.6 GeV (after background subtraction) are assumed to be a_1.

3.5 *Final State Interaction*

The factorization assumes that effect of final state interaction is negligible. Therefore any test that is sensitive to final state interaction is also a test of factorization.

One way is to perform an isospin analysis on a set of isospin-related modes. For example, assuming that the relevant Hamiltonian has isospin $|I, I_z\rangle = |1, -1\rangle$ (i.e. $b \to c\overline{u}d$ - simply a creation of $\overline{u}d$ pair as long as isopin is concerned), the three decay amplitudes of $\overline{B}^0 \to D^+\pi^-$, $D^0\pi^0$, and $B^- \to D^0\pi^-$ can be written as

$$\begin{aligned} Amp(D^+\pi^-) &= \sqrt{\frac{1}{3}}A_{\frac{3}{2}} - \sqrt{\frac{2}{3}}A_{\frac{1}{2}} \\ Amp(D^0\pi^0) &= \sqrt{\frac{2}{3}}A_{\frac{3}{2}} + \sqrt{\frac{1}{3}}A_{\frac{1}{2}} \\ Amp(D^0\pi^-) &= \sqrt{3}A_{\frac{3}{2}} \end{aligned} \tag{47}$$

where $A_{\frac{3}{2}}$ and $A_{\frac{1}{2}}$ are the isospin 3/2 and 1/2 amplitudes respectively. There are three unknown parameters: $|A_{\frac{3}{2}}|$, $|A_{\frac{1}{2}}|$, and $\delta = \arg(A_{\frac{3}{2}}/A_{\frac{1}{2}})$. Since there are three measurements of decay rates, one can solve for the three unknowns. Then the non-zero phase δ signifies the existence of final state interaction. Unfortunately, the $D^0\pi^0$ mode is not observed yet at this point; we expect, however, that it will be observed sometime soon as mentioned earlier.

One could go further along this line if one is enough. One can set $\delta = 0$ and recalculate the decay rates that would have been without the final state interaction. Then those rates may be compared with what is expected by factorization. In fact, a phenomenologically successful analysis of charm decay was performed in such manner.[28] However, there is no guarantee that all the effect of final state interaction can be taken away by this method. There may be interactions with other final states, for example.

Another possibility is to look at the azimuthal angular distribution in $B \to VV$ decays. Taking $B \to D^*\rho$ as an example, the angular distribution is given by

$$\begin{aligned}\frac{d\Gamma}{dc_D dc_\rho d\chi} \propto\ & (|H_+|^2 + |H_-|^2)s_D^2 s_\rho^2 + 4|H_0|^2 c_D^2 c_\rho^2 \\ & +2\mathrm{Re}(H_+^* H_-)s_D^2 s_\rho^2 \cos 2\chi + 2\mathrm{Im}(H_+^* H_-)s_D^2 s_\rho^2 \sin 2\chi \\ & +4\mathrm{Re}(H_+^* H_0 + H_-^* H_0)s_D c_D s_\rho c_\rho \cos\chi + 4\mathrm{Im}(H_+^* H_0 - H_-^* H_0)s_D c_D s_\rho c_\rho \sin\chi\end{aligned} \tag{48}$$

where $\theta_{D,\rho}$ are the polar decay angle of D and ρ decays as before, and χ is the azimuthal angle between the two decay planes. We have used a short hand: $c_D = \cos\theta_D$, $s_D = \sin\theta_D$ etc. If there is no final-state interaction and there is no CP violation, then all the helicity amplitudes are relatively real. The effect of CP violation would show up as difference of angular distribution (as well as difference in total decay rate) between B and $\overline{B}$ decays.[62] For Cabbibo-favored modes such as $D^*\rho$, we do not expect significant CP violation. Thus, existence of terms proportional to $\sin\chi$ or $\sin 2\chi$ signals final state interaction.[63] This analysis should be able to be done with dataset presently available, but thus far not completed.

4. SUPPRESSED DECAYS

Now we move to rare decays which are typically Cabbibo-suppressed. We start from charm-less two-body decays.

4.1 B Decays to Two Charmless Mesons

Each of the processes $B^0 \to K^-\pi^+$, $\pi^+\pi^-$ could proceed through two types of diagrams: spectator and penguin (Figure 10). When there exist more than one diagram with different weak interaction phases and different final state interaction phases (i.e. strong interaction), there can be CP violating decay asymmetries[64] as seen below. Suppose two diagrams contribute to a decay $B \to f$ with amplitudes A_1 and $A_2 e^{i\delta}$ where $A_{1,2}$ are the weak amplitudes and δ is the FSI phase difference. Since only relative phases matter, the weak and strong phases of the first diagram are assumed to be zero. For the corresponding $\overline{B} \to \overline{f}$ decay, the weak phase changes its sign but the strong phase does not. This leads to a decay asymmetry:

$$Amp(B \to f) = A_1 + A_2 e^{i\delta}, \quad Amp(\overline{B} \to \overline{f}) = A_1^* + A_2^* e^{i\delta} \quad (A_1 : \text{real}). \tag{49}$$

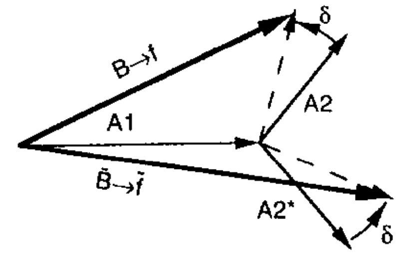

(50)

In our case, the weak phase of each diagram is given by that of the CKM matrix elements which multiply the entire amplitude as coefficients. Thus we expect that there is a weak phase difference as shown in the figure. The strong phases, however, are difficult to estimate.

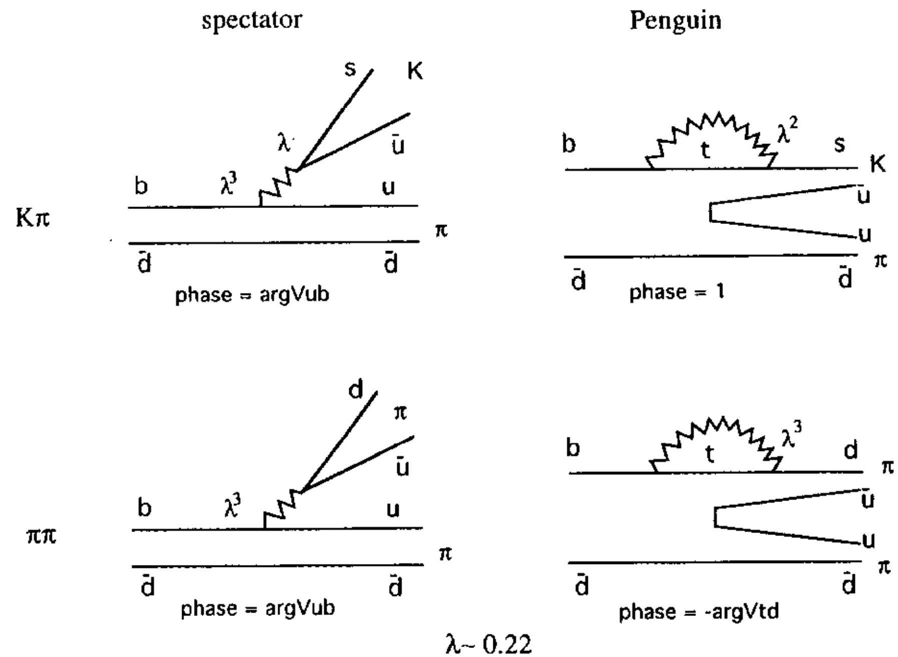

Figure 10. Diagrams that can contribute to $B \to K\pi, \pi\pi$.

If we assume the flavor $SU(3)$ symmetry, then the ratio of amplitudes are

$$\left.\frac{K\pi}{\pi\pi}\right|_{\text{spectator}} \sim \lambda \qquad \left.\frac{K\pi}{\pi\pi}\right|_{\text{penguin}} \sim \frac{1}{\lambda} \tag{51}$$

where λ is the Cabbibo suppression factor (~ 0.2). It is expected that the spectator diagram will dominate in $B^0 \to \pi^+\pi^-$. Then if there is no penguin contribution, the $K^-\pi^+$ branching ratio should be $\lambda^2 \sim 0.04$ times smaller than that of $\pi^+\pi^-$. Thus, if the rate of $K^-\pi^+$ is comparable or greater than $\pi^+\pi^-$, then it is likely that the $K^-\pi^+$ rate is dominated by the penguin diagram. When there is a large disparity in magnitudes of the two diagrams, the expected CP violation will be small independent of the phases.

One should note, however, that there is a possibility that $B \to K\pi$ can occur through final state re-scatterings. This could occur through intermediate states involving two charmed mesons as

$$B^0 \to D^- D_S^+ \to K^+\pi^-, \qquad B^0 \to D^- D^+ \to \pi^-\pi^+ \tag{52}$$

which corresponds to replacing the top quark loop in the penguin diagrams by a charm quark which will be on-shell as shown below and can be considered to be a dispersive version of penguin diagram.

(53)

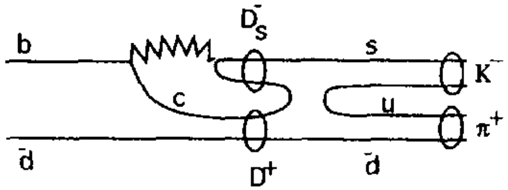

Such process will result in a large FSI phase, and can interfere with the top quark penguin diagram to generate a CP violation as originally postulated by Bander, Silverman and Soni.[65]

Approximate rate of $\pi^+\pi^-$ can be estimated from the measured $B^0 \to D^-\pi^+$ rate quite reliably:

$$Br(\pi^+\pi^-) \sim \left|\frac{V_{ub}}{V_{cb}}\right|^2 \sim 1 \times 10^{-5} \tag{54}$$

where the effect of form factor will reduce it somewhat and that of phase space will increase it somewhat. The estimation of the $K\pi$ rate requires the coefficient of the penguin operator, and the uncertainty is greater; the theoretical estimates are in the same range as the $\pi\pi$ mode.[66]

Experimentally, the signature on $\Upsilon(4S)$ is a rather spectacular high-momentum back-to-back tracks of $p \sim 2.6$ GeV. This is the maximum momentum a B-decay can emit and thus the background is dominated by continuum events; thus, cuts are made on event shapes to reject 2-jet like events and the fast back-to-back tracks are required not to be aligned with the jet axis of event. For a $B\overline{B}$ pair event, the event shape is spherical and there is little correlation between the event axis and the direction of the back-to-back tracks. Then, as before, the energy difference ΔE and the beam-constrained mass M_B is used to select the candidates [see (3)].

When masses are correctly assigned to the tracks, the ΔE resolution is 25 MeV. The dE/dx information in the drift chamber is used to separate kaon and pion. The dE/dx resolution is 6.5% and provides 1.8σ $K-\pi$ separation per track. Each candidate is assigned the most likely masses ($\pi\pi$, $K\pi$, or KK), then ΔE is calculated. The beam-constrained mass, on the other hand, does not depend on the mass assignments and the resolution is 2.5 MeV. Figure 11(a) shows the M_B distribution for $K\pi$ and $\pi\pi$ candidates after 2-σ cut on ΔE around zero. The shaded events are the $\pi\pi$ candidates. One can see an enhancement at the nominal B mass of 5.280 GeV. The ΔE distribution after the 2-σ cut on M_B is shown in Figure 11(b). Again, there is a peak around the nominal region near $\Delta E = 0$. For the final extraction of numbers, an un-binned maximum likelihood fit is performed with ΔE, M_B, dE/dx, and an event shape variable as parameters. Here ΔE is calculated assuming $\pi\pi$. The result is shown in Table 7.[67]

When ΔE is calculated assuming $\pi\pi$, the value shifts down by 42 MeV if the actual tracks are $K\pi$. Since the ΔE resolution is 25 MeV, this by itself can provide 1.7σ separation between $K\pi$ and $\pi\pi$. The available particle identifications are not good enough to cleanly separate the two. When $K\pi$ and $\pi\pi$ are combined there is a substantial signal of about 3.5σ. The central value of $\pi^+\pi^-$ mode is consistent with the expected value of 1×10^5. If we take the central value of the $K^+\pi^-$ mode at its face value, then penguin diagrams (t-loop or the re-scattering c-loop) are likely to be dominating the $K^+\pi^-$ mode.

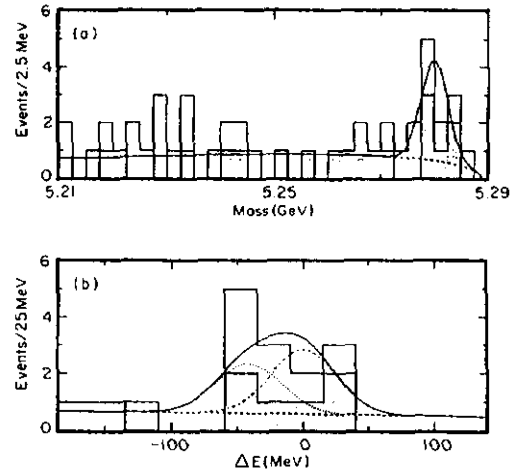

Figure 11. Sum of $K\pi$ sample and $\pi\pi$ sample. (a) The beam-constrained mass M_B after the 2-σ cut on ΔE. (b) ΔE distribution after the 2-σ cut on M_B. The shaded events are the events assigned to be $\pi\pi$.

Table 7. Measured branching fractions and 90% confidence level upper limits.

Mode	Br(10^{-5})	Upper Limit (10^{-5})
$\pi^+\pi^-$	$1.3^{+0.8}_{-0.6} \pm 0.2$	2.9
$K^+\pi^-$	$1.1^{+0.7}_{-0.6} \pm 0.2$	2.6
K^+K^-		0.7
$K^+\pi^- + \pi^+\pi^-$	$2.4^{+0.8}_{-0.7} \pm 0.2$	

4.2 b to s Radiative Decays

Another rare process a penguin diagram is expected to contribute is the radiative $b \to s$ transition through emission and re-absorption of W.

(55)

At the lowest order, the GIM suppression is operative and it depends on the top mass (m_t) strongly, and $Br(B \to X_s\gamma)$ changes from 0.5×10^{-4} at $m_t = 100$ GeV to 1.4×10^{-4} at $m_t = 200$ GeV. With QCD correction,[68] the GIM suppression is loosened ('soft' GIM suppression) and as a result the rate is substantially enhanced and becomes a slow function of m_t. The enhancement factor is ~ 5 at $m_t = 120$ GeV to give $Br(B \to X_s\gamma) = \sim 3.5 \times 10^{-4}$. Theoretical estimate for the exclusive mode $B \to K^*\gamma$ is more uncertain due to the unknown transition matrix element $B \to K^*$.[69] One estimate based on HQET gives $Br(B \to K^*\gamma) = (1.4 - 4.9) \times 10^{-5}$.[70]

The experimental signature[71] is a monochromatic hard photon (2.6 GeV) recoiling against $K^* \to K\pi$ decay. We look for both $B^0 \to K^{*0}\gamma$ and $B^- \to K^{*-}\gamma$. The K^*'s are searched for in the modes $K^{*0} \to K^+\pi^-$ and $K^{*-} \to K^-\pi^0, K_s\pi^-$. Again the background is dominated by continuum events since such high-energy photon is at the kinematic limit of B decay. The continuum backgrounds are reduced by requiring that the events be not 2-jet like and that the hard photon be not aligned to the event axis. If the photon forms a π^0 or η with another photon then it is rejected. Figure 12 shows the M_B distribution after the cut $|\Delta E| < 90$ MeV (2.2σ). There is a clear signal observed with 6.6 ± 2.8 events in B^0 mode and 4.1 ± 2.3 events in B^- modes. The branching fractions are

$$\begin{aligned} Br(B^0 \to K^{*0}\gamma) &= (4.0 \pm 1.7 \pm 0.8) \times 10^{-5}, \\ Br(B^- \to K^{*-}\gamma) &= (5.7 \pm 3.1 \pm 1.1) \times 10^{-5} \qquad \text{(CLEO)}. \end{aligned} \tag{56}$$

If we assume isospin symmetry, then

$$Br(B^0 \to K^{*0}\gamma) = Br(B^- \to K^{*-}\gamma) = (4.5 \pm 1.5 \pm 0.9) \times 10^{-5} \tag{57}$$

which is consistent with theoretical estimates based on the standard model where the penguin contribution dominates. Another possibility is that the $B \to K^*\gamma$ transition may occur through $\psi K*$ by vector dominance[72]

$$B \to \psi K^* \to \gamma K^* \qquad \text{(vector dominance)} \tag{58}$$

or other long distance effects.[73] Such processes have been estimated and found to be at least an order of magnitude smaller than the observed rate.

The inclusive transition $B \to X_s\gamma$ can be searched by looking for the hard photon without reconstructing X_s where the mass of X_s lies in the typical strange meson region (0.5 to 2 GeV). Similar cuts as before to reduce continuum backgrounds are applied. Figure 13 shows the continuum-subtracted (see Section 1) photon spectrum. The signal region is around 2.2 to 2.7 GeV. There seems to be some enhancement, but it is not statistically significant; thus, we set an upper limit

$$Br(b \to s\gamma) < 5.4 \times 10^{-4} \qquad \text{(CLEO}^{74}\text{)}. \tag{59}$$

Such measurement places stringent constraints on non-standard physics, in particular two-Higgs-doublet models.[75] The W-top loop can be replaced by loops involving charged Higgs, neutralinos, gluinos, and squarks etc. For example, in the minimal supersymmetric model with two Higgs doublets, the mass of the CP-odd neutral Higgs A^0 is ruled out for $m_{A^0} <$ 250 GeV ($\tan\beta > 1$).[77]

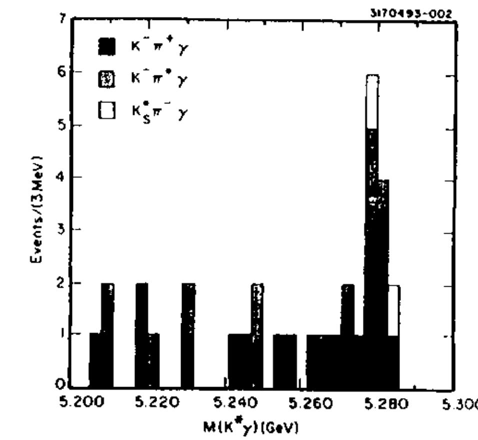

Figure 12. The M_B distribution for $B \to K^*\gamma$ after ΔE cut.

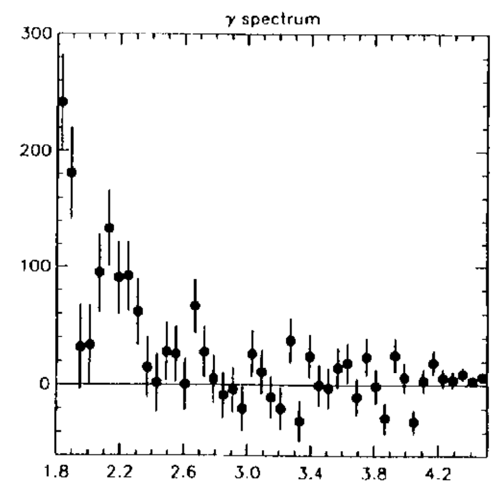

Figure 13. Single photon spectrum after continuum subtraction. The signal $b \to s\gamma$ would show up in the region 2.2 to 2.7 GeV.

5. ACKNOWLEDGEMENTS

The author would like to thank Mike Dugan, Guilia Ricciardi, Thorsten Ohl, and Mitch Golden for fruitful discussions. A major credit should go to the editing staff whose extraordinary patience made it possible that this article be completed.

6. REFERENCES

1. Particle Data Group, Phys. Rev. **D45** Part II (1992).
2. D. Bortoletto *et al.* (CLEO collaboration), Phys. Rev.**D45** (1992) 21.
3. H. Albrecht *et al.* (ARGUS collaboration), Z. Phys.**C48** (1990) 543.
4. S. Alam *et al.* (CLEO collaboration), to be published. Also, presented at the 1993 Lepton-photon conference at Cornell University.
5. An early attempt to predict charmed meson masses is in, A. De Rujula, H. Georgi, and S. Glashow, Phys. Rev. Lett. **37** (1976) 398. For a review, see for example, J. Gasser and H. Leutwyler, Phys. Rep **87** (1982) 78, and references therein.
6. J. Goity and W-S Hou, Phys. Lett. **B282** (1992) 243.
7. F. Abe *et al.* (CDF collaboration), FERMILAB-PUB-93-141-E (Jun 1993).
8. D. Buskulic *et al.* (ALEPH collaboration), Phys. Lett. **B311** (1993) 425.
9. P. D. Acton *et al.* (OPAL collaboration), Phys. Lett. **B295** (1992) 357.
10. Y. Arnoud *et al.* (DELPHI collaboration), Paper submitted to the "HEP 93" conference, Marseille, 1993.
11. W. Kwong and J. Rosner, Phys. Rev. **D44** (1991) 212, and references therein.
12. K. Han *et al.*, Phys. Rev. Lett. **55** (1985) 36; J. Lee-Franzini *et al.*, Phys. Rev. Lett. **65** (1990) 2947.
13. D. Akerib *et al.* (CLEO collaboration), Phys. Rev. Lett. **67** (1991) 1692.
14. The references quote the photon energy in the B^* rest frame. A correction of $\Delta M^2/2M_{B^*}$ is applied to convert it to the mass difference.
15. M. Frank and P. O'Donnel, Phys. Lett. **159B** (1985) 174; Z. Phys. **C34**, (1987) 39; K. Igi and S. Ono, Phys. Rev. **D32** (1985) 232.
16. E. Eichten *et al.*, Phys. Rev. **D21** (1980) 203; S. Godfrey and N. Isgur, Phys. Rev. **D32** (1985) 189.
17. The electromagnetic hyperfine splitting can be cleanly separated by measuring the difference of the hyperfine splittings within isospin multiplet; e.g. $[M(D^{*+}) - M(D^+)] - [M(D^{*0}) - M(D^0)]$ for D mesons: J. Amundson *et al.*, Phys. Rev. **D47**, (1993) 47.
18. M. Gronau, A. Nippe, and J. Rosner, Phys. Rev.**D47** (1993) 1988.
19. See for example, R. E. Marshak, 'Conceptual Foundations of Modern Particle Physics' (World Scientific, 1993); T-P Cheng and L-F Li, 'Gauge Theory of Elementary Particle Physics', (Oxford, 1984); T. D. Lee, 'Particle Physics and Introduction to Field Theory', (Harwood, 1988), to name a few.
20. See for example, J. Rosner, in 'B Decays' p312 ed. S. Stone, (World Scientific) and references therein.
21. A popular parametrization of the CKM matrix which is accurate to λ^3 is:
$$V \sim \begin{pmatrix} 1-\frac{1}{2}\lambda^2 & \lambda & A\lambda^3(\rho - i\eta) \\ -\lambda & 1-\frac{1}{2}\lambda^2 & A\lambda^2 \\ A\lambda^3(1-\rho-i\eta) & -A\lambda^2 & 1 \end{pmatrix}$$
where $\lambda \sim 0.22$ and A, ρ, η are real numbers of order 1. L. Wolfenstein Phys. Rev. Lett. **51** (1983) 1945.
22. F. G. Gilman and M. B. Wise, Phys, Rev. **D20** (1979) 2392.
23. K. G. Wilson, Phys. Rev. **179** (1969) 1499.
24. Originally, the calculations were done in the context of $\Delta I = 1/2$ enhancement. M. K. Gaillard and B. W. Lee, Phys. Rev. Lett. **33** (1974) 108; G. Altarelli and L. Maiani, Phys. Lett. **32B** (1974) 351.
25. G. Altarelli, G. Curci, G. Martinelli, and S. Petrarca, Phys. Lett. **99B** (1981) 141; Nucl. Phys. **B187** (1981) 461.
26. M. A. Shifman, A. I. Vainshtein, and V. I. Zakharov, Nucl. Phys. **B120** (1977) 316. The purpose was to explain the $\Delta I = 1/2$ enhancement in the non-leptonic strange particle decays.
27. A good review is found in, M. Neubert, V. Rieckert, B. Stech, and Q.P. Xu, in 'Heavy Flavors' p286, ed. A. Buras (World Scientific, 1992).
28. M. Bauer, B. Stech, and M. Wirbel, Z. Phys. **C34** (1987) 103.
29. J. Schwinger, Phys. Rev. Lett. **12** (1964) 630.
30. R. P. Feynman, 'Symmetries in Elementary Particle Physics' Ed. A. Zichichi, p111 (Academic Press, 1965).
31. N. Isgur and M. Wise, Phys. Lett. **B232** (1989) 113; **B237** (1990) 527.
32. B. Grinstein, W. Kilian, T. Mannel, and M. Wise, Nucl. Phys. **B363** (1991) 19.
33. J. Bjorken, Nucl. Phys. **B** (Proc. Suppl.) **11** (1989) 325.
34. S. Brodsky and A. Mueller, Phys. Lett. **B206** (1988) 685.
35. M. Dugan and B. Grinstein, Phys. Lett. **B255** (1991) 583.
36. A. Buras, J.-M. Gérard, and R. Rückl, Nucl. Phys. **B268** (1986) 16.
37. C. Reader and N. Isgur, Phys. Rev. **D47** (1993) 1007.
38. See for example the appendix of L. B. Okun, 'Leptons and quarks' (North Holland, 1982).
39. It is important to note that the current operator $(\bar{q}q')$ and the 'factorized hadron operator' $(\bar{q}q')_{\rm had}$ are two different objects. A same current operator can contribute to more than one factorized hadron operators.
40. B. Blok and M. Shifman, Nucl. Phys. **B389** (1993) 534; M. Shifman, Nucl. Phys. **388** (1992) 346.
41. M. Wirbel, B. Stech, and M. Bauer, Z. Phys. **C29** (1985) 637; M. Bauer and M. Wirbel, Z. Phys. **C 42** (1989) 671.
42. N. Isgur and M. Wise, Phys. Lett. **B237** (1990) 527.

43. M. Bauer and B. Stech, Phys. Lett. **B152** (1985) 380.

44. V. Mathur and T. Rizzo, Phys. Rev. **D16** (1977) 3343.

45. J. Ellis, M. Gaillard, D. Nanopoulos, Nucl. Phys. **B100** (1975) 313.

46. D. Fakirov and B. Stech, Nucl. Phys. **B133** (1978) 313.

47. H. Fritzsch and P. Minkowski, Phys. Lett. **90B** (1980) 455; M. Bander, D. Silverman, A. Soni, Phys. Rev. Lett. **44**, (1980) 7; B. Bernreuther, O. Nachtmann, and B. Stech, Z. Phys. **C4** (1980) 257. The last article also speculated a deviation from $V-A$ interaction due to soft gluon effects.

48. J. Rosner, Phys. Rev. **D42** (1990) 3732.

49. One may add a_1^2 to the expression, but what to take for ξ is not clear and the uncertainty is of order 10%. One has to be careful not to use the value of a_1 which is obtained by phenomenological fit to hadronic rates together with semileptonic form factors. That would be a biased test of factorization.

50. H. Albrecht *et al.* (ARGUS collaboration), Phys. Lett. **B219** (1989) 121; H. Albrecht *et al.*, Phys. Lett. **B197** (1987) 452.

51. D. Bortoletto *et al.*, Phys. Rev/ Lett. **63** (1989) 1667. D. Bortoletto, Ph.D. thesis, Syracuse University, 1989.

52. N. Isgur, D. Scora, B. Grinstein, and M. Wise, Phys. Rev. **D39** (1989) 799. B. Grinstein, M. Wise, and N. Isgur, Phys. Rev. Lett. **56** (1986) 298.

53. J.G. Korner and G.A. Schuler, Z. Phys. **C38** (1988) 511.

54. In principle, one can make a QED radiative correction; the result, however, does not vary significantly for the purpose of this analysis. See Ref. 1, p VII.1.

55. The parameter c_V is the charge squared of the valence quark properly averaged over the quarks. For example, $c_V = 1/9$ and $4/9$ for ϕ and ψ, respectively. For ρ^0, $c_V = |Q_u\langle u\overline{u}|\rho^0\rangle + Q_d\langle d\overline{d}|\rho^0\rangle|^2 = 1/2$, where Q_i is the charge of quark type i.

56. X.-Y. Pham and X.C. Vu, Phys. rev. **D46** (1992) 261.

57. D. Akerib *et al.* (CLEO collaboration), Phys. Rev. Lett. **71** (1993) 3070.

58. F. Butler *et al.* (CLEO collaboration), Phys. Rev. Lett. **69** (1992) 2041.

59. D. Bortolleto *et al.* (CLEO collaboration), Phys. Rev. Lett. **64** (1990) 2117.

60. H. Albrecht *et al.* (ARGUS collaboration), Z. Phys. **C54** (1992) 1.

61. CLEO paper submitted to the EPS conference, Marseille 1993 (CLEO CONF 93-17).

62. G. Kramer and W.F. Palmer, Phys. Lett. **B279** (1992) 181.

63. J.G. Korner and G.R. Goldstein, Phys. Lett. **89B** (1979) 105.

64. A. Pais and S.B. Treiman, Phys. Rev. **D12** (1975) 218; L.B. Okun, V.I Zakharov, and B.M. Pontecorvo, Lett. Nuovo. Cim **13** (1975) 218; For a modern treatment including B decays, see for example, L. Wolfenstein, Phys. Rev. **D43** (1991) 151.

65. M. Bander, D. Silverman, and A. Soni, Phys. Rev. Lett. **43** (1979) 242. Also, see J.-M. Gerard and W.-S. Hou, Phys. Rev. Lett. **62** (1989) 855; D. London and R.D. Pecce, Phys. Lett. **B223** (1989) 257; I.I. Bigi, V.A. Khoze, N.G. Uraltzev, and A.I. Sanda in 'CP Violation', Ed. C. Jarlskog (1988) World Scientific, and references therein.

66. N.G. Deshpande and J. Tranpetic, Phys. Rev. **D41** (1990) 895; Phys. Rev. **D41** 2926; L.-L. Chau *et al.*, Phys. Rev. **D43** (1991) 2176.

67. M. Battle *et al.* (CLEO collaboration), Phys Rev. Lett **71** (1993) 3922.

68. B. Grinstein, R. Springer, and M.B. Wise, Phys. Lett. **B202** (1988) 138; G. Cella, G. Curci, G. Ricciardi, and A. Vicere, Phys. Lett. **B248** (1990) 181; M. Misiak, Phys. Lett. **B269** (1991) 161.

69. T. Altomari, Phys. Rev. **D37** (19 8) 677.

70. A. Ali, T. Ohl, and T. Mannel, Phys. Lett. **B298** (1993) 195.

71. R. Ammer *et al.* (CLEO collaboration), Phys Rev. Lett. **71** (1993) 674.

72. N.G. Deshpande *et al.*, Phys. Lett. **B214** (1988) 467.

73. P. Colangelo *et al.*, Z. Phys. **C45** (1990) 575.

74. P. Kim, to appear in the proceedings of the heavy flavor conference, McGill University, 1993.

75. W.-S. Hou and R.S. Willey, Phys. Lett. **202** (1988) 591; S. Bertolini *et al.*, Nucl. Phys. **B353** (1991) 591; V. Barger *et al.*, Phys. Rev. Lett. **70** (1993) 1368.

76. S. Bertolini, 'Heavy Flavors' p202, ed. A. Buras (World Scientific, 1992)

77. J. Hewett, Phys. Rev. Lett. **70** (1993) 1045.

DESIGN CHOICES AND ISSUES FOR COLLIDER EXPERIMENTS

JEFF SPALDING
Fermi National Accelerator Laboratory
Batavia, IL 60510

1. INTRODUCTION

This talk was given on the first day of the workshop. It discusses the technical considerations in the design of B physics experiments at hadron colliders. Since the talk was given on the first day of the workshop, it is an overview of the issues which will be more fully addressed in the working groups.

B particles are copiously produced in hadronic collisions at both FNAL and SSC energies. However, the high rates and relatively soft p_t distribution for B production present severe challenges for the experiments. In terms of detector technologies the main issues are:

- **Triggering and DAQ at very high rates, and the collection and analysis of very large data sets**
- **Tracking and vertexing over a large rapidity range in a high radiation environment**
- **Particle ID - in particular lepton ID and good π and K separation, again over a large rapidity range**

These technical issues result from underlying physics properties and requirements, including:

- **The small ratio of σ_B (per decay mode)/σ_{TOT}**
- **The need for precision measurements -- for example in the measurement of the time evolution in Bs-mixing**
- **The need to tag the flavor of the B particle at its production**

The large cross-section for B production (about 0.1% of the total hadronic cross-section) is a major advantage for hadron colliders. As illustrated in Table 1, these cross-sections lead to the production of very large numbers of B particles. For example at Fermilab energies, $\sqrt{s}$ = 2 TeV, an integrated luminosity of 1 fb^{-1} will produce about 5-10 x 10^{10} B decays, and the yields are 5 to 10 times higher at the SSC. The main issue for B physics at hadron machines is not the production of sufficient B particles, but rather the development of the experimental techniques to fully exploit the enormous yield.

Table 1: Beauty cross-sections and production rates at hadron colliders.

	FNAL (1.8 ->2.0 TeV)	FNAL Main Injector	SSC (40 TeV)
$b\bar{b}$ cross-section	QCD ~ 50μb Expt ~ 100 μb	QCD ~ 50μb Expt ~ 100 μb	QCD ≥ 500 μb
Luminosity	5×10^{30} $cm^{-2}s^{-1}$	5×10^{31} $cm^{-2}s^{-1}$	$10^{33}/10^{34}$ * $cm^{-2}s^{-1}$
$b\bar{b}$ produced in 10^7 seconds	$2.5 - 5 \times 10^9$	$2.5 - 5 \times 10^{10}$	$10^{11} - 10^{12}$ *

* Although the accelerator will run at higher luminosities, trigger rate limitations and radiation damage to vertex detectors will limit the luminosity for B experiments to about 10^{32}.

The B particles are produced at relatively low p_t, and over a broad range in rapidity y, with a rather loose correlation in Δy between the B and $\bar{B}$. Figure 1 illustrates the rapidity and polar angle distributions of the B's and the p_t of their decay products. These distributions necessitate a broad coverage in rapidity for tracking and triggering, especially for studies involving the reconstruction of decay products from both the B and $\bar{B}$. There are conceptually two classes of detector geometry; central (typically with coverage out to one to three units of rapidity on each side of zero) and forward (with coverage above plus one or two units or below minus one or two units of rapidity, perhaps in a two-arm configuration). The present CDF and D0 detectors at Fermilab are central detectors optimized for high-p_t physics, but are nevertheless capable of extensive B physics. CDF has a solenoidal field, while D0 in its present configuration has no magnetic field. The B physics capabilities of these detectors will be upgraded by extending the rapidity range of the tracking and triggering, and by adding a solenoidal field for D0. [1] The BCD collaboration has proposed a central detector at Fermilab and at the SSC with a broad rapidity range and a dipole field to improve forward tracking for low p_t particles. [2] Forward detectors using planar (fixed-target like) geometry have been proposed at Fermilab, LHC and the SSC. [3]

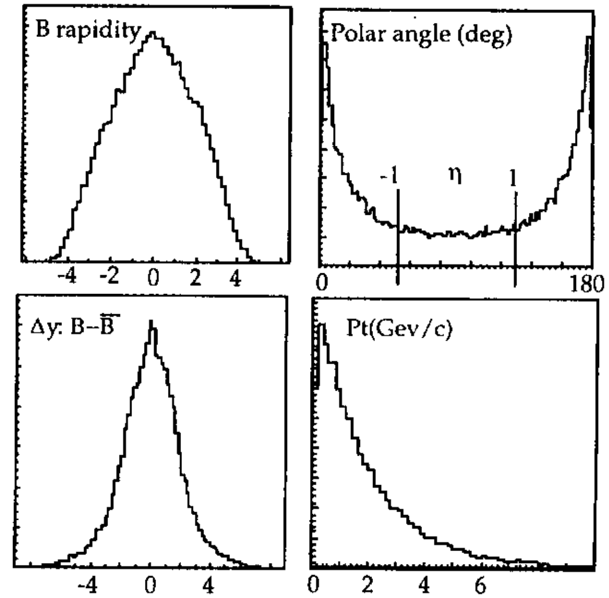

Figure 1: Rapidity and polar angle distributions of B-particles, the difference in rapidity for the B and $\bar{B}$, and the p_t distribution for the B decay products (generated by ISAJET).

Extended rapidity coverage is essential for analyses in which the flavor of a B at production is tagged via the decay of the partner $\bar{B}$, either using the lepton from semi-leptonic decays or with the kaon charge from the subsequent charm decay. These tags require particle ID, charge measurement, and probably p_t selection and impact parameter cuts for the tag particle over this broad range. An alternative method for tagging, using the charge of a pion associated with the signal B, may prove to be very important. [4] Such a correlation may result from the decay of B** states, or from the non-resonant fragmentation of the b quark. This correlation, if it is found to exist, will alleviate much of the need for extended rapidity coverage.

At high luminosities the B production rate is several kHz. The challenge of isolating the B decays from the even larger number of background events presents the main problem encountered in hadron experiments, both in triggering and in event reconstruction.

Since the characteristics of $B\bar{B}$ events, in terms of particle p_t, rapidity spread and multiplicity are not particularly distinctive, it is difficult to design experiment triggers and analysis criteria which separate B $\bar{B}$ events from the much larger total cross-section. At high luminosities, the total $B\bar{B}$ event rate is itself too high, and mode-specific triggers are needed. The most obvious feature of a generic $B\bar{B}$ event is the presence of the B (and the subsequent charm) decay vertices. Silicon vertex detectors have been used for some time with great success in fixed-target experiments to isolate and study charm decays. They have more recently been used in the LEP experiments. [5]

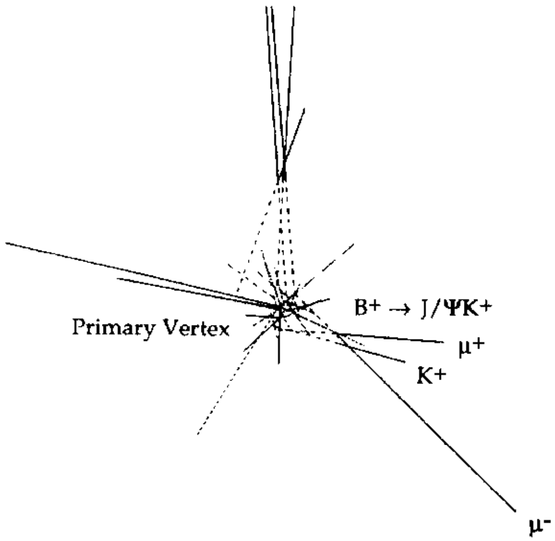

Figure 2: CDF event display showing the vertex reconstruction of an event with a primary vertex and two secondary vertices, one of which includes a J/ψ. The length of the tracks is proportional to their momenta.

CDF is using the first silicon detector to be installed in a full hadron collider experiment. [6] (The first use of a silicon detector at a hadron machine was in the $Sp\bar{p}S$ test P-238 for a dedicated forward B experiment.) [7] The power of vertex reconstruction to isolate B decays is illustrated by the first results of CDF using the SVX. Figure 2 shows a reconstructed event in CDF. A J/ψ resulting from a B decay is seen, well separated from the primary interaction vertex, and from a second decay vertex, presumably the decay of the second B. Events like this will yield valuable information on the correlations between the B and $\bar{B}$.

Currently $B\bar{B}$ events are selected by triggering on semi-leptonic or multi-leptonic B decay modes, since these are more easily identified at the trigger level. Future triggers will include impact parameter information, and eventually vertex reconstruction to greatly reduce the trigger rate and enhance the B content of the data set.

In addition to the need for vertex finding and tracking over a wide rapidity range, and for fast DAQ and triggering, another area of detector development important for B physics is particle ID. This not only contributes to the reduction in combinatoric background to the B signals, but also allows the use of kaons to "tag" the b or $\bar{b}$ flavor of the decaying B. The branching ratio for a charged kaon from the decay chain $b \to c \to s$ is higher than direct semi-leptonic branching. The BCD and COBEX proposals estimate that the tagging efficiency using kaons and leptons can be over three times higher than that for leptons alone. Of course this improvement is only fully realized for triggers which do not themselves rely on observing a semi-leptonic decay.

We now discuss each of these three issues for hadron collider B experiments.

2. TRIGGERING FOR B'S AND THE NEED FOR HIGH DATA ACQUISITION RATES

Experiments so far have relied on triggers based on semi-leptonic B decays, or the decays into J/ψ modes. Even so, single lepton trigger rates are dominated by background due to decays in flight and "punch-through" for muons. Several groups are working on strategies based on the use of vertex detector information by a trigger processor at "Level 2" (in a typical 3-level trigger system). Such processors must produce rejection factors of order 10^2 or higher and make the trigger decision within a few μsec. Trigger processor technology will continue to improve, with more complete event reconstruction becoming possible in shorter times. This then puts severe requirements on the speed of the front-end electronics and Level 1 trigger.

With such processors in the on-line triggers, the high event rates result in the accumulation of very large data sets. Even with the expected reduction in the cost of workstation farms on which we have come to rely, the scale of the offline computing is a serious problem for many experiments.

As an illustration we look at the approaches adopted by BCD, COBEX and CDF.

2.1 BCD

The BCD proposals were perhaps the first to really grapple with this problem of triggering, data aquisition rate, and data set size (see Figure 3). Their solution is to emphasize speed of readout and to send the data to a huge online workstation farm. The size of farm required is estimated to be one million MIPs, or 10 thousand 100-MIP workstations! Similarly the quantity of data archived, and the off-line computing required, are on a very large scale. Of course computing costs continue to drop and it is difficult to estimate the cost to purchase and support computing on this scale in, say, the year 2000.

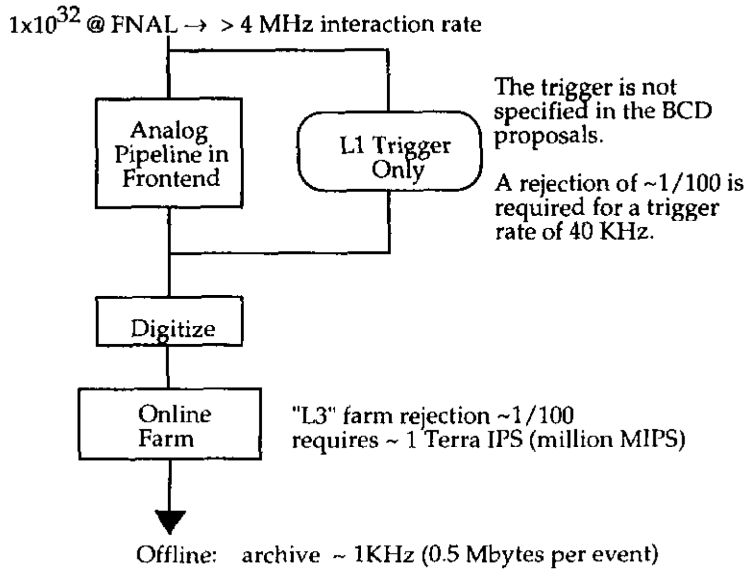

Figure 3: BCD Trigger-DAQ Scheme.

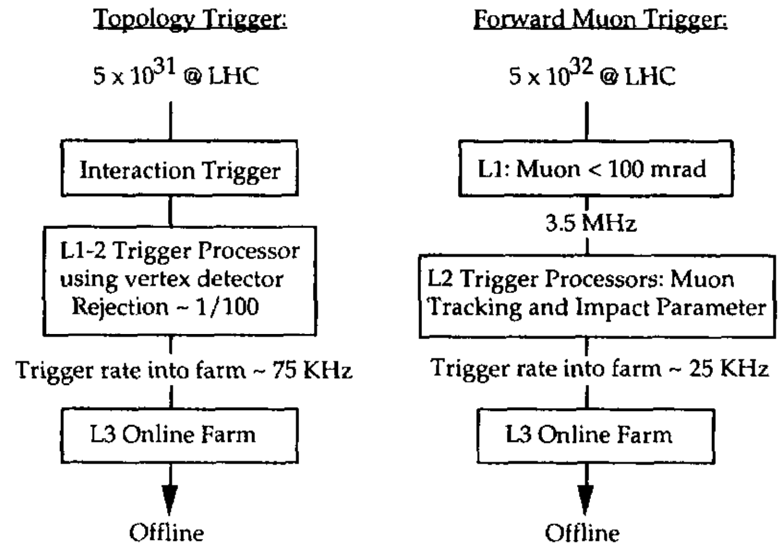

Figure 4: COBEX Trigger-DAQ Scheme.

2.2 *COBEX*

Two trigger schemes are discussed in the COBEX proposals (see Figure 4). The "topology trigger" uses a pipeline trigger processor to process the vertex detector information and determine inconsistency with a single vertex. The vertex detector consists of a series of silicon planes perpendicular to the beam. In order to achieve high acceptance the silicon planes come to within a few millimeters of the beam itself. The trigger processor reconstructs tracks in each view separately, and determines a chi-squared assuming only one vertex. This trigger is limited to a maximum luminosity of a few 10^{31} $cm^{-2}s^{-1}$ by the rate of multiple beam interactions. For higher luminosities a muon trigger is proposed, including processors for tracking and impact parameter cuts.

The L3 farm and offline computing are not specified in the COBEX proposals, but it is interesting to note that with extensive L1 and L2 trigger processors the event rate into the farm at LHC is similar to the BCD FNAL proposal.

2.3 *CDF*

CDF also emphasizes the need for L1 and L2 trigger processors (see Figure 5). The XFT (eXtremely Fast Tracker) will find tracks in the central tracking chamber in the level 1 trigger. At level 2, the Silicon Vertex Tracker or SVT will use an array of processors and associative memories to extend these tracks in the r-Φ view in the vertex detector and impose impact parameter cuts. This will allow the p_t threshold for single-lepton triggers to be lowered, and will provide a trigger for exclusive B final states such as $\pi\pi$. [8]

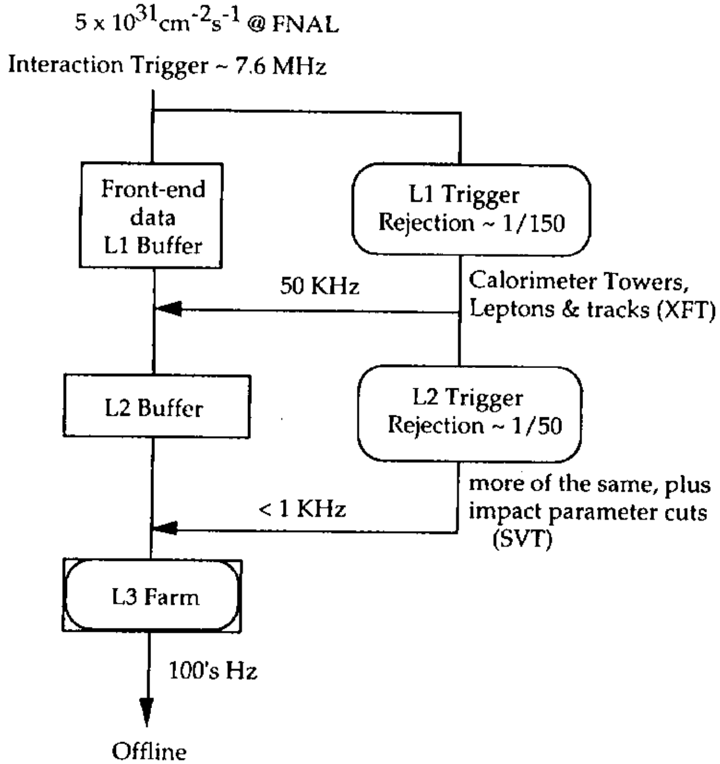

Figure 5: CDF Trigger-DAQ Scheme.

Use of the vertex detector information at L2 requires a very fast digitization and readout, within 7 μs. Groups at Fermilab, LHC and SSC are designing readout schemes using high speed optical links to provide the vertex detector information both to the data acquisition and trigger systems.

3. VERTEX DETECTORS

Silicon vertex detectors are an essential component of heavy flavor experiments. Hadron colliders present a severe environment for these detectors in terms of requirements on high rate operation, low mass construction (particularly since the B decay products are low p_t, and hence multiple scattering is of particular concern in the central region), extended rapidity coverage, and exposure to radiation doses up to a few Mrad. Improved pattern recognition and 3D vertex reconstruction are provided by double-sided vertex detectors with little increase in multiple scattering. Pixel detectors hold out the promise of significant further improvements for the future. To extend the rapidity range the next generation of silicon vertex detectors will be significantly larger than the present CDF SVX. Both CDF and D0 are planning detectors with 250K readout channels, compared to 46K channels for SVX, and the central detectors at SSC and LHC are designed with several million channels. Extended rapidity coverage requires detectors in both barrel and disk geometry. The forward geometry experiments achieve their coverage with detectors in a disk geometry, resulting in a simplified mechnical design.

The short interbunch spacing at future hadron colliders (132 nsec at FNAL with the Main Injector, and 25 nsec at the SSC), and the need for fast DAQ places challenging demands on the vertex detector readout. New readout chips are being developed to meet the needs of the high data rates, and large scale of detectors (see Figure 6). Like the present SVX chip (SVX-H) these chips will all be radiation hard. For precision vertex reconstruction the analog information from the strips is important to locate the centroid of a cluster. Chips being developed at FNAL and LBL for the CDF and D0 upgrades, and those developed by the RD2 collaboration [9] include ADCs on-board the chip. Of course, keeping this analog information greatly increases the quantity of digital data which must then be read from the chip.

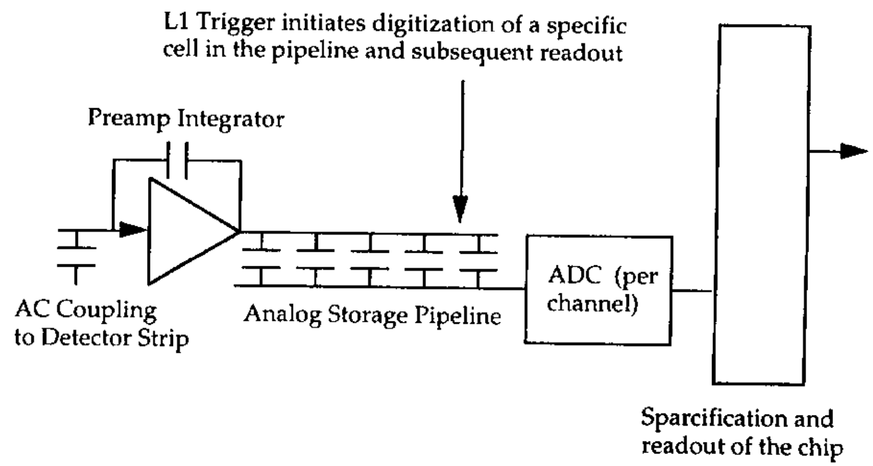

Figure 6: Conceptual Chip Components. Each chip contains 128 such readout channels at 50 μm spacing.

The position resolution may be less crucial for tracking devices. The silicon tracker designed for SDC keeps only hit information, not the value of the charge. In the present SVX II design the analog input is halted during digitization and readout (which are expected to take about 5 μsec), leading to a deadtime at very large level 1 rates. Operating the analog and digital functions concurrently on the same chip is a challenge. The RD2 group is developing a design to do this in one CMOS chip. In the SDC design the analog front-end is bipolar with the digital section in a separate CMOS chip.

Whereas the readout electronics mounted on the detectors can be made rad-hard to above 1 Mrad (the SVX-H chip, fabricated in the UTMC radiation hard CMOS process has so far been tested above 2 Mrad), the issues for the detectors themselves are of more concern. Several groups have studied the effects of radiation on detectors [10]. Ionization can increase the detector capacitance, at least on the n-side, and bulk damage leads to increased leakage current, which can be reduced by running the detectors at lower temperatures. At exposures of about 0.5 Mrad the bulk silicon changes from n-type to p-type, and following this the voltage required to fully deplete the detector increases. The life of the detector will finally be limited to a few Mrad when this increase in the depletion voltage reaches the point where the detectors break down.

Exposing the silicon to high doses cannot be avoided. For precision measurements of the time evolution of B_s-mixing or CP-asymmetries vertex detectors should be close to the beam. For CDF and D0 running at full Main Injector luminosities, with the inner silicon 2 to 3 cm from the beam, the detectors are likely to experience an integrated dose of about 1 Mrad over 4 x 10^7 seconds. This is about the same as the dose which will be experienced by the inner layer of the SDC silicon tracker at 10 cm at the SSC. In the forward geometry of COBEX, with the silicon about 3 mm from the beam the dose is much higher, scaling something like radius^2. Such proximity to the beam is required for a high acceptance for vertex reconstruction and triggering at high rapidities. In order to run at a few 10^{32} $cm^{-2}s^{-1}$ it is likely that the silicon would have to be replaced several times during a data run.

4. PARTICLE ID

It is clear that muon and electron identification with a large geometric coverage is important for B experiments. In 40% of beauty events one of the B's decays semi-leptonically, and the charge of the lepton then tags the flavor of that B at the time of decay. Similarly, hadronic ID can play a critial role. The identification of kaons in particular not only allows a reduction in combinatorial backgrounds and reflections, but also the possibility of tagging using the kaon from the subsequent charm decay. While lepton coverage is fairly standard in all experiments, hadron ID is more challenging, especially in the central region. In a forward geometry the B momentum is typically a few tens of GeV [3], which puts the kaons into a momentum range which is typical for fixed-target experiments. Also, this geometry allows significant real estate to be devoted to Cerenkov counters. Standard Cerenkov counters can therefore be used, although the high occupancy levels suggest the need for finely segmented RICH counters rather than traditional threshold counters.

For the central geometries the momentum range of the decay products extends up to only a few GeV. Depending on the trigger, the momentum spectrum of kaons in triggered events can extend quite high, so one would like K/π separation from a p_t of, say, 0.4 GeV to above 6 GeV. Also, the space available for detectors dedicated to particle ID is very limited in a central magnetic field. Time-of-flight systems can in principal provide adequate separation up to perhaps 1.5 to 2 GeV/c, depending on the time resolution and the path length of the system. The present CLEO system provides 2σ K-π separation to above 1 Gev [11]. dE/dX information using the tracking systems can contribute to higher pt, with a gap in coverage where the K and π dE/dX curves cross. The performance of such systems depends largely on the number of samples, for example the OPAL and ALEPH dE/dX measurements provide good K-π separation to high p_t [12], whereas the smaller number of samples with the central tracking chamber at CDF limits the significance of the separation at higher p_t. In combination with a TOF system studies for CDF indicate that a 2σ separation can be achieved out to a p_t of 5 Gev. [13]

Compact Cerenkov counters could extend this p_t range higher, and the development work looks very promising for counters using a liquid or solid radiator, a low gain gaseous chamber to allow the Cerenkov ring to spread, and a solid photocathode with, for example, CsI pads on a substrate. [14] These counters are thin, fast, and are efficient for Cerenkov light while being insensitive to minimum ionizing particles. While substantial development is still needed, it is possible that such counters can be built with a total thickness of 5 to 10 cm, making this technology suitable for placement between the tracking and magnetic coil or calorimeters in the central region.

5. CONCLUDING REMARKS

B physics at hadron colliders is already a broad on-going program and we are just learning how to do it, both in terms of the technology and the analysis techniques. The initial results from CDF are very encouraging and the upgrades to CDF and D0 will extend this program in the future to include the study of rare decays, B_s-mixing, and CP-asymmetries. Over the next few years the efficiencies and dilutions will be measured for lepton tagging, and for tagging via associated pions, allowing reliable estimates to be made for the future.

Achieving sufficiently high data rates and background rejection requires the development of high speed data acquisition and triggering, and precision vertex detectors. While the D0 and CDF detectors, and the major detectors planned at SSC and LHC are primarily intended for high p_t physics, they will be capable of extensive B physics. The full exploitation of the potential at hadron colliders may however require a dedicated experiment, optimized for low p_t and very high rates, perhaps with a forward geometry. The choice of rapidity coverage, forward versus central, is driven by the issues of trigger strategies and rates, vertex detector design and tracking performance, and particle ID. The requirements for these capabilities, and the performace of the different approaches are studied by the working groups at this workshop.

6. ACKNOWLEDGEMENTS

This talk covers just some of the technical issues, those which the author considers most critical. It of course includes information from many sources, some of which are referenced. The author wishes to thank many people for their illuminating discussions and comments which are represented here. Any errors and omissions are his.

7. REFERENCES

1 D0 Upgrade Proposal : Fermilab p-823
2 SSC Expression of Interest: Bottom Collider Detector SSCL-SR-1163
Proposal for a B Physics Experiment at TeV I - The μBCD and addendum: Fermilab p827
3 A Dedicated Beauty Experiment for the TeVatron Collider: Fermilab p-845. A similar experiment, COBEX, is proposed for the LHC
4. Gronau, Nippe, Rosner, Phys. Rev. D 47(1993)1988
5. For example:
Aleph, Nuc. Inst. and Meth. A315(1992)121
Delphi, Nuc. Inst. and Meth. A303(1991)233
L3, Nuc. Inst. and Meth. A315(1992)191
6. Nuc. Inst. and Meth. A289(1990)388,
Nuc. Inst. and Meth. A315(1992)125
7. Nuc. Inst. and Meth. A315(1992)139
8. CDF note #1872: The Silicon Vertex Tracker
9. Progress Report on the RD2 Project CERN/DRDC/93-18
10. For example:
Study of the Effects of Neutron Radiation on Silicon Detectors, Nuc. Inst. and Meth. A315(1992)156
Type Inversion in Silicon Detectors, Nuc. Inst. and Meth. A311(1992)98
11. For example: CLEO, Nuc. Inst. and Meth. A320(1992)60
12. For example:
OPAL, Nuc. Inst. and Meth. A305(1991)91
ALEPH, Nuc. Inst. and Meth. A306(1991)446
13. Proposal for an Upgraded CDF Detector : CDF Note # 1172
14. For example:
B. Hoeneisen, D. Anderson and S. Kwan, Nuc. Inst. and Meth. A302 (1991) 447
S. Kwan And D. Anderson, Nuc. Inst. and Meth. A309 (1991) 190
D. Anderson, S. Kwan, V. Peskov and B. Hoeneisen, Nuc. Inst. and Meth. A323 (1992) 626

DESIGN CHOICES AND ISSUES IN FIXED-TARGET B EXPERIMENTS

LESLIE CAMILLERI
PPE Division, CERN
1211 Geneva 23, Switzerland

1. THE PHYSICS MEASUREMENTS

1.1 CP Violation

The main priority of any experiment on B physics in the years to come will be an endeavour to observe CP violation in the B sector [1]. This can be attempted in several ways as described in the theoretical talks in this workshop.

a) A measurement of the CP asymmetry

$$A = \frac{\left(\overline{B}^0 \to f\right) - \left(B^0 \to f\right)}{\left(\overline{B}_0 \to f\right) + \left(B^0 \to f\right)},$$

where f is a self-conjugate state, will yield a measure of the angles α, β, and γ through a measurement of $B_d^0 \to \pi^+\pi^-$, $B_d^0 \to \psi K_S^0$, and $B_s^0 \to \rho^0 K_S^0$ respectively. In order to determine whether the observed decay originated from a B^0 or a $\overline{B}^0$, the nature of the companion B must be ascertained, most probably through the sign of the lepton or the kaon it decays to. A measurement of these three angles will overconstrain the unitary triangle shown in Fig. 1.

b) The angle γ can also be determined by measuring six self-tagging reactions [2].

$$B_d^0 \to \overline{D}^0 K^{*0},\ D^0 K^{*0},\ D_1^0 K^{*0} \quad \text{and} \quad \overline{B}_d^0 \to \overline{D}_0 K^{*0},\ D^0 \overline{K}^{*0},\ D_1^0 \overline{K}^{*0},$$

where D_1^0 denotes the decay of a D^0 into CP eigenstates, such as $\pi\pi$, $\pi\pi\pi\pi$, KK, and $KK\pi\pi$. Constructing the triangles shown in Fig. 2 will yield a measurement of γ. Note that all six reactions are characterized by at least four tracks not coming from the primary vertex.

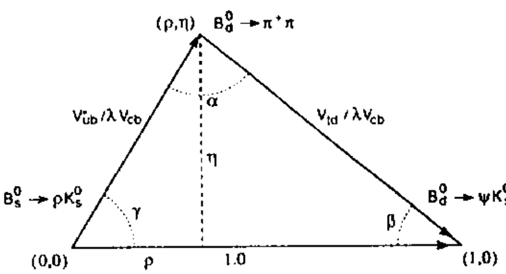

Figure 1. The unitary triangle.

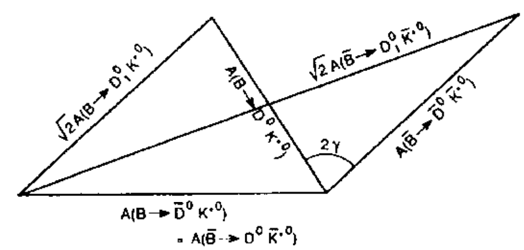

Figure 2. Self-tagging processes arranged in two triangles giving the angle γ.

1.2 B_s^0 *Oscillations*

These are expected to be very fast and hadron machines may well be the only way to observe them. They could be observed in the decay

$$B_s^0 \rightarrow D_s^{\pm}\pi^{\mp}$$
$$\hookrightarrow \phi\,\pi^{\pm}$$
$$\hookrightarrow K^+K^-$$

Here again the reaction involves four tracks originating at secondary vertices. At LHC fixed-target conditions ($\sqrt{s}$=114 GeV) the oscillation length is of the order of 1 cm for $x_s \approx 12$. Vertex resolutions of ≈ 1 mm are therefore needed.

1.3 *Rare Decay Modes*

The inclusive reactions $B \rightarrow \mu^+\mu^-X$ and $B \rightarrow e^+e^-X$ as well as the exclusive channels $B \rightarrow \mu^+\mu^-$ and $B \rightarrow e^+e^-$ could be observed using a lepton trigger. In the latter case the Standard Model predicts [3] a branching ratio of ~ 10^{-9}. Any deviations from this number could point to new physics. For instance a two Higgs Doublet extension would predict [4] a branching ratio of 10^{-8} for $m_t \approx 150$ GeV/c^2, $m_H < 400$ GeV/c^2, and small tan β.

1.4 *Tagging*

For those reactions which are not self-tagging the nature of the companion B must be determined. Experimentally this is most easily done by determining the sign of the lepton in its semi-leptonic decays. However, this is costly in event numbers as only 21% of the B's decay to an electron or a muon. Furthermore, mistags can occur because of the observed leptons originating from the $B \rightarrow D \rightarrow {}^-$ chain, from π/K decays, or from π/μ or π/e misidentifications. These mistags can be reduced by requiring the lepton to have $p_T > 1.2$ GeV/c. The efficiency of this cut is 0.8 for B's and results in

$$\omega = \frac{\text{wrong tags}}{\text{all tags}} = 0.17.$$

The nature of the companion B can also be determined by measuring the sign of the charged kaon in the $B \rightarrow D \rightarrow K$ chain. More events are retained this way as 50% of the B's result in a charged kaon. Mistags are due to $B \rightarrow D\overline{D}$ decays and Cabibbo suppressed decays. For kaons $\omega = 0.16$.

In principle, it is also possible to tag by directly measuring the charge of the companion $B^{\pm}$, either in a very strong magnetic field or by reconstructing all the decay charged particles.

Finally, as explained in an earlier talk, the effect of oscillations of the companion B results in a value of

$$\overline{\omega} = \frac{\text{wrong tag}}{\text{all tag}} = 0.25.$$

1.5 *Checks*

Because the initial state is pp rather than $\overline{p}p$, the B^0 and $\overline{B}^0$ production rates will not necessarily be the same [5]. Before a CP asymmetry can be measured these production rates will, of course, have to be known. This can be done by measuring the reactions

$$B^0 \rightarrow J/\psi K^* \qquad \overline{B}^0 \rightarrow J/\psi \overline{K}^*$$
$$\hookrightarrow K^+\pi^- \qquad\qquad \hookrightarrow K^-\pi^+$$

These reactions are expected to have a branching ratio that is three times bigger than the $J/\psi K_S^0$ decays and they will of course be automatically included in a J/ψ trigger. Furthermore, they are not expected to exhibit CP violation and they are self tagging. Because of this latter property an observation of this reaction will yield a measurement of dilution effects in "companion B tagging".

The production rates for B^+ and B^- will also need to be known in order to compute $\overline{\omega}$. Here the reaction $B^{\pm} \rightarrow J/\psi K^{\pm}$, which will also be included in a J/ψ trigger, can be used.

Both these reactions will need particle identification.

These measurements imply the following requirements of the experiment.

a) *Trigger*
- A muon trigger will be sensitive to J/ψ reactions and muon tags.
- An electron trigger will double the number of lepton events.
- In order to include kaon tags and self-tagging reactions, the experiment must not rely entirely on lepton triggers. Secondary vertex triggers and hadron p_T triggers should be included in order to have the maximum flexibility.

b) *Detector*
- Vertex detector.
- Particle identification.
- Good momentum resolution.
- Electromagnetic and hadronic calorimeters.
- Muon detector.

2. QUESTIONS AND ISSUES

The following issues have to be addressed.

- Collider or fixed-target mode?
- If fixed target, extracted beam or internal target?
- If internal target, gas jet or wire target?
- If a gas jet, hydrogen or a heavy gas?
- Beam pipe design.
- Silicon microvertex design and radiation damage.
- K_S^0 decay path.
- Particle identification.
- Momentum resolution.
- Order of detectors.

2.1 *Collider or Fixed Target*

- The mean B flight path is much longer in a fixed-target mode than in a collider mode (Fig. 3). Furthermore, the target region in fixed-target can be limited to a few millimetres compared with several centimetres in a collider mode. This makes for much easier separation of a secondary vertex from the primary vertex, even at the trigger level.
- Owing to the lower $\sqrt{s}$ in fixed-target mode, the associated multiplicity is lower (Fig. 4). Comparing a fixed-target spectrometer having an acceptance of 3.5–87 mrad with a forward collider [6] one having an acceptance of 5–600 mrad, the mean charged multiplicity associated with a B is 9.5 as against 30.3 and the mean number of associated K_S^0 is 0.9 as against 1.9.
- Whereas the p_T distribution of secondaries from B decays is the same for fixed-target and collider modes, the p_T distribution of minimum bias events is much steeper in fixed-target than in collider modes. This results in a hadronic p_T trigger having a rejection of 6×10^{-4}

against minimum bias events in fixed-target mode and only 5×10^{-2} in collider mode for an efficiency for $B \rightarrow \pi^+\pi^-$ of 0.80 in both cases.

- The momenta are higher in fixed-target mode resulting in less multiple scattering.
- In the case of an extracted beam there is no need for a beam pipe or roman pots.

But of course the cross-section [7] is smaller in fixed-target mode by a factor of 500 and the signal to noise ratio is also worse by a factor of 200.

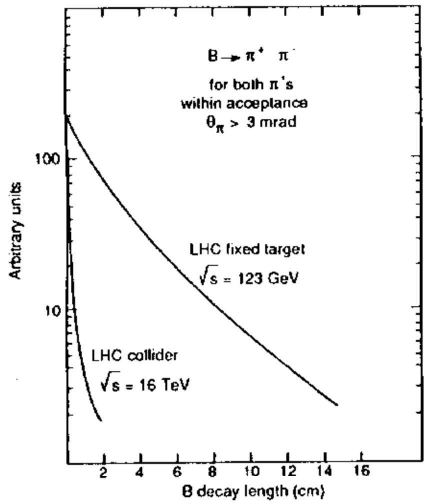

Figure 3. The decay path distributions of B mesons decaying to $\pi^+\pi^-$ for fixed-target and collider modes at the LHC. The π^+ and π^- are required to have a production angle greater than 3 mrad.

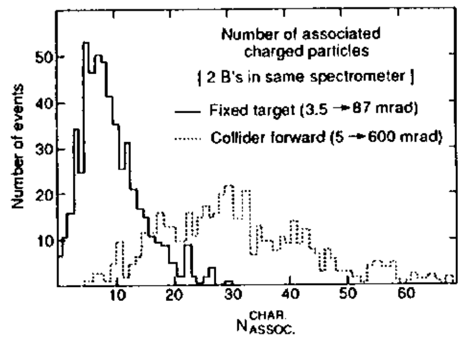

Figure 4. The charged-particle multiplicity associated with B mesons for fixed-target (3.5–87 mrad) and collider (5–600 mrad) geometries at the LHC.

2.2 *Extracted Beam*

At the LHC and SSC a continuously extracted beam can be obtained using channeling by a bent crystal placed in the halo of the beam. The halo particles are guided by the bent crystal planes and deviated by ~ 0.7 mrad. The principle was tested [8] using a 120 GeV beam at the CERN SPS. The counting rate in a counter telescope is shown in Fig. 5 as a function of crystal orientation. A clear peak is observed. Channeling efficiencies of 10–12% have been measured. Both the SFT [9] and LHB [10] proposals intend to use this technique.

Table 1 is a summary of running or proposed extracted beam B experiments. It can be seen that the longitudinal target dimension varies from 0.2 cm to 18 cm and that the target thicknesses are several tens of per cent of a radiation length and several per cent of an interaction length. This results in many conversions and secondary interactions thus increasing the multiplicity in an event and producing "fake" secondary vertices. The beam intensities vary from 2.5×10^6 to 4×10^9 particles per second (2×10^8 for SFT and LHB)

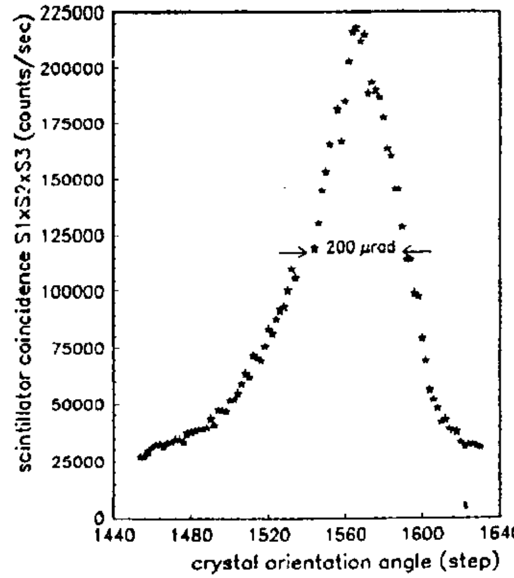

Figure 5. The counting rate in a scintillator counter telescope as a function of crystal orientation in a bent crystal extraction test at the SPS.

Table 1. A summary of extracted beam experiments.

Experiment	Beam intensity (protons/s)	Target Type	(%X_0)	(%λ_{int})
WA92 [11]	$2.5 \times 10^6(\pi^-)$	2 mm Cu	14	1.3
E771 [12]	4.6×10^7	24 mm Si	25	4.1
E789 [13]	3.0×10^9 [During flat top]	3 mm W	86	3.1
P865 [14]	4×10^9 [During flat top]	2 mm W	57	2.1
P867 [15]	1.2×10^8	24 mm Si	25	4.1
SFT [9]	2×10^8	18 mm Si 90 planes over 18 cm	19	7.7
LHB [10]	2×10^8	7.5 mm Cu	52	5

2.3 *Internal Target*

2.3.1 Gas jet

An experiment using a gas jet in the circulating beam of a collider uses a beam of

$$\text{EFFECTIVE INTENSITY} = \text{NUMBER OF CIRCULATING PROTONS} \times \text{REVOLUTION FREQUENCY}$$
$$= (1.5 \times 10^{14}) \times 3441 = 5.2 \times 10^{17} \text{ p/s at SSC}$$
$$= (4.8 \times 10^{14}) \times 11246 = 5.4 \times 10^{18} \text{ p/s at LHC.}$$

This is ten orders of magnitude more than an extracted beam and therefore allows the use of a very thin target such as a gas jet. This in turn implies no conversions, no secondary interactions, and no multiple scattering in the target.

A molecular hydrogen cluster target has been used [16] for seven years in the SPS collider by experiment UA6. The design is shown in Fig. 6. Hydrogen gas is pumped through a 0.1 mm nozzle cooled to 25 K. Saturation occurs on the other side of the nozzle and clusters of ~ 10^5 molecules are formed. This cluster jet is collimated using a skimmer and diaphragms. It then traverses the circulating beam and is absorbed in a cryopump. In UA6 the jet profile at the beam was 2.5 mm transverse to the beam and 8 mm along the beam, and its density was 4×10^{14} p/cm^3. The integrated density along the beam was 3.2×10^{14} p/cm^2. For use in the proposed GAJET B experiment [17] the longitudinal dimension of the jet must be reduced to about 2 mm, while maintaining approximately the same integrated density. This can be done by reducing the size of the diaphragm and skimmer holes, reducing the distance between the nozzle and the circulating beam from 22 cm to 13 cm, and increasing the gas throughput by a factor of 1.7. This should result in a 2 mm long jet with an integrated density of 3.8×10^{14} p/cm^2. It must be ascertained that no diffuse gas remains in the vicinity of the jet. The upper limit on this number from UA6 is 5% of the peak density.

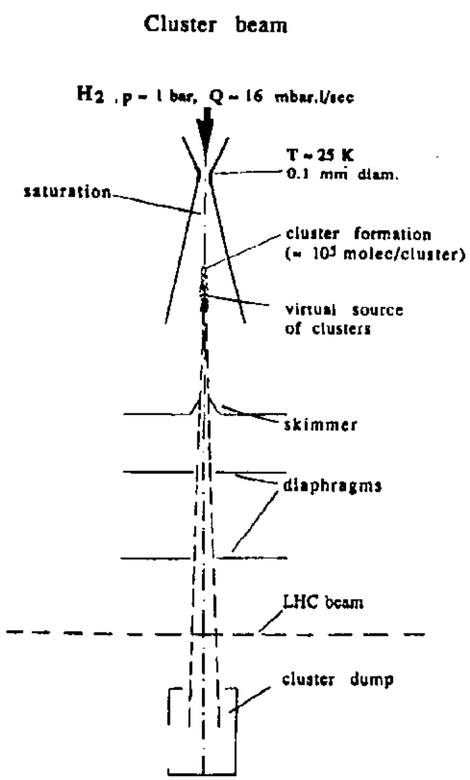

Figure 6. The UA6 molecular cluster jet design.

2.3.2 Wire target

This is a method advocated by the proponents of the HERA B experiment [18]. Eight 50 μm steel wires would be placed in the halo of the 820 GeV proton beam at about 4 beam σ's from the centre. They would be arranged in two groups of four wires 5 cm apart, as shown in Fig. 7. A wire target is favoured by this group over a gas jet as it only affects the particles in the halo, which are in any case lost to the main ep experiments; it needs a simple scraper type mechanism rather than big pumping stations and it produces no diffuse gas. However, a sudden movement of the beam could result in large increases in counting rates, whereas with a gas jet a movement of the beam can only reduce the counting rate. The technique was tested with a single wire and was shown to produce stable counting rates five minutes after moving the wire into position. Also, no background increase was observed in the ep experiments.

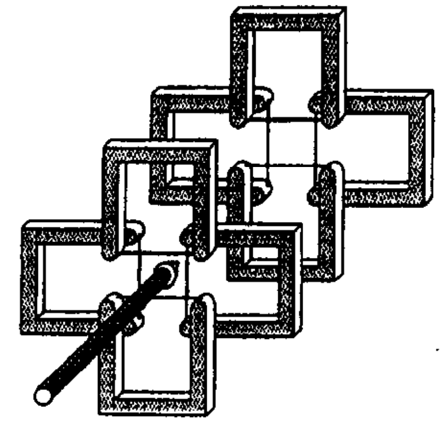

Figure 7: The eight-wire configuration of the HERA B proposed internal target.

2.4 The Use of Heavy Gases in a Jet

The following applies to metallic targets as well. It is expected that the $B\overline{B}$ production cross-section will be proportional to A^{α}, where A = atomic weight of the target and $0.9 < \alpha < 1.0$. On the other hand, the total cross-section is known to be proportional to $A^{0.72}$. The ratio of the $\sigma_{B\overline{B}}$ to σ_{tot} will therefore be F times what it is in hydrogen where $F = A^{\alpha - 0.72}$. For argon (A = 40) and $\alpha = 0.95$, F is equal [19] to 2.3. Therefore, for a given number of minimum bias events there will be 2.3 times more $B\overline{B}$ events in argon than in hydrogen. Hence a better signal-to-noise ratio for $A \neq 1$ targets.

There is however a price to pay.

- Both the multiplicity associated with a $B\overline{B}$ pair and the multiplicity in minimum bias events are about a factor of 2 higher in pA collision than in pp collisions, thus increasing the complexity of events [20].
- In pA collisions the production cross-section for pions [21] of $p_T > 2.0$ GeV/c is proportional to $A^{1.15}$. As an example, for a copper target (A = 64) the cross-section for pion production per nucleon is 1.9 times bigger than the pp cross-section. The difference in p_T distribution between minimum bias events and B events is thus reduced in pA collisions.

A summary of the luminosities, interaction rates, and numbers of minimum bias events per bunch is given in Table 2 for SFT, LHB, GAJET, and HERA B. The number of interaction rates varies from 0.1 per bunch for SFT to 4.0 per bunch for HERA B.

Table 2. Cross-sections, luminosities and interaction rates for proposed fixed-target experiments on CP violation.

	$\sigma_{B\overline{B}}$ per nucleon (μb)	σ^{pA}/A = effective σ^{inel} per nucleon (mb)	Luminosity	Interaction rate (MHz)	Bunch spacing (ns)	Min. bias events per bunch
SFT	1.5	14	5×10^{32}	7	16	0.1
LHB	1.0	11	8×10^{32}	9	25	0.2
GAJET	1.0	35	2×10^{33}	70	25	1.8
HERA B	0.01	10	4×10^{33}	40	100	4.0

2.5 *Beam Pipe Design*

For experiment using an internal target, the B decay products must traverse the storage ring beam pipe. It must therefore be carefully designed to minimize the amount of material. In particular, heavy flanges and septum plates must be avoided. Glancing incidence on even very thin pipes can result in traversals of several radiation lengths of material [22]. The silicon microvertex detector must be housed inside the beam pipe in roman pots.

2.6 *Silicon Microvertex Detector*

In the case of experiments using an external beam, the microvertex detector can be placed immediately following the target (LHB) or can actually constitute the target (SFT). In both cases the B's have enough flight path to decay within the microvertex detector. This makes the pattern recognition problem much easier, as demonstrated by the WA92 experiment at CERN [23]. The direct observation of decay vertices within the microvertex detector is a distinct advantage of an extracted beam over all other methods of studying B production.

The SFT active target design consists of 90 planes of 200 μm thick silicon planes spread over 18 cm along the beam and followed by further reconstruction planes occupying 120 cm along the beam.

For a gas jet target or a wire target the silicon planes must be housed in roman pots. The minimum distance of approach to the beam, dictated either by radiation dose or by disturbance to the beam, together with the minimum production angle to be observed determines the position of these detectors along the beam. In the case of GAJET the detectors consists of nine 300 μm thick double sided reconstruction planes of 25 μm pitch. These reconstruction planes, together with six additional trigger planes, are located at distances varying between 40 cm and 400 cm from the jet. They can be located in individual pots or grouped in a few pots following the design pioneered by P238: partial vacuum within the pots allows very thin walls [24]. The decay vertices can be reconstructed with a precision of ± 1 mm along the beam and ± 20 μm transverse to the beam.

2.7 *Radiation Damage to the Silicon Microvertex*

The radiation dose, D, absorbed in 10^7 s by a strip located at a distance of R cm from the beam is given by [25]

$$D = 2.66\times10^{-14}\Phi$$
$$= 4.2\times10^{-13} + \sigma_{tot}\frac{dN}{d\eta}\cdot\frac{1}{R^2}\ \text{MRad}$$

where

Φ = fluence (particles per cm^2)
+ = instantaneous luminosity
σ_{tot} = total cross-section
$dN/d\eta$ = number of particles per unit of rapidity.

The dose is essentially independent of the distance ALONG the beam at which the detector is placed but depends critically on the transverse distance R from the beam. For a given luminosity, the maximum dose tolerable [26] by the silicon will determine the minimum distance R_{min} at which the detectors can be placed. For a desired angular coverage, this in turn will fix the distance along the beam at which the detectors must be placed.

As an example, for GAJET running at 2×10^{33} cm^{-2} s^{-1} a dose of 20 MRad/year is expected for a strip 7 mm from the beam.

In the case of an extracted beam there is an extra complication because, in order to capitalize on the fact that in these experiments the B decay vertex can occur within the vertex detector, the beam must also go through the vertex detector. This would quickly destroy the silicon at the spot traversed by the beam. The solution is to spread the radiation damage due to the beam over an area S cm^2. The LHB solution is to move the vertex detector over an area of 10×10 cm^2, whereas SFT intends to use a beam of 8 cm diameter. Either solution necessitates a vertex detector of much larger dimensions than would be needed with a fixed narrow beam. The fluence is than given by [25].

$$\Phi = (10^7 s)\,(N_p)\times(1 + L_T\langle N_{ch}\rangle f_{pA}\, f_{SI})/s$$

where

N_p = Number of protons per second in the beam
L_T = Target thickness in units of interaction length
$\langle N_{ch}\rangle$ = Mean number of charged particles per interaction
f_{pA} = Nuclear enhancement of multiplicity ≈ 2
f_{SI} = Enhancement of multiplicity due to secondary interactions and conversions ≈ 2.

A comparison of LHB with GAJET, both at a luminosity of 10^{33} cm^2 s^{-1}, results in LHB expecting a dose of 2.4 MRad everywhere, whereas GAJET expects a maximum of 7.5 MRad at 0.7 cm from the beam. The extracted beam experiment expects a smaller maximum dose because of its ability to spread the radiation damage of the beam over a large area.

2.8 K^0_S *Decay Region*

It is necessary to allow a significant distance for the K^0_S to decay before the magnetic analysis. The mean decay length at the LHC fixed target is 8.6 m. In order to maximize the distance available for K^0_S decay GAJET is investigating the possibility of installing the RICH in front of the magnet.

2.9 *Particle Identification*

Discrimination between pions and kaons is necessary for kaon tagging and to avoid the contamination of the $B\to\pi\pi$ sample by $B\to K\pi$ decays. The latter is the most difficult problem because of the high momenta of the pions in $B\to\pi\pi$ events (Fig. 8). Rejecting candidate events with momenta larger than 250 GeV/c would result in an efficiency of only 50%. Extending the upper momentum cut to 600 GeV/c would recover most of the lost events.

The SFT Collaboration proposes to use a 12 m long neon-filled RICH. The Cherenkov photons are to be observed in an array of multianode photomultipliers. These are preferred over TEA or TMAE filled wire chambers because of

- small (< 2 ns) dispersion in collection time
- no need for high temperature or low pressure
- no need for ultra-pure radiator gas (TEA is only sensitive to UV photons and hence is very sensitive to oxygen contamination).

The upper limit in momentum for π/K discrimination at the 2 standard deviation level is shown in Fig. 9 as a function of anode pad size. It can be seen that discrimination can be obtained for momenta up to 300 GeV/c for a pad size of 3 × 3 mm^2.

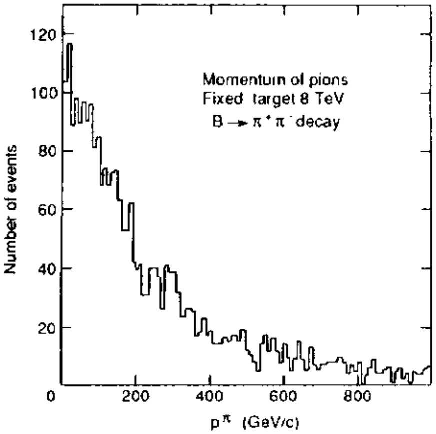

Figure 8. The momentum distribution of π's from $B \to \pi^+\pi^-$ in a LHC fixed-target mode.

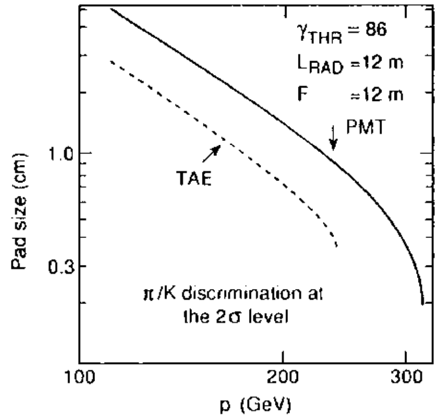

Figure 9. The momentum up to which pions and kaons can be separated as a function of the pad size of the multianode photomultiplier used to detect the Cherenkov photons.

Another very interesting new idea, currently being investigated by P865, is the use of Visible Light Photon Counters instead of phototubes or wire chambers.

Beyond these momenta it should be possible to use transition radiation detectors for π/K separation. GAJET is proposing to use 100 modules of the type developed for ATLAS in the RD6 project [27]. Each module consists of 12×15 µm thick polypropyiene foils separated by 370 µm and of one plane of 4 mm diameter Xe-filled straw tubes separated by 8 mm. Defining a "hit" as a tube containing an energy deposition greater than 5 keV (where a minimum ionizing particle deposits 1.8 keV), the distribution of the number of hits along a track is plotted for pions and kaons of 400 GeV/c (Fig. 10a). The particles cannot be distinguished at low momenta, where both of them do not give transition radiation and at very high momenta where both of them do. However, between 150 and 450 GeV/c a kaon suppression factor of 10 can be obtained (Fig. 10b).

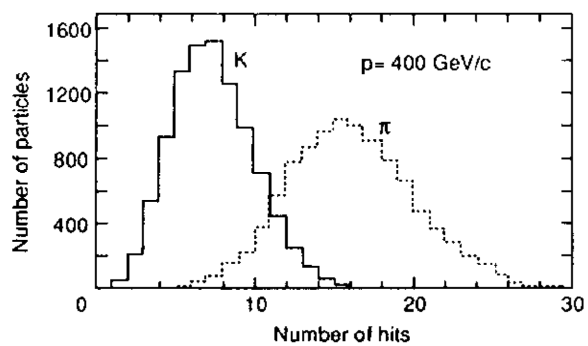

Figure 10a. The distribution of hits in a 100 plane TRD for pions and kaons of 400 GeV/c momentum.

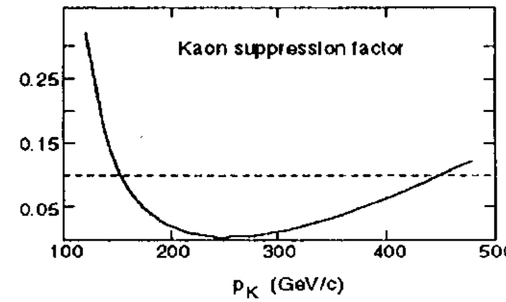

Figure 10b. The kaon suppression factor provided by the TRD as a function of momentum.

2.10 The magnetic spectrometer

It is expected that it will not be possible to link observed π^0's to a given decay vertex. It is therefore important to be able to distinguish between $B \to \psi K^0_S$ and $B \to \psi K^0_S \pi^0$ on the basis of the reconstruction of the ψ and the K^0_S only. The ψK^0_S invariant mass for the two modes is shown in Fig. 11 for a momentum resolution $\sigma_p/p = 10^{-4}$ p. For this momentum resolution the background for $\psi K^0_S \pi^0$ under the peak from ψK^0_S is small. However, worsening the momentum resolution would clearly broaden the peak and move more background to higher masses. Similarly for $B \to \pi^+\pi^-\pi^0$ and $B \to \pi^+\pi^-$.

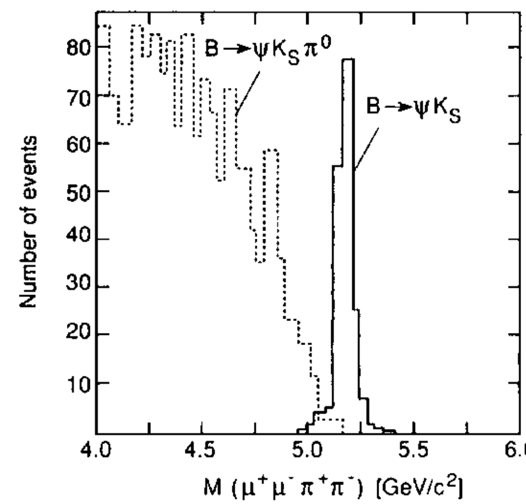

Figure 11. The invariant mass of ψK^0_S for $B \to \psi K^0_S$ and $B \to \psi K^0_S \pi^0$ assuming a momentum resolution of $\sigma(p)/p = 10^{-4}$ p.

2.11 Order of Detector Components

Several possibilities can be envisaged. GAJET, HERA B, P865 and P867 envisage the use of a single magnet, whereas SFT and LHB are thinking of two. As mentioned earlier, GAJET is advocating placing the RICH before the magnet unlike the other proposals. This maximizes the K_S^0 decay volume, and results in straight tracks from a point source in the RICH. In this configuration the magnet is closer to the calorimeter thus minimizing the effect of the magnetic bend on the p_T of a particle as calculated from calorimeter information alone.

3. FIRST-LEVEL TRIGGERS

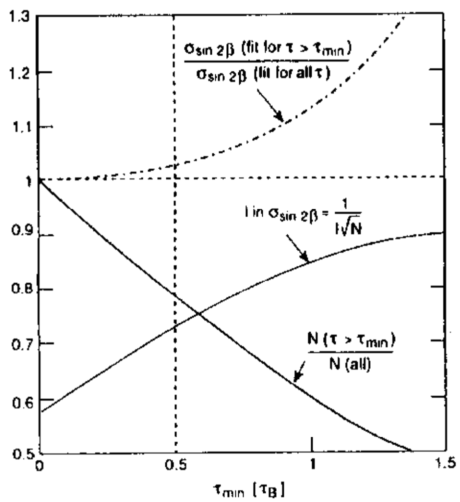

Figure 12. The proportion of the number of events retained, the fitting factor I, and the degradation in the error in sin 2β as a function of the lowest value of proper time, τ_{min}, used in the analysis.

It is assumed that the data will be pipelined over about 2.5 μs and that the first-level triggers should give a rejection of about 1000 in that time. Four types of triggers will be discussed – an optical discriminator, a silicon trigger, a p_T trigger, and a muon trigger. The first two select events with tracks not originating at the target and give rejections which are therefore correlated. In selecting events with a displaced second vertex, these two triggers necessarily reject B decays at small proper time. However, the CP asymmetry of these events is small and therefore rejecting them does not significantly worsen the error on the asymmetry. This is demonstrated in Fig. 12, which shows, as a function of the lower cut of the proper time τ_{min}, the number of events retained, the error on the asymmetry, and the fitting factor I, all normalized by their value at $\tau_{min} = 0$ (all events retained). For a cut at $\tau > 0.5\ \tau_B$, 22% of the events are lost but the error only worsens by 2%. This is therefore a useful cut.

3.1 The Optical Discriminator [28]

It consists of a shell of transparent material centred on the target. The index of refraction of the material is chosen such that Cherenkov light emitted in the shell by charged particles originating at the target is refracted out, whereas some of the light emitted by particles not pointing to the target is trapped in the shell by total internal reflection and emerges at the edge of the shell (Fig. 13). The principle was tested [29] by placing a LiF shell in a parallel beam (Fig. 14). For each particle a pseudo-impact parameter, b, could be calculated. It increased with distance from the middle of the crystal. The mean number of photoelectrons observed at the edge of the shell is plotted in Fig. 15 as a function of b. It can be seen that, as expected, very little light is trapped and collected at the edge for particles with b = 0 (i.e. particles simulating those originating from the target). Furthermore, the amount of collected light increases with b. However, it is obvious from the figure that the device tested is only sensitive to impact parameters above ~ 4 mm, whereas in a B experiment an optical discriminator must be able to trigger on impact parameters of a few hundred microns. The result of a Monte Carlo calculation which includes Fresnel reflection, refraction, chromaticity mirror collection efficiency, and quantum efficiency of the photomultiplier is also shown in Fig. 15 and agrees very well with the data. This program was therefore used to predict the behaviour of different optical configurations. For a shell of index of refraction n_1, immersed in a medium of index n_2, the condition NOT to collect light for particles with b = 0 is

$$1-\left(n_1^2-n_2^2\right)>0\ .$$

The closer this quantity is to zero the smaller will be the impact parameters that result in collected light. Furthermore, in order to obtain a sharp threshold and a large amount of collected light, this condition must be satisfied by as large a range of wavelengths as possible. Such an achromatic combination of n_1 and n_2 would be obtained with sapphire (Al_2O_3, n_1 = 1.8) coated with SiO_2 (n_2 = 1.5). For small impact parameters only light emitted in the last part of the shell is trapped. The amount of collected light can therefore be increased by replacing a single thick shell by several thinner concentric achromatic shells. The efficiency for retaining $B \to \pi^+\pi^-$ and minimum bias events as a function of a cut on the number of observed photoelectrons, N_{opt}, was calculated using the Monte Carlo described earlier, for the GAJET geometry (Fig. 16). An efficiency for $B \to \pi^+\pi^-$ of 0.62 and for minimum bias of 0.1 was obtained for $N_{opt} \geq 8$. This trigger has a very fast response time ~ 25 ns and could even give a decision in less than the bunch crossing time. It relies heavily on having a point target. Its rejection of minimum bias events worsens by a factor of 3 in going from a 2 mm long to a 7 mm long target because of minimum bias events produced at the edges of the target simulating b ≠ 0 events.

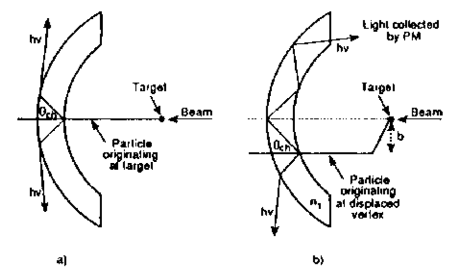

Figure 13: The principle of the optical discriminator. a) Cherenkov light refracted out of the shell for a particle originating at the target. b) Some Cherenkov light totally internally reflected to the edge of the shell for a particle not originating at the target.

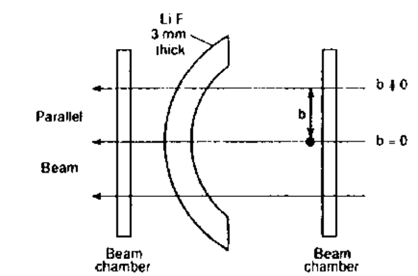

Figure 14. Test of an optical discriminator in a parallel beam. The off-axis particles simulate particles not originating at the target.

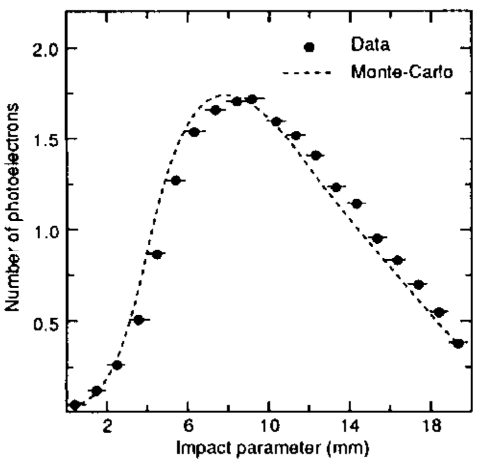

Figure 15. The mean number of photoelectrons as a function of impact parameter for data and Monte Carlo.

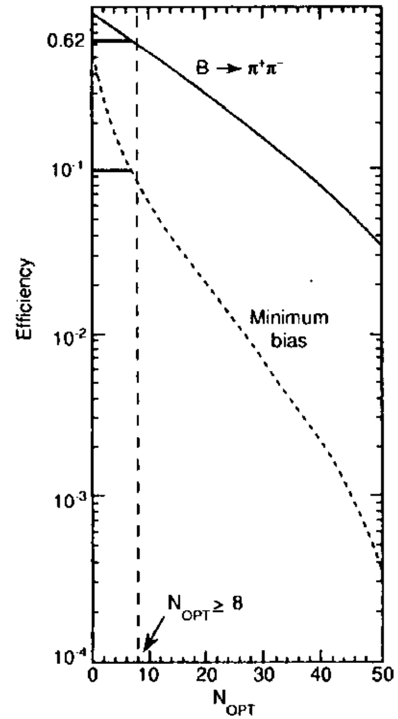

Figure 16. The efficiency of the optical trigger as a function of the lower cut on the number of detected photoelectrons for $B \to \pi^+\pi^-$ and for minimum bias.

3.2 *Secondary Vertex Trigger*

This would be based on silicon planes. For experiments with point targets (gas jets or wire targets) in which the primary vertex is automatically known, the preferred geometry to capitalize on the long flight path of the B is an r–Φ geometry. To reduce combinatorial background, each r–Φ strip can be divided into striplets. The trigger could be based on 3 planes, the number of striplets in each plane being the same but their dimensions increasing in proportion to the distance of the plane from the target. Thus a track originating at the target will intersect striplets of the same order number in the 3 planes and can be easily rejected. The trigger algorithm would

- reject hits that form 3-hit combinations, pointing to the target;
- form 3-hit combinations that point downstream of the target;
- require at least 3 such combinations.

A Monte Carlo program which includes multiple scattering indicates that a rejection of minimum bias events by more than a factor of 100 can be obtained for a 50% B efficiency. It is expected that this rejection can be obtained in less than 2.5 µs.

3.3 *Transverse Momentum Trigger for Hadrons and Electrons*

The energy and position information to form the p_T trigger can be obtained:

- either from the calorimeter; this is fast but has a worse resolution and is affected by the magnetic deflection;
- or from pad chambers and the magnet; this is slower and is affected by chamber occupancy; however, it is more accurate and computes the true p_T.

It may be that the best solution would be to use the magnetic bend algorithms in which the position information of the last pad plane is replaced by position information obtained from the calorimeter. The following calculation is based on calorimeter information only in the GAJET geometry.

An individual calorimeter cell (4×4 cm^2) consists of a scintillator tile S_1, 2 X_0 of lead, a scintillator tile S_2, an electromagnetic calorimeter cell of lead scintillator tile design, a hadron calorimeter cell. Using appropriate combinations of S_1, S_2, an electromagnetic cell and a hadronic cell, we can define signatures for charged hadrons, electrons, and photons. Overlapping clusters of 3×3 cells for electrons and 5×5 cells for hadrons can be formed. A Monte Carlo which includes multiple interactions, calorimeter resolutions, and the effect of the magnetic bending results in the efficiencies for triggering on a single hadronic cluster of $p_T \geq p_T^{HADR}$ shown in Fig. 17. In GAJET for $p_T^{HADR} > 2.6$ GeV/c the efficiency for $B \to \pi^+\pi^-$ is 54% to be compared with 0.9% for minimum bias events. The trigger efficiencies are 96% for $B \to J/\psi K_S^0$, $J/\psi K_S^0 \to e^+e^-$ compared with 1.7% for minimum bias events when triggering on $p_T^{elec} > 1$ GeV/c.

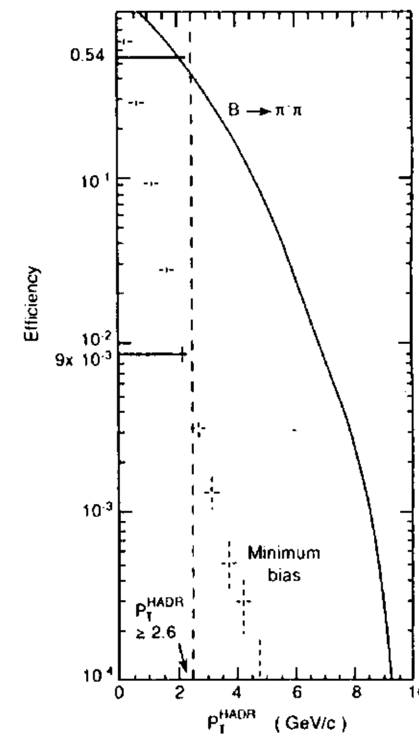

Figure 17. The efficiency of a hadronic p_T trigger as a function of the threshold on p_T^{HADR} for $B \to \pi^+\pi^-$ and minimum bias.

3.4 *Muon Trigger*

Both SFT and LHB advocate the use of three planes of Resistive Pad Chambers (RPC) for their muon trigger and Programmable Array Logic (PAL). SFT plans to use two planes between the magnet and the muon filter and one plane after the filter. For a given pad combination in chambers 1 and 3, the range of pads in chamber 2 corresponding to the minimum p_T to be triggered on is stored in the PAL.

In LHB all three RPC planes are placed behind the filter, thus reducing the occupancy (Fig. 18). Two magnets of equal and opposite deflection are used such that after the two magnets a track emerges parallel to its original direction but displaced by an amount which decreases with increasing momentum. The trigger is therefore based on selecting 3-pad combinations that point close to the target.

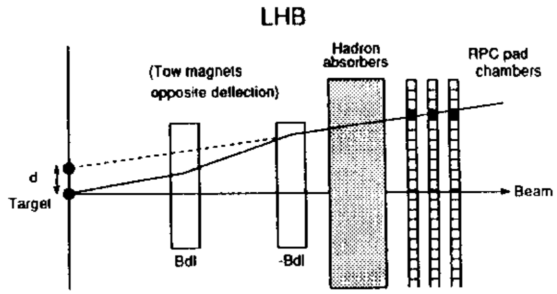

Figure 18. The LHB trigger scheme for muons.

4. COMPARISON OF SENSITIVITIES AND DIFFICULTIES

4.1 *Sensitivities*

The sensitivities of SFT, LHB, GAJET, and HERA B are contrasted in Table 3. The branching ratios of $B \to J/\psi K^0_S$, $J/\psi \to {}^{+},{}^{-}$, and $K^0_S \to \pi^+\pi^-$ have been taken to be 3.3×10^{-4}, 0.12, and 0.69 respectively. It is assumed that the angle β will be obtained from a time-dependent fit which minimizes the effect of oscillations in the primary B. Note that in the numbers presented by the collaborations.

- LHB has only used a lepton tag.
- HERA B, because of the very low B production cross-section, assumes a run lasting five times longer than the other proposals (but it proposes to use an existing machine!).
- There are still large differences in assumed reconstruction efficiencies (0.27 for GAJET compared with 0.57 for LHB).
- HERA B would benefit from an increase of the HERA proton energy from 0.8 TeV to 1 TeV.

Table 3. Sensitivity of SFT, LHB, GAJET, and HERA B for the $B \to J/\psi K^0_S$ channel

	SFT	LHB	GAJET	HERA
Time (s)	10^7	10^7	10^7	5.4×10^7
$b\bar{b}$	1.2×10^{10}	1×10^{10}	2×10^{10}	1.6×10^9
Hadronization	0.8	0.8	0.8	0.8
$\varepsilon_{acceptance}$	0.30	0.52	0.4	0.08
$\varepsilon_{reconstruc}$	0.66	0.57	0.27	
$\varepsilon_{trigger}$	0.70	0.64	0.62	0.7
ε_{tag}	0.57	0.16	0.36 (0.14 + 0.22)	0.67
$N(J/\psi K^0_S)$	33000	6800	10440	2610
D	0.26	0.75	0.5	0.5
I		0.57	0.72	0.82
$\Delta(\sin 2\beta) = 1/(ID\sqrt{N})$	±0.021	±0.038	±0.027	±0.065 (±0.050 at 1 TeV)

Errors on $\sin 2\beta$ of the order of ± 0.03 could be achieved with about 10,000 observed events in one year.

The corresponding numbers for the $\pi^+\pi^-$ mode are shown in Table 4. HERA B is not proposing to investigate this channel at present. Errors on $\sin 2\alpha$ of the order of ± 0.03 to 0.08 are anticipated.

Table 4. Sensitivity of SFT, LHB, and GAJET for the $B \to \pi^+\pi^-$ channel.

	SFT	LHB	GAJET
$\varepsilon_{acceptance}$	0.76	0.75	0.62
$\varepsilon_{reconstruc}$	0.55	0.23	0.39
$\varepsilon_{trigger}$	0.50	0.85	0.19
ε_{tag}	0.65	0.16	
$N(\pi^+\pi^-)$	2700	2200	7600
$\Delta(\sin 2\alpha)$	± 0.077	± 0.056	± 0.032

4.2 *Difficulties*

An attempt has been made to summarize the difficulties of the extracted beam, gas jet, and wire target approaches in Table 5. A "+" in a given column favours the corresponding method.

An extracted beam offers the advantages of a well-defined target (no surrounding halo), larger signal-to-noise ratio due to its use of a $A \neq 1$ target, better vertex resolution because of its ability to place silicon planes in the extracted beam, no beam pipe and roman pots, and smaller radiation damage. Its disadvantages are its thick target which results in multiple scattering, secondary interactions and conversions, its long target which makes triggering on secondary vertices more difficult, its increased associated multiplicity due to nuclear effects.

Table 5. Advantages (+) and disadvantages of the various fixed-target approaches to B physics.

	Extracted beam	H2 gas jet	Wire target
Well-defined target. (no diffuse gas)	+	?	+
Thin target (no sec. inter.)		+	+
$A \neq 1$			
Large $\sigma_{B\bar{B}}B/\sigma_{tot}$	+		+
Assoc. mult.		+	
Target length		+	+
Easy trigger on sec. vertex (optical+silicon)		+	+
p_T trigger		+	
Vertex resolution	+		
Beam pipe and roman pots	+		
Acceptance	?		
Radiation damage	+		

A gas jet offers a thin target with no secondary interactions, a short target making secondary vertex trigger algorithms faster, a lower associated multiplicity, and a better p_T trigger. However, it has a smaller signal-to-noise ratio, worse vertex resolution, a beam pipe and roman pots, and worse radiation damage.

A wire target offers a thin target with no multiple scattering, secondary interactions or conversions, a short target making it easy to trigger on secondary vertices, and a better signal-to-noise ratio. But it has a worse associated multiplicity, a beam pipe, roman pots, and worse radiation damage.

5. CONCLUSIONS

No single method stands out as the "obvious one". An extracted beam yields better vertex resolution and an internal target easier triggering.

A flexible and diverse triggering scheme is of prime importance in order to be sensitive to as many reactions as possible; the experiment should not be limited to lepton triggers only.

Proposed experiments (P865, P867, HERA B) at existing machines will be invaluable for testing new devices and strategies for the LHC and SSC experiments.

6. ACKNOWLEDGEMENTS

The help of the members of the various collaborations, and in particular of the GAJET Collaboration, in preparing this report is gratefully acknowledged.

7. REFERENCES

1. For a review of CP violation problems see, for instance, T. Nakada, *CP Violation in K and B Meson Decays*, PSI-PR-91-02.
2. I. Dunietz, *CP Violation with Self Tagging* B_d *Modes*, CERN TH-6161/91 (1991).
3. T. Inami and C.S. Lim, *Prog. Theor. Phys.* **65** (1981) 297.
4. J.L. Hewett et al., *Phys. Rev.* **D39** (1989) 250.
5. M. Chaichian and A. Fridman, *Measurement Possibilities of CP Violation for B-Decays in* pp *Collisions*, CERN TH-6068/91 (1991);
   A. Fridman, CERN EP/90-87 (1987);
   PYTHIA, H.U. Bengtsson and T. Sjöstrand, *Comp. Phys. Commun* **46** (1987) 43.
6. S. Erhan et al., *A Dedicated Collider B Experiment, Nucl. Instrum. and Methods* **A333** (1993) 101.
7. P. Nason et al., *Nucl. Phys.* **B303** (1988) 607, **B327** (1989) 49, **B335** (1990) 260.
8. H. Akbari et al., CERN/SL/93-28 (DI), submitted to Physics Letters.
9. *An Expression of Interest in a Super Fixed Target Beauty Facility (SFT) at the Superconducting Super Collider*;
   Fixed Target B Physics at Fermilab and the SSC, S. Conetti, *Nucl. Instrum. Methods* **A333** (1993) 142.
10. F. Costantini, LHB, *Nucl. Instrum. Methods.* **A333** (1993) 125.
11. *A Measurement of Beauty Particle Lifetimes and Hadroproduction Cross-Section*, CERN SPSC 90-10, SPSC/P251 (1990).
12. *A Proposal to Study Beauty Production and other Heavy Quark Physics associated with Dimuon Production in 800 (925)* GeV/c pp *Interactions*, Fermilab proposal 771 (1986).
13. *Study of Two-Prong Decays of Neutral B Mesons and* Λ_b, Fermilab proposal P789 (1988).
14. *High Sensitivity Study of Charm and Beauty Decays*, Fermilab proposal P865 (1993).
15. *A Proposal to Continue the Study of Hidden Charm and Beauty States by Triggering on High Transverse Momentum Single Muons and High Mass Dimuons in 800* GeV/c pN *Interactions*, Fermilab proposal P867 (1993).
16. A. Bernasconi et al., Phys. Lett. **206** (1988) 163;
    L. Dick and W. Kubischta, *Physics with Jet Targets at the SPS* $p\bar{p}$ *Collider in Hadronic Physics at Intermediate Energies*, ed. T. Bressani and R.A. Ricci (Elsevier Science Publishers B.V., 1986), p. 209.
17. Y. Lemoigne, *A CP Violation Gas Jet Experiment for the CERN LHC, Nucl. Inst. Meth.* **A333** (1993) 113.
18. *An Experiment to Study CP Violation in the B System Using an Internal Target at the HERA Proton Ring*, DESY PRC 92/04 (1992) and W. Hofman, *Nucl. Instrum. Methods* **A333** (1993) 153.
19. A. Fridman and B. Penzo, *Remarks about* B *Production in* pA *Collisions with a* p-*Beam of* 8 TeV, CERN PPE/91-58 (1991).
20. FRITIOF, B. Andersson et al., LU-TP-92-20 (1992).
21. J.W. Cronin et al., *Phys. Rev.* **D11** (1975) 3105.
22. K.T. McDonald, *Beam Pipes for Foward Collider Detectors*, Princeton/HEP/92-05 (1992).
23. L. Rossi, private communication.
24. *Study of Beauty Physics at the SPS Collider with Real Time Use of Silicon Microvertex Information*, CERN SPSC/88-33, 89-43, 89-55 and 89'-61, SPSC/P238, and J. Ellett et al., *Nucl. Instrum. Methods* **A317** (1992) 28.
25. G. Carboni, *Radiation Damage to Microvertex Detectors*, LHB-Note-1 (1991).
26. G. Hall, *Radiation Resistance of Semiconductor Detectors and Associated Electronics*, in *Proceedings of the Large Hadron Collider* Workshop, Aachen 1990, eds. G. Jarlskog and D. Rein, CERN 90-10 (1990) Vol. III, p. 693, .
27. *Integrated High Rate Transition Radiation Detector and Tracking Chamber for the LHC*, CERN/DRDC/90-38, DRDC/P8 (1990).
28. *Study of Optical Trigger to be used for Beauty Search in Fixed Target Mode at LHC*, CERN DRDC 91-32 and 92-53, G. Charpak et al., *Nucl. Instrum. Methods* **A306** (1991) 439.
29. G. Charpak et al., *Nucl. Instrum. Methods* **A332** (1993) 91.

RECENT RESULTS ON B PHYSICS WITH CDF

JAMES A. MUELLER
Department of Physics and Astronomy, Rutgers University
Piscataway, NJ 08855, USA

1. INTRODUCTION

The existence of working b experiments at hadron colliders is a vital component in planning for CP violation studies in the B system. Not only do they extend our current knowledge of the production and decay of the b quark, they reduce the amount of extrapolation necessary in making decisions for the future. As our experimental and theoretical prejudices confront the reality of data, we obtain benchmarks with which to better design new experiments and upgrade existing ones. In May 1992, the drought of CDF data ended, as the Fermilab Tevatron resumed operations. This began what turned out to be a very successful year of running. Between the completion of detector commissioning and the end of the run, CDF wrote $\sim$ 21 pb$^-$1 of data to tape. Analysis is proceeding rapidly, and already two papers on b physics have been submitted for publication.

I will discuss the improvements made to CDF[1] for the 1992 run, as well as give a broad description on how we triggered on b events CDF. I will briefly review the results from the 1988 run on inclusive b production, with a little more detail on a study of $b\bar{b}$ correlated production. Then, I will discuss a measurement of the differential cross section made using fully reconstructed B mesons from a portion of the new data. The addition of a silicon vertex detector has made the study of b lifetimes possible at CDF, and I will discuss results on inclusive and exclusive measurements. Finally, I give some indication of what, we hope, is yet to come from the data we have taken and will take in the coming year. I will not discuss the longer range upgrade plans for CDF, as that as been covered elsewhere in this workshop.[2]

1.1 Detector Upgrades for Run 1A

A number of improvements were made to CDF in the long shutdown between the 1988 and 1992 runs. The Central Muon eXtension chambers (CMX) have been added which extend the η coverage from 0.6 to 1.0. Behind the original muon chambers(CMU), extra steel has been added, followed by the Central Muon uPgrade chambers (CMP), increasing the number of absorption lengths in this region from 5 to 8. The Central PreRadiator multiwire proportional chambers (CPR) were installed in front of the Central ElectroMagnetic calorimeter (CEM), but outside the 1.09 radiation lengths of material in the CDF solenoid.

These allow additional e/π discrimination. The readout electronics for the Central Tracking Chamber (CTC) have been modified to allow for dE/dX measurements. Calibration of the dE/dX information is in progress.

Finally, we added a silicon microstrip detector (SVX).[3] This is a four layer DC coupled, single sided silicon device. The hit resolution is 13 μm, with radii ranging from 3 to 8 cm. This gives an impact parameter resolution that varies from 40 μm for a 1.0 GeV/c track, to < 15 μm for high P_T tracks. It covers $|z| < 26$ cm, but since this is also the RMS spread of the interaction region in z, not all events in CDF have vertices within the fiducial volume of the SVX.

1.2 b Triggers for Run 1A

Currently and for the near future, CDF is primarily a high P_T experiment. Triggers for low P_T physics must obey the rule, "Contribute no deadtime to the top search." A brief discussion of the triggers relevant for b physics, may help people understand what physics might be done at CDF and on what time scale. These triggers are based identification of electrons and muons.

The trigger is divided into three levels. At Level1, we require at least one central muon stub or one CEM trigger tower ($\eta \times \phi = 0.2 \times 0.25$) with a $P_T(E_T) > 6$ GeV. For events with two or more lepton candidates, the threshold is lowered to 4 for the CEM tower and 3 for the muon stub. Since the P_T of the muon stub is measured only in the muon chambers, the resolution is poor, and the trigger turn on soft. For instance, the 3 GeV/c threshold has an efficiency that rises from 50% at 1.6 GeV/c to 90% at 3.1 GeV/c and reaches a plateau of 94%

At Level2, hardware EM clustering, and track finding[4] are run. The tracks are matched to the EM clusters or muon stubs, cuts are placed on the E_T of EM clusters and the P_T of tracks. The electron(muon) cuts are 9 GeV (9 GeV/c) for the single lepton triggers, and 5 GeV (3 GeV/c) for the ee, $e\mu$ and $\mu\mu$ triggers. In order to increase the acceptance for J/ψ events in the dimuon triggers, only one of the muon stubs was required to have a hardware track matched to it. In addition, a lower threshold single lepton trigger was installed specifically for b physics. The threshold was 6 GeV, but not all events were written to tape. The fraction of these triggers that was passed by Level 2 was automatically adjusted to soak up any available bandwidth, without violating the prime rule stated above.

Level3[5] consisted of a 1000 MIP microprocessor farm, in which a subset of the offline reconstruction software was run. The thresholds for the lepton triggers were matched to their Level 2 values, except the dimuon trigger, where the thresholds were lowered to down to 1.4 GeV/c. This matched the range out energy for muons passing through calorimeter. In addition to filtering, Level3 also selected 10% of the events for a special high priority data set. Since this split was made in the trigger, these events were available to the collaboration within hours of the data being taken. This stream mainly consisted of top candidates, W's, and other high P_T events. We were able to include a data set containing opposite sign dimuon events with mass between 2.8 and 3.4 GeV/c^2. All of the results from the 1992 run presented here come from these J/ψ events.

2. b PRODUCTION STUDIES

Determining b production cross sections provide an interesting test of QCD. Measuring B spectra also provide important engineering numbers for predicting the sensitivity of future experiments. CDF has used many methods of studying b production, and is using the

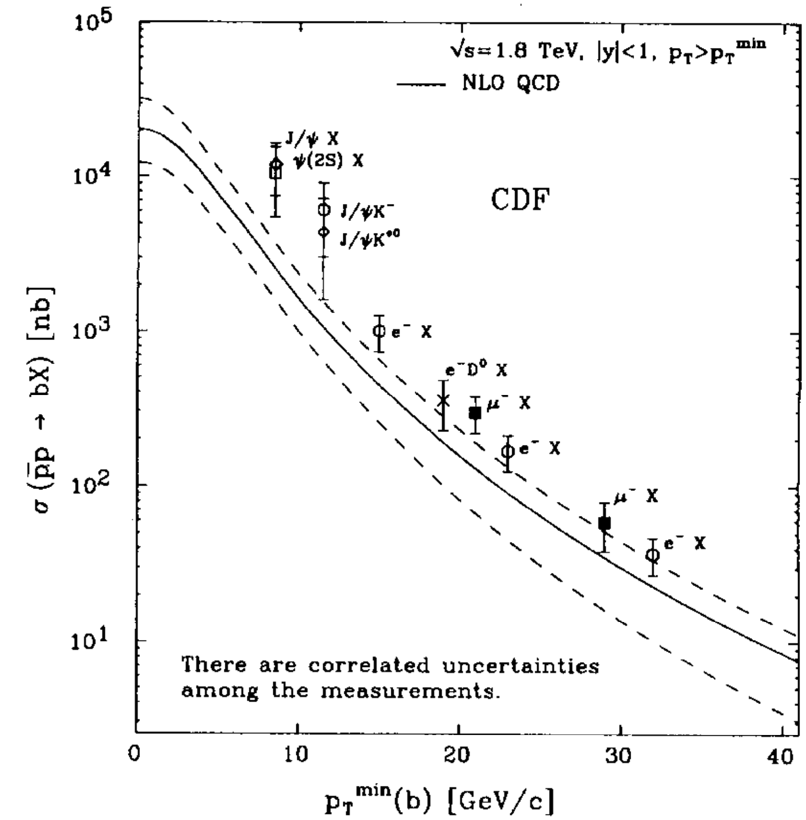

Figure 1: Summary of various CDF measurements of the cross section for b quark production with $P_T^b > P_T^{min}$. The solid line is a next-to-leading order calculation along with those obtained from varying parameters in the calculation.

new data to extend and refine these measurements.

2.1 Overview of 1988 data

A summary of the published CDF b cross section measurements is shown in Figure 1. Although measurements at lower energy[6] were in good agreement with the next-to-leading-order (NLO) QCD calculations,[7] the theory seems to slightly underestimate the cross section at the Tevatron. Here, I will try to list what the major sources of uncertainty were in the individual measurements, and how we will be able to reduce them with the 1992 data set.

Inclusive lepton cross sections[8,9] provided a high statistics measure of the b cross section at the Tevatron. The systematic uncertainties in these measurements, come from our level of knowledge of the backgrounds. Using the detector improvements in the current data we will be able to greatly reduce these uncertainties. The CPR will allow us to better estimate and reduce the amount of hadron fakes in the electron sample, while the level of hadron punch-through in the muon sample can be reduced by requiring muon confirmation in the CMP. Studies of lepton impact parameters in the SVX will allow a more accurate determination of what fraction of the leptons actually come from the decay of b hadrons.

We also measured the b cross section[8] using the semi-exclusive decay $B \rightarrow e^- D^0 X$. The improvements listed above will also lead to a better measurement in this channel. Just as important will be the increase in statistics that the lower lepton trigger thresholds and increased luminosity are providing.

Studies of charmonium production[10] provide an estimate of the b cross section at lower P_T. The excellent mass resolution of CDF, allows us to easily separate J/ψ, χ_c, and $\psi(2S)$ states from the background. Converting charmonium cross sections to b cross sections requires knowledge of the fraction of these ψ states that come from b decays. In these measurements we have used the theoretical assumption that charmonium production at the Tevatron is dominated by b and χ_c production. This predicts that the 100% of the $\psi(2S)$ events come from b's. Using the measured J/ψ and χ_c cross sections we can also determine this model dependent b cross section. With the addition of the SVX we now have vertex resolutions that are small compared to the b lifetime. This will allow us to separate the J/ψ's from prompt charmonium production from those from b decays in a model independent manner. As will be seen in the discussion on the lifetime analysis, there are indications that the fraction of J/ψ's that come from b might be smaller than derived from the above assumption.

The last two points on the curve come from fully reconstructed B meson decays![11] These measurement were limited by statistics. The triggers implemented for the 1992 run increased the acceptance for J/ψ events by over a factor of five. The integrated luminosity written to tape was also about a factor of 5 greater than in 1988. As will be discussed later, this increase in statistics are substantially increasing our physics reach with these decay modes.

2.2 $b\bar{b}$ Correlated Cross Section

The NLO calculations[12] predict correlations between the b and $\bar{b}$ quark. In addition to being an interesting check of the theory, measurements of these correlations indicate how we can use these models to predict tagging rates in future experiments. We have used the $e\mu$ data set from the 1988 run to examine some of these correlations![13]

Since a fake lepton will have no sign correlation with the other lepton, we use the difference in number of same sign and opposite sign $e\mu$ events ($\Delta_{e\mu}$) to measure the $b\bar{b}$ cross section. To calculate the number of $b\bar{b}$ events, we correct $\Delta_{e\mu}$ for events lost due to mixing, using the average mixing parameter χ. The number of $b\bar{b}$ events is then,

$$N_{b\bar{b}} = \frac{f_{b\bar{b}} \Delta_{e\mu}}{(1-2\chi)^2 \delta}, \tag{1}$$

where delta corrects for events where one of the leptons comes from the sequential decay, $b \rightarrow c \rightarrow l$. $f_{b\bar{b}}$ is the fraction of sign subtracted events due to $b\bar{b}$ as opposed to $c\bar{c}$ production. This is measured from the distribution of the component of the lepton momentum transverse to the direction of the associated jet (P_T^{rel}). This distribution is shown in Figure 2 for same sign (dashed histogram) and opposite sign (solid histogram) events. The difference of these distributions (points) is then fit to the shapes of the P_T^{rel} distributions for b and c decays obtained from Monte Carlo. The fit indicates $f_{b\bar{b}} = 1.0^{+0.0}_{-0.1}$.

We measure $N_{b\bar{b}}$ for electron $P_T \geq 5.0$ GeV/c and muon $P_T \geq 3.0$, 4.0, and 5.0 GeV/c. These cuts imply $P_T \geq 8.75$ GeV/c for one b and $P_T \geq 6.5$, 7.5, and 8.75 GeV/c for

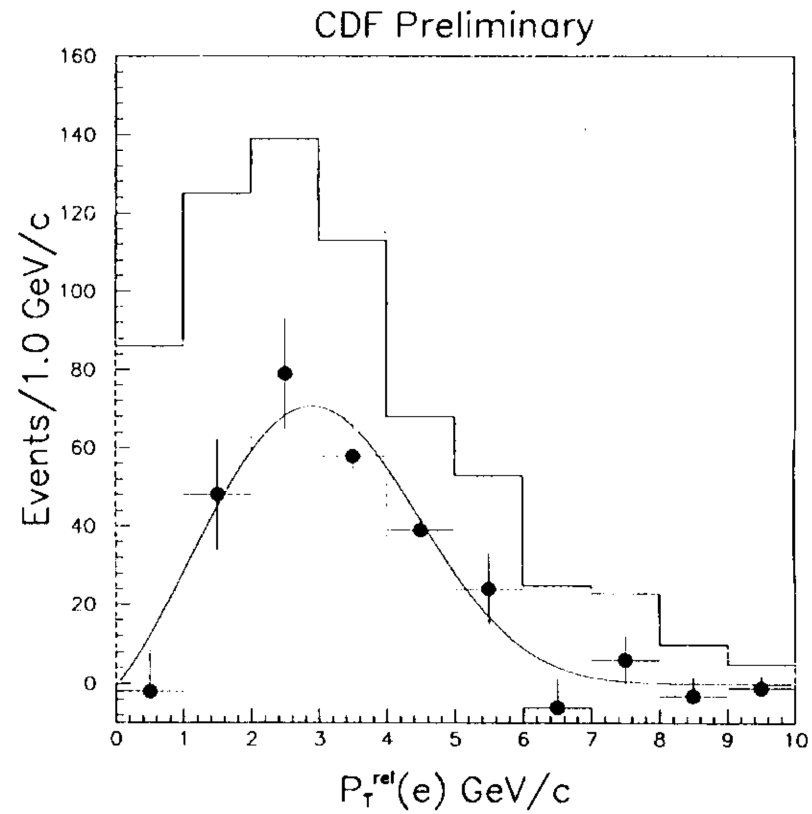

Figure 2: P_T^{rel} for electrons in the e-μ data. Opposite sign (solid) and same sign (dashed) distributions are shown along with the difference (points). The curve is described in the text.

the second b. The derived cross section as a function of the second b quark's P_T is shown in Figure 3. Again, the NLO prediction seems to be slightly low with respect to the data, but within errors the agreement is good. Although the plot shows little sensitivity to the shape of the distribution, the uncertainties in the measurements are highly correlated. Work is proceeding to unfold the correlated from the uncorrelated errors, in order to get a more precise determination of the shape.

2.3 $d\sigma_B/dPt$

The statistics available in the decay $B^+ \rightarrow J/\psi K^+$ allow us to directly measure the differential cross section of B mesons as a function of P_T. This measurement[14] is currently based on $14pb^{-1}$ of the 1992 data.

Events were selected by requiring opposite sign dimuons with track-stub matching consistent with the multiple scattering in the material before the muon chambers. In order to be in a region of well understood trigger efficiency, each muon was required to have

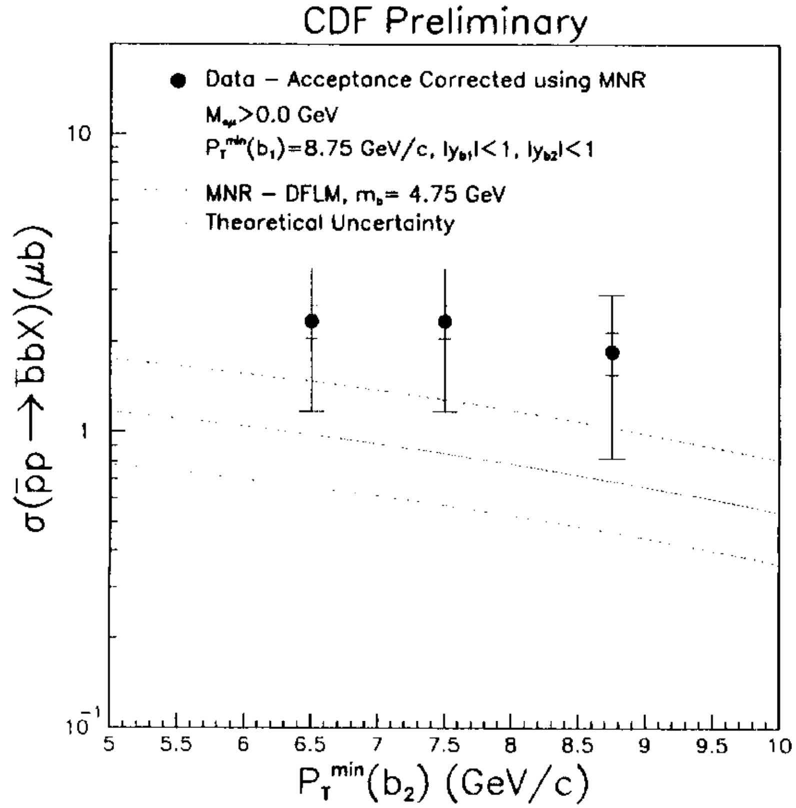

Figure 3: The cross section for $p\bar{p} \to b\bar{b}X$. The cross section is plotted as a function of the P_T^{min} of the second b given the P_T^{min} of the first b. Also shown is a theoretical prediction and associated uncertainty.

$P_T \geq 1.8$ GeV/c, and at least one was required to have $P_T \geq 2.8$ GeV/c. The dimuons were constrained to come from a common point in space, which improves the mass resolution. J/ψ candidates were selected by requiring that the invariant mass be within 3 sigma of the world average,[16] where sigma was determined by fitting a gaussian to the mass distribution.

Any track with $P_T \geq 2.0$ GeV/c was assigned the kaon mass and combined with the J/ψ. The P_T cut reduces the combinatoric background due to tracks from the underlying event. All three tracks were then refit with the constraints that they all come from a common point and the dimuon invariant mass be equal to the world average J/ψ mass. The mass distribution for $J/\psi K^+$ candidates with $P_T \geq 6.0$ GeV/c is shown in Figure 4. A fit to the data gives 104 ± 21 events.

The data was divided into three bins in P_T, 6-9, 9-12, and 12-15 GeV/c. Mass plots for each bin were fit with mean and width fixed to the values obtained in the full sample. The cross section is shown in Figure 5, along with a NLO calculation[12] convoluted with Peterson fragmentation.[15] A common normalization uncertainty, dominated by the uncertainty in the

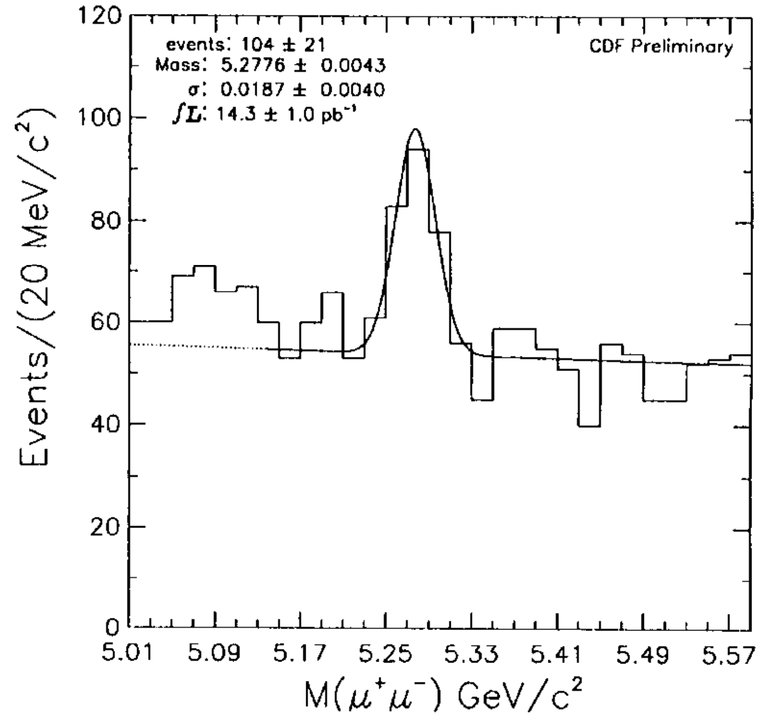

Figure 4: B meson invariant mass from the decay $B^+ \to J/\psi K^+$.

product branching ratio[16] for this decay is shown separately. The measured values are about a factor of two higher than the NLO predictions[12], and the shape may be steeper at low P_T than was predicted. Work is ongoing to determine the best way to use the SVX information in this analysis.

3. b LIFETIMES

The b lifetime can be combined with measures of semileptonic b decays, to determine the Cabbibbo-Kobayashi-Maskawa[17] matrix element V_{cb}. The most promising method employs Heavy Quark Effective Theory[18] to interpret exclusive semileptonic decays.[19] In the past they have used a lifetime determined as an inclusive average over hadronic states, but as statistics improve over the next year or so, I expect that exclusive lifetimes will naturally be combined with exclusive decay rates, to obtain V_{cb}. Exclusive lifetime measurements also allow comparisons between hadrons. The spectator model predicts that the B^0 and B^+ lifetime should be nearly equal, although this didn't turn to be true in the charm system![16] CDF

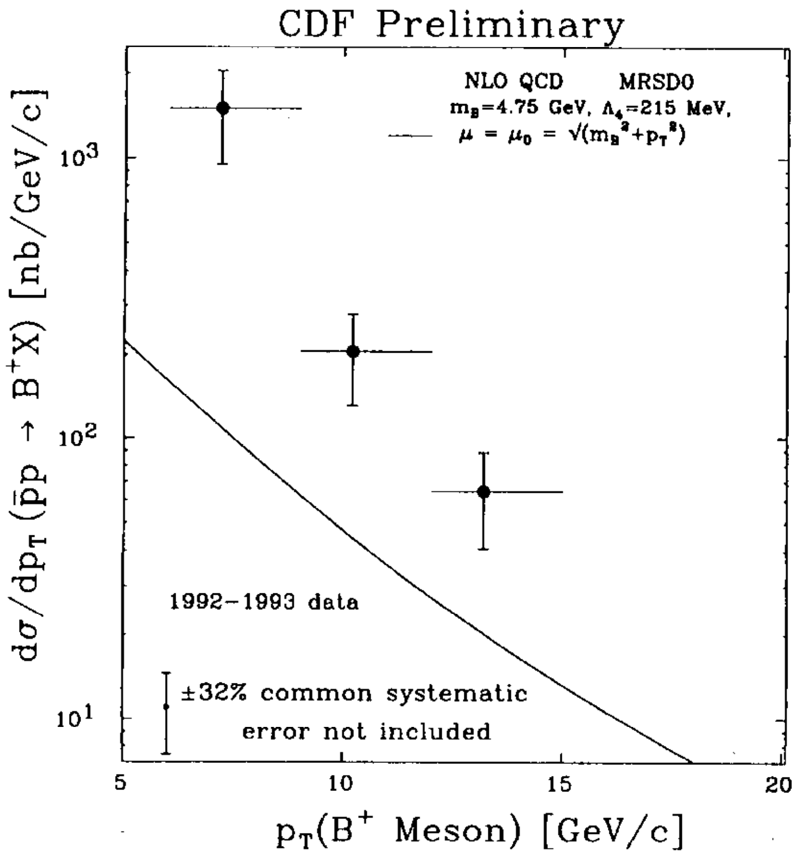

Figure 5: The B meson differential cross section compared to a NLO calculation convoluted with Peterson fragmentation.

has completed a measurement of the inclusive b lifetime,[20] and is now pursuing a program of individual measurements of bottom hadron lifetimes.

3.1 Inclusive Lifetime

In the past two years, LEP experiments have used semileptonic b decays, to obtain statistically precise measurements of the average b lifetime.[21] The theoretical models of semileptonic decays are now the dominant source of uncertainty. The decay $B \to J/\psi X$ provides an alternative determination of the b lifetime with different systematic uncertainties. Using the 1992 data, CDF has obtained the first high statistics measurement of the b lifetime using J/ψ decay vertices.

To obtain a sample sample of J/ψ's for measuring the lifetime, the P_T requirements for the muons were reduced slightly to increase the acceptance. To ensure a well measured vertex, both muon tracks were required to be reconstructed in the SVX with hits on at least

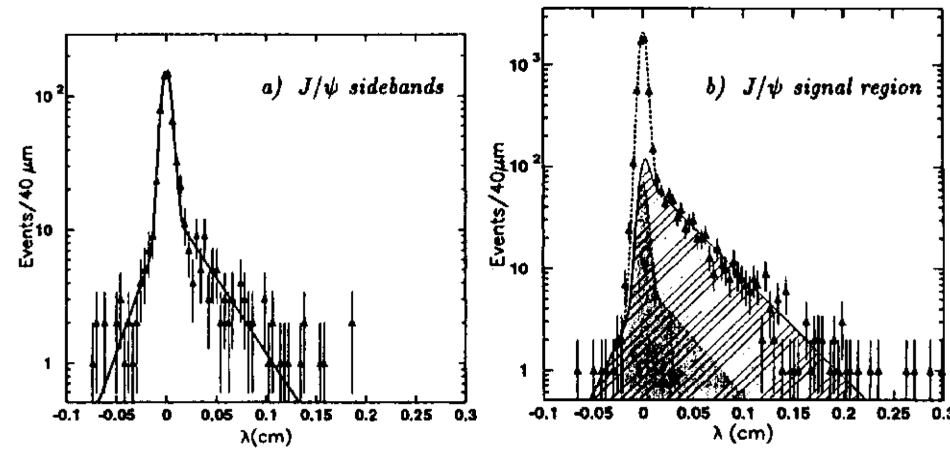

Figure 6: The λ distributions from a) the J/ψ sideband regions and b) the J/ψ signal region. The fits (curves) are described in the text.

three out of the four layers. None of these hits could have total charge deposition greater than four times that expected for a minimum ionizing particle, and all of them had to have a small residual. The total χ^2 contribution of these residuals had to be less than 20. If any of the SVX hits matched to the muons could be assigned to another track, the muon was not considered further. Finally, the two muons were refit with a constraint that they come from a common vertex. Only those events consistent with this constraint were retained. About 20% of the triggered J/ψ events survived all these cuts.

The transverse decay distance (L_{xy}) is the projection of the vector pointing from the primary to the secondary vertex, both measured in the transverse plane. The secondary vertex that obtained in the constrained fit, while the primary is approximated by the average beam position, determined run-by run. The beam is circular and has an rms of $\approx 40\mu m$. Contrary to some peoples expectations, many of these events are too clean to allow an event-by-event determination of the primary with better accuracy. We convert L_{xy} to a proper lifetime (λ) using the $\beta\gamma$ of the J/ψ,

$$\lambda = L_{xy}\frac{M_\psi}{P_T^\psi F(P_T^\psi)}, \tag{2}$$

where $F(P_T^\psi)$ corrects from $(\beta\gamma)_\psi$ to $(\beta\gamma)_b$. It is depends on the b production and decay as convoluted with the trigger and is determined as a function of P_T^ψ using Monte Carlo.

We fit the λ distribution using curves representing the three sources of dimuon events in the J/ψ region.

- J/ψ from b decays: This is parameterized by an exponential convoluted with a gaussian resolution. From the fit, we also obtain the fraction of J/ψ's arising from b decays (f_b).
- Prompt charmonium production: This yields a zero lifetime contribution, smeared with a gaussian resolution.

- Background processes whose invariant mass happens to fall in the J/ψ mass window: There are many possible sources to this component, and the shape could be complex. It can, however be measured using the J/ψ sidebands. The distribution of the sideband events has been fit to the sum of a gaussian and both a positive and negative exponential, each with different slope. Both the shape and size of this component are determined from the sidebands and are not free parameters in the fit to the signal region.

Figure 6a shows the λ distribution with the fit for the J/ψ sidebands. Figure 6b shows the results of an unbinned likelihood fit to the data. The dark shaded area is the contribution from the background fit. The light shaded area shows the sum of the background plus the component due to b decays. The remaining unshaded gaussian is due to prompt decays. The fit results are $\tau_b = 1.46 \pm 0.06$ ps and $f_b = 15.1 \pm 0.6\%$. This value is much lower than the model dependent fraction obtained in the cross section measurement of the last run. The track quality cuts, however, tend to favor isolated muons. Therefore, the value of f_b can not be used to measure the b cross section until relative efficiencies for different sources of b decays are understood.

The uncertainty in $F(P_T)$ is the dominant source of systematic uncertainty in this measurement (3.0%). We have estimated this by varying the b quark production spectrum and fragmentation, and J/ψ momentum spectrum and polarization in the B rest frame. Other sources are the due to any residual SVX misalignment (2.0%), our uncertainty in the event-by-event calculation of the error on λ (1.6%), possible trigger biases (1.4%), beam instabilities over the course of a Tevatron store (1.0%), and the statistical uncertainty in the determination of the background shape (0.5%). The final result is

$$\tau_b = 1.46 \pm 0.06(\text{stat.}) \pm 0.06\text{syst.})\text{ps}. \tag{3}$$

This represents the average lifetime for b-hadrons produced at the Tevatron, weighted by their decay fraction into a J/ψ. This result is final and has been submitted for publication.

3.2 *Exclusive Lifetimes*

Measurements of the B^+ and B^0 lifetimes have been made[22] at LEP and PEP using partially reconstructed decays containing a lepton and a D^0 or D^*+. Although CDF is also pursuing this technique, the large cross section at the Tevatron allows us to measure the lifetimes directly using fully reconstructed B meson decays.[23] Measuring the lifetime of B^+ and B^0 lifetimes using this method is, at the moment, statistically limited by the number of fully reconstructed B's. In order to increase the sample, we have relaxed some of the track quality cuts applied in the inclusive lifetime analysis. Only two SVX hits are required on each track, and the muons are allowed to be in the new CMX chambers. B's are reconstructed in eight decay modes:

$$\begin{array}{lll} B^+ & \to J/\psi K^+ & \to \mu^+\mu^- K^+ \\ B^+ & \to J/\psi K^{*+} & \to \mu^+\mu^- K^0_s\pi^+ \\ B^+ & \to \psi(2S)K^+ & \to \mu^+\mu^-\pi^+\pi^- K^+ \\ B^+ & \to \psi(2S)K^{*+} & \to \mu^+\mu^-\pi^+\pi^- K^0_s\pi^+ \\ B^0 & \to \psi K^0_s & \to \mu^+\mu^- K^0_s \\ B^0 & \to \psi K^{*0} & \to \mu^+\mu^- K^+\pi^- \\ B^0 & \to \psi(2S)K^0_s & \to \mu^+\mu^-\pi^+\pi^- K^0_s \\ B^0 & \to \psi(2S)K^{*0} & \to \mu^+\mu^-\pi^+\pi^- K^+\pi^- \end{array} \tag{4}$$

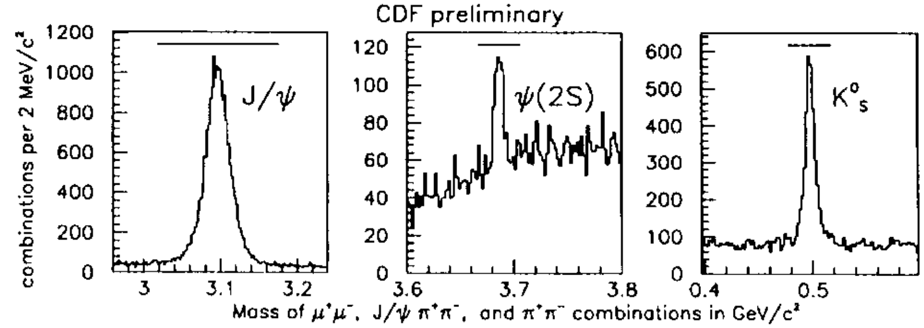

Figure 7: Mass distributions of the J/ψ, $\psi(2S)$, and K^0_S candidates. The mass cuts are indicated by the horizontal lines above the histograms.

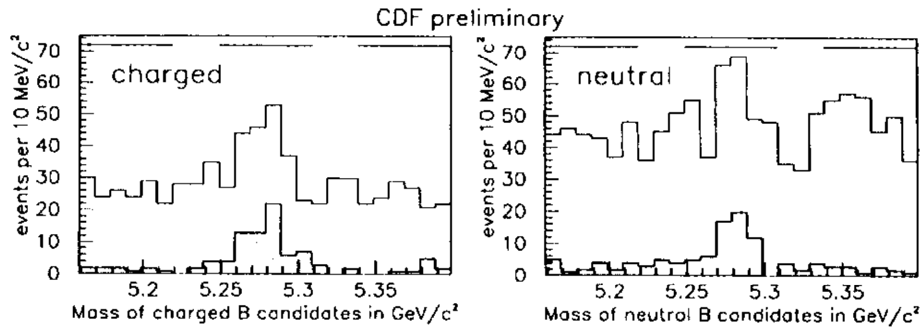

Figure 8: Mass distributions of the fully reconstructed B samples. The shaded histograms are obtained by requiring $c\tau > 100\ \mu m$. The signal and sideband regions are indicated by the horizontal lines above the histograms.

K^0_S are selected by combining two tracks with impact parameters greater than 2σ, where σ is the measurement error on the impact parameter added in quadrature with the size of the beam spot. The K^0_S is required to have a positive decay length, and an impact parameter with respect to the J/ψ vertex of less than 2 mm. Since K^0_S's can decay outside the SVX outer radius, the tracks used to reconstruct them are not required to have hits in the SVX. The invariant mass distributions of some of the intermediate states are shown in Figure 7. $\psi(2S)$ and K^0_S candidates are required to be within 20 MeV of the world average,[16] while J/ψ and K^* candidates are required to be within 80 MeV of the world average.[16] To be used for reconstructing B's, the K^+, K^0_S, or K^* candidates must have a $P_T \geq 1.25$ GeV/c.

In the final B reconstruction, all the decay tracks, except those from a K^0_S, are vertex constrained, and the J/ψ and $\psi(2S)$ candidates are mass constrained to their known values. Any B's with $P_T < 6.0$ GeV/c are rejected. In the case of multiple candidates, we keep the one with the best χ^2 for the constrained fit. The mass distributions for these candidates are shown in Figure 8. The shaded region shows the same distribution for candidates with $c\tau > 100\mu m$. There are clear B signals, albeit with a large zero lifetime background. For the lifetime analysis, we define the signal region to be ± 30 MeV of the world average[16] B

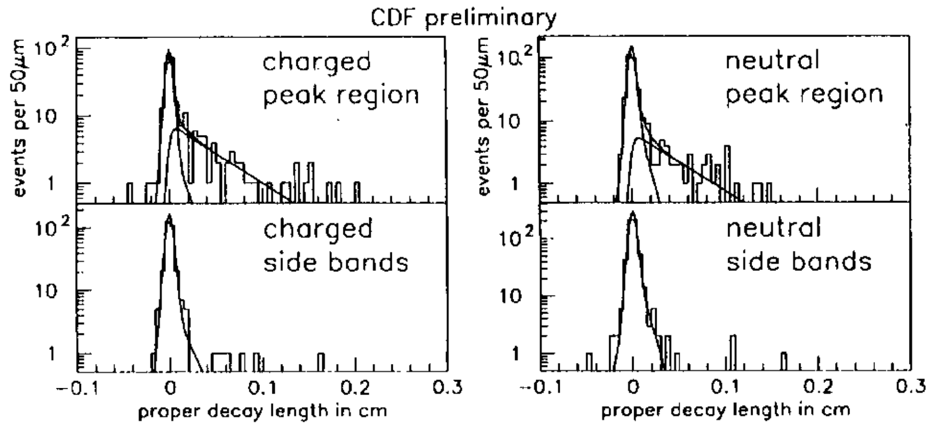

Figure 9: The proper decay length ($c\tau$) distributions of the fully reconstructed B samples. The fits (curves) are described in the text.

mass. Sideband regions are are defined to be between 60 and 120 MeV away from the world average. This excludes the region where B's with a missing π would be reconstructed.

The decay length distributions for charged and neutral B's, for both the signal and sideband regions is shown in Figure 9. The superimposed curves are the results of separate unbinned likelihood fits for the B^+ and B^0. As for the inclusive analysis, the signal is parameterized as an exponential convoluted with the gaussian resolution, while the background is gaussian plus asymmetric exponential tails. The signal and background distributions have been fit simultaneously. The fits indicate that there are 75 ± 10 charged and 61 ± 9 neutral B mesons in the signal regions. As can be seen, there are events at large decay length in the sideband regions. The preliminary measurement of the lifetimes of the B^+ and B^0 mesons is,

$$\begin{aligned} \tau^+ &= 1.63 \pm 0.21(\text{stat.}) \pm 0.16(\text{syst.})\text{ps} \\ \tau^0 &= 1.54 \pm 0.22(\text{stat.}) \pm 0.10(\text{syst.})\text{ps}. \end{aligned} \tag{5}$$

The systematic uncertainty is dominated by the lack of statistics in the sideband regions, and hence our inability to accurately measure the shape of the positive tails of their lifetime distribution. Assuming that this systematic is uncorrelated, we obtain the lifetime ratio

$$\tau^+/\tau^0 = 1.06 \pm 0.20(\text{stat.}) \pm 0.12(\text{syst.}). \tag{6}$$

Work is ongoing to further increase both the statistics and the signal to noise ratio of the B mesons, and to understand the shape of the background distribution better. We also will add in the second half 1992 data.

4. The B_s Mass

The B_s meson is a bound state of a of a b-s quark-antiquark pair. Its mass is determined from the QCD potential between them. It has been observed in the decay to a lepton plus a D_s meson.[24,25] This allowed measurements of the B_s lifetime, but due to missing neutrals, not the mass. An indirect mass measurement was obtained by CUSB using the photon spectrum in $\Upsilon(5S)$ decays.[26] Recently, experiments at LEP have reported fully reconstructing candidate events.[25,27] The CDF search[28] uses the decay mode $B_s \to J/\psi\phi$.

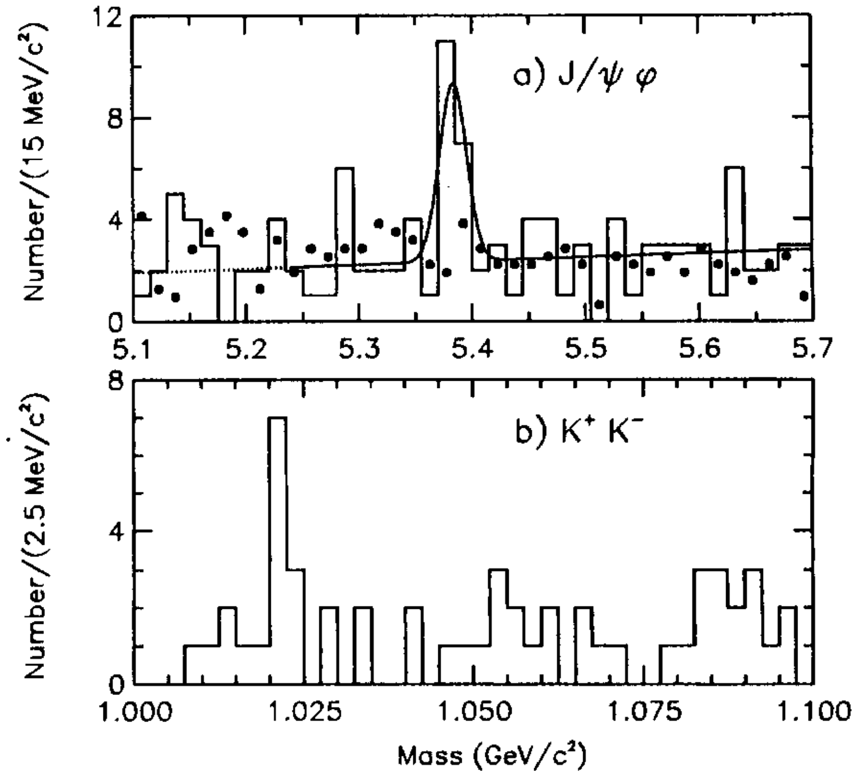

Figure 10: a)The $J/\psi\ K^+K^-$ mass distribution for K^+K^- within 10 MeV/c^2 of the ϕ mass (solid). The dots are the normalized ϕ sideband region ($M_K^+K^-$ between 1050-1090 MeV/c^2). b) The K^+K^- mass distribution for $J/\psi\ K^+K^-$ combinations within 20 MeV/c^2 of 5380 MeV/c^2.

We follow the general reconstruction procedures tuned on the $B_u \to J/\psi K^+$ and $B_d \to J/\psi K^*$ decays. To ensure high efficiency, all well matched mouns are considered, and tracks are not required to pass be reconstructed in the SVX. We combine tracks, assigned the K mass, and keep combinations where the invariant mass is within 10 MeV of the ϕ mass. These are combined with $J/\psi \to \mu^+\mu^-$ candidates, where the four tracks are vertex constrained and the dimuon pair is mass constrained to the J/ψ mass. The probability of this fit must be greater than 1%. In order to reject combinatoric background, the resulting combination is required to have a positive decay length. The mass spectrum of the resulting events is shown in Figure 10. A signal is clearly visible and remains significant under variation of the selection criteria. A binned likelihood fit result gives 14.0 ± 4.7 B_s events at a mass of 5383.3 ± 4.5 (stat.) MeV/c^2.

The estimate of the systematic error is based on the uncertainty in the magnetic field (1 MeV), varying the fitting procedure (2 MeV), and the selection criteria (2 MeV), alternative methods for constraining the 4-track system (2 MeV), and the current uncertainty in the tracking calibration (3 MeV). Our ability to estimate these uncertainties is limited by the size of the data sample. Thus the final result is,

$$M_{B_s} = 5383.3 \pm 4.5(\text{stat}) \pm 5.0(\text{syst})\text{MeV}/c^2. \tag{7}$$

Although this measurement has been submitted for publication, we expect it to be further improved with the addition of the second half of the data.

5. NEAR TERM GOALS AT CDF

While this workshop was going on, processing the "express" data stream with the "final" version of the production executable was completed. Thus the entire J/ψ data sample is now available for analysis. The main data set is expected to be completed by the end of September. In these data sets, we will have $\sim$ 80K J/ψ events, and $\sim$ 300 fully reconstructed B decays; a few 10^5 semileptonic b decays, and $\sim$ 1000 partially reconstructed lepton + charm hadron events.

Using these data, we expect a rich program of b physics at CDF. We will improve our understanding of b production at the Tevatron. The study of $b\bar{b}$ production will be extended using the dilepton correlations in the new data. (We also look forward to seeing results on this from our friends at D0.)

We will measure the exclusive B lifetimes with at least a factor of $\sqrt{2}$ reduction in errors over what is presented here. We should also have a measurement using semileptonic decays sometime this fall. We will improve our measurement of the B_s mass. We will either observe or greatly improve our upper limit on Λ_b production. We will set limits on or observe B_c production. Searches for the rare decays including $B \to \mu^+\mu^-$, $B \to \mu^+\mu^- K^*/K/\phi$ are in progress, and in some we hope our sensitivity will approach the standard model expectations. We will improve our measurement of time integrated B mixing, and use the SVX to measure the time dependence of it.

We are looking forward to the continuation of the collider run, this fall through next spring. We are still improving the detector, and optimizing the trigger, to obtain the maximum physics output from CDF. For instance, we are studying the feasibility of instituting a dedicated trigger for the decay $B \to \gamma\ K^*/\phi$. The observation[29] of this decay at CLEO is one of the more interesting events of the year. We feel obliged, if it appears possible, to try to confirm it.

If this years run goes well, we should have 1000 fully reconstructed and self-tagged B decays by next summer. This will allow us to study tagging rates and mis-tag fractions in the kinematic region of interest for CP violation. We hope to have measurements of these numbers using both lepton tagging and B-π correlations. This will allow us to begin to optimize our strategies for the future.

6. ACKNOWLEDGEMENTS

I would like to thank the people who helped me with the preparation of this talk. In particular, I would like to thank F. DeJongh, T. LeCompte, O. Schneider, B. Mattingly, and M. Bailey.

7. REFERENCES

1. F.Abe *et. al.*. *Nucl. Instrum. Methods Phys. Res.* **A271** (1988) 387 and references therein.
2. J. Spalding, these proceedings.
3. D. Amidei *et. al.*, *Nucl. Inst. and Meth.* **A289** (1990) 388.
4. G.W. Foster *et. al.*, *Nucl. Inst. and Meth.* **A269** (1990) 93.
5. J.T. Carroll *et. al.*, *Nucl. Inst. and Meth.* **A300** (1991) 552. U. Joshi *et. al.*, *Nucl. Phys. B. (Proc. Suppl.)* **23A** (1991) 365.
6. C.Albajar *et. al.*, *Phys. Lett.* **B186** (1987) 237, *Phys. Lett.* **B213** (1988) 405, *Phys. Lett.* **B256** (1991) 121.
7. P. Nason, S. Dawson and R.K. Ellis,, *Nucl. Phys.* **B303** (1988) 607, **B237** (1989) 49, **B335** (1990) 260.
8. F.Abe *et. al.*, *Phys. Rev. Lett.* **71** (1993) 500.
9. F.Abe *et. al.*, Preprint FERMILAB-PUB-93/145-E, submitted to Phys. Rev. Lett.
10. F.Abe *et. al.*, Preprint FERMILAB-PUB-93/106-E, submitted to Phys. Rev. Lett.
11. F.Abe *et. al.*, *Phys. Rev. Lett.* **68** (1992) 3403
12. M. Mangano, P. Nason, and G. Ridolfy, *Nucl. Phys.* **B373** (1992) 295
13. CDF Collaboration, submitted to the XVI *International Symposium on Lepton Photon Interactions*. Preprint FERMILAB-CON-93/200-E.
14. CDF Collaboration, submitted to the XVI *International Symposium on Lepton Photon Interactions*. Preprint FERMILAB-CON-93/199-E.
15. C. Peterson *et. al.*, *Phys. Rev.* **D27** (1983) 105; J. Chrin, *Z. Phys.* **C36** (1987) 163.
16. Particle Data Group, K. Hikasa *et. al.*, *Phys. Rev.* **D45** (1992) 1.
17. N. Cabbibio., *Phys. Rev. Lett.* **10** (1963) 531; M. Kobayashi and T. Maskawa, *Prog. Theor. Phys.* **49** (1973) 652.
18. N. Isgur and M. Wise,, *Phys. Lett.* **B232** (1989) 113, **B255** (1991) 297.
19. H. Albrecht *et. al.*, *Phys. Lett.* **B229** (1989) 175; D. Bortoletto and S. Stone, *Phys. Rev. Lett.* **65** (1990) 2951; M. Neubert, *Phys. Lett.* **B264** (1991) 455; H. Albrect *et. al.*, *Z. Phys.* **C57** (1993) 533.
20. F.Abe *et. al.*, Preprint FERMILAB-PUB-93/158-E. submitted to Phys. Rev. Lett. (1993).
21. P. Abreu *et. al.*, *S. Phys.* **C53** (1992) 567; B. Adeva *et. al.*, *Phys. Lett.* **B270** (1992) 111; P.D. Acton *et. al.*, *Phys. Lett.* **B274** (1992) 513; D. Buskulic *et. al.*, *Phys. Lett.* **B295** (1992) 174; P.D. Acton *et. al.*CERN PPE/93-02, submitted to Z. Phys.
22. S. Wagner, *et. al.*, *Phys. Rev. Lett.* **64** (1990) 1095; P. Abreu, *et. al.*, *Z. Phys.* **C57** (1993) 181; D. Buskulic, *et. al.*, *Phys. Lett.* **B297** (1992) 449,, *Phys. Lett.* **B307** (1993) 194; P.D. Acton *et. al.*, *Phys. Lett.* **B307** (1993) 247.

23. CDF Collaboration, submitted to the XVI *International Symposium on Lepton Photon Interactions.* Preprint FERMILAB-CON-93/198-E.

24. D. Buskulic *et. al.*, *Phys. Rev. Lett.* **B294** (1992) 145; P. Abreu *et. al.*, *Phys. Lett.* **B289** (1992) 199;

25. P.T. Acton *et. al.*, *Phys. Lett.* **B295** (1992) 357.

26. J. Lee-Franzini *et. al.*, *Phys. Rev. Lett.* **65** (1990) 2947.

27. D. Buskulic *et. al.*, *Phys. Lett.* **B311** (1993) 425; W. Venus, talk presented at the XVI *International Symposium on Lepton Photon Interactions.*

28. F.Abe *et. al.*, *Phys. Rev. Lett.* **71** (1993) 1685.

29. R. Ammar *et. al.*, *Phys. Rev. Lett.* **71** (1993) 674.

B PHYSICS AT THE D0 DETECTOR

MARY ANNE C. CUMMINGS
Department of Physics and Astronomy, University of Hawaii
Honolulu, Hawaii 96896

ABSTRACT

This article describes the current b physics program at the DØ experiment at Fermilab[1]. Results from single and dimuon events produced in $p\bar{p}$ collisions at $\sqrt{s}$ = 1.8 TeV include the inclusive muon and J/ψ differential cross sections and a measurement of the time-averaged $B^\circ - \bar{B}^\circ$ mixing parameter χ. Plans for the near future b physics program at DØ are discussed, and an overview of the DØ upgrade, scheduled for implementation beginning with Fermilab collider run II are presented with emphasis on the prospects for continuing b physics research.

1. INTRODUCTION

The DØ detector was originally designed and constructed to study high mass states and large p_T final products from proton-antiproton collisions at $\sqrt{s}$ = 2 TeV in the FNAL Tevatron Collider. Several gross features of the current detector reflect the original intent: 1) large muon coverage, $|\eta| < 3.4$, with thick magnetised iron to provide muon momentum determination with small hadron punchthoughs 2) stable, unity-gain, finely segmented, hermetic, radiation-hard calorimetry 3) non-magnetic tracking with emphasis on suppressing backgrounds to electrons. The design and optimisation of the DØ tracking system has, naturely, been very much influenced by the absence of a magnetic field.

These features serve the primary physics goals of DØ , namely, searches for new phenomena (the top quark, supersymmetric and other particles outside of the standard model) and high precision studies of the W and Z bosons. The detector design has allowed for accurate identification, complete angular acceptance and precise measurement of charged leptons (both electrons and muons), quarks and gluons which emerge as collimated jets of particles, and neutrios. The fine segmentation of the calorimeter makes DØ and excellent tool for jet and QCD studies. However, in addition to the original goals, the large muon coverage, both in triggering and track reconstruction, and the large $b\bar{b}$ cross section at $\sqrt{s}$ = 1.8 TeV (the current c.o.m. energy of the FNAL machine) also allow for a viable study of b quark production in single muon and multi-muon channels.

This presentation will describe the DØ b physics program as carried out in the recent '92-'93 FNAL collider run. This was the first time that DØ operated in colliding mode, and an ambitious physics program was carried out despite having also to commission the detector, electronics, and data acquisition system. The priority was to collect data for top search and W and Z studies; however, by the end of the run, all the necessary trigger hardware was in place and functioning for single and dimuon triggers over the entire design coverage for muons. The results of the inclusive muon and J/ψ cross sections can be used to extract the $b\bar{b}$ cross sections which, in turn, can be compared directly to QCD next-to-leading (NLO) calculations. A precise measurement of the combined mixing parameter χ can be used to set a lower limit on the B_s° mixing strength, x_s. Measurement of heavy quark production at large pseudorapidity would provide a useful probe of the gluon density function at small x.

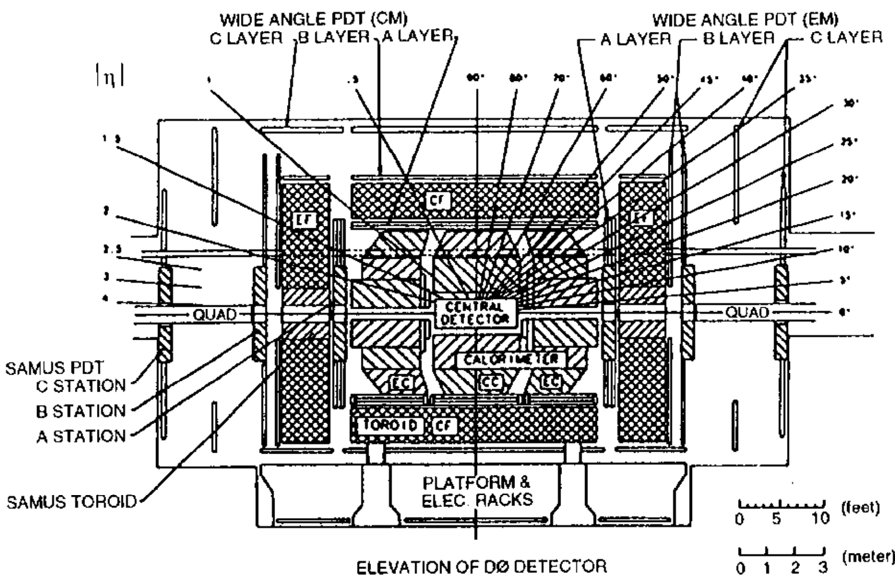

Figure 1. Elevation of the DØ detector.

The next section (2) will briefly describe the DØ detector, emphasising features salient to b quark detection. The results from single and dimuon triggers are summarised in sections 3-5. The plans for the imminent collider run Ib are discussed in section 6. The penultimate section summarises the long term plans for the b physics program in the DØ upgrade.

2. D0 DETECTOR

Figure 1 shows an elevation of the DØ detector. The DØ detector comprises (in order from the beamline), a vertex detector, transition radiation detectors, central tracking (drift chambers), a uranium-liquid argon calorimeter, and an extensive, three-layer system of muon chambers. The calorimeter is contained in three cryostats, one central and two endcaps. The central tracking is in three corresponding sections (central and two forward). The fine segmentation ($\Delta\eta$ x $\Delta\phi$ = 0.1 x 0.1) and good energy resolution ($\sigma \approx 0.41\%/\sqrt{E}$) along with coverage up to $|\eta| \approx 4.0$ provides good measurement of jet energies.

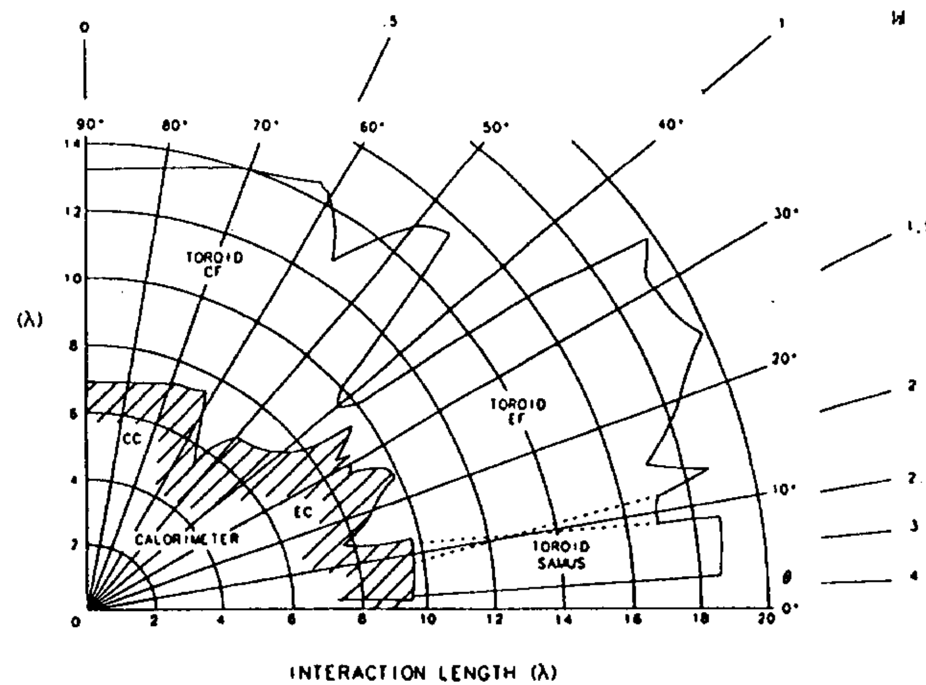

Figure 2. Thickness, in interaction lengths, of the DØ calorimeter and toroids.

The muon system comprises two different detector types. The "wide angle" (WAMUS) muon chambers are made of aluminum extrusions, 3 or 4 decks of 10.0 cm wide proportional drift cells. These chambers are mounted three layers deep around three iron toroids (one central, two ends). The 4-deck chambers form the layer inside the toroids, the 3-deck chambers form the two outer layers. In addition to the drift times, the WAMUS chamber cells are paired with a common anode wire to produce a longitudinal position through the time division (ΔT) measurement. Vernier pads arranged in repeating patterns inside each cell provide finer longitudinal position resolution within their "half" patterns ($\approx$ 30.0 cm) by the ratios of induced charges on the inner and outer pads (see Figure 3). Signals from these pads are also latched to form the trigger elements of the various muon triggers. The "small angle" (SAMUS) system extends the reach of the muon system to $|\eta| \approx 3.4$. SAMUS comprises three stations of 3.0 cm wide proportional drift tubes at x, y and u planar orientations, with a smaller toroid between the first and second stations, at either end of the detector. In both detectors, the combination of chambers and toroids provide a measurement of the signed momentum of the muon by the bend of the track. Thus, the momentum resolution is limited by multiple scattering in the iron to be $\geq$ 18%. The thickness of the calorimeter plus the iron is 14-18λ over the η coverage (Figure 2). This makes the punchthrough probability quite small ($\approx 10^{-4}$). For details of the DØ detector, and the muon system in particular, see refs. [2] and [3].

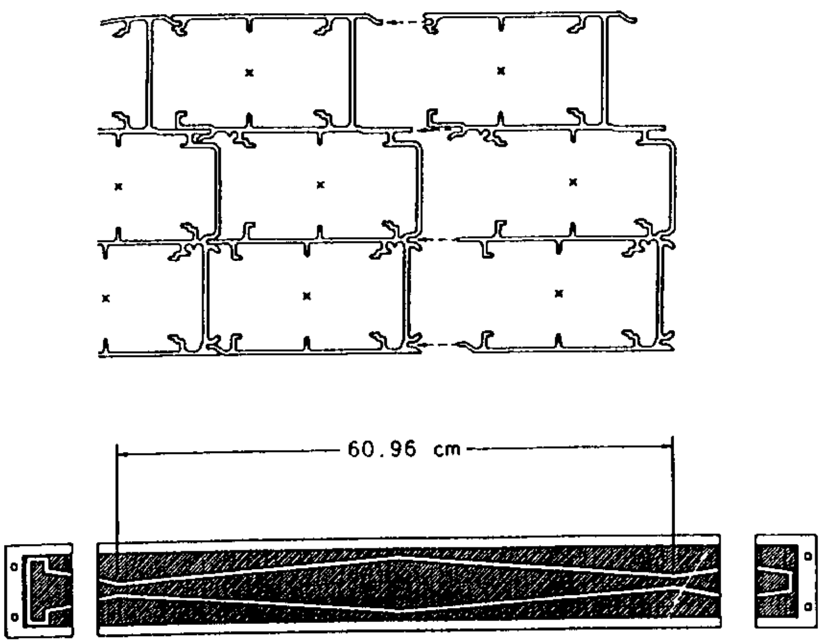

Figure 3. Cross section of the muon drift cells (top) and a section of the vernier pad pattern along the length of the cell (bottom).

3. INCLUSIVE MUON CROSS SECTION

3.1 *Single Muon Trigger*

The DØ trigger comprises a hierarchical system which reduces the 43 mb of inelastic cross section to 2 Hz of interesting physics events which are written to 8mm tapes. There are three main levels. The Level 0 trigger is a scintillator array around the beam pipe that detects the presences of an inelastic event. The Level 1 trigger is actually any number of trigger elements from the calorimete and muon systems. For the b physics program, the triggers consist of muon elements; a combination of hit cells that are contained within 60 cm roads. These combinations are required to have at least 2 hits from at least 2 or 3 layers (depending on the detector geometry). The Level 1 muon trigger efficiency, including geometrical acceptance, has a maximum of 60%, and is 30% efficient at p_T= 4.0 GeV. The Level 2 trigger is a software trigger, using a farm of 48 micro Vaxes (4000/60). Several routines, or filters, can run, depending on the physics requirements, that use code similar to the offline reconstruction. At Level 2, a good quality muon track, with $p_T^\mu > 3.0$ GeV is required.

In addition, there is another hardware trigger, Level 1.5, which in the last run was implemented only in the high p_T muon triggers used in the top and W/Z analyses. This imposes a rough p_T cut on the muon track. It was not used for the run Ia b physics data, but has been fully implemented for the next run, and should provide enough rejection for single muon low p_T triggers over most of the η coverage. This is discussed in section 6.

3.2 *Data Analysis*

Data for the inclusive muon cross section measurement was taken in several special runs as the trigger rate was too high to run concurrently with other physics triggers. Data was collected for the η regions $|\eta| < 1.0$, $1.0 < |\eta| < 1.6$, and $2.2 < |\eta| < 3.3$ with integrated luminosities of 89 nb^{-1}, 12 nb^{-1}, and 6.3 inb respectively. Approximately 70% of the data from the regions $|\eta| < 1.0$ and $1.0 < |\eta| < 1.6$ have been fully reconstructed and are used for the cross section measurement.

A good quality muon is defined after the following offline cuts:

1. Good vertex projection in the bend and non-bend views;
2. Track hits in all three layers of the muon system;
3. 1 GeV energy deposition in the hit plus nearest neighbour calorimeter cells;
4. Matching central tracking detector;
5. Muon drift t_0 within 100 ns of the beam crossing for $|\eta| < 1.0$.

The overall acceptance for single muons was calculated using b$\rightarrow$c$\mu^-\bar{\nu}X$ ISAJET events. These events were passed through a complete GEANT detector simulation, Level 1 and Level 2 trigger simulators, full reconstruction and offline cuts. The overall efficiency is shown in Figure 4 26% for $|\eta| < 1.0$ and 18% for $1.0 < |\eta| < 1.6$.

3.3 *Results*

The inclusive muon cross section is found by dividing the number of observed muon events in a given p_T bin by the efficiency and integrated luminosity. The results for $|\eta| < 1.0$, $1.0 < |\eta| < 1.6$ and $2.2 < |\eta| < 3.3$ are shown in Figures 5(a-c). The various dotted/dashed lines show the contributions to the cross section from $b \to \mu X$ $c \to \mu X$ π or K decays and their summed contribution.

Sources of systematic error arise from uncertainties in backgrounds from cosmic rays and combinatorics (20%), and luminosity (12%). The combined systematic error is shown as the larger error bars in the Figures 5(a-c).

The fact that the data agree well with the summed contributions from ISAJET is NOT equivalent to the statement that the data agree with QCD predictions for the $b\bar{b}$ cross section, since the ISAJET events did not necessarily sample the full $b\bar{b}$ cross sections. The predictions for the observed muon cross section depend on the heavy quark fragmentation functions folded into the QCD calculation. Work is still going on to extract $b\bar{b}$ cross sections from the inclusive muon cross section measurements.

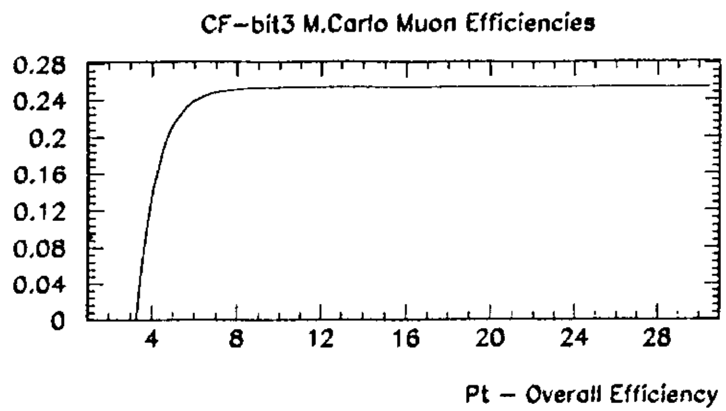

Figure 4. Combined trigger, reconstruction and offline cuts efficiency for muons with $|\eta| < 1.0$

4. INCLUSIVE J/ψ CROSS SECTION

4.1 The Dimuon Trigger

Dimuon events were collected by requiring that two muons are found in the Level 1 muon trigger as described above, and that two "quality" muons be reconstructed with the Level 2 muon trigger. The integrated luminosity for the data sample used in the cross section analysis is 3.5 pb^{-1}.

4.2 The Dimuon Analysis

After an event has passed the above requirements, additional cuts are applied offline:

1. At least two "high quality" muon tracks are found;
2. Both tracks have good vertex projection in the bend and non-bend views;
3. $\Delta\phi <$ deg160 and $\Delta\theta < 170°$ cosmic ray rejection);
4. 1 GeV energy deposition in the hit plus nearest neighbour cells for both tracks;
5. $p_T^{\mu\mu} > 8.0$ GeV;
6. $|\eta| < 0.8$ for both muons.

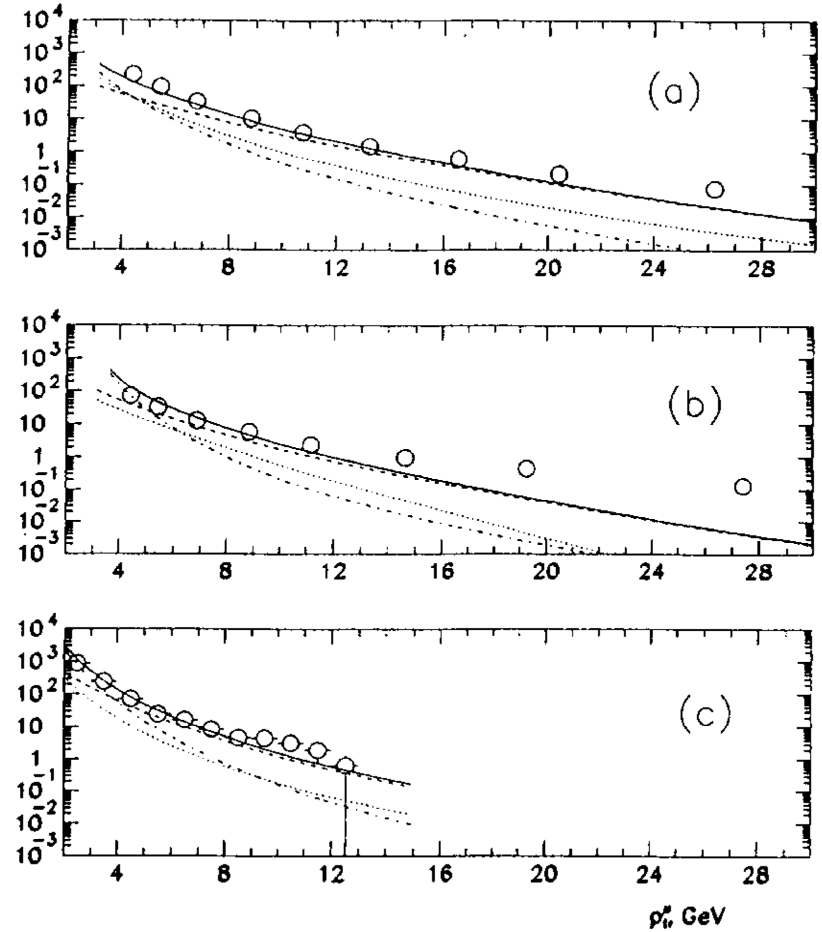

Figure 5. Inclusive muon cross sections for (a) $|\eta| < 1.0$, (b) $1.0 < |\eta| < 1.7$ and (c) $2.2 < |\eta| < 3.3$. Shown with Monte Carlo predictions for muons from $b \to \mu X$ (dashed line), $c \to \mu X$ (dotted line), π or K decays (dashed-dotted line), and their sum (solid line).

Jets are defined using a $\Delta R = \sqrt{\Delta\eta^2 + \Delta\phi^2}$ cone of 0.7 and have $E_{tjet} > 8.0$ GeV. Isolated dimuons are defined such that the ΔR distance between each muon and the nearest jet be greater than 0.7. Non-isolated dimuons are defined to have at least one muon within a ΔRcone of 0.7 about the nearest jet. The invariant mass plots for both like and unlike-sign dimuons and for both non-isolated and isolated dimuon samples are shown in Figures 5. This particular data sample corresponds to an integrated luminosity of 7.0 pb^{-1}. Both unlike-sign samples show a clear J/ψ peak. The isolated unlike- sign sample shows evidence of the J/ψ. Neither of the like-sign samples shows any evidence of mass peaks.

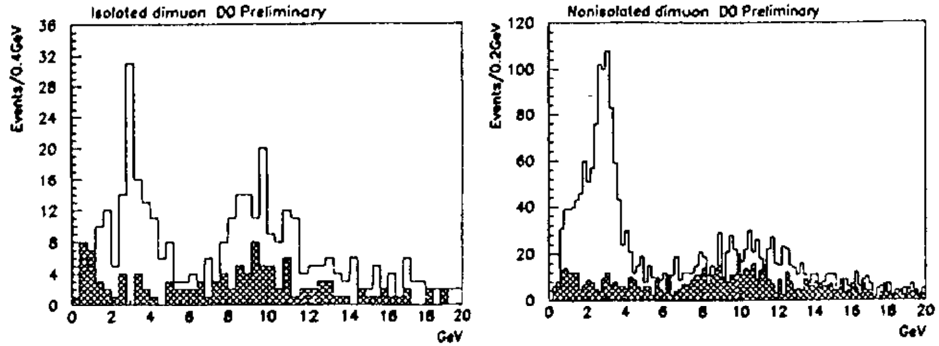

Figure 6. Unlike-sign (unshaded) and like-sign (shaded) invariant mass for: (a) non-isolated and (b) isolated dimuons.

4.3 *Comments on Dimuons*

For the inclusive J/ψ cross section, both isolated and non-isolated dimuons were used. The number of J/ψ's in each mass bin was estimated by fitting the invariant mass distribution to a Gaussian (signal) plus a polynomial (background) which matched the tails of the distribution above 4.0 GeV and below 2.0 GeV. The total number of J/ψ's is found to be 138 $\pm$ 15 events.

The acceptance was determined by generating J/ψ's with the ISAJET Monte Carlo, passing them through the complete GEANT detector and trigger simulators, reconstructing them fully, and applying the offline cuts. The overall efficiency for J/ψ's is shown in Figure 6(a), where the bounds indicate systematic uncertainties. The inclusive J/ψ cross section is gotten by dividing the number of J/ψ's in each p_T bin by the efficiency, and the integrated luminosity. The results are shown in Figure 6(b). The error bars are for statistical uncertainties only. Also shown are the ISAJET predictions for the J/ψ from χ and direct production (CPM) and for J/ψ's from B decay (BPM). That the data lie above the summed contributions is significant, however. The determination of the $b\bar{b}$ cross section using inclusive J/ψ's and of the fraction of J/ψ's which come from χ's or direct production is still in progress.

5. $B^\circ - \bar{B}^\circ$ MIXING PARAMETER

5.1 *Mixing Probabilities*

Mixing between B° and its anti-particle can occur in the Standard Model via well-known box diagrams. The time averaged mixing probability χ is given in terms of the mixing parameter x as

$$\chi \approx \frac{x^2}{2+2x^2}, \qquad (1)$$

where x is the mass difference of the mass eigenstates divided by their average decay width. The mixing parameters x_d and x_s are of interest because they can be written in terms of parameters of the Standard Model. In particular, they depend on the CKM matrix elements V_{td} and V_{ts}. An accurate measurement of χ (or χ_s) can be used to set a lower limit on x_s and thus help constrain elements of the CKM matrix.

The combined mixing probability χ is defined as

$$\chi = \frac{BR(b \to B^0 \to \bar{B}^0 \to \mu^+)}{BR(b \to \mu^\pm)}, \qquad (2)$$

which is an average over both B_d° and B_s° mesons which can mix as well as charged B mesons which can not. The b or $\bar{b}$ can be tagged by the sign of the muon from the semi-leptonic decay of the B.

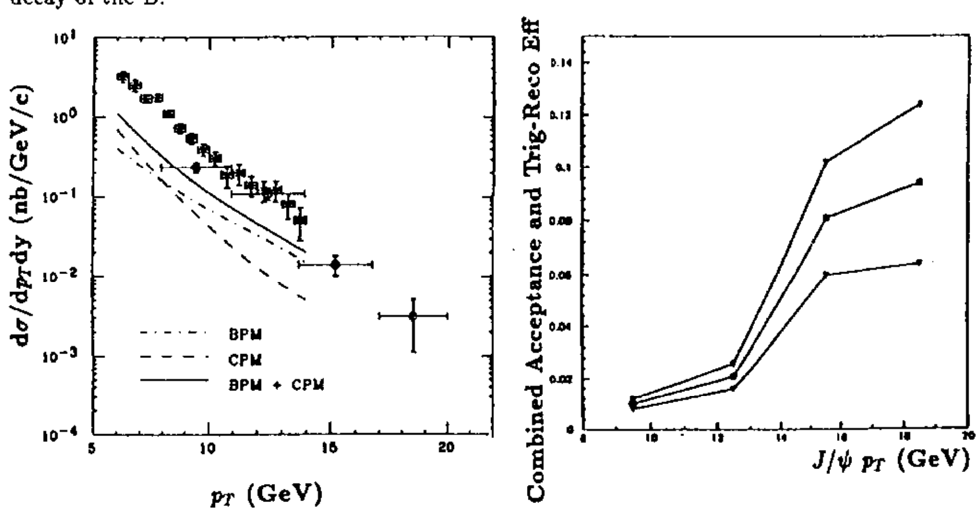

Figure 7. (a) Inclusive J/ψ cross sections; (b) Overall J/ψ efficiency.

The semi-leptonic decay of a $B^\circ\bar{B}^\circ$ pair into muons (direct decay) will give rise to unlike-sign dimuons. Flavor mixing of a B° or $\bar{B}^\circ$ will result in like sign dimuons. Like sign dimuons can also be produced by secondary decays in which one muon comes from $b \to \mu$ decay while the other comes from $b \to c \to \mu$ decay. In the presence of mixing the fraction of like and unlike-sign dimuons for various processes is given in Table 1.

Experimentally, one measures the ratio R of like- to unlike-sign dimuons. In order to extract χ from R it is necessary to model the relative contributions of all processes

Table 1: Fraction of like and unlike sign dimuons from contributing processes

Process	Type	Like Sign	Unlike Sign
P1	$b \to \mu^-, \bar{b} \to \mu^+$	$2\chi(1-\chi)$	$(1-\chi)^2 + \chi^2$
P2	$b \to \mu^-, \bar{b} \to \bar{c} \to \mu^-$	$(1-\chi)^2 + \chi^2$	$2\chi(1-\chi)$
P3	$b \to c \to \mu^+, \bar{b} \to \bar{c} \to \mu^-$	$2\chi(1-\chi)$	$(1-\chi)^2 + \chi^2$
P4	$b \to c\mu^-, c \to \mu^+$	0%	100%
P5	$c \to \mu^+, \bar{c} \to \mu^-$	0%	100%
P6	Drell-Yan, J/ψ, Υ	0%	100%
P7	decay background	50%	50%

contributing to dimuon production. For this we use the ISAJET Monte Carlo event generator and a fast detector simulator described below. Once the relative fractions of the contributing processes are known, χ can be extracted from R as the solution to a quadratic equation.

5.2 Data Reduction and Analysis

Data was collected using the dimuon Level 1 and Level 2 muon trigger described in section 4.1. The data used in the mixing analysis corresponds to a total integrated luminosity of 8.4 pb^{-1}. Offline cuts for the mixing analysis include:

1. Two or three high quality muon tracks in $|\eta| < 1.1$;
2. 1.0 GeV energy deposition in hit plus nearest neighbor calorimeter cells;
3. $\int B \cdot dl$ for each muon > 0.5 GeV;
4. $\Delta\phi < 160°$ (cosmic ray rejection);
5. $m_{\mu\mu} > 6.0$ GeV (removes J/ψ's);
6. $3 < p_T^{\mu} < 25.0$ GeV (ensures proper sign determination).

In addition, each event is required to have at least one associated jet where an associated jet is defined as a jet with $E_T^{jet} > 8$ GeV within $\Delta R = 0.8$ of the muon. Further, all muons having associated jets in the event must satisfy $p_T^{rel} > 1.2$ GeV where p_T^{rel} is the transverse momentum of the muon relative to the jet axis. These cuts serve to enhance the fraction of dimuons coming directly from $b\bar{b}$ decay.

Using these cuts we find a total of 116 like sign and 234 unlike-sign events. The ratio of like to unlike-sign events does not change significantly if we relax the associated jet requirement and ask only that at least one jet be found anywhere in the event. The fraction of cosmic rays in these events is estimated to be $\approx 15\%$ based on visual scan of a subset of the sample. Correcting for cosmic ray background we find the ratio of like to unlike-sign dimuons to be

$$R = \frac{like}{unlike} = 0.51 \pm 0.06(stat) \pm 0.02(sys), \tag{3}$$

where the systematic error reflects the uncertainties associated with our estimated fraction of cosmic rays.

5.3 Monte Carlo Analysis

Table 2: Relative fraction of contributing processes

Process	Fraction
Direct $b\bar{b}$(P1)	0.66 ± 0.15
Secondary $b\bar{b}$(opp. side) (P2)	0.15 ± 0.06
Tertiary $b\bar{b}$(P3)	0.09 ± 0.04
$c\bar{c}$, J/ψ, secondary $b\bar{b}$(same side) (P4-P6)	0.02 ± 0.02
Background (P7)	0.08 ± 0.04

To determine the relative fraction of the processes listed in Table 1, a sample of 10000 dimuon events from $b\bar{b}$ and $c\bar{c}$ were generated using the ISAJET Monte Carlo. The events were then passed through the fast DØ simulator which employs parameterizations of the DØ detector response to hadrons and leptons and the Level 1 and Level 2 trigger efficiencies. The offline cuts described above were then applied and the relative fractions of contributing processes resulting are shown in Table 2.

The accuracy of the fast simulation model has been checked by processing 5000 dimuon ISAJET events through full GEANT detector simulation, complete trigger and reconstruction packages, and offline cuts. Similar fractions are observed within statistical errors.

5.4 Results

Assuming the relative fractions of contributing processes given in Table 2 and using the measured value of R from equation (3) we find for the combined time averaged mixing parameter χ

$$\chi = 0.14 \pm 0.03(stat) \pm 0.06(sys), \tag{4}$$

where the systematic error is dominated by uncertainties in our estimation of the fractions of contributing processes from our procedure. This value of χ is in agreement with results from CDF and LEP[4-9]. Work in reducing the systematic error by increasing Monte Carlo statistics and improving the technique for estimating the fractions of contributing processes is in progress, along with determining a lower limit on x_s.

6. RUN IB

The results presented in the previous sections are largely preliminary. Because of the higher priority of top search, W/Z, and QCD physics programs, all of the single muon data were taken with special, low luminosity runs. This, naturally, severely limits the data sample, and low luminosity runs will become increasingly rare in the next run. Our plan for run Ib is to implement single muon triggers to run in the regular trigger set. This will require a a high enough rejection rate from the Level 1, 1.5 and 2.0 triggers to get to an overall rate that is some acceptable fraction of the 4 Hz bandwith limit to tape, with a minimum of prescaling.

The biggest contribution to this reduction will come from the Level 1.5 hardware muon trigger. The Level 1.5 trigger defines much narrower roads than the Level 1 hardware trigger. The determination of muon hits consistent with these roads allows a rough determination

Table 3: Single Muon Rates with Level 1.5 Rejection, luminosity $\approx 10^{31}$

η Region	Level 1 (μb)	Level 1.5 (μb)	Level 2 (hz)
$\|\eta\| < 1.0$	50.0	8.0	1.6
$\|\eta\| < 1.7$	65.0	20.0	20.0
$\|\eta\| < 2.2$	115.0	30.0	30.0
$\|\eta\| < 3.3$	625.0	50.0	35.0

Table 4: Single Muon Rates plus Jets with Level 1.5 Rejection

η Region	Level 1 (μb)	Level 1.5 (μb)	Level 2 (hz)
$\|\eta\| < 1.0$	2.0	0.8	0.6
$\|\eta\| < 1.7$	3.0	1.2	1.0
$\|\eta\| < 2.2$	4.0	1.6	1.5
$\|\eta\| < 3.3$	20.0	2.0	4.0

of muon momentum, and p_T cuts can be applied at this level. For the last run this Level 1.5 rejection was only applied to high p_T W, Z and top triggers in the central region during regular data taking. The Level 1.5 is now in place for the entire muon coverage. The very high rates at $|\eta| > 1.0$ will force an additional requirement on the single muon triggers. If a jet is also required in the Level 1.0 trigger, the single muon trigger should be able to run unprescaled for all but the highest η region.

The dimuon data sample was taken during normal data runs, but prescaled significantly. A Level 1.5 requirement on one or both muons would eliminate the need for any prescaling of the dimuon triggers. Dedicated runs were taken near the end of run 1a to test the Level 1.5 hardware on single muon, single muon plus jet and dimuon triggers. Figures 7(a-c) show the results for each trigger in increasing regions of η. Further rejection rate is expected for both Single muon and Dimuon triggers as the Level 1.5 is better understood and the tables refined, and from improved code in the Level 2 (software) trigger.

7. RUN II AND BEYOND

7.1 *DØ Detector Upgrade*

The upgrade in the Tevatron luminosity has made it necessary for an extensive upgrade of the DØ detector for higher luminosity operation. To keep a viable physics program at DØ running through the decade, a detailed detector upgrade plan has been proposed for

Table 5: Dimuon Rates with Level 1.5 Rejection on one Muon

η Region	Level 1 (μb)	Level 1.5 (μb)	Level 2 (hz)
$\|\eta\| < 1.0$	2.5	1.3	0.3
$\|\eta\| < 1.7$	3.5	1.8	0.5
$\|\eta\| < 2.2$	4.5	2.0	0.6
$\|\eta\| < 3.3$	215.0	43.0	1.0

implementation begin- ing with collider run II. These plans have been described extensively in several documents[10-13]. The basic scheme calls for the replacement of the entire current central tracking system. The vertex tracking (VTX), transiton radiation detector (TRD) and the central and forward drift chambers (CDC and FDC) will be replaced by a combination of silicon microstrip barrel and disk detectors, and a full scintillating fiber tracker. Another major addition will be a superconducting solenoid magnet, surrounding the new tracking system, with a preshower detector located just outside the magnet.

The current scintillating fiber design consists of four "super-layers" at radii of 20.0, 33.0, 44.0, and 55.0 cm inside a 2.0 Tesla superconducting magnet. In each super-layer the fiber layers are arranged in four doublets with half-fiber width offsets. Two of the fiber doublets (axial) are oriented parallel to the beam axis, and the other two are oriented with offset angles to the axial doublets of one to three degrees (*i.e* a constant pitch of 0.001 rad/cm along z). There is a total of 90,000 fibers in this system which are individually read out. The silicon disks and barrels are located inside the fiber barrels and close to the beam. The full DØ upgrade tracker is shown in Figure 8.

A full simulation of the proposed upgrade is available and is used in extensive studies of event reconstruction, track resolutions and efficiencies. In particular, $b\bar{b}$ events with selected $b \to \mu$ decays and J/ψ events have been generated to study tracking performance of the upgrade central tracker.

7.2 *b Physics at the Upgraded DØ Detector*

The copious production of hadrons containing the b quark at the Tevatron will permit a broad range of studies. Results from CDF and the very preliminary DØ sample show that it will be possible to obtain high-statistics, clean samples of B states and J/ψ's. This, and the results from DØ upgrade simulation studies[11], give an optimistic outlook for detecting CP violation in the B-sector at the upgraded DØ . In addition, several more crucial measurements are possible with the upgraded DØ detector, many of them inaccessible to experiments in an e^+e^- collider. Among these unique studies are 1) B_s mixing and determination of V_{ts}; 2) Study of the B_c meson (with its unique spectroscopy of two heavy dissimilar quarks); 3) Exploration of the b-baryon spectroscopy; 4) Rare decays involving flavour changing neutral currents.

As in the original design, a major thrust of the DØ upgrade has been toward high mass, high p_T physics. However, as with the current muon system, the acceptances and resolutions for tracks are adequate to make a significant contribution to b-physics. The phase space of the B-meson decay products fully populates the geometric acceptance of the tracking down to $|\eta| = 3$ and beyond, and also down to very low p_T. In particular, for b-quark physics at the upgrade, there must be a high reconstruction efficiency for tracks which traverse all components of the tracking system: scintilling fibers, silicon barrels and silicon disks. Thus b-physics tracking necessitates a deeper level of tracking system integration than does the high p_T top and W tracking.

Studies have been made with generated $b\bar{b}$ events and selected $b \to \mu$ decays into 2 distinct η regions: $|\eta| \approx 2.0$ and $|\eta| \approx 2.5$. In the first case the muon traverses four silicon disks, two silicon barrels and two fiber barrels; in the second case it traverses seven silicon disks and one silicon barrel. In either case, the track finding efficiency is 100%, with no distortion of the resolutions compared with those found earlier for isolated muon tracks. Figure 8 shows the geometry of the η divisions in the upgrade central tracking - the arrangement of the silicon and fiber elements are such that for any η a track goes through a minimum of 7 tracking devices.

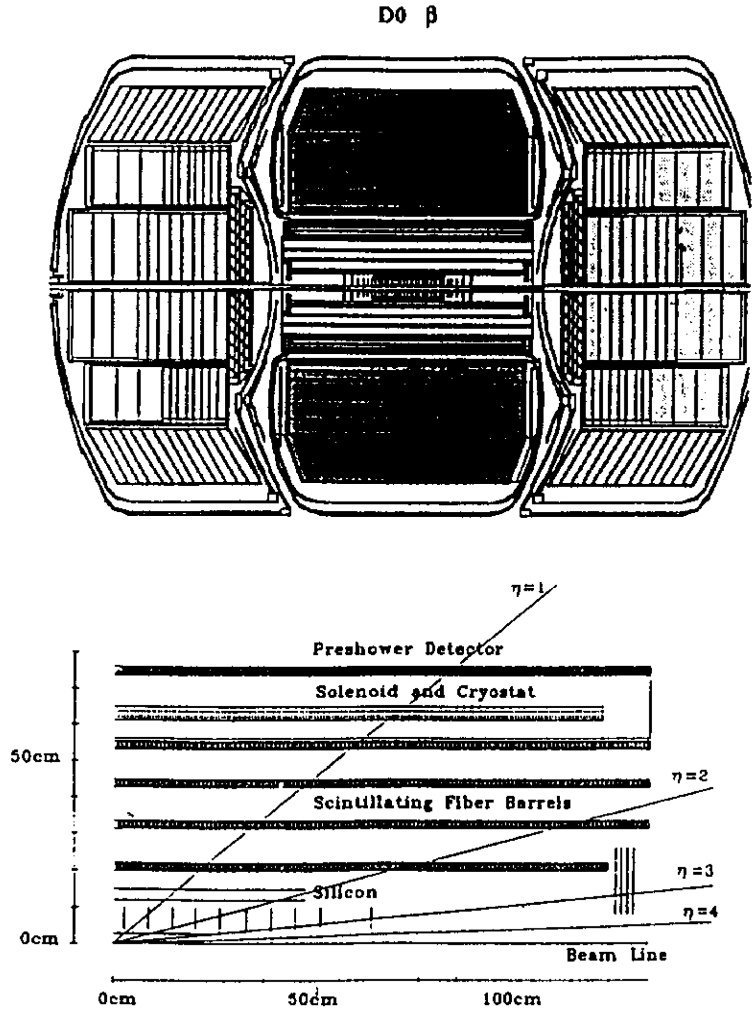

Figure 8. Upgraded DØ detector. The existing central detector is to be replaced by silicon barrels and disks and scintillating fibers, with a solenoid just inside the calorimeter cryostats (top). Details of the Upgrade central tracking shown w.r.t. η (bottom).

A $b\bar{b}$ sample has also been generated where one of the B-mesons decay to a J/ψ and subsequently to a muon pair. The b quark p_T was between 10.0 and 20.0 GeV and that of the muons greater than 2.0 GeV with $|\eta| < 4.0$. Several reconstruction studies have been done on these events. The J/ψmass resolution for 2 different η regions: 1) both muons accepted in the scintillating fiber barrels and 2) both not accepted. These are shown in Figure 9. The resolution obtained in the masses is compatible with that used in previous simulation studies of CP violation. The study here uses full pattern recognition in both disks and barrels.

The results show a favourable outlook for the tracking design to support a strong b physics program. Integrated with the current muon chambers, the upgraded tracking system combines the resolution, vertex reconstruction and the current system's low background from punchthroughs and direct decays needed for CP violation search. The inclusion of the solenoid for the inner tracking effectively doubles the b event sample by identifying the electron B decay channels analogous to those of the muon. With the new central tracking, and the planned electronics upgrades on the existing detector elements, the upgraded DØ detector will be able to satisfy all requirements for a sustained, competitive b physics program for the next decade.

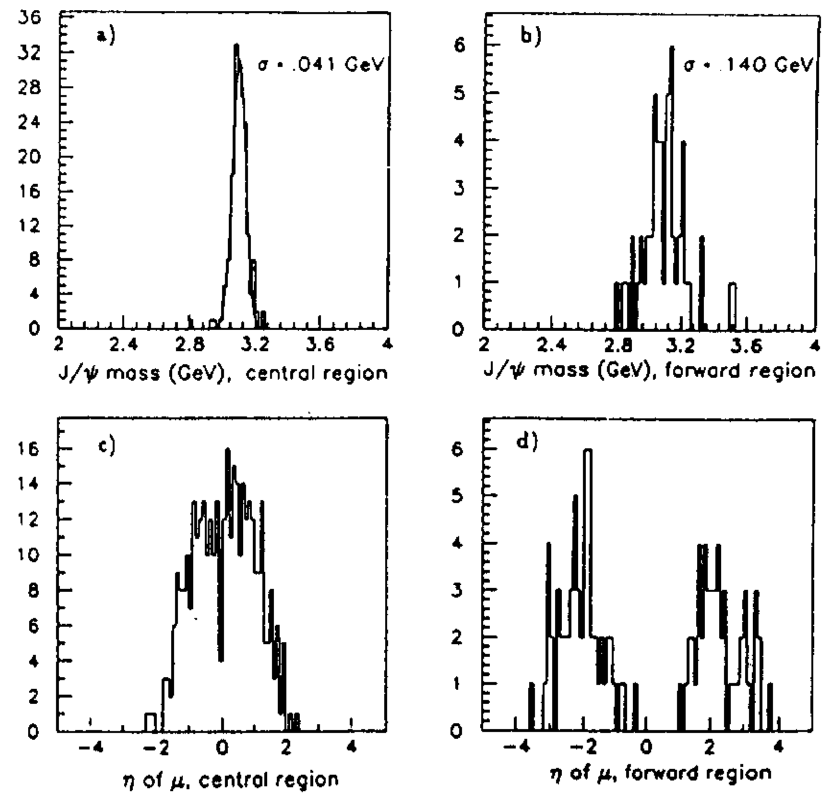

Figure 9.DØ Upgrade simulation. Invariant mass of $\mu\mu$ system in the (a) central and (b) forward region with associated η distributions (c) and (d).

8. SUMMARY

The DØ experiment has completed its first collider run with notable success. Despite the priority given to top, W/Z and QCD programs, the b physics group managed to solve most major outstanding problems in triggering and reconstruction of b-quark produced muons, and demonstrated that the DØ detector has impressive reach to low p_T high η regions where the high cross section for b-quark production can be exploited. DØ produced preliminary results on the inclusive muon cross section out to $|\eta| < 3.3$, and for J/ψ out to $|\eta| < 0.8$. Also produced was a preliminary measurement of the time-averaged mixing probability χ. Prospects for reducing both systematic and statistical errors in these measurements using the full run Ia (1992-1993) data sample are excellent. Since the entire muon trigger was in place by the end of run Ia, the collaboration anticipates all b physics measurements to be made out to the design coverage of $|\eta| < 3.4$ during run Ib. Work on the determination of the $b\bar{b}$ cross sections using the inclusive muon and J/ψ cross sections is in progress. Searches for additional particles such as γ's and $K^o_S s$ associated with J/ψ's are ongoing. The data sample is expected increase by more than an order of magnitude during run Ib. The proposed DØ upgrade will greatly improve the DØ detector's continued b physics programs, in particular, enhancing its prospects for CP violation search in the B system and providing a strong b physics program at Fermilab into the next century.

9. REFERENCES

1. The DØ Collaboration consists of the Universidad de los Andes (Colombia), University of Arizona, Brookhaven National Laboratory, Brown University, University of California,Riverside, Centro Brasiliero de Pesquisas Fisicas (Brazil), CINVESTAV (Mexico), Columbia University, Delhi University (India), Fermilab, Florida State University, University of Hawaii, University of Illinois, Chicago, Indiana University, Iowa State University, Korea University (Korea), Lawrence Berkeley Laboratory, University of Maryland, University of Michigan, Michigan State University, Moscow State University (Russia), New York University, Northeastern University, Northern Illinois University, Northwestern University, University of Notre Dame, Panjab University (India), Institute for High Energy Physics (Russia), Purdue University, Rice University, University of Rochester, CEN Saclay (France), State University of New York,Stony Brook, SSC Laboratory, Tata Institute of Fundamental Research (India), University of Texas, Arlington, and Texas A&M University.
2. S. Abachi et al., "The DØ Detector", submitted to Nucl. Inst. and Methods, and Fermilab PUB 93/179.
3. M. Fortner, et al., *IEEE Transactions on Nuclear Science*, **38**, 480 (1991)
4. C. Albajar, et al., *Phys. Lett.* **B262** (1991) 171.
5. F. Abe et al., *Phys. Lett.* **B67** (1991) 3351.
6. B. Adeva et al., *Phys. Lett.* **B288** (1992) 395.
7. D. Decamp et al., *Phys. Lett.* **B236** (1991) 236.
8. P. Acton et al., *Phys. Lett.* **B276** (1992) 379.
9. C. Albajar, et al., *Phys. Lett.* **B301** (1993) 345.
10. The DØ Upgrade, unpublished (1990)
11. P823 (DØ Upgrade): Responses to the Physics Advisory Committee, DØ note 1148 (1991).
12. P823 (DØ Upgrade): R & D and Optimisation Progress Report, DØ note 1322 (1992).
13. P823 (DØ Upgrade): Step-1 and Beyond, DØ note 1619 (1993).

Extracting CKM parameters from B decays

Isard Dunietz
Fermi National Accelerator Laboratory
Theoretical Physics Department
P.O. Box 500, Batavia, IL 60510

Abstract

This note extracts CKM (Cabibbo-Kobayashi-Maskawa) parameters from currently triggerable B-decay modes. The classic $B_d \to J/\psi K_S$ asymmetry measures the angle β, one of the angles of the CKM unitarity triangle. The other angles of that triangle are more difficult to extract. A tagged, time-dependent study of $B_s \to J/\psi\phi$ extracts the angle γ. Such a study of $B_d \to J/\psi\rho^0$ independently determines γ, where $B_d \to J/\psi K^*$ needs to be studied for normalization purposes. A tagged study of the classic $B_d \to \pi^+\pi^-$ extracts α if the penguin amplitude is negligible. The penguin may be sizeable, however. An involved isospin analysis is then required. It measures α by disentangling the penguin from the tree amplitude. At hadron accelerators, this isospin analysis would require a tagged, time-dependent study of $B_d \to \pi^0\pi^0$, which is currently impossible. This note presents alternatives for measuring α. The angle could be obtained from studies of exclusive modes that are governed by $b \to d\ \ell^+\ell^-$, such as $B \to \rho\ell^+\ell^-$. The branching ratio for such an exclusive mode is tiny, at the few 10^{-8} level. Another method for measuring this angle requires the study of both $B_d \to \pi^+\pi^-$ and $B_s \to K^+K^-$. Many more modes could be used to extract CKM parameters, if triggering on secondary vertices becomes feasible. The methods discussed here require high precision. They require tremendous effort experimentally and theoretically. Experiment will guide us toward the feasible modes and theory must accurately estimate ratios of related strong matrix elements.

1. Introduction

Not all the three angles α, β, and γ of the CKM (Cabibbo-Kobayashi-Maskawa) [1] unitarity triangle [2] can be straightforwardly extracted; see Figure 1. The angle β is the easiest to extract and can be obtained from the $B_d \to J/\psi\ K_S$ asymmetry with negligible hadronic uncertainty [3]. The uncertainty of strong matrix-elements cancels in a ratio which determines the $B_d \to J/\psi K_S$ asymmetry.

The determination of α and γ is more difficult on two fronts. First, the straightforward asymmetries, such as for $B_d \to \pi^-\pi^+$ and $B_s \to \rho^0 K_S$, may not suffice to determine the angles of the CKM triangle, because of penguin diagrams. Elaborate methods have been proposed to overcome this problem [4] - [11]. Second, all existing methods employ modes that cannot currently be triggered on at hadron accelerators.

This note shows how triggerable modes, those with di-leptons in the final state, can extract all the angles of the unitarity triangle: α, β and γ. Further, all the angles can be obtained from triggerable B_d modes alone. Additional triggerable B_s modes are available for the extraction, if the resolution is good enough to observe time-dependent effects of the B_s. Time-integrated rate-asymmetries are not as useful, because they are badly diluted by the large mixing parameter x_s,

$$\frac{\int_0^\infty dt \left[\Gamma\left(B_s(t) \to f\right) - \Gamma\left(\bar{B}_s(t) \to \bar{f}\right)\right]}{\int_0^\infty dt \left[\Gamma\left(B_s(t) \to f\right) + \Gamma\left(\bar{B}_s(t) \to \bar{f}\right)\right]} \sim \frac{\mathrm{Im}\lambda}{x_s} \quad \text{for large } x_s\,. \tag{1}$$

Before turning to the triggerable modes, we briefly review the existing methods. The angle α can be determined from the $B_d \to \pi^+\pi^-,\ \rho^\pm\pi^\mp, a_1^\pm\pi^\mp$ asymmetries [4], when penguin contributions are negligible. For sizeable penguins, elaborate isospin analyses extract α by disentangling the penguin from the tree [5]. Since the $\pi\pi$ isospin analysis requires time-dependent studies of $B_d \to \pi^0\pi^0$ decays at hadron machines, it will not work in the foreseeable future [6]. A combined Dalitz plot and isospin analysis of $B \to \rho\pi$ may be able to determine α [7]. The angle α can also be extracted from six decay modes related to $B_d \to D^0 K_S$ [8], or variants thereof [9].

Most methods extract γ from tagged, time-dependent studies of specific B_s-decays. Experimentalists will have to learn how to observe the rapid B_s-oscillations for very large B_s mixing,

$$x_s \gtrsim 20\,. \tag{2}$$

The $B_s \to \rho^0 K_S$ asymmetry would measure γ, if penguins could be neglected. But penguins may not be negligible, and γ cannot be cleanly extracted from the asymmetry. Anyway, the branching ratio of this color-suppressed mode is expected to be tiny, at the 10^{-7} level [10].

The angle γ can be extracted from tagged, time-dependent studies of [10] $B_s \to D_s^\pm K^\mp$ or $B_s \to D^0\phi$ [8]. Penguins cannot contribute and the branching ratio for the color-favored $B_s \to D_s^\pm K^\mp$ mode is expected to be large,

$$B(B_s \to D_s^\pm K^\mp) \sim 2 \times 10^{-4}\,. \tag{3}$$

Modes of beautiful hadrons with neutral D's can be used to extract γ. Neither tagging nor time-dependence is required for this extraction. The angle γ is obtained by measuring the rates of six processes, $B \to D^0 K, \bar{D}^0 K, D^0_{CP} K$ and their CP-conjugated partners [8], [11]. Here D^0_{CP} denotes that the neutral D is seen in modes with definite CP parity.

We designate by K^r those resonances of K^0 which can appreciably be seen both in modes that determine their kaon flavor and in modes where the kaon flavor is lost. The K^r_{CP} denotes CP-eigenmodes of the K^r resonance, which are modes with undetermined kaon flavor. Two such resonances are K^{*0} and $K_1(1270)$. The K^{*0} is seen in its $K^+\pi^-$ mode two-thirds of the time and in its $K_S\pi^0$ mode one-sixth of the time. Because the π^0 may be difficult to detect in a hadronic environment, we consider the $K_1(1270)$. It is not too broad, $\Gamma \simeq 90$ MeV, and is seen appreciably in the $K_0^{*+}(1430)\pi^-$ and $K^{*+}\pi^-$ modes that tag the original kaon-flavor. A mode where the original kaon-flavor is lost is

$$B(K_1(1270) \to K_S\rho^0) = 0.07\,. \tag{4}$$

A Dalitz plot analysis distinguishes among the various modes of $K_1(1270)$.

Time-dependent studies are reviewed in Section 2. Section 3 shows that a tagged, time-dependent study of $B_s \to J/\psi\phi$ measures γ or alternatively α. It notes, in passing, that a similar study of color-allowed modes, $B_s \to D_s^+ D_s^-, D_s^{*+}D_s^{*-}, D_s^+ D_s^{*-}, D_s^{*+}D_s^-$, extracts the same CKM angle. Section 4 mentions that the $b \to d + c\bar{c}$ transition involves non-spectator amplitudes at the few percent level compared to the dominant spectator one. The interference between the non-spectator with the spectator amplitude could result in direct CP violation [12]. Section 5 exploits this interference to measure γ from a tagged, time-dependent study of any of the following processes of $B_d \to J/\psi\ \rho^0, J/\psi\omega, J/\psi\pi^0, B_s \to J/\psi\ K_S, B_s \to J/\psi\ \bar{K}^{*0}, B_s \to J/\psi\ \bar{K}^r$. The measurement of γ can be performed regardless of whether direct CP violation occurs. Section 6 sketches the extraction of the angle α from CKM suppressed exclusive rare decays governed by $b \to d + \ell^+\ell^-$, such as $B \to \rho\ \ell^+\ell^-, B \to \pi\ \ell^+\ell^-, B \to \omega\ \ell^+\ell^-$. If we could succeed in triggering on secondary vertices, many more modes could be used to measure CKM parameters. Although some of those modes are briefly discussed in Sections 3 and 5, Sections 7 and 8 are devoted entirely to them. Section 7 determines α from the $B_d \to \pi^+\pi^-$ mode when the penguin graph contributes sizeably, without recourse to an isospin analysis. The determination of CKM parameters from many additional modes, governed by $b \to d$ + charmless, is covered in Section 8. The short hand $b \to d$ + charmless denotes any of the $b \to du\bar{u}, b \to dd\bar{d}$ and $b \to ds\bar{s}$ quark transitions. Sections 5 - 8 extract the CKM angles up to discrete ambiguities. We chose not to discuss them because the treatment would become more cumbersome. The time to analyze all the possible ambiguities is when data has been accumulated. Unfortunately this lies many years into the future. Conclusions can be found in Section 9.

The CKM angles can be extracted only when ratios of related strong matrix elements are accurately known, except in the method described in Section 3. Those ratios will have to be analyzed carefully.

We have organized this report in terms of measuring the CKM angles α, β, and γ, because this has become the popular description of the CKM model. However, on a more fundamental level, the CKM matrix can be parametrized by a single CP-violating parameter and three magnitudes. Within that context, the report extracts various CKM combinations. The extractions allow the overdetermination of the CKM model.

2. Time-Dependence

This section reviews time-dependent amplitudes for the decay of a neutral B to a final state f [13, 14, 4]. This intriguing phenomenon occurs because of $B^0 - \bar{B}^0$ mixing. The time-evolutions of initially unmixed B^0 and $\bar{B}^0$ are

$$|B^0(t)\rangle = c(t)\,|B^0\rangle + i\,\frac{q}{p}\,s(t)\,|\bar{B}^0\rangle\,, \tag{5}$$

$$|\bar{B}^0(t)\rangle = c(t)\,|\bar{B}^0\rangle + i\,\frac{p}{q}\,s(t)\,|B^0\rangle\,, \tag{6}$$

where

$$c(t) = e^{-i\,\frac{m_L+m_H}{2}t}\,e^{-\frac{\Gamma}{2}t}\,\cos\frac{\Delta m t}{2}\,, \tag{7}$$

$$s(t) = e^{-i\,\frac{m_L+m_H}{2}t}\,e^{-\frac{\Gamma t}{2}}\,\sin\frac{\Delta m t}{2}\,. \tag{8}$$

The parameters q and p are the coefficients which relate the B^0 and $\bar{B}^0$ to the mass-eigenstates. The CKM model predicts

$$|q/p| \approx 1, \tag{9}$$

to an accuracy of 10^{-3} for the B_d system, and to 10^{-4} for the B_s system. The ratio q/p is essentially a phase given by

$$\frac{q}{p} = \frac{V_{tb}^* V_{tx}}{V_{tb} V_{tx}^*} \tag{10}$$

where $x = d$ or s for the B_d or B_s system. Define the CP-conjugated final-state as

$$|\bar{f}\rangle = CP|f\rangle\,. \tag{11}$$

Consider the four time-dependent rates of an initially unmixed neutral B to f and $\bar{f}$.

$$\begin{aligned}\Gamma\left(B^0(t) \to f\right) &= e^{-\Gamma t}\Big\{|\langle f|B^0\rangle|^2\cos^2\frac{\Delta m t}{2} + |\langle f|\bar{B}^0\rangle|^2\sin^2\frac{\Delta m t}{2}\\ &- |\langle f|B^0\rangle|^2 \mathrm{Im}\,\lambda\sin\Delta m t\Big\}\,,\end{aligned} \tag{12}$$

$$\begin{aligned}\Gamma\left(\bar{B}^0(t) \to f\right) &= e^{-\Gamma t}\Big\{|\langle f|\bar{B}^0\rangle|^2\cos^2\frac{\Delta m t}{2} + |\langle f|B^0\rangle|^2\sin^2\frac{\Delta m t}{2}\\ &+ |\langle f|B^0\rangle|^2 \mathrm{Im}\,\lambda\sin\Delta m t\Big\}\,,\end{aligned} \tag{13}$$

$$\begin{aligned}\Gamma\left(\bar{B}^0(t) \to \bar{f}\right) &= e^{-\Gamma t}\Big\{|\langle \bar{f}|\bar{B}^0\rangle|^2\cos^2\frac{\Delta m t}{2} + |\langle \bar{f}|B^0\rangle|^2\sin^2\frac{\Delta m t}{2}\\ &+ |\langle \bar{f}|B^0\rangle|^2 \mathrm{Im}\,\lambda'\sin\Delta m t\Big\}\,,\end{aligned} \tag{14}$$

$$\begin{aligned}\Gamma\left(B^0(t) \to \bar{f}\right) &= e^{-\Gamma t}\Big\{|\langle \bar{f}|B^0\rangle|^2\cos^2\frac{\Delta m t}{2} + |\langle \bar{f}|\bar{B}^0\rangle|^2\sin^2\frac{\Delta m t}{2}\\ &- |\langle \bar{f}|B^0\rangle|^2 \mathrm{Im}\,\lambda'\sin\Delta m t\Big\}\,,\end{aligned} \tag{15}$$

where

$$\lambda \equiv \lambda\,(B^0 \to f) \equiv \frac{q}{p}\,\frac{\langle f|\bar{B}^0\rangle}{\langle f|B^0\rangle}\,, \tag{16}$$

$$\lambda' \equiv \lambda(B^0 \to \bar{f}) \equiv \frac{q}{p}\,\frac{\langle \bar{f}|\bar{B}^0\rangle}{\langle \bar{f}|B^0\rangle}\,. \tag{17}$$

The distinction between an initial unmixed B^0 and $\bar{B}^0$ is called tagging. Whenever we speak about a tagged, time-dependent study of $B^0 \to f$, we mean the study of all four time-dependent rates, Eqs. (12)-(15). For final states which are CP eigenstates, only two distinct time-dependent rates exist.

A tagged, time-dependent study measures the magnitudes of the unmixed amplitudes,

$$|\langle f|B^0\rangle|,\ \ |\langle f|\bar{B}^0\rangle|,\ \ |\langle \bar{f}|\bar{B}^0\rangle|,\ \ |\langle \bar{f}|B^0\rangle| \tag{18}$$

and

$$\mathrm{Im}\ \lambda(B^0 \to f),\ \ \mathrm{Im}\ \lambda(B^0 \to \bar{f}). \tag{19}$$

Strictly speaking the four time-dependent rates of Eqs. (12)-(15) were derived under the assumption that there is no lifetime difference ($\Delta\Gamma$) between the heavy and light B^0. While $\Delta\Gamma$ may be observable in the B_s system [15, 16],

$$\Delta\Gamma/\Gamma \sim 10\%, \tag{20}$$

it is negligible for the B_d system. Tagged, time-dependent fits with non-zero $\Delta\Gamma$ extract, in addition to the above observables, Eqs. (18)-(19), the quantities [13]

$$\mathrm{Re}\ \lambda(B^0 \to f)\ \text{ and }\ \mathrm{Re}\ \lambda(B^0 \to \bar{f}). \tag{21}$$

The λ's will be known without any ambiguity.

3. γ (or α) from $B_s \to J/\psi\phi$

The angle γ can be extracted from tagged, time-dependent measurements of $\bar{B}_s \to J/\psi\ \phi$ [13, 17]. The unmixed $\bar{B}_s \to J/\psi\ \phi$ amplitude is dominated by the CKM combination $V_{cb}V_{cs}^*$, and $B(\bar{B}_s \to J/\psi\ \phi) \approx 10^{-3}$ can be inferred from the measured $B(B_d \to J/\psi K^{*0})$ [18]. The amplitude with the different CKM combination $V_{ub}V_{us}^*$ is negligible, because it is suppressed by three orders of magnitude [12]. A tagged, time-dependent study of $B_s \to J/\psi\ \phi$ measures

$$\lambda = \frac{V_{tb}^*\ V_{ts}}{V_{tb}\ V_{ts}^*}\ \ \frac{V_{cb}\ V_{cs}^*}{V_{cb}^*\ V_{cs}}\,. \tag{22}$$

The final state has both CP-even and CP-odd components, diluting the CP asymmetry. An angular analysis can disentangle the CP-odd from the CP-even contributions [19, 20]. It extracts λ without loss in statistical accuracy when one CP-parity dominates. But even when no CP-parity dominates, the full angular distribution measures Imλ with a statistical accuracy that at worst would require no more than four times the statistics compared to a definite CP eigenstate [20]. CLEO and ARGUS results indicate that the helicity-zero $B_d \to J/\psi\ K^{*0}$ amplitude is dominant [21]. This result suggests that the final state of $B_s \to J/\psi\ \phi$ is mainly CP-even.

The tagged, time-dependent distribution (for the CP-even part) is

$$\Gamma\left(\overset{(-)}{B_s^0}(t) \to J/\psi\ \phi\right) \sim e^{-\Gamma t}\left\{1 \overset{(+)}{-} \mathrm{Im}\ \lambda\ \sin\ \Delta m t\right\}, \tag{23}$$

where Γ denotes the B^o lifetime, Δm the positive $B^o - \bar{B}^o$ mass difference, and

$$\mathrm{Im}\lambda = 2|V_{cd}|\left|\frac{V_{ub}}{V_{cb}}\right|\sin\gamma\left(1+\mathcal{O}\left(\theta^2\right)\right) \tag{24}$$

$$= 2|V_{cd}|\left|\frac{V_{td}}{V_{cb}}\right|\sin\beta\left(1+\mathcal{O}\left(\theta^2\right)\right) \tag{25}$$

$$= 2\left|\frac{V_{td}\ V_{ub}}{V_{cb}^2}\right|\sin\alpha\left(1+\mathcal{O}\left(\theta^2\right)\right) \tag{26}$$

The sine of the Cabibbo angle is denoted by $\theta \equiv \sin\ \theta_c = 0.22$.

Measuring Imλ requires the tagged, time-dependent study of $B_s \to J/\psi\ \phi$. Once Imλ is measured, we can either choose to determine $\sin\gamma$ by using Eq. (24) with the by then accurate measurement of $|V_{ub}/V_{cb}|$. Or $\sin\alpha$ can be extracted from Eq. (26) with the by then well known quantities $|V_{td}V_{ub}/V_{cb}^2|$.

The CKM model predicts large values for γ,

$$0.3 \lesssim \sin\gamma \le 1. \tag{27}$$

Equation (27) and present measurements of $|V_{ub}/V_{cb}|$ guarantee that the interference term never vanishes,

$$0.01 \lesssim \mathrm{Im}\lambda \lesssim 0.05. \tag{28}$$

Thus the CKM model predicts *nonvanishing* CP violation at the θ^2 level. Measuring Imλ = 0.05 (to 3σ) requires the observation of 3600 tagged $B_s \to J/\psi\ \phi$ decays, assuming perfect tagging and time-resolution.

The same CP violating interference term occurs for the modes governed by $b \to c\bar{c}s$, such as $B_s \to D_s^+D_s^-, D_s^{*+}D_s^{*-}, D_s^+D_s^{*-}, D_s^{*+}D_s^-$. Those modes are dominantly CP-even [16]. To increase the data sample, they could be added and measure Imλ up to a correction that depends upon the dilution coming from the CP-odd parity.

4. Direct CP Violation with $b \to d(c\bar{c})$

The branching ratio for the color and CKM suppressed exclusive decay mode $H_b \to H_d J/\psi$ is,

$$B(H_b \to H_d J/\psi) \sim 5 \times 10^{-5} . \tag{29}$$

Here H_b (H_d) denotes a bottom (down)-quark flavored hadron. Rate asymmetries at the few percent level are possible [12]. They require neither tagging nor time-dependences, except for modes of neutral B mesons where H_d decays into a CP eigenstate.

The comparison between the $H_b \to H_d J/\psi$ process with its CP-transformed partner may exhibit CP violation not only in a rate comparison, but in other decay parameters as well. For instance, compare

$$\begin{aligned}
B^- \to J/\psi\pi^- &\text{ versus } B^+ \to J/\psi\pi^+, \\
B^- \to J/\psi a_1^- &\text{ versus } B^+ \to J/\psi a_1^+, \\
B^- \to J/\psi\rho^- &\text{ versus } B^+ \to J/\psi\rho^+, \\
\bar{B}_s \to J/\psi K^{*0} &\text{ versus } B_s \to J/\psi \bar{K}^{*0}, \\
\bar{B}_s \to J/\psi K^+\pi^- &\text{ versus } B_s \to J/\psi K^-\pi^+, \\
\Xi_b^0 \to J/\psi\Lambda &\text{ versus } \bar{\Xi}_b^0 \to J/\psi\bar{\Lambda}, \\
\Omega_b^- \to J/\psi\Xi^- &\text{ versus } \bar{\Omega}_b^+ \to J/\psi\bar{\Xi}^+ .
\end{aligned}$$

The amplitude for the process is

$$A \equiv A(H_b \to H_d J/\psi) = \xi_c a_2 + \xi_u a_u , \tag{30}$$

while that for the CP-conjugated process is

$$\bar{A} \equiv A(\bar{H}_b \to \bar{H}_d J/\psi) = \xi_c^* a_2 + \xi_u^* a_u. \tag{31}$$

Here

$$\xi_q = V_{qb} V_{qd}^*, \quad q = u, c, t, \tag{32}$$

are CKM combinations, and a_2 and a_u strong matrix elements which probably differ in their final-state phases. Unitarity of the CKM matrix eliminated the ξ_t contribution to the amplitude. One CP violating observable is the rate asymmetry,

$$\begin{aligned}
\text{Asym} &\equiv \frac{|A|^2 - |\bar{A}|^2}{|A|^2 + |\bar{A}|^2} \simeq \\
&\simeq -2\sin\gamma \ \text{Im}\left(\frac{a_u}{a_2}\right) \left|\frac{V_{ub}V_{ud}}{V_{cb}V_{cd}}\right|
\end{aligned} \tag{33}$$

The CKM model predicts $\sin\gamma$ to be large, Eq. (27). A recent report has shown that [12]

$$|a_u/a_2| \simeq 0.05 , \tag{34}$$

where a_u is estimated from the one-loop electroweak contributions. The conventional non-leptonic penguin amplitude requires at least three gluons to create the J/ψ. The final-state phase difference is currently being investigated [22].

There is no need to limit ourselves to the $H_b \to J/\psi H_d$ modes. CP asymmetries at the 1% level occur for the truly semi-inclusive $b \to c\bar{c}d$ mode. For instance, the asymmetry would show up when all the B^- modes governed by $b \to dc\bar{c}$ are summed over, such as $B^- \to D^- D^0$, $D^{*-}D^0, D^-D^{*0}, D^{*-}D^{*0}, J/\psi\pi^-, J/\psi\rho^-, J/\psi a_1^-$, etc. Neither tagging nor time-dependences are required to observe this CP violating effect. The inclusive $b \to dc\bar{c}$ asymmetry can be more reliably calculated than the exclusive ones. It is trivial to obtain the asymmetry from the existing literature which considered $b \to d$ + charmless. Some choice exclusive modes have been studied [23, 24]. The CPT theorem requires that [25]

$$\Gamma(b \to dc\bar{c}) - \Gamma\left(\bar{b} \to \bar{d}c\bar{c}\right) = -\left(\Gamma(b \to d + \text{charmless}) - \Gamma\left(\bar{b} \to \bar{d} + \text{charmless}\right)\right) \tag{35}$$

Thus the inclusive $b \to dc\bar{c}$ asymmetry can be estimated from the published calculations of $b \to d$ + charmless [26]. But let us review what is involved in calculating the inclusive $b \to dc\bar{c}$ asymmetry. First, the q^2 dependence of the virtual gluon of the penguin graph is tightly constrained, $4m_c^2 < q^2 < m_b^2$. The gluon is hard and can be treated perturbatively. Further, the absorptive part relevant for CP violation emerging from the u-quark loop is not kinematically suppressed. Asymmetries at the percent level result. This perturbative treatment is more justifiable for the inclusive $b \to dc\bar{c}$ process than for the exclusive modes, such as $B^- \to D^0D^-$, $D^0D^{*-}, D^{*0}D^-, D^{*0}D^{*-}$, because of rescattering among them. It is possible that some of the exclusive modes will show larger CP-violating effects, which will be compensated by smaller effects with other modes.

In conclusion, the CKM-suppressed modes governed by the $b \to d\, c\bar{c}$ transition may show direct CP violating effects at best at the few percent level. Although $\sin\gamma$ is proportional to the rate asymmetry, we cannot extract it, due to our lack of understanding about final-state interactions. The effects of final state interactions largely cancel in ratios of related processes. Such ratios may then allow the extraction of CKM parameters, which will be the topic of the next sections.

5. γ from $B_d \to J/\psi\rho^0$

Section 4 focussed on exclusive modes governed by $b \to d c\bar{c}$. Those modes involve two interfering amplitudes with the relative CKM angle γ. If the strong matrix elements could be calculated from first principles, the CKM parameters could be extracted from CP-violating effects and other observables. However, our ability to estimate strong matrix elements is meager. Although we are currently not able to estimate strong matrix elements, we may be able to estimate their ratios more reliably. This note extracts CKM parameters by using such ratios. The extraction of γ will be illustrated with the $B_d \to J/\psi\rho^0$ mode, where $B_d \to J/\psi K^{*0}$ serves as normalization. However, each of the modes, $B_d \to J/\psi\pi^0, J/\psi\omega, D^+D^-, D^{*+}D^-, D^+D^{*-}, D^{*+}D^{*-}$, etc., extracts γ, with the normalization coming from $B_d \to J/\psi K_S, J/\psi K^{*0}, D_s^+D^-, D_s^{*+}D^-, D_s^+D^{*-}, D_s^{*+}D^{*-}$, etc., respectively.

For the exclusive modes governed by $b \to d c\bar{c}$, factorization applied to the effective Hamiltonian predicts a penguin to tree amplitude-ratio of a few percent [12, 22], $|a_u/a_2| \sim 0.05$. This section demonstrates that γ can be extracted regardless of whether or not the final-state phase difference—that is, the phase of a_u/a_2—vanishes.

Consider then the $B_d \to J/\psi\rho^0$ mode and use $B_d \to J/\psi K^{*0}$ as normalization. The amplitude of the unmixed $\bar{B}_d \to J/\psi\rho^0$ is

$$\bar{A} \equiv \langle\, J/\psi\rho^0|\bar{B}_d\rangle = \xi_c a_2 + \xi_u a_u = \xi_c a_2[1 + ze^{-i\gamma}] = \xi_c a_2 \bar{b}\,, \tag{36}$$

while that for the unmixed $B_d \to J/\psi\rho^0$ is

$$A \equiv \langle\, J/\psi\rho^0|B_d\rangle = \xi_c^* a_2[1 + ze^{i\gamma}] = \xi_c^* a_2 b\,. \tag{37}$$

The normalization comes from the CKM favored mode $B_d \to J/\psi K^{*0}$,

$$\langle\, J/\psi K^{*0}|B_d\rangle = -\sqrt{2}\,(v_c^* a_2 + v_u^* a_u) = -\sqrt{2}\,v_c^* a_2[1 + \mathcal{O}(10^{-3})]\,, \tag{38}$$

where $v_q = V_{qb}V_{qs}^*$. Since the final state consists of two spin one particles, three helicity amplitudes contribute. A full angular analysis disentangles them, as shown in Appendix A. The helicity zero amplitude probably dominates the decay, as in $B_d \to J/\psi K^{*0}$ [21]. We assume that to be the case so as to illustrate the point most simply. Otherwise a full angular analysis will obtain the CKM-parameter; see Appendix A. A tagged, time-dependent $B_d \to J/\psi\rho^0$ study determines

$$|A|^2,\ |\bar{A}|^2\,,\ \text{ and }\ \mathrm{Im}\lambda(B_d \to J/\psi\rho^0)\,. \tag{39}$$

The last observable combined with the observation of CP-violation in $B_d \to J/\psi K_S$ yields $\arg(\bar{b}/b)$, because

$$\lambda(B_d \to J/\psi\rho^0) = -\lambda(B_d \to J/\psi K_S)\frac{\bar{b}}{b}\,. \tag{40}$$

In fact, the isospin related processes, $B^{\mp} \to J/\psi\rho^{\mp}$, measure $|\bar{A}|$ and $|A|$ without tagging and without time-dependence. Then the determination of $\mathrm{Im}\lambda(B_d \to J/\psi\rho^0)$ might not require time-dependence. It does require tagging, however. By normalizing with $B_d \to J/\psi K^{*0}$, we measure $|b|^2, |\bar{b}|^2$, since

$$\begin{aligned} \left|\frac{\langle\, J/\psi\rho^0|B_d\rangle}{\langle\, J/\psi K^{*0}|B_d\rangle}\right|^2 &= \frac{1}{2}\left|\frac{V_{cd}}{V_{cs}}\right|^2 r\left|1 + ze^{+i\gamma}\right|^2 = \\ &= \frac{1}{2}\left|\frac{V_{cd}}{V_{cs}}\right|^2 r\left|b\right|^2. \end{aligned} \tag{41}$$

Here r is the ratio of the strong matrix elements a_2 and will come from theory [27],

$$r \equiv \left|\frac{a_2(B_d \to J/\psi\rho^0)}{a_2(B_d \to J/\psi K^{*0})}\right|^2. \tag{42}$$

It must be accurately calculated and need not be close to 1. Eq. (41) determines $|b|$, since $|V_{cd}/V_{cs}| \approx \theta$, r will be given from theory, and the left-hand side of Eq. (41) is a ratio of rates. Fig. 2 shows the two amplitude triangles,

$$\bar{b} = 1 + ze^{-i\gamma}, b = 1 + ze^{i\gamma}\,. \tag{43}$$

The points B and $\bar{B}$ are equidistant from O, and the angle between $O\bar{B}$ and OB is 2γ. Let us extract γ from the observables, which are $|b|, |\bar{b}|$ and $\arg(\bar{b}/b)$.

We measure the lengths of b and $\bar{b}$ and the angle between them. Let us draw them. The point O is not yet fixed. It is equidistant from points B and $\bar{B}$, that is–point O is somewhere on line d, see Fig. 2. However, normalization demands that EO is of unit length. The location of point O is thus determined, and the angle γ can be obtained.

Studies of $B_d \to J/\psi\rho^0$ and $B_d \to J/\psi K^{*0}$ extract the angle γ. The extraction is accomplished by observing the interference between the spectator and non-spectator diagrams. The angle γ can be extracted whether or not direct CP violation occurs—that is, whether z has a phase or is real—as long as $|z|$ does not vanish. The extraction requires the knowledge of the ratio of matrix elements, r.

The specific mode $B_d \to J/\psi\rho^0$ suffers from drawbacks. The small phase of $\bar{b}/b$ must be disentangled from the large CP violating interference terms, $\lambda(B_d \to J/\psi K_S)$ and $\lambda(B_d \to J/\psi\rho^0)$, see Eq. (40). The final-state interactions may differ for the $J/\psi K^{*0}$ and $J/\psi\rho^0$ modes, and thus r may not be able to be calculated accurately. Furthermore, even within the $SU(3)$ limit, the ratio r is not exactly 1, because the W-exchange diagram contributes to $B_d \to J/\psi\rho^0$ but does not to $B_d \to J/\psi K^{*0}$. This is an academic problem, because the W-exchange diagram is expected to be highly suppressed compared to the spectator one. Those drawbacks can be overcome by tagged, time-dependent studies of specific B_s modes as shown in Appendix B.

What makes this method difficult is that the interfering amplitudes, which are governed by different CKM combinations, are so unequal, $|z| \ll 1$. Tagged, time-dependent studies of $B_s \to D_s^{\pm}K^{\mp}$ and $B_s \to J/\psi\phi$ are most likely superior in extracting γ. Our motivation to present the $B_d \to J/\psi\rho^0$ method is two-fold. It may not be possible to study time-dependences of B_s accurately, if x_s is large. Secondly, we wanted to point out that, in principle, triggerable B^0-modes allow the extraction of CKM parameters in addition to β.

An analogous method extracts α from exclusive modes governed by the $b \to d\ell^+\ell^-$ transition. This is the topic of the next section. The interfering amplitudes are of similar strength, and the interference term yields the phase between the two unmixed amplitudes without any disentangling. Those are two important advantages over the modes discussed in this section. The branching ratio is miniscule, however.

6. α from $B \to \rho\, \ell^+\ell^-$

The angle α can be extracted from the once CKM-suppressed exclusive rare processes, governed by $b \to d\ell^+\ell^-$. The branching ratio is tiny, at the few $\times 10^{-8}$ level.

$$B(B \to \rho\, \ell^+\ell^-) \sim 10^{-7} - 10^{-8}\,. \qquad (44)$$

The modes of interest are three body decays, such as $B \to \rho\ell^+\ell^-, \pi\ell^+\ell^-, a_1\ell^+\ell^-, B_s \to \bar{K}^*\ell^+\ell^-$, etc. The amplitude varies around the Dalitz plot. The variation [28] and the short- and long-distance [29] contributions have been theoretically analyzed for the CKM-favored $b \to s\ell^+\ell^-$ modes. The analyses can be modified to apply to the modes of interest here $b \to d\ell^+\ell^-$ [30]. Our aim is only to sketch several ways to extract α. We thus simplify and treat the amplitude as a complex number. We are currently investigating how to optimize the extraction of α. The unmixed amplitudes are

$$\begin{aligned} \langle\, \rho^0\ell^+\ell^-|B_d\rangle &= \xi_t^* z_t[1 + z\, e^{-i\alpha}] = \xi_t^* z_t E, \\ \langle\, \rho^0\ell^+\ell^-|\bar{B}_d\rangle &= \xi_t z_t[1 + z\, e^{i\alpha}] = \xi_t z_t \bar{E}, \end{aligned} \qquad (45)$$

where z_t is a strong matrix element, and z depends on ratios of strong matrix elements and on the magnitude of the CKM combination $|V_{ub}V_{ud}|/|V_{tb}V_{td}|$. This parameter z differs from the one in Section 5 and varies around the Dalitz plot. An honest determination of α must take the variation into account, which however is ignored here as stated above.

Large direct CP violation occurs with exclusive rare modes governed by $b \to d\ell^+\ell^-$ [30]. The parameter z is of order unity with a large final state phase difference [30]. A few options exist to determine α. The $B_d \to K^{*0}\ell^+\ell^-$ mode can be used as normalization,

$$\langle\, K^{*0}\ell^+\ell^-|B_d\rangle = -\sqrt{2}\, v_t^* z_t[1 + \mathcal{O}(10^{-2})]\,. \qquad (46)$$

Then we get

$$\left|\frac{\langle\, \rho^0\ell^+\ell^-|B_d\rangle}{\langle\, K^{*0}\ell^+\ell^-|B_d\rangle}\right|^2 = \frac{1}{2}\left|\frac{V_{td}}{V_{ts}}\right|^2 |1 + ze^{-i\alpha}|^2 = \frac{1}{2}\left|\frac{V_{td}}{V_{ts}}\right|^2 |E|^2\,, \qquad (47)$$

where we omit an $SU(3)$ breaking ratio of order unity, for simplicity. Clearly, by the time experiments capable of measuring this ratio will be feasible, the CKM ratio $|V_{td}/V_{ts}|$ will be well-known. A tagged, time-dependent study of $B_d \to \rho^0\ell^+\ell^-$ yields

$$|E|,\ |\bar{E}| \text{ and} \qquad (48)$$

$$\mathrm{Im}\lambda(B_d \to \rho^0\ell^+\ell^-) = \mathrm{Im}\frac{\bar{E}}{E}\,. \qquad (49)$$

The moduli of the unmixed amplitudes can also be obtained from the isospin related charged B decays, $B^{\pm} \to \rho^{\pm}\, \ell^+\ell^-$. Neither tagging nor time-dependence is required. Note that the interference term informs us directly about the relative phase between E and $\bar{E}$, without having to involve another CP-violating measurement, in contrast to Eq. (40). The angle α is extracted "in analogy" to the extraction of γ from $B_d \to \rho^0 J/\psi$ [31]. If time-dependent B_s-measurements are feasible, α could also be determined from B_s modes; see Appendix B.

A second variant could be to measure only the moduli of the two "unmixed" amplitudes and use the calculated z. This suffices to extract α. The moduli could be obtained from the charged B-decays, $B^{\pm} \to \pi^{\pm}\ell^+\ell^-, a_1^{\pm}\ell^+\ell^-$, etc. The mode $B \to K^{(*)}\ell^+\ell^-$ would provide the normalization. The two moduli could alternatively come from $B_s \to \bar{K}^{*0}\ell^+\ell^-$ and $\bar{B}_s \to K^{*0}\ell^+\ell^-$, which are self-tagging since K^{*0} is seen in its $K^+\pi^-$ mode. Theoretical uncertainties are probably reduced since the B_d-mode with identical particle content $B_d \to K^{*0}\ell^+\ell^-$ could be used for normalization. Neither tagging nor time-dependence would ever be necessary. A third variant eliminates normalization. The two moduli of the unmixed amplitudes, the interference term $\arg(\bar{E}/E)$, and the calculated z suffice to determine α.

The amplitude ratio z is of order unity for the exclusive $b \to d\, \ell^+\ell^-$ processes, in contrast to the exclusive $b \to dJ/\psi$ modes where it is tiny at the few percent level. Thus, the angle α may be more readily extracted than the angle γ by the method discussed here.

The extraction of α is also possible from modes with a photon, by using variant 2. The angle α cannot be extracted from methods that involve an interference term λ, for modes with a photon. The interference term vanishes because only one helicity occurs from the B^0-decay and the other from the $\bar{B}^0$-decay [32]. Variant 2 measures the moduli of the two amplitudes of $B^+ \to a_1^+\gamma$ and $B^- \to a_1^-\gamma$, or $B^\pm \to \rho^\pm\gamma$. It normalizes from $B \to K^*\gamma$. The two moduli of $B_s \to \bar{K}^{*0}\gamma$ and $\bar{B}_s \to K^{*0}\gamma$ also extract α, where the normalization comes from $B_d \to K^*\gamma$ or alternatively from $B_s \to \phi\gamma$. The parameter z here is different from that of $B_d \to \rho^0\ell^+\ell^-$ or $B \to \rho^0 J/\psi$, and is in principle calculable. A first step was taken by Soares, who calculated [32]

$$z \approx (0.09 + i\,0.13)|V_{ub}/V_{td}| \,. \tag{50}$$

More theoretical work is required in calculating this z reliably. Because the final state is simpler than non-leptonic modes, there is more hope that theory will estimate z reliably.

In summary, exclusive modes governed by the $b \to d$ transition extract the angle α. In addition to the information coming from the relevant modes, the extraction requires experimental and theoretical input. Experiments must inform us about $|V_{td}/V_{ts}|$, and theory about z and about ratios of strong matrix elements.

7. α from $B_d \to \pi^+\pi^-$ and $B_s \to K^+K^-$

The tagged $B_d \to \pi^+\pi^-$ mode extracts α, for negligible penguin amplitudes. It may occur, however, that penguin contributions are significant compared to the tree one. An elaborate isospin analysis could determine α by disentangling the tree from the penguin [5]. At hadron accelerators, it requires a tagged, time-dependent study of the $B_d \to \pi^0\pi^0$ mode, which at present cannot be achieved [6].

This section presents alternative measurements of α in the case of large penguins. We assume that flavor $SU(3)$ for B-decays [33] and its breaking terms will be well understood. One way could be to have a tagged, time-dependent $B_d \to \pi^+\pi^-$ study with the normalization coming from $B_d \to K^+\pi^-$. This method is analogous to the extraction of γ from the tagged, time-dependent $B_d \to J/\psi\rho^0$ study, where the normalization comes from $B_d \to J/\psi K^*$, see Section 5.

The accuracy on α depends on how dominant the penguin is over the tree amplitude in $B_d \to K^+\pi^-$. The more dominant the penguin compared to the tree, the more accurately α could, in principle, be extracted. Information as to the strength of the penguin amplitudes could be obtained by comparing the branching ratio of the $\pi^+\pi^-$ mode to the $K^+\pi^-$ one and to those of pure penguin modes, such as $B^- \to K^-\phi, K_S\pi^-, B_d \to \phi K_S$.

Another alternative uses tagged, time-dependent studies of the charged two-body modes, $B_d \to \pi^+\pi^-$ and $B_s \to K^+K^-$. This method will be the focus of the section. The unmixed B_d-amplitudes are

$$\langle \pi^+\pi^-|\bar{B}_d\rangle = \xi_t a_t + \xi_u a_u = \xi_t a_t(1 + z\,e^{i\alpha}) = \xi_t a_t \bar{a} \,, \tag{51}$$

$$\langle \pi^+\pi^-|B_d\rangle = \xi_t^* a_t(1 + z\,e^{-i\alpha}) = \xi_t^* a_t a \,. \tag{52}$$

The interference term is given by

$$\lambda_d = \frac{\bar{a}}{a} = \frac{1 + ze^{i\alpha}}{1 + ze^{-i\alpha}} \,. \tag{53}$$

Here ξ_q are the relevant CKM combinations, a_t, a_u are the two strong matrix elements, and z depends on their ratio and on the ratio $|\xi_u/\xi_t|$. Note that a_t, a_u, and z denote different quantities from the ones of previous sections. The two unmixed B_s-amplitudes and the interference term are

$$\begin{aligned} \langle K^+K^-|\bar{B}_s\rangle &= v_t a_t + v_u a_u = v_t a_t[1 + rze^{-i\gamma}] = v_t a_t \bar{b} \,, \\ \langle K^+K^-|B_s\rangle &= v_t^* a_t[1 + rze^{i\gamma}] = v_t^* a_t b \,, \\ \lambda_s &= \frac{\bar{b}}{b} = \frac{1 + rze^{-i\gamma}}{1 + rze^{i\gamma}} \,. \end{aligned} \tag{54}$$

The b, $\bar{b}$ and r differ from the ones defined in Section 5. For simplicity, $SU(3)$ flavor symmetry is assumed, although much effort will have to be directed toward estimating corrections to it. The parameter r is a ratio of CKM elements and will be well known:

$$r = \left|\frac{V_{us}V_{td}}{V_{ud}V_{ts}}\right| . \tag{55}$$

and so will the relative normalization of the unmixed B_d- and B_s-amplitudes,

$$\left|\frac{\xi_t}{v_t}\right| = \left|\frac{V_{td}}{V_{ts}}\right| . \tag{56}$$

The tagged, time-dependent study of $B_d \to \pi^+\pi^-$ informs about $|a|, |\bar{a}|$, and arg $(\bar{a}/a)$, while that of $B_s \to K^+K^-$ measures $|b|, |\bar{b}|$, and arg $(\bar{b}/b)$. Figure 3 shows the two B_d-amplitude triangles,

$$a = 1 + ze^{-i\alpha} \,,\ \bar{a} = 1 + ze^{+i\alpha} \,, \tag{57}$$

and the two B_s ones,

$$b = 1 + rze^{+i\gamma} \,,\ \bar{b} = 1 + rze^{-i\gamma} \,. \tag{58}$$

The angle $\angle AC\bar{A}$ is 2α, while $\angle BC\bar{B}$ is 2γ.

We wish now to demonstrate the extraction of the CKM parameters α and γ. The tagged, time-dependent $B_d \to \pi^+\pi^-$ study obtains the phase, arg$(\bar{a}/a)$, and the moduli of the unmixed amplitudes, $|a|$ and $|\bar{a}|$. The two moduli are determined up to an overall constant that can be chosen *arbitrarily*. The choice of the overall constant fixes the magnitudes of $|b|$ and $|\bar{b}|$. The two magnitudes, $|b|$ and $|\bar{b}|$, as well as $\arg(\bar{b}/b)$ are obtained from the tagged, time-dependent B_s-study. Draw the triangle $AO\bar{A}$. The lengths of its two sides and its angle $\angle AO\bar{A}$ are known. Point C lies on the straight line d that bisects $A\bar{A}$. The shape of the $BO\bar{B}$ triangle is known. Its orientation relative to $AO\bar{A}$ is fixed because points B and $\bar{B}$ must be equidistant from d. Point C is found since the ratio of lengths is known,

$$CB/CA = r\,, \tag{59}$$

thus determining the angles α and γ. If the penguin of $B_d \to \pi^+\pi^-$ is sizeable, b and $\bar{b}$ will be indistinguishable and γ will not be determined, because $CB \ll CA$. For a negligible penguin of $B_d \to \pi^+\pi^-$—that is, $z \gg 1$—the interference term λ_d determines α, and γ could be obtained from the method outlined here.

Instead of extracting the CKM angles α and γ when $|V_{td}/V_{ts}|$ is used as input, the procedure could be inverted by supplying a CKM angle and determining $|V_{td}/V_{ts}|$ and the other CKM angle. The key point is that a simultaneous study of $B_d \to \pi^+\pi^-$ and $B_s \to K^+K^-$ can be used to extract CKM parameters.

8. α from $b \to d$ + charmless

The method used in the previous section can be extended to many additional modes, where the B_d and B_s modes are related by flavor $SU(3)$. There may be doubts as to the validity of flavor $SU(3)$ for the final state. For instance, the symmetry is badly broken for D^0 modes [18],

$$\frac{\Gamma(D^0 \to K^+K^-)}{\Gamma(D^0 \to \pi^+\pi^-)} \simeq 2\,. \tag{60}$$

Perhaps the invariant mass of D^0 still lies within the resonance region, and the breakdown is due to different resonance structures. If so, flavor $SU(3)$ would be a rather good symmetry for B-decays, because the B-mass is much above the resonance region. We do not really understand the symmetry breakdown for the final states of D^0 that are related by flavor $SU(3)$. We could, however, consider final states that are identical in particle content and differ only in their invariant mass, one coming from decays of the heavy hadron and the other coming from the $SU(3)$-related heavy hadron. For the B-mass region, the final state interactions are expected to be similar for the modes with identical particle content coming from decays of the B_d and $\bar{B}_s$. *Only* the $SU(3)$ relation between the initial states (B_d and $\bar{B}_s$) and between the transition currents must be investigated. Table 1 lists examples of such modes. In analogy to the last section, the angles α (and perhaps γ too) can be extracted. For classes 1-2, the phase between the two unmixed amplitudes can be disentangled; for a similar discussion, see Section 5. For modes that involve a single K^0 resonance, K^r, the moduli of the two unmixed amplitudes can be obtained from untagged and time-integrated data samples. Determining the interference term requires a tagged, time-dependent study with K^r_{CP}, however. Theory and experiment will guide us to those modes that have small theoretical uncertainties and that are experimentally feasible.

Many neutral B modes may be used in the future to extract CKM parameters. The extraction is done by disentangling the CKM parameters from strong matrix elements. The disentangling is accomplished by simultaneously studying related modes, where most theoretical uncertainties cancel. We could either study $SU(3)$ related modes, or B_d and $\bar{B}_s$ modes with identical particle content.

Table 1: $\bar{B}_s$ and B_d modes with identical particle content.

Class	$\bar{B}_s$ transition	B_d transition	Examples
1	$b \to d\, u\bar{u}$	$\bar{b} \to \bar{s}\, u\bar{u}$	$\rho^0 K_S, \omega K_S, \eta K_S, \eta K^r, \rho^0 K^r, \omega K^r$
2	$b \to d\, s\bar{s}$	$\bar{b} \to \bar{s}\, s\bar{s}$	$\phi K_S, \phi K^r$
3	$b \to s\, d\bar{d}$	$\bar{b} \to \bar{d}\, s\bar{s}$	$K^0\bar{K}^0, K^r\bar{K}^{r\prime}, K^0\bar{K}^r, K^r\bar{K}^0$

9. Conclusion

Triggerable B_d modes can extract each of the three angles of the unitarity triangle. It is well known that a tagged study of $B_d \to J/\psi K_S$ measures β. It is, however, not as well known that a tagged, time-dependent study of $B_s \to J/\psi\phi, D_s^+D_s^-$ determines γ [13, 17]. The determination requires the value of $|V_{ub}/V_{cb}|$ as input. The angle γ can still be measured, even if accurate time-dependent B_s-studies are not feasible, perhaps because x_s is too large.

The measurement could come from a tagged, time-dependent study of $B_d \to J/\psi\rho^0$, where $B_d \to J/\psi K^{*0}$ would serve as normalization. Although it could be done, it is a challenge in both experimental and theoretical aspects. The small phase between the two unmixed amplitudes must be disentangled from two large interference terms; see Eq. (40). Further, the magnitudes of those two unmixed amplitudes must be measured very well. On the theoretical front, much effort must be expended to accurately calculate a ratio of strong matrix elements, $a_2(B_d \to J/\psi\rho^0)/a_2(B_d \to J/\psi K^{*0})$. The exclusive modes governed by $b \to d\ell^+\ell^-$ extract the angle α. Here the phase between the two unmixed amplitudes is generally large. It is measured from an interference term without any disentangling. The rate is tiny, however.

If triggering on secondary vertices becomes feasible, many more modes could be used to measure CKM parameters. For instance, a combined $B_d \to \pi^+\pi^-$ and $B_s \to K^+K^-$ analysis can measure CKM parameters. Extractions with other such modes are discussed throughout the note.

In conclusion, precision measurements with beautiful hadrons allow the extraction of various CKM parameters. The CKM model will thus be tested by overconstraining it. The extractions require copious amounts of beautiful hadrons and additional theoretical input as to ratios of strong matrix elements. The first requirement can be fulfilled at hadron accelerators. The second one requires much additional study. We look forward to stimulating interactions between experimentalists and theorists as to what modes are feasible and as to what methods have the least theoretical uncertainties.

Acknowledgements

We appreciate helpful comments from R. Aleksan, J. Appel, F. DeJongh, C. O. Dib, E. Eichten, M. Gronau, C. Hill, W.-S. Hou, D. Kaplan, B. Kayser, J. Lewis, H. J. Lipkin, D. London, J. Mueller, C. Quigg, J. Rosner, J. Soares, P. Sphicas, J. Taron, A. Yagil and particularly from P. Grosse-Wiesmann, T. Takeuchi and E. Yehudai. We are grateful to all the participants and organizers of the Snowmass workshop for creating a stimulating atmosphere. We thank C. Quigg for insisting that we determine CKM angles. Special thanks go to Lois Deringer for her fast typing of the manuscript, for her many extra hours of work and for her constant encouragement. This work was supported in part by the Department of Energy under Contract No. DE-AC02-76CHO3000.

Appendix A: Helicity Amplitudes and the Extraction of CKM Angles

The extraction of the relevant CKM angle is possible even when several helicity amplitudes exist. We prefer to explain the main idea by an example instead of keeping the discussion abstract. The generalization to other cases is straightforward. Although Section 5 focuses on $B_d \to J/\psi\rho^0$, this appendix discusses the $\bar{B}_s \to J/\psi K^{*0}$ mode, because additional subtleties occur. Consider the mode

$$\bar{B}_s \to J/\psi \quad K^{*0} \hookrightarrow K^+\pi^- . \tag{61}$$

Three helicity amplitudes contribute,

$$A_{\lambda\lambda} = \langle\, J/\psi(\lambda)\ K^{*0}(\lambda)|\bar{B}_s\rangle,\quad \lambda = \pm 1,\ 0\,. \tag{62}$$

The CP-conjugated partner,

$$B_s \to J/\psi \quad \bar{K}^{*0} \hookrightarrow K^-\pi^+ , \tag{63}$$

involves

$$\bar{A}_{\lambda\lambda} = \langle\, J/\psi(\lambda)\ \bar{K}^{*0}(\lambda)|B_s\rangle,\ \lambda = \pm 1,\ 0. \tag{64}$$

We find it useful to define

$$H_+ \equiv A_{++} + A_{--}\,, \tag{65}$$

$$H_- \equiv A_{++} - A_{--}\,, \tag{66}$$

$$H_0 \equiv 2A_{00}\,. \tag{67}$$

A full angular analysis can determine the following observables [34, 20],

$$|H_+|^2,\ |H_-|^2,\ |H_0|^2\,, \tag{68}$$

$$\mathrm{Re}\ H_+\ H_0^*\,, \tag{69}$$

$$\mathrm{Im}\ H_+\ H_-^*,\ \ \mathrm{Im}\ H_-\ H_0^*\,. \tag{70}$$

The magnitudes and relative phases of H_+, H_-, H_0 are observables [35].

The CP-conjugated process involves

$$\bar{H}_+ \equiv \bar{A}_{++} + \bar{A}_{--}\ , \tag{71}$$

$$\bar{H}_- \equiv \bar{A}_{++} - \bar{A}_{--}\ , \tag{72}$$

$$\bar{H}_0 \equiv 2\bar{A}_{00}\ . \tag{73}$$

CP invariance requires

$$|\bar{H}_+| = |H_+|,\ |\bar{H}_-| = |H_-|,\ |\bar{H}_0| = |H_0|\ , \tag{74}$$

$$\mathrm{Re}\ \bar{H}_+\ \bar{H}_0^* = \mathrm{Re}\ H_+\ H_0^*\ , \tag{75}$$

$$\mathrm{Im}\ \bar{H}_+\ \bar{H}_-^* = -\mathrm{Im}\ H_+\ H_-^*,\ \mathrm{Im}\ \bar{H}_-\ \bar{H}_0^* = -\mathrm{Im}\ H_-\ H_0^*\ . \tag{76}$$

In terms of strong matrix elements (denoted by $p_c, p_u, m_c, m_u, z_c, z_u$) and CKM combinations ξ_q,

$$H_+ = \xi_c\ p_c + \xi_u\ p_u, \tag{77}$$

$$H_- = \xi_c\ m_c + \xi_u\ m_u, \tag{78}$$

$$H_0 = \xi_c\ z_c + \xi_u\ z_u\ . \tag{79}$$

The CP-conjugated process involves

$$\bar{H}_+ = \eta(\xi_c^* p_c + \xi_u^* p_u)\ , \tag{80}$$

$$\bar{H}_- = -\eta(\xi_c^* m_c + \xi_u^* m_u)\ , \tag{81}$$

$$\bar{H}_0 = \eta(\xi_c^* z_c + \xi_u^* z_u)\ . \tag{82}$$

The phase η is arbitrary when the $\bar{K}^{*0}$ is seen in its $K^-\pi^+$ mode. It is $+1(-1)$ when $\overset{(-)}{K}{}^{*0}$ is seen in its $K_S\pi^0(K_L\pi^0)$ mode. Were the $B_d \to J/\psi\rho^0$ mode considered, η would be $+1$.

The $K_S\pi^0$ mode of the $\overset{(-)}{K}{}^{*0}$ allows the $B_s \to J/\psi\ \bar{K}^{*0}$ and $\bar{B}_s \to J/\psi\ K^{*0}$ amplitudes to interfere. The time-dependences of the helicity amplitudes are

$$H_k(t) = H_k\left[c(t) + i\ s(t)/\lambda_k\right], \tag{83}$$

$$\bar{H}_k(t) = \bar{H}_k\left[c(t) + i\ \lambda_k\ s(t)\right], \tag{84}$$

where

$$\lambda_k \equiv \frac{q}{p}\frac{H_k}{\bar{H}_k}, \tag{85}$$

for $k = +, -, 0$.

As discussed after Eq. (70), the observables are the magnitudes and relative phases of the three $H_k(t)$. Obviously that is true also for the three $\bar{H}_k(t)$. A tagged time-dependent study of $\bar{B}_s \to J/\psi(K_S\pi^0)_{K^*}$ determines the relevant interference terms. By disentangling them, we measure

$$\arg\left(H_k/\bar{H}_k\right)\ \text{ for }\ k = +, -, 0\ . \tag{86}$$

The much more copious self-tagged data sample of $\bar{B}_s \to J/\psi(K^+\pi^-)_{K^*}$ obtains

$$|H_k|\ \text{ and }\ |\bar{H}_k|,\ \ k = +, -, 0\ . \tag{87}$$

In the $m_d = m_s$ limit, a full angular analysis of the process

$$B_d \to J/\psi \quad K^{*0} \hookrightarrow K^+\pi^-\ , \tag{88}$$

provides the magnitudes and relative phases of

$$p_c,\ m_c,\ z_c\ . \tag{89}$$

For instance,

$$H_+\left(B_d \to J/\psi\ K^{*0}\right) \cong \frac{V_{cs}}{V_{cd}}\ \xi_c^*\ p_c \tag{90}$$

and similarly for H_0 and H_-. Statistics are doubled when the CP-conjugated mode $\bar{B}_d \to J/\psi\ \bar{K}^{*0}$ is considered as well. The angle γ can now be extracted in several independent ways. Alternatively the magnitudes and relative phases of p_c, m_c, z_c could be obtained from an untagged, time-integrated study of $B_s \to J/\psi\phi$.

Appendix B: CKM Extraction With B_s Modes

The angles γ and α can be extracted from time-dependent B_s-studies. Specific B_s-modes probably reduce theoretical uncertainties, because the $\bar{B}_d$-mode with identical particle content could be used as normalization. The uncalculable final state interactions mostly cancel in ratios of amplitudes. The latter part of Section 5 discussed drawbacks of the extraction of γ from the $B_d \to J/\psi\rho^0$ mode. Those drawbacks can be overcome by studies of specific B_s modes governed by $b \to d + J/\psi$, such as $\bar{B}_s \to J/\psi K_S$ or $\bar{B}_s \to J/\psi K^r$. A tagged, time-dependent study of such B_s-modes extracts γ. The normalization could come from the untagged, time-integrated, CKM-favored mode of the other neutral B-species, $B_d \to J/\psi K_S$ or $B_d \to J/\psi K^r$, respectively [36]. The final states have identical particle content and differ only in their invariant mass by about 100 MeV [37]. The uncalculable final-state interactions cancel to a large extent in the ratio of strong matrix elements,

$$r' = \left|\frac{a_2(B_s \to J/\psi K_S)}{a_2(B_d \to J/\psi K_S)}\right|^2 . \tag{91}$$

Perhaps this ratio will be estimated more accurately than r; see Eq. (42). The phase between the two unmixed amplitudes of $\bar{B}_s \to J/\psi K_s (J/\psi K^r)$ and $B_s \to J/\psi K_s (J/\psi \bar{K}^r)$ is determined by disentangling it from two interference terms,

$$\lambda(B_s \to J/\psi K_s (J/\psi K^r_{CP})) = -\lambda(B_s \to J/\psi\phi|_{CP=+})\bar{b}'/b' . \tag{92}$$

The b' and $\bar{b}'$ describe the unmixed amplitudes of $B_s \to J/\psi K_s (J/\psi \bar{K}^r)$ and $\bar{B}_s \to J/\psi K_s$ $(J/\psi K^r)$, in analogy to b and $\bar{b}$ of Eq. (43). And $\lambda(B_s \to J/\psi\phi|_{CP=+})$ denotes the right-hand side of Eq. (22), and is obtained from a CP study of $B_s \to J/\psi\phi$; see Section 3.

Whereas the imaginary parts of the two interference terms of Eq. (92) are small at order θ^2, the ones of $\lambda(B_d \to J/\psi\rho^0)$ and $\lambda(B_d \to J/\psi K_s)$ are much larger. It thus may be easier to disentangle the phase between the two unmixed amplitudes for $B_s \to J/\psi K_s (J/\psi \bar{K}^r)$ than for $B_d \to J/\psi\rho^0$. Finally, there are no W-exchange diagrams for $\bar{B}_d$ and B_s decay modes to $J/\psi K_s (J/\psi \bar{K}^r)$.

What is the merit of extracting γ from $B_s \to J/\psi \bar{K}^r$ compared to $B_s \to J/\psi K_S$? A tagged, time-dependent study of $B_s \to J/\psi K_S$ has to determine simultaneously three observables, the moduli of the two unmixed amplitudes and the interference term $\lambda(B_s \to J/\psi K_s)$. In contrast, a tagged, time-dependent study of $B_s \to J/\psi K^r_{CP}$ needs to measure only the interference term $\lambda(B_s \to J/\psi K^r_{CP})$. The moduli of the two unmixed amplitudes $B_s \to J/\psi \bar{K}^r$ and $\bar{B}_s \to J/\psi K^r$ are provided from the *much larger* untagged and time-integrated data sample. On the other hand, the $J/\psi K^r$ mode involves several helicity amplitudes. Angular correlations need to disentangle them, unless $J/\psi K^r$ is dominated by a single helicity amplitude. In contrast, the $J/\psi K_s$ mode involves only one helicity amplitude.

The modes $B_s \to K_S \ell^+\ell^- (\bar{K}^r \ell^+\ell^-)$ extract α. A tagged time-dependent study of $B_s \to K_S \ell^+\ell^- (\bar{K}^r \ell^+\ell^-)$ determines the moduli of the two unmixed amplitudes and the interference term. The moduli of the two unmixed amplitudes with a $\overset{(-)}{K}{}^r$ can be determined without tagging and without time-dependence, as explained above. The normalization could use the same final state from $\bar{B}_d, B_d \to K_S \ell^+\ell^- (\bar{K}^r \ell^+\ell^-)$. The phase between the unmixed amplitudes requires some disentangling, however,

$$\lambda(B_s \to K_S \ell^+\ell^- (K^r_{CP} \ell^+\ell^-)) = -\lambda(B_s \to J/\psi\phi|_{CP=+})\lambda^*(B_d \to J/\psi K_S)\bar{E}/E . \tag{93}$$

$\overset{(-)}{E}$ denotes the relevant unmixed amplitude of $B_s \to K_S \ell^+\ell^- (\bar{K}^r \ell^+\ell^-)$, in analogy to Eq. (45). The observables are the two magnitudes of the unmixed amplitudes and their relative phase. They allow the determination of α .

References

[1] N. Cabibbo, Phys. Rev. Lett. **10** (1963) 531; M. Kobayashi and T. Maskawa, Prog. Theor. Phys. **49** (1973) 652.

[2] L.L. Chau and W.-Y. Keung, Phys. Rev. Lett. **53** (1984) 1802; J.D. Bjorken, private communication; Fermilab report (1988) unpublished; C. Jarlskog and R. Stora, Phys. Lett. **B208** (1988) 268.

[3] A.B. Carter and A.I. Sanda, Phys. Rev. Lett. 45 (1980) 952; Phys. Rev. D23 (1981) 1567; I.I. Bigi and A.I. Sanda, Nucl. Phys. B193 (1981) 85. For a review, see for instance, B. Kayser, NSF report, NSF-PT-92-01 (1991); Y. Nir, SLAC report, SLAC-PUB-5874 (1992), lectures given at 20th Annual SLAC Summer Institute on Particle Physics, and references therein.

[4] R. Aleksan, I. Dunietz, B. Kayser and F. Le Diberder, Nucl. Phys. B361 (1991) 141.

[5] M. Gronau and D. London, Phys. Rev. Lett. 65 (1990) 3381; Y. Nir and H.R. Quinn, Phys. Rev. Lett. 67 (1991) 541; H.J. Lipkin, Y. Nir, H.R. Quinn and A. Snyder, Phys. Rev. D44 (1991) 1454; M. Gronau, Phys. Lett B265 (1991) 389.

[6] For a gigantic data sample, the secondary vertex may be observed from Dalitz conversion, $\pi^0 \to \gamma e^+ e^-$. If the tiny opening angle of the e^+e^- pair can be seen, time-dependent studies of $B_d \to \pi^0\pi^0$ may be possible.

[7] A.E. Snyder and H.R. Quinn, SLAC report, SLAC-PUB-6056, February, 1993.

[8] M. Gronau and D. London, Phys. Lett. B253 (1991) 483.

[9] I. Dunietz, Fermilab report, Fermilab-Pub-93/150-T, in progress.

[10] R. Aleksan, I. Dunietz and B. Kayser, Z. Phys. C54 (1992) 653.

[11] M. Gronau and D. Wyler, Phys. Lett. B265 (1991) 172; I. Dunietz, Phys. Lett. B270 (1991) 75; Z. Phys. C56 (1992) 129; in "B Decays," ed. by S. Stone, p. 393, World Scientific, Singapore, 1992.

[12] I. Dunietz, Fermilab report, Fermilab-Pub-93/089-T, June 1993, to appear in Phys. Lett. B.

[13] I. Dunietz and J.L. Rosner, Phys. Rev. D34 (1986) 1404.

[14] M. Gronau, Phys. Rev. Lett. 63 (1989) 1451; M. Gronau, Phys. Lett. B233 (1989) 479.

[15] J.S. Hagelin, Nucl. Phys. B193 (1981) 123; E. Franco, M. Lusignoli and A. Pugliese, Nucl. Phys. B194 (1982) 403; A.J. Buras, W. Slominsky and H. Steger, Nucl. Phys. B245 (1984) 369; M.B. Voloshin, N.G. Uraltsev, V.A. Khoze, M.A. Shifman, Sov. J. Nucl. Phys. 46 (1987) 112; A. Datta, E.A. Paschos, U. Türke, Phys. Lett. B196 (1987) 382.

[16] R. Aleksan et al., Orsay report, LPTHE 93/17, May 1993.

[17] D. Du, I. Dunietz, D.-D. Wu, Phys. Rev. D34 (1986) 3414; C.O. Dib, I. Dunietz, F.J. Gilman, Y. Nir, Phys. Rev. D41 (1990) 1522.

[18] Particle Data Group, K. Hikasa et al., Phys. Rev. D45 (1992) S1.

[19] B. Kayser, M. Kuroda, R.D. Peccei and A.I. Sanda, Phys. Lett. B237 (1990) 508.

[20] I. Dunietz, H. Quinn, A. Snyder, W. Toki and H.J. Lipkin, Phys. Rev. D43 (1991) 2193.

[21] S. Ball, in "The Fermilab Meeting, DPF 92," ed. by C.H. Albright et al., p. 533, World Scientific, Singapore, 1993; M.V. Danilov, in "Joint International Lepton-Photon Symposium and Europhysics Conference on High Energy Physics," ed. by S. Hegarty et al., p. 331, vol. 2, World Scientific, Singapore, 1992.

[22] I. Dunietz and J. M. Soares, in preparation.

[23] J. Bernabéu and C. Jarlskog, Z. Phys. C8 (1981) 233; L.-L. Chau and H.-Y. Cheng, Phys. Rev. Lett. 53 (1984) 1037; Phys. Lett. B165 (1985) 429.

[24] H. Simma and D. Wyler, Phys. Lett. B272 (1991) 395; H. Simma, dissertation submitted to the Swiss Federal Institute of Technology, Diss ETH No. 9781, 1992.

[25] J.-M. Gérard and W.-S. Hou, Phys. Rev. **D43** (1991) 2909; L. Wolfenstein, Phys. Rev. D43 (1991) 151. We thank J. Soares for reminding us about this consequence of the CPT theorem.

[26] J.-M. Gérard and W.-S. Hou, Phys. Rev. **D43** (1991) 2909; H. Simma, G. Eilam and D. Wyler, Nucl. Phys. **B352** (1991) 367; R. Fleischer, Technische Universität München report, TUM-T31- 26/92 (1992), unpublished; N. G. Uraltsev, University of Notre Dame report, UND-HEP-92-BIG08 (1992), talk given at DPF meeting at Fermilab (Nov. 1992).

[27] In the $m_d = m_s$ limit, the strong matrix element a_2 is identical for the two processes $B_d \to J/\psi K^{*0}$ and $B_d \to J/\psi\rho^0$ (and so is the a_u matrix element), for a negligible W-exchange amplitude of $B_d \to J/\psi\rho^0$.

[28] N.G. Deshpande et al., Phys. Rev. Lett. 57 (1986) 1106; N.G. Deshpande and J. Trampetic, Phys. Rev. Lett. 60 (1988) 2583; B. Grinstein, M.J. Savage and M.B. Wise, Nuc. Phys. B319 (1989) 271; M. Misiak, Nucl. Phys. B393 (1993) 23; P.J. O'Donnell et al., Phys. Rev. D46 (1992) 4091.

[29] N.G. Deshpande et al., Phys. Rev. D39 (1989) 1461; C.S. Lim, T. Morozumi and A.I. Sanda, Phys. Lett. B218 (1989) 343; P.J. O'Donnell and H.K.K. Tung, Phys. Rev. D43 (1991) 2067.

[30] I. Dunietz and J.M. Soares, in preparation.

[31] The extraction is complicated by the fact that z varies around the Dalitz plot, while it is a complex number for a helicity amplitude of $B_d \to J/\psi\rho^0$.

[32] J.M. Soares, Carnegie Mellon University report, CMU-HEP 92-13, revised version of May 14, 1993.

[33] M.J. Savage and M.B. Wise, Phys. Rev. D39 (1989) 3346; E-ibid D40 (1989) 3127.

[34] M. Jacob and G.C. Wick, Ann. Phys. (NY) 7 (1959) 404; J.D. Richman, Ph. D. thesis, Caltech report, CALT-68-1231, 1985; G. Kramer and W.F. Palmer, Phys. Rev. D45 (1992) 193; Phys. Rev. D46 (1992) 2969; Phys. Lett. B279 (1992) 181.

[35] The relative phases are known only within a two-fold discrete ambiguity. A study of the interference between the mode and the S-wave $K\pi$ background may remove the ambiguity.

[36] In the case of the $\bar{B}_s \to J/\psi K^{*0}$ study, the normalization could alternatively come from the untagged, time-integrated rate of $\bar{B}_s \to J/\psi\phi$. The W-exchange diagram contributes to $\bar{B}_s \to J/\psi\phi$ but does not to $J/\psi K^{*0}$.

[37] F. Abe, et al. (CDF Collaboration), Fermilab-Pub-93/141-E, report the mass of the B_s meson as 5383.3±4.5 (stat.)±5.0 (sys.) MeV; D. Buskulic et al. (ALEPH Collaboration), CERN-PPE/93-97, report 5368.6 ± 5.6 (stat.) ± 1.5 (sys.) MeV. See also P. D. Acton et al. (OPAL Collaboration), Phys. Lett. B295 (1992) 357.

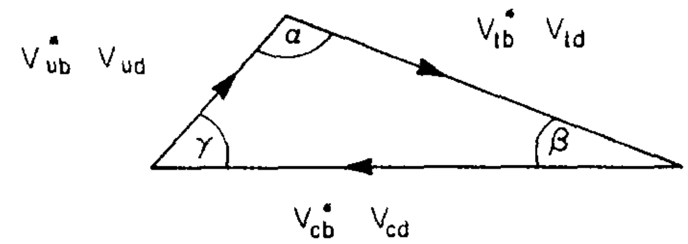

Figure 1: The CKM unitarity triangle.

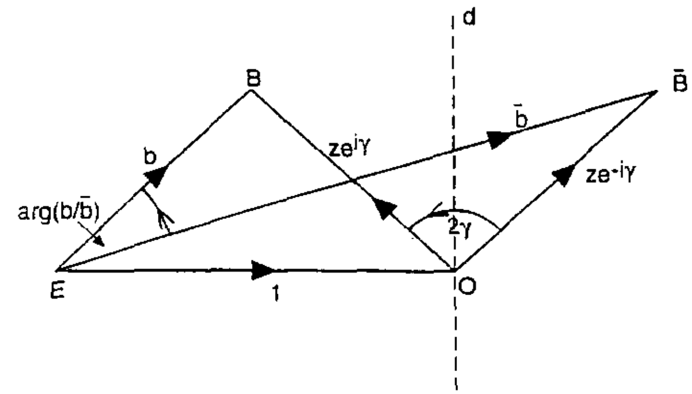

Figure 2: The two amplitude triangles b and $\bar{b}$, see Eq. (43). The angle between $O\bar{B}$ and OB is 2γ.

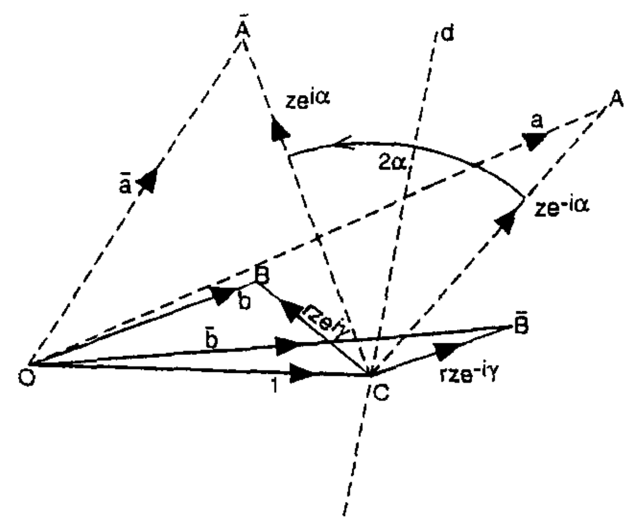

Figure 3: The four amplitude triangles $a, \bar{a}, b$ and $\bar{b}$. The angle between $\bar{A}C$ and AC is 2α, and the one between BC and $\bar{B}C$ is 2γ.

B MESON SEMILEPTONIC DECAYS FROM $\Upsilon(4S)$ RESONANCE DATA

MARINA ARTUSO
Department of Physics, Syracuse University
Syracuse, NY 13244, USA

1. INTRODUCTION

B meson semileptonic decays are an exceptional laboratory to study a very important sector of the Standard Model, namely the quark mixing parametrized by the Cabibbo-Kobayashi-Maskawa (CKM) matrix. Two CKM elements are directly measured in semileptonic decays, ($|V_{ub}|$ and $|V_{cb}|$). Figure 1 shows the Feynman diagrams associated with these decays. In principle, another CKM element, ($|V_{td}|$), can be extracted from measurements of $B^0\bar{B}^0$ mixing. A precise determination of quark mixing parameters is a crucial test of the Standard Model. Eventually, the determination of the complex phase in this mixing matrix, through measurement of CP asymmetries in B decays is likely to provide the most sensitive probe of possible physics beyond the Standard Model. However the measurement of the absolute values of these CKM elements already provide very interesting constraints and are important inputs in the prediction of the expected magnitude of these asymmetries.

Wolfenstein[1] proposed an approximate representation of the CKM matrix which provides a natural parametrization of the hierarchy of the quark couplings :

$$V = \begin{pmatrix} 1-\lambda^2 & \lambda & A\lambda^3(\rho - i\eta) \\ -\lambda & 1-\lambda^2/2 & A\lambda^2 \\ A\lambda^3(1-\rho-i\eta) & -A\lambda^2 & 1 \end{pmatrix} + \mathcal{O}(\lambda^4),$$

where $\lambda = \sin\theta_c \approx 0.22$ is the sine of the Cabibbo angle.

The most attractive feature of semileptonic decays is that the virtual W decays into a lepton-$\bar{\nu}$ pair and therefore this vertex is governed by a purely electroweak interaction, which is amenable to precise theoretical calculations. On the other hand, the evaluation of the matrix element relating the hadronic system in the final state and the initial meson must take into account the strong interaction between quarks in the initial and final state. This is the realm of non-perturbative QCD, which is so far elusive to precise theoretical determination. In principle, hadronic B decays can also be used to study quark mixing, but in this case the effects of the strong interactions are even more difficult to evaluate because the particles produced in the W decay are quarks too. The exceptional increase in statistical accuracy which we are expecting to achieve in the near future with the CESR e^+e^- collider at Cornell University and with the b-factories, will enable us to probe this sector of the Standard Model with high sensitivity, if a parallel progress in the theoretical evaluations of the hadronic matrix elements governing these processes is achieved.

A precision study of the phenomenology of $B^0\bar{B}^0$ is quite crucial in several respects. In fact the most promising avenue to measure CP violation in B decays appears to be the study of decays where the interference producing observable CP asymmetry is between direct decay of a neutral B^0 meson to a CP eigenstate and decay occurring after flavour oscillation. In addition, when the top quark mass is measured accurately, a reliable value of the B meson decay constant is available and QCD effects are better understood, it can provide a precise determination of $| V_{td} |$.The high statistics samples presently available and the even higher ones which will be accumulated in the near future will allow to reduce significantly both statistical and systematical error in $\Delta M/\Gamma$.

2. THEORETICAL EVALUATIONS OF STRONG INTERACTION EFFECTS

Lattice gauge calculations are supposed to provide us, in due time, with values of the hadronic matrix element based on the 'exact theory' of the strong interaction according to the Standard Model. The progress made in recent years is quite impressive[2], but it is crucial to have a better understanding of the errors introduced by the approximations made in doing the calculation[3] (most notably the quenched approximation).

In absence of lattice final results, phenomenological models and approaches based on limits of QCD in specific kinematical regimes have been employed to study these decays. Most of them focus on semileptonic decays for the reasons discussed above. It is worth summarizing their most salient features in order to understand their success and shortcoming with respect to experimental information.

One approach is based on pure parton phenomenology. The electroweak interaction is calculated treating the decaying quark as a free parton. Strong interactions effects are introduced in some cases. For instance, in the model developed by Altarelli and collaborators (ACCMM),[4] bound state effects are accounted for by introducing an effective mass for the decaying b quark and smearing the lepton momentum spectrum in the B meson center of mass system by the motion of the initial b parton inside the decaying meson. Alternatively, in an ultrarelativistic treatment,[5] the decay rate is calculated in the infinite momentum frame and partons are related to hadrons through structure functions. These models are expected to be more suitable to the study of decays which involve many channels in the final state, because the quark–hadron duality is expected to be valid on the average if a continuum of states are involved. It is more difficult to see how this treatment can apply to decays dominated by a few resonances in the final state. Nonetheless, as it will be discussed below, the ACCMM model seems to be as good as any other model to describe the lepton spectrum from the $b \to c$ decay, which is dominated by two resonances ($B \to D$ and $B \to D^*$) which constitute at least 60% of the total rate.

"Exclusive" quark models calculate the hadronic current $< X \mid J_\mu \mid B >$ between the decaying B meson and specific meson final state. Generally only the low lying resonances of the $\mid Q\bar{q} >$ state are considered, (Q indicates the quark produced in the weak decay and $\bar{q}$ indicates the spectator quark in the B meson). This approach is more useful for decays involving only a few resonances in the final state. It has been relatively successful in describing $b \to c$ semileptonic decays. Also in this case, the non-relativistic approach[6–7] and the infinite momentum frame approach[8–9] have been applied. The hadronic current is expressed in terms of form factors using a covariant expansion. For instance, for the $B \to D$ transition we have:

$$< D(p_2) \mid V_\mu \mid B(p_1) >= F_+^V(q^2)(p_1 + p_2)_\mu + F_-^V q_\mu \tag{1}$$

where p_1 and p_2 are respectively the B and D momenta and $q = p_1 - p_2$ is the momentum transfer to the lepton–$\bar{\nu}$ system or, equivalently, the 4-momentum of the virtual W. Each model assumes a q^2 dependence of the form factors, as a more or less educated conjecture and calculates their normalization by relating quarks and hadrons at some q^2 scale, which typically is q^2_{max} for non-relativistic models and $q^2 = 0$ for ultrarelativistic calculations.

A different approach to the calculation of the form factors is proposed by the QCD sum rule technique, originally proposed to study non-perturbative aspects of QCD by Shifman, Vainshtein and Zakharov.[10] This method evaluates the form factors in terms of the three point current correlator with the suitable Lorentz structure.[11,12] For instance, in the case of the $B \to D$ transition the relevant three point correlator is:

$$\Pi_\mu(p_1, p_2, q) = i^2 \int dx dy e^{(ip_1 x - ip_2 y)} < 0 \mid T\{\bar{q}(x)\gamma_5 c(x), J_\mu^V(0), \bar{b}(y)\gamma_5 q(y)\} \mid 0 > \tag{2}$$

where

$$J_\mu^V = \bar{c}\gamma_\mu b \tag{3}$$

is the vector component of the current involved in the weak decay between a b and a c quark and T identifies a time ordered product in the integral. The current correlator is in turn decomposed into a covariant expansion. In the case of the $B \to D$ transition, we have:

$$\Pi_\mu(p_1, p_2, q) = \Pi_+(p_1^2, p_2^2, q^2)(p_1 + p_2)_\mu + \Pi_-(p_1^2, p_2^2, q^2)q_\mu \tag{4}$$

The amplitudes appearing in this expansion can be evaluated evaluated in two different ways. The first expression is obtained by expanding each amplitude in terms of operator product expansion and the other is obtained by saturating the correlator with the low lying resonances and a continuum of states above a certain threshold, generally modeled by perturbative QCD. By matching the two expressions, one gets a value for the form factors at $q^2 = 0$.

Finally, in the last few years much interest has been stirred by the "Heavy Quark Effective Theory" (HQET)[13] which studies several aspects of B meson decay phenomenology by exploiting an effective Hamiltonian which is the correct limit of QCD for large quark masses. This theory can be considered the analogy of the chiral limit of QCD, which holds for infinitely small quark masses, in the opposite kinematical regime. The interest is motivated by the hope to overcome the model dependence which plagues purely phenomenological approaches, especially in cases where the b and c quark masses can legitimately be considered close to infinity. Radiative corrections induced by gluons attached to the heavy and light quark lines have been studied extensively. In addition, the effective theory is the first order term in an expansion in terms of $1/m_Q$, where m_Q is the heavy quark mass. Effects of higher order terms in this expansion need to be evaluated for each specific process. The hope is that this approach will lead to a less model dependent evaluation of the CKM parameters. The present prospects for $\mid V_{cb} \mid$ and $\mid V_{ub} \mid$ will be discussed below.

3. EXPERIMENTAL HANDLES

3.1 *Study of Inclusive Semileptonic Decays*

A first observable which is amenable to experimental study and is interesting in several respects is the lepton spectrum from B decays. Figure 2 shows the lepton spectra from B decays recently measured by CLEO. These spectra can be fitted with two dominant components, produced respectively in 'cascade decays', where the B meson decays to a charmed meson which subsequently undergoes a semileptonic decay, and in direct B meson semileptonic decays to a charmed final state. There is an additional component which affects the shape of the end point of this spectrum and corresponds to B meson semileptonic decays to charmless hadrons in the final state. This tiny portion of the spectrum plays crucial importance on our ability to determine the CKM parameter $\mid V_{ub} \mid$ and will be discussed in great detail below.

The main physical information coming from the study of the inclusive lepton spectrum is the rate for $b \to cl\nu$. In order to determine it precisely, it is necessary to eliminate the contribution from cascade decays as accurately as possible. The CLEO collaboration performs this subtraction by convoluting the measured spectrum for $D \to Xl\nu$ from the DELCO collaboration[14] and convoluting it to the measured D^0 and D^+ momentum distributions from CLEO data. There is some uncertainty in this procedure associated with the lack of knowledge of the effective smearing induced by detector resolution effects in the DELCO measurements. The fit is performed with three different models: the model by Altarelli and collaborators,[4] the model by Isgur, Scora, Grinstein and Wise[7] (ISGW) and a modified version of ISGW (referred as ISGW*), where the fraction of D^{**} mesons in $B \to X_c l\nu$ is taken as one of the parameters of the fit. This last model was motivated by the evidence shown in the previous CLEO data sample (CLEO 1.5) for a substantial fraction of semileptonic decays not accounted for by the channels $Dl\nu$ and $D^*l\nu$ (totaling only 62±12% of the $X_c l\nu$).[15] The ARGUS collaboration measured a consistent fraction of $B \to D^{**}l\nu$ (roughly 26%).[16] It should be pointed out that the ARGUS analysis claims to identify a contribution from P-wave charmed mesons, and that the new CLEO results with the ISGW* fit indicate a smaller D^{**} fraction $(21.2 \pm 1.6 \pm 8\%)$,[17] with a systematic error which is still large and in part reflects our poor knowledge of the composition of the D^{**} states and the corresponding form factors. The fit results are summarized in Table 1.

Table 1. CLEO II $b \to xl\nu$ branching fractions from inclusive lepton spectrum analysis.

	$b \to xl\bar{\nu}$
ACCMM	$10.65 \pm 0.05 \pm 0.33$
ISGW	$10.42 \pm 0.05 \pm 0.33$
ISGW*	$10.98 \pm 0.10 \pm 0.33$

These results are consistent with previous CLEO[18] and ARGUS[19] measurements summarized in Table 2 for the ACCMM model.

Table 2. Previous $b \to xl\nu$ branching fractions obtained with ACCMM model.

	$b \to xl\bar{\nu}$
CLEO 1.5	$10.5 \pm 0.2 \pm 0.4$
ARGUS	$10.2 \pm 0.5 \pm 0.2$

These measurements give $< b >$, defined as:

$$< b > = f_0 b_0 + f_- b_- \tag{5}$$

where b_0, b_- are the charged and neutral B semileptonic branching fractions and f_0 and f_- are the branching fractions for $\Upsilon(4S)$ decay to $\bar{B}^0$ and B^- respectively. Here and throughout the paper charge conjugate reactions are also used. It is of great interest to measure the individual semileptonic branching fractions for charged and neutral B separately and this can be accomplished with samples of tagged B's. The most relevant quantity which can be extracted from these measurements is the ratio between lifetimes τ^-/τ^0, which gives a direct measurement of non spectator effects in B decays and, assuming equal semileptonic widths for B^- and B^0, is given by:

$$\frac{\tau^-}{\tau^0} = \frac{b_-}{b_0} \tag{6}$$

CLEO takes advantage of the high statistic sample of tagged B's[20] to obtain b_0 and b_+. There are four subset in the tagged sample used:

1- 492±31 fully reconstructed B^0's and 919 ± 42 fully reconstructed B^-,

2- 378± 30 semileptonic decays $B^0 \to D^{*+}l\bar{\nu}$ and 231 ± 30 $B^- \to D^{*0}l\bar{\nu}$, where the ν is the only missing particle.

3- 7100± 182 semileptonic decays $B^0 \to D^{*+}l\bar{\nu}$, where only the slow π from D^* decay is explicitly reconstructed.

4- 754± 51 partially reconstructed $B^0 \to D^{*+}\pi^-$, where only the slow π from D^* decay is explicitly reconstructed.

This analysis gives:

1. $\mathcal{B}(B^- \to X^0 l^- \bar{\nu}) = 12.0 \pm 1.7 \pm 1.8\%$
2. $\mathcal{B}(\bar{B}^0 \to X^+ l^- \bar{\nu}) = 11.4 \pm 0.7 \pm 1.3\%$
3. $\tau^-/\tau^0 = \mathcal{B}(B^- \to X^0 l^- \bar{\nu})/\mathcal{B}(\bar{B}^0 \to X^+ l^- \bar{\nu}) = 1.05 \pm 0.16 \pm 0.15$

A quantity related to τ^-/τ^0 can be extracted from the yields of exclusive semileptonic decays $\bar{B}^0 \to D^{*+}l\bar{\nu}$ and $\bar{B}^- \to D^{*0}l^-\bar{\nu}$. Assuming isospin invariance, we have:

$$\frac{\mathcal{B}(B^- \to D^{*0}l\bar{\nu})}{\mathcal{B}(\bar{B}^0 \to D^{*+}l\bar{\nu})} = \frac{\tau^-}{\tau^0} \tag{7}$$

CLEO[21] recently presented a measurement of a related quantity R_B:

$$R_B = \frac{\mathcal{B}(B^- \to D^{*0}l\bar{\nu})}{\mathcal{B}(\bar{B}^0 \to D^{*+}l\bar{\nu})} \cdot \frac{f_-}{f_0} = 1.20 \pm 0.20 \pm 0.19; \tag{8}$$

the method involves full reconstruction of the D^{*+} and D^{*0} mesons, both in the $D\pi^0$ channel. The second error quoted is systematic and is dominated by the uncertainty in the ratio $\mathcal{B}(D^+ \to K^-\pi^+\pi^+)/\mathcal{B}(D^0 \to K^-\pi^+)$. These results are consistent with values of τ^-/τ^0 recently reported by LEP experiments.[22]

3.2 *Study of Exclusive Semileptonic Decays*

Exclusive semileptonic decays to the dominant charmed final states ($Dl\bar{\nu}$ and $D^*l\bar{\nu}$) have been studied by the CLEO and ARGUS collaborations quite extensively. Unfortunately, the published results[15-16,23-26] have been normalized to different absolute branching fractions of the D^0 and D^+ decay modes chosen to reconstruct the specific decay channel investigated. In addition, some results have been obtained by performing a constrained fit tho the MM^2 distributions from $D^+Xl\bar{\nu}$ and $D^0Xl\bar{\nu}$ simultaneously, imposing typically that the vector to pseudoscalar ratio is the same in the charged and neutral B semileptonic decays. Although this assumption is a good one, it makes it difficult to unfold the results when the D^0 or D^+ branching fractions Therefore this information will be neglected in the summary shown in Table 3. The published branching ratios are rescaled to the D absolute branching ratios $\mathcal{B}(D^0 \to K^-\pi^+) = (3.91 \pm 0.08 \pm 0.17)\%$, recently measured by CLEO[27] and $\mathcal{B}(D^+ \to K^-\pi^+\pi^+) = (9.1 \pm 1.3 \pm 0.4)\%$,[28]) and to the most recent values of the D^* branching fractions.[29] In addition, all the measurements assume $f_- = f_0 = 0.5$.

Table 3. CLEO and ARGUS average semileptonic exclusive branching fractions

	CLEO 1.5	CLEO II	ARGUS	Average
$\mathcal{B}(\bar{B}^0 \to D^+l\bar{\nu})$			$1.9 \pm 0.6 \pm 0.4$	1.9 ± 0.7
$\mathcal{B}(\bar{B}^0 \to D^{*+}l\bar{\nu})$	$4.1 \pm 0.5 \pm 0.7$	$4.5 \pm 0.44 \pm 0.44$	$4.7 \pm 0.6 \pm 0.6$	4.5 ± 0.4

These branching fractions can be related to the CKM parameter $|V_{cb}|$ through hadronic matrix elements evaluated through some of the approaches discussed in the previous section. In order to reduce the model dependence of the result obtained, it is important to provide more stringent constraints on the various models. In particular, several variables for the decay $B \to D^*l\bar{\nu}$ can be studied to extract information about the form factors discussed above. The differential decay width for this decay is generally parametrized in terms of the helicity amplitudes:[30]

$$\begin{aligned}\frac{d\Gamma(B \to D^*l\bar{\nu})}{dq^2 d\cos\theta d\cos\theta^* d\chi} &= \frac{3G_F^2}{8(4\pi)^4} \mid V_{cb} \mid^2 \frac{Kq^2}{m_B^2}((\mid H_+ \mid^2 + \mid H_- \mid^2)(1+\cos^2\theta)\sin^2\theta^* + \\ &4 \mid H_0 \mid^2 \sin^2\theta\cos^2\theta^* - 2Re[H_+H_-^*]\sin^2\theta\sin^2\theta^*\cos 2\chi \\ &-Re[(H_+ + H_-)/H_0^*]\sin 2\theta \sin 2\theta^* \cos\chi \\ &+2\eta\xi\{Re[(H_+ + H_-)/H_0^*]\sin\theta\sin 2\theta^*\cos\chi \\ &+(\mid H_+ \mid^2 - \mid H_- \mid^2)\cos\theta\sin^2\theta^*\}), \end{aligned} \tag{9}$$

where q^2 is the virtual W invariant mass, θ is the lepton polar angle in the $l\bar{\nu}$ rest frame, θ^* is the polar angle of the D in the D^* rest frame, m_B is the B mass, G_F is the Fermi coupling constant, K is the D^* momentum in the B rest frame, η=+1 describe the handedness of the $l\bar{\nu}$ current and $\xi = +1$ describe the $V - A$ behaviour of the leptonic current.

The helicity amplitudes are related to the form factors appearing in the hadronic currents by the relationships[30]:

$$H_\pm(q^2) = (m_B + m_{D^*})A_1(q^2) \mp \frac{2m_bK}{m_B + m_{D^*}}V(q^2) \tag{10}$$

$$H_0(q^2) = \frac{1}{2m_{D^*}\sqrt{q^2}}\left[(m_B^2 - m_{D^*}^2 - q^2)(m_B + m_{D^*})A_1(q^2) - \frac{4m_B^2K^2}{m_B + m_{D^*}}A_2(q^2)\right] \tag{11}$$

The form factor $A_1(q^2)$ can be factored out Equations 10 and 11 and the differential decay rate can be expressed as a function of the ratios $A_2(q^2)/A_1(q^2)$ and $V(q^2)/A_1(q^2)$. The absolute scale of this decay width is determined by the product $|V_{cb}|^2 A_1^2\tau_B$. If an estimate of $|V_{cb}|$ and the lifetime of the B meson are taken, the normalization of the decay rate gives $A_1(q^2)$.

The procedure chosen by CLEO[31] to extract the form factors is to build a χ^2 with nine different measurements of observables related to the differential decay width in Equation 9. They are:

1. The forward backward asymmetry defined as:

$$A_{fb} = \frac{d\Gamma(\theta) - d\Gamma(\pi - \theta)}{d\Gamma(\theta) - d\Gamma(\pi - \theta)}, \quad \frac{\pi}{2} \le \theta \le \pi \tag{12}$$

   where the notation implies that the differential decay width has been integrated over all the remaining observables. This observables is sensitive to the chirality of the $b \to c$ transition[32] and has been measured by CLEO to be $0.14 \pm 0.06 \pm 0.03$ for a lepton momentum $p_l > 1$ GeV. The background subtracted A_{fb} is shown in Figure 3, which shows also the results of the fits of these data with the ISGW model assuming pure $V - A$ and $V + A$ currents for the $b \to c$ transition. It can be seen that a $V - A$ current is clearly favoured. This test is valid under the assumption that the lepton current is $V - A$. Gronau and Wakaizumi[33] have shown that it is possible to construct some non Standard Model in which this test is not sufficient to determine the chirality of the $b \to c$ transition.

2. The shape of the distribution $d\Gamma/dq^2$ from a weighted average of the CLEO1.5 and ARGUS data.[34]

3. The value of Γ_L/Γ_T from measurements of the D^* polarization.[35,23]

The fit parameters are only the form factor ratios at $q^2 = q^2_{max}$, using two different assumptions for the q^2 dependence, a) an exponential dependence a la ISGW and b) the fitting function used by Neubert.[36] These two fits should give a rough idea of the sensitivity of the results to the q^2 dependence assumed. The results are shown in Table 4 together with the predictions by different models. It can be seen that the results are in qualitative agreement with all the models, but the experimental errors need to be reduced in order to be able to enhance the discriminatory power of the measurement.

Table 4. Form factor ratios at $q^2 = q^2_{max}$.

	A_2/A_1	V/A_1
Fit a	1.02 ± 0.24	1.07 ± 0.57
Fit b	0.79 ± 0.28	1.32 ± 0.62
ISGW	1.14	1.27
KS	1.39	1.54
WSB	1.06	1.14
HQET[37]	1.26	1.26
HQET[38]	1.14	1.74

4. DETERMINATION OF $|V_{cb}|$

A precise determination of $|V_{cb}|$ is a very important goal as it determines the parameter A in the Wolfenstein representation of the CKM quark mixing matrix. In turn, this has crucial importance, as pointed our recently by Marciano,[39] to constraint some Supersymmetric Grand Unified Theories (SUSY GUTS) , which predict some natural relationships between quark and lepton masses and couplings. In particular a relatively high value of $|V_{cb}|$ is predicted (≈ 0.047): a firm evidence that it is be much smaller than this value would cast serious doubts on the validity of this minimal SUSY GUT. Several approaches can be adopted to extract from the data discussed so far a value of $|V_{cb}|$. Some methods have a better statistical accuracy but are plagued by a higher sensitivity to the theoretical model used in extracting $|V_{cb}|$ from the data, some others appear promising but more data are necessary to improve the statistical error.

4.1 $|V_{cb}|$ from Exclusive Semileptonic Decays

In principle both the $B \to Dl\bar{\nu}$ and $B \to D^*l\bar{\nu}$ can be used to extract $|V_{cb}|$. The present discussion will focus on $B \to D^*l\bar{\nu}$ because the difficulties in combining different experimental values of this branching fraction discussed above make the present errors too big to be a useful determination. In order to extract $|V_{cb}|$ it is necessary to transform the semileptonic branching fraction into a decay width. The value of τ_B chosen in the present analysis and in all the subsequent determinations of $|V_{cb}|$ is 1.51 ± 0.1,[22] which is the present world average of τ_0. The error in this lifetime is bigger than the one associated with the commonly used $<\tau_b>$, but this choice eliminates the additional systematic error in $|V_{cb}|$ associated with the effects of the lifetimes of the B_S and b baryons in the latter quantity.

In this average value of $\mathcal{B}(B \to D^*l\bar{\nu}) = 4.45 \pm 0.44$ is used; $|V_{cb}|$ is obtained through the relationship:

$$|V_{cb}| = \sqrt{\Gamma_{SL}/\Gamma_{TH}}, \tag{13}$$

where Γ_{SL} is given by $\mathcal{B}(B \to D^*l\bar{\nu}/\tau_B$ and Γ_{TH} is the model dependent theoretical hadronic matrix element. Table 5 summarizes the predicted values of Γ_{TH} and the corresponding values of $|V_{cb}|$.

Table 5. $|V_{cb}|$from $\mathcal{B}(B \to D^*l\bar{\nu})$.

Model	$\Gamma_{TH}(\text{ps}^{-1})$	$\vert V_{cb}\vert$
ISGW	25.2	0.034 ± 0.004
KS	25.7	0.034 ± 0.004
WBS	21.9	0.037 ± 0.004

It can be seen that the models considered in this case are in a reasonable good agreement: if we take the somewhat dubious approach of averaging over models and associating an additional error with the spread in predictions, we get $<|V_{cb}|> = 0.035 \pm 0.004 \pm 0.002$ and the relatively low value of $<|V_{cb}|>$ with respect to previously published numbers[40] is due to the increased value of τ_B.

4.2 $|V_{cb}|$ from Inclusive Lepton Spectrum

The same procedure followed in extracting $|V_{cb}|$ from the exclusive decay $B \to D^*l\bar{\nu}$ can be adopted to extract $|V_{cb}|$ from the inclusive $b \to xl\bar{\nu}$ spectra discussed before. In this case the theoretical width Γ_{TH} is taken either from an inclusive model, like ACCMM, which does not consider explicit hadronic final states or from the sum of the Γ^i_{TH} for each final state i included in the calculation. It was originally thought that exclusive models were the best to describe semileptonic B decays, dominated by the $b \to c$ transition, as the D and D^* hadronic final states appeared to saturate the rate. There was even some theoretical justification for this[41] because of the relatively high mass of the quarks involved in the decay. Now it appears that other final states compose between 20 to 30 % of the semileptonic rate. Parton models are justified by quark-hadron duality which applies when a continuum of hadronic final states are involved. This hardly seems the case here. On the other hand , the relatively sizable component which is presently labeled "$D^{**}l\bar{\nu}$" indicates that exclusive models may need some refinement to be able to give reliable predictions for the inclusive Γ_{TH}.

With these caveats, the values of $|V_{cb}|$ extracted with the ACCMM and the ISGW* models in the CLEO II analysis are shown in Table 6.

Table 6. $|V_{cb}|$ from $\mathcal{B}(B \to Xl\bar{\nu})$.

Model	$\Gamma_{TH}(\text{ps}^{-1})$	$\vert V_{cb}\vert$
ISGW*	42	0.042 ± 0.005
ACCMM	40	0.041 ± 0.005

4.3 $|V_{cb}|$ from q^2 Dependence of the Decay Width for $B \to D^*l\bar{\nu}$

HQET has stirred a new interest in a precision study of the q^2 distribution for the exclusive decay $B \to D^*l\bar{\nu}$: Luke's theorem[42] guarantees that the $1/m_q$ corrections to the infinite mass limit form factors vanish near the point $q^2 = q^2_{max}$, which, in the formalism of HQET corresponds to the limit $y = v \cdot v' = 1$, where v and v' correspond to the 4-velocity of the B and D^* meson respectively. The differential decay rate is given by[36]:

$$\frac{1}{\sqrt{(y^2-1)}}\frac{d\Gamma}{dy} = \frac{G_F^2}{48\pi^3} m^3_{D^*}(m_B - m^*_D)^2 \eta^2_{QCD} \, |V_{cb}|^2 \, \xi^2(y) f(y) \tag{14}$$

where $\xi(y)$ is the Isgur – Wise function, giving the shape of the form factors in the decays $B \to D(D^*)l\bar{\nu}$, η_{QCD} represents the strong interaction radiative correction, $r = m^*_D/m_B$ and the function $f(y)$ is given by:

$$f(y) = 4y(y+1)\frac{1 - 2yr + r^2}{1 - r^2} \tag{15}$$

for D^* with transverse polarization and:

$$f(y) = (y+1)^2 \tag{16}$$

for D^* with longitudinal polarization.

The theoretical claim is that, up to $1/m_q^2$ corrections, $d\Gamma/dy$ $(y = 1)$ is given exactly by the HQET prediction. The only theoretical uncertainty the error in η_{QCD} which is presently quoted as $\eta_{QCD} = 0.99 \pm 0.04$.[43], which corresponds to an 8% uncertainty in the absolute scale of $d\Gamma/dy$. In addition, there has been some discussion on the effects of different assumptions for the unknown function $\xi(y)$ in extracting $|V_{cb}|$ from present measurements of $d\Gamma/dy$.[44,26]

Figure 4 shows the CLEO II data . Their fit results are summarized in Table 7. An estimate of $|V_{cb}|$ with this method was performed previously by Neubert[36], which used the compilation of CLEO 1.5 and ARGUS data performed by Bortoletto and Stone[34]. Note that the value of $|V_{cb}|$ reported by Neubert (0.045 ± 0.007) was obtained with a different assumed value of $\tau_B = 1.18$ ps and η_{QCD}=0.95. If we use $\tau_B = 1.51$ ps and η_{QCD}=0.99, his result becomes $|V_{cb}| = 0.037 \pm 0.006$ in full agreement with the CLEO II data.

Table 7. $| V_{cb} |$ from $d\Gamma/dy$ for $\mathcal{B}(B \to D^* l\bar{\nu})$.

$\xi(y)$	Model	$\hat{\rho}^2$	$\mid V_{cb} \mid$
$\frac{2}{(y+1)} \exp(-(2\hat{\rho}^2 - 1)\frac{(y-1)}{(y+1)})$	BSW	$1.2 \pm 0.6 \pm 0.3$	$0.038 \pm 0.006 \pm 0.004$
$\frac{2}{(y+1)}^{2\hat{\rho}^2}$	POLE	$1.1 \pm 0.5 \pm 0.2$	$0.038 \pm 0.005 \pm 0.004$
$\exp(-\hat{\rho}^2(y-1))$	ISGW	$1.0 \pm 0.4 \pm 0.2$	$0.037 \pm 0.005 \pm 0.004$
$1 - \hat{\rho}^2(y-1) + \epsilon^2(y-1)^2$	Burdman	$1.2 \pm 0.5 \pm 0.3$	$0.038 \pm 0.010 \pm 0.004$

where the parameter $\hat{\rho}^2$ By combining the Neubert's and CLEO results, we get as our best estimate of $| V_{cb} |$ with this method $0.038 \pm 0.004 \pm 0.004 \pm 0.004$. The last error reflects the theoretical uncertainty on the value of η_{QCD}.

4.4 Summary

Figure 5 summarizes the $| V_{cb} |$ values extracted with the different methods discussed before. If we use the value extracted from $d\Gamma/dy$ to get the value of the parameter A in the Wolfenstein parametrization of the CKM matrix, we get $A = 0.79 \pm 0.14$. A smaller error is necessary in order to make a stringent test of the validity of the minimal SUSY GUTS theoretical expectations.

5. DETERMINATION OF $|V_{ub}|$

The only positive evidence for $b \to u$ transitions is the study of the end-point of the lepton spectrum. The discovery of an excess of leptons beyond the kinematical end-point for $b \to c$ transitions was performed by CLEO[45] and was soon confirmed by ARGUS.[46] Figure 6 shows the end-point lepton spectra from the new CLEO data sample,[47] which shows a robust signal, which however implies a value of $| V_{ub} |$ smaller that in the previous measurements.

In this case, the theoretical uncertainties are much bigger than in the extraction of $| V_{cb} |$. This is due to the fact that the quark in the final state is light. Therefore the phase space available in the $q^2 - E_l$ plane is much larger than in the $b \to c$ case and the model sensitivity is more pronounced. In particular, there is a significant difference between "inclusive" models (e.g. ACCMM) and exclusive models which sum up contributions from discrete resonances (π, ρ, ω...). There is general consensus that the "exclusive" models cannot account for the whole lepton spectrum from $b \to u$ transitions, but it was argued that they could describe the end-point quite adequately.[7] On the other hand, even when leptons have energy close to the kinematical end-point, the q^2 of the lepton-$\bar{\nu}$ spans the whole range between $q^2 = 0$ and q^2_{max}. If q^2 is close to q^2_{max}, the hadronic final state is likely to be composed by a single low mass resonance. On the other hand, if q^2 is close to $q^2 = 0$, a continuum of final states is more likely, and inclusive models appear more appropriate.[48] Artuso[49] has shown that the q^2 distribution predicted by an inclusive model is quite different from the one predicted by exclusive models, as shown in Figure 7. In addition, exclusive models give quite different predictions because they assume different q^2 dependence of the form factors. Therefore a study of the q^2 distribution in $b \to u$ semileptonic decay may be a very sensitive test to the validity of different theoretical approaches and may reduce the model dependence of the results .

Table 8 summarized the CLEO II $| V_{ub} |$ estimates, which represent the most precise knowledge so far of this parameter. It can be seen that the dominant uncertainty is associated with the spread of model predictions, which needs to be reduced until significant progress is made in determining $| V_{ub} |$.

Table 8. $| V_{ub} |$ from $\mathcal{B}(B \to X_u l\bar{\nu})$ for $2.3 \leq p_l \leq 2.6$ GeV.

Model	$10^6 \Delta\mathcal{B}_{ub}(p_l)$	$10^2 \mid V_{ub}/V_{cb} \mid^2$	$\mid V_{ub} \mid / \mid V_{cb} \mid$
ISGW	$121 \pm 17 \pm 15$	1.02 ± 0.20	0.101 ± 0.010
KS	$115 \pm 16 \pm 15$	0.31 ± 0.06	0.056 ± 0.006
WBS	$122 \pm 17 \pm 16$	0.53 ± 0.11	0.073 ± 0.007
ACCMM	$154 \pm 22 \pm 20$	0.57 ± 0.11	0.075 ± 0.008

Exclusive decays, like $B \to \rho l\bar{\nu}$, could provide some discrimination between exclusive models, especially if enough statistics were available to measure the form factors. We are still a long way from this goal: so far only upper limits are available for these decays. In particular, CLEO measures an upper limit for $\mathcal{B}(B^- \to V^0 l\bar{\nu}) < (1.6 - 2.7) \times 10^{-4}$ at 90% C.L,[50] where V^0 is a neutral vector meson (ρ^0 or ω) and the range covers the different theoretical predictions.

6. $B^0\bar{B}^0$ MIXING

The discovery of $B^0\bar{B}^0$ mixing, performed by ARGUS[51] in 1987 and soon confirmed by CLEO,[52] had several important ramifications. It implied a much higher top quark mass than previously expected and opened up new prospects for measuring CP violations in B decays. In these measurements the flavour of the B meson is tagged by the charge of the lepton from B^0 semileptonic decays.

The first measurements were given in terms of the parameter r defined as:

$$r = \frac{\Gamma(B^0 \to \bar{B}^0)}{\Gamma(B^0 \to B^0)} \tag{17}$$

A related parameter which is used in recent CLEO measurements [53] and in measurements performed at higher energies is χ_d:

$$\chi_d = \frac{\Gamma(B^0 \to \bar{B}^0)}{\Gamma(B^0 \to B^0) + \Gamma(B^0 \to \bar{B}^0)} \tag{18}$$

The experimental value of χ_d is obtained from the measured ratio of like-sign to opposite-sign dileptons via :

$$\chi_d = \frac{1}{1-\Lambda} \cdot \frac{N(l^\pm)N(l^\pm)}{[N(l^+l^-) + N(l^\pm l^\pm)]} \tag{19}$$

where $\Lambda = f_+ b_+^2/(f_+ b_+^2 + f_0 b_0^2)$ is the fraction of leptons coming from charged B's semileptonic decays. Presently the uncertainty in Λ represents the largest source of systematic uncertainty in χ_d. This is the reason why both CLEO and ARGUS tried to perform this measurement on an enriched sample of neutral B mesons using several different tagging techniques.

CLEO[53] uses the decay $\bar{B}^0 \to D^{*+} l^- \bar{\nu}$ to tag $\bar{B}^0$ events. In order to increase the statistical accuracy, D^{*+} are partially reconstructed, that is only the slow π from the D^* is explicitly detected and the low Q value in the decay $D^{*+} \to D^0\pi^+$ is used to select these events without explicitly reconstructing the D^0. It measures:

$$\chi_d = 0.149 \pm 0.023 \pm 0.019 \pm 0.010 \tag{20}$$

where the third error corresponds to a $\pm15\%$ variation in Λ. This has to be compared with

$$\chi_d = 0.157 \pm 0.016 \pm 0.018^{+0.028}_{-0.021} \tag{21}$$

which is obtained from the same data sample from the untagged analysis. The two results are in good agreement and confirm previous results and the recent ARGUS [54] evaluation $\chi_d = 0.173 \pm 0.038 \pm 0.044^{+0.031}_{-0.023}$, with smaller errors.

The parameter χ_d is related to the parameter $\Delta M/\Gamma$, which is relevant to the measurement of CP violation occurring via mixing, through the relationship:

$$x_d = \frac{\Delta M}{\Gamma} = \sqrt{2\chi_d/(2-\chi_d)} \tag{22}$$

The tagged measurement from CLEO corresponds to $x_d = 0.652 \pm 0.074$.

7. SUMMARY ON EXPERIMENTAL CONSTRAINTS ON CKM PARAMETERS

The experimental information from semileptonic B decays discussed in the previous section can be combined with the data on the parameter ϵ_K, describing CP violation in the $K^0 - \bar{K}^0$ system. It is usual to display these constraints as bands in the ρ and η plane, where ρ and η are the CKM parameters in the Wolfenstein representation. Figure 8 shows the region allowed by the present experimental information[55] for three values of the top quark mass m_t.

The measured value of $\mid V_{ub}/V_{cb} \mid$ defines a region comprised between two circles having radius $\mid V_{ub}/V_{cb} \mid /\lambda$. The boundaries correspond to $\mid V_{ub}/V_{cb} \mid /\lambda = 0.34 \pm 0.13$, where the central value corresponds to the value obtained by CLEO II with the ACCMM model and the error reflects mostly the theoretical uncertainty in the extraction of $\mid V_{ub} \mid$ from experimental data. The measurement of the mixing parameter x_d defines an allowed region between two circles centered at $(\rho = 1, \eta = 0)$. In this case the major uncertainty, for a given m_t, comes from the uncertainty in the B meson decay constant f_B: the two boundaries corresponding to the allowed region correspond to $f_B = 160$ MeV (leftmost boundary) and $f_B = 240$ MeV (rightmost boundary). Finally the measured value of ϵ_K defines the region between the two almost horizontal lines.

The shaded areas in the three plots correspond to the region consistent with all these constraints. In the middle figure, the triangle describing CP violation is shown. The angle with the vertex at $(\rho = 1, \eta = 0)$ is the one which is related to the CP asymmetry in the decay $B^0 \rightarrow \psi K_S$. It can be seen that the constraints from the Standard model seem to indicate that a rather large asymmetry should be measured in this channel. An increased value of f_B with respect to present lattice gauge calculation expectations would increase this angle towards its maximum allowed value of 45°.[55]

8. ACKNOWLEDGEMENTS

The author would like to give a very special thank to J. Donoghue, N. Isgur, J. Körner, S. Stone, and M. Wirbel for interesting conversations. In addition Julia Stone should be thanked for helping me enjoy the stay in Snowmass and for cheerful breaks during the completion of this work.

9. REFERENCES

1. L. Wolfenstein, *Phys. Rev. Lett.* **51** (1983) 1945.
2. C. T. Sachrajda, *Talk given at the Advanced Study Conference on Heavy Flavours*, Pavia, Italy, 1993.
3. P. McKenzie, *Talk given at the Vth International Conference on Heavy Flavour Physics*, Montreal, Canada, 1993.
4. G. Altarelli et al., *Nucl. Phys.* **B208** (1982) 365.
5. A. Bareiss and E. Paschos, *Nucl. Phys.* **B327** (1989) 353.
6. T. Altomari and L. Wolfenstein , *Phys. Rev. Lett.* **58** (1987) 1583.
7. N.Isgur et al., *Phys. Rev.* **D39** (1989) 799.
8. M. Wirbel et al., *Zeit. für Phys.* **C29** (1985) 637.
9. J. Körner and G. Schuler, *Zeit. für Phys.* **C38** (1988) 511 and *Zeit. für Phys.* **C41** (1989) 690 (*erratum*).
10. M. A. Shifman, A.J. Vainstein and V.I. Zacharov, *Nucl. Phys.* **B147** (1979) 385.
11. G. Nardulli, *Nucl. Phys.* **B27** (Proc. Suppl.) (1992) 47.
12. P. Ball, *Phys. Lett.* **B281** (1992) 133.
13. N. Isgur and M. Wise, in *B Decays*. ed. S. Stone, (World Scientific, Singapore, 1992) p. 158.
14. W. Bacino et al. (DELCO), *Phys. Rev. Lett.* **43** (1979) 1073.
15. R. Fulton et al. (CLEO), *Phys. Rev.* **D43** (1991) 651.
16. H. Albrecht et al. (ARGUS), *Zeit. für Phys.* **C57** (1993) 533.
17. B. Ong et al. (CLEO), *Contributed Paper to XVI International Symposium on LEPTON-PHOTON INTERACTIONS*, Cornell University, Ithaca, NY 1993.
18. S. Henderson et al. (CLEO), *Phys. Rev.* **D45** (1992) 2212.
19. H. Albrecht et al. (ARGUS), *Phys. Lett.* **B249** (1990) 359.
20. M. Artuso et al. (CLEO), *Contributed Paper to XVI International Symposium on LEPTON-PHOTON INTERACTIONS*, Cornell University, Ithaca, NY 1993.
21. D. Akerib et al. (CLEO), *Contributed Paper to XVI International Symposium on LEPTON-PHOTON INTERACTIONS*, Cornell University, Ithaca, NY 1993.
22. T. Bowcock, *Talk given at the Advanced Study Conference on Heavy Flavours*, Pavia, Italy, 1993.
23. D. Bortoletto et al. (CLEO), *Phys. Rev. Lett.* **63** (1989) 1667.
24. G. Crawford et al. (CLEO), *Contributed Paper to XVI International Symposium on LEPTON-PHOTON INTERACTIONS*, Cornell University, Ithaca, NY 1993.
25. H. Albrecht et al. (ARGUS), *Phys. Lett.* **B275** (1992) 195.
26. H. Albrecht et al. (ARGUS) *DESY Preprint* **DESY-92-029** (1992) .
27. J. Bartelt et al. (CLEO), *Contributed Paper to XVI International Symposium on LEPTON-PHOTON INTERACTIONS*, Cornell University, Ithaca, NY 1993.

28. J. Adler et al. (MARK III), *Phys. Rev. Lett.* **60** (1988) 89.
29. F. Butler et al. (CLEO), *Phys. Rev. Lett.* **69** (1992) 2041.
30. F. Gilman and R. L. Singleton, *Phys. Rev.* **D41** (1990) 142.
31. S. Sanghera et al. (CLEO), *Phys. Rev.* **D47** (1993) 791.
32. J. Körner and G. Schuler, *Phys. Lett.* **B226** (1989) 185.
33. M. Gronau and S. Wakaizumi, *Phys. Lett.* **280** (1992) 79 and *Phys. Rev. Lett.* **68** (1992) 1814.
34. D. Bortoletto and S. Stone, *Phys. Rev. Lett.* **65** (1990) 2951.
35. H. Albrecht et al. (ARGUS), *Phys. Lett.* **B219** (1989) 121.
36. M. Neubert, *Phys. Lett.* **B264** (1991) 455.
37. N. Isgur and M. Wise, *Phys. Lett.* **B237** (1990) 527.
38. M. Neubert in *Heavy Flavours* eds. A. J. Buras and M. Lindner, (World Scientific, Singapore, 1991)
39. W. Marciano, *Talk given at the Vth International Conference on Heavy Flavour Physics*, Montreal, Canada, 1993.
40. S. Stone, in *B Decays*. ed. S. Stone, (World Scientific, Singapore, 1992) p. 210.
41. M.B. Voloshin and M.A. Shifman, *Sov. J. Nucl. Phys.* **47** (1988) 511.
42. M.E. Luke, *Phys. Lett.* **B252** (1990) 447 .
43. Z. Ligeti, *Talk given at the Advanced Study Conference on Heavy Flavours*, Pavia, Italy, 1993 .
44. G. Burdman, *Phys. Lett.* **B284** (1992) 133.
45. R. Fulton et al. (CLEO), *Phys. Rev. Lett.* **64** (1990) 16.
46. H. Albrecht et al. (ARGUS), *Phys. Lett.* **B234** (1990) 409.
47. J. Bartelt et al. (CLEO), *Contributed Paper to XVI International Symposium on LEPTON-PHOTON INTERACTIONS*, Cornell University, Ithaca, NY 1993.
48. C. Ramirez et al., *Phys. Rev.* **D41** (1990) 1496.
49. M. Artuso, *Phys. Lett.* **B311** (1993) 307.
50. A. Bean et al. (CLEO), *Phys. Rev. Lett.* **70** (1993) 18.
51. H. Albrecht et al. (ARGUS), *Phys. Lett.* **B192** (1987) 245.
52. M. Artuso et al. (CLEO), *Phys. Rev. Lett.* **62** (1989) 2233.
53. J. Bartelt et al. (CLEO), *Cornell Preprint.* **CLNS 93/1207** (1993) .
54. H. Albrecht et al. (ARGUS), *Zeit. für Phys.* **C55** (1992) 357.
55. S. Stone, *Talk given at the Vth International Conference on Heavy Flavour Physics*, Montreal, Canada, 1993.

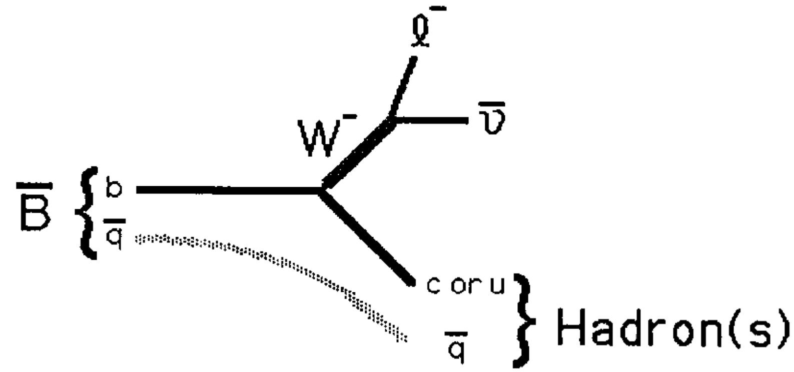

Figure 1. Spectator diagram for semileptonic *b* quark decay.

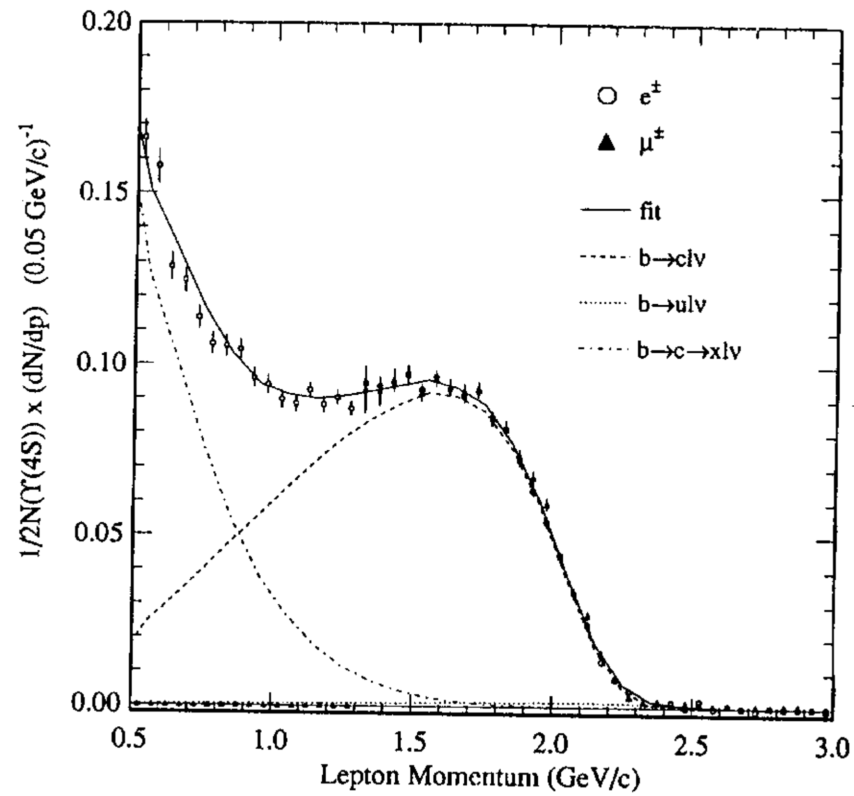

Figure 2. Lepton spectra from *B* decays (CLEO). The fit with ACCMM model is superimposed.

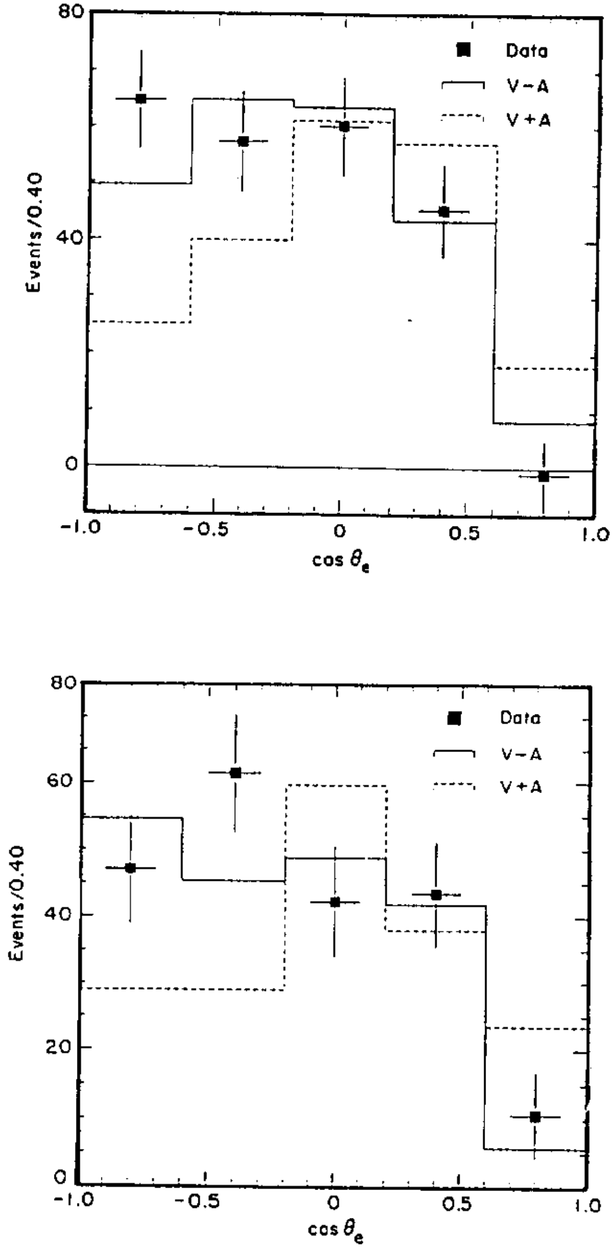

Figure 3. $dN/d\cos\theta$ (CLEO) distributions in a)$\bar{B}^0 \to D^{*+} l\bar{\nu}$ and b)$B^- \to D^{*0} l\bar{\nu}$.

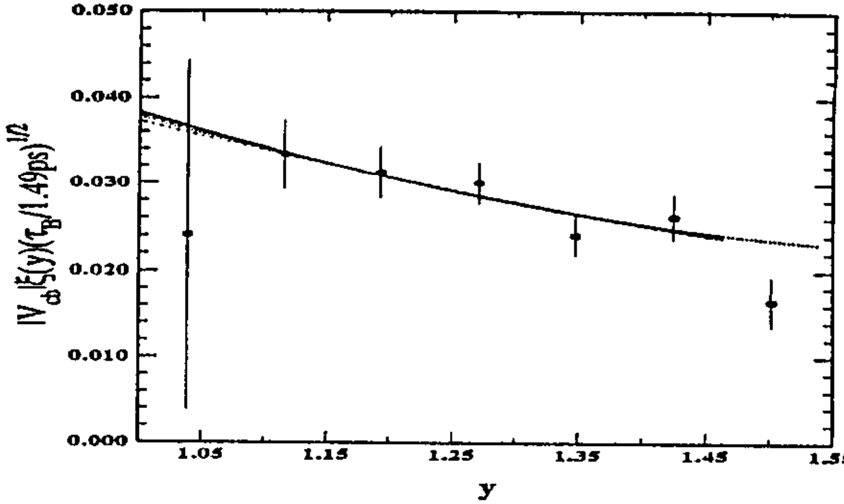

Figure 4. $d\Gamma/dy$ in the decay $\bar{B}^0 \to D^{*+} l\bar{\nu}$ (CLEO).

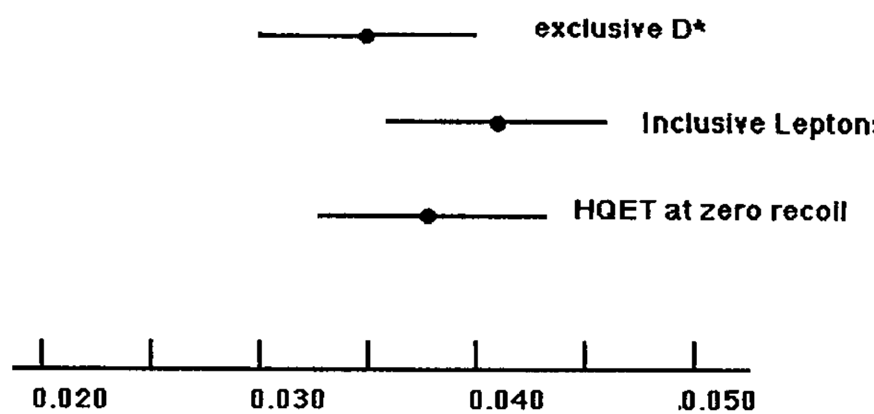

Figure 5. Summary of V_{cb} determinations.

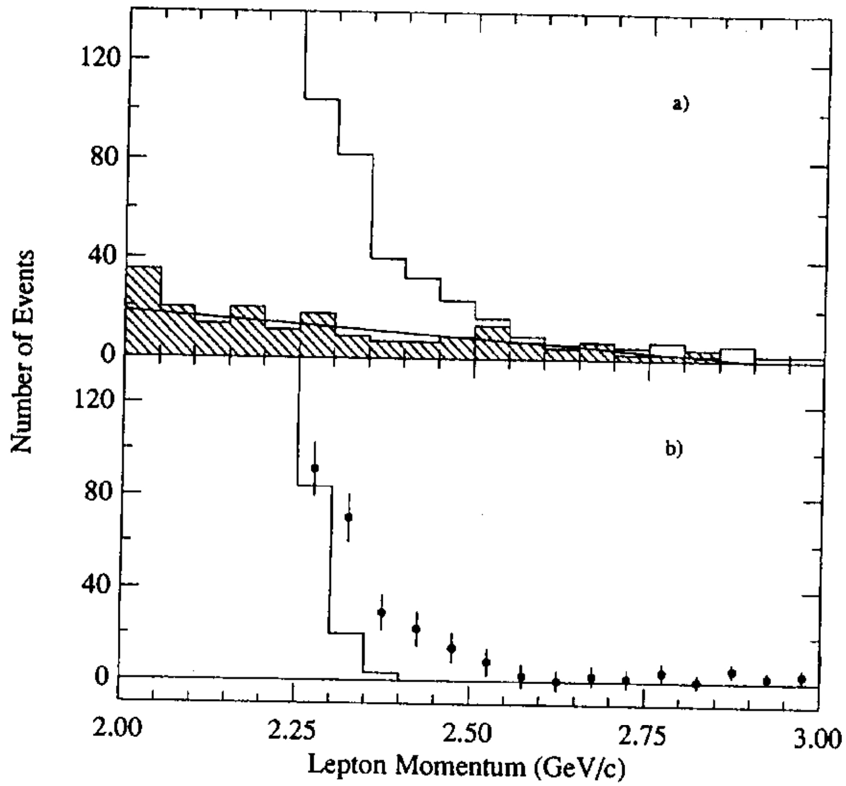

Figure 6. End-point lepton momentum spectra (CLEO) (histogram shows the ON $\Upsilon(4S)$ data whereas the hatched area shows the OFF data. In b) the dots show the ON data after the fitted and scaled OFF data have been subtracted.)

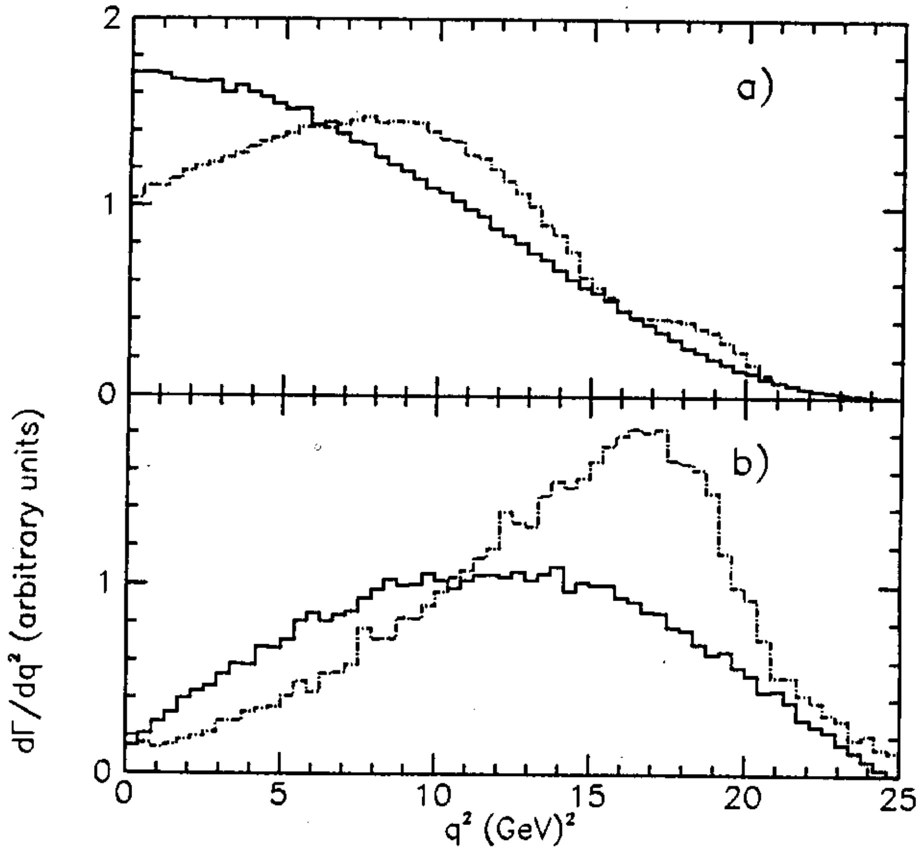

Figure 7. q^2 distribution for $b \to ul\bar{\nu}$ decay from Ref. 46 (solid histogram) and ISGW model (dash-dotted histogram) a) for all P_l, b) for $P_l \geq 2.4$ GeV/c in $\Upsilon(4S)$ rest frame (all the resonances studied ISGW model have been included).

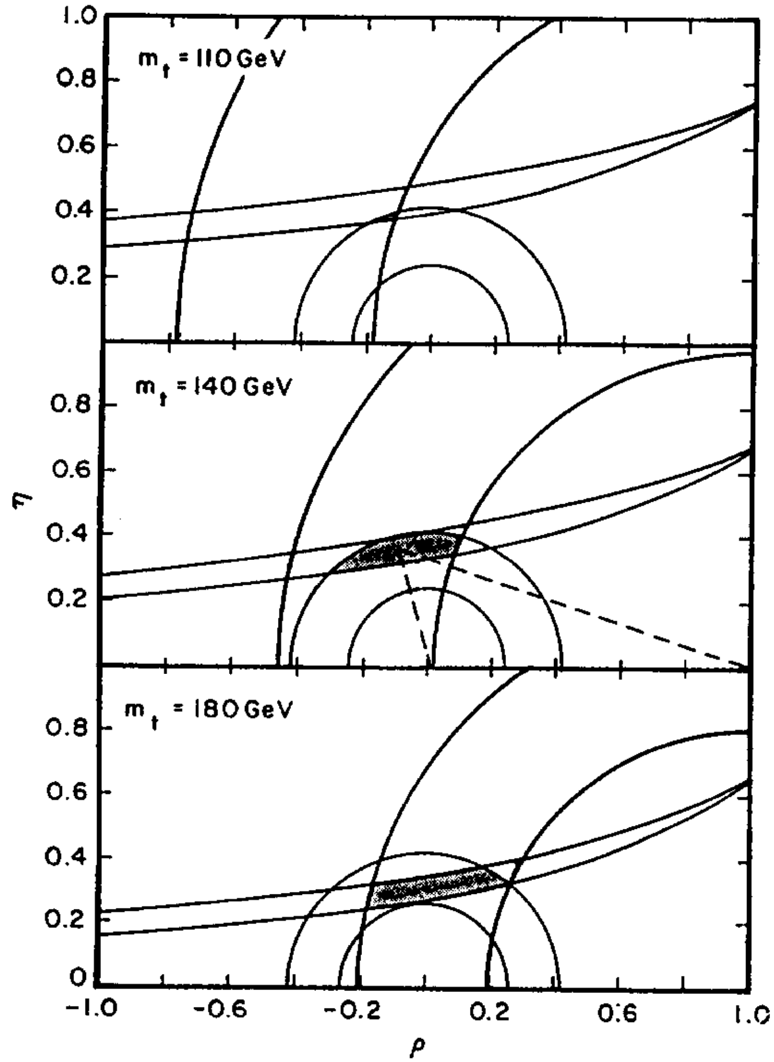

Figure 8. Experimental constraints in the $\rho - \eta$ plane for different values of the top quark mass.

LIGHT-QUARK, HEAVY-QUARK SYSTEMS: AN UPDATE

BENJAMIN GRINSTEIN
SSC Laboratory, 2550 Beckleymeade Ave., MS-2007
Dallas, Texas 75248 USA

We review many of the recently developed applications of Heavy Quark Effective Theory techniques. After a brief update on Luke's theorem, we describe striking relations between heavy baryon form factors, and how to use them to estimate the accuracy of the extraction of $|V_{cb}|$. We discuss factorization and compare with experiment. An elementary presentation, with sample applications, of reparametrization invariance comes next. The final and most extensive chapter in this review deals with phenomenological lagrangians that incorporate heavy-quark spin-flavor as well as light quark chiral symmetries. We compile many interesting results and discuss the validity of the calculations.

1. INTRODUCTION

It seems hardly appropriate to devote any time to reviewing the fundamentals of Heavy Quark Effective Theory (HQET), both because this is a meeting of experts and because several good reviews of the subject are now available.[1,2] Instead of wasting any space introducing conventions, I simply choose to use the notation of Ref. 2. Thus, I will be able to devote more energy towards a description of recent developments in this field.

I view this paper as updating and expanding on Ref. 2. There the HQET was presented and a few applications discussed at length. Other applications where briefly discussed. Much has changed since Ref. 2 was written, and it seems the time is ripe for an extension of that work. Because of time and space limitations this is not intended as an extensive overview of progress in the field since Ref. 2 was written. Rather, I shall pick and choose according to my taste, familiarity with the subjects, and what I perceived as relevant to the participants of the workshop.

2. AN UPDATE ON LUKE'S THEOREM

Presumably the best known consequence of heavy quark symmetries is that the form factors for semileptonic $B \to D$ and $B \to D^*$ decays are determined at the point of zero recoil (equal B and D velocities). Luke's theorem states that this normalization of the meson form factors has no $1/M_Q$ corrections.[3] It is not widely appreciated that Luke's original proof did not exclude possible *short distance* corrections of order $(\alpha_s(m_c)/m_c)$. It turns out it is easy to extend Luke's proof to exclude corrections of this sort to any order in the strong coupling.[4]

Similarly, the normalization of form factors for $\Lambda_b \to \Lambda_c$ semileptonic decay is computable up to corrections of order $1/M_Q^2$.[4, 5]

3. HEAVY BARYON FORM FACTOR RELATIONS

3.1 Relations to First Order in $1/M_Q$

Six form factors encode the semileptonic decay amplitude $\Lambda_b \to \Lambda_c e\overline{\nu}$. The transition lends itself particularly well to HQET analysis because it is tightly constrained by the heavy quark spin symmetry.[6] Like their mesonic counterparts, the six form factors that parameterize this baryonic process are predicted at leading order in the $1/M_Q$ expansion in terms of a single Isgur-Wise function. In contrast with their mesonic counterparts, one can prove that this is still the case at order $1/M_Q$.[5] In other words, five relations among these six form factors remain after $O(1/m_c)$ and $O(1/m_b)$ corrections are included.

Remarkably, that such relations can be written is not precluded by short distance effects to any order in the strong coupling constant.[4] However the relations themselves get corrected order by order in perturbation theory. To see how this works, define the form factors through

$$\langle\Lambda_c(v',s')|V^\mu|\Lambda_b(v,s)\rangle = \overline{u}(v',s')[F_1(v{\cdot}v')\gamma^\mu + F_2(v{\cdot}v')v^\mu + F_3(v{\cdot}v')v'^\mu]u(v,s) \quad (1)$$

$$\langle\Lambda_c(v',s')|A^\mu|\Lambda_b(v,s)\rangle = \overline{u}(v',s')[G_1(v{\cdot}v')\gamma^\mu + G_2(v{\cdot}v')v^\mu + G_3(v{\cdot}v')v'^\mu]\gamma^5 u(v,s) \quad (2)$$

where v and s refer to the velocity and spin of the state Λ_b and of the Dirac spinor u. Then, the relations between form factors are[4]

$$\frac{F_1}{G_1} = 1 + \left[\frac{\overline{\Lambda}}{2m_c} + \frac{\overline{\Lambda}}{2m_b}\right]\frac{2}{(v{\cdot}v'+1)} + \frac{4}{3}\frac{\alpha_s(m_c)}{\pi}r + \frac{4}{3}\frac{\alpha_s(m_c)}{\pi}\frac{\overline{\Lambda}}{2m_c}\frac{2(1+r-v{\cdot}v'r)}{(v{\cdot}v'+1)} \quad (3)$$

$$\frac{F_2}{G_1} = \frac{G_2}{G_1} = -\frac{\overline{\Lambda}}{2m_c}\frac{2}{(v{\cdot}v'+1)} - \frac{4}{3}\frac{\alpha_s(m_c)}{\pi}r - \frac{4}{3}\frac{\alpha_s(m_c)}{\pi}\frac{\overline{\Lambda}}{2m_c}\frac{2(1+r-v{\cdot}v'r)}{(v{\cdot}v'+1)} \quad (4)$$

$$\frac{F_3}{G_1} = -\frac{G_3}{G_1} = -\frac{\overline{\Lambda}}{2m_b}\frac{2}{(v{\cdot}v'+1)} \quad (5)$$

where

$$r = \frac{\log(v{\cdot}v' + \sqrt{(v{\cdot}v')^2-1})}{\sqrt{(v{\cdot}v')^2-1}}\,. \quad (6)$$

and $\overline{\Lambda}$ is an undetermined constant with unit mass dimensions, expected to be of order of the hadronic scale, $\overline{\Lambda} \sim 500$ MeV. If in Eqs. 3 – 5 one sets $\alpha_s(m_c) = 0$ and $\overline{\Lambda} = 0$, one recovers the zeroth order results of Ref. 6, while the results of Ref. 5 are obtained by allowing $\overline{\Lambda} \neq 0$ but with $\alpha_s(m_c) = 0$. Clearly there are also corrections of order $\alpha_s(m_b)$ and of higher order in $1/M_Q$.

Heavy quark symmetries give the value of the form factors at zero recoil. In the leading-log approximation

$$G_1(1) = \left(\frac{\alpha_s(m_b)}{\alpha_s(m_c)}\right)^{a_I} \quad (7)$$

There are no corrections of order $1/M_Q$ to this relation.[5, 4] The counterpart of this prediction for mesons is used in the measurement of the mixing angle $|V_{cb}|$.

The form factor relations 3 – 5 provide a valuable means for assessing the uncertainty in future measurements of the mixing angle $|V_{cb}|$. It is reasonable to expect the prediction in Eq. 7 to hold to the same accuracy with which the form factors satisfy the predicted relations, at least for small or moderate $v{\cdot}v' - 1$.

3.2 Relations To All Orders In $1/m_c$

The relations above were obtained by expanding both in $1/m_c$ and $1/m_b$. Because the charm quark is only a few times heavier than typical hadronic scales, the corrections to the relations 3 – 5 may be large. Remarkably, Mannel and Roberts obtain four relations among the six form factors without assumptions on the size of m_c.[7] Expanding in $1/m_b$, *i.e.*, using the HQET for the b quark, the spin symmetry acting on the b quark alone is enough to limit to two the number of independent form factors in $\Lambda_b \to \Lambda_q$, where $q = u, c$:

$$\langle\Lambda_q(p',s')|\bar{q}\Gamma h_v^{(b)}|\Lambda_b(v,s)\rangle = \overline{u}(p',s')[f_1(v{\cdot}p') + \not{v}f_2(v{\cdot}p')]\Gamma u(v,s) \quad (8)$$

It is straightforward to write the six form factors in Eqs. 1 – 2 in terms of the two form factors in Eq. 8. Explicit relations between the form factors follow from eliminating $f_{1,2}$ from Eq. 8:

$$F_1 = G_1 - G_2 \quad (9)$$

$$F_2 = G_2 \quad (10)$$

$$F_3 = 0 \quad (11)$$

$$G_3 = 0 \quad (12)$$

These remarkably simple expressions receive corrections in order $1/m_b$ and $\alpha_s(m_b)/\pi$, but are valid for arbitrary m_q (provided $m_q < m_b$). Moreover, the perturbative corrections $\sim \alpha_s(m_b)/\pi$ are computable; the leading correction is obtained by replacing[8]

$$\Gamma \to \Gamma - \frac{\alpha_s(m_b)}{6\pi}\gamma_\mu\not{v}\Gamma\not{v}\gamma^\mu \quad (13)$$

in Eq. 8.

By taking the limit $m_b \to \infty$, one readily checks that Eqs. 3 – 5 are consistent with Eqs. 9 – 12.

4. FACTORIZATION

4.1 Summary of Theory

Consider purely hadronic B-meson decays into singly charmed final states. I have in mind the class of processes that includes $B \to D\pi$, $B \to D^*\pi$, $B \to D\rho$, etc. The interaction Hamiltonian density mediating these decays is

$$\mathcal{H} = \frac{G_F}{\sqrt{2}}V_{cb}V_{ud}^*[c_1\bar{b}_L\gamma_\mu c_L\bar{u}_L\gamma^\mu d_L + c_2\bar{b}_L\gamma_\mu T^a c_L\bar{u}_L\gamma^\mu T^a d_L]\,, \quad (14)$$

where $c_{1,2}$ are calculable short distance QCD corrections, T^a are color octet matrices, and q_L stands for a left handed quark. The second term in $\mathcal{H}$ arises from short distance QCD effects. Factorization in a particular decay, say $B \to D\pi$ is the statement that the following equation is true:

$$\langle D\pi|\mathcal{H}|B\rangle = \frac{G_F}{\sqrt{2}} V_{cb}V_{ud}^* c_1 \langle D|\bar{b}_L\gamma_\mu c_L|B\rangle\langle\pi|\bar{u}_L\gamma^\mu d_L|0\rangle \tag{15}$$

If factorization holds, the rate for the hadronic decay (the left hand side in eq. (9)) is given in terms of a meson decay constant ($\langle\pi(q)|\bar{u}_L\gamma^\mu d_L|0\rangle = if_\pi q^\mu$) and the form factors for $B \to D$ at a fixed momentum transfer (that is $\langle D|\bar{b}_L\gamma_\mu c_L|B\rangle$ at $q^2 = M_\pi^2$).

Whether a particular matrix element factorizes is a dynamical issue that involves non-perturbative strong interactions, and is therefore hard to settle from first principles. We do know, nevertheless, that factorization does not hold for a large class of two body decays. In the case of K decays, the $\Delta I = 1/2$ rule is a stark reminder that simple factorization does not hold. More recently, a wealth of evidence *against* factorization in D-meson decays (as in $D \to K\pi$) has been amassed.[9]

To my knowledge there are two known theoretical approaches to demonstrating factorization. It holds in leading order in the $1/N_c$ expansion, where N_c is the number of colors in QCD.[10] And it holds in the leading order in the $1/M_Q$ expansion.[11]

Now, these approaches are rather different. The large N_c limit is fairly democratic: effectively, it predicts factorization in any meson decay into two meson final states, regardless of which flavors are involved in the transition. It does not predict, as far as I can tell, factorization in baryon decays (because the number of non-spectator diagrams, each suppressed by $1/N_c$, scales like N_c).

*The large M_Q limit is fairly restrictive as to which transitions may exhibit factoriza-*tion. It must be a transition of the form M $\to$ M′X where M and M′ are heavy hadrons, with their masses in a fixed ratio, both scaling with the large parameter M_Q, and X is a hadronic state with small invariant mass, that is, it's mass does not grow with M_Q. To the extent that the b and c quarks can be considered heavy, this approach can be used for $B \to D\pi$, and even for baryons as in $\Lambda_b \to \Lambda_c\pi$. But in the case of D decays this approach says nothing, since the final state does not involve any heavy quarks.

I will have nothing to say about phenomenological approaches to factorization.[12] My interest here is on what can be obtained from first principles, even if only in some approximation. Clearly we have a better chance of learning about dynamics if we concentrate *on results that follow directly from QCD than on phenomenological approaches. It is for this* reason also that we have nothing to say about decays such as $B \to \psi K$ which may very well factorize, but we don't know of any first principles justification for that to be the case. (In fact, one expects factorization in the inclusive resonant rate $B \to \psi X_s$, where by resonant we mean that the ψ is directly produced. P-wave charmonium production in B-meson decays is known not to factorize.[13] Consequently nonresonant inclusive ψ production won't either).

4.2 Comparison With Experiment

The large N_c approach is far too democratic: experimentally it is found that factorization does not hold in decays of heavy mesons to light mesons, or in light-to-light decays. In this section I intend to investigate the predictions of the large mass limit as far as factorization is concerned.

We start by considering qualitative statements implied by the arguments of Ref. 11. Feynman diagrams that don't factorize on account of the light quark in the initial heavy meson ending up in the light hadron in the final state are suppressed by $1/M_Q$. Now, the only diagrams that contribute to $\bar{B}^0 \to D^0\pi^0$ are of this kind (and therefore $\bar{B}^0 \to D^0\pi^0$ does not itself factorize). Hence if factorization is to hold to some accuracy ϵ, the rate for $\bar{B}^0 \to D^0\pi^0$ ought to be suppressed relative to the rate for $\bar{B}^0 \to D^+\pi^-$ or $B^- \to D^0\pi^-$ by roughly ϵ^2.

A quick glance at the particle data book shows that $\bar{B}^0$ decays into $D^+\pi^-$, $D^+\rho^-$, $D^+a_1(1260)^-$, $D^*(2010)^+\pi^-$, $D^*(2010)^+\rho^-$ and $D^*(2010)^+a_1(1260)^-$ have been observed and have branching fractions in the 0.3% to 1.8% range. Non of the corresponding decays into D^0 or $D^*(2010)^0$ plus a neutral light meson have been observed. An upper bound exists on the branching fraction for $\bar{B}^0 \to D^0\rho^0$ of 6×10^{-4}. This is all as expected from the factorization argument in the paragraph above.

Quantitative, model independent,[14] tests of factorization are readily available. We will consider three kinds of such tests. The first two compare different two body decays which are related by a combined use of factorization and either isospin or heavy quark spin symmetries. In the third we compare some two body decays to corresponding semileptonic rates. The third is the most direct test, but is not available for as many processes. Also, it is interesting to see how well the other symmetries, and in particular heavy quark spin symmetry, work.

Using isospin symmetry on the factorized amplitudes, one obtains that the partial widths for the charged and the neutral meson decays into charmed two body decays should be equal. That is, one expects $\Gamma(\bar{B}^0 \to D^+\pi^-) \approx \Gamma(B^- \to D^0\pi^-)$ and similar relations for the other modes. These results are not predicted by isospin symmetry alone. The hamiltonian in Eq. 14 has $\Delta I = 0, 1$, while the B and D mesons are both $I = 1/2$ states, so the final $D\pi$ *state is a combination of $I = 1/2$ and $I = 3/2$.* There are three independent amplitudes, but they are not independent if factorization holds.

This can be tested assuming the total widths of the charged and neutral B-mesons are equal. It is seen that these relations hold to the present experimental accuracy. For example, the particle data book gives

$$\mathrm{Br}(B^- \to D^0\pi^-) = (3.8 \pm 1.1) \times 10^{-3} \tag{16}$$

while

$$\mathrm{Br}(\bar{B}^0 \to D^+\pi^-) = (3.2 \pm 0.7) \times 10^{-3} \tag{17}$$

and similar results for the other three modes mentioned above.

Since the factorized amplitude is given in terms of the semileptonic form factors, one can use heavy quark spin symmetry to relate the rates into D and D^* final states:

$$\Gamma(\bar{B} \to DX) = \Gamma(\bar{B} \to D^*X)\ . \tag{18}$$

This seems to work well, too. For example, from the particle data book

$$\mathrm{Br}(\bar{B}^0 \to D^*(2010)^+\pi^-) = (3.2 \pm 0.7) \times 10^{-3} \tag{19}$$

to be compared with $\mathrm{Br}(\bar{B}^0 \to D^+\pi^-)$ in Eq. 17 above. It is remarkable that both factorization and heavy quark spin symmetry can be tested simultaneously and that both seem to work rather well.

Table 1 shows CLEO II measured branching fractions.[15] The two columns are related by spin symmetry (if factorization holds). We group lines into pairs for the neutral and charged B decays. Thus the combined result of factorization, isospin symmetry, heavy quark spin symmetry and the assumption of equal B^0 and B^+ lifetimes, is that all entries in each 2×2 block are equal. It can be seen that, within experimental errors this is the case. It is intriguing that the central values of all of the $\bar{B}^0$ decays are about 70% of the corresponding B^-. If this is a real effect it could be evidence against factorization. It could also be interpreted as evidence for different B^0 and B^+ lifetimes, $\tau(B^0)/\tau(B^+) \sim 0.7$. But this is hard to reconcile with direct results from the DELPHI[16] and ALEPH[17] experiments, which tend to favor $\tau(B^0)/\tau(B^+) > 1$.

Table 1. Some CLEO II Branching Fractions

Decay	Branching Fraction	Decay	Branching Fraction
$B^- \to D^0\pi^-$	$0.40 \pm 0.03 \pm 0.09$	$B^- \to D^*(2010)^0\pi^-$	$0.35 \pm 0.05 \pm 0.12$
$\bar{B}^0 \to D^+\pi^-$	$0.26 \pm 0.03 \pm 0.06$	$\bar{B}^0 \to D^*(2010)^+\pi^-$	$0.27 \pm 0.04 \pm 0.06$
$B^- \to D^0\rho^-$	$1.02 \pm 0.11 \pm 0.29$	$B^- \to D^*(2010)^0\rho^-$	$1.14 \pm 0.16 \pm 0.37$
$\bar{B}^0 \to D^+\rho^-$	$0.71 \pm 0.10 \pm 0.21$	$\bar{B}^0 \to D^*(2010)^+\rho^-$	$0.73 \pm 0.10 \pm 0.16$

If factorization holds, the degree of polarization in the decay $\bar{B}^0 \to D^*(2010)^+\rho^-$ can be predicted in terms of the degree of polarization in the semileptonic decay:[15]

$$\frac{\Gamma_L}{\Gamma}(\bar{B}^0 \to D^*(2010)^+\rho^-) = \frac{d\Gamma_L}{d\Gamma}(\bar{B}^0 \to D^*(2010)^+\ell\nu)|_{m^2_{\ell\nu}=m^2_\rho} \tag{20}$$

Here the differential rates on the right hand side are with respect to the invariant lepton pair mass, $m^2_{\ell\nu}$. The CLEO collaboration finds

$$\frac{\Gamma_L}{\Gamma}(\bar{B}^0 \to D^*(2010)^+\rho^-) = 0.90 \pm 0.07 \pm 0.05 \tag{21}$$

while the expected value from the semileptonic decay is 85% - 88%.

Finally, the most direct test of factorization is obtained by comparing directly both sides of Eq. 15, or equivalently by testing whether Bjorken's ratio

$$R_\pi \equiv \frac{\Gamma(\bar{B}^0 \to D^*(2010)^+\pi^-)}{d\Gamma(\bar{B}^0 \to D^*(2010)^+\ell\nu)/dm^2_{\ell\nu}|_{m^2_{\ell\nu}=M^2_\pi}} \tag{22}$$

agrees with the expectation from factorization:

$$R_\pi = 6\pi^2 f_\pi^2 c_1^2 \tag{23}$$

Similar expressions can be written with the pion replaced by some other final state. Experimentally, the ratios R_π and R_ρ for the neutral meson decay have been studied. The results of CLEO II measurements and the expectations from factorization are summarized in Table 2.[15]

Table 2. CLEO II Results on Bjorken's Ratios

	Experiment	Factorization
R_π	$1.3 \pm 0.2 \pm 0.3$	1.2 ± 0.2
R_ρ	$3.2 \pm 0.4 \pm 0.7$	3.3 ± 0.6

5. REPARAMETRIZATION INVARIANCE

There is an ambiguity in assigning a four-velocity, v, and residual momentum, k, to a particle in the HQET. Recall that only the momentum $p = Mv + k$ has physical significance. One may shift both the velocity and residual momentum to obtain the same physical momentum:

$$v \to v + q/M \tag{24}$$
$$k \to k - q \tag{25}$$

The only constraint on the vector q is that the new four-velocity be properly normalized:

$$(v + q/M)^2 = 1 \tag{26}$$

The effective field theory must be invariant under these reparametrizations.[18] The reparametrizations mix different orders in $1/M$. Hence, one can use reparametrization invariance to put constraints on the form of the $1/M$ corrections.[19]

As an example of an application consider the matrix element of the vector current between two pseudoscalar mesons. When using the HQET to order $1/M$ it is important to include in the description of the states both the velocity label v and the residual momentum k:

$$\langle v,k'|V_\mu|v,k\rangle = f_1 v_\mu + f_2(k_\mu + k'_\mu) + f_3(k_\mu - k'_\mu)\ . \tag{27}$$

Here V_μ stands for the heavy quark current including $1/M$ corrections. Now, in the "full theory", that is, the theory without any large mass expansion, there are only two independent form factors, usually denoted by f_+ and f_-. It shouldn't be necessary to introduce three form factors in the effective theory. This is implied by reparametrization invariance, which gives the relation

$$f_2 = \frac{1}{2M} f_1 \tag{28}$$

Of more practical importance is the use of reparametrization invariance to constrain the form of the heavy quark current in the effective theory. The heavy quark vector current has a $1/M$ expansion[2]

$$\sum_i C^{(i)}(v{\cdot}v')\mathcal{O}_i^{(0)} + \frac{1}{2M_Q}\sum_j D^{(j)}(v{\cdot}v')\mathcal{O}_j^{(1)} + \frac{1}{2M_{Q'}}\sum_j D'^{(j)}(v{\cdot}v')\mathcal{O}_j^{(1)} \tag{29}$$

where $\mathcal{O}_i^{(0)}$ and $\mathcal{O}_j^{(1)}$ stand for vector operators of dimension three and four respectively with $\overline{Q}'_{v'}Q_v$ quantum numbers, and their coefficients C, D and D' are perturbatively calculable. For example, at tree level the current is

$$\overline{Q}'_{v'}\gamma_\mu Q_v + \frac{1}{2M_Q}\overline{Q}'_{v'}\gamma_\mu i\not{D}Q_v - \frac{1}{2M_{Q'}}\overline{Q}'_{v'}i\overleftarrow{\not{D}}\gamma_\mu Q_v \tag{30}$$

where we have used the equations of motion, $v{\cdot}DQ_v = 0$. Now, the vector current in Eq. 29 will be reparametrization invariant if and only if it depends on the velocities v and v' in the combinations

$$v_\mu + k_\mu/M_Q \qquad \text{and} \qquad v'_\mu + k'_\mu/M_{Q'} \tag{31}$$

or in operator language

$$v_\mu + iD_\mu/M_Q \qquad \text{and} \qquad v'_\mu - i\overleftarrow{D}_\mu/M_{Q'} \tag{32}$$

Consider, for example, the following leading term in Eq. 29

$$C^{(1)}(v\cdot v')\overline{Q}'_{v'}\gamma_\mu Q_v = \overline{Q}'_{v'}\left(\frac{1+\not{v}'}{2}\right)C^{(1)}(v\cdot v')\gamma_\mu\left(\frac{1+\not{v}}{2}\right)Q_v \tag{33}$$

It must appear in the following combination to be invariant under separate reparametrizations of v and v'

$$\begin{aligned}\overline{Q}'_{v'}\left(\frac{1+\not{v}'-i\overleftarrow{\not{D}}/M_{Q'}}{2}\right)&C^{(1)}((v'-i\overleftarrow{D}/M_{Q'})\cdot(v+iD/M_Q))\gamma_\mu\left(\frac{1+\not{v}+i\not{D}/M_Q}{2}\right)Q_v\\ &= C^{(1)}(v\cdot v')\left[\overline{Q}'_{v'}\gamma_\mu Q_v + \frac{1}{2M_Q}\overline{Q}'_{v'}\gamma_\mu i\not{D}Q_v - \frac{1}{2M_{Q'}}\overline{Q}'_{v'}i\overleftarrow{\not{D}}\gamma_\mu Q_v\right]\\ &\quad+\frac{dC^{(1)}}{dv\cdot v'}\left[\frac{1}{M_Q}\overline{Q}'_{v'}\gamma_\mu v'\cdot DQ_v - \frac{1}{M_{Q'}}\overline{Q}'_{v'}v\cdot\overleftarrow{D}\gamma_\mu Q_v\right]+\cdots\end{aligned} \tag{34}$$

In a similar manner the coefficients of other dimension four operators can be constrained by applying the same method to the other two dimension three operators, $\overline{Q}'_{v'}v_\mu Q_v$ and $\overline{Q}'_{v'}v'_\mu Q_v$.

The calculation leading to the $1/m_c$ corrections in $\Lambda_b \to \Lambda_c e\nu$ required the coefficients of the vector and axial currents to order $1/m_c$. It is easy to check that the coefficients used[4] to obtain the relations in Eqs. 3 – 5 satisfy the constraints from reparametrization invariance. The calculation there would have been simplified vastly had reparametrization invariance been used to obtain the result. (Alternatively, reparametrization invariance gives an independent test of the calculation).

6. CHIRAL SYMMETRY TOO

6.1 Generalities

Chiral symmetry and soft pion theorems have been used in particle physics for several decades now with great success. The most efficient way of extracting information from chiral symmetry is by writing a phenomenological lagrangian for pions that incorporates both the explicitly realized vector symmetry and the non-linearly realized spontaneously broken axial symmetry.[20] Theorems that simultaneously use heavy quark symmetries and chiral symmetries are most expediently written by means of a phenomenological lagrangian for pions and heavy mesons that incorporates these symmetries.[21, 22]

In the limit $m_b \to \infty$, the $\overline{B}$ and the $\overline{B}^*$ mesons are degenerate, and to implement the heavy quark symmetries it is convenient to assemble them into a "superfield" $H_a(v)$:

$$H_a(v) = \frac{1+\not{v}}{2}\left[\overline{B}^{*\mu}_a\gamma_\mu - \overline{B}_a\gamma^5\right]. \tag{35}$$

Here v^μ is the fixed four-velocity of the heavy meson, and a is a flavor $SU(3)$ index corresponding to the light antiquark. Because we have absorbed mass factors $\sqrt{2m_B}$ into the fields, they have dimension 3/2; to recover the correct relativistic normalization, we will multiply amplitudes by $\sqrt{2m_B}$ for each external $\overline{B}$ or $\overline{B}^*$ meson.

The chiral lagrangian contains both heavy meson superfields and pseudogoldstone bosons, coupled together in an $SU(3)_L \times SU(3)_R$ invariant way. The matrix of pseudogoldstone bosons appears in the usual exponentiated form $\xi = \exp(i\mathcal{M}/f)$, where

$$\mathcal{M} = \begin{pmatrix} \frac{1}{\sqrt{2}}\pi^0 + \frac{1}{\sqrt{6}}\eta & \pi^+ & K^+ \\ \pi^- & -\frac{1}{\sqrt{2}}\pi_0 + \frac{1}{\sqrt{6}}\eta & K^0 \\ K^- & \overline{K}^0 & -\sqrt{\frac{2}{3}}\eta \end{pmatrix}, \tag{36}$$

and f is the pion (or kaon) decay constant. The bosons couple to the heavy fields through the covariant derivative and axial vector field,

$$\begin{aligned} D^\mu_{ab} &= \delta_{ab}\partial^\mu + V^\mu_{ab} = \delta_{ab}\partial^\mu + \tfrac{1}{2}\left(\xi^\dagger\partial^\mu\xi + \xi\partial^\mu\xi^\dagger\right)_{ab}, &(37)\\ A^\mu_{ab} &= \frac{i}{2}\left(\xi^\dagger\partial^\mu\xi - \xi\partial^\mu\xi^\dagger\right)_{ab} = -\frac{1}{f}\partial_\mu\mathcal{M}_{ab} + \mathcal{O}(\mathcal{M}^3). &(38)\end{aligned}$$

Lower case roman indices correspond to flavor $SU(3)$. Under chiral $SU(3)_L \times SU(3)_R$, the pseudogoldstone bosons and heavy meson fields transform as $\xi \to L\xi U^\dagger = U\xi R^\dagger$, $A^\mu \to UA^\mu U^\dagger$, $H \to HU^\dagger$ and $(D^\mu H) \to (D^\mu H)U^\dagger$, where the matrix U_{ab} is a nonlinear function of the pseudogoldstone boson matrix $\mathcal{M}$.

The chiral lagrangian is an expansion in derivatives and pion fields, as well as in inverse powers of the heavy quark mass. The kinetic energy terms take the form

$$\mathcal{L}_{\rm kin} = \frac{1}{8}f^2\,\partial^\mu\Sigma_{ab}\,\partial_\mu\Sigma^\dagger_{ba} - \mathrm{Tr}\left[\overline{H}_a(v)iv\cdot D_{ba}H_b(v)\right], \tag{39}$$

where $\Sigma = \xi^2$. Here the trace is in the space of 4×4 Dirac matrices that define the "superfields" $H_a(v)$ in Eq. 35. The leading interaction term is of dimension four,

$$\mathcal{L}_{\rm int} = g\,\mathrm{Tr}\left[\overline{H}_a(v)H_b(v)\not{A}_{ba}\gamma^5\right], \tag{40}$$

where g is an unknown parameter, of order one in the constituent quark model. The analogous term in the charm system is responsible for the decay $D^* \to D\pi$. Expanding the term in the lagrangian in 40 to linear order in the Goldstone Boson fields, $\mathcal{M}$, we find the explicit forms for the $D^*D\mathcal{M}$ and $D^*D^*\mathcal{M}$ couplings

$$\left[\left(\frac{-2g}{f}\right)D^{*\nu}\partial_\mu\mathcal{M}D^\dagger + \mathrm{h.c.}\right] + \left(\frac{2gi}{f}\right)\epsilon_{\mu\nu\lambda\kappa}D^{*\mu}\partial^\nu\mathcal{M}D^{*\lambda}v^\kappa. \tag{41}$$

Using this one can compute the partial width

$$\begin{aligned}\Gamma(D^{*+}\to D^0\pi^+) &= \frac{g^2}{6\pi f^2}|\vec{p}_\pi|^3 &(42)\\ \Gamma(D^{*+}\to D^+\pi^0) &= \frac{g^2}{12\pi f^2}|\vec{p}_\pi|^3 &(43)\end{aligned}$$

The ACCMOR collaboration has reported an upper limit of 131 KeV on the D^* width.[23] The branching fractions for $D^{*+}\to D^0\pi^+$ and $D^{*+}\to D^+\pi^0$ are $(68.1\pm1.0\pm1.3)\%$ and $(30.8\pm0.4\pm0.8)\%$, respectively, as measured by the CLEO collaboration.[24] Using $f = 130$ MeV, one obtains the limit $g^2 < 0.5$. Even if the D^* decay width is too small to measure, radiative D^* decays provide an indirect means for determining the coupling g, and provide a lower bound $g^2 \gtrsim 0.1$.[25]

Since charmed and beauty baryons are long lived, one can write down phenomenological lagrangians for their interactions with pions. These are as well justified and should be as good an approximation as the lagrangian for heavy mesons discussed above. The treatment is rather similar, and due to space limitations, we refer the interested reader to the literature.[26]

6.2 $B \to De\nu$ and $B \to D^*\pi e\nu$

As a first example of an application consider a soft pion theorem that relates the amplitudes for $B \to D^* e\nu$ and $B \to D^*\pi e\nu$.[22] The heavy quark current is represented in the phenomenological lagrangian approach by

$$J_\mu^{\bar{c}b} = \bar{h}_{v'}^{(c)}\gamma_\mu(1-\gamma_5)h_v^{(b)} \to \xi(v\cdot v')\mathrm{Tr}\overline{H}_a^{(c)}(v')\gamma_\mu(1-\gamma_5)H_a^{(b)}(v) + \cdots \tag{44}$$

where the ellipsis denote terms with derivatives, factors of light quark masses m_q, or factors of $1/M_Q$, and $\xi(v\cdot v')$ is the Isgur-Wise function. The leading term in Eq. 44 is independent of the pion field. Therefore, it is pole diagrams that dominate the amplitude for semileptonic $B \to D\pi$ and $B \to D^*\pi$ transitions; see Fig. 1. These pole diagrams are calculable in this approach, and are determined by the Isgur-Wise function and the coupling g.

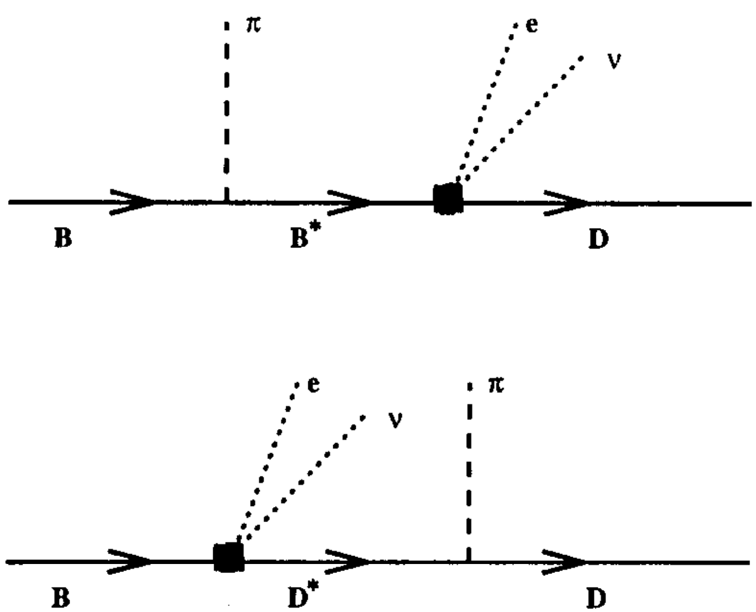

Figure 1. Feynman diagrams for $B \to De\nu$

A straightforward calculation gives

$$\begin{aligned}\langle D(v')\pi^a(q)|J_\mu^{\bar{c}b}|B(v)\rangle &= iu(B)^*\tfrac{1}{2}\tau^a u(D)\sqrt{M_B M_D}\frac{g}{f}\xi(v\cdot v')\\ &\times \left\{\frac{1}{v\cdot q}[i\epsilon_{\mu\nu\lambda\kappa}q^\nu v'^\lambda v^\kappa + q\cdot(v+v')v_\mu - (1+v\cdot v')q_\mu\right.\\ &\left.-\frac{1}{v'\cdot q}[i\epsilon_{\mu\nu\lambda\kappa}q^\nu v'^\lambda v^\kappa + q\cdot(v+v')v'_\mu - (1+v\cdot v')q_\mu\right\}\end{aligned} \tag{45}$$

where $u(M)$ stands for the isospin wavefunction of meson M. A similar but lengthier expression is found for $B \to D^*\pi e\nu$.[22] If the coupling g is close to its upper limit, this process could be an important correction to the inclusive semileptonic rate. It may, perhaps, account for some of the anomalously large "D^{**}" contributions observed by CLEO.[27]

6.3 Violations To Chiral Symmetry

Phenomenological lagrangians are particularly well suited to explore deviations from symmetry predictions. In the context of heavy mesons, several quantities of considerable interest have been studied. Moreover, the self-consistency of the approach has been explored. It would be impossible to cover all of this in this talk. I will briefly comment on a few of those results, and invite you to consult the references for further details.

In order to study violations of chiral symmetry, one must introduce symmetry breaking terms into the phenomenological lagrangian. The light quark mass matrix $m_q = \mathrm{diag}(m_u, m_d, m_s)$ parametrizes the violations to flavor $SU(3)_V$. To linear order in m_q and lowest order in the derivative expansion, the correction to the phenomenological lagrangian is

$$\begin{aligned}\Delta\mathcal{L} &= \lambda_0\ \left[m_q\Sigma + m_q\Sigma^\dagger\right]^a{}_a\\ &+ \lambda_1\mathrm{Tr}\bar{H}^{(Q)a}H_b^{(Q)}\left[\xi m_q\xi + \xi^\dagger m_q\xi^\dagger\right]^b{}_a\\ &+ \lambda'_1\mathrm{Tr}\bar{H}^{(Q)a}H_a^{(Q)}\ \left[m_q\Sigma + m_q\Sigma^\dagger\right]^b{}_b\end{aligned} \tag{46}$$

The coefficients λ_0, λ_1 and λ'_1 are determined by non-perturbative strong interaction effects, but may be determined phenomenologically. We postpone consideration of mass relations obtained from this lagrangian until we have introduced heavy quark spin symmetry breaking terms into the lagrangian too.

The decay constants for the D and D_s mesons, defined by

$$\langle 0|\bar{d}\gamma_\mu\gamma_5 c|D^+(p)\rangle = if_D p_\mu \tag{47}$$

and

$$\langle 0|\bar{s}\gamma_\mu\gamma_5 c|D_s(p)\rangle = if_{D_s} p_\mu\ , \tag{48}$$

determine the rate for the purely leptonic decays $D^+ \to \mu^+\nu_\mu$ and $D_s \to \mu^+\nu_\mu$. These are likely to be measured in the future.[28] In the chiral limit, where the up, down and strange quark masses go to zero, flavor $SU(3)_V$ is an exact symmetry and so $f_{Ds}/f_D = 1$. However $m_s \neq 0$, so this ratio will deviate from unity. Calculating this involves, at one loop, the Feynman diagrams in Fig. 2, where a dashed line stands for a light pseudoscalar propagator.

Neglecting the up and down quark masses in comparison with the strange quark mass, this deviation has been calculated to be[29, 30]

$$f_{D_s}/f_D = 1 - \frac{5}{6}\left(1+3g^2\right)\frac{M_K^2}{16\pi^2 f^2}\ln\left(M_K^2/\mu^2\right) + \lambda(\mu)M_K^2 + \ldots \tag{49}$$

where the ellipsis denote terms with more powers of the strange quark mass (recall $M_K^2 \sim m_s$). The dependence of λ on the subtraction point μ cancels that of the logarithm. If μ is of order the chiral symmetry breaking scale then λ has no large logarithms and for very small m_s the explicit logarithm dominates the deviation of f_{D_S}/f_D from unity. In Eq. 49 the contribution from η loops has been written in terms of M_K using the Gell-Mann-Okubo formula $M_\eta^2 = 4M_K^2/3$, and the contribution from pion loops, proportional to $M_\pi^2 \ln M_\pi^2$, has been neglected. Numerically, using $\mu = 1$ GeV, the result is that

$$f_{D_s}/f_D = 1 + 0.064\ (1+3g^2), \tag{50}$$

or $f_{D_s}/f_D = 1.16$ for $g^2 = 0.5$.

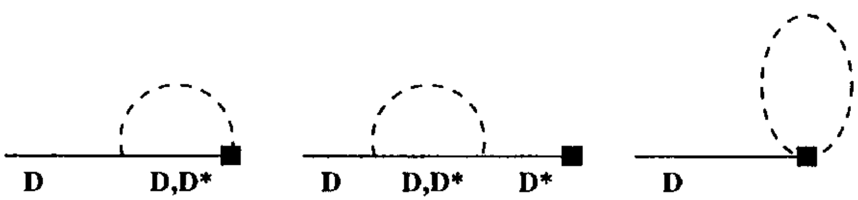

Figure 2. Feynman Diagrams in the calculation of f_{D_s}/f_D.

The same formula also holds for f_{B_s}/f_B. In fact, to leading order in $1/M_Q$ the ratio is independent of the the flavor of the heavy quark. Consequently,

$$\frac{f_{B_s}/f_B}{f_{D_s}/f_D} = 1 \tag{51}$$

to leading order in $1/M_Q$ and all orders in the light quark masses. Now, Eq. 51 also holds as a result of chiral symmetry, for any m_c and m_b. That is f_{B_s}/f_B and f_{D_s}/f_D are separately unity in the limit in which the light quark masses are equal. This means that deviations from unity in Eq. 51 must be small, $O(m_s) \times O(1/m_c - 1/m_b)$.[31] This ratio of ratios is observed to be very close to unity in a variety of calculations.[32] This may be very useful, since it suggests obtaining the ratio f_{B_s}/f_B of interest in the analysis of $B-\bar{B}$ mixing (see below) from the ratio f_{D_s}/f_D, measurable from leptonic D and D_s decays.

The hadronic matrix elements needed for the analysis of $B-\bar{B}$ mixing are

$$\langle\bar{B}(v)|\bar{b}\gamma^\mu(1-\gamma_5)d\ \bar{b}\gamma^\mu(1-\gamma_5)d|B(v)\rangle = \frac{8}{3}f_B^2 B_B\ , \tag{52}$$

$$\langle\bar{B}_s(v)|\bar{b}\gamma^\mu(1-\gamma_5)s\ \bar{b}\gamma^\mu(1-\gamma_5)s|B_s(v)\rangle = \frac{8}{3}f_{B_s}^2 B_{B_s}\ , \tag{53}$$

where the right hand side of these equations define the parameters B_{B_s} and B_B. In the $SU(3)_V$ symmetry limit $B_{B_s}/B_B = 1$. For non-zero strange quark mass, the ratio is no longer unity. The chiral correction is[29]

$$\frac{B_{B_s}}{B_B} = 1 - \frac{2}{3}\left(1-3g^2\right)\frac{M_K^2}{16\pi^2 f^2}\ln\left(M_K^2/\mu^2\right)\ . \tag{54}$$

Again, $M_\eta^2 = 4M_K^2/3$ has been used. Using $\mu = 1$ GeV, $f = f_K$, and $g^2 = 0.5$, the correction is $B_{B_s}/B_B \approx 0.95$.

Violations to chiral symmetry in $B \to D$ semileptonic decays have also been studied. One obtains that a different Isgur-Wise function must be used for each flavor of light spectator quark[30]

$$\frac{\xi_s(v\cdot v')}{\xi_{u,d}(v\cdot v')} = 1 + \frac{5}{3}g^2\Omega(v\cdot v')\frac{M_K^2}{16\pi^2 f^2}\ln\left(M_K^2/\mu^2\right) + \lambda'(\mu, v\cdot v')M_K^2 + \cdots \tag{55}$$

where

$$\Omega(x) = -1 + \frac{2+x}{2\sqrt{x^2-1}}\ \ln\left(\frac{x+1+\sqrt{x^2-1}}{x+1-\sqrt{x^2-1}}\right) + \frac{x}{4\sqrt{x^2-1}}\ \ln\left(\frac{x-\sqrt{x^2-1}}{x+\sqrt{x^2-1}}\right) \tag{56}$$

or, expanding about $x = 1$,

$$\Omega(x) = -\frac{1}{3}(x-1) + \frac{2}{15}(x-1)^2 - \frac{2}{35}(x-1)^3 + \cdots \tag{57}$$

Using $g^2 = 0.5$ and $\mu = 1$ GeV, and neglecting the counterterm one obtains

$$\frac{\xi_s(v\cdot v')}{\xi_{u,d}(v\cdot v')} = 1 - 0.21\,\Omega(v\cdot v') + \cdots \tag{58}$$

or a 5% correction at $v\cdot v' = 2$.

6.4 Violations to Heavy Quark Symmetry

In a similar spirit one can consider the corrections in chiral perturbation theory to predictions that follow from heavy quark spin and flavor symmetries. These are effects that enter at order $1/M_Q$, so the first step towards this end is to supplement the phenomenological lagrangian with such terms. In particular, the only $SU(3)_V$ preserving term of order $1/M_Q$ that violates spin symmetry in the lagrangian is[29]

$$\Delta\mathcal{L}_{\rm int} = \frac{\lambda_2}{M_Q}\mathrm{Tr}\,\bar{H}^{(Q)a}\sigma^{\mu\nu}H_a^{(Q)}\sigma_{\mu\nu}\ . \tag{59}$$

In addition there are contributions to the lagrangian in order $1/M_Q$ that violate flavor but not spin symmetries. These can be characterized as introducing M_Q dependence in the couplings g, λ_1 and λ_1' of Eqs. 40 and 46. At the same order as these corrections, there is a term that violates both spin and $SU(3)_V$ symmetries

$$\Delta\mathcal{L}_{\rm int} = \frac{\lambda_3}{M_Q}\mathrm{Tr}\left[\bar{H}^{(Q)a}\sigma^{\mu\nu}H_b^{(Q)}\sigma_{\mu\nu}\right]m_q{}^b{}_a \tag{60}$$

Spin symmetry violation is responsible for "hyperfine" splittings in spin multiplets. To leading order these mass splittings are computed in terms of the spin symmetry violating coupling of Eq. 59

$$\Delta_B \equiv M_{B^*} - M_B = -\frac{8\lambda_2}{m_b} \tag{61}$$

That the mass splittings scale like $1/M_Q$ seems to be well verified in nature:

$$\frac{M_{D^*} - M_D}{M_{B^*} - M_B} \approx \frac{M_B}{M_D} \tag{62}$$

Table 3. Measured Mass Splittings

$X - Y$	$M_X - M_Y$ (MeV)
$D_s - D^+$	99.5 ± 0.6[33]
$D^+ - D^0$	$4.80 \pm 0.10 \pm 0.06$[34]
$D^{*+} - D^{*0}$	$3.32 \pm 0.08 \pm 0.05$[34]
$D^{*0} - D^0$	$142.12 \pm 0.05 \pm 0.05$[34]
$D^{*+} - D^+$	$140.64 \pm 0.08 \pm 0.06$[34]
$D_s^* - D_s$	141.5 ± 1.9[33]
$B_s - B$	82.5 ± 2.5[34] or 121 ± 9[35]
$B^0 - B^+$	0.01 ± 0.08[33]
$B^* - B$	$46.2 \pm 0.3 \pm 0.8$[36] or 45.4 ± 1.0[35]
$B_s^* - B_s$	47.0 ± 2.6[35]
$(D^{*0} - D^0) - (D^{*+} - D^+)$	$1.48 \pm 0.09 \pm 0.05$[34]

Armed with the machinery of chiral lagrangians that include both spin and chiral symmetry violating terms, one can compare hyperfine splitting for different flavored mesons. There is a wealth of experimental information to draw from; see Table 3. Breaking of flavor $SU(3)_V$ and heavy quark flavor symmetries by electromagnetic effects is not negligible. It is readily incorporated into the lagrangian in terms of the charge matrices $Q_Q = \mathrm{diag}(2/3, -1/3)$ and $Q_q = \mathrm{diag}(2/3, -1/3, -1/3)$,[37] which must come in bilinearly. For example, terms involving Q_q^2 correspond to replacing $m_q \to Q_q$ in Eqs. 46 and 60. The electromagnetic effects of the light quarks can be neglected if one considers only mesons with d and s light quarks. The electromagnetic shifts in the hyperfine splittings Δ_{X_q} and Δ_{X_q} ($X = D, B$, $q = d, s$) differ on account of different b and c charges, but they cancel in the difference of splittings

$$\Delta_{X_s} - \Delta_{X_d} = (M_{X_s^*} - M_{X_s}) - (M_{X_d^*} - M_{X_d}) \tag{63}$$

The only term in the phenomenological lagrangian that enters this difference is Eq. 60. This immediately leads to

$$(M_{B_s^*} - M_{B_s}) - (M_{B_d^*} - M_{B_d}) = (m_c/m_b)\left(\frac{\bar\alpha_s(m_c)}{\bar\alpha_s(m_b)}\right)^{9/25}\left[(M_{D_s^*} - M_{D_s}) - (M_{D_d^*} - M_{D_d})\right] \tag{64}$$

We have included here the short distance QCD effect that is usually neglected.[38]

The accuracy with which Eq. 64 holds is to be much better than the separate relations for each hyperfine splitting in Eq. 61. Recall that $SU(3)_V$ breaking by light quark masses and electromagnetic interactions have been accounted for in leading order. Moreover, the result is trivially generalized by replacing the quark mass matrix in Eqs. 46 and 60, by an arbitrary function of the light quark mass matrix. It is seen from Table 3 that this relation works well. The left side is 1.2 ± 2.7 MeV while the right side is 3.0 ± 6.3 MeV.

Since both sides of Eq. 64 are consistent with zero and both are proportional to the interaction term in Eq. 60, it must be that the coupling λ_3 is very small.[37] From the difference of hyperfine splittings in the charm sector

$$-\frac{8\lambda_3}{m_c}(m_s - m_d) = 0.9 \pm 1.9 \text{ MeV} \tag{65}$$

while

$$M_{D_s} - M_{D_d} = 4\lambda_1(m_s - m_d) - \frac{12\lambda_3}{m_c}(m_s - m_d) = 99.5 \pm 0.6 \text{ MeV} \tag{66}$$

leading to $|\lambda_3/\lambda_1|$ less than ~ 20 MeV. This is smaller than expected by about an order of magnitude. With such a small coefficient it is clear that the next-to-leading terms and the loop corrections may play an important role. In particular they may invalidate the simple $1/M_Q$ scaling of Eq. 64.[39] There is no obvious breakdown of chiral perturbation theory, even though the leading coupling (λ_3) is anomalously small.[40]

At one loop, the expressions for the mass shifts involve large $O(m_s \ln m_s)$ and $O(m_s^{3/2})$ (non-analytic) terms.[30, 40] The coupling λ_3 is not anomalously small at one loop. Instead, the smallness of the difference of hyperfine splittings in Eq. 64 is the result of a precise cancellation between one loop and tree level graphs. Explicitly,[40]

$$\left(M_{X_s} - M_{X_s^*}\right) - \left(M_{X_d} - M_{X_d^*}\right) = \frac{5}{3}g^2\left(\frac{8\lambda_2}{M_Q}\right)\frac{M_K^2}{16\pi^2 f^2}\ln\left(M_K^2/\mu^2\right) - \frac{8\lambda_3}{M_Q}m_s \tag{67}$$

With $g^2 = 0.5$ and $\mu = 1$ GeV, the chiral log is 30 MeV, so the λ_3 counterterm must cancel this to a precision of better than 10%.

The $1/M_Q$ corrections to the masses M_X and M_{X^*} drop out of the combination $M_X + 3M_{X^*}$. The combination $(M_{X_s} + 3M_{X_s^*}) - (M_{X_d} + 3M_{X_d^*})$ is a measure of $SU(3)_V$ breaking by a non-vanishing m_s (or $m_s - m_d$ if the d quark mass is not neglected). It can be computed in the phenomenological lagrangian. To one loop[40]

$$\frac{1}{4}\left(M_{X_s} + 3M_{X_s^*}\right) - \frac{1}{4}\left(M_{X_d} + 3M_{X_d^*}\right) = 4\lambda_1 m_s - g^2\left(1 + \frac{8}{3\sqrt{3}}\frac{1}{2}\right)\frac{M_K^3}{16\pi f^2}$$
$$-4\lambda_1 m_s\left(\frac{25}{18} + \frac{9}{2}g^2\right)\frac{M_K^2}{16\pi^2 f^2}\ln\left(M_K^2/\mu^2\right) \tag{68}$$

The pseudoscalar splittings $(M_{D_s} - M_{D_d})$ and $(M_{B_s} - M_{B_d})$ have been measured; see Table 3. Also, $\frac{1}{4}(M_{X_s} + 3M_{X_s^*}) - \frac{1}{4}(M_{X_d} + 3M_{X_d^*}) = \frac{3}{4}[(M_{X_s^*} - M_{X_s}) - (M_{X_d^*} - M_{X_d})] + (M_{X_s} - M_{X_d})$, and the term in square brackets is less than a few MeV, as we saw above. The combination $(M_{X_s}+3M_{X_s^*})-(M_{X_d}+3M_{X_d^*})$ in Eq. 68 is first order in m_s but has no corrections at order $1/M_Q$. Thus, one expects a similar numerical result for B and D systems. Experimentally, $(M_{B_s}-M_{B_d})/(M_{D_s}-M_{D_d})$ is consistent with unity; see Table 3. The formula in Eq. 68 has a significant contribution from the M_K^3 term which is independent of the splitting parameter λ_1. The M_K^3 term gives a negative contribution to the splitting of ~ -250 MeV for $g^2=0.5$. The chiral logarithmic correction effectively corrects the tree level value of the parameter λ_1; for $\mu = 1$ GeV and $g^2=0.5$, the term $4\lambda_1 m_s$ gets a correction ≈ 0.9 times its tree level value. Thus, the one-loop value of $4\lambda_1 m_s$ can be significantly greater than the value determined at tree-level of approximately 100 MeV.

Chiral perturbation theory can be used to predict the leading corrections to the form factors for semileptonic $B\to D$ or D^* decays which are generated at low momentum, below the chiral symmetry breaking scale. Of particular interest are corrections to the predicted normalization of form factors at zero recoil, $v{\cdot}v'=1$. According to Luke's theorem (see section 2), long distance corrections enter first at order $1/M_Q^2$. Deviations from the predicted normalization of form factors that arise from terms of order $1/M_Q^2$ in either the lagrangian or the current are dictated by non-perturbative physics. But there are computable corrections that arise from the terms of order $1/M_Q$ in the lagrangian. These must enter at one-loop, since Luke's theorem prevents them at tree level, and result from the spin and flavor symmetry breaking in the hyperfine splittings Δ_D and Δ_B. Retaining only the dependence on the larger Δ_D, the correction to the matrix elements at zero recoil are[41]

$$\langle D(v)|J_\mu^{cb}|B(v)\rangle = 2v_\mu\left(1-\frac{3g^2}{2}\left(\frac{\Delta_D}{4\pi f}\right)^2\left[F(\Delta_D/M_\pi)+\ln(\mu^2/M_\pi^2)\right]+C(\mu)/m_c^2\right) \tag{69}$$

$$\langle D^*(v,\epsilon)|J_\mu^{cb}|B(v)\rangle = 2\epsilon^*_\mu\left(1-\frac{g^2}{2}\left(\frac{\Delta_D}{4\pi f}\right)^2\left[F(-\Delta_D/M_\pi)+\ln(\mu^2/M_\pi^2)\right]+C'(\mu)/m_c^2\right) \tag{70}$$

where C and C' stand for tree level counter-terms and

$$F(x)\equiv\int_0^\infty dz\frac{z^4}{(z^2+1)^{3/2}}\left(\frac{1}{[(z^2+1)^{1/2}+x]^2}-\frac{1}{z^2+1}\right) \tag{71}$$

As before, no large logarithms will appear in the functions C and C' if one takes $\mu\approx 4\pi f\sim 1$ GeV. With this choice, formally, their contributions are dwarfed by the term that is enhanced by a logarithm of the pion mass. Numerically, with $g^2=0.5$ the logarithmically enhanced term is -2.1% and -0.7% for D and D^*, respectively.

The function F accounts for effects of order $(1/m_c)^{2+n}$, $n=1,2,\ldots$ It is enhanced by powers of $1/M_\pi$ over terms that have been neglected. Consequently it is expected to be a good estimate of higher order $1/m_c$ corrections. With $\Delta_D/M_\pi\approx 1$, one needs $F(1)=14/3-2\pi$ and $F(-1)=14/3+2\pi$ for a numerical estimate; with μ and g^2 as above, this term is 0.9% and -2.0% for D and D^*, respectively.

6.5 *Trouble on the Horizon?*

I would like to point out a peculiar aspect of this result. The function $F(x)$ can be expanded in x starting at order x, as expected.[41] But it can also be expanded in $1/x$, and the leading term is a logarithmic singularity $\sim -2\ln x$. Physically this limit corresponds to $M_\pi\to 0$ (rather than the absurd alternative $\Delta_D\to\infty$), and the logarithmic singularity is canceled by the $\ln(\mu^2/M_\pi^2)$ in Eqs. 69 and 70. Thus, the expansions in powers of x and $1/x$ correspond, in terms of physical limits, to expansions in powers of $1/m_c$ and M_π, respectively. These are alternative, but not equivalent, expansions. This troubles me some. It seems to indicate that the order of the limits $1/m_c\to 0$ and $M_\pi\to 0$ matters. But the phenomenological lagrangian for pions and heavy mesons implicitly assumes that one can systematically expand about the origin in $1/m_c - M_\pi$ space.

Frequently the non-analytic corrections to relations that follow from the symmetries are uncomfortably large. A case of much interest is the relation between the form factors $f_\pm$ and h for $B\to K$ transitions, relevant to the short distance process $b\to se^+e^-$,

$$\langle\overline{K}(p_K)\,|\,\bar s\gamma^\mu b\,|\,\overline{B}(p_B)\rangle = f_+(p_B+p_K)^\mu + f_-(p_B-p_K)^\mu\,, \tag{72}$$

$$\langle\overline{K}(p_K)\,|\,\bar s\sigma^{\mu\nu}b\,|\,\overline{B}(p_B)\rangle = ih\left[(p_B+p_K)^\mu(p_B-p_K)^\nu-(p_B+p_K)^\nu(p_B-p_K)^\mu\right], \tag{73}$$

and the form factors for $B\to\pi e\nu$,

$$\langle\overline{\pi}(p_\pi)\,|\,\bar u\gamma^\mu b\,|\,\overline{B}(p_B)\rangle = \hat f_+(p_B+p_\pi)^\mu + \hat f_-(p_B-p_\pi)^\mu\,. \tag{74}$$

In the combined large mass and chiral limits only one of these form factors is independent:

$$m_b h = f_+ = -f_- = \hat f_+ = -\hat f_- \tag{75}$$

In this limit, the ratio of rates for $B\to Ke^+e^-$ and $B\to\pi e\nu$ is simply given, in the standard model of electroweak interactions, by $|V_{ts}/V_{ub}|^2$, times a perturbatively computable function of the top quark mass. If the relation 75 held to good accuracy one could thus measure a ratio of fundamental standard model parameters.*

The non-analytic, one-loop corrections to the relations in Eq. 75 have been computed.[42] The results are too lengthy to display here. Numerically, the violation to $SU(3)_V$ symmetry is found to be at the 40% level.†

The phenomenological lagrangian that we have been considering extensively neglects the effects of states with heavy-light quantum numbers other than the pseudoscalar – vector-meson multiplet. The splitting between multiplets is of the order of 400 MeV and is hardly negligible when one considers $SU(3)_V$ relations involving both π and K mesons. For example, consider the effect of the scalar – pseudovector-meson multiplet. One can incorporate its effects into the phenomenological lagrangian. To this end, assemble its components into a "superfield", akin to that in Eq. 35 for the pseudoscalar – vector multiplet:[43]

$$S_a(v)=\frac{1+\not v}{2}\left[B_{1a}'^{\mu}\gamma_\mu\gamma^5 - B_{0a}^*\right]. \tag{76}$$

The phenomenological lagrangian has to be supplemented with a kinetic energy and mass for S,

$$\mathrm{Tr}\left[\overline{S}_a(v)(iv\cdot D_{ba}-\Delta\delta_{ba})S_b(v)\right], \tag{77}$$

*Another application of this relation was discussed by I. Dunietz in this workshop. Assuming factorization in $B\to\psi X$, ratios of CKM elements can be extracted from these two body hadronic decays. For more details, consult the talk by Dunietz, these proceedings.

†The large violation of $SU(3)_V$ symmetry affects as well the results of Dunietz (see previous footnote).

where Δ is the mass splitting for the excited S from the ground state H, and with coupling terms

$$g' \operatorname{Tr}\left[\overline{S}_a(v)S_b(v)\, \not{A}_{ba}\gamma^5\right] + (h \operatorname{Tr}\left[\overline{H}_a(v)S_b(v)\, \not{A}_{ba}\gamma^5\right] + \text{h.c.})\,. \tag{78}$$

In terms of these one can now compute additional corrections to quantities such as f_{D_s}/f_D in Eq. 49. Numerically the corrections are not small,[44] $f_{D_s}/f_D = 1 + 0.13h^2$ for $M_{D_0^*} =$ 2300 MeV (or $f_{D_s}/f_D = 1 + 0.08h^2$ for $M_{D_0^*} = 2400$ MeV), assuming the strange mesons to be 100 MeV heavier. Similarly, corrections to the Isgur-Wise function can be computed, and are not negligible.[44]

7. CONCLUSIONS

Applications of heavy quark symmetries and of heavy quark effective theory methods abound. Many specific predictions have been made and can be tested. If the predictions work well we may feel confident in using these methods for a more lofty goal, that of interpreting experiments, be it for the measurement of fundamental parameters (as in $|V_{cb}|$) or in probing new physics at very short distances (as in $B \to K\ell^+\ell^-$).

Theorists are starting to understand the precision and limitations of the method. The warning flags of the previous section are a sign of the maturity research in this field has attained.

This is not to say the work is done. Many open questions remain. A salient issue is that of computation of form factors for semileptonic $b \to u$ decays. Even the inclusive rate cannot be computed at large electron energies,[‡] where it is measured with an aim at determining $|V_{ub}|$. Some remaining issues require improved input from experiment. For example, a better measurement of the entries in Table 1 and of the lifetimes of B^+ and B^0 would settle the issue of factorization discussed above.

Regardless of the nature of the machine that conducts the next generation beauty and charm experiments, Heavy Quark Effective Theory methods will play a salient role in the interpretation of the results.

8. ACKNOWLEDGEMENTS

I thank Glenn Boyd for illuminating discussions. This work was supported in part by the Department of Energy under contract number DE-AC35-89ER40486.

[‡] Space limitations keep me from discussing recent work on this issue. The interested reader may consult the literature.[45]

9. REFERENCES

1. M. B. Wise, in *Particle Physics - The Factory Era, Proceedings of the Sixth Lake Louise Winter Institute*, B. A. Campbell *et al*, eds., World Scientific (1991)222;
   H. Georgi, in *Proceedings of the Theoretical Advanced Study Institute*, R. K. Ellis *et al*, eds., World Scientific (1992)589;
   B. Grinstein, in *Proceedings of the Workshop on High Energy Phenomenology*, M. A. Pérez and R. Huerta, eds., World Scientific (1992)161
2. B. Grinstein, *Ann. Rev. Nucl. Part. Sci.* **42** (1992)101
3. M.E. Luke, *Phys. Lett.* **B252** (1990)447
4. P. Cho and B. Grinstein, *Phys. Lett.* **B285** (1992)153
5. H. Georgi, B. Grinstein and M. B. Wise, *Phys. Lett.* **B252** (1990)456
6. N. Isgur and M. B. Wise, *Nucl. Phys.* **B348** (1991)276; H. Georgi, *Nucl. Phys.* **B348** (1991)293; T. Mannel, W. Roberts and Z. Ryzak, *Nucl. Phys.* **B355** (1991)38; *Phys. Lett.* **B255** (1991)593
7. T. Mannel and W. Roberts, *Phys. Rev.* **D47** (1993)4963
8. A. Falk, H. Georgi, B. Grinstein and M. Wise, *Nucl. Phys.* **B343** (1990)1
9. H. Yamamoto, these proceedings
10. M. Fukugita, T. Inami, N. Sakai and S. Yazaki, *Phys. Lett.* **B72** (1977)237;
    A. Buras, J. Gerard and R. Rückl, *Nucl. Phys.* **B268** (1986)16
11. M. Dugan and B. Grinstein, *Phys. Lett.* **B255** (1991)583
12. M. Bauer, B. Stech and M. Wirbel, *Z. Phys.* **C34** (1987)103
13. G. Bodwin, E. Braaten, T. Yuan and P. Lepage, *Phys. Rev.* **D46** (1992)3703;
    G. Bodwin, E. Braaten and P. Lepage, *Phys. Rev.* **D46** (1992)1914
14. C. Reader and N. Isgur, *Phys. Rev.* **D47** (1993)1007
15. S. Ball, in the proceedings of the *7th Meeting of the American Physical Society, Division of Particles and Fields*, eds. C. Albright *et al*,, (World Scientific,1993), p. 533
16. G. Maehlum, in the proceedings of the *7th Meeting of the American Physical Society, Division of Particles and Fields*, eds. C. Albright *et al*,, (World Scientific,1993), p. 567
17. F. Weber, in the proceedings of the *7th Meeting of the American Physical Society, Division of Particles and Fields*, eds. C. Albright *et al*,, (World Scientific,1993), p. 571
18. M. Dugan, M. Golden and B. Grinstein, *Phys. Lett.* **B282** (1992)142
19. M. Luke and A. Manohar, *Phys. Lett.* **B286** (1992)348
20. A good introduction can be found in H. Georgi, *Weak Interactions and Modern Particle Physics*(The Benjamin/Cummings Publishing Company, California,1984)
21. G. Burdman, J. F. Donoghue, *Phys. Lett.* **B280** (1992)287;
    M. B. Wise, *Phys. Rev.* **D45** (1992)2188
22. T.-M. Yan, H.-Y. Cheng, C.-Y. Cheung, G.-L. Lin, Y. C. Lin and H.-L. Yu, *Phys. Rev.* **D46** (1992)1148
23. The ACCMOR Collaboration (S. Barlag *et al*), *Phys. Lett.* **B278** (1992)480

24. The CLEO Collaboration (F. Butler *et al*), *Phys. Rev. Lett.* **69** (2041)1992

25. J. Amundson, C. Boyd, E. Jenkins, M. Luke, A. Manohar, J. Rosner, M. Savage and M. Wise, *Phys. Lett.* **B296** (1992)415;
P. Cho and H. Georgi, *Phys. Lett.* **B296** (1992)408

26. H.-Y. Cheng, C.-Y. Cheung, G.-L. Lin, Y. C. Lin, T.-M. Yan and H.-L. Yu, *Phys. Rev.* **D46** (1992)5060

27. The CLEO collaboration (S. Henderson, *et al.*) *Phys. Rev.* **D45** (1992)2212

28. The CLEO Collaboration (D. Acosta, *et al.*), *First Measurement Of* $\Gamma(D_s^+ \to \mu^+\nu)/\Gamma(D_s^+ \to \phi\pi^+)$, CLNS-93-1238, Aug 1993.

29. B. Grinstein, E. Jenkins, A. Manohar, M. Savage and M. Wise, *Nucl. Phys.* **B380** (1992)369

30. J. Goity, *Phys. Rev.* **D46** (1992)3929

31. B. Grinstein, *On a precise calculation of* $(f_{B_s}/f_B)/(f_{D_s}/f_D)$ *and its implications on the interpretation of* $B-\bar{B}$ *mixing*, SSCL-Preprint-492(hep-ph:9308226), August 1993

32. See, for example, C. Bernard, J. Labrenz and A. Soni, *A Lattice Computation Of The Decay Constants Of B And D Mesons*, UW-PT-93-06(hep-lat:9306009), June 1993;
C. Dominguez, *Leptonic Decay Constants of Charm and Beauty Mesons in QCD: An Update*, SISSA Ref. 139/93/EP(hep-ph:9309260), September 1993

33. Particle Data Group, *Phys. Rev.* **D45** (1992)

34. The Cleo Collaboration (D. Bortoletto *et al*) *Phys. Rev. Lett.* **69** (1992)2046

35. The CUSB-II Collaboration (J. Lee-Franzini *et al*), *Phys. Rev. Lett.* **65** (1990)2947

36. The Cleo II Collaboration (D.S. Akerib *et al*), *Phys. Rev. Lett.* **67** (1991)1692

37. J. Rosner and M. Wise, *Phys. Rev.* **D47** (1992)343

38. A. Falk, B. Grinstein, M. Luke, *Nucl. Phys.* **B357** (1991)185

39. L. Randall and E. Sather, *Phys. Lett.* **B303** (1993)345

40. E. Jenkins, *Heavy Meson Masses In Chiral Perturbation Theory With Heavy Quark Symmetry*, CERN-TH-6765-92(hep-ph:9212295), Dec 1992

41. L. Randall and M. Wise, *Phys. Lett.* **B303** (1993)135

42. A. Falk and B. Grinstein, $\overline{B} \to \overline{K}e^+e^-$ *in Chiral Perturbation Theory*, SLAC-PUB-6237, SSCL-Preprint-484(hep-ph:9306310), June 1993

43. A. Falk, *Nucl. Phys.* **B378** (1992)79;
A. Falk and M. Luke, *Phys. Lett.* **B292** (1992)119

44. A. Falk, *Phys. Lett.* **B305** (1993)268

45. I. Bigi, M. Shifman, N. Uraltsev and A. Vainshtein *Phys. Rev. Lett.* **71** (1993)496;
A. Manohar and M. Wise, *Inclusive Semileptonic B And Polarized* Λ_b *Decays From Qcd*, UCSD-PTH-93-14(hep-ph:9308246), August 1993;
T. Mannel, *Operator Product Expansion For Inclusive Semileptonic Decays In Heavy Quark Effective Field Theory*, IKDA-93-26(hep-ph:9308262), August 1993

B PHYSICS AT LEP

ROBERT V. KOWALEWSKI
CERN
1211 Geneva 23, Switzerland

1. INTRODUCTION

Each LEP experiment has accumulated approximately 250 000 $Z^0 \rightarrow b\bar{b}$ events through 1992. The analysis of these data has produced results on b production and decay properties. This talk will discuss LEP results on b hadron lifetimes, B meson mixing, and b hadron masses. Measurements of the forward-backward asymmetry in $Z^0 \rightarrow b\bar{b}$ decays and of the partial width of the Z^0 into $b\bar{b}$ are being actively pursued at LEP, but will not be discussed here.

LEP has certain advantages for studying b physics. The event rate, while small in comparison to hadron machines, is far above the levels seen at PEP and PETRA and approaches those of DORIS-II and CESR. The LEP luminosity has improved each year, and has recently exceeded the design figure of $1.5 \cdot 10^{31}/\mathrm{cm/s}$ in 8×8 bunch running. Further improvements to the luminosity are planned.

The triggering and selection of $q\bar{q}$ final states is done with high efficiency and negligible background, and $b\bar{b}$ final states account for roughly 22% of all hadronic Z^0 decays. The b hadrons are boosted and typically travel a few millimeters before decaying, and their decay products are collimated into easily identifiable jets. The cleanliness of the final states allows inclusive studies of b hadron decays. The B_s and b baryon states have been observed and can be studied at LEP, in contrast to the experiments at the $\Upsilon(4S)$.

2. EXPERIMENTS AT LEP

The experiments at LEP as of 1992 are

OPAL Good charged particle tracking in the $r\phi$ plane, 2 layers of silicon in $r\phi$, good lepton identification, excellent dE/dx.

L3 Small tracking volume, excellent electromagnetic energy resolution, good lepton identification.

DELPHI Good charged particle tracking from silicon (3 layers in $r\phi$), good muon identification, RICH detectors for particle identification.

ALEPH Good charged particle tracking including silicon in 3-d, excellent invariant mass resolution, good lepton identification, finely segmented electromagnetic calorimeter, good dE/dx.

Some characteristics relevant to studying b hadron decays are listed for each detector. L3 and OPAL have silicon vertex detectors with $r\phi$ and rz readout installed for the 1993 run. Several experiments are proposing further improvements in silicon vertex detectors.

Lepton identification and charged track impact parameter measurements are two important tools used in the study of b hadrons at LEP. The semileptonic decay of b hadrons is responsible for about 80% of the identified leptons in hadronic events with p greater than 3 GeV/c and p_t, the momentum transverse to the jet with which the lepton candidate is associated, greater than 1 GeV/c. These leptons are used to discriminate b from non-b final states and to determine the charge of the decaying b quark.

The tracking resolutions achieved with silicon vertex detectors in OPAL, DELPHI, and ALEPH on the impact parameter (30-100 μm depending on p) and vertex decay length (200-400 μm) are small compared to the average impact parameter of tracks from b hadrons ($\simeq$ 400 μm) and the average b hadron decay length ($\simeq$ 3 mm). Vertex information is used to tag the presence of long-lived b hadron decays, to measure b hadron lifetimes, and to reduce combinatorial background in b hadron reconstruction. The most precise measurements of the partial width of the Z^0 into $b\bar{b}$ now come from comparing single and double lifetime tags.

The number of $Z^0 \to b\bar{b}$ events collected per experiment per year is roughly

- 1990: 30 000,
- 1991: 70 000,
- 1992: 150 000.

Not all of the analyses presented here include the data collected in 1992. The year(s) in which the data set for a particular measurement was collected is indicated in each table in the sections which follow.

3. LIFETIMES OF b HADRONS

3.1 *Average b Hadron Lifetime*

The average lifetime of the b hadrons produced at LEP has been measured by all 4 experiments. The standard technique is to perform a maximum likelihood fit to the impact parameter distribution of high p, high p_t leptons. The lepton candidate sample is typically 70-80% $b \to \ell\nu X$ and 8-12% $b \to c \to \ell\nu X$, the remainder coming from primary charm decay, non-prompt lepton backgrounds, and misidentified hadrons. The fitting function is a convolution of the distributions expected in a detector with perfect impact parameter resolution with the observed resolution of the experiment. This resolution is determined from the impact parameter distribution of those tracks which satisfy the same kinematic criteria as the lepton candidate tracks, but which appear to have originated from the hemisphere opposite to which their momentum points. These tracks come predominantly from the primary vertex, and thus provide a measure of the true resolution of the detector. The lifetime results, in ps, are given in table 1. In this and all the following tables, the first error quoted is statistical and the second systematic.

Table 1. Measurements of the average b hadron lifetime.

ALEPH [1]	1.49	±0.03	±0.06	91 ℓ
(DELPHI preliminary	1.36	±0.04	±0.05	91 μ)
(DELPHI preliminary	1.41	±0.03	±0.05	91 hadrons)
(DELPHI preliminary	1.57	±0.03	±0.05	91 vertices)
DELPHI preliminary	1.48	±0.03	±0.05	91 average
L3 preliminary	1.36	±0.04	±0.05	91 ℓ
OPAL [2]	1.52	±0.03	±0.04	90,91 ℓ
LEP	1.474	±0.035		$\chi^2 = 4.1/3$

The lifetime measured is an average weighted by the production fractions and semileptonic branching ratios of the b hadrons in Z^0 decays. Systematic errors come mostly from uncertainties in the detector resolution and in the modelling of fragmentation and weak decays. A common systematic error of 0.02 ps was assumed in forming the LEP average.

The LEP results on $\langle\tau_b\rangle$ from $B \to J/\psi X$ decays, given in table 2, are statistically weaker.

Table 2. Lifetime measurements using J/ψ decays.

ALEPH [3]	1.35	$^{+0.19}_{-0.17}$	±0.05	90,91
ALEPH preliminary	1.41	$^{+0.13}_{-0.12}$	±0.04	90-92
DELPHI preliminary	1.10	$^{+0.33}_{-0.25}$	$^{+0.11}_{-0.06}$	90,91
DELPHI preliminary	1.47	$^{+0.23}_{-0.19}$	$^{+0.09}_{-0.17}$	92
OPAL [4]	1.32	$^{+0.31}_{-0.25}$	±0.15	90
LEP	1.38	$^{+0.10}_{-0.09}$		$\chi^2 = 1.1/4$

The combined precision one might obtain from LEP using J/ψ decays when each experiment updates their results with the 1992 data is $\simeq$ 6%, corresponding to roughly 600 decays.

3.2 *B^+/B^0 Lifetime Ratio*

The B^0 and B^+ lifetimes at LEP have been measured indirectly using the following modes:

- $B \to D^{*-}\ell^+\nu X$,
- $B \to \overline{D}^0\ell^+\nu X$, and
- $B \to D^-\ell^+\nu X$.

The D mesons are reconstructed primarily in all charged modes of the type $K^-n\pi$, but modes with a missing π^0 are also used for the D^{*-} decays. The apparent lifetimes of these samples are determined from the reconstructed decay lengths and estimated energies of the B decays. As mentioned above, the decay length resolution is typically 200-400 μm. The uncertainty in the estimate of the B energy varies considerably as a function of the invariant mass of the $D\ell$ pair, but is typically 15-20%.

The different samples do not provide perfect separation between B^+ and B^0, since "X" can be charged. Estimates of the sample composition are based partly on measurements of $B \to D^{**}\ell\nu$ and partly on assumptions, e.g. isospin symmetry. The uncertainties in these estimates are the major source of systematic error on the lifetime ratio. Table 3 gives the results.

Table 3. Measurements of the B^+/B^0 lifetime ratio.

ALEPH [5]	0.96	$^{+0.19}_{-0.15}$	$^{+0.18}_{-0.12}$	91 $D\ell$
DELPHI [6]	1.11	$^{+0.51}_{-0.39}$	±0.11	91 $D\ell$
DELPHI [7]	1.09	$^{+0.28}_{-0.23}$	±0.11	91 vertex
OPAL [8]	1.00	$^{+0.33}_{-0.25}$	±0.08	91 $D\ell$
LEP	1.02	$^{+0.16}_{-0.13}$		$\chi^2 = 0.2/3$

DELPHI have also used the charge of reconstructed vertices to separate B^+ from neutral b hadrons[7]. The charge of reconstructed secondary vertices is estimated to be correct 71% of the time, allowing a partial separation between charged and neutral b hadrons.

The average of the B^+ and B^0 lifetime measurements is

$$\langle \tau(B^+), \tau(B^0) \rangle = 1.49 \pm 0.10\,\mathrm{ps},$$

in good agreement with measurements of the average b hadron lifetime.

3.3 The B_s Lifetime

Semi-exclusive decays of the type

- $B_s \to D_s^- \ell^+ \nu X$

with

- $D_s^- \to \phi\pi^-$ or
- $D_s^- \to K^{*0}K^-$

have been used to measure the B_s lifetime. The decay time estimate is determined from the measured $D_s\ell$ vertex and the estimated relativistic boost. The analysis is the similar to the B^+/B^0 case, but is simpler in that the sample is not significantly contaminated by decays of a different b hadron. DELPHI have also used $\phi\ell$ correlations and inclusive D_s decays to tag the presence of B_s and measure its lifetime. These channels yield less pure samples of B_s, and a correction must be made for the charm flight path in the inclusive D_s case. Table 4 summarizes the B_s lifetime measurements.

Table 4. Measurements of the B_s lifetime.

ALEPH preliminary	2.26	$^{+0.68}_{-0.48}$	±0.12	91,92
DELPHI preliminary	1.00	±0.30		91
OPAL [9]	1.13	$^{+0.35}_{-0.26}$	±0.09	90-92
LEP	1.53	$^{+0.30}_{-0.23}$		$\chi^2 = 6.3/2$

The background from improper reconstruction of B^0 and B^+ decays is small. The uncertainty in the size and lifetime content of the combinatorial background in the $KK\pi$ invariant mass distribution is the major source of systematic error. This error will decrease as statistics improve.

3.4 The b Baryon Lifetime

The b baryon signatures used for lifetime measurements so far are

- $(\Lambda_b) \to \Lambda\ell^- X$,
- $(\Lambda_b) \to \Lambda_c\ell^- X$, with $\Lambda_c \to pK^-\pi^+$.

The symbol (Λ_b) represents all b baryons; the mixture of b baryons at LEP is not well known, although the b flavor changing decays are expected to be dominated by Λ_b and Ξ_b. A method similar to that used in the B meson lifetime analyses is used by ALEPH on a sample of $(\Lambda_b) \to \Lambda_c\ell^- X$ candidates. OPAL fit a decay length to $(\Lambda_b) \to \Lambda\ell^- X$ candidates, while ALEPH use only the lepton impact parameter in their $(\Lambda_b) \to \Lambda\ell^- X$ candidates, using an analysis similar to the one used in measuring the average b hadron lifetime. DELPHI reconstruct a vertex around the lepton candidate in the $(\Lambda_b) \to \Lambda\ell^- X$ sample using additional tracks to obtain a more precise decay time estimator. The results are given in table 5.

Table 5. Measurements of the average b baryon lifetime.

ALEPH [10]	1.12	$^{+0.32}_{-0.29}$	±0.16	90,91 ℓ i.p.
ALEPH preliminary	1.16	$^{+0.42}_{-0.32}$	±0.07	91,92 $\Lambda_c\ell$
DELPHI [11]	1.04	$^{+0.48}_{-0.38}$	±0.09	90,91 $\Lambda\ell$+vertex
OPAL [12]	1.05	$^{+0.23}_{-0.20}$	±0.08	90-92 $\Lambda\ell$
LEP	1.07	$^{+0.16}_{-0.14}$		$\chi^2 = 0.2/3$

The systematic errors come principally from uncertainties in the background and biases in the fit (especially for $(\Lambda_b) \to \Lambda\ell^- X$ candidates). The effect of uncertainties in b baryon polarization is small (2-3% conservatively). The measurement of separate Λ_b and Ξ_b lifetimes awaits higher statistics.

The measurement of the lifetimes of specific b hadrons has just begun at LEP, and all measurements to date are statistics limited. The LEP average values for each of the scalar B mesons is consistent with the measured average b hadron lifetime, and the b baryon lifetime is about 2σ below the average.

4. MEASUREMENTS OF B MESON MIXING

4.1 Time Integrated Measurements

LEP experiments are sensitive to the mixing of B_s and B_d mesons. Measurements of the time-integrated mixing parameter $\chi = N(b \to \bar{b} \to \ell^+)/N(b \to \ell^\pm)$ have been made using like and unlike-sign dileptons, and using a combination of leptons and jet charge,

$$Q_H = \frac{\sum_i |p_i \cdot e_T|^\kappa \cdot q_i}{\sum_i |p_i \cdot e_T|^\kappa},$$

where p_i and q_i are, respectively, momentum and charge, e_T is the direction of the summed momentum vector of the jet, and the sum runs over all particles in the jet. These two methods have slightly different sensitivity to B_s and B_d mixing. Leptons from the cascade decay $b \to c \to \ell^+$ are an intrinsic source of incorrect flavor tagging, and are an important source of systematic error in the dilepton measurement. The largest systematic error in the jet charge analysis comes from uncertainties in fragmentation. Table 6 summarizes the measurements of $\langle\chi\rangle$.

Table 6. Measurements of $\langle\chi\rangle$ at LEP.

ALEPH [13]	.113	$\pm.018$	$\pm.027$	90 ℓ-jet charge
ALEPH preliminary	.113	$\pm.014$	$\pm.008$	90,91 grand ℓ fit
DELPHI preliminary	.131	$^{+.014}_{-.015}$	$\pm.012$	91,92 dilepton
DELPHI preliminary	.144	$\pm.014$	$^{+.019}_{-.017}$	91,92 ℓ-jet charge
L3 [14]	.121	$\pm.017$	$\pm.006$	90,91
OPAL [15]	.143	$^{+.022}_{-.021}$	$\pm.007$	90-91 grand ℓ fit
LEP	.129	$\pm.010$		$\chi^2 = 2.2/5$

Interpretation of $\langle\chi\rangle$ is complicated by production rates and branching fractions. CLEO[16] and ARGUS[17] have determined $\chi_d = 0.167 \pm 0.037$. Using this value and assuming 40% of the b quarks result in B_d mesons at LEP, one expects $\langle\chi\rangle = 0.067$ in the absence of B_s mixing.

4.2 Time Dependent Measurements

Recently, ALEPH[18] have made a first observation of the time dependence of B_d mixing. A $D^{*\pm}$ decay is fully reconstructed in one jet and a lepton with large p and p_t is tagged in a second, well separated jet. The lepton tag is used to enrich the sample in $b\bar{b}$ events and to infer the flavor of the b which produced the charged D^*. The reconstructed $D^{*\pm}$ vertex forms the basis for the decay time measurement, and the $D^{*\pm}$ charge tags the b flavor at the time of decay. An oscillation is observed in the plot of the $D^{*\pm}$-ℓ charge correlation versus reconstructed decay length. After correcting for the additional decay length of the D^0, they find

$$\begin{aligned} \Delta m &= (3.44^{+.65+.26}_{-.70-.20})10^{-4}\,\mathrm{eV} \quad , \\ \frac{\Delta m}{\Gamma} &= 0.75^{+0.15+0.08}_{-0.14-0.05} \quad , \end{aligned}$$

compatible with mixing measurements from CLEO and ARGUS. DELPHI see a time dependence for B_d mixing in the ratio of like to unlike sign dileptons versus the lepton impact parameter, and find $\Delta m/\Gamma = 0.54^{+0.20}_{-0.15} \pm 0.10$. The resolution on the decay time is approximately $0.7\,t$, precluding any search for B_s mixing. ALEPH have studied dilepton events, where they achieve a decay time resolution of $0.3\,\mathrm{ps} \oplus 0.2\,t$ by reconstructing vertices around the tagged leptons. They observe an oscillation corresponding to B_d mixing, but do not yet extract a value for Δm. The dilepton technique allows one to search for both B_d and B_s mixing, and has a sensitivity to B_s mixing if $\Delta m/\Gamma < 8$, given sufficient statistics.

5. EXCLUSIVE RECONSTRUCTION OF b HADRONS

5.1 Reconstruction of B_u and B_d

ALEPH, DELPHI, and OPAL have reported a few dozen B_u and B_d reconstructed in the following modes:

$$J/\psi\,K, \quad J/\psi\,K^*,$$
$$\psi'K, \quad \psi'K^*,$$
$$D^{*+}n\pi, \quad D^+n\pi, \quad D^0 n\pi.$$

The statistics are modest, but observation of these events shows that exclusive b hadron reconstruction can be done at LEP.

5.2 Reconstruction of B_s

ALEPH, DELPHI and OPAL have searched for exclusive B_s decays in the modes

$$\begin{array}{cc} J/\psi\,\phi & J/\psi\,K^+K^- \\ \psi'\,\phi & \psi'K^+K^- \\ D_s n\pi. & \end{array}$$

The J/ψ are reconstructed in their $\ell^+\ell^-$ decay, the ψ' into either $\ell^+\ell^-$ or $J/\psi\,\pi\pi$, and the D_s into $\phi\pi$ or K^*K. Based on two 'unambiguous' exclusive events, ALEPH quote[19]

$$m(B_s) = 5.3686 \pm 0.0056 \pm 0.0015\,\mathrm{GeV}/c^2$$

The event which dominates the mass measurement is

$$B_s \to \psi'\phi \to \mu^+\mu^- K^+K^- \quad ,$$

for which the uncertainty in the measured mass is $5.6\,\mathrm{MeV}/c^2$. DELPHI report a preliminary measurement of

$$\begin{aligned} m(B_s) - m(B_d) &= 78 \pm 9 \pm 11\,\mathrm{MeV}/c^2 \\ m(B_s) &= 5.357 \pm 0.009 \pm 0.011\,\mathrm{GeV}/c^2 \end{aligned}$$

based on 11 B_s candidates in 6 decay modes (0-3 events/mode). An OPAL candidate[20] in the $J/\psi\,\phi$ channel gave a mass of $5.36 \pm 0.07\,\mathrm{GeV}/c^2$. Combining these numbers,

$$m(B_s) = 5.369 \pm 0.005\,\mathrm{GeV}/c^2$$

6. OTHER TOPICS

6.1 Observation of $B^* \to B$ Transitions

L3 have seen evidence for B^* production in their inclusive photon energy spectrum. They take all photon candidates passing quality criteria and boost them back to the presumed B rest frame. The resulting rest frame energy spectrum has a large excess near 50 MeV which is attributed to photons from the $B^* \to B$ transition. From the number observed and a calculation of the efficiency they determine the vector to pseudo-scalar B production ratio to be $0.82 \pm 0.08 \pm 0.12$, consistent with the spin-counting expectation of 0.75.

6.2 Branching Fraction $B \to \tau\nu X$

ALEPH have measured $B(B \to \tau\nu X)$ to be[21] $4.08 \pm 0.76 \pm 0.62\%$. This value is consistent with theoretical expectations. The measurement is performed by looking for the missing energy carried away by the ν_τ and $\bar{\nu}_\tau$.

6.3 *Searches for B_s Penguin Decays*

ALEPH have set a 90% c.l. upper limit on the decay $B_s \rightarrow \phi\gamma$ of

$$B(B_s \rightarrow \phi\gamma) < 4.1 \cdot 10^{-4} \quad .$$

This is near the theoretical upper limit on the branching fraction for $b \rightarrow s\gamma$ penguin decays.

7. CONCLUSION

The experiments at LEP now dominate the world average b hadron lifetime, and have measured individual lifetimes for the pseudo-scalar B mesons and for b baryons with precisions of 15-20%. Measurements of the average mixing parameter $\langle\chi\rangle$ at LEP suggest substantial B_s mixing. Flavor oscillations have been observed directly for the B_d, and searches for B_s oscillations are underway. Some exclusive B decays have been reconstructed, and the mass of the B_s has been measured. Most analyses are statistics limited, so further improvements can be expected as the data sample increases.

8. REFERENCES

[1] ALEPH Collab., D. Buskulic *et al.*, *Phys. Lett.* **B295** (1992) 174.
[2] OPAL Collab., P. Acton *et al.*, CERN/PPE 93-92, submitted to *Zeit. fur Physik* **C**.
[3] ALEPH Collab., D. Buskulic *et al.*, *Phys. Lett.* **B295** (1992) 396.
[4] OPAL Collab., G. Alexander *et al.*, *Phys. Lett.* **B266** (1991) 485.
[5] ALEPH Collab., D. Buskulic *et al.*, CERN/PPE 93-42, submitted to *Phys. Lett.* **B**.
[6] DELPHI Collab., P. Abreu *et al.*, *Zeit. fur Physik* **C57** (1993) 181.
[7] DELPHI Collab., P. Abreu *et al.*, CERN/PPE 93-80, submitted to *Nuclear Phys.* **B**.
[8] OPAL Collab., P. Acton *et al.*, *Phys. Lett.* **B307** (1993) 247.
[9] OPAL Collab., P. Acton *et al.*, CERN/PPE 93-95, submitted to *Phys. Lett.* **B**.
[10] ALEPH Collab., D. Buskulic *et al.*, *Phys. Lett.* **B297** (1992) 449.
[11] DELPHI Collab., P. Abreu *et al.*, CERN/PPE 93-32, submitted to *Phys. Lett.* **B**.
[12] OPAL Collab., R. Akers *et al.*, CERN/PPE 93-132, submitted to *Zeit. fur Physik* **C**.
[13] ALEPH Collab., D. Buskulic *et al.*, *Phys. Lett.* **B284** (1992) 177.
[14] L3 Collab., B. Adeva *et al.*, *Phys. Lett.* **B288** (1992) 395.
[15] OPAL Collab., R. Akers *et al.*, CERN/PPE 93-106, submitted to *Zeit. fur Physik* **C**.
[16] CLEO Collab., M. Artuso *et al.*, *Phys. Rev. Lett.* **62** (1989) 2233.
[17] ARGUS Collab., H. Albrecht *et al.*, *Zeit. fur Physik* **C55** (1992) 357.
[18] ALEPH Collab., D. Buskulic *et al.*, CERN/PPE 93-97, submitted to *Phys. Lett.* **B**.
[19] ALEPH Collab., D. Buskulic *et al.*, CERN/PPE 93-99, submitted to *Phys. Lett.* **B**.
[20] OPAL Collab., P. Acton *et al.*, *Phys. Lett.* **B295** (1992) 357.
[21] ALEPH Collab., D. Buskulic *et al.*, *Phys. Lett.* **B298** (1993) 479.

B–PHYSICS IN HADRON COLLIDERS

CHRISTOPHER T. HILL
Fermi National Accelerator Laboratory
P.O. Box 500, Batavia, Illinois, 60510

1. INTRODUCTION

1.1 Generalities

The b–quark offers a window on the standard model that is open to experimentalists at hadron colliders, where the largest yields of b–quarks occur. With existing facilities, such as CDF, it should be possible to achieve $\sim 10^9$ observable B–decays within the next few years. This entails evolution of the high resolution vertex detectors, e.g., CDF's SVX, including full r-θ-z information, and especially generalized triggers, such as single lepton displaced vertices for semileptonic weak decay studies.[1,2] With a modest yet dedicated program, perhaps involving a new detector, $> 10^{10}$ observed B's should be achievable at Tevatron to Main Injector luminosities within this decade. Such a program is essential to break the ground for future hadron-based B-physics programs at LHC and SSC. An ultimate hadron collider based program at Fermilab, LHC and SSC can look forward to recording the decays of $> 10^{12}$ produced B's.

The present discussion is intended to be primarily a prospectus for such a program. We will, however, indulge in some speculations about tagging of flavors and the all–important kinematic reconstruction needed to do semileptonic weak studies. This reflects recent interest that has arisen in the possibility of "daughter pion" tagging, i.e., using the pions from the decays of parent resonances to tag the flavor.[3]

The major advantages of the hadron based B–physics environment are the relatively large cross–section for b–quark production and the the "broad–band" nature of the beam. b–quark pairs are produced by (predominantly) gluon fusion[4] and arbitrarily massive states are available. Thus, all of the spectroscopy, including $B_c \sim \bar{b}c$ and the resonances, B^{**} etc., are produced in hadronic collisions. This sharply contrasts with the situation in e^+e^- machines that make use of the $\Upsilon(4S)$ and $\Upsilon(5S)$ resonances in which only the low–lying $\bar{b}(u,d)$ combinations can be produced. Moreover, in e^+e^- machines that operate in the continuum or on the Z–peak the cross-section for b production is many orders of magnitude below that in the hadronic environment.

On the other hand these advantages imply major challenges as well.[1,2] The copious production at hadron machines implies that a substantial parsing of data must occur quickly on–line, i.e., a trigger that can keep interesting candidate events must be provided. To date in hadronic colliders the semileptonic decay modes have been largely discarded in favor of the much easier ψ modes. A trigger capable of recovering the semileptonic decays is possible, and demonstrating its feasibility is of high priority for a number of reasons (e.g., conventional flavor tagging requires it).

Another issue is the extent to which decays involving missing mass, such as the semileptonic decays involving neutrinos, can be fully reconstructed. In e^+e^- machines that make use of the $\Upsilon(4S)$ the B–mesons are produced with a known energy, the beam energy.

In combination with the visible decay momentum, this completely determines the decay kinematics, e.g., the Q^2 of the lepton pair is determined even though the neutrino is never seen. In a hadronic mode we observe a B-meson flight direction and the visible momentum of the decay products, but this yields a two-fold ambiguity in the B energy. Thus, to make maximal use of a semileptonic decay sample it is imperative that efficient techniques evolve for resolving this ambiguity!

One technique would "bludgeon" the semileptonic processes with high statistics by insisting on keeping only those special kinematic configurations for which the ambiguity disappears[5]. While inefficient, this technique is guaranteed to work. However, we will suggest another approach presently that is speculative, but may ultimately prove to be an efficient way of fully reconstructing B processes with relatively high efficiency. It makes use of the fact that B-mesons will often be produced as decay fragments of a resonance as in $B^{**} \to B + \pi$. The π meson here we will call a "daughter pion," and it has previously been suggested as a flavor tagging mechanism for neutral B-mesons.[2] The observation of daughter π-mesons from resonances is established by ARGUS, E-691 and CLEO, and E-687.[6] However, we suggest here that it can potentially be used to resolve the two-fold kinematic ambiguity in the B-meson 4-momentum. We describe this approach in Section 2.4 below. It may prove workable in some form as our understanding of B production evolves.

The physics goals of a $> 10^{10}$ B-meson program are very rich and diverse. Heavy quark physics allows us to map out the CKM matrix of the standard model through the detailed studies of inclusive and exclusive decay modes. It will allow us to test the standard model beyond the leading order in radiative corrections, and through rare decay modes and mixing phenomena which are sensitive to m_{top} and V_{tq}, etc. This will lead ultimately to experimental tests of the CKM theory of CP-violation, which is expected to manifest itself in many interesting new channels in the b-system. High statistics studies of the b-system will furthermore enable searches for exotic physics, signals of which might be expected to emerge in heavy quark processes.

We begin first with a brief overview of the physics considerations that are relevant to doing heavy quark physics in the hadronic collider environment.

1.2 *Prima Facie Considerations of Hadronic B's*

B-physics at hadron colliders is often casually dismissed out-of-hand, preference given to e^+e^- production, because the hadronic environment is "too noisy." It is important to realize that the "noise," i.e., the background of high multiplicity, mostly low p_T pions in a hadronic collision, is largely spread out over a large range of rapidity. The low-mass particle production follows an approximately constant distribution in the pseudo-rapidity:

$$\eta = -\ln[\tan(\theta/2)] \approx \tanh^{-1}(p_z/E) \tag{1}$$

Typically at Tevatron energies the number of pions per unit rapidity is given by:

$$\frac{dN_\pi}{d\eta} \approx 3.0 \quad \text{charged}; \qquad \approx 1.5 \quad \text{neutral} \tag{2}$$

Thus, in a rapidity range of $|\eta| < 1$ we expect of order $\bar{n} = 6$ charged pions, and 6 π^0 gamma's emanating from the beam collision spot.

On the other hand, the finite and relatively large mass of the b-quark leads to a longitudinal momentum distribution that is centered on $\eta = 0$, and is fairly broad depending upon the *cm* energy scale and the p_t cut (see, e.g., Alan Sill in ref.[1]). In rapidity, the range of significant b-quark production with high p_t is for the Tevatron $\sim \pm 3$; for the LHC $\sim \pm 4.5$; and for the SSC $\sim \pm 7$. Moreover, the transverse momentum distribution, p_t, of heavy quarks is set by the mass scale of the quark (generally, it requires a parton subprocess of larger $\hat{s}$ to make a heavier quark, hence larger values of p_t become relatively more probable).

Moreover, b-hadrons have a fortuitously long life-time, and they therefore drift a resolvable distance away from the primary vertex before they decay. With high resolution vertex detectors it is easy to resolve the secondary vertex and isolate the heavy hadron decay. The typical displacement of a b-hadron secondary decay vertex is ~ 400 microns, while a resolution to better than ~ 15 microns is achieved with the SVX. With this secondary vertex separation there is only a very small combinatorial background to these displaced vertices coming from minimum bias physics. There remains, however, a significant background from charmed mesons which also have displaced secondary vertices. These can generally be controlled by demanding partial reconstruction of the heavy hadron decay with mass cuts, i.e., demand that the visible decay products have masses exceeding those of charmed particles, typically $\gtrsim 2.5$ GeV.

Table I: Indicated yields of usable B-mesons running for a 3 year, 30% duty cycle, period for: (a) Tevatron at present attainable $\mathcal{L} = 10^{31}$ cm^{-2} sec^{-1} (b) Main Injector assuming $\mathcal{L} = 10^{32}$ cm^{-2} sec^{-1} (twice the design goal; multiply by 10 if the rapidity range is $|\eta| \leq 3$ and $p_t > 5$ GeV). (c) ABF - Asymmetric B-factory proposal at $\mathcal{L} = 10^{34}$ cm^{-2} sec^{-1} operating on the $\Upsilon(4S)$ (d) LEP at Z^0-pole with $\mathcal{L} = 2 \times 10^{31}$ cm^{-2} sec^{-1} (see M. Artuso in ref.[2]).

Mode	Tevatron$^{(a)}$	Main Injector$^{(b)}$	ABF$^{(c)}$	LEP II$^{(d)}$
$B_{u,d}$	6×10^9	6×10^{10}	3×10^8	4×10^6
B_s	1.6×10^9	1.6×10^{10}	none	8×10^5
B_c	10^7	10^8	none	4×10^3
Λ_b	10^9	10^{10}	none	4×10^5

At the luminosity of 10^{31} cm^{-2} sec^{-1} in a $p\bar{p}$ collider, for which we assume $\sqrt{s} = 1.8$ GeV, B-meson pairs are produced in a rapidity range of $|\eta| \leq 1$ and $p_t > 10$ GeV, with a total cross-section of ~ 10 μb or 100 Hz (ref.[1]; M. Artuso in ref.[2]). With the main injector, and the experience to date at the Tevatron, an ultimate luminosity of 10^{32} cm^{-2} sec^{-1} is thinkable (the present peak Tevatron luminosity is $\sim 0.8 \times 10^{31}$). Running at 10^{32} (10^{31}) for a total of 3 years, with a 33% duty factor yields $\sim 3 \times 10^{10}$ (3×10^9) *usable* B-mesons. If we can triple the rapidity range to $|\eta| \leq 3$ and reduce the lower limit to $p_t > 5$ GeV the yields for useful B's approach $\sim 3 \times 10^{11}$ (3×10^{10}). Of this, the yield of B_s is $\sim 18\%$, Λ_B is $\sim 10\%$ and of B_c is $\sim 0.1\%$. The yield of b-quark containing baryons is expected to be of order 10%, though these are crude estimates at present, and should actually be measured at the end of run I.

This compares with the idealized luminosity of 10^{34} cm^{-2} sec^{-1} in an e^+e^- storage ring, such as the proposed asymmetric B-factory (ABF) at SLAC or CESR (the present peak luminosity at CESR is 2.5×10^{32}). The cross-section for $B\overline{B}$ production on the $\Upsilon(4S)$ is ~ 1 nb, which yields B pairs on the $\Upsilon(4S)$ at a rate of ~ 10 Hz. The yield for the same 3 year 30% duty cycle period is $\sim 3 \times 10^8$ B-mesons (note this is the proposed ultimate

300 fb^{-1}, lifetime $\int \mathcal{L}dt$ for the asymmetric B-factory). On the Z^0 pole the cross-section is ~ 7.0 nb. Hence operating an e^+e^- collider at the LEP luminosity of 2×10^{31} on the Z^0 pole for the same 3 year continuous duty cycle period yields $\sim 3 \times 10^6$ b's. For continuum e^+e^- machines the cross-sections are $\sim 10^{-2}$ those on the Z^0 pole and we will not consider them for comparison.

We see from Table I that various new states and decay modes are available in the hadronic facility that are inaccessible, or of lower statistics in the e^+e^- environment. Moreover, it appears that a reasonable goal for a dedicated hadron collider based program in the pre-SSC era is to produce a total of $> 10^{10}$ usable b hadrons. In what follows we will take 10^{10} B-mesons to be our standard reference normalization and give a preliminary consideration of what might be achieved in such a program.

2. PHYSICAL STATES AND LEADING PROCESSES

2.1 *Resonance Spectroscopy*

The spectrum of resonances of the B-mesons imitates that of the charm system. We see this by comparison in Fig.(1), where the known and predicted resonances of $\ell = 0$ and $\ell = 1$ are indicated. The spectroscopy is actually reflecting a remarkable aspect of heavy quark symmetry, i.e., the heavy quark spin symmetry.[7]

Put simply, heavy quark spin can be ignored in the dynamics, and acts effectively like a flavor symmetry. As a result, states which differ only by flipping the heavy quark spin will be degenerate (up to $O(1/M)$). It is convenient to describe this by classifying mesons as (j_1, j_2), where j_1 is the spin of the heavy quark subsystem and j_2 is the spin of the remaining system. So, for a heavy-light meson $j_1 = \frac{1}{2}$, and the states of lowest mass will have $j_2 = \frac{1}{2}$ as well. Thus $(\frac{1}{2}, \frac{1}{2})$ describes the ground state and this corresponds to total $J = 0$ or $J = 1$. Therefore, the groundstate consists of a degenerate 0^- and 1^- multiplet. We see the D and D^* are actually split by slightly more than a pion mass, while the splitting between the B and B^* decreases by m_c/m_b in the B system. It is important to note that j_2 is the quantum number of the "brown muck;" we cannot *a priori* separate the light quark and gluon degrees of freedom under rotations in QCD, though potential models do so (potential models refer to constituent quarks, and work remarkably well even in light heavy-light systems).[8] A fancier way of stating this is to note that spin is the classification of a state under the "little group;" the little group is the subgroup of the Lorentz group which commutes with the momentum of the state (i.e., it is just $O(3) = SU(2)$ for a massive particle, or $O(2) = U(1)$ for a massless particle). Remarkably, we see that the little group of a heavy-light meson is enlarged to $SU(2) \times SU(2)$, since we can rotate the heavy quark independently of the brown muck. The states for which $|j_1 - j_2|$ is an integer are equivalent to representations of $O(4) = SU(2) \times SU(2)$. Thus the ground state is equivalent to a 4-plet under $O(4)$, containing the 0^- and the 1^- mesons.

The masses and decay widths of heavy-light resonances have been estimated recently by Eichten, Hill and Quigg (EHQ)[8]. The masses of these states seem to be well fit by using a Buchmüller-Tye potential for a static massive quark with a constituent light quark bound statebound state. Their decay widths were obtained by rescaling the known strange and charm widths with smearing. The spectra are presented here:

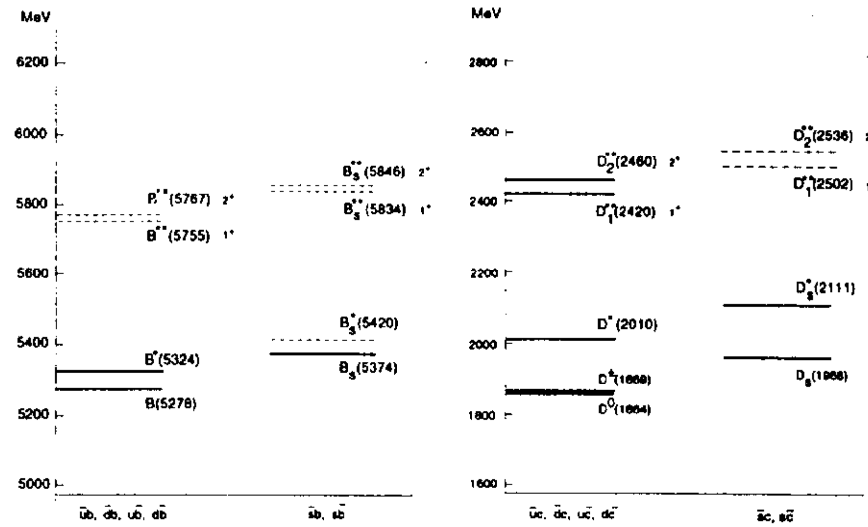

Figure 1. The low-lying spectra of D and B states from EHQ.[8] Solid lines are established, dashed lines are predictions (we omit the broad $(0^+, 1^+)$ p-waves[9]).

There will generally occur a $(\frac{1}{2}, \frac{1}{2}) = 0^+ + 1^+$ parity partner of the ground state (a p-wave in the constituent quark model) which has a very large $\sim GeV$ width and will generally be unobservable.[9] This state may be viewed as the "chiral partner" of the ground state:[9] if we imagine restoring the broken chiral symmetry the ground state would have to linearly realize the chiral symmetry, thus becoming doubly degenerate (thus, the left-handed iso-doublet is $0^+ - 0^-$, while the right-handed iso-doublet is $0^+ + 0^-$ when the chiral symmetry is restored).

2.2 *Daughter Mesons*

The resonances can be observed by studying the π's and K's produced in association with B-mesons. Some of the π-mesons will be decay relics from processes like:

$$p + \bar{p} \to X + (B^{**} \to B + (\pi, K)) \tag{3}$$

The first objective is to establish the existence and masses of the resonant states and the fraction $f = \sigma_{B^{**}}/\sigma_B$ by which a B-meson is produced through the decay of parent resonance. f is likely to be sensitive to the decay and production kinematics.

Experience in e^+e^- (ARGUS and CLEO) and charm photo-production experiments[6] suggests $f \sim 13\%$ for the fraction of D^* coming from the D^{**}, and $f \sim 7\%$ for the fraction of D coming from the D^{**}. We note that photoproduction on a hadronic target (E-691, E-687 in ref.[6]) bears some formal resemblance to the gluon fusion process, and might be a good analogue process for calibrating our understanding of detailed production in $\bar{p}p$ collisions. We would expect (heavy quark symmetry) that apart from normalization the charm production distributions can be taken over to B-physics directly. Thus, for tagging purposes an inclusive rate of $f \sim 20\%$ of B's coming from the $B^{**} \to B^* \to B$ and $B^{**} \to B$ chains might be expected. The experience in photoproduction suggests that the efficiency for finding the daughter pion is $\sim 50\%$. We will therefore assume an overall tagging efficiency of $\sim 10\%$ by daughter mesons is possible.

The production tagging efficiency is probably sensitive to p_T and to angular cuts (or rapidity cuts). The heavy quark limit ensures that the 4-velocity of the produced B^{**} is approximately equal to the 4-velocity of the B, i.e., zero-recoil of the b-system is a good approximation. In hadronic collisions it is probably reasonable to assume that the B^{**} system at low p_T is produced in an unpolarized initial state and, thus, the distribution of decay pions in the process $B^{**} \to B + \pi$ is spherical in the B^{**} rest frame. The (unit normalized) polar distribution of pions relative to the B flight direction is then obtained by boosting the spherical distribution:

$$\frac{dN}{d\Omega} = \frac{1}{4\pi}\left[\frac{\gamma(1-\beta^2\omega^2 - ((\beta^4 - 2\beta^2)\omega^2 + \beta^2)\cos^2\theta) + 2A\beta\omega\cos\theta}{A\gamma^2(\beta^2\cos^2\theta - 1)^2}\right] \tag{4}$$

where:

$$A = (1 - \beta^2\omega^2 - \beta^2(1-\omega^2)\cos^2\theta)^{1/2} \tag{5}$$

and $\omega = 1/\sqrt{1 - m_\pi^2/(\Delta M)^2} \approx 1.04$. In the massless pion limit, $\omega = 1$ and this reduces to $dN/d\Omega = 1/[4\pi\gamma^2(1-\beta\cos\theta)^2]$ valid to order $\frac{1}{2}O(m_\pi^2/(\Delta M)^2) \approx 4\%$. Note that 50% of the pions will occur within a cone of opening angle $\theta_{50\%}$ given by (for $\omega = 1$):

$$\tan\theta_{50\%} = \frac{1}{\gamma\beta} = \frac{1}{\sqrt{\gamma^2 - 1}} \tag{6}$$

For $\gamma \approx 2$ we see that $\theta_{50\%} \sim 30°$, and this defines a cone of small solid angle of $0.07 \times 4\pi$ steradians. The aligned daughter pions, coming from the primary vertex, are also expected be more energetic than typical minimum bias pions. Thus, the conical cut on pions with $\theta < \theta_{50\%}$ should lead to a significant gain in signal to background for low-p_T (at high p_T the B-meson is enveloped in a jet with higher π multiplicity within small conical angle). We do not consider the more general possibility of rapidity correlations here.[3]

2.3 Semileptonic Weak Decays involving V_{cb}

High statistics measurements of exclusive semileptonic branching ratios such as $B \to l + \nu + (D^{**}, D^*, D)$, etc., are possible at the level of $\sim 10^9$ decays. These are important processes for establishing the overall normalization of weak transitions in hadron colliders since the CLEO and ARGUS experiments are significantly improving the statistics of these processes. The key physics goal here is to obtain the highest precision determination of V_{cb} possible. This requires exploiting the heavy quark symmetry result, together with QCD and $1/M$ corrections, which fixes at special kinematic point $w = v \cdot v' \to 1$ the normalization of the Isgur-Wise function. The normalization of $\xi(w \to 1)$ is known to a precision approaching 3%.[10] Therefore, the goal of experiment should be to approach a 3% determination of V_{cb}.

Much effort to date has gone into the measurements of semileptonic weak inclusive decays and exclusive decays of heavy mesons. In e^+e^- experiments such as CLEO or ARGUS, and as proposed for the asymmetric B-factory, one tunes the beam energy to produce the $\Upsilon(4S)$ resonance, which decays to pairs of B^+B^- or $B^0\overline{B}^0$ mesons that are nearly at rest in their *cm* system. With tagging this can produce a clean sample of B's for the exclusive decay modes. The B-mesons can then decay to a final state lepton either directly, semileptonically as $B \to (l\nu)X$, or hadronically, cascading as $B \to X \to (l\nu)X'$.

Various models[11] are used to fit the leptonic energy distribution to the various component subprocesses (see discussion of S. Stone in ref.[2]). The error in these results is dominated by the theoretical models used to fit the spectra, and is of order $\sim 15\%$. At PEP, PETRA and the LEP experiments the semileptonic decays are studied at much higher energies. These results are consistent with the $\Upsilon(4S)$ results to order $\sim 15\%$.[2] Alternatively, one can study exclusive modes using a tagged B, and determine the missing M^2 distribution from the mass of the visible decay fragments of the other B. The missing M^2 distribution will contain endpoint peaks from contributing subprocesses, such as $B^0 \to l^-\nu(D^{*+}) \to \pi^+(D^0) \to K^-\pi^+$. The subprocesses are then fit to the observed missing M^2 distribution. These methods, using different theoretical models, have broadly consistently yielded our first determinations of branching ratios and again yield results to order $\sim 15\%$.[2,11]

However, ultimately we want to minimize the sensitivity to theoretical models in extracting V_{cb}, V_{ub}. Here we can use heavy quark symmetry in a model independent way,[10] from the w distribution. The decay distribution in w for $B \to \ell\nu D_i$ is:

$$\frac{d\Gamma_{D_i}}{dw} = \frac{G_F^2}{48\pi^3}|V_{cb}|^2 m_B^2 m_D^2(1+w)^2\sqrt{w^2-1}\,(F_{D_i}(r,w)) \tag{7}$$

where $r = m_{D_i}/m_B$ and $F_{D_i}(r,w)$ is a form factor.[10] In the $m_{B,D} \to \infty$ limit F is given in terms of the Isgur-Wise function $\xi(w)$ and the known ratio r. At the special "zero recoil" point $\xi(1) = 1 + \epsilon$ where ϵ is composed of (a) QCD corrections computed to NLLA order $\pm 1\%$ and (b) $1/M$ effects that are dominant $\pm 3\%$. Hence, the strategy is to extract the functional dependence of $F(r,w)$, or $\xi(w)$ upon w and extrapolate to $w = 1$ where theoretical corrections are under control. This implies that the experimental statistical uncertainties must become significantly smaller than $\sim 1\%$ and the limiting attainable precision of V_{cb} is expected to be $\sim 3\%$, modulo improvements in the theoretical uncertainties.

Neubert[10] has carried out this analysis with the existing CLEO and ARGUS data on the q^2 distributions, based upon $\sim$ (a few 100) events, to extract the model independent result $|V_{cb}| = 0.042 \pm 0.007$. This is indicative of the current statistical extrapolation errors attained with ~ 300 events, and this should improve in the near future. It would appear that with 10^4 fully reconstructed events the statistical error in this approach will scale downward by a factor of 10. The key point here is that the theoretical modeling in the hadronic environment is now relegated to the corrections, and not to the result itself. The highest experimental statistics will drive the future determinations of V_{cb}.

The challenge for this approach in the hadronic experiments is the requirement to fully reconstruct the decaying B-meson, particularly with respect to kinematics. In e^+e^- experiments the the beam energy, together with the flight direction of the B, supplies sufficient kinematic information to know the B energy unambiguously. In the broad-band hadronic environment we are *a priori* limited to knowing only the flight 3-vector of the B, and the visible 4-momenta; the unobserved neutrino momentum leads to the ambiguity.

Let us consider the semileptonic decay $B \to D + \ell^\pm + X$. Of course, X contains the neutrino but may also contain missing neutrals as well. The first question is, can we select events in which $w \to 1$ using this information alone? If we consider events for which *we hypothesize that* the missing (mass)^2 is M_X^2, then the energy of the B is determined up to a a two-fold ambiguity,

$$E_B = \frac{\Delta^2 E_{vis} \pm [\Delta^4 E_{vis}^2 - (E_{vis}^2 - \vec{p}_{vis}^{\,2}\cos^2\theta)(\Delta^4 + M_B^2 \vec{p}_{vis}^{\,2}\cos^2\theta)]^{1/2}}{(E_{vis}^2 - \vec{p}_{vis}^{\,2}\cos^2\theta)}, \tag{8}$$

where $(E_{vis}, \vec{p}_{vis}) = p_{vis}^\mu = p_D^\mu + p_\ell^\mu$ is the visible 4-momentum $(M_{vis}^2 = p_{vis}^2)$ and $\Delta^2 = \frac{1}{2}(M_B^2 + M_{vis}^2 - M_X^2)$.

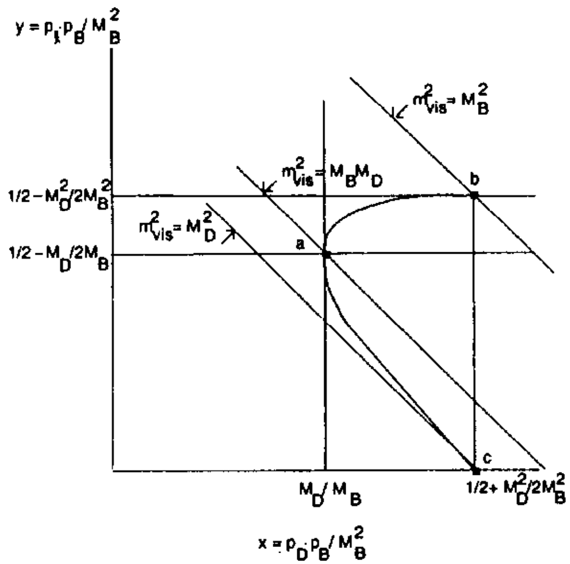

Figure 2: The phase space for $B \to D+\ell+\nu$ $(M_X^2 = 0)$ in the variables $x \sim E_D/M_B$, $y \sim E_\ell/M_B$. The phase space is bounded by the points (a) (ℓ and ν back-to-back), (b) (D and ℓ back-to-back), and (c) (D and ν back-to-back). The point (a) corresponds to $w = v_D \cdot v_B = 1$.

Here θ is the angle subtended by the flight vector of the B (primary to secondary vertex vector) and $\vec{p}_{vis}$. Let us now further assume $M_X = 0$ (no missing neutrals, etc.). To observe $w = v_D \cdot v_B = 1$ we must have in the B rest-frame, $M_B = M_D + 2E_\ell$, i.e., the massless leptons are back-to-back, whence

$$M_{vis}^2 = (p_D + p_\ell)^2 = M_D^2 + 2M_D E_\ell = M_D M_B \tag{9}$$

The condition $M_{vis}^2 = M_D M_B$, using,

$$0 = M_X^2 = (p_D + p_\ell - p_B)^2 \qquad \text{implies} \qquad x + y = \frac{1}{2}(1 + M_D/M_B), \tag{10}$$

which defines a line in the phase space of the decay Fig.(2) intersecting point (a). Unfortunately this line cuts accross the physical region (interior to (abc)) and does not uniquely select $w = 1$, while $M_{vis}^2 = M_D^2$ and $M_{vis}^2 = M_M^2$ do uniquely select points (b) and (c). Thus, for $w = 1$:

$$E_B = \frac{E_{vis}}{2}\left(\frac{M_B}{M_D} + 1\right) \pm \frac{|\vec{p}_{vis}|}{2}\left(\frac{M_B}{M_D} - 1\right) \tag{11}$$

Therefore, we see that we cannot uniquely reconstruct the Isgur–Wise point $w = 1$ from M_{vis}^2 alone. To uniquely reconstruct the kinematic point $w = 1$ using the information about the B decay alone we must have (i) $M_X^2 = 0$ (ii) $M_{vis}^2 = M_D M_B$, (iii) and $|\vec{p}_{vis}| = 0$. Note that for $|\vec{p}_{vis}| = 0$ the B-energy is determined uniquely as $E_B = \Delta^2/E_{vis}$.

P. Sphicas[5] has examined by Monte Carlo the fraction of (hypothetical) events for which the two-fold energy ambiguity of the B-meson is less than 10%. For $\sim 10^9$ decays he finds (few)$\times 10^3$ decays in which $\delta E_B/E_B < 10\%$. The slope of the Isgur–Wise function near $v \cdot v' = 1$ is $\xi'/\xi \sim -0.4$, thus a 10% precision in the B energy yields about an additional 4% uncertainty in the normalization, or about $\sim 6\%$ overall. With 10^{11} B's this would approach the desired limiting resolution.

How well does this do in excluding missing neutrals? If we allow $M_X^2 = m_\pi^2$, which occurs for a fast pion collinear to the neutrino, then one finds that the point (a) shifts by $\delta x_a \sim \delta y_a \sim O(m_\pi^2/M_B^2)$ (the points (b) and (c) shift by $O(m_\pi/M_B)$, which is easier to resolve). This is much less than the experimental momentum resolution, and is therefore problematic. However, the typical pion contribution is not collinear with the neutrino and $M_X^2 \sim m_\pi M_B$, whence $\delta x_a \sim \delta y_a \sim O(m_\pi/M_B) \sim 3\%$, and is marginally resolvable.

2.4 Kinematic Tagging with Daughter Pions?

Let me indulge here in a speculative proposal. Clearly we can sacrifice the huge statistics available at the hadron machine to achieve reasonable kinematic reconstruction for a (few)$\times 10^3$ events. However, we would prefer a method which is efficient, covers all of phase space, not just $\vec{p}_{vis} = 0$, and ideally which offers greater leverage in momentum resolution.

Perhaps we can exploit the fact that a fraction $f \sim 20\%$ of B-mesons will be produced as the daughters of the B^{**} resonance, together with the daughter pion. Thus, let us ask if we can select the B-meson energy in a typical process $B \to D^* + \ell + \nu$, where the two hypothetical 4-momenta of the B are $p_\mu^{(1)}$, $p_\mu^{(2)}$. We demand that we find a pion which matches a hypothetical solution for the B-meson 4-momentum, p_B, satisfying either:

$$(p_\pi + p_B^{(1)})^2 = M_{B^{**}}^2 \qquad \text{or} \qquad (p_\pi + p_B^{(2)})^2 = (M_{B^{**}} + \delta M_{B^{**}})^2 \tag{12}$$

where $\delta M_{B^{**}}$ is the width of the resonance parent. Then a difference between the hypothetical 4-momentum has a resolution given by the width:

$$p_\pi^\mu(p_B^{(1)} - p_B^{(2)}) = M_{B^{**}}\delta M_{B^{**}} = E_\pi\, \delta_r E_B\, (1 - (1 + \beta - \beta^2)\cos\theta) \tag{13}$$

where $\delta_r E_B$ is the *minimum resolvable B-energy*. Hence, apparently we can directly reconstruct the B energy by this method to a limiting resolution of only:

$$\frac{\delta_r E_B}{M_{B^{**}}} \sim \frac{\delta M_{B^{**}}}{E_\pi} \gtrsim 5\% \tag{14}$$

where we use $E_\pi \sim 1$ GeV, $\delta M_{B^{**}} \sim 50$ MeV, typically, and $\theta \approx 90^\circ$. On the other hand, we see in eq.(11) that, using $\vec{p}_{vis}$ the energy ambiguity is:

$$\delta E_B = |\vec{p}_{vis}|\left(\frac{M_B}{M_D} - 1\right). \tag{15}$$

Note that $|\vec{p}_{vis}|$ can be quite large; as we approach the Isgur-Wise point (a) in Fig.(2) and, taking for example the B rest-frame, we have $|\vec{p}_{vis}| \sim \frac{1}{2}(M_B - M_D)$. The value $\delta_r E_B$ is then sufficiently small to allow a selection between the two solutions, since:

$$\frac{\delta_r E_B}{\delta E_B} \sim \frac{M_{B^{**}} \delta M_{B^{**}}}{E_\pi |\vec{p}_{vis}|} \left(\frac{M_B}{M_D} - 1 \right)^{-1} \sim 10\% \tag{16}$$

using $|\vec{p}_{vis}| \sim \frac{1}{2}(M_B - M_D)$. In other words, the energy ambiguity can be $\sim 10\sigma$ of the minimum resolvable energy of the B-meson, using the daughter pion in combination.

Note that we are not then restricted to the special kinematic configurations $|\vec{p}_{vis}| = 0$; indeed, this approach would be complimentary to $|\vec{p}_{vis}| = 0$, and preferably requires that $|\vec{p}_{vis}|$ be large. It does rely on being able to "cut hard" to reduce the background pions that fake a B^{**} daughter, and it is subject to background fakes that favor the wrong solution. This probably favors low p_T B's with less of an enveloping jet structure, and then a $< \theta_{50\%}$ cut. Again, this cannot resolve the missing collinear pion ambiguity, but it is potentially able to resolve the typical missing neutral pion ambiguity. We have given here only a sketchy analysis of this. It requires serious study by Monte Carlo simulation, or direct application to the existing data of charm photoproduction experiments, and eventually in B decays where the B-momentum is known (all decay products visible). With $f \sim 10\%$ we may hope to be able to select between kinematic options with efficiencies of order 1%, allowing $\sim 10^7$ fully reconstructed semileptonic weak decays.

2.5 *Semileptonic Weak Decays involving V_{ub}*

High statistics measurements of exclusive semileptonic branching ratios such as $B \to \ell + \nu + (\overline{u}, (d, s))$, etc., are possible at the level of a (few)$\times 10^6$ decays. These are important processes to establish the general normalization of weak transitions involving V_{ub}. The statistical limitations together with theory imply better than a 3% determination of the quantity $f_B\sqrt{B}|V_{ub}|$ may be possible. The quantity $f_B\sqrt{B}$ is known poorly to about 20% precision, implying an overall determination of $V_{ub} \pm 20\%$.

Table II. Branching ratios estimated by rescaling charm analogues, assuming $|V_{bu}/V_{bc}| = 0.05$. The yields assume 33% $B^\pm$, 33% B^0, 18% B_s.

Mode	Br	yield/10^{10} B's	comment
$B \to \rho l \nu$ ($\rho \to \pi^+\pi^-$)	5.0×10^{-5}	1.5×10^5	$\star$ lattice
$B \to X_{charmless} l \nu$	2.5×10^{-4}	1.7×10^6	inclusive models
$B \to \omega l \nu$ ($\omega \to \pi^+\pi^-$)	1.0×10^{-6}	3.3×10^3	
$B \to \phi l \nu$ ($\phi \to K^+K^-$)	2.7×10^{-7}	8.3×10^2	
$B \to \pi l \nu$	3.0×10^{-5}	10^5	$\star$ chiral symmetry
$B \to \eta l \nu$ ($\eta \to \pi^+\pi^- e^+ e^-$)	1.0×10^{-7}	10^3	chiral symmetry
$B \to D_s(\pi, \rho, \omega)$	10^{-4}	10^6	Argus limit $\lesssim 1\%$
$B_s \to K l \nu$	3×10^{-5}	6×10^4	$\star$ yields $f_{B_s}/f_{B_{(u,d)}}$
$B_s \to K^* l \nu$	5×10^{-5}	10^5	$\propto f_{B_s}$

The present determinations of $|V_{ub}/V_{cb}|$ are based upon the endpoint of the lepton spectrum for inclusive semileptonic decay rates (see the S. Stone review in ref.[2]). There have been searches for the exclusive decay mode $B \to \rho \ell \nu$. On the $\Upsilon(4S)$ the measurement of E_ℓ near the endpoint where the background from $b \to c \ell \nu$ and continuum e^+e^- production becomes small in principle yields a determination of $|V_{ub}/V_{cb}|$, however it is subject to limitations from the knowledge of m_b and m_c, and is highly model dependent. The extracted V_{ub}/V_{cb} values range from 0.075 ± 0.008 for the ACM model to 0.101 ± 0.010 for the ISGW model.[2] The statistical errors are large. The exclusive decay mode $B \to \rho \ell \nu$ has been studied, with greater model dependence, lower statistics < 100 events and a larger scatter of $0.1 < |V_{ub}/V_{cb}| < 0.3$.

With a reasonable extrapolation to the SVX technology, and the copious yield of B's we can imagine rather conservative cuts allowing the study of final states such $X = \rho$, $X = \pi$, $X = \omega$, $X =$ many π's, etc. In the decay $B^- \to \rho \ell^- \nu$ and the subsequent $\rho \to \pi^+\pi^-$ ($P = 0.5$) we demand that the pions reconstruct to the ρ mass, and connect to the lepton at the decay vertex of the B. The estimated $Br(B^- \to \rho l^- \nu) \sim (Br(B^- \to D^* l^- \nu) \sim 4\%) \times |V_{bu}/V_{bc}|^2 \times 1/2 \sim 5.0 \times 10^{-5}$, thus with 10^{10} produced B's we will have $\sim 1.5 \times 10^5$ events. The problematic backgrounds are from $B \to D \ell \nu$ and $D \to 2\pi$ or $D \to \rho \pi^0$, with the π^0 undetected, $B \to \rho D$ and $D \to \ell \nu$. The ρ tends to be diluted by the pion background, which may require cutting on events in which the other B is seen in a semileptonic mode ($\sim 10\%$). The rejection of γ's and the mass reconstruction of the ρ, and a veto on more than 2 pions are important constraints to consider in fishing the ρ out of hadronic events.

Thus, a high statistics study of Cabibbo suppressed decay modes seems possible with 10^{10} B-mesons, but we are in a learning situation at present that must evolve considerably. This yields of order 10^5 decays. A form factor analysis may be possible for the $\pi \ell \nu$ mode if daughter pion kinematic tagging is possible, yielding $\sim 10^3$ fully reconstructed decays. One can hope to exploit the fact that chiral symmetry fixes the normalization of this matrix element at $w = 1$. It should certainly be possible to achieve V_{ub} to better than $\pm 20\%$ using models, and perhaps better precision by use of chiral symmetry. The quantity $f_{Bs}/f_{Bu,d}$ would be probed to $\pm 1\%$ precision.

2.6 *B_s and B_c*

The $B_s = (\bar{b}s)$ has been seen at ALEPH, OPAL and CDF.[12] CDF has observed 14 fully reconstructed $\psi\phi$ events, and reports a mass of $M_{B_s} = 5383 \pm 7$ MeV. With a yield of 10^{10} usable B's there are expected to be produced 1.8×10^9 $B_s + \overline{B}_s$. This will allow survey of various decay modes, such as DK^*, D^*K, $D_S^* D_S^*$, $D_S^* \ell \nu$, etc. Also, of great interest will be the study of higher resonances producing daughter K-mesons in association with the B_s, e.g.,

$$p\overline{p} \to B_u^{***}(2^-, 3^-) \to K + B_s \tag{17}$$

The prospects for the application of this to, e.g., flavor tagging for study of $B_s\overline{B}_s$ mixing, is discussed below.

Perhaps the most interesting new mesonic system will be the $B_c = (\bar{b}c)$. This is remarkable because we can say with certainty that non-relativistic potential models apply, and the spectrum is completely determined by those methods. Indeed, this is the true Hydrogen atom of QCD. Eichten and Quigg[13] have estimated the spectrum and widths of the B_c system. They use the Buchmüller-Tye potential as fit to the ψ and Υ systems (and use other potentials, e.g., the Cornell and Richardson potentials, for error estimation), finding:

$$M_{B_c} = 6258 \pm 20\ MeV \qquad M_{B_c^*} - M_{B_c} = 73 \pm 5\ MeV \tag{18}$$

The prospects for observation of B_c hinge upon the production cross-section. There is reasonable agreement amongst several groups[14] that the ratio $\sigma(B_c)/\sigma(\bar{b}b) \sim 10^{-3}$ Thus, for $|\eta| \leq 1$ and $p_t > 10$ GeV/c we have $\sigma(B_c) \sim 10^{-2}\ \mu b$, and a yield of $\sim 10^7$ B_c's for 10^{10} B's. Some of the principal detectable decay modes are listed in Table III.[12]

Table III. (a) Yields are for detectable decays and include the branching fractions $\psi \to \mu^+\mu^- \sim 7\%$ (b) includes $(\psi \to \mu^+\mu^-) \times (D_s^* \to \pi^+(\phi \to K^+K^-) \sim 2\%)$.

Mode	Br	yield/10^{10} B's	yield/100 pb^{-1}
$B_c \to \pi^+\psi$	4.0×10^{-3}	2.8×10^3 $^{(a)}$	276 $^{(a)}$
$B_c \to D_s^*\psi$	5.0×10^{-2}	7.0×10^2 $^{(b)}$	few $^{(b)}$
$B_c \to \psi\ell\nu$	10%	7.0×10^4 $^{(a)}$	

Note that the decay mode $B_c \to \psi\ell\nu$ is the B_c analogue of the $B_u \to D^*\ell\nu$ decay for which the Isgur-Wise function at $w = 1$ sets the normalization. Here the process is completely determined, and $w = 1$ involves only the overlap of the known ψ and B_c wave-functions. Thus, this is an interesting toy laboratory for the heavy quark symmetry methods where everything is perturbative. We should also mention that processes containing CP-violation, like $B_c \to D_s\phi$, involve both a direct short-distance penguin and interference terms with short-distance contributions to the imaginary parts. Here the factorization approximation is exact, and the short-distance imaginary parts are also in principle computable. Thus, CP-violation in the B_c system may ultimately prove to be a fundamental issue in the B-physics program. The B_c is a remarkable system in which much of the QCD dynamics is solvable by perturbative methods. It will thus provide a powerful laboratory for theorists and experimentalists, and possibly a probative system for new physics in the future.

2.7 *Heavy Baryons*

The spectroscopy and interactions of baryons consisting of two heavy quarks and one light quark simplify in the heavy quark mass limit, $m_Q \to \infty$. The heavy quarks are bound into a diquark whose radius r_{QQ} is much smaller than the typical length scale $1/\Lambda$ of QCD. In the limit $r_{QQ} \lesssim 1/\Lambda$ the heavy diquark has interactions with the light quark and other light degrees of freedom which are identical to those of a heavy antiquark. Hence as far as these light degrees of freedom are concerned, the diquark is nothing more than the pointlike, static, color antitriplet source of the confining color field in which they are bound, i.e., these QQq baryons are in a sense "dual" to heavy mesons $\overline{Q}q$.

The spectrum of QQq baryons is thus related to the spectrum of mesons containing a single heavy antiquark. The ground state is essentially a $(1, \frac{1}{2})$ or $(0, \frac{1}{2})$ heavy spin multiplet. The form factors describing the semileptonic decays of these objects may be directly related to the Isgur-Wise function, which arises in the semileptonic decay of heavy mesons. The production rates for baryons of the form ccq, bbq and bcq have been estimated in the approximation that the QQ diquark is formed first by perturbative QCD interactions, and then this system fragments to form the baryon like a heavy meson.[15] (In the cc system the heavy diquarks are not particularly small relative to $1/\Lambda$, so there may be sizeable corrections to these results). Essentially the fragmentation of a heavy quark Q into a QQq (or $QQ'q$) baryon factorizes into short-distance and long-distance contributions. The heavy quark first fragmentation into a heavy diquark may be trivially related to the fragmentation of Q into quarkonium $Q\overline{Q}$. This initial short distance fragmentation process is analogous to fragmentation into charmonium, $c \to \psi c$, which has been analyzed recently by Braaten, et al., and others[14,15] The subsequent fragmentation of the diquark QQ to a baryon is identical to the fragmentation of a $\overline{Q}$ to a meson $\overline{Q}q$.[15] Experimental data on production of heavy mesons can be used here.

The probability for $c \to \Sigma_{cc}, \Sigma_{cc}^*$ is estimated to be $\sim 2 \times 10^{-5}$, for $b \to \Lambda_{bc}$ to be $\sim 2 \times 10^{-5}$, and for $b \to \Sigma_{bc}, \Sigma_{bc}^*$ to be $\sim 3 \times 10^{-5}$. The probabilities for $b \to \Sigma_{bb}, \Sigma_{bb}^*$, $c \to \Lambda_{bc}$ and $c \to \Sigma_{bc}, \Sigma_{bc}^*$ are down by roughly $(m_c/m_b)^3$, or two orders of magnitude.

Table IV. Hadronically produced double heavy baryons for Tevatron (3×10^9 $B_{u,d}$'s) and Main Injector (3×10^{10} $B_{u,d}$'s).

Mode	Tevatron	Main Injector
$\Sigma_{cc}, \Sigma_{cc}^*$	6×10^4	6×10^5
Λ_{bc}	6×10^4	6×10^5
$\Sigma_{bc}, \Sigma_{bc}^*$	$\sim 10^5$	$\sim 10^6$
$\Sigma_{bb}, \Sigma_{bb}^*$	$\sim 10^3$	$\sim 10^4$
Λ_{bc}	6×10^2	6×10^3
$\Sigma_{bc}, \Sigma_{bc}^*$	6×10^2	6×10^3

Detection of these objects is probably very difficult at best. Consider the Σ_{bb} decay chain:

$$\begin{aligned} \Sigma_{bb} \quad \to \quad & D^* + X + (\Sigma_{bc} \\ & \to D^* + X + (\Lambda_b \\ & \quad \to D^* + X + (\Lambda_c \\ & \qquad \to K^* + X + \Lambda \end{aligned} \tag{19}$$

Each vertex above must be reconstructed, in spite of a high probability of missing neutrals, including the drift of $D^* \to D$'s away to branch vertices. A rough estimate is that a handful of such decay chains might be available in a 10^{10} program admitting reconstruction of the parent doubly-heavy baryon. However, there will come insights as to how to do this well as experience is gained.

3. RARE PROCESSES

In this section we will briefly discuss some of the interesting "rare" processes that are the far-reaching goals of the initiatives of this decade. Much greater detail is afforded these topics in other talks in this conference, so we will focus only on issues that involve some of the aforementioned ideas. Clearly the ultimate structure of CP-violation is of great interest, but the first observation of CP-violation in the B-system will be an achievement of enormous importance. We will comment as to how this observation may be feasible in the hadronic collider mode by making use of daughter pion flavor tagging, in comparison to the conventional strategy. Indeed, many of the tools necessary to see the CP-asymmetry in $B \to \psi K_S$ are now in place at CDF, and this exciting observation may be only a few years away!

We describe the important observation of $B_s\overline{B}_s$ mixing. This process will be quite a bit more difficult to observe than CP-violation. This is likely, given that the large top mass implies a large x_s, and mandates very high statistics for flavor tagged, and kinematically tagged B_s semileptonic decays. It may be a leap of faith to extrapolate to this process, given that there is limited experience with semileptonic decays of any B-system to date.

In conjunction with flavor tagging, our experience here is $O(\epsilon^2)$ at present. We will also discuss the rare leptonic modes. Here we have made extensive use of a presentation by S. Willenbrock and G. Valencia from our in-house workshop. Thus, the last subsection is really their effort, more than mine.

3.1 *CP violation*

There are well-known modes for the observation of CP-violation, such as $B^0 \to \psi\, K_S$, etc., and $B_s \to D_s^{\pm}\, K^{\mp}$, and self-tagging modes.[16] To observe CP-violation we must tag the flavor of the initial state, which taxes the available statistics. CP-violation with self-tagging modes is experimentally attractive, but there exists no guarantee that observable CP-effects will be present in these modes.[16] Since the volume of the Snowmass Proceedings is consumed with the intimate details of CP-violation in the B-system, we will simply focus on how one might use the conventional or daughter-meson tagging methods to observe the straightforward $B^0 \to \psi\, K_S$ CP-asymmetry.

The decay mode $(B^0,\ \overline{B}^0) \to \psi\, K_S$ involves CP-violation. Thus the partial widths for B^0 and $\overline{B}^0$ to decay into the $\psi\, K_S$ final state differ, and the time integrated asymmetry is defined as:

$$a = \frac{\Gamma(\overline{B} \to \psi K_S) - \Gamma(B \to \psi K_S)}{\Gamma(\overline{B} \to \psi K_S) + \Gamma(B \to \psi K_S)} = \frac{x_d}{1+x_d^2}\sin(2\beta) \sim 0.1\ -0.5 \qquad (20)$$

Note that the branching ratio for $B^0 \to K_S + (\psi \to \mu^+\mu^-)$ is $\sim 2\times 10^{-5}$ (including the 7% dimuon mode of ψ).

To observe a one must flavor-tag the neutral B-meson at production $t=0$ to determine if it is a particle or anti-particle. Since b-quarks are produced in pairs, this is conventionally achieved by observing the semileptonic decay mode of the other B in the event. For example, if the other meson is a B^- ($\overline{B}^+$) it can decay semileptonically to a charge $-$ ($+$) lepton, with a $Br(B \to \ell\nu D) \sim 10\%$. This does not require full reconstruction of the semileptonic decay, so for CP-violation one is effectively measuring $\Gamma(\ell^+\psi K_S) - \Gamma(\ell^-\psi K_S)$ (Note that this does not require a new single lepton trigger since one can trigger on the ψ dimuons). Including geometric efficiencies this conventional tagging efficiency is expected to be of order $\epsilon_1 \sim 10^{-2}$.

Gronau, Nippe and Rosner[3] have pointed out that resonance daughter pions (as well as rapidity correlations associated with the jet fragmentation) are possible flavor-tags. A stunning implication of the daughter mesons from parent resonances is that all CP-violating processes in hadron machines are expected to be self-tagging! We should recognize that at low-p_T the b-production mechanism is somewhat more akin to threshold production and the resonance mechanism may be favored. At higher p_T the b-jet is forming and there would be more pions expected (a source of dilution), and perhaps the rapidity correlation idea is favored. This is not to advocate any theory of production, but rather to emphasize that the optimization may involve tuning of p_T, etc. For example, we may prefer operating at low p_T's below the present cuts. While with optimization cuts it is possible that significant improvements in the tagging efficiency may occur, the charm photoproduction experiments suggest that a tagging efficiency of $\epsilon_2 \sim 10\%$ from daughter pions is possible. The flavor of a neutral $B^0 \sim \bar{b}d$ ($\overline{B}^0 \sim b\bar{d}$) is tagged by the presence of a π^+ (π^-) daughter, and the CP-asymmetry we measure in practice is effectively $\propto \Gamma(\pi^+\psi K_S) - \Gamma(\pi^-\psi K_S)$.

The overall efficiency for observing $B \to K_s(\psi \to \mu\mu)$ involves the physics branching ratio $\sim 2\times 10^{-5}$ times the detection efficiency (including geometric efficiencies). The latter is $\sim 3\%$ at the CDF SVX at present, and we assume it in Table IV. Thus, the overall efficiency for $B \to K_s(\psi \to \mu\mu)$ is $\sim 6\times 10^{-7}$, and, for 100 pb^{-1}, we expect 3×10^8 usable neutral B's, therefore ~ 180 ψK_s events. Larger η coverage, and other detector gains might boost this $\sim 5\times$.

Table V. Statistical significance σ_i for tagging efficiencies ϵ_1, ϵ_2 and asymmetries a, for various integrated luminosities. We show the 100 pb^{-1}, i.e., prospects for run I(b) at Fermilab (10^{10} B's corresponds to $\int \mathcal{L}dt = 10^3\ pb^{-1}$).

a	$\epsilon_2 - \epsilon_1$	$\int \mathcal{L}dt$	$\sigma_2 - \sigma_1$
0.5	0.1 − 0.01	100 pb^{-1}	2.1 − 0.7
0.1	0.1 − 0.01	100 pb^{-1}	0.4 − 0.13
0.5	0.1 − 0.01	10^3 pb^{-1}	6.7 − 2.1
0.1	0.1 − 0.01	10^3 pb^{-1}	1.3 − 0.4
0.5	0.1 − 0.01	10^4 pb^{-1}	21.2 − 6.6
0.1	0.1 − 0.01	10^4 pb^{-1}	4.1 − 1.3

The prospects for observing the CP-asymmetry at a statistical deviation σ are indicated in Table V. Significant limits on CP-violation in the B system will begin to be placed by end of run I. In the best case, $a = 0.5$ we can begin to see a signal with the conventional semileptonic tagging efficiency, $\epsilon = 0.01$, for 10^{10} produced B's, or with the daughter pion tagging $\epsilon_2 = 0.1$ and the larger asymmetry a discovery is likely. We note that the $\bar{p}p$ collision mode is charge symmetric, while pp is not, and this suppresses a fake CP background in daughter pion tagged neutral B's which contributes to a. This background is expected not to exceed $\sim 4\%$ at the SSC in ψK_S, which is tolerable, but potentially problematic in other modes (Note that a charge asymmetric detector can give a background in the $\bar{p}p$ mode). Evidently a discovery is assured for $> 10^{11}$ B's with daughter pion tagging.

3.2 *$B_s\overline{B}_s$ Mixing*

We have for the mixing parameter:

$$\begin{aligned} x_s &= \frac{G_F^2 m_{B_s}\tau_{B_s}}{6\pi^2} B_s f_{B_s}^2 \eta_B |V_{ts}^* V_{tb}|^2 m_t^2 F(m_t/M_W) \\ &\approx \Delta M_{B\overline{B}}/\Gamma \sim (14\pm 6)(f_{B_s}/200\ MeV)^2 \qquad (21) \end{aligned}$$

where $F(z)$ is an Inami-Lim function. An expression for x_d is gotten by replacing s by d everywhere. Note that:

$$\frac{x_s}{x_d} = \left|\frac{V_{ts}}{V_{td}}\right|^2 (1+\delta) \qquad \delta = \left(\frac{m_{B_s} f_{B_s}^2}{m_{B_d} f_{B_d}^2} - 1\right) \sim 0.2 \qquad (22)$$

x_s is very sensitive to m_{top} and we find:

$$\begin{aligned} x_s &\sim 8.0 \leftrightarrow 18.0, \qquad m_t = 140\ GeV;\ \sqrt{B} f_B = 200\ MeV \qquad (23) \\ x_s &\sim 17.0 \leftrightarrow 40.0, \qquad m_t = 200\ GeV;\ \sqrt{B} f_B = 220\ MeV \end{aligned}$$

and we must prepare ourselves for the possibility of large x_s, $8 \lesssim x_s \lesssim 40$. For large values the system oscillates many times per decay length ($x = \frac{1}{2}$(radians)/(e-attenuation), thus $x = 10$ corresponds to 20 radians per decay length). This requires observing the time evolution of the system, which implies that fully reconstructed (energy and flavor), tagged B_s decays are necessary. In contrast, $x_d = 0.66$ and is readily observed in time–integrated measurements. These requirements make the observation of $B_s\overline{B}_s$ mixing more challenging than the observation of CP–violation! However, it should be emphasized that this important phenomenon is likely to be the exclusive province of hadron collider experiments because of the large statistical requirements.

The key to observing oscillations is achieving the smallest proper time resolution, σ_t (for a good schematic discussion of this see Mike Gold in ref.(1); we also thank John Skarha for discussions on this topic). σ_t is composed of the beam-spot resolution $\delta L_{xy}/L_{xy}$ where L_{xy} is the transverse path length (this is the dominant contribution), together with the momentum resolution $\delta p_T/p_T$ as:

$$\sigma_t = \left((\delta L_{xy}/L_{xy})^2 + (\delta p_T/p_T)^2\right)^{\frac{1}{2}} \tag{24}$$

With $\delta_{xy} \sim 40\ \mu m$, $L_{xy} \sim 600\ \mu m$, we find $\sigma_t \sim 0.07$ characteristic of CDF-SVX.

The conventional triggers would use a produced $B_s \rightarrow l\nu(D_s \rightarrow \phi X)$ or $B_s \rightarrow \pi^+\pi^-\pi^+(D_s \rightarrow \phi X)$ and the opposite $B \rightarrow l\nu X$ for flavor tagging. By fully reconstructing the B_s decay (requiring exclusively charged particles in X) and partially reconstructing the tagging decay, it has been estimated that one can reconstruct the oscillation in τ with ~ 4000 events.[1] With the estimated efficiencies this requires about 3×10^{10} to 10^{11} produced B's. This appears to be a significant challenge!

Can we tag the B_s flavor and kinematics by using the daughter K mesons associated with it's resonance production? For example, we expect the D-wave $B(2^-)$ and $B(3^-)$ to be above threshold for decay to $K^+ + B_s$ or $K^- + \overline{B}_s$. These resonances are estimated to be broad (250 to 400 MeV), but with a decay fraction to B_s and B_s^* of about 30%. Thus, with the favorable production and branching fractions we may have a flavor tag for B_s, but a kinematic tag seems less likely. The charm system process $D_s^{**} \rightarrow D^*K$ has been demonstrated,[5] which is the opposite to $D^{***} \rightarrow D_sK$, The higher resonances have not yet been seen.

3.3 Some Other Rare Modes

Length considerations preclude our giving any comprehensive discussion of the additional interesting rare modes in B-physics. We will, however, briefly mention a few of the leptonic modes. Rare B decays encompass such processes as:

$$\begin{array}{llll} (I) & B_{d,s} & \rightarrow & (e\overline{e},\ \mu\overline{\mu},\ \tau\overline{\tau}) \\ (II) & B_{d,s} & \rightarrow & (e\overline{\mu},\ \mu\overline{\tau},\ e\overline{\tau}) \end{array} \tag{25}$$

and additional hadrons in the final state may be included. We should remark that the τ containing final states are unique to B, never available in K decays, and at best phase space suppressed for D's.

Such processes as (I) have low standard model rates and are probes of V_{td}, V_{ts}, and m_t. Thus, they are good probes of the standard model if they are seen at the expected rates. Moreover, they are excellent probes of new physics, such as charged Higgs and flavor changing neutral Higgs couplings, which are generally $\propto$ mass. The conventional SM estimates are as follows:

Table VI. Rare leptonic mode branching ratios.

	$\tau\overline{\tau}$	$\mu\overline{\mu}$	$e\overline{e}$
Br($B_s \rightarrow$)	10^{-7}	10^{-9}	10^{-14}
Br($B_d \rightarrow$)	5.0×10^{-9}	5.0×10^{-11}	5.0×10^{-16}

A crude estimate of the background due to Valencia and Willenbrock is as follows. UA1 has measured the continuum μ-pair background cross-section near the B-mass, $M^2_{\mu^+\mu^-} = M^2_B$ with momentum resolution $\delta p \sim 100$ MeV to be $\sigma(\mu^+\mu^-) \sim 10^{-5}\sigma_B$, where σ_B is the hadronic B cross-section. This can presumably be reduced to $\sigma(\mu^+\mu^-) \sim 10^{-6}\sigma_B$ with improved momentum resolution from silicon vertex detectors. The probability that two stray muons make a vertex is geometrically $\sim 10^{-2}$ and the probability that this yields a momentum vector pointing toward the primary vertex is $\sim 10^{-2}$. Thus we have an overall background approaching $\sim 10^{-10}\sigma_B$ and a 3-σ B_s-peak is therefore possible. With a yield of 10^{11} B's we expect therefore ~ 30 events from $B_s \rightarrow \mu\overline{\mu}$. Since the signature is a clean displaced muon pair event with mass reconstruction, it is likely that this can be searched over a rapidity range of $|\eta| \lesssim 3$, and a p_t threshold of $O(5)$ GeV/c.

Valencia and Willenbrock (VW) have given a nice characterization of the lepton-number violating processes (class II, above) which we describe here. First, note that (τ e) and (τ μ) are unique to the B-system (not available in rare K decays). Since such processes can be generated in principle by Higgs-scalar exchange, which is a coupling constant $\propto$ mass, it is possible that the B system becomes sensitive to these processes at a level that is readily experimentally accessible, and complimentary to rare K decay searches, such as at KTEV.

VW begin by postulating general four–fermion interactions describing such processes as $B \rightarrow e\mu$ and $K \rightarrow e\mu$ as:

$$c_B(\overline{s}\Gamma d\ \overline{\mu}\Gamma e) + c_K(\overline{b}\Gamma s\ \overline{\mu}\Gamma e) \tag{26}$$

with arbitray Dirac structures Γ. VW then consider the effects of different Γ's and c_X's on the ratio of branching ratios $R_1 = Br(B \rightarrow \mu e)/Br(K_L \rightarrow \mu e)$ and $R_2 = Br(B \rightarrow \mu e + h)/Br(K_L \rightarrow \mu e + h)$ (where h is an extra hadron system, e.g., pions) as follows:

$$\begin{array}{lllll} R_1 & \approx & \dfrac{c_B^2 f_B^2}{c_K^2 f_K^2}\left(\dfrac{m_B\tau_B}{m_K\tau_K}\right) \approx 10^{-4}\dfrac{c_B^2}{c_K^2} & & \Gamma = (\gamma_\mu, \gamma_\mu\gamma^5) \\ R_1 & \approx & \dfrac{c_B^2 f_B^2}{c_K^2 f_K^2}\left(\dfrac{m_B^3\tau_B}{m_K^3\tau_K}\right) \approx 10^{-2}\dfrac{c_B^2}{c_K^2} & & \Gamma = (1, \gamma^5) \\ R_2 & \approx & \dfrac{c_B^2 f_B^2}{c_K^2 f_K^2}\left(\dfrac{m_B^5\tau_B}{m_K^5\tau_K}\right) \approx \dfrac{c_B^2}{c_K^2} & & \end{array} \tag{27}$$

Thus, to proceed we need input as to the magnitude of the ratio c_B/c_K. VW distinguish three cases: (i) (Current-like) $c_B/c_K \sim 1$ (ii) (Higgs-like) $c_B/c_K \sim m_B/m_K \sim 10^1$ (iii) (Box-like) $c_B/c_K \sim V_{tb}V_{ts}/V_{td}V_{ts} \sim 10^2$. The latter "box-like" result assumes that the process is induced via a top quark containing box diagram. Thus, we have the following table:

Table VII. Valencia and Willenbrock's characterization of lepton-number violating modes of B and K.

$Br(B \to X)/Br(K \to X)$	Current-like	Higgs-like	Box-like
$\Gamma = (\gamma_\mu, \gamma_\mu\gamma^5)$; $X = e\mu$	$\sim 10^{-4}$	$\sim 10^{-2}$	~ 1
$\Gamma = (1, \gamma^5)$; $X = e\mu$	10^{-2}	1	10^2
Any Γ; $X = e\mu + h$	1	10^2	10^4

Thus, in the "box-like" and "Higgs-like" limits the B system maybe a better probe than the K system for new physics. The VW characterization is general, and covers all possible models. It illustrates the possibility that B decays are sensitive to new physics in a manner complimentary to rare K's.

4. SUMMARY

A program of producing $> 10^{10}$ detectable B's is conservatively achievable within this decade. This offers an excellent conventional physics program of $\sim 10^9$ $B \to D^*\ell\nu$ decays and $\sim 10^5$ $B \to \rho\ell\nu$ decays, allowing a determination of $V_{cb} \pm 3\%$ and $V_{ub} \pm 20\%$. This also probes the quantities such as $\sqrt{B} f_B$ and f_{B_s} with high statistics.

The resonances of the B-system and the prospects for flavor and kinematic tagging will emerge within the next few years. New states such as B_c will be surveyed, and the list of B_s and B_c decay modes will grow. CP-violation with conventional or bachelor pion tagging may be first observed in the ψK_S asymmetry within such a 10^{10} program. $B_s\overline{B}_s$ mixing looks difficult, though $x_s \lesssim 20$ may be probed. Rare and radiative decays will be subject to their first probative examination.

In conclusion, we have seen that B-physics based in a hadron collider offers a rich and diverse, unique and powerful scientific program. It can peacefully coexist with a high-p_T program and dominate the post-high-p_T era at such facilities as Fermilab. Indeed, the prospects for observation of CP-violation in the $p\bar{p}$ collider environment are great. There are, in fact, advantages of the charge-symmetric $p\bar{p}$ mode over pp in the observation of CP-violation. A dedicated B-physics program at Fermilab is important to the evolution of the world-wide effort and a healthy base program for at least the next ten years and probably beyond.

5. ACKNOWLEDGEMENTS

This work was performed at the Fermi National Accelerator Laboratory, which is operated by Universities Research Association, Inc., under contract DE-AC02-76CH03000 with the U.S. Department of Energy. Much of it has been influenced strongly by an in-house B-physics working group at Fermilab which we convened in March '93, and which met approximately weekly throughout the spring. I wish to thank CDF and D0 experimentalists, in particular Fritz DeJongh, Dan Green, Jim Mueller, John Skarha, Paris Sphicas, and especially Tom LeCompte, who were active contributors in this group. Also, I wish to thank my theoretical colleagues, I. Dunietz, E. Eichten, R. Ellis, A. Kronfeld, C. Quigg, J. Rosner, J. Soares, G. Valencia and S. Willenbrock for numerous contributions and discussions. I also thank A. Yagil and S. Stone for several useful discussions and C. Quigg for proof-reading an earlier version. This view of a B-physics program was subsequently presented to the Fermilab PAC. My present talk is essentially that sketch, embellished with a lot of personal biases.

6. REFERENCES

1. "B Physics at Hadron Accelerators," *4th Workshop in a FNAL/SSCL Series* Fermilab, ed. J. Appel, November (1992)

2. "B Decays," ed. S. Stone, World Scientific (1992); see also, D. Besson, "B Weak Decays from Threshold Experiments," *XVI Int'l. Symposium on Lepton-Photon Interactions*, (Cornell U.), (Aug. 1993).

3. M. Gronau, A. Nippe, and J. Rosner, *Phys. Rev.* **D47**, 1988 (1993);
L. Randall and E. Sather, "The Rate for $B\overline{B}$ Production Accompanied by a Single Pion," MIT-CTP-2214, May (1993);
M. Gronau, and J. Rosner, "Identification of Neutral B Mesons Using Correlated Hadrons" TECHNION-PH-93-32, EFI 93-41 (1993);
Tom LeCompte, (private communication); see also ref.(8).

4. P. Nason, S. Dawson, R. K. Ellis, *Nucl. Phys.* **B303** 607 (1988); ibid., **B327** 49 (1988);
W. Beenakker, H. Kuijf, W. L. Van Neerven and J. Smith, *Phys. Rev* **D40** 54 (1989);
W. Beenakker, W. L. Van Neerven, R. Meng, G. Schuler and J. Smith, *Nucl. Phys.* **B351** 507 (1991);
A. D. Martin, R. G. Roberts, W. J. Stirling, *Phys. Lett.* **B306**, 145 (1993); erratum, ibid., **B309**, 492 (1993)
E. Berger and R. Meng, *Phys. Rev* **D46** 169 (1992); see also ibid., "Bottom Quark Cross Sections at Collider and Fixed-Target Energies at the SSC and LHC" CERN-TH.6987/93.

5. I thank Paris Sphicas (M.I.T. and CDF) for discussing his preliminary Monte Carlo studies of this.

6. ARGUS Collaboration: H. Albrecht et al. *Phys. Lett.* **B221**, 422 (1989); **B232**, 398 (1989); **B231**, 208 (1989); **B230**, 162 (1989); **B297**, 425 (1989).
E-691, Tagged Photon Spectrometer Collaboration: J. C. Anjos et.al. *Phys. Rev. Lett.* **62**, 1717 (1989).
CLEO Collaboration: P. Avery, et al. *Phys. Rev* **D41** 774 (1990); *Phys. Lett.* **B303** 377 (1993);
E-687 Collaboration: P.L. Frabetti, et.al., "Measurement of the Masses and Widths of $L = 1$ Charm Mesons," FERMILAB-Pub-93/249-E, (1993); Joel Butler (private communication); S. Shukla, (private communication).

7. E. Eichten and F. Feinberg, *Phys.Rev.* **D23**, 2724 (1981);
M. Suzuki, *Nucl. Phys.* **B258** 553 (1985).
M.B. Voloshin and M.A. Shifman, Yad. Fiz. **45**, 463 (1987) [Sov. J. Nucl. Phys. **45**, 292 (1987)]; **47**, 801 (1988) [**47**, 511 (1988)].
N. Isgur and M.B. Wise, Phys. Lett. **B 232**, 113 (1989); **B 237**, 527 (1990), Nucl. Phys. **B 348**, 276 (1991).
E. Eichten and B. Hill, Phys. Lett. B **234**, 511 (1990); **243**, 427 (1990).

8. E. Eichten, C. T. Hill, and C. Quigg, "Properties of Orbitally Excited Heavy-Light Mesons," FERMILAB-Pub-93/255-T (1993); C. Quigg, in these proceedings.

S. Godfrey, R. Kokoski, *Phys.Rev.* **D43**, 1679 (1991);
W. Kwong and J. Rosner, *Phys.Rev.* **D44**, 212 (1991).

9. A. Falk, M. Luke. *Phys. Lett.* **B292**, 119 (1992);
W. A. Bardeen and C. T. Hill, "Chiral dynamics and heavy quark symmetry in a solvable toy field-theoretic model," Superconducting Super Collider Laboratory preprint SSCL-PP-243 (1993, to appear Phys. Rev. D).

10. M. Neubert, Phys. Lett. B **264,** 455 (1991); P. Cho, B. Grinstein, Phys. Lett. B **285,** 153 (1992).

11. N. Isgur, D. Scora, B. Grinstein, M. Wise, *Phys. Rev* **D39** 799 (1989).
G. Altarelli, N. Cabibbo, G. Corbo, L. Maiani, *Nucl. Phys.* **B207** 1 (1990);
see S. Stone in ref.[2] for a comprehensive review.

12. CDF Collaboration: F. Abe, et al., Fermilab-Pub-93/141-E (1993) [5383.3 $\pm$ 4.5 $\pm$ 5.0 MeV]; ALEPH Collaboration: D. Buskulic et al., CERN-PPE/93-97 (1993) [5368.6 $\pm$ 5.6 $\pm$ 1.5 MeV]; OPAL Collaboration: P. Acton et al., *Phys. Lett.* **B295**, 357 (1992).

13. E. Eichten, C. Quigg, (in preparation); see C. Quigg in these proceedings.

14. M. Lusignoli, M. Masetti, S. Petrarca, *Phys. Lett.* **B266** 142 (1991); C.-H. Chang, Y.-Q. Chen, *Phys. Lett.* **B284** 127 (1992) and *Phys. Rev.* **D46** 3845 (1992); E. Braaten, K. Cheung and T.C. Yuan, NUHEP-TH-93-2,UCD-93-1, and "QCD Fragmentation Functions for B_c and B_c^* Production," NUHEP-TH-93-6,UCD-93-9 (1993).

15. see, e.g., A. F.Falk, M. Luke, M. Savage, M. B. Wise, "Baryons Containing Two Heavy Quarks," UCSD/PTH 93-11, CALT-68-1868, SLAC-PUB-6226 (1993).

16. I. Dunietz, "CP-Violation in $b \to \bar{c}c$ Without Tagging," Fermilab-Pub-93/089-T (1993).

17. G. Valencia and S. Willenbrock (private communications and working–group presentation).

SECONDARY PARTICLE BACKGROUND LEVELS AND EFFECTS ON DETECTORS AT FUTURE HADRON COLLIDERS

TRIVAN PAL
Physics Research Division,
Superconducting Super Collider Laboratory, 2550 Beckleymeade Avenue*
Dallas, Texas 75237

1. INTRODUCTION

The next generation of hadron colliders, the Superconducting Super Collider (SSC) and the Large Hadron Collider (LHC), will operate at high center-of-mass energies and luminosities. Namely, for the SSC (LHC) $\sqrt{s} = 40$ TeV ($\sqrt{s} = 16$ TeV) and $\mathcal{L} = 10^{33}$ cm^{-2}s^{-1} ($\mathcal{L} = 3 \times 10^{34}$ cm^{-2}s^{-1}). These conditions will result in the production of large backgrounds as well as radiation environments. Ascertaining the backgrounds, in terms of the production of secondary charged and neutral particles, and the radiation environments are important considerations for the detectors proposed for these colliders. An initial investigation of the radiation levels in the SSC detectors was undertaken by D. Groom and colleagues, in the context of the "task force on radiation levels in the SSC interaction regions."[1] The method consisted essentially of an analytic approach, using standard descriptions of average events in conjunction with simulations of secondary processes.

Following Groom's work, extensive Monte Carlo simulations were performed to address the issues of backgrounds and radiation environments for the GEM[2] and SDC[3] experiments proposed at the SSC, and for the ATLAS[4] and CMS[5] experiments planned for the LHC. The purpose of the present article is to give a brief summary of some aspects of the methods, assumptions, and calculations performed to date (principally for the SSC detectors), and to stress the relevance of such calculations to the detectors proposed for the study of B-physics in particular.

At the SSC, the GEM and SDC experiments will be located in the interaction regions (IRs), where the beam optics will provide a high value of the luminosity and hence small β^*. In these regions, the dominant source of background is due to the p-p collisions themselves. The interaction rate will be approximately 10^8 Hz, corresponding to the nominal luminosity of $\mathcal{L} = 10^{33}$ cm^{-2}s^{-1}. There also exist other, smaller sources of backgrounds arising from beam-gas collisions in the vacuum pipe and beam losses in the collider lattice elements. In contrast to the above, IRs are also foreseen that will have larger free space for the experiments (for example, detectors for B-physics). However, the corresponding beam optics will result in higher values of β^* and lower luminosity.[6]

*Operated by the Universities Research Association, Inc., for the U.S. Department of Energy under Contract No. DE-AC35-89ER40486.

2. SYNOPSIS OF THE ANALYTIC APPROACH

Various processes contribute to the charged and neutral particle backgrounds and the radiation levels in the experimental apparatus. The following were considered by the task force:[7] the minimum ionizing particles (MIPs) produced in the p-p collisions; photon conversions; electromagnetic and hadronic showers in the calorimeters; and albedo particles (mostly neutrons and photons) from the showers induced in the calorimeters. We note that there are other considerations to incorporate, and these are described in the next section.

2.1 *Particle Production Characteristics*

The p-p interaction cross sections have been measured as a function of $\sqrt{s}$ (Figure 1) at lower energies and extrapolated to the energies of interest to us. The cross sections have also been calculated using QCD, and are subject to theoretical uncertainties arising from, for example, the parametrization of the parton distributions (i.e., structure functions). It has been assumed that 1/4 of the total cross section is elastic and 3/4 of the total cross section has been assigned to the inelastic cross section (including diffractive processes). Thus, at the SSC and LHC the values assumed are: $\sigma_{\rm inel} = 100$ mb and 84 mb, respectively.

The distribution of charged particles produced in an inelastic p-p interaction is described as a function of the pseudorapidity (η) of the particle. The pseudorapidity is defined as $\eta = -\ln(\tan\theta/2)$, where θ is the polar angle of the particle with respect to the beam axis. Figure 2 shows the differential distribution ($dN/d\eta$) obtained using the DTUJET Monte Carlo[8] for p-p collisions at $\sqrt{s} = 40$ TeV. The Monte Carlo is based on the dual parton model and incorporates both soft and hard transverse momentum processes. The distribution in Figure 2 is approximately constant over the "central rapidity plateau." This is referred to as the "height" (H) of the rapidity plateau. The dip in the distribution at $\eta = 0$ is due to a kinematical effect.

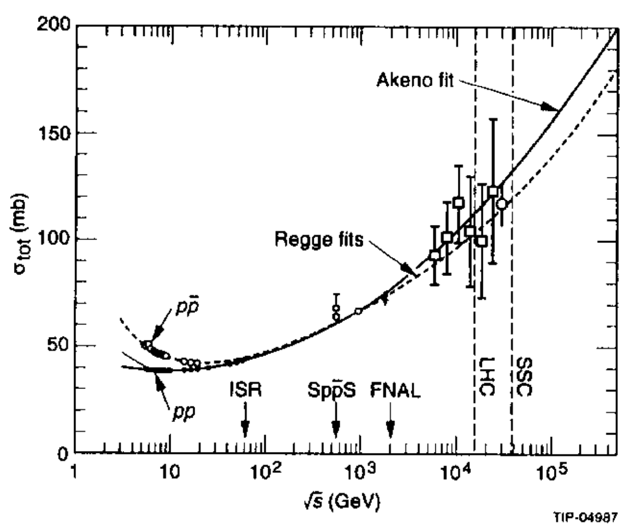

Figure 1. Data points and extrapolations to higher energies of the p-p and $\bar{p}$-p total cross sections (Reference 9).

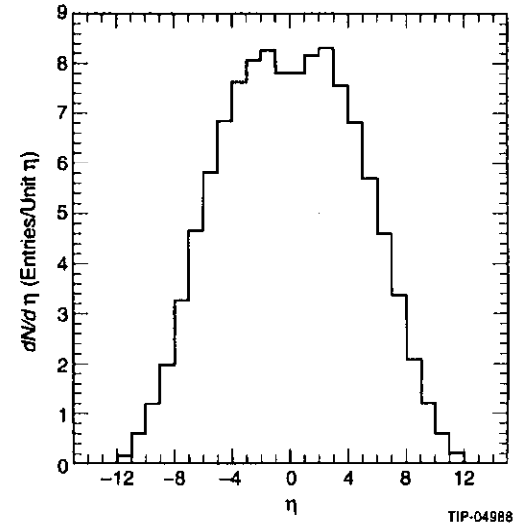

Figure 2. Distribution of charged particles as a function of the pseudorapidity, η, obtained by the DTUJET Monte Carlo. The central rapidity plateau corresponds to ~ 7.5 charged particles per unit rapidity, for p-p interactions at $\sqrt{s} = 40$ TeV.

The mean charged particle multiplicity as a function of $\sqrt{s}$ is shown in Figure 3. The lower energy data have been obtained from the ISR, Sp$\bar{p}$S, and FNAL, and extrapolated to higher energies.[9] The value for H per unit η is 6.2 at the LHC and 7.5 at the SSC. It is observed that the momentum (p) distribution for a given value of η is an η-independent function of the transverse momentum (p_t). The studies of the task force suggest that radiation levels scale as $\langle p_t \rangle^\alpha$, where $\alpha \lesssim 1$. Furthermore, in the analytic approach the approximation $f(p_t) = \delta(p_t - \langle p_t \rangle)$ was used, which is estimated to result in a systematic error of $\sim 6\%$.[7] The (dN/dp_t) distribution for the charged particles produced in p-p collisions at $\sqrt{s} = 40$ TeV is shown in Figure 4, with $\langle p_t \rangle \sim 0.6$ GeV; whereas at LHC, $\langle p_t \rangle \sim 0.55$ GeV.

Figure 5 shows the cumulative energy fraction emitted from the interaction point (IP) as a function of η. The figure indicates typical intervals in pseudorapidity covered by the different components of the experimental apparatus, i.e., the tracking region, the barrel and end-cap regions of the calorimeter, the forward calorimeter region, and the regions of the low-beta quadrupoles, including their shielding.

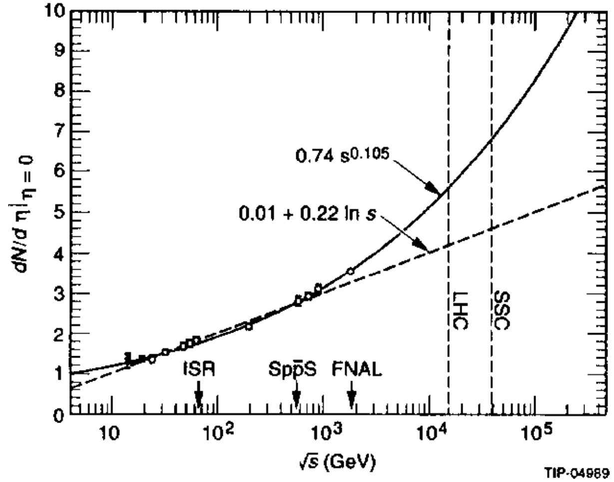

Figure 3. Evolution of the number of charged particles per unit rapidity as a function of the center-of-mass energy (Reference 9).

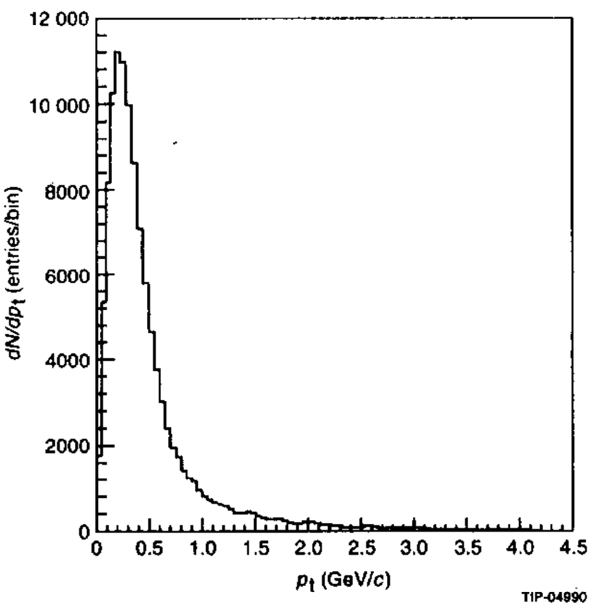

Figure 4. p_t distribution of charged particles obtained using the DTUJET Monte Carlo, for p-p interactions at $\sqrt{s} = 40$ TeV. Average p_t is approximately 0.6 GeV/c.

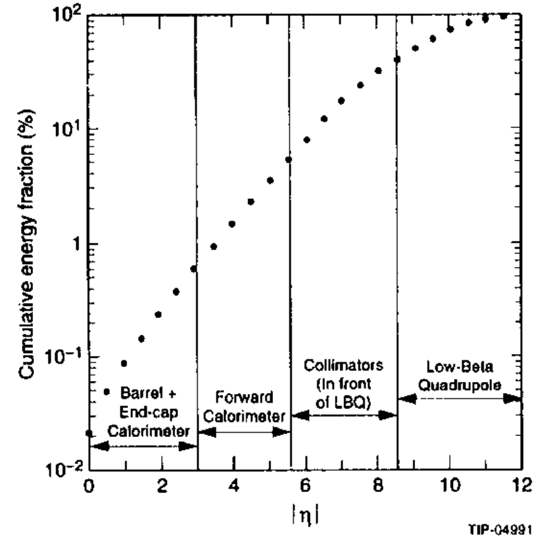

Figure 5. Cumulative energy fraction emitted from the p-p interactions at $\sqrt{s} = 40$ TeV, as a function of the pseudorapidity. Regions covered by the various detector elements are also indicated.

2.2 *Quantitative Parametrizations*

2.2.1 *Charged Particle Flux*

The charged particle flux in a unit area, A, perpendicular to the radius vector from the IP, with a polar angle θ with respect to the beam line, is given by:

$$\begin{aligned}\frac{dN}{dA} &= \left(\frac{dN}{d\eta}\right)\left(\frac{d\eta}{d\Omega}\right)\left(\frac{d\Omega}{dA}\right)\\ &= H \times \left(\frac{1}{2\pi\sin^2\theta}\right) \times \left(\frac{1}{r^2}\right)\\ &= \frac{H}{2\pi r_\perp^2}, \qquad (1)\end{aligned}$$

where $d\Omega = 2\pi\sin\theta d\theta$ is the solid angle (after integration over the azimuthal angle), and $r_\perp = r\sin\theta$ is the perpendicular distance from the beam line.

2.2.2 *Dose Rate*

The dose rate is obtained from Eq. (1):

$$\text{Dose rate} = \frac{H \times \mathcal{L} \times \sigma_{\text{inel}}}{2\pi r_\perp^2} \times \left(\frac{dE}{dx}\right), \qquad (2)$$

where $\mathcal{L} \times \sigma_{\text{inel}}$ is the event rate, and dE/dx is the usual energy loss of a particle as it goes through a thin absorber. Note that this expression does not include the effects due to secondary interactions and photon conversions, nor low-momentum particles ascribing loops in the presence of the solenoidal magnetic fields in the tracking volume of the detectors. These effects will increase the flux, typically by a factor of two.

2.2.3 Parametrization for Cascades

A derivation of the ionizing dose and fluence of neutrons in a cascade process is given in Reference 9. The essential steps of the argument are as follows: from Eq. (1) and since the mean energy ($E \approx p$) of a particle at polar angle θ is $E \approx p = p_t/\sin\theta$, then the energy flow in the solid angle $d\Omega \propto 1/\sin^3\theta$, and thus the energy flow in a unit area, $dE/dA \propto 1/r^2\sin^3\theta$. Thus, one can write:

$$\text{Dose or Fluence} = \frac{C}{r^2\sin^{2+\alpha}\theta} \equiv \frac{A}{r^2}\cosh^{2+\alpha}\eta, \tag{3}$$

where C is an appropriate variable used to scale the above quantities for different colliders: $C \propto \sigma_{\text{inel}} \times \mathcal{L}_{\text{ave}} \times H \times \langle p_t\rangle^\alpha$. Note that $\mathcal{L}_{\text{ave}}$ is an average luminosity over the canonical 10^7 sec assumed to be the operation time for the colliders per calendar year. From the experimental data and Monte Carlo simulations, it is observed that α is in the range of $0.5 \leq \alpha < 1$.

2.2.4 Reflections in a Cavity

For the tracking detectors that are contained within the cavity of the calorimeters, the flux of backscattered neutrons (and photons) is an important consideration. A derivation of this albedo flux (Φ) in terms of the characteristic radius (R) of the cavity, and the average number of reflections that the neutrons undergo (A) are given in Reference 7:

$$\Phi = \frac{N}{\pi R^2}(1 + A), \tag{4}$$

where N represents the number of neutrons "injected" in the cavity. The simulation studies suggest that $(1 + A) \approx 2$ for spherical calorimeters. For neutrons, this represents the number of reflections before absorption, or degradation in energy, such that it will not damage the material (e.g., silicon for the tracker).

3. NUMERICAL TECHNIQUES

In addition to the considerations of the preceding section, we have ascertained from the extensive Monte Carlo simulations performed that the details concerning the geometry and material composition of the detector halls and the collider tunnel are also important to include. Likewise, it has been quantified by the results of the simulations that the details of the low-beta quadrupoles (LBQs) and the collimators designed to protect them (from the impinging particles produced at the IP) are rather crucial to implement, in order to predict accurately the backgrounds at various locations.

In the following sections a brief description is given of the processes involved leading to secondary particle production and radioactivation. Likewise, a summary of the various Monte Carlo codes employed to estimate the particle fluences and activity, as well as the shielding requirements, is also given.

3.1 Summary of the Mechanisms

Each high-energy particle interacting with a nucleus may be absorbed or may dislodge some nucleons out of the struck nucleus. In this process, additional high-energy particles can also be created. If the resulting nucleus is excited, it will de-excite by "boiling off" neutrons, also referred to as "evaporation neutrons." The nuclear reaction above is called a "star" due to the numerous particles radiating from it.

The various cross sections for producing specific nuclides depend on the target nucleus as well as on the energy and species of the incident particle. These cross sections are determined from experimental data, or else empirical formulae are employed to approximate the cross sections over orders of magnitude. Further details can be found in Reference 10. Similarly, to calculate the radioactivity, it is required to have radiological data, such as nuclear lifetimes, decay schemes, transport of β's and γ's out of the activated object (i.e., self-shielding considerations), and conversion factors that will convert the particle flux to dose.

For the Monte Carlo calculations, one has to be careful in the interpretation of the results, since these codes have low-energy cutoffs below which the particles are not followed. Depending on the cutoff, it may be higher than the thresholds of certain activation reactions. Thus, using the flux or the star density calculated by Monte Carlo would result in a lower value for the activation with respect to the true value.

Various Monte Carlo programs have been developed for the purpose of estimating the secondary particle backgrounds in terms of charged and neutral particles produced by the mechanisms described above. Likewise, there exist specific codes to calculate the radioactivity and to perform calculations to optimize the shielding required for the detectors and for personnel safety considerations. While a detailed description of the individual codes is beyond the scope of the present article, some of the salient features are listed below. The GEM and SDC experiments have used the LAHET[11] and CALOR[12] packages. Similarly, the ATLAS and CMS experiments have employed the FLUKA code.[13]

The LAHET system of codes, developed at the Los Alamos National Laboratory, consists of several "modules" for specific purposes. The transport of hadrons is done using the models of FLUKA and HETC, in the energy range < 1 MeV for charged hadrons and < 20 MeV for neutrons. The MCNP model is used for neutron transport down to thermal energies. All electromagnetic processes are simulated using the EGS code. There exists an interface to the CINDER code in order to calculate the residual radioactivity. The information of the spallation products in conjunction with the low-energy neutron spectra, calculated previously, is used to estimate the nuclide densities, activation, and dose rates as a function of the time and specific location.

The CALOR Monte Carlo package was developed at the Oak Ridge National Laboratory. The models employed consist of HETC, which uses the high-energy fragmentation scheme of FLUKA; an evaporation model for low energies; and MORSE, which is used for the transport of neutrons with kinetic energy < 20 MeV. As in the preceding case, the EGS code is used for the propagation of the electromagnetic cascades. Recently, a version of CALOR has been interfaced to the GEANT program,[14] enabling the use of a detailed detector geometry package as well as other well established features—familiar in the simulation of detector response—contained in GEANT. The combined package is called GCALOR.

In addition to the above, extensive simulations have also been performed using the MARS code.[15] In particular, since the code utilizes inclusive particle production and statistical weighting techniques, it allows for relatively fast simulation as compared to the two cases described previously. This approach is particularly useful when considering the backgrounds produced by beam losses in the accelerator lattice elements and the transport of particles over large distances. The typical threshold energies for particle species, below which they are not followed, are: 2 MeV for charged hadrons; 0.025 eV $< E <$ 14 MeV for neutrons, and 0.1 MeV for electrons and photons.

3.2 Code Comparison and Systematics

In order to ascertain the reliability of the results obtained from the Monte Carlo calculations, it is important to compare the values with experimental data, when available, and to compare the simulation results among themselves. As an illustrative example, the test geometry shown in Figure 6 was used to calculate the neutron fluence at various locations of the setup, corresponding to punchthrough, side leakage, and albedo, which are important to quantify in the actual experiments. The energy range of the incident protons as well as the dimensions and materials used in the test geometry were selected to simulate a typical shielding requirement for the collider experiments. The comparison was performed using the three sets of simulation codes described previously: GCALOR, LAHET, and MARS. The results are summarized in Table 1. There appears to be fair agreement between the codes. The discrepancy observed between GCALOR and the other codes for the side leakage is being investigated.[16]

Another example is from the ROSTI and FLUKA collaborations[17] at CERN. The experiment was motivated by the lack of experimental information concerning the number of neutrons with energies between 0.1 MeV and 10 MeV in the cascades originating from hadrons with energy in the range 1 GeV to several hundred GeV. The ROSTI series of experiments consisted of calorimeter-like structures, constructed from 5-cm-thick slabs of iron or lead with dimensions between 30×30 cm^2 and 50×50 cm^2. In between the slabs, 6-mm-wide gaps were present that contained thin aluminium plates that were equipped with neutron activation detectors and dosimeters. From the information of these detectors, one could infer the longitudinal and radial profiles as well as the energy distribution of the neutrons. Thus, one can compare the ratios of neutrons at cascade maximum and the albedo neutrons as a function of the kinetic energy (E) of the incident primary hadron, with those of the task force.[1] These results are summarized in Table 2. The value for the ratio at cascade maximum determined from the experiment is higher than the value obtained by the task force. This would suggest an exponent $n = 0.8$ in the power law E^n, as compared to $n = 0.67$ assumed in the task force. The albedo ratio, however, is in good agreement with the value quoted by the task force.

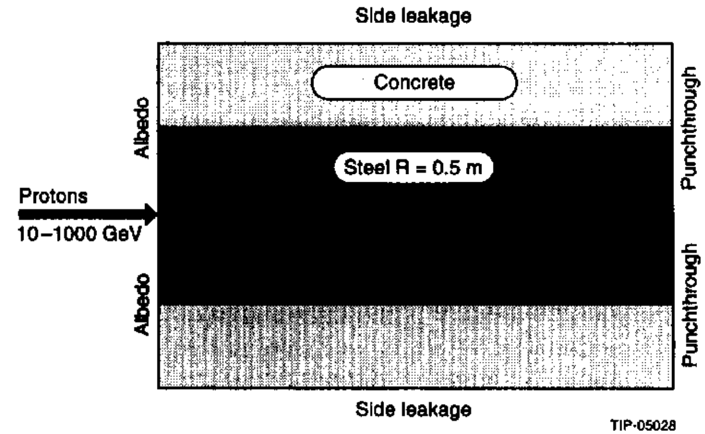

Figure 6. Details of the test geometry used to compare the neutron fluences at various locations using different Monte Carlo simulation packages.

Table 1. Results of code comparison for the test geometry shown in Figure 6. The numbers in the columns indicate the number of neutrons emerging from the surface of the cylinder per incident proton.

Incident p Energy	Monte Carlo Code	Punchthrough	Side Leakage	Albedo
10 GeV	GCALOR	0.041	1.47	32.6
	LAHET	0.027	0.72	39.2
	MARS	0.06	0.67	35.2
100 GeV	GCALOR	0.96	12.2	173.0
	LAHET	0.67	5.3	176.1
	MARS	0.96	4.2	153.5
1000 GeV	GCALOR	23.12	96.6	827.5
	LAHET	18.17	37.0	807.3
	MARS	14.75	24.1	658.1

Table 2. Comparison of fluences at cascade maximum and albedo neutrons for the ROSTI experiment and the SSCL task force.

	Cascade Maximum	Albedo
ROSTI Experiment	5.4 ± 0.1	2.8 ± 0.4
SSCL Task Force	4.1	2.9

3.3 Strategies for Shielding

The details of the shielding configurations adopted for the detectors are specific to the particular requirements. However, it is possible, albeit simplified, to list the strategy employed to design the shielding around the various sources of the backgrounds in the collider experiments, from the primary pp interactions.

There are essentially four criteria that have been identified to reduce the backgrounds:

1. to suppress the high-energy hadronic cascade by the use of dense materials;
2. to "slow down" the flux of neutrons present to thermal energies;
3. to reduce the low-energy neutron background using materials that have a high cross section for thermal neutron capture; and
4. to suppress the resulting low-energy gamma flux from the neutron capture process by using materials with high Z.

For the high-energy hadronic cascade, it is desirable to have a material with a relatively small interaction length. Likewise, the choice of the material should be such that it does not generate additional neutrons from the nuclear fission process. Taking into account practical considerations, materials such as tungsten, lead, and steel are commonly used.

Concerning the neutron flux, it is well known that hydrogen effectively shifts the energy of the neutrons downward to thermal energies, by the elastic scattering process. Thermal neutrons can also be captured by the hydrogen nucleus, producing deuterium and yielding a photon of energy 2.2 MeV. Polyethylene, for example, is a "good candidate" with the above limitation. Similarly, the Boron-10 isotope has a large cross section for neutron capture, and in the process it yields photons with energy ~ 0.4 MeV. In order to suppress the residual photon flux, high-Z materials such as lead are employed.

Figure 7(a) shows a quadrant of the GEM detector with the proposed shielding, and Figure 7(b) shows the distributions of the neutrons and photons with the shielding implemented, as estimated from the CALOR/GEANT Monte Carlo package.

In analogy, Figure 8 shows the proposed shielding for a quadrant of the SDC detector. Also indicated on the figure are the neutron and photon fluxes and their ratios for the different locations in the apparatus, obtained using the MARS and LAHET code systems.

The dimensions of the shieldings are variable, and depend on the requirements as well as the constraints present. However, the typical "size" can be estimated from the scale of the relevant figures. For both experiments, a suppression factor between 100 and 1000 has been achieved, depending on the location, by the implementation of the proposed shielding with respect to typical values of the neutron flux in the range 10^{12}–10^{13} $n/\mathrm{cm}^2/\mathrm{SSCY}$.

It is worthwhile to recall that all these calculations have been performed assuming the standard luminosity of 10^{33} cm^{-2}s^{-1} and the canonical SSC year (SSCY) operating time of 10^7 s. It is important to stress that the desired reduction in the particle fluences (in particular neutrons and gammas) is principally motivated by the low occupancy requirements in the large-area muon detector apparatus and by the radiation damage considerations to the silicon devices in the central tracking systems.

Similar considerations have been made for the shielding requirements in the ATLAS and CMS experiments, bearing in mind that the LHC luminosity is expected to be over an order of magnitude higher ($\sim 3 \times 10^{34}$ cm^{-2}s^{-1}) than the SSC. Further details can be found in References 4 and 5.

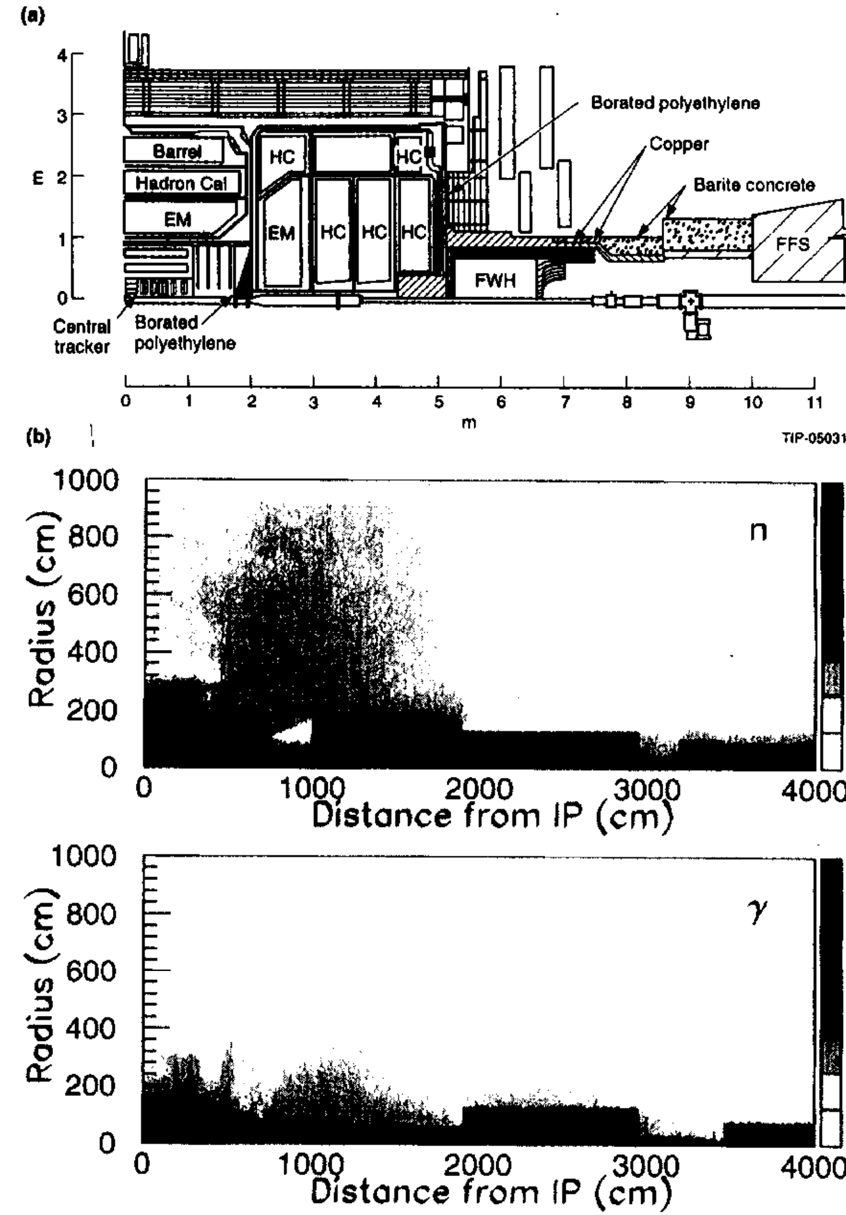

Figure 7. (a) A quadrant of the GEM experiment, showing details of the proposed shielding. (b) Results obtained for the neutron fluence and photon fluence, with the shielding implemented. The simulation code CALOR-GEANT was employed. The scale on the right-hand-side indicates the value of the exponent (m). The units are 10^m neutrons or photons per cm^2 per SSCY (Reference 2).

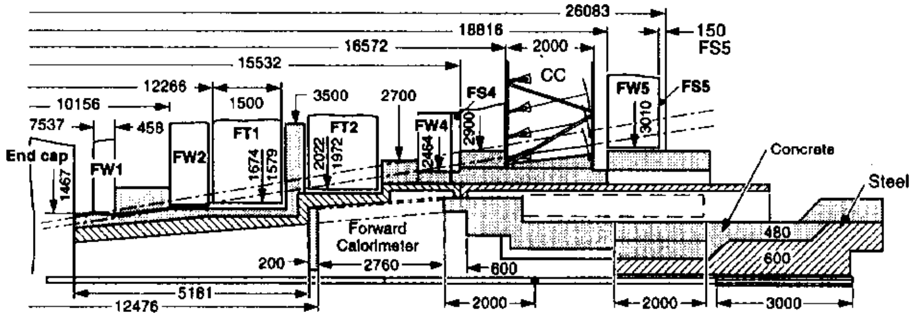

	FW1		FW2		FW4		FW5	
	n	γ/n	n	γ/n	n	γ/n	n	γ/n
MARS	4×10^{10}	0.5	2.8×10^{10}	0.3	0.98×10^{10}	0.2	0.26×10^{10}	0.6
LAHET	1.1×10^{10}	1.4	0.6×10^{10}	1.3	1.2×10^{10}	0.9	1.0×10^{10}	1.0
	(n/cm^2/SSCY)		(n/cm^2/SSCY)		(n/cm^2/SSCY)		(n/cm^2/SSCY)	

TIP-05027

Figure 8. A quadrant of the SDC experiment, showing details of the proposed shielding. The neutron and photon fluence, as well as their ratio, is also indicated at various locations of the detector, corresponding to the muon detector subsystem.

3.4 Beam-Line Considerations

From the results of the previous section it can be ascertained that among the predominant sources of backgrounds are the LBQs and the collimators on either side of the IP (at a typical distance of 25–30 m with respect to the center of the detector), as well as the beam pipe. Thus, care has been taken to optimize the design of these components. As an example, Figure 9 shows the mean number of hadronic interactions in a beam pipe as a function of the longitudinal distance along it for two geometries. In the case of the GEM apparatus, the beam pipe design[2] in the region of the central tracker consists of a beryllium section of diameter 80 mm and thickness 1.5 mm. The section of the beam pipe near the endcap calorimeter region has a larger diameter (200 mm) and is proposed to be made of stainless steel with a thickness of 2 mm. The figure serves to illustrate that the larger diameter ensures that only a small fraction of the forward emitted particles at low angles and high energies intercept the beam pipe.

Other, smaller sources of backgrounds in comparison to the particle production in the pp interaction themselves are due to beam losses in the LBQs and beam-gas interactions in the evacuated beam pipe.[18] Figure 10 shows a comparison of the magnitude of the low-energy neutron fluence from these sources. The beam loss in the LBQs is approximately 5×10^4 p/m/s in the region shown in Figure 10, and corresponds to $\sim 10\%$ of the pp interaction energy at $\sqrt{s} = 40$ TeV, which in turn is 4×10^9 TeV/s. Similarly, for the beam-gas interactions, assuming a residual pressure of 10^{-8} torr nitrogen equivalent in the "warm region" of the evacuated beam pipe and $\sim 4 \times 10^8$ N_2 molecules per cc in the "cold region," the loss rate is $\sim 2 \times 10^4$ p/m/s, which is small compared to the pp interaction rate.

In terms of systematic uncertainties concerning the results of the two previous subsections, it is noteworthy that the inclusion of the magnetic fields in the simulations, in particular for the LBQs, is rather important.

Finally, we note that the relevance of such calculations to the detectors proposed for the study of B-physics (e.g., the FAD apparatus[19]), for various collider luminosities is presented in the section dealing with machine-detector interface issues of these proceedings.[20]

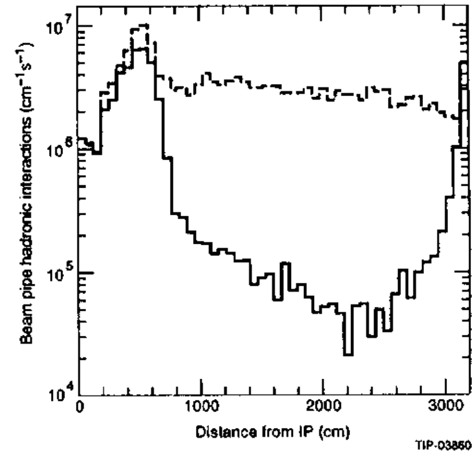

Figure 9. Average number of hadronic interactions in the beam pipe as a function of the longitudinal dimension from the IP, for the GEM apparatus. The dashed line represents a pipe with a constant diameter, and the solid line a pipe with a variable diameter (Reference 2).

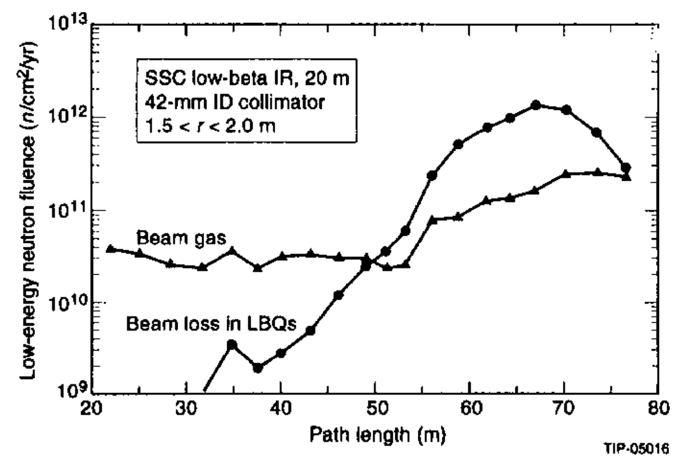

Figure 10. Low-energy neutron fluence from sources corresponding to beam-gas interactions in the beam pipe and beam losses in the collider lattice, in the vicinity of the LBQs. The abscissa refers to the distance from the IP (Reference 18).

3.5 *Parametrization of the Spectrum*

For the purpose of calculating the response of a detector to the background flux of neutrons and photons, it is important to be able to parametrize the energy distribution of these backgrounds obtained from the Monte Carlo simulations. D. Groom[21] has studied this in the context of the background particles' energy distributions that are calculated in the context of the SDC apparatus.[22] As a specific example, Figure 11 (upper figure) shows the spectrum of the neutron flux for the air over the detector itself; the lower figure shows the contributions to the theoretical model used to parametrize the spectrum.

The following essential features of the spectrum have been identified by D. Groom:

- Evaporation peak: this is centered near 0.5 MeV, and is due to the evaporation process of neutrons after the collisions.
- Hole peak: this occurs at approximately 460 keV, and corresponds to an increase in the n-Fe cross section.
- Notch: this is characterized by a sharp peak at 26 keV, and corresponds to a dip in the n-Fe cross section.
- Skirt: this is analogous to a smooth "background" under the spectrum going almost linearly "downhill" from the 500-keV peak to thermal energy values. This is most likely the result of repeated neutron scatterings (downscattering) with some energy loss.
- Thermal peak: this thermal neutron peak is well described by a Maxwellian distribution.

Additional details pertinent to the interpretation of the spectrum can be found in the original document.[21]

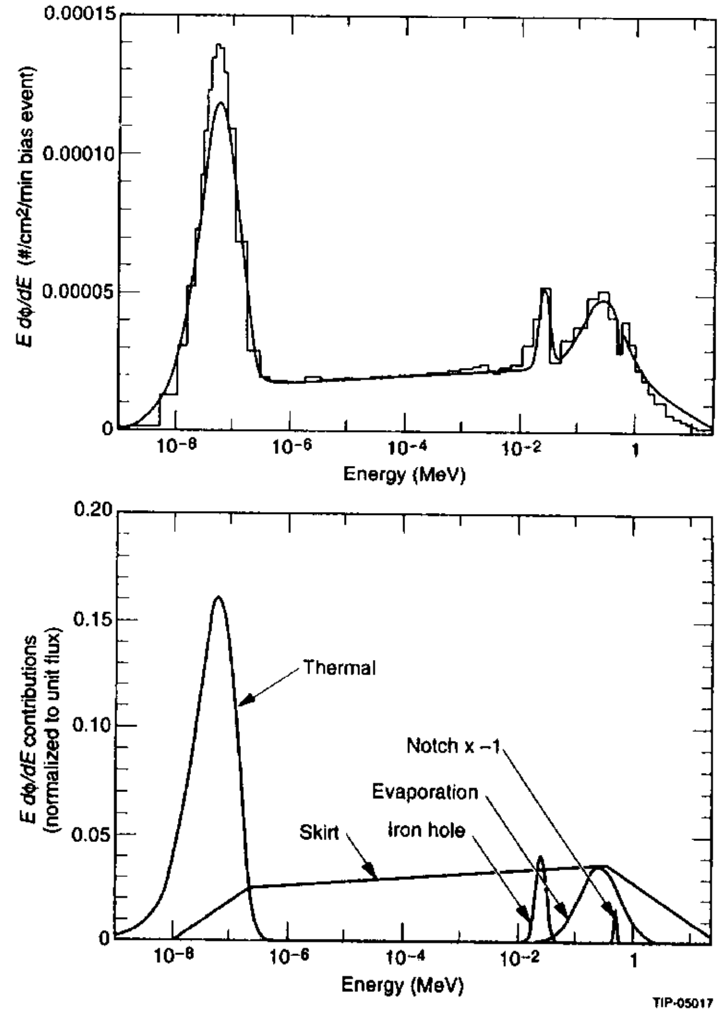

Figure 11. Differential neutron flux spectra corresponding to the "air over the detector" for the SDC apparatus, upper figure (Reference 22). The lower figure indicates the contributions to the theoretical model used to describe the spectra (Reference 21).

3.6 *Charged Particle Fluence and Dose*

In the preceding sections, emphasis has been put on understanding the neutron and photon fluence. In order to be complete, one should also discuss the charged-particle backgrounds as well as the overall issue of dose and activation. For the latter, since the values for the doses and activation levels are specific to the individual detectors, the appropriate details may be found in References 2 and 3 and in References 4 and 5 for the SSC and LHC detectors, respectively.

However, the charged-particle fluence is indeed an important consideration for the silicon detectors proposed for particle tracking and event as well as secondary vertex reconstruction, in particular for the proposed B-physics experiments. In order to obtain a quantitative comparison, Table 3 lists the charged-particle fluences (and corresponding doses) calculated for various luminosities (corresponding to existing and proposed future collider facilities), as a function of the radial distance where it is proposed to implement the silicon devices.

Table 3. List of charged particle fluence (for 10^7 s) from the primary interactions as a function of the perpendicular distance ($r_\perp$) from the IP, for various colliders. The σ's represent the inelastic cross sections.

$r_\perp \rightarrow$	2.5 cm	5.0 cm	10.0 cm	20.0 cm
SSC H: 7.5 $\mathcal{L}$: 10^{33} cm^{-2}s^{-1} σ: 100 mb	19×10^{13} part/cm^2 5 mrad	4.8×10^{13} part/cm^2 1.3 mrad	1.2×10^{13} part/cm^2 0.3 mrad	0.3×10^{13} part/cm^2 0.08 mrad
LHC H: 6.2 $\mathcal{L}$: 1.7×10^{34} cm^{-2}s^{-1} σ: 84 mb	225×10^{13} part/cm^2 60 mrad	56×10^{13} part/cm^2 15 mrad	14×10^{13} part/cm^2 3.7 mrad	3.5×10^{13} part/cm^2 0.9 mrad
TEV H: 3.9 $\mathcal{L}$: 2×10^{30} cm^{-2}s^{-1} σ: 56 mb	0.011×10^{13} part/cm^2 2.9×10^{-3} mrad	0.003×10^{13} part/cm^2 0.74×10^{-3} mrad	0.0007×10^{13} part/cm^2 0.18×10^{-3} mrad	0.0002×10^{13} part/cm^2 0.05×10^{-3} mrad
TEV H: 3.9 $\mathcal{L}$: 10^{32} cm^{-2}s^{-1} σ: 56 mb	0.55×10^{13} part/cm^2 0.15 mrad	0.14×10^{13} part/cm^2 0.04 mrad	0.035×10^{13} part/cm^2 0.009 mrad	0.009×10^{13} part/cm^2 0.002 mrad

4. EFFECTS ON DETECTORS

The purpose of this section is to present a brief overview concerning the consequences of radiation damage to the operation of silicon detector devices. As indicated in the previous section, these silicon detectors will be placed around the beam pipe, at small radii with respect to the interaction point for purposes of particle track reconstruction and vertex reconstruction. It is beyond the scope of this paper to attempt to summarize the consequences of radiation damage to other detector devices and electronics. Details may be found in recent workshop proceedings.[23]

4.1 *Damage Mechanisms*

The damage mechanisms in silicon devices can essentially be separated into bulk effects and surface effects. The typical energy of the neutrons in the tracking cavity of the apparatus is ~ 1 MeV, characteristic of the nuclear evaporation process. Neutrons in this energy range are effective in creating displacement damage. Figure 12 shows the relative damage of neutrons as a function of the incident n energy, calculated from a knowledge of the n-Si cross sections.[24] Recently, there has been evidence from investigation of electronic devices that the displacement damage is proportional to non-ionizing energy loss (NIEL). This has been calculated by Van Ginneken,[25] and is shown in Figure 13 for different particle species as a function of their incident energy. From this figure it can be ascertained that for a particular value of the incident energy (1–2 MeV), the ratio of the damage coefficient of electrons to neutrons is $\sim 10^{-2}$. Some of the consequences of the bulk damage are:

- an increase in the leakage current of the reverse-biased p-n junction;
- trapping of the mobile charge carriers, leading to incomplete charge collection;
- effective compensation of the material, thus modifying the electrical field characteristics in the device.

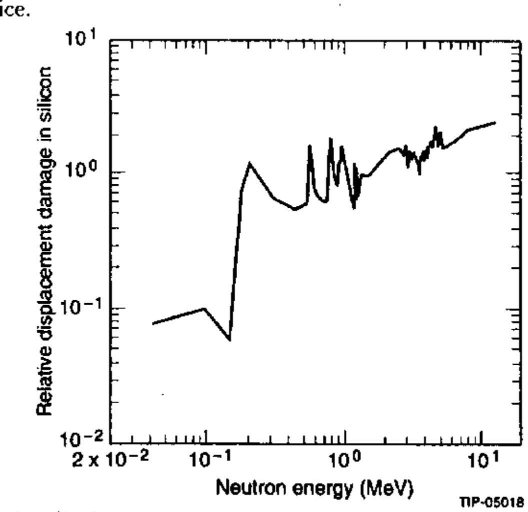

Figure 12. Relative displacement damage by neutrons in silicon, as a function of the neutron energy (Reference 24).

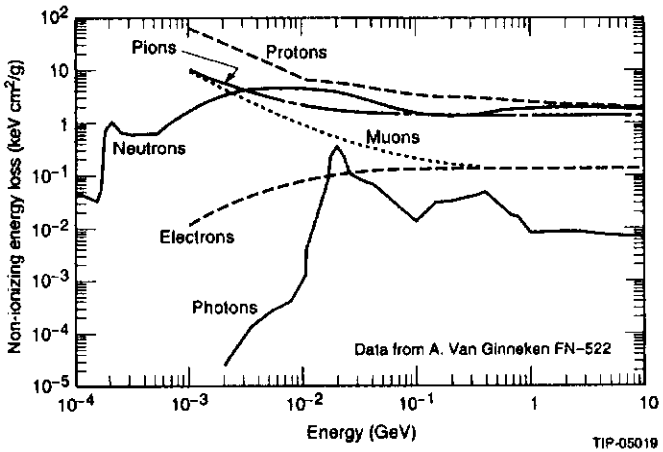

Figure 13. Calculated non-ionizing energy loss for different particle species, as a function of the incident particle energy (Reference 25).

Surface damage affects the passivation layer (SiO_2) and the SiO_2-Si interface region in the *p-n* junction diode.[23] Also, there could be the creation of "mid-gap" interface states, which are mobile. Likewise, there may be charge trapping due to oxide defects. A partial list of some of the important consequences includes:

- an increase in the surface leakage current;
- a decrease in the charge carrier mobility;
- a decrease in the "interstrip" resistivity of the device;
- the formation of charge "inversion" layers.

These phenomena lead to a degraded performance of the devices. In the following, a brief sample of some of these phenomena is listed.

- Leakage current: an increase in the leakage current of the device will, in turn, lead to an increase in the electronic noise as well as increased power consumption. It is rather well established that the increase in the current density (ΔI) is related to the particle fluence (Φ), as in the expression $\Delta I = \alpha \times \Phi$, where α is referred to as the damage constant. Numerous experiments have measured this constant[23] with different incident particles. Typical values are: $\alpha \simeq 2 \times 10^{-17}$ A/cm for incident neutrons with energy ~ 1 MeV; and $\alpha \simeq 3 \times 10^{-17}$ A/cm for incident protons of energy ~ 800 MeV.

- Effective doping concentration: this is a phenomenon where the initial, *n*-type (bulk) material gradually becomes intrinsic and then inverts to *p*-type material with increased particle fluence. The effective donor concentration (N_D) decreases during irradiation as a consequence of the creation of charged damage sites in the bulk. The electric field characteristics, and thus the depletion voltage ($V_{\rm dep}$), will be affected. The depletion voltage is related to the donor concentration by the equation: $V_{\rm dep} = (e \times N_D \times d^2)/(2 \times \epsilon)$, where e is the electric charge, d is the detector thickness (usually 300 μ), and ϵ is the permittivity of silicon. Figure 14 shows the variation of the depletion voltage as a function of the fluence for 800-MeV incident protons.[26] The phenomenon of "type inversion" occurs at a fluence between 1 and 2×10^{13} p/cm^2. The curves are a fit to the data, using a model in which $N_D = N_o e^{-c\phi} + \beta\phi$, where N_o is the initial doping concentration, and c and β are coefficients to be determined from the fit to the data points. The model is consistent with a two-component process, which incorporates donor removal and acceptor creation in the silicon bulk. Additional details may be found in Reference 26.

It should be noted that similar conclusions are obtained with incident neutrons, where type inversion is also observed at a fluence of $\sim 2 \times 10^{13}$ n/cm^2.[26] We note, however, that recent results from the RD-2 collaboration[27] at CERN indicate that type inversion is observed at a fluence of $\sim 3 \times 10^{12}$ n/cm^2, which is approximately an order of magnitude lower. It is clear that the systematics concerning the actual neutron fluence have to be quantified. These could be quite large.

The effect of the change in the depletion voltage of the *p-n* junction device in terms of the charge collection (i.e., peak position) is illustrated in Figure 15. The typical values for the depletion voltage prior to irradiation were in the range $30 < V_{\rm dep} < 65$ V. After irradiation, a bias voltage of 100 V is required to attain the same charge collection.

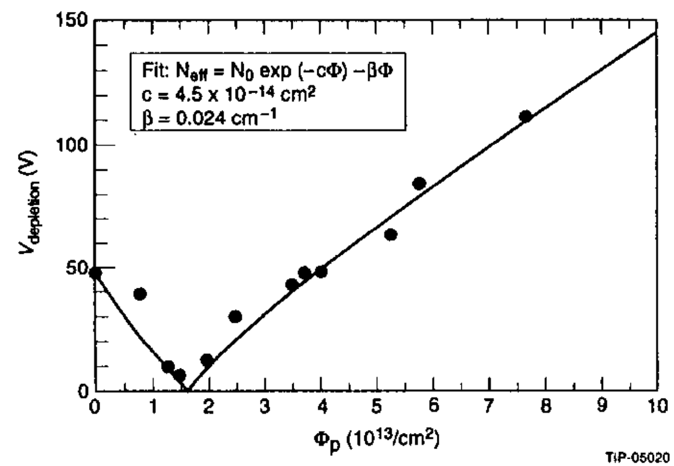

Figure 14. Variation of the depletion voltage in a reverse-biased silicon *p-n* junction diode as a function of the particle fluence. The solid lines represent a fit to the data in the context of the model described in the text.

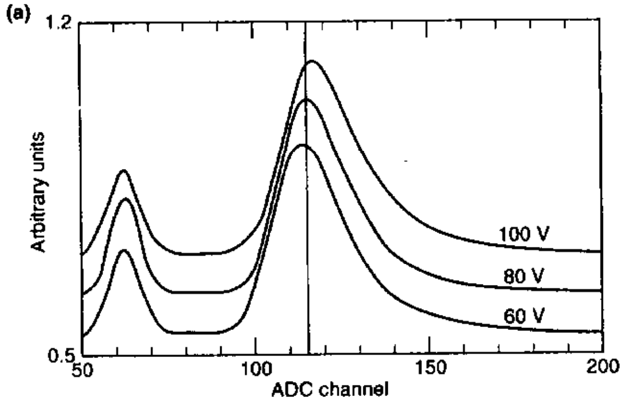

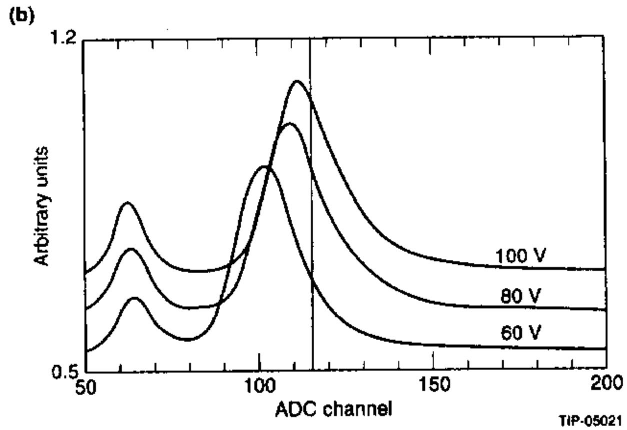

Figure 15. Pulse height spectrum obtained from a reverse-biased silicon p-n junction diode, using a β-source. The upper figure shows the variation in the peak position of the pulse height spectrum for the different applied bias voltages, after the detector has received a fluence of 1.7×10^{12} n/cm^2. In analogy, the lower figure shows the same, but for a larger fluence corresponding to 6×10^{12} n/cm^2. The detectors are required to be significantly overdepleted after irradiation with respect to the original values in order to ensure complete charge collection.

4.2 Consequences for Operation

The silicon devices operating at the SSC, with the nominal luminosity of 10^{33} cm^{-2}s^{-1}, will be exposed to a fluence of $\sim 10^{14}$ particles/cm^2 over approximately a decade of operation, at a typical radius of 10 cm from the interaction point. The consequences of radiation damage suggest that it would be desirable to operate the devices at relatively low temperatures (0°C) as compared to ambient temperature. The reason is essentially that the leakage current is lowered by a factor two for every 7°C reduction in the temperature. Thus, experimental results[28] suggest that, for example, operating the devices at 0°C as opposed to 24°C would lead to approximately a factor 10 reduction in the leakage current. Even if one takes into account the lack of annealing at 0°C, the overall reduction in the leakage current would be a factor ~ 5, with respect to the higher temperature. Likewise, from the point of view of the operating voltage, the experimental observations favor the lower temperature. It is important to stress that the study of the annealing phenomenon and its temperature dependence is the subject of extensive investigation at present. The annealing phenomenon is rather complicated, and the characteristic time constants involved can be long (of the order of hundreds of days), requiring large time periods of monitoring and analysis. Further details and an update on recent experimental results can be found in Reference 28.

5. ACKNOWLEDGEMENTS

It is a pleasure to acknowledge my colleagues from the GEM experiment neutron task force and the SDC experiment neutron task force. In particular, I am most grateful to T. Gabriel, D. Groom, V. Kubarovsky, N. Mokhov, and L. Waters for their valuable guidance.

6. REFERENCES

1. D. E. Groom, *Nucl. Instr. and Meth.* **A279** (1989) 1.
2. Technical Design Report, GEM Experiment, SSCL-SR-1219 (1993).
3. Technical Design Report, SDC Experiment, SSCL-SR-1215 (1992).
4. Letter of Intent, ATLAS Experiment, CERN/LHCC/92-4 (1992).
5. Letter of Intent, CMS Experiment, CERN/LHCC/92-3 (1992).
6. Y. M. Nosochkov, these Proceedings.
7. D. E. Groom, ed., SSC Report SSC-SR-1033 (1988).
8. J. Ranft et al., UL-92-7 and UL-HEP-93-01, Leipzig, Germany.
9. D. E. Groom, SDC Report SDC-93-448 (1993); and references contained therein.
10. M. Barbier, *Induced Radioactivity*, North-Holland Publishing Company (1969).
11. Radiation calculations using LAHET/MCNP/CINDER 90, LANL Report LA-UR-89-3014 (1992); and references contained therein.
12. T. A. Gabriel et al., ORNL Report ORNL/TM-5619 (1977); and references contained therein.
13. A. Ferrari et al., in *Proceedings of the Second International Conference on Calorimetry in High Energy Physics*, p. 101 (1991); and references contained therein.
14. C. Zeitnitz and T. A. Gabriel, private communication. R. Brun et al., CERN-DD/78/2 (1978); and references contained therein.
15. N. Mokhov, Fermilab report FNAL-FN-509 (1989); and references contained therein.
16. V. Kubarovsky, private communication.
17. G. R. Stevenson, *Nucl. Instr. and Meth.* (Proc. Suppl.) **32** (1993) 37.
18. N. Mokhov, private communication; and N. Mokhov in the collected minutes of the SSCL Collider-Detector interface meetings (1993).
19. J. D. Bjorken, *Inter. Jour. of Mod. Phys.*, **A7**, N18 (1992) 4189.

20. V. Bharadwaj (ed.), these proceedings.

21. D. E. Groom, SDC Report SDC-93-492 (1993).

22. A. Palounek et al., SDC Report SDC-93-467 (1993).

23. G. Hall, CERN-LHC Report CERN 90-10 (1990); and T. Dombeck et al., (eds.), in *Proceedings of the Symposium on Detector Research and Development for the Superconducting Super Collider*, Fort Worth, Texas (1990); and references contained therein.

24. J. E. Gover and J. R. Srour, Sandia Lab. Report SAND85-0776 (1985).

25. A. Van Ginneken, Fermilab Note FN-522 (1989).

26. A. Weinstein et al., SDC Report SDC-91-133 (1991); and references contained therein.

27. The RD-2 Collaboration Status Report: CERN/DRDC/93-18, March 1993.

28. H. Ziock et al., "Temperature dependence of the radiation induced change of depletion voltage in silicon PIN detectors." In preparation.

PHYSICS OPPORTUNITIES AT ASYMMETRIC e^+e^- COLLIDER AT Υ
- KEK ASYMMETRIC B-FACTORY -

YOSHIHIDE SAKAI
National Laboratory for High Energy Physics
1-1 Oho, Tsukuba-city, Ibaraki, 305, Japan

ABSTRACT

The prospects of various physics are discussed for an Asymmetric e^+e^- B-Factory, which is considered as a next project after TRISTAN at KEK. The potential reach of CP asymmetry measurements are presented for various decay modes based on the Monte Carlo simulation studies. Combining various decay modes, the angles in the unitarity triangle of the CKM-matrix could be measured with precisions of $\delta \sin 2\phi_1 \sim 0.05$, $\delta \sin 2\phi_2 \sim 0.07$, and $\delta\phi_3 \sim 13°$ with an integrated luminosity of 100 fb^{-1}.

1. INTRODUCTION

An asymmetric e^+e^- collider at $\Upsilon(4S)$[1] is considered as a next generation B-Factory and studies for accelerators[2-4] and experiments[5-9] have been made in great detail. It is considered as a next project after TRISTAN at KEK (National Lab. for High Energy Physics) in Japan. It collides e^+ and e^- with different energies at a c.m. energy of $\Upsilon(4S)$ and therefore $B\bar{B}$ are produced moving along the higher energy beam direction. This provides an ability to measure the decay time evolution by measuring vertex points of B decay.

An asymmetric e^+e^- B-Factory essentially covers all nice features of an ordinary symmetric e^+e^- collider; Running at $\Upsilon(4S)$, only $B^\circ\bar{B}^\circ$ or B^+B^- are produced without any associated particles. Signal to noise ratio is $\sim 1/3$ and kinematical constraint can be used for event reconstruction since energy of B is equal to $E_{cm}/2$ in the C.M. frame. These provide the cleanest B signals, which are the most advantage of e^+e^- collider at $\Upsilon(4S)$. This is in contrast to the hadron machine case where S/N ratio is $10^{-5} \sim 10^{-2}$ and $B\bar{B}$ are imbedded in particles with multiplicity of $15 \sim 100$ (depending on collision energy). As in usual e^+e^- collider, the trigger efficiency for $B\bar{B}$ events are $\sim$ 100% and no special triggers are needed.

An asymmetric collision provides further unique physics possibilities. CP asymmetry is the most important and unique physics possible with an asymmetric e^+e^-

B-Factory. In the standard model, CP violation is explained by the complex phase of the quark mixing matrix (CKM matrix)[10] (in the Wolfenstein representation[11]):

$$\begin{pmatrix} V_{ud} & V_{us} & V_{ub} \\ V_{cd} & V_{cs} & V_{cb} \\ V_{td} & V_{ts} & V_{tb} \end{pmatrix} = \begin{pmatrix} 1-\lambda^2/2 & \lambda & \lambda^3 A(\rho - i\eta) \\ -\lambda & 1-\lambda^2/2 & \lambda^2 A \\ \lambda^3 A(1-\rho-i\eta) & -\lambda^2 A & 1 \end{pmatrix}$$

A sizable CP violation effect in B system is predicted. The observation of CP violation in B system would be the first CP violation effect other than in the Kaon system. It will provide new information on the mechanism of CP violation and redundant measurements on CKM matrix elements.

On the other hand, an asymmetric e^+e^- B-Factory has limitations compared to hadron machine; A production cross section for $B\bar{B}$ is 1.15 nb and orders of magnitude smaller than hadron machine, which limits the total number of produced events. Heavy b-flavored states such as B_c and Λ_b can not be studied because they are not produced at Υ energy. Therefore, they are complementary each other, while they are competitors at the same time.

In this report, the design and status of the KEK asymmetric B-Factory accelerator is briefly described in Sec. 2 and physics goal and potential is overviewed in Sec. 3. Then in Sec. 4, the potential of CP asymmetry measurements by KEK B-Factory experiments are described, which are mostly based on simulation work by KEK B-Factory Physics Task Force group[7-9]. Similar studies have been reported for other proposed asymmetric B-Factories[5, 6]. Those reported here also apply to the other asymmetric B-Factories.

2. KEK B-Factory Accelerator

The KEK B Factory is a 3.5 × 8 GeV asymmetric e^+e^- collider[4]. The present TRISTAN Main Ring tunnel will be used for 3.5 GeV e^+ and 8 GeV e^- rings. The present design parameters of the accelerator are listed in Table 1.

The luminosity goal is $10^{34} cm^{-2} sec^{-1}$ and the design is based on the following philosophies:

- A small β_y^* (1 cm) and high $\xi_{x,y}$ (0.05) are chosen in order to achieve the desired luminosity with the smallest current.
- All RF buckets are filled with the beam in order to reduce the RF voltage. An RF frequency of 508 MHz results in a beam crossing interval of 2 nsec. Also, a low α lattice is proposed for the Low Energy Ring.
- A low emittance ratio ($\epsilon_y/\epsilon_x = 0.01$) together with the same β_y^*/β_x^* ratio is chosen. This serves to reduce the background problem to the detector.

Table 1. Parameters for KEK Asymmetric B-Factory accelerator. Values in parentheses are for Phase-I.

		LER		HER
Energy(GeV)	E	3.5		8.0
Momentum compaction factor		normal	low	normal
Circumference(m)	C	3018		3018
Luminosity($cm^{-2}s^{-1}$)	$\mathcal{L}$	1×10^{34} (2×10^{33})		
Tune shifts	ξ_x/ξ_y	0.05/0.05		0.05/0.05
Beta function(m)	β_x^*/β_y^*	1.0/0.01		1.0/0.01
Beam current(A)	I	2.6 (0.52)		1.1 (0.22)
Bunch length(cm)	σ_z	0.5		0.5
Energy spread(10^{-3})	σ_ϵ	0.78	0.74	0.73
Bunch spacing(m)	S_B	0.6 (3.0)		0.6(3.0)
Particles/bunch(10^{10})	N	3.3		1.4
Emittance(nm)	ϵ_x/ϵ_y	19/0.19		19/0.19
Synchrotron tune	ν_s	0.064	0.014	0.070
Betatron tune	ν_x/ν_y	~ 39	~ 43	~ 39
Momentum compaction(10^{-3})	α	0.88	0.20	1.0
Energy loss/turn(MeV)	U_0	0.91	0.84	4.1
RF voltage(MV)	V_c	20	4.4	47
RF frequency(MHz)	f_{RF}	508		508
Harmonic number	h	5120		5120
Energy damping decrement(10^{-3})	T_0/τ_E	0.26	0.24	0.5
Bending radius(m)	ρ	15.0	16.2	91.3
Length of bending magnet(m)	ℓ_B	0.42	0.85	2.56

Since the achievement of $10^{34} cm^{-2} sec^{-1}$ requires several breakthroughs from the present situation, the accelerator construction will go through two steps. In phase-I, it will start with a luminosity of $2 \times 10^{33} cm^{-2} sec^{-1}$ by filling every fifth bucket in the beams. This considerably reduces the problems (like beam-beam instability) and enables a quick start of the accelerator operation and physics program. During phase-I operation, further R&D and machine studies will be pursued aiming towards the luminosity goal of $10^{34} cm^{-2} sec^{-1}$ in phase-II.

The present linac will be upgraded as an injector for the B-Factory:

1) The linac energy will be increased from the present 2.5 GeV to 8.0 GeV, so that both electrons and positrons can be directly injected into the main rings and the complexity of having a booster ring can be avoided. This energy upgrade will be achieved by adding RF units (10 ~ 20) and an increase of RF power with SLED or recirculation method.

2) The intensity of the positron source will be increased at least a factor 10 by increasing the energy on the positron production target from the present 0.25 GeV to ~ 4 GeV.

3) The repetition rate will be increased from the present 25 Hz to 50 Hz.

A linac upgrade has started from FY 1993. R&D work on accelerator hardware components (RF cavity, vacuum system, feed back, and so on) as well as design and simulation work (on lattice, dynamic aperture, and beam-beam effect) have been intensively performed. We hope construction of the B-Factory accelerator starts from FY 1994 and phase-I operation begins by the end of 1998.

3. Physics Goal of Asymmetric B-Factory

The physics goal of an asymmetric B-factory can be divided into following 3 steps.

1. Discover and confirm CP violation in B system as soon as possible.
2. Precise determination of CKM-matrix elements.
3. Find keys beyond the Standard Model.

In each step, experiments at hadron machine would be strong competitors, but also complementary in some aspects.

Even though no experimental evidence beyond the standard model has been observed so far, a fact which can not be explained within the standard model is the matter - antimatter asymmetry of the present universe. In interpreting this fact, baryon number non-conservation is required, which should involve CP violation. Therefore, investigation of CP violation would provide a key to beyond the standard model.

An unitarity condition of CKM-matrix gives triangle relation shown in Fig. 1. Because of the direct relation between As described below, CP asymmetries are directly related to angle ϕ_i's of unitarity triangle. Any observation of inconsistency between measurements of lengths and angles of unitarity triangle would be a manifestation beyond the standard model. Therefore, measurements of CP asymmetries still have a special importance even after the first discovery and following points should be stressed:

- The precise measurements of length of triangle have same importance as CP asymmetry in order to make an over-constraints for CKM parameters.
- The ambiguity in extracting CKM-parameters from experimentally measured quantities should be reduced theoretically or by additional experimental measurements. Otherwise, measurements are not so useful even if they are very precise.

3.1. Measurements of Triangle Length

The lengths of the sides alone uniquely determine triangle. However, constraints on the unitarity triangle from the present measurements are yet not strict enough[9, 15] because of both experimental and theoretical uncertainties. Though improvement of these measurements are being made by CLEO, it is also one of the important roles of an asymmetric e^+e^- B-Factory since it accumulates much more luminosity and potentially better signal to noise ratio provided by decay vertex measurement.

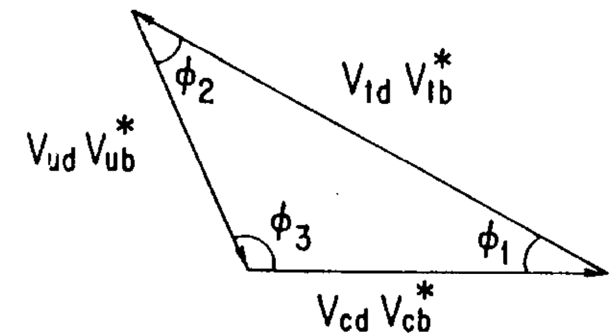

Fig. 1. Unitarity triangle of the CKM matrix.

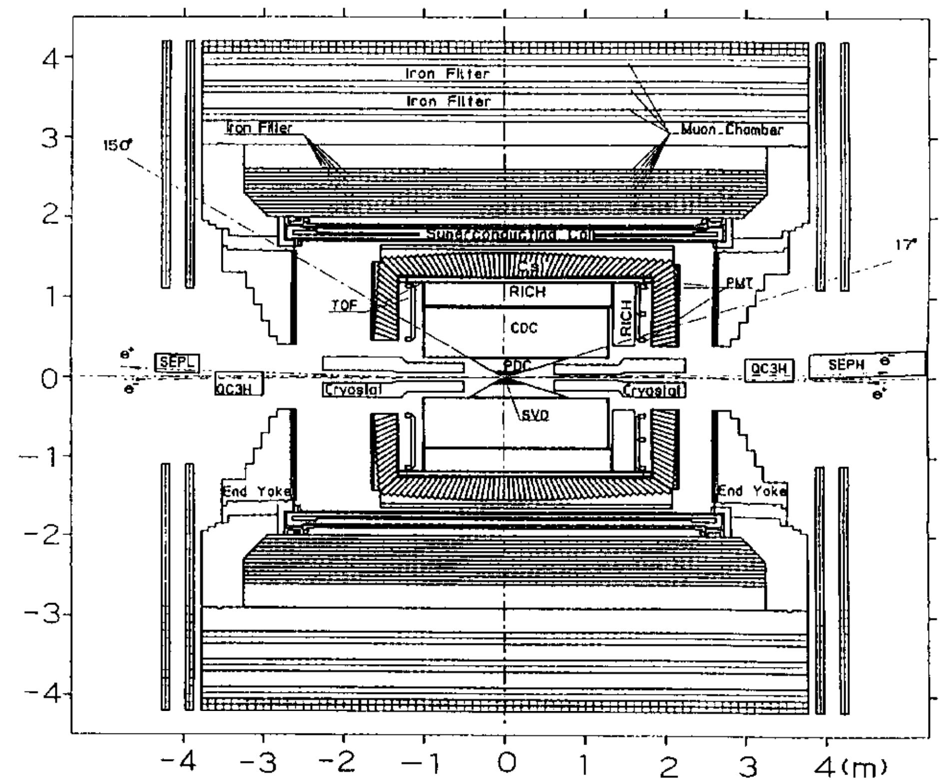

Fig. 2. The detector configuration of KEK B Factory.

The following improvement is expected in an asymmetric e^+e^- B-Factory.

1) $|V_{cb}|$: Inclusive semi-leptonic B decay modes have been used to measure $|V_{cb}|$, but this suffers the model dependence. According to Heavy Quark Effective Theory (HQET), hadronic form factors can be expressed by a single universal function $\xi(v \cdot v')$ which is absolutely normalized to 1 at kinematical end point $v \cdot v' = 1$ for exclusive semi-leptonic decays like $B \to D^* \ell \nu$. (Here v and v' are four-velocities of heavy particles.) Therefore, measurement of differential decay rate at $v \cdot v' = 1$ provides model independent $|V_{cb}|$. However, an application of this method to presently available data still gives similar uncertainty as inclusive mode due to the quite limited statistics around kinematical end point and extrapolation errors [12]. Both uncertainties can be reduced by accumulating more statistics, especially around kinematic end point. We expect to measure $|V_{cb}|$ with accuracy of a few % by an asymmetric B-Factory with 100 fb^{-1}.

2) $|V_{ub}|$: The end point of lepton spectrum has been used to extract $|V_{ub}|$ so far. This suffers large model dependence since only small part of spectrum is measured. Exclusive semi-leptonic decay modes $B \to \rho(\pi, \omega)\ell\nu$ allow to measure wider kinematic region and help to reduce uncertainties. We expect several hundreds of exclusive decay events with 100 fb^{-1} at asymmetric B-Factory. Theoretical uncertainty still needs to be reduce in the future.

3) $|V_{td}|$: A measurement of $B_d^\circ - \bar{B}_d^\circ$ mixing provides $|V_{td}|$. However, it suffers a large uncertainty due to poorly known $f_B\sqrt{B}$ whose theoretical prediction ranges 100 to 250 MeV. The uncertainty of $f_B\sqrt{B}$ can be reduced in some extent by measuring $B_s^\circ - \bar{B}_s^\circ$ mixing and taking ratio of x_s/x_d. However, it is difficult to measure $B_s^\circ - \bar{B}_s^\circ$ mixing at asymmetric B-Factory. Another method which would be suitable for asymmetric B-Factory is a measurement of the ratio of radiative Penguin decay branching ratios $\Gamma(B \to \rho\gamma)/\Gamma(B \to K^*\gamma)$ which is proportional to $|V_{td}|^2$[13]. Recently CLEO has reported $\mathrm{Br}(B \to K^*\gamma) = (4.5 \pm 1.7) \times 10^{-5}$[14]. Taking into account Cabbibo suppression factor, we expect about 100 $B \to \rho\gamma$ events and $\sim 5\%$ measurement error in $|V_{td}|$ with 100 fb^{-1} at asymmetric B-Factory.

3.2. CP Violation at Asymmetric B-Factory

In a B° decay into CP eigenstate f, CP violation appears as a consequence of interference between the amplitude for $B^\circ \to f$ and that for $B^\circ \to \bar{B}^\circ \to f$ through B° - $\bar{B}^\circ$ mixing. In e^+e^- collider at $\Upsilon(4S)$ case, the CP asymmetry is written as

$$A = \frac{R(B^\circ \to f) - R(\bar{B}^\circ \to f)}{R(B^\circ \to f) + R(\bar{B}^\circ \to f)} = \sin 2\phi_i \cdot \sin(\Delta m \cdot \Delta t)$$

It should be noted that Δt ($= t_f - t_{tag}$) ranges from $-\infty$ to $+\infty$ and the asymmetry vanishes for time integrated rate. Therefore, it is essential to measure Δt to observe CP asymmetry. ϕ_i is a phase difference between amplitude of B° - $\bar{B}^\circ$ mixing and decay

Table 2. Decay modes for CP asymmetry measurements and angle ϕ_i of CKM unitarity triangle for B_d° decays. A final state shown is just a representative.

Tree	ϕ_i	$O(\lambda)$	Decay	Penguin	ϕ_i	$O(\lambda)$
$\bar{b} \to \bar{c}(c\bar{s})$	ϕ_1	λ^2	$J/\psi K_S$	$\bar{b} \to \bar{s}(c\bar{c})$	ϕ_1	λ^2
$\bar{b} \to \bar{c}(c\bar{d})$	ϕ_1	λ^3 λ^3	$J/\psi\pi^\circ$ D^+D^-	$\bar{b} \to \bar{d}(c\bar{c})$	0	λ^3
$\bar{b} \to \bar{c}(u\bar{d})$	ϕ_1	λ^2	$D^\circ_{CP}\pi^\circ$	-	-	-
$\bar{b} \to \bar{c}(u\bar{s})$	ϕ_1	λ^3	$D^\circ_{CP}K_S$	-	-	-
$\bar{b} \to \bar{u}(c\bar{s})$	ϕ_2	λ^3	$D^\circ_{CP}K_S$	-	-	-
$\bar{b} \to \bar{u}(c\bar{d})$	ϕ_2	λ^4	$D^\circ_{CP}\pi^\circ$	-	-	-
$\bar{b} \to \bar{u}(u\bar{d})$	ϕ_2	λ^3 λ^3	$\pi^+\pi^-$ $\eta\pi^\circ$	$\bar{b} \to \bar{d}(u\bar{u})$ $\bar{b} \to \bar{d}(d\bar{d})$	0	λ^3
$\bar{b} \to \bar{u}(u\bar{s})$	ϕ_2	λ^4	$\pi^\circ K_S$	$\bar{b} \to \bar{s}(u\bar{u}), (d\bar{d})$	ϕ_1	λ^2
-	-	-	ϕK_S	$\bar{b} \to \bar{s}(s\bar{s})$	ϕ_1	λ^2
-	-	-	K_SK_S $\phi\pi^\circ$	$\bar{b} \to \bar{d}(s\bar{s})$	0	λ^3

amplitude and is directly related to the angles of the unitarity triangle of CKM-matrix as shown in Fig. 1.

Depending on the CKM-matrix elements involved in decay modes, one can measure different ϕ_i. Table 2 lists the relation of various decay modes and ϕ_i for B_d° case. The final state shown in the table is just representative and any CP eigenstates with the same quark content gives exactly the same ϕ_i. One can get those for B_s° by replacing $\phi_1 \to 0$, $\phi_2 \to \phi_3$, and $0 \to \phi_1$.

In order to determine the CKM-matrix elements, it is quite important to have small theoretical ambiguities in extracting the desired quantities. There is no theoretical ambiguity in extracting ϕ_i from a measured asymmetry, as long as a decay goes through amplitudes with a single CKM phase. This condition can be always satisfied if a decay is completely dominated by a single diagram. Unfortunately, as shown in Table 2, in addition to a tree diagram there is usually another diagram (so called Penguin) which provides same final state. Also, two tree diagrams with different phases contribute to the same final states for $D^\circ_{CP}\pi^\circ$ and $D^\circ_{CP}K_S$ cases. Only $J/\psi K_S$ ($\bar{b} \to \bar{c}c\bar{s}$) is a special case where two diagrams have same phase ϕ_1 and the condition is satisfied. The effect of Penguin diagram to ϕ_i measurement can not be reliably calculated yet. A rough estimation indicates that it amounts to $\sim 40\%$ for $\pi^+\pi^-$ case[16], for example. Recently, it has been shown that Penguin effects can be extracted out using Iso-spin relations between amplitudes[17], which will be described later. However, decay modes to which Iso-spin analysis can be applied are quite limited[17, 18] and for other modes we need to wait for more knowledge on Penguin decay, which is also one of roles of

e^+e^- B-Factories.

The existence of two diagrams decaying into the same final state with different phases could lead to a CP asymmetry in an integrated decay rate (so called "direct" CP violation). This type of CP asymmetry can also be observed at a symmetric e^+e^- B-Factory. Although, it is important to discriminate between some models (such as superweak model[19]), it does not give much information to constrain the CKM-matrix because of unknown hadronic phases, except D^oK modes described later.

The best advantage of an e^+e^- asymmetric B-Factory is that it can provide not only CP asymmetries but also most of the information needed to determine the CKM-matrix within one experiment, which enhances the reliability of measurements.

4. CP Reaches by Asymmetric B-Factory

Measurement errors of CP asymmetries for various decay modes have been estimated by Monte Carlo simulation[8] using the KEK B-Factory detector design shown in Fig. 2. A fast simulation program (FSIM) is used for the study, which simulates the detector performance as following:

1. Detector has acceptance of $17° < \theta < 150°$ for all particles.
2. It smears the particle momenta, energies, and vertex with expected resolutions.

$$\sigma_{p_t}/p_t = (0.61 \cdot p_t \oplus 0.49)\%$$
$$\sigma_E/E = [(1.6/\sqrt{E} + 0.86E^{0.3}) \oplus 0.45/E]\%$$
$$\sigma_{\Delta_z} \sim 80\mu m$$

3. Particle identification includes TOF ($\sigma_T = 150ps$), dE/dx from CDC ($\sigma = 7.2\%$), and RICH (3σ at p = 3 GeV).
4. Effect of track finding and reconstruction is not included.
5. Effect of materials in front of CsI calorimeter or effect of clustering are not included for photon detection.

Items 4 and 5 are now under investigation using full simulation program based on GEANT.

The statistical error of $\sin 2\phi_i$ from a CP asymmetry measurement is given by:

$$\delta \sin 2\phi_i = \sqrt{\frac{1 + N_{BG}/N_{obs}}{N_{obs}}} \frac{1}{d(1-2w)}.$$

Here d is a dilution factor which comes from a factor $\sin(\Delta m \cdot \Delta t)$ and the finite resolution of vertex measurement. By fitting the Δt distribution of simulated events, we get $d = 0.53$. This value weakly depends on the vertex resolution. w is a fraction of wrong B^o tagging. N_{obs} and N_{BG} represent the expected number of signal and background events, respectively. N_{obs} is given by;

$$N_{obs} = L \cdot \sigma_{\Upsilon(4S)} \cdot 2f_0 \cdot Br(B) \cdot Br(f) \cdot \epsilon_{rec} \cdot \epsilon_{tag},$$

where,

L : integrated luminosity,
$\sigma_{\Upsilon(4S)} = 1.15$ nb $= 1.15 \times 10^{-33}$ cm^2,
$f_0 = Br(\Upsilon(4S) \to B^0\bar{B}^0) = 0.5$,
$Br(B) = Br(B^o \to f)$,
$Br(f) = Br(f \to$ observed particles),
ϵ_{rec} : event reconstruction efficiency,
ϵ_{tag} : tagging efficiency of the other B^o.

Various methods of tagging have been studied. The commonly used method is with high momentum leptons ($p_l^* \geq 1.4$ GeV) and charged Kaons, which gives $\epsilon_{tag} = 0.42$ and $w = 0.09$. Further, methods using low and medium momentum leptons and the reconstruction of missing $D^{(*)\pm}$ in $D^{(*)\pm}n\pi$ decay modes have been studied[6, 8]. Combining all methods, we obtain $\epsilon_{tag} = 0.58$ and $w = 0.10$, which gives a 30% increase in the figure of merit $\epsilon_{tag}(1-2w)^2$ for CP asymmetry measurement. However, conventionally, $\epsilon_{tag} = 0.42$ and $w = 0.09$ are used below.

In the error estimation below, we use $L = 10^{41}cm^{-2}$ ($= 100\ fb^{-1}$) which is our milestone luminosity corresponding to 5 years running at Phase-I or 1 year running at Phase-II. With this luminosity, 1.15×10^8 $B\bar{B}$ events are produced, which are orders of magnitude smaller than for the hadronic machine case. Since it is considered quite hard to get a luminosity much greater than $10^{34}cm^{-2}sec^{-1}$, the number of $B\bar{B}$ is the most serious limitation of an e^+e^- B-Factory. Therefore, it is quite important to measure as many decay channels as possible for an asymmetric e^+e^- B-Factory to increase the number of observed events to increase sensitivities for CP asymmetry measurements.

4.1. ϕ_1 Measurement

4.1.1 $\bar{b} \to \bar{c}(c\bar{s})$ Mode

As mentioned previously, this mode does not suffer Penguin pollution in deriving ϕ_1 from CP asymmetry. The most promising decay mode is $B_d^o \to J/\psi K_S \to \ell^+\ell^-\pi^+\pi^-$ and called the "Gold Plated Mode (GPM)" because of its clean signature. As demonstrated by ARGUS[20] and CLEO[21], this mode is free from background. As seen from Table 3, we expect $N_{obs} = 837$ and $\delta \sin 2\phi_1 = 0.081$. CP asymmetry measurement using this mode guarantees the possibility of CP violation observation at a certain level.

However, as mentioned above, it is quite important to increase the sensitivity by using other decay modes if possible. We have explored the following decay modes:

Table 3. Summary of expected sensitivity for $\sin 2\phi_1$ measurements with $L = 100 fb^{-1}$. For all modes, tagging efficiency $\epsilon_{tag} = 0.42$, wrong tag fraction $w = 0.09$, dilution factor $d = 0.53$ are used. See text for $d_{\pm}$. (a) sum for $(cc) = \eta_c$, J/ψ, χ_{c0}, and χ_{c1}. (b) sum of $D^{\pm} \to K^{\mp}\pi^{\pm}\pi^{\pm}$, $K^-K^+\pi^{\pm}$, and $K_S\pi^{\pm}\pi^+\pi^-$.

decay mode	final states	Br(B)	$Br(f) \times \epsilon_{rec}$	N_{obs}	N_{BG}	$\delta \sin 2\phi_1$
$J/\psi K_S$	$\ell^+\ell^-\pi^+\pi^-$	3.0×10^{-4}	0.095×0.61	837	0	0.081
$J/\psi K_S$	$\ell^+\ell^-\pi^0\pi^0$	3.0×10^{-4}	0.042×0.33	201	22	0.17
$J/\psi K_L$	$\ell^+\ell^- K_L$	3.0×10^{-4}	0.140×0.34	611	75	0.099
$J/\psi K^{*0}$	$\ell^+\ell^-\pi^+\pi^-\pi^0$	1.2×10^{-3}	0.016×0.34	314	38	$0.14 \times d_{\pm}$
$\chi_{c1} K_S$	$\gamma\ell^+\ell^-\pi^+\pi^-$	5.0×10^{-4}	0.026×0.45	280	112	0.16
$\psi' K_S$	$\pi^+\pi^-\ell^+\ell^-\pi^+\pi^-$	3.0×10^{-4}	0.031×0.52	231	0	0.15
$(c\bar{c})K_S$	(hadrons)$\pi^+\pi^-$	1.4×10^{-3}	0.0055 [a]	381	252	0.15
D^+D^-	(vis)^2 [b]	5.0×10^{-4}	0.015×0.34	125	202	0.33

1) $J/\psi K_S \to \ell^+\ell^-\pi^0\pi^0$: The branching ratio is about half of GPM and this mode requires good photon detection to reconstruct the two π^0's. MC study shows $N_{obs} = 0.22 \times$ GPM.

2) $J/\psi K_L$ decay mode: K_L can be detected by observing charged particles coming from K_L interacting in the material. CsI and chambers inserted in a finely segmented iron filter can detect such a signal. Monte Carlo simulation of the hadron shower shows that about 63% of K_L can be detected. This can provide information on K_L direction and gives a kinematical constraint on the $J/\psi K_L$ event reconstruction. As shown in Fig. 3, background from $J/\psi K^*$ can be removed by kinematic cuts. Because of the clean signature of $J/\psi \to \ell^+\ell^-$, background from the continuum is expected to be small. We expect $0.73 \times$ GPM events from this mode.

3) $J/\psi K^{0*} \to J/\psi K_S\pi^0$: Since both J/ψ and K^{0*} are vector boson, CP = ±1 states are generally mixed. However, ARGUS recently showed that J/ψ and K^{0*} are highly polarized and one CP state dominates over the other.[22] If this is true, we can use the $J/\psi K^{0*}$ mode as same way as other modes. Even if two CP states are mixed with some fraction, we can extract the CP asymmetry by using a transversity analysis.[23] Fig. 4 shows the result of a transversity analysis using simulation events. The degradation factor ($d_{\pm}$) of CP measurements ranges from 1 to 2.7 depending on the mixing ratio of CP states. If the fraction of other states is less than 30%, $d_{\pm}$ is less than 1.5.

4) $(c\bar{c})K_S \to XJ/\psi K_S$ decay modes: Recently ARGUS and CLEO reported that the branching ratios of B decaying into $(c\bar{c})^{LJ}$ are similar to that into J/ψ. Especially, $Br(B^- \to \chi_{c_1}K^-)$ was measured to be 0.11 ± 0.055 %[22]. Simulation was done for decay modes $\chi_{c1}K_S \to \gamma J/\psi K_S$ and $\psi' K_S \to \pi^+\pi^- J/\psi K_S$, where $J/\psi \to \ell^+\ell^-$ and $K_S \to \pi^+\pi^-$. As shown in Table 3, both modes give about twice larger error than GPM.

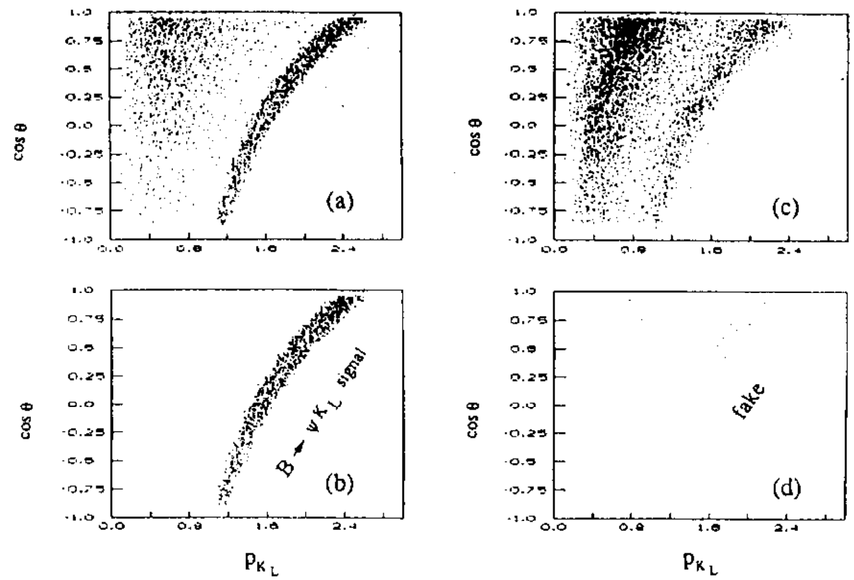

Fig. 3. $\cos\theta$ vs p_{K_L} plots: (a) for $B^0 \to J/\psi K_L$ events before cuts, (b) after selection cuts. (c) for $B^0 \to J/\psi K^*$ events before cuts, (d) after selection cuts.

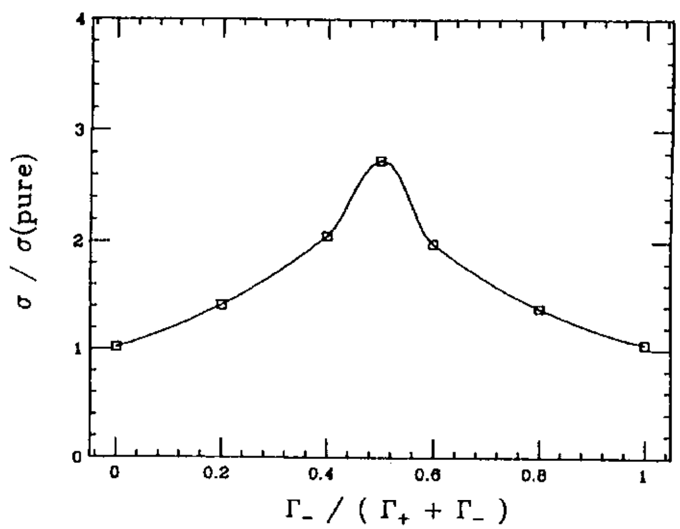

Fig. 4. The ratio of expected error on CP asymmetry for $J/\psi K_S\pi^0$ mode extracted using transversity analysis to that for pure CP state. The ratio is plotted as a function of the mixing ratio.

5) $(c\bar{c})K_S \to (hadrons)\pi^+\pi^-$ decay modes: $J/\psi \to \ell^+\ell^-$ decay mode provides a clean signature but the branching ratio is limited. An alternative way is to use decay modes into hadrons. Four charged hadronic decay modes have been studied by simulation. In this case, decays $(c\bar{c})K_S \to$ hadrons + $\pi^+\pi^-$ can be reconstructed simultaneously for $(c\bar{c}) = \eta_c$, J/ψ, χ_{c_0}, and χ_{c_1}. Branching ratios are assumed to be 5×10^{-4} for $\chi_{c1}K_S$ and 3×10^{-4} for other modes. Fig. 5 shows the invariant mass distribution of 4-charged particles after various kinematic and vertex cuts. A mass constrained fit is done to improve the mass resolution with constraint of m_{K_S} and m_{B°. The mass distribution shows clear peaks corresponding to each $(c\bar{c})$ state, although the background from the continuum is at a comparable level.

If all above modes are combined (assuming $d_\pm = 1.4$), $\delta \sin 2\phi_1$ reduces to 0.048 from 0.081 with GPM alone.

4.1.2. Non $(c\bar{c})(s\bar{d})$ final states

As shown in Table 2, there are several other decay modes which provide ϕ_1 measurements in the standard model. However, this might not be true if a CP asymmetry does not come from the CKM scheme. Therefore, it is important to measure CP asymmetry with such modes also. The following decay modes belong this category;

1) $B^\circ \to J/\psi\pi^\circ$ mode: A branching ratio is expected to be $\sim \lambda^2 \times \mathrm{Br}(B^\circ \to J/\psi K_S)$ $\sim 2 \times 10^{-5}$ because decay amplitude ($|V_{cb}V_{cd}| \sim \lambda^3$) is suppressed by λ compared to $J/\psi K_S$ ($|V_{cb}V_{cs}| \sim \lambda^2$). MC simulation showed similar detection efficiency as GPM case and this mode give $\sim 0.1 \times$ GPM.

2) D^+D^- mode: This mode has the same CKM coupling elements as the $J/\psi\pi^\circ$ mode but with external W emission diagram (no color suppression). The theoretically expected branching ratio is $\sim 5 \times 10^{-4}$ and is similar to $J/\psi K_S$. However, detection of the $D^\pm$ is difficult because it does not have a dominant decay mode. Using $D^\pm \to K^\mp\pi^\pm\pi^\pm$, $K^-K^+\pi^\pm$, and $K_S\pi^\pm\pi^+\pi^-$ (total Br = 12%), MC gives a detection efficiency of 0.34 and $N_{obs} \sim 0.15 \times$ GPM. In this mode, B° decay vertex can not be directly seen. A multi-vertex fit is performed to determine B° vertex from two $D^\pm$ decay particles. A similar vertex resolution as in the GPM case is achieved for the D^+D^- case.

As in Table 2, the above two modes suffer Penguin pollution with the same order of $\sim \lambda^3$ as tree diagram. D^+D^- mode has smaller effect because of larger branching ratio. Iso-spin analysis is not applicable because only the $\Delta I = 1/2$ amplitude contributes.

3) $\mathrm{D}^\circ_{1,2} + \pi^\circ, \eta, \rho^\circ$ mode: This mode is free from Penguin pollution and contamination from $\bar{b} \to \bar{u}(c\bar{d})$ is suppressed by λ^2. A branching ratio of this mode is expected to be $\mathrm{O}(10^{-3} \sim 10^{-4})$. However, branching ratios for $\mathrm{D}^\circ \to$ CP eigenstate are small (only 1 to 0.1%). Furthermore, MC study shows that the combinatorial background from the continuum is too severe and is not acceptable for CP asymmetry measurement.

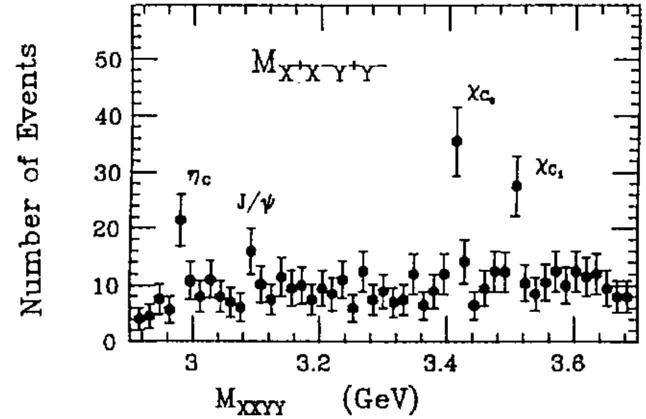

Fig. 5. Invariant mass distribution of 4-charged particles after all selection cuts for $B^\circ \to (c\bar{c})K_S$ events. Continuum, $B\bar{B}$, and $B^\circ \to (c\bar{c})K_S$ events are mixed together corresponding to $10^7 B\bar{B}$ events.

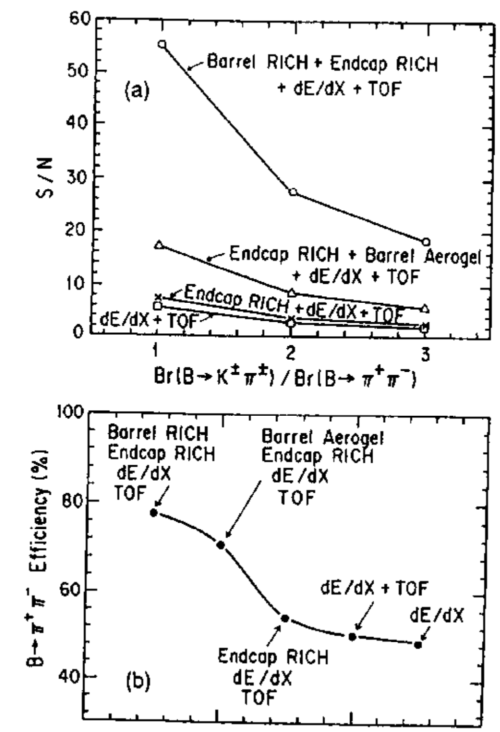

Fig. 6. (a) S/N ratio vs ratio of $K^\pm\pi^\mp$ and $\pi^\pm\pi^\mp$ branching fractions, and (b) Detection efficiency for $B^0 \to \pi^+\pi^-$ for different combinations of K/π identification devices.

At present, it has unfortunately not been possible to find good decay modes which provide a N_{obs} comparable to GPM.

4.2. ϕ_2 Measurement

4.2.1. $B^\circ \to \pi^+\pi^-$

The $B^\circ \to \pi^+\pi^-$ mode is usually mentioned as a bench mark for ϕ_2 measurement. Experimentally, the background and the branching ratio are the main concerns. Recently, CLEO observed positive signal with $Br(\pi^+\pi^- + K^\pm\pi^\mp) = 2.3\ ^{+0.8}_{-0.7} \times 10^{-5}$[24] which is consistent with the theoretical expectation [25, 26]. However, individual branching ratio has large uncertainty. Two kinds of background are important: one is from $B^\circ \to K^-\pi^+$ decay which has a similar branching ratio in theoretical estimation[26], and the other is from the continuum ($e^+e^- \to q\bar{q}$). We have made simulation studies in detail on these issues.[9]

1) $K^\pm\pi^\pm$ background: Rejection of $K^\pm\pi^\pm$ background requires good K/π identification in the high momentum region (up to 4 GeV or so) and we need a special device such as RICH or Aerogel. Detection efficiencies for $\pi^+\pi^-$ and S/N ratios are estimated for various combination of particle identification devices, as shown in Fig. 6. The detection efficiency is about 50% if only a combination of dE/dx and TOF is used which gives about 1.5 σ K/π separation for high momentum tracks. Adding RICH only in the forward region does not significantly improve the efficiency. The detection efficiency improves significantly if Aerogel counter or RICH is added in the barrel region. However the difference between using RICH over aerogel is not very large. The background fraction due to $K^\pm\pi^\mp$, on the other hand, is greatly improved if RICH is used. Study also shows that the detection efficiency and S/N ratio only weakly depend on the average number of photoelectrons (for $< N_{p.e.} > = 2 \sim 5$)

2) Continuum background: For CP asymmetry measurements we like to achieve S/N > 1, i.e. $\epsilon_c/\epsilon_B < 10^{-5}/3$ for $Br(B^0 \to \pi^+\pi^-) \sim 1 \times 10^{-5}$. Here ϵ_B (ϵ_c) is fraction of selected events for $B^0 \to \pi^+\pi^-$ (continuum) events. CLEO reported that their selection gave $\epsilon_B \sim 0.31$ and $\epsilon_c \sim 5 \times 10^{-6}$ with particle-ID using dE/dx and TOF[27]. We have checked the same selection cuts as CLEO and obtained $\epsilon_B = 0.52$ and $\epsilon_c \sim 16 \times 10^{-6}$ without particle-ID. ϵ_c reduces to 4×10^{-6} with particle-ID. In this study, we use $\sigma_{p_T}/p_T \sim 0.0024 p_T \oplus 0.0033$ which is expected when CDC, PDC, and SVD data are combined. We have also studied another set of cuts: (1) $M_{\pi^+\pi^-} < m_{B^\circ} \pm 2\sigma$, (2) $0.2 < P^*_{sum} < 0.44$ GeV, (3) Fox-Wolfman parameter ratio[28] $R_2 < 0.45$, and (4) $|\cos\theta_{spher}| < 0.7$, where θ_{spher} is an angle between the sphericity axis of $\pi^+\pi^-$ and that of the rest of the particles. This selection gives $\epsilon_B \sim 0.51$ and $\epsilon_c \sim 8 \times 10^{-6}$ without particle-ID, which is similar to CLEO's cuts. In addition, the following vertex cuts are tried: (5) $P_{\pi\pi} > 0.05$ and $P_{all} < 0.05$ where $P_{\pi\pi}$ and P_{all} are χ^2 probability of vertex fit for $\pi^+\pi^-$ and all tracks, respectively. This gives $\epsilon_B \sim 0.28$ and $\epsilon_c \sim 1.5 \times 10^{-7}$. We need further study on the optimization of cuts and their effects on the asymmetry measurement. However, from the above study, we can expect $\epsilon_c \sim 10^{-6}$ with $\epsilon_B \sim 0.45$.

Another concern for the $\pi^+\pi^-$ mode is a Penguin pollution. For $\pi^+\pi^-$ case, the effect of Penguin can be extracted out using Iso-spin relation between amplitudes of $B^\circ \to \pi^+\pi^-$, $B^\circ \to \pi^\circ\pi^\circ$, and $B^- \to \pi^-\pi^\circ$[17]. Iso-spin analysis leads to the following relations:

$$\begin{aligned}
A(B^+ \to \pi^+\pi^\circ) &\equiv A^{+0} = 3A_2 \\
A(B^\circ \to \pi^+\pi^-) &\equiv A^{+-} = \sqrt{2}(A_2 - A_0) \\
A(B^\circ \to \pi^\circ\pi^\circ) &\equiv A^{00} = 2A_2 + A_0
\end{aligned}$$

$$\begin{aligned}
A(B^- \to \pi^-\pi^\circ) &\equiv \bar{A}^{+0} = 3\bar{A}_2 \\
A(\bar{B}^\circ \to \pi^+\pi^-) &\equiv \bar{A}^{+-} = \sqrt{2}(\bar{A}_2 - \bar{A}_0) \\
A(\bar{B}^\circ \to \pi^\circ\pi^\circ) &\equiv \bar{A}^{00} = 2\bar{A}_2 + \bar{A}_0
\end{aligned}$$

where A_2 and A_0 are the amplitudes for I = 2 and 0. The Penguin diagram contributes to A_0 only and hence $A_2 = \bar{A}_2$. The above relation can be represented by two triangles shown in Fig. 7. By measuring branching ratios for the above 6 (5 independent) decay modes, one can determine all $|A_i|$'s, and therefore θ and $\bar{\theta}$ in Fig. 7. Then, real $\sin 2\phi_2$ can be determined from measured $\sin 2\phi_{meas}$ from $B^\circ \to \pi^+\pi^-$ with a 4-fold ambiguity:

$$\sin 2\phi_{meas} = Im\left(e^{i2\phi_2}\frac{1 - |\bar{A}_0/\bar{A}_2|e^{\pm i\bar{\theta}}}{1 - |A_0/A_2|e^{\pm i\theta}}\right).$$

Thus, an effect of Penguin to $\sin 2\phi_2$ measurement can be removed. Usefulness of Iso-spin analysis in actual experiment has been studied by several people[29], but further study is needed.

There are also decay modes to CP eigenstates with both neutrals through V_{ub} transition, such as $\rho^\circ\pi^\circ$, $\omega\pi^\circ$, $\eta\pi^\circ$ etc. These modes have the same CKM coupling as $\pi^+\pi^-$ but are color suppressed ($\sim 1/10$ in Branching ratio). Hence, the expected branching ratios are $O(10^{-6})$ and seems too small to be useful.

4.2.2. $B^\circ \to \rho^\pm\pi^\mp$ and $a_1^\pm\pi^\mp$

In these modes, the final states are not CP eigenstates but CP self-conjugate at the quark level. Therefore, both B° and $\bar{B}^\circ$ can decay into the same final states. In this case, CP asymmetry arises in the same way as for the CP eigenstate case. However, an additional dilution factor

$$d_\rho = \frac{2\rho}{\rho^2 + 1}, \qquad \rho = \frac{|A(\bar{B}^\circ \to f)|}{|A(B^\circ \to f)|}$$

appears because the final state is not a CP eigenstate[30]. If f is a CP eigenstate, $\rho = 1$ and $d_\rho = 1$.

Theoretically, branching ratios of these decay modes are expected to be about 3 times larger than $\pi^+\pi^-$. A MC simulation study has been done for the $\rho^\pm\pi^\mp \to \pi^\circ\pi^+\pi^-$

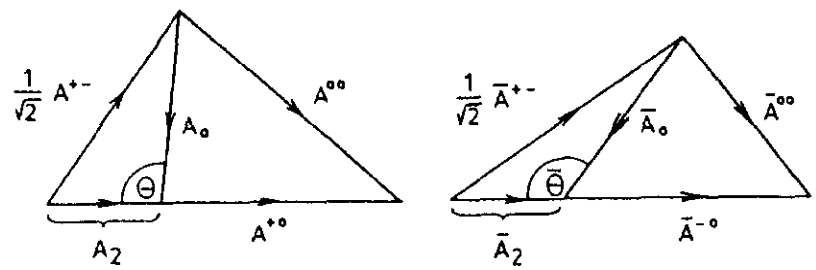

Fig. 7. Triangle relation between amplitudes for $B \to \pi\pi$ decays.

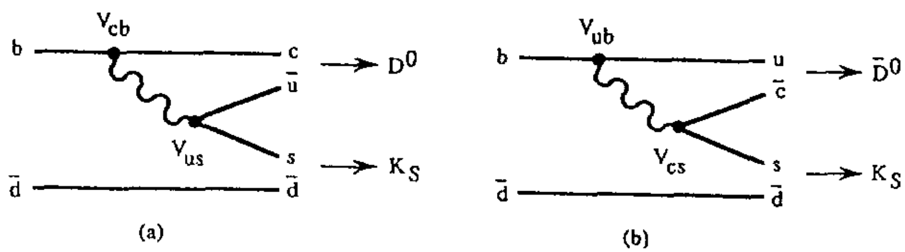

Fig. 8. Decay diagrams for $B \to D^\circ K$ and $B \to \bar{D}^\circ K$ decay modes.

Table 4. Summary of expected sensitivity for $\sin 2\phi_1$ measurements with $L = 100 fb^{-1}$. A dilution factor $d = 0.53$ are used. See text for d_ρ.

decay mode	final states	Br(B)	$\epsilon_{rec+tag}$	N_{obs}	N_{BG}	$\delta \sin 2\phi_2$
$\pi^+\pi^-$	$\pi^+\pi^-$	1.5×10^{-5}	0.45×0.42	326	73	0.14
$\rho^\pm\pi^\mp$	$\pi^\circ\pi^+\pi^-$	6.0×10^{-5}	0.215	1480	532	$0.07/d_\rho$
$a^\pm\pi^\mp$	$\pi^+\pi^-\pi^+\pi^-$	6.0×10^{-5}	0.095	656	476	$0.12/d_\rho$

and $a_1^\pm\pi^\mp \to \pi^+\pi^-\pi^+\pi^-$ modes. The background from continuum is more severe than in the $\pi^+\pi^-$ case. With kinematic cuts similar to the $\pi^+\pi^-$ case, S/N ratios are still $\sim 1/20$ and are not acceptable for CP measurements. To improve background rejection, a more elaborate selection which optimizes cuts for lepton and Kaon tags separately has been reported[30]. They obtain $\epsilon_{rec+tag} = 0.215$ and $\epsilon_c = 1.9 \times 10^{-6}$ for $\rho^\pm\pi^\mp$ case, and $\epsilon_{rec+tag} = 0.095$ and $\epsilon_c = 1.7 \times 10^{-6}$ for $a_1^\pm\pi^\mp$ case, respectively. This mode also suffers Penguin pollution. A suggestion has made to remove Penguin contribution by fitting to Dalitz plot and time distribution for $B^\circ \to \rho^\pm\pi^\mp$ mode[31].

The expected errors for $\sin 2\phi_2$ are shown in Table 4. Combining the three modes with the assumptions of $d_\rho = 0.75$ and no Penguin effect, we get $\delta \sin 2\phi_2 = 0.07$.

4.3. ϕ_3 Measurement

4.3.1. $B_s^\circ \to \rho^\circ K_S$

As seen from Table 2, one can not measure ϕ_3 using B_d° in an analogous way as for ϕ_1 and ϕ_2. Instead, one needs to use $B_s^\circ \to \rho^\circ K_S$, as is often mentioned. However, there are several inconveniences to use B_s° decay modes at an asymmetric e^+e^- B-Factory:

- B_s° can not be produced at $\Upsilon(4S)$ and one has to run at $\Upsilon(5S)$.
- Both the production cross section of $\Upsilon(5S)$ and $\mathrm{Br}(\Upsilon(5S) \to B_s^\circ \bar{B}_s^\circ)$ are considerably smaller than $\Upsilon(4S)$ and $B_d^\circ \bar{B}_d^\circ$ case.
- The expected value of x_s is too large (> 5) to measure an oscillation of CP asymmetry with a modest boost by an asymmetric B-Factory.
- This mode also suffers Penguin pollution, but Iso-spin analysis can not be applied for B_s°.

4.3.2. $B \to D^\circ K(X)$ Modes

Fortunately, a method to measure ϕ_3 using $B_{d,u} \to D^\circ K$ has been proposed[32]. This method uses branching ratio measurements only and is not specific to an asymmetric B-Factory.

B can decay into D° K or $\bar{D}^\circ K$ through diagrams shown in Fig. 8. Decay amplitudes are written as follows;

$$\begin{aligned}
B \to D^\circ K: &\quad A_D = |A_D|e^{i\delta} \\
B \to \bar{D}^\circ K: &\quad A_{\bar{D}} = |A_{\bar{D}}|e^{i\bar{\delta}}e^{i\phi_3} \\
\bar{B} \to \bar{D}^\circ \bar{K}: &\quad \bar{A}_{\bar{D}} = |\bar{A}_D|e^{i\delta} \\
\bar{B} \to D^\circ \bar{K}: &\quad \bar{A}_D = |A_{\bar{D}}|e^{i\bar{\delta}}e^{-i\phi_3}
\end{aligned}$$

where δ and $\bar{\delta}$ are hadronic phases. Since a CP eigenstate of D° can be written as $D_{1,2} = (D^\circ \pm \bar{D}^\circ)/\sqrt{2}$, the decay amplitudes can also be written;

$$\begin{aligned}
B \to D_{1,2}K: &\quad A_{D_{1,2}} = (A_D - A_{\bar{D}})/\sqrt{2}) \\
\bar{B} \to D_{1,2}\bar{K}: &\quad \bar{A}_{D_{1,2}} = (\bar{A}_D - \bar{A}_{\bar{D}})/\sqrt{2})
\end{aligned}$$

Therefore, (A_D, $A_{\bar{D}}$, $A_{D_{1,2}}$) and ($\bar{A}_D$, $A_{\bar{D}}$, $\bar{A}_{D_{1,2}}$) form triangles as shown in Fig. 9. The angle between A_D and $A_{\bar{D}}$ is $|\Delta + \phi_3|$ and the one between $\bar{A}_D$ and $\bar{A}_{\bar{D}}$ is $|\Delta - \phi_3|$, where $\Delta = \bar{\delta} - \delta$. When the absolute values of all 6 amplitudes (4 are independent) are measured, two triangles are fixed and then ϕ_3 and Δ can be obtained. The absolute values of amplitudes can be obtained from the branching ratios. $|A_{D_{1,2}}| \neq |\bar{A}_{D_{1,2}}|$ indicates direct CP violation. This method can be applied to both B° and charged B, and any $B \to D^\circ K + X$ mode can be used.

A simulation study has been done for $B^\circ \to D^\circ K_S$ and $B^- \to D^\circ K^-$ modes. D° and $\bar{D}^\circ$ are reconstructed with $K^\pm\pi^\mp$ (Br = 3.7%) and $K^\pm\pi^\mp\pi^\circ$ (Br = 11.9%) decay modes, where a Kaon charge identifies D° or $\bar{D}^\circ$. D_1 can be identified by decay modes into CP eigenstates and $K_S\pi^\circ$ (Br = 1.4%) and $K_S\omega$ (Br = 1.7%) decay modes (CP = -1) are used. Unfortunately, the branching ratio is small for D_1 which actually carries CP asymmetry. $D^\circ K$ events are selected with similar kinematic cuts as other modes already mentioned. $B^\circ \to D^\circ K_S$ mode requires tagging of the other B°, while $B^\pm$ mode is self-tagging. For $D^\circ K^\pm$ mode, good K/π separation is required in momentum region between 2.5 and 3.5 GeV, since branching ratio of $B^\pm \to D^\circ\pi^\pm$ is expected to be orders of magnitude larger. In the simulation, perfect K/π separation is assumed.

Results are summarized in Table 5. The error of ϕ_3 measurement depends on values of ϕ_3, Δ, and r, where $r = |A_{\bar{D}}|/|A_D|$. r is expected to be $\sim |V_{ub}/V_{cb}|/\lambda \sim 0.4$ for $B^\circ \to D^\circ K_S$, while ~ 0.1 for $B^- \to D^\circ K^-$ modes because of an extra contribution of non-color-suppressed diagram. From the numbers in Table 5, the error of ϕ_3 is estimated and shown in Fig. 10 for various values of ϕ_3, Δ and r. The error of ϕ_3 for B° is less than 25° (for $\phi_3 < 90°$), if $|\Delta|$ is between 50° and 150° and r is larger than 0.25. That for $B^\pm$ is less than 15° (for any ϕ_3), if $|\Delta|$ is larger than 50° and r is larger than 0.1. Combining the B° and $B^\pm$ modes, the error of ϕ_3 becomes less than 13°.

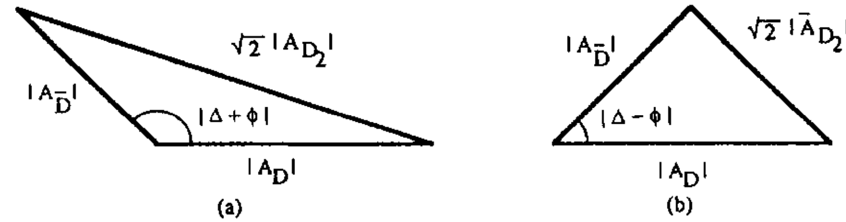

Fig. 9. Triangle relations for $B \to D^\circ K$ and $B \to \bar{D}^\circ K$ decay modes.

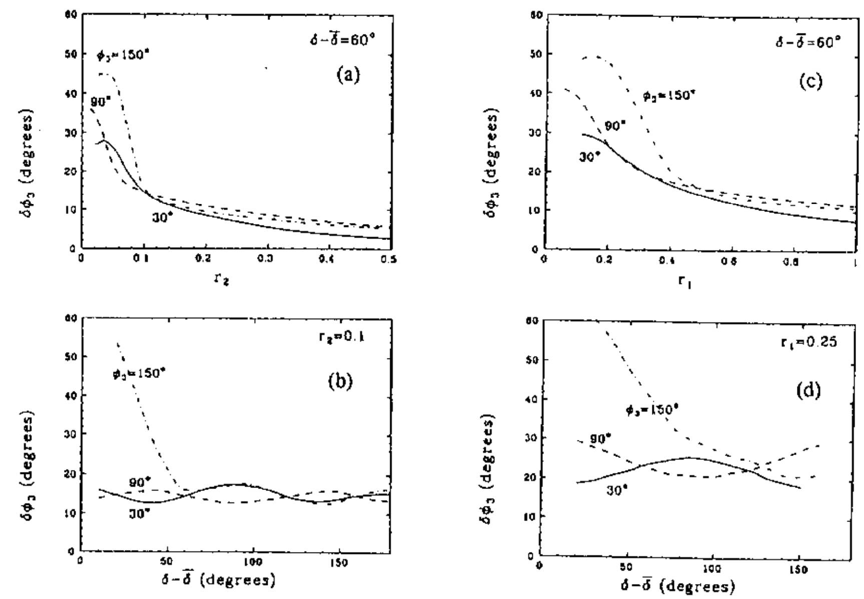

Fig. 10. (a) Expected error of ϕ_3 measurement by $B^\circ \to D^\circ K_S$ as a function of r, (b) as a function of $\delta - \bar{\delta}$. (c) Expected error of ϕ_3 measurement by $B^\pm \to D^\circ K^\pm$ as a function of r, (d) as a function of $\delta - \bar{\delta}$.

Table 5. Summary of simulation for $B \to D^\circ K$ mode for ϕ_3 measurements with $L = 100 fb^{-1}$. (a) see text

decay mode	Br(B)	final states	$Br(f) \times \epsilon_{rec}$	ϵ_{tag}	N_{obs}	N_{BG}	$\delta\phi_3^{(a)}$
$B^\circ \to D^\circ K_S$	5.0×10^{-5}	$D^\circ \to K^\pm \pi^\mp$	0.037×0.75	0.42	238	214	$\leq 25^\circ$
		$D^\circ \to K^\pm \pi^\mp \pi^\circ$	0.119×0.56				
		$D_1 \to K_S \pi^\circ$	0.014×0.43	0.42	34	29	
		$D_1 \to K_S \omega$	0.019×0.44				
$B^\pm \to D^\circ K^\pm$	3.5×10^{-4}	$D^\circ \to K^\pm \pi^\mp$	0.037×0.83	self tag	4021	176	$\leq 15^\circ$
		$D^\circ \to K^\pm \pi^\mp \pi^\circ$	0.119×0.55				
		$D_1 \to K_S \pi^\circ$	0.014×0.43	self tag	652	89	
		$D_1 \to K_S \omega$	0.019×0.49				

5. Summary

An asymmetric e^+e^- B-Factory at $\Upsilon(4S)$ provides an unique opportunity to measure CP asymmetries in B decays with many redundancies. It will shed light in understanding the origin of CP violation.

Using a "Gold Plated Mode" $B^\circ \to J/\psi K_S \to \ell^+\ell^-\pi^+\pi^-$, we can measure CP asymmetry with accuracy of $\delta \sin 2\phi_1 \cong 0.081$ with $L = 10^{41}$ cm^{-2} ($= 100\ fb^{-1}$). This is more or less"guaranteed". Adding other decay modes into $(c\bar{c})K^\circ$, we may be able to achieve $\delta \sin 2\phi_1 \sim 0.048$.

ϕ_2 could be measured with $\delta \sin 2\phi_2 \sim 0.07$ using $B^\circ \to \pi^+\pi^-$ decay as well as $\rho^\pm\pi^\mp$ and $a_1^\pm\pi^\mp$ decay modes.

A method to measure ϕ_3 using $B_{d,u} \to D^\circ K$ decay modes has been proposed. This will enable us to measure ϕ_3 at $\Upsilon(4S)$, without using B° - $\bar{B}^\circ$ mixing. The error of ϕ_3 for B° is estimated to be less than 25° (for $\phi_3 < 90°$), if $|\Delta|$ is between 50° and 150° and r is larger than 0.25. That for $B^\pm$ is estimated to be less than 15° (for any ϕ_3), if $|\Delta|$ is larger than 50° and r is larger than 0.1. Combining the B° and $B^\pm$ modes, the error of ϕ_3 becomes less than 13°.

Besides CP asymmetry measurements, asymmetric B-Factory will provide improved measurements of the length of unitarity triangle, which are also important roles of asymmetric B-Factory. This offers a stringent check of the standard model and opportunity to explore beyond the standard model.

References

[1] P.Oddone, in *Proceedings of the UCLA Workshop: Linear Collider $B\bar{B}$ Factory Conceptual Design*, ed. by D.Stoke, World Scientific, p.243 (1987).

[2] "An Asymmetric B-Factory Based on PEP - Conceptual Design Report", LBL PUB-5303, SLAC-372, CALT 68-1715, UCRL-10-106426, UC-IIRPA-91-01 (February 1991).

[3] "CESR B-Factory-CESR B Conceptual Design", CLNS 91-1050 (January 1991).

[4] "Acceler Design of KEK B-Factory", ed. by S.Kurokawa *et al.* , KEK Report 90-24 (March 1991); K.Sato, talk presented at *International Workshop on B-Factories: Accelerators and Experiments*, Tsukuba, Japan (Nov. 1992), proceedings is in preparation.

[5] "The Physics Program of a High Luminosity Asymmetric B FActory at SLAC", SLAC-353, LBL-27856, CALT-68-1588 (October 1989)

[6] "CESR B-Factory - Physics Rationale for a B-Factory", CLNS 91-1043 (January 1991).

[7] "Physics and Detector of Asymmetric B Factory at KEK" (B Physics Task Force), KEK Report 90-23 (February 1991).

[8] "Progress Report on Physics and Detector at KEK Asymmetric B Factory" (B Physics Task Force), KEK Report 92-3 (April 1992).

[9] "1992 Progress Report on B Physics Task Force Activities" (B Physics Task Force), to appear in KEK Report (March 1993).

[10] M.Kobayashi and T.Maskawa, Progr. Theor. Phys. **49**, 652 (1973).

[11] L.Wolfenstein, Phys. Rev. Lett. **51**, 1945 (1983).

[12] M.Neubert, Phys. Lett. **264B**, 455 (1991); H.Albrecht *et al.* , Z. Phys. **C57**, 533 (1993).

[13] A.Ali *et al.* , DESY 93-016 (1993).

[14] R.Ammar *et al.* , CLNS 93/1212 (1993).

[15] G.R.Harris and J.L.Rosner, Phys. Rev. **D45**, 946 (1992); M.Schmidtler and K.R.Schubert, Z. Phys. **C53**, 347 (1992).

[16] A.I.Sanda, "Towards testing the Standard Model at the level of 1%", KEK Report 90-7, page 44 (1990); M.Gronau, Phys. Lett. **300B**, 163 (1993).

[17] M.Gronau and D.London, Phys. Rev. Lett. **65**, 3381 (1990).

[18] Y.Nir *et al.* SLAC-PUB-5408 (1991).

[19] L.Wolfenstein, Phys. Rev. Lett. **13**, 562 (1964).

[20] H.Albrecht *et al.* , Z. Phys. **C48**, 453 (1990).

[21] D.Bortoletto *et al.* , Phys. Rev. **D45**, 21 (1992).

[22] M.Danilov, plenary talk presented at LP-HEP 91, July 1991.

[23] I.Dunietz, H.Quin, A.Snyder, and W.Toki, SLAC-PUB-5270 1990).

[24] H.Yamamoto, talk in this workshop.

[25] M.Bauer, B.Stech, and M.Wirbel, Z. Phys. **C34**, 103 (1987).

[26] L.L.Chau *et al.* , Phys. Rev. **D45** 3143 (1992).

[27] K.Lingel, talk given at *XXVIIth Recontres de Moriond*, France (March 1992).

[28] G.Fox and S.Wolfman, Phys. Rev. Lett. **41**, 1481 (1987).

[29] R.Aleksan, A.Gaidot and G.Vasseur, page 588 in *proceedings of B Factories - The state of the Art in Accelerators, Detectors and Physics*, SLAC-400, SLAC, April 1992; A.Snyder, SLAC B-Factory BaBar Note (1993).

[30] R.Aleksan, I.Dunietz, B.Kayser, and F. Le Diberder, DPhPE 90-17 / SLAC - 373 (1990).

[31] A.Snyder and H.Quinn, SLAC-PUB-6056 (1993).

[32] M.Gronau and D.London, Phys. Lett. **253B**, 483 (1991); I.Dunietz, CERN-TH-6161/91 (1991).

CHARM AND BEAUTY MEASUREMENTS AT FERMILAB FIXED TARGET

C. S. Mishra
Fermi National Accelerator Laboratory*
Batavia, Illinois 60510

ABSTRACT

Eighteen months after a successful run of the Fermilab fixed target program, interesting results from several experiments are available. This is the first time that more than one Fermilab fixed target experiment has reported the observation of beauty mesons. In this paper we review recent results from charm and beauty fixed target experiments at Fermilab.

I. INTRODUCTION

The Fermilab fixed target program is quite diverse. Several experiments have studied the production and decay of charm and beauty quark hardons during the past two fixed target runs, 1987-88 and 1990-91. These experiments will provide better understanding of the dynamics of charm and beauty production, better lifetime measurements, improved understanding of semileptonic and hardonic decays, searches for new bound states, studies of rare and forbidden decays such as B°, D° $\rightarrow \mu^+\mu^-$, and $D^\circ\bar{D}^\circ$ mixing. A detailed discussion of the physics of all these heavy quark production experiments is beyond the scope of this paper. These high statistics heavy quark experiments have been made possible by advances in silicon microstrip detector and data acquisition technology. All the experiments use silicon microstrip detectors to search for detached secondary vertices. Experiment E653 is a hybrid emulsion experiment measuring charm and beauty production and decay. The photoproduction of charm quark hardons has been studied by E687 and E691. E687 ran both periods and has several new results. The hadroproduction of charm has been studied by E791. B meson decays have also been reported by E672. During the last fixed target run the

*Operated by the Universities Research Association under contract with the U.S. Department of Energy

hadroproduction of beauty mesons was studied by two experiments, E771 and E789. These two experiments were planned to be the initial phase of further experiments to investigate the possibility of a high sensitivity B experiment. Experiment E771 was designed to study B production and decay by measuring B$\rightarrow J/\psi K_s$ and B$\rightarrow \mu X$. Experiment E789 studied two body decays of charm and beauty mesons in a high rate fixed target environment, and has measured dihadron decays of D^o mesons and also B$\rightarrow J/\psi$ X.

It is not possible to discuss all of these experiments in detail here, only important features of these experiments and their physics results will be discussed. Each experiment's results will be presented separately. We discuss the luminosity limitations of fixed target heavy flavor production experiments at the end of this paper.

II. Charm Production and Decay

Charmed hadron production and decay have been studied by using photon, pion and proton beams. In photoproduction, the charm pair production cross section is about 1% of the total cross section. Photoproduced charm events have low primary multiplicity, but the lack of a primary vertex can make the event reconstruction difficult. The photon beam intensity is lower than typical hadron beams.

On the other hand, in hadroproduction the charm to total cross section ratio is only about 0.1% ($30\mu b$/40 mb). The advantage of hadroproduction is the presence of a primary vertex and higher intensity beams. The total hadroproduction cross section is much larger which thus requires a selective trigger and/or a high bandwidth data acquisition system. Fig.1 shows a comparison between the photoproduction experiment E691 [1] and the hadroproduction experiment E791 [2]. The signal to background of the hadroproduction experiment is better. This figure also shows how much the capability of charm experiments has increased in about three years. In this section we will limit our discussion to the hadronic decays of charm. There are several new results on the semileptonic decays of charm which are described in detail elsewhere [3].

A. E687

Experiment E687 [4] is a high rate multiparticle spectrometer dedicated to the photoproduction of charm. The goal of the experiment is to reconstruct a large sample of charm quark decays in order to study the dynamics of heavy quark photoproduction, to study charm quark weak decays, and to study J/ψ photoproduction.

During the 1990/91 run more than 500 million events were collected. The data contains more than 10^5 fully reconstructed charm decays [5]. E687 is currently analyzing their data and has several new results. This experiment has measured the lifetime of charmed mesons and baryons more accurately than before, providing information on the relative importance of different weak decay diagrams and various modifying hadronic effects. Fig.2 shows the invariant mass plot of $\phi\pi^+$ combinations as a function of various cuts on the distance of the decay vertex from the primary vertex (L) and the error on that quantity (σ). The two peaks in the plots are the Cabibbo suppressed decay of D^+ and the Cabibbo flavored decay of the D_s^+. As the L/σ cut is increased the peak gets cleaner and the relative size of the D^+ increases due to its longer lifetime.

A comparison of the D_s lifetime from different experiments is shown in Fig.3. Due to the high statistics of E687, the new result is the most accurate and allows a comparison of the D_s and D^o lifetimes with better precision [6]. The E687 measurements give $\tau_{D_s}/\tau_{D_o} = 1.13 \pm 0.05$, suggesting that the D_s is sightly longer lived than the D^o.

Experiment E687 has also observed and measured the lifetime of the charmed baryons $\Lambda_c, \Xi_c^+, \Xi_c^o$, and Ω_c^o. Fig.4 shows the mass plot of these four charmed baryons. The lifetime measurements of charmed baryons provide important tests of theoretical models which include light quark interference effects and exchange diagrams. The measured lifetime hierarchy of charmed baryons, shown in Fig.5, is consistent with the theoretical prediction [7]. According to this model the exchange diagram and light quark interference play a significant role in the lifetime of charmed baryons. The E687 measurement of lifetimes, $\Lambda_c^+ = 0.215^{+0.025}_{-0.017} \pm 0.008ps, \Xi_c^+ = 0.41^{+0.11}_{-0.08} \pm 0.02ps$, and $\Xi_c^o = 0.101^{+0.025}_{-0.017} \pm 0.01ps$, have smaller uncertainties than previous measurements by NA32.

The Cabibbo suppressed decays $D^o \rightarrow \pi^+\pi^-$ and $\Lambda_c^+ \rightarrow pK^-K^+$ have been observed by E687. Fig.6 shows the invariant mass distribution of $D^o \rightarrow K^-K^+\pi^+\pi^-$, $D^o \rightarrow K^-K^+K^-\pi^+$, and $\Lambda_c^+ \rightarrow pK^-K^+$. These decay modes contain two or three charged kaons.

The D^{**} charmed meson states, in which the relative angular momentum between the charm quark and lighter quark equals one, have also been observed by E687 [8]. These previously observed D^{**} states [9] are $D^{**o}(2460) \rightarrow D^+\pi^-$, $D^{**o}(2420) \rightarrow D^{*+}\pi^-$, and $D_s^{**+}(2536) \rightarrow D^{*+}K_s^o$. The mass difference ($M_{D^+\pi^-}$ - M_{D^+}) distribution, Fig.7, shows a pronounced peak at $\Delta M \sim 600$ MeV. This peak is due to $D^{**o}(2460)$ decaying into $D^+\pi^-$. The natural width of this peak has been calculated to be 42 ± 10 MeV. Fig.8 shows the invariant mass difference plot for $M_{D^{*+}\pi^-}$ - $M_{D^{*+}}$ with a peak at about 420 MeV. This peak is due to the $D^{**o}(2420)$ and has a natural width of 14 ± 8 MeV. Fig.9 shows the mass difference distribution of the $D_s^{**+} \rightarrow D^*K$ decay. This observed peak is due to the $D_s^{**+}(2536)$ state and has a natural width of 12 ± 6 MeV.

E687 has enough statistics to study the production dynamics (the xf and pt distributions) of the charmed hadrons and to study correlations between charm pairs.

B. E791

Experiment E791 is a charm hadroproduction experiment built reusing the same basic spectrometer as a series of charm experiments, photoproduction E691 [10] and hadroproduction E769 [11]. The goals of E791 are to collect a large unbiased charm sample in order to make precision, high statistics charm measurements and to search for rare and forbidden charm decays. Using a 500 GeV/c π^- beam incident on a segmented target, this experiment has collected over 20 billion "minimally biased" events. A high E_t trigger was made possible by the segmented nature of their electromagnetic and hadronic calorimeters. The large data set (50 Terabytes) was made with a high speed parallel data acqusition system [12].

The analysis of the E791 data is currently in progress, Fig.10 shows some of their preliminary charm signals. Based on the preliminary analysis of 10% of data, they expect to reconstruct more than 200k charm decays [2]. This large sample of charm decays will enable them to set limits on flavor changing neutral current decays of D^o and search for $D^o\bar{D}^o$ mixing. The current data sample is about 20 times larger than the predecessor experiment E691.

III. Beauty Production and Decay

The recent observation [13] of large mixing of neutral B mesons suggests [14] the possibility that CP-violation could be observed in a high statistics study of B^o decays. The luminosity and the small cross section at existing e^+e^- colliders severely limit the B production rate. An alternative is the detection of B decays at a high energy proton accelerator, FNAL or CERN, either in fixed target or collider mode. At proton colliders both the cross section and luminosity are high. The crucial questions to be addressed by these initial experiments are how many b's can be produced, and can one distinguish the b-decay events from the non b quark backgrounds. The large number of $b\bar{b}$ pairs produced at the Fermilab Tevatron makes it interesting to explore different methods to trigger, detect, and reconstruct both the inclusive and exclusive b quark hadrons. Experiments E653 and E672 have studied b quark production cross sections and dynamics. Experiments E771 and E789 are exploring possible ways to do high yield b quark experiments at Fermilab fixed target in order to reach CP sensitivity.

A. E653

Experiment E653 [15] is the first fixed target experiment to report more than one reconstructed B pair. The hybrid emulsion spectrometer used in this experiment has been described in detail elsewhere [16]. The experiment uses an active nuclear emulsion target in which both the primary interaction and short lived decays are observed. A silicon spectrometer with 18 planes of silicon microstrip vertex detectors provides tracking information for selecting events to be scanned in the emulsion. During the second run of E653, data was taken with a 600 GeV/c π^- beam. The trigger required an interaction in the target and a muon that penetrated 3900 gm/cm^2 of absorber. A total of 8.2×10^6 events, selected from 2.5×10^8 interactions, were recorded during the run. Reconstructed events with a muon of transverse momentum greater than 1.5 GeV/c were selected for scanning in the emulsion.

The first scan of the data sample yielded 9 $b\bar{b}$ pair candidates. The decay modes and topologies of these 9 pairs are shown schematically in Fig.11. There are 12 neutral and 6 charged b decays, produced in 4 neutral-neutral, 4 neutral-charged and 1 charged-charged combinations. The production x_f and p_t^2 distributions [17] are shown in Fig.12. The inclusive x_f distribution is described by $d\sigma/dx_f = (1 - |x_f - xo|^n)$ with $n = 5.0^{+2.7+1.5}_{-2.1-0.9}$ and a positive offset $xo = 0.06^{+0.06}_{-0.07}$. The inclusive p_t^2 distribution is broader than that of charm and is described by $d\sigma/dp_t^2 = \exp(-bp_t^2)$ with $b = 0.13^{+0.05}_{-0.04}$. Based on these 9 pair events, the pair production cross section, assuming a linear A dependence, is $33 \pm 11 \pm 6$ nb/nucleon [15,17], consistent with QCD predictions [18].

The measured lifetime of the 12 neutral and 6 charged beauty decays is [19] $\tau_{b^o} = 0.81^{+0.34+0.08}_{-0.22-0.02}$ ps and $\tau_{b^\pm} = 3.84^{+2.73+0.08}_{-1.36-0.16}$ ps. The combined sample lifetime is $\tau_b = 1.88^{+0.66+0.16}_{-0.45-0.07}$ ps, where the first errors are statistical and the second are systematic. A second scan of the data with a reduced p_t cut on the muon has so far yielded three more beauty pair candidates.

B. E672

Experiment E672 has investigated B$\rightarrow J/\psi X$ decays in π^- nucleon collisions at 530 GeV/c by analyzing the J/ψ vertex distribution [20]. They have reported evidence for the exclusive B decay modes B$\rightarrow J/\psi K^\pm$ and $J/\psi K^{o*}$. Experiment E672 sits behind Experiment E706 at Fermilab. The experiment triggers on final states containing two muons. This experiment uses the E706 vertex spectrometer to search for secondary J/ψ vertices in their J/ψ sample. The data was collected during the 1990 fixed target run with a 530 GeV/c π^- beam incident on a segmented Cu and Be target. About 5 million triggers were recorded during this run.

Of the 11,000 reconstructed J/ψ events, 11% have more than one vertex. About 64% of these events have a detached J/ψ vertex. A vertex fit was done for dimuon pairs in the J/ψ mass range 2.85 GeV/c^2 < $M_{\mu\mu}$ <3.35 GeV/c^2. The J/ψ vertex z-position distribution is shown in Fig.13. The target, two 0.8mm thick pieces of Cu followed by 3.71 and 1.12cm thick Be, is clearly separated in the J/ψ vertex distribution plot. They reconstruct the difference of the primary and secondary vertex in each event. Fig.14 shows the Z position difference of the primary and J/ψ vertices. The J/ψ's from the primary vertex are centered at zero, while events with a difference greater than 1 mm are J/ψ's from a secondary vertex. The false event reconstruction rate is given by the events reconstructed with a negative δZ. The sample contains 857 J/ψ events with a downstream vertex, of which only 73 events survive different selection cuts to eliminate backgrounds. The Z position of the primary and secondary vertex of the 73 events is shown in Fig.15(a,b). From Monte Carlo simulations, the estimated backgrounds are 4 ± 2 events due to false secondary vertices and 33 ± 7 due to secondary interactions.

The experiment then searched for secondary vertices in the mass free regions of the target-SSD system. They report a preliminary signal of 9 ± 3 secondary vertex J/ψ events from B decays in the mass free region. Fig.16 shows the secondary J/ψ vertex position in the y-z plane in the mass free region, with errors. Based on 9 ± 3 B$\rightarrow J/\psi X$ candidate events, the J/ψ cross section, assuming linear A dependence and a B$\rightarrow J/\psi X$ branching fraction of 1.57×10^{-3}, is $\sigma_{B\bar{B}}(X_f > 0.1) = 28 \pm 9 \pm 8$ nb/nucleon.

Experiment E672 has also searched for the exclusive B decays, B$\rightarrow J/\psi K^\pm$ and B$\rightarrow J/\psi K^{o*}$, in their sample of 73 secondary vertex J/ψ events. The experiment has no hadron identification and considers all non-muon tracks as hadrons. In three prong events with, two muons plus another track, the third track was assigned a kaon identification if it had a pt > 0.5 GeV and satisfied all other secondary vertex requirements. In four prong events, K^{o*} was observed by its decays into $K\pi$. A non-muon track in these four prong events was assigned a kaon mass if it had a momentum greater than twice the other. The combined $J/\psi K^{\pm}$ and $J/\psi K^{o*}$ invariant mass distribution is shown in Fig.17. There is an excess of events near the B mass. A background analysis using primary vertex events subjected to same cuts shows no evidence of enhancement in the B mass region.

This experiment has also measured the production of χ states. During the 1991 run, E672 collected 10 million triggers with 530 GeV/c and 800 GeV/c protons incident on Be and Cu targets.

C. E771

Experiment E771 [21] is a high rate 800 GeV proton fixed target beauty experiment using the upgraded E705 spectrometer. The main goals of the experiment are to measure the total cross section for $B\bar{B}$ production at 800 GeV, to study inclusive distributions and correlations and reconstruct exclusive B final states, measure beauty lifetimes in both exclusive and inclusive modes, and observe $B\bar{B}$ mixing. E771 has a magnetic spectrometer which follows an array of target foils and 18 planes of silicon vertex detectors. During 1990-91, experiment E771 could instrument only 60% of the original design number of silicon readout channels. In a four week running period the experiment recorded 127 million dimuon and 62 million single muon triggers.

The experiment targets 800 GeV/c protons on a distributed foil target at a 2 MHz interaction rate. Data acquisition is triggered by dimuons or single high pt muons. The data analysis from the last run is currently in progress. The dimuon invariant mass from the preliminary analysis of 10% of the data is shown in Fig.18, J/ψ and ψ' peaks are clearly resolved. The preliminary cross section for 800 GeV protons is $\sigma(J/\psi) = 339 \pm 10 \pm 74$ nb and $\sigma(\psi(2s)) = 72 \pm 16 \pm 16$ nb [21].

Using the silicon vertex spectrometer, a search for downstream J/ψ vertices has been made on about 10% of the data. Fig.19 shows one four prong event which reconstructed with a downstream vertex consistent with a B mass. This event is consistent with a B$\rightarrow$ $J/\psi K\pi \rightarrow \mu^+\mu^- K\pi$ (non resonant) decay.

D. E789

Experiment E789 studies low multiplicity decays of neutral D and B mesons in a high rate environment. The experiment used the upgraded E605 [22], E772 [23] spectrometer used in previous experiments to detect hadron and lepton pairs with good mass resolution and high rate capability. The spectrometer was upgraded with the addition of a silicon vertex spectrometer, drift chambers, a vertex trigger processor, and an upgraded high capacity data acquisition system. The main goals E789 are to measure the B production cross section at 800 GeV via B$\rightarrow$ $J/\psi X$ decays and to search for charmless dihadron decay modes such as B$\rightarrow \pi^+\pi^-$.

A schematic view of the E789 [24] spectrometer and its silicon vertex spectrometer is shown in Fig.20(a,b). The silicon spectrometer consists of sixteen 50μm pitch silicon strip detectors, each $5 \times 5cm^2$ in area and 300μm thick, covering an angular range of 20 to 60 mr above and below the beam axis. Unlike other fixed target experiments where a defocused beam is incident on foil targets and the silicon spectrometer intercepts the incident beam, the E789 silicon spectrometer has a beam hole. This enables the spectrometer to take a high interaction rate but reduces the acceptance. An 800 GeV proton beam was incident on one of several thin wire targets ranging from 0.1 mm to 0.3 mm high and 0.8 mm to 3 mm thick. The signals from silicon microstrips were read by DC coupled Fermilab 128 channel amplifiers [25] and LBL discriminators [26] synchronized to the accelerator RF. The electronics were designed to have 1 RF bucket (19 ns) resolution time; on average only 2 RF bucket resolution was achieved due to several limitations. The use of a thin target localizes the primary interaction vertex and greatly simplifies the offline event reconstruction.

Two different spectrometer settings were needed to span the mass regions of the D$\rightarrow h^+h^-$, B$\rightarrow$ $J/\psi X$, and B$\rightarrow h^+h^-$ decays. A total of 1.5×10^9 events were recorded in 8×10^4 spills. The beauty data corresponds to a total of 3×10^{13} interactions. The charm setting was used to study the performance of the newly installed silicon spectrometer. The nuclear dependence of D meson production, measured with gold and beryllium targets, should give valuable insight into the origin of the J/ψ A dependence observed at the same beam energy [23]. A vertex reconstruction trigger processor was used online for the D data taking. For the beauty setting, a proton beam of 5×10^{10} protons per pulse was incident on a 3mm thick gold target yielding a 50 MHz interaction rate.

Fig.21 shows the E789 dihadron mass spectra for the charm data sample. The $D^o \rightarrow \pi^+K^-, \bar{D}^o \rightarrow K^+\pi^-$ and $D^o, \bar{D}^o \rightarrow \pi^+\pi^-, K^+K^-$ decays are clearly visible in this figure. Information from the ring imaging Cherenkov detector has not been used in this analysis for π/K identification. Fig.22 shows the D^o lifetime distribution obtained by making a side band subtraction at the D^o peak. The estimated D^o lifetime is 0.41 ± 0.03 ps consistent with other published measurements [27]. The nuclear dependence of D production was also measured in this experiment by measuring D^o production from Be and Au targets. The preliminary value of α is 1.02 ± 0.06. Analysis of the D$\rightarrow$ dilepton mode data is in progress. E789 is expected to set a 90% C.L. upper limit of 5×10^{-6} for D$\rightarrow e^+e^-, \mu^+\mu^-$, and $e\mu$.

The dimuon mass spectrum from a preliminary analysis of data at the beauty mass setting is shown in Fig.23. These events are required to have silicon tracks but no vertex cut is applied. There are approximately 50k J/ψ and 600 ψ' events in this sample. Requiring that the impact parameters for both muon tracks are greater than 150μm and that the decay vertex is between 0.7 cm and 5.0 cm yields the dimuon mass spectra in Fig.24a. A J/ψ peak is clearly visible. These 24 events are candidate events for B$\rightarrow$ $J/\psi X \rightarrow \mu^+\mu^- X$ decays. Backgrounds caused by silicon tracking errors are estimated by selecting events with an apparent vertex upstream of the target, $-5.0cm < Z_{vert} < -0.7cm$, see Fig.24b. The Z_{vert} symmetry of the silicon tracking is confirmed using a dihadron data sample, where no signal is expected to be observed. A more detailed analysis, currently underway, using a different silicon tracker should confirm the b signal and allow the calculation of the b production cross section. This experiment is also studying B$\rightarrow J/\psi X \rightarrow e^+e^-X$, B$\rightarrow \mu^+\mu^-, e^+e^-, e\mu, h^+h^-$ decays. Extrapolating from the current yield, the full sample should provide about 75 reconstructed B$\rightarrow J/\psi X$ events. Assuming no decays are observed after all cuts, a 90% confidence level upper limit for rare decays of about 1.0×10^{-4} should be obtained.

V. Limitations of Fixed Target heavy quark experiments

This is a controversial topic; opinions vary considerably. It is not directly related to the topic of this paper, but is an important issue at this workshop. The experiences gained from the current experiments are the best guide to future high rate beauty experiments. At 800 GeV, the beauty production cross section is predicted to be about 10 nb compared to 40 mb of total cross section. The experiment must be capable of handling a very high trigger rate and must find a very small signal in a very large background. There are two major types of background. The first is due to the copious production of light hadrons at the primary vertex. The second arises from pairs of long lived particles, each decaying at different distances downstream of the target. Accurate multiple vertex reconstruction in the presence of these two backgrounds is extremely difficult, especially when the soft pions from either source multiple scatter in the silicon detectors.

The silicon detector can be placed either in the beam (E771), or very close to the beam (E789), to accept the maximum number of B decays. To accumulate high statistics these experiments must run at a high interaction rate, which results in very high track rates in the silicon and radiation damage of the silicon detectors. The high track density makes it difficult to correctly identify tracks, one must devise a very sophisticated and highly segmented vertex spectrometer to reduce this problem. Besides the hard and soft tracks produced in the target, there are tracks present in the events which are due to the decay of long lived strange and charmed hadrons. Such tracks, paired with a misreconstructed primary vertex track, yield fake downstream vertices. The high rate of tracks also limits the capability of the downstream charged particle spectrometer. Experiment E789, which has a very limited acceptance (about 1%), was rate limited in almost all of its detectors. One must deal with higher rates if one increases the angular acceptance to achieve higher statistics or broaden the physics potential. It is not enough to simulate the signal to claim the potential of an experiment. In designing future experiments, we must use the backgrounds and hit density information gathered in recent runs to estimate realistically the signal to background ratios.

It is my impression that doing a high rate, high yield beauty experiment with Fermilab fixed target beams is difficult. It might be possible to do an experiment to measure the cross section, lifetime, production dynamics, with reasonable statistics and to observe some rare decays in a long run. It is unlikely that a Fermilab fixed target B experiment will be able to reach CP sensitivity by only the same means that have been very successful for present Charm experiments. On the other hand it does appear that an order of magnitude over current charm statistics can be achieved in a newly designed charm experiments [28].

VI. Acknowledgments

I would like to thank C. N. Brown for much assistance and the opportunity to give this talk. I would also like to thank the different collaborations, and specifically J. N. Butler and P. Garbincius (E687), J. A. Appel and M. V. Purohit (E791), R. Lipton (E653), A. Zieminski (E672), and L. Spiegel (E771) for providing their data.

VII. REFERENCES

[1] J. C. Anjos et al., Phys. Rev. D48 (1993) 56.

[2] J. V. Appel and M. V. Purohit, private communication.

[3] J. P. Cumalat, Proc. of DPF92, Nov 10-14, 1992, Fermilab.

[4] P. L. Frabetti et al., NIM A320 (1992) 519.

[5] P. H. Garbincius, private communication; J. Butler and P. H. Garbincius, Fermi Report, April 1993.

[6] P. L. Frabetti et al., Fermilab Pub 93/030E, submitted to Phys. Rev. Lett.

[7] B. Guberina et al., Z. Phys C33 (1986) 297.

[8] S. Shukla, Proc. of DPF92, Nov 10-14, 1992, Fermilab.

[9] J. C. Anjos et al., Phys. Rev Lett 62 (1989) 1717; H. Albrecht et al. Phys. Lett. B221 (1989) 422; P. Avery et al. Phys. Rev. D41 (1990) 774; H. Albrecht et al. Phys. Lett. B323 (1989) 398, B230 (1989) 162; A. E. Asratyan, Z. Phys. C40 (1988) 483.

[10] J. R. Raab et al., Phys. Rev D37 (1988) 2391.

[11] G. A. Alves et al., Phys. Rev. Lett. 69 (1992) 3147.

[12] S. Amato et al., E791 Collaboration, Submitted to NIM.

[13] H. Albrecht et al., Phys. Lett B192 (1987) 245; C. Albajar et al., Phys. Lett B186 (1987) 247.

[14] F. J. Gilman, Proc. of the workshop on high sensitivity Beauty Physics at Fermilab, 1987.

[15] R. Lipton, private communication, Fermi-Conf 92/06 and in the Proc. of 1991 SLAC summer Institute, SLAC, Aug 1991; K. Kodama et al., Phys. Lett B305(1993)359.

[16] K. Kodama et al., NIM A289 (1990) 146.

[17] K. Kodama et al., Phys. Lett B284 (1992) 961.

[18] E. Berger, Argonne National Lab, ANL-HEP-CP-88-26.

[19] K. Kodama et al., Prog. of Theoretical Physics, Vol 89, No 3, pp679, March 1993.

[20] R. Jesik, Ph. D. thesis 'Beauty Production in π^- A collision at 530 GeV/c', Univ. of Illinois at Chicago, Aug 1993; R. Jesik et al., Proc. XXVI Int conf. on High Energy Physics, Dallas,1992; L. Dauwe et al., Proc of DPF92, page 759, Fermilab, 1992.

[21] L. Spiegel, private communication.

[22] J. A. Crittenden et al., Phys. Rev. D34 (1986) 2548; G. Moreno et al., Phys. Rev. D43(1991)2815.

[23] D. M. Alde et al., Phys. Rev. Lett. 66 (1991) 133, Phys. Rev. Lett. 66 (1991) 2285.

[24] J. C. Peng et al., Proc. XXVI Int. Conf. on High Energy Physics, Dallas, 1992; M. H. Schub et al., Proc. of DPF92, 10-14 Nov 1992, Fermilab; D. Jansen et al., Fermi-Conf93/129E and in the Proc. of 28th Recontres de Moriond:QCD and High Energy Hadronic Interactions, Les Arcs, France, March 1993.

[25] D. Christian et al., IEEE Trans. Nucl Sci NS36 (1989) 507.

[26] B. T. Turko et al., IEEE Trans. Nucl Sci N39 (1992) 758.

[27] Particle Properties Data Booklet, Particle Data Group, Phys. Rev D45, 1992.

[28] Fermilab Experiment E831, J. Cumalat Spokesperson; Fermilab Proposal P829, D. Christian and M. Sokoloff Spokesperson.

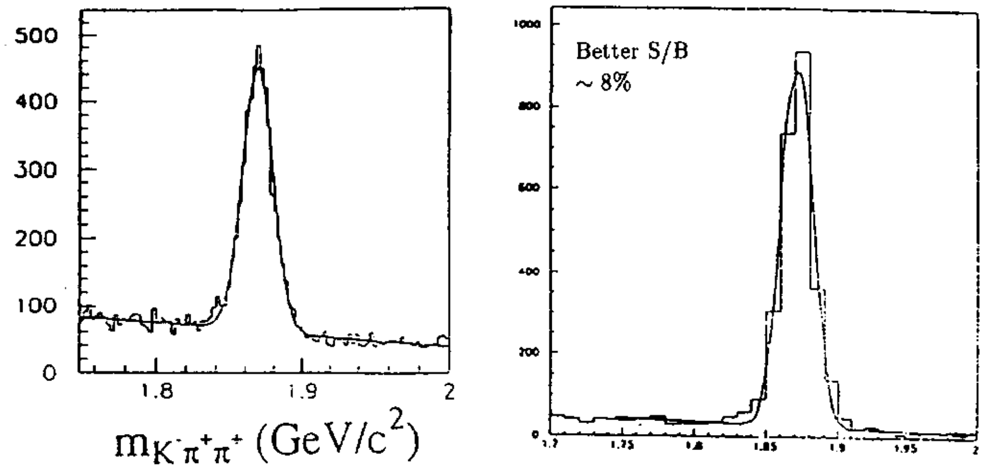

Fig. 1 Comparision between photoproduction (E691) and hadroproduction (E791) of charm experiments.

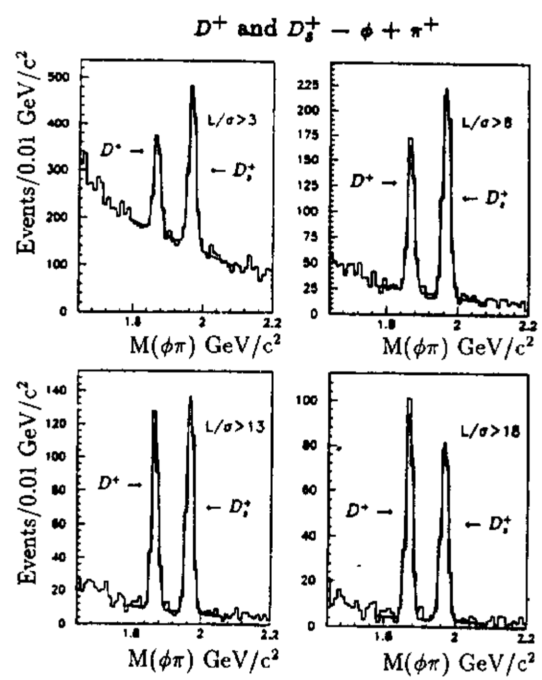

Fig. 2 Invariant Mass distributions for $\phi\pi$ combination, subject to various detachment cuts.

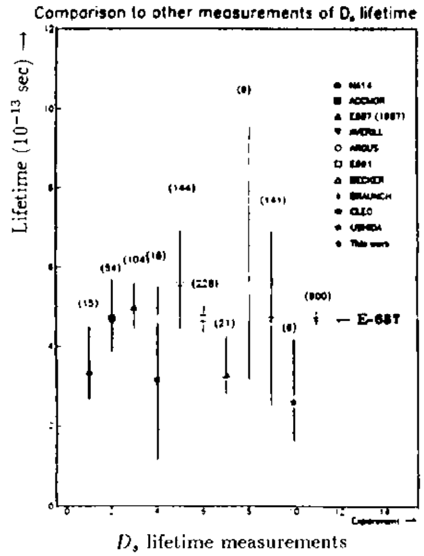

Fig. 3 World data of the D_s lifetime.

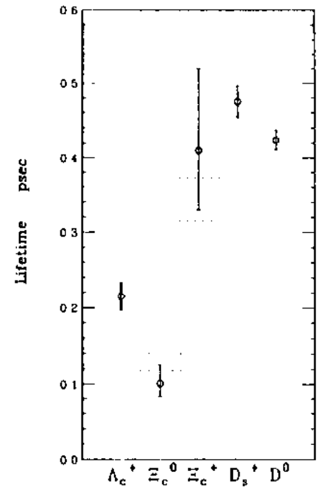

Fig. 5 Lifetime hierarchy for charmed baryons and theoretical predictions (dotted region)

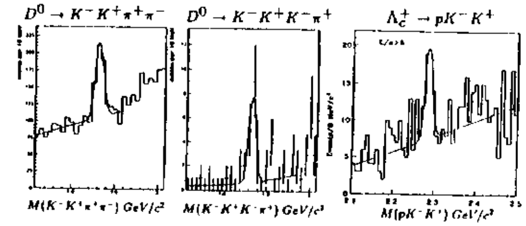

Fig. 6 Invariant Mass distributions for $K^-K^+\pi^+\pi^-$, $K^-K^+K^-\pi^+$, and pK^+K^-.

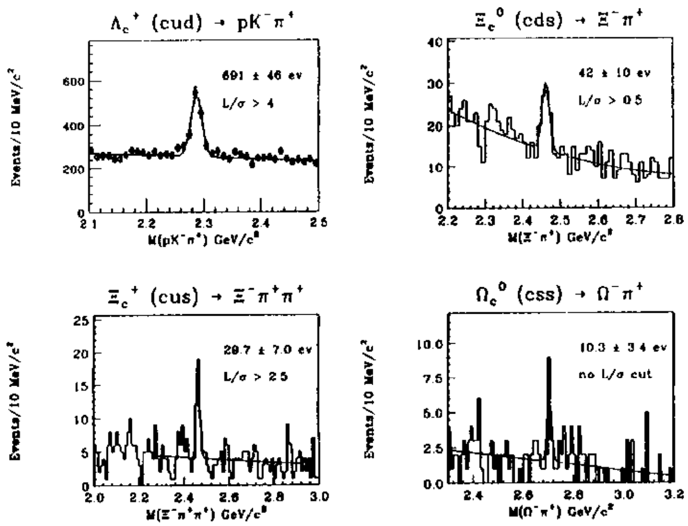

Fig. 4 Signal of four Charmed baryons.

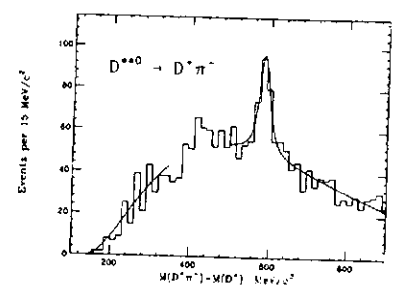

Fig. 7 Invariant Mass distributions for $M_{D^+\pi^-} - M_{D^+}$. The peak is due to $D^{**0}(2460)$.

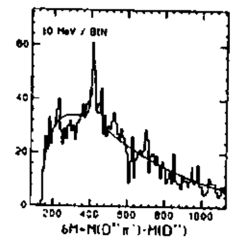

Fig. 8 Invariant Mass distributions for $M_{D^{*+}\pi^-} - M_{D^{*+}}$. The peak is due to $D^{**0}(2420)$.

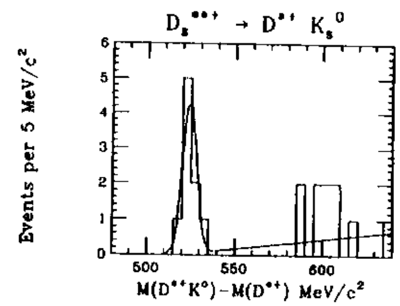

Fig. 9 Invariant Mass distributions for $M_{D_s^{*+}} - M_{D^{*+}}$. The peak is due to $D_s^{**+}(2536)$.

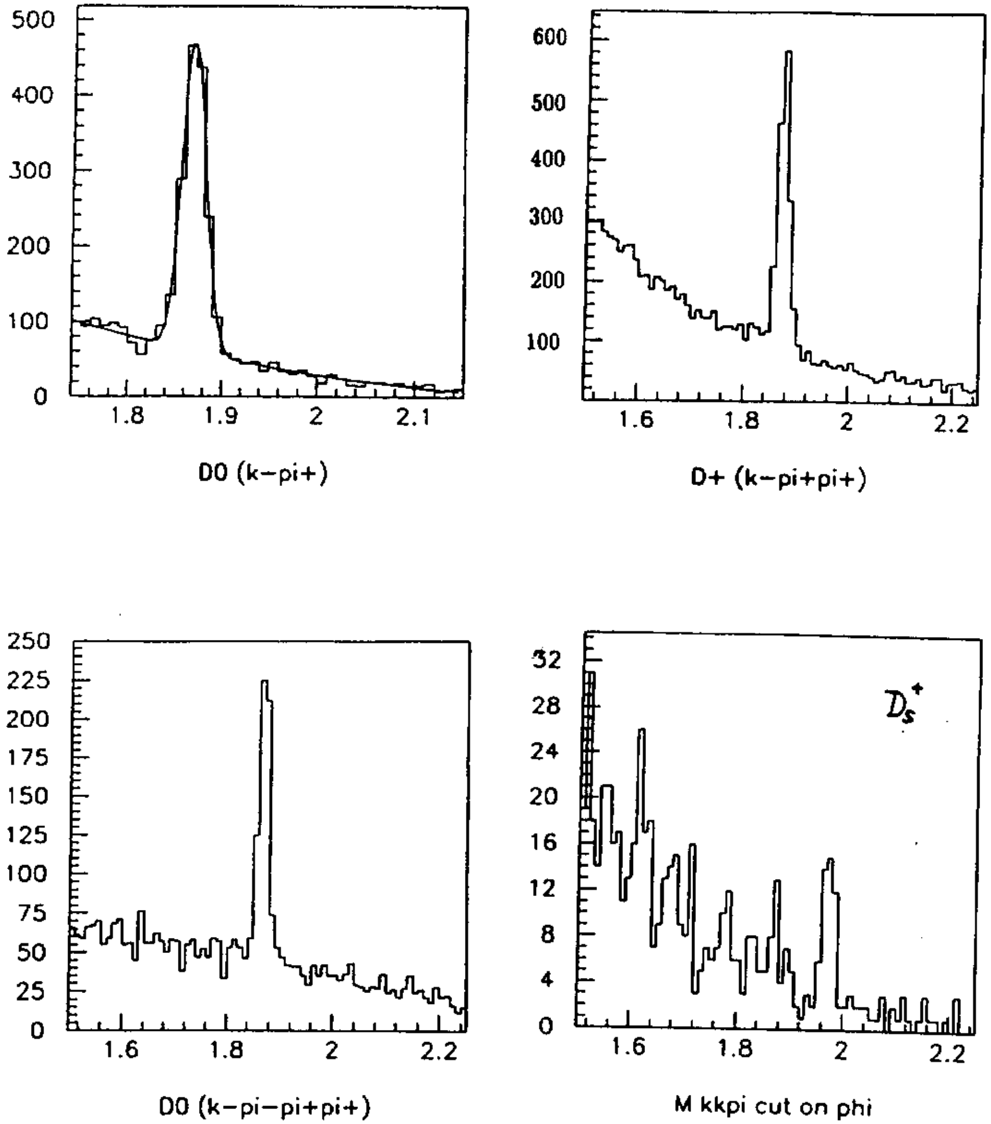

Fig. 10 Preliminary mass distribution from E791.

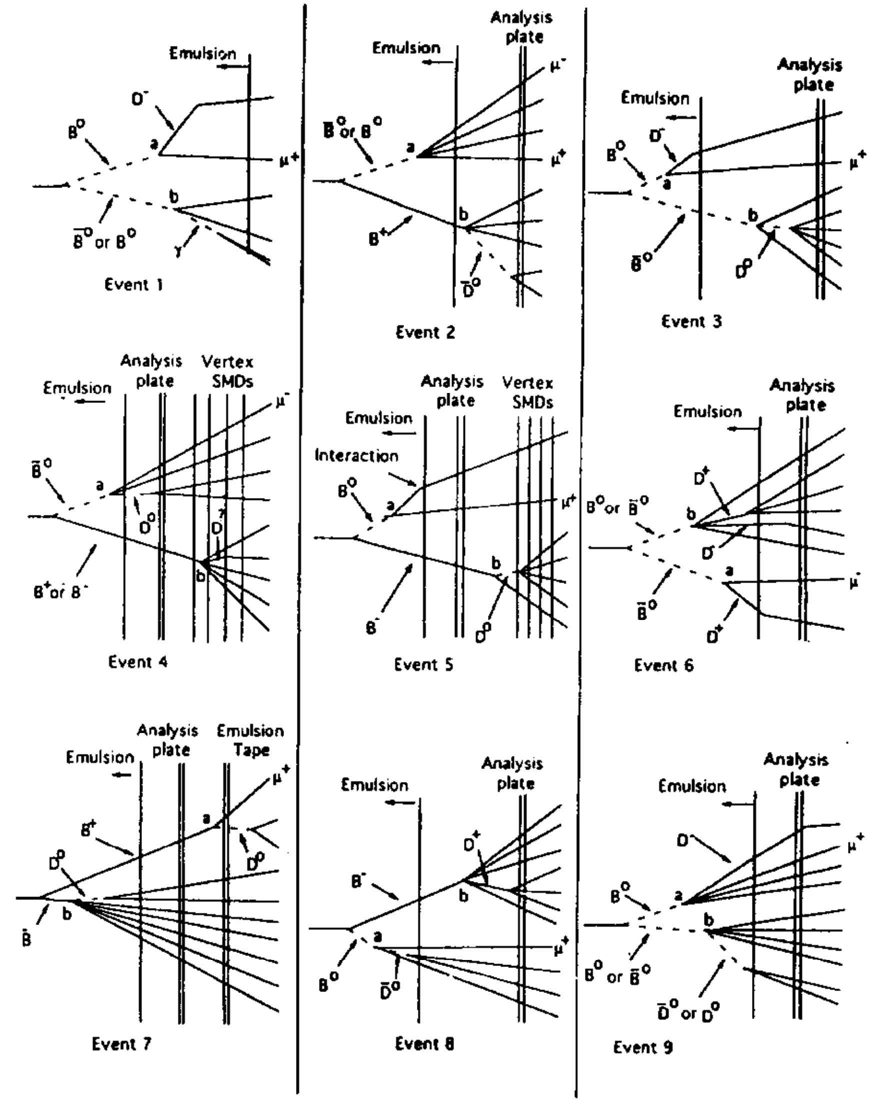

Fig. 11 Decay modes and topologies of 9 $B\bar{B}$ pairs.

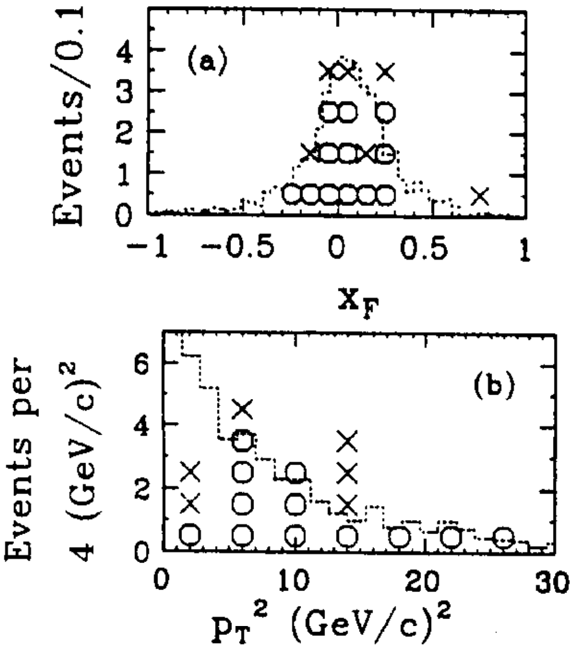

Fig. 12 a) Histogram of inclusive xf for 6 neutral(circles) and 6 charged (crosses) beauty mesons. The dashed histogram is simulation with n=5.0 and x_o = 0.06.

b) Histogram of inclusive pt². The dashed histogram is a simulation with b=0.13.

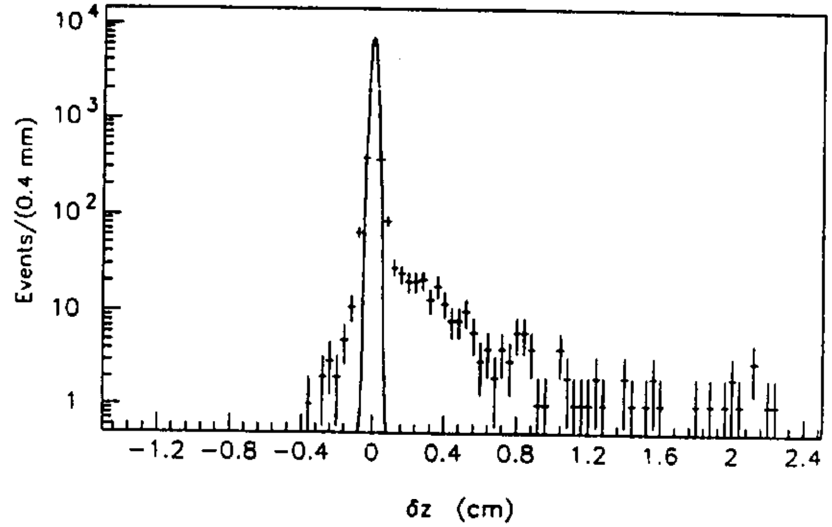

Fig. 14 Difference between primary vertex Z position and J/ψ vertex Z position.

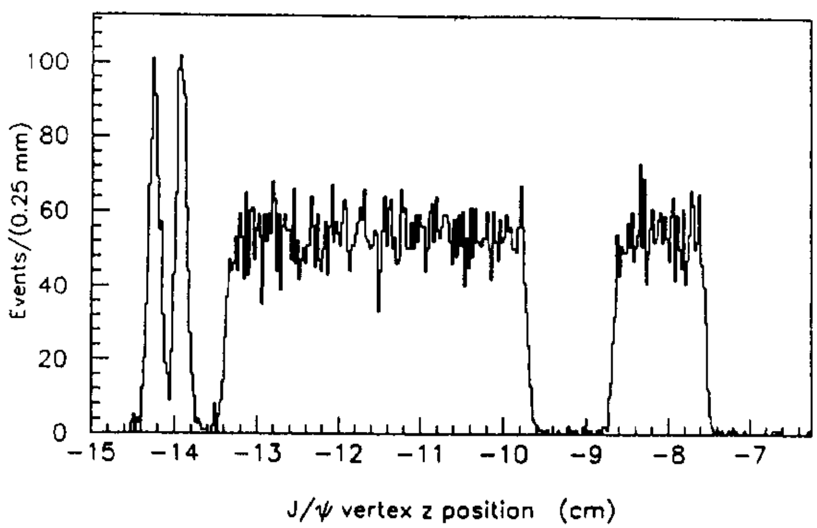

Fig. 13 Reconstructed J/ψ Z vertex position from E672.

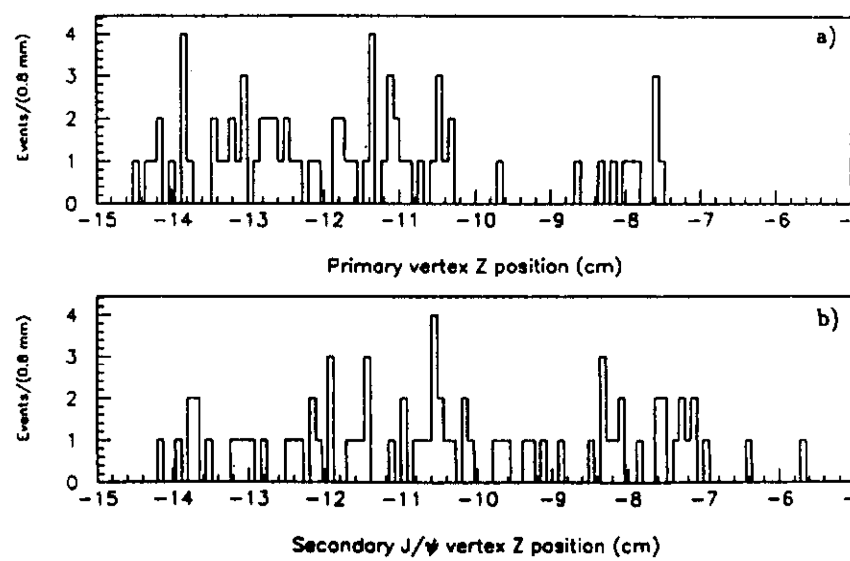

Fig. 15 a) Primary vertex position for events with a secondary J/ψ vertex.
b) Secondary J/ψ vertex position for these events.

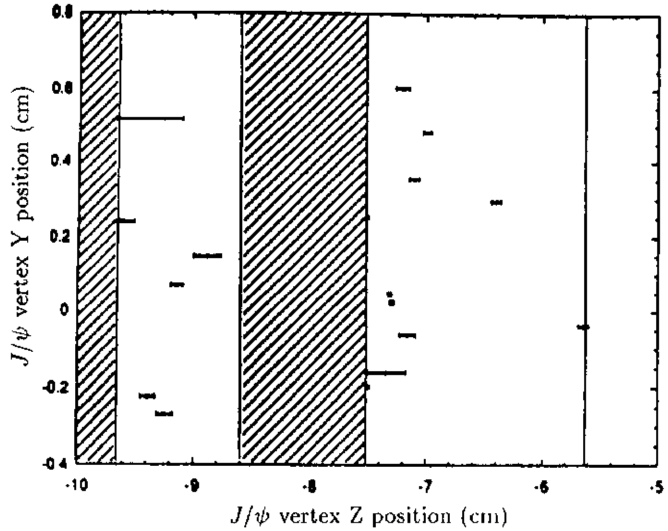

Fig. 16 Distribution of secondary vertices in material free region around the target.

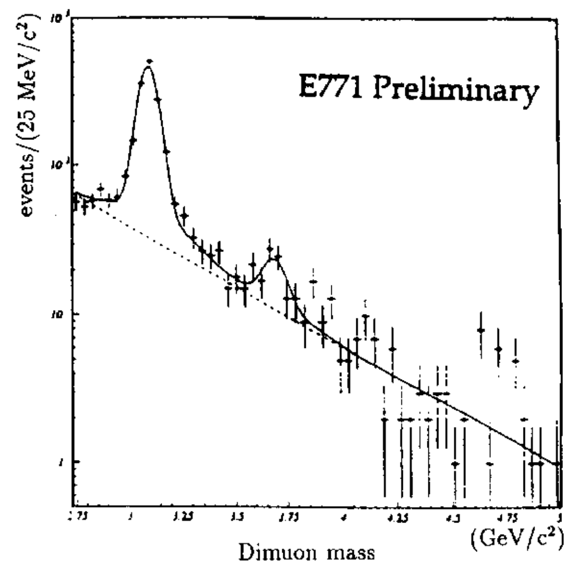

Fig. 18 Dimuon invariant mass distribution from the preliminary analysis of 10% of data.

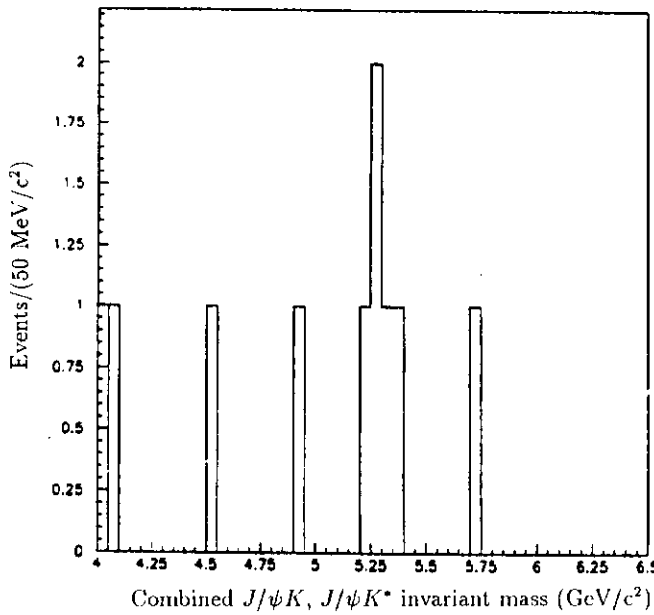

Fig. 17 Combined $J/\psi K^*$ and $J/\psi K$ invariant mass distribution (GeV/c^2).

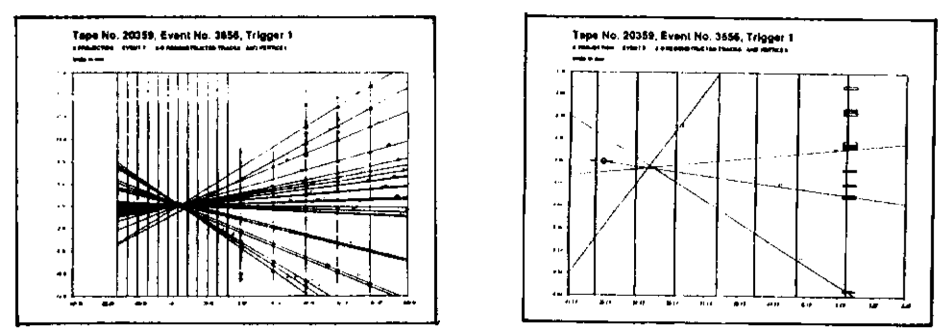

Fig. 19 Candidate B event.

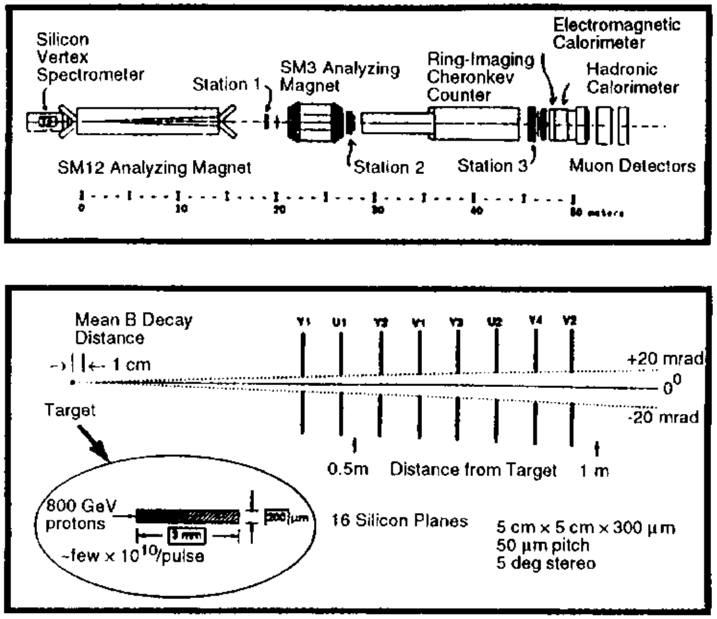

Fig. 20 A schematic view of E789 spectrometer and silicon vertex spectrometer.

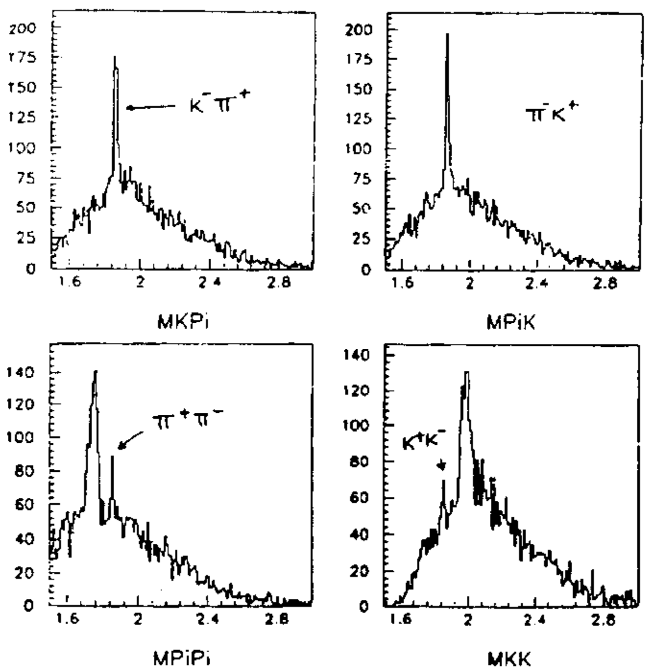

Fig. 21 Mass spectra for dihadron events reconstructed with various assumption for the hadron species.

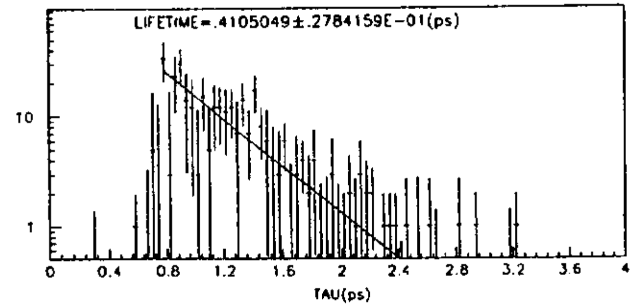

Fig. 22 D° lifetime distribution.

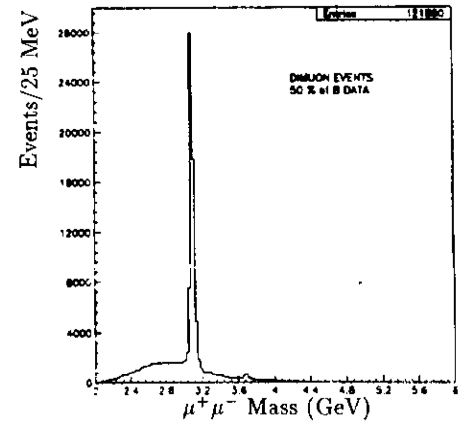

Fig. 23 Mass Spectrum for dimuon events (50% of the data).

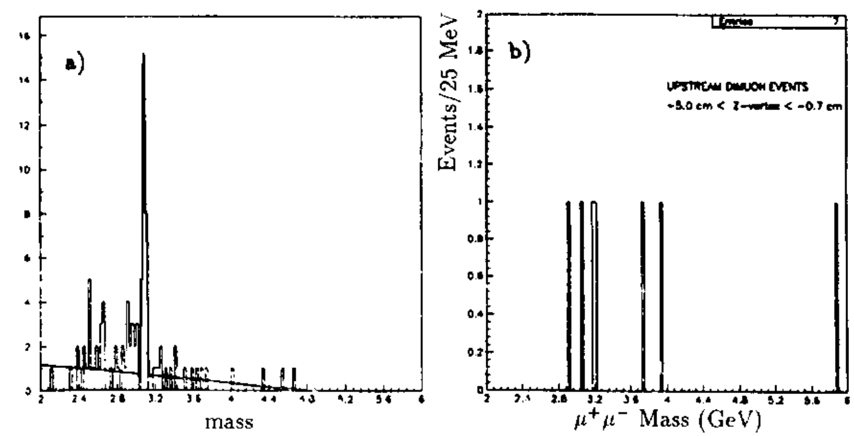

Fig. 24 Mass spectra for dimuon events passing a) downstream Z vertex cuts b) upstream Z vertex cuts.

BEAUTY AND THE BEAST: WHAT LATTICE QCD CAN DO FOR B PHYSICS*

Andreas S. KRONFELD

Theoretical Physics Group, Fermi National Accelerator Laboratory, P.O. Box 500, Batavia, IL 60510, USA

1. INTRODUCTION

One of the reasons why b-hadrons are interesting is that their properties (decays, mixing, CP violation) help determine the least well-known elements of the Cabibbo-Kobayashi-Maskawa (CKM) matrix. (For a review of the CKM matrix, see Ref. 1.) Leptonic and semileptonic B-meson decay amplitudes are proportional to the CKM matrix elements V_{cb} or V_{ub}. Through top-quark box diagrams, B^0_q-$\bar{B}^0_q$ mixing is sensitive to V_{tq}, where q denotes a d or an s quark. In each case, however, the standard-model expression for the (differential) decay rate follows the pattern

$$\begin{pmatrix} \text{experimental} \\ \text{measurement} \end{pmatrix} = \begin{bmatrix} \text{known} \\ \text{factors} \end{bmatrix} \begin{pmatrix} \text{QCD} \\ \text{factor} \end{pmatrix} \begin{pmatrix} \text{CKM} \\ \text{factor} \end{pmatrix} \tag{1.1}$$

The known factors consist of well-known constants and experimentally measurable quantities such as masses and kinematic variables. But, as a rule, the QCD factor is nonperturbative and cannot be deduced from other experiments. Therefore, to extract the CKM factor from the measurement one must have reliable theoretical calculations in nonperturbative QCD.

The only systematic, first-principles approach to nonperturbative QCD is the formulation on the lattice.[2] The most promising calculational method has proven to be large-scale numerical computations. Much like an experimentalist, a lattice theorist must contend with statistical and systematic errors in numerical data. Hence, the reliability of the calculation boils down to the care and control of the uncertainties. Only recently, however, have methods and machines become powerful enough to produce reasonably reliable estimates for the quantities needed to pin down standard-model parameters. Although this report focuses on B physics, a recent review is more general.[3]

How does lattice QCD compare to other theoretical approaches to properties of b hadrons? The main strength of lattice QCD is that it *is* QCD. Given enough computing resources the numerical results are derived from the first principles of the path integral, the renormalization group and the QCD Lagrangian. There are only $n_f + 1$ free parameters, corresponding to quark masses and the gauge coupling. Once these are fixed by experiment,

*This work was performed at the Fermi National Accelerator Laboratory, which is operated by Universities Research Association, Inc., under contract DE-AC02-76CH03000 with the U.S. Department of Energy

using meson masses to fix the quark masses and the 1P–1S splitting of quarkonium* Δm_{1P-1S} to fix Λ_{QCD}, there are no more adjustable parameters. By contrast, both QCD sum rules and effective field theories introduce additional parameters—condensates or coupling constants, respectively, which are not calculable in a self-consistent fashion.

Of course, numerical lattice QCD is not omnipotent. Computational physics is more labor intensive than theoretical physics, though less so than experimental physics. In the case of lattice QCD, the field is just starting to mature. Other aspects of the numerical technique—imaginary time and the finite volume—make some calculations less feasible. Nevertheless, the origins of the uncertainties in the numerical calculations are conceptually understood. In B physics results for leptonic and semileptonic decays and neutral-meson mixing are limited only by computer and human resources. But by the end of the decade the uncertainty in the QCD factor of eq. (1.1) for these measurments should be less than or comparable to the experimental uncertainties.

For the time being, one must live with something called the "quenched approximation" (cf. sect. 2), if other errors are to be brought under control. The quenched approximation is easy to describe: it omits the vacuum polarization of the quarks. For heavy quarks (c, b, t) this is probably tolerable, because their vacuum polarization is short-distance, and hence mostly perturbative. Similarly, one ought to be able to compensate for short-distance, light-quark (u, d, s) vacuum polarization. Long-distance effects of light quarks is harder to characterize. Nevertheless, the quenched approximation can be hoped to provide a useful phenomenology, because it embodies more of QCD than, say, the naive quark models do. But, as with an empirical model, presuming predictions in one arena after success in another may be subject to trial and error.

This paper is organized as follows: Because of the importance of the uncertainty estimates sect. 2 reviews some of the theoretical foundation and the origin of systematic errors in the numerical calculations. To illustrate the advantages of a systematic approach, recent calculations of light hadron masses[4] and decay constants[5] are briefly discussed in sect. 3. The emphasis of sect. 4 is on properties of the B meson—leptonic (sect. 4.1) and semileptonic (sect. 4.2) decays and neutral-meson mixing (sect. 4.3)—for which reliable QCD calculations will be available within the next few years. Prospects for studying nonleptonic decays are discussed in sect. 4.4, and results on the B meson wave function are mentioned in sect. 4.5. Sect. 5 shows how a combination of experimental measurements and the lattice QCD calculations discussed in sect. 4 can be assembled to determine the sides of the celebrated unitarity triangle. Together with the assumption of 3-generation unitarity (i.e., the unitarity polygon is indeed a triangle), the three sides yield the angles α, β, and γ describing CP asymmetries.

2. THEORETICAL AND NUMERICAL BASICS

According to Feynman, vacuum expectation values can be represented as a path integral. In field theory, a mathematically sound definition starts with a lattice of finite volume, depicted in Fig. 1. For QCD the degrees of freedom are gluons $A^a_\mu(x)$ (a is a color index), quarks $\psi_i(x)$ (i is an index for spin, color, and flavor), and anti-quarks $\bar\psi_i(x)$. Then an expectation value is given by

$$\langle\bullet\rangle = \lim_{L\to\infty} \lim_{\substack{a\to 0\\ L=Na\text{ fixed}}} \frac{1}{Z_{L,a}} \int \prod_{x,\mu,a} dA^a_\mu(x) \prod_{x,i} d\psi_i(x) \prod_{x,i} d\bar\psi_i(x)\ \bullet\ e^{-S(A,\psi,\bar\psi)}, \tag{2.1}$$

*This quantity is especially insensitive to the quark masses.

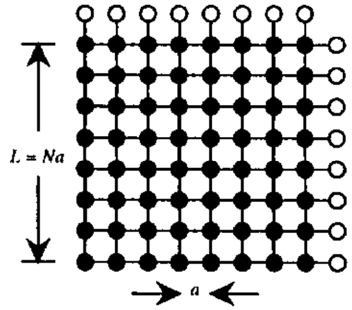

Figure 1: The finite lattice consists of a discrete set of points x separated by lattice spacing a. If the number of points on each side is N, the linear size of the finite volume is $L = Na$. Usually one uses periodic boundary conditions, which would identify the white sites at the top (far right) with the sites at the bottom (far left).

where S is (a lattice version of) the QCD action. The normalization factor $Z_{L,a}$ is defined so that $\langle 1\rangle = 1$ for each L and a.

As an application of eq. (2.1), let $\hat\Phi$ denote an operator with well-specified quantum numbers, built out of A^a_μ, ψ_i, and $\bar\psi_i$, and consider

$$\langle\Phi(t)\Phi^\dagger(0)\rangle = \langle 0|\hat\Phi e^{-\hat Ht}\hat\Phi^\dagger|0\rangle. \tag{2.2}$$

Note that the evolution is through imaginary time ($e^{-\hat Ht}$ instead of $e^{i\hat Ht}$), which makes the integral in eq. (2.1) converge better (weight e^{-S} instead of e^{iS}). Inserting complete sets of states

$$\langle\Phi(t)\Phi^\dagger(0)\rangle = \sum_n \left|\langle 0|\hat\Phi|n\rangle\right|^2 e^{-E_n t} \overset{\text{large } t}{\approx} \left|\langle 0|\hat\Phi|1\rangle\right|^2 e^{-E_1 t}, \tag{2.3}$$

where E_n is the energy of the n-th state. For large enough t the lowest-lying state dominates, so its energy E_1 can be read off from the exponential fall-off. If Φ has the quantum numbers of a B meson at rest, then $E_1 = m_B$. By a similar approach, one can determine matrix elements. Substituting a current J for Φ in eq. (2.2) yields

$$\langle J(t)\Phi^\dagger(0)\rangle \overset{\text{large } t}{\approx} \langle 0|\hat J|1\rangle\langle 1|\hat\Phi^\dagger|0\rangle e^{-E_1 t}, \tag{2.4}$$

for large t. Once E_1 and $\langle 1|\hat\Phi^\dagger|0\rangle$ have been determined from eq. (2.3), eq. (2.4) yields $\langle 0|\hat J|1\rangle$. If J is the charged weak current and Φ again has the quantum numbers of a B meson at rest, $\langle 0|\hat J|1\rangle$ is proportional to f_B, cf. sect. 4.1. In an obvious jargon, eqs. (2.2) and (2.4) are called two-point functions. For matrix elements with hadrons in the final state too, one calculates a *three*-point function

$$\langle\Phi_f(t_1)J(t_2)\Phi_i^\dagger(0)\rangle \overset{\text{large } t_1,t_2}{\approx} \langle 0|\hat\Phi_f|f_1\rangle\langle f_1|\hat J|i_1\rangle\langle i_1|\hat\Phi_i^\dagger|0\rangle e^{-E_{f_1}t_1-E_{i_1}t_2}, \tag{2.5}$$

to obtain $\langle f_1|\hat J|i_1\rangle$. Matrix element of this kind are needed for semileptonic form factors and neutral-meson mixing.

Nonperturbative calculations of eqs. (2.2), (2.4), and (2.5) actually yield masses and matrix elements in "lattice units," e.g. am_B rather than m_B. Physical results are obtained by extrapolating dimensionless ratios. For example,

$$\frac{f_B}{m_B} = \lim_{L\to\infty} \lim_{\substack{a\to 0 \\ L=Na \text{ fixed}}} \frac{af_B(L,a)}{am_B(L,a)}. \tag{2.6}$$

Fortunately, both limits are constrained by theoretical considerations. The infinite-volume limit $L \to \infty$ must conform with general properties of massive quantum field theories in a finite volume.[6] In QCD the *pattern* of approach to the continuum limit $\substack{a\to 0 \\ L=Na \text{ fixed}}$ can be deduced from perturbation theory, because of asymptotic freedom.

Familiar units of MeV are restored by using a standard mass in the denominator of eq. (2.6) and setting it to its physical value. Owing to the renormalization group, this equivalent to eliminating the bare gauge coupling, one of the free parameters of QCD. Rather than m_B, as indicated in eq. (2.6), typical choices are m_ρ or the 1P–1S splitting of quarkonium $\Delta m_{1P\text{-}1S}$. The latter is especially insensitive to the quark masses, i.e. the other parameters of QCD. The quark masses are also parameters that must be set by experimental input. For example, m_b is fixed by tuning $m_\Upsilon/\Delta m_{1P\text{-}1S}$ to its physical value.

Eq. (2.1) makes an explicit mathematical analogy between quantum field theory and statistical mechanics. Starting from eq. (2.1), therefore, a wide variety of nonperturbative techniques from statistical physics can be applied to field theory. For QCD the most promising has proven to be a numerical method. First a and L are fixed. Then the left-hand-sides of eqs. (2.2), (2.4), and (2.5) are merely integrals of a finite, though huge, dimension $\sim (L/a)^4 \times 4 \times 8$. In practice, available memory in the largest supercomputers limits the dimension to 10^7–10^{10}. The only practical way to evaluate integrals of such high dimension is Monte Carlo integration with importance sampling, almost always with weight e^{-S}. Then the whole procedure is repeated for a sequence of a's holding $L = Na$ fixed, and for sequences of L's holding a fixed.

There are two ways to reduce the statistical errors. One is to carry out longer Monte Carlo runs. This puts a premium on computer speed. The other is to choose the largely arbitrary operator Φ, above, to maximize the signal-to-noise ratio of the two- and three-point functions. This puts a premium on computer programmability. From eq. (2.6) it is clear that the statistical errors must be under control if sensible extrapolations in a and L are to be made.

There are also two ways to take the continuum limit, and, hence, to control finite lattice-spacing errors. One is by brute force, making a smaller and smaller, using a simple form of the action S. The other way, which should save computer time, is to improve the accuracy of the lattice action. This is the generalization to field theory of methods familiar from the numerical solution of differential equations. In the past, statistical errors were often too large to notice any practical improvement from this theoretical improvement. Now, however, there are several examples, and one should expect "improved actions" to play an important role in B physics.

For complicated technical reasons the most time-consuming part of the numerical calculations involve treating the light quarks. The physical root of these problems is the Pauli principle: a fermion over here always "knows" something about a fermion way over there. It turns out that one can save a factor of 10^2–10^3 in computer time by neglecting the back reaction of quarks on the gluons. As mentioned in the Introduction, this amounts to omitting vacuum polarization while treating the interaction between the valence quarks and the gluons exactly. This approximation is therefore sometimes called the valence approximation. More often it is called the quenched approximation (calling on an technical analogy to condensed matter physics). Fig. 2 illustrates examples of quark-flow diagrams that are kept (a, c) or omitted (b, d) in the quenched approximation. In particular, the quenched approximation spoils the mechanism generating the mass of the η', with consequences that could affect other masses through self-energy interactions.[7]

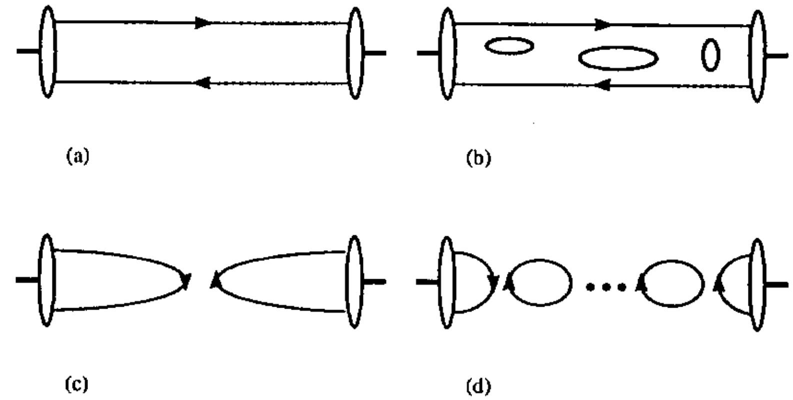

Figure 2: (a) A meson consisting of valence quarks (lines) interacting with the glue (gray shading); this quark-line topology is kept in the quenched approximation. (b) Same as (a) but with some sea quarks; this topology is omitted in the quenched approximation. (c) A flavor-singlet topology kept in the quenched approximation. (d) Flavor-singlet topologies omitted in the quenched approximation; such diagrams generate the η' mass.

Another way to assess the quenched approximation is at the quark-gluon level. As shown in Fig. 3, the gauge coupling runs too quickly in the quenched approximation. In quenched QCD one effectively adjusts the quenched gauge coupling (dotted line in Fig. 3) at the cutoff, so that it agrees with the real coupling (solid line in Fig. 3) at the scale of the physics (denoted μ_{ph} in Fig. 3). If the quenched approximation is at all successful, many quantities with typical scale μ_{ph} should be verifiable. On the other hand, one need not expect quantities with a typical scale rather different from μ_{ph} to be verified. Usually this consideration is merely heuristic. For nonrelativistic systems, i.e. the ψ and Υ families, the two-body wave function provides the probability of each scale, so one can account quantitatively for the effects of the difference between the two curves.[8]

To conclude this section, let us offer a handful of questions the nonexpert should keep in mind when appraising lattice QCD calculations:

1. Are the statistical errors small enough to understand anything?
2. Is the lattice spacing large enough? Or, even better, have lattice-spacing errors been extrapolated away?
3. Is the physical volume large enough? Or, even better, have finite-volume errors been extrapolated away?

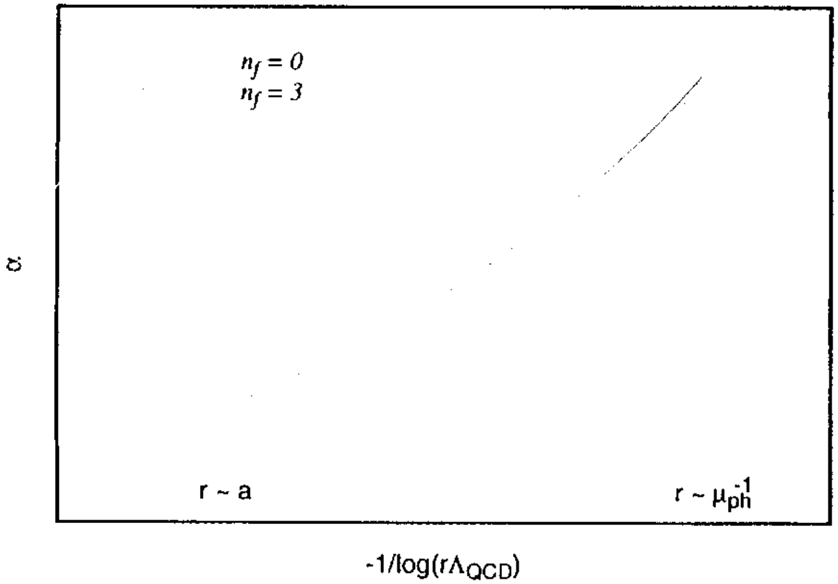

Figure 3: Sketch of the gauge coupling in quenched and "full" QCD. The flavor-dependence of the β-function coefficient $b_0 = 11 - 2n_f/3$ implies that the coupling in the quenched ($n_f = 0$) case runs more quickly at short distances.

4. Have the quark masses been adjusted precisely enough?

5. Is the quenched approximation acceptable?

With a little luck the lattice mavens will always answer, "At the x% level, yes."

3. LIGHT HADRON SPECTRUM

One of the original goals of lattice QCD was a first principles calculation of the light hadron mass spectrum. A recent paper[4] employing the quenched approximation reports a significant step towards that goal. Using the GF-11, a special purpose computer designed at IBM,[9] Weingarten, et al, have evaluated the path integral at three values of a (and fixed L) and, at the coarsest lattice spacing, three values of L. With m_ρ to convert from lattice units to MeV (cf. eq. (2.6)) and m_π and m_K to set the light and strange quark masses, their results for two vector mesons and six baryons are summarized in Fig. 4. The error bars represent the authors' estimates of the accumulated uncertainties from all sources except the quenched approximation.

The agreement between these quenched QCD results and nature is tantalizing. Experts[3, 10, 11] in the field might quibble about some details of the analysis, but they cannot deny that such a systematic attack on the errors is basically sound. A "bottom-line" example is the ratio m_N/m_ρ, which without extrapolation is too large.[10] After extrapolation, however, this ratio agrees to an accuracy much better than the quoted precision. Moreover, there are

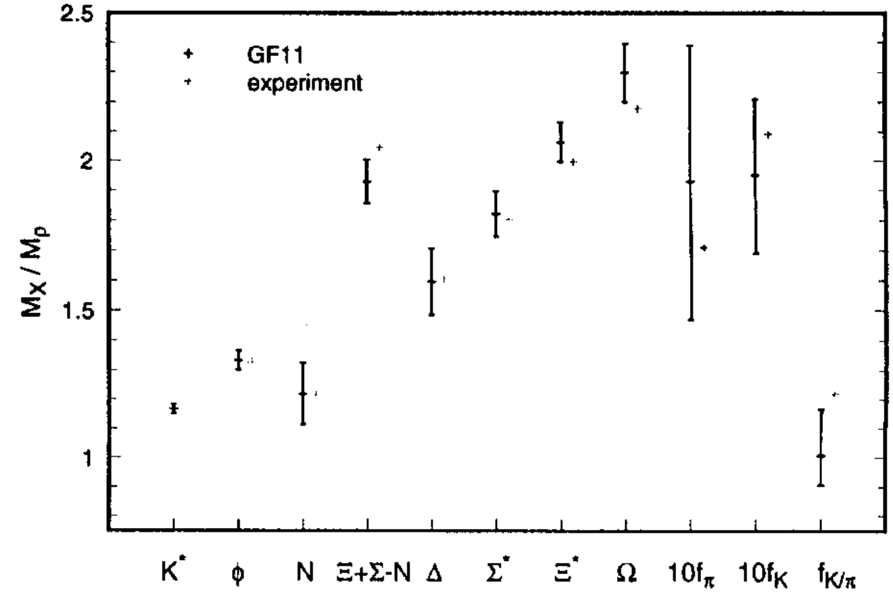

Figure 4: Spectrum and decay constants of the light hadrons. Error bars are from lattice calculations in the quenched approximation,[4, 5] and + denotes experiment.

some nontrivial cross-checks: The value of $\Lambda^{(0)}_{\rm lat}$ (= $\Lambda_{\rm QCD}$ in the "lattice" scheme with $n_f = 0$ active flavors) agrees with the value obtained in lattice QCD studies of charmonium.[8, 12] In charmonium, however, it is possible to correct for the quenched approximation, because most of the error comes from short distances. The same calculations[8] obtain a value of $\Lambda^{(4)}_{\overline{\rm MS}}$ that agrees with deep, inelastic scattering and other high-energy processes.

Fig. 4 also shows results for the π and K decay constants.[5] We have converted the results to the convention of eq. (4.2), below, in which $f_\pi = 131$ MeV. The relative uncertainties are larger than for the mass ratios. Because the decay constants are more sensitive to short distances, one might hope that the ratio f_K/f_π would be less sensitive to the errors of the quenched approximation. Unfortunately, the numerical results do not support this idea.

4. *B*-PHYSICS

In contrast to the light hadron physics discussed above, the lattice-spacing and finite-volume dependence of B meson properties has not yet been thoroughly investigated. An exception to this rule is the study of the decay constant in the theoretically interesting limit of an infinitely heavy b quark.[13, 14] This limit is often called the static limit, because the heavy quark is anchored in one place. It seems, however, that the $1/m_b$ correction to the decay constant is large, so that these results are not directly applicable to phenomenology.

The dynamics of a hadron with one heavy quark is surprisingly simple, because the energy scale associated with the heavy quark mass decouples. For this reason, it is possible to treat a heavy quark on the lattice,[15, 16, 17] even when $m_q a \sim 1$.

In this section, subsection titles indicate the product of CKM matrix element and B-meson property, where appropriate.

4.1 Leptonic Decays: $f_B|V_{ub}|$

The leptonic width of the charged B meson is given by

$$\Gamma[B \to l\nu] = \left[\frac{G_F^2 m_l^2 m_B}{8\pi}\eta_{em}\left(1 - \frac{m_l^2}{m_B^2}\right)\right] f_B^2|V_{ub}|^2. \tag{4.1}$$

Eq. (4.1) is a concrete example of eq. (1.1). The numerical value of the bracket is well known, although the electromagnetic radiative correction η_{em} is uncertain at the 0.1% level. To determine $|V_{ub}|$ through a measurement* of a leptonic decay, one must first know the decay constant f_B, defined by

$$\langle 0|\bar{u}\gamma_\mu\gamma_5 b|B^-(p)\rangle = ip_\mu f_B \tag{4.2}$$

with the normalization convention $\langle B^-(q)|B^-(p)\rangle = 2E_B(2\pi)^3\delta^{(3)}(\boldsymbol{p} - \boldsymbol{q})$.

The two-point function in eq. (4.2) [cf. eq. (2.4)] is one of the most straightforward of lattice QCD calculations. A recent preprint,[18] for example, finds

$$\begin{aligned} f_B &= 187(10) \pm 12 \pm 32 \pm 15 \text{ MeV}, \\ f_{B_s} &= 207(\ 9) \pm 10 \pm 32 \pm 22 \text{ MeV}, \\ f_D &= 208(\ 9) \pm 11 \pm 33 \pm 12 \text{ MeV}, \\ f_{D_s} &= 230(\ 8) \pm 10 \pm 28 \pm 18 \text{ MeV}. \end{aligned} \tag{4.3}$$

The uncertainty in parentheses is statistical; the others are systematic. From left to right, they are due to the following sources:

1. Fitting, interpolation, and extrapolation. The t dependence of the numerical two-point functions is fit to eqs. (2.2) and (2.4) once the lowest-lying pseudoscalar has been isolated. The mass of the heavy quark is adjusted by interpolating to m_b or m_c; the mass of the light quark is adjusted by extrapolating to $(m_u + m_d)/2$ or m_s. These could be reduced somewhat in concert with a reduction in the statistical error.

2. Large m_b effects. Two $1/m_b$ contributions modify the static limit, the kinetic energy and a chromomagnetic $i\boldsymbol{\Sigma}\cdot\boldsymbol{B}$ term. Owing to lattice artifacts in the standard lattice action, the quark mass is tuned so that the kinetic energy has the correct strength, the chromomagnetic term is too weak.[17, 19] This could be reduced with an improved action, as done in Ref. 20. The results with the improved action agree extremely well with eq. (4.3), especially when one compares f_P/f_π from both.[18, 20]

3. Uncertainty in the conversion from lattice units to MeV. As in Ref. 5, it turns out that $(af_\pi/am_\rho)_{\text{Ref. 18}} \neq (f_\pi/m_\rho)_{\text{expt}}$. This could be an artifact either of non-zero lattice spacing or of finite volume, but these possibilities are unlikely because Ref. 18 agrees with Ref. 5, which extrapolates these two effects away. Another culprit could be the quenched approximation, which is, perhaps, more likely.

*Because of helicity mismatch, the rate is proportional to m_l^2, which makes the measurement difficult. This example is worth pursuing—at least pedagogically—because it is so simple.

A remarkable feature of Ref. 18 is that the number of systematic uncertainties quoted equals the number of authors.

In ratios many of the errors cancel, because of statistical and systematic correlations. The result from Ref. 18

$$\frac{f_D}{f_{D_s}} = \frac{f_B}{f_{B_s}} = \frac{f_B}{f_D} = \frac{f_{B_s}}{f_{D_s}} = 0.90 \pm 5\%. \tag{4.4}$$

is easy to remember. If f_{D_s} were experimentally determined to 5%, eq. (4.4) would perhaps be more relevant than eq. (4.3).

The uncertainty estimates do not explicitly include quenched, finite-volume, or non-zero lattice spacing errors. As indicated above, however, some of these errors are implicitly included in the estimates quoted. From the studies of the static limit[13, 14] one expects the volume dependence to be insignificant once the volume is "large enough." The lattice-spacing dependence, on the other hand, is surprisingly large.

The results shown in eq. (4.3) may disagree with previous lattice calculations. Some older results were higher, quoting values larger than 300 MeV for f_B. Such numbers came typically from early calculations in the static limit, neglecting the dependence on the heavy quark mass. In addition, the early studies were at larger lattice spacings and often used operators that were unsuccessful in isolating the lowest-lying states. Other older results were lower. These results typically started with heavy quark that were relatively light, and extrapolated. These extrapolations were done using an incorrect normalization of the current. The correct normalization is now understood[17, 19] and Ref. 18, for example, uses it. The difference is most noticeable on coarse lattices; the impact of the correct normalization and an associated mass shift[17, 19] is shown in Fig. 5, using numerical data from Ref. 21.

4.2 Semileptonic Decays: $A_1^{B\to D^*}(q^2)|V_{cb}|$ and $A_1^{B\to\rho}(q^2)|V_{ub}|$

The rates of semileptonic decays exceed those of pure leptonic decays, because they do not suffer from helicity suppression. They therefore lend themselves particularly well to the determination of elements of the CKM matrix. The rates are measurable and the reliability of theoretical calculations is better than for nonleptonic decays (sect. 4.4). For example, the best determination of $|V_{us}|$ comes from $K \to \pi l\nu$, and the best determination of $|V_{cb}|$ comes from $B \to D^* l\nu$.

We shall focus on mesons, because they are easier than baryons to study, both experimentally and theoretically. A generic semileptonic decay can be denoted $A \to Xl\nu$, where A is a flavored meson. The process is depicted in Fig. 6. The differential decay rate follows the pattern of eq. (1.1):

$$\frac{d\Gamma}{dq^2} = \left[\frac{G_F^2\lambda^{3/2}}{192\pi^3 m_A^3}\right] |f_+(q^2)|^2|V_{ax}|^2, \tag{4.5}$$

when X is a pseudoscalar meson, and

$$\frac{d\Gamma}{dq^2} = \left[\frac{G_F^2\lambda^{1/2}q^2}{64\pi^3 m_A}\right] |A_1(q^2)|^2|V_{ax}|^2, \tag{4.6}$$

when X is a vector meson. In eqs. (4.5) and (4.6), q^2 is the invariant mass of the virtual W $[0 < q^2 \leq q^2_{\max} = (m_A - m_X)^2]$, V_{ax} is the element of the CKM matrix associated with the quark-W vertex in Fig. 6, and $\lambda = (m_A^2 + m_X^2 - q^2)^2 - 4m_A^2 m_X^2$. For brevity and a reason

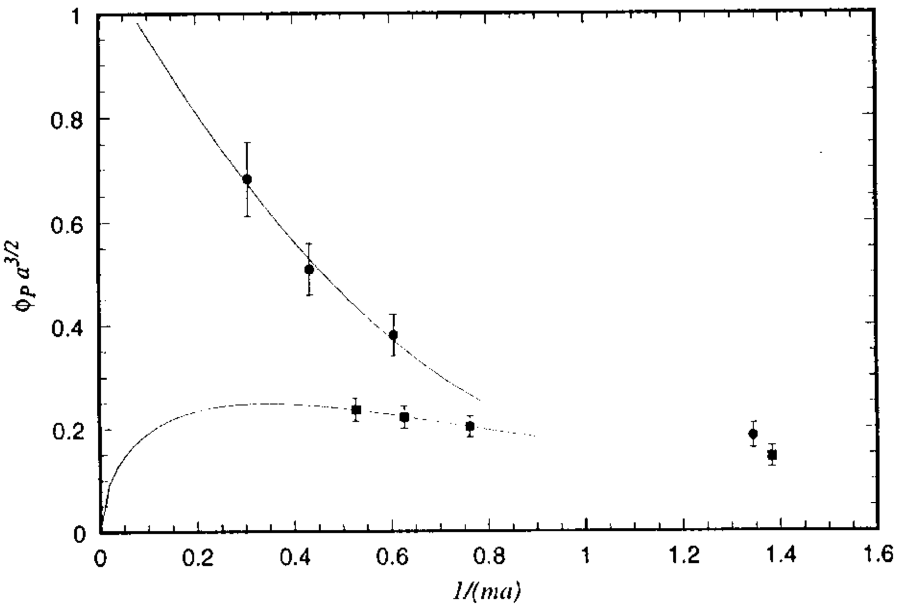

Figure 5: Putative calculations of $\phi_P = \sqrt{m_P} f_P$, where P denotes a heavy-light pseudoscalar meson, as a function of (inverse) mass. The squares denote an incorrect current normalization, which systematically underestimates ϕ_P. The circles use a current normalization and mass definition derived in Ref. 17. The curves indicate the large mass behavior in each case.

explained below, eq. (4.6) is valid only for q^2 near $q^2_{\rm max}$. The form factors f_+ and A_1 are defined by hadronic matrix element of the $V - A$ current

$$J_\mu = \bar{x}\gamma_\mu(1 - \gamma_5)a \tag{4.7}$$

turning flavor a into flavor x. When X is a pseudoscalar meson

$$\langle X|J_\mu|A\rangle = f_+(q^2)(p + p')_\mu + f_-(q^2)(p - p')_\mu, \tag{4.8}$$

where p (p') is the initial (final) state meson's momentum and $q = p - p' = p_l + p_\nu$. Similarly, when X is a vector meson there are four independent form factors:

$$\begin{aligned}\langle X|J_\mu|A\rangle = \epsilon^*_\lambda \Bigg[& \frac{2\varepsilon_{\mu\lambda\rho\sigma}p_\rho p'_\sigma}{m_A + m_X} V(q^2) - \delta_{\mu\lambda}(m_A + m_X)A_1(q^2) \\ & + \frac{(p+p')_\mu p_\lambda}{m_A + m_X} A_2(q^2) - \frac{2m_X(p-p')_\mu p_\lambda}{q^2} A(q^2)\Bigg],\end{aligned} \tag{4.9}$$

where ϵ^*_λ is the polarization vector of the final-state meson. The form factors f_- and A do not appear in the expressions for the differential decay rates because the lepton mass has been neglected; A_2 and V do not appear for q^2 near $q^2_{\rm max}$ because they are suppressed by a higher power of λ.

Table 1: Semi-leptonic decays and the CKM matrix elements they determine. For brevity only pseudoscalar final states are listed; vector final states are ρ, K^* and D^*, as appropriate.

$A \to X$	V_{ax}	COMMENT
$K \to \pi$	V_{us}	calibrate quenched approximation
$D \to \pi$	V_{cd}	uncertainty in $\lvert V_{cd}\rvert$ dominated first by BR($D \to \pi l\nu$), then by f_+
$D \to K$	V_{cs}	uncertainty in $\lvert V_{cs}\rvert$ dominated by f_+
$B \to D$	V_{cb}	test/compute corrections to heavy quark limit
$B \to \pi$	V_{ub}	ρ final state more useful; cf. text

Table 1 lists a variety if semileptonic decays and their utility in either testing numerical lattice QCD methods or extracting CKM matrix elements. For B decays two entries are of note, depending on whether the quark-level decay is $b \to c$ or $b \to u$.

For $B \to D^{(*)}$ both the charm and bottom quarks are reasonably heavy and one can apply heavy-quark symmetry. The kinematic endpoint $q^2_{\rm max} = (m_B - m_{D^{(*)}})^2$ is especially interesting, because then one can determine the $B \to D^* l\nu$ differential decay rate up to corrections of order[22, 23] $1/m^2_{D^*}$. A similar analysis shows that the leading correction to the $B \to Dl\nu$ differential decay rate is $O(1/m_D)$. For $q^2 < q^2_{\rm max}$ the corrections are $O(1/m_{D^{(*)}})$ for both final states. Using estimates from QCD sum rules for the $1/m^2_{D^*}$ and $1/m^2_B$ corrections to $A_1(q^2_{\rm max})$ enables one to limit the theoretical uncertainty on $|V_{cb}|$ to 4%. It seems unlikely that lattice QCD can improve on this bottom line any time soon, although verification of the QCD sum rule calculations would be important. Another contribution that lattice QCD can make is a model-independent determination of the q^2 dependence. This would assist the extrapolation of the experimental data towards the statistics-poor endpoint, possibly reducing the overall uncertainty on $|V_{cb}|$. Exploratory results in this direction have appeared recently.[24, 25]

Lattice QCD can make a more significant impact on the determination of V_{ub}. Since the π or ρ is light, heavy-quark symmetry could only be used to relate, say, $D \to (\pi$ or $\rho)$

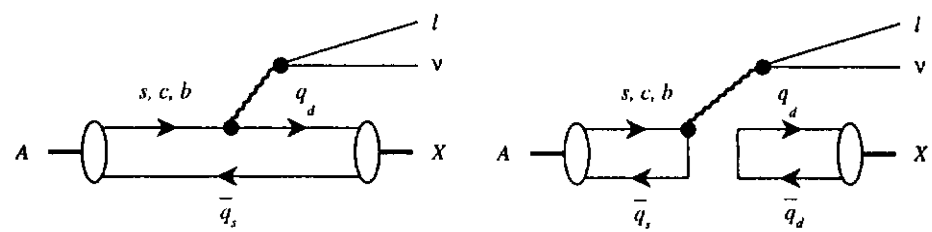

Figure 6: Quark-flow diagrams for meson semileptonic decays. For the weak interactions, the diagram may be interpreted as a Feynman diagram. The strong interactions binding quarks into mesons must be treated nonperturbatively, however, as indicated by the gray shading. The second diagram contributes only when X is an isoscalar. It is usually neglected, because it is difficult to calculate and because diagrams similar to Fig. 2(d) are omitted in the quenched approximation anyway.

form factors to $B \to (\pi \text{ or } \rho)$ form factors.[26] As above either models or lattice QCD would be needed to compute the $1/m_D - 1/m_B$ corrections. Strictly speaking, the end result would be $|V_{ub}/V_{cd}|$. It seems more reasonable to use lattice QCD to calculate the form factors and use the experiments to determine $|V_{ub}|$ and $|V_{cd}|$ separately. As pointed out in Ref. 27 the cleanest procedure is to use ρ final states with q^2 near $q^2_{\max}$. The calculations are most reliable at $q^2_{\max}$, because $q^2 < q^2_{\max}$ is obtained for $\mathbf{p}' \neq \mathbf{0}$, and when $|\mathbf{p}'|a \sim 1$ there are additional lattice artifacts. Near $q^2_{\max}$ the phase spaces suppression is less drastic for vector mesons than for pseudoscalar mesons. No calculation of $A_1^{B\to\rho}(q^2)$ with a thorough error analysis is available yet, although it seems to feasible to complete a calculation with 5–10% errors by the time experimental data for $d\Gamma/dq^2$ become available.

Let us sketch how this will come about, starting from the estimates of the systematic uncertainties for $D \to K^{(*)}l\nu$ in Refs. 28 and 27. One ought to be able to reduce the 10-20% statistical uncertainty of published calculations[29, 28, 30, 27] to 2-5%. At that level it is possible to treat the systematic quantitatively. (Refs. 28 and 27 made semi-quantitative estimates; other papers[29, 30] felt that their large statistical uncertainties made estimates of systematic errors premature.) The previous 20-40% uncertainty from $O(a)$ effects should be reduced to below the statistical error, by extrapolating in a. The 5-20% uncertainty owing to inadequate knowledge of quark masses should fall to the level limited by mass calculations, which is presently estimated to be 2-6%.[4] Finally, although volume dependence is probably not a problem, momentum and, hence, q^2 take on discrete values in a finite volume. A variety of volumes would make available more values of q.

4.3 B^0_q-$\bar{B}^0_q$ Mixing: $f_B^2 B_B |V_{td}|^2$ and $f_{B_s}^2 B_{B_s} |V_{ts}|^2$

Neutral-meson mixing is interesting from the point of view of the CKM matrix, because it offers a handle on the third row. The rate of mixing is related to

$$x_d = \frac{\Delta m_{B^0}}{\Gamma_{B^0}} = \left[\frac{G_F^2 m_t^2 \tau_B}{16\pi^2 m_B} f_2(m_t^2/m_W^2)\right] \eta_{\rm pQCD} \tfrac{8}{3} m_B^2 f_B^2 B_B |V_{td}^* V_{tb}|^2, \tag{4.10}$$

where

$$\tfrac{8}{3} m_B^2 f_B^2 B_B = \langle \bar{B}^0 | \bar{b}_i \gamma_\mu (1-\gamma_5) d_i \bar{b}_j \gamma_\mu (1-\gamma_5) d_j | B^0 \rangle. \tag{4.11}$$

Similar expressions hold for the B_s meson, substituting an s quark for the d quark throughout. The perturbative QCD factor $\eta_{\rm pQCD}$ has been grouped outside of the bracket of known factors, even though it is known, because both $\eta_{\rm pQCD}$ and B_B depend on the renormalization scheme, but the product $\eta_{\rm pQCD} B_B$ does not. Even though the top-quark mass m_t is not yet known, the dependence on it is grouped with the known factors, because it should be known soon; the function f_2 is known.

The peculiar but traditional notation B_B is useful for lattice QCD calculations, because B_B is then a ratio of matrix elements for which many uncertainties cancel. Although the analogous quantity in the kaon system represents one of the most reliable lattice QCD calculations,[31] calculations of B_B are still exploratory.[32] At the 20-40% level, there is no evidence yet for a significant deviation from the naive expectation $B_B = 1$.

The dependence on the top-quark mass and some other "known" factors, cancel in the ratio, leaving

$$\frac{x_d}{x_s} = \left[\frac{\tau_B m_B}{\tau_{B_s} m_{B_s}}\right] \frac{f_B^2 B_B}{f_{B_s}^2 B_{B_s}} \left|\frac{V_{td}}{V_{ts}}\right|^2. \tag{4.12}$$

Hence, an experimental measurement of x_d/x_s together with a lattice QCD calculation of $f_B^2 B_B/(f_{B_s}^2 B_{B_s})$ determines $|V_{td}/V_{ts}|$. As in eq. (4.4) the uncertainty in the B-to-B_s ratio should be smaller than in numerator or denominator separately.[32]

4.4 Nonleptonic Decays

Nonleptonic decays, such as $B \to J/\psi K_S$ or $B \to \pi^+\pi^-$, receive almost all of the attention in discussions of CP violation. A serious obstacle to the treatment of nonleptonic decays is the presence of two (or more) hadrons in the final state. The technical aspect is the difficulty of separating the particles in the finite volume. The conceptual aspect is the determination of final-state phase shifts from purely real quantities computed in Euclidean field theories.[33, 34] It is rigorously known[35] how to determine the resonance properties of the ρ, which decays through an interaction in the QCD Hamiltonian. The stumbling block for weak B decays is evidently the application of the ideas in Ref. 35 when the particle decays through an interaction being treated as a perturbation. Note that these difficulties do *not* stem from the lattice cutoff, but from other features, finite volume and imaginary time, introduced to make the computational method tractable. Nevertheless, until these issues are resolved, lattice results for nonleptonic decays probably will not warrant attention from non-experts.

With the lattice QCD calculations discussed above, however, it *will* be able to determine the angles of the unitarity triangle, as discussed in sect. 5

4.5 Qualitative Information

An interesting qualitative result for the B meson is its valence wave function. The intriguing result[36] is that the wave functions in the static limit are completely consistent with wave functions of the semi-relativistic potential model with Hamiltonian

$$H = \sqrt{p^2 + m^2} + V_{q\bar{q}}(x), \tag{4.13}$$

where m is the (reduced) mass of the light quark and $V_{q\bar{q}}(x)$ is Buchmüller-Tye potential or any other empirical potential consistent with asymptotic freedom, linear confinement, and quarkonium phenomenology. Because of the relativistic kinetic energy, the wave functions are much broader than in a nonrelativistic model. In particular, the true wave function seems to be much broader than those used in phenomenological quark models.

5. FUTURE PROSPECTS

The standard model has around 20 parameters and, in the long run, precision lattice QCD calculations are needed to determine half of them ever more precisely.[3] In particular, properties of the B meson are needed to pin down the four parameters associated with the CKM matrix. Indeed, in the standard 3-generation parameterization $|V_{us}|$, $|V_{cb}|$, and $|V_{ub}|$ yield (to good approximation) θ_{12}, θ_{23}, and θ_{13}, respectively. These three together with $|V_{td}|$ yield the phase δ responsible for CP violation. Hence, semileptonic decays and mixing of the B meson, together with the calculations described above, are essential to determining three out of the four CKM parameters.

To put an even finer point on this observation, consider the unitarity triangle. The magnitudes of its sides are $|V_{ud}V_{ub}^*|$, $|V_{cd}V_{cb}^*|$, and $|V_{td}V_{tb}^*|$. Sect. 4.2 shows how to determine $|V_{cb}|$ and $|V_{ub}|$ with semileptonic decays; a similar technique for charm decays determines

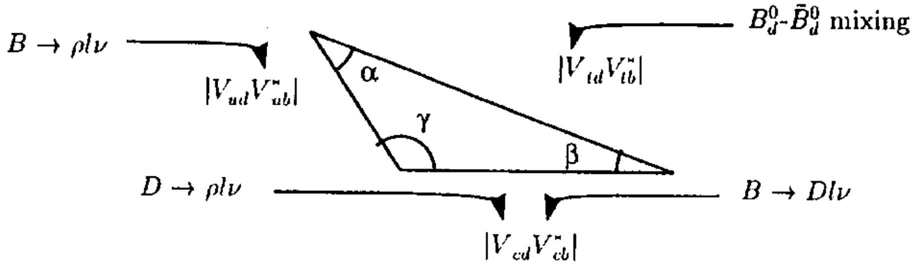

Figure 7: The unitarity triangle and the B properties needed to determine the sides. $|V_{ud}|$ is known from $K \to \pi l \nu$ and $|V_{tb}|$ is known from three-generation unitarity.

$|V_{cd}|$. Sect. 4.3 shows how to determine $|V_{td}|$ from neutral-meson mixing. Now assume three-generation unitarity. (Eq. (4.10) already does so.) That implies that the three sides form a triangle, as shown in Fig. 7. It also implies $|V_{tb}| = 1$, $|V_{ud}| = 0.976$, and $|V_{ts}| = |V_{cb}|$; the latter can improve the determination of $|V_{td}|$ through $|V_{td}/V_{ts}|$, cf. eq. (4.12). Of all these CKM matrix elements $|V_{ub}|$ is the most poorly known, but the experimental and theoretical work of the next few years will improve the determination. Once is it precise enough, all three sides will be known, and, as any child will tell you, then the angles are known too.

Most theoretical descriptions of CP asymmetries cast them as measurements of the angles α, β, and γ. But three-generation unitarity is often assumed and penguin contributions are almost always assumed to be unimportant. Using the calculations discussed above, however, one need only assume three-generation unitarity to determine α, β, and γ. Because the measurements involved all conserve CP, they will most likely be available before the CP asymmetries are. If that is indeed so, it is more accurate to say that measurements of CP asymmetries test the CKM theory of CP violation, than to say that they determine the CKM parameters.

ACKNOWLEDGEMENTS

I would like to thank M. Uchima for nursing my ailing Exabyte tapes, while I was enjoying the mountain air of Snowmass.

6. REFERENCES

1. F. Gilman and Y. Nir, *Annu. Rev. Nucl. Part. Sci.* **40** (1991) 213;
   Y. Nir, in *Perspectives in the Standard Model*, edited by R.K. Ellis, C.T. Hill and J.D. Lykken (World Scientific, Singapore, 1992).
2. K.G. Wilson, *Phys. Rev.* **D10** (1974) 2445;
   K.G. Wilson, in *New Phenomena in Subnuclear Physics*, edited by A. Zichichi (Plenum, New York, 1977).
3. A.S. Kronfeld and P.B. Mackenzie, *Annu. Rev. Nucl. Part. Sci.* **43** (1993) 793.
4. F. Butler, H. Chen, A. Vaccarino, J. Sexton, and D. Weingarten, *Phys. Rev. Lett.* **70** (1993) 2849.
5. F. Butler, H. Chen, A. Vaccarino, J. Sexton, and D. Weingarten, "Meson Decay Constant Predictions of the Valence Approximation to Lattice QCD," IBM preprint (1993); erratum (private communication)
6. M. Lüscher, *Commun. Math. Phys.* **104** (1986) 177; **105** (1986) 153.
7. S.R. Sharpe, *Phys. Rev.* **D41** (1990) 3233, **D46** (1992) 3146; C.W. Bernard and M. Golterman, *Phys. Rev.* **D46** (1992) 853.
8. A.X. El-Khadra, G. Hockney, A.S. Kronfeld and P.B. Mackenzie, *Phys. Rev. Lett.* **69** (1992) 729.
9. D. Weingarten, *Nucl. Phys. B (Proc. Suppl.)* **17** (1990) 272.
10. A. Ukawa, *Nucl. Phys. B (Proc. Suppl.)* **30** (1993) 3.
11. S.R. Sharpe, in *The Fermilab Meeting, DPF '92*, edited by C.H. Albright, P.H. Kasper, R. Raja, and J. Yoh (World Scientific, Singapore, 1993).
12. S.M. Catterall, et al., *Phys. Lett.* **B300** (1993) 393.
13. C. Alexandrou, S. Güsken, F. Jegerlehner, K. Schilling, and R. Sommer, CERN preprint CERN-TH 6692/92.
14. A. Duncan, E. Eichten, A.X. El-Khadra, J.M. Flynn, B.R. Hill, and H.B. Thacker, *Nucl. Phys. B (Proc. Suppl.)* **30** (1993) 433.
15. E. Eichten and B. Hill, *Phys. Lett.* B234:511 (1990).
16. G.P Lepage, L. Magnea, C. Nakhleh, U. Magnea, and K. Hornbostel, *Phys. Rev.* D46:4052 (1992).
17. A.X. El-Khadra, A.S. Kronfeld, and P.B. Mackenzie, Fermilab preprint FERMILAB-PUB-93/195-T.
18. C.W. Bernard, J.N. Labrenz and A. Soni, Univ. of Washington preprint UW/PT-93-06.
19. A.S. Kronfeld, *Nucl. Phys. B (Proc. Suppl.)* **30** (1993) 445; P.B. Mackenzie, in *The Fermilab Meeting, DPF '92*, edited by C.H. Albright, P.H. Kasper, R. Raja, and J. Yoh (World Scientific, Singapore, 1993).
20. S.P. Booth, et al (UKQCD Collaboration), Edinburgh Univ. preprint 93/526 and Southampton Univ. preprint SHEP 92/93-24.
21. C. Bernard, T. Draper, G. Hockney, and A. Soni, *Phys. Rev.* **D38** (1988) 3540.
22. M.E. Luke, *Phys. Lett.* **B252** (1990) 447.
23. M. Neubert, *Phys. Lett.* **B264** (1991) 455.
24. C.W. Bernard, Y. Shen, and A. Soni, Boston Univ. preprint BUHEP-93-15.
25. S.P. Booth, et al (UKQCD Collaboration), Edinburgh Univ. preprint 93/525 and Southampton Univ. preprint SHEP 92/93-17.
26. C.O. Dib and F. Vera, *Phys. Rev.* **D47** (1993) 3938.
27. C.W. Bernard, A.X. El-Khadra, and A. Soni, *Nucl. Phys. B (Proc. Suppl.)* **26** (1992) 204; *Phys. Rev.* **D47** (1993) 998.
28. C.W. Bernard, A.X. El-Khadra, and A. Soni, *Phys. Rev.* **D43** (1991) 2140.

29. M. Crisafulli, G. Martinelli, V.J. Hill, and C.T. Sachrajda, *Phys. Lett.* **B223** (1989) 90; V. Lubicz, G. Martinelli, M.S. McCarthy, and C.T. Sachrajda, *Phys. Lett.* **B274** (1992) 415.

30. V. Lubicz, G. Martinelli, M.S. McCarthy, and C.T. Sachrajda, *Nucl. Phys.* **B356** (1991) 301.

31. G.W. Kilcup, S.R. Sharpe, R. Gupta, and A. Patel, *Phys. Rev. Lett.* **64** (1990) 25; N. Ishizuka, M. Fukugita, H. Mino, M. Okawa, Y. Shizawa, and A. Ukawa, *Phys. Rev. Lett.* **71** (1993) 24; G.W. Kilcup, *Phys. Rev. Lett.* **71** (1993) 1677.

32. A. Abada, et al, *Nucl. Phys. B376* (1992) 172.

33. C. Bernard and A. Soni, *Nucl. Phys. B (Proc. Suppl.)* **9** (1989) 155.

34. L. Maiani and M. Testa, *Phys. Lett.* **B245** (1990) 585.

35. M. Lüscher, *Nucl. Phys.* **B354** (1991) 531; **B364** (1991) 237.

36. A. Duncan, E. Eichten, and H.B. Thacker, *Phys. Lett.* **B303** (1993) 109.

NEW PHYSICS EFFECTS ON CP VIOLATION IN B DECAYS

YOSEF NIR

Physics Department, Weizmann Institute of Science,

Rehovot 76100, Israel

1. INTRODUCTION

We review new physics effects on CP violation in B decays. For previous reviews on this subject, we refer the reader to refs. [1, 2, 3, 4]. A discussion of CP violation in B decays within the Standard Model (and a guide to the literature) can be found in [5].

In chapter 2 we introduce our formalism, and discuss the Standard Model picture of CP violation in B decays, with special emphasis on the cleanliness of the predictions. Chapter 3 gives a general discussion of new physics effects: we point out the ingredients in the analysis that are sensitive to new physics and deduce the type of new physics that is most likely to modify the Standard Model predictions. Explicit examples are given in chapter 4: a model with Z-mediated flavor changing neutral currents (FCNC) demonstrates in which ways will new physics manifest itself in CP asymmetries in B decays; a supersymmetric model with "quark–squark alignment" mechanism shows that supersymmetry may affect CP asymmetries in B decays, even though the minimal supersymmetric Standard Model (MSSM) does not; multi-scalar models may affect the asymmetries even in the absence of new CP violating phases; schemes for quark mass matrices will be crucially tested by the CP asymmetries. In chapter 5 we explain how, if deviations from the Standard Model predictions are measured, we will be able to learn detailed features of the New Physics that is responsible for that.

2. THEORETICAL BACKGROUND

Let us first describe our basic formalism. A more detailed discussion can be found in ref. [3]. If B and $\bar{B}$ are the CP conjugate bottom mesons (*i.e.* B^0 and $\bar{B}^0$, B^+ and B^-, B_s and $\bar{B}_s$), and f and $\bar{f}$ are CP conjugate final states, then we denote by A and $\bar{A}$ the two CP conjugate amplitudes:

$$A \equiv \langle f|\,H\,|B\rangle\,, \quad \bar{A} \equiv \langle \bar{f}|\,H\,|\bar{B}\rangle\,. \tag{1}$$

For the neutral B mesons, we define p and q to be the components of the interaction eigenstates B^0 and $\bar{B}^0$ within the mass eigenstates B_H and B_L (H and L stand for Heavy and Light, respectively):

$$|B_L\rangle = p\,|B^0\rangle + q\,|\bar{B}^0\rangle\,, \quad |B_H\rangle = p\,|B^0\rangle - q\,|\bar{B}^0\rangle\,. \tag{2}$$

For final CP eigenstates f_{CP}, we define the product

$$\lambda \equiv \frac{q}{p}\frac{\bar{A}_{f_{CP}}}{A_{f_{CP}}}. \tag{3}$$

The quantities $|\bar{A}/A|$, $|q/p|$ and λ are free of phase conventions and physical.

We distinguish three types of CP violation in meson decays:

(i) CP violation in decay:

$$|\bar{A}/A| \neq 1. \tag{4}$$

Here, CP violation arises from the interference between direct decay amplitudes. CP violation of the type (4) can be observed in non-leptonic charged B decays, *e.g.* a difference in the rate of $B^+ \to K^+\pi^0$ and $B^- \to K^-\pi^0$.

(ii) CP violation in mixing:

$$|q/p| \neq 1. \tag{5}$$

Here, CP violation arises from the mass eigenstates being different from the CP eigenstates. CP violation of the type (5) can be observed in semi-leptonic neutral B decays, *e.g.* a difference in the rate of $\bar{B}^0_{\rm phys}(t) \to \ell^+\nu X$ and $B^0_{\rm phys}(t) \to \ell^-\nu X$.

(iii) CP violation in the interference of mixing and decay:

$$\mathrm{Im}\lambda \neq 0, \quad |\lambda| = 1. \tag{6}$$

Here, CP violation arises from the interference between the direct decay, $B^0 \to f_{CP}$, and the "first - mix, then - decay" process, $B^0 \to \bar{B}^0 \to f_{CP}$. Of course, $|\lambda| \neq 1$ also reflects CP violation, but it belongs to either or both of the types (4) and (5). CP violation of the type (6) can be observed in neutral B decays into final CP eigenstates that are dominated by a single weak phase, *e.g.* a difference in the rate of $\bar{B}^0_{\rm phys}(t) \to \psi K_S$ and $B^0_{\rm phys}(t) \to \psi K_S$.

There is a significant difference in the cleanliness of the theoretical calculations in the three types of CP violation. If a certain decay gets contributions from various amplitudes with absolute values A_i, strong phases δ_i and weak, CP violating phases ϕ_i, then

$$\left|\frac{\bar{A}}{A}\right| = \left|\frac{\sum_i A_i e^{i\delta_i} e^{-i\phi_i}}{\sum_i A_i e^{i\delta_i} e^{+i\phi_i}}\right|. \tag{7}$$

It follows that direct CP violation requires both non-trivial strong phase difference ($\delta_i - \delta_j \neq 0$) and non-trivial weak phase difference ($\phi_i - \phi_j \neq 0$). Conversely, the calculation of direct CP violation requires knowledge of strong phase shifts and absolute values of various amplitudes and, therefore, necessarily involves hadronic uncertainties.

In the neutral B system, where the width difference between the two mass eigenstates is much smaller than the mass difference,

$$\left|\frac{q}{p}\right| = 1 - \frac{1}{2}\mathrm{Im}\frac{\Gamma_{12}}{M_{12}}. \tag{8}$$

While M_{12} is measured by the mass difference, Γ_{12} needs to be theoretically calculated. This is basically a long-distance physics calculation, and therefore involves large hadronic uncertainties. While it is clear that $|q/p| - 1$ is very small ($\mathcal{O}(10^{-3})$), the actual value is uncertain by a factor of a few [1].

In contrast, CP asymmetries of the type (6) are theoretically clean. Take, for example, the $B \to \psi K_S$ mode. The deviation of $|\lambda|$ from unity due to CP violation in mixing is, as mentioned in the previous paragraph, of order 10^{-3}. The deviation of $|\lambda|$ from unity due to direct CP violation is even smaller: not only is the penguin diagram much smaller than the tree diagram, it also carries to a good approximation the same weak phase. Thus, the interpretation of the measured CP asymmetry in terms of electroweak parameters, $a_{CP}(B \to \psi K_S) = \sin 2\beta$, is accurate to better than 10^{-3}. In other modes, where the penguin contribution differs in phase from the tree diagrams, hadronic uncertainties are larger, *e.g.* of order 10% in $B \to \pi\pi$.

The Standard Model predictions for direct CP violation in various semi-inclusive $B^\pm$ decays are given in Table 1. We take the results for the purely hadronic modes from refs. [6, 7]. The results in these two references agree, except for the modes marked with a star, where [6] quotes very small asymmetries. The quoted values should be taken as representative numbers and not as exact predictions. The asymmetries in the radiative decays were calculated in ref. [8].

1. Direct CP Violation		
Decay	BR	a_{CP}
$\bar b \to \bar u u \bar s$	5×10^{-3}	0.006*
$\bar b \to \bar d d \bar s$	3×10^{-3}	0.005
$\bar b \to \bar s s \bar s$	3×10^{-3}	0.005
$\bar b \to \bar u u \bar d$	8×10^{-3}	−0.004*
$\bar b \to \bar s s \bar d$	3×10^{-4}	−0.04
$\bar b \to \bar d d \bar d$	3×10^{-4}	−0.04
$\bar b \to \bar s \gamma$	3×10^{-4}	0.005
$\bar b \to \bar d \gamma$	1×10^{-5}	0.1

It is difficult, however, to see how these inclusive asymmetries can be experimentally measured. It is more likely that direct CP violation would be measured in exclusive modes. On the one hand side, the asymmetries for exclusive modes could be much larger. On the other hand, their calculation suffers from larger hadronic uncertainties and is sometimes very sensitive to the value of q^2 being used. Examples of exclusive asymmetries are [6, 7]

$$\begin{aligned} a_{CP}(B^+ \to K^+\pi^0) &\sim 0.01, \\ a_{CP}(B^+ \to K^+ K^{*0}) &\sim 0.05. \end{aligned} \tag{9}$$

Again, the Standard Model prediction is uncertain by at least a factor of a few in either direction. However, if the measured asymmetries are very large, say $\gg 0.2$, it would be very difficult to accommodate them in the Standard Model even if one stretches the hadronic uncertainties, and would probably signal new physics.

An estimate of the Standard Model value of the CP asymmetry in semi-leptonic B decays,

$$a_{SL} \equiv \frac{\Gamma(B^0_{phys}(t) \to \ell^-\nu X) - \Gamma(\bar B^0_{phys}(t) \to \ell^+\nu X)}{\Gamma(B^0_{phys}(t) \to \ell^-\nu X) + \Gamma(\bar B^0_{phys}(t) \to \ell^+\nu X)} = \frac{|q/p|^4 - 1}{|q/p|^4 + 1}, \tag{10}$$

can be made on the basis of quark diagrams calculation of Γ_{12} (see refs. [1, 3] and references therein):

$$\begin{aligned} a_{SL}(B^0) &\approx \frac{8\pi}{f_2(y_t)} \frac{m_c^2}{m_t^2} \frac{J}{|V_{tb}V_{td}^*|^2} \sim 10^{-3}, \\ a_{SL}(B_s) &\approx \frac{8\pi}{f_2(y_t)} \frac{m_c^2}{m_t^2} \frac{J}{|V_{tb}V_{ts}^*|^2} \sim 10^{-4}, \end{aligned} \tag{11}$$

(J is the Jarlskog measure of CP violation). The estimates (11) have hadronic uncertainties of a factor of 2–3. In addition, the estimate of $a_{SL}(B^0)$ has a large uncertainty from the poorly determined CKM parameter $|V_{td}|$. Again, a very large leptonic asymmetry, say $\gtrsim 10^{-2}$, would be difficult to explain by hadronic uncertainties and would imply new physics.

The cleanliness of CP violation in the interference of mixing and decay makes it the prime candidate for discovery of New Physics. The Standard Model predictions for various classes of asymmetries are given in Tables 2 and 3. (The signs of the asymmetries in the last column corresponds to CP even final hadronic states and not necessarily for the actual example in the first column.)

2. CP Asymmetries in B^0 Decays		
Final State	Quark Sub-Process	SM Prediction
ψK_S	$\bar{b} \to \bar{c}c\bar{s}$	$-\sin 2\beta$
D^+D^-	$\bar{b} \to \bar{c}c\bar{d}$	$-\sin 2\beta$
$\pi^+\pi^-$	$\bar{b} \to \bar{u}u\bar{d}$	$\sin 2\alpha$
ϕK_S	$\bar{b} \to \bar{s}s\bar{s}$	$-\sin 2(\beta - \beta')$
K_SK_S	$\bar{b} \to \bar{s}s\bar{d}$	0

3. CP Asymmetries in B_s Decays		
Final State	Quark Sub-Process	SM Prediction
$\psi\phi$	$\bar{b} \to \bar{c}c\bar{s}$	$-\sin 2\beta'$
ψK_S	$\bar{b} \to \bar{c}c\bar{d}$	$-\sin 2\beta'$
ρK_S	$\bar{b} \to \bar{u}u\bar{d}$	$-\sin 2(\gamma + \beta')$
$\phi\phi$	$\bar{b} \to \bar{s}s\bar{s}$	0
ϕK_S	$\bar{b} \to \bar{s}s\bar{d}$	$\sin 2(\beta - \beta')$

The various angles that appear in Tables 2 and 3 are defined by

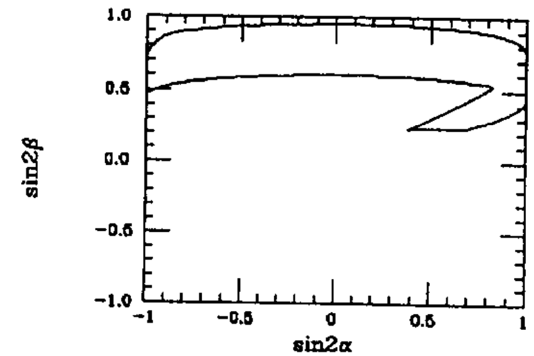

Fig. 1. The Standard Model predictions in the $\sin 2\alpha$(horizontal) – $\sin 2\beta$(vertical) plane for $110 \le m_t \le 180$ GeV. (The allowed ranges for all other parameters are taken from [29].)

$$\alpha = \arg\left[-\frac{V_{td}V_{tb}^*}{V_{ud}V_{ub}^*}\right], \quad \gamma = \arg\left[-\frac{V_{ud}V_{ub}^*}{V_{cd}V_{cb}^*}\right],$$
$$\beta = \arg\left[-\frac{V_{cd}V_{cb}^*}{V_{td}V_{tb}^*}\right], \quad \beta' = \arg\left[-\frac{V_{cs}V_{cb}^*}{V_{ts}V_{tb}^*}\right]. \tag{12}$$

Of these angles, β' is constrained to be very small,

$$|\sin 2\beta'| \le 0.06. \tag{13}$$

The Standard Model constraints on $\sin 2\alpha$ and $\sin 2\beta$ are given in Fig. 1. (We focus on these two angles because they are likely to be measured first.)

It follows that there are several clean signals of new physics:

(*i*) $a_{CP}(B \to \psi K_S)$ that is significantly smaller than $+0.2$ (and certainly if it is negative).

(*ii*) $a_{CP}(B \to \psi K_S)$ and $a_{CP}(B \to \pi\pi)$ both significantly smaller than $+0.5$.

(*iii*) Any of $a_{CP}(B_s \to \psi\phi)$, $a_{CP}(B_s \to \psi K_S)$ and $a_{CP}(B_s \to \phi\phi)$ above a few percent in absolute value.

3. BEYOND THE STANDARD MODEL - GENERAL

CP asymmetries in B decays are a sensitive probe of new physics in the quark sector, because they are likely to differ from the Standard Model predictions if there are sources of CP violation beyond the CKM phase of the Standard Model. This can contribute in two ways:

1. If there are significant contributions to $B-\bar{B}$ mixing (or $B_s-\bar{B}_s$ mixing) beyond the box diagram with intermediate top quarks; or

2. If the unitarity of the three-generation CKM matrix does not hold, namely if there are additional quarks.

Actually, there is a third way in which the Standard Model predictions may be modified even if there are no new sources of CP violation:

3. The constraints on the CKM parameters may change if there are significant new contributions to $B-\bar{B}$ mixing and to ϵ_K.

On the other hand, the following ingredients of the analysis of CP asymmetries in neutral B decays are likely to hold in most extensions of the Standard Model:

4. $\Gamma_{12} \ll M_{12}$. In order for this relation to be violated, one needs a new dominant contribution to tree decays of B mesons, which is extremely unlikely, or strong suppression of the mixing compared to the Standard Model box diagram, which is unlikely (though not impossible for the B_s system). The argument is particularly solid for the B_d system as it is supported by experimental evidence: $\Delta M/\Gamma \sim 0.7$, while branching ratios into states that contribute to Γ_{12} are $\leq 10^{-3}$.

5. The relevant decay processes (for tree decays) are dominated by Standard Model diagrams. Again, it is unlikely that new physics, which typically takes place at a high energy scale, would compete with weak tree decays. (On the other hand, for penguin dominated decays, there could be significant contributions from new physics.)

Within the Standard Model, both B decays and $B-\bar{B}$ mixing are determined by combinations of CKM elements. The asymmetries then measure the relative phase between these combinations. Unitarity of the CKM matrix directly relates these phases (and consequently the measured asymmetries) to angles of the unitarity triangles. In models with new physics, unitarity of the three-generation charged-current mixing matrix may be lost and consequently the relation between the CKM phases and angles of the unitarity triangle violated. But this is not the main reason that the predictions for the asymmetries are modified. The reason is rather that if $B-\bar{B}$ mixing has significant contributions from new physics, the asymmetries measure different quantities: the relative phases between the CKM elements that determine B decays and the elements of mixing matrices in sectors of new physics (squarks, multi-scalar, etc) that contribute to $B-\bar{B}$ mixing.

Thus, when studying CP asymmetries in models of new physics, we look for violation of the unitarity constraints and, even more importantly, for contributions to $B-\bar{B}$ mixing that are different in phase and not much smaller in magnitude than the Standard Model contribution. This leads to the following general description of the potential for large effects in various directions of new physics:

1. In extensions of the quark sector, CKM–unitarity is violated and there are new contributions to $B-\bar{B}$ mixing. Potentially, large effects are possible.

2. In Supersymmetry, there are new contributions to $B-\bar{B}$ mixing. Potentially, large effects are possible. (Note, however, that in the minimal SUSY Standard Model (MSSM), FCNC and new phases are "switched-off" by hand, and no new effects are possible.)

3. In extensions of the scalar sector, there are new contributions to $B-\bar{B}$ mixing. Potentially, large effects are possible. (Note, however, that in the two Higgs doublet Model with NFC, there are no new phases, and no new effects are possible.)

4. In extensions of the gauge sector, the new gauge bosons couple universally

in flavor space. Typically, the strong constraints from K-physics imply that it is unlikely to have observable effects in B-physics.

In what follows, we describe several specific examples of extensions of the Standard Model that affect CP asymmetries in B decays. The following models were discussed in detail in the literature: 4th generation quarks [9, 10, 11, 12, 13, 14]; Z-mediated FCNC [15, 16, 17], Left-Right Symmetry [18, 19]; extensions of the scalar sector [20, 21, 22, 23, 24, 25, 26]; Supersymmetry [27, 28]; schemes of quark mass matrices [29, 30]; modifications of the CKM constraints [31, 24]. Effects of new physics on direct CP violation have been studied in refs. [32, 33] and on CP violation in mixing in refs. [34, 35].

4. SPECIFIC EXAMPLES

4.1 Extra Quark Singlets [15, 16, 17]

We describe here an extension of the quark sector with an $SU(2)_L$-singlet of charge $-1/3$. (This represents well the case when there is such an additional quark for each generation, as in E_6 models.) With this extension, all the ingredients relevant to CP asymmetries in B decays are indeed affected by new physics.

In such models, the charged current mixing matrix V is 3×4 and, most important, it is not unitary. (It is a submatrix of the unitary 4×4 matrix that relates the down mass eigenstates to the interaction eigenstates.) This leads to non-diagonal Z couplings, as the neutral current mixing matrix, $U = V^\dagger V \neq 1$. In particular,

$$U_{db} = V_{ud}^* V_{ub} + V_{cd}^* V_{cb} + V_{td}^* V_{tb} \neq 0. \tag{14}$$

Eq. (14) shows that the two ingredients relevant to CP asymmetries in B decays are indeed modified in this extension:

1. Unitarity of the CKM matrix is violated. In particular, the unitarity triangle turns into a unitarity quadrangle, with U_{db} being the fourth side.

2. There are new contributions to $B - \bar{B}$ mixing from Z mediated tree diagrams:

$$M_{12}^Z = \frac{\sqrt{2}}{12} G_F (B_B f_B^2) m_B \eta (U_{db})^2. \tag{15}$$

3. There are new sources of CP violation, as the matrices V and U depend on three CP violating phases.

It is a peculiar property of this model that all three new ingredients are related to each other. Let us define the following new two angles in the unitarity quadrangle:

$$\bar{\alpha} = \arg\left(\frac{V_{ud} V_{ub}^*}{U_{db}^*}\right), \quad \bar{\beta} = \arg\left(\frac{U_{db}^*}{V_{cd} V_{cb}^*}\right). \tag{16}$$

Then, if the Z-mediated tree diagrams dominate $B - \bar{B}$ mixing,

$$a_{CP}(B \to \psi K_S) \approx \sin 2\bar{\beta}, \quad a_{CP}(B \to \pi\pi) \approx \sin 2\bar{\alpha}. \tag{17}$$

The significant modification is then not in the new range for α and β but rather that the asymmetries now depend on new phases, $\bar{\alpha}$ and $\bar{\beta}$. As there are no experimental constraints on the values of $\bar{\alpha}$ and $\bar{\beta}$ (but only on the magnitude $|U_{db}|$), the asymmetries in (17) could have any value [15], unlike the Standard Model case described in Fig. 1. (If the extra singlet quarks are much heavier than a few TeVs, $|U_{db}|$ is expected to be very small, the Z-mediated FCNC contribute negligibly to $B - \bar{B}$ mixing, and the deviations from the Standard Model predictions are unobservably small.)

In ref. [16] it was shown that the upper bound on $|U_{sb}|$ from the UA1 measurement of $b \to s\mu^+\mu^-$ implies that the effects on CP asymmetries in B_s decays cannot be maximal. For example, the zero asymmetries predicted for various B_s decays (see Table 3), could be modified to, at most, $\mathcal{O}(0.3)$. In ref. [17] it was observed that even if the Z contributions do not dominate the mixing but are just not much smaller than the box diagrams, they could still have large effects on the asymmetries. In this case, the asymmetries in (17) would have a more complicated dependence on α, β, $\tilde{\alpha}$ and $\tilde{\beta}$.

4.2 Quark-Squark Alignment [36, 28]

We describe here a supersymmetric extension of the Standard Model that is different from the MSSM. In particular, the mechanism that suppresses SUSY-induced FCNC is not squark degeneracy. Instead, the quark mass matrices and the squark mass-squared matrices are naturally aligned in models of abelian horizontal symmetry [36], namely the are both approximately diagonal in the same basis. If this alignment is precise enough, the mixing matrix for quark-squark-gluino couplings is very close to the unit matrix, and FCNC are highly suppressed even if squarks are not degenerate at all.

The motivation for this extension [37] was to explain the hierarchy in the quark sector parameters,

$$\begin{aligned} 1 &\sim m_t/\langle\phi_u\rangle\,; \\ \lambda &\sim V_{us}; \\ \lambda^2 &\sim V_{cb},\ m_d/m_s,\ m_s/m_b; \\ \lambda^3 &\sim V_{ub},\ m_u/m_c,\ m_c/m_t. \end{aligned} \tag{18}$$

(with $\lambda \sim 0.2$ these relations hold to within a factor of 2.) These relations are predicted and the alignment of quarks and squarks is precise enough to satisfy the constraints from neutral meson mixing if the mass matrices have the following form (for details see [28]):

$$M^d \sim \langle\phi_d\rangle \begin{pmatrix} \lambda^4 & 0 & \lambda^3 \\ 0 & \lambda^2 & \lambda^2 \\ 0 & 0 & 1 \end{pmatrix}, \quad M^u \sim \langle\phi_u\rangle \begin{pmatrix} \lambda^6 & \lambda^4 & \lambda^3 \\ \lambda^5 & \lambda^3 & \lambda^2 \\ \lambda^3 & \lambda^2 & 1 \end{pmatrix}. \tag{19}$$

(All entries here are just order of magnitude estimates.)

Such a structure for the quark mass matrices can be a result of a horizontal (discrete subgroup of) $U(1)_a \times U(1)_b$ symmetry, that is spontaneously broken by the VEVs of two Standard Model singlet scalars:

$$S_a(-1,0):\ \frac{\langle S_a\rangle}{M} \sim \lambda; \quad S_b(0,-1):\ \frac{\langle S_b\rangle}{M} \sim \lambda^2. \tag{20}$$

M is a high scale where the information about the horizontal symmetry breaking is communicated to the light quarks. An example of charge assignments that lead to M^d as in (19) is the following:

$$\begin{aligned} &Q_1(3,0),\ \ Q_2(0,1),\ \ Q_3(0,0); \\ &\bar{d}_1(-1,1),\ \ \bar{d}_2(2,-1),\ \ \bar{d}_3(0,0). \end{aligned} \tag{21}$$

Here, the Q_i are quark-doublet supermultiplets, while $\bar{d}_i$ are down-quark singlet supermultiplets. The charge assignments in (21) determine the form of the squark mass-squared matrices as well. Most important for our study are the diagonal blocks in the down-squark mass-squared matrix:

$$\tilde{M}^{d2}_{LL} \sim \tilde{m}^2 \begin{pmatrix} 1 & \lambda^5 & \lambda^3 \\ \lambda^5 & 1 & \lambda^2 \\ \lambda^3 & \lambda^2 & 1 \end{pmatrix}, \quad \tilde{M}^{d2}_{RR} \sim \tilde{m}^2 \begin{pmatrix} 1 & \lambda^7 & \lambda^3 \\ \lambda^7 & 1 & \lambda^4 \\ \lambda^3 & \lambda^4 & 1 \end{pmatrix}. \tag{22}$$

The structure of M^d and $\tilde{M}^{d2}$ allows an estimate of the mixing matrix for quark-squark-gluino interaction which, in turn, gives an estimate of the SUSY contribution to neutral meson mixing. With the mass matrices of eqs. (19) and (22), SUSY contribution to $B - \bar{B}$ mixing (with $\tilde{m} \sim m_{\tilde{g}} \sim 1\ TeV$) is about 20% of the Standard Model one. On the other hand, the SUSY contribution to mixing in the K system is negligibly small. Actually, it is small enough to obey the more stringent ϵ_K constraints even for phases of order 1.

As the SUSY diagram is, in magnitude, about 20% of $M_{12}(B^0)$ but with a phase that could be very different from the Standard Model one, the Standard

Model predictions for CP asymmetries in B^0 decays may be modified by as much as 0.4, a sizable effect. On the other hand, a similar analysis for B_s mixing shows that it cannot be significantly affected by the SUSY contributions, so that the Standard Model predictions for CP asymmetries in B_s decays remain unchanged.

The quark-squark alignment mechanism has strong testable predictions, namely that squarks are not degenerate and that $D - \bar{D}$ mixing is close to the experimental upper bound. Large effects on CP asymmetries in B decays are not a necessary result of quark-squark alignment, but their measurement would be extremely useful in distinguishing between various explicit models that incorporate this mechanism. Furthermore, the model above shows that the absence of modifications to the Standard Model predictions for CP asymmetries in B decays in the MSSM is a special property of this model and not a generic feature of SUSY models.

4.3 Charged Scalar Exchange [24]

In models of three or more scalar doublets, the mixing matrix for charged scalars contains one or more CP violating phases. This phase could, in principle, affect CP asymmetries in B decays [24]. However, recent experimental constraints imply that the effect is too small to be observed. Still, the Standard Model predictions may be violated because the constraints on the CKM parameters change.

In multi-scalar models, $B - \bar{B}$ mixing gets additional contributions from box diagrams where one or two of the Standard Model W-boson propagators are replaced by the charged scalar H propagators. This situation can be presented in the following way:

$$M_{12}(B^0) = \frac{G_F^2}{64\pi^2}(V_{td}^* V_{tb})^2 (I_{WW} + 2I_{WH} + I_{HH}), \tag{23}$$

where I_{WW}, I_{HW} and I_{HH} are functions of the intermediate particle masses (m_W, m_H and m_t) and of the Yukawa couplings. The Standard Model contribution is I_{WW}. The functions I_{HW} and, in a more significant way, I_{HH} depend on the phase in the charged scalar mixing matrix.

Let us define a phase θ_H according to

$$\theta_H = \arg(I_{WW} + 2I_{WH} + I_{HH}). \tag{24}$$

(I_{WW} is real, so that in the Standard Model $\theta_H = 0$.) The angles measured by CP asymmetries in B^0 decays will be universally shifted by θ_H. Specifically,

$$a_{CP}(B \to \psi K_S) = -\sin(-2\beta + \theta_H), \quad a_{CP}(B \to \pi\pi) = \sin(2\alpha + \theta_H). \tag{25}$$

The magnitude of this effect depends on how large θ_H is. Existing constraints from CP violating processes, most noticeably the electric dipole moment of the neutron, still allow for very large θ_H. However, the CP violating charged scalar couplings contribute also to the CP conserving decay $b \to s\gamma$. The recent CLEO bound on the rate of this decay gives the strongest constraint on CP violation from charged scalar exchange [24]. It implies that the effect on CP asymmetries in B^0 decays cannot be larger than 2%, too small to stand out as a signal of new physics.

Modifications of the Standard Model predictions for CP asymmetries in B decays may also arise from the different constraints on CKM parameters. This holds even for two scalar doublet (type I and type II) models where indeed there are no new phases. The most significant effect is that the lower bounds on $|V_{tb}V_{td}^*|$ from $B - \bar{B}$ mixing and from ϵ_K are relaxed, because charged scalar exchange may contribute significantly. This situation is actually much more general than our specific multi-scalar framework, and the results below apply to all models with significant contributions to x_d and ϵ_K: a new region (forbidden in the Standard Model) opens up in the plane of $\sin 2\alpha - \sin 2\beta$, as shown in Fig. 2 [24]. If experiment finds a relatively low value of $\sin 2\beta$ (below 0.5) and a negative value

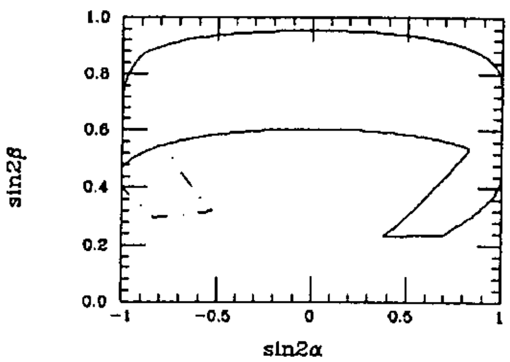

Fig. 2. The allowed region in the $\sin 2\alpha - \sin 2\beta$ plane in the Standard Model (solid) and the new allowed region in multi-scalar models (dot-dashed).

for $\sin 2\alpha$, it may be an indication that there are significant contributions from new physics to $B - \bar{B}$ mixing, even if these contributions carry no new phases.

Multi-scalar models without NFC are much less constrained, and may give large effects on the CP asymmetries [25]. An interesting case is that of light scalars with small couplings to quarks protected by approximate symmetries, where close to zero asymmetries are expected for all B decays [26].

4.4 Schemes for Quark Mass Matrices [29]

As far as CP asymmetries in B decays are concerned, extensions of the Standard Model that provide relations between the quark sector parameters are unique: instead of relaxing the Standard Model constraints on CP asymmetries in B decays, they actually narrow down considerably the allowed ranges. This means that while none of the extensions discussed in previous sections can be excluded on the basis of measurements of CP asymmetries, schemes for quark mass matrices can.

We will not go to any details concerning the various schemes for quark mass

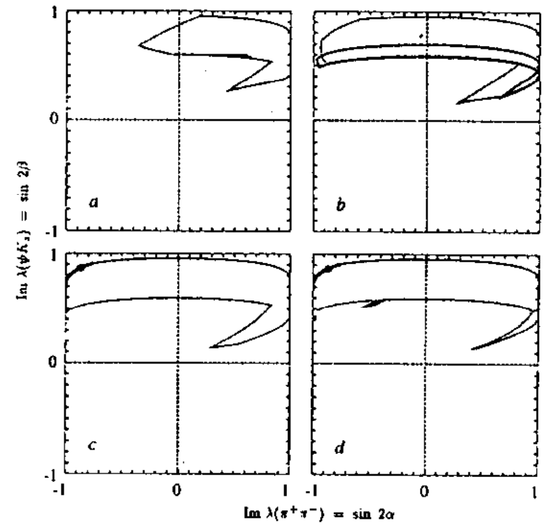

Fig. 3. The regions predicted by various mass matrix schemes in the $\sin 2\alpha - \sin 2\beta$ plane for m_t = (a) 90 GeV, (b) 130 GeV, (c) 160 GeV, (d) 185 GeV. The Standard Model predictions are outlined in grey, and those of the various schemes in black. (See the text for details.)

matrices discussed here. Instead, we present in Fig. 3 [29] the predictions for $a_{CP}(B \to \psi K_S)$ and $a_{CP}(B \to \pi\pi)$ from schemes by Fritzsch (the thin black wedge in Fig. 3.a); Giudice (the black band in Fig. 3.b); Dimopoulos-Hall-Raby (the black region in Fig. 3d); and the "symmetric - CKM" scheme (the black curves in Figs. 3.c and 3.d). (For detailed references, see [29].) It is clear from the figure that CP asymmetries in the above-mentioned modes would crucially test each of these schemes.

5. HOW TO DISTINGUISH BETWEEN VARIOUS TYPES OF NEW PHYSICS?

If deviations from the Standard Model predictions are found, how can we tell which extension of the Standard Model (among the many extensions that allow large effects) is responsible for that? In this chapter, we show that the richness of experimental measurements, reflected in the large number of modes in Tables 2 and 3, can be used to study very detailed features of the new physics that might affect the CP asymmetries [38, 31].

More specifically, various relations among the asymmetries do not depend on all the assumptions that go into the analysis and thus may hold beyond the Standard Model or, conversely, if they are violated can help pinpoint which ingredients must be added to the Standard Model. Here are a few examples.

(i) Violation of

$$a_{CP}(B \to D^+D^-) = -a_{CP}(B \to \psi K_S) \tag{26}$$

(the minus sign comes from the opposite CP of the final states) would imply that (a) there is new physics contribution to $K - \bar{K}$ mixing and (b) the approximate unitarity relation $V_{ud}^* V_{us} + V_{cd}^* V_{cs} \approx 0$ (where we neglected $V_{td}^* V_{ts}$) is violated.

(ii) Violation of

$$a_{CP}(B_s \to \psi\phi) \approx 0 \tag{27}$$

would imply that there is new physics contribution to $B_s - \bar{B}_s$ mixing. As shown in ref. [38], this condition is equivalent to

$$\alpha + \beta + \gamma = \pi \tag{28}$$

(where α, β and γ are deduced from the CP asymmetries in $B \to \pi\pi$, $B \to \psi K_S$ and $B_s \to \rho K_S$, respectively).

(iii) Violation of

$$a_{CP}(B \to \psi K_S) = \sin 2\beta, \quad a_{CP}(B \to \pi\pi) = \sin 2\alpha, \tag{29}$$

(where $\sin 2\alpha$ and $\sin 2\beta$ are calculated from the constraints on the unitarity triangle) would imply that there is new physics contribution to $B^0 - \bar{B}^0$ mixing.

(iv) Violation of

$$a_{CP}(B_s \to \psi\phi) \approx a_{CP}(B_s \to \phi\phi) \tag{30}$$

would most likely imply that the approximate unitarity relation $V_{cb}^* V_{cs} + V_{tb}^* V_{ts} \approx 0$ (where we neglected $V_{ub}^* V_{us}$) is violated.

As an example, we explain the test (i) above. The phases measured by the two modes are:

$$\begin{aligned} \arg\lambda(B \to D^+D^-) &= \arg(M_{12}(B^0)) - 2\arg(A(\bar{b} \to \bar{c}c\bar{d})), \\ \arg\lambda(B \to \psi K_S) &= \arg(M_{12}(B^0)) - 2\arg(A(\bar{b} \to \bar{c}c\bar{s})) - \arg(M_{12}(K^0)). \end{aligned} \tag{31}$$

It is clear that the phase of the B^0 mixing amplitude does not affect the relation of eq. (26) (even though it affects the actual values of the asymmetries). As decay amplitudes are dominated by W-mediated tree diagrams, (26) does hold if

$$\arg(M_{12}(K^0)) = \arg((V_{cd} V_{cs}^*)^2). \tag{32}$$

This is trivially the case if $K - \bar{K}$ mixing is dominated by the Standard Model box diagram with virtual c quarks. Therefore, a necessary condition for violating (26) is a new mechanism for $K - \bar{K}$ mixing. However, the extremely small experimental value of ϵ_K implies that $\arg(M_{12}(K))/\Gamma_{12}(K)) \sim 10^{-3}$. Therefore, model-independently

$$\arg(M_{12}(K^0)) \approx \arg((V_{ud} V_{us}^*)^2). \tag{33}$$

Consequently, another necessary condition for violating (26) is that $V_{ud} V_{us}^* + V_{cd} V_{cs}^* \neq 0$.

We conclude that with CP asymmetries measured in many B decay modes, we can learn many detailed features of the new physics that affects their values.

ACKNOWLEDGEMENTS

This work is based on collaborations with Claudio Dib, Yuval Grossman, Miriam Leurer, David London, Helen Quinn, Uri Sarid, Nati Seiberg and Dennis Silverman. YN is an incumbent of the Ruth E. Recu Career Development Chair, and is supported in part by the Israel Commission for Basic Research, by the United States – Israel Binational Science Foundation (BSF), and by the Minerva Foundation.

REFERENCES

1. I.I. Bigi *et al.*, in *CP Violation*, ed. C. Jarlskog (Singapore, World Scientific, 1989).
2. Y. Nir and H.R. Quinn, Ann. Rev. Nucl. Part. Sci. 42 (1992) 211.
3. Y. Nir, in the Proc. of the 20th SLAC Summer Institute on Particle Physics, SLAC-REPORT-412, ed. L. Vassilian (1992).
4. C.O. Dib, D. London and Y. Nir, Int. J. Mod. Phys. A6 (1991) 1253.
5. M. Gronau, these proceedings.
6. J.-M. Gerard and W.-S. Hou, Phys. Rev. D43 (1991) 2909.
7. H. Simma and D. Wyler, Phys. Lett. B272 (1991) 395.
8. J.M. Soares, Nucl. Phys. B367 (1991) 575.
9. I.I. Bigi and S. Wakaizumi, Phys. Lett. B188 (1987) 501.
10. M. Tanimoto, Y. Suetaka and K. Senba, Z. Phys. C40 (1988) 539.
11. S. Wakaizumi, T. Hayashi and M. Tanimoto, Phys. Rev. D39 (1989) 2792.
12. T. Hasuike *et al.*, Int. J. Mod. Phys. A4 (1989) 2465; Phys. Rev. D41 (1990) 1691.
13. S. Wakaizumi *et al.*, Phys. Rev. D44 (1991) 3582.
14. D. London, Phys. Lett. B234 (1990) 354.
15. Y. Nir and D. Silverman, Phys. Rev. D42 (1990) 1477.
16. D. Silverman, Phys. Rev. D45 (1992) 1800.
17. G.C. Branco, P.A. Parada, T. Morozumi and M.N. Rebelo, Phys. Rev. D48 (1993) 1167.
18. G. Ecker and W. Grimus, Z. Phys. C30 (1986) 293.
19. D. London and D. Wyler, Phys. Lett. B232 (1989) 503.
20. J. Liu and L. Wolfenstein, Phys. Lett. B197 (1987) 536.
21. J.F. Donoghue and E. Golowich, Phys. Rev. D37 (1988) 2542.
22. J.-M. Gerard and T. Nakada, Phys. Lett. B261 (1991) 474.
23. J.M. Soares and L. Wolfenstein, Phys. Rev. D46 (1992) 256.
24. Y. Grossman and Y. Nir, Phys. Lett. B, in press.
25. J.M. Soares and L. Wolfenstein, Phys. Rev. D47 (1993) 1021.
26. L. Hall and S. Weinberg, Phys. Rev. D48 (1993) 979.
27. I.I. Bigi and F. Gabbiani, Nucl. Phys. B352 (1991) 309.
28. M. Leurer, Y. Nir and N. Seiberg, in preparation.
29. Y. Nir and U. Sarid, Phys. Rev. D47 (1993) 2818.
30. L. Hall and A. Rasin, LBL-33668 (1993).
31. Y. Nir and H.R. Quinn, Phys. Rev. D42 (1990) 1473.
32. M. Tanimoto, Phys. Rev. Lett. 62 (1989) 2797.
33. M. Tanimoto, K. Hirayama, T. Shinmoto and K. Senba, Z. Phys. C48 (1990) 99.
34. D. Cocolicchio and L. Maiani, Phys. Lett. B291 (1992) 155.

35. G.C. Branco, P.A. Parada, T. Morozumi and M.N. Rebelo, Phys. Lett. B306 (1993) 398.

36. Y. Nir and N. Seiberg, Phys. Lett. B309 (1993) 337.

37. M. Leurer, Y. Nir and N. Seiberg, Nucl. Phys. B398 (1993) 319.

38. Y. Nir and D. Silverman, Nucl. Phys. B345 (1990) 301.

Measurement of Angle α

Convenors:

A. Jawahery
University of Maryland

K.B. Luk
Lawrence BerkeleyLaboratory

D. London
University of Montreal

List of Participants

F. Azfar
University of Pennsylvania

L. Camilleri
CERN

E. Dukes
University of Virginia

P. Eerola
CERN

K. Gounder
University of Mississippi

M. Halling
Cornell University/
Fermi National Accelerator Laboratory

J. Heinrich
University of Pennsylvania

W. Hofmann
Max-Planck-Institut für Kernphysik

J. Izen
University of Texas at Dallas

T. Lawry
University of Virginia

J. Lewis
Fermi National Accelerator Laboratory

P. Karchin
Yale University

C. Kennedy
Yale University

S. Kwan
Fermi National Accelerator Laboratory

K. McDonald
Princeton University

A. McManus
University of Virginia

S. Mishra
Fermi National Accelerator Laboratory

J. Mueller
Rutgers University

G. Punzi
INFN-Pisa

J. Spalding
Fermi National Accelerator Laboratory

P. Wilson
University of Chicago

Measurement of Angle α

Summary Report of the Working Group on: Measurement of the Angle α

A. Jawahery
Department of Physics, University of Maryland
College Park, MD 20742

D. London
Laboratoire de physique nucléaire, Université de Montréal
C.P. 6128, succ. A, Montréal, Québec, CANADA, H3C 3J7.

and

K. B. Luk
Department of Physics and Lawrence Berkeley Laboratory
University of California, Berkeley, CA 94720

1. INTRODUCTION

In the framework of the standard model, CP violating asymmetries in decays of kaons or B hadrons can be described using the parameters of the CKM matrix [1], which includes a CP violating phase. The unitarity of the CKM matrix implies several triangular relations in the complex plane such as:

$$V_{ud}V_{ub}^* + V_{cd}V_{cb}^* + V_{td}V_{tb}^* = 0 \ . \tag{1}$$

This relation can be described in terms of three angles, $\alpha = arg(V_{ud}V_{ub}^*V_{td}V_{tb}^*)$, $\beta = arg(V_{cd}V_{cb}^*V_{td}V_{tb}^*)$, $\gamma = arg(V_{ud}V_{ub}^*V_{cd}V_{cb}^*)$. A test of the unitarity relation and the CKM scheme for CP violation can be performed by measuring these angles and testing the relation, $\alpha + \beta + \gamma = 180°$.

The charge of this working group was to consider the feasibility of measuring the angle α using a hadron accelerator and to compare the capabilities of the various experimental options. For this study we focussed on experiments at the SSC with $E_{beam} = 20$ TeV and at the Tevatron with $E_{beam} = 1$ TeV. For detector configurations, we formed three subgroups studying central collider experiments, forward collider experiments and fixed target experiments. In each subgroup we compared the capabilities of several proposed or existing experiments using, for the most part, the results of the simulation studies provided by the proponents of each experiment. The results of these comparisons are discussed in detail in the reports of the subgroups and are summarized here in Tables 1 to 3, where as a figure of merit we present the number of years required to measure the CP asymmetry in the mode $B^0 \to \pi^+\pi^-$ with an accuracy of $\delta A_{CP} = 0.1$.

This report consists of a theoretical introduction, a brief description of some of the principal experimental issues involved in the measurements of CP asymmetries in modes sensitive to the angle α, followed by a set of Tables comparing the capabilities of various experimental options. Following the summary report are the reports of subgroups which contain more detailed discussions of the experiments considered in this study. Also included in the report are several papers on talks presented at the workshop sessions on issues related to the measurement of the angle α.

2. THEORETICAL OVERVIEW

We begin with a brief review of the formalism describing CP violation in the neutral B-meson system [2].

Due to B^0-$\overline{B^0}$ mixing, a meson which is born as a B^0 or a $\overline{B^0}$ will evolve in time to a mixture of B^0 and $\overline{B^0}$:

$$
\begin{aligned}
|B^0(t)\rangle &= f_+(t)|B^0\rangle + \frac{q}{p} f_-(t)|\overline{B^0}\rangle \\
|\overline{B^0}(t)\rangle &= \frac{p}{q} f_-(t)|B^0\rangle + f_+(t)|\overline{B^0}\rangle \, ,
\end{aligned} \tag{2}
$$

in which $|B^0\rangle$ ($|\overline{B^0}\rangle$) represents a pure B^0 ($\overline{B^0}$) state at $t=0$, and

$$
\begin{aligned}
f_+(t) &= e^{-imt}e^{-\Gamma t/2}\cos(\Delta mt/2) \\
f_-(t) &= e^{-imt}e^{-\Gamma t/2} i \sin(\Delta mt/2) \, .
\end{aligned} \tag{3}
$$

In Eq. (2) the factor q/p represents the CP violation in the mixing. To a good approximation this is a pure phase and can be written as

$$
\frac{q}{p} \equiv e^{-2i\phi_M} \, . \tag{4}
$$

For the B_d and B_s systems, this phase is

$$
\left(\frac{q}{p}\right)_{B_d} = \frac{V_{td}}{V_{td}^*} \, , \qquad \left(\frac{q}{p}\right)_{B_s} = 1. \tag{5}
$$

Here and below we implicitly assume the Wolfenstein parametrization [3] of the CKM matrix, in which only V_{td} and V_{ub} have non-negligible phases.

The standard way to look for CP violation in the neutral B system is to look for a difference between $\Gamma(B^0(t)\to f)$ and $\Gamma(\overline{B^0}(t)\to \bar{f})$, in which f is some final state and $\bar{f}$ is its CP-conjugate. As we will see, it may not always be possible to obtain clean information on the CKM phases using this asymmetry, so it is necessary to perform a more general analysis. The quantities which will be of interest to us are the rates for $B^0(t)$ and $\overline{B^0}(t)$ to decay into both f and $\bar{f}$. Defining

$$
\begin{aligned}
A_f &\equiv \langle f|B^0\rangle \quad , \quad & A_{\bar{f}} &\equiv \langle \bar{f}|B^0\rangle \, , \\
\overline{A}_f &\equiv \langle f|\overline{B^0}\rangle \quad , \quad & \overline{A}_{\bar{f}} &\equiv \langle \bar{f}|\overline{B^0}\rangle \, ,
\end{aligned} \tag{6}
$$

it is straightforward to calculate

$$
\begin{aligned}
\Gamma(B^0(t)\to f) &= e^{-\Gamma t}|A_f|^2\left[\cos^2\frac{\Delta mt}{2} + |\alpha_f|^2\sin^2\frac{\Delta mt}{2} - \mathrm{Im}\,\alpha_f \sin\Delta mt\right]; \\
\alpha_f &\equiv \frac{q}{p}\frac{\overline{A}_f}{A_f} \, ,
\end{aligned} \tag{7}
$$

$$
\begin{aligned}
\Gamma(B^0(t)\to \bar{f}) &= e^{-\Gamma t}|A_{\bar{f}}|^2\left[\cos^2\frac{\Delta mt}{2} + |\alpha_{\bar{f}}|^2\sin^2\frac{\Delta mt}{2} - \mathrm{Im}\,\alpha_{\bar{f}} \sin\Delta mt\right]; \\
\alpha_{\bar{f}} &\equiv \frac{q}{p}\frac{\overline{A}_{\bar{f}}}{A_{\bar{f}}} \, ,
\end{aligned} \tag{8}
$$

$$
\begin{aligned}
\Gamma(\overline{B^0}(t)\to f) &= e^{-\Gamma t}|\overline{A}_f|^2\left[\cos^2\frac{\Delta mt}{2} + |\bar{\alpha}_f|^2\sin^2\frac{\Delta mt}{2} - \mathrm{Im}\,\bar{\alpha}_f \sin\Delta mt\right]; \\
\bar{\alpha}_f &\equiv \frac{p}{q}\frac{A_f}{\overline{A}_f} = \frac{1}{\alpha_f} \, ,
\end{aligned} \tag{9}
$$

$$
\begin{aligned}
\Gamma(\overline{B^0}(t)\to \bar{f}) &= e^{-\Gamma t}|\overline{A}_{\bar{f}}|^2\left[\cos^2\frac{\Delta mt}{2} + |\bar{\alpha}_{\bar{f}}|^2\sin^2\frac{\Delta mt}{2} - \mathrm{Im}\,\bar{\alpha}_{\bar{f}} \sin\Delta mt\right]; \\
\bar{\alpha}_{\bar{f}} &\equiv \frac{p}{q}\frac{A_{\bar{f}}}{\overline{A}_{\bar{f}}} = \frac{1}{\alpha_{\bar{f}}} \, .
\end{aligned} \tag{10}
$$

Thus far, the calculations have been completely general. The procedure for measuring CP violation depends on the assumptions made regarding the final state and the weak decay amplitudes.

2.1 $f=\bar{f}$; One Weak Amplitude in $B^0\to f$

Consider the case in which the final state is a CP eigenstate [4], that is, $f=\bar{f}$. Suppose further that one weak amplitude contributes to the decay $B^0\to f$. In this case we can write [5]

$$
\begin{aligned}
A_f &= A(B^0\to f) = |A_f|e^{i\phi_D}e^{i\delta} \, , \\
\overline{A}_f &= A(\overline{B^0}\to f) = |A_f|e^{-i\phi_D}e^{i\delta} \, ,
\end{aligned} \tag{11}
$$

in which ϕ_D is the weak phase in the decay and δ is the strong phase. The value of the weak decay phase depends on whether a $b\to c$ or a $b\to u$ transition is involved:

$$
(\phi_D)_{b\to u} = arg\left(\frac{V_{ub}}{V_{ub}^*}\right) \, , \qquad (\phi_D)_{b\to c} = 0 \, . \tag{12}
$$

The above assumptions imply two things. First, we have

$$
|A_f|^2 = |\overline{A}_f|^2 \equiv |A|^2 \, . \tag{13}
$$

The second implication is that $|\alpha_f|=1$, that is, α_f is a pure phase:

$$
\alpha_f = \frac{q}{p}\frac{\overline{A}_f}{A_f} = e^{-2i\phi_M}e^{-2i\phi_D} \tag{14}
$$

The four equations for the B decay rates in Eqs. (7)-(10) now simplify considerably to the following two expressions:

$$
\begin{aligned}
\Gamma(B^0(t)\to f) &= e^{-\Gamma t}|A|^2\left[1 - \mathrm{Im}\,\alpha_f\sin\Delta mt\right] \, , \\
\Gamma(\overline{B^0}(t)\to f) &= e^{-\Gamma t}|A|^2\left[1 + \mathrm{Im}\,\alpha_f\sin\Delta mt\right] \, .
\end{aligned} \tag{15}
$$

The difference between these two rates (time-dependent or time-integrated) is the measure of CP violation, with $\mathrm{Im}\,\alpha_f = \sin 2(\phi_M+\phi_D)$. Note that the above rates depend only on weak phases; there is no contamination from the strong phase δ.

Thus, if the final state f is a CP eigenstate, and if we assume that only one weak amplitude contributes to the B-decay process, we find that there are three classes of B decays which can have sizeable CP-violating asymmetries [6], represented by the angles α, β and γ:

- B_d decays with $b \to u$ (e.g. $B_d \to \pi^+\pi^-$): $\sin 2\alpha$.
- B_d decays with $b \to c$ (e.g. $B_d \to \Psi K_s$): $\sin 2\beta$.
- B_s decays with $b \to u$ (e.g. $B_s \to \rho K_S$): $\sin 2\gamma$.

(The fourth class, B_s decays with $b \to c$ (e.g. $B_s \to D_s^+ D_s^-$), is expected to have no CP asymmetry.) In this report we will focus on the possibilities for measuring the angle α, principally via the final state $\pi^+\pi^-$.

There are, however, a number of good reasons to consider other final states than $\pi^+\pi^-$. First, although the branching ratio is expected to be about 1×10^{-5}, it has not been measured, and could conceivably be smaller. Second, $\pi^+\pi^-$ might be a difficult final state to observe in a hadron collider, due to the large backgrounds. Finally, penguin diagrams might contribute significantly to this decay [7], which would ruin the assumption of the dominance of a single weak decay amplitude. In this case the CP violation in $B_d \to \pi^+\pi^-$ would no longer depend cleanly on the angle α. For all these reasons it is necessary to consider relaxing the above assumptions regarding the final state and the weak decay amplitudes, and to consider other final states for measuring α.

2.2 $f \neq \bar{f}$; One Weak Amplitude in $B^0 \to f(\bar{f})$

Consider now the case in which the final state f is not a CP eigenstate, but that still one weak amplitude contributes to the decays $B^0 \to f$, $B^0 \to \bar{f}$, $\overline{B^0} \to f$ and $\overline{B^0} \to \bar{f}$. In this case we have

$$\begin{aligned} A_f &\equiv A(B^0 \to f) = |A_f| e^{i\phi_D} e^{i\delta} , \\ \overline{A}_{\bar f} &\equiv A(\overline{B^0} \to \bar{f}) = |A_f| e^{-i\phi_D} e^{i\delta} , \end{aligned} \tag{16}$$

which implies that $|A_f| = |\overline{A}_{\bar f}|$. Similarly,

$$\begin{aligned} A_{\bar f} &\equiv A(B^0 \to \bar{f}) = |A_{\bar f}| e^{i\phi_D'} e^{i\delta'} , \\ \overline{A}_f &\equiv A(\overline{B^0} \to f) = |A_{\bar f}| e^{-i\phi_D'} e^{i\delta'} , \end{aligned} \tag{17}$$

with $|A_{\bar f}| = |\overline{A}_f|$. It is therefore clear that α_f and $\alpha_{\bar f}$ are not pure phases:

$$\begin{aligned} \alpha_f &= \frac{|A_{\bar f}|}{|A_f|} e^{-i\left(2\phi_M + \phi_D + \phi_D' + \delta - \delta'\right)} , \\ \alpha_{\bar f} &= \frac{|A_f|}{|A_{\bar f}|} e^{-i\left(2\phi_M + \phi_D + \phi_D' - \delta + \delta'\right)} . \end{aligned} \tag{18}$$

From the above we see that there are four independent parameters: $|A_f|$, $|A_{\bar f}|$, $2\phi_{CKM} \equiv 2\phi_M + \phi_D + \phi_D'$, and $\Delta \equiv \delta - \delta'$. The *time-dependent* measurement of the four decay rates in Eqs. (7)-(10) permits the extraction of the two quantities $\sin(2\phi_{CKM} + \Delta)$ and $\sin(2\phi_{CKM} - \Delta)$. It is then straightforward to obtain $\sin 2\phi_{CKM}$, up to a 4-fold ambiguity [8].

In order for this technique to be practical, it is necessary to consider final states for which A_f, $A_{\bar f}$, $\overline{A}_f$ and $\overline{A}_{\bar f}$ are about the same size. This can be accomplished by choosing states for which f and $\bar{f}$, though not CP-conjugates of one another, have the same quark content. In this case, $\phi_D = \phi_D'$. For the measurement of the angle α, examples of such states are $(\rho^+\pi^-, \rho^-\pi^+)$ and $(a_1^+\pi^-, a_1^-\pi^+)$. The $a_1\pi$ state might be particularly interesting for hadron colliders, since the signal will be four charged pions coming from a single secondary vertex.

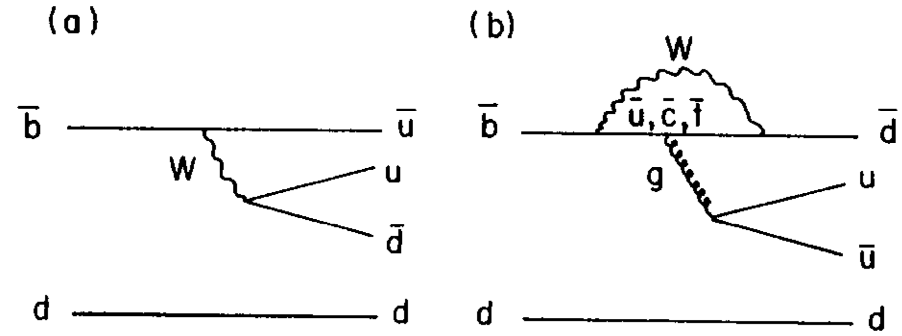

Figure 1: Tree level (a) and penguin (b) diagrams for the decay $B_d^0 \to \pi\pi$.

2.3 $f = \bar{f}$; More than One Weak Amplitude in $B^0 \to f$)

If the final state is a CP eigenstate, but more than one weak amplitude contributes to the decay $B^0 \to f$, then the asymmetry between the rates $\Gamma(B^0(t) \to f)$ and $\Gamma(\overline{B^0}(t) \to f)$, as described in Sec. 1.1, will *not* provide clean information on the CKM phases – there will be inevitably be some uncertainty due to both strong phases and the presence of more than one weak phase. In this case, it is necessary to perform a more intricate analysis.

One example of such a situation is the final state $\pi^+\pi^-$, in the case in which penguin diagrams contribute significantly to the decays $B_d^0(t), \overline{B_d^0}(t) \to \pi^+\pi^-$ (see Fig. 1). Since the weak phase of the penguin contribution is not equal to that of the tree diagram, the CP asymmetry does not cleanly measure the angle α. It is, however, possible to disentangle the various effects by using isospin [9].

The analysis proceeds by considering the decays $B_d^0 \to \pi^+\pi^-$, $B_d^0 \to \pi^0\pi^0$ and $B_u^+ \to \pi^+\pi^0$. The amplitudes for these three processes, denoted A^{+-}, A^{00} and A^{+0}, respectively, can be related by isospin. We begin by noting the following points. First, due to Bose statistics, the final $\pi\pi$ states can have only $I = 0$ or $I = 2$. Second, the tree diagram can produce $\pi\pi$ pairs in either state of total isospin. On the other hand, since the gluon carries no isospin, the penguin diagrams can contribute to final states with $I = 0$ only. Therefore the $\Delta I = 3/2$ operator comes purely from the tree diagram, while the $\Delta I = 1/2$ operator has contributions from both tree and penguin diagrams. Finally, the decay $B_u^+ \to \pi^+\pi^0$ arises solely from the tree diagram, since the final state can have only $I = 2$.

Using the Wigner-Eckart theorem, it is straightforward to express A^{+-}, A^{00} and A^{+0} in terms of the $I = 0$ and $I = 2$ amplitudes (A_0 and A_2, respectively):

$$\begin{aligned} \frac{1}{\sqrt{2}} A^{+-} &= A_2 - A_0 , \\ A^{00} &= 2A_2 + A_0 , \\ A^{+0} &= 3A_2 , \end{aligned} \tag{19}$$

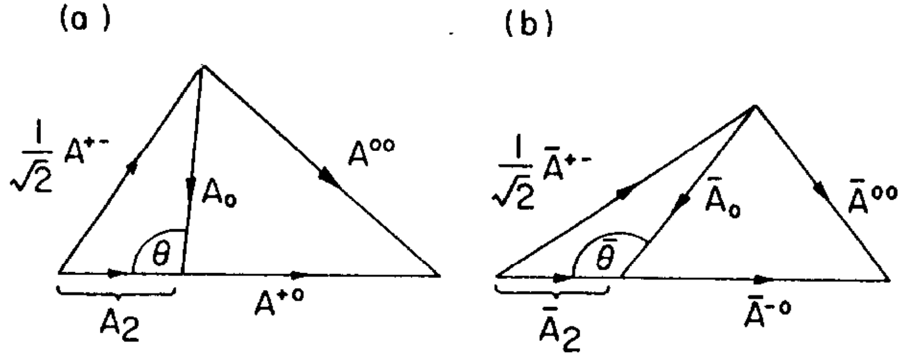

Figure 2: Complex triangles of Eqs. (20) and (21).

which immediately leads to the triangle relation

$$\frac{1}{\sqrt{2}}A^{+-} + A^{00} = A^{+0} . \tag{20}$$

There is a similar relation for the charge-conjugated processes $\overline{B_d^0} \to \pi^+\pi^-$, $\overline{B_d^0} \to \pi^0\pi^0$ and $B_u^- \to \pi^-\pi^0$, whose amplitudes are denoted $\overline{A}^{+-}$, $\overline{A}^{00}$, $\overline{A}^{-0}$, respectively:

$$\frac{1}{\sqrt{2}}\overline{A}^{+-} + \overline{A}^{00} = \overline{A}^{+0} . \tag{21}$$

The $\overline{A}$-amplitudes are obtained from the A-amplitudes by changing the sign of the weak phases, while leaving the strong phases unchanged.

The key point here is that only one weak amplitude – the tree-level diagram – contributes to the $I = 2$ final state, so that

$$A_2 = |A_2| e^{i\phi_t} e^{i\delta_2} , \qquad \overline{A}_2 = |\overline{A}_2| e^{-i\phi_t} e^{i\delta_2} , \tag{22}$$

in which ϕ_t is the weak phase of the tree diagram and δ_2 is the $I = 2$ final-state-interaction phase. This implies that $|A^{+0}| = |\overline{A}^{-0}|$. On the other hand, due to the presence of penguin contributions there is no simple relation between A^{+-} and $\overline{A}^{+-}$, or between A^{00} and $\overline{A}^{00}$. One can, however, obtain information by looking at the time-dependent decay rates. For f a CP eigenstate, the four rates of Eqs. (7)-(10) reduce to the two equations

$$\Gamma(B_d^0(t) \to f) = e^{-\Gamma t}|A_f|^2 \left[\cos^2\frac{\Delta m t}{2} + |\frac{\overline{A}_f}{A_f}|^2 \sin^2\frac{\Delta m t}{2} - \mathrm{Im}\left(\frac{q}{p}\frac{\overline{A}_f}{A_f}\right)\sin\Delta m t\right], \tag{23}$$

$$\Gamma(\overline{B_d^0}(t) \to f) = e^{-\Gamma t}|\overline{A}_f|^2 \left[\cos^2\frac{\Delta m t}{2} + |\frac{A_f}{\overline{A}_f}|^2 \sin^2\frac{\Delta m t}{2} + \mathrm{Im}\left(\frac{q}{p}\frac{\overline{A}_f}{A_f}\right)\sin\Delta m t\right]. \tag{24}$$

For $f = \pi^+\pi^-$, the time-dependent measurements of the above rates allow the extraction of $|A^{+-}|$ and $|\overline{A}^{+-}|$. For the $\pi^0\pi^0$ final state, in principle one could perform similar measurements to obtain $|A^{00}|$ and $|\overline{A}^{00}|$. In practice, however, it is extremely unlikely that such a measurement could be performed at a hadron collider. Such information must probably come from e^+e^- colliders.

In fact, at an e^+e^- machine operating at the $\Upsilon(4s)$, it is not even necessary to do a time-dependent measurement [10]. The $B_d^0\overline{B_d^0}$ pair resulting from the decay of the $\Upsilon(4s)$ is necessarily in a $C = -1$ eigenstate. The time-dependent rates for such a $B_d^0\overline{B_d^0}$ pair to decay to a final CP eigenstate f plus a semileptonic tag are

$$\begin{aligned}\Gamma(B_d^0(t)\overline{B_d^0}(\bar{t}) \to f + (D\ell\overline{\nu}X)_{tag}) &= e^{-\Gamma(t+\bar{t})}|A_f|^2 \\ &\times \left[\cos^2\frac{\Delta m(t+\bar{t})}{2} + |\frac{\overline{A}_f}{A_f}|^2 \sin^2\frac{\Delta m(t+\bar{t})}{2} - \mathrm{Im}\left(\frac{q}{p}\frac{\overline{A}_f}{A_f}\right)\sin\Delta m(t-\bar{t})\right],\end{aligned} \tag{25}$$

$$\begin{aligned}\Gamma(\overline{B_d^0}(t)B_d^0(\bar{t}) \to f(\overline{D\ell\nu X})_{tag}) &= e^{-\Gamma(t+\bar{t})}|\overline{A}_f|^2 \\ &\times \left[\cos^2\frac{\Delta m(t+\bar{t})}{2} + |\frac{A_f}{\overline{A}_f}|^2 \sin^2\frac{\Delta m(t+\bar{t})}{2} + \mathrm{Im}\left(\frac{q}{p}\frac{\overline{A}_f}{A_f}\right)\sin\Delta m(t-\bar{t})\right].\end{aligned} \tag{26}$$

Integrating over t and $\bar{t}$ symmetrically from 0 to ∞ yields

$$\Gamma(B_d^0\overline{B_d^0} \to f + (D\ell\overline{\nu}X)_{tag}) \propto \left(|A_f|^2 + |\overline{A}_f|^2\right) + \frac{1}{1+x_d^2}\left(|A_f|^2 - |\overline{A}_f|^2\right), \tag{27}$$

$$\Gamma(B_d^0\overline{B_d^0} \to f + (\overline{D\ell\nu X})_{tag}) \propto \left(|A_f|^2 + |\overline{A}_f|^2\right) - \frac{1}{1+x_d^2}\left(|A_f|^2 - |\overline{A}_f|^2\right), \tag{28}$$

where x_d is the mixing parameter, $\Delta m/\Gamma$. From these two expressions $|A_f|$ and $|\overline{A}_f|$ can be obtained. Thus, the tagged, time-integrated measurements at the $\Upsilon(4s)$ of the rates for the decay into $\pi^0\pi^0$ will yield $|A^{00}|$ and $|\overline{A}^{00}|$.

Given the magnitudes of the A- and the $\overline{A}$-amplitudes, this allows us to specify the triangles of Eqs. (20) and (21) (Fig. 2). The final piece of information is the measurement of CP violation in Eqs. (23) and (24). For the $\pi^+\pi^-$ final state, this is

$$\mathrm{Im}\left(\frac{q}{p}\frac{\overline{A}^{+-}}{A^{+-}}\right) = \mathrm{Im}\left(e^{2i\alpha}\left[\frac{1-\bar{z}}{1-z}\right]\right), \tag{29}$$

in which $z \equiv A_0/A_2$ and $\bar{z} \equiv \overline{A}_0/\overline{A}_2$. Here one sees explicitly that, indeed, in the presence of penguins, the asymmetry in $B_d^0(\overline{B_d^0}) \to \pi^+\pi^-$ does not cleanly measure the angle α – there is additional phase information, a priori unknown, in z and $\bar{z}$. However, and this is the main point, z and $\bar{z}$ can be obtained from the triangles of Fig. 2, each up to a twofold ambiguity, using elementary trigonometry. In this way the isospin analysis permits the clean measurement of $\sin 2\alpha$, even in the presence of large penguin contributions, up to a fourfold ambiguity. (If, in addition, it were possible to measure CP violation using the final state $\pi^0\pi^0$, then the ambiguity could, in general, be lifted completely.) This same technique can in principle be used to extract α using the decays $B_d^0 \to \pi K$, $\pi\rho$, [11] although here there tend to be a larger number of ambiguities [12].

Another example of a case in which the final state is a CP eigenstate, but more than one weak amplitude contributes to $B^0 \to f$, is the decay $B_d^0 \to D_{CP}^0 K_S$, in which $D_{CP}^0 = (D^0 + \overline{D^0})/\sqrt{2}$ is identified by its CP-even decay products. Here there are no penguin contributions, but rather two tree-level diagrams (Fig. 3), so that once again the technique elaborated in Sec. 1.1 will not yield clean information on the CKM phases.

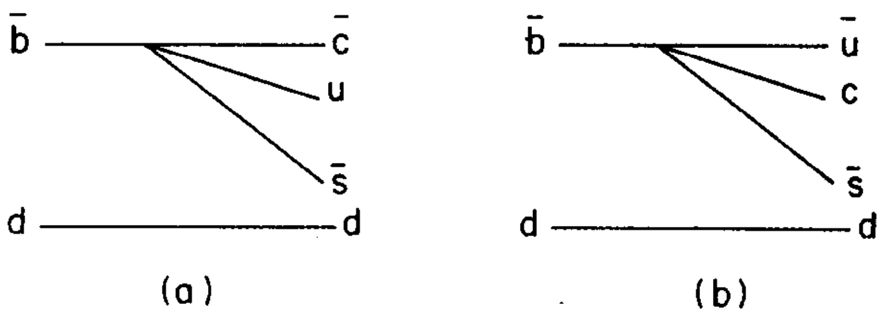

Figure 3: The two diagrams for (a) $B_d^0 \to \overline{D^0} K_s$, (b) $B_d^0 \to D^0 K_s$.

This situation can be resolved [13] by considering also the amplitudes for the decays $B_d^0 \to \overline{D^0} K_s$ and $B_d^0 \to D^0 K_s$. The weak CKM phases of diagrams Figs. 3a and 3b are 0 and γ, respectively, with corresponding strong phases $\delta_{\overline{D}}$ and δ_D. We can therefore write

$$\begin{aligned} A_{\overline{D}} &\equiv A(B_d^0 \to \overline{D^0} K_s) = |A_{\overline{D}}| e^{i\delta_{\overline{D}}} \\ A_D &\equiv A(B_d^0 \to D^0 K_s) = |A_D| e^{i\gamma} e^{i\delta_D} \\ A_{D^0_{CP}} &\equiv A(B_d^0 \to D^0_{CP} K_s) = \frac{1}{\sqrt{2}} (A_D + A_{\overline{D}}), \end{aligned} \tag{30}$$

where the third equation is due to the definition of D^0_{CP}. The magnitudes $|A_{\overline{D}}|$ and $|A_D|$ are expected to be of comparable size. The amplitudes for the charge-conjugated processes, $\overline{B_d^0} \to D^0 K_s$, $\overline{B_d^0} \to \overline{D^0} K_s$ and $\overline{B_d^0} \to D^0_{CP} K_s$, denoted $\overline{A}_D$, $\overline{A}_{\overline{D}}$ and $\overline{A}_{D^0_{CP}}$, respectively, are obtained from the A-amplitudes by changing the sign of the weak CKM phases. We therefore have $|A_{\overline{D}}| = |\overline{A}_D|$ and $|A_D| = |\overline{A}_{\overline{D}}|$, but $|A_{D^0_{CP}}| \neq |\overline{A}_{D^0_{CP}}|$.

As with the previous examples, it is necessary to measure the time-dependence of B_d^0 decays to the three final states $D^0 K_s$, $\overline{D^0} K_s$ and $D^0_{CP} K_s$ (Eqs. (7) and (8)). From these measurements, it is possible to obtain the magnitudes of A_D, $A_{\overline{D}}$ and $A_{D^0_{CP}}$. These same measurements will also give the CP-violating parameters

$$\begin{aligned} -\mathrm{Im}\,\alpha_{\overline{D}} &= \frac{|A_D|}{|A_{\overline{D}}|} \sin(2\beta + \gamma - \Delta), \\ -\mathrm{Im}\,\alpha_D &= \frac{|A_{\overline{D}}|}{|A_D|} \sin(2\beta + \gamma + \Delta), \end{aligned} \tag{31}$$

where $\Delta \equiv \delta_D - \delta_{\overline{D}}$ and we have used the fact that the phase of B_d^0-$\overline{B_d^0}$ mixing (q/p) is 2β.

It is now just straightforward algebra to show that these five quantities – the three magnitudes and the 2 CP-violating parameters – along with the triangle relation of Eq. (30) suffice to determine *both* $\sin 2\alpha$ and $\sin 2\beta$ with no hadronic uncertainty (we use the relation $\sin 2(\beta + \gamma) = -\sin 2\alpha$, which follows from the unitarity triangle). Note that, in fact, we are not obliged to consider only the CP-even final state $D^0_{CP} K_s$ – one can also include the CP-odd state $D'^0_{CP} K_s$, where $D'^0_{CP} = (D^0 - \overline{D^0})/\sqrt{2}$. In this case it is necessary to appropriately modify the triangle relation of Eq. (30).

The one drawback of this method is that the branching ratios are likely to be rather small, since the decays are color-suppressed. A rough estimate yields [14] $B(B_d^0 \to \overline{D^0} K_s) \sim 2 \times 10^{-6}$ and $B(B_d^0 \to D^0 K_s) \sim 5 \times 10^{-7}$. Since about 10% of D decays are to CP eigenstates, the branching ratios to the final states $D^0_{CP} K_s$ and $D'^0_{CP} K_s$ should be $O(10^{-7})$.

2.4 $f \neq \bar{f}$; *More than One Weak Amplitude/Partial Wave in* $B^0 \to f(\bar{f})$

For the case in which the final state f is not a CP eigenstate, and where more than one weak amplitude contributes to $B^0 \to f(\bar{f})$, in general it is impossible to obtain clean information on the CKM phases. This is also true if there is only one weak amplitude, but many different partial waves. The one exception to the rule is if the different partial waves have different CP parities. In this case one can perform an angular correlation analysis to distinguish the partial waves, and then measure CP asymmetries within each partial wave. Since the method of angular analysis is rather involved, we will not describe it here – we refer the reader to the original articles [15].

As far as the angle α is concerned, a partial list of final states to which this method applies includes $\omega\omega\rho^0$, $\omega\rho^0\pi^0$, $\omega\omega\pi^0$, $\omega\omega\omega$, $\rho^+\rho^-$, $\rho^0\rho^0$, $a_1^+ a_1^-$, $a_1^0 a_1^0$, ωa_1^0, $\Delta\overline{\Delta}$, $\omega\pi^0 K_s$, $\omega\omega K_s$, and $\omega\rho^0 K_s$. Although elegant, the method of angular correlations has a number of drawbacks. First, one needs a larger data sample in order to perform such an analysis. Second, the branching ratios to baryons and to 3-body states are likely to be considerably smaller than those to pairs of mesons. Finally, for most, if not all, of the above states, it will be necessary to combine the angular analysis with the isospin analysis described in Sec. 1.3 in order to eliminate the contributions from penguin diagrams. For all of these reasons, more work is required to determine if this method will be useful in the first generation of CP-violation experiments at hadron colliders.

3.0 EXPERIMENTAL OVERVIEW

Since the detector options and the related technology largely depend on the geometrical configuration of the experiments, we grouped the experiments into three categories: (a) central collider experiments, (b) forward collider experiments, and (c) fixed target experiments. The central collider experiments typically cover the pseudorapidity range of $|\eta| < 3$. However, the acceptance of these experiments for doing B physics is generally limited to a smaller η range because of requirements on the detector performance, particularly in regard to the momentum and vertex reconstruction resolution. The forward collider experiments with a single arm cover the pseudorapidity range of $1 < \eta < 6$. The fixed target experiments, benefitting from the large Lorentz boost of the final state particles, cover the small angular range of about 100 mrad around the incident beam direction.

Aside from the experimental and technological issues, there are several physics-related quantities that determine the capabilities of the experiments. These include the $\overline{B}B$ cross section, the production branching ratio $(\sigma_{b\bar{b}}/\sigma_{total})$, and the momentum distribution of the b-flavored hadrons and their decay products. The collider experiments, being at higher center-of-mass energies compared to the fixed target experiments, have the advantage of a larger $\overline{B}B$ cross section as well as a higher production branching ratio. However, the very high momenta of the decay products in the fixed target experiments significantly reduce the effect of multiple scattering, thus allowing for a more accurate determination of the secondary vertices. In addition, the decay vertices are in general well separated from the primary interaction point because of the longer mean decay distance in the fixed target experiments.

The overall comparison of the merits of the experimental options must take into account issues involving the detector technology and accelerator conditions. These are covered in the relevant detector and accelerator sessions.

In the following we will briefly discuss some of the principal issues relevant to the measurement of CP asymmetries related to the angle α. Our considerations include the choice of decay mode, triggers, criteria for the selection and reconstruction of events, tagging and dilution effects.

3.1 Choice of the Decay Mode

As discussed in Section 2, a large class of B decays is sensitive to the angle α. Among these, the decay $B^0 \to \pi^+\pi^-$ has been extensively simulated for the different experimental options considered here. However, the measurement of the CP asymmetry in the decay $B^0 \to \pi^+\pi^-$ does not directly lead to the determination of the angle α. In the presence of penguin processes, α can be extracted from the time-dependent decay rates and the CP asymmetries of the modes $B^0 \to \pi^+\pi^-$, $B^+ \to \pi^+\pi^0$, and $B^0 \to \pi^0\pi^0$. Since π^0 reconstruction in hadron beam experiments is considered to be very difficult, we assumed that the information on modes involving π^0's must come from e^+e^- experiments. Here we simply focussed on the feasibility of measuring the time-dependent decay rate and the CP asymmetry for the decay mode $B^0 \to \pi^+\pi^-$. We also briefly considered the decay mode $B \to a_1^+\pi^-$.

The reconstruction of the $B^0 \to \pi^+\pi^-$ decay is rather simple. It requires two tracks with a displaced vertex from the primary vertex of the event. However, because of its simple two-body topology, the signature for this mode can also be easily mimicked by random combinatorial processes, including the combination of particles from other decays of B mesons. Monte Carlo studies have shown that the level of combinatorial background can be several orders of magnitude larger than the expected signal in this mode. Therefore, background suppression is the most challenging task for any measurement involving this mode.

The kinematic features of this decay offer some discrimination against background processes. In Fig. 4 the transverse momentum distribution of the pions from the $B^0 \to \pi^+\pi^-$ decay, based on a simulation study for the GAJET proposal at LHC [16], is compared with that of the minimum bias events and the decay products from $B \to \psi K$ decay. The distinctly hard distribution of the π from the $B^0 \to \pi^+\pi^-$ decay is obvious. Furthermore, owing to the long lifetime of b hadrons, the pions tend to have a larger impact parameter on average, hence providing further discrimination against the background. These are some of the features of the $B^0 \to \pi^+\pi^-$ decay that are exploited in dedicated triggers for this process [17]. In the offline analysis additional cuts can be developed based on the decay length of the B meson and information from particle identification.

3.2 Trigger

The most common scheme for a $\overline{B}B$ trigger in hadron accelerator experiments is a lepton trigger, where an event is recorded if it contains a lepton which is consistent with having originated from the semileptonic decay of a B hadron. The selection of the decay $B^0 \to \pi^+\pi^-$ is subsequently performed in the offline analysis of the data. The overall trigger efficiency is then the product of the semileptonic branching ratio of B hadrons, the kinematic acceptance for the lepton, and the efficiency for detecting and identifying the lepton. In such events, the charge of the lepton is also used to tag the flavor of the B meson at the production point. Considerations have also been given to a dedicated trigger, where the event is recorded if a candidate $B^0 \to \pi^+\pi^-$ decay is present [17]. The main advantage of a dedicated trigger is that, given an event containing an identified $B^0 \to \pi^+\pi^-$ decay, one could envisage using various complementary tagging techniques, hence enhancing the statistical power of the measurement.

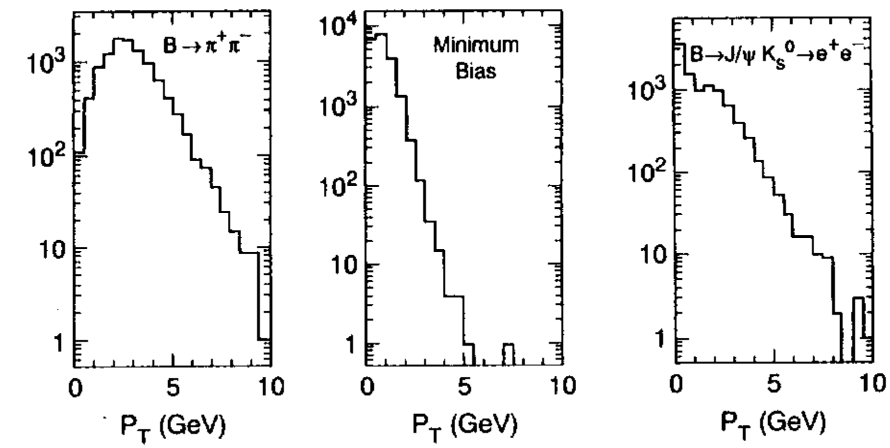

Figure 4: Simulation of calorimetric p_T distribution in GAJET: (a) the decay products in $B^0 \to \pi^+\pi^-$, (b) minimum bias events, and (c) the decay products in $B \to \psi K$

3.3 Background Rejection and Event Selection

The criteria for the reconstruction and selection of $B^0 \to \pi^+\pi^-$ events are primarily dictated by the requirements for the suppression of the background processes. Several detailed studies of the sources and the suppression of the combinatorial background have been performed. One study for the BCD proposal at SSC, which is reported here in the contributed papers, considers the background from $\overline{B}B$ events in detecting the decay $B^0 \to \pi^+\pi^-$ [18]. It demonstrates that, by applying cuts on the distributions of the transverse momentum and impact parameter of the decay products and the decay vertex of the B candidates (required to be separated from the primary vertex by at least 15 standard deviations), a signal to noise ratio of 1:1 can be achieved. Although this result is specific to the BCD detector, it provides a general indication of the severity of the background contamination and the need for accurate measurement of the secondary vertices.

Another background is the overlapping of signals from other exclusive decay modes of B mesons. Examples of such backgrounds are $B^0 \to K^+\pi^-$, $B_s \to K^-K^+$, which, if reconstructed as a $\pi\pi$ combination, would produce a peak near the expected signal for the

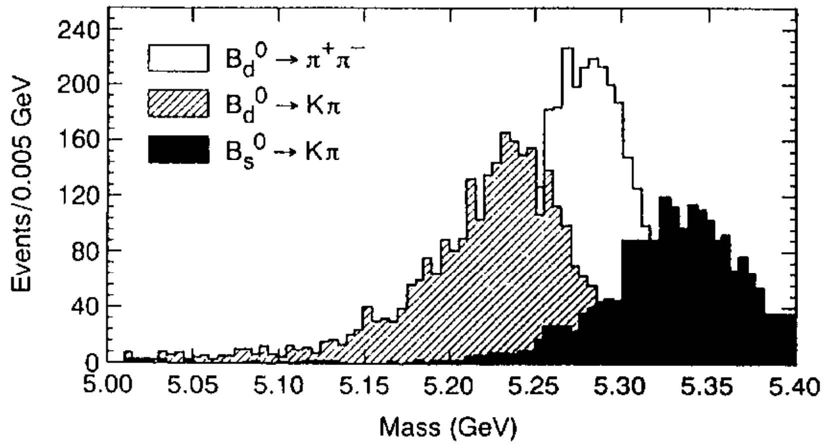

Figure 5: Invariant mass distribution of $\pi\pi$ combinations from the decay $B^0 \to \pi^+\pi^-$ (from a simulation for the BCD proposal). Shown are also the invariant mass distributions of the track combinations from the decays $B_s \to K\pi$ and $B^0 \to K\pi$, interpreted as $\pi\pi$. The relative normalizations are arbitrary.

decay $B^0 \to \pi^+\pi^-$. The decay $B^0 \to \rho^+\pi^-$, where $\rho^+ \to \pi^+\pi^0$, can also result in a structure overlapping with the $B^0 \to \pi^+\pi^-$ signal. As an example, in Fig. 5 we show the $\pi\pi$ invariant mass distributions for various final states interpreted as $\pi^+\pi^-$, for a BCD-like detector at SSC [19]. The presence of the background dilutes the measured CP asymmetry for the mode $B^0 \to \pi^+\pi^-$ by an unknown factor which is a function of the mass resolution and the CP asymmetry of the background decay modes. There are, however, ways of reducing these background events. According to Monte Carlo simulations, a mass resolution on the order of 5 MeV, though difficult to achieve, can either resolve or reduce the contamination of the different decay modes in the $\pi\pi$ invariant mass distribution. In addition, the level of the reflected peaks can be further suppressed by means of particle identification. Clearly, the message here is that excellent mass resolution and particle identification capability are needed.

3.4 Tagging

In order to determine the CP asymmetry for a decay channel, the particle anti-particle nature (the flavor) of the B meson at production ($t = 0$) must be known. For decays in which the final state is a CP eigenstate, the flavor of the B meson cannot be determined from the decay products – it must be extracted from the accompanying B hadron in the event. This can be achieved by using the charge of a lepton originating from the semileptonic decay of the accompanying B meson. For lepton-triggered events, this is readily done by using the trigger lepton. However, in order to reduce the mistagging probability, one may have to apply somewhat harder kinematic cuts to the lepton. The tagging efficiency is then just the acceptance of the additional kinematic cuts on the trigger lepton.

For $\pi^+\pi^-$-triggered events, the tagging efficiency would include a factor due to the semileptonic decay branching ratio times the lepton selection and identification efficiencies. Other methods for tagging include the kaon tag, in which the sign of the leading kaon in the accompanying B decay is used, and the so-called "soft pion" tag. The latter is based on a proposal by M. Gronau, A. Nippe and J. Rosner [20], which makes use of the presence of a soft pion accompanying the B meson in the fragmentation of the b quark or from the decay of an excited B^{**} meson. The charge of the soft pion is correlated with the original flavor of the B meson. Preliminary studies show that this method offers a potentially powerful tagging method. However, currently there are no experimental results on B^{**} production or on the production rate of an accompanying soft pion in B-meson production. Future data from LEP and Tevatron experiments will allow us to address these issues.

3.5 Dilution Factors

For a given decay, the observed CP asymmetry is diluted by the background, wrong-sign tagging of the B flavor, and flavor oscillation of the B meson before decay. Assuming that the combinatorial background is symmetric, the dilution due to this effect is simply a factor of $\sqrt{\frac{S}{S+B}}$ where S refers to the number of signal events, and B is the number of background events. Lacking a detailed Monte Carlo study of the combinatorial background for most of the experimental options, we assumed a signal to noise ratio of 1:1 for all experiments considered here. This is a very optimistic assumption. Wrong sign tagging of the flavor of the B mesons can occur because of contamination in the lepton sample from the cascade process $B \to D \to \ell$, misidentification of hadrons, or $B \to \bar{B}$ oscillations in the accompanying B meson. The dilution factor due to mistagging is a strong function of the kinematic cuts applied to the lepton or the hadron used for the tag. In general an optimum setting for an experiment can be determined by maximizing the product $D^2 \times \epsilon$, where D is the total dilution factor and ϵ is the total efficiency [21]. Finally, for cases in which the CP asymmetry is determined using a time-integrated signal, the CP asymmetry is reduced by the factor $x^2/(1+x^2)$, where $x = \delta m/\Gamma$, assuming that the time integration is performed from $t = 0$.

4. COMPARISON OF VARIOUS APPROACHES

In order to compare the capability of different experiments to measure the CP asymmetry for the $B^0 \to \pi^+\pi^-$ decay, a figure of merit was calculated for each experiment we have considered. This figure of merit is defined as the number of nominal SSC years (10^7 seconds/year) required to measure the CP asymmetry with an accuracy of $\delta A_{CP} = 0.1$. The basic ingredients of these calculations are the estimates for the factors described in the previous Section and some quantities which are common to all experiments, including the branching ratio $B(B^0 \to \pi^+\pi^-)$, and the probability of producting a B^0 meson in the fragmentation of a b quark, f_{B^0}. Guided by theoretical arguments and existing measurements we have assumed $B(B^0 \to \pi^+\pi^-) = 1 \times 10^{-5}$ and $f_{B^0} = 0.375$. Results from Monte Carlo studies of the experiments are then used to determine the acceptance, trigger and tagging efficiency and the related dilution effects. Some results of the comparison of the fixed target and forward collider experiments at the SSC, and central collider experiments at Tevatron are summarized in the following Tables. We refer the reader to the subgroup reports for further details. We did not have time in this workshop to compare the central collider experiments at SSC.

Table 1. Central Collider Experiments

	CDF at Tevatron			D0 at Tevatron
$\sqrt{s}$	2 TEV			2 TEV
Luminosity	$10^{32}\ cm^2 s^{-1}$			$10^{32}\ cm^2 s^{-1}$
$\sigma(b\bar{b})$	50 μb			50 μb
$\sigma(total)$	50 mb			50 mb
	ℓ trigger ℓ tag	$\pi\pi$ trig. ℓ tag	$\pi\pi$ trig. soft $\pi\pi$ tag	ℓ trigger ℓ tag
Total efficiency	9.3×10^{-4}	6.9×10^{-4}	6.9×10^{-3}	2.34×10^{-3}
Total dilution	0.36	0.33	0.19	0.23
$N(B_d^0)$ for δA_{CP}=0.1	8.3×10^{10}	1.3×10^{11}	4.1×10^{10}	8.1×10^{10}
Time ($\times 10^7 s$)	2.3	3.5	1.1	2.2

It should be noted that although the results presented here for the combination of lepton trigger and lepton tag suggests a similar capability for the CDF and D0 experiments, the assumptions and the analysis leading to these results are quite different. For example, the CDF analysis uses a limited acceptance of $|\eta| < 1.1$ in order to achieve a mass resolution of better 20 MeV. The D0 analysis uses $|\eta| < 3$. However, the loss of efficiency in the CDF analysis is somewhat compensated for by their higher dilution factor which is claimed to correctly account for the effects of cuts on track impact parameter and vertex separation.

Table 2. Forward Collider Experiments

	BCD at SSC		COBEX at SSC	
$\sqrt{s}$	20 TeV		20 TeV	
Luminosity	$10^{32}\ cm^2 s^{-1}$		$10^{32}\ cm^2 s^{-1}$	
$\sigma(b\bar{b})$	1 mb		1 mb	
$\sigma(total)$	100 mb		100 mb	
	ℓ trig. ℓ tag	ℓ trig. Kaon tag	ℓ trig. muon tag	topology trig. kaon tag
Total efficiency	6.0×10^{-4} (μ & e)	4.0×10^{-4} (μ & e)	6.8×10^{-4}	5.3×10^{-3}
Total dilution	0.12	0.32	0.27	0.32
$N(B_d^0)$ for δA_{CP}=0.1	2.3×10^{12}	4.9×10^{11}	2.0×10^{11}	1.9×10^{11}
Time ($\times 10^7 s$)	1.5	0.33	0.27	0.025

Table 3. Fixed Target Experiments

	SFT at SSC	GAJET at LHC
$\sqrt{s}$	194 GeV	123 GeV
Interaction rate	1×10^7	7×10^7
$\sigma(b\bar{b})$	$2.0 \times (A = 28)\ \mu b$	1.0 μb
$\sigma(total)$	$32 \times (A = 28)^{0.71}\ mb$	32 mb
	ℓ and hadron trig. ℓ and hadron tag	ℓ and hadron trig. ℓ and hadron tag
Total efficiency	0.119	0.073
Total dilution	0.47	0.25
$N(B_d^0)$ for δA_{CP}=0.1	3.8×10^8	2.2×10^9
Time ($\times 10^7 s$)	0.03	0.11

5. CONCLUSIONS

As shown in Tables 1-3 both the fixed target and collider experiments at SSC claim that they could measure the CP asymmetry in the $B^0 \to \pi^+\pi^-$ decay with a precision of $\delta A_{CP} = 0.1$ in a fraction of a year. The time scale of the collider experiments at Tevatron is between 1 to 2 years. There are, however, significant uncertainties in these conclusions. To date none of the experiments has simulated in detail the background processes, including the minimum bias, $c\bar{c}$ and $b\bar{b}$ events. All estimates are based on an assumed signal to background ratio of 1/1. Without a detailed simulation of the background for each experimental setup it is difficult to obtain a reliable estimate of the efficiencies and dilution factors corresponding to this level of signal to background. One study of the $b\bar{b}$ background done for the BCD proposal claims that it is possible to achieve a signal to background ratio of 1/1. Understanding the background processes is certainly the most important issue for any further studies of the feasibility of measuring the angle α using the $B^0 \to \pi^+\pi^-$ mode. The background issue also points to the need for excellent mass resolution and particle identification in order to suppress overlapping signals from other low multiplicity B decays, such as $B \to K^-\pi^+$, $B_s \to K^-K^+$ and $B \to \rho^+\pi^-$. In addition it is also important to study other modes, such as $B \to a_1\pi$, which can be used to determine the the angle α.

6. ACKNOWLEDGEMENTS

We would like to thank the organizers for organizing this stimulating workshop that provided us an excellent opportunity for exploring the exciting frontier in B physics. This work is supported in part by the US Department of Energy, by the Alfred P. Sloan Foundation, by the Natural Sciences and Engineering Research Council of Canada, and by FCAR, Québec.

7. REFERENCES

1. N. Cabibbo, *Phys. Rev. Lett.* **10** (1963) 531; M. Kobayashi and T. Maskawa, *Prog. Theor. Phys.* **35** (1977) 252.

2. See also M. Gronau, these proceedings.
3. L. Wolfenstein, *Phys. Rev. Lett.* **51** (1983) 1945.
4. A. Carter and A.I. Sanda, *Phys. Rev. Lett.* **45** (1980) 952; *Phys. Rev.* **D23** (1981) 1567; I.I. Bigi and A.I. Sanda, *Nucl. Phys.* **B193** (1981) 85; **B281** (1987) 41.
5. I. Dunietz and J. Rosner, *Phys. Rev.* **D34** (1986) 1404.
6. P. Krawczyk, D. London, R.D. Peccei and H. Steger, *Nucl. Phys.* **B307** (1988) 19; A.B. Blinov, V.A. Khoze and N.G. Uraltsev, *Int. J. Mod. Phys.* **A4** (1989) 1933.
7. D. London and R.D. Peccei, *Phys. Lett.* **B223** 257 (1989); M. Gronau, *Phys. Rev. Lett.* **63** 1451 (1989); B. Grinstein, *Phys. Lett.* **B229** 280 (1989); M. Gronau, SLAC Report SLAC-PUB-5911 (1992).
8. R. Aleksan, I. Dunietz, B. Kayser and F. LeDiberder, *Nucl. Phys.* **B361** (1991) 141.
9. M. Gronau and D. London, *Phys. Rev. Lett.* **65** (1990) 3381.
10. We thank M. Gronau for pointing this out.
11. Y. Nir and H.R. Quinn *Phys. Rev. Lett.* **67** (1991) 541; H.J. Lipkin, Y. Nir, H.R. Quinn and A.E. Snyder, *Phys. Rev.* **D44** (1991) 1454.
12. M. Gronau, *Phys. Lett.* **B265** (1991) 389; L. Lavoura, *Mod. Phys. Lett.* **A7** (1992) 1553.
13. M. Gronau and D. London, *Phys. Lett.* **B253** (1991) 483.
14. R. Aleksan, I. Dunietz and B. Kayser, *Z. Phys.* **C54** (1992) 653.
15. B. Kayser, M. Kuroda, R.D. Peccei and A.I. Sanda, *Phys. Lett.* **B237** (1990) 508; I. Dunietz, H.R. Quinn, A. Snyder, W. Toki and H.J. Lipkin, *Phys. Rev.* **D43** (1991) 2193.
16. See L. Camilieri, these proceedings.
17. G. Punzi et al, Contributed paper to this session.
18. O. Long, et al, Contributed paper to this session.
19. Presented by F. Azfar at the workshop sessions.
20. M. Gronau, A. Nippe and J.L. Rosner, *Phys. Rev.* **D47** (1993) 1988.
21. K. McDonald, private communication. It was pointed out to us that such a study has been performed for the BCD proposal.

8. FOOTNOTE

Participants in the α working group:
F. Azfar, L. Camilleri, C. Dukes, P. Eerola, K. Gounder, M. Halling, J. Heinrich, W. Hoffmann, J. Izen, A. Jawahery, T. Lawry, J. Lewis, D. London, K.B. Luk, P. Karchin, C. Kennedy, S. Kwan, K. McDonald , A. McManus, C. S. Mishra, J. Mueller, G. Punzi, J. Spalding and P. Wilson

Fixed Target B Experiments and the Angle Alpha using $B^0 \to \pi\pi$ and $B^0 \to a_1\pi$

A.P. McManus, B. Cox, E.C. Dukes, T. Lawry
Physics Department, University of Virginia, McCormick Rd.
Charlottesville, Va 22901, USA

1. INTRODUCTION

Fixed target beauty (B) experiments proposed at the SSC or LHC come in two basic types. The first type is the extracted beam experiments using a bent crystal of silicon or some other method to extract a beam of protons parasitically from the circulating beam as the collider experiments are taking data. The two chief experiments proposing this method are the LHB[1] collaboration which would use the LHC at CERN and the SFT[2] collaboration which would use the SSC. The second type of fixed target experiment is one that would place the detector around the circulating beam using a gas jet or thin wire(s) as a target. Two experiments of this type are the one proposed at CERN for LHC (GAJET[3]) and the Hera-B[4] experiment proposed at DESY using the Hera collider.

2. GENERAL COMMENTS ON FIXED TARGET EXPERIMENTS

The basic difference affecting design between fixed target experiments and collider experiments is the large Lorenz boost that all decay products are given in fixed target experiments. Because of the large boost, all fixed target experiments are long (50-100 meters) and cover a small solid angle ($\theta \sim 100$ mrad) unlike the typical collider experiment which attempts to cover a 4π solid angle and on average has much lower momentum decay products. The basic layout of a fixed target B experiment[5] is a follows: the target (internal/external) is followed by a silicon microvertex detector, wire chambers, a dipole magnet (or perhaps two magnets), some more wire chambers and a calorimeter followed by a muon detector. There is also some kind of hadron ID system placed before or after the magnet(s).

The one main advantage that all fixed target experiments share is very good primary vertex resolution either because the target is small (internal target or external target) or because the vertex detector is very close to the target (external target). In addition, coupled with the good primary resolution offered by the fixed target experiments, the large Lorenz boost gives very long decay paths for B particles in the lab frame. The average B decay length is 16mm for an 800 GeV proton beam or 95mm for a 20 TeV proton beam. These two effects will favorably impact the reconstruction efficiency of fixed target experiments as will be seen later.

3. EXTRACTED BEAM EXPERIMENTS

Extracted beam experiments offer several advantages over internal target experiments. The chief advantages are the ability to bring the silicon microvertex detector as close as needed to the target and to cover an angular range down to zero mrad without having to Increase the length of the spectrometer beyond practical limits. This gives the extracted beam experiments the ability to get a complete view of the event, since all charged tracks can be seen by some part of the detector. This also means that extracted beam experiments have better vertex resolution and impact parameter resolution than achievable by any other type of experiment with similar detector technology. Another advantage of extracted beam experiments is the ability to use a live target (SFT experiment) and determine the charge of the B's from the presence or absence of a charged track leading into the secondary vertex. This would also allow the reconstruction of more complicated decay topologies and the use of partly reconstructed states to help in determining the particle or antiparticle state of the tagging B.

External target experiments allow much less expensive and easier to build detectors than either internal target or collider experiments and the radiation damage of the detectors can be tuned by "blowing up" the beam or scanning the beam across the surface area of the silicon strip detectors. Extracted beam experiment can exist either in a separate hall some distance away from the circulating beam or be placed in a hall designed for collider experiments. An advantage of a separate fixed target hall would be the ability to install and repair detectors without affecting collider experiments.

4. INTERNAL TARGET EXPERIMENTS

The internal target experiments propose to operate at very high beam intensities and use a very thin target of either gas (GAJET) or wire (HERA-B). Unfortunately because of the high intensity, internal target experiments will have multiple interactions per bucket. GAJET would expect 2 interactions per bucket and Hera-B 5 interactions per bucket as compared to 0.2 interactions per bucket for a extracted beam experiment. Also, like collider experiments, internal beam experiments must be designed around a beam pipe and can not bring the silicon vertex detector too close to the beam without suffering severe radiation damage.

5. PHYSICS CAPABILITIES AT SSC/LHC

5.1 *General Considerations*

The abilities of fixed target experiments to extract the angle alpha using the decay $B^0 \to \pi\pi$ will be discussed using one example from the extracted beam experiments (SFT) and one from the internal target experiments (GAJET). The LHB collaboration at CERN uses a spectrometer almost identical to the SFT spectrometer. Other than the lower $\sqrt{s}$ for a LHC fixed target experiment, the only difference between the LHB and SFT spectrometers is the use of an active target in SFT and a thin non-active target in LHB. The mode $B^0 \to a_1\pi$ will be briefly discussed for the SFT experiment.

Listed in Table 1 are the physics quantities that were assumed to make an estimation of the physics potential of the fixed target experiments. The branching ratio for $B^0 \to \pi\pi$ is assumed to be 10^{-5}. Both SFT and GAJET assume that they can use μ, e, and K as a tag for the other B in the event.

Table 1. Assumptions for physical quantities and experiment parameters.

	SFT ($B \to \pi\pi$ or $a_1\pi$)	GAJET ($B \to \pi\pi$)
$\sqrt{s}$	194 GeV	123 GeV
interaction rate	1×10^7	7×10^7
# of interactions/bunch	0.17	1.6
$b\bar{b}$ cross section	2.0 μb	1.0 μb
total cross section/nucleon	32 mb	32 mb
target material	silicon	hydrogen
Neutral B fraction	0.76	0.76
Number of $B^0/\overline{B}^0$ produced/y	1.3×10^{10}	2.0×10^{10}
Branching ratio	10^{-5} for $\pi\pi$ mode	10^{-5} for $\pi\pi$ mode
Branching ratio	0.75×10^{-5} for $a_1^+\pi^-$ mode	—
Branching ratio	3×10^{-5} for $a_1^-\pi^+$ mode	—
Physics final state	$B^0 \to \pi\pi$, $B^0 \to a_1\pi$	$B^0 \to \pi\pi$
Particle used as tag	μ,e,K	μ,e,K
Angular acceptance	2-75* mrad	5-87.5 mrad

* The silicon microstrip detector acceptance is 0-75 mrad.

5.2 *Reconstruction Efficiencies and Acceptance*

Listed in Table 2 are the efficiencies and acceptances for reconstructing the decays of $B^0 \to \pi\pi$ and $B^0 \to a_1\pi$ for SFT and GAJET.

The efficiency ε_{decays} which is the probability for the decay into the CP eigenstate, is 1.0 for the $B^0 \to \pi\pi$ decay since the decay is always into two charged pions and 0.5 from isospin for the decay of $B^0 \to a_1\pi$ into all charged pions.

The triggers used by SFT and GAJET are similar with both experiments expecting to use a single lepton (l) trigger with a P_t threshold of 1.5 GeV/c for SFT and 1.0 GeV/c for GAJET. Both experiments also plan to use a dihadron (2h) trigger with SFT using a P_t threshold of 3.0 GeV/c for the high P_t hadron and 1.0 GeV/c for the low P_t hadron. GAJET would use a single P_t threshold of 2.6 GeV/c for both hadrons. The trigger efficiency, ε_{trig}, is defined to be the probability of the trigger particle(s) being above threshold and the effect of a vertex trigger which is a first level optical trigger (62% efficient) in the case of GAJET and a second level secondary vertex trigger processor (81% efficient) in the case of SFT. Also for SFT, the efficiency of the trigger hardware (97% efficient) is taken into account. The Monte-Carlo studies for using the hadronic P_t trigger were not done for the $B^0 \to a_1\pi$ decay. The hadronic P_t trigger should be very useful for triggering on the $B^0 \to a_1\pi$ decay, but will not be quite as efficient as for the $B^0 \to \pi\pi$ decay.

The efficiency for reconstructing the CP eigenstate, ε_{CP}, includes the acceptance for all the secondary tracks to be in the tracking volume, the track reconstruction efficiency, the vertex reconstruction efficiency, and a secondary vertex cut that requires the secondary vertex to be 15 σ from the primary. For the SFT detector, all of the above numbers are based on a GEANT simulation with detector efficiency, noise, secondary interactions, delta rays and pattern recognition. The efficiency, ε_{CP}, also includes the acceptance of the tagging particle (μ, e, K). The GAJET efficiency, ε_{CP}, includes a "safety factor" of 80% to account for effects not present in the the simpler GAJET Monte-Carlo.

The tagging efficiency, ε_{tag}, includes the branching ratio for the other B in the event to provide a tagging particle. In the case of SFT, the efficiency to reconstruct the tag and identify it is also included.

The total efficiency, ε_{total}, is complicated for the $B^0 \to \pi\pi$ decay since there are two triggers and two tags that must be added up together and their overlaps accounted for[6]. The branching ratio for the kaonic and leptonic decays of the B are 21% and 85% respectively. If one assumes that 15% of the events have both tags, the total number of events with a tag are 91% rather than 100% for maximally uncorrelated tags. This means that only 30% of the lepton tags (6% of the total events) in 2 hadron triggered events were not also in the lepton trigger sample. For the effect of overlapping triggers, if one assumes that they are uncorrelated then the fraction (30%) of dihadron triggers overlapping with a lepton trigger must be subtracted from the dihadron trigger sample. The final efficiency for fully reconstructed $B^0 \to \pi\pi$ decays after taking both triggers and both tags into account is:

$$\varepsilon_{total} = [\varepsilon_{trig}(l) \times \varepsilon_{cp}(l,l) \times \varepsilon_{tag}(l)] + [\varepsilon_{trig}(2h) \bullet 0.70 \times \varepsilon_{cp}(K,2h) \times \varepsilon_{tag}(K)] + [\varepsilon_{trig}(2h) \times \varepsilon_{cp}(l,2h) \times \varepsilon_{tag}(l) \bullet 0.30] \quad (1)$$

where the symbol in brackets is the tag or trigger, lepton tag or trigger=l, kaon=K and 2 hadron trigger=$2h$. The efficiency for fully reconstructed $B^0 \to a_1\pi$ decays is just the product of the individual efficiencies. Only lepton tags were considered for the $B^0 \to a_1\pi$ decays, but in principle the dihadron trigger with K tagging should work almost as well for this decay as it does for the $B^0 \to \pi\pi$. Further study of the ε_{CP} for the $B^0 \to a_1\pi$ decay is clearly needed but the trigger efficiency for this decay with dihadron trigger has been calculated (Table 2).

Table 2. Reconstruction efficiency of the CP state

	SFT: $B \to \pi\pi$	SFT: $B \to a_1\pi$	GAJET: $B \to \pi\pi$
ε_{decay}	1.0	0.5	1.0
ε_{trig}: l $P_t$trigger	0.35	0.34	0.39
ε_{trig}: $2h$ P_t trigger	0.45	0.35	0.34
ε_{CP}:l tag,l trig	0.54	0.30	0.24
ε_{CP}:l tag,$2h$ trig	0.40	—	0.24
ε_{CP} K tag,$2h$ trig	0.37	—	0.24
ε_{tag}: l tag, l trigger	$0.85 \bullet BR = 0.18$	$0.85 \bullet BR = 0.18$	$BR = .21$
ε_{tag}: l tag, $2h$ P_t trigger	$0.85 \bullet BR = 0.18$	$0.85 \bullet BR = 0.18$	$BR = .21$
ε_{tag}: K tag, $2h$ P_t trigger	$0.77 \bullet BR = 0.65$	$0.77 \bullet BR = 0.65$	$BR = .85$
ε_{total}: all triggers	0.119	0.009	0.073

5.3 *Dilution Factors*

The dilution factors are listed in Table 3. The dilution factor, D_{mix}, is the time dependent mixing dilution including the dilution from the tag. The dilution factor, D_{tag}, is 1-2w where w is the probability of incorrectly tagging the "other" B either though faulty particle identification or assigning the tag to the wrong vertex, for example, $B \to D \to \mu, e$. For SFT with a 1.5 GeV P_t cut and an impact parameter cut on the lepton, the probability of a wrong tag from a lepton tag is 5%. The dilution factor, D_{bg}, is the dilution from background under the $\pi\pi$ or 4π peak. From a monte-carlo simulation, SFT has a mass resolution of less than 13 MeV. Experience from FNAL E771[7] data analysis shows that a signal to noise of at least 5:1 can be achieved for the J/ψ decay into two muons with a tight 5σ vertex cut and a 35 MeV mass resolution. For further information on backgrounds in SFT see the paper by T. Lawry in this section.

The total dilution is:

$$D_{total} = D_{mix} \bullet D_{bg} \bullet \overline{D_{tag}} \quad (2)$$

where $\overline{D_{tag}}$ is the weighted average of the dilution from the K and l tags. There are 3.4 times as many K tags as l tags in SFT and 3.5 times as many K tags as l tags in GAJET.

Table 3. Dilution factors

	D_{mix}	D_{tag} e tag	D_{tag} μ tag	D_{tag} K tag	D_{bg}	D_{total}
SFT	0.67	0.85	0.93	0.75	0.90	0.47
GAJET	0.70	0.50	0.50	0.50	0.70	0.25

6. CP MEASUREMENTS & CONCLUSIONS

The time needed for these experiments to reach an asymmetry error of 10% and the total asymmetry error for a one year run is listed in Table 4. The CP asymmetry measurement from the $B^0 \to a_1\pi$ decay is more complicated than the measurement from the $B^0 \to \pi\pi$ decay and only the total number detected for each state in listed in Table 4. Clearly the fixed target option to measure the angle alpha is very attractive with measurements of the angle alpha to less than 10% in well under a year with either option, and in particular the external fixed target option (SFT) would yield a measurement of alpha of 2% in one year of operation.

An important point that impacts the physics goals of all SSC B physics experiments is the survivability of silicon microstrip detectors. Experience on FNAL E771[8] has shown, that the maximum radiation dose that the current generation silicon strip detectors can survive is about 2 Mrad. This would imply that GAJET would need to replace their silicon detector 3-4 times in the course of a 1 year run, since they expect a radiation dose of 7.5 Mrad in 1 year. The SFT experiment would expect to experience about 4 Mrad with a 5cm beam or 2 Mrad with a 7cm beam in a 1 year run and might expect to replace detectors at the rate on no more than once per year. As a worst case, COBEX[9] would have a dose of 30 Mrad in 1 year and would have to replace detectors more often than once per month.

Table 4. CP asymmetry measurements

	SFT:$B \to \pi\pi$	SFT:$B \to a_1\pi$ $a_1^+\pi^-$, $a_1^-\pi^+$	GAJET
Number produced in 1 year	15500	900,3600*	14600
Time for $0.1\delta A$	0.03 Years	—	0.11 Years
δA in 1 year	0.020	—	0.038

* Only events with lepton tags considered.

7. REFERENCES

1. G. Carboni *et al*, LHB Collaboration, INFN PI/AE91/04, (1991).
2. B. Cox *et al*, EOI-14, SSC Laboratory (1990).
3. Y. Lemoigne, GAJET Collaboration, Nucl. Instr. Meth. **A333** (1993).
4. W. Schmidt-Parzefall *et al*, An Experiment to Study CP Violation Using an Internal Target at the HERA Proton Ring, Letter of intent, DESY-PRC 92/04 (1992)
5. B. Cox *et al*, The SFT a Super Fixed Target Beauty Facility at the SSC, Workshop on B physics, snowmass, July 1993.
6. B. Cox, Fixed Target Beauty Experiments at SSC and LHC, Workshop on Heavy Quarks, Frascati, May 1993.
7. B. Cox *et al*, P-867 proposal, FNAL Laboratory (1992).
8. A. Boden *et al*, "Characteristics of Radiation Damage Seen in the Silicon Microstrip Detector of Fermilab Experiment E771", Accepted to be published in NIM.
9. S. Erhan *et al*, Nucl. Instr. Meth. **A333** 101-112, (1993).

Report of the α subgroup on Forward Collider Experiments*

S. Kwan
Fermilab, Batavia, Illinois 60510

K.B. Luk
Lawrence Berkeley Laboratory, Berkeley, California 94720

1. Introduction

The subgroup studied the potential of forward collider experiments for measuring the angle α using the $B^0 \rightarrow \pi^+\pi^-$ decay. In particular, we tried to answer the questions of what sensitivites the two different proposals (COBEX[1] and forward BCD[2]) could probe CP violation in the above decay mode in units of 10^7 seconds. A detailed comparison of the capabilities of the experiments would require extensive Monte Carlo estimates of the total number of reconstructed and tagged exclusive B meson decays as well as realistic estimates of the background. Both experiments have performed most of these calculations and their numbers have been used as the basis of discussion. Given the short time available in the workshop, we took the approach of examining the numbers presented by the proponents of the two experiments at the workshop and estimated what would be achievable.

2. Overview of the Forward Collider Experiments

Details of the experimental setup, trigger strategy and tracking/vertexing capability of both BCD and COBEX are covered in this workshop in relevant sessions. Here we will just summarize some of the essential features that are important for our discussion.

The COBEX detector covers pseudorapidity from 1 to 6 with a spectrometer based on a quadrupole and a dipole magnet. Its vertex detector, which consists of uniformly spaced disks, is in a field free region inside the beampipe at an inner radius of 2 mm. The disks are placed inside the accelerator vacuum system in 'Roman Pots'. The massive support structure prevents the expansion of the spectrometer into the central region. A more serious penalty of placing the vertex detector so close to the beam is the radiation dosage. It has been estimated that at a luminosity of 10^{32} cm^{-2}s^{-1} and at a radius of

*The members of the subgroup on forward collider geometry for measuring α included: K. Gounder, J. Izen, C. James, C. Kennedy, S. Kwan, K.B. Luk and D. Wagoner.

5mm from the beam, the radiation dosage is 10.8 Mrad per year. Either COBEX has to run at a much lower luminosity or the vertex detector has to be replaced every couple of months. For triggering, COBEX plans to use a high p_t muon trigger, with a p_t threshold set between 1 and 1.5 GeV/c, as well as a topology trigger which selects events not compatible with a single production vertex. But the latter trigger is only effective up to a luminosity of 10^{31} $cm^{-2}s^{-1}$.

The BCD detector strives to cover a broad pseudorapidity range from -6 to +6. Early stages of the detector plan to use a dipole magnet and a spectrometer in the forward region to cover the rapidity interval from 1.5 to 5.5 without compromisng the possibility of later expansion into the central region. The BCD vertex detector has rapidity space disks in the forward region and is outside the beampipe at an inner radius of 1 cm. Radiation dosage is expected to be about 1.7 Mrad per a year of running. For triggering, BCD plans to use a high p_t lepton (muon or electron) trigger but they also plan to do a vertex trigger with a large processor farm.

The conclusion from the tracking/vertex group in this workshop is that there is little difference between COBEX and forward BCD in terms of efficiency and vertex resolution. Furthermore, they also conclude that from the tracking perspective, there is no compelling evidence that a forward collider experiment is better than a dedicated central collider experiment. However, it is also clear that for a decay mode like $B^0 \to \pi^+\pi^-$, good mass resolution and particle identification are important. Both COBEX and forward BCD claim to have a mass resolution of about 20 MeV for this mode.

3. Comparison of COBEX and forward BCD

Table 1 summarizes the CP reach in $B \to \pi^+\pi^-$ decay mode for COBEX[3] and forward BCD[4] at the SSC. Most of the numbers are produced by the proponents of the experiments. The assumptions used in the generation of these numbers have to be checked carefully and systematically. The feasibility of running the experiments at such a high luminosity and at the proposed trigger rate has not been considered thoroughly. Nor are the effects of losses due to having more than one interaction per bunch crossing included.

COBEX have evaluated the muon trigger using a Pythia-based Monte Carlo simulation for minimum biased events and for $B^0 \to \pi^+ \pi^-$. Using a three level trigger system, and with a $p_t > 1.2$ GeV, they estimated that the total rejection factor would be about 1300. The efficiency for $B \to \pi^+ \pi^-$ in which both decay π's are accepted is about 3%, including the inclusive branching ratio of $B \to \mu X$. In table 1, the geometrical acceptance, tracking and vertexing efficiency are combined to give the number ε_{CP}. We show the physics potential of COBEX for the two triggers that they proposed. An advantage of the topology trigger is that it does not bias the tag particle. To suppress the combinatorial background, various cuts have been studied by both COBEX and BCD. BCD assummed that with their analysis cuts, a S/B of 1 could be obtained. The study by COBEX, on the other hand, showed that while a S/B of greater than 20 is achievable, S/B of 1 has not yet been demonstrated. In the table, a value of S/B of 1 was assummed.

Since the final state is a CP eigenstate, tagging information has to be obtained from the accompanying B meson. Both COBEX and BCD plan to use lepton(only muon in COBEX, and both electron and muon in BCD) and K tag. The soft pion tag discussed in this workshop has not been studied at all. There are several sources of wrong tags, such as the oscillation of the accompanying B before decay, or from tags which do not come from the b->c transitions. These wrong tags dilute the measured asymmetry. Two dilution factors are given: d_{tag} is the dilution due to mistagging and d_{mix} is due to oscillation. For B_d, using $X_d=0.7$, d_{mix} is equal to $X/(1+X^2)$ which is 0.47 using $X_d=0.7$. COBEX claim that when one fits the time dependence of the oscillation, one can get a better d_{mix}. BCD, on the other hand, claim that even with perfect time resolution, d_{mix} can only be as high as 0.58.

To estimate background, both COBEX and BCD have done extensive Monte Carlo studies. COBEX have estimated that in the time required to trigger on 100 accepted $B \to \pi^+\pi^-$ events, there will be 5×10^{10} minimum bias interactions in their apparatus. Assuming 10% reconstruction efficiency, one has to suppress the combinatorial background from minimum bias events by more than 5×10^9. Their studies show that a minimum overall suppression of 10^9 from the minimum bias background is achievable with loose analysis cuts combining with trigger efficiency and tight mass cut on the $\pi\pi$ invariant mass. Their conclusion is that the signal to background ratio greater than 1/20 is achievable. BCD have done a similar study from a different perspective[5]. They have generated a million beauty events and the B^0 in these events are forced to decay into the $\pi^+\pi^-$ channel. Backgrounds were studied with b, c and light-quark events by trying various cuts. Their conclusions are that the principle source of background comes from bb events and not from charm or light quark events. After all cuts, they found an efficiency of 4% for finding $B_d \to \pi^+\pi^-$ with a signal to noise ratio of >0.42, at the 90% confidence level. Both experiments agree that in the $\pi^+\pi^-$ invariant mass distribution, there would be significant contamination under the mass peak from reflections of the decays: $B_d \to K^+\pi^-$, $B_s \to K^+K^-$, $B_s \to K^+\pi^-$. Therefore, good K/π separation would be necessary. Both experiments plan to use a fast RICH for particle identification. Aside from the formidable technical challenge of constructing and operating a fast RICH, there may not be a realistic estimate on the particle identification efficiency and contamination for the analysis cuts used for $B_d \to \pi^+\pi^-$ and tagging in the table.

4. Discussion

As one can see from the table, both forward BCD and COBEX claim that they can measure α in a year of running at the SSC. However, the COBEX numbers seem to imply that it is a better experiment. Their total efficiency is higher, particularly so in the topology trigger although it is highly doubtful if this trigger is practical in a luminosity of 10^{32} cm^{-2}s^{-1}. A small fraction of their higher ε_{CP} could be attributed to the fact that they cover one more unit of pseudorapidity but it seems that the crucial difference between the two experiments is the number used for the tracking and vertexing efficiencies. Naively, one would expect the vertex and impact parameter resolutions are better for COBEX. However, a remarkable conclusion of the forward tracking group at this workshop is that both experiments are about the same in terms of vertex resolution and tracking efficiency; in this case, it is hard to justify the advantages of placing the vertex detectors inside the beampipe. What might be causing the difference in the numbers could be the looser cuts used by COBEX which give them a higher efficiency as well as a higher background. Instead of asumming S/B to be 1, if we used 0.05 which is what COBEX have demonstrated to be achievable, the figure of merit for COBEX would be increased by about 10, bringing the CP reach of the two experiments about the same to within a factor of two.

5. References

[1] S. Erhan et al. NIM A333 (1993) 101.

[2] BCD Collaboration, Expression of Interest for a Bottom Collider Detector at the SSC (EO10008), May 1990 & Proposal for a B-Physics Experiment at TEV I: The μBCD (P827).

[3] S. Erhan , NIM A333 (1993) 213.

[4] K.T. McDonald, these proceedings.

[5] O.R. Long et al. , SSCL/PP/139 and Princeton/HEP/92-07.

Table 1: Comparison of the yield estimates of forward BCD and COBEX at the SSC for measurment the CP asymmetry: angle α using $B^0 \to \pi^+\pi^-$.

Experiment	Forward BCD at SSC		COBEX at SSC	
TRIGGER TAG	Lepton trig. Lepton tag	Lepton trig. Kaon tag	Lepton trig. muon tag	Topology trig. Kaon tag
ε_{dec}	1.0	1.0	1.0	1.0
ε_{trig}	0.058	0.058	0.03	0.18
ε_{CP}	0.015	0.015	0.03	0.11
ε_{tag}	0.34	0.23	0.76	0.27
d_{mix}	0.58	0.58	0.75	0.75
d_{tag}	0.30	0.79	0.50	0.60
d_{bg}	0.70	0.70	0.70	0.70
Total Efficiency	3.0×10^{-4}	2.0×10^{-4}	6.8×10^{-4}	5.3×10^{-3}
Total dilution	0.12	0.32	0.27	0.32
Fig. of merit	2.3×10^5	4.9×10^4	2.0×10^4	1.9×10^3
N_{prod} for δA_{CP} =0.1	2.3×10^{12}	4.9×10^{11}	2.0×10^{11}	1.9×10^{11}
Time (10^7s)	3 (μ) 1.5 (e,μ)	0.65 (μ) 0.33(e,μ)	0.27	0.025

Central Collider Experiments: A Feasibility Study of Measuring the Angle α with CDF

J. D. Lewis
Fermi National Accelerator Laboratory, Batavia, Illinois 60510

J. Mueller
Rutgers University, Piscataway, New Jersey 08854

J. Spalding
Fermi National Accelerator Laboratory, Batavia, Illinois 60510

and

P. Wilson
University of Chicago, Chicago, Illinois 60637

1. Introduction

The "central region" in hadron collider experiments is generally defined as the region $\eta < 1$ or 1.5, although "central experiments" certainly have some coverage well beyond this region. CDF and D0 at FNAL are principally "high-p_T" experiments, with an emphasis on this central region. Nevertheless they are capable of significant b physics and are upgrading their capabilities over an extended η region. The high-p_T experiments proposed for LHC and SSC again stress the central region. In this section we discuss the capabilities of the CDF detector at FNAL.

In the central region, it is natural to use a solenoidal magnetic field with p_T as the relevant parameter for charged particle tracking. CDF has such a field. Solenoids are not ideal for tracking in the far forward direction (beyond $|\eta|$ of 2.5 or so), and the proposed forward experiments have dipole or quadrupole fields. The BCD proposals cover both central and forward region with a single dipole field.

The principal issues for studying the angle α via the $\pi^+\pi^-$ decay mode are:

Triggering: Present triggers are based on the semileptonic decay of the partner B. Using tracking and vertex information, triggers based on the $\pi^+\pi^-$ decay itself are being developed by CDF.

Background Rejection: The combinatoric background is expected to be very high in this mode, so isolation of the $\pi^+\pi^-$ decay vertex is essential. Even so, B_d and B_s decays into $K\pi$ and KK will contaminate the signal. Good mass resolution is essential to reduce this contamination in particular, and the background in general, and K-π separation in particle identification is important. The CDF upgrades have no specific plans for particle identification, although CDF has implemented the use of dE/dx in the central tracking system and is studying the feasibility of adding a time-of-flight system.

Tagging: Because the correlation in rapidity between the decaying B and its partner is loose, tagging via the semileptonic decay of the partner B requires charge identification, a p_T cut, and perhaps an impact parameter cut over a wide range of rapidity. Including the semileptonic branching ratio, the tagging efficiency is relatively low, a few percent. Similarly tagging using the kaon resulting from the decay of the partner B requires kaon identification over a large rapidity range. CDF has no plans for hadron identification over a wide rapidity range at this time. An alternative method for tagging, using the charge of a pion associated with the signal B, may prove to be very important! We will refer to this method as $B\pi$ tagging. Such a correlation may result from the decay of excited B meson states (B^{**}) or from the non-resonant fragmentation of b quarks. If such a correlation is found, the efficiency may well be much higher than in lepton tagging. For either of these tagging methods the efficiency and dilution can be measured for decays into self-tagging modes. CDF will be able to make these measurements in the next year or so.

2. The CDF Detector for Run II and Beyond

The CDF detector[2] is a solenoidal detector designed originally for probing high-mass phenomena. However, it has a number of advantages for b physics. The current configuration includes charged particle tracking accomplished with an 84-layer drift chamber with momentum resolution $\delta p_T/p_T{}^2 < 0.002$ GeV^{-1} for $|\eta| < 1.2$ and a four-layer silicon strip detector with impact parameter resolution $\delta d < 10$ μm for $p_T > 1$ GeV. A trigger processor finds tracks with $p_T > 2$ GeV with resolution $\delta p_T/p_T{}^2 < 0.04$ GeV^{-1}. The lead and scintillator central electromagnetic calorimeter covers the region $|\eta| < 1$. It is segmented into towers that cover 15° in azimuth and 0.1 in pseudorapidity. The resolution is $\delta E_T/E_T = 13.5\%/\sqrt{E_T}$ (E_T in GeV). Wire chambers at shower maximum are also used in electron identification. Electron triggers are formed from a electromagnetic energy cluster matched to a charged track. Muon chambers in the range $|\eta| < 1$ lie behind 4-8 hadronic interaction lengths of material. At the trigger level, the p_T of track stubs in the muon chambers is determined from the drift-time difference of hits on radially aligned wires. Muon candidates are formed from matching tracks to muon chamber stubs. Triggers currently used for b physics include dileptons with $p_T(\mu) > 3$ GeV and/or $p_T(e) > 5$ GeV and single leptons with $p_T > 9$ GeV and with $p_T > 6$ GeV at a reduced rate. Gas calorimeters covering $1 < |\eta| < 3.5$ and torroidal muon spectrometers $2 < |\eta| < 3.5$ do not provide trigger signals efficient for b physics.

For collider Run II, the CDF data aquisition and trigger systems are being replaced to accommodate the planned 400 ns (and ultimately 132 ns) bunch spacing of the Tevatron. The silicon vertex detector will be replaced with a new detector (SVX II) with a length of 1 m along the beam axis, twice the extent of the current SVX. SVX II will have 4 layers of double-sided detectors with r-ϕ resolution of 10 μm and r-z resolution of 25 μm. The readout electronics will incorporate a trigger processor to determine the impact parameters of charged tracks of $p_T > 2$ GeV with 40 μm resolution. Single-lepton triggers with lower thresholds and multi-track triggers will become feasible when track impact-parameter information is included. Other improvements for Run II include replacing the gas calorimeter systems with an upgraded plug calorimeter incorporating scintillator tiles with optical fiber light guides, filling azimuthal gaps in muon coverage in $0.6 < |\eta| < 1.0$, and moving the forward muon torroids closer to the central detector to cover $1.5 < |\eta| < 3$.

We envision that a future CDF upgrade optimized for b physics would include silicon disks for tracking coverage over $|\eta| < 3$. Further, new trigger electronics would take advantage of this increased tracking range to provide single-lepton triggers over the full instrumented range; however, resolution for the $B \to \pi^+\pi^-$ still degrades beyond about $|\eta| > 1.0$. New muon chambers would cover the region between the central and forward detectors, and hadron identification using either time-of-flight or RICH technology would be added inside the solenoid without compromising momentum resolution.

3. CDF Capabilities for $\pi^+\pi^-$

To estimate CDF's capabilities for studying the $B \to \pi^+\pi^-$ mode, we consider two triggering approaches (lepton and $\pi^+\pi^-$) and two tagging methods (lepton and $B\pi$). For lepton triggering and tagging, the efficiency and trigger rate estimates are taken from the studies of P. Sphicas[3] and G. Punzi[4] In Run II, CDF will have single electron and muon triggers with p_T thresholds of 3 GeV and rapidity range $|\eta| < 1.2$ (1.0) for electrons (muons). We assume that a 100 μm impact parameter cut will be applied to these single lepton triggers[4] in order to reduce the trigger backgrounds and rates. The trigger efficiency is 0.5% (0.32%), and the trigger rate is 0.2 μb (0.45 μb). It is expected that further upgrades beyond Run II, with a new forward muon system and improved tracking in the forward region will provide lepton identification to $|\eta| < 3$. The lepton trigger efficiency then increases to 1.5% (1.5%) and the trigger rate increases to 0.5 μb (1.5 μb). The $\pi^+\pi^-$ trigger requires two opposite-sign charged tracks with $p_T > 2.0$ GeV that each have an impact parameter greater than 100μm. The efficiency and rate for the $\pi^+\pi^-$ trigger in the region $|\eta| < 1.0$ are determined by G. Punzi[4] to be 4.4% and 3.0μb.

The $\pi^+\pi^-$ reconstruction efficiency is quite different for the two classes of trigger, since a 100 μm impact parameter cut and a $p_T > 2.0$ GeV cut are already applied to each pion in the $\pi^+\pi^-$ trigger. For the lepton triggers the pion p_T cut is relaxed to 1.0 GeV. The reconstruction efficiency is estimated from a simulation of the vertex detector and tracking system within $|\eta| < 1.0$. The error on the vertex separation is expected to be about 25 μm in the r-ϕ plane and 65 μm in r-z. The mass resolution is determined to be better than 20 MeV rms if both tracks have $|\eta| < 1.1$ and $p_T < 10$ GeV. No estimate of the background level has been made at this time. In the spirit of the working group we apply a 15σ vertex-separation cut and assume a signal-to-background ratio $S/B = 1$ implying a dilution factor $d_{\rm back} = 0.7$. Figure 1 shows the mass distribution of $B_d \to \pi^+\pi^-$, $B_d \to K\pi$, $B_s \to K\pi$ and $B_s \to KK$ where kaons have been assigned the pion mass in the reconstruction of the B's and the cuts outlined above have been applied. Figure 2 shows the efficiency of the trigger and reconstruction cuts as a function of the proper lifetime of the B, as determined in Monte Carlo simulations. The result is a reconstruction efficiency of 3.1% for the lepton triggers and 25.6% for the $\pi^+\pi^-$ trigger, including the $p_T < 10$ GeV cut. Upgrades beyond Run II will not increase the η coverage of the reconstruction or the $\pi^+\pi^-$ trigger since the mass resolution is degraded significantly beyond $|\eta| = 1$ by multiple scattering.

The tagging efficiency is also dependent on the tagging and triggering methods. For the lepton trigger, the requirements for the tag are taken to be the same as those for the trigger, including the impact parameter cut, and the dilution is estimated to be 0.61. For lepton tagging with the $\pi^+\pi^-$ trigger, cuts similar to those used with the lepton trigger are applied with two exceptions: the p_T threshold for tagging muons is 2 GeV rather than the 3 GeV threshold applied in the trigger, and the impact parameter cut is not applied to electron tags. For electrons there is an additional factor 0.7 for fiducial and reconstruction cuts. The tag efficiency is 1.5% (0.6%) for the Run II configuration and increases to 4% (2%) with increased η coverage of upgrades beyond Run II. The false-tag fraction for the lepton tags is estimated to be 8% for a 3 GeV threshold and 11% for 2 GeV which in combination with a factor 0.73 for mixing of the partner B yields a dilution factor $d_{\rm tag}$ of 0.62.

The effectiveness of the $B\pi$ tag is completely unknown at this time. CDF will be able to measure both the efficiency and dilution for this method in the next year. We use here some values only as an illustration of how valuable such a tagging method could be. The numbers are not unreasonable, but they are not substantiated. We assume that 60% of reconstructed $B \to \pi^+\pi^-$ decays have a charged pion within some Δm, Δp_T and cone selection, of which 2/3 are the right sign and 1/3 the wrong sign, yielding a dilution factor d_{tag} of 0.33.

The dilution effect due to mixing of the signal B before decaying to $\pi^+\pi^-$ depends strongly on the method of analysis (time dependent or independent) and on the vertex separation cuts. The standard numbers quoted for $d_{\rm mix}$ are 0.47 and 0.58 for time-integrated and time-dependent asymmetry measurements. These, however, assume an efficiency that is constant with respect to decay time. When applying impact parameter or vertex separation cuts, one must calculate their effect on the dilution factors as well as the efficiency. For a time-integrated measurement, $d_{\rm mix}$ is the average dilution, weighted by the number of produced events $N(t)$ and the efficiency $\epsilon(t)$:

$$d_{\rm mix} = \frac{\int N(t)\,\epsilon(t)\,d(t)\,dt}{\int N(t)\,\epsilon(t)\,dt} \tag{1}$$

where $d(t) = \sin(x_d t)$, and t is the proper decay time in units of the lifetime. It is possible to make an unfortunate choice of decay cuts, such that the $d_{\rm mix}$ will average to zero. For a time-dependent measurement, one can think of binning the data in proper time and taking a weighted average of all the measurements of α. The weight is proportional to $1/N_i\epsilon_i d_i^2$:

$$N\epsilon d_{\rm mix}^2 = \sum N_i\epsilon_i d_i^2, \tag{2}$$

$$d_{\rm mix}^2 = \sum N_i\epsilon_i d_i^2 / \sum N_i\epsilon_i. \tag{3}$$

The case where one requires a minimum proper decay time has been derived elsewhere with a slightly different technique and taking into account resolution in the decay time.[5] For B_d mixing the resolution is much smaller than the oscillation period and can safely be ignored. As an example, if one removed all events with proper time less than 1.5 lifetimes, $d_{\rm mix}$ would rise from 0.58 to 0.89, with a 78% loss in efficiency, but $\epsilon d_{\rm mix}^2$ would fall only from 0.34 to 0.18. Making cuts in the trigger or in the reconstruction can sculpt the efficiency as a function of decay time, and it is necessary to evaluate the effect of such cuts on $d_{\rm mix}$ as well as the efficiency. Using the results shown in Figure 2 and the above expressions, we calculate the time-integrated $d_{\rm mix} = 0.73$ and the time-dependent $d_{\rm mix} = 0.82$.

Table 1 lists the net efficiencies and dilution factors for each of the trigger, tag and detector combinations. The last column of the table gives estimates of the number of years required to measure the CP assymetry with an error $\delta A_{CP} = 0.1$ assuming a luminosity of 1×10^{32} cm^{-2}s^{-1} at Fermilab with the Main Injector. It takes at least 2.3 years with lepton tagging if lepton coverage reaches out to $\eta = 3$ but only 1 year if $B\pi$ tagging were to work as well as in the example used here. However, it should be stressed that the reliability of these estimates and any comparison with other experiments depends on understanding the relationship between the $\pi^+\pi^-$ cuts and the background. It is possible that S/B of 1 can be achieved with less than 15σ separation between the primary and decay vertices, resulting in a significantly higher efficiency. A full Monte Carlo simulation is required to estimate the background, including effects of pattern recognition. Since the branching ratio for $B \to \pi^+\pi^-$ is 10^{-5}, very large Monte Carlo samples are needed to determine sources of background due to tracking errors.

Table 1: Efficiencies and dilutions for CDF.

	ϵ	d	$1/\epsilon d^2$	Time (10^7 sec)
CDF Run II				
Lepton Trigger, Lepton Tag (e and μ)	2.5×10^{-4}	3.6×10^{-1}	3.2×10^4	8.5
$\pi^+\pi^-$ Trigger, Lepton Tag	2.4×10^{-4}	3.3×10^{-1}	3.8×10^4	10
$\pi^+\pi^-$ Trigger, $B\pi$ Tag	6.3×10^{-3}	1.9×10^{-1}	4.1×10^3	1.1
CDF Upgrade beyond Run II				
Lepton Trigger, Lepton Tag (e and μ)	9.3×10^{-4}	3.6×10^{-1}	8.5×10^3	2.3
$\pi^+\pi^-$ Trigger, Lepton Tag	6.9×10^{-4}	3.3×10^{-1}	1.3×10^4	3.5
$\pi^+\pi^-$ Trigger, $B\pi$ Tag	6.9×10^{-3}	1.9×10^{-1}	4.1×10^3	1.1

4. Comments and Conclusions

Use of the $\pi^+\pi^-$ trigger allows a lower threshold to be applied for lepton tagging than can be allowed for leptons at the trigger level because of trigger rate considerations. However, in the estimates here, this is partly compensated by a somewhat worse dilution factor for lepton tagging at lower p_T. The lepton trigger has the advantage of pushing the pion p_T threshold down to 1 GeV. For tagging that does not require leptonic decays, for example the $B\pi$ tagging assumptions used here, the $\pi^+\pi^-$ trigger gains significantly over the lepton triggers. The numbers are striking if the $B\pi$ tagging works this well.

5. REFERENCES

1. M. Gronau, A. Nippe and J. Rosner, *Phys. Rev.*, **D47**, 1988 (1993).
2. F. Abe, *et al.*, *Nucl. Instrum. and Meth.*, **A271**, 387 (1988).
3. P. Sphicas and R. Mattingly, "$B\overline{B}$ Correlations," CDF Memorandum CDF/2034 (1993).
4. G. Punzi and L. Ristori, "SVT: The Silicon Vertex Tracker," CDF Memorandum CDF/1872 (1992).
5. K.T. McDonald, "Maximum-Likelihood Analysis of CP-Violating Asymmetries," Preprint PRINCETON/HEP/92-04.

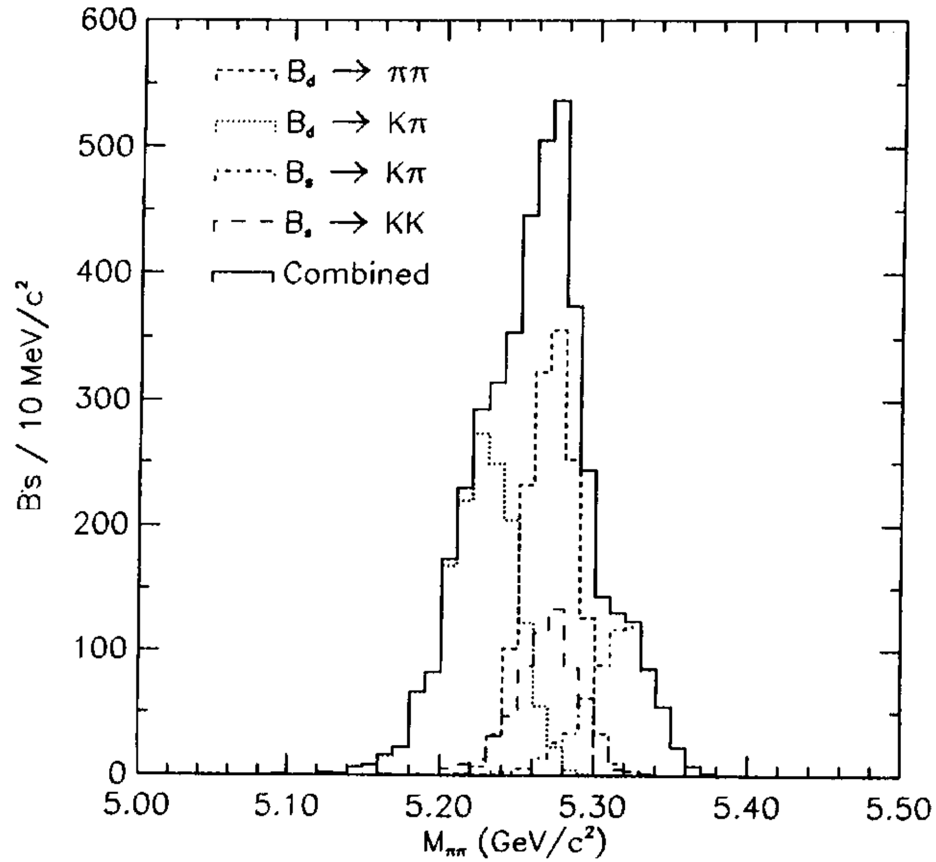

Figure 1: Mass distribution for the combination of $B_d \to \pi^+\pi^-$, $B_d \to K\pi$, $B_s \to K\pi$, and $B_s \to KK$ assuming all K's to be π's. The solid histogram is the combination and the dashed histograms show the 4 separate components.

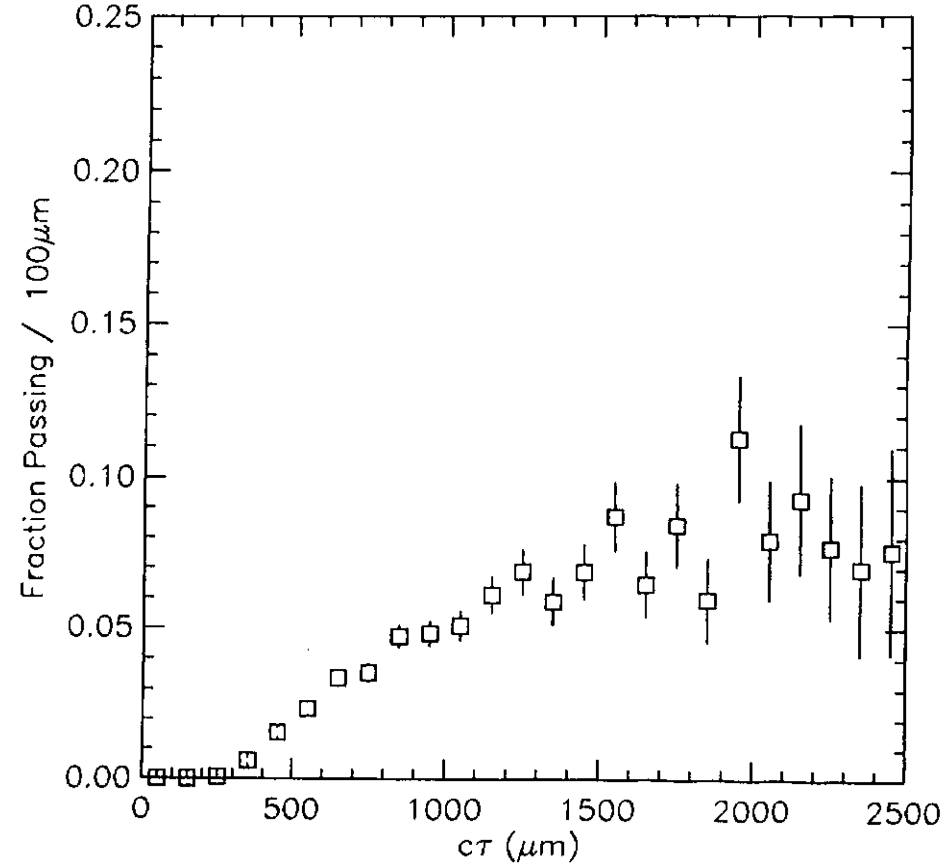

Figure 2: Trigger and offline efficiency as a function of proper lifetime.

D0 Upgrade: Feasibility Study of Measuring Alpha By $B^o \rightarrow \pi^+\pi^-$

C. S. Mishra and R. Lipton
For D0 Collaboration,
Fermi National Accelerator Laboratory*,
Batavia, Illinois 60510

ABSTRACT

The upgrade plans of the Fermilab collider detectors opens the possibility of measuring CP violation in B decays. In this paper we discuss the planned D0 upgrade and present simulation results to explore the feasibility of measuring angle of the CKM matrix using $B^o \rightarrow \pi^+\pi^-$ decays.

I. INTRODUCTION

The D0 Collider detector at Fermilab has finished its successful first run and is preparing for its second run. The current D0 detector's emphasis is on high pt physics. A major upgrade of the D0 detector is planned which will improve its capability in many aspects of the collider physics including B Physics. This planned upgrade is also compatible with the improvements in the Tevatron luminosity. The Tevatron luminosity will increase from its current luminosity of 5×10^{30} to $10^{32} cm^{-2} s^{-1}$ after the Main Injector is operational, at the same time the bunch crossing time will reduce from $3.5 \mu s$ to 132ns. In this paper we only discuss the experimental issue, a theoretical overview of measuring angle alpha by $B^o \rightarrow \pi^+\pi^-$ decays is discussed elsewhere[1]. The major components of the upgrade include a solenoidal magnet, replacement of the central tracking detectors by silicon micro strip detector surrounded by a scintillating fiber tracker inside the solenoidal magnet. Surrounding the superconducting coil will be a preshower detector, which will aid in electron identification. Upgrades to the calorimeter electronics, the muon system, the triggers and the DAQ are also planned to meet the requirements of the high luminosity and shorter bunch crossing interval.

*Operated by the Universities Research Association under contract with the U.S. Department of Energy

II. THE D0 UPGRADE

A significant part of the D0 upgrade will be in place for the RUN II (1996) of the Tevatron just before the Main Injector. The full upgrade is anticipated to complete for the first run of the Tevatron with the Main Injector Run III(1999). In this section, we will briefly describe the planned D0 upgrade, the details are described elsewhere[2].

Full replacement of the current D0 Tracking system is the major part of the D0 upgrade. A schematic view of the tracking system is given in Fig. 1. This system is designed to operate at luminosity of $10^{32} cm^{-2} s^{-1}$ with 132 ns bunch crossing time. The momentum resolution of this detector is $dpt/pt = 0.0008pt + 0.015$ for the central part and about $0.0025pt + 0.03$ in the forward region. This tracker will also determine the sign of the charge of particles and will have sufficient vertex resolution to identify B decays near jets to reconstruct exclusive B decays. The tracker will enhance the identification of electrons in calorimeter through energy and momentum comparisons, and by extrapolating candidate tracks into the preshower detector.

The silicon tracker system as shown at the center of Fig 1. consists of three layers of silicon barrel and 28 silicon disks. The detector is designed to provide good coverage up to $|\eta| \leq 3$, while covering a large interaction region of $\sigma = 25$ cm. All the silicon detectors used will have $50\mu m$ pitch. The silicon barrel detectors are made of single sided silicon wafers. The inner barrel (radius =2.7 cm) is 48 cm long, whereas the outer two barrels (at radius =11.9 cm and 14.9 cm) are 96 cm long. The double sided silicon disks (called F type) are placed in between the first and second barrel layer. The F type Si disk, consists of twelve double sided wedge detectors with strips running parallel to one of the radially extending edge on one side, and parallel to the other edge on other side providing 30° stereo angle. In the forward region, to provide better tracking there are large Si-disks (called H-type). H type disks covers the radial region from 9.5 cm to 26 cm with single sided silicon detectors. The silicon detectors will be readout with a 128 channel AC-coupled SVX-II chip with onboard digitization. Each chip contains shaping, an analog delay pipeline and 7 bit A/D circuitry with subsequent multiplexing.

The scintillating fiber tracking system consists of four concentric fiber (765 μm diameter) detectors in the space between silicon tracker and the solenoid coil, $20cm < radius < 55cm$. Each scintillating fiber superlayer contains 8 layers of fibers arranged in 4 layers of axial fibers and two layers each of stereo fibers. The photons are carried to the photo detector by coupling the scintillating fibers to clear wave guide fibers. The visible light photon counter (VLPC) developed by Rockwell Inc [3] is the proposed photo detectors for this system. The VLPC is a compact, low power and high speed device with quantum efficiency > 60 % which operates at cryogenic temperature (6 – 8° K). A large scale cosmic ray test of this system is underway at Fermilab.

The superconducting solenoidal magnet for D0 upgrade will be a 2 Tesla magnet with good field uniformity. This will add about one radiation length X_o material to the central tracker.

A preshower detector will be installed between the coil of the superconducting solenoid and calorimeter cryostat to correct for the electromagnetic energy lost in the coil. The preshower detector consists of a tapered lead absorber to provide a constant $2X_0$ radiator when combined with the coil material and six layers of scintillating strips with wavelength shifting fiber readout, arranged in two axial and two stereo layers with ±10° stereo angle. The readout system is the same as VLPC readout of scintillating fiber tracker. A preshower electron trigger is under study.

Shorter beam bunch crossing time and higher luminosity also requires upgrades to the D0 calorimeter electronics, the muon system, the triggers and the DAQ. The upgrade of the calorimeter electronics requires a re-optimization of the shaping time, addition of a delay in the signal path to accommodate the signal formation time of $2\mu s$ and a change in timing of the baseline measurement. Muon PDT system gas will be replaced with a faster gas ($ArCO_2CF_4$) to reduce the drift time from about 1.2 μs to 800 ns. This drift time will be longer than the bunch crossing time. A full scintillator coverage of the muon PDT's will help provide a time stamped associated with the beam crossing number for every event. The small angle muon system (SAMUS) will have a small cell chamber and significant improvements to its readout electronics, i.e. double hit capability for drift time measurements, increased spatial resolution at trigger level and increase in digitization speed.

The raw event rate will increase by about two orders of magnitude to 5 MHz at a luminosity of $10^{32} cm^{-2} s^{-1}$ over the current D0 capability. A dead time less Level 1 trigger and increase of the bandwidth into Level 2 by providing additional data path is planned to deal with the higher rates. The Level 2 output is estimated to increase from 2 Hz to 50 Hz. We are also investigating more sophisticated triggers and processor to increase the physics throughput of the data.

III. SIMULATION OF $B^o \to \pi^+\pi^-$

The simulations presented in this paper are done by using a fast simulation program[4]. The detector simulated in this study is the current D0 upgrade design[2]. The detector geometry is specified in files specifying resolution, radiation length, and orientation of each detector. A set of tracks are generated binned in momentum, vertex position, and eta. Fits are made to the track and the error matrices are saved in a file. These error matrices are then used to produce a special smearing matrix, V, which can be stored and used to produce smeared tracks. The idea is to find the matrix V such that the measured vector Y = Y0 + VxR, where R is a vector of 5 normalized Gaussian distributed random numbers. These five vectors are xslope, yslope, inverse momentum, x intercept and y intercept. Y then is the set of "measured" variables with the proper errors and correlations.

We have used ISAJET (D0 Version) to generate $B^o \to \pi^+\pi^-$ and B$\to \mu X$ decays. These two decays were generated separately, so our tagging efficiency could be higher than if both the B were required to be reconstructed in the detector simultaneously. In both of these simulations B's were generated as TWOJETS and were forced to decay in $B^o \to \pi^+\pi^-$ and B$\to D\mu\nu$ respectively. The code takes as input a standard D0 ISAJET ZEBRA file and a set of routines which describe the measured parameters (momentum, slopes, intercepts, error matrix) of tracks as a function of the ISAJET Z, Px, Py, Pz. The output is an NTUPLE which contains the generated and fitted parameters for the B and charm vertices. Using the full error matrices, fit are made to the vertices. A muon trigger simulator was used to set flags for muon trigger acceptance. Informations are also available on effective mass, particle identification, and the eta range of the decay products from each vertex.

At present there is no scheme to trigger on hadrons specifically from B decays in D0. We will use the semileptonic decays of B ($B\rightarrow \mu X$ and $B\rightarrow eX$) to trigger and tag the B event. The most important factor is how low in pt one can go to improve the trigger and tagging efficiency without saturating the available bandwidth for the readout. After triggering on a B event we will look in the other parts of the detector for a $B^o \rightarrow \pi^+\pi^-$, hence all of the detected $B^o \rightarrow \pi^+\pi^-$ will be tagged by our trigger.

a. $B^o \rightarrow \pi^+\pi^-$ acceptance

We have generated B^o events using ISAJET and forced them to decay into $\pi^+\pi^-$. This ISAJET file is then tracked with the fast simulation program. In all the simulations presented here tracking efficiency per track is assumed to be 90%. B^o lifetime used in these calculation is 1.29×10^{-12} sec [5]. Fig. 2 shows the plot of decay length over error in decay length for the $B^o \rightarrow \pi^+\pi^-$ events. The mass resolution of $B \rightarrow \pi^+\pi^-$ is an important issue considering the backgrounds. Mass resolution of $B \rightarrow \pi^+\pi^-$ degrades significantly above η of 2.5 for upgraded D0 detector[6a]. We have also applied a 2 GeV cut on the B^o pt. It is also necessary to impose decay length over error in decay length cut to improve signal to background ratio. Fig. 3 shows our acceptance ϵ_{CP} a function of this parameter. During this workshop[6b] there were some cuts selected and all the experiments were supposed to use the same cut for comparison. BCD collaboration, has done a simulation of the background contributions to $B^o \rightarrow \pi^+\pi^-$[7]. In their simulation study they claim that the ratio of decay length over error in decay length > 15 is a powerful tool to reduce the background. Detailed simulations of the background for Tevatron energy have not been done, so for the purpose of comparison we will use the same cut for estimating the acceptance. Although it seems to be a tight for Tevatron experiment.

b. $B\rightarrow \mu X$ *acceptance*

We have also simulated our trigger and tagging efficiency by generating $B\rightarrow \mu X$ decay using ISAJET and tracking it through the same simulation program. Muons from $B\rightarrow \mu X$decay are required to satisfy the current muon trigger and be with in $|\eta| \leq 3.0$. The $BR(B\rightarrow \mu X)$ is 10.3%[5]. Fig. 4 shows our trigger and tagging efficiency as a function of the muon pt cut. At present we do not have a simulation for $B\rightarrow eX$. For calculations purpose we have assumed that muon and electron trigger efficiencies are equal.

c. *Calculation of Dilution factors*

The dilution of the measured asymmetry is from three principal sources, mixing of the neutral B mesons prior to its decay, decays that are mistagged and the presence of background in the observed sample. There exists an extensive discussion of dilution factor and its calculation in the literature. Here we will present only the relevant informations.

Using the Silicon vertex detector one can perform the time dependent analysis of the mixing. The mixing parameter x for B_d^0 is 0.69 ± 0.17 [5]. The dilution due to mixing using the time dependent information is given by[8]

$d_{mix}(t_{dep}) = \sqrt(2x^2/(1+4x^2)) = 0.57$

At the workshop[6b] we agreed to use the signal to background ratio of 1, which is the current estimate from CDF in their $B \rightarrow J/\psi K$ events.

$d_{bkg} = \sqrt(S/S+B) = 0.71$

The flavor of the B^0 or $\bar{B}^0$ can be tagged by the decay of the second B particle. A fraction of B will be incorrectly tagged either because the tagging B mixes before decaying or because the tagging lepton does not originate from the decay of B, but instead comes from cascade decay of a charmed meson, decay of other light mesons or hadron punchthrough. If we denote the fraction of tags due to these processes by F_B, F_C, F_D, and F_P respectively, then the wrong sign tagging fraction is given by [9]

$w = \alpha F_B + (1-\alpha)F_C + (F_D + F_P)/2$

where α is given by

$\alpha = f_s/2 + f_d(x^2/(2+2x^2)) = 0.15$

f_s and f_d are the fractions of b quarks which hadronize to strange and down type neutral B's respectively, and α is therefore the fraction of B's which mixes before decaying. The dilution due to mistagging is given by $d_{tag} = (1-2w)$. Since the pt distribution of these processes are significantly different, the dilution due to tagging depends on the pt cut used in the trigger. We have used the value of w from the simulations presented in [9] which is shown in Fig. 5.

IV. Calculation of Sensitivity to Alpha measurement

We are still in the process of planning of the D0 upgrade for B physics. It is not yet clear how soft lepton we can trigger on or will we use a online vertex processor to trigger on large impact parameter particles. We believe that with not too modest effort we can trigger on leptons with pt above 3 GeV. The number of produced $B^o\bar{B}^o$ needed to obtain a given error on δA_{cp} is given by

$N_{prod} = (1/\delta^2 A_{cp})(1/D^2\epsilon\ \mathrm{BR})$

Where D and ϵ are the products of different factors contributing to dilution and efficiency and BR is the branching ratio. The summary of D0's sensitivity in measuring angle Alpha using the simulation results and other informations is presented in Table 1. We have done separate simulations for $B^o \rightarrow \pi^+\pi^-$ and $B \rightarrow \mu X$, rather than doing a more realistic simulation where both the B's are required to decay simultaneously.

V. Remarks

This study is very preliminary and points that the measurement of asymmetry by $B^o \to \pi^+\pi^-$ is difficult with the current D0 upgrade plans. The detector efficiencies used in this simulation for muons are from current run. They are expected to improve significantly after the full upgrade. It should be noted that with improved triggering scheme, where we can trigger on particles with large impact parameter or on mass from two reconstructed tracks, the measurement will improve significantly. We are in the process of evaluating all of these options including the design of our central tracker, such as using double sided silicon in some of the silicon barrel detectors.

Table 1. Measurement of CP Asymmetry: Alpha

Energy Ecm (TeV)	2.0
Luminosity L	$10^{32} cm^{-2} s^{-1}$
Cross Section $\sigma_{b\bar{b}}$	50 μb
Cross Section σ_{tot}	50 mb
B0 fraction, f0	0.375
N(B0) produced/10^7 sec	3.75×10^{10}
Branching Ratio $B^o \to \pi^+\pi^-$	1.0×10^{-5}
CP final state	$B \to \pi^+\pi^-$
B flavor tag	μ/e (Semileptonic Decays on B)
ϵ_{dec}	1.0
$\epsilon_{trig}, \lvert\eta\rvert \leq 3.0$,pt$\mu \geq 3.GeV$	0.018
$\epsilon_{CP}, \lvert\eta\rvert \leq 2.5$,pt $B^o \geq 2.GeV$	0.13
ϵ_{tag}	1.0
d_{mix}	0.57
d_{tag}	0.56
d_{bkg}	0.71
Total efficiency ϵ	2.34×10^{-3}
Total Dilution D	0.23
Figure of Merit, $1/(D^2)\epsilon$	8078
N_{prod} for $\delta A_{cp} = 0.1$	8.1×10^{10}
Time for Measurement (10^7 sec)	2.2 years

VI. REFERENCES

[1] David London, Theoretical review Alpha group summary, Proceeding of Workshop on B Physics at Hadron Accelerators, Snowmass, June 21-July 2 1993.

[2] D0 upgrade proposal, D0 note 1148, D0 note 1322, D0 note 1426.

[3] M. Atac, Proceeding of the 3rd International Conf. on Advanced Technology and Particle Physics, Como, Italy, 22-26 June 1992. M. Petrov, Proceeding of the 3rd International Conf. on Advanced Technology and Particle Physics, Como, Italy, 22-26 June 1992.

[4] Heidi Schellman and Tacy Joffe-Minor, Private communications.

[5] Particle Properties Data Booklet, Particle Data Group, Phys. Rev D45, 1992.

[6] Proceeding of Workshop on B Physics at Hadron Accelerators, Snowmass, June 21-July 2 1993. a) Tracking and Vertexing Group Summary ; b) Alpha Group summary.

[7] O. R. Long et al.,Princeton/HEP/92-07, Aug 13, 1992.

[8] K. T. McDonald, Princeton/HEP/92-04, Sept 4, 1992.

[9] Natalie Roe, D0 Note 1122. Jun 12, 1991.

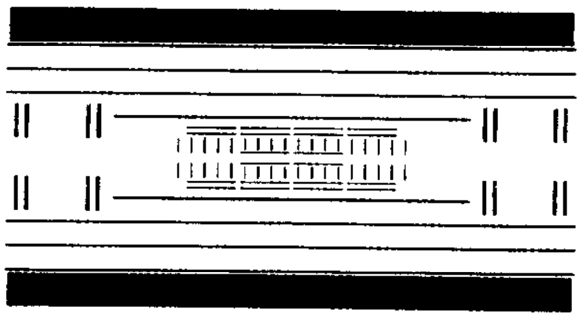

Fig. 1 A schematic View of the tracking system.

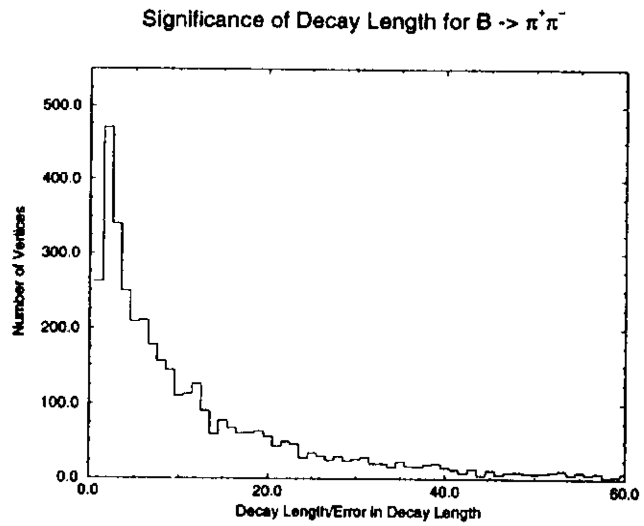

Fig. 2 Plot of decay length/error in decay length for $B \to \pi^+\pi^-$ events.

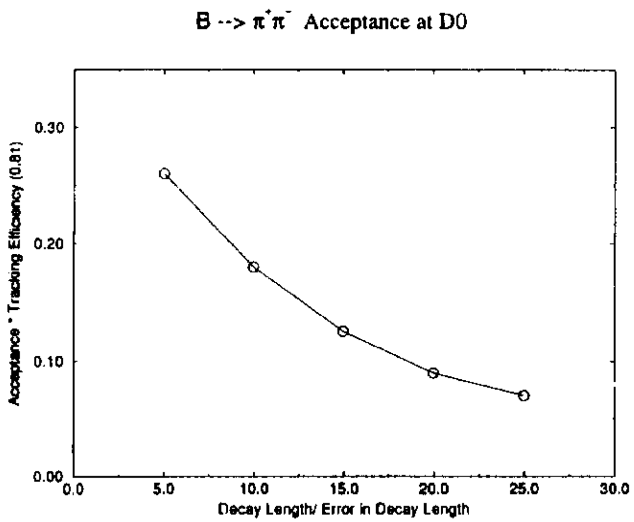

Fig. 3 Acceptance of $B \to \pi^+\pi^-$ as a function of cut on decay length/error in decay length.

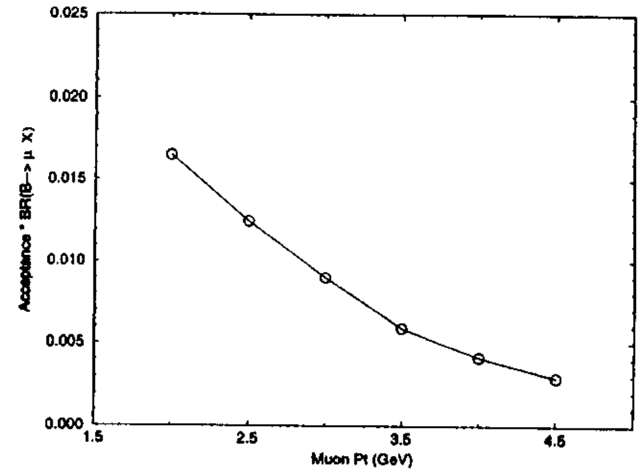

Fig. 4 Trigger and tagging efficiency as a function of pt cut on muon.

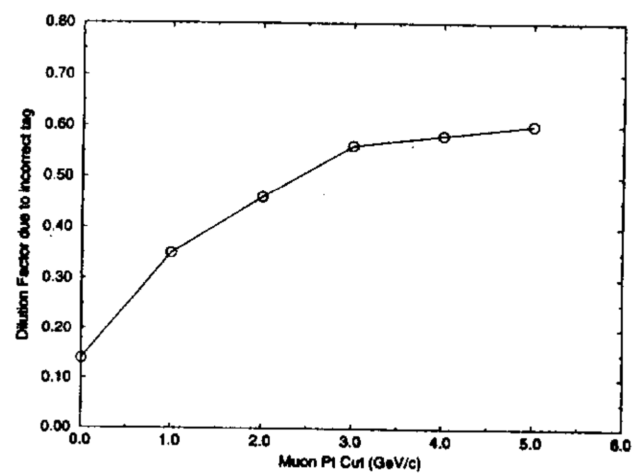

Fig. 5 Dilution factor due to mixing as a function of pt cut.

A $B^0 \to \pi^+\pi^-$ TRIGGER FOR CDF

GIOVANNI PUNZI
Scuola Normale Superiore and INFN
Via Livornese, S. Piero a Grado, Pisa 56100, Italy

and

SIMONE DONATI, GUIDO GAGLIARDI
INFN, Via Livornese, S. Piero a Grado, Pisa 56100, Italy

1. INTRODUCTION

We have studied how to implement in CDF a trigger for the process $B^0 \to \pi^+\pi^-$, exploiting the new trigger hardware being built for Run II (1996/1997).

The trigger we propose is based on online measurement of impact parameters, a very important handle for a decay channel that is otherwise almost featureless. The new devices that will make this trigger possible are, at Level 1, the new fast tracker for the Central Drift Chamber (XFT[1]) and, at Level 2, the Silicon Vertex Tracker (SVT[2]), allowing online tracking in the new Silicon Vertex detector (SVX II[3]). We evaluate rates and efficiency of the proposed trigger, and discuss its feasibility.

2. METHOD

We describe in the following the tools used in performing this study. All rates are estimated from a sample of real Minimum Bias data collected in the CDF run IA (1992/1993), amounting to about $2.4 \cdot 10^5$ events. We believe that using real data is crucial, since the evaluation of the background when very high rejection factors are needed (as in this case) is very uncertain if based on simulated data.

We have crudely simulated the XFT by smearing the track momenta with the expected resolution and making the appropriate acceptance cut ($|\eta| < 1$ and $P_T > 2$ GeV). This is expected to be good enough for our purpose, since the efficiency and background rate should be almost ideal in events with low multiplicity like those we are considering. The SVX II detector is simulated by the actual SVX of Run IA, which is very similar except for Z acceptance. This is taken into account by scaling the resulting rates by the appropriate factor.

For the SVT, we have used a fully detailed simulation program that includes the algorithms for online correction of SVX misalignment and beam position. We expect this simulation to be very accurate in predicting the behaviour of the real device. Given the small number of MB events written on tape for each run, the beam finding algorithm yields large statistical errors on the beam position. This leads to a pessimistic estimation of the SVT performance, since in the actual running conditions a huge statistics will be available. For this reason, we also made alternative rate estimates using the full off-line reconstruction in place of the SVT simulator, that has a much larger available statistics, given the lower P_T threshold. This provides an upper limit to the expected performance, and it is likely to be closer to reality than the lower limit, since the SVT resolution has been determined to be almost identical to the offline resolution.

Efficiency estimates are based on a sample of 10,000 simulated $B^0 \to \pi^+\pi^-$ decays, generated according to theoretical calculations[4] of B-meson P_T and rapidity distributions. No detector simulation was performed in evaluating the efficiency, but simply resolution smearing and acceptance cuts were applied. We deemed this appropriate, since the largest uncertainties on signal size come from the theoretical uncertainties on cross sections and branching ratios.

3. RESULTS

We have performed the cuts both on the signal and background samples, and we report in the table below the efficiency on both the signal and the background after each cut. All rates are estimated at the expected Run II luminosity of $5 \cdot 10^{31}$.

At Level 1, we require two tracks within the XFT acceptance ($|\eta| < 1$ and $P_T > 2$ GeV), and this simple requirement gives an acceptable, though high, trigger rate. At Level 2, we require the presence of at least two oppositely-charged tracks with impact parameter greater than 100 μm. This gives a substantial rate reduction. A further cut is made on the impact parameter of the reconstructed B particle, to make sure it points back to the primary vertex, and that the decay is in the forward direction. A cut at 140 μm on this variable helps in reducing the background and is almost fully efficient.

Table 1. Trigger cuts, efficiencies and rates

CUT	Signal	MB (OFF.)	MB(SVT)	RATE
Eta	0.20	-	-	
P_T	0.12	0.026	0.026	
Opp. charge	0.12	0.017	0.017	30 kHz (L1)
Impact par.	0.044	$1.2 \cdot 10^{-4}$	$4 \cdot 10^{-4}$	
B imp. par.	0.043	$2.2 \cdot 10^{-5}$	$11 \cdot 10^{-5}$	40÷190 Hz (L2)
Invariant Mass	0.043	$< 10^{-6}$	$< 10^{-5}$	< 18 Hz (L3)

The expected bandwidths are:

- L1: 50 to 100 kHz
- L2: $\approx$ 1 kHz
- L3: 50 Hz or more

We can see that the rates are easily fit in the available bandwidth, and we are able to preserve a significant fraction of the signal (4%). Note that the eta acceptance alone is responsible for cutting the efficiency down to 20%.

4. CONCLUSIONS

Assuming a b-quark cross section of 50 μb, a BR($B^0 \to \pi^+\pi^-$) $= 10^{-5}$, and a B^0 fraction of 40%, we expect to be able to put about 8.5 Kevents of signal on tape in $10^7 s$ run at the Run II design luminosity. This is a sizable sample, and if the tagging efficiency is not too small (we expect 4% or better), it could yield the first observation of CP-violation in $B^0 \to \pi^+\pi^-$.

The initial signal/noise ratio is 1:3,000,000, and reduces to about 1:1,500 on tape. That is still a large background and, in order to actually make a measurement, further tight cuts will be needed in the offline analysis. It is still to be understood how much additional rejection is obtainable in the offline. Unfortunately, this is not easy to figure out with some level of confidence until a huge sample of real data becomes available.

5. ACKNOWLEDGEMENTS

We wish to thank Peter Wilson for many interesting discussions.

6. REFERENCES

1. P. Wilson, these proceedings, in Trigger Subgroup Report.
2. G. Punzi and L. Ristori, CDF-note 1872 and CDF-note 2037.
3. *SVX II Upgrade Proposal*, CDF-note 1922.
4. P. Nason, S. Dawson, R.K. Ellis, *Nucl. Phys.* **B327** (1989)

STUDY OF COMBINATORICAL BACKGROUND IN THE DECAY $B_d^0 \to \pi^+\pi^-$ FROM p-p INTERACTIONS AT $\sqrt{s} = 40$ TeV

O. LONG, F. AZFAR and J. HEINRICH
Department of Physics, University of Pennsylvania, 209 S 33 Street
Philadelphia, PA 19104-6396, USA

1. INTRODUCTION

The $b\bar{b}$ cross section at the SSC is predicted to be 1–3 mb, and 1–3% of the p-p interactions will produce a $b\bar{b}$ pair.[1] Based on the experience of the CDF collaboration it has been established that the $B \to J/\psi X$ modes can be found with acceptable background levels in a hadron collider.

This paper reports studies of the efficiency for reconstructing the decay $B_d^0 \to \pi^+\pi^-$ and of rejection of background due to $b\bar{b}$. Identification of this decay mode is expected to be more difficult than the $B \to J/\psi X$ modes due to severe combinatoric backgrounds. Nonetheless, two aspects of B decays will make it possible to extract the $B_d^0 \to \pi^+\pi^-$ signal at a hadron collider. The relatively long lifetime of the B meson allows the vertex for the decay $B_d^0 \to \pi^+\pi^-$ to be easily isolated from the primary vertex. In addition, the pions from this decay have the maximum momentum of daughters from any B decay and so are more readily separated from low-P_T hadron backgrounds.

The results reported here are based on detailed simulation of pattern recognition in vertex fitting using information from a silicon vertex detector. However, the separate issue of track pattern recognition is not addressed, and it is assumed that detector hits are all properly associated with tracks. A study that combines the issues of track and vertex pattern recognition has been reported in Ref. 2.

2. DETECTOR PARAMETERS

We simulated a vertex detector that consisted of 3 coaxial silicon barrels and 33 silicon disks normal to the beam, 21 of which were interleaved with the barrels. The vertex detector surrounded a beryllium beam pipe. The detector is symmetrical about z=0 with the central 21 discs spaced uniformly in length and the rest uniformly in pseudorapidity with $|\eta| < 5$. The simulated detector has been described in more detail in Ref. 3.

3. EVENT GENERATION

Based on previous experience we have concluded that the main source of background for this decay mode comes from other B decays, and not from minimum-bias events or charm decays. ISAJET was used to generate 1,040,000 $b\bar{b}$ events at 40 TeV center of mass energy.[4] The detector simulation-package GEANT was used to track and decay the particles taking into account multiple scattering, nuclear interactions, and electromagnetic cascades. Roughly 42% of the $b\bar{b}$ events contained B_d^0 mesons; these were forced to decay to $\pi^+\pi^-$. The detector simulation contained a beam pipe, a silicon vertex detector and no magnetic field. The simulation was run on Intel iPSC/860 processors at U. Pennsylvania and the SSC Laboratory.[5] Up to 16 independent processors (nodes) were used simultaneously.

4. VERTEX RECONSTRUCTION

Only charged tracks with at least three hits in either the barrels or the disk detectors were used for vertex reconstruction. A hit was defined as a track intercepting a silicon detector at an angle of incidence $< 55°$. The hits were smeared with Gaussian errors based on angle dependent resolution.[6] A straight line was then fit to the hits for each track returning a slope, intercept, and error matrix based on an estimate of multiple scattering. The momentum of the particle was assumed known due to an outer detector (not simulated). Fitted tracks with a $P_T > 0.6$ GeV/c and $|\eta| < 4$ were passed on to the CERN program library routine VERTEX. All selected tracks were initially fit to the hypothesis of a single vertex and those contributing a $\chi^2 > 3$ were excluded from this vertex. In the next iteration this set of previously excluded tracks were considered to come from a single vertex and the whole procedure repeated until no more vertices were found. All secondary vertices with two oppositely charged tracks were considered as $B_d^0 \to \pi^+\pi^-$ candidates.

5. ANALYSIS

Only 11% of the true $B_d^0 \to \pi^+\pi^-$ events passed the inital set of cuts and the vertexing algorithm described above, after which three additional cuts were used:

1. The closest-distance-of-approach (CDA) cut, where CDA is the distance between between the reconstructed primary vertex and the three-momentum of the B_d^0 . Where CDA is required to be < 0.01 cm.

2. The vertex-separation cut ($S/\Delta S$), where S is the two dimensional displacement of the fitted vertex from the beam and ΔS is the error on this quantity. $S/\Delta S$ is requried to be >15.

3. The track-P_T cut. This cut was on the P_T of both the charged tracks from the secondary vertex. P_T is required to be >1.75 GeV/c.

The efficiencies and the background rejection of each cut is shown in the table given below:

Table 1. Efficiency and Background Rejection of the Cuts.

CUT	EFFICIENCY	BACKGROUND REJECTION
$P_T > 1.75$ GeV/c	67%	98%
CDA<0.01cm	95%	50%
$S/\Delta S > 15$	48%	97%

No background remains in a ± 0.25 GeV/c^2 window about the B_d^0 mass, after all cuts are applied. Assuming a branching ratio of 10^{-5} for the decay $B_d^0 \to \pi^+\pi^-$, we calculate a signal-to-noise ratio of greater than 1, at a confidence level of 90%.

6. CONCLUSIONS

We have studied the feasibility of observing the decay mode $B_d^0 \to \pi^+\pi^-$ in a hadron collider such as the SSC, using the ISAJET Monte Carlo and GEANT detector-simulation package. The large combinatoric background from other B decays was the main concern. After cuts, principally on secondary-vertex quality, we achieved an efficiency for finding $B_d^0 \to \pi^+\pi^-$ decays of 4% and a signal-to-noise ratio of > 1.0, 90% CL. This simulation indicates that the SSC collider environment provides an opportunity to detect a large sample of $B_d^0 \to \pi^+\pi^-$.

7. REFERENCES

1. E.L. Berger and R. Meng, *Heavy Quark Cross Sections at Hadron Collider Energies*, ANL-HEP-PR-92-11 (January 1992).
2. *Response to the SSC PAC*, (July 11, 1990). *Bottom Collider Detector: A Low- and Intermediate-P_t Detector for the SSC*, SSC-240 (Sept. 30, 1989); *Bottom Collider Detector, Expression of Interest* (EOI008), submitted to the SSCL (May 25, 1990).
3. L.A. Roberts, *Monte Carlo Simulation of Vertex Detector for Bottom Collider Detector*, Fermilab preprint FN-488 (June, 1988).
4. F.E. Paige and S.D. Protopopescu. *ISAJET 6.36*, Brookhaven National Laboratory.
5. P.T. Keener *et al.*, *Porting of Standard High Energy Physics Physics Codes to the Intel iPSC*, submitted to Comp. Phys. Comm. (June 1992).
6. M. Lambrecht *et al.*, *Beam Tests of Silicon Microstrip Detectors with VLSI Readout*, IEEE Trans. Nucl. Sci. **NS-38** (1991).

Background to $B_d \to \pi^+\pi^-$ From Secondary Interactions in a Silicon Microvertex Detector at the SFT

T.J. Lawry, E.C. Dukes, A.P. McManus
Physics Dept., U. of Virginia, McCormick Rd.
Charlottesville, Va., 22901 USA

1. INTRODUCTION

The decay $B_d \to \pi^+\pi^-$ is very important for CP violation studies. We propose to study this decay using a Silicon Microvertex Detector (SMVD) at the SFT[1] (SSC Fixed Target) experiment. The target region of the SMVD has 0.04 interaction lengths so the probability of secondary interaction is 2% per hadron from the primary vertex. These secondary interactions are a background to the decay $B_d \to \pi^+\pi^-$. This background is peculiar to the SFT since in collider, gas jet, and wire experiments the B_d decays take place in vacuum.

In this note we show that the background from secondary interactions is negligible after simple kinematic cuts, at least for the channel $B_d \to \pi^+\pi^-$. The background could be further reduced, if necessary, by requiring that the production vertex of the $\pi^+\pi^-$ pair lie in one of the spaces between the silicon foils.

The PYTHIA simulations were run with $P_h^T = 0.7\ GeV/c$, rather than $P_h^T = 0.35\ GeV/c$ which is the PYTHIA default. P_h^T is the parameter which controls the transverse momentum of primary hadrons. The large value of P_h^T gives a much larger tail at high mass. The value of $P_h^T = 0.7\ GeV/c$ is probably much too large but we use it anyway to be conservative.

2. VARIOUS CUTS

Using PYTHIA we simulate the energy distribution of B particles produced at the SFT. For $B_d \to \pi^+\pi^-$ with both pions in the acceptance, only 1% have $E_B < 100\ GeV$. This is reasonable since a particle of mass 5.278 GeV/c^2 has lab frame energy below 100 GeV only if $x_{Feynmann} < -0.14$.

We require $B_d \to \pi^+\pi^-$ candidates to have exactly two charged tracks (of opposite sign) in the spectrometer acceptance (2 - 75 mrad), the energy of the two tracks must exceed 100 GeV, and the invariant mass of the two tracks must be within 25 MeV/c^2 of the B_d mass. (The mass resolution of the spectrometer is 13.0 MeV/c^2 at the B_d mass.)[1]

In Table 1 we summarize the mass spectrum for 10^6 $\pi^- p$ secondary interactions with $E_\pi = 300\ GeV$, and $E_\pi = 3\ TeV$. The fraction of secondary interactions which pass our cuts is almost independent of the hadron energy so this crude simulation of the energy spectrum of primary hadrons is sufficient. The mass region $5.0-5.5\ GeV/c^2$ has 18 events at 300 GeV and 29 events at 3 TeV. So we expect 1.8-2.9 events (per 10^6 secondary interactions) in our 50 MeV/c^2 wide mass window. Further cuts eliminate these events completely.

Let θ be the angle between the momentum of the primary hadron and the sum of the momenta of the two secondary tracks in the spectrometer. We make a conservative cut $|\theta| < 1$ mrad and require that there should be no "other" charged tracks from this vertex. "Other" tracks are charged tracks which fall outside the spectrometer acceptance but inside the acceptance of the SMVD. We make the very conservative assumption that the SMVD can detect tracks out to 250 mrad.

An orthogonal cut can be applied to the P^T of the $\pi^+\pi^-$ pair. In Table 2 we give the percentage of B_d, and of primary hadrons in minimum bias events, whose P^T exceeds a given value.

Table 1. Number of secondary interaction which produce $\pi^+\pi^-$ in given mass ranges, for different cuts and energies of the primary hadron. In the θ cut and "other" cut columns, the first number is the number of events, the second number is the background reduction due to the cut.

$E = 300\ GeV$				
Mass Range	No Cuts	θ cut	"other" cut	both cuts
0 – 1	44,910	235/191.1	7,158/6.27	51
1 – 2	24,636	444/55.5	4,679/5.26	97
2 – 3	5,470	169/32.4	1,097/4.99	41
3 – 4	932	33/28.2	164/5.68	5
4 – 5	173	9/19.2	29/5.96	0
5 – 6	28	3/9.33	3/9.33	0
$E = 3\ TeV$				
Mass Range	No Cuts	θ cut	"other" cut	both cuts
0 – 1	26,420	135/195.7	166/159.2	0
1 – 2	12,438	213/58.4	76/163.7	2
2 – 3	2,931	76/38.5	19/154.3	1
3 – 4	689	17/40.5	6/114.8	0
4 – 5	150	6/25	1/150	0
5 – 6	46	2/23	1/46	0

Table 2. P^T distribution of particles.

Particle type	$P^T > 0.0$	$P^T > 1.0$	$P^T > 1.5$	$P^T > 2$	$P^T > 2.5$	$P^T > 3$
B_d	100.0	92.6	85.5	76.1	65.6	55.8
Primary hadron	100.0	17.5	4.69	1.19	0.33	0.11

3. RESULTS

In Table 1 we summarize the effects of the θ and "other" track cuts. Note that after both cuts there are no events with mass pairs above 4 GeV/c^2 in 10^6 π^-p secondary interactions. To get a conservative upper limit we suppose that there is one pair in the mass range 5.0 – 5.5 GeV/c^2, or 0.1 pairs in the 50 MeV/c^2 mass window. The average event has 12 primary hadrons with energy above 100 GeV, giving 0.24 secondary interactions per event. One background pair per 10^7 secondary interactions, times 0.24 interactions per event, gives a background of 2.4×10^{-8} per triggered event, if one triggers on the other B in the event. We assume that the θ and "other" track cuts cause negligible loss of signal, since the cuts are very conservative this assumption is a good approximation.

From Table 2, a P^T cut on the $B_d \to \pi^+\pi^-$ candidate of 2 or 3 GeV/c retains 76.1% or 55.8% of the signal while suppressing the background by a factor of 84.0 or 909, giving background rates of 2.9×10^{-10} or 2.6×10^{-11} respectively.

The nominal branching ratio for $B_d \to \pi^+\pi^-$ is 10^{-5}, so secondary interactions in $B-\bar{B}$ events are a negligible background. High P_T lepton triggers yield event samples with about 50 times more minimum bias events than $B-\bar{B}$ events[1]. So at the first trigger level minimum bias events would be a 12% contamination to the $B_d \to \pi^+\pi^-$ sample with no P^T cut, or 0.2% contamination with a cut of $P^T > 2\ GeV/c$. Applying impact parameter or vertex cuts on the trigger lepton, which can be done both offline and in a second level trigger, will reduce the background from minimum bias by a large factor.

Minimum bias events are 6300 times more common than $B-\bar{B}$ events[1], so a trigger on high mass $\pi^-\pi^+$ events would have 24.0% or 2.9% contamination from minimum bias with P^T cuts of 2 GeV/c or 3 GeV/c. The background can be reduced further by requiring evidence for a second B in the event.

We conclude that the background to $B_d \to \pi^+\pi^-$ from secondary interactions can be reduced to levels of $\approx 1\%$ by simple kinematic cuts.

4. REFERENCES

1. The SFT: A Super Fixed Target Beauty Experiment at the SSC.

VERTEX RESOLUTION IN EXPERIMENT 791

Krishnaswamy Gounder
Department of Physics and Astronomy, University of Mississippi
Oxford, MS 38677, U. S. A.

1. Introduction

The experiment E791 is fourth in the series of experiments using the Tagged Photon Spectrometer at Fermilab devoted to the study of production and decay of charm particles. During the 1991-92 Fixed Target Run, it acquired an unprecedented 20 billion triggers (with a mild E–T trigger of about 4.5 GeV) with an expected reconstructed charm sample of over 200K decays. The components of the E791 version of the Tagged Photon Spectrometer along with the high speed parallal data acquisition system are described in detail elsewhere [1,2] . Here, only the relevant elements for the detection of the primary interaction and the secondary charm decay vertices will be addressed.

2. Vertex Detection

The detector components for the vertex detection consist of 8 PWC (Proportional Wire Chamber) and 23 SMD (Silicon Microstrip) planes. The immediate pair of SMD planes upstream and downstream of the target have a pitch of 25 microns while the rest of the SMD planes have 50 microns. The outer regions of th six most downstream SMD planes have en effetive pitch of 200 microns. The PWC planes have 1mm wire spacing and are located upstream of the target. The primary interaction is produced by colliding a beam of 500 GeV/c negative pions on a target made up of a platinium and four carbon foils separated by about 1.5 cm. The beam is tracked with the aid of 8 PWC and 6 SMD planes located upstream of the target foils. Locating the primary interaction foil and in turn the primary vertex is greatly aided by this beam tracking, especially in the transverse (X-Y) plane. The tracks originating from primary and secondary vertices are reconstructed using the hits in 17 SMD planes consisting of X, Y and V views. The momentum for these tracks are determined to an accuracy of few MeV by a system of drift chambers, PWCs and two magnets located downstream of the SMD planes.

The three dimensional track segments are reconstructed after forming segments in X, Y and V views in the SMD planes. A complete track fitting procedure is applied and the covariant error matrix for these tracks are determined in the SMD region alone. There is about 40-60 track segments for each triggered event. These 3-d track segments are projected and swum through magnets to obtain linked tracks. The two downstream magnets bend the tracks only in the horizontal direction thus allowing straight projection of SMD track segments in Y. The downstream pattern recognition algorithm functions using the method of triplets. Each linked downstream track is refitted to obtain its momentum. The tracking efficiency for the SMD tracks is about 0.90 and the ghost rate is 0.25.

3. Primary Vertex

A number of vertex algorithms exist for finding vertices in E791. Usually, the primary vertex is found using the beam track as a seed track. Candidate tracks for the primary are found by means of an impact parameter technique and then, taking mutiple scattering into account, subjected to a full vertex fit. The average number of tracks in the primary is about 6 excluding the beam track. The primary vertex finding efficiency is about 0.95. Using a popular CERNLIB vertex fitter, the primary foil and the z-resolution are plotted in figures 1 and 3. The error in x, y and z of the primary are given in table 1.

4. Secondary Vertex

The two major methods of finding secondary vertices in use are (i) topological vertexing and (ii) candidate (mass) vertexing. In the former, one searches topologically for secondary vertices using tracks excluded from the primary without any regard to a given decaying particle or its mode of decay. In the latter case, a candidate set of tracks (decay products such as kaons, pions, muons, etc.) are combined such that their effective mass is in a large interval that includes the parent particle mass. This interval is chosen such that there is enough range on both the lower and upper ends of the parent mass for determining background. While the topological vertexing technique is useful for identifying new decays, the candidate driven method is more efficient for searching for a given decay.

Table I. Mean Vertex Resolutions

Vertex	Prong	X (in cm)	Y(in cm)	Z(in cm)
Primary	--	0.0004	0.0004	0.0171
Secondary	2	0.0009	0.0010	0.0410
Secondary	3	0.0009	0.0009	0.0340
Secondary	4	0.0008	0.0008	0.0310

Besides detector resolution, tracking and vertexing algorithms, multiple scattering plays a major role in determining the quality (χ^2 per degree of freedom) of a vertex. In E791, a complete Kalman filtering[3] treatment of multiple scattering is applied to the candidate tracks as a part of the vertex fitting procedure. The vertex resolution also depends on decay topology such as opening angle, the number of decay products and their momenta, etc.. Again using the CERN vertex package and candidate driven method, the secondary foil and z-resolution for a three prong decay is shown in figures 2 and 4 respectively. The secondary vertex resolutions in x, y, and z for two, three and four prong decays are listed in Table I.

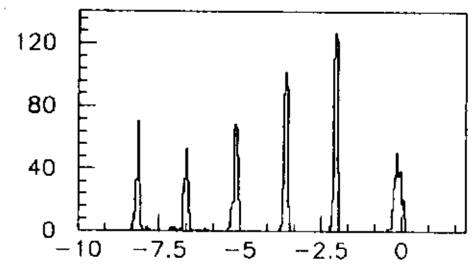

Fig. 1 Primary Foil (in cm)

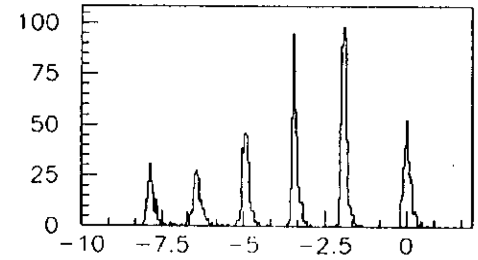

Fig. 2 Secondary Foil (in cm)

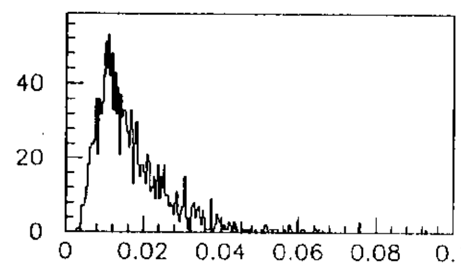

Fig. 3 Primary z−resolution (in cm)

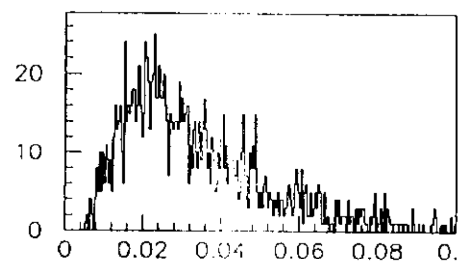

Fig. 4 Secondary z−resolution (in cm)

From the above table, it is evident the x and y vertex resolution is very small compared to the z-resolution as one might expect. The z-resolution of secondary vertex is worse compared to that of the primary. As a result, the significance of charm decay distance (secondary vertex separation from the primary divided by the errors in quadratures) is dominated by the secondary vertex resolution.

5. Conclusion

Due to efficient beam tracking and the high multiplicity in the primary, the vertex separation is dominated by the error in reconstructing the secondary vertex. In E791, the majority of charm mesons and baryons travel a few thousand microns before they decay. With the present mean vertex separartion z resolution of 400-500 microns, we are able to recontruct charm meson and baryon decays with considerable efficiency.

6. Acknowledgements

The author likes to thank his E791* colleagues for their support and making this effort possible. This work was supported by the U.S. Department of Energy under contract DE-FG05-91ER40622.

7. References

1. S. Amato *et al.*, "The E791 Parallel Architecture Data Acquisition System", *Nucl. Inst. and Meth.*, **A324**, 535 (1993).

2. G. A. Alves *et al.*, *Phys. Rev. Lett.* **70**, 722 (1992).

3. E. J. Wolin and L. Ho, "Covariant Matrices for Track Fitting with Kalman Filter", *Nucl. Inst. and Meth.* **A329**, 493 (1993).

* **E791 Collaboration:** University of California (Santa Cruz), CBPF (Rio de Janeiro), University of Cincinatti, CINVESTAV, Fermilab, Illionis Institute of Technology, University of Mississippi, The Ohio State University, Princeton University, Universidade Federal de Rio de Janeiro, Tel Aviv University, Tufts University, UNESP, University of Wisconsin, Yale University.

RECONSTRUCTION OF $B_d^0 \to \pi^+\pi^-$ DECAYS IN THE ATLAS EXPERIMENT AT LHC

S. Gadomski
Institute of Nuclear Physics, Cracow, Poland

P. Eerola, N. Ellis, D. Froidevaux
CERN, Geneva, Switzerland

A study of the capability of the ATLAS experiment at the Large Hadron Collider to measure the CP-violation parameter α by using the decay channel $B_d^0 \to \pi^+\pi^-$ is described.

1. INTRODUCTION

One of the Cabibbo-Kobayashi-Maskawa (CKM) triangles, constructed by using the unitarity constraint of the CKM matrix and sensitive to the CP-violating complex phase, is formed by the matrix elements $V_{cb}^* V_{cd}$, V_{ub}^* and V_{td}. The angle opposite to the side $V_{cb}^* V_{cd}$ is called α. It can be measured from the asymmetry of the rates of the neutral B-decays $B_d^0 \to \pi^+\pi^-$ and $\bar{B}_d^0 \to \pi^+\pi^-$. B and $\bar{B}$ mesons are distinguished by the charge of the lepton originating from a semileptonic decay of the other b-quark in the event.

When the decay rates for B_d^0 and $\bar{B}_d^0$ mesons are integrated starting from time t_0, the observed asymmetry is

$$\begin{aligned} A^{obs} &= \frac{N_{total}(\pi^+\pi^-\ell^+) - N_{total}(\pi^+\pi^-\ell^-)}{N_{total}(\pi^+\pi^-\ell^+) + N_{total}(\pi^+\pi^-\ell^-)} \\ &= D_{tag} D_{back} \frac{1}{1+x_d^2} \sin 2\alpha (\sin \Delta m t_0 + x_d \cos \Delta m t_0), \end{aligned} \tag{1}$$

if the tree-level amplitude dominates the decay. The statistical significance of the signal is reduced by wrong sign tags ($D_{tag} = (N_{right\,tags} - N_{wrong\,tags})/(N_{right\,tags} + N_{wrong\,tags})$), background ($D_{back} = \sqrt{N_S/N_{total}}$) and mixing $(1/(1+x_d^2) \cdot (\sin \Delta m t_0 + x_d \cos \Delta m t_0))$, where $x_d = \Delta m/\Gamma \simeq 0.71 \pm 0.11$ [1].

The expected error on $\sin 2\alpha$ is

$$\delta(\sin 2\alpha) \simeq \frac{1}{D_{tag} D_{back} x_d/(1+x_d^2)\sqrt{N_S}}, \; A^{obs} << 1, t_0 << \tau_b/x_d \tag{2}$$

where $N_S = N_S(\pi^+\pi^-\ell^+) + N_S(\pi^+\pi^-\ell^-)$, and τ_b is the lifetime of the b.

The ATLAS experiment is described in detail in [2], and a short summary of the detector parts relevant to B-physics is given elsewhere in these proceedings [3].

The total $b\bar{b}$ production cross-section is estimated to be between 100 and 700 μb [4] for LHC operating at a center of mass energy of 16 TeV. The total cross-section given by the PYTHIA Monte Carlo program [5] was 560 μb.

In ATLAS, events from b-quarks will be triggered with the muon trigger, based on coincidences in trigger chambers in the outer toroid magnet. The lowest feasible p_T threshold for the muon trigger is about 6 GeV/c. The trigger cross-section given by PYTHIA was 1.7 μb with a muon p_T threshold of 6 GeV/c and $|\eta| < 1.6$. At the initial luminosity of $\mathcal{L} = 10^{33}$ cm^{-2}s^{-1}, the single muon trigger rate from b- and c-decays is expected to be about 3 kHz with a p_T threshold of 6 GeV/c. The second level trigger should reduce the rate giving a maximum output rate of 1 kHz.

2. THE DECAY $B_d^0 \to \pi^+\pi^-$

Events triggered with a high-p_T muon trigger are predominantly b-events. Background to the signal $B_d^0 \to \pi^+\pi^-$ can be produced by:

1. B-meson decays $B_d^0 \to K^+\pi^-$, $B_s^0 \to K^+\pi^-$, $B_s^0 \to K^+K^-$. Since the branching fractions of these channels have not been measured, it was assumed that the fractions are the same as for the signal, $2 \cdot 10^{-5}$. The mass difference between B_d^0 and B_s^0 was set to 100 MeV/c^2 according to the latest measurements [6]. B-meson production fractions were assumed to be 0.40 and 0.14 for B_d^0 and B_s^0, respectively.

2. B-baryon decay $\Lambda_b \to p\pi$. The branching fraction for this decay was assumed to be $1 \cdot 10^{-4}$ [7]. The Λ_b production fraction was taken to be 0.1 and the mass was assumed to be 5.62 GeV/c^2.

3. Three-body B-decays: $B_d^0 \to \rho^\pm\pi^\mp$ and $B_d^0 \to \pi^+\pi^-\pi^0$. These branching fractions were each assumed to be four times that of the signal.

4. Combinatorial background with one particle from a B-hadron decay and the other from the primary vertex.

5. Combinatorial background with both particles from the primary vertex.

6. Combinatorial background with the two particles from two different B-hadron decays, or one from a B-hadron decay and the other from a decay of a long-lived particle (K_S^0, Λ).

To estimate reconstruction efficiencies and background rejection, signal events and background events were generated with the PYTHIA Monte Carlo program, including direct $b\bar{b}$ production, gluon splitting and flavour excitation. The nominal beam energy was 7.7 TeV. Subsequently, the charged particle tracks were parametrized in terms of momentum resolution and impact parameter resolution. The angular acceptance was assumed to be $|\eta| < 2.5$, the track finding efficiency 95% and the lepton identification efficiency 80%.

Events were accepted if the trigger muon had a p_T larger than 6 GeV/c, and a pseudorapidity in the range $|\eta| < 1.6$. Events passing the level-2 trigger must contain two oppositely charged particles with $p_T > 3$ GeV/c, $|\eta| < 2.5$. The two particles were required to be nearby in space ($\Delta(\varphi_{\pi\pi}) < 29°$, $\Delta(\theta_{\pi\pi}) < 17°$).

The final event selection criteria were based on the decay characteristics of a B-hadron:

- The scaled impact parameters ($f = d/\sigma_d$) of the two particles greater than 3, and the angle between the reconstructed B-meson transverse momentum vector and the line joining the primary and the secondary vertices in the transverse plane less than 6°. The acceptance for signal events was 44%. The impact parameter cut rejects the combinatorial background with at least one particle coming from the primary vertex, and reduces background where both particles originate from the primary vertex to a negligible level.

- The closest distance of the two tracks in space less than 150 μm. The acceptance for signal events was 94%. This cut is powerful in rejecting fake secondary vertices.

- The reconstructed $\pi^+\pi^-$ mass within one standard deviation of the nominal value ($\pm$50 MeV/c^2). This cut reduces the background coming from reflections from other B-hadron two- or three-body decays.

The mass distributions for the signal and the different backgrounds are shown in Figures 1 and 2 after all the other cuts except for the final mass cut.

The fraction of wrong sign muons with the ATLAS trigger was found to be 0.14 from sources other than oscillations. The dominant contribution is cascade $b \to c \to \mu$ decays (0.085). The rest originates from multiple quark pair production (0.04), hadron decays and J/ψ decays. Including the effect of mixing the total fraction of wrong sign muons is 0.24, which corresponds to a dilution factor D_{tag} equal to 0.52.

The fraction of wrong sign tags can be measured directly from data using CP-conserving B-decays like $B^+ \to J/\psi K^+$. The same decay mode can be used to control the production asymmetry of B_d^0 and $\bar{B}_d^0$ at LHC, estimated to be at the per cent level [8].

The results are summarized in Table 1.

3. CONCLUSIONS

The CP-reach of the ATLAS experiment in measuring the angle α using the decay channel $B_d^0 \to \pi^+\pi^-$ was investigated. In the absence of particle identification, the good secondary vertex resolution results in a signal to background ratio of about 1:2 under the signal mass peak, where the background is dominated by other two-body B-decays. Taking into account the background, $\sin 2\alpha$ can be measured with a statistical precision of 0.12 with the data collected during the first year of running with LHC at the luminosity of 10^{33} cm^{-2}s^{-1}.

4. REFERENCES

1. H. Albrecht et al., ARGUS Coll., Z. Phys. C55 (1992) 357;
   M. Artuso et al., CLEO Coll., Phys. Rev. Lett. 62 (1989) 2233.
2. Letter of Intent 'ATLAS', CERN/LHCC/92-4, LHCC/I 2, October 1992.
3. P. Eerola, N. Ellis, D. Froidevaux and S. Weinzierl, 'Reconstruction of $B_d^0 \to J/\psi K_S^0$ decays in the ATLAS experiment at LHC', these proceedings (Workshop on B Physics at Hadron Accelerators, Snowmass, Colorado, June 21-July 2, 1993).
4. J.P. Guillot, P. Nason and H. Plothow-Besch, in Large Hadron Collider Workshop, Aachen 4-9 October 1990, CERN 90-10, ECFA 90-133, Vol. II, p. 116.
5. H.-U. Bengtsson, T. Sjöstrand, Computer Phys. Comm. 46 (1987) 43.

6. A. Bonissent, talk given in Rencontres de Moriond, QCD and Heavy Flavours, Les Arcs, March 20-277, 1993;
D. Buskulic et al., ALEPH Coll., 'First Measurement of the B_s Meson Mass', CERN-PPE/93-97, submitted to Phys. Lett. B.
7. S. Rudaz and M. Voloshin, Phys. Lett. B252 (1990) 443.
8. M. Botlo et al., 'Further Comments about B-Physics in pp Interactions', SSCL-538, SLAC-PUB-5795, June 1992.

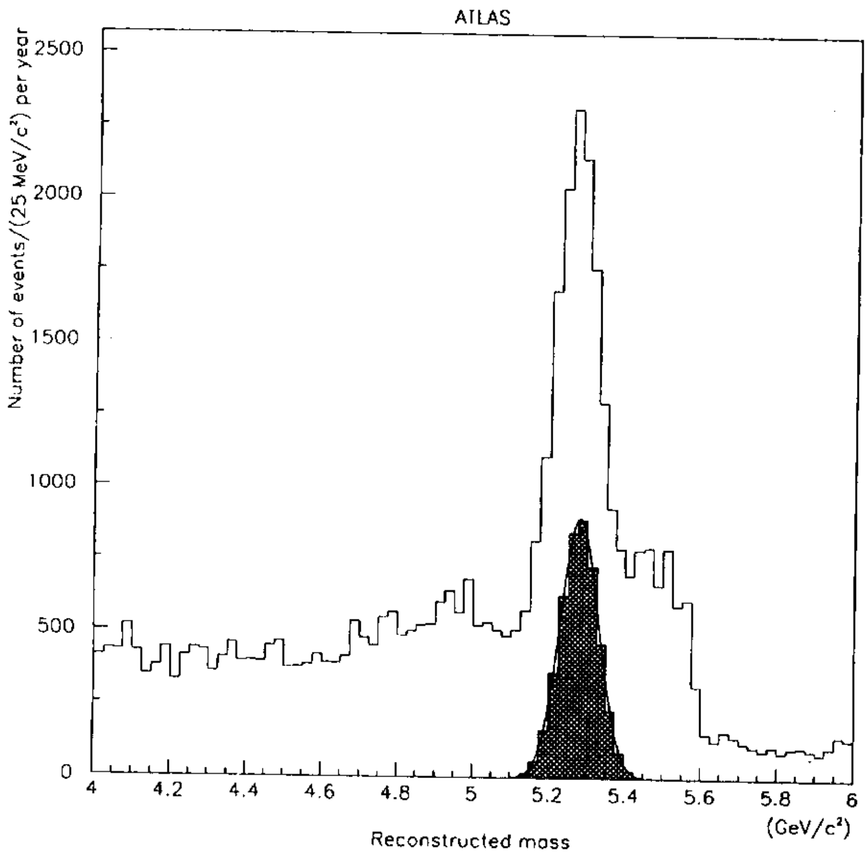

Figure 1: *Reconstructed $(\pi^+\pi^-)$-mass for signal (dark region) and signal plus background (white region).*

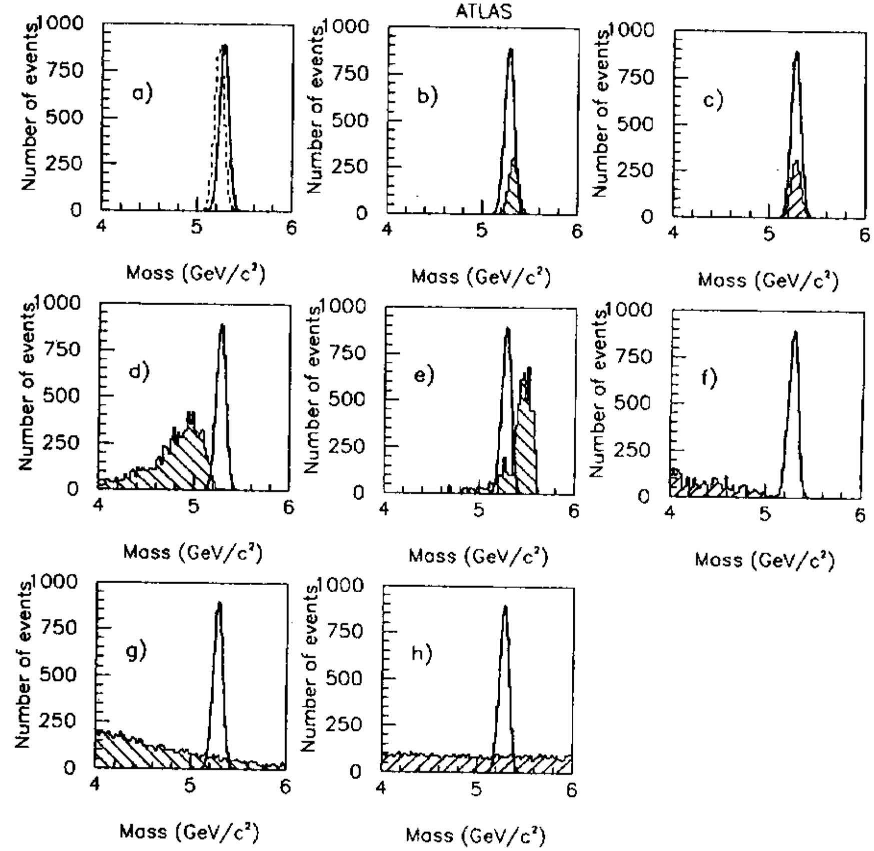

Figure 2: *Reconstructed $(\pi^+\pi^-)$-mass for signal and background from a)* $B^0_d \to K^+\pi^-$, *b)* $B^0_s \to K^+\pi^-$, *c)* $B^0_s \to K^+K^-$, *d)* $B^0_d \to \rho^\pm\pi^\mp$, *e)* $\Lambda_b \to p\pi^-$, *f)* $B^0_d \to \pi^+\pi^-\pi^0$, *g) a B- and a primary track, h) a B- and a secondary track.*

Table 1. ATLAS summary on measuring $\sin 2\alpha$.

Parameter	Value	Comment
$\mathcal{L}$ [$cm^{-2}s^{-1}$]	10^{33}	
t [s]	10^{7}	
$\sigma(b\bar{b} \to \mu X)$ [μb]	1.7	$p_T^{\mu} > 6$ GeV/c, $\lvert\eta^{\mu}\rvert < 1.6$. Includes $2 \cdot Br(b \to \mu) = 0.2$, $Br(c \to \mu) = 0.1$
$N(b\bar{b} \to \mu X)$	$1.7 \cdot 10^{10}$	
$f(b \to B_d^0)$	0.4	
$Br(B_d^0 \to \pi^+\pi^-)$	$2 \cdot 10^{-5}$	
$N(\pi^+\pi^-)$ triggered	136,000	
Level-2 trigger acceptance	0.11	η, p_T, $\Delta\varphi$, $\Delta\theta$ cuts for pions
Impact and angle cut acceptance	0.44	
Distance cut acceptance	0.94	
Lepton identification	0.8	
Track efficiency	$(0.95)^2$	
$N(\pi^+\pi^-)$ reconstructed	4,500	
$m = m_{B_d^0} \pm 50$ MeV/c^2		
$N(B_d^0 \to \pi^+\pi^-) = N_S$	3,070	
$N(B_d^0 \to K^+\pi^-)$	2,170	
$N(B_s^0 \to K^+K^-)$	1,060	
$N(B_s^0 \to K^+\pi^-)$	750	
$N(B_d^0 \to \rho^{\pm}\pi^{\mp}, \pi^+\pi^-\pi^0)$	37	
$N(\Lambda_b \to p\pi^-)$	640	
N(a B- and a primary track)	300	
N(a B- and a secondary track)	430	
N(total)	8,460	
D_{back}	0.60	$\sqrt{N_S/N_{total}}$
δA (stat.)	0.03	$\delta A \simeq 1/(D_{back}\sqrt{N_S})$, $A << 1$
D_{tag}	0.52	$W = 0.24$
Time integration	0.47	$x_d = 0.71$, $t_0 << \tau_b/x_d$
$\delta(\sin 2\alpha)$ (stat.)	0.12	if tree-level decay only

Measurement of Angle β

Convenors:

F. DeJongh
Fermi National Accelerator Laboratory

V. Sharma
University of Wisconsin

List of Participants

G. Apollinary
Rockefeller University/
Fermi National Accelerator Laboratory

C. Campagnari
Fermi National Accelerator Laboratory

J. Chen
Colorado State University

D. Christian
Fermi National Accelerator Laboratory

S. Conetti
University of Virginia

G. Corti
University of Virginia

D. Coupal
Superconducting Super Collider Laboratory

P. Eerola
CERN

H. Frisch
University of Chicago

J. Gonzalez-A
University of Pennsylvania

J. Hassard
Imperial College

J. Heinrich
University of Pennsylvania

W. Hofmann
Max-Planck-Institut für Kernphysik

J. Izen
University of Texas at Dallas

B. Kayser
National Science Foundation

R. Kephart
Fermi National Accelerator Laboratory

T. Lohse
Max-Planck-Institut für Kernphysik

T. LeCompte
University of Illinois at Urbana-Champaigns

S. Loucatos
CEN Saclay

P. McBride
Superconducting Super Collider Laboratory

K. McDonald
Princeton University

N. Neumeister
Institut für Hochenergiephysik
d. Österreichische

V. Papadimitriou
Fermi National Accelerator Laboratory

N. W. Reay
Ohio State University

P. Schlein
University of California–Los Angeles

W. Selove
University of Pennsylvania

A. Sill
Texas Tech University/
Fermi National Accelerator Laboratory

N. Stanton
Kansas State University

W. Toki
Colorado State University

A. Yagil
Fermi National Accelerator Laboratory

BETA GROUP SUMMARY

Fritz DeJongh
Fermilab
Batavia, IL 60510, USA

1. INTRODUCTION

The angle β of the unitarity triangle can be measured through CP asymmetries in several decay modes. The most commonly considered decay mode is $B^0 \to J/\psi K_s$, $J/\psi \to ee, \mu\mu$, and $K_s \to \pi^+\pi^-$. The dilepton in a secondary vertex provides a distinctive signature for triggering and reconstruction.

Other modes in this class have a χ_c instead of a J/ψ, detected through $\chi_c \to J/\psi\gamma$. Also, there are modes with a K^{*0} instead of a K_s, detected through $K^{*0} \to K_s\pi^0$. The consensus of the group was that detection efficiencies for the photons would not be high enough to make these modes useful. In a contribution to this session, Giorgio Apollinari demonstrates this for the case of a central hadron collider.

In a contribution to this session, Boris Kayser discusses another class of decay modes, $B \to D^+D^-$, $B \to D^{*+}D^-$, $B \to D^+D^{*-}$, and $B \to D^{*+}D^{*-}$. He points out that CP asymmetries in these modes provide a signal to measure $\sin(2\beta)$ through different quark level diagrams than those for $B \to J/\psi K_s$. Comparing the values obtained by the two methods is thus a useful consistency check.

There are a couple of strategies that may enable a measurment of the CP asymmetry in this class of decay modes. In the first, a D^+ is detected in the $K^-\pi^+\pi^+$ final state. In the second, a D^{*+} is detected in the π^+D^0 final state. The signature is a soft pion and a tertiary vertex (partially reconstructed) for the D^0. Some collaborations thought this measurement may be feasible, and were interested in investigating the possibility for their proposals.

Tagging whether the meson was produced as a B^0 or $\bar{B}^0$ is necessary. This is usually done through the partial reconstruction of the second B hadron in the event. Efficiencies as well as fake rates need to be considered. In many proposals, the tag signature is exploited in the trigger. Electron and muon tagging are most commonly considered, and are relatively straightforward to incorporate into a trigger. Kaon tagging has a potentially large advantage in the high branching ratio to taggable final states. Charged vertex tagging (tagging by measuring the total charge of a secondary vertex) also has a potentially large efficiency, but it is not clear whether a high dilution factor can be acheived. The soft pion in the decay chain $B^{**} \to B\pi$ can be used for flavor tagging, but the fraction of B mesons produced in this decay chain must still be measured.

2. COMPARISONS OF DIFFERENT PROPOSALS

John Hassard and Walter Toki, in a contribution to this session, have compiled a table comparing the capabilities of the various proposals and have shown in a graphical format how the different factors enter for the measurement of the CP asymmetry. It is apparent that different proposals at different center of mass energies claim to achieve similar sensitivity through much different combinations of b cross-section and acceptance. For example, fixed target geometries with the same beam energy as a collider geometry compensate for the lower bottom cross-section by attaining a higher acceptance.

Many people in our session have pointed out that when making these comparisons it is important to keep in mind that many proposals with lesser sensitivity are planned to begin at a much earlier date.

3. CURRENT STATUS

A milestone has recently been achieved on the route to measuring the CP asymmetry in $J/\psi K_s$: The CDF collaboration has reconstructed a B signal of approximately 40 $J/\psi K_s$ events, as shown by Julio Gonzalez in a contribution to these proceedings. This has been accomplished by a combination of low trigger thresholds, silicon vertex tracking and other detector upgrades, and an integrated luminosity of 20 pb^{-1} . This was also the first run for the D0 collaboration, which has presented b signals in inclusive lepton and J/ψ channels.

The CDF data set marks the start of the study of B decays in hadronic collisions. Many interesting measurements will become possible in the near- and medium-term. CDF and D0 are planning to take more data starting in fall 1993, with the goal of accumulating an integrated luminosity of 75 pb^{-1}. CDF and D0 are also planning major upgrades for a run to start approximately in 1997. The data from these runs will provide valuable information on improving $J/\psi K_s$ efficiency, and the feasibility of various tagging methods.

4. PROSPECTS WITH UPGRADES OF EXISTING EXPERIMENTS

When the Fermilab Main Injector is completed, it will become possible to accumulate 1 fb^{-1} of data per year. Furthermore, the machine group at this workshop has formulated a plan they call "Tevatron-99" to extend beyond this. By using 99 bunches and bunched beam cooling, they estimate that it may be possible to accumulate 7 fb^{-1} per year.

The challenge for CDF and D0 is therefore to simultaneously improve trigger and reconstruction efficiency and the data rate capability. Both collaborations have plans to do this.

One approach is to expand the pseudorapidity coverage for muons. The current CDF results use only the region $|\eta| < 1$. D0 has coverage to $|\eta| < 3.1$ and CDF, with planned upgrades, will have coverage to $|\eta| < 2.5$. This could result in a factor of 4 gain in acceptance for $J/\psi K_s$ events times a factor of 2 gain in muon tagging efficiency. It still needs to be demonstrated that the difficulties of this approach can be overcome. The mass resolution gets worse as $|\eta|$ increases, and track reconstruction becomes less robust as there are fewer measurements in the central tracking chambers. The mass resolution must be at least good enough to reject low mass background from $B \to J/\psi K^*$, $K^* \to K_s \pi$.

Another approach for CDF would be to continue to concentrate on the region $|\eta| < 1$. By completing the muon coverage, lowering trigger thresholds, and in addition using $J/\psi \to e^+e^-$, it may be possible to gain a factor of 3 in $J/\psi K_s$ trigger efficiency. Improvements would also be necessary in the tagging efficiency. Lepton tagging may not yield more than 4% efficiency. Kaon tagging is possible in principle, but would require a very difficult upgrade in practice. Charged vertex tagging and B^{**} tagging may help but remain unproven.

In summary, using the current CDF data set as a baseline, a factor of 50 increase in luminosity and 10 in efficiency while maintaining a high dilution factor would allow a 10% measurement of $\sin(2\beta)$ in 3 years. The current data set and new data to be acquired in the near term will allow additional feasibility studies.

5. NEW EXPERIMENTS AT EXISTING ACCELERATORS

There is an proposal called HERA-B to build a fixed target experiment in the Hera proton ring. The target would consist of wires moved into the beam halo. The feasibility of this type of target has been investigated in test runs.

The B cross-section is expected to be 12 nb at 820 GeV, and 20 nb if the energy is upgraded to 1000 GeV. The total cross-section is expected to be about 10^6 higher.

The goal is to obtain an efficiency for tagged $J/\psi K_s$ of 0.02, with a dilution factor of 0.5. This would allow an asymmetry measurement to a precision of 0.07 in 5 or 6 years.

6. LARGE CENTRAL LHC AND SSC DETECTORS

The SDC and GEM collaborations at the SSC and the CMS and ATLAS collaborations at the LHC have been investigating the possibility of applying these large central detectors, designed primarily for the Higgs boson search, to B physics. Typically, the proposal is to do the B physics at a luminosity 1/10 that of the design.

The triggers envisioned typically involve 2 muons from the J/ψ as well as a muon from the tag. It may be possible to require only 1 or 2 muons, but with higher thresholds. This appears to allow a measurement of $\sin(2\beta)$ with a precision of about 0.07 in one year of running if detectors are ready during accelerator commissioning and DAQ bandwidth is allocated.

7. DEDICATED B DETECTORS AT THE LHC and SSC

There are many proposals for dedicated B detectors at the LHC and SSC. The BCD and COBEX collaborations propose forward collider experiments. SFT and LHB are proposals for extracted beam fixed target experiments, and GAJET is a proposal for a gas jet fixed target experiment.

The total b cross-section is of course much higher for the forward collider, and the ratio of b cross-section to total cross-section is also higher. However, since the B hadrons are much more boosted in the fixed target case, the acceptance is higher. Also, minimum transverse momentum requirements suppress the extra background from the total cross-section in the fixed target case. From the presentations at this workshop, it appeared that both approaches have similar capabilities.

Within each approach, there are various designs, differing in the areas of of detector configuration, trigger signature used, trigger hardware and DAQ system, etc. These areas are highly coupled to each other, and the optimal configuration is not yet clear. There was general agreement though among the various proponents that a measurement of $\sin(2\beta)$ to a precision of 2% would be possible for one year of running.

8. CONCLUSIONS

The study of b decays at hadron colliders has started at the Tevatron. There are still many steps to take to achieve a measurement of $\sin(2\beta)$. CDF and D0 have plans to take the next step in a program that may culminate in an initial measurement. An internal wire fixed target experiment in the HERA ring may also be able to measure $\sin(2\beta)$ with several years running.

The large central detectors at SSC and LHC appear to have the ability to measure $\sin(2\beta)$ in one year of running at a luminosity one tenth of design. However, the dedicated forward and fixed target B detector proposals claim to have significantly better precision. At this workshop, while we gained much information about the various proposals, we were not able to evaluate which approach was the best.

COMPARING THE PHYSICS REACH OF DETECTORS IN MEASURING CP VIOLATING ANGLE β

W. TOKI
Colorado State University, Fort Collins
J.F. HASSARD
Imperial College, London

1. COMPARING EXPERIMENTS

There have been attempts in the past[1] to make quantitive comparison among present and proposed experiments seeking to measure the internal angles of the CKM unitarity triangle. The best known, which we shall call the Harrison Plot (figure 1), puts the attainable error in sin (2β) against the year that error might be reached. Since there is huge uncertainty in the luminosity profiles of the proposed accelerators, the slope of these curves is recognised to be suspect. Furthermore, this representation makes no statement about the relative sizes of efficiency, dilution and number of events which determine the error. Here we present a complementary representation which allows a simple comparison to be made, and which can be later extended to accommodate systematic erros and contributions to, say, the efficiencies to be compared.

2. THE ERROR ON β

The error on CP reach is given by

$$\delta(sin(2\beta)) \approx \frac{\sqrt{(1-D\prime^2(sin(2\beta))^2}}{D\prime\sqrt{N_{prod}}} \approx \frac{1}{D\prime\sqrt{N_{prod}}} \tag{1}$$

where

$$D\prime = D\frac{x_d}{1+x_d^2} \tag{2}$$

and D = 0.51, N_{prod} being the number of events. Consequently, the inverse log error in the measured asymmetry $A_{CP}(\beta)$ is simply:

$$ln(\frac{1}{\delta A_{CP}}) \approx ln(D\sqrt{\epsilon Br N_{prod}}) \tag{3}$$

We can therefore add linearly the logarithms of the components which contribute to the error and compare experiments in a bar chart. This is shown in figure 2, where the error attainable in one year's running is shown. In effect, what is left of the number of events N_{prod} after branching fraction, efficiency and dilution have been subtracted is the height of the white histogram, which is shown as a percentage error on the right.

The reader can factor in believable luminosities as required. On the left we show that all experiments apart from CDF (without Main Injector) are to some degree viable, that is, have errors less than 100% after 1 year running.

3. CONCLUSION

While absolute values shown above for individual experiments not even yet approved must remain suspect, the above representation does at least reveal some interesting - even anomalous - differences, and can be used to hone known parameters, and focus on areas which clearly need more work.

4. REFERENCES

[1] Paul Harrison, EPS Conference, Marseille, July 22nd 1993; Paul Harrison, B Physics Workshop, Liblice Castle, Czech Republic, November 1992.

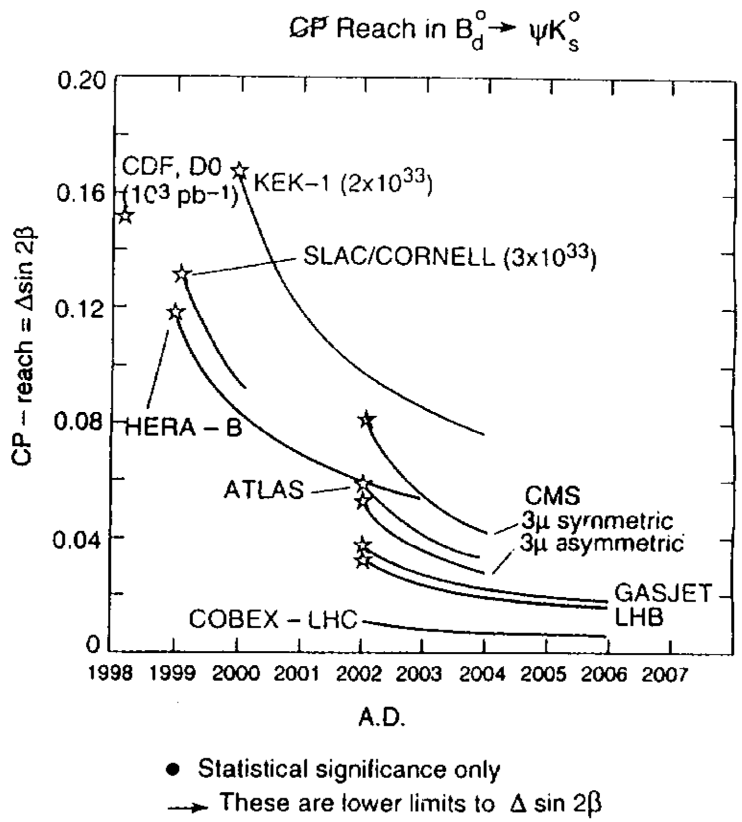

Figure 1. The Harrison plot: CP reach vs. year.

Graphical Estimate of Asymmetry Errors

$$\sigma(A) = \frac{1}{D \cdot \sqrt{N \cdot \varepsilon \cdot Br}}$$

$$\ln\left(\frac{1}{\sigma(A)}\right) = .5 \times \ln N - |.5 \times \ln \varepsilon| - |.5 \times \ln Br| - |\ln D|$$

since N>1 and ε, Br, D < 1

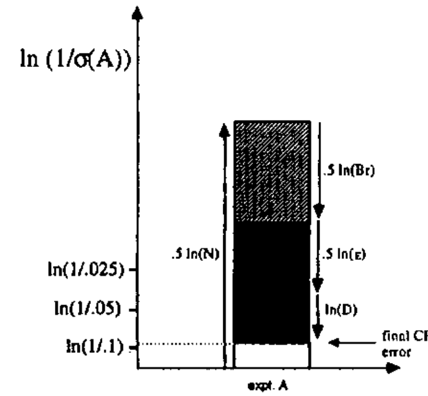

$$\ln(1/\delta A_{cp}) = \ln(D(\varepsilon\, Br\, N_{prod})^{1/2})$$

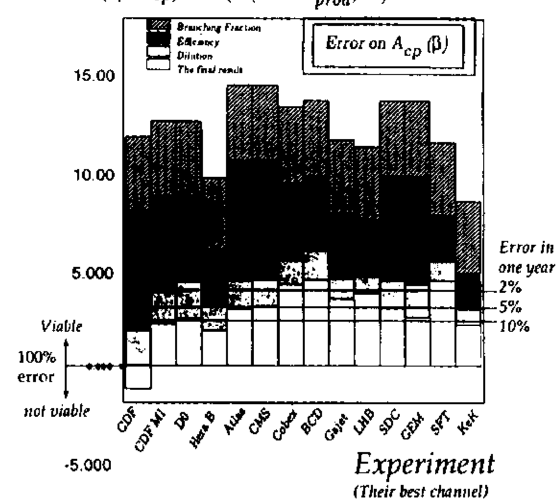

figure 2: The comparison for 14 Experiments in one year's running.

Reference Table for sin2β

Experiment	#B's in 1 year at 10^7 seconds	Decay modes J/ψKs	Tag modes	Eff., not icluding B(B→J/ψKs)	dilution factor	final error in sin2β for 1 year	reference
CDF 1A	$1.1\times10^{9}(2\times10^{30})$	μμππ	μ	3.7×10^{-6}	.165	>1	T.LeCompte
CDF III	$9.5\times10^{10}(1\times10^{32})$	μμππ	μ+e	4×10^{-5}	.2	.11	T.LeCompte
D0 upgrade	$9.5\times10^{10}(1\times10^{32})$	μμππ	μ	$1{,}24\times10^{-4}$	.15	.09	J.Wilcox
HERA-B	3.2×10^{8} (@820GeV)	(μμ+ee)ππ	μ+e+K	8.27×10^{-4} 2.95×10^{-3}	.38 .28	.23 .16	T.Lohse
ATLAS	$4\times10^{12}(1\times10^{33})$	(μμ+ee)ππ	μ	3.14×10^{-6}	.24	.06	P.Eerola
CMS	$4\times10^{12}(1\times10^{33})$	μμππ	μ	3.7×10^{-6}	.25	.046	J. Hassard
COBEX	$4\times10^{11}(1\times10^{32})$	(μμ+ee)ππ	μ	.0002489	.3	.016	Proposal
BCD	$8\times10^{11}(1\times10^{32})$	(μμ+ee)ππ	μ+e+K	3.3×10^{-5} 3.6×10^{-4}	.17 .22	.051 .012	K.McDonald
GAJET	1.6×10^{10}	(μμ+ee)ππ	μ+e+K	0.001	.36	.031	L.Camilleri
LHB	0.8×10^{10}	(μμ+ee)ππ	μ	0.0025	.427	.023	L.Camilleri
SDC	$8\times10^{11}(1\times10^{32})$	μμππ	μ	1.68×10^{-5}	.24	.051	D.Coupal
GEM	$8\times10^{11}(1\times10^{32})$	μμππ	μ+e	1.175×10^{-5}	.18	.081	R.Frey
SFT	1.28×10^{10}	(μμ+ee)ππ	μ+e+K	.008	.36	.012	S.Conetti
KEK	$3\times10^{7}(3\times10^{33})$	(μμ+ee)ππ	μ+e+K	.02434	.4346	.12(.09*)	Y.Sakai

B(B→J/ψKs)=5×10^{-4}
σ(bb)=1000μb(SSC),500μb(LHC),50x2.5μb(CDF,CDFIII&D0),1μb(FT-LHC),1.14nb(Υ(4s).
* including $\pi^\circ\pi^\circ$ and K_L

PROBING BETA

Boris Kayser
Division of Physics, National Science Foundation
Washington, DC 20550 USA

The angle β of the unitarity triangle may be measured by studying CP violation in the decay $B_d \to \psi + K_S^0$. However, to test the Standard Model (SM) of CP violation, one would like to do more than merely *measure* β. Rather, one would like to measure it *in a variety of decay modes* which differ at the quark level, but which, if the SM is correct, all yield this same angle. Do these different decay modes actually yield the same angle, as predicted?

From the standpoint of testing the SM of CP violation, decay modes which are identical at the quark level may be considered to be equivalent, even if they involve different hadrons. Results on β from equivalent decay modes may be combined to improve the statistics.

In this note we explain which B decay modes probe β, and identify several such modes which might be amenable to experimental study. Among these are modes which differ at the quark level, so that their results can be *compared* to test the SM, and ones which are identical at the quark level, so that their results can be *combined* to improve statistics.

In the Wolfenstein approximation[1] to the Cabibbo-Kobayashi-Maskawa (CKM) matrix V, the only elements which are not real are V_{td} and V_{ub}. In this approximation, the angles α, β, and γ of the unitarity triangle are given by

$$\begin{aligned} \alpha &= \pi + \arg(V_{td}) + \arg(V_{ub}) \\ \beta &= -\arg(V_{td}) \\ \gamma &= -\arg(V_{ub}). \end{aligned} \tag{1}$$

Thus, in this approximation, to experimentally probe β is to probe the phase of V_{td}.

As is well known, the B decays which promise to provide the cleanest information on phases in the CKM matrix are those of the neutral B mesons, B_d and B_s. Consider the decay of a neutral B born as a pure B_q, q = d or s, into a final state f that can come either from a pure B_q or from a pure $\overline{B_q}$. The B_q can decay to f directly, or, taking advantage of B-$\overline{B}$ mixing, it can transform itself into a $\overline{B_q}$ which then decays to f. The CP violation in the decay of the initially pure B_q to f probes the relative CKM phase of the amplitudes for these two decay paths. That is, it probes

$$\text{CKM Phase}\left[\frac{A(B_q \to f)}{A(B_q \to \overline{B}_q)^* A(\overline{B}_q \to f)}\right] , \tag{2}$$

where A stands for amplitude.

In the Wolfenstein approximation, the CKM phase of $A(B_d \to \overline{B}_d)$ is

$$\arg(V_{td}/V_{td}^*) = -2\beta. \tag{3}$$

Thus, from (2), we can probe β by studying B_d decays in which the CKM elements occurring in the decay amplitudes $A(B_d \to f)$ and $A(\overline{B}_d \to f)$ are real. In the Wolfenstein approximation, these CKM elements will be real when, at the quark level, the B_d decay is dominated by a single tree diagram involving one of the processes

$$\overline{b} \to \overline{c} + \begin{cases} c\overline{d} \\ c\overline{s} \\ u\overline{d} \\ u\overline{s} \end{cases} , \tag{4}$$

and the $\overline{B}_d$ decay is dominated by the CP-conjugate diagram. Thus, to probe β, we need to find B_d decays which are hadronic embodiments of the quark processes (4), and which have reasonable branching ratios. As we shall discuss, information on β can be extracted even from decays which do not yield CP eigenstates. However, if a final state f is to be useful, then the amplitudes $A(B_d \to f)$ and $A(B_d \to \overline{B}_d)^* A(\overline{B}_d \to f)$, whose interference will probe β, should be of comparable size so that the interference is large. Since $|A(B_d \to \overline{B}_d)| = 1$,[2] this means that $A(B_d \to f)$ and $A(\overline{B}_d \to f)$ should be of comparable size. In addition, $A(B_d \to f)$ must not contain significant contributions from penguin diagrams. For, unlike the tree diagrams for the processes (4), a penguin diagram can involve one of the non-real CKM elements V_{td} and V_{ub}.

In Table 1 we list B_d decays produced largely by tree diagrams for the quark-level processes (4), together with crude estimates of their branching ratios. Each listed estimate is meant to be the branching ratio for a typical decay in the collection of decays listed in the given row of the Table. The estimate was obtained by relating the decay of interest to another decay whose branching ratio is already known. In the Table, K^o_{CP} stands for a K^o_S or a K^o_L. The symbol K^{*o}_{CP} stands for a K^{*o} which is required to decay to $\pi^o K^o_S$ or to $\pi^o K^o_L$. By D^o_{CP} we mean a neutral D which is required to decay to a CP eigenstate, such as K^+K^- or $\pi^+\pi^-$. (One pays a price of a factor of ~100 in the overall branching ratio for the B_d decay by imposing this requirement.) Finally, by D^{*o}_{CP} we mean a neutral D^* which is required to decay to $\pi^o D^o_{CP}$. Table 1 lists only final states f for which, as desired, the amplitudes $A(B_d \to f)$ and $A(\overline{B}_d \to f)$ are not only both nonvanishing but are of comparable magnitude.

Table 1. Decays of beauty mesons born as pure B_d that probe β. See text for explanation.

Quark Process	Hadronic Processes	Rough Branching Ratio	Penguins Worrisome?
$\overline{b} \to \overline{c} + c\overline{d}$	$B_d \to D^+D^-, D^{*\pm}D^{\mp}, D^{*+}D^{*-}$	6 x 10^{-4}	Perhaps As in $B_d \to \pi^+\pi^-$
"	$B_d \to (\psi, \psi', \eta_c, \text{ or } \chi_c) + (\rho^o \text{ or } \pi^o)$	2 x 10^{-5}	Perhaps
$\overline{b} \to \overline{c} + c\overline{s}$	$B_d \to (\psi, \psi', \eta_c, \text{ or } \chi_c) + K^{(*)o}_{CP}$	3 x 10^{-4}	No
$\overline{b} \to \overline{c} + u\overline{d}$	$B_d \to D^{(*)o}_{CP} + (\rho^o \text{ or } \pi^o)$	10^{-4}	No

Among the decays in Table 1, those to D^+D^-, $D^{*\pm}D^{\mp}$, $D^{*+}D^{*-}$, ψK^o_S, and ψK^{*o}_S have relatively advantageous branching ratios and might be amenable to experimental study. (By K^{*o}_S we mean a K^{*o} which decays to $\pi^o K^o_S$.) Since the $D^{(*)}\overline{D}^{(*)}$ decay modes differ at the quark level from the $\psi K^{(*)o}_S$ modes, it would be desirable to study both of them in order to test the SM. Results from the $D^+D^-, D^{*\pm}D^{\mp}$, and $D^{*+}D^{*-}$ modes may be combined to improve statistics, as may those from the ψK^o_S and ψK^{*o}_S modes.

To extract information on β from the decay $B_d \to D^+D^-$ or the decay $B_d \to \psi K^o_S$, either of which yields a CP eigenstate, one would use the usual method for obtaining CKM phase information from the time dependence of the decay of a neutral B to a CP eigenstate.[3] To extract information from $B_d \to D^{*+}D^{*-}$ or $B_d \to \psi K^{*o}_S$, in either of which the final state may not be a CP eigenstate because it may be a mixture of partial waves, one can use angular distribution measurements to disentangle the partial waves.[4,5] To extract information from $B_d \to D^{*+}D^-$ and $B_d \to D^{*-}D^+$, where the final states are not CP eigenstates because of their particle content, one would use the technique[6] for extracting clean CKM phase information from final states of this kind.

To be useful, the decay to $D^{*+}D^-$ of an initially pure B_d must involve interfering amplitudes $A(B_d \to D^{*+}D^-)$ and $A(\overline{B}_d \to D^{*+}D^-)$ which are of comparable magnitude. A general argument[7,2] suggests that these amplitudes *are* of comparable magnitude. Indeed, according to the heavy quark effective theory (HQET),[8] we have[9]

$$A(B_d \to D^{*+}D^-) = -A(B_d \to D^{*-}D^+) \ . \tag{5}$$

But, by CP in the approximation where penguin diagrams are neglected,

$$A(B_d \to D^{*-}D^+) = -A(\overline{B}_d \to D^{*+}D^-) \ . \tag{6}$$

Thus, according to HQET, $A(B_d \to D^{*+}D^-)$ and $A(\overline{B}_d \to D^{*+}D^-)$ are of *equal* magnitude.[10,11] Moreover, the equality (5) implies that the decays $B_d \to D^{*\pm} D^{\mp}$ actually yield a CP eigenstate: $\frac{1}{\sqrt{2}}\left| D^{*+} D^- - D^{*-} D^+ \right\rangle$.[9] If this is true, then these decays enjoy many of the advantages of other decays to CP eigenstates as probes of β.[9]

Interestingly, according to HQET, the decay $B_d \to D^{*+}D^{*-}$ also yields a CP eigenstate (at least to a good approximation).[11,9] If this is true, then this decay also enjoys many of the advantages of any decay to a CP eigenstate.

Again interestingly, a naive quark picture suggests that $B_d \to \psi K_S^{*o}$ yields a CP eigenstate as well; namely, the state in which the ψ and K_S^{*o} have helicity zero.[4] Here, there is already experimental evidence that this CP eigenstate is at least the dominant component of the final state.[12,13] Thus, $B_d \to \psi K_S^{*o}$ is yet another rather promising probe of β.[14]

In conclusion, there are a number of decay modes which appear to be potentially useful probes of β. These modes merit consideration, both with a view to testing the Standard Model, and in order to improve the statistical accuracy of the measurement of β.

REFERENCES

1. L. Wolfenstein, *Phys. Rev. Lett.* **51**, 1945 (1983).
2. B. Kayser, *Proceedings of the Second International Symposium on Particles, Strings, and Cosmology,* edited by P. Nath and S. Reucroft (World Scientific, Singapore, 1992) p. 837.
3. See, for example, I. Bigi, V. Khoze, A. Sanda and N. Uraltsev, *CP Violation*, edited by C. Jarlskog (World Scientific, Singapore, 1989) p. 175.
4. B. Kayser, M. Kuroda, R. Peccei, and A. Sanda, *Phys. Lett.* **B237**, 508 (1990).
5. I. Dunietz, H. Lipkin. H. Quinn, A. Snyder, and W. Toki, *Phys. Rev.* D**43**, 2193 (1991).
6. R. Aleksan, I. Dunietz, B. Kayser, and F. Le Diberder, *Nucl. Phys.* **B361**, 141 (1991). See also D. London, and R. Aleksan, B. Kayser, and D. London, in these Proceedings.
7. R. Aleksan, I. Dunietz, B. Kayser, and F. Le Diberder, Ref. 6.
8. N. Isgur and M. Wise, *Phys. Lett.* **B232**, 113 (1989).
9. R. Aleksan, A. Le Yaouanc, L. Oliver, O. Pène, and J.-C. Raynal, Orsay preprint LPTHE 93/18. This reference also predicts branching ratios for $B_d \to D^{(*)}\overline{D}^{(*)}$ larger than our own crude estimates.
10. T. Mannel, W. Roberts, and Z. Ryzak, *Phys. Lett.* **B248**, 392 (1990).
11. J. Rosner, *Phys. Rev.* D **42**, 3732 (1990). This reference also predicts the branching ratio for $B_d \to D^{*+}D^{*-}$ to be 6×10^{-4}.
12. M. Danilov, *Proceedings of the Joint International Lepton-Photon Symposium and Europhysics Conference on High Energy Physics*, edited by S. Hegarty, K. Potter, and E. Quercigh (World Scientific, Singapore, 1992) Vol. **2**, p. 333.
13. S. Ball, *The Fermilab Meeting, DPF 92*, edited by C. Albright, P. Kasper, R. Raja, and J. Yoh (World Scientific, Singapore, 1993) p. 533.
14. The feasibility of studying $B_d \to \psi K_S^{*o}$ at a hadron accelerator is discussed by W. Toki in these Proceedings.

A FIXED TARGET B EXPERIMENT AT THE HERA PROTON RING

THOMAS LOHSE

MPI für Kernphysik, 69029 Heidelberg, Germany

1. Introduction

Amongst the multitude of proposed fixed target B experiments at proton machines, the HERA B detector is in several ways unique: Firstly, it is the only experiment for which the machine already exists and would be continuously available with peak luminosity for many years. Secondly, it would have to operate at very low center of mass energies, slightly above 40 GeV, where the B cross section of 10 to 20 nb is 6 orders of magnitude smaller than that of normal inelastic events. It is therefore the first but also the most challenging fixed target B experiment dedicated to the phenomenon of CP violation. At the same time it has to be regarded as an ideal test-ground to gain experience for future more sophisticated experiments at the large machines.

The project will be briefly described in this article. More details can be found in references [1, 2].

2. Detector

The detector is sketched in Fig. 1. It is a single-stage spectrometer of 22 m length with an angular acceptance of 300 mrad horizontally and 130 mrad vertically.

The target consists of a set of wires grouped around the beam. Interactions are produced by collisions of beam halo protons with the wires. This technique allows to reach high rates without significantly reducing the beam lifetimes and the e–p luminosity of HERA. Preliminary beam tests indicate [3] that the required interaction rates of 20 to 40 MHz are achievable once HERA runs with design currents.

The target is followed by a moveable silicon vertex detector of 2 m length. The device is mounted in an evacuated target tank and is planned to be operated in 1 cm distance to the beam during data taking. At high momenta it provides impact parameter measurements with resolutions around 20 to 30 μm. The longitudinal vertex resolution is better than 400 μm. The inner edge of the detector will have to stand considerable radiation doses; 10 Mrad per year are expected at full luminosity. The detector will be replaced in the long machine shutdown once per year. If the radiation hardness of the device proves insufficient, the detector might (at least initially) be operated at a slightly larger distance to the beam.

The main tracking chambers inside the magnet are followed by a TRD tracker and further tracking chambers behind the magnet. The latter are vital for the first level trigger. Pion/kaon/proton separation, necessary for kaon tagging, is provided by a RICH counter. Leptons are detected in the SPACAL electromagnetic calorimeter and the muon filter.

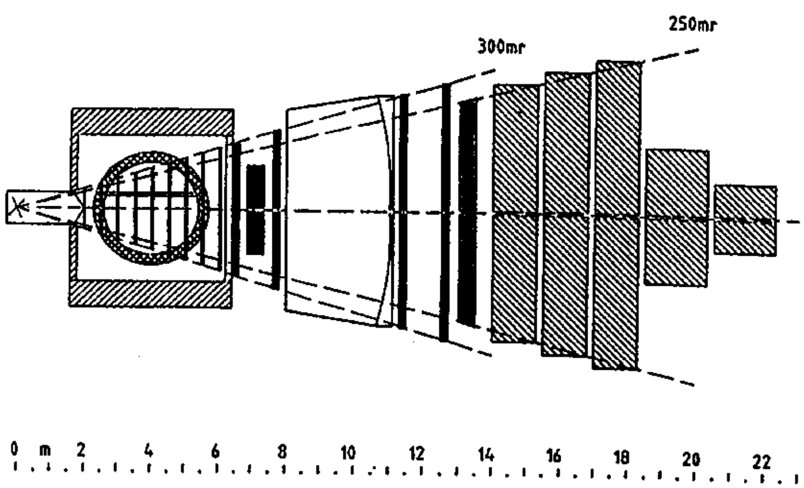

Figure 1: *Sketch of the HERA B detector.*

3. First Level Trigger

Given the enormous background of inelastic events and from charm production, first level triggering at the HERA experiment deserves special attention. We require a reduction of the 20 to 40 MHz event rate[1] by three orders of magnitude while keeping more than 50% of the signal.

The trigger is based on the invariant mass of lepton pairs from J/Ψ decays. Electron candidates are given by energetic clusters in the calorimeter, muon candidates by hit coincidences in the muon chambers. Electron candidates might be further restricted by using fast information of the TRD. These candidates start a track search procedure in four dedicated tracking chambers behind the magnet. Processors mapped onto small regions of these chambers with memory boards containing the local wire information exchange current track parameters via short messages. A processor receiving a message checks in its wire memory whether a hit is found in the predicted region and, if successful, updates the track information and issues a new message to the next relevant processor. Since no detector raw data information is moved around, this strategy avoids transfer of huge amounts of data. Successful track candidates are finally combined in processors which compute the invariant masses from the track parameters. If an electron or muon pair exceeds a mass of 2.5 GeV the trigger fires.

The trigger algorithm has been tested by software simulation. The trigger efficiency, folded with detector acceptance and energy cuts was found to be 47% for $J/\Psi \to e^+e^-$ and 60% for $J/\Psi \to \mu^+\mu^-$ with trigger rates around 10 to 30 kHz.

[1]The HERA bunch crossing rate is 10 MHz. The detector therefore has to handle several simultaneous interactions for every bunch crossing, the vertices of which are distributed over the targets.

A preliminary hardware implementation has been designed and tested by circuit simulations. The latency of the trigger ranges from 5 to 8 μs which has to be compared to the upper limit of 12.3 μs for 128 element front-end pipelines and a 96 ns bunch crossing time.

4. CP Reach

Because of lack of space the sensitivity of the detector is summarized in form of two tables. Details can be fiound in [1].

Table 1 shows the relevant factors for the rate estimations (from [1]). Numbers are given

Table 1: *Rate estimates for $B^0 \to J/\psi K_s$.*

$b\bar{b}$ production rate	40 s^{-1} for p_{beam} = 820 GeV (70 s^{-1} for p_{beam} = 1000 GeV)
$b\bar{b} \to b\bar{d}$	0.8
$B^0 \to J/\psi K^0_s$	$4 \cdot 10^{-4}$
$\mathrm{Br}(J/\psi \to \ell^+\ell^-) \cdot \mathrm{Br}(K^0_s \to \pi^+\pi^-)$	0.1
Average geometrical and reconstruction efficiency	0.33
Trigger efficiency	0.7
Lepton quality cuts	0.75
Vertex cut	0.50
Kinematical cuts	0.65
15000 h running time	$5.4 \cdot 10^7$ s
Number of events	3900 for p_{beam} = 820 GeV (6800 for p_{beam} = 1000 GeV)

for the nominal HERA energy of 820 GeV and the maximum reachable energy of 1 TeV. The experiment is assumed to run for $5.4 \cdot 10^7$s (corresponding to five "snowmass years"). It should be noted that unlike collider experiments, where the luminosity decreases during the run and where the average luminosity is well below the peak luminosity, the proposed experiment is designed to operate throughout a run at a constant trigger rate, controlled by the distances of the target wires to the beam. The expected number of B events with a decay $B^0 \to J/\Psi K^0_s$ after all cuts is about 3900 for the 820 GeV beam, and 6800 for the 1 TeV beam.

To measure CP asymmetries, the initial flavor of the B^0 under study has to be determined by tagging the flavor of the second B in the event. We considered only two single-particle tags, namely kaons and high-p_t leptons. Additional tags, such as charge counting at a secondary vertex, are conceivable and may serve to enhance the tagging efficiency further.

Various cuts have to be applied on the tagging tracks in order to optimize the quality of the tagging. They are summarized together with the resulting tagging efficiencies in Table 2. Kaon tags are more frequent than lepton tags but are less clean and therefore more strongly diluted. The statistical precision for the measurement in $\sin 2\beta$ is therefore comparable for the two tags. Combining lepton and kaon tags results in $\Delta \sin 2\beta = 0.065$ for an 820 GeV proton beam, and $\Delta \sin 2\beta = 0.050$ for a 1000 GeV beam.

Table 2: *Tagging efficiencies and dilution factors.*

	Lepton tag	Kaon tag
Cuts in impact parameter	none	$\sigma > 2$ S.D. $\sigma < 1$ mm
Cuts in momentum	$p > 5$ GeV/c $p > 0.7\mathrm{GeV/c} \cdot \theta^{-0.85}$ $p_t > 1$ GeV/c	$p > 4.5$ GeV/c $p < 50$ GeV
Geometrical acceptance	82%	83%
Detection efficiency after cuts	55%	55%
Probability c to detect correct sign tag from B^0 or B^+ (incl. mixing)	9.6%	24.7%
Probability w to detect wrong-sign tag from B^0 or B^+ (incl. mixing)	2.0%	5.6%
Probability f to detect fake tag	3.1%	22.1%
Total tagging efficiency $c + w + f$	14.7%	52.4%
Tagging dilution $(c - w)/(c + w + f)$	0.52	0.36
Number of tagged events (for $p_{beam} = 820$ GeV/c)	570	2040
Error in $\sin 2\beta$	0.11	0.08
Combined error in $\sin 2\beta$	0.065	

References

[1] H. Albrecht et al., *An Experiment to Study CP Violation in the B System Using an Internal Target at the HERA Proton Ring*, Letter of Intent, **DESY-PRC 92/04** (1992).

[2] H. Albrecht et al., *An Experiment to Study CP Violation in the B System Using an Internal Target at the HERA Proton Ring*, Progress Report, **DESY-PRC 93/04** (1993).

[3] T. Lohse, *Test of an Internal Wire Target at the HERA Proton Ring*, Contribution to the Machine Interface working group.

Measuring the Angle β in $B_d \to D^*\bar{D}^*$ Decays at the SFT

T.J. Lawry, S. Conetti, G. Corti
Physics Dept., U. of Virginia, McCormick Rd.
Charlottesville, Va., 22901 USA

1. INTRODUCTION

Even though the most popular reaction to measure the angle β is without any doubt the decay $B \to J/\psi K_s^0$, it would be extremely useful to achieve an independent measurement exploiting some different decay mode. It has been suggested[1] that one possibility is given by the decays $B \to D\overline{D}$ or $B \to D^*\overline{D}^*$. In the following we discuss the capability of the SFT[2] in reconstructing such decay modes; as discussed below, the live target environment is particularly suitable in recognizing the unique signatures of the modes under consideration. The $D^*\bar{D}^{*-}$ mode is expected to have a larger branching ratio than $D\bar{D}$ and provides a more striking signature.

We consider only the decay chain $B_d \to D^{*+}D^{*-}, D^{*\pm} \to \pi^{\pm}D^0$. We require one neutral D to decay to all charged tracks, we reconstruct the other D from the missing P_T and the D and D^* mass contraints.

2. ACCEPTANCE

The topology of the decay chain is two soft charged pions from the B_d decay vertex and two D^0 decay vertices. For the $D^* \to \pi^{\pm}D^0$ decays, the median opening angle in the lab between the π and the D^0 is 1.4 mrad. The median distance of closest approach of the pion to the D^0 vertex is 19 microns, so each pion will appear to pass through or very near a 2 or 4 prong vertex. The kinematic limits on the $\pi^+\pi^-$ mass are 313.6 MeV/c^2 and 448.5 MeV/c^2. We take the initial signature for the decay $B_d \to D^{*+}D^{*-}$ to be a pair of tracks with mass in the range 310-450 MeV/c^2.

We require both pions to be in the spectrometer acceptance of 2-75 mrad, and to have $E_\pi > 5\ GeV$, which gives an acceptance of 55.2%.

To reconstruct the B_d, we require that for one of the D^0s all of the daughter tracks are charged, have energies greater than 5 GeV, and are in the spectrometer acceptance. We make no requirement on the other D^0. The sum of the branching ratios for D^0 decay to two or four charged particles (and no neutral particles)[3] is 12.8 %, which gives an acceptance of 24.0% since there are two D^0s in the event. The probability for all the charged daughters of the D^0 to be in the spectrometer acceptance is 82.1%, assuming the π from the D^* is in the acceptance.

The reconstruction efficiency in the spectrometer[4] is 0.95 per track. Since we must detect the two pions from the D^*'s and the two or four daughters of the D^0, the tracking efficiency is $(0.95)^4(.33 + .67(0.95)^2) = 0.761$.

We reconstruct the other D^0 by requiring that it satisfies the D^0 and D^* mass constraints and that the momentum perpendicular to the flight path of the B_d be zero. To account for the spectrometer resolution, the momenta of the charged tracks were smeared using the formula $\sigma_p/p = 0.0009+0.00000841p$ and the vertices using[5] $\sigma_x = 3\mu$, $\sigma_y = 4\mu$, $\sigma_z = 58\mu$ for the primary vertex and $\sigma_x = 6\mu$, $\sigma_y = 8\mu$, $\sigma_z = 300\mu$ for the B_d decay vertex. The resulting invariant mass distribution of the $D^{*+}D^{*-}$ is shown in Figure 1. Without the vertex error, the mass peak would have a σ of 30 MeV/c^2. The mass range $5.1 - 5.4$ GeV/c^2 contains 62.6% of the B_d.

The final acceptance is then

$$(0.55)^2(0.552)(0.240)(0.821)(0.626)(0.761) = 0.0156$$

The 0.55 is the branching ratio for $D^{*\pm} \to \pi^\pm D^0$. The other numbers are given above.

3. SAMPLE SIZE

In one year of running at the SFT[6] we expect to have 1.6×10^{10} $B - \bar{B}$ events. We expect that 9.6% will have a Level II high P_T lepton trigger, 85% will be successfully tagged by the lepton[7], and in 38% of the triggered events the other B will be a B_d. Given our acceptance of 1.56% we expect $7.7 \times 10^6 \times BR$ events per year. The decay $B_d \to D^{*+}D^{*-}$ will be Cabibbo suppressed by a factor of about 20 relative to $B_d \to D^{*+}D_S^-$ which has branching ratio $1.6 \pm 1.1\%$. There should also be a spin enhancement of three. Therefore we expect a branching ratio $\approx 2 \times 10^{-3}$ and a total sample of 15,400 events per year.

4. BACKGROUNDS

We consider three background decay modes, $B_d \to D^{*+}D^{*-}K^0$, $B_d \to D^{*+}D^{*-}\pi^0$, and $B_d \to D^{*+}\bar{D}^0\pi^-$, $\bar{D}^0\pi^-$ nonresonant. We wish to find their acceptances relative to $B_d \to D^{*+}D^{*-}$.

To reduce the background we make the mass cut $0.31\ GeV/c^2 < M_{\pi\pi} < 0.45\ GeV/c^2$ on the pions from the D^* decay. We require $2.26\ GeV/c^2 < M_{D^*\pi} < 2.42\ GeV/c^2$ where the D^* is the one whose D^0 decays to all charged tracks, the π comes from the other D^*. These cuts do not remove any signal since they are outside the kinematic limits for $B_d \to D^{*+}D^{*-}$.

Figures 2 and 3 show the invariant mass distribution of the $\pi^+\pi^-$ and the $D^*\pi$ respectively. The solid line is the mass spectrum for $B_d \to D^{*+}D^{*-}$, the dashed line is the mass spectrum for $B_d \to D^{*+}\bar{D}^0\pi^-$, and the dotted line is the mass spectrum for $B_d \to D^{*+}D^{*-}K^0$.

The two mass cuts combined cut 93.2% of the K^0 decays, 76.4% of the π^0 decays, and 91.5% for the $D^0\pi$ nonresonant decays.

After requiring the mass of the reconstructed B_d to be in the range $5.1\ GeV/c^2 - 5.4\ GeV/c^2$, the final acceptance for $B_d \to D^{*+}D^{*-}K^0$ is only 2.0% of the acceptance for $B_d \to D^{*+}D^{*-}$. For $B_d \to D^{*+}D^{*-}\pi 0$ and $B_d \to D^{*+}\bar{D}^0\pi^-$ the acceptances are 10.5% and 6.1% respectively. The acceptance for the π^0 decay is larger than for the K^0 decay, but we expect the branching ratio to be larger for the K^0 decay since it is not Cabibbo suppressed.

Another background comes from triggered events with a secondary interaction which produces $D^{*+}D^{*-}$ and no detectable charged tracks. In the SFT target we expect 0.24 secondary interactions with energy greater than 100 GeV per triggered event[3]. Approximately one secondary interaction in a thousand produces charmed particles.

The rate of lepton triggers is the product of the interaction rate of 10^7 Hz and the Level I and Level II trigger supression factors[8] $(10^7)(1.6 + .44) \times 10^{-3}(0.1) = 2.04 \times 10^3$, where the 1.6 and the 0.44 refer to the electron and muon triggers respectively. Since $B - \bar{B}$ events are 6300 less common than minimum bias, the rate of $B - \bar{B}$ events with Level II lepton triggers is $(10^7)(1/6300)(0.096) = 1.52 \times 10^2$. So 1 in 13.5 Level II lepton triggers will be a due to a $B - \bar{B}$ event.

We assume that all $C - \bar{C}$ interactions produce D^*D^* and that one in four produce $D^{*+}D^{*-}$. Hence in 13,500 triggered events there are about $(13.5 \times 10^3)(10^{-3})(0.24)(.25) = 0.81$ with a secondary interaction which makes $D^{*+}D^{*-}$, and $(10^3)(2 \times 10^{-3})(0.38) = 0.76$ with $B_d \to D^{*+}D^{*-}$.

From PYTHIA simulations of π^-p interactions with $E_\pi = 1000$ GeV, 1.4% of $D^{*+}D^{*-}$ events have no detectable charged tracks. We consider a charged track to be detectable if its momentum is greater than 20 GeV/c and it falls within the spectrometer acceptance of 2-75 mrad. Both the momentum and angle cuts are very conservative since the silicon can detect charge tracks out to at least 250 mrad.

The acceptance of $C - \bar{C}$ background events relative to $B_d \to D^{*+}D^{*-}$ is 4.1% for the cuts on track energy, track angle, and mass of track pairs given above. Hence the ratio of $C - \bar{C}$ background events relative to $B_d \to D^{*+}D^{*-}$ is

$$(0.81/0.76)(0.014)(0.041) = 6.2 \times 10^{-4}$$

5. CONCLUSIONS

In one year of running at the SFT we expect 15,400 events $B_d \to D^{*+}D^{*-}, D^{*\pm} \to \pi^\pm D^0$ where the other B provides a high P_T lepton trigger and tag. The background is dominated by B_d decays and is of the order of ten percent. The error on the angle β for time independent measurements is $1/(D\sqrt{N})$ where D is the dilution factor and N is the number of observed decays[9]. Taking D = 3.45 from the average of lepton tags[10] we find the error on $\sin(2\beta)$ from one year of running is 0.028.

6. REFERENCES

1. B. Kayser, presentation at the Snowmass Workshop
2. B. Cox et. al., "The SFT: A Super Fixed Target Beauty Experiment at the SSC", these proceedings
3. Ref [2] Table 11
4. A.P. McManus et. al., "Tracking Considerations for Fixed Target Experiments at the SSC and the LHC", these proceedings
5. Ref [2] Table 3 and following
6. Ref [2] Section 4
7. Ref [2] Table 14
8. Ref [2] Table 12 and following
9. Ref [2] Section 3
10. Ref [2] Table 8

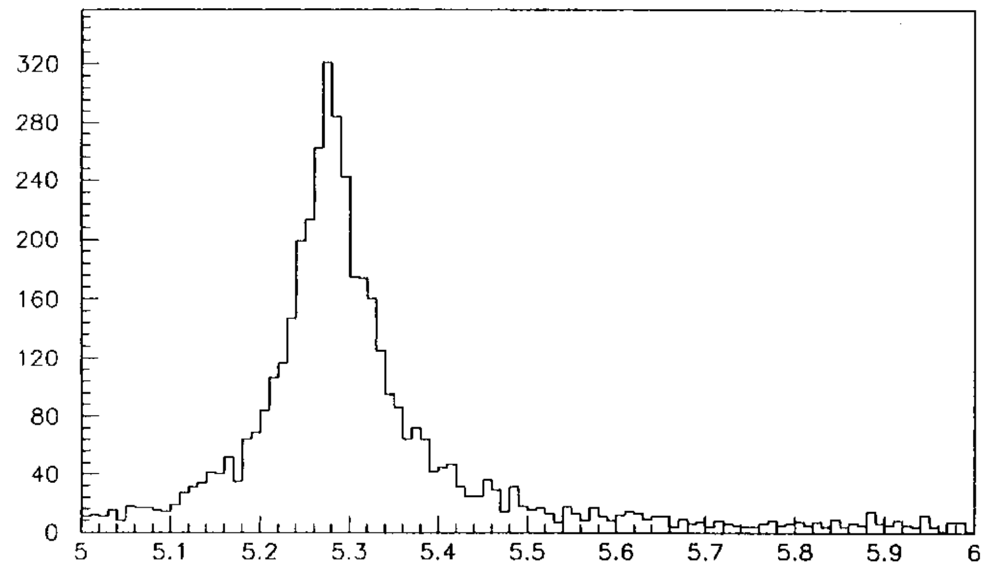

Fig. 1 Reconstructed B_d Mass

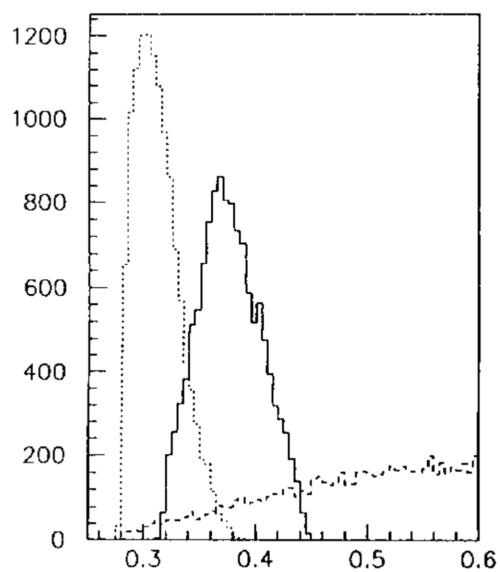

Fig. 2 $\pi^+\pi^-$ Mass from $B_d \to D^{*+}D^{*-}$

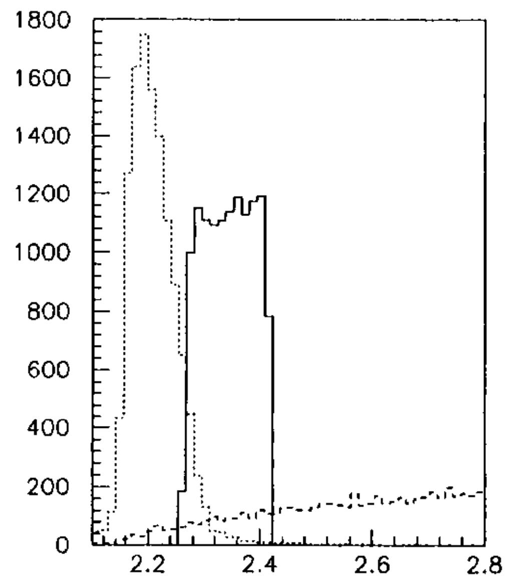

Fig. 3 πD^* Mass from $B_d \to D^{*+}D^{*-}$

MEASUREMENT OF CP-VIOLATION WITH THE GEM DETECTOR

HIROAKI YAMAMOTO

Lauritsen Laboratory, California Institute of Technology

Pasadena, CA 91125, USA

1. INTRODUCTION

In this note, the feasibility of measuring CP-violation in the B-meson system with the GEM detector[1] at SSC is described, using the decay mode $B_d \rightarrow J/\psi + K_S^0 \rightarrow \mu^+\mu^-\pi^+\pi^-$ for the β angle measurement. In Section 2, the signature of the signal is discussed. Section 3 is devoted to a description of the GEM performance, including the estimation of the backgrounds. The rate of the signal is discussed in Section 4, and the summary is given in Section 5. More details of this study are published in a separate paper.[2]

2. CP-VIOLATION SIGNATURE

CP violation is signalled by a difference of the branching ratios of B_d and $\overline{B}_d$ decaying into the same CP eigenstate $J/\psi + K_S^0$ in the production of $b-\bar{b}$ quark pairs in proton-proton collisions. The flavor of the B-meson can be determined by the sign of the decay lepton from the other B hadron. The error of the sin2β measurement can be expressed as

$$\delta(\sin 2\beta) \simeq \frac{1}{D\sqrt{\epsilon \cdot Br \cdot N_{prod}}} \tag{1}$$

where the parameters in this equation are summarized in Table 1.

One significant uncertainty in judging the feasibility of a CP violation signal measurement is the total production rate of $b - \bar{b}$ quark pairs. A big systematic error comes from theoretical and MC implementation uncertainties.[3,4,5] As is explained in Ref. 3, the comparison between the analytical and MC calculations is not straight forward.

The prediction of PYTHIA 5.6[6], with the CTEQ PDF set CTEQ1L[4], is used in the following calculations without an additional multiplicative factor. The three processes to produce $b - \bar{b}$ pairs, flavor production, shower and flavor excitation process, were simply added together assuming that the ambiguity due to the double counting is less important than other ambiguities.[7] The total cross section strongly depends on the choice of the minimum p_t of the produced partons, but the cross sections which pass the signal event selection are not. The total cross section in Table 1 was calculated using $p_{t_{min}} = 0$ for the flavor production and 10 GeV for the other processes.

Table 1. Parameters for sin2β measurement

Parameter	Description	Value
N_{prod}	Number of B_d, $\overline{B}_d$: $\int \mathcal{L}dt \cdot \sigma_{b\bar{b}} \cdot 2f_d$	9.3 $\times 10^{11}$
$\int \mathcal{L}dt$	int. luminosity per year at $\mathcal{L} = 10^{32}$ cm^{-2}sec^{-1}	1 fb^{-1}
$\sigma_{b\bar{b}}$	cross section for b $-$ $\bar{\text{b}}$ production	1.2 mb (Sec.2)
f_d	fraction of B_d mesons from b quark	0.39 (f_s=0.13,f_{baryon}=0.1)
Br	Branching faction of $B_d \to J/\psi + K^0_S$	0.032 $\times 10^{-2}$ (Ref. 8)
ϵ	Total detection efficiency : $\epsilon_{dec} \cdot \epsilon_{trig} \cdot \epsilon_{CP} \cdot \epsilon_{tag}$	2.2 $\times 10^{-6}$
ϵ_{dec}	$Br(J/\psi \to \mu^+\mu^-) \cdot Br(K^0_S \to \pi^+\pi^-)$	4.12 $\times 10^{-2}$
ϵ_{trig}	trigger efficiency	0.10 (Sec.4)
ϵ_{CP}	detect and reconstruct the signal	4.6 $\times 10^{-3}$ (Sec.3,4)
ϵ_{tag}	B flavor tagging using muons	0.11 (Sec.4)
D	Dilution factors : $d_{mix} \cdot d_{tag} \cdot d_{bg}$	0.27
d_{mix}	mixing of B_d prior to decay	0.47
d_{tag}	$= 1 - 2\times$W, incorrect flavor tagging	0.6 (Sec.4)
d_{bg}	$= \sqrt{S/(S+B)}$, backgrounds in the "signal"	0.95 (Sec.3)

The cross section using CTEQ1L was compared with that using the set 2 of the PDF by Morfin and Tung[9]. Although the total cross sections differ by a factor of 2, the cross sections passing the event selection differ only by 15%. This indicates how the cross section depends on the parametrization at small x, but the effect of the O(α_s^3) correction can be still large, and the predicted number of the signal can be off by a factor of 2.

Finally, note that PYTHIA was modified to include the correct longitudinal polarization of vector mesons decaying from B mesons to calculate the acceptance of J/ψ correctly.

3. GEM DETECTOR, PARTICLE PROPERTIES, AND BACKGROUNDS

The GEM detector performance was estimated using the MC GEMFAST[1] based on detailed GEANT simulation. The GEM detector includes a central tracker and a muon system covering $|\eta| \leq 2.5$ in a 0.8 T magnetic field. The central tracker consists of an inner silicon strip detector, and a barrel and two endcaps made by interpolating pad chambers. The silicon tracker is around 200 cm long and extends in radius from 10 to 35 cm. The muon momentum is reconstructed using the muon system measurement and the energy loss measured in the calorimeter, which is then combined with the measurement of the central tracker to improve the resolution at low momentum. The acceptance below 5 GeV is not well understood, but studies are in progress. The single muon trigger with a minimum p_t of 8 - 10 GeV at the origin is feasible.

The particle properties are summarized in Table 2. Both K^0_S and J/ψ were reconstructed by 1) combining a pair of particles with invariant mass requirements shown in the last column of Table 2, 2) applying the mass constraint fit, and 3) requiring the χ^2 of the constraint fit less than 5 and 20 respectively. The constraint fit improves the momentum resolution of K^0_S by a factor of 5. It is assumed that the secondary vertex can be reconstructed if those two tracks are well reconstructed, i.e., each track has at least 4 silicon hits and 6 IPC hits. This condition is almost equivalent to requiring that the K^0_S decays within a cylinder of radius ρ = 15 cm and half length z = 70 cm in the beam direction. The $M_{J/\psi K^0_S}$ distribution of the signal with and without mass constraint is shown in Figure 1. The efficiency of the signal below $p_t(B_d)$ = 20 GeV strongly depends on the muon efficiency at $p_t(\mu) \sim 5$ GeV.

Table 2. Particle Properties (Eff. includes all effects)

Particle	$\Delta p_t/p_t$ (%)	Efficiency	σ(mass) (MeV)	Particle Selection
π	$3.5 \oplus 0.115 \cdot p_t$	0.97		
μ	3 (p_t=5GeV) 2 ($p_t \geq$20GeV)	0.83		
J/ψ	1.5 (p_t=10GeV) 2 ($p_t \geq$30GeV)	0.55	77	$M_{\mu\mu}$ = 2.8 - 3.4 GeV $\chi^2 \leq 20$
K^0_S	2 (p_t=2GeV) 0.5 ($p_t \geq$6GeV)	0.6 (p_t=2GeV) 0.15 (p_t=15GeV)	8.3	$M_{\pi\pi}$ = 0.45 - 0.55 GeV $\chi^2 \leq 5$
B_d		0 (p_t=10GeV) 0.09 ($p_t \geq$20GeV)	24 (p_t=15GeV) 42 (p_t=35GeV)	$M_{J/\psi K^0_S}$= 5.2 - 5.36 GeV

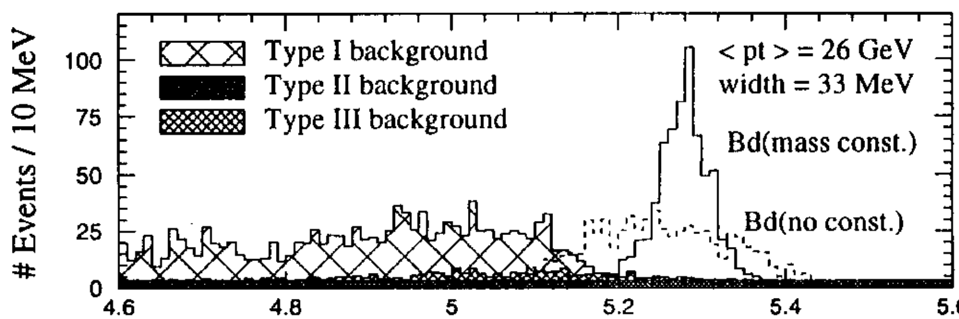

Figure 1. $M_{J/\psi K^0_S}$ (GeV) distribution

Three kinds of backgrounds were studied, which are summarized in Table 3. Type I backgrounds contain J/ψ and K^0_S decaying from a B hadron. Backgrounds involving ψ' and χ_{cJ} decays were also studied, and their contributions were negligibly small above $M_{J/\psi K^0_S}$= 5.18 GeV. Type II are combinatorial backgrounds of of 2μ's and a K^0_S in jets. The estimated backgrounds include 1) J/ψ from B hadron decay + K^0_S in the same jet (2.5%), 2) other J/ψ + X (2.5%) and 3) muon pairs in heavy quark jets (2.5%). Type III contains K^+ and π^- which are combined to form K^0_S. These backgrounds can be reduced by the requirement of a

Table 3. Backgrounds / Signal (%) in $M_{J/\psi K^0_S}$ = 5.2 to 5.36 GeV

	Background process	BR (%)	N_B/N_S (%)
I	$B_d \to J/\psi + K^{*0} \to J/\psi + K^0_S + \pi^0$	$Br(B_d \to J/\psi + K^{*0}) = 0.153^8$	0.3
	$B_u \to J/\psi + K^{*+} \to J/\psi + K^0_S + \pi^+$	$Br(B_d \to J/\psi + K^{*+}) = 0.153^8$	0.3
II	Combinatorial background	$Br(B \to J/\psi + X) = 1.09^8$	7.5
III	$B_d \to J/\psi + K^{*0} \to J/\psi + K^+ + \pi^-$	$Br(B_d \to J/\psi + K^{*0}) = 0.153^8$	2.4
	$B_d \to J/\psi + K^+ + \pi^-$ (non-resonant)	Br assumed = 0.153	0.6
	Total background		11

finite flight length of the K^0_S candidate, and though not simulated, Table 3 shows the result assuming the rejection by a factor of 20. These backgrounds are also shown in Figure 1.

4. SIGNAL SELECTION EFFICIENCIES AND DILUTION

The efficiencies to select the signal is summarized in Table 4. To clarify each effect, the calculation was done using PYTHIA, and the particle detection efficiencies were multiplied at the end. Among these efficiencies, the lower limit of the muon p_t coverage and the detection of the K^0_S secondary vertex are the major detector dependent factors. Table 4 also shows the efficiencies for different cases.

Including all the effects, the total efficiency to observe the signal is 5.4×10^{-10}, and

Table 4. Efficiency

Contribution	Acceptance Factor	Comment
Trigger μ $p_t \geq 8$GeV,$\lvert\eta\rvert \leq 2.5$	0.12	$\times 0.6$ if $p_t(\text{trig}) \geq 13$GeV
3μ's $p_t \geq 5$GeV,$\lvert\eta\rvert \leq 2.5$	0.039	$\times 1.7$ if $p_t(\text{threshold}) \geq 4$GeV
2π's $p_t \geq 0.5$GeV,$\lvert\eta\rvert \leq 2.5$	0.79	$\times 0.76$ if $p_t(\pi) \geq 1$GeV
$z(K^0_S\text{decay}) \leq 70$ cm	0.71	$\times 1.06$ if $z \leq 100$cm
$\rho(K^0_S\text{decay}) \geq 1$ cm	0.97	
$\rho(K^0_S\text{decay}) \leq 15$ cm	0.42	$\times 1.5$ if $\rho \leq 30$cm
Particle Efficiencies	0.43	$0.83(\mu)\cdot 0.66(J/\psi)\cdot 0.81(K^0_S)\cdot 0.96(M_{Bd})$
Sub total (Detector dep.)	4.6×10^{-4}	
$b \to \mu$ for flavor tagging	0.23	$2\cdot\epsilon_{tag}$ (including b and $\bar{b}$ decay)
$f_d \cdot Br(B_d \to J/\psi + K^0_S) \cdot \epsilon_{dec}$	5.1×10^{-6}	
Total	5.4×10^{-10}	650 evts / 1 fb^{-1}

the detector dependence is a factor of 2 to 3. As has been discussed before, the ambiguity of this number is a factor of 2 coming from the $O(\alpha_s^3)$ correction.

The cascade decay, $b \to c \to \mu + s$, gives the wrong sign for the flavor tagging. The fraction of tagging by this cascade muon is dependent on the p_t of the tagging muon, and is around 10% with $p_t(\mu)$ above 4 GeV. The contribution of decay muons from K and π and the punch through are negligible compared to other effects. Including the flavor oscillation, the wrong sign tagging fraction W in Table 1 was 0.2.

5. SUMMARY

Applying the mass constraint fits for J/ψ and K^0_S, the mass resolution of the B_d signal was improved by a factor of 2.5 to 33 MeV. With this resolution, the background fraction was around 11%.

Combining all these numbers in Equation (1), the error on $\sin 2\beta$ comes out to be

$$\delta(\sin 2\beta) \simeq \frac{1}{0.27\sqrt{650 \cdot T}} = \frac{0.15}{\sqrt{T}} \tag{2}$$

where T is the total luminosity in units of 1 fb^{-1}, i.e., 10^7 seconds at $\mathcal{L} = 10^{32}cm^{-2}sec^{-1}$.

6. ACKNOWLEDGMENTS

I would like to thank B. Barish and R-Y. Zhu for the support and encouragement for this study, and to thank F. Paige, J. Urheim, S. Mrenna and X. Shi for valuable discussions.

7. REFERENCES

1. GEM Collaboration, *GEM Technical Design Report*, **GEM TN-93-262** and **SSCL-SR-1219**, April 30, 1993.
2. H. Yamamoto, *Measurement of CP-violation using* $B_d \to J/\psi + K^0_S$ *decay mode with GEM Detector*, **GEM TN-93-457, CALT-68-1888**, Sep. 1993.
3. J. R. Cudell, O. Di Rosa, I. ten Have, A. Nisati, R. Odorico and T. Sjostrand, *Large Hadron Collider Workshop*, **CERN 90-10, ECFA 90-133** Vol-II p 164, Dec. 1990.
4. J. Botts, J. G. Morfin, J. F. Owens, J. Qui, W. K. Tung and H. Weerts, **MSUHEP-92-27, Fermilab-Pub-92/371, FSU-HEP-92-1225, ISU-NP-92-17.**
5. J. Collins and R. K. Ellis, Nucl. Phys. **B360**, 3 (1991); E. M. Levin, M. G. Ryskin, Yu. M. Shabelski, and A. G. Shuvaev, *DESY Reports Nos. 91-065 and 91-054* (unpublished); D. Kuebel, M. Pundurs, C.-P. Yuan, E. L. Berger, and F. E. Paige, *Phys. Rev.* **D43**, 767 (1991); P. Nason, S. Dawson, and R. K. Ellis, *Nucl. Phys.* **B303**, 607 (1988); **B327**, 49 (1989).
6. T. Sjostrand, *PYTHIA 5.6 and JETSET 7.3 Physics and Manual*, **CERN-TH.6488/92**, May 1992.
7. T. Sjostrand, private communication.
8. CLEO Collaboration, *Exclusive B Decays to Charm and Charmonium Final States* and *Inclusive Decays of B Mesons to J/ψand ψ'*, papers submitted to Lepton Photon Conference, Cornell, 1993.
9. J. G. Morfin and W. K. Tung, *Z. Phys.* **C52**, 13 (1991).

PROSPECTS FOR MEASURING CP VIOLATION IN SDC USING $B_d^0 \to \psi K_S^0$

DAVID P. COUPAL

*Superconducting Super Collider Laboratory,**
2550 Beckleymeade Avenue, Dallas, TX 75237

1. INTRODUCTION

This note describes results of a study of acceptance and backgrounds in the SDC detector for the neutral B meson decay $B_d^0 \to \psi K_S^0$. The aim here is to explore the possibility of observing CP violation in the B system – a significant physics measurement that may be possible at the SSC during the period of time when the accelerator is ramping up to design luminosity.

Section 2 describes the theoretical predictions for b$\bar{\text{b}}$ quark production at the SSC and the signal for CP violation in the B meson system. The following section outlines the cuts used to isolate $B_d^0 \to \psi K_S^0$ decays and presents the expected rates for signal and background. The next section discusses the sensitivity to CP violation parameters and the final section contains some additional comments.

2. b$\bar{\text{b}}$ PRODUCTION AND CP VIOLATION

Berger and Meng[1] present calculations of the b$\bar{\text{b}}$ production up to SSC energies based on next-to-leading-order QCD hard scattering cross sections.[2] At $\sqrt{s} = 40TeV$ they find a total cross section of 1-3 mb. A central detector like SDC would probably trigger on the p_t components of the b quark decay products (at least at level 1). We therefore limit the study to b quarks with p_t greater than 10 GeV/c, a region dominated by higher-order gluon splitting diagrams. Berger and Meng predict a cross section $\sigma(pp \to bX, p_T(b) > 10) = 80 - 170\mu b$ with resummation effects boosting it to around ~ 250 μb. This number will be used in the signal and background estimates that follow.

We look for CP violation in the decay of the neutral B_d^0 meson to the CP eigenstate ψK_S^0. The time-integrated asymmetry is:

$$A = \frac{N - \bar{N}}{N + \bar{N}} = \frac{x_d}{1 + x_d^2} sin2\beta \tag{2.1}$$

The sensitivity to $sin2\beta$ is diluted due to mixing ($x_d = \Delta m_d/\Gamma_d$ = degree of mixing in B_d^0). The above equations assume a knowledge of the initial state(B^0 or $\bar{B}^0$). In practice one uses the fact that b and $\bar{b}$ are pair produced and tags the flavor of the B meson by observing the sign of the lepton in the semileptonic decay of the other B. This demand introduces additional dilution due to mixing of the tagging B meson and mistagging contributions

* Operated by the Universities Research Association, Inc., for the U.S. Department of Energy under Contract No. DE-AC35-89ER40486.

from cascade decays or detector limitations (e.g. π or K decay, punchthrough, etc.). The measured asymmetry can be written $A_{meas} = (1-2\omega)A$ where ω is the fraction of wrong tags from mixing, cascade decays and detector effects .

The probability of mistagging from mixing of the tagging B meson is $\omega_{mix} = \alpha \times F_B$ where

$$\alpha = .5 \times f_s + f_d \times \frac{x_d^2}{2+2x_d^2} \tag{2.2}$$

is the probability of mixing, F_B is the relative fraction of tags from B semileptonic decays and f_s and f_d are the relative fractions of B_s^0 and B_d^0 production. B_s^0 is assumed to be fully mixed. For tags from cascade decays to charm, a wrong-sign tag is produced only if the initial B meson does not mix, otherwise a correct sign tag will result. Therefore the cascade term is $\omega_{cascade} = (1-\alpha)F_C$ where F_C is the fraction of tags from charm. Similarly, decay in flight and punchthrough backgrounds will have a random charge so $\omega_{decay} = F_D/2$ and $\omega_{punch} = F_P/2$ where F_D and F_P are the decay in flight and punchthrough fractions, respectively. Assuming relative fractions: $f_\pm : f_d : f_s : f_\Lambda = 0.38 : 0.38 : 0.14 : 0.10$ and $x_d = .7$, then $\alpha = .132$. An estimate of the tagging fractions (F_B,etc.) derived from a Monte Carlo simulation of the detector response is given in section 5.

3. CP VIOLATION SIGNAL

Bottom quark production via gluon splitting was simulated with ISAJET by generating lowest order parton-parton scattering to non-b partons and accepting only events in which a b quark with $p_t > 10 GeV/c$ is produced in the parton shower. This study used the decays $B_d^0 \to \psi K_S^0$, $\psi \to \mu^+\mu^-$and tagged the flavor using the semileptonic decay $B \to \mu + X$. K_S^0's were required to decay to $\pi^+\pi^-$. Half of the MC data sample selected on the $\bar{b}$ quark rather than the b. The mean p_t of the B_d^0 is ~12 GeV/c; the mean momentum is ~27 GeV/c.

Fig. 3.1 shows the SDC detector, with tracking, calorimetry and muon identification out to $|\eta| < 2.5$. For triggering and eliminating low p_t backgrounds such as π and K decay we impose a minimum p_t cut on the muons. For events with all 3 muons within $|\eta| < 2.5$, Fig. 3.2 shows the acceptance versus the minimum p_t cut for one, two or all three muons passing the cut. The acceptance for 3 muons with $p_t > 5$ is roughly equal to requiring 2 muons with $p_t > 10$ or one muon with $p_t > 20$. The effect of different combinations of p_t cuts is discussed further in section 5.

The B meson is reconstructed by first taking opposite sign muon pairs to reconstruct the J/ψ. A cut of $\pm 50 MeV/c^2$ around the J/ψ mass is used. The J/ψ are combined with K_S^0's in the event that satisfy $|\eta| < 2.5$ and $p_t > 1.0$ GeV/c. K_S^0 were required to decay within a cylinder of .33 meter radius (layer 6 of SDC silicon barrel) and .33 meter in z (layer 1 of forward disks) to insure efficient K_S^0 reconstruction. The $\pi^+\pi^-$ are not tracked to insure that they are within the η acceptance (though we do so for the parent K_S^0) so there will be a small additional loss in acceptance due to this approximation. Cuts on $p_t(K_S) > 1.0$ and $\cos(\Theta(J/\psi, K_S)) > .8$, where Θ is the angle between the J/ψ and the K_S^0, remove much of the background discussed in the next section.

The contributions to the total rate for $B_d^0 \to \psi K_S^0$ in SDC are given in Table 3.1. Assuming a run of 10^7 seconds at a luminosity of $10^{32} cm^{-2} sec^{-1}$(.1 × design) and a b quark production cross section of $\sigma(b\bar{b}, p_t(b) > 10 GeV/c) = 250 \mu b$, the above acceptance predicts a sample of 1050 events.

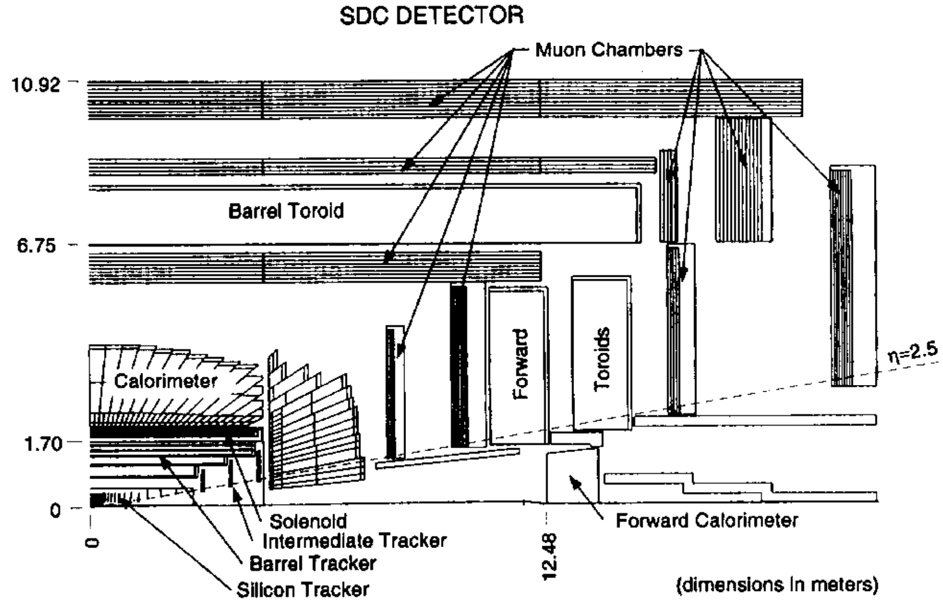

Figure 3.1: The SDC detector.

Table 3.1: Contributions to the rate for $B_d^0 \to \psi K_S^0$ detected in SDC

Contribution	Acceptance factor
$b \to \bar{B}_d^0$ or $\bar{b} \to B_d^0$	.38 × 2
$B_d^0 \to \psi K_S^0, \psi \to \mu^+\mu^-, K_S^0 \to \pi^+\pi^-$	1.9×10^{-5}
$b \to \mu + X$	.12
3μ's with $\eta < 2.5$	.46
3μ's with $p_t > 5$ GeV/c	.025
K_S^0 with $\eta < 2.5, p_t > 1$ GeV/c	.91
K_S^0 decaying within $r < 33cm, z < 33cm$	.50
$cos\Theta(J/\psi, K_S^0) > .8$	.90
Tracking and μ id efficiency	$(0.80)^3$
Total	4.2×10^{-9}

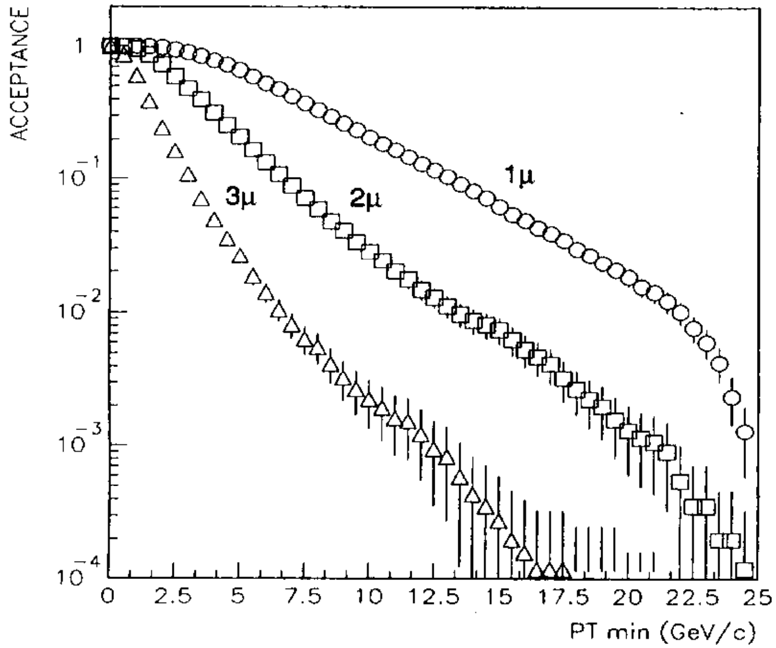

Figure 3.2: Acceptance versus minimum p_t after requiring that the 3 final state muons fall within $|\eta| < 2.5$ for one, two or three muons above p_t cut.

4. BACKGROUNDS

The large $b\bar{b}$ cross section at SSC (1-3 mb) implies of order 2×10^{12} produced $b\bar{b}$ pairs. Hence, even limiting consideration to backgrounds from b quarks, there is the computational problem of generating such a large number of events and one must make guesses of modes likely to contribute to the 3μ final state. The backgrounds considered in this study are:

1. Muons from semileptonic decay of b or $\bar{b}$.
2. Muons from semileptonic decay of c or $\bar{c}$.
3. Muons from π or K decay.
4. Inclusive J/ψ production in B meson decay together with a tagging muon from above sources.

Punchthrough is a possibly significant background not studied in this analysis.

Pion and kaon decay-in-flight backgrounds are evaluated by assigning a weight corresponding to the probability of decay to $\mu+X$ before the calorimetry, assigning the direction of the decay muon to be the same as the parent, the p_t to be .79 (.53) of parent π (K) and assuming that all such muons are identified in the muon system. The $p_t > 5$ cut eliminated much of the π and K decay background so we do not consider events where all 3 muons come from this background source. Given the 3 background muons, we apply the same reconstruction outlined in the previous section. To boost statistics, the background is measured with wider cuts around the J/ψ and B mass and scaled down to the smaller cuts.

A predominant background is inclusive J/ψ production by b quarks combined with other K_S^0's in the event. The branching ratio BR($B \to J/\psi + X$) is measured to be approximately 1%. Cuts on the K_S^0 momentum and angle relative to the J/ψ direction reduce this background significantly.

The number of background events is still limited by MC statistics. The 90% CL limit is 2500 events for one μ from b and two from charm or π/K decay, 600 events for one μ from b, one from $\bar{b}$ and one from charm or π/K decay and 300 events for inclusive J/ψ plus one other muon from b,c or π/K decay. Based on extrapolating the p_t distribution of μ's from charm or π/K decay the first background is probably small in spite of the size of the limit quoted.

5. IMPLICATIONS

Assuming 1050 $B_d^0 \to \psi K_S^0$ events in one year of running at $10^{32}\mathrm{cm}^{-2}\mathrm{sec}^{-1}$ and the background is indeed negligible, the expected error on $\sin 2\beta$ is:

$$\delta\,(sin2\beta) = \frac{1}{D}\frac{1}{\sqrt{N}} \tag{5.1}$$

where N is the number of events, D is the *dilution factor*

$$D = (1-2\omega)\frac{x_d}{1+x_d^2} \tag{5.2}$$

and ω is the mis-tagging probability. Monte Carlo simulations were used to get the tagging fractions from bottom and charm. π and K decay contributions to mistagging are assumed to be negligible. No estimate was done of punchthrough probabilities. The fraction of B tags is found to be $F_B = .77$ and for charm $F_C = .23$. Using these numbers in the equations of section 2, gives $\omega_{total} = .30$. The predicted error then is:

$$\delta\,(sin2\beta) = .16 \tag{5.3}$$

6. FURTHER COMMENTS

1. Referring to Fig. 3.2, the acceptance for requiring 3 μ's with $p_t > 5$ is about the same as requiring 2 μ's with $p_t > 10$ and one μ with $p_t > 20$, so there is some flexibility in how one might consider triggering on these events. Tracks with p_t around 5 GeV/c will barely penetrate the calorimeter+toroid. The case where one requires 2 μ's with $p_t > 10$ then adds a third μ with $p_t > 5$ reduces the total acceptance of Table 3.1 by 0.32. One μ with $p_t > 20$ and 2 μ's with $p_t > 5$ reduces it by 0.43. Finally requiring one μ with $p_t > 10$ and 2 μ's with $p_t > 5$ reduces it by 0.81. A J/ψ mass cut at level 2 could also be considered to significantly cut the rate into level 3.
2. Electrons have not been considered. If one can make similar cuts then the statistics increase by a factor of 4. The error then is $\delta(sin2\beta)_{e+\mu} = .08$. An isolation requirement on the electrons will likely reduce the acceptance but a study of this is yet to be done. In addition, SDC studies[3] indicate that a trigger of one muon with $p_t > 20$ is viable at a luminosity of 10^{33}. Given the acceptance loss mentioned above, a one-year run at 10^{33} will give a muon-only measurement error of $\delta(sin2\beta)_{\mu-only,10^{33}} = .08$
3. Also lacking in this study is any estimate of muon punchthrough backgrounds. Tools now exist for studying this possible source of background and mistagging.
4. No use was made of the displaced vertex of the B meson decays. It doesn't appear to be necessary for this clean decay mode but could be considered if the backgrounds increase (from punchthrough, for example). For SDC to measure other decay modes (for example, measuring sin2α through the decay mode $B_d^0 \to \pi^+\pi^-$ or sin2γ using $B_s^0 \to \rho K_S^0$) would likely require vertexing in the reconstruction and probably at the trigger level. This is left to future studies.

7. ACKNOWLEDGEMENTS

The author thanks F. Bird, A. Fridman, P. McBride and E. Wang for useful discussions.

8. REFERENCES

1. E.L. Berger and R. Meng, Phys. Rev. D46, 169 (1992).
2. P. Nason, S. Dawson, and R.K. Ellis, Nucl. Phys. B303, 607 (1988);**B327**,49 (1989).
3. Z.Y. Feng and T. Zhao, "Level 1 Muon Trigger Rate of SDC Central Muon Detector," SDC-93-506, June (1993).

RECONSTRUCTION OF $B_d^0 \to J/\psi K_S^0$ DECAYS IN THE ATLAS EXPERIMENT AT LHC

P. Eerola, N. Ellis, D. Froidevaux, S. Weinzierl

CERN, Geneva, Switzerland

A study of the feasibility for the ATLAS experiment at the Large Hadron Collider to measure the CP-violation parameter β by using the decay channel $B_d^0 \to J/\psi K_S^0$ is described. Both time-integrated and time-dependent analyses are presented, and estimates on the sensitivities of the measurements are updated.

1. INTRODUCTION

The angle β, one of the angles in the Cabibbo-Kobayashi-Maskawa complex triangle, can be measured from the asymmetry of the rates of the neutral B-decays $B_d^0 \to J/\psi K_S^0$ and $\bar{B}_d^0 \to J/\psi K_S^0$. B and $\bar{B}$ mesons are distinguished by the charge of the lepton originating from a semileptonic decay of the other b-quark in the event.

When the decay rates for B_d^0 and $\bar{B}_d^0$ mesons are integrated starting from time $t_0 = 0$, the observed asymmetry is

$$A^{\rm obs} = \frac{N_{\rm total}(J/\psi K_S^0 \ell^+) - N_{\rm total}(J/\psi K_S^0 \ell^-)}{N_{\rm total}(J/\psi K_S^0 \ell^+) + N_{\rm total}(J/\psi K_S^0 \ell^-)} = D_{\rm tag} D_{\rm back} \frac{x_d}{1+x_d^2} \sin 2\beta, \qquad (1)$$

where $N_{\rm total} = N_{\rm Signal} + N_{\rm Background}$. The statistical significance of the signal is reduced by wrong sign tags ($D_{\rm tag} = (N_{\rm right\,tags} - N_{\rm wrong\,tags}) / (N_{\rm right\,tags} + N_{\rm wrong\,tags})$), background ($D_{\rm back} = \sqrt{N_S/N_{\rm total}}$) and mixing ($x_d/(1+x_d^2)$), where $x_d = \Delta m/\Gamma \simeq 0.71 \pm 0.11$ [1]. Assuming $A^{\rm obs} << 1$, the expected error on $\sin 2\beta$ is

$$\delta(\sin 2\beta) \simeq \frac{1}{D_{\rm tag} D_{\rm back} x_d/(1+x_d^2)\sqrt{N_S}}, \qquad (2)$$

where $N_S = N_S(J/\psi K_S^0 \ell^+) + N_S(J/\psi K_S^0 \ell^-)$.

This note describes both time-integrated and time-dependent analyses of $\sin 2\beta$ with the ATLAS experiment at LHC, and is an update to previous estimates [2].

2. THE ATLAS DETECTOR

The ATLAS detector [3] is a general purpose pp collider detector with a tracking system situated in a 2 T solenoidal field, consisting of silicon detectors and a transition radiation straw tube tracker (TRT) in the central region, and microstrip gas chambers interspersed with TRT wheels in the forward part. The innermost radius of the tracking system is at 11.5 cm and the outer radius is at 1.10 m. The tracker length is 6.9 m, thus covering $|\eta| < 2.7$. The momentum resolution is expected to be $5 \cdot 10^{-4} p_T \oplus 1.2\%$, and the asymptotic impact parameter resolution 27 μm. The resolution in z at the point of closest approach is 40 μm.

Together with a lead-LAr electromagnetic calorimeter, the TRT provides electron identification down to energies of about 1 GeV. Muons are identified with the outer muon system, consisting of a superconducting air-core toroid magnet with three chamber superlayers.

Events containing b-quarks will be triggered with the muon trigger, based on coincidences in trigger chambers in the outer toroid magnet. The lowest feasible p_T threshold for a single muon trigger at low luminosity is about 6 GeV/c. $b\bar{b}$ events with the muon coming from primary b-decay are expected to dominate beyond a trigger threshold of about 5 GeV/c [4]. The ATLAS muon trigger is thus well optimized for detecting $b\bar{b}$ events and rejecting background. The luminosity was assumed to be the initial LHC luminosity of 10^{33} cm^{-2} s^{-1}, thus minimising pile-up effects. At this luminosity, the expected single muon trigger rate from b- and c-decays is about 3 kHz with a p_T threshold of 6 GeV/c, assuming a muon trigger pseudorapidity coverage of ± 1.6 corresponding to the barrel toroid. The second level trigger should reduce this rate well below the maximum tolerable rate of 1 kHz. It will do this by refining the muon trigger and by identifying the $J/\psi \to \ell^+\ell^-$ decay using the TRT.

3. THE DECAY $B^0_d \to J/\psi K^0_S$

The total $b\bar{b}$ production cross section is estimated to be between 100 and 700 μb [5] for LHC operating at a center of mass energy of 16 TeV. The total cross-section given by the PYTHIA Monte Carlo program [6] was 560 μb, corresponding to 1.7 μb with the ATLAS muon trigger.

Background to the signal can be produced by other B-meson decays with a true J/ψ and K^0_S in the final state: $B^0_d \to J/\psi K^{*0} \to J/\psi K^0_S \pi^0$, and $B^+ \to J/\psi K^{*+} \to J/\psi K^0_S \pi^+$. Including the branching ratios of $K^{*0+} \to \pi^+\pi^-\pi^{0+}$, the number of background events in each mode is roughly the same as the number of signal events. The decay modes $B^0_d \to J/\psi K^+\pi^-$ (non-resonant) and $B^0_d \to J/\psi K^{*0} \to J/\psi K^+\pi^-$ (resonant) could also be a source of background, when a K^+ misidentified as a π^+ produces a fake K^0_S. It has been shown that after cuts on the decay length and the mass of the K^0_S candidate this background is negligible [2].

An accidental background can be produced by combining a real J/ψ from a B-decay and a K^0_S from fragmentation. This is potentially the most dangerous background from accidental correlations. Background from fake J/ψ's and any K^0_S can be reduced by cuts on the $J/\psi \to \ell^+\ell^-$ impact parameters or decay vertex. These cuts also suppress the background from real J/ψ's coming directly from hadronization.

To estimate reconstruction efficiencies and background rejection, signal events and background events were generated with the PYTHIA Monte Carlo program, including direct $b\bar{b}$ production, gluon splitting and flavour excitation. The nominal beam energy was 7.7 TeV. Subsequently, the charged particle tracks were parametrized in terms of momentum resolution. The angular acceptance was assumed to be $|\eta| < 2.5$, track finding efficiency 95% and lepton identification efficiency 80%.

The simulated mass resolution for K^0_S varies from 3 to 8 MeV/c^2 depending on the K^0_S decay position and transverse momentum. The mass resolution for J/ψ is 27 MeV/c^2, ignoring bremsstrahlung effects for $J/\psi \to e^+e^-$ decays. A mass resolution of 35 MeV/c^2 can be obtained for the B^0_d meson without using mass constraints. Constraining the K^0_S and the J/ψ masses to their nominal values, a resolution of 7.5 MeV/c^2 can be obtained for the B^0_d.

The reconstruction efficiencies were calculated by demanding that the events satisfied the following cuts. The first set of cuts corresponds to the requirements set by the trigger:

- For $J/\psi \to e^+e^-$ decays, the electrons were required to be within $|\eta| < 2.5$, and to have a transverse momentum greater than 1 GeV/c. The low p_T threshold for electrons is possible because of the electron identification in the TRT. Events were required to contain a tag muon with a transverse momentum greater than 6 GeV/c and with $|\eta| < 1.6$.
- For $J/\psi \to \mu^+\mu^-$ decays, three muons were required to be found within pseudorapidity range of $\pm$ 2.5. The transverse momenta of two of the muons (one of them being the tag muon) were required to be greater than 5 GeV/c (muons identified in the muon chambers), and greater than 1 GeV/c for the third muon (no muon identification required). In addition, one of the muons was required to satisfy the single muon trigger conditions: $p_T > 6$ GeV/c, $|\eta| < 1.6$.

The second set of cuts corresponds to 'offline' analysis requirements:

- The two charged pions from the K^0_S decay within the tracking volume $|\eta| < 2.5$, and the transverse momenta of the pions greater than 0.5 GeV/c.
- K^0_S decay length in the transverse plane with respect to the beam axis greater than 1 and less than 50 cm. The upper limit ensures that the charged pion tracks from the K^0_S decay start before the inner radius of the TRT, and that the first measurement point is the space point from the innermost layer of the outer silicon tracker. The lower limit reduces the combinatorial background from particles originating from the primary vertex.
- Reconstructed K^0_S and J/ψ masses within two standard deviations of the nominal values.

The reconstructed $(J/\psi K^0_S)$ mass distributions for the signal and background are shown in Fig. 1 after all the other cuts except for the final mass cut.

The main sources of wrong assignments, 'tags', are

1. Cascade decays of the b and additional c- and b-quark pairs created in the parton shower. The fraction of wrong sign muons was found to be (0.135 ± 0.026) with a dominant contribution from cascade $b \to c \to \mu$ decays. The error is due to the simulation statistics.
2. Hadron background (π, K-decays, punchthrough). The fake muon background from hadron decays is about 1% [7], contributing equally to the right and wrong sign muon classes. This gives a total fraction of wrong sign muons equal to 0.14 from sources other than oscillations.

3. $B^0 - \bar{B}^0$ mixing. Including the effect of mixing using mixing probabilities $P(B^0_d \to \bar{B}^0_d) = 0.17$, $P(B^0_s \to \bar{B}^0_s) = 0.5$, the total fraction of wrong sign muons is 0.24, which corresponds to a dilution factor D_{tag} equal to 0.52.

In Fig. 2, the dilution factor including the different contributions is shown as a function of the transverse momentum threshold of the trigger muon.

The fraction of wrong sign tags can be measured directly from data using CP-conserving B-decays like $B^+ \to J/\psi K^+$. The same decay mode can be used to control the production asymmetry of B^0_d and $\bar{B}^0_d$ at LHC, estimated to be at the per cent level [8].

The results are summarized in Table 1.

Table 1. ATLAS summary on measuring $\sin 2\beta$.

Parameter	Value	Comment
$\mathcal{L}$ [cm^{-2}s^{-1}]	10^{33}	$\sim$ 1.5 interactions/event
t [s]	10^7	
$\sigma(b\bar{b} \to \mu X)$ [μb]	1.7	$p_T^\mu > 6$ GeV/c, $\lvert\eta^\mu\rvert < 1.6$ Includes 2$\cdot$ Br$(b \to \mu) = 0.2$, Br$(c \to \mu) = 0.1$
$N(bb \to \mu X)$	$1.7 \cdot 10^{10}$	
$f(b \to B^0_d)$	0.4	
$Br(B^0_d \to \ell^+\ell^-\pi^+\pi^-)$	$2.76 \cdot 10^{-5}$	$\ell = \mu$ or e. Br's from ref. [9]
$N(J/\psi K^0_S)$ triggered	187,000	
$N(e^+e^-K^0_S)$ reconstructed	9,950	
$N(\mu^+\mu^-K^0_S)$ reconstructed	6,370	
N_S	15,500	$m = m_{B^0_d} \pm 2\sigma$
$N_B(B^0_d \to J/\psi K^{*0})$	< 3	Br $= 1.3 \times 10^{-3}$ [9]
$N_B(B^+ \to J/\psi K^{*+})$	3	Br $= 1.4 \times 10^{-3}$ [9]
$N_B((B \to J/\psi \to e^+e^-) \oplus K^0_S)$	600	
$N_B((B \to J/\psi \to \mu^+\mu^-) \oplus K^0_S)$	250	
N_{total}	16,360	
D_{back}	0.95	$\sqrt{N_S/N_{total}}$
D_{tag}	0.52	
Time integration	0.47	$x_d = 0.71$
$\delta(\sin 2\beta)$ (stat.)	0.035	

4. TIME-DEPENDENT MEASUREMENT

A measurement of the CP-violation parameter $\sin 2\beta$ using decays $B^0_d, \bar{B}^0_d \to J/\psi K^0_S$ could also be performed by measuring directly the proper time of the B-decay from the secondary vertex of the J/ψ-decay, if secondary vertex reconstruction in B-decays is feasible. CP-violation should reveal itself as a deviation from the exponential decay rate, which is of different sign for B^0_d and $\bar{B}^0_d$. Measurement of the time-variation of the asymmetry is also an important confirmation of the origin of the observed time-integrated asymmetry.

In ATLAS, a secondary vertex resolution in the transverse plane of about 400 μm is expected for two-body decays of B-mesons, when the decay particles have a transverse momentum above 2 GeV/c.

In this study, the sample consisted of 14000 events using only events with $p_T^B > 5$ GeV/c. Requiring proper time $t > 1.0$ ps, 7265 events were selected. The value of $\sin 2\beta$ was then extracted from a χ^2 fit to the asymmetry of the two proper time distributions for the positive and negative tags. The results are shown in Table 2.

Table 2. Results of the time-dependent measurement of $\sin 2\beta$. Errors are statistical.

Parameter	Input value	Fitted value
$\sin 2\beta$	1.	0.948 ± 0.027
$\sin 2\beta$	0.6	0.552 ± 0.029
$\sin 2\beta$	0.2	0.184 ± 0.030

5. CONCLUSIONS

The CP-reach of the ATLAS experiment in measuring the angle β using the decay channel $B^0_d \to J/\psi K^0_S$ was investigated. The signal selection cuts were optimized to use the full potential of the experiment in electron and muon identification as well as in K^0_S reconstruction. A statistical error of ± 0.035 in the measurement of $\sin 2\beta$ can be reached during the first year of running of LHC. A measurement of the time-dependence of the asymmetry has been shown to be feasible as well, with comparable statistical accuracy.

6. REFERENCES

1. H. Albrecht et al., ARGUS Coll., Z. Phys. C55 (1992) 357; M. Artuso et al., CLEO Coll., Phys. Rev. Lett. 62 (1989) 2233.
2. P. Eerola, Nucl. Instrum. and Meth. A333 (1993) 73.
3. Letter of Intent 'ATLAS', CERN/LHCC/92-4, LHCC/I 2, October 1992.
4. A. Nisati, in Large Hadron Collider Workshop, Aachen 4-9 October 1990, CERN 90-10, ECFA 90-133, Vol. III, p. 442.
5. J.P. Guillot, P. Nason and H. Plothow-Besch, in Large Hadron Collider Workshop, Aachen 4-9 October 1990, CERN 90-10, ECFA 90-133, Vol. II, p. 116.
6. H.-U. Bengtsson, T. Sjöstrand, Computer Phys. Comm. 46 (1987) 43.
7. A. Cheplakov et al., 'Muon Rates at LHC', ASCOT/EAGLE Note MUON-NO-006 (1992).
8. M. Botlo et al., 'Further Comments about B-Physics in pp Interactions', SSCL-538, SLAC-PUB-5795, June 1992.
9. Particle Data Group, Phys. Rev. D45, Part 2 (June 1992).

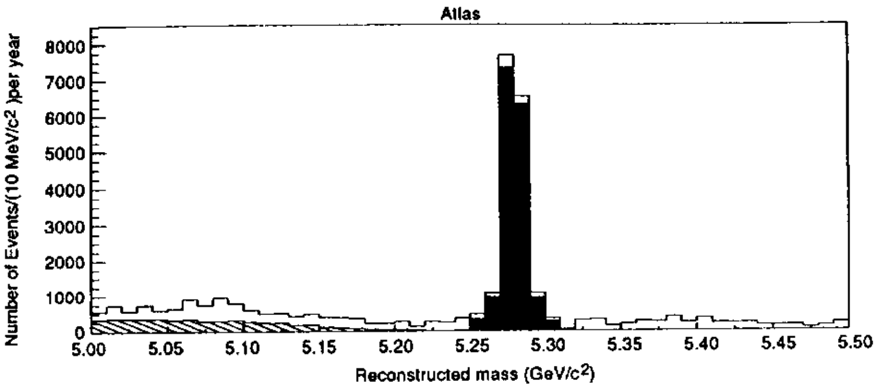

Figure 1: *Reconstructed ($J/\psi K^0_S$)-mass. The dark shaded histogram shows the signal, the hatched histogram shows the background from $J/\psi K^{*+}$ and $J/\psi K^{*0}$, and the white region shows the signal added together with all the considered sources of background.*

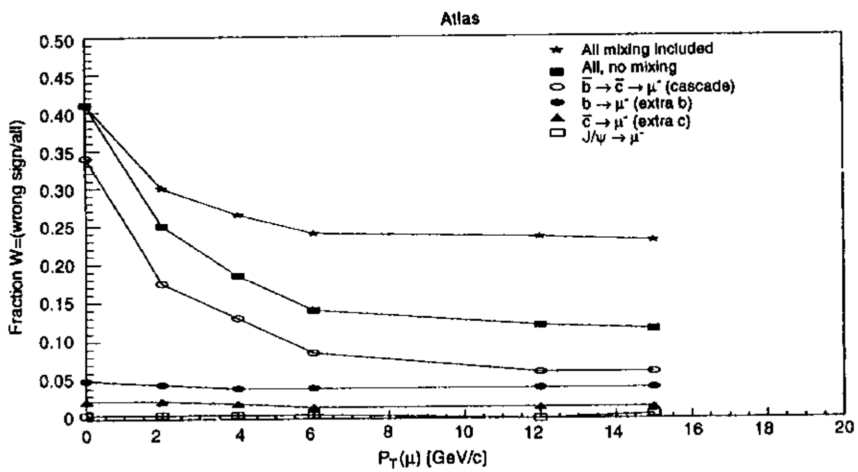

Figure 2: *The fraction of wrong sign tags as a function of the transverse momentum threshold of the trigger muon.*

MEASUREMENT OF sin(2β) WITH THE CMS DETECTOR AT LHC

N. Neumeister
Institut für Hochenergiephysik,
Österreichische Akademie der Wissenschaften,
Nikolsdorfergasse 18, A-1050 Vienna, Austria

1. INTRODUCTION

The large number of $B\bar{B}$ events at LHC will offer the possibility to search for CP-violation in the $B^0 - \bar{B}^0$ system. The unitarity of the 3×3 CKM matrix implies a relation between the elements: $V_{ub}^* + V_{tb} \simeq \lambda V_{cb}$, which can be visualized as a triangle in the complex plane. In principle all three angles of this unitarity triangle are accessible to direct experimental measurements, for instance from the neutral B-decays $B_d^0 \to \pi^+\pi^-$, $B_d^0 \to J/\psi K_s^0$ and $B_s^0 \to \rho K_s^0$ [1].

For this study we explored the possibility to determine CP-violation by measuring the time-integrated asymmetry in $B_d^0, \bar{B}_d^0 \to J/\psi K_s^0$ decays, to determine the angle β of the unitarity triangle. The time-independent asymmetry A for this channel is:

$$A = \frac{\Gamma(B_d^0 \to J/\psi K_s^0) - \Gamma(\bar{B}_d^0 \to J/\psi K_s^0)}{\Gamma(B_d^0 \to J/\psi K_s^0) + \Gamma(\bar{B}_d^0 \to J/\psi K_s^0)} = \sin(2\beta) \cdot \frac{x_d}{1 + x_d^2} \tag{1}$$

where x_d has been measured to be 0.71 [2].

Because of the mixing phenomena, the nature of the B_d^0 (particle or antiparticle) has to be determined. This can be done by measuring the charge of the $\mu^\pm$ in the semileptonic decay of the associated beauty hadron ($b \to \mu^- X$).

2. THE CMS DETECTOR

The CMS (Compact Muon Solenoid) is designed as a general purpose detector for discoveries at the highest luminosity in proton-proton collisions at LHC. However, during the initial period of LHC operation, it is expected that there will be an opportunity to carry out heavy flavour studies, such as CP-violation, at lower luminosity. Here I will just concentrate on the detector parts most important for measuring CP-violation, i.e. the muon-system, the muon trigger and the inner tracker. A detailed description of the CMS detector can be found in ref. [3].

The detector will be built around a 14 m long 4 T superconducting solenoid. The 4 T central field together with a powerful tracking leads to a good momentum resolution. The muon momentum is measured three times almost independently, which makes the muon identification very robust. Starting from the primary vertex, centrally produced muons are first measured in the inner tracker inside the uniform 4 T magnetic field. They then traverse the calorimeters (7λ at 90°), still inside the 4 T magnetic field, the coil (1.1λ) and a non-magnetic "tail catcher" (2λ). They are then identified and measured in four identical muon stations inserted in the return yoke. Each muon station consists of several planes of drift chambers designed to give a muon vector in space, with $100\mu m$ precision in position and better than 1 mrad in direction. The four muon stations also include triggering planes which identify the bunch crossing and cut on the muon transverse momentum. The transverse position of the vertex is known to an accuracy of better than 20 μm.

The muon trigger should be very flexible and therefore various options are considered for the first-level muon trigger (adjustable p_T-cut from 4-100 GeV):
- inclusive single μ trigger in the $|\eta| < 2.0$ region with a p_T threshold $\sim$ 25 GeV (dependent on luminosity) for large p_T^μ, W, W', top physics, etc.
- inclusive double μ trigger in the $|\eta| < 2.4$ region with p_T threshold down to 4 GeV for inclusive Z, top physics, CP-violation, etc.

The muons from b's have relatively low p_T and therefore one needs a low-p_T muon trigger and high statistics to study CP-violation.

The CMS inner tracker consists of several planes of microstrip gas chambers ($\sigma \sim$ 50 μm) and silicon strip detectors with 50 μm pitch for the innermost part of the tracker. The silicon detectors at a radial distance of 20 to 40 cm from the beam improve the resolution significantly. The planes of the inner tracker are distributed in a cylindrical tracking volume of dimensions $|z| < 3.5$ m, $R < 1.3$ m. The tracking system has been optimized for pattern recognition and track finding efficiency [3]. For straight tracks there are on average 12 points per track in the barrel region and about 20 points per track in the forward region. With the distributed tracking of CMS it should be possible to reconstruct K^0s with sufficient efficiency.

3. SIMULATION OF THE $B_d^0 \to J/\psi K_s^0$ CHANNEL

The most realistic decay-channel to measure CP-violation is: $B_d^0 \to J/\psi K_s^0$ followed by $J/\psi \to \mu^+\mu^-$ and $K_s^0 \to \pi^+\pi^-$, because it has the clearest signature and the most tractable background [4]. Moreover it is the only channel for which a lower bound of the CP-violation parameter can be predicted, depending on the top quark mass. For m_t = 100, 140, 180 GeV the lower bound of $\sin(2\beta)$ becomes 0.16, 0.21, 0.24 respectively [5]. Further advantages are the relatively high branching ratio and the fact that triggering on $J/\psi \to \mu^+\mu^-$ is relatively easy. The experimentally measurable time-integrated asymmetry (1) for this decay-channel is related to the CP-violation parameter $\sin(2\beta)$. The total branching fraction for this decay-channel including the semileptonic branching ratio of the associated b is: $PR[b\bar{b} \to B_d^0\bar{b}] \cdot BR[B_d^0 \to \psi K_s^0] \cdot BR[J/\psi \to \mu^+\mu^-] \cdot BR[K_s^0 \to \pi^+\pi^-] \cdot BR[b \to \mu X] = 0.8 \cdot 3.3 \times 10^{-4} \cdot 0.0597 \cdot 0.6861 \cdot 0.103 = 1.114 \times 10^{-6}$. The production cross-section of $b\bar{b}$ at LHC, operating at a center of mass energy of 14 TeV, is estimated to be between 300 and 700 μb [6]. For this study we assume $\sigma_{b\bar{b}}$ to be 500 μb.

To avoid problems due to multiple events per bunch-crossing we are assuming a luminosity of $\mathcal{L} = 10^{33}\ cm^{-2}s^{-1}$ (corresponding to an integrated luminosity of $10^4\ pb^{-1}$), which might be realistic for the first years of LHC operation. At this luminosity the total number of produced events per year is 5.6×10^6.

To calculate the total signal-efficiency for this decay-channel we simulated events with PYTHIA Monte Carlo [7] and used a simple detector simulation to estimate the detector effects. For the trigger we assume a low-p_T 2μ-trigger. For the kinematical selection of the 3 muons we consider two different options:

- 3 μ's with $|\eta^\mu| \leq 2.4$ and $p_T^\mu \geq 4.0$ GeV/c.
- 3 μ's with $|\eta^\mu| \leq 2.4$ and $p_T^\mu \geq$ 6.0, 4.5 and 2.5 GeV/c, where the two higher-p_T muons are triggered and the third muon is just accepted.

The following cuts were applied to all events: 2 π's from K^0 with $|\eta| \leq 2.4$ and $p_T \geq$ 0.7 GeV/c and the K_S^0 decay length in the transverse plane between 2 and 60 cm in order to avoid problems due to the pattern recognition.

The kinematical parameters (p,λ,Φ) of all charged particles have been smeared according to a parametrization obtained by a full detector simulation. According to our simulation, the fitted values for the mass resolutions are: $\sigma(K^0) = 6.5$ MeV, $\sigma(J/\psi) = 15.5$ MeV, $\sigma(B_d^0) = 21$ MeV.

In addition we considered the trigger efficiency and the efficiency of tracking and identification of 3 muons with $\epsilon = (0.8)^2 \cdot 0.9$ and the pattern recognition efficiency for K_s^0 (in the case of 2 π's from K^0 with $p_T \geq 0.7$GeV/c) with 35%. Finally the numbers of reconstructed events (for $10^4\ pb^{-1}$) for the two options are given in table 1. These numbers include the kinematical acceptance, the effective mass resolution, trigger efficiencies, efficiencies for a tracking and identification and K_s^0 reconstruction efficiency.

SELECTION	number of events per year
3μ with $p_T \geq 4.0$ GeV/c	2280
3μ with $p_T \geq 6.0, 4.5, 2.5$ GeV/c	4780

Table 1: Total number of tagged and reconstructed events per year

The background to this channel can be produced by the following B-decays: $B^\pm \to J/\psi K^{*\pm}$, $B_d^0 \to J/\psi K^{*0}$ and $B \to \psi(2S)K/K^*$. Applying our cuts we end up with a signal to background ration in the B-mass region of $\sim$ 50. Furthermore there will be a combinatorial background from inclusive J/ψ production of approximatly 15%.

4. DILUTION EFFECTS

Equation (1) deals with the ideal but unrealistic case that the second beauty hadron is perfectly tagged. Practically the measured asymmetry A is affected by a dilution effect due to the mistagging of muons ($A \to D \cdot A$), and the dilution factor D is dependent on the p_T-threshold of the tagging muon [8, 9]. The muon mistagging can be due to:

1. mixing of B_d^0 or B_s^0 before decaying into muons
2. cascade-decays of b's
3. μ's from hadron decays (K's and π's)
4. punchthrough in the detector.

The dominant contribution to the dilution effect is due to mixing and cascade decays. Without mixing the dilution factor D_c can be defined as:

$$D_c = \frac{N(good\,tags) - N(bad\,tags)}{N(good\,tags) + N(bad\,tags)} = 1 - 2 \times w$$

where w is the fraction of wrong sign muons. The tagging-quality increases with higher p_T-cuts, as does the detection efficiency. In fig. 1 the fraction of wrong sign muons is plotted as a function of the p_T^μ-cut. With a muon p_T^μ-threshold of 4.0 GeV/c, the fraction of wrong sign muons (excluding mixing) was found to be 15%. Therefore we obtain a dilution factor of $D_c = 0.70$ and including the mixing our final dilution factor is $D = D_m \cdot D_c = 0.73 \cdot 0.70 = 0.51$.

The punchthrough has not been included yet, but the fraction of punchthrough muons is expected to be lower than the fraction of muons from hadron decays.

To measure the dilution effect we consider the following channels: $B^\pm \to J/\psi K^\pm$ and $B_d^0 \to J/\psi K^{*0}$. After applying all kinematical cuts and efficiencies we estimate to obtain approximately ten times more reconstructed events for these control channels than for the signal channel.

5. CONCLUSION

The error on the CP-violation parameter $\sin(2\beta)$ is related to:

$$\delta(\sin 2\beta) \simeq \frac{\sqrt{1 - (D' \cdot \sin 2\beta)^2}}{D' \cdot \sqrt{N}} \simeq \frac{1}{D' \cdot \sqrt{N}} \qquad \text{with} \qquad D' = D_m \cdot D_c \cdot \frac{x_d}{1 + x_d^2}$$

where N is the number of reconstructed events. For 3 muons with $|\eta^\mu| \le 2.4$ and $p_T^\mu \ge 6.0, 4.5, 2.5$ GeV/c with 10^4 pb^{-1} the error on $\sin(2\beta)$ is therefore 0.06. Fig. 2 shows the number of reconstructed events necessary to measure $\sin(2\beta)$ with 3 and 5 standard deviations. The present expected theoretical lower limit on $\sin(2\beta)$ is 0.16 [6].

Although this is just a preliminary study it is clear that the CMS-detector is well suited to study CP-violation in the $B_d^0 \to J/\psi K_S^0$ channel. After 1 year's running (10^4 pb^{-1}) we would measure CP-violation at 3σ provided $\sin(2\beta) \ge 0.18$.

6. ACKNOWLEDGEMENTS

It is a pleasure to thank D.Denegri, A. Fridman, J.Hassard and M.Konecki for many useful discussions.

7. REFERENCES

1. S. Erhan et al., *Collider Beauty Physics at LHC* in Proceedings of LHC Workshop, Aachen 1990, CERN 90-10 (1990) vol. II.
2. H. Albrecht et al. (*ARGUS Collab.*), Z. Phys. C55 (1992) 357.
3. CMS (Compact Muon Solenoid) Letter of Intent, October 1992, CERN/LHCC 92-3, LHCC/I 1.
4. M. Botlo et al., *Further Comments about B-Physics in pp-Interactions*, SSCL-538 (1992).
5. G. Carboni et al., *Beauty at the LHC* in Proceedings of LHC Workshop, Aachen 1990, CERN 90-10 (1990) vol. II.
6. D. Denegri *Standard Model Physics at the LHC* in Proceedings of LHC Workshop, Aachen 1990, CERN 90 10 (1990) vol. I.
7. H.-U. Bengtsson and T. Sjostrand, Computer Phys. Comm. **46** (1987) 43.
8. M. Chaichian and A. Fridman, *Measurement Possibilities of CP Violation for B-Decays in pp Collisions.* CERN-TH/6068-91 (1991).
9. M. Cannalire and A. Fridman, *Dilution Effects for CP Violation Measurement in B Decays*, SSCL-566 (1992).

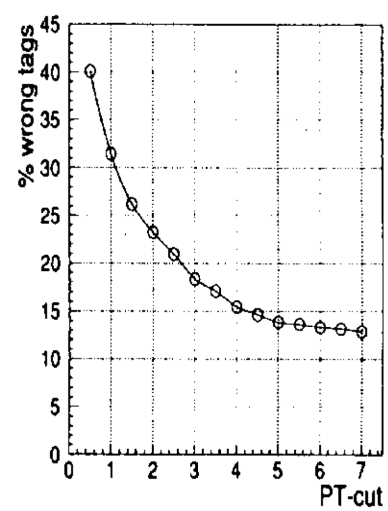

Figure 1: Number of wrong tags as a function of p_T^μ

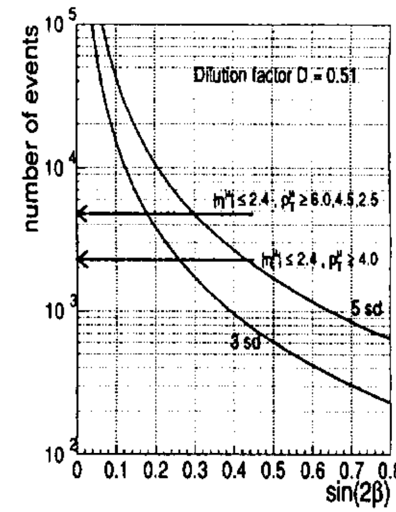

Figure 2: Number of reconstructed events required for measuring 3σ and 5σ effects as a function of the CP-violation parameter

K^0 FINDING EFFICIENCIES IN INCREASING LUMINOSITIES

J.F. HASSARD and S. MARGETIDES
Imperial College, London

1. THE pp ENVIRONMENT

In early LHC running it is anticipated that we will obtain luminosities of 10^{32} $cm^{-2}sec^{-1}$, during which typically only one interaction per event will be obtained. But at higher luminosities, necessary for any Higgs and myriad other searches, we will have to deal with up to 50 distinct primary processes. Most will be minimum bias, and easily distinguished in terms of trigger. They can still, of course, confuse analysis of high P_T events. When it comes to B events, the confusion even from minimum bias events becomes more acute, since B events are not "high P_T" in this environment. The need for vertex discrimination, particularly in z, is well understood; however, a collateral effect—the increasing difficulty in finding tracks at all—has received little attention. In Figure 1, we show the distribution of the K^0 in the Pythia[1] process $B \rightarrow J|\psi K^0$ in the space γ vs. η. Confusion in reconstructing the K^0 is acute for many reasons, note least of which is the way their pions are boosted forward, and even out of acceptance. Extra luminosity merely increases the problems in finding K^0s, so it must not be assumed that 10^{33} $cm^{-2}sec^{-1}$ is ten times better than 10^{32} $cm^{-2}sec^{-1}$.

2. THE LUMINOSITY DEPENDENCE IN $B \rightarrow J|\psi K^0$

We have described the CMS trackfinder CMSTR elsewhere.[2] To illustrate the problem outlined above, we show here how it copes with increasing luminosity and the subsequent effect on finding Bs. Figure 2 shows the track finding luminosity as a function of P_T for varying numbers of events overlying each other. Figure 3 shows the effect on the efficiency of finding a given number of K^0s in increasing track density. The ψ reconstruction efficiency is barely affected, depending on isolated tracks in the muon system. The subsequent reconstruction efficiency of Bs in increasing luminosity comes from the convolution of the two daughter particle efficiencies, and as we go from 1 to 2 to 3 overlying events, resembles, therefore, the K^0 graphs.

3. CONCLUSIONS

Estimates of CP reach[3] as a function of time are fraught with danger. Track finders at future colliders must be robust.

4. REFERENCES

1. Pythia version 5.3 by H.U. Bengtsson, T. Söstrand, Lund Monte Carlo Programs, CERN 1989.
2. J. Hassard, S. Margetides; "Studies of CP Violation in CMS: The Case for Vertexing," Imperial College IC-HEP 93-12.
3. W. Toki, J. Hassard, "Comparing the CP reach of Different Experiments," these proceedings.

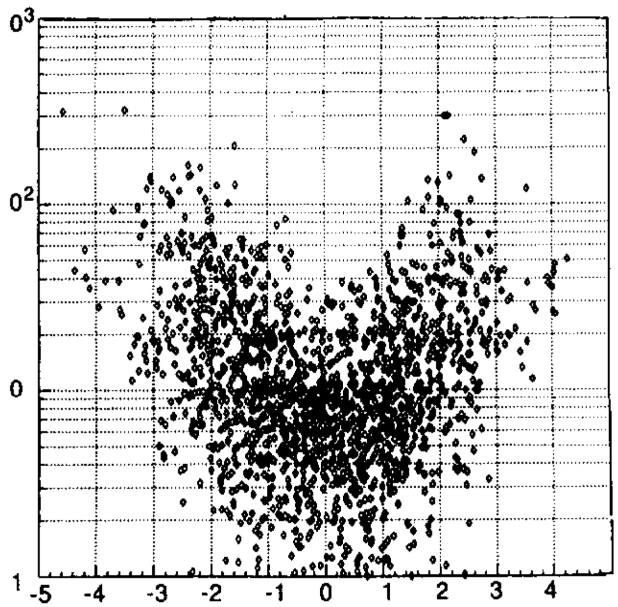

Figure 1. The distribution of K^0s from B decay in γ (boost) vs. η space.

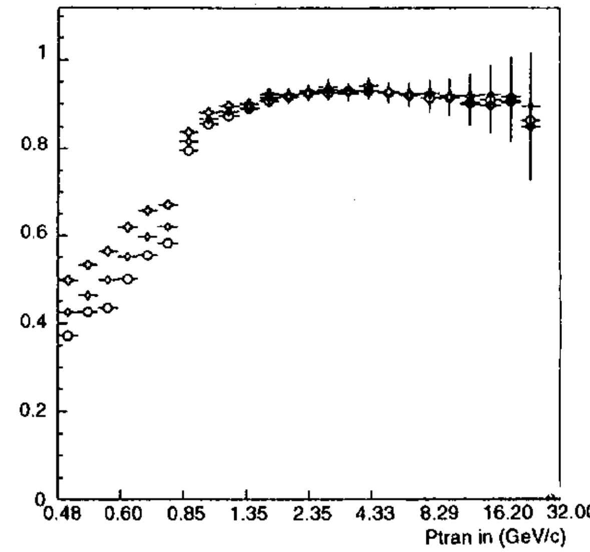

Figure 2. The trackfinding efficiency as a function of P_T. Different symbols refer to 1,2,3-event pile-up.

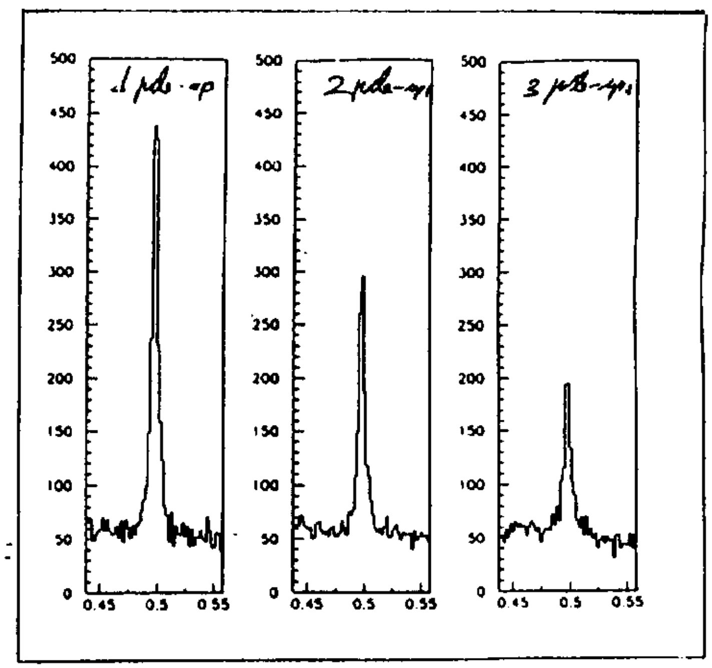

Figure 3. K^0 peaks in 1,2,3-event pile-up from same number of events.

A NOVEL TRACK FINDING TECHNIQUE FOR $pp \rightarrow b\bar{b}$ EVENTS

J.F. HASSARD AND S. MARGETIDES
Imperial College, London

1. WHY BOTHER?

Track finding techniques are in many senses a mature technology, with many highly effective working examples. This note describes in a preliminary way a novel method to be used in the LHC detector CMS. We have written trackfinder CMSTR for several reasons, among them:

- We wanted to develop a speedy method which would be suitable for highly parallel, probably online, hardwired VLSI treatment;
- We wanted to optimise for heavy quark decays in the CMS environment[1]: that means decoupling the trackfinder from a known vertex, and reaching down to the relatively low P_Ts of 0.7 - 1 GeV/c, momenta characteristic of the pions from the K^os in the decay B$\longrightarrow J|\psi K^o$.
- We wanted to exploit - rather than be hurt by - the CMS tracker high magnetic field.
- We wanted to be relatively insensitive to misalignments between detector sub-components;
- We wanted an algorithm which was robust enough to allow pain-free adaptation from the "Basic" design[2] to the four or five options still being discussed: changes characteristic of an evolving detector.

For a more detailed analysis of the decay reconstruction of CP eigenstates B$\longrightarrow J|\psi K^o$ and B$\longrightarrow Dl^{\pm}\nu$ read Neumeister's talk in these proceedings.

2. THE CMS DETECTOR

CMS is one of the two detectors expected to exploit the LHC collider from its turn on later this century. The CMS tracker geometry is shown in figure 1. In the barrel, you may see 9 layers of detectors, the outer 6 MicroStrip Gas Counter (MSGC) layers, the inner 3 silicon strip detectors. In the endcaps we have 9 layers of MSGC. CMS has a 4T solenoid, so tracks of $P_T \leq 800$ MeV/c and can loop many times. Given the huge particle multiplicity (even at low luminosity, typically 200 charged tracks per 15 ns crossing time) the confusion can be considerable for a track finder.

3. CMSTR

The detector is simulated in a way which includes multiple scattering, positional resolution, which is strongly momentum dependent, and alignment errors. Resolutions of MSGC's were unknown during this study but were assumed to be 60 μ, independent of P_T, folded with a 50 μ alignment error. Silicon strips had 15 -30 μ resolution. In fact a strong P_T dependence of resolution exists for MSGC's. Work done since Snowmass has included these extra effects[3].

Pairs of hits, whether in barrel, or endcap, are combined to make vectors. The natural grouping of layers in CMS, their concentricity in the barrel and their parallelity in the endcaps, and the high magnetic field allow us to calculate radii of curvature from different pairs of vectors. Angular "roads" are defined within which vectorial combinations can be made, these roads being radius dependent. From pairs of vectors, one radius can be calculated. From a low P_T track which loops, many radii can therefore be found, and if an adjustment is made for energy loss, those radii will coincide. Note how this is optimised for B physics. The dependence on radius of the road makes finding tracks coming from a point away from the origin easier: they have a smaller angle of incidence. Low P_T tracks spike more; smaller circles are measured with much greater accuracy (until we get smaller than the outer detector plane radius).

For a given event, we store all found radii in all the superlayers, and interrogate the array for spikes. It is important to note that the worst of the effects of multiple scattering and intersuperlayer misalignments are minimised by keeping calculations of radii to within any superlayer. Note also that for all but very stiff tracks ($P_T \geq 40 GeV/c$) the positions of the circle centres (x_j, y_j) can be used to check the track's validity. Any cut on the clustering of the circle centres has to be strongly P_T dependent, since the errors δx_j, δy_j grow large with the track radius of curvature, and therefore this information is not used except in certain ambiguities. Extra redundancy comes from the fact that we still have z hit information (2mm resolution in both MSGCs and silicon) which is used in fitting the track and resolving ambiguities.

All associated hits (ie. those found in tracks of acceptable χ^2) are removed from the hit array, and the method is reiterated, with looser cuts to mop up remaining hits. This process can repeated an arbitrary number of times, nominally two.

In the region $1.0 \leq \eta \leq 2.5$ we must measure tracks which, when projected onto an endcap plane, have a small effective path length $\Delta s^{r-\phi}$. Since $\frac{\Delta P_T}{P} = \frac{\kappa P_T \Delta s}{BL^2}$ where $\kappa = 0.027$, the sagitta to this becomes comparable to the errors δx_j, δy_j with which the j points are measured.

Any point in the endcap is defined by z (unique to a detector plane), azimuthal ϕ and polar θ. We get z for free, and have seen that for hard tracks, ϕ contains little information. Our strategy is to look first for the very low $P_T \times P_L$ tracks using the radii method outlined. Having found them, we leave the hits in the hit array to avoid losing ambiguous hits from harder tracks. For the tracks too stiff to find using radii, we note that s is close to $\sqrt{x^2+y^2+z^2}$, and so we look for sequences of hits in the endcaps which satisfy clustering in the analogous angle θ, starting restrictively with $\pm$ 1 deg to get those tracks with large $P_T \times P_L$ and about $\pm$ 2 deg in $\Delta\phi$. Associated hits are withdrawn. We then repeat with angle cuts of increasing magnitude.

4. RESULTS

A typical event at $\sqrt{s} = 16$ TeV and luminosity 10^{32} is shown[4] in figure 2. The trackfinding efficiency as a function of pseudorapidity for *all* tracks above $P_T = 350$ Mev/c is shown in figure 3, and in figure 4 the track efficiency for tracks as a function of P_T.

We find that the track finder and fitter[5] takes a period per event almost - surprisingly - linear in the number of tracks in the event. The fit package is a 3% overhead. Figure 5 shows the relationship for a VAX station 4000. CMSTR has been written in a way which should make its translation to hardwired processors reasonably possible.

5. REFERENCES

[1] J.Hassard, S. Margetides; "Studies of CP Violation in CMS: The Case for Vertexing", Imperial College IC-HEP 93-12

[2] CMS Letter of Intent, CERN/LHCC/92-1, LHCC/I1, 1992; CMS Staging Document, LHCC I1 Add. 1, CERN/LHCC/93-22, 1993

[3] CMS B Paper for LHCC, Sept 1993, to be published

[4] J. Hassard, S. Margetides, S. Woon; "$^{S_w}o_{o_N}$: Graphics à la Carte, A Menu Driven Interactive Analysis Package", IC-HEP 92-32

[5] Veikko Karimäki, "Fast Code to Fit Circular Arcs" Computer Physics Communications, 69, 1992 133-141.

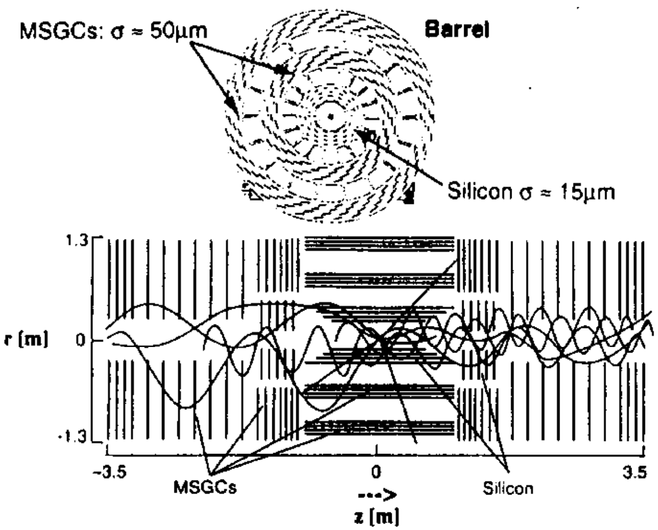

Figure 1. The CMS staged detector.

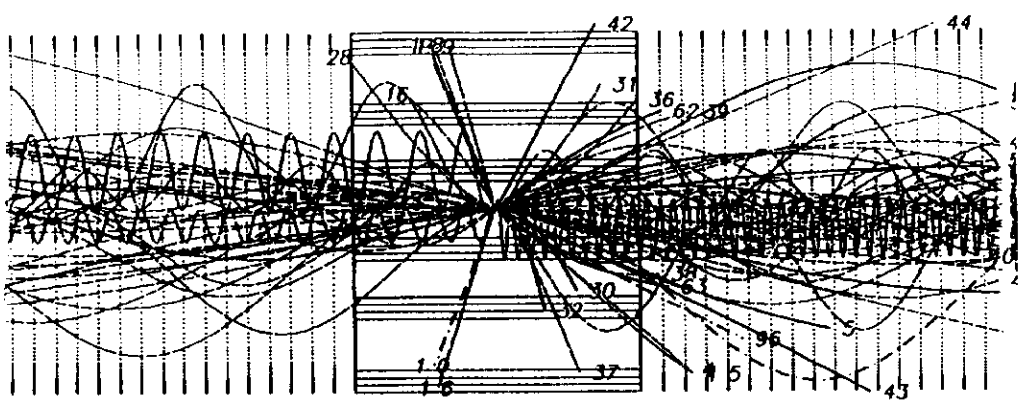

Figure 2. A CP eigenstate in the CMS LOI detector.

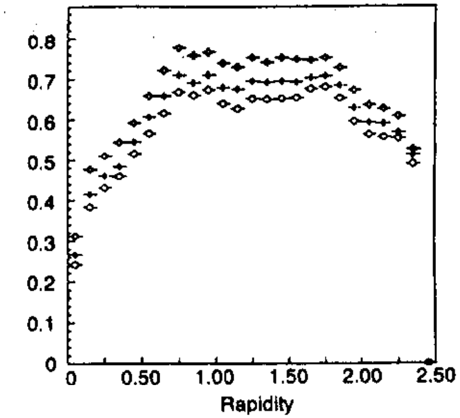

Figure 3. Trackfinding efficiency- all tracks vs. η.

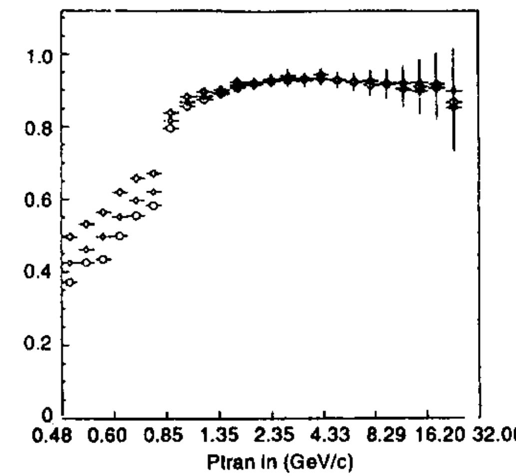

Figure 4. Trackfinding efficiency vs. P_T.

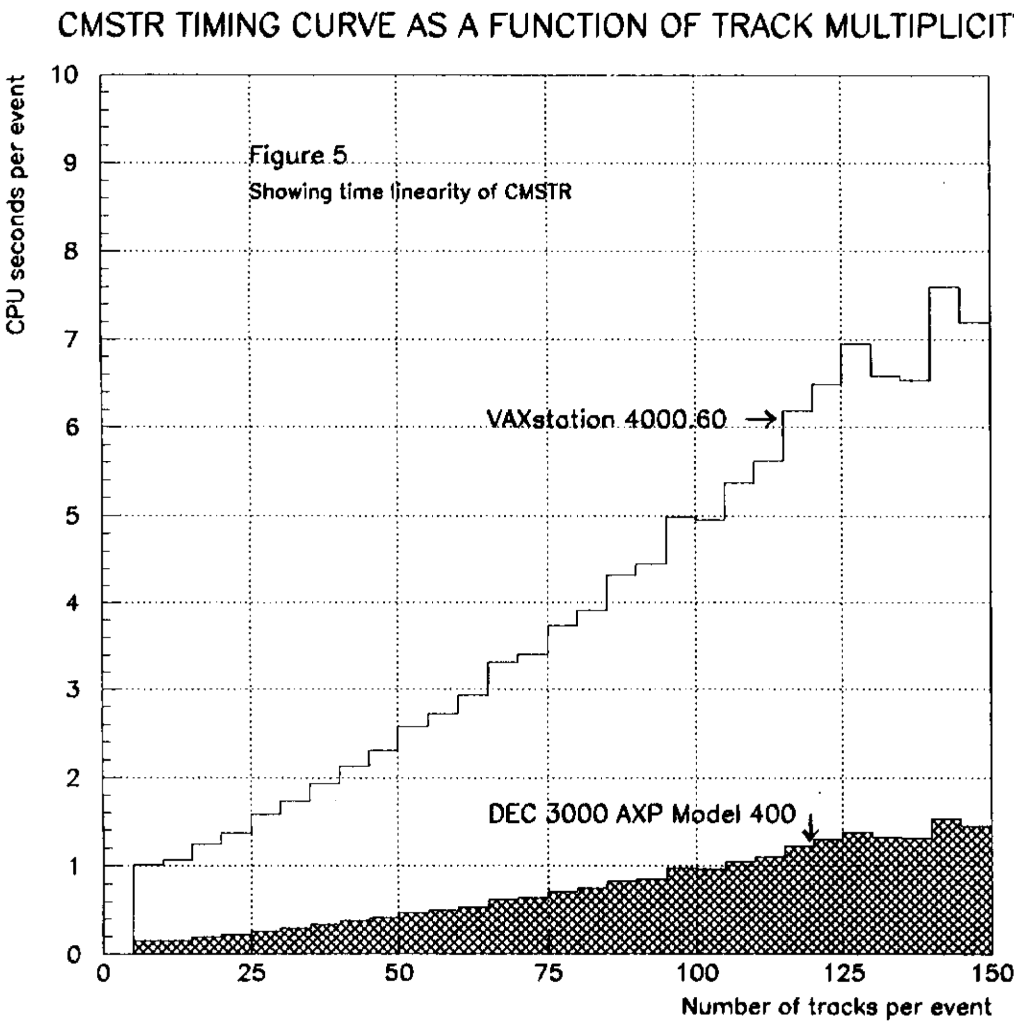

Figure 5. CMSTR timing curve in VAX 4000.

MEASUREMENT OF RATIO OF BRANCHING RATIOS

$BR(B^+ \to J/\psi K^+)/BR(B^0 \to J/\psi K^0)$

JULIO GONZALEZ-A
Department of Physics, University of Pennsylvania, 209 S 33rd Street
Philadelphia, PA 19104-6396, USA

1. INTRODUCTION

This paper reports a preliminary measurement of the ratio of branching ratios $BR(B^+ \to J/\psi K^+)/BR(B^0 \to J/\psi K^0)$. The reconstruction of J/ψ's is done via the decay $J/\psi \to \mu^+\mu^-$ while the K^0_S's are identified through the decay $K^0_S \to \pi^+\pi^-$. The data used was obtained at the Collider Detector at Fermilab from $p\bar{p}$ collisions at $\sqrt{s}$ =1.8 TeV. There are several reasons why this measurement is important. It embodies the first observation of the decay mode $B^0 \to J/\psi K^0_S$ at a hadronic machine and it permits us to measure the ratio of charged to neutral lifetimes and the $BR(B^0 \to J/\psi K^0)$.

1.1 Ratio of Lifetimes

There are recent predictions [1] that the ratio of lifetimes should be in the range

$$1.02 \leq \tau(B^+)/\tau(B^0) \leq 1.08 \tag{1}$$

By assuming that

$$\Gamma(B^+ \to J/\psi K^+) = \Gamma(B^0 \to J/\psi K^0) \tag{2}$$

with Γ the decay rate, we have the following relation

$$\begin{aligned} \frac{BR(B^+ \to J/\psi K^+)}{BR(B^0 \to J/\psi K^0)} &= \frac{\Gamma(B^+ \to J/\psi K^+)/\Gamma(B^+ \to X)}{\Gamma(B^0 \to J/\psi K^0)/\Gamma(B^0 \to X)} \\ &= \frac{1/\Gamma(B^+ \to X)}{1/\Gamma(B^0 \to X)} \\ &= \tau(B^+)/\tau(B^0) \end{aligned} \tag{3}$$

1.2 Branching Ratio

By using the $BR(B^+ \to J/\psi K^+)$ from **CLEO** we can obtain the $BR(B^0 \to J/\psi K^0)$ with higher precision than the present PDG value which has 50% error.

2. METHOD

The basic necessary relationships are

$$\begin{aligned} \mathcal{L} \times \sigma(p\bar{p} \to B^+) & \\ \times BR(B^+ \to J/\psi K^+) \times \epsilon_{B^+} &= N(J/\psi K^+) \end{aligned}$$

$$\begin{aligned} \mathcal{L} \times \sigma(p\bar{p} \to B^0) & \\ \times BR(B^0 \to J/\psi K^0) \times \epsilon_{B^0} &= N(J/\psi K^0) \end{aligned} \quad (4)$$

Here $\mathcal{L}$ is the integrated luminosity, σ is a cross section, ϵ represents the reconstruction efficiency and N is the number of reconstructed events for the specific decay mode.

Assuming that

$$\sigma(p\bar{p} \to B^+) = \sigma(p\bar{p} \to B^0) \quad (5)$$

(this is a good assumption because of the smallness of the u and d quark masses compared to the b quark mass) we then have

$$\frac{BR(B^+ \to J/\psi K^+)}{BR(B^0 \to J/\psi K^0)} = \frac{N(J/\psi K^+)}{N(J/\psi K^0)} \times \frac{\epsilon_{B^0}}{\epsilon_{B^+}} \quad (6)$$

3. PARTICLE SELECTION

3.1 J/ψ Selection

We require a good match between the stubs from the muon chambers and the corresponding track from the Central Tracking Chamber (CTC). The softer muon is required to have a transverse momentum > 1.7 GeV while the harder muon must be > 2.7 GeV. This requirement is needed only because these are the minimum momentums above which the level 1 and level 2 muon triggers are understood. The track parameters are then constrained to a common vertex and the J/ψ candidates are selected as di-muons with mass within $\pm 2.5\sigma$ of the world average.

3.2 $K^\pm$ Selection

All tracks with $P_t > 1.5$ GeV are considered $K^\pm$ candidates.

3.3 K^0_S Selection

We require both π tracks to have an impact parameter (with respect to the beam position) over its error greater than 1.0. We then constrain the parameters to a common vertex and require the decay distance to be > 1.0 cm and the K^0_S impact parameter to be < 0.3 cm if both tracks only have CTC information or 0.03 cm if both tracks have information from the Silicon Vertex Detector. The K^0_S candidates are selected as di-pions with mass within $\pm 2.5\sigma$ of the world average.

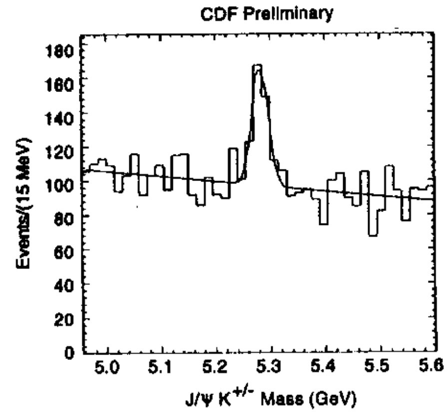

Figure 1: J/ψ $K^\pm$ mass distribution. The smooth line is a log likelihood fit of a gaussian plus a straight line. There are 167 $\pm$ 38 (stat) fitted events in the peak.

3.4 $B^\pm$ Reconstruction

Mass constrain all J/ψ candidates and simultaneously vertex constrain the di-muons plus the $K^\pm$ candidates to a common vertex. The $B^\pm$ candidate must have $P_t > 6$ GeV and a positive displacement with respect to the primary vertex. Figure 1 shows the resulting mass distribution. The smooth line is a log likelihood fit of a gaussian plus a straight line. There are 167 $\pm$ 38(stat) fitted events in the peak.

3.5 B^0 Reconstruction

Mass and vertex constrain all J/ψ candidates. Then mass, point and vertex constrain all K^0_S candidates. Require that the K^0_S transverse momentum be greater than 1.5 GeV. The B^0 candidate must have $P_t > 6$ GeV and a positive displacement with respect to the primary vertex. Figure 2 shows the resulting mass distribution. The smooth line is a log likelihood fit of a gaussian plus a straight line. There are 31 $\pm$ 5(stat) fitted events in the peak.

4. RECONSTRUCTION EFFICIENCY

For this measurement we assume all efficiencies common to both modes cancel in the ratio. Now we present a list of the efficiencies that are particular to each mode. The cuts are studied in succession in order to properly consider the correlation among them. Some efficiencies are determined by using a simple B-decay Monte Carlo (no underlying event or fragmentation) and a full simulation of the detector.

4.1 $B^\pm$ Mode

Use the M.C. simulation to determine the following two efficiencies

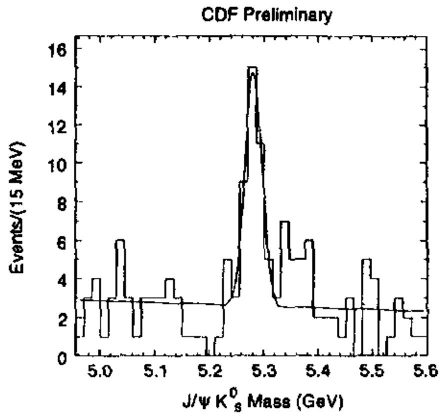

Figure 2: $J/\psi K^0_S$ mass distribution. The smooth line is a log likelihood fit of a gaussian plus a straight line. There are 31 $\pm$ 5 (stat) fitted events in the peak.

$\epsilon_{K^\pm}$ detection

Count number of found J/ψ within a $\pm 2.5\sigma$ mass window of the PDG value. Then count the number of B candidates. No cuts applied to the K. The ratio of these two numbers is $\epsilon_{K^\pm \text{ detection}}$.

$$\epsilon_{K^\pm \text{ detection}} = 0.878 \pm 0.028 \tag{7}$$

$\epsilon_{P_t(K^\pm)}$

Ratio of number $K^\pm$ after requiring $P_t(K^\pm) > 1.5$ GeV to the number before.

$$\epsilon_{P_t(K^\pm)} = 0.627 \pm 0.023 \tag{8}$$

4.2 B^0 Mode

Use the M.C. simulation to determine the following three efficiencies

$\epsilon_{K^0_S}$ detection

Count number of found J/ψ within a $\pm 2.5\sigma$ mass window of the PDG value. Count the number of K^0_S within a $\pm 2.5\sigma$ mass window. The ratio of these two numbers is $\epsilon_{K^0_S \text{ detection}}$.

$$\epsilon_{K^0_S \text{ detection}} = 0.611 \pm 0.017 \tag{9}$$

$\epsilon_{P_t(K^0_S)}$

Ratio of number K^0_S after requiring $P_t(K^0_S) > 1.5$ GeV to the number before.

$$\epsilon_{P_t(K^0_S)} = 0.748 \pm 0.024 \tag{10}$$

$\epsilon_{dist(K^0_S)}$

Ratio of number K^0_S after requiring $dist(K^0_S) > 1$ cm to the number before.

$$\epsilon_{dist(K^0_S)} = 0.926 \pm 0.031 \tag{11}$$

Use inclusive K^0_S sample to determine

$$\epsilon_{\text{other cuts}} = 0.789 \pm 0.040 \tag{12}$$

4.3 Ratio of Efficiencies

It comes to

$$\frac{\epsilon_{J/\psi K^0_S}}{\epsilon_{J/\psi K^\pm}} = 0.57 \pm 0.05 \tag{13}$$

An efficiency correction of 0.94 has been applied to account for the extra track in the $J/\psi K^0_S$ mode. This is needed as the M-C does not have a simulation of fragmentation or of the underlying event and the presence of extra tracks lowers the tracking efficiency.

5. RATIO OF BRANCHING RATIOS

$$\begin{aligned} \frac{BR(B^+ \to J/\psi K^+)}{BR(B^0 \to J/\psi K^0)} &= \frac{N_{J/\psi K^\pm}}{N_{J/\psi K^0_S}} \times \\ &\quad \frac{\epsilon_{J/\psi K^0_S}}{\epsilon_{J/\psi K^\pm}} \times 0.686 \times 0.5 \\ &= 1.05 \pm 0.3 \pm 0.2 \end{aligned} \tag{14}$$

where 0.686 is the $K^0_S \to \pi^+\pi^-$ branching ratio and 0.5 is the $K^0 \to K^0_S$ ratio. The 20% systematic uncertainty reflects our best guess for a conservative upper limit.

6. REFERENCES

1. I.I. Bigi, B. Blok, M. Shifman, N.G. Uratselv and A. Vainshtein, *A QCD "Manifesto" on Inclusive Decays of Beauty and Charm*, (DPF meeting of APS, November 1992).

Measurement of Angle γ

Convenors:

R. Aleksan
CEN Saclay

B. Kayser
National Science Foundation

P. Sphicas
Massachusetts Institute of Technology

List of Participants

A. Abashian
Virginia Polytechnic Institute

G. Abrams
Lawrence Berkeley Laboratory

M. Artuso
Syracuse University

P. Avery
University of Florida

F. Bird
Superconducting Super Collider Laboratory

E. Blucher
University of Chicago

D. Cords
Stanford Linear Accelerator Center

B. Cox
University of Virginia

J. Cunningham
Brandeis University

J. Dorenbosch
Superconducting Super Collider Laboratory

A. Erwin
University of Wisconsin

L. Garren
Fermi National Accelerator Laboratory

M. Johnson
Fermi National Accelerator Laboratory

P. Karchin
Yale University

J. Kroll
Fermi National Accelerator Laboratory

K. Nelson
University of Virginia

W. Selove
University of Pennsylvania

F. Snider
Johns Hopkins University

J. Slaughter
Yale University

I. Tzamouranis
University of Virginia

MEASUREMENT OF THE ANGLE GAMMA

R. Aleksan
Centre d'Etude Nucléaire Saclay
DAPNIA/SPP
F-91191 Gif-sur-Yvette Cedex, France

B. Kayser
Division of Physics
National Science Foundation
Arlington, VA 22230, USA

P. Sphicas
Physics Department and Laboratory for Nuclear Science
Massachusetts Institute of Technology
Cambridge, MA 02139, USA

1 INTRODUCTION

In the unitarity triangle, the angle γ is the phase between the legs $V_{ud}V_{ub}^*$ and $V_{cd}V_{cb}^*$. As such, it is the only angle that does not touch on the $V_{td}V_{tb}^*$ leg. This last combination of CKM elements enters in the amplitude of $B_d\bar{B}_d$ mixing. Therefore, both the α and β angles, which do have $V_{td}V_{tb}^*$ on one side can be measured by using B_d decays, which, unfortunately, do not yield any information on γ.

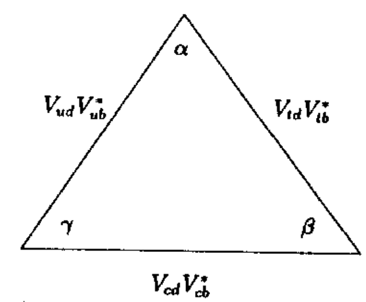

Therefore, the analog of the "golden" mode traditionally studied in association with the angle β, i.e. $B_d \to J/\psi K_s$, in the case of the angle γ involves the decay of a B_s meson. The mode cited frequently as a probe of γ is thus the decay $B_s \to \rho K_s$. And here lies the difficulty associated with γ: its measurement involves the decay of a B_s meson into an all-hadronic final state with a very small branching ratio. For an e^+e^- collider, this implies very small production cross-sections whereas for a hadron collider, the backgrounds would be formidable while the natural trigger provided by the J/ψ is no longer present. Moreover, the extraction of the angle γ from $B_s \to \rho K_s$ is not clean because of contributions from penguin and rescattering diagrams[1,5].

This situation, at least seemingly hopeless, has prompted intense theoretical work in search of more suitable decay modes. The result is a host of new possible decay modes. The most notable examples, some of which had been proposed prior to the workshop, together with the expected branching ratios, are listed in Table 1. Also listed in Table 1 are the requirements of each decay mode, i.e. whether a time-dependent analysis and tagging are required. With the exception of the $B_s \to J/\psi\phi$ decay, all the modes listed have all-hadronic final states. Furthermore, these new modes are still not easily triggerable in a hadronic environment. Experimentally, this puts severe demands on the trigger, the data acquisition system, the acceptance to be covered by the detectors, and certainly their background rejection capabilities.

Table 1. Decay modes for the angle γ.

Decay Mode	Branching fraction	Tagging required	Time-Dependent Analysis
$B_s \to \rho K_s$	5×10^{-7}	Yes	Yes
$B_s \to D_s^- K^+$	2×10^{-4}	Yes	Yes
$B^+ \to D_1^0 K^+$	2×10^{-4}	No	No
$B_s \to \psi\phi$	10^{-3}	Yes	Yes

In this paper we summarize the results of a first attempt to study the feasibility of using these modes in a hadronic machine. To this end, different accelerator-detector configurations have been examined:

1. The "Central Collider" option: a detector such as CDF covering the central rapidity ($|\eta| < 1$, $\theta > 40°$) region of a $p\bar{p}$ interaction[2] at $\sqrt{s} = 2$ TeV.

2. The "Forward Collider" option: a detector such as the one envisaged in the COBEX and BCD proposals, covering the large rapidity region ($1.5 < \eta < 5.5$, $0.3° < \theta < 34°$) of a pp interaction[3] at SSC-type energies.

3. The "Fixed Target" option: a detector such as the one proposed by the SFT collaboration with a proton beam on a fixed target at SSC-type energies.[4]

The goal of the γ working group was defined as a full comparison of the above three different options, hoping that at least one of them is sufficient for measurement of the angle γ. If none of the options could yield a measurement of γ with sufficiently small errors, then the next goal was defined as the description of a fourth option, the "Dream Detector" option, i.e. a non-existent, yet feasible, detector-accelerator option that would be needed for the measurement of γ.

Whenever possible, the capabilities of these different approaches have been compared. The task of defining a "γ" detector option, clearly capable of measuring γ accurately enough for a test of the closedness of the unitarity triangle, very quickly became one of requiring extremely large Trigger and Data Acquisition rates to tape. As such, very little has been concluded on this front.

The organization of this paper is as follows: in section 2 the details of the analysis of the $D_s^- K^+$ mode is presented. This is then used to compare the expectations for each of the three options. Section 3 contains the same information regarding the $B^+ \to D_1^0 K^+$ mode. In section 4, we examine the J/ψ-related modes proposed by Dunietz. No extensive analysis of these modes is attempted, since – with the exception of the time-dependent part of the analysis explained in section 2 – they are very similar to the $B_d \to J/\psi K_s$ analysis. Finally, we summarize an unexpected theoretical result that was obtained in the course of the workshop, regarding the meaning of the "measurement of "γ" in general. The subject is analyzed in detail in review of the subject by Aleksan, Kayser and London in these proceedings[1].

2. $B_s \to D_s^- K^+$

The study of this mode was first proposed in reference 5. Briefly, the B_s can decay into both $D_s^+ K^-$ and $D_s^- K^+$. Therefore, one can observe CP violation in this mode from the interference of the two amplitudes for the decay of the B_s, namely the direct decay and that via mixing, or, schematically,

$$B_s \to D_s^- K^+|seen = B_s \to D_s^- K^+ + B_s \to \bar{B}_s \to D_s^- K^+$$

One can then write[5]

$$\begin{aligned} Br(\bar{B}_s \to D_s^+ K^-) &\sim e^{-t}\{1 \mp R\cos x_s t \mp D\sin(-\gamma + \Delta\alpha)\sin x_s t\} \\ Br(\bar{B}_s \to D_s^- K^+) &\sim e^{-t}\{1 \pm R\cos x_s t \mp D\sin(-\gamma - \Delta\alpha)\sin x_s t\} \end{aligned} \tag{1}$$

where $R = \frac{\rho^2-1}{\rho^2+1}$, $D = \sqrt{1-R^2}$ and $\rho = \frac{|A_1|}{|A_2|}$; $\Delta\alpha$ is the strong phase difference between the two decays $D_s^+ K^-$ and $D_s^- K^+$; $|A_1|$ and $|A_2|$ are the amplitudes for the $B_s \to D_s^- K^+$ and $B_s \to D_s^+ K^-$ respectively. In equation (1) the first sign refers to the B_s whereas the second sign refers to the $\bar{B}_s$. Theoretical expectations yield $D \approx 0.94$. Denoting the decay of the B_s into either $D_s^+ K^-$ or $D_s^- K^+$ as $B_s \to D_s K$ an asymmetry is then expected in the quantity

$$A_{CP}(t) = \frac{N(B_s \to D_s K) - N(\bar{B}_s \to D_s K)}{N(B_s \to D_s K) + N(\bar{B}_s \to D_s K)} = D\cos\Delta\alpha\sin\gamma\sin x_s t$$

Depending on the value of the strong phase difference $\Delta\alpha$, an asymmetry may be visible. This measurement requires knowledge of the flavor of the decaying particle, i.e. whether it is a B_s or a $\bar{B}_s$. This "tagging" of the flavor of the decaying meson can be achieved by determining the flavor of the second b-flavored meson in the event. Lepton tagging refers to only using events in which the second b decays semileptonically, the sign of the lepton thus determining its flavor with a high efficiency. Another possibility arises from using kaons from the second b. In either case, the flavor of the meson that decayed into the $D_s K$ state is then determined and one computes the ratio A. Experimentally, the quantity measured is however not A_{CP} but rather

$$A_{meas} = A_{CP} D_{bkg} D_{tag} D_{mistag} D_{res} D_{fit}$$

where the factors D_x are various "dilution factors". These are:

1. D_{bkg} : this is the dilution due to the presence of background in the data sample, i.e. events not due to $B_s \to D_s K$ decays. If S is the signal and B is the background

$$D_{bkg} = \frac{S}{S+B}$$

2. D_{tag} : this is the dilution due to the mixing of the second b which is used for tagging. Using χ, the average B mixing parameter (averaged over all b-hadron species)

$$D_{tag} = 1 - 2\chi$$

3. D_{mistag} : this is the dilution due to mistagging. An example of mistagging is a lepton from the second b decay which does not arise from a direct decay of the b but from a sequential decay: $b \to c \to l$. Clearly, the sign of the lepton then does not corrrespond to the sign of the second b. If w is the mistagging probability,

$$D_{mistag} = 1 - 2w$$

4. D_{res} : this is the dilution arising from the resolution in the measurement of the decay length[6] (and therefore of the decay time t also).

$$D_{res} = e^{-\sigma_t x_s^2/2}$$

5. D_{fit}: this is the dilution arising from the statistics of the CP decay[6]. Simply put, the difference between the particle and antiparticle yields is maximum when the statistics on the lower of the two is minimum, and vice-versa.

$$D_{fit} = \sqrt{\frac{2x_s^2}{1+4x_s^2}}$$

The error on A_{meas} is given by $\delta A_{meas} = \frac{1-A_{meas}^2}{\sqrt{N}}$ where N is the total number of events observed. Including the background fraction in the events observed, the statistical error on A_{CP} is then given by

$$\delta A_{CP} = \frac{1}{D_{tag}}\frac{1}{D_{mistag}}\frac{1}{D_{res}}\frac{1}{D_{fit}}\frac{1}{\sqrt{D_{bkg}}}\frac{1}{\sqrt{N_{prod}}}$$

where N_{prod} is the number of events produced. In the above list of dilutions some terms are global, i.e. common to all experiments, while other terms are experiment-dependent. Clearly, the D_{bkg} and D_{res} are different for the three detector options under consideration. Also, since tagging is performed with different P_T thresholds, and in some experiments only leptons are being used, whereas in others kaons are also used, the factor D_{mistag} is also experiment-dependent. On the other hand, the dilution due to mixing of the tag and the fit statistics are common across experiments. To facilitate a comparison, we use $x_s = 10$ and $\chi = 0.15$ in what follows. We then apply the common factor $D_{tag}D_{fit} = 0.5$ to all experiments.

2.1 Time resolution

Clearly, the resolution on the measurement of the decay length of the B varies considerably across the three options. Table 2 lists the measured or expected secondary vertex resolution, the average B momentum, the average B decay length and the ratio of the decay length to its error for the three options. A B lifetime of 450 μm was assumed.

Clearly, the fixed-target option benefits greatly from the high boost of the B meson in the lab frame, resulting in a negligible fractional error on the decay length, and thus essentially no dilution due to this effect. On the other end of the spectrum, the Central Collider option refers to the measured quantities at CDF, and results in a sizable dilution of 0.6. These factors are assumed throughout this paper, whenever a time-dependent B_s analysis is involved.

Table 2. Decay length resolution and resulting Dilution factor for the three options.

	Central Collider (CDF)	Forward Collider (COBEX)	Fixed Target (SFT)
σ(Decay Length)	60 μm	0.15 mm	0.25 mm
$< P_B >$ (GeV)	7 – 10	45	450
$< \gamma c\tau >$	630 – 900 μm	4 mm	4 cm
l/σ_l	10 – 15	26	160
D_{res}	0.6	0.9	1.0

2.2 Background and Mistagging

With the exception of the CDF calculation, for which real data has been used to evaluate the signal to background ratio from the observed $D_s \to \phi\pi$ signal[2], the dilutions from backgrounds are based on Monte Carlo studies. As such, they entail large errors, and one should treat these numbers with caution. They are presented in table 3.

Table 3. Background and Mistagging fractions and resulting Dilution factor for the three options.

	Central Collider (CDF)	Forward Collider (COBEX)	Fixed Target (SFT)
$\sqrt{D_{bkg}}$	0.7	1.0	0.89
$D_{mistag}(e)$	0.8		0.85
(μ)	0.8		0.93
(K)			0.75
(average)	0.8	0.7	

The $D_{bkg} = 1$ for COBEX is simply due to the absence of a background calculation. CDF and COBEX use the decay chain $D_s \to \phi\pi$, $\phi \to K^+K^-$. SFT uses a host of decay modes for the D_s, including K^*K. These extra modes should have higher backgrounds (e.g. due to the large width of the K^*). The expected SFT dilutions, especially due to backgrounds, may be overly optimistic, due to the absence of data. Overall, however, there is not a big difference between the three options with the exception of Kaon tagging. CDF does not quote a fraction due to the lack of a particle identification system. This will result in much smaller tagging rates for the central collider option. COBEX lists an average dilution across the lepton and kaon tags.

The total dilution factor for the three options is thus computed as $D_{TOT} = 0.17, 0.31, 0.33$ for the three options (CDF, COBEX and SFT respectively). Note that in the Forward Collider contribution in these proceedings[3], the dilution factor due to tagging is equal to $D_{tag}D_{mistag}$ here; this is the difference between the dilutions presented here and those in reference 3: the product does yield the same dilution factor. Also note that the total dilution factor, *extracting* the contribution due to the time resolution, is approximately the same across experiments. The inclusion of a small background fraction in COBEX, for example, would yield a number very close to that from CDF - and similarly for the SFT.

2.3 Signal Expectations

We now turn to the expected signal. The relevant quantities are (a) the trigger effifiency (ϵ_{trig}), (b) the acceptance to the decay products (α), (c) the reconstruction efficiency (ϵ_{rec}) and (d) the tagging efficiency (ϵ_{tag}).

A direct comparison of the above factors for the three detector options is not always possible due to the overlap between the trigger and acceptance factors. Perhaps the most meaningful comparison can be made by examining the product of $\alpha \times \epsilon_{trig}$ across options. Even then, in some cases the tag is included in the trigger, and thus its efficiency - or at least part of it - is sometimes included in the trigger efficiency. Table 4 lists the above factors, and also the total efficiency, i.e. the product of the efficiencies listed. The luminosities assumed are 5×10^{31} cm^{-2}sec^{-1} at the Tevatron and 10^{32}cm^{-2}sec^{-1} at the SSC.

Table 4. Efficiencies and Expected yield for $B_s \to D_sK$

	Central Collider (CDF)	Forward Collider (COBEX)	Fixed Target (SFT)
$\epsilon_{trig} \times \alpha$	0.028	0.05	0.21
ϵ_{tag}	0.02	0.76	0.85
ϵ_{rec}	1.0	0.02	0.60
ϵ_{tot}	5.6×10^{-4}	7.6×10^{-4}	0.11
N_{exp} in 10^7 sec	7	412	1500

In the above, the CDF group has assumed the existence of a high impact parameter two-track trigger at level 1. Given the kinematic cuts of $P_T > 2$ GeV, this translates to the low trigger efficiency of ≈ 0.03. For comparison, the COBEX scheme, which also involves a secondary vertex trigger (the actual requirement is inconsistency with a single primary vertex) has a trigger efficiency of ≈ 0.05. The SFT group estimates a total trigger efficiency$\times$acceptance of 0.21. Presumably, the factor ~ 4 superior efficiency is due to SFT plans to trigger on very low P_T leptons in association with hadrons. The reader is referred to reference 4 for details on this subject. Finally, the 100% efficiency for reconstruction at CDF is due to the inclusion of the reconstruction requirements in the $\epsilon_{trig} \times \alpha$ factor[2].

From Table 4, it can be seen that the expected efficiency for SFT is ~ 100 times better than the CDF and COBEX efficiencies. This is because the SFT group has chosen to include factors like the Branching ratio of $B \to l$ into the total branching ratio for the decay, and not in the acceptance to leptons. A detailed comparison with the other two options is thus not possible. Perhaps the bottom line is just the number of events expected. Clearly, the Central Collider option at FNAL energies is far worse than the Forward and Fixed Target options at SSC-type energies. This can be traced to the small tagging efficiency expected in a central collider detector. In fact, were it not for this big difference, a CDF-type detector would be quite competitive (at least in principle) with the other two alternatives.

2.4 Error on γ

Combining the expected number of events with the dilution factors yields the estimated error on the quantity $\cos\Delta\alpha \sin\gamma$. This is listed in table 5. Taken at face value, the measurement is hopeless at CDF and - assuming the background estimates and trigger efficiencies of SFT are correct - possible with a fixed-target experiment at high energy.

Table 5. Error on $\sin\gamma$ from $B_s \to D_sK$ for 10^7 sec; $\cos\Delta\alpha = 1$.

	Central Collider (CDF)	Forward Collider (COBEX)	Fixed Target (SFT)
$\delta(\sin\gamma\cos\Delta\alpha)$	2.4	0.16	0.08

In the course of the workshop, attention was drawn to the possibility that use of higher B resonances (such as the B^{**}) or charge correlations between the B meson and fragmentation tracks could enhance significantly the tagging rate of a single B meson[7]. Clearly, CDF stands to gain the most from such a possibility. This fact is noted, and no further analysis of this possibility is attempted at this point, until more experimental input on the feasibility of such a tagging method is received.

It should be noted that the above analysis does not yield a value for $\sin\gamma$, since the strong phase difference, $\Delta\alpha$, is unknown - even though we expect $\Delta\alpha \sim 0$. As explained in the theoretical contribution to the γ group[1], the actual solution for $\sin\gamma$ involves discrete ambiguities. Thus, even if one fits the independent B_s and $\bar{B}_s$ time distributions in (1), there remains an ambiguity between $\Delta\alpha$ and γ. Thus, this decay mode can be used only as long as an external means of distinguishing between the two solutions exists. Ideally, one would have multiple measurements of $\sin\gamma$ using various decay modes. It is conceivable that these extra decay modes can help in determining the correct $\sin\gamma$, without the ambiguity with $\cos\Delta\alpha$.

In conclusion, the proposed designs are at least capable of observing an asymmetry in $B_s \to D_sK$, for values of $\cos\Delta\alpha$ not too small. It should also be noted here that this result depends crucially on the assumed value of x_s and also on the backgrounds quoted by the proponents of the COBEX and SFT proposals.

3. $B^\pm \to D_1K^\pm$

The details of this decay mode are discussed in the theoretical review of the γ angle in [1]. The method was proposed in reference [8]. Briefly, CP violation in $B^+ \to D_1K^+$ arises from the interference of the two amplitudes for $B^+ \to \bar{D}^oK^+$ (the favored "right" decay mode) and $B^+ \to D^oK^+$ (the "wrong" i.e. unfavored mode). Here, D_1 refers to a CP eigenstate of the D^o meson, as deduced from, say, the decay $D^o \to K^+K^-$. The branching ratios for the two modes differ by a factor 100. Schematically[8],

$$\sqrt{2}A(B^+ \to D_1^o K^+) = A(B^+ \to D^o K^+) + A(B^+ \to \bar{D}^o K^+)$$
$$\sqrt{2}A(B^- \to D_1^o K^-) = A(B^- \to D^o K^-) + A(B^- \to \bar{D}^o K^-)$$

where

$$A(B^+ \to D^o K^+) = M e^{i\gamma} e^{i\alpha_1} \qquad A(B^+ \to \bar{D}^o K^+) = \bar{M} e^{i\alpha_2}$$

where, as usual, α_1, α_2 are the strong phases. A similar expression holds for the B^-. An asymmetry is then expected in the two rates for $B^+ \to D_1^o K^+$ and $B^- \to D_1^o K^-$:

$$|A(B^+ \to D_1^o K^+)|^2 - |A(B^- \to D_1^o K^-)|^2 = 2M\bar{M} \sin\Delta\alpha \sin\gamma$$

where $\Delta\alpha = \alpha_1 - \alpha_2$.

Unfortunately, there is still the unmeasurable factor $\sin\Delta\alpha$ - which leads to a discrete ambiguity in determining $\sin\gamma$ just like in the $B_s \to D_s K$ case. The question, experimentally, is whether one can measure this asymmetry, and to a lesser extent, what the "error" on γ is, given the discrete ambiguity. Once one accounts for the branching ratio of D^o mesons into observable final states, such as $K\pi$, and with the assumption that both $D^o \to \pi^+\pi^-$ and $D^o \to K^+K^-$ decays can be used for observing the $B^+ \to D_1 K^+$ decay, the final branching ratios for the "right", the "CP" and the "wrong" mode are roughly in the ratio 100 : 10 : 1. Clearly, measurement of the angle γ will be dominated by the statistics in the "wrong mode".

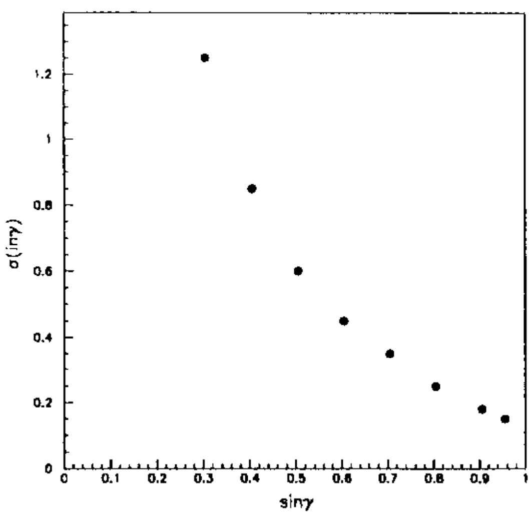

Figure 1: The error on $\sin\gamma$ as a function of $\sin\gamma$, for COBEX-type statistics.

Table 6. Expectations for $B^\pm \to D_1 K^\pm$ in 10^7 sec.

	Central Collider (CDF)	Forward Collider (COBEX)	Fixed Target (SFT)
N_{exp}	122	627	1100

Experimentally, this decay is attractive - compared to $B_s \to D_s K$ - because the B is self tagged from its decay products, via the sign of the kaon in the decay. Given the input from the previous section, we expect results roughly similar to the $B_s \to D_s K$ case for the fixed target and forward collider options, and a significant enhancement of the expected signal for the central collider option.

This indeed turns out to be the case, as can be seen in table 6 which lists the expected number of events for the three options. The numbers listed are the expectations for the CP eigenstate, which after all is the most important decay mode, since an asymmetry has to be observed before any attempts at measuring γ can be made. It can be seen that the gain of a factor 50 in CDF (by avoiding the tagging requirement) results in a considerably increased event yield.

None of the groups has included a dilution due to background. With this caveat, an asymmetry - dependent on the strong phase difference again - may actually be observed. This is shown for the CDF case by explicit calculation of the error on the expected asymmetry for various values of $\sin\gamma$ and $\sin\Delta\alpha$ [2]. As an example, the best case of $\sin\Delta\alpha = 1$ and $\sin\gamma = 1$ would result in an asymmetry of 0.20, measured with an error of 0.09.

The error on $\sin\gamma$ is more complicated to calculate, because of the discrete ambiguity. A calculation by Avery[9] in this workshop yields an error which is dependent on the value of $\sin\gamma$. This is shown in Figure 1. The calculation assumes the best-case scenario, that in which $\Delta\alpha = \pi/2$.

4. $B_s \to J/\psi\phi$

It has been suggested by Dunietz[10] that CP violation can also be observed in the decays $B_s \to J/\psi\phi$. In the Wolfenstein approximation, $V_{cb}V_{cs}^*$ has no phase and this decay does not exhibit CP violation. Thus,

$$B_s \to J/\psi\phi$$

was considered as a good mode to *search* for CP violation as a sign of new physics. When one treats the CKM phases exactly, instead of within the Wolfenstein approximation, and *assuming* unitarity leads to a small CP violation effect given by

$$A_{CP}(t) = 2|V_{cd}|\left|\frac{V_{ub}}{V_{cb}}\right| \sin\gamma \sin x_s t$$

Clearly, the factor multiplying $\sin\gamma$ is quite small (~ 0.03). And since it finally represents a dilution factor, the statistics required for measurement of γ with a certain precision is increased by a factor $\sim 10^3$. The presence of the J/ψ in the final state, however, makes this analysis possible: a natural trigger is provided.

This mode, involving a B_s, again, implies a time-dependent analysis. In addition, it requires tagging. The expected yields for CDF are therefore too small to discern an asymmetry (due to the extra factor 10^3 required in this mode). The analysis has, however, been attempted by the two other options. The expected yields, total dilution factor and error on $\sin\gamma$ are shown in table 7.

Table 7. Expectations for $B_s \to J/\psi\phi$ in 10^7 sec.

	Forward Collider (COBEX)	Fixed Target (SFT)
N_{exp}	74,000	101,000
D_{tot}	0.25	0.33
$\delta(\sin\gamma)$	0.5	0.32

In determining the values in Table 7, the efficiencies predicted by the COBEX and SFT groups have been used. The total dilution factor used differs from the one cited by COBEX[3] because a factor 0.71 to account for the missing D_{fit} dilution in COBEX – referred to a "d(mix)" in [3] – and a resolution factor $D_{res} = 0.9$ have been applied in order to facilitate the comparison. It should be noted that the SFT group cites a very small mistagging fraction, whereas COBEX has no background estimate. The yields listed should therefore be regarded as optimistic. To compensate for this, the dilution factor due to $2|V_{cd}|\left|\frac{V_{ub}}{V_{cb}}\right|$ was taken to be 0.03, i.e. on the low side of the expected range for $\left|\frac{V_{ub}}{V_{cb}}\right|$. The estimate on the error on $\sin\gamma$ differs from the one in [4]. This is probably to the non-inclusion of this extra dilution factor.

At any rate, the measurement seems to be quite possible at SSC-type energies, over a span of 2 – 3 years. In addition, this mode remains an excellent probe of new physics in the event that an abnormally high asymmetry is observed.

Another suggestion by Dunietz has been to use the decay mode $J/\psi\rho$. The analysis is similar to the one for $J/\psi\phi$ The width of the ρ will certainly introduce more background. In addition, in this case the asymmetry also depends on the angle β:

$$A_{CP} \sim Im\lambda; \qquad \lambda = e^{-2i\beta}\frac{1 + re^{-i\gamma}}{1 + re^{i\gamma}}$$

where r is in general a complex number with magnitude in the range 0.01 – 0.10. This decay mode clearly suffers from the small dilution factor r and also the dependence on β. A preliminary analysis by the SDC group[11] yields that a measurement, excluding background contaminations, etc. which could be significant, will require the equivalent of ~ 5 SSC years.

5. $B_s \to \rho K_s$

This mode is the direct analog of the $B_d \to J/\psi K_s$ decay mode for the angle β. It requires tagging and a time-dependent analysis. These have been investigated by the Forward Collider and Fixed Target groups. The reader is directed to the contributions from the Forward Collider and SFT groups[3,4].

It should be noted that this decay mode can receive considerable contributions from penguin diagrams, thus making extraction of the angle γ theoretically unclear (one really measures a linear combination of the β and γ angles that only theoretical calculations can decipher).

6. Measuring γ

A closer examination by Aleksan, Kayser and London of what one actually measures in all the decay modes considered so far yielded a host of interesting results[1]. Briefly stated, none of the decay modes examined here actually measures the angle γ directly, without reference to either (a) other angles in the unitarity triangles, or (b) invoking an approximation.

For example, the $B^o \to \pi^+\pi^-$ decay probes the angle α via the mixing of $B_d^o \leftrightarrow \bar{B}_d^o$. The asymmetry in $B^o \to \pi^+\pi^-$ vs $\bar{B}^o \to \pi^+\pi^-$ decays is proportional to the phase of the CKM product $V_{ub}^*V_{ud}/V_{ub}V_{ud}^* \times V_{td}^*V_{tb}/V_{td}V_{tb}^*$. This angle is 2α. The term $V_{td}^*V_{tb}/V_{td}V_{tb}^*$ arises from the mixing $B_d^o \leftrightarrow \bar{B}_d^o$. In B_s decays, the equivalent factor is $V_{ts}^*V_{tb}/V_{ts}V_{tb}^*$ and thus, B_s decays do not measure the angle γ.

It is then shown [1] that the $B_s \to D_sK$ decay results in a CP asymmetry which is proportional to $\sin(\gamma + O(\lambda^2))$. Similarly, the $B_s \to \rho K_s$ decay results in an asymmetry proportional to $\sin 2(\gamma + O(\lambda^2))$. The $O(\lambda^2)$ terms disappear only upon using the Wolfenstein approximation. Thus, in general, the "γ" modes do not yield a measurement of γ but an approximation to it. The Dunietz suggestion of using the $J/\psi\phi$ mode probes the small λ^2 angle in the unitarity triangle formed by the unitarity condition applied to the sb row-column combination of the CKM matrix:

$$V_{us}V_{ub}^* + V_{cs}V_{cb}^* + V_{ts}V_{tb}^* = 0$$

i.e. it corresponds to the measurement of the angle between the sides $V_{ts}V_{tb}^*$ and $V_{cs}V_{cb}^*$. Using unitarity, this small angle can be expressed approximately in terms of γ and the magnitudes of certain CKM elements.

Further theoretical work by Aleksan, Kayser and London has yielded a much more general statement regarding measurement of the complete CKM matrix via four angles. This work is reviewed in [1] also.

7. Conclusion

The angle γ at least as defined in the Wolfenstein approximation is not completely out of reach of current or proposed dedicated B experiments. This conclusion certainly depends crucially on the assumed trigger and tagging efficiencies and also on the expected backgrounds. The work summarized here represents but a first step in the direction of extracting the third angle of the unitarity triangle. The theoretical developments during the workshop have resulted in a clearer understanding of the quantities studied. On the experimental side, new decay modes (i.e. in addition to the traditional ρK_s decay) have resulted in expectations for observing CP violation in B_s decays which are not unreasonable. It is conceivable that a dedicated B experiment can probe a fundamental aspect of the Standard Model, the CKM matrix, in multiple ways. In the process, new physics can appear anywhere along the line.

8. Acknowledgements

We would like to thank the organizers of the workshop for their efforts in creating a pleasant environment in which it was possible to work efficiently and productively. The computing and library facilities were exceptional.

9. REFERENCES

1. R. Aleksan, B. Kayser, D. London, "In Pursuit of Gamma", in these proceedings.
2. E. Blucher et al., "Measuring γ with the Decays $B_s \to D_s K$ and $B_u \to D^o K$ with the CDF detector at the Tevatron", in these proceedings.
3. P. Karchin et al., "Measurement of the angle gamma with a Forward Collider Detector", in these proceedings.
4. B. Cox et al., "The Measurement of the Angle Gamma in the SFT, an SSC Fixed Target B Experiment", in these proceedings.
5. R. Aleksan, I. Dunietz and B. Kayser, *Zeit. Phys.* **C54** (1992) 653.
6. R. Aleksan, I. Dunietz, B. Kayser and F. Le Diberder, *Nucl. Phys.* **B361** (1991) 141; also see K. McDonald, "Maximum-Likelihood Analysis of CP-violating Asymmetries", Princeton Preprint Princeton/HEP/92-04.
7. M. Gronau, A. Flippe and J. Rosner, *Phys. Rev.* **D47** (1993) 1988.
8. M. Gronau and D. Wyler, *Phys. Lett.* **B265** (1991) 172.
9. P. Avery, private communication, this workshop.
10. I. Dunietz, *Phys. Lett.* **B270** (1991) 75. Also see the proceedings in this workshop.
11. F. Bird, "The Prospect for Determining the Angle γ in the decay $B_d^0 \to J/\psi\rho$ at the SSC", in these proceedings.

In Pursuit of Gamma

R. Aleksan
DAPNIA, CE Saclay
F-91191 Gif-sur-Yvette Cedex, France

B. Kayser
Division of Physics, National Science Foundation
4201 Wilson Blvd., Arlington, VA 22230 USA

and

D. London
Laboratoire de physique nucléaire, Université de Montréal
C.P. 6128, succ. A, Montréal, Québec, CANADA, H3C 3J7

ABSTRACT

After reviewing techniques for extracting clean information on CP-violating phase angles from B decays, we explain the rules for finding decay modes that can probe the phase angle γ of the unitarity triangle. We identify the more promising of these "γ modes," estimate their branching ratios, and examine the degree to which they are theoretically clean. We then show that when the quark mixing matrix is not approximated as usual, but is treated exactly, none of the "γ modes" actually measures γ. Rather, each of them measures γ plus some correction. In all modes, the correction is small enough to be disregarded in first-generation experiments, but in some of them, it may be large enough to be observed in second-generation experiments.

Our treatment of the γ modes calls attention to the fact that when the quark mixing matrix is treated exactly, there are six unitarity triangles, rather than just one triangle. However, only four of the angles in these six triangles are independent. Examining the role played by these four angles, we discover that, in principle at least, measurements of nothing but CP-violating asymmetries in B decays are sufficient to determine the entire quark mixing matrix.

1. INTRODUCTION

In the Standard Model, CP violation is caused by complex elements in the unitary C(abibbo)-K(obayashi)-M(askawa) quark mixing matrix, V. If this Model is correct, then in many B decays there should be large CP-violating asymmetries from which theoretically clean information on the phases in V can be extracted. This information can then be used to confirm in detail that phases in V really are the origin of CP violation, or to exhibit an inconsistency of the theory.

In the Wolfenstein approximation[1] to V, there is a phase convention in which this matrix is real except for the elements V_{ub} and V_{td}. In this approximation, experiments on CP violation in B decays are usually described as probes of the angles α, β and γ of the "unitarity triangle," shown in Fig. 1. That the legs in this Figure form a closed triangle follows from the unitarity constraint that the d and b columns of V must be orthogonal, and the assumption that there are only three generations. From Fig. 1 we see that in the

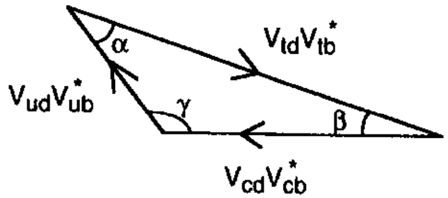

Figure 1: The unitarity triangle expressing orthogonality of the d and b columns of the CKM matrix.

Wolfenstein approximation,

$$\gamma \simeq -arg(V_{ub}) \ , \qquad \beta \simeq -arg(V_{td}) \ , \qquad \alpha \simeq \pi + arg(V_{ub}) + arg(V_{td}). \tag{1}$$

Thus, probing the angle γ – the focus of the Gamma Working Group within this Snowmass Workshop – amounts to probing the phase of V_{ub}.

In Sec. 2, we recall what must be measured to extract clean CKM phase information from the decays of *neutral* B mesons. We then identify a number of B decay modes which potentially can yield the phase of V_{ub}. We estimate the branching ratios, and comment on the degree of theoretical cleanliness, of these modes.

In Sec. 3, we ask what happens if one treats the CKM matrix exactly, rather than in the Wolfenstein approximation. The single unitarity triangle of Fig. 1 is then replaced by the six unitarity triangles of Fig. 9, which express the orthogonality of any pair of columns, or any pair of rows, of V. We find that when the Wolfenstein approximation is not made, *none* of the B decays modes proposed so far as "probes of the angle γ" actually measure γ. Instead, each of these modes measures γ plus corrections which are small angles in the triangles other than the one of Fig. 1. We explore the degree to which these corrections may undermine the interpretation of these decay modes as probes of γ.

In Sec. 4, we report on a general analysis of the unitarity triangles and CP-violating phases when the CKM matrix is treated exactly. We find that the CKM phase yielded by a theoretically-clean decay mode is always a simple linear combination of angles in the unitarity triangles. Moreover, at least in principle, measurements of CP-violating asymmetries in B decays are sufficient to determine, not only some angles in one unitarity triangle, but the entire CKM matrix.

2. POTENTIAL PROBES OF GAMMA

2.1 *Extraction of CKM Phases*

In general, *theoretically clean* CKM phase information can be extracted only from the decays of the *neutral* B mesons, B_d and B_s. In the decays of either of these mesons, we are usually interested in some final state which can come both from the pure B and from the pure $\overline{B}$. Now, owing to B-$\overline{B}$ mixing, a particle born at time $t=0$ as a pure $|B_q\rangle$, $q=d$ or s, evolves in time t into a state $|B_q(t)\rangle$ which is a linear superposition of $|B_q\rangle$ and $|\overline{B}_q\rangle$.[2,3] In the (excellent) approximation that B-$\overline{B}$ mixing is dominated by a t-quark box diagram, this superposition is given by

$$|B_q(t)\rangle = exp\left(-i(m_q - i\frac{\Gamma_q}{2})t\right)\left[c_q|B_q\rangle + i\,\omega_q s_q|\overline{B}_q\rangle\right]. \tag{2}$$

Here, m_q is the average mass of the two mass eigenstates of the B_q-$\overline{B}_q$ system, and Γ_q is their common width.[4] With Δm_q their mass difference,

$$c_q \equiv \cos\left(\frac{\Delta m_q}{2}t\right), \text{ and } s_q \equiv \sin\left(\frac{\Delta m_q}{2}t\right). \tag{3}$$

Finally, ω_q is the CKM phase of the amplitude $A(B_q \to \overline{B}_q)$ for $|B_q\rangle \to |\overline{B}_q\rangle$, and is given by

$$\omega_q = \frac{V_{tq}V_{tb}^*}{V_{tq}^*V_{tb}}. \tag{4}$$

In a similar fashion, a particle born at $t=0$ as a pure $|\overline{B}_q\rangle$ evolves in time t into a linear superposition $|\overline{B}_q(t)\rangle$ of $|\overline{B}_q\rangle$ and $|B_q\rangle$ given by an expression analogous to that of Eq. (2). Suppose, now, that f is some final state which can come both from a pure B_q and from a pure $\overline{B}_q$. From Eq. (2), the amplitude $A(B_q(t) \to f)$ for the meson $B_q(t)$ which at time $t=0$ was a pure B_q to decay into f at time t is

$$A(B_q(t) \to f) = exp\left(-i(m_q - i\frac{\Gamma_q}{2})t\right)\left[c_q\,A(B_q \to f) + i\,\omega_q s_q\,A(\overline{B}_q \to f)\right]. \tag{5}$$

The corresponding time-dependent decay rate, $\Gamma_{q,f}(t) \equiv |A(B_q(t) \to f)|^2$, then contains a term representing the interference between the $A(B_q \to f)$ and $A(\overline{B}_q \to f)$ terms in Eq. (5).

Let us now turn to the CP-mirror-image process $\overline{B}_q(t) \to \bar{f}$, in which the meson $\overline{B}_q(t)$ born at $t=0$ as a pure $\overline{B}_q$ decays into the final state $\bar{f}$, the CP-mirror-image of f. The rate for this process, $\overline{\Gamma}_{q,\bar{f}}(t) \equiv |A(\overline{B}_q(t) \to \bar{f})|^2$, also contains an $A(B_q \to f)$-$A(\overline{B}_q \to f)$ interference term. However, when the CKM matrix elements are complex, this interference term has, in general, a different magnitude than its counterpart in $\Gamma_{q,f}(t)$. This difference leads to a CP-violating difference between $\overline{\Gamma}_{q,\bar{f}}(t)$ and $\Gamma_{q,f}(t)$, which one would like to observe. In order to observe it, one must know in each event whether the decaying meson was born as a B_q or a $\overline{B}_q$. That is, one must tag it as one of these by observing a flavor-revealing decay of an accompanying beautiful meson or baryon. It may also be possible to use an interesting, recently-proposed "self-tagging" method.[5]

Suppose that the final state f is a CP eigenstate, so that $\bar{f}$ is the same as f. If f has intrinsic CP parity η_f, the decay rates $\Gamma_{q,f}(t)$ and $\overline{\Gamma}_{q,\bar{f}}(t) = \overline{\Gamma}_{q,f}(t)$ are given by[2]

$$\begin{aligned}\Gamma_{q,f}(t) &\propto exp(-\Gamma_q t)\left[1 + \eta_f \sin\varphi_{q,f}\sin(\Delta m_q t)\right],\\ \overline{\Gamma}_{q,f}(t) &\propto exp(-\Gamma_q t)\left[1 - \eta_f \sin\varphi_{q,f}\sin(\Delta m_q t)\right].\end{aligned} \tag{6}$$

Here, $\varphi_{q,f}$ is the phase of some product of CKM elements whose identities depend on q and f. It is $\varphi_{q,f}$ that we would like to determine from the asymmetry in the decay rates (6). We shall be interested in decays where $\varphi_{q,f}$ is γ, or perhaps 2γ.

Suppose, next, that the final state f is not a CP eigenstate, but has a CP conjugate $\bar{f}$ distinct from itself. An example of interest is $f = D_s^+K^-$, $\bar{f} = D_s^-K^+$. Theoretically clean CKM phase information can still be extracted.[6] There are now four decay rates which can be measured. They are given by

$$\begin{aligned}
\Gamma_{q,f}(t) &= exp(-\Gamma_q t)\left[c_q^2 M_{q,f}^2 + s_q^2 \overline{M}_{q,f}^2 + 2c_q s_q M_{q,f}\overline{M}_{q,f}\sin(\varphi_{q,f}+\theta_{q,f})\right] \\
\overline{\Gamma}_{q,\bar{f}}(t) &= exp(-\Gamma_q t)\left[c_q^2 M_{q,f}^2 + s_q^2 \overline{M}_{q,f}^2 + 2c_q s_q M_{q,f}\overline{M}_{q,f}\sin(-\varphi_{q,f}+\theta_{q,f})\right] \\
\overline{\Gamma}_{q,f}(t) &= exp(-\Gamma_q t)\left[c_q^2 \overline{M}_{q,f}^2 + s_q^2 M_{q,f}^2 - 2c_q s_q M_{q,f}\overline{M}_{q,f}\sin(\varphi_{q,f}+\theta_{q,f})\right] \\
\Gamma_{q,\bar{f}}(t) &= exp(-\Gamma_q t)\left[c_q^2 \overline{M}_{q,f}^2 + s_q^2 M_{q,f}^2 - 2c_q s_q M_{q,f}\overline{M}_{q,f}\sin(-\varphi_{q,f}+\theta_{q,f})\right] . \qquad (7)
\end{aligned}$$

Here, $\Gamma_{q,f}(t)$ is the rate for decay of $B_q(t)$ into f, $\overline{\Gamma}_{q,\bar{f}}(t)$ is the rate for decay of $\overline{B}_q(t)$ into $\bar{f}$, etc. The angle $\varphi_{q,f}$ is, as before, the phase of some product of CKM elements whose identities depend on q and f. As before, $\varphi_{q,f}$ is the quantity we would like to determine, and we shall be interested here in decays where $\varphi_{q,f}$ is γ or 2γ. The constants $M_{q,f}$ and $\overline{M}_{q,f}$ are, respectively, the magnitudes of the amplitudes $A(B_q \to f)$ and $A(\overline{B}_q \to f)$. It is desirable that $M_{q,f}$ and $\overline{M}_{q,f}$ be comparable, so that the rates (7) will be sensitive to $\varphi_{q,f}$. Finally, $\theta_{q,f}$ is a strong-interaction phase.

With Γ_q and Δm_q known, measuring the decay rates (7) more than suffices to determine the quantities $s_\pm(q,f) \equiv \sin(\pm\varphi_{q,f}+\theta_{q,f})$. In turn, these quantities determine $\sin^2\varphi_{q,f}$, up to a two-fold ambiguity, via the expression

$$\sin^2\varphi_{q,f} = \frac{1}{2}\left[1 - s_+(q,f)s_-(q,f) \pm \sqrt{(1-s_+^2(q,f))(1-s_-^2(q,f))}\right] . \qquad (8)$$

If, contrary to what we have assumed here, the two mass eigenstates of the B_q-$\overline{B}_q$ system have widths which differ enough to result in measurable effects, it becomes possible to experimentally resolve some of the ambiguities in the determination of $\varphi_{q,f}$.

The decay rates (6) and (7) hold when $A(B_q \to f)$ and $A(\overline{B}_q \to f)$ are each dominated by a single Feynman diagram, so that they each have a well-defined CKM phase. When, instead, $A(B_q \to f)$ receives significant contributions from several Feynman diagrams with different CKM phases, the extraction of clean CKM phase information from experimental decay rates is either impossible or requires measurement of rates for several isospin-related decays.[7] When several diagrams contribute significantly, the largest one is usually a tree diagram, and the others are usually penguin diagrams. In exploring the usefulness of each decay mode proposed as a probe of the angle γ, we will consider the degree to which penguin or other diagrams with CKM phases different from that of the dominant diagram might contribute significantly to the mode.

In the decay rates (6) and (7), the violation of CP invariance, and the information on the CKM phase $\varphi_{q,f}$ producing this violation, are in the term proportional to $2c_q s_q = \sin(\Delta m_q t)$. To learn about $\varphi_{q,f}$, one would like to measure the time dependence of the rates and uncover this term. When f is not a CP eigenstate and the rates are described by Eqs. (7), measurement of their time dependence is absolutely essential. Not all four decay rates need be measured. Indeed, it is easy to see[3] that, say, $\Gamma_{q,f}(t)$ and $\overline{\Gamma}_{q,\bar{f}}(t)$ alone suffice to determine $\sin^2\varphi_{q,f}$. However, if we measure only the time integrals of the rates (7), then we cannot determine $\sin^2\varphi_{q,f}$, even if we measure the time integrals of all four of the rates. For, if Eqs. (7) hold, then clearly we must have

$$\Gamma_{q,f}(t) + \overline{\Gamma}_{q,f}(t) = \Gamma_{q,\bar{f}}(t) + \overline{\Gamma}_{q,\bar{f}}(t) . \qquad (9)$$

Now, when the decay rates in this constraint are replaced by their time integrals, they become merely four numbers, instead of four functions of time, and the constraint implies that only *three* of these four numbers are independent. But the decay rates (7), and their time-integrated analogues, depend on *four* unknowns: $M_{q,f}$, $\overline{M}_{q,f}$, $\varphi_{q,f}$, and $\theta_{q,f}$. Hence, it is impossible to determine $\varphi_{q,f}$ from the time-integrated rates. When f is a CP eigenstate and the decay rates are described by Eqs. (6), then in principle one can extract $\sin\varphi_{q,f}$ from a knowledge of the time-integrated rates alone. However, in the case of B_s decay, this will be extremely difficult if, as we expect,[8] Δm_s is an order of magnitude larger than Γ_s. When $x_s \equiv \Delta m_s/\Gamma_s$ is large, the fractional contribution of the CP-violating $\sin\varphi_{q,f}\sin(\Delta m_s t)$ term in Eqs. (6) to the decay rate gets reduced by a factor of $\sim 1/x_s$ when the rate is integrated over time.

In view of these circumstances, we assume here that when one is seeking to extract CKM phase information from a neutral B decay, the time dependence of the decay rate must be measured, except perhaps in B_d decay to a CP eigenstate.

2.2 *Neutral B Decay Modes That Can Probe Gamma*

In which neutral B decays can we identify the CKM phase $\varphi_{q,f}$ that is probed as γ or 2γ? As we have discussed, the CP violation that we study in the decay $B_q(t) \to f$ results from interference between the two terms in the decay amplitude (5). The CKM phase $\varphi_{q,f}$ that is probed by $B_q(t) \to f$ is, therefore, just the relative CKM phase of these two terms. Thus, remembering that ω_q is the CKM phase of $A(B_q \to \overline{B}_q)$, we see from Eq. (5) that the $\varphi_{q,f}$ probed by $B_q(t) \to f$ is given by

$$\varphi_{q,f} = CKM\ Phase\ \left[\frac{A(B_q \to f)}{A(B_q \to \overline{B}_q) \times A(\overline{B}_q \to f)}\right] . \qquad (10)$$

Instead of referring to Eq. (5), we may think of the CP violation in $B_q(t) \to f$ as resulting from interference between the amplitude $A(B_q \to f)$ for the particle born as a pure B_q to decay directly to f, and the amplitude $A(B_q \to \overline{B}_q) \times A(\overline{B}_q \to f)$ for this particle to convert, via mixing, into a $\overline{B}_q$ which then decays into f. Once again we conclude that the $\varphi_{q,f}$ probed by $B_q(t) \to f$ is given by (10).

Now, recall that in the Wolfenstein approximation to the CKM matrix, all CKM elements are real save V_{ub} and V_{td}, and $\gamma = -arg(V_{ub})$. In this approximation, the CKM phase of $A(B_d \to \overline{B}_d)$ is

$$arg(V_{td}/V_{td}^*) = -2\beta , \qquad (11)$$

while that of $A(B_s \to \overline{B}_s)$ is

$$arg(V_{ts}/V_{ts}^*) = 0 . \qquad (12)$$

Thus, from Eq. (10), we can probe γ by studying $B_s(t)$ decays in which the phase of $A(B_s \to f)/A(\overline{B}_s \to f)$ is essentially γ. This will be the case when each of $B_s \to f$ and $\overline{B}_s \to f$ is dominated by a tree diagram, and either (a) the tree diagram for $B_s \to f$ involves one of the processes

$$\bar{b} \to \bar{u} + \begin{cases} c\bar{s} \\ c\bar{d} \\ u\bar{s} \\ u\bar{d} \end{cases} , \qquad (13)$$

or (b) the tree diagram for $\overline{B}_s \to f$ involves one of the processes

$$b \to u + \begin{cases} \bar{c}s \\ \bar{c}d \\ \bar{u}s \\ \bar{u}d \end{cases} , \qquad (14)$$

Decay Mode	Branching Ratio
$B_s \to D_s^{\pm} K^{\mp}$	2×10^{-4}
$B_s \to D^0 \phi, \overline{D^0}\phi$	2×10^{-5}
$B_s \to \rho^0 K_S$	5×10^{-7}

Table 1: B_s decay modes that can probe the angle γ.

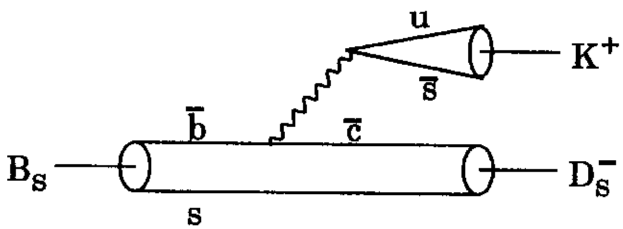

Figure 2: The dominant diagram for $B_s \to D_s^- K^+$.

or both. When both (13) and (14) are involved, the CKM phase of $A(B_s \to f)/A(\overline{B}_s \to f)$ is obviously $arg(V_{ub}^*/V_{ub}) = 2\gamma$. When only one of them is involved, the other is replaced by a (real) $b \to c$ or $\bar{b} \to \bar{c}$ transition, so that the phase of $A(B_s \to f)/A(\overline{B}_s \to f)$ is γ.

We have considered the hadronic B_s decay modes produced by tree diagrams for the quark processes (13,14). We have tried to identify the modes that have advantageous branching ratios, and in which the interfering decay amplitudes $A(B_s \to f)$ and $A(\overline{B}_s \to f)$ are each dominated by a single Feynman diagram[9] and have comparable magnitudes. The most promising modes we found are listed, together with their estimated branching ratios, in Table 1. These branching ratios were obtained by comparing the modes of interest to others whose branching ratios are already known. We now discuss the modes in Table 1 in turn.

• $B_s(t), \overline{B}_s(t) \to D_s^{\pm} K^{\mp}$:[10]

Here the final state $f \equiv D_s^+ K^-$ is distinct from its CP conjugate, $\bar{f} \equiv D_s^- K^+$, and one uses the expressions (7) to analyze the time-dependent decays of $B_s(t)$ and $\overline{B}_s(t)$ into f and $\bar{f}$. Tagging of the parent meson and study of the time dependence of the decays are essential.

The expected branching ratio is relatively large. The value quoted in Table 1, 2×10^{-4}, is for the decay $B_s \to D_s^- K^+$. Like all the values quoted, it assumes the parent to be a pure B_s and neglects mixing. The value 2×10^{-4}, which should be fairly reliable, is obtained by comparing the dominant diagram for $B_s \to D_s^- K^+$, shown in Fig. 2, to the very similar one for the decay $B_d \to D^- \pi^+$, whose branching ratio is known. The branching ratio for the decay $B_s \to D_s^+ K^-$ (again of a pure B_s neglecting mixing) is estimated, both in Ref. 10 and by the present authors, to be $\sim 1 \times 10^{-4}$. This estimate is obtained by comparing the dominant diagram for $B_s \to D_s^+ K^-$, shown in Fig. 3, to the related but somewhat different diagram for $B^- \to \Psi K^-$. Accordingly, it is not as reliable as the estimate for $B_s \to D_s^- K^+$.

In $B_s(t) \to D_s^+ K^-$, the interfering decay amplitudes are, of course, $A(B_s \to D_s^+ K^-)$

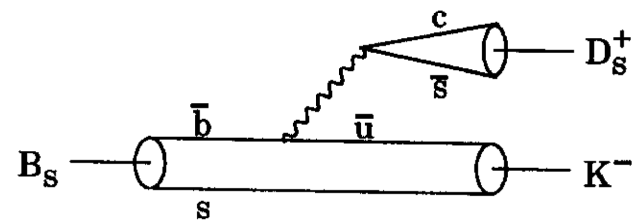

Figure 3: The dominant diagram for $B_s \to D_s^+ K^-$.

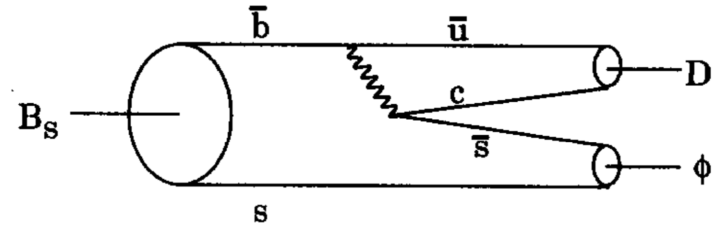

Figure 4: The dominant diagram for $B_s \to D^0 \phi$.

and $A(\overline{B}_s \to D_s^+ K^-)$. The amplitude $A(B_s \to D_s^+ K^-)$, being dominated by the diagram of Fig. 3, has a CKM phase which is $arg(V_{ub}^* V_{cs}) \simeq \gamma$. This amplitude receives no other tree-level contributions except from a W-exchange diagram with the same CKM phase. Penguin diagrams cannot contribute at all. The amplitude $A(\overline{B}_s \to D_s^+ K^-)$ is dominated by the diagram which is the CP-mirror-image of that in Fig. 2. Thus, it has a CKM phase which is $arg(V_{cb} V_{us}^*) \simeq 0$. It receives no other tree-level contributions except from a W-exchange diagram with the same CKM phase, and no penguin contributions. Thus, from Eq. (10), the CKM phase $\varphi_{s,D_s^+K^-}$ probed by the rates (7) for the decays $B_s(t), \overline{B}_s(t) \to D_s^{\pm} K^{\mp}$ is γ. Moreover, from our branching ratio estimates, the magnitudes $M_{s,D_s^+K^-} = |A(B_s \to D_s^+ K^-)|$ and $\overline{M}_{s,D_s^+K^-} = |A(\overline{B}_s \to D_s^+ K^-)|$ $(= |A(B_s \to D_s^- K^+)|)$ of the two interfering decay amplitudes in $B_s(t) \to D_s^+ K^-$ are in the ratio $(1 \times 10^{-4}/2 \times 10^{-4})^{1/2} \simeq 0.7$. Thus, the desire that these magnitudes be comparable is very nicely satisfied.

• $B_s(t), \overline{B}_s(t) \to D^0 \phi, \overline{D^0}\phi$:

Once again, we have a final state, $f = D^0 \phi$, which is distinct from its CP conjugate, $\bar{f} = \overline{D^0}\phi$, and we use the expressions (7) to analyze the four time-dependent decays $B_s(t) \to D^0 \phi$, $B_s(t) \to \overline{D^0}\phi$, $\overline{B}_s(t) \to D^0 \phi$, and $\overline{B}_s(t) \to \overline{D^0}\phi$. Tagging of the parent B is essential.

In $B_s(t) \to D^0 \phi$, the interfering decay processes are $B_s \to D^0 \phi$, which is dominated by the tree diagram in Fig. 4, and $\overline{B}_s \to D^0 \phi$, which is dominated by the tree diagram in Fig. 5. Penguin diagrams cannot contribute. Thus, the CKM phase $\varphi_{s,D^0\phi}$ probed by $B_s(t) \to D^0 \phi$ and the related decays is γ.

The branching ratio estimate quoted in Table 1, 2×10^{-5}, is for $B_s \to \overline{D^0}\phi$, or for its CP-mirror-image $\overline{B}_s \to D^0 \phi$, and is obtained by comparing this process to $B_d \to \Psi K^{*0}$.

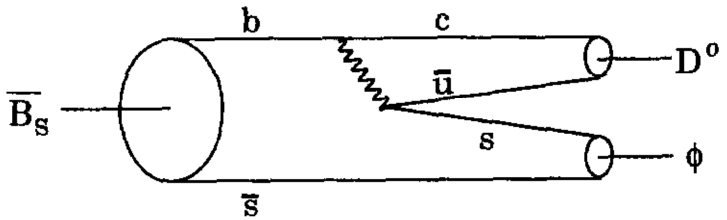

Figure 5: The dominant diagram for $\overline{B}_s \to D^0\phi$.

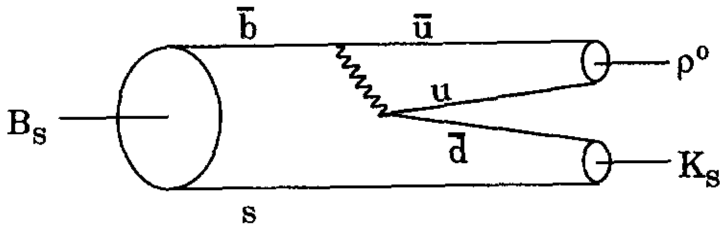

Figure 6: The dominant diagram for $B_s \to \rho^0 K_S$.

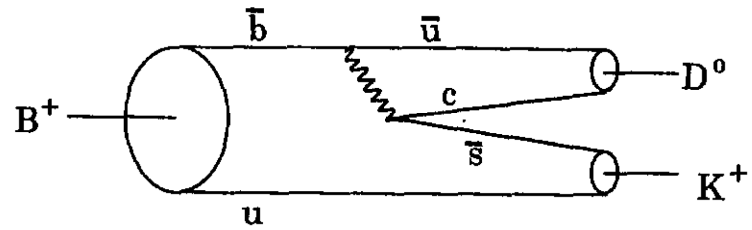

Figure 7: The dominant diagram for $B^+ \to D^0K^+$.

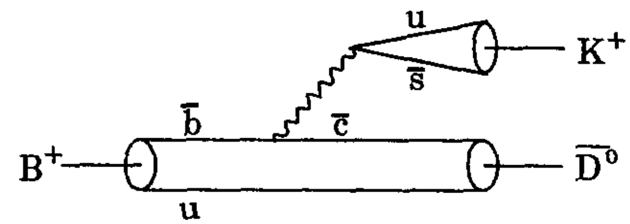

Figure 8: The dominant diagram for $B^+ \to \overline{D^0}K^+$.

The diagram which dominates $B_s \to D^0\phi$ is almost identical to that which dominates $\overline{B}_s \to D^0\phi$, apart from CKM factors, and we estimate the branching ratio for $B_s \to D^0\phi$ to be 4×10^{-6}. The magnitudes $M_{s,D^0\phi} = |A(B_s \to D^0\phi)|$ and $\overline{M}_{s,D^0\phi} = |A(\overline{B}_s \to D^0\phi)|$ of the two interfering decay amplitudes in $B_s(t) \to D^0\phi$ then have the ratio $(4\times10^{-6}/2\times10^{-5})^{1/2} \simeq 0.4$, which is $O(1)$, as desired.[11]

• $B_s(t), \overline{B}_s(t) \to \rho^0 K_S$:

This mode, oft-proposed as a probe of γ, has the advantage of yielding a CP eigenstate, so that the analysis is simplified. However, the estimated branching ratio, obtained by comparing $B_s \to \rho^0 K_S$ to $B_d \to \Psi K_S$, is very small.

The decay amplitudes $A(B_s \to \rho^0 K_S)$ and $A(\overline{B}_s \to \rho^0 K_S)$ that interfere in $B_s(t) \to \rho^0 K_S$ are dominated, respectively, by the tree diagram in Fig. 6 and by its CP-mirror-image. Thus, from Eq. (10), the CKM phase $\varphi_{s,\rho^0 K_S}$ probed by $B_s(t), \overline{B}_s(t) \to \rho^0 K_S$ via Eqs. (6) is 2γ. Furthermore, as in all decays to a CP eigenstate, if one diagram dominates $A(B_q \to f)$ and its CP-mirror-image dominates $A(\overline{B}_q \to f)$, these two interfering decay amplitudes are of identical size. However, unlike the other modes in Table 1, $B_s(t), \overline{B}_s(t) \to \rho^0 K_S$ does involve penguin contributions. Possibly, these are significant, and some of them have CKM phases other than γ. Thus, in addition to having a small branching ratio, $B_s(t), \overline{B}_s(t) \to \rho^0 K_S$ may not be a clean probe of γ.

2.3 *Non-B_s Decay Modes That Can Probe Gamma*

While most decays of charged B mesons cannot yield clean CKM phase information, the decays $B^\pm \to DK^\pm$ are an exception, and they probe γ.[12] The technique for using these decays, explained in Ref. 12, requires one to measure the branching ratios for $B^\pm \to D^0K^\pm$, $B^\pm \to \overline{D^0}K^\pm$, and $B^\pm \to D_{CP}K^\pm$, where D_{CP} is a neutral D that decays to a CP eigenstate such as K^+K^- or $\pi^+\pi^-$. As in all charged B decays, there is, of course, no need to tag, and no non-exponential time dependence.

The decay $B^+ \to D^0K^+$ is dominated by the diagram in Fig. 7, while $B^+ \to \overline{D^0}K^+$ is dominated by the diagram in Fig. 8. Since D_{CP} is a coherent superposition of D^0 and $\overline{D^0}$, in $B^+ \to D_{CP}K^+$ the diagrams of Figs. 7 and 8 interfere. Now, the CKM phase of the $B^+ \to D^0K^+$ diagram, Fig. 7, is $arg(V_{ub}^*V_{cs}) \simeq \gamma$. That of the $B^+ \to \overline{D^0}K^+$ diagram, Fig. 8, is $arg(V_{cb}^*V_{us}) \simeq 0$. Hence, the interference between these diagrams probes γ. There are no penguin contributions, so this probe is quite clean.

By comparing the diagram for $B^+ \to \overline{D^0}K^+$ to that for $B^+ \to \overline{D^0}\pi^+$, we readily estimate that $BR(B^+ \to \overline{D^0}K^+) \simeq 2\times10^{-4}$. This is a promising value. However, by comparing the diagram for $B^+ \to D^0K^+$ to that for $B^+ \to \Psi K^+$, we estimate that $BR(B^+ \to D^0K^+) \sim 2\times10^{-6}$. In addition, by comparing $B^+ \to D^0K^+$ to $B_d \to \overline{D^0}\pi^0$, for which there is an interesting upper limit,[13] we estimate that $BR(B^+ \to D^0K^+) \lesssim 6\times10^{-6}$. Thus, if these estimates prove to be right, this branching ratio may be hard to measure. So may the branching ratios for $B^\pm \to D_{CP}K^\pm$, since study of these processes requires that the neutral D decay to a CP eigenstate, a requirement which costs a factor of $\sim 10^{-2}$ in overall branching ratio. The initial $B^\pm$ decay will be dominated by the diagram of Fig. 8 or its CP-mirror-image, and so will have a branching ratio of $\simeq 2\times10^{-4}$. Thus, the overall branching ratio will be $\sim 2\times10^{-6}$.

As in all studies of CP violation in B decay, one would like the two diagrams which interfere in $B^+ \to D_{CP} K^+$ to be of comparable magnitude. From our branching ratio estimates, their magnitudes will be in the ratio $\sim (2\times 10^{-6}/2\times 10^{-4})^{1/2} \simeq 1/10$. While not as close to unity as one might wish, this ratio is perhaps close enough to yield measurable interference effects.

A variant of the $B^\pm \to DK^\pm$ approach utilizing the self-tagging B_d decays $B_d(\overline{B}_d) \to DK^{*0}(D\overline{K}^{*0})$ has been proposed as an alternate way to probe γ.[14] By comparing to $B^+ \to D^0K^+$, we estimate that $BR(B_d \to D^0K^{*0}) \sim 2\times 10^{-6}$, and by comparing to $B_d \to \overline{D}^0 K^{*0}$, that $BR(B_d \to \overline{D^0}K^{*0}) \sim 2\times 10^{-5}$.

3. WHAT ANGLES DO THE "GAMMA" MODES ACTUALLY MEASURE?

We have identified a number of B decay modes which, *within the Wolfenstein approximation to the CKM matrix*, probe the angle γ. In each of these modes, the decay amplitude consists of two interfering terms, as illustrated in Eq. (5), and each of these terms is dominated by a single Feynman diagram. *In the Wolfenstein approximation*, the CKM phases of these dominating diagrams are such that the interfering terms in the decay amplitude have relative CKM phase γ, or 2γ. In this approximation, the statement that our "γ modes" probe γ entails only the error, which we have argued is in most cases small or absent, corresponding to the neglect of the non-dominating diagrams. However, suppose that one does not make the Wolfenstein approximation. The CKM phases of Feynman diagrams are then altered. Neglecting the non-dominating diagrams, do the "γ modes" still probe γ? If not, what phase angle does each of them actually probe? How big an error do we make if we identify this angle as being approximately γ?

To explore these questions, we note that a very useful framework for dealing with phases in the CKM matrix is provided by the "unitarity triangles." One of these triangles is shown in Fig. 1. When the CKM matrix is treated exactly, rather than in the Wolfenstein approximation, one has, not just this one triangle, but six triangles. These triangles correspond to the unitarity constraint that any pair of columns, or any pair of rows, of the CKM matrix be orthogonal. That is, they correspond to the orthogonality requirements

$$\begin{array}{llll}
ds & V_{ud}V_{us}^* & + \; V_{cd}V_{cs}^* & + \; V_{td}V_{ts}^* = 0 \\
 & \lambda & \quad\lambda & \quad\lambda^5 \\[6pt]
sb & V_{us}V_{ub}^* & + \; V_{cs}V_{cb}^* & + \; V_{ts}V_{tb}^* = 0 \\
 & \lambda^4 & \quad\lambda^2 & \quad\lambda^2 \\[6pt]
db & V_{ud}V_{ub}^* & + \; V_{cd}V_{cb}^* & + \; V_{td}V_{tb}^* = 0 \\
 & \lambda^3 & \quad\lambda^3 & \quad\lambda^3 \\[6pt]
uc & V_{ud}V_{cd}^* & + \; V_{us}V_{cs}^* & + \; V_{ub}V_{cb}^* = 0 \\
 & \lambda & \quad\lambda & \quad\lambda^5 \\[6pt]
ct & V_{cd}V_{td}^* & + \; V_{cs}V_{ts}^* & + \; V_{cb}V_{tb}^* = 0 \\
 & \lambda^4 & \quad\lambda^2 & \quad\lambda^2 \\[6pt]
ut & V_{ud}V_{td}^* & + \; V_{us}V_{ts}^* & + \; V_{ub}V_{tb}^* = 0 \\
 & \lambda^3 & \quad\lambda^3 & \quad\lambda^3
\end{array} \tag{15}$$

To the left of each of these equations, we have indicated the pair of columns, or pair of rows, whose orthogonality it expresses. Also, under each term in the equations, we have indicated the rough magnitude of the term as a power of the Wolfenstein parameter $\lambda = 0.22$.

The unitarity triangles, depicted somewhat schematically in Fig. 9, are simply pictures in the complex plane of the conditions (15). Apart from signs and extra π's, the angles in any triangle are just the relative phases of the various terms in the corresponding condition. Let us refer to a specific triangle by stating the columns (rows) whose orthogonality it expresses, and a specific leg in this triangle by stating which up-type (down-type) quark it involves. Denoting up-type quarks by Greek letters, and down-type ones by Latin letters, let

$$\omega_{\alpha\beta}^{ij} \equiv arg\left(V_{\alpha i}V_{\alpha j}^*/V_{\beta i}V_{\beta j}^*\right) \tag{16}$$

be the relative phase of the α and β legs in the ij triangle. Since

$$arg\left(V_{\alpha i}V_{\alpha j}^*/V_{\beta i}V_{\beta j}^*\right) = arg\left(V_{\alpha i}V_{\beta i}^*/V_{\alpha j}V_{\beta j}^*\right), \tag{17}$$

$\omega_{\alpha\beta}^{ij}$ is also the relative phase of the i and j legs in the $\alpha\beta$ triangle. That is, each angle in a triangle expressing orthogonality of rows is also an angle in one expressing orthogonality of columns. Hence, for our discussion of CKM phases, we can forget about the row triangles. From the first two of Eqs. (15) (c.f. also Fig. 9), we see that

$$\begin{aligned}
\omega_{uc}^{ds} &\leq O(\lambda^4), \\
\omega_{ct}^{sb} &\leq O(\lambda^2).
\end{aligned} \tag{18}$$

That is, one of the angles in the sb triangle is small ($\lesssim 0.05$), and one in the ds triangle is extremely small ($\lesssim 0.003$). (There is no reason to suppose that the remaining angles in these triangles are small.)

Now, when the CKM matrix is treated exactly, what CKM phases do the decay modes we have discussed in Sec. 2 actually probe? Any neutral B mode probes the phase given by Eq. (10). Applied to any $B_s(t)$ decay, this equation involves the mixing phase $arg(B_s \to \overline{B_s})$, which from Eq. (4) is $arg(V_{ts}V_{tb}^*/V_{ts}^*V_{tb})$. Moreover, the V_{ts}/V_{ts}^* in this expression cannot be cancelled by the decay amplitudes $A(B_s \to f)$ and $A(\overline{B_s} \to f)$ so long as these amplitudes are dominated by tree diagrams, which can never involve a t quark. However, from Fig. 1, apart from a π,

$$\gamma \equiv \omega_{uc}^{db} = arg(V_{ud}V_{ub}^*/V_{cd}V_{cb}^*). \tag{19}$$

Since the CKM elements in this expression do not include V_{ts}, it is clear that the phase probed by a $B_s(t)$ decay cannot be γ.

For the decay $B_s(t) \to D_s^+K^-$, $A(B_s \to f)$ is dominated by the diagram in Fig. 3, proportional to $V_{cs}V_{ub}^*$. Similarly, $A(\overline{B_s} \to f)$ is dominated by the CP-mirror-image of the diagram in Fig. 2, and so is proportional to $V_{cb}V_{us}^*$. Thus, from Eqs. (10) and (4), the phase probed by $B_s(t) \to D_s^+K^-$ is

$$\begin{aligned}
\varphi_{s,D_s^+K^-} &= arg\left[\frac{V_{cs}V_{ub}^*}{\dfrac{V_{ts}V_{tb}^*}{V_{ts}^*V_{tb}}\,V_{cb}V_{us}^*}\right] \\
&= arg\left[\frac{V_{ud}V_{ub}^*}{V_{cd}V_{cb}^*}\left(\frac{V_{cs}V_{cb}^*}{V_{ts}V_{tb}^*}\right)^2\frac{V_{us}V_{ud}^*}{V_{cs}V_{cd}^*}\right] \\
&= \gamma + 2\,\omega_{ct}^{sb} - \omega_{uc}^{ds}\,.
\end{aligned} \tag{20}$$

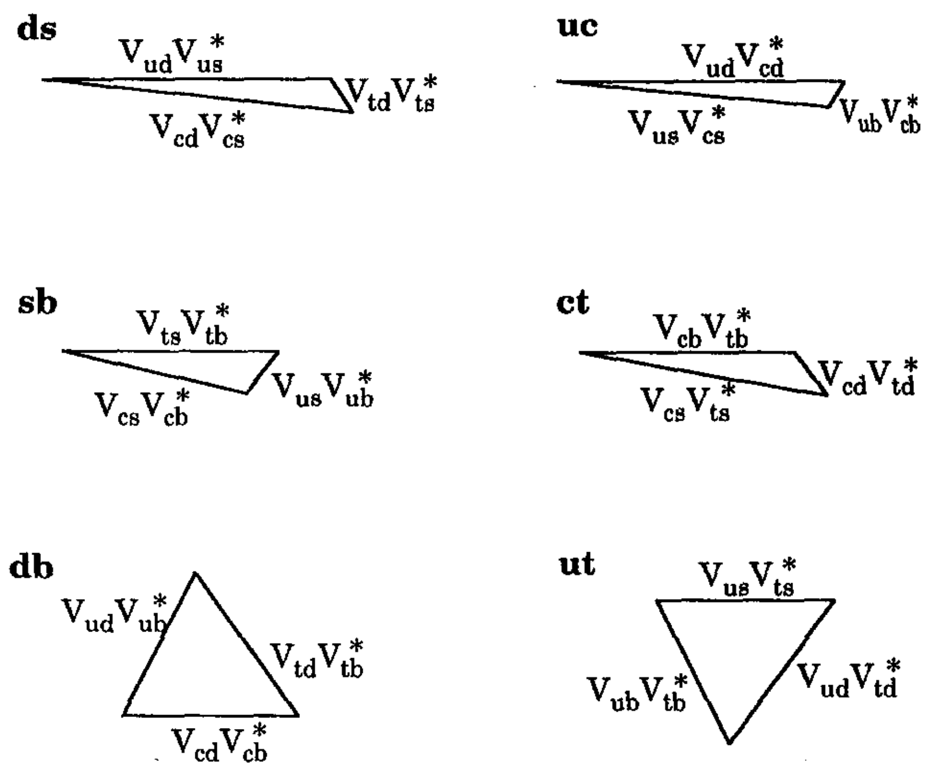

Figure 9: The unitarity triangles. To the left of each triangle is indicated the pair of columns, or of rows, whose orthogonality this closed triangle expresses.

Decay Mode	CKM Phase Probed
$B_s, \overline{B}_s \to D_s^{\pm} K^{\mp}$	$\gamma + 2\omega_{ct}^{sb} - \omega_{uc}^{ds}$
$B_s, \overline{B}_s \to D^0\phi, \overline{D^0}\phi$	$\gamma + 2\omega_{ct}^{sb} - \omega_{uc}^{ds}$
$B_s, \overline{B}_s \to \rho^0 K_S$	$2(\gamma + \omega_{ct}^{sb})$
$B^{\pm} \to DK^{\pm}$ [with $D \to K^+K^-$]	$\gamma - \omega_{uc}^{ds}$
$B_d(\overline{B}_d) \to DK^{*0}(D\overline{K}^{*0})$ [with $D \to K^+K^-$]	$\gamma - \omega_{uc}^{ds}$

Table 2: CKM phases probed by the "γ modes" when the CKM matrix is treated exactly.

We see that this phase is γ plus angles in the sb and ds triangles. From Eq. (18), we note that the particular sb and ds angles involved are the small ones, so that $\varphi_{s,D_s^+K^-}$ is γ plus a $\leq O(\lambda^2)$ correction.

In the same way, we can find the CKM phases probed by the other $B_s(t)$ decay modes listed in Table 1. For the decays

$$B^{\pm} \rightarrow D + K^{\pm}, \quad D \hookrightarrow f_{CP} \tag{21}$$

where f_{CP} is the CP eigenstate (e.g. K^+K^-) into which the neutral D decays, we must find the relative CKM phase of the two interfering terms in the decay amplitude

$$\begin{aligned} A\left(\begin{matrix} B^+ \to D + K^+ \\ \hookrightarrow f_{CP} \end{matrix}\right) &= A(B^+ \to D^0K^+)A(D^0 \to f_{CP}) \\ &\quad + A(B^+ \to \overline{D^0}K^+)A(\overline{D^0} \to f_{CP}). \end{aligned} \tag{22}$$

If D^0-$\overline{D^0}$ mixing is slow compared to the D^0 decay rate, then, as suggested by Eq. (22), the D-system phases which influence the decay sequence (21) are the D *decay* phases, not the D^0-$\overline{D^0}$ mixing phase. But then the phase probed by the sequence depends on f_{CP}. For $f_{CP} = K^+K^-$, we find from the diagrams of Figs. 7 and 8, and the tree diagrams for $D^0 \to K^+K^-$ and $\overline{D^0} \to K^+K^-$, that the relative CKM phase of the two terms in Eq. (22) is

$$\begin{aligned} arg\left[V_{us}V_{ub}^*/V_{cs}V_{cb}^*\right] &= \omega_{uc}^{sb} \\ &= arg\left[\frac{V_{ud}V_{ub}^*}{V_{cd}V_{cb}^*}\frac{V_{us}V_{ud}^*}{V_{cs}V_{cd}^*}\right] = \gamma - \omega_{uc}^{ds}. \end{aligned} \tag{23}$$

Thus, the decay chain (21) with $f_{CP} = K^+K^-$ probes a CKM phase which is one of the "large" angles in the sb triangle, and this angle is in turn γ plus a $\leq O(\lambda^4)$ correction.

In Table 2 we show what CKM phases are actually probed by the various "γ modes" we have considered when the CKM matrix is treated exactly. These phases are expressed in terms of γ and angles in the sb and ds triangles. We see from Table 2 that *none* of the modes we have discussed actually measures γ. Every one of them yields γ, or 2γ, plus nonzero corrections. On the other hand, in every case the corrections involve only the $\leq O(\lambda^2)$ angle in the sb triangle and/or the $\leq O(\lambda^4)$ angle in the ds triangle. Thus, the corrections are always less than 0.1 radians. One might wonder whether the correction angles ω_{ct}^{sb} and ω_{uc}^{ds} can represent a *fractionally* large correction in the event that γ itself is small. It can be

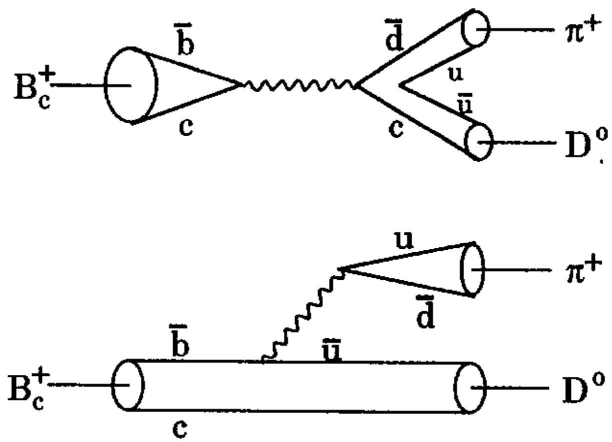

Figure 10: Diagrams for $B_c^+ \to D^0\pi^+$.

shown that they cannot. When γ goes to zero, ω_{ct}^{sb} and ω_{uc}^{ds} also go to zero, at the same rate as γ. Furthermore, given what is already known about the CKM matrix, the proportionality constant relating ω_{ct}^{sb} to γ for small γ is ~ 0.015, and that relating ω_{uc}^{ds} to γ is still smaller. Thus, the corrections to γ are always fractionally small.

As the examples in Table 2 suggest, *any* B decay mode which probes γ in the Wolfenstein approximation probes γ plus, at most, corrections involving only the small angles ω_{ct}^{sb} and ω_{uc}^{ds} when the CKM matrix is treated exactly. For, as discussed in Sec. 4, the exact CKM phase probed by an arbitrary B decay mode can be expressed as a linear combination of γ, β, ω_{ct}^{sb} and ω_{uc}^{ds}, with integer coefficients. Now, for a B decay which yields γ in the Wolfenstein approximation, this linear combination obviously does not involve β. Thus, apart from γ, it can involve only ω_{ct}^{sb} and ω_{uc}^{ds}.

While the angles measured by the various "γ modes" differ only slightly from γ, they do differ, and in some modes they may differ by as much as 0.05 to 0.1. In contrast, neglecting penguin contributions, the "α modes" $B_d, \overline{B}_d \to \pi^+\pi^-$ and $B_d, \overline{B}_d \to \rho^\pm\pi^\mp$ yield precisely α, even when the CKM matrix is treated exactly. Similarly, assuming as usual that K^0-$\overline{K^0}$ mixing is dominated by the $d\bar{s} \to c\bar{c} \to s\bar{d}$ box diagram, the "β mode" $B_d, \overline{B}_d \to \Psi K_S$ yields precisely β. Thus, in the second generation experiments on CP violation in B decays, it would be interesting to test the Standard Model by showing that the angles extracted from, say, the modes $B_d, \overline{B}_d \to \pi^+\pi^-$, $B_d, \overline{B}_d \to \Psi K_S$ and $B_s, \overline{B}_s \to D_s^\pm K^\mp$ *fail* to add up to π by an amount of order 0.05 to 0.1. To carry out this precision test of the angles probed by the leading diagrams in various modes, one would have to eliminate from $B_d, \overline{B}_d \to \pi^+\pi^-$ the possible penguin contributions, using an isospin analysis.[7]

It is tempting to ask whether there is *any* B decay mode which, unlike all the modes we have discussed, actually measures precisely γ when the CKM matrix is not approximated. In principle, the mode $B_c^+ \to D^0\pi^+$ does this via interference between the diagrams shown in Fig. 10. The relative CKM phase of these diagrams is just $arg(V_{ud}V_{ub}^*/V_{cd}V_{cb}^*) = \gamma$. However, it is not clear that the penguin diagrams for this decay are small relative to the annihilation diagram in Fig. 10,[15] and, in any case, this mode, like most charged B decays, cannot yield clean CKM phase information.

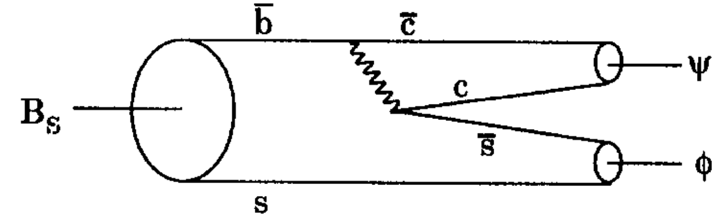

Figure 11: The dominant diagram for $B_s \to \Psi\phi$.

It would, of course, be very interesting to probe directly angles in the sb and ds triangles. One decay mode that would do this is $B_s(t), \overline{B}_s(t) \to \Psi\phi$.[16] In this mode, the interfering decay amplitudes are $A(B_s \to \Psi\phi)$,which is dominated by the diagram in Fig. 11, and $A(\overline{B}_s \to \Psi\phi)$, which is dominated by its CP conjugate. From Eqs. (10) and (4), the CKM phase probed by $B_s(t) \to \Psi\phi$ is then[17]

$$\begin{aligned}
\varphi_{s,\Psi\phi} &= arg\left[\frac{V_{cs}V_{cb}^*}{\frac{V_{ts}V_{tb}^*}{V_{ts}^*V_{tb}}\,V_{cb}V_{cs}^*}\right] \\
&= 2\,arg\left[\frac{V_{cs}V_{cb}^*}{V_{ts}V_{tb}^*}\right] = 2\,\omega_{ct}^{sb}\,, \qquad (24)
\end{aligned}$$

just twice the small angle in the sb triangle.

To use this mode, tagging and measurement of the time dependence will, of course, be necessary. The final state $\Psi\phi$ is technically not a CP eigenstate, because it may be a mixture of helicity configurations. However, it appears that the outgoing particles in the decay $B_d \to \Psi K^*$ have zero helicity much of the time.[18] We then expect the same to be true of the outgoing particles in $B_s(t), \overline{B}_s(t) \to \Psi\phi$. The final state then *is* largely a CP eigenstate, and the decay rates are described by the simple equations (6).

By comparing to the very similar decay $B_d \to \Psi K^*$, one readily estimates that $BR(B_s \to \Psi\phi) \simeq 10^{-3}$, a very promising value.

It has been pointed out[16] that $\sin\varphi_{s,\Psi\phi}$, the quantity probed by $B_s(t), \overline{B}_s(t) \to \Psi\phi$ via Eqs. (6), can be rewritten as

$$|\sin\varphi_{s,\Psi\phi}| = 2\left|V_{cd}\frac{V_{ub}}{V_{cb}}\sin\gamma\right|(1 + O(\lambda^2)). \qquad (25)$$

Thus, if $|V_{ub}/V_{cb}|$ is known, this decay mode becomes another way to determine γ. Of course, the mode does not "probe γ" in the sense of involving two interfering amplitudes whose relative CKM phase is γ or 2γ. Rather, the relative phase is, as we saw in Eq. (24), the small phase $2\omega_{ct}^{sb}$. The CP-violating asymmetry in the mode will be correspondingly small, rather than being of order $\sin\gamma$ or $\sin 2\gamma$. Indeed, if we assume that $|V_{ub}/V_{cb}| \sim 0.07$,[13] then Eqs. (25) and (6) indicate that the asymmetry will be $\sim 0.03 \sin\gamma$, which is necessarily quite small. Nevertheless, perhaps the large branching ratio for the mode will make this small asymmetry observable. Needless to add, if $B_s(t), \overline{B}_s(t) \rightarrow \Psi\phi$ should be found to have an asymmetry much larger than, say, 0.06, then we would have evidence for a CP-violating mechanism beyond that in the Standard Model.

4. THE UNITARITY TRIANGLES AND THE CKM MATRIX

The discussion of the previous Section calls attention to the unitarity triangles beyond the db triangle, and to the angles in those other triangles. We would now like to briefly report the results of a general analysis of how the angles in the full set of six unitarity triangles are related to CP-violating asymmetries in B decay, and of how they are related to the CKM matrix. A more complete discussion, including the proofs of the results, will be presented elsewhere.[19]

There are three main results, which we shall describe in turn.

- As we have already noted (see Eq. 17), each angle in a "row" triangle is also an angle in a "column" triangle. Thus, there are at most nine, not eighteen, distinct angles in the six unitarity triangles. We find that exactly four of these nine angles are independent. The remaining five angles are very simple linear combinations of the independent four. The independent angles may be chosen, for example, as two of the angles α, β and γ in the db triangle, plus two of the angles in one of the other column triangles. They may also be chosen as two of the angles α, β and γ, plus the two small angles ω_{ct}^{sb} and ω_{uc}^{ds}.

- As we have seen, any CP-violating asymmetry in B decay probes the relative CKM phase of two interfering amplitudes. Thus, the asymmetry probes the phase of some product and quotient, or, equivalently, of some product, of CKM elements. Now, not every conceivable product of CKM elements has a phase which is invariant under phase redefinitions of the quark fields. However, if the phase of some product of CKM elements is determined by an experiment, then, obviously, this phase must be invariant under quark-field rephasing.

  We find that if the phase φ of some product of CKM elements is rephasing-invariant, then

  $$\varphi = \sum_{i=1}^{4} n_i \varphi_i + k\pi \ , \tag{26}$$

  where the φ_i are the four independent angles in the unitarity triangles, the n_i are integers, and k is zero or one. For any specific φ and choice of the independent angles φ_i, the n_i and k will, of course, be known quantities.

  The relation (26) states that the CKM phase probed by any CP-violating asymmetry in a B decay is a simple linear combination, with integer coefficients, of the four independent angles in the unitarity triangles. Thus, these angles form a complete set of variables for the description of CP violation in B decay. Moreover, these variables are very closely and simply related to the quantities – the phases φ – to be measured in B decay experiments.

- Suppose that the four independent angles φ_i have been determined by CP-violation experiments. What have we learned about the CKM matrix? The answer is that once the φ_i are known, the entire CKM matrix follows from them! That is, in principle at least, we can determine the whole CKM matrix, including the magnitudes of all its elements, and all its physically-meaningful phases, through measurements of nothing but CP-violating asymmetries in B decays. Thus, albeit at varying levels of sensitivity, these CP-violating asymmetries probe *everything* in the CKM matrix. Consequently, they are potentially a very rich test of the Standard Model explanation of CP violation.

ACKNOWLEDGEMENTS

It is a pleasure to thank A. Ali, I. Dunietz, M. Gronau, J. Rosner and P. Sphicas for helpful conversations. We thank the organizers for their thoughtful, supportive and gracious efforts, which made possible a very fruitful Workshop. Two of us (BK and DL) are grateful for the hospitality of Fermilab, where part of this work was done. One of us (BK) is also grateful for the hospitality of DESY, where another part was done, and for that of the Université de Montréal, where the paper was completed. This work was supported in part by the SSC Laboratory, the Natural Sciences and Engineering Research Council of Canada, and by FCAR, Québec.

5. REFERENCES

1. L. Wolfenstein, *Phys. Rev. Lett.* **51** (1983) 1945.
2. I. Bigi, V. Khoze, A. Sanda and N. Uraltsev, in *CP Violation*, ed. C. Jarlskog (World Scientific, Singapore, 1989) p. 175.
3. B. Kayser, in *Proceedings of the Second International Symposium on Particles, Strings and Cosmology*, eds. P. Nath and S. Reucroft (World Scientific, Singapore, 1992) p. 837.
4. The mass eigenstates of the B_d-$\overline{B}_d$ system are expected to have very nearly equal widths. Those of the B_s-$\overline{B}_s$ system are expected to have widths differing by 15%, a difference we shall neglect. See R. Aleksan et. al., *Phys. Lett.* **B316** (1993) 567.
5. M. Gronau, A. Nippe and J.L. Rosner, *Phys. Rev.* **D47** (1993) 1988; M. Gronau and J.L. Rosner, TECHNION-PH-93-31, EFI 93-43 and TECHNION-PH-93-32, EFI 93-41; M. Gronau, these proceedings. See also C. Hill, these proceedings.
6. R. Aleksan, I. Dunietz, B. Kayser and F. LeDiberder, *Nucl. Phys.* **B361** (1991) 141.
7. See, for example, M. Gronau and D. London, *Phys. Rev. Lett.* **65** (1990) 3381. See also Y. Nir and H.R. Quinn *Phys. Rev. Lett.* **67** (1991) 541; H.J. Lipkin, Y. Nir, H.R. Quinn and A.E. Snyder, *Phys. Rev.* **D44** (1991) 1454; M. Gronau, *Phys. Lett.* **B265** (1991) 389; L. Lavoura, *Mod. Phys. Lett.* **A7** (1992) 1553; H.R. Quinn and A.E. Snyder, *Phys. Rev.* **D48** (1993) 2139; J.P. Silva and L. Wolfenstein, DOE-ER/40682-43, CMU-HEP93-18.
8. For a review of B_s-$\overline{B}_s$ mixing, see A. Ali and D. London, *J. Phys. G: Nucl. Part. Phys.* **19** (1993) 1069.
9. Of course, it is equally acceptable for each decay amplitude to be dominated by several diagrams which have the same CKM phase.
10. This decay mode is proposed as a probe of γ in R. Aleksan, I. Dunietz and B. Kayser, *Z. Phys.* **C54** (1992) 653.

11. A related approach to probing γ utilizes the B_s decays we have been discussing plus those into $D_{CP}\phi$, where D_{CP} is a neutral D which decays into a CP eigenstate such as K^+K^- or $\pi^+\pi^-$. See M. Gronau and D. London, *Phys. Lett.* **B253** (1991) 483.

12. M. Gronau and D. Wyler, *Phys. Lett.* **B265** (1991) 172.

13. D. Besson, talk presented at the *1993 International Symposium on Lepton and Photon Interactions at High Energies*, Cornell University, August, 1993.

14. I. Dunietz, *Phys. Lett.* **B270** (1991) 75.

15. We thank Isi Dunietz for helpful comments on this point.

16. I. Dunietz, these proceedings.

17. We thank M. Gronau for participating with us in an analysis which verified that subleading contributions to this decay may be neglected.

18. M. Danilov, in *Proceedings of the Joint International Lepton-Photon Symposium and Europhysics Conference on High Energy Physics*, eds. S. Hegarty, K. Potter and E. Quercigh (World Scientific, Singapore, 1992) Vol. 2, p. 333; S. Ball, in *The Fermilab Meeting, DPF 92*, eds. C. Albright, P. Kaspar, R. Raja and J. Yoh (World Scientific, Singapore, 1993) p. 533.

19. B. Kayser, R. Aleksan and D. London, to be published.

Measuring γ with the Decays $B_s^0 \to D_s K$ and $B_u \to D^0 K$ with the CDF Detector at the Tevatron

E. Blucher
The University of Chicago
Chicago, Illinois 60637

J. Cunningham
Brandeis University
Waltham, Massachusetts 02254

J. Kroll
Fermilab
Batavia, Illinois 60510

F. D. Snider
The Johns Hopkins University
Baltimore, Maryland 21218

and

P. Sphicas
Massachusetts Institute of Technology
Cambridge, Massachusetts 02139

1. INTRODUCTION

This report summarizes a study of the sensitivity of the present CDF detector[1], with a trigger upgrade[2], to the following decay modes (and their charge conjugates) of the B_s and B_u mesons:

1. $B_s^0 \to D_s^- K^+$ and $D_s^+ K^-$

2. $B^+ \to \bar{D}^0 K^+$, $B^+ \to D^0 K^+$, and $B^+ \to D^0_{CP+} K^+$,

where D_{CP+} refers to the even CP state $(|D^0\rangle + |\bar{D}^0\rangle)/\sqrt{2}$. These decays are of interest for measuring[3] the angle γ, which is one of the three angles of the unitary triangle defined by $V_{ud}V_{ub}^* + V_{cd}V_{cb}^* + V_{td}V_{tb}^* = 0$.

For this study, we use a b quark cross section of $\sigma = 20\mu b$ for $|\eta| < 1$ for $p\bar{p}$ collisions at $\sqrt{s} = 1.8$ TeV[4]. We take a luminosity of $5 \times 10^{31}\text{cm}^{-2}\text{s}^{-1}$, which for a year of 10^7 seconds corresponds to an integrated luminosity of 0.5 fb^{-1}. This integrated luminosity yields 1.0×10^{10} b quarks per year in $|\eta| < 1$ (and 1.0×10^{10} $\bar{b}$ quarks). We assume that a b quark hadronizes into b hadrons in the following proportions: 37.5% $\bar{B}_d^0$, 37.5% B^-, 15% $\bar{B}_s^0$, and 10% b baryons.

2. TRIGGER RATES

For this study, we have considered a track-based trigger that exploits the relatively long lifetime of b hadrons.

The CDF trigger upgrade includes (1) a first level trigger with a track processor[5] (XFT), which uses azimuthal information from the central detector to reconstruct charged tracks, and (2) a second level trigger, with a Silicon Vertex Tracker[6] (SVT), which combines XFT tracks with clusters from the silicon vertex detector to determine track impact parameters. In the present design, the XFT is only efficient for finding tracks with $p_t > 2$ GeV/c. The first level trigger is designed to have no deadtime. The second level trigger is designed to take 20 microseconds; this second level will not introduce deadtime as long as the input from the first level is less than 50 kHz. The output from the second level must be less than 1 kHz.

We have used CDF minimum-bias data from the 1992-1993 data taking period to investigate the feasibility of a trigger based on track transverse momentum (p_t) at the first level and track impact parameter at the second level. Table 1 summarizes the fraction of minimum-bias events with the following combinations of tracks passing a p_t cut: (1) one track, (2) two tracks with opposite charge, (3) two tracks with opposite charge and an additional track, and (4) two pairs of oppositely charged tracks. All tracks were required to have $|\eta| < 1$. The quoted rates are based on a luminosity of 5×10^{31} cm^{-2}s^{-1}, a minimum-bias cross section of 50 mb, and assume ~ 1 interaction per crossing.

Table 1: Measured Minimum-Bias Rejection Factors

p_t (GeV)	1 track		2 opp.-ch.		2 opp.-ch. +1		2 opp.-ch. pairs	
	Eff.	Rate (kHz)	Eff.	Rate (kHz)	Eff.	Rate (kHz)	Eff.	Rate (kHz)
> 0.5	0.72	1807	0.50	1260	0.44	1100	0.31	775
> 1.0	0.43	1083	0.18	451	0.13	315	0.06	140
> 1.5	0.22	553	0.05	134	0.03	70	0.007	19
> 2.0	0.11	273	0.016	40	0.005	13	0.0012	3
> 2.5	0.05	130	0.005	13	0.0016	4	0.0002	0.5

For further studies, we require two oppositely-charged tracks with $p_t > 2$ GeV/c, which results in a first level output of 40 kHz.

Using SVT information at the second level, we require that both tracks have impact parameters greater than 100 μm. In the minimum-bias data, this impact parameter requirement reduces the rate by an additional factor[7] of 200. The combined rejection of the first and second levels of the trigger is 8×10^{-5}; this rejection corresponds to an output rate of 200 Hz.

3. DETECTION EFFICIENCIES

To determine the detector acceptance and the efficiency of the above trigger requirements for $B_s^0 \to D_s^- K^+$ and $B^+ \to \bar{D}^0 K^+$, we have used a Monte Carlo that generates a single b hadron with a p_t spectrum that agrees with data. The b hadron is required to have $|\eta| < 1$. For the D_s and D^0, we consider the following decay modes: $D_s \to \phi\pi$ with $\phi \to K^+K^-$ and $D^0 \to K^-\pi^+$. In addition to the above trigger requirements, all decay products are required to have $p_t > 250$ MeV/c and $|\eta| < 1$. These requirements ensure that the decay products will be reconstructed with high efficiency in the central detector of CDF. No simulation of the CDF detector is made for these efficiency calculations. The 35 μm beam spot size and resolution on the impact parameter of the track have been ignored, which makes our estimates slightly pessimistic. We have included a track-finding efficiency of 0.95 per track.

The detection efficiencies for the two decay modes of interest are expressed as the product of two numbers: (1) the acceptance, which is the fraction of the decays for which all tracks have $|\eta| < 1$ and $p_t > 250$ MeV/c, and (2) the trigger efficiency, which is defined as the fraction of events in the acceptance that pass the trigger requirements described above. Table 2 summarizes these efficiencies. The total given in the table is the product of the acceptance and trigger efficiencies multiplied by an additional factor of $(0.95)^4 = 0.82$ for the B_s decays, and $(0.95)^3 = 0.86$ for the B_u decays, to account for the reconstruction efficiency in the central detector of the charged tracks in the final state of each of the two modes.

Table 2: Detection Efficiencies for $B_s \to D_s^- K^+$ and $B^+ \to \bar{D}^0 K^+$

	$B_s \to D_s^- K^+$	$B \to \bar{D}^0 K^+$
Acceptance (%)	0.34	0.37
Trigger (%)	0.12	0.09
Total (%)	0.029	0.029

4. The Determination of $\sin\gamma$

We have examined two methods of extracting $\sin\gamma$. The first method is based on the comparison of the branching fraction of $B_s^0 \to D_s^- K^+$ and $D_s^+ K^-$ to the branching fraction of $\bar{B}_s^0 \to D_s^+ K^-$ and $D_s^- K^+$. Experimentally we compare the measured combined number of $D_s^- K^+$ and $D_s^+ K^-$ decays when the initial state produced in the $p\bar{p}$ interaction is a B_s^0 to the measured combined number of $D_s^+ K^-$ and $D_s^- K^+$ decays when the initial state is a $\bar{B}_s^0$. This comparison, therefore, requires that we tag whether the state produced in the $p\bar{p}$ interaction is a B_s^0 or $\bar{B}_s^0$. In this study, we consider only a tagging method that uses the semileptonic decay of the other b hadron produced in the collision. As discussed in reference[8], the extraction of $\sin\gamma$ from just the measured rates alone is diluted by an overwelming factor, $x_s/(1+x_s^2)$, due to the rapid $B_s^0 - \bar{B}_s^0$ oscillation. It is necessary, therefore, to compare the rates as a function of the proper decay time of the B meson, that is, a time dependent measurement is required.

The second method[9] of extracting $\sin\gamma$ comes from the measurement of the following branching fractions (and the branching fractions of the charge conjugate modes as well): $B^+ \to \bar{D}^0 K^+$, $B^+ \to D^0 K^+$, and $B^+ \to D^0_{CP+} K^+$, where D_{CP+} refers to the even CP state $(|D^0\rangle + |\bar{D}^0\rangle)/\sqrt{2}$. Flavour tagging using the other b hadron in the event and a measurement of the proper decay time of the B meson are not required in this method.

The numbers of events given below are based on the following branching ratios:

$B(B_s^0 \to D_s^- K^+) = 2 \times 10^{-4}$,
$B(B_s^0 \to D_s^+ K^-) = 1 \times 10^{-4}$,
$B(B^+ \to \bar{D}^0 K^+) = 2 \times 10^{-4}$,
$B(B^+ \to D^0 K^+) = 2 \times 10^{-6}$.

4.1 $B_s \to D_s^- K^+$

The total number of produced $\bar{B}_s^0$ and B_s^0 mesons in $|\eta| < 1$ in one year (using the cross sections and hadronization probabilities given in Section 1) is 3.0×10^9. Using $B(\bar{B}_s^0 \to D_s^- K^+$ and $D_s^+ K^-) = 3 \times 10^{-4}$ gives 9.0×10^5 $\bar{B}_s^0$ and B_s^0 decaying to $D_s^- K^+$ and $D_s^+ K^-$. We look for $D_s \to \phi\pi$ with $\phi \to K^+K^-$: the combined branching ratio[10] is 1.38%. The trigger and detection efficiencies for this final state are given in Section 3. The total detected number of events in one year is $(9.0 \times 10^5) \cdot (0.0138) \cdot (0.029) = 360$.

To tag the initial flavour of the B meson, we use the charge of the lepton coming from the semileptonic decay of the other b hadron produced in the $p\bar{p}$ collision. We use either electrons or muons with $p_t > 2$ GeV/c. The total tagging efficiency is 2%[11]. This efficiency includes the geometric acceptance (the lepton must have $|\eta| < 1$), the semileptonic branching fractions of b hadrons, and the lepton identification criteria. With this tagging efficiency, the total number of tagged events in one year is 7.2.

To determine the statistical precision on the extraction of $\sin\gamma$, we follow the prescription described in reference[8]. The statistical precision depends on the total number of tagged $\bar{B}_s^0$ and B_s^0 decays and on the following dilution factors:

- incorrect tagging of the flavour of the initial B_s meson. Mistags can arise from mixing of the other b hadron in the event, hadrons that are misidentified as leptons, and leptons that come from the semileptonic decays of charmed particles produced in the decay of the other b hadron. We take D_{tag} equal to $D_{tag} = 0.58$.
- The time dependent measurement has an inherent dilution factor[8] D_{t-dep} given by $D_{t-dep} = [2x_s^2/(1+4x_s^2)]^{1/2}$. This dilution factor approaches a maximum value of 0.71 for large values of x_s. Since x_s is expected to be large, we take $D_{t-dep} = 0.71$
- There is a dilution factor due to the experimental resolution on the proper decay time of the B_s meson. This dilution factor is given by[8] $D_{res} = \exp(-x_s^2\sigma_t^2/2)$, where σ_t is the experimental resolution on the B_s decay distance in units of proper time. We assume that σ_t is 0.1 lifetimes and take $x_s = 10$ to get $D_{res} = 0.61$.
- There is a dilution D_{bkg} due to background in the B_s signal. Using the signal to background ratio in the $D_s \to \phi\pi$ signal observed in the CDF data, we estimate $D_{bkg} = 0.70$

The total dilution factor D is the product of all the above dilution factors:

$$D = D_{tag} \cdot D_{t-dep} \cdot D_{res} \cdot D_{bkg} = 0.18.$$

We have not made an explicit minimum decay length requirement on the reconstructed B_s meson. The impact parameter requirements in the trigger cause the acceptance to turn on for decay lengths that are well beyond any minimum we might impose to reduce background. This loss of acceptance has been taken into account in the detection efficiencies.

The statistical precision on the determination of $\sin\gamma$ is given by $\sigma(\sin\gamma) = [D\sqrt{N}]^{-1}$ where N is the total number of tagged decays in the time dependent analysis performed with our above assumed resolution on the proper decay time (1/10 of a lifetime) and our assumed value of x_s (10). The number of tagged events needed for a 10% determination of $\sin\gamma$ is 3200 events, which corresponds to 450 years.

Additional statistics could be obtained by using other decay modes of the D_s^+, such as K^+K^{*0}. The K^+K^{*0} mode has a detection efficiency similar to the $\phi\pi^+$ mode. The dilution due to background, however, is expected to be higher in K^+K^{*0}.

4.2 $B_u \to D^0 K$

This second method of extracting $\sin\gamma$ involves the measurement of six decay amplitudes:

1. $B^+ \to \bar{D}^0 K^+$,
2. $B^- \to D^0 K^-$,
3. $B^+ \to D^0 K^+$,
4. $B^- \to \bar{D}^0 K^-$,
5. $B^+ \to D^0_{CP+} K^+$,
6. $B^- \to D^0_{CP+} K^-$.

The charge of the kaon indicates whether a B^+ or B^- decayed. In reactions (1) through (4), the D^0 and $\bar{D}^0$ are detected using the $K^-\pi^+$ and $K^+\pi^-$ decay modes, respectively. The charge of the kaon in the D decay tells us whether it was a D^0 or $\bar{D}^0$. We detect the CP even state with the decay $D^0 \to K^+K^-$ and the decay $D^0 \to \pi^+\pi^-$.

We expect $B(B^+ \to \bar{D}^0 K^+)$ to equal $B(B^- \to D^0 K^-)$ and $B(B^+ \to D^0 K^+)$ to equal $B(B^- \to \bar{D}^0 K^-)$. The rate for $B^- \to D^0_{CP+} K^-$ might be different than the rate of $B^+ \to D^0_{CP+} K^+$, and the observation of such a difference would be evidence for direct CP violation. The expected asymmetry is proportional to $\sin\Delta\delta \sin\gamma$, where $\Delta\delta$ is the difference of the phases of the final state strong interactions in the B^+ and B^- decays[9]. If $\Delta\delta = 0$, then no asymmetry is observed. If an asymmetry is observed, it is difficult to extract $\sin\gamma$ from the asymmetry, since there is a large theoretical uncertainty in $\Delta\delta$. Gronau and Wyler[9] have proposed a method for using all six reactions listed above to determine both $\sin\gamma$ and $\sin\Delta\delta$. The estimated observed rates of events for these six reactions are given below.

The number of B^+ mesons produced in one year is 3.8×10^9. Using the branching fractions given above and $B(D^0 \to K^-\pi^+) = 3.65 \times 10^{-2}$, this implies 27400 produced $B^+ \to \bar{D}^0 K^+$ with $\bar{D}^0 \to K^+\pi^-$, and 274 $B^+ \to D^0 K^+$ with $D^0 \to K^-\pi^+$; equal numbers are expected for the charge conjugate modes. The total detection efficiency for (1) is (see Table 2) 0.0286, and we have used this efficiency for reactions (2) through (5) as well. The detected numbers of events per year are 780 for process (1), and 7.8 for process (3). To get the combined rate from B^+ and B^-, these numbers must be multiplied by two.

The observed rates for reactions (5) and (6) are given in Table 3 for different values of γ and $\Delta\delta$. To obtain these numbers, we have used[11] $B(D^0 \to K^-K^+) = 4.1 \times 10^{-3}$, $B(D^0 \to \pi^-\pi^+) = 1.63 \times 10^{-3}$. The observed asymmetry in the Table is defined as $A \equiv (N_+ - N_-)/(N_+ + N_-)$. No dilution due to backgrounds has been taken into account. In particular, we have neglected backgrounds from $D^0 \to K^-\pi^+$ decays misidentified as $D^0 \to K^+K^-$ or $D^0 \to \pi^+\pi^-$ decays. For the best case (*i.e.*, $\Delta\delta = \pi/2$ and $\gamma = \pi/2$), one year of data results in about a 44% measurement of the asymmetry.

Table 3: Expected numbers of events and asymmetry for $B^+ \to D^0_{CP+}K^+$ (N_+) and $B^- \to D^0_{CP+}K^-$ (N_-) as a function of γ and $\Delta\delta$ after one year of data. Note that the results are identical if the values of γ and $\Delta\delta$ are interchanged.

γ	$\Delta\delta$	N_+	N_-	A	ΔA
$\pi/2$	$\pi/2$	74	50	0.20	0.09
$\pi/2$	$\pi/4$	71	53	0.14	0.09
$\pi/2$	$\pi/8$	67	57	0.08	0.09
$\pi/4$	$\pi/4$	74	62	0.09	0.09
$\pi/4$	$\pi/8$	73	67	0.05	0.08
$\pi/8$	$\pi/8$	74	71	0.02	0.08
0	0	74	74	0.00	0.08

The method of Gronau and Wyler[9] results in an equation for $\sin\gamma$ that has four solutions: two solutions correspond to $\pm\sin\gamma$, and the other two solutions correspond to $\pm\sin\Delta\delta$. An independent measurement of $\sin\gamma$ is required to resolve which of these four solutions is correct. Assuming this independent information is available, we have studied the statistical precision of the determination of $\sin\gamma$. To exploit the technique of Gronau and Wyler, $\sin\gamma$ and $\sin\Delta\delta$ should be determined using a maximum-likelihood method. We have not performed such an analysis; we have, however, considered a specific case: $\gamma = \pi/4$ and $\Delta\delta = \pi/2$. For these values of γ and $\Delta\delta$, $\sin\gamma$ is determined to 70% after one year of running. Other values of $\sin\gamma$ and $\sin\Delta\delta$ would lead to a determination of $\sin\gamma$ with a different statistical precision.

5. REFERENCES

1. F. Abe *et al.*, *Nucl. Instrum. Methods Phys. Res.*, **A271** (1988) 387.
2. E. Blucher et al., *Conceptual Design of a Deadtimeless Trigger for the CDF Trigger Upgrade*, CDF Internal Report 2038 (1993).
3. P. Sphicas, summary of the γ working group, these proceedings.
4. P. Nason, S. Dawson, R. K. Ellis, *Nucl. Phys.* **B327** (1989) 49. This cross section is taken from the solid curve in Fig. 15.
5. P. Wilson, summary of Trigger working group report, these proceedings.
6. G. Punzi and L. Ristori, *SVT: The Silicon Vertex Tracker*, CDF Internal Report 1872 (1992).
7. G. Punzi, private communication.
8. K. T. McDonald, *Maximum-Likelihood Analysis of CP-Violating Asymmetries*, Princeton/HEP/92-04 (1992).
9. M. Gronau and D. Wyler; *Phys. Lett.* **B 265** (1991) 172.
10. Review of Particle Properties, K. Hikasa *et al.*, *Phys. Rev.* **D45 Part II** (1992) 1.
11. P. Sphicas and B. Mattingly, *$B\overline{B}$ Correlations*, CDF Internal Report 2034 (1992).

MEASUREMENT OF THE ANGLE GAMMA WITH A FORWARD COLLIDER DETECTOR

Paul Karchin, Chris Kennedy, Robert Harr
Physics Department, Yale University
J.W. Gibbs Laboratory, P.O. Box 6666, New Haven, CT 06511

Lynn Garren
Fermi National Accelerator Laboratory
P.O. Box 500, Batavia, IL 60510

Paul Avery
Physics Department, University of Florida
Gainesville, FL 32611

Dieter Cords
Stanford Linear Accelerator Center
P.O. Box 4349, Stanford, CA 94309

1. INTRODUCTION

1.1 Decay Modes of Interest

The γ group considered a variety of ways to directly or indirectly extract the angle γ. A representative sample of these methods was chosen for detailed evaluation by sub-groups examining a specific detector or class of detectors. Our sub-group considered the measurement of γ with a forward collider detector. The decay modes chosen for detailed study are listed in Table 1.

Table 1. Decay modes for the angle γ.

decay	branching fraction	tag required?	time dependence required?
$B_s \to \psi\phi$	10^{-3}	yes	yes
$B_s \to \rho K_s$	3.5×10^{-7}	yes	yes
$B_s \to D_s^- K^+$ (See ref. 1.)	2.5×10^{-4}	yes	yes
$B^+ \to D_1^0 K^+$ (See ref. 2,3.)	2×10^{-4}	no	no

Note that decay modes of both B_s and B_u are considered. Some decay modes require flavor-tagging of the accompanying B while others are self-tagging. The theoretical basis for the various techniques are described in the published literature[1-3] and/or in the proceedings of this workshop. The theoretical estimates for branching fractions, given in the table, were agreed upon as standards for the γ group. The analysis for sensitivity to the angle γ is straightforward for decays to a tagged CP eigenstate. This analysis is summarized in the note by V. Luth which was distributed to all conference participants. For the other types of decays considered by the γ group, the determination of the error on γ is described in the report of the γ group. In this article, we report only the total number of expected observed decays for these modes.

2. OUR GENERIC FORWARD COLLIDER DETECTOR

2.1 *Coverage in Polar Angle*

Our definition of a forward collider detector is one that covers a pseudo-rapidity (η) range from 1.5 to 5.5. We've also considered a detector covering only 2 units of η, from 1.5 to 3.5. The smaller range detector is considered as a less costly alternative to the full detector, which is comparable to the (upgraded) CDF in the number of units of η covered. Furthermore, if trigger rate is a limiting factor in the larger detector, the smaller one may be justified simply to limit the trigger rate to a manageable level. For our forward detector, the minimum η is taken to be 1.5 as this corresponds to a laboratory angle of 25 degrees which can be reasonably covered with a planar geometry. The angular coverage is summarized below.

Table 2. Polar Angle Coverage of Generic Forward Collider Detector.
A larger detector covers the range $1.5 < \eta < 5.5$ and a smaller one covers $1.5 < \eta < 3.5$.

η	1.5	3.5	5.5
$tan(\theta)$	.470	.060	.008
degrees	25	3.5	0.5

Our estimates of geometric acceptance and trigger efficiency are based on Monte Carlo studies using Pythia. We require a trigger muon with $P_T > 1.2$ GeV and we require that each track in the final state of interest have $P > 0.5$ GeV, to insure good tracking.

We've taken the estimates of tagging efficiency and tagging dilution from the COBEX design[4] which has η coverage of 1.2 to 6.0, as tabulated below.

Table 3. Parameters of the COBEX design.

η	1.2	6.0
$tan(\theta)$	.684	.005
$\theta(rad)$	.600	.005
degrees	34	0.3

Another difference between our generic detector and COBEX is that we take the silicon vertex detector to be at a minimum distance of 6 mm from the beam line, as opposed to 2 mm for COBEX. This is discussed in more detail below.

Our design has coverage over the full η range for muon detection, vertexing, magnetic spectrometry, and Cerenkov detection.

For the smaller forward detector, we found that to a good approximation the combined trigger and geometric acceptance for the final states of interest is about half that for the larger forward detector. Thus, estimates for the smaller detector can be easily extrapolated from those of the full forward detector. In this article, our detailed analysis for specific decay modes is for the larger forward detector.

2.2 *The Muon Trigger and Tagging*

Since muons can generally be detected with lower background and at lower energies than electrons, we assume that a muon system is favored for the trigger and for tagging B's. For events triggered with a muon, we expect that electron and kaon tagging will not be competitive with muon tagging, except in cases where the final state has a ψ. Then, kaon and electron tagging will significantly add to the overall tagging efficiency. So in these studies, we allow kaon and muon tagging only for final states with a ψ.

We do not consider the recently proposed idea of tagging the B with an associated pion either from a B^{**} decay or from a quark anti-quark pair shared between the B meson and the associated pion. This method has yet to be established.

For self-tagging modes, the μ requirement in the trigger is still useful. This is because the b and $\bar{b}$ are correlated in η and so if a muon from the accompanying B falls in the acceptance, then the chance that the B decay of interest also falls in the acceptance is enhanced.

For the special case of a ψ decay in the final state, a muon trigger is very effective, since the muon could come from the ψ decay or from the accompanying B. The only such decay we consider here is $B_s \rightarrow \psi\phi$. This decay must also be time tagged.

Note that the trigger efficiencies quoted in our studies take into account the branching fraction for $B \rightarrow \mu X$.

We've studied a muon trigger for minimum bias events using Pythia. Since a $b\bar{b}$ pair can be generated by Pythia in minimum bias events, we excluded these events in order to study explicitly the trigger rate due to non-beauty events. We allowed a 10 meter radius sphere in which particles such as pions and kaons could decay and studied the efficiency of retaining minimum bias events as a function of a cut on the highest P or P_T muon in the acceptance. We found that we could get a rejection of about 100 by cutting on either P or P_T at the values shown below.

Table 4. Values of the minimum P or P_T for the trigger muon
for a background rejection factor of 100.

Machine	η range	P_T cut (GeV)	P cut (GeV)
SSC	1.5 - 5.5	1.2	20
FNAL	1.5 - 5.5	0.9	15

Furthermore, the P and P_T cuts listed above resulted in about the same efficiency for various final states of interest. Thus, we found that for the single muon trigger, a cut on P or P_T is equally effective. The cut used in all the studies that follow is $P_T > 1.2GeV$.

For a final state without a ψ, the muon trigger is still useful. We found that for a muon trigger cut giving a factor of 100 in rejection of minimum bias events, there is about a factor of 100 reduction in the efficiency for all B's. However, the B's that are retained by the trigger have a tagging muon in the acceptance, whereas all B's have only a 10% chance of being accompanied by a tagging muon, and this muon may not be in the acceptance. Even for final states that are self tagging, the muon trigger still helps compared to a minimum bias trigger because the B events that are retained have a better geometric acceptance than all B events. This is because the tagging muon is correlated in polar angle with the decay products from the other B.

We also considered a di-muon trigger for final states with a ψ. We found that such a trigger, although operating at a lower P or P_T threshold than the single muon trigger, gave no better rejection and efficiency than the single muon trigger. Thus, we confine our detailed analysis of final states to the case of a single muon trigger.

So far, there has been no study of the effect of secondary interactions in the beam pipe on the muon trigger rate. This problem was discussed by CDF at this workshop. If secondary interaction products enter the muon detectors without passing through the muon absorber, they create a false muon signal. However, timing and fiducial cuts, such as employed by CDF, may be sufficient to eliminate these triggers, even at higher luminosity and energy.

For decays without a muon in the final state, it would certainly be advantageous to have a trigger that does not require a muon. There was discussion at the workshop of the trigger for $B \rightarrow \pi^+\pi^-$ being considered for CDF based on track P_T and impact parameter. Schemes of vertex triggers for forward collider detectors were also discussed during the workshop, but none was specific enough to be included in our considerations. If the technique of vertex triggering can be successfully developed, it may provide a promissing way of obtaining a substantially enriched sample of B decays for which electron and kaon tagging can be employed as well.

2.3 Vertex Detector Minimum Radius

In the COBEX design, the silicon vertex detector is at a radial distance of 2 mm from the beam line. At the luminosities considered here, a more likely location is a radius of 6 mm, which reduces the radiation dose by a factor of 9 compared to a radius of 2 mm. The minimum radius affects the vertex resolution primarily because of multiple Coulomb scattering in the silicon detectors. This, in turn, effects the reconstruction efficiency of the final state, the efficiency of flavor tagging, and the dilution factors for tagging and final state oscillation. However, in a detailed simulation of vertex detectors for a forward collider geometry[5], R. Harr et al. show that the multiple scattering contribution to vertex resolution does *not* dominate at radial distances up to about 2 cm. Hence, we expect that the event reconstruction efficiency estimated for COBEX will not significantly change when the minimum radius increases from 2 mm to 6 mm.

2.4 Data Acquisition Rate

The DA rate to tape is an important parameter in the (likely) case that the number of beauty events recorded in the experiment is limited simply by the ability to read out the detector fast enough and write out the data to tape. Let's examine the factors affecting the DA rate. We estimate the event size for a forward detector to be 10K byte. This is to be compared to CDF, which currently has an event size of about 100 Kbyte. The forward detector can have a smaller event size if the readout electronics is specifically designed to exploit zero-suppression and data compaction to the fullest extent possible. The next important factor is the data rate to tape. Fixed target experiments specifically designed for high DA rate have achieved 10 Mbyte/sec, while CDF can currently write to tape at about 100 Kbyte/sec. So the planned forward experiment could sustain a trigger rate of 1 KHz. At the SSC, the interaction rate is 10 MHz at $L = 10^{32}$ cm^{-2} sec^{-1}. Thus a reduction in the trigger rate of 10^4 is required.

Since the muon trigger alone can give a rate reduction of only about 100, even with adding other trigger requirements, such as a vertex condition, the reduction in the trigger rate is likely to be only about 10^3. An additional factor of 10 is needed which could come from a prescaler or cutting very hard on the trigger variables, such as muon P_T and vertex separation. However, there are alternatives.

A higher rate to tape can be considered, such as 100 Mbyte/sec, the design goal for the SDC detector. Then, the forward detector could tolerate a trigger rate of 10 KHz. However, a large data set is expensive to manage. One estimate[6] is that at current prices, 3 million dollars will buy enough computing power to analyze, in one calendar year, the data produced at 100 Mbytes/sec for 10^7 seconds. We take this amount of data as an upper limit.

Another possibility is a sophisticated level 3 trigger: if the trigger rate can be reduced to 1 KHz, then a rate of only 10 MByte/sec is required.

In our estimates below, we will assume that a 1 KHz rate to tape is achieved (with 10 kbyte events) with a trigger that requires a muon above a certain P_T *in combination* with a vertex requirement giving a rate reduction of 10^4. Such a trigger implies that for decays to final states without a muon, the only useful tagging for the events written to tape is a muon tag. This is because in events triggered on a muon, the tagging efficiency for muons will be high, while the tagging with kaons will not benefit from the trigger condition. If a vertex-only trigger with a rate reduction of 10^4 is possible, then kaon and electron tagging will also be useful for final states without a ψ.

2.5 Luminous Region at Fermilab

At the Tevatron, the longitudinal extent of the luminous region has σ_z of 30 cm, which is also the length of the current CDF vertex barrel. Even with a 60 cm long vertex detector, there is a 32% loss of luminosity, assuming a Gaussian distribution. However, we do not include this factor in estimates.

3. CASE STUDIES OF SENSITIVITY FOR CP ASYMMETRIES

3.1 Common Considerations

Standard values for luminosity and cross section were adapted at the conference to facilitate comparison of the results of the various sub-groups. These values are listed in Table 5.

For B_d and B_s decaying to CP final states, the expression for the error on asymmetry is given in the document by V. Luth distributed at the conference. We follow the method given there.

For all of the decay modes, we used Pythia to evaluate the efficiency of the muon trigger (for the cuts described in section 2.2) and the efficiency due to the geometrical acceptance. All four B decay modes considered have four particles in the final state. We took the reconstruction efficiency to be 0.1, slightly less than the COBEX estimate of 0.12 for $B_d \to \psi K_S^0$ final state.

The factor $d(mix)$ describes the dilution of the decay rate asymmetry due to the mixing of the decaying particle. With no measurement of the time development of the decaying particle, this factor is $d(mix) = x/(1+x^2)$. In principle, with perfect measurement of the time development, the mixing factor is one, i.e., there is no dilution. In practice, the time development of the mixing is hard to measure for B_d because of the relatively rapid rate of decay compared to mixing ($x_d = 0.7$). For B_s, many mixing oscillations are expected to occur within the period of a mean lifetime ($x_s \sim 15$), so that the mixing can be accurately measured if the time resolution is much smaller than a mean lifetime. We assume this to be the case for B_s decay and hence set $d(mix) = 1$.

Table 5. Common parameters for specific decay mode studies.

Parameter	SSC	FNAL
Energy E_{cm} (TeV)	40	2
Luminosity ($10^{33} cm^{-2} s^{-1}$)	.1	.1
$b\bar{b}$ cross section (μb)	1000	50
Total cross section (mb)	100	50

3.2 $B_s \to \psi\phi$

Since the trigger muon may have come from the ψ, the trigger efficiency is higher for this mode than for modes without a ψ in the final state. However, the muon tag efficiency in recorded events is not as high as for a state without a ψ. Kaon tagging will help significantly with this mode, enhancing the tagging efficiency over muons only. We assume kaon tagging is possible. The parameters for this decay are summarized in Table 6.

3.3 $B_s \to \rho K_s$

This decay is considered here because it was the first one widely discussed for measurement of γ. However, because of the small expected branching fraction, this decay is not likely to provide a measurement, as can be seen from Table 7.

3.4 $B_s \to D_s^- K^+$

The analysis for this mode is not the same as for the CP eigenstates previously considered. The charge conjugate mode is also required and is expected to have a somewhat lower branching fraction. In Table 8 we estimate only the number of flavor-tagged, reconstructed decays of $B_s \to D_s^- K^+$. The analysis for γ, which also requires measurement of the time distribution of the decays, was discussed by P. Sphicas in the summary talk for the γ group. The error on $sin(\gamma)$ depends on the value of $sin(\gamma)$ and size of the strong interaction phase factor. For a few hundred tagged decays, the sensitivity to $sin(\gamma)$ is only of order 0.2 Thus, a measurement of γ would be difficult with this mode.

The decay $B_s^* \to B_s\gamma$ could be useful to reduce background if the single γ could be detected. However, we do not consider this case here.

3.5 $B^+ \to D_1^0 K^+$

The analysis for this mode is both different from the previous one and different than that for a CP eigenstate. This mode is self-tagged, and the time dependence of the decay is not required. However, the mode $B^+ \to D^0 K^+$ is also required for a joint analysis and is considered separately. In fact, it turns out that the sensitivity ultimately depends on the statistics from this related mode. The parameters for the two decay modes are given in Tables 9 and 10.

The sensitivity to $sin(\gamma)$ was analyzed by P. Avery and reported in the summary talk of the γ group by P. Sphicas. The error on $sin(\gamma)$ depends on the value of $sin(\gamma)$. For the order of magnitude of the number of tagged, reconstructed events shown below, the error on $sin(\gamma)$ is of order 1 or worse for a wide range of values of $sin(\gamma)$. This technique does not appear to be useful.

4. CONCLUSIONS

Four different techniques were considered which are sensitive, in principle, to the angle γ. The only one which appears promising is the decay $B_s \to \psi\phi$ measured at the SSC.

5. REFERENCES

1. R. Aleksan, I. Dunietz and B. Kayser, *Zeit. Phys.* **C54** (1992) 653.
2. M. Gronau and Wyler, *Phys. Lett.* **B265** (1991) 172.
3. I. Dunietz, *Phys. Lett.* **B270** (1991) 75.
4. Erhan et al., *Nucl. Instr.* **A333** (1993) 101.
5. R.F. Harr et al. in these proceedings.
6. D. Summers, University of Mississippi, private communication in discussions at this workshop.

Table 6. $B_s \to \psi\phi$

B_s fraction	.15	
$N(B_s + \overline{B}_s)/10^7$ sec	3×10^{11} (SSC)	1.5×10^{10} (FNAL)
branching ratio	10^{-3}	
B flavor tag	μ, K	
ϵ(decay)	.035	(branching for $\mu^+\mu^-$ and K^+K^-)
ϵ(trig).AND.ϵ(acceptance)	.19 (SSC)	.14 (FNAL)
ϵ(recon.)	.1	
ϵ(tag)	.37	(COBEX proposal for ψK_s)
d(mix)	1	
d(tag)	.4	(COBEX proposal for ψK_s)
d(bkd)	1	(ie., no estimate yet)
total efficiency	2.5×10^{-4}	
total dilution	.4	
$1/D^2\epsilon$	2.5×10^4	
$N(B_s + \overline{B}_s)$ for $\delta(A) = 0.01$	2.5×10^{11}	(expected asymmetry is 0.03)
time for measurement (10^7 seconds)	0.8 (SSC)	23. (FNAL)

Table 7. $B_s \to \rho K_s$

B_s fraction	.15	
$N(B_s + \overline{B}_s)/10^7$ sec	3×10^{11} (SSC)	1.5×10^{10} (FNAL)
branching ratio	3.5×10^{-7}	
B flavor tag	μ	
ϵ(decay)	.69	
ϵ(trigger and acceptance)	.009 (SSC)	.006 (FNAL)
ϵ(reconstruction)	.1	
ϵ(tag)	.76	(from COBEX, $B \to \pi^+\pi^-$)
d(mix)	.7	
d(tag)	.5	(from COBEX, $B \to \pi^+\pi^-$)
d(bkd)	1	(ie., no estimate yet)
total efficiency	4.7×10^{-4}	
total dilution	.35	
$1/D^2\epsilon$	1.7×10^4	
$N(B_s + \overline{B}_s)$ for $\delta(A) = 0.1$	4.9×10^{12}	
time for measurement (10^7 seconds)	16 (SSC)	

Table 8. $B_s \to D_s^- K^+$

B_s fraction	.15	
$N(prod)/10^7$ sec	1.5×10^{11}	7.5×10^9 (FNAL)
branching ratio	2.5×10^{-4}	
B flavor tag	μ	
ϵ(decay)	.015	($D_s^+ \to \phi\pi^+$, $\phi \to K^+K^-$)
ϵ(trigger)	.053	.039 (FNAL)
ϵ(acceptance)	.19	.16 (FNAL)
ϵ(reconstruction)	.1	
ϵ(tag)	.76	(from COBEX, $B \to \pi^+\pi^-$)
d(tag)	.5	(.58 in COBEX, $B \to \pi^+\pi^-$)
d(bkd)	1	(ie., no estimate yet)
total efficiency	1.1×10^{-5}	7.1×10^{-6}
N(reconstructed & tagged) per 10^7 sec.	412 (SSC)	16 (FNAL)

Table 9. $B^+ \to D_1^0 K^+$

B_u fraction	.375	
$N(B^+$ and $B^-)/10^7$ sec	7.5×10^{11}	3.75×10^{10} (FNAL)
branching ratio	2×10^{-4}	
B flavor tag		self tagging
ϵ(decay)	.004	($D^0 \to K^+K^-$)
ϵ(trigger)	.055	
ϵ(acceptance)	.19	
ϵ(reconstruction)	.1	
total efficiency	4.1×10^{-6}	
N(reconstructed)/10^7 sec.	627 (SSC)	32 (FNAL)

Table 10. $B^+ \to D^0 K^+$

B_u fraction	.375	
$N(B^+$ and $B^-)/10^7$ sec	7.5×10^{11}	3.75×10^{10}
branching ratio	2×10^{-6}	
B flavor tag		self tagging
ϵ(decay)	.1	($D^0 \to K^-\pi^+$)
ϵ(trigger)	.055	
ϵ(acceptance)	.19	
ϵ(reconstruction)	.1	
d(bkd)	1	(ie., no estimate yet)
total efficiency	10^{-4}	
N(reconstructed)/10^7 sec.	157 (SSC)	8 (FNAL)

THE MEASUREMENT OF THE ANGLE GAMMA IN THE SFT: AN SSC FIXED TARGET B EXPERIMENT

B. Cox, G. Corti, K. Nelson
University of Virginia, Charlottesville, Virginia 22901

A. Erwin
University of Wisconsin, Madison, WI 53706

ABSTRACT

The measurement of the gamma angle of the CKM triangle defined by the unitarity relationship $V_{ud} V^*_{ub} + V_{cd} V^*_{cb} + V_{td} V^*_{tb} = 0$ is difficult since most B decay modes only give direct access to this angle in the limit of the Wolfenstein approximation. In addition, even assuming this approximation is valid, determination of the gamma angle from many of the B decay modes requires measurements of the rapid oscillations of B^0_s decay distribution. Since the superior time resolution possible in fixed target experiments permits better measurements of mixing and time dependent CP violation effects in B_s decays than with other options, the SFT fixed target option is particularly suited for determination of the gamma angle.

1. INTRODUCTION

The fixed target experimental configuration[1,2,3,4] has many technical advantages in the measurement of CP violating asymmetries compared to e^+e^- or hadron collider experiments (see as examples, Ref. 5 and 6) and is more economical to implement. The long decay lengths of the Lorentz boosted B's combined with superior vertex resolution (σ_L/L for B decays $\approx$ 380) make possible very good resolution measurements of the time dependent CP asymmetries in both B^0_d and B^0_s decay distributions, minimizing "dilution" effects due to mixing and minimum decay length criteria. The superior ratio of resolution to decay length of fixed target experiments also significantly decrease the dilution effects due to mistagging by allowing association of the tagging particle with a given secondary or tertiary vertex. The overall effect is to make possible precise measurements of the gamma angle of the unitarity triangle in cases where the rapid oscillations of the B^0_s must be measured.

Furthermore, because the measurement of the gamma angle in CP eigenstate and "almost" CP eigenstate modes involves B^0_s mixing, we do not measure gamma directly except in the Wolfenstein approximation[14]. For example, in the case of $B^0_d \to \pi^+\pi^-$ where the interference that allows observation of CP violation comes from B^0_d mixing, the angle determined from fitting the time distributions for B^0_d and $\bar{B}^0_d$ decay into $\pi^+\pi^-$ is

$$\phi\left[\frac{V_{ub}^{*}V_{ud}}{V_{td}^{*}V_{tb}}\right]$$

which is just the angle α of the particular unitarity triangle indicated by unitarity relation $V_{ud}V^*_{ub} + V_{cd}V^*_{cb} + V_{td}V^*_{tb} = 0$. On the contrary, for $B^0_s \to \rho K^0_s$, we measure an angle "γ" which is the following combination of CKM matrix elements[7]

$$"\gamma" = 2\bullet\left(\phi\left[\frac{V^*_{ub}V_{ud}}{V_{td}V^*_{tb}}\right]+\phi\left[\frac{V_{td}V^*_{tb}}{V_{cd}V^*_{cb}}\right]+\phi\left[\frac{V^*_{ts}V_{tb}}{V^*_{cs}V_{cb}}\right]\right)$$
$$= 2\bullet\left(\alpha+\beta+O\left[\lambda^2\right]\right) = 2\bullet\left(\gamma+O\left[\lambda^2\right]\right)$$

Therefore, we use "γ" to indicates that, in most cases, the measurement proposed does not determine γ directly. In the limit of the Wolfenstein approximation, only Vub and Vtb have phases so "γ"=γ. However, with the precision of the measurement possible with the SFT, the effect of the Wolfenstein approximation should be visible and the $O(\lambda^2)$ significant. In some cases combinations of two different measurements provides enough information to extract gamma cleanly independent of the Wolfenstein approximation. For example, a measurement of $B^0_s \to J/\Psi/\phi$ measures the small angle (call it γ) in the triangle appropriate to unitary relation $V_{us}V^*_{ub} + V_{cs}V^*_{cb} + V_{ts}V^*_{tb} = 0$. This turns out to be just the correction term needed to extract gamma (to order λ^4) from the measurement of $B^0_s \to D^+K^-$ which measures an angle, "γ" = $\gamma + \gamma + O(\lambda^4)$.

Following the development of Aleksan et al.[11] for particular class I or II type B decays where only one amplitude dominates the decay, the error in sin (2φ) is given by

$$\delta(\sin 2\phi) \equiv \frac{1}{d_{tag}}\bullet\frac{1}{d_{CP}}\bullet\frac{1}{d_p}\bullet\frac{1}{d_{Bkg}}\bullet\frac{1}{d_{mistag}}\bullet\frac{1}{d_{res}}\bullet\frac{1}{\sqrt{N_{recon}}}$$

where N_{recon} is the sum of the reconstructed and tagged B^0 and $\bar{B}^0$ decays in the selected mode for which a measurement of CP asymmetries is being analyzed. The various "dilution" factors in the error are

$$d_{tag} = \text{dilution of } B_{tag} \text{ mixing } = \left[p_\pm + p_\Lambda\right] + \frac{p_s \bullet x_s}{\left[1+x_s^2\right]} + \frac{p_d \bullet x_d}{\left[1+x_{d,s}^2\right]}$$

where $p_\pm, p_d, p_s, p_\Lambda$ are the hadronization fractions for $B^\pm_u$, B^0_d, B^0_s, Λ_b

d_{CP} = dilution due to CP decay statistics

$$= e^{-\tau_{cut}}\bullet\left[1+\frac{2x_{d,s}\sin 2x_{d,s}\tau_{cut} - \cos 2x_{d,s}\tau_{cut}}{1+4x_{d,s}^2}\right]\xrightarrow[\tau_{cut}\Rightarrow 0]{}\sqrt{\frac{2x_{d,s}^2}{1+4x_{d,s}^2}}$$

d_ρ = dilution due to deviation of final state from a CP eigenstate

$$= \frac{2\rho}{1+\rho^2}\xrightarrow[f\Rightarrow CP\ eigenstate]{} 1$$

$$d_{bkg} = \text{dilution due to background} = \sqrt{\frac{S}{S+B}}$$

$$d_{mistag} = \text{dilution due to mistagging } = (1-2w)$$

$$d_{res} = \text{dilution due to time resolution} = e^{-\sigma_t^2 x^2/2}$$

Table 1 below gives an evaluation of the dilution factors appropriate to the SFT detector[4] for Class I and II decays of neutral B's.

Table 1
Dilution Factors

B_{CP}	B_{tag}	$1/d_{tag}$	$1/d_{CP}$	$1/d_\rho$	$1/d_{bkg}$	$1/d_{mistag}$	$1/d_{res}$	$1/d_{total}$
B^0_d	$\mu^\pm$ $e^\pm$ $K^\pm$	1.49	1.77	1.0,1.03	1.12	1.075 1.18 1.33	≈1	3.17,3.27 3.48,3.59 3.93,4.05
B^0_s	$\mu^\pm$ $e^\pm$ $K^\pm$	1.49	1.40	1.0,1.03	1.12	1.075 1.18 1.33	1.001	2.51,2.59 2.76,2.84 3.11,3.20

The number of reconstructed and tagged events, N_{recon} is given by

$$N_{recon} = N_B \bullet f_B \bullet BR_{CP} \bullet BR_{tag} \bullet A_{accep} \bullet \varepsilon \quad \text{where } \varepsilon = \varepsilon_{CP} \bullet \varepsilon_{tag} \bullet \varepsilon_{trig}$$

N_B ≡ Number of B's produced per year of operation in the SFT
BR_{CP} ≡ Composite Branching ratio for the CP decay
BR_{tag} ≡ Composite Branching ratio for the tag decay
f_B ≡ Hadronization ratio for specific CP and tagging B configuration
Accp ≡ Composite acceptance for the B_{CP}, B_{tag} and trigger particles.
ε_{CP} ≡ Composite detector and reconstruction efficiencies for CP B decay
ε_{tag} ≡ Composite detector and reconstruction efficiency for tagging B decay
ε_{trig} ≡ Composite detector efficiency for trigger

3. YIELDS OF B DECAYS SUITABLE FOR MEASUREMENT OF γ

As described in Ref. 4, using the Snowmass standard cross section of 2μb with an A^1 dependence and hadronization fractions $p_{\pm}/p_d/p_s/p_{\Lambda}$ = 0.38/0.38 /0.14 /0.10 for pp-> $B\bar{B}$ production in 20 TeV fixed target experiment together with 32 mb and an atomic number dependence of $A^{0.72}$ for the pN total cross section, we expect one $B\bar{B}$ pair for every 6300 pSi interactions in the SFT. With the 2.5×10^8 crystal extracted proton beam producing 10^7 interactions in the SFT live target ($0.04\lambda_0$), $\approx10^{14}$ interaction will be produced per year of operation yielding the numbers of various B species given in Table 2.

Table 2

Production per Year (10^7 sec) of B Pairs in SFT

B Pair Cross Section for pN	2 μb
B Pair Production Cross Section for pSi	56 μb
Number of B Pairs	1.6×10^{10}
Number of $B^{\pm}_u$	1.3×10^{10}
Number of B^0_d	1.3×10^{10}
Number of B^0_s	4.5×10^9
Number of B^0_c	3.2×10^7
Number of Λ_b	3.2×10^9

The yields of B decay • B tagging topologies suitable for "γ" measurements are given in Table 3.

Table 3

Production per Year of B Decays in the SFT Appropriate for "γ" Measurements

∠	Class	B_{CP}	Tag	BR	#/year	Trig	Requirements
"γ"	I	$B^0_s \to \rho K^0_s$	$B \to l^{\pm}$	1.1×10^{-7}	5.0×10^2	$l^{\pm}$	Time/Tag
	I	$B^0_s \to D^+_s D^-_s$	$B \to l^{\pm}$	1.4×10^{-5}	6.4×10^4	$l^{\pm}$	Time/Tag
	II	$B^0_s \to D^+_s K^-$	$B \to l^{\pm}$	3.2×10^{-6}	1.4×10^4	$l^{\pm}$	Time/Tag
		$\bar{B}^0_s \to D^+_s K^-$	$B \to l^{\pm}$	2.3×10^{-6}	1.0×10^4	$l^{\pm}$	
	III	$B^0_d \to \bar{D}^0 K^{0*}$	self	2.7×10^{-5}	3.2×10^5	$l^{\pm}$	
		$B^0_d \to D^0 K^{0*}$		2.7×10^{-6}	3.2×10^4		
		$B^0_d \to D^0_1 K^{0*}$		0.6×10^{-6}	0.6×10^3		
	III	$B^+ \to \bar{D}^0 K^+$	self	5.5×10^{-6}	3.8×10^5	$l^{\pm}$	
		$B^+ \to D^0 K^+$		5.5×10^{-7}	5.1×10^3		
		$B^+ \to D^0_1 K^+$		1.2×10^{-7}	1.4×10^3		
	I	$B^0_d \to \Psi\rho^0$	$B \to l^{\pm}$	1.2×10^{-6}	5.4×10^3	l^+l^-	Time/Tag
		$B^0_d \to \Psi\rho^0$	$B \to K^{\pm}$	5.2×10^{-6}	2.3×10^4	l^+l^-	
	I	$B^0_s \to \Psi\phi$	$B \to l^{\pm}$	2.6×10^{-5}	1.2×10^5	l^+l^-	Time/Tag
		$B^0_s \to \Psi\phi$	$B \to K^{\pm}$	1.0×10^{-4}	4.7×10^5	l^+l^-	

The branching ratios of Table 3 are composite branching ratios for the required B decay configuration. They include branching ratios for all secondary decays such as $K^0_s \to \pi\pi$, $J/\Psi \to \mu\mu$, $\phi \to K^+K^-$ and a composite of D branching ratios for modes which produce experimentally detectable final state as described in Ref. 4. The composite branching ratio also contains the branching ratios for the tagging and trigger decays of the "other" B.

The three level triggering strategy described in References 4 and 15 adopted for the SFT detector is based on detection of high p_t leptons and hadrons. Level I, II, and III of the trigger necessarily result in loss of B signal in the various "γ" decay modes. Preliminary results for acceptances and trigger efficiencies and the trigger level retention factors for modes appropriate to measurements of "γ" are given in Table 4 for both CP and tag B's

Table 4

Signal Retention for "γ" Decay Modes and "Other" Tagging B Decays

B Decay Topology	Accp. charged tracks	Eff_{trig} Level I	Eff_{trig} Level II	Overall Fraction A*Trig	Trigger/ Threshold GeV/c
$B^0_s \to \rho K^0_s$ • $B \to l^{\pm}$	0.28	0.45•0.96	0.81	0.10	μ/e•$h^{\pm}$ (1.5,1)
$B^0_s \to D^+_s D^-_s$ • $B \to l^{\pm}$	0.40	0.45•0.96	0.81	0.17	μ/e•$h^{\pm}$ (1.5,1)
$B^0_s \to D^+_s K^-$ • $B \to l^{\pm}$	0.50	0.45•0.96	0.81	0.22	μ/e•$h^{\pm}$ (1.5,1)
$B^+ \to D^0 K^+$ • $B \to l^{\pm}$	0.50	0.45•0.96	0.81	0.17	μ/e•$h^{\pm}$ (1.5,1)
$B^0_d \to J/\Psi\rho$ • $B \to l^{\pm}, K^{\pm}$	0.56,.51	0.91•0.97	0.81	0.40,0.36	l^+l^- (1,.5)
$B^0_d \to J/\Psi\phi$ • $B \to l^{\pm}, K^{\pm}$	0.60,.51	0.91•0.97	0.81	0.43,0.36	l^+l^- (1,.5)

Using these trigger retention factors and collecting all other efficiencies and acceptances, we obtain the yields of reconstructed events in each channel shown in Table 5. Details of how these estimates were arrived at are given in Ref. 4.

Table 5

# of Reconstructed/Tagged B Topologies Useful for Measurement of "γ" in the SFT / Year

B (CP • tag • trig)	Prod.	Accp	ε_{trig}	ε_{tag}	ε_{CP}	N_{recon}	N_{corr}
$B^0_s \to \rho K^0_s$ • $B \to l^{\pm}$(trig/tag)	5.0×10^2	0.28	0.37	0.85	0.60	30	30
$B^0_s \to D^+_s D^-_s$ • $B \to l^{\pm}$(trig/tag)	6.4×10^4	0.40	0.37	0.85	0.35	2900	2900
$B^0_s \to D^+_s K^-$ • $B \to l^{\pm}$(trig/tag)	1.4×10^4	0.50	0.37	0.85	0.40	900	900
$\bar{B}^0_s \to D^+_s K^-$ • $B \to l^{\pm}$(trig/tag)	1.0×10^4	0.50	0.37	0.85	0.40	640	640
$B^0_d \to \bar{D}^0_d K^{0*}$ • $B \to l^{\pm}$(trig/tag)	3.2×10^5	0.45	0.37	0.85	0.38	17600	17600
$B^0_d \to D^0 K^{0*}$ • $B \to l^{\pm}$(trig/tag)	3.2×10^4	0.45	0.37	0.85	0.38	1760	1760
$B^0_d \to D^0_1 K^{0*}$ • $B \to l^{\pm}$(trig/tag)	0.6×10^3	0.45	0.37	0.85	0.42	370	370
$B^+ \to \bar{D}^0_d K^+$ • $B \to l^{\pm}$(trig)	3.8×10^5	0.50	0.37	0.85	0.42	25800	25800
$B^+ \to D^0 K^+$ • $B \to l^{\pm}$(trig)	5.1×10^3	0.50	0.37	0.85	0.42	350	350
$B^+ \to D^0_1 K^+$ • $B \to l^{\pm}$(trig)	1.4×10^3	0.50	0.37	0.85	0.47	110	110
$B^0_d \to \Psi\rho^0$ • $B \to l^{\pm}$(tag)	5.4×10^3	0.56	0.70	0.85	0.60	1,100	4600
$B^0_d \to \Psi\rho^0$ • $B \to K^{\pm}$(tag)	2.3×10^4	0.51	0.70	0.77	0.60	3900	
$B^0_s \to \Psi\phi$ • $B \to l^{\pm}$(tag)	1.2×10^5	0.60	0.70	0.85	0.54	24000	94700
$B^0_s \to \Psi\phi$ • $B \to K^{\pm}$(tag)	4.7×10^5	0.55	0.70	0.77	0.54	80000	

The acceptance factors in Tables 4 and 5 are the composite acceptances for all the charged decay products of the B_{CP} and $B_{trig/tag}$. For some triggers, both lepton and kaon tagging are used. In these cases the first number in the acceptance column is for lepton tagging and the second number for kaon tagging.

4. ESTIMATED ERRORS IN 'γ' PER YEAR OF SFT OPERATION

To demonstrate the sensitivity of the fixed target method and specifically the SFT for measuring the angles of the unitarity triangle, we have estimated the error in "γ" as given in Section 2 for CP eigenstate modes (Class I B decays) per year of SFT operation for several B-> CP eigenstate modes. Only Class I decays have been used at this point since these decays have fewer uncertainties in the theoretical treatment than Class II decays and the error does not depend on the actual magnitude of the angle as it does for Class III and IV. The results are given in Table 6 below.

Table 6
Expected Errors in "γ" per Year of SFT Operation

∠	B (CP • tag • trig)	Prod.	Accp	ϵ_{tot}	N_{recon}	$1/d_{tot}$*	$\delta\sin 2\phi$	$\delta\phi$
'γ'	$B^0_s \to \rho K^0_s \cdot B \to l^\pm$(trig/tag)	5.0×10^2	0.28	0.19	30	2.64	0.242	7.0°
	$B^0_s \to D^+_s D^-_s \cdot B > l^\pm$(trigtag)	6.4×10^4	0.40	0.11	2900	2.64	0.050	1.4°
	$B^0_d \to \Psi\rho^0 \cdot B \to l^\pm$(tag) $B^0_d \to \Psi\rho^0 \cdot B \to K^\pm$(tag)	5.4×10^3 2.3×10^4	0.56 0.50	0.36 0.34	4600	3.00	0.045	1.3°
	$B^0_s \to \Psi\phi \cdot B \to l^\pm$(tag) $B^0_s \to \Psi\phi \cdot B \to K^\pm$(tag)	1.2×10^5 4.7×10^5	0.60 0.55	0.33 0.31	94700	3.00	0.010	0.3°

*Weighted by the proportion of the μ, e and K tags

5. SUMMARY

In conclusion, the SFT live target/extracted beam configuration allows measurement of the γ angle of the unitarity triangle to one to two degrees even if Class I decays are considered. When all possible methods are considered, errors of less than a degree should be possible.

6. REFERENCES

1. B. Cox et al, EOI-14, SSC Laboratory (May, 1990).
2. G. Carboni et al, LHB Collaboration, INFN PI/AE91/04, (1991).
3. Y.Lemoigne, GAJET Collaboration, Nucl. Instr. Meth. **A333**, 13(1993).
4. B. Cox et al., "The SFT, A Super Fixed Target Beauty Experiment at the SSC", these proceedings.
5. K. Foley et al., "Experiments, Detectors and Experimental Areas for the Super Collider", eds. R. Donaldson and M.G.D. Gilchriese, 701(1987).
6. A Feasibility Study for Asymmetric B Factory Based on PEP, SLAC-353.
7. M. Kobayashi and T.Maskawa, Prog. Theor. Phys. **49**, 652(1973).
8. L. Wolfenstein, Phys. Rev. Lett. **51**, 1945(1983).
9. I.I. Bigi, UND-HEP-92-BIG01, (1992).
10. I.I. Bigi and A.I. Sanda, Nulcear Physics B281, 41(1987).
11. R. Aleksan, I.Dunietz, B. Kayser and F. Le Diberder, Nuclear Physics B361, 141(1991).
12. M. Gronau and D. Wyler, Phys. Lett. **B265**, 172(1991).
13. M. Gronau and D. London, Phys. Lett. **B253**, 483(1991).
14. B. Kayser, "What Do Gamma Modes Measure", presentation at the 1993 Snowmass Workshop on B Physics.
15. S. Conetti, "Triggering at the SFT", these proceedings.

THE PROSPECT FOR DETERMINING THE ANGLE γ IN THE DECAY $B_d^0 \to \psi\rho^0$ AT THE SSC

FRED BIRD
Superconducting Super Collider Laboratory, 2550 Beckleymeade Avenue, Dallas, TX 75237*

1. INTRODUCTION

The most compelling understanding of the evidence for CP violation in the neutral B meson system will require many redundant measurements of the angles of the unitarity triangle. The angle γ is presently considered to be the most difficult angle to measure. This is primarily due to mounting evidence that the mixing is almost complete in the neutral B_s system, which implies rapid oscillations between $B_s^0 - \overline{B_s^0}$ mesons. A large oscillation rate will preclude the experimental observation of the B_s mixing due to inadequate detector resolution, where the most optimistic designs promise to allow measurement to no better than $x_s \approx 25$.

Due to this complication, alternative methods for extracting γ have been proposed. A candidate mode which has recently been proposed would require a study of the neutral B_d system in the $B_d^0 \to \psi\rho^0$ decay mode[1]. The measurement of the γ angle is via an asymmetry measurement as in the case of the β angle measurement in the $B_d^0 \to \psi K_s^0$ mode. Here, the extraction of γ necessarily depends upon, and so is coupled to, the measurement of β. However, as will become apparent, the measurement of the β angle will be known with sufficient precision by the time that a γ measurement can be attempted that the proposed technique remains interesting. In fact, many of the techniques required to observe β and those necessary to determine γ are identical so that both numbers can, in principle, be extracted within the same experiment, given a sufficient statistical sample and favorable decay parameters.

The theoretical motivation for the measurement is discussed below, followed by the experimental potential for such a measurement from one of the large high p_t detectors, SDC, proposed for the Superconducting Supercollider[2]. In all likelihood this measurement will require the SSC (at least), where the primary b yield is expected to be $\approx 10^{13}$ at the design luminosity of $10^{33}\text{cm}^{-2}\text{sec}^{-1}$, since the expected branching ratio for $B_d^0 \to \psi\rho^0$ is small, $\approx 5 \times 10^{-5}$. The final state will be readily observable in SDC. There are 4 tracks, 2 μ's (or e's, though they are not explicitly studied here) and 2π's, from the signal B_d^0, each pair of which should reconstruct to a resonance, and an additional μ from the $B_d^0 \to \mu\nu_\mu X$ decay

*Operated by the Universities Research Association, Inc., for the U.S. Department of Energy under Contract No. DE-AC35-89ER40486.

of the associated tag B. Good tracking efficiency, good μ identification, and good mass resolution allow the signal to be observed.

2. THE THEORY

The theoretical motivation for studying this channel is discussed by Dunietz[1]; only the salient experimental points are reviewed here. First, this decay is not the most apparent one in which to measure γ. For instance, measuring the asymmetry in the $B_s \to \psi\phi$ final state would yield γ, through a second-order penguin contribution. This final state is very accessible to experiment; however, it must be stressed that it requires clean tagging and excellent vertexing (required to observe the time-dependent mixing oscillations) which may both be precluded if x_s is large. The same comment applies to other potentially interesting B_s decays, e.g., $B_s^0 \to D_s^{(\pm)} K^{(\mp)}$.

The γ measurement in $B_d^0 \to \psi\rho^0$ is extracted from the measurement of the $Im\lambda(B_d^0 \to \psi\rho^0)$ which follows from a measurement of the asymmetry

$$A_{CP}(t) = \frac{\Gamma(B_d^0 \to \psi\rho^0) - \Gamma(\overline{B_d^0} \to \psi\rho^0)}{\Gamma(B_d^0 \to \psi\rho^0) + \Gamma(\overline{B_d^0} \to \psi\rho^0)} = Im\lambda \sin \Delta mt. \tag{1}$$

From eq. 40 of [1],

$$\lambda(B_d^0 \to \psi\rho^0) = -\lambda(B_d^0 \to \psi K_s^0)\frac{\bar{b}}{b}, \tag{2}$$

which can be rewritten as

$$\lambda(B_d^0 \to \psi\rho^0) = -e^{-2i\beta}\frac{1 + z^* e^{-i\gamma}}{1 + ze^{-i\gamma}} = -e^{-2i\beta}e^{i\phi}, \tag{3}$$

where $b(\bar{b}) = 1 + z^{(*)}e^{(-)i\gamma}$. Figure 2 of [1] depicts the geometrical relationship of γ to the observables in the experiment. Due to strong matrix element effects in the final state, a measurement of $B_d^0 \to \psi K^{*0}$ is also required when determining b. However, that mode will be well known by the time that the present measurement could be attempted.

Now z (considering only case $z = z^*$) is expected to be a small number, $0.01 \leq z \leq 0.1$. In that case, neglecting second order terms in z, write

$$\lambda(B_d^0 \to \psi\rho^0) = -e^{-2i\beta}e^{i\phi} \approx -e^{-2i\beta}e^{-i2z\sin\gamma}. \tag{4}$$

Then,

$$Im\lambda \approx \sin(2z\sin\gamma + 2\beta) \tag{5}$$

and so the time integrated asymmetry is given by

$$A_{CP} = \sin(2z\sin\gamma + 2\beta). \tag{6}$$

Clearly, a good measurement of γ requires a good knowledge of β, which is expected to be well known by the time the γ measurement can be attempted.

3. THE SIGNAL SAMPLE

This work is closely coupled to that of the proposed measurement of the β angle in the $B_d^0 \to \psi K_s^0$ channel with the SDC detector[3]. ISAJET is used to generate the pair-produced b quarks via gluon splitting. Events are selected which contain a b quark jet with $p_t \geq 10$ GeV/c^2 within the acceptance of SDC. The $\psi\rho^0$ decay is studied in the $\mu^+\mu^-\pi^+\pi^-$ final state. The initial flavor of the b quark in the final state is determined (tagged) by the sign of the μ from the associated $\bar{b}$ semileptonic decay. The trigger discussion follows that of the ψK_s^0 decay[3]. However, here the SDC nominal single μ trigger with a $p_t = 20$ GeV/c threshold is chosen.

The B_d^0 is reconstructed by first reconstructing the two final state resonances. The ψ is made from a pair of oppositely charged μ's which have a mass within ± 50 MeV/c^2 of the nominal ψ mass. Each μ must have $p_t \geq 1$ GeV/c and $|\eta| \leq 2.5$. A pair of unlike sign π's, each of which meet the same kinematic criteria as the ψ decay muons, which reconstruct within ± 50 MeV/c^2 of the ρ^0 mass are also selected. It is also required that $p_t(\rho^0) \geq 1$ GeV/c. To further suppress background, the ψ and the ρ^0 are required to be close together, here $\cos\theta(\psi, \rho^0) \geq 0.9$.

The full set of cuts required to isolate a clean $\psi\rho^0$ sample is shown in table 1. For 1 SSC year of running at design luminosity (10^7 seconds at 10^{33} cm^{-2} sec^{-1}), and a b quark production cross section of 250μb [3], there will be of order 2000 $B_d^0 \to \psi\rho^0$ events reconstructed.

Table 1: Contributions to the rate for $B_d^0 \to \psi\rho^0$ detected in SDC. †From figure 3.2 of Coupal[3].

Contribution	Acceptance factor
$b \to B_d^0$ or $\bar{b} \to \bar{B}_d^0$	2×0.38
$B_d^0 \to \psi\rho^0, \psi \to \mu^+\mu^-, \rho^0 \to \pi^+\pi^-$	3×10^{-6}
$b \to \mu + X$	0.12
1 trigger $\mu, p_t > 20$, $\lvert\eta\rvert \leq 2.5^{\dagger}$	0.015
2 other μ's, $p_t \geq 3, \lvert\eta\rvert \leq 2.5$	0.46
$p_t(\rho) \geq 1$	0.97
$\cos\theta(J/\psi, \rho^0) > 0.9$	0.95
tracking and μ id efficiency	$(0.8)^3$
Total (ϵBr)	9×10^{-10}

4. BACKGROUNDS

Much of the background to the $\psi\rho^0$ signal arises from the same sources as in the background discussion of the ψK_s^0 channel[3]. Briefly, spurious μ's which could give rise to false signals will arise from other true c, b decays, decays in flight, or punchthrough. In particular, μ's due to inclusive ψ production from b decays in combination with other unassociated π's and ρ^0's in the event are the most serious. The angle cut reduces the fake rate. The μ's from charm decays and from decays in flight are generally at low p_t and so of less concern. The punchthrough contamination has not been evaluated. If these background μ's prove unwieldy, there can be loose requirements placed on a common vertex for the ψ and ρ^0 which should reduce the problem considerably at a minimal cost to the signal. A very serious problem may arise from the production of $B_d^0 \to \psi\omega$, where the π^0 from the ω decay is very soft. Future studies should address and quantify these points.

5. MEASUREMENT OF γ

For the present purposes then, assume that the background to the signal can be neglected. Then, the measured asymmetry will be given by $A = DA_{CP}$ where the dilution factor, D, represents the loss of analyzing power due to incorrect identification of the final state. There are several contributions to D including that due to mixing of both the signal and tag Bs, those due to the cascade decays of the tagging b, and to detection difficulties. A thorough Monte Carlo study of these errors has been made[3] and gives $D \approx 0.19$. The number of events required to measure the angle to a given precision follows from eq. (6);

$$N = \frac{1}{\delta^2 A_{CP}} \frac{1}{D^2 \varepsilon Br} = \frac{1}{\delta^2(\sin\gamma)} \frac{1}{D^2} \frac{1}{\cos^2 2\beta} \frac{1}{z^2}, \tag{7}$$

where it has been assumed that $2z \sin\gamma \ll 2\beta$. Again, this will require that $\sin 2\beta$ has been well measured, in fact well enough that $\delta\beta < z \sin\gamma$.

At this point, some assumptions must be made regarding the sizes of the different parameters in order to extract an example γ measurement. In the most optimistic scenario, with z near a maximum ($z = 0.1$) and $\cos 2\beta \approx 1$ (or $2\beta \approx 0$), the analysis indicates that it would take on the order of 10 SSC years at design luminosity to reach $\delta(\sin\gamma) \approx 0.2$.

Unfortunately, full vertexing of the $\psi\rho^0$ pair will probably be required, which would cost signal. However, a factor of perhaps four in improvement could be expected if the e's from $B_d^0 \to e\nu_e X$ on the tagging side and $\psi \to e^+e^-$ from the signal side can be used. It is clear that a good measurement of γ will require a great deal of patience...and luck.

6. ACKNOWLEDGMENTS

Thanks to D. Coupal (SSCL), I. Dunietz (FNAL), and P. Sphicas (MIT) for useful discussions.

7. REFERENCES

1. I. Dunietz,"Extracting CKM parameters from B Decays," Fermilab-CONF-93/90-T and these proceedings.
2. SDC Technical Design Report, SDC-92-201, SSCL-SR-1215, 1 Apr 1992.
3. D. Coupal,"Prospects for Measuring CP Violation in SDC Using $B_d^0 \to \psi K_s^0$," these proceedings.

Other B Physics

Convenors:

S. Wojcicki
Stanford Linear Accelerator Center /
Superconducting Super Collider Laboratory

A. Zieminski
Indiana University

Y. Nir
Weizmann Institute of Science

List of Subgroups

Hadro- and Photo-Production

B_S Mixing

B Decays

Other Spectroscopy

Hadro- and Photo-Production

Leaders:

D. Hedin
Northern Illinois University

V. Papadimitriou
Fermi National Accelerator Laboratory

W.K. Tung
Michigan State University

List of Participants

G. Álvarez
Indiana University

J. Appel
Fermi National Accelerator Laboratory

B. Choudhary
University of California (Riverside)

R. Demina
Northwestern University

E. Engels
University of Pittsburgh

V. Glebov
Superconducting Super Collider Laboratory

E. Hartouni
University of Massachusetts

D. Hedin
Northern Illinois University

P. Lebrun
Fermi National Accelerator Laboratory

E. Levin
Fermi National Accelerator Laboratory

S. Mani
University of California (Davis)

H. Melanson
Fermi National Accelerator Laboratory

R. Meng
Argonne National Laboratory

M. Mohammadi
State University of New York at Stony Brook

V. Papadimitriou
Fermi National Accelerator Laboratory

A. Peryshkin
Fermi National Accelerator Laboratory

S. Riemersma
Southern Methodist University

J. Smith
State University of New York at Stony Brook

W. Tung
Michigan State University

D. Zieminska
Indiana University

AN OVERVIEW of the δ WORKING GROUP

ANDRZEJ ZIEMINSKI
Department of Physics
Indiana University
Bloomington, Indiana 47405, USA

0. INTRODUCTION

The δ group was charged to encompass all other b-physics topics not covered by the α, β and γ groups. It turned out to be quite a challenge. The convenors of the group: Y. Nir, S. Wojcicki and A. Zieminski decided that the topics discussed by the group should reflect the interests of the participants. With over 80 physicists, who signed up for our group, we were able to cover a large area of exciting physics. All topics were first presented at the group plenary sessions, and then the actual work was done by smaller working groups, with a well balanced input from both experimentalists and theorists. The δ group split into 3 major subgroups: (1) hadro- and photo- production, (2) B_s mixing, (3) B-decays plus a small subgroup dedicated to (4) other spectroscopy. The B-decays subgroup split even further into: (3.1) B_c spectroscopy and pentoquarks, (3.2) leptonic and semileptonic decays and (3.3) rare decays. The leaders and contributors to individual subgroups are listed at the end of this overview.

There are 18 δ papers included in these proceedings. They summarize majority of the topics discussed by the group and their order reflects the group organization described above.

1. HADRO- and PHOTO- PRODUCTION

The first four papers are concerned with the b-quark hadroproduction. There was a natural overlap between the hadroproduction δ subgroup and the "theory" group. Whereas the theory group concentrated primarily on theoretical uncertainties of the QCD calculations, the δ subgroup tried to provide experimentalists with a consistent set of predictions for total and differential beauty cross sections. A lot of activity was spent testing the small x resummation approach by Levin et al. Unfortunately, the current results from this approach are at best very preliminary. Therefore the cross section predictions are based on a fixed-order perturbative QCD, which is expected to be more reliable at the Fermilab fixed target c.m. energy range than at the Tevatron or the SSC collider energies. The two δ papers included in these proceedings provide predictions for b-quark cross sections calculated in the regions of phase space covered by various experiments. The papers by **S. Riemarsama and R. Meng** and by **E. Berger and R. Meng** should serve as pinacotheques of b-cross sections, consistently calculated in the fixed-order perturbative QCD. Contributions from **V. Papadimitriou** and **B. Choudhary** present the most recent (as of September 1993) results from CDF and $D0$ Fermilab collider experiments.

2. B_s MIXING

A precise measurement of B_s mixing could lead to a determination of the CKM unitarity triangle through a measurements of its sides, rather than angles. Present estimates predict a value of the mixing parameter x_s within a range of 10-30. Papers included in these proceedings cover majority of experimental approaches to the subject. **J. Skarha and B. Wicklund** introduce the subject and discuss CDF B_s mixing potential. They also provide extensive lists of B_s decay modes most suitable for the measurement. **K. Johns** summarizes $D0$ measurements of the time integrated and flavor averaged mixing. The LEP results and approach to mixing measurements are described by **X. Lou**. The SLD plans are presented by **C. Baltay**. The LEP experiments do not have enough statistics to study exclusive B_s decay modes and the time resolution for semileptonic decays limits the measurable x_s range to $x_s<10$. The SLD group proposes to use the electron beam polarization to tag b quarks at the production time. Under optimistic assumptions, with an upgraded vertex detector, this technique can reach x_s values of 15. The x_s range around 20 is available only to the hadroproduction experiments. The methodology for evaluating B_s mixing measurement capabilities for various experiments, developed by the subgroup, is described by **T. Burnett**. The summary Tables are contained in a paper by **D. Ritchie, J. Skarha and A. Zieminski**. They conclude that the upgraded CDF and $D0$ experiments should accumulate enough events to measure x_s up to 20 in less than a year of running with the Main Injector. Many of the Monte Carlo assumptions used in this study should be verified by CDF during the forthcoming run in 1994.

3. B DECAYS

3.1 B_c spectroscopy and Pentaquarks

C. Quigg addresses many aspects of the production and decay of B_c , a bound state of two heavy quarks $c\bar{b}$, yet to be discovered. He discusses the B_c mass spectrum, its lifetime, exclusive decay modes and chances of its discovery during the forthcoming Tevatron collider run.

3.2 Leptonic and semileptonic decays

An article by **K. Kinoshita et al.** summarizes the conclusions of this subgroup. The leptonic and semileptonic decay modes are the modes of choice for measurement of the CKM matrix elements $|V_{cb}|$ and $|V_{ub}|$. The theoretical uncertainties involved in determinations of CKM matrix elements will improve in the near future as a result of heavy-quark symmetry applications and improved lattice QCD calculations. The vector meson decays $B \to D^{*}l\nu$ should soon lead to a $|V_{cb}|$ measurement with a 2% statistical accuracy, diluted by a 7% systematic errors combined with a 4% theoretical uncertainty. The projection for statistical errors on $|V_{ub}|$ is (5-15)% within five years.

3.3 Rare decays

H. Lipkin introduces, at a level aimed at pedestrians, the difficulties and future possibilities of two types of CP-violation experiments, neutral meson mixing and direct charge asymmetry in $B^{\pm}$ decays.

Discussions of the B rare decays subgroup are summarized in a paper by **Y. Nir**. The group concentrated on three type of processes: (1) neutral B decays into final CP eigenstates, for which CP asymmetries are predicted to be close to zero, (2) rare decays with two final charged leptons, (3) CP asymmetries in charge B-mesons and baryons. Specific aspects of processes (2) and (3) are also discussed in papers by **D. Cline** and **A. Schwartz**, respectively. The B decay modes that seem to be experimentally most feasible are: the $B_s \to \psi\phi$ mode (among the "clean zeros" B_s decays), the $B \to K\mu^+\mu^-$ mode (among the flavor changing decays), and the $B^- \to \phi K^-$ and $\Lambda_b \to pK^-$ modes for the observation of direct CP violation.

D. Cline discusses selected topics of rare B Flavor Changing Neutral Currents ($FCNC$) processes and their sensitivity to physics beyond the standard model. The paper also addresses potentials of various fixed target and collider experiments to detect these processes. Results of specific Monte Carlo studies of the process $b \to s + \gamma$ for the Fermilab fixed target proposal $P867$ are described by **D. Cline et al.** in a companion paper.

Experimental methods of observing some of the self-tagging B decays are discussed by **A. Schwartz**. He concentrates on decay modes producing two charged K's in the final states. These K's can be used to trigger the detector with a reasonably high level of background rejection.

4. OTHER SPECTROSCOPY

Finally, **J.Rosen,J. Marques and L. Spiegel** discuss heavy flavor spectroscopy. They stress that there are many undiscovered states among both: (1) hidden flavor states and (2) open flavor states. A special effort should be made to identify possible hadro-molecular states. The authors also suggest that the richness of the exited B-states may undermine the efficacy of self-tagging schemes using excited B-mesons - a topic discussed in C. Hill's report at this workshop.

B-QUARK PRODUCTION AT HADRON COLLIDERS

STEPHAN RIEMERSMA
Department of Physics, Southern Methodist University, Fondren Science Building
Dallas, TX 75275-0175, U.S.A.

and

RUIBIN MENG
High Energy Physics Division
Argonne National Laboratory, Argonne, IL 60439, U.S.A.

1. INTRODUCTION

Studying B-physics at hadron accelerators requires a good understanding of the total and differential cross sections for b-quark production. This knowledge gives those involved in $B\bar{B}$ mixing, rare B decays, and those trying to determine the CKM angles α, β, and γ an idea of how many events they can expect, given the luminosity and the branching ratios. It is particularly important for those studying rare B decays as they set limits on where we can hope to see new physics. For these reasons and others, the complete $\mathcal{O}(\alpha_S^3)$ corrections to heavy-quark production at hadron accelerators were calculated in [1] and [2]. Also three groups [3],[4],[5] have attempted to calculate heavy-quark production using resummation techniques in the small-x kinematic region. These resummation techniques are necessary since the b-quark mass m_b is small relative to the center-of-mass energies $\sqrt{S}$ of the TeVatron and the SSC. While these techniques offer some hope of obtaining reasonable predictions for b-production at these machines, the current results can best be considered as preliminary.

Thus we must turn to fixed-order perturbative QCD for guidance, as we have no other real choice at this point. However, let us submit a *caveat* here: fixed-order perturbative QCD works best when all the scales are roughly comparable, *i.e.* $\sqrt{s} \approx m_b \approx p_t$, $\sqrt{s}$ being the partonic center-of-mass energy. When we are not in this regime, for example at the TeVatron and the SSC, our predictions will then be less reliable. Bearing this in mind, let us continue to the results section.

2. RESULTS

A number of fixed-target pp experiments have been proposed for HERA, LHC, and SSC. The cross sections given in Table 1. are total cross sections without any cuts applied. The purpose is to give an idea of the overall rate of b-production at these proposed experiments. Note that these cross sections are for inclusive b-production, so if one wants to calculate rates for b- or $\bar{b}$-production, one needs to multiply these results by a factor of two.

Table 1. Cross Sections for Proposed Fixed-Target Experiments.

$\sqrt{S}$ (GeV)	Born	$\mathcal{O}(\alpha_S^3)$
43	8.3 nb	17 nb
124	0.32 μb	0.58 μb
200	0.89 μb	1.6 μb

These cross sections were generated using programs created by [2] with the following inputs: m_b was chosen to be 4.75 GeV/ c^2, the mass factorization scale M^2 was chosen to be m_b^2, and the parton distribution set used was CTEQ1M [6]. We would also like to mention here that similar results have been obtained earlier in [7] using a similar parton distribution set and our numbers in Table 1. as well as in Table 2. below agree with theirs. From Table 1., we see that the corrections even at these low energies are sizeable. For $\sqrt{S} = 43$ GeV, one should probably take into account resummation effects at large-x (see [8]). However, at these energies, we expect that the results are fairly accurate.

The situation for b-production at the TeVatron, LHC, and SSC is more problematic. We are no longer in a region where we expect fixed-order perturbative QCD to give experimentally valid results. Nevertheless, the predictions made are worth noting, to get a quantitative idea of which regions in phase space our predictions are lacking and how much of an improvement needs to be made. Having given sufficient warning, we present Table 2., cross sections for the TeVatron, LHC, and SSC.

Table 2. Cross Sections for the Various Colliders.

$\sqrt{S}$ (TeV)	Born	$\mathcal{O}(\alpha_S^3)$
1.8	17 μb	37 μb
15.4	92 μb	270 μb
40	170 μb	550 μb

As in Table 1., no cuts were applied and the input parameters chosen were the same. We see rather large increases when the $\mathcal{O}(\alpha_S^3)$ corrections are included. The 'K-factors' are 2.2, 2.9, and 3.2 for the TeVatron, LHC, and SSC, respectively. The size of these 'K-factors' might give one cause to worry, however they are slightly misleading since the massless t-channel exchanges present in the $\mathcal{O}(\alpha_S^3)$ corrections are absent in the Born approximation calculation. A better indication of the convergence should be found in comparing the $\mathcal{O}(\alpha_S^4)$ results with the $\mathcal{O}(\alpha_S^3)$ corrections. We were also presented with a list of cuts from various experimental groups, and what was settled upon was the following: for CDF, we were asked for pseudorapidities $|\eta| < 1$ and $p_t > 4$ GeV/c in the central region. The D0 cuts were $|\eta| < 3.4$ and $p_t > 5$ GeV/c in the central region. In the forward region at the TeVatron, the request was for $2.5 < |\eta| < 5.5$ and $p_t > 1.5$ GeV/c. At the SSC, the central region was determined to be $|\eta| < 2.5$ and $p_t > 10$ GeV/c, and the forward region given was $1.5 < |\eta| < 5.5$ and $p_t > 1.5$ GeV/c. The calculations are done with cuts in rapidity not pseudorapidity, but the difference should be small. Table 3. shows the results for these cuts.

Table 3. Cross Sections with Cuts Implemented.

CDF Central	D0 Central	TeVatron Forward	SSC Central	SSC Forward
7.2 μb	13 μb	7.0 μb	62 μb	300 μb

The forward region results include the sum of the positive and negative rapidity results. The result for the central SSC region seems low until one considers the large p_t-cut made. Also, the large rapidity coverage of D0 helps considerably in enlarging the cross section.

For additional enlightenment, we have plotted $d\sigma/dp_t$ versus p_t for the central and forward regions for both the TeVatron and the SSC. Before we discuss the $d\sigma/dp_t$ plots we would also refer interested readers to [7] for rapidity distributions giving additional useful information. In Figure 1., we see that the expanded rapidity coverage of D0 makes the cross section larger by a factor of two over CDF rather uniformly over the entire p_t-range. Most of the cross section lies in the low-p_t range. Therefore if one could lower the p_t-cut, the event increase would be sizeable. For these plots, we have chosen $M^2 = p_t^2 + m_b^2$. Also, these plots were produced by running the programs for the Born approximation p_t-distributions and multiplying by the 'K-factors' previously introduced; 2.2 for the TeVatron plots and 3.2 for the SSC plots. The justification for this was 1) time was of the essence and the higher-order calculations would have taken a day each to compute and 2) in discussions [9], it was revealed that the higher-order calculations generally raise the Born approximation results by a fairly uniform amount across the entire p_t-range.

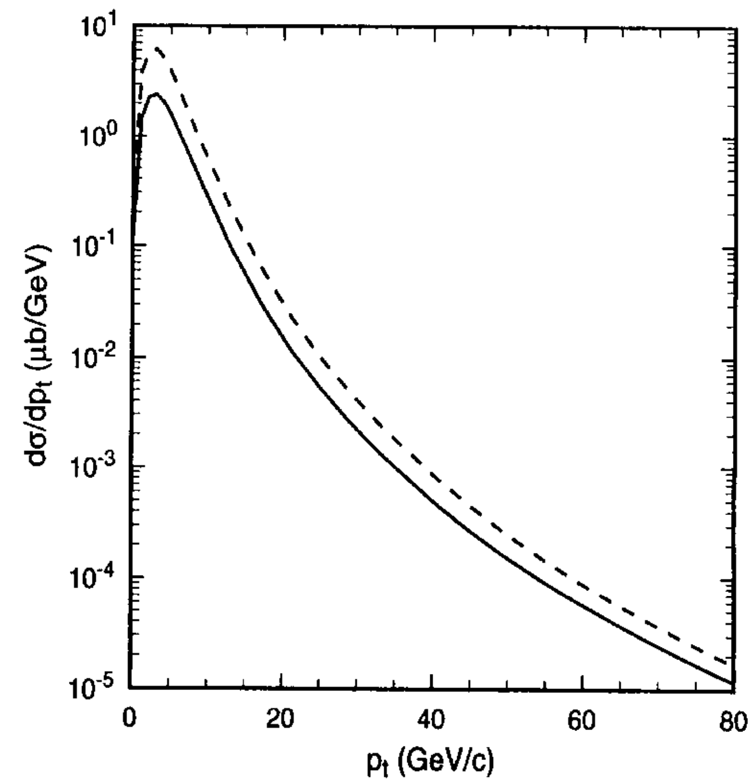

Figure 1. $d\sigma/dp_t$ vs. p_t for the kinematic cuts imposed for the CDF collaboration (solid line) and the D0 collaboration (dashed line) in the central region.

Figure 2. shows a dramatic fall-off in the forward region as p_t increases, again with most of the cross section in the low-p_t region. In the low-p_t range, the cross section is reduced by a factor of three to five compared to the central region, depending on the cut made.

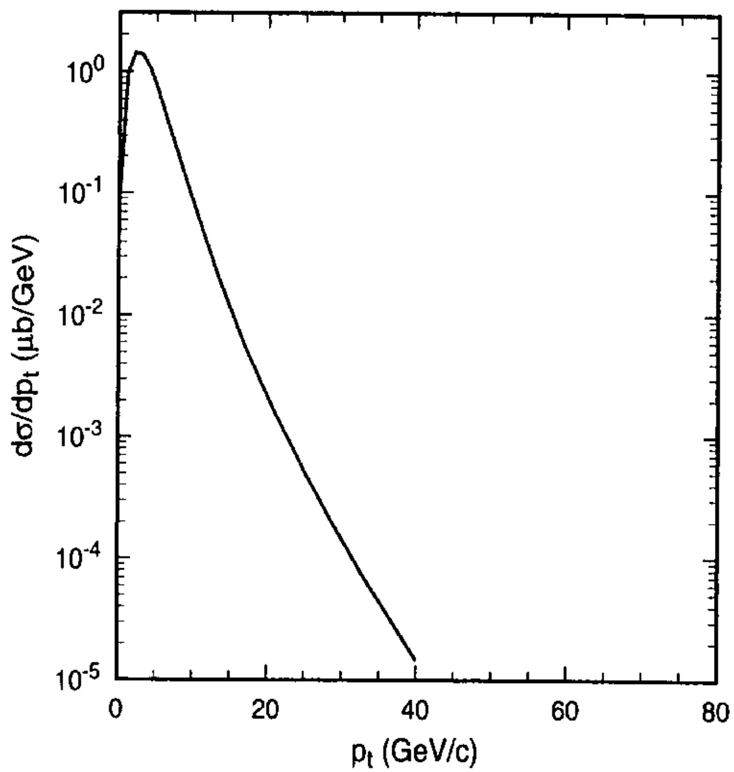

Figure 2. $d\sigma/dp_t$ vs. p_t for the kinematic cuts imposed in the forward region at the TeVatron.

Turning to the SSC, Figure 3. shows that by imposing a p_t-cut of 10 GeV/c, most of the cross section is lost in the central region. At large p_t, we find that the contribution is still appreciable.

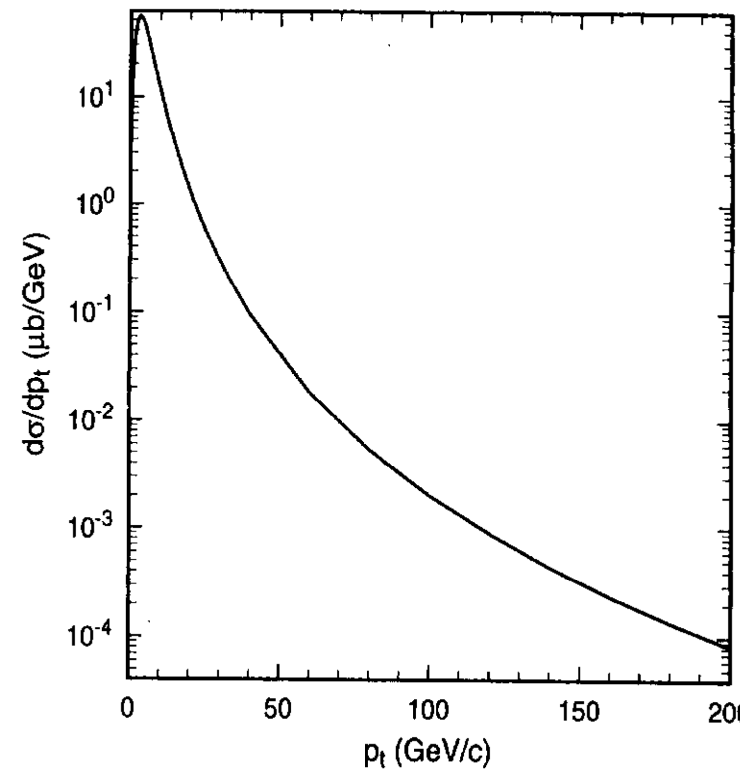

Figure 3. $d\sigma/dp_t$ vs. p_t for the kinematic cuts imposed in the central region at the SSC.

Finally, in the forward region, Figure 4. reveals the large-p_t region is again still significant, but again the majority of the cross section comes from the low-p_t region. The loss of cross section as p_t increases is not so dramatic as it is in the forward region at the TeVatron.

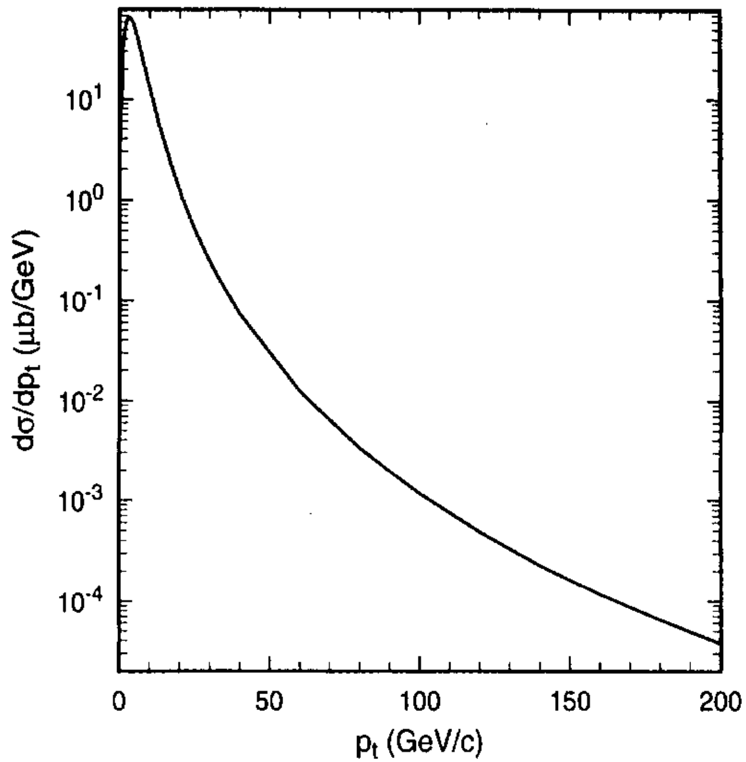

Figure 4. $d\sigma/dp_t$ vs. p_t for the kinematic cuts imposed in the forward region at the SSC.

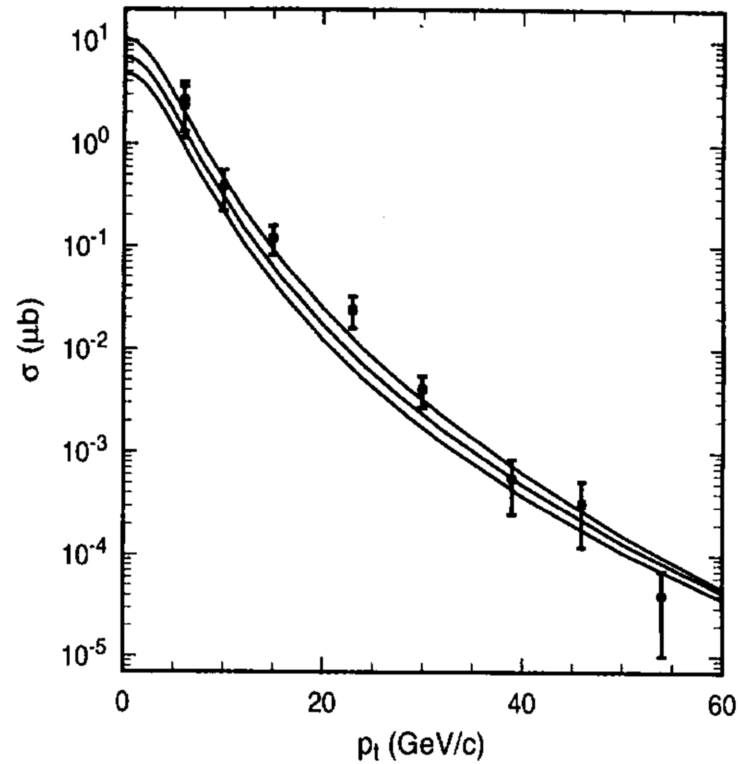

Figure 5. σ vs. p_t^{min} for $\sqrt{S} = 630$ GeV with $|y| < 1.5$. The data are taken from Table 2. of [10]. The high curve was run with $m_b = 4.5$ GeV$/c^2$, and $M = m_b/2$. The middle curve was run with $m_b = 4.75$ GeV$/c^2$, and $M = m_b$. The low curve was run with $m_b = 5.0$ GeV$/c^2$, and $M = 2m_b$. CTEQ1M distribution functions were used.

3. CONCLUSIONS

What can we conclude from these results? First, the fixed-target results are probably solid, since we can see from Figure 5. the results from UA1 [10] are in good agreement with the $\mathcal{O}(\alpha_S^3)$ results, and the energies for the fixed-target experiments are lower than that of UA1.

Looking at Figure 6., we compare the $\mathcal{O}(\alpha_S^3)$ calculations of [1,2] with the 1988-89 and 1992-93 results of CDF[11]. Some of these data are still preliminary, of course, but it appears that the data do not fit the calculation.

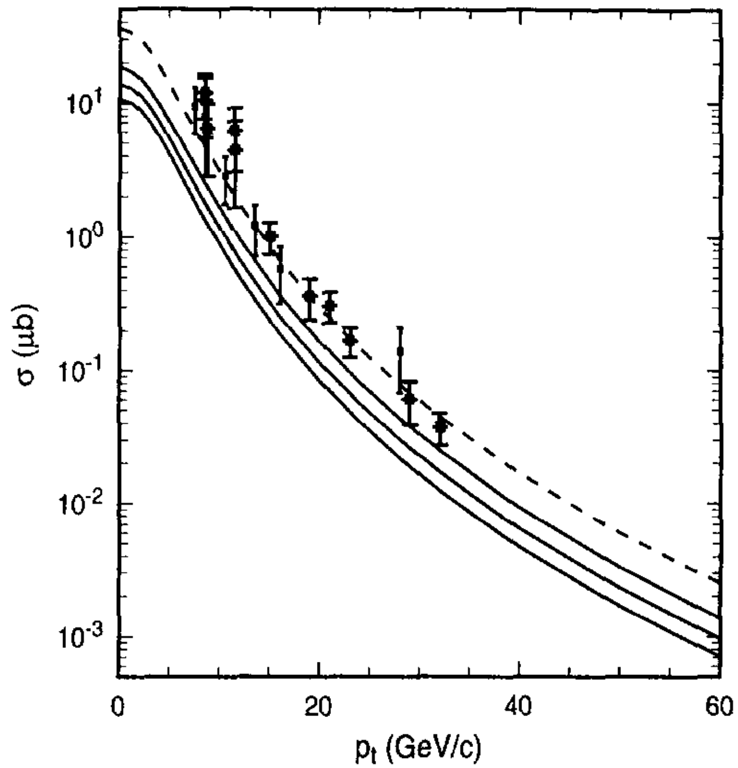

Figure 6. σ vs. p_t^{min} for $\sqrt{S} = 1.8$ TeV with $|y| < 1$. The high solid curve was run with b-quark mass $m_b = 4.5$ GeV$/c^2$, and $M = m_b/2$. The middle solid curve was run with $m_b = 4.75$ GeV$/c^2$, and $M = m_b$. The low solid curve was run with $m_b = 5.0$ GeV$/c^2$, and $M = 2m_b$. CTEQ1M distribution functions were used. The data with the thick error bars are taken from the 88-89 and the thin error bars from the 92-93 runs of CDF[11]. The dashed curve is the middle solid curve multiplied by a factor of 2.6.

From the figure caption we see that we are off by about a factor of 2.6. But we have some consolation because the shape is approximately correct, although a steeper distribution as discussed in [12] would fit better. This factor of 2.6 will only be magnified when we look at the results for the SSC. Clearly, we have a problem.

What are the possible solutions? Calculate the $\mathcal{O}(\alpha_S^4)$ corrections and see what difference that makes. That is an enormous endeavor and would take years. Try to make further headway on the small-x front. This is possible but large uncertainties remain. As an example, one interesting mechanism to accommodate the CDF data shown in Figure 6. is to alter the form of the gluon distribution in the small-x region[12]. But for a 'ballpark estimate' that probably is not too bad, why not do the following: try

$$\sigma_{exp} = \sigma_0 \, e^{(K-1)}, \tag{1}$$

where σ_0 is the Born cross section, K is the appropriate 'K-factor,' and σ_{exp} is the expected cross section. In the case of the TeVatron, $\sigma_0 = 17$ microbarns and $K = 2.2$. We would get $\sigma_{exp} = 56$ microbarns. For the SSC, $\sigma_0 = 170$ microbarns and $K = 3.2$. Here $\sigma_{exp} = 1.5$ millibarns. The distributions would also have the factor $e^{(K-1)}$ multiplying the lowest-order distributions. This is of course rather *ad hoc*, but the results look reasonable. More theoretically valid calculations are still well off in the distance, and the numbers are needed now.

Finally, in the course of many discussions [13], it was decided that approximate cross section numbers for each of the colliders, current and proposed, should be provided so an estimate of B-physics event rates could be made. Toward that end, we present Table 4., a compilation of cross section numbers that should be correct within a factor of two.

Table 4. Cross Section Figures for Reference.

$\sqrt{S}$	43 GeV	124 GeV	200 GeV	1.8 TeV	15.4 TeV	40 TeV
σ	20 nb	0.5 μb	2 μb	100 μb	0.5 mb	1 mb

The numbers for the lower energies were arrived at essentially by rounding the results of the $\mathcal{O}(\alpha_S^3)$ calculation. The 1.8 TeV result was derived in the following way: we took the fact that the curve that fits the data of CDF is 2.6 times the $\mathcal{O}(\alpha_S^3)$ result. Multiplying the 37 microbarns by the factor of 2.6, we get a convenient number of 100 microbarns for the TeVatron with no cuts. The numbers for the LHC and the SSC were based on various estimates obtained using various parton distribution sets. They were also agreed upon in [13] and further detailed discussions about the uncertainties can be found in [7,13].

4. ACKNOWLEDGEMENTS

The authors would like to thank Jack Smith for his careful reading of the manuscript. This work was supported by the Lightner Sams Foundation, Inc., the U.S. Department of Energy, Division of High Energy Physics, Contract W-31-109-ENG-38, and the Texas National Research Laboratory Commission.

5. REFERENCES

1. P. Nason, S. Dawson, and R.K. Ellis, *Nucl. Phys.* **B303** (1988) 607; *Nucl. Phys.* **B327** (1989) 49; *Nucl. Phys.* **B335** (1990) 260.
2. W. Beenakker, H. Kuijf, J. Smith, and W.L. van Neerven, *Phys. Rev.* **D40** (1989) 54; W. Beenakker, W.L. van Neerven, R. Meng, G.A. Schuler, and J. Smith, *Nucl. Phys.* **B351** (1991) 507.
3. J.C. Collins and R.K. Ellis, *Nucl. Phys.* **B360** (1991) 3.
4. E.M. Levin, M.G. Ryskin, Yu.M. Shabelskii, and A.G. Shuvaev, DESY-91-054; E.M. Levin, M.G. Ryskin, and Yu.M. Shabelskii, *Phys. Lett.* **B260** (1991) 429.
5. S. Catani, M. Ciafaloni, and F. Hautmann, *Nucl. Phys.* **B366** (1991) 135.
6. J. Botts, J.G. Morfín. J.F. Owens, J. Qiu, W-K. Tung, and H. Weerts, *Phys. Lett.* **B304** (1993) 159.
7. E. Berger, and R. Meng, *Phys. Rev.* **D46** (1992) 169.

8. E. Laenen, J. Smith, and W.L. van Neerven, *Nucl. Phys.* **B369** (1992) 543.

9. J. Smith, *private communication.*

10. UA1 Collaboration, C. Albajar *et al*, *Phys. Lett.* **B256** (1991) 121.

11. V. Papadimitriou, *private communication*: F. Abe et al., *Phys. Rev. Lett.* **68**, (1992) 3403; F. Abe et al., *Phys. Rev. Lett.* **69**, (1992) 3704: F. Abe et al., FERMILAB-PUB-93/091-E (April 1993), submitted to *Phys. Rev. Lett.*: F. Abe et al., FERMILAB-PUB-93/106-E (May 1993), submitted to *Phys. Rev. Lett.*: F. Abe et al., FERMILAB-PUB-93/131-E (June 1993), submitted to *Phys. Rev.* **D**: F. Abe et al., FERMILAB-PUB-93/145-E (June 1993), submitted to *Phys. Rev. Lett.*

12. E. Berger, and R. Meng, in the *Proc. DPF92*, Fermilab, 1992: E. Berger, R. Meng, and J.-W. Qiu, in the *Proc. XXVI Int. Conf. on High Energy Physics*, Dallas, 1992: E. Berger, R. Meng, and W.-K. Tung, *Phys. Rev.* **D46** (1992) 1859.

13. E.M. Levin, J. Smith, and W.-K. Tung, *private communication.*

Bottom Quark Cross Sections at Collider and Fixed-Target Energies at the SSC and LHC

Edmond L. Berger[a,b] and Ruibin Meng[a]

[a]High Energy Physics Division
Argonne National Laboratory, Argonne, IL 60439, USA
[b]CERN, Geneva, Switzerland

Abstract

Calculations of inclusive cross sections for the production of bottom quarks in proton-proton collisions are presented as a function of energy, transverse momentum, and Feynman x_F for values of $\sqrt{s}$ from 100 GeV to 40 TeV. In addition, we provide simple parametrizations of our theoretical results that should facilitate estimates of rates, acceptances, and efficiencies of proposed new detectors.

Calculations of heavy flavor cross sections at the planned energies of future hadron colliders assist in the design of experiments and in the evaluation of the merits of various options, such as experiments in fixed target modes and/or with detection concentrated in forward or central regions of phase space. In this paper, calculations are presented of inclusive cross sections for bottom quark production at energies from $\sqrt{s} = 100$ GeV to 40 TeV. For several energies, cross sections are displayed as functions for transverse momentum (p_T) for selected values of Feynman x_F. In addition, we provide simple analytic parametrizations of our theoretical predictions that should make our results easy to use in studies of expected acceptances and efficiencies of proposed new detectors. The theoretical computations are based on next-to-leading order QCD hard-scattering cross sections[1,2] and the latest two-loop evolved parton densities obtained from a global fit of data from deep-inelastic lepton scattering and other reactions[3]. The work presented here is an update of an earlier publication[4] to which we refer for the theoretical formalism and summary of its limitations.

The heavy quark inclusive cross section in perturbative QCD is obtained as a convolution of parton densities $f_{i/h}(x,\mu)$ with a hard-scattering cross section $\hat{\sigma}_{ij}(\hat{s}, M_Q, \mu, \alpha_s(\mu))$. The heavy quark mass is M_Q; $\hat{s}$ is the square of the parton-parton center-of-mass energy, $\hat{s} = x_1 x_2 s$; and μ is the renormalization/factorization scale that serves to separate long- and short-distance effects.

$$\sigma(s, M_Q^2) = \int_0^1 dx_1 \int_0^1 dx_2 f_{i/h_1}(x_1,\mu) f_{j/h_2}(x_2,\mu) \hat{\sigma}_{ij}(\hat{s}, M_Q, \mu, \alpha_s(\mu)).$$

For the total cross sections reported here and for the cross sections differential in p_T, we use the scale choice $\mu = \sqrt{M_b^2 + p_T^2}$. We adopt $M_b = 4.75$ GeV. Poor knowledge of the gluon density is a principal source of uncertainty for predictions of bottom quark cross sections at

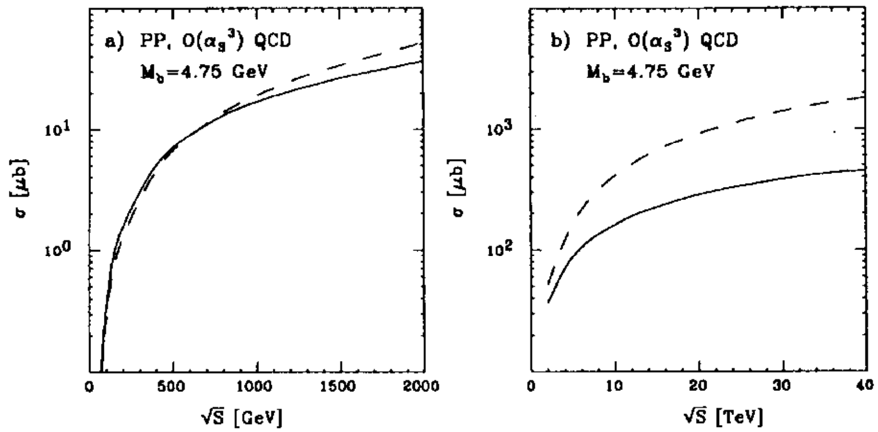

Figure 1. a) The calculated cross section $\sigma(pp \to b\bar{b}X)$ at order α_s^3 in QCD is shown as a function of $\sqrt{s}$ for $100 < \sqrt{s} < 2000$ GeV. The solid line is obtained from the parton densities of MRS D'_o ("regular" gluon), and the dashed curve from the MRS D'_-("singular" gluon). b) As in (a), but for $\sqrt{s} \geq 2$ TeV.

collider energies. In earlier work, we showed that measurements of the bottom quark cross sections by the CERN UA1 and FNAL CDF collaborations provide valuable constraints on the gluon density at intermediate values of Bjorken x[5]. For LHC and SSC energies, the values of x of interest extend over the range 10^{-6} to 10^{-2}, or so. To explore the uncertainties associated with relative ignorance of the gluon density in this range, we adopt for part of our study the "singular" and "regular" gluon density parametrizations of the MRS collaboration. These are denoted, respectively, MRS D'_- and MRS D'_o.

In Fig. 1 we show calculations of the inclusive cross section $\sigma(pp \to b\bar{b}X)$ obtained from an integration of the inclusive yield over all rapidity and transverse momentum. For the energy range $100\ GeV < \sqrt{s} < 2\ TeV$ shown in Fig. 1 (a), the singular and regular parametrizations of the gluon density yield similar results. The differences become increasingly significant as $\sqrt{s}$ increases above $\sqrt{s} = 2\ TeV$, as shown in Fig. 1 (b).

A 20 TeV proton beam incident on a fixed proton target provides a center-of-mass energy $\sqrt{s} = 200\ GeV$. For this SSC fixed-target option, we calculate $\sigma(b\bar{b}X) = 1.27\ \mu b$ for the singular set D'_- and 1.56 μb for the regular set D'_o. Including uncertainties associated with variations of the choice of scale μ and b quark mass M_b, we estimate

$$\sigma(b\bar{b}X, \sqrt{s} = 200\ GeV) = 1.0 \text{ to } 2.0\mu b$$

At $\sqrt{s} = 40\ TeV$, the calculations yield $\sigma(b\bar{b}X) \simeq 0.45\ mb$ for set D'_o and nearly 2 mb for set D'_-. However, at this energy, gluon resummation effects[6] are expected to be very significant, providing enhancement factors[6] of ~ 4 for a regular gluon starting distribution

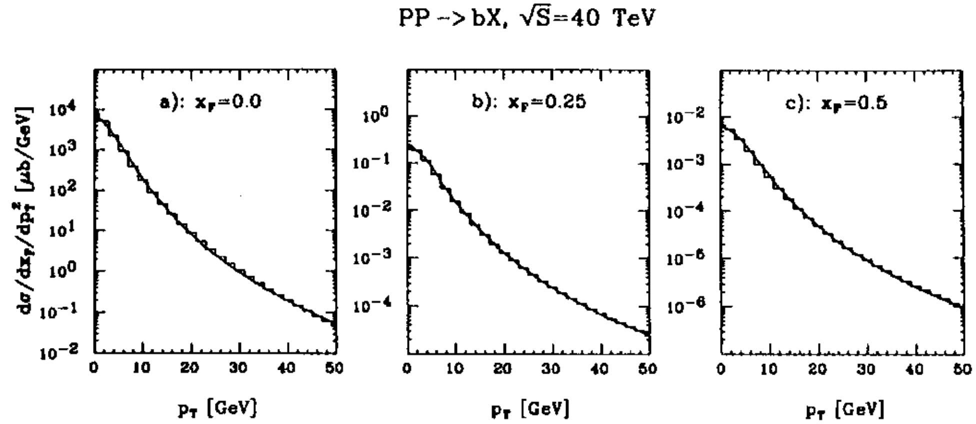

Figure 2. The calculated order α_s^3 QCD differential cross section $d\sigma/dx_F/dp_T^2$ vs. p_T for the SSC collider energy $\sqrt{s} = 40$ TeV is shown (solid curves) for (a)$x_F = 0$; (b)$x_F = 0.25$; (c)$x_F = 0.50$. Phenomenological parametrizations fitted to the theoretical calculations are presented as the histograms.

($xG(x) \to$ constant) and ~ 1.5 for a singular distribution ($xG(x) \sim x^{-\frac{1}{2}}$). Using these factors, we may multiply our $O(\alpha_s^3)$ results at $\sqrt{s} = 40\ TeV$, obtaining $\simeq 1.8mb$ for set D'_- and $\simeq 3mb$ for set D'_o. Including estimates of other uncertainties, we quote

$$\sigma(b\bar{b}X, \sqrt{s} = 40\ TeV) = 1 \text{ to } 3mb$$

Similar reasoning leads to an estimate appropriate at the LHC energy $\sqrt{s} = 15.4\ TeV$:

$$\sigma(b\bar{b}X, \sqrt{s} = 15.4\ TeV) = 0.5 \text{ to } 0.9mb.$$

In Fig. 2, we present the QCD order α_s^3 differential cross section $d\sigma/dx_F dp_T^2$ as a function of p_T for the SSC collider energy, for three values of Feynman x_F. For these results, we use the regular gluon density MRS D'_o. In our earlier paper[4], we showed that the influence of the more singular gluon density is felt most strongly at small p_T ($p_T \leq 25\ GeV$) at $\sqrt{s} = 40\ TeV$. Our theoretical results are shown as the solid curves in Fig. 2. Notable in Fig. 2 is the dramatic decrease in the cross section at $p_T = 0$ by more than four orders of magnitude when x_F is increased from 0. to 0.25. Comparison of Figs. 2 (b) and 2 (c) shows that this large drop is followed by a less remarkable decrease by a factor of 30 or so as x_F is increased from 0.25 to 0.5. At small x_F and small p_T, the cross section is sensitive to the small x behavior of the gluon density. In our previous paper, we provided calculations of rapidity and pseudo-rapidity distributions[4].

The theoretical results shown in Fig. 2 may be fitted with a fairly simple analytic

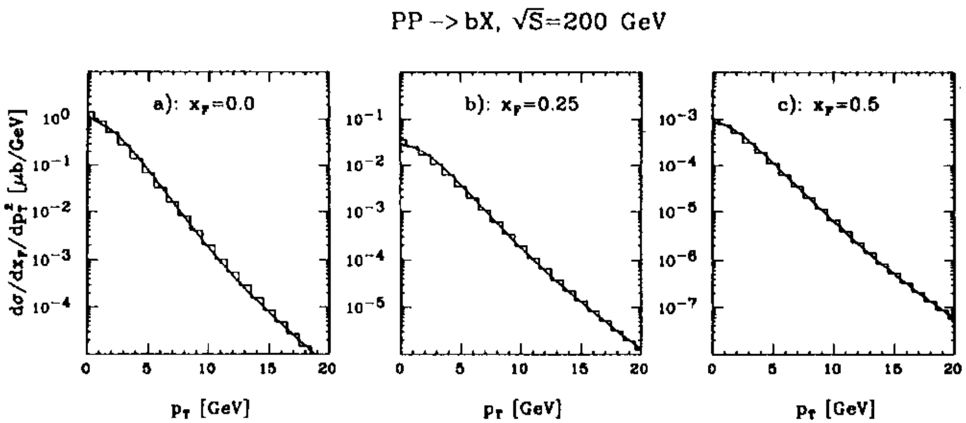

Figure 3. As in Fig. 2 but for the proposed SSC fixed target energy $\sqrt{s} = 200$ GeV.

expression. The form we adopted is

$$\frac{d\sigma}{dp_T^2 dx_F} = \frac{1}{(p_T^2 + m_b^2)^2} \exp(A + B\, p_T)$$

We treat quantities A, B, and m_b as three free parameters whose values vary with $\sqrt{s}$ and x_F. The histograms in Fig. 2 show the results of our fits to the theoretical calculations. Fitted values of the three parameters are provided in Table I.a. The fitted value of our parameter m_b is close to the value we used for the physical bottom quark mass M_b in our calculation, to be anticipated since $< p_T >$ is approximately M_b, but no great significance should be attached to the fact that our fitted m_b varies somewhat with x_F and $\sqrt{s}$. The good agreement of the simple fit with the full theoretical calculation should make the fitted expression useful for estimates of rates, acceptances, and efficiencies.

Table I.a Fitted Parameters for $d\sigma/dp_T^2/dx_F$ for: $0 < p_T < 50$ GeV at SSC Collider Energy.

x_F	m_b (GeV)	A	$B(GeV^{-1})$
0.0	5.00	15.4	-0.0559
0.25	6.16	5.84	-0.0152
0.50	6.60	2.55	-0.0145

Table I.b Fitted Parameters for $d\sigma/dp_T^2/dx_F$ for: $0 < p_T < 20$ GeV at $\sqrt{s} = 200$ GeV.

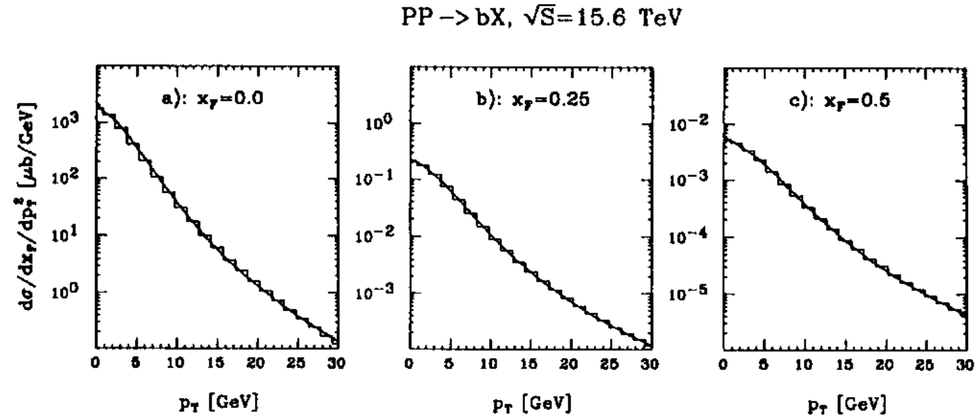

Figure 4. As in Fig. 2 but for the LHC collider energy $\sqrt{s} = 15.4$ TeV.

x_F	m_b (GeV)	A	$B(GeV^{-1})$
0.0	5.53	7.16	-0.363
0.25	6.34	4.06	-0.274
0.50	6.14	0.383	-0.246

Table I.c Fitted Parameters for $d\sigma/dp_T^2/dx_F$ for: $0 < p_T < 30$ GeV at LHC Collider Energy.

x_F	m_b (GeV)	A	$B(GeV^{-1})$
0.0	5.35	14.2	-0.0873
0.25	5.96	5.58	-0.0318
0.50	6.81	2.46	-0.0376

Table I.d Fitted Parameters for $d\sigma/dp_T^2/dx_F$ for: $0 < p_T < 15$ GeV at $\sqrt{s} = 120$ GeV.

x_F	m_b (GeV)	A	$B(GeV^{-1})$
0.0	6.76	6.80	-0.516
0.25	7.95	4.58	-0.440
0.50	7.74	1.02	-0.408

In Fig. 3 and Table I.b, we provide analogous results for the SSC fixed target energy of $\sqrt{s} = 200$ GeV. The x_F dependence is less dramatic at this energy.

In Fig. 4 and Table I.c, we present results for the LHC collider energy of $\sqrt{s} = 15.4$ TeV. The x_F dependence at this energy shows a steep decrease from $x_F = 0$ to 0.25, followed by a more gradual decrease from 0.25 to 0.5, as we saw above at $\sqrt{s} = 40\ TeV$. Fitted values for the LHC cross section at $\sqrt{s} = 120\ GeV$ are provided in Table I.d

We acknowledge valuable communications with Stanley Wojcicki. We are grateful to W. James Stirling for providing a copy of the Martin, Roberts, and Stirling parton densities. This work was supported in part by the U.S. Department of Energy, Division of High Energy Physics, Contract W-31-109-ENG-38.

References

1. P. Nason, S. Dawson, and R. K. Ellis, Nucl. Phys. **B303**, 607 (1988); **B327**, 49 (1989).

2. W. Beenakker, H. Kuijf, W. L. van Neerven, and J. Smith, Phys. Rev. **D40**, 54 (1989); W. eenakker, W. L. van eerven, R. Meng, G. Schuler, and J. Smith, Nucl. Phys. **B351**, 507 (1991).

3. A. D. Martin, R. G. Roberts, and W. J. Stirling, Phys. Lett. **B306**, 145 (1993), Erratum-ibid. **B309**, 492 (1993).

4. E. L. Berger, and R. Meng, *Phys. Rev.* **D46**, 169 (1992).

5. E. L. Berger and R. Meng, *Phys.Lett.* **B304**, 318 (1993); E. L. Berger and R. Meng, in the *Proc. DPF92*, Fermilab, 1992, edited by C. Albright, P. Kasper, R. Raja, and J. Yoh, vol. 2, p. 954; E. L. Berger, R. Meng, and J.-W. Qiu, in the *Proc. XXVI Int. Conf. on High Energy Physics*, Dallas, 1992, edited by J. R. Sanford, vol. 1, p. 853; E. L. Berger, R. Meng, and W.-K. Tung, *Phys. Rev.* **D46**, 1859 (1992).

6. J.C. Collins and R.K. Ellis, *Nucl. Phys.* **B360**, 3 (1991); S. Catani, M. Ciafaloni, and F. Hautmann, *Nucl. Phys.* **B366**, 135 (1991); E.M. Levin *et al.*, *Sov. J. Nucl. Phys.* **54**, 867 (1991).

QUARKONIA PRODUCTION, b-QUARK PRODUCTION AND $b\bar{b}$ CORRELATION STUDIES WITH CDF

VAIA PAPADIMITRIOU
Fermi National Accelerator Laboratory
P.O. Box 500, Batavia, IL 60510

1. INTRODUCTION

The high rate of $B\bar{B}$ production at the Tevatron makes it a unique place for the study of B production and decay. Although e^+e^- colliders provide a cleaner environment than hadron colliders for the study of B decays, CDF has shown that exclusive B channels can be succesfully reconstructed in a harsh environment. Our data have been taken in $p\bar{p}$ collisions at $\sqrt{s}$ = 1.8 TeV with the CDF detector[1] during the 1988-89 and the 1992-93 collider runs. The CDF detector has been upgraded before the start of the 1992-93 run. The upgrades relevant to this presentation are the muon chamber upgrade and the employment of a silicon vertex detector (SVX). The original CDF Central Muon detector, which covers the pseudorapidity region $|\eta| < 0.6$, has been complemented by the addition of four layers of drift tubes behind 2 feet of steel. As a result, hadronic punch-through backgrounds to the muon signal have been reduced by a factor of $\sim$ 10. We have also added layers of drift tubes in the pseudorapidity region of $0.6 < |\eta| < 1.0$ in order to increase our muon coverage. Finally four layers of DC coupled, single sided, silicon detectors with R-ϕ readout have been added around the beam-pipe and provide a very good resolution in the transverse position of primary and secondary vertices. The primary vertex resolution in a typical event is 35 μm, similar to the transverse beam size. The impact parameter resolution is better than 40(15) μm for tracks with $P_T > 1$ (10) GeV/c. We have collected $\sim$21 pb^{-1} of data with this upgraded detector during the 1992-93 run.

2. QUARKONIA PRODUCTION STUDIES

2.1 1988-89 data

In the 1988-89 collider run we studied the reactions $p\bar{p} \rightarrow J/\psi(\psi(2S))X \rightarrow \mu^+\mu^- X$ by using 2.6 ± 0.2 pb^{-1} of data. This allowed us to shed some light on the quarkonia production mechanisms at the Tevatron energy. The production mechanisms of the J/ψ's($\psi(2S)$'s) are B decays, direct charmonium production and the recently suggested[2] gluon fragmentation. We obtained the J/ψ and $\psi(2S)$ differential cross sections which are displayed in Fig. 1 as functions of P_T. The number of J/ψ and $\psi(2S)$ events used in the measurement of the cross section was 889 $\pm$ 30 and 35 $\pm$ 8 respectively. Theoretical predictions for the two types of

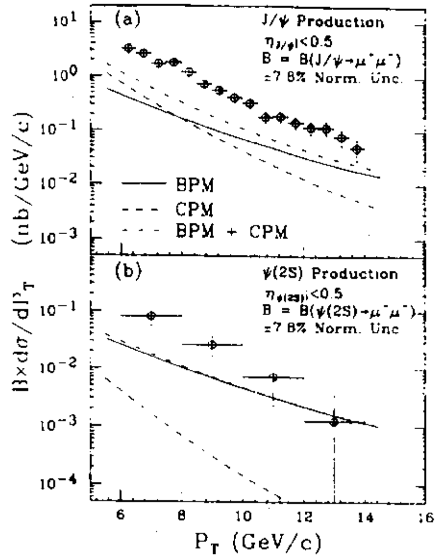

Figure 1: The product $B \times \left(\frac{d\sigma}{dP_T}\right)$ vs. P_T for (a) $J/\psi \to \mu^+\mu^-$ and (b) $\psi(2S) \to \mu^+\mu^-$. The circles correspond to the data. The solid curve corresponds to $J/\psi(\psi(2S))$'s produced from B meson decays. The dashed curve corresponds to $J/\psi(\psi(2S))$'s from direct charmonium production. The dot-dashed curve is their sum.

processes expected to dominate J/ψ and $\psi(2S)$ production are also plotted. The solid curve in Fig. 1a (1b) is a next-to-leading-order (NLO) calculation of the production of b-quarks by Nason, Dawson, & Ellis (NDE)[3] leading to B-mesons and subsequent decay to J/ψ ($\psi(2S)$) as discussed in Ref. 4. We refer to this overall calculation as B-production model (BPM). The dashed curve in Fig. 1a (1b) corresponds to J/ψ's ($\psi(2S)$'s) from direct charmonium production[5], that is, either from the decay of a higher charmonium state or from direct production through gluon fusion. We refer to this overall calculation as the charmonium production model (CPM). The sum of these two contributions (BPM and CPM) is also plotted in Fig. 1. In Fig. 1a we fit the theory to the data by summing the two theoretical contributions with independent normalization factors. With no normalization constraints a good fit is obtained with ~69% J/ψ production from CPM and ~31% J/ψ production from BPM. Using additional information which is described in Ref. 4 we found that the 90% C.L. upper limit on the BPM contribution is ~60%; we concluded as well that if future measurements exceed this value, then either at least one of the two models considered above is wrong or there are additional production mechanisms with a significant contribution.

We have also reconstructed χ_c mesons through the decay chain $\chi_c \to J/\psi\gamma$, $J/\psi \to \mu^+\mu^-$. In the 1988-89 collider run we reconstructed 67 ± 8 χ_c's and we calculated the cross section for the process $p\bar{p} \to \chi_c X$ to be $\sigma(\chi_c \to J/\psi\gamma) = 3.2 \pm 0.4(stat)\ {}^{+1.2}_{-1.1}\ (syst)$ nb[6]. We found that the fraction, f_χ, of J/ψ's coming from χ_c decays is $f_\chi = (44.9 \pm 5.5\ {}^{+15.4}_{-14.1})\%$,

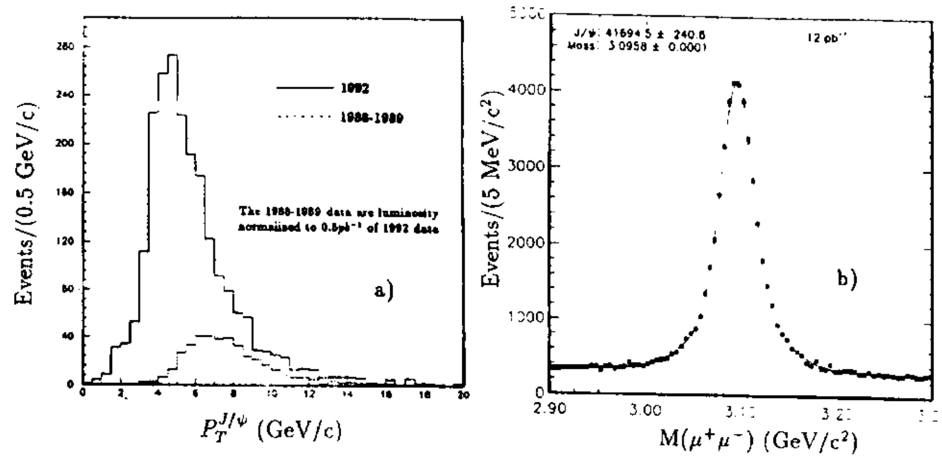

Figure 2: a) J/ψ P_T spectrum in the dimuon channel. b) J/ψ mass spectrum in the dimuon channel from $12pb^{-1}$ of the 1992-93 data.

but we did not have enough statistics to measure this fraction as a function of P_T. Assuming that the only processes for J/ψ production are B decays and χ_c decays, the fraction f_b turns out to be $(63 \pm 17)\%$. This value of f_b was used to derive the b-quark production cross section from the inclusive J/ψ sample (see Fig. 7).

2.2 *1992-93 data*

Due to improvements in the trigger, in the 1992-93 run we have approximately a factor of 5 more J/ψ's per pb^{-1} than in the previous run (see Fig. 2a)). In Fig. 2b) we show the J/ψ mass spectrum from a 12 pb^{-1} sample which represents ~ 60% of the 1992-93 data. In Fig. 3 we compare the differential J/ψ cross section from the 1988-89 data to the one from 7.5 pb^{-1} of 1992-93 data. In the 1992-93 run we have extended the measurement to both lower and higher P_T values. The agreement with the 1988-89 data is pretty good. In the 1992-93 data, by using the SVX we can measure the fraction of J/ψ's coming from B's directly and without any assumptions. From the measurement[7] of the B lifetime with inlusive J/ψ's we have indications that the fraction of J/ψ's coming from B's is lower than the one we assumed in the previous run. The fraction derived from the lifetime fit is 15%. Although this is the right b fraction in the lifetime sample, it should not be automatically interpreted as the fraction of J/ψ's from b's to be used for the b cross section measurement. The reason is that the applied track quality cuts favor isolated muons and systematically decrease the fraction. This fraction should not be directly compared with the one we derived from the 1988-89 data either, because the fraction is a P_T dependent quantity and the P_T regions for the inclusive J/ψ sample were different in the 1988-89 and 1992-93 collider runs. The measurement of an unbiased fraction f_b from the 1992-93 run is work in progress.

A $\psi(2S)$ mass distribution reconstructed through the decay chain $\psi(2S) \to J/\psi\pi^+\pi^-$ is shown in Fig. 4 from ~ 11 pb^{-1} of 1992-93 data. All the tracks in the event have been

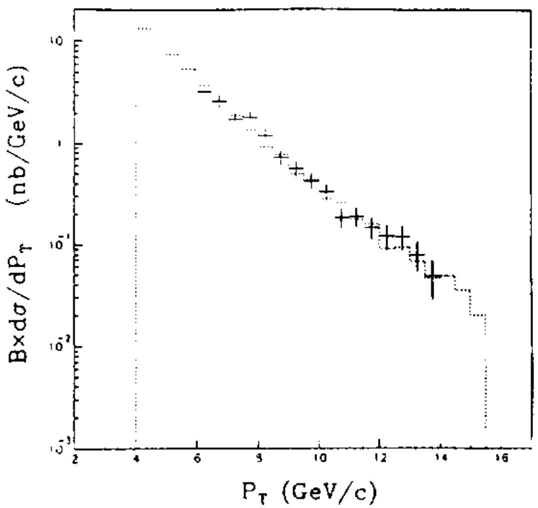

Figure 3: Comparison of the differential J/ψ cross section between the 1988-89 (points with error bars) and the 1992-93 (histogram) data for the region $|\eta_{J/\psi}| < 0.5$.

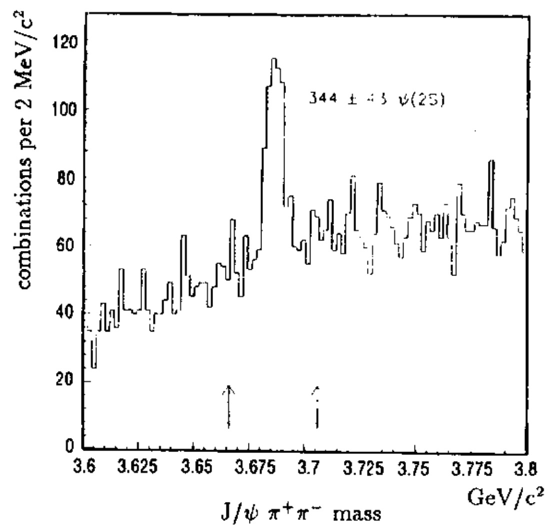

Figure 4: $\psi(2S)$ mass spectrum in the dimuon channel from $\sim 11\ pb^{-1}$ of the 1992-93 data.

reconstructed by using the SVX. The use of the SVX in the calculation of the $\psi(2S)$ decay length indicates that the $\psi(2S)$ state has a non negligible prompt component.

With the new data set we are also reconstructing a respectable sample of χ_c decays (see Fig. 5). This sample will be used to measure the fraction f_χ and to cross check the fraction f_b measured with the SVX. Since we can now measure the J/ψ differential cross section from b's and from χ_c's, it will be much easier to disentangle the different J/ψ production mechanisms. By measuring with the SVX the fraction of prompt χ_c's we can also measure the ratio of the inclusive rates of $B \to \chi_c X$ and $B \to J/\psi X$.

Finally in Fig. 6 we show the Υ mass distribution from $\sim 12\ pb^{-1}$ of the 1992-93 data. Since Υ's are not produced from B meson decays but they are produced either directly or from χ_b's, we can use the measurement of $\left(\frac{d\sigma}{dP_T}\right)$ versus P_T in order to check if the direct production spectrum predicted by QCD is correct. Since the $\Upsilon(3S)$ state is produced only directly, it will be especially useful for this comparison. The Υ sample offers also the possibility to check the differential production cross section at P_t values as low as $0.5 - 1.0\ GeV/c$.

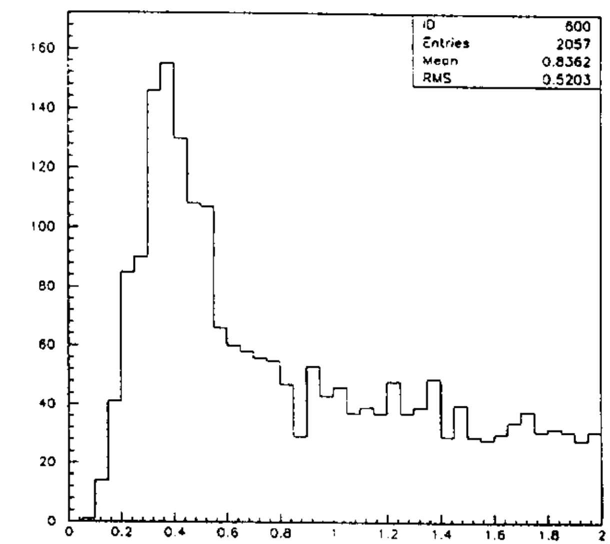

Figure 5: The mass difference ΔM for the χ_c mass region from $\sim 12\ pb^{-1}$ of the 1992-93 data.

3. b-QUARK PRODUCTION STUDIES

3.1 1988-89 data

In Fig. 7 we show the b-quark production cross sections that we derived by studying various b decay channels in the 1988-89 data. The curves in the same figure represent the theoretical predictions based on the NDE calculation. The uncertainty in the predictions arising from choices of the renormalization scale μ, the b-quark mass and the QCD Λ parameter are also shown. The dashed lines correspond to the central value and the upper and

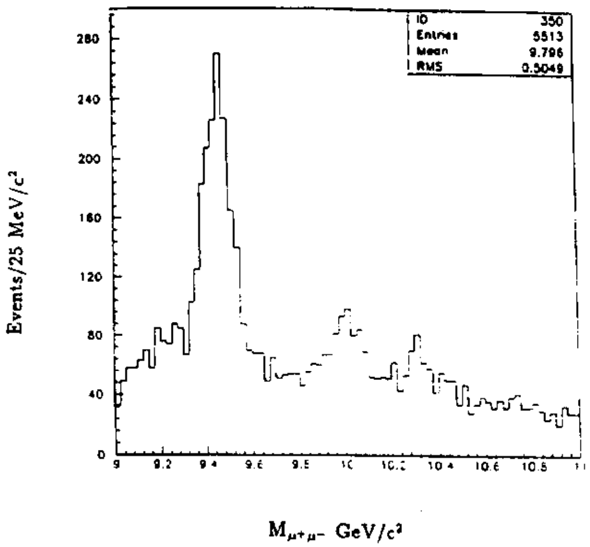

Figure 6: The dimuon mass distribution for the Υ mass region in the 1992-93 data.

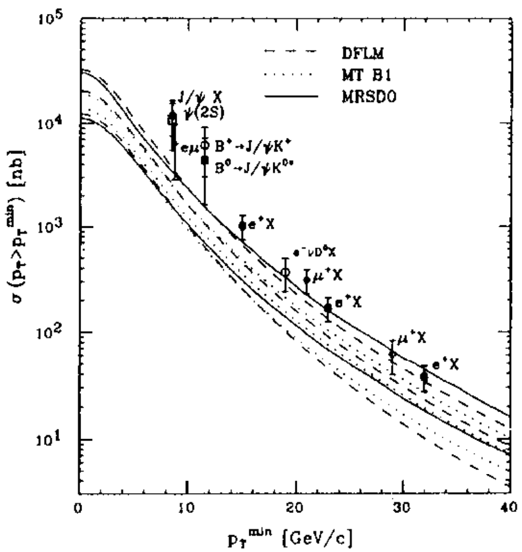

Figure 7: Integrated b P_T distribution at 1.8 TeV: 1988-89 CDF data versus NLO QCD.

lower allowed predictions by using the DFLM structure functions[3]. The dotted lines correspond to similar predictions by using the MT structure functions[8]. Finally the solid lines represent the central value and the upper allowed prediction by using the MRSD0 structure functions[9].

The b-quark production cross section from the inclusive $J/\psi(\psi(2S)) \to \mu^+\mu^-$ channels was based on the measurement of the integrated $J/\psi(\psi(2S))$ cross section for $P_T > 6\ GeV/c$ (see section 2.1) and on the fraction f_b of $J/\psi(\psi(2S))$'s coming from b's. For the J/ψ's we used the fraction discussed in section 2.1. For the $\psi(2S)$'s we assumed that they all originate from B decays[10]. The b cross section measurement based on the $\psi(2S)$ sample will have a considerably improved statistical error in the 1992-93 data.

The b-quark cross section from the $e\mu$ sample shown in Fig. 7, is a single-b inclusive cross section based on the observation of a correlated lepton pair that originates from the $b\bar{b}$ produced in the event. This measurement has been based on $\sim$ 1000 lepton pairs. It is interesting that although this cross section is measured at a similar P_T^b as the cross section from inclusive J/ψ's and $\psi(2S)$'s, it has a lower central value. This is an indication that there might be something wrong with the assumptions we made to derive f_b from the inclusive J/ψ and $\psi(2S)$ channels.

The B meson production cross sections from the exclusive decay channels $B^\pm \to J/\psi K^\pm$ and $B^0 \to J/\psi K^{0*}$ were based on 14.1±4.3 and 9.6±4.6 events respectively from the 1988-89 data and therefore they were statistically limited. The corresponding b-quark cross sections were $\sigma^b(P_T > 11.5\ GeV/c,\ |y^b| < 1) = 6.1\pm3.1\ \mu b$ and $\sigma^b(P_T > 11.5\ GeV/c, |y^b| < 1) = 4.4\pm2.8\ \mu b$

From the inclusive electron production rate and the associated electron-D^0 production rate we derived the b-quark cross section for four different ranges of P_T^b; from the inclusive muon production rate in the same data we derived the b-quark cross section for two different ranges of P_T^b. The major systematic uncertainty in these inclusive lepton measurements was the level of the knowledge of the background. This is greatly improved in the 1992-93 run due to the upgrades of the detector.

From the comparison of the data with the theoretical predictions we observe that the experimental b cross section is larger than the theoretical one at the Tevatron energy (see Fig. 7). There is a clear excess in the observed rate at small P_T^b. At larger values of P_T^b, the data are consistent with the upper extreme of the theoretical band. The measurements of b-quark production cross sections from the UA1 experiment in $p\bar{p}$ collisions at $\sqrt{s} = 630\ GeV$ agree much better with the theoretical predictions than the CDF measurements at $\sqrt{s} = 1.8\ TeV$ do[9]. There have been several attempts to explain the difference, such as consideration of higher order corrections to the next-to-leading order theoretical calculation, higher order small-x corrections to the partonic cross sections and modification of the gluon densities[11].

We know that several of the 1988-89 CDF b-quark cross section measurements were statistically limited or were derived under certain assumptions; we expect that the analysis of the data set we collected during the 1992-93 run will shed light onto the problem.

3.2 1992-93 data

Since we know that the measured fraction f_b for both J/ψ's and $\psi(2S)$'s is smaller than the one we assumed in the 1988-89 analyses (see section 2.2), we expect that the b cross sections based on the inclusive quarkonia samples will become more consistent with the theory.

From $(14.3 \pm 1.0)\ pb^{-1}$ of the 1992-93 data we also reconstructed $104 \pm 21\ J/\psi K^\pm$

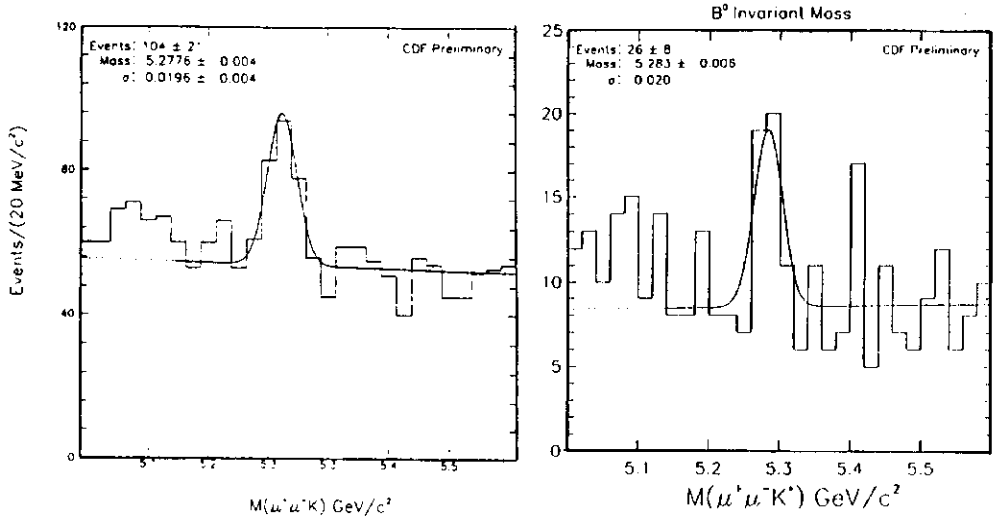

Figure 8: Reconstructed B mass from the decays $B^{\pm} \to J/\psi K^{\pm}$ and $B^0 \to J/\psi K^{0*}$ from 14 pb^{-1} of the 1992-93 data.

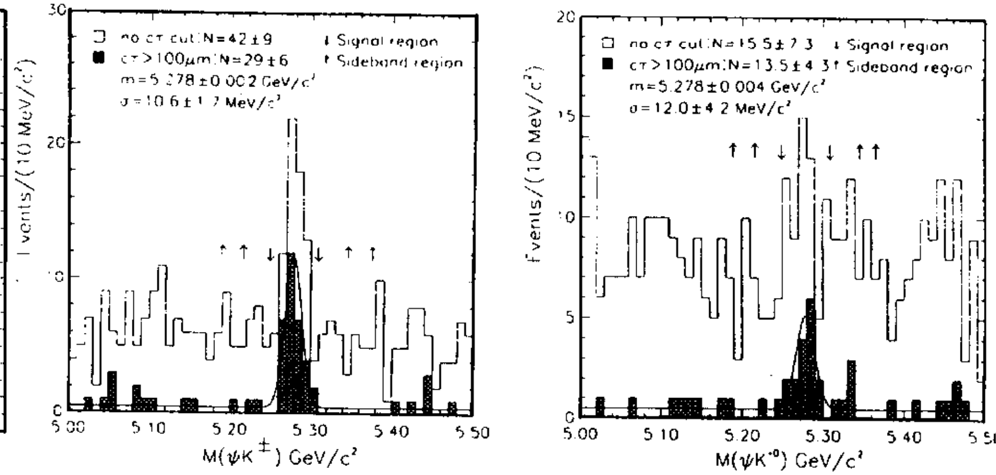

Figure 9: Reconstructed B mass from the decays $B^{\pm} \to J/\psi K^{\pm}$ and $B^0 \to J/\psi K^{0*}$ using the SVX (9 pb^{-1} of the 1992-93 data).

and 26 ± 8 $J/\psi K^{0*}$ events for $P_T^B > 6.0\ GeV/c$ and $P_T^B > 9.0\ GeV/c$ respectively (see Fig. 8). The reconstruction of these exclusive channels has not used any decay length or SVX related cuts yet, and therefore the signal to noise ratio is not optimal. Such additional cuts reduce drastically the background as can be seen in Fig. 9. Since there are sufficient statistics in the $B^{\pm} \to J/\psi K^{\pm}$ decay channel it has been used to determine the differential B meson cross section which is shown in Fig. 10. The measurement suggests that the shape of the theoretical cross section differs from the experimental result since there is an excess in the observed rate at low P_T^B (see Ref. 12). We derived the b-quark cross sections to be $\sigma^b(P_T^b > 7.5\ GeV/c, |y^b| < 1) = 9.43 \pm 3.69\ \mu b$, $\sigma^b(P_T^b > 10.5\ GeV/c, |y^b| < 1) = 2.85 \pm 1.12\ \mu b$, $\sigma^b(P_T^b > 13.5\ GeV/c, |y^b| < 1) = 1.22 \pm 0.51\ \mu b$ from $B^{\pm} \to J/\psi K^{\pm}$ decays and $\sigma^b(P_T^b > 10.5\ GeV/c, |y^b| < 1) = 2.61 \pm 1.29\ \mu b$ from $B^{\pm} \to J/\psi K^{0*}$ decays. The error is statistical and systematic combined in quadrature. These new b-quark cross section measurements (see Fig. 11), although statistically consistent with the corresponding ones of the 1988-89 data, they are closer to the theoretical predictions.

Finally we have derived the b-quark cross section for two different ranges of P_T^b from the associated muon-D^0 production rate. These two measurements are based on 8.8 and 4.4 pb^{-1} of 1992-93 data respectively, and they will certainly improve when we use the full data set.

4. $b\bar{b}$ CORRELATION STUDIES

As already mentioned in section 3.1, the NLO QCD prediction is in good agreement with the data at $\sqrt{s} = 630$ GeV but is systematically low when compared to the CDF measurements at $\sqrt{s} = 1.8$ TeV. The process $p\bar{p} \to b\bar{b}X$ provides further opportunities for comparison between experiment and NLO QCD.

In order to obtain a high enough rate for our studies we chose to tag the $b\bar{b}$ pair by

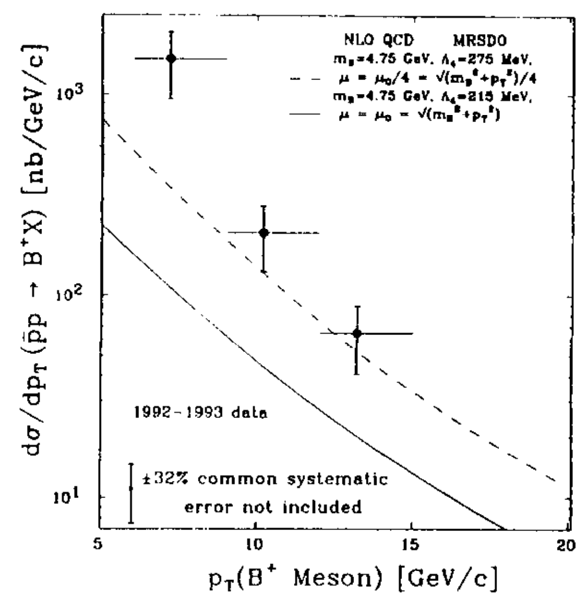

Figure 10: B meson differential cross section.

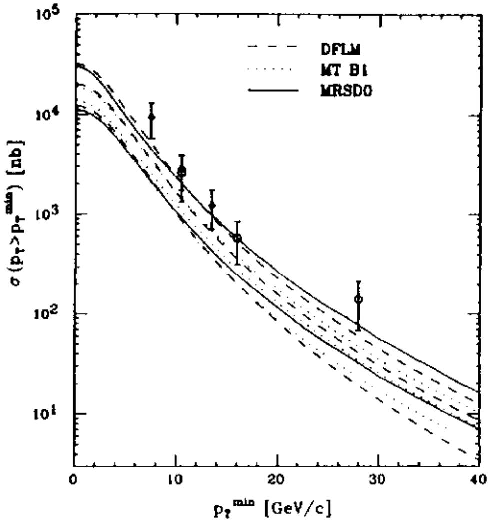

Figure 11: Integrated b P_T distribution at 1.8 TeV: 1992-93 CDF data versus NLO QCD. The diamonds correspond to the decay $B^{\pm}\rightarrow J/\psi K^{\pm}$, the square to $B^0\rightarrow J/\psi K^{0*}$ and the circles to $B\rightarrow\mu D^0\nu X$.

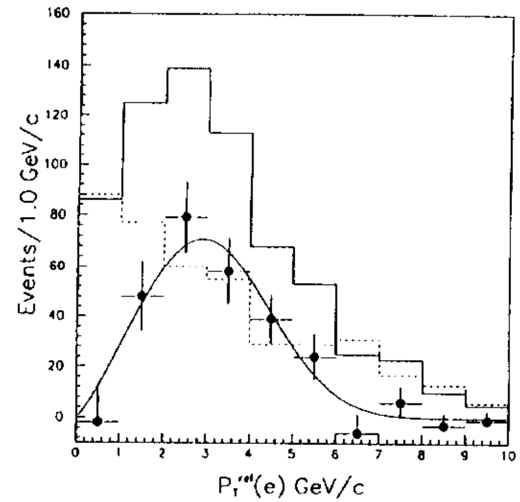

Figure 12: P_T^{rel} for electrons from the data. OS (SS) events are shown in solid (dashed) lines. The difference of the OS and SS distributions is shown with points. The curve is a fit of the sum of the normalized b and c distributions to the subtracted data.

the semileptonic decay of the b and $\bar{b}$ quarks. More specifically, we chose to look for events in which one b decayed to an electron and the other to a muon, thus avoiding potential backgrounds such as Drell Yan and leptonic decays of the J/ψ, $\psi(2S)$, Υ and Z. We made this study using (2.65 ± 0.17) pb^{-1} of the 1988-89 collider run data. The data were collected with the dilepton trigger which requires an electron in the Central Electromagnetic calorimeter with minimum E_T of 5 GeV and a muon in the Central muon chambers with a minimum P_T of 3 GeV/c. Events with electron-muon pairs in the final state come from $b\bar{b}$ production, $c\bar{c}$ production, a cascade decay of a single bottom quark and "fakes", that is events with misidentified particles. To determine the number of $e\mu$ events due to $b\bar{b}$ production, we separated the data into events with leptons of same sign (SS) or opposite sign (OS). The $b\bar{b}$ production, although it produces mainly opposite sign pairs, it contributes to the SS sample as well due to $B^0\bar{B}^0$ mixing. The $c\bar{c}$ production contributes only to the OS sample since the mixing is negligible. We get rid of lepton pairs from the decay of a single B by requiring that $m_{e\mu} > 5$ GeV/c^2. Fakes contribute equally to the SS and OS samples and they are removed by subtracting the SS $e\mu$ pairs from the OS. The fraction, $f_{b\bar{b}}$, of the sign subtracted events due to $b\bar{b}$ production is determined by examining the distribution of the component of the lepton momentum transverse to the direction of the associated jet, P_T^{rel}. The P_T^{rel} distribution for leptons from b decays is stiffer than the corresponding one from c decays. We obtain $f_{b\bar{b}}$ by fitting the difference of the P_T^{rel} distribution for the SS and OS samples (see Fig. 12) to the sum of the normalized b and c distributions. It turns out that $f_{b\bar{b}} = 1.0\,^{+0.0}_{-0.1}$. The electron and muon acceptances are calculated using the full NLO calculation of $b\bar{b}$ production by Mangano, Nason and Ridolfi (MNR)[13]. In Fig. 13 we show our measured cross section for the process $p\bar{p}\rightarrow b\bar{b}X$ versus the P_T^{min} of the second b given the P_T^{min} of the first b (see Ref. 14). The inner error bars correspond to the statistical uncertainty and the outer error bars represent the combined statistical and systematic uncertainty. In the same plot we also show the MNR theoretical prediction using the DFLM structure functions. The upper and lower uncertainty bands correspond to variations in the mass of the b-quark, in Λ_4 and in the normalization scale μ. In Fig. 14 we show the sign-subtracted distribution of the angle between the electron and the muon in the transverse plane for events passing all the analysis cuts, and we compare it with the MNR prediction.

The data is seen to be consistent with the shape of the $b\bar{b}X$ cross section as predicted by NLO QCD. The absolute normalization though is found to be lower than the data by a factor of 4. The shape of the $\Delta\phi_{e\mu}$ distribution from $b\bar{b}$ production is seen to be in good agreement with the theory.

1. SUMMARY

During the 1988-89 collider run CDF has shown that one can study quarkonia physics and b physics even in a harsh $p\bar{p}$ collider environment. The 21 pb^{-1} we collected with the upgraded CDF detector during the 1992-93 run are leading us to a rich program which focuses on the production and decay of quarkonia and b-quarks, and which will answer many of the questions posed during the 1988-89 collider run.

7. REFERENCES

1. F. Abe et al., *Nucl. Inst. Meth.* **A271**, (1988) 387; F. Bedeschi et al., *Nucl. Inst. Meth.* **A268**, (1988) 50; G. Ascoli et al., *Nucl. Inst. Meth.* **A268**, (1988) 33.
2. E. Braaten and T. C. Yuan, *Phys. Rev. Lett.* **71**, (1993) 1673.

3. P. Nason, S. Dawson, and R.K. Ellis, *Nucl. Phys.* **B303**, (1988) 607, *Nucl. Phys.* **B327**, (1989) 49, *Nucl. Phys.* **B335**, (1990) 260.
4. F. Abe et al., *Phys. Rev. Lett.* **69**, (1992) 3704.
5. E.W.N.Glover, A.D.Martin, W.J.Stirling, *Z. Phys.* **C38**, (1988) 473.
6. F. Abe et al., FERMILAB-PUB-93/106-E (May 1993), submitted to *Phys. Rev. Lett.*.
7. F. Abe et al., FERMILAB-PUB-93/158-E (June 1993), submitted to *Phys. Rev. Lett.*; M. Shaw, these Proceedings.
8. E. L. Berger, R. Meng and W. K. Tung, Phys. Rev. **D46**, 1895 (1992).
9. M. L. Mangano, *Z. Phys.* **C58**, 651 (1993).
10. S. D. Ellis, M. B. Einhorn, C. Quigg, *Phys. Rev. Lett.* **36**, 1263 (197); C. E. Carlson, R. Suaya, *Phys. Rev.* **D15**, 1416 (1977).
11. E. L. Berger, R. Meng and W. K. Tung, *Phys. Rev.* **D46**, 1895 (1992); J. C. Collins and R. K. Ellis, *Nucl. Phys.* **B360**, 3 (1991); S. Catani, M. Ciafaloni and H. Hautmann, *Nucl. Phys.* **B366**, 135 (1991); E. M. Levin, M. G. Ryskin and Yu. M. Shabelsky, *Phys. Lett.* **B260**, 429 (1991); E. L. Berger, R. Meng and J. Qui, ANL-HEP-CP-92-79.
12. F. Abe et al., FERMILAB-CONF-93/200-E, submitted to *International Symposium on Lepton and Photon Interactions*, Cornell, August 10-15, 1993.
13. M. Mangano, P. Nason and G. Ridolfi, *Nucl. Phys.* **C373**, (1992) 295-345.
14. F. Abe et al., FERMILAB-CONF-93/199-E, submitted to *International Symposium on Lepton and Photon Interactions*, Cornell, August 10-15, 1993.

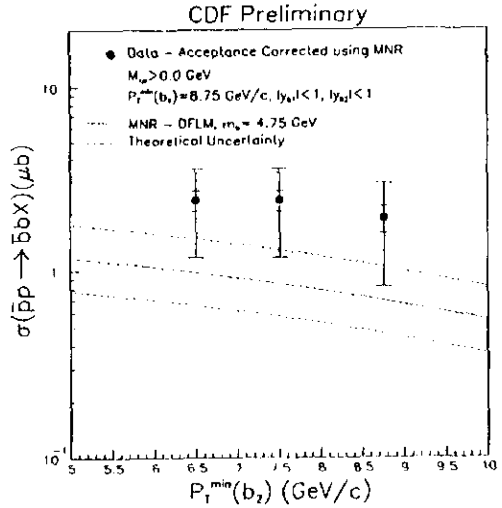

Figure 13: The cross section for $p\bar{p}\rightarrow b\bar{b}X$. The theoretical prediction and associated uncertainty are represented by the solid and dashed lines respectively.

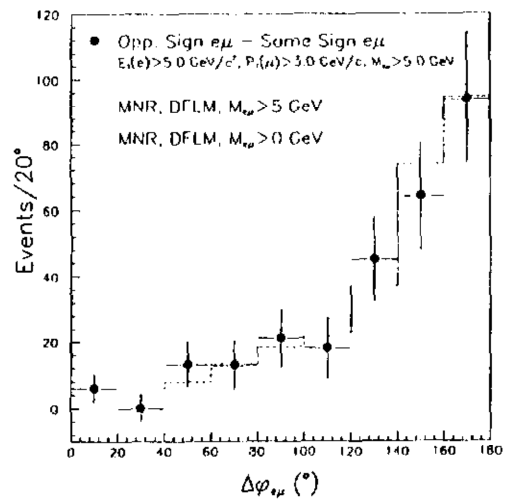

Figure 14: The opening angle between the electron and the muon in the transverse plane.

B PRODUCTION AT DØ

Brajesh C. Choudhary
Department of Physics, University of California
Riverside, CA, 92521, USA

For the DØ Collaboration

ABSTRACT

Preliminary results on B production using single and dimuon events produced in $p\bar{p}$ collisions at $\sqrt{s} = 1.8$ TeV, are presented from the DØ experiment at FNAL. Results from inclusive muon and J/ψ studies are compared to the theory.

1. INTRODUCTION

The B-production cross section has been calculated in next-to-leading order [1]. Although the DØ experiment is optimized to do high p_T physics, the large $b\bar{b}$ cross section of ≈ 50 μb at $\sqrt{s} = 1.8$ TeV can be used to study the b production mechanisms. The inclusive single muon and J/ψ cross sections as a function of muon transverse momentum p_T^μ and pseudorapidity η can be used to infer the $b\bar{b}$ cross section which can then be directly compared to QCD calculations. The shape of the rapidity distribution can be used to constrain the gluon distribution function.

2. DØ DETECTOR

The DØ detector [2] is a large general purpose detector with no central magnetic field. It is optimized for the detection and measurement of muons, electrons, jets and missing transverse energy. The detector consists of tracking chambers, a transition radiation detector, a highly segmented liquid-argon uranium calorimeter with good energy resolution and an extensive array of muon detectors with thick magnetized iron absorber to provide sufficient momentum measurement and minimize backgrounds from hadron punchthrough.

The muon system consists of five separate solid-iron toroids with different sets of proportional drift tubes (PDT's) to measure track coordinates down to $|\eta|$ of ≈ 3.3. The muon momentum is measured by its bend in the 1.8 Tesla field of the toroid. Multiple Coulomb scattering limits the muon momentum resolution to $\geq 20\%$. The spatial resolution of 700 μm is currently limited by the accuracy of the geometric alignment. Test beam data indicates that the intrinsic diffusion limit is ≈ 200 μm. The central tracking chamber is used to identify muons coming from the vertex. The calorimeter coverage extends down to $|\eta|$ of ≈ 4.4 and is used to measure jets associated with the muon. The total interaction length (λ) for the calorimeter plus the toroid varies from 13-18 λ and reduces the hadron

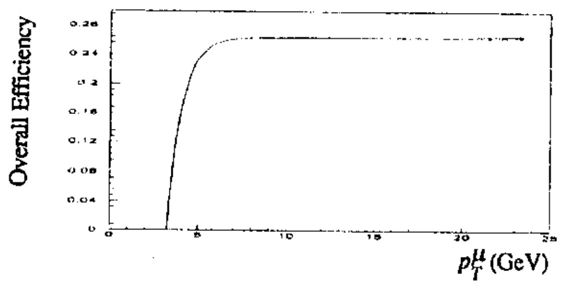

Figure 1: Overall efficiency for muons with $|\eta| < 1$.

punchthrough to negligible level in the final data sample.

3. INCLUSIVE MUON CROSS SECTION

3.1. Event Selection

The DØ event selection consists of 3 levels of trigger [2] which reduces $\approx$ 43 mb [3] of inelastic cross section to 2 Hz of data written to magnetic tape. The Level 0 trigger selects inelastic collisions from beam-beam scintillator coincidences and measures the vertex position. Depending on the detector geometry, Level 1 hardware muon trigger requires 2 hits in either 2 or 3 layers of the muon system from the hit information stored in the muon latch bit in a coarse road of 60 cm width. The efficiency of the Level 1 muon trigger for a high p_T^μ is $\approx$ 60%, where the losses are mostly geometric. The Level 2 software muon trigger requires a "good" muon with $p_T^\mu > 3$ GeV.

3.2. Data Analysis

Special muon runs were taken at low luminosity for the inclusive muon cross section measurement. These runs used single muon triggers for $|\eta| < 1$, $1 < |\eta| < 1.7$ and $2.2 < |\eta| < 3.3$, with integrated luminosities of $100nb^{-1}$, $10nb^{-1}$, and $6nb^{-1}$ respectively. Almost 70% of the data for the regions $|\eta| < 1$ and $1 < |\eta| < 1.7$ has been analyzed and is presented here.

For the offline analysis the muon was required to have $p_T^\mu > 5$ GeV. Quality cuts require that: the muon has hits in all the three layers of the muon system; the muon track matches with a central detector track; the candidate has at least 1 GeV energy deposition in the calorimeter; the muon has good impact parameter vertex projection in both bend and non-bend views; the muon track passes cosmic rejection cuts and is synchronized within $100ns$ of the beam crossing time.

For single muon analysis the overall efficiency was evaluated using ISAJET $b\bar{b} \rightarrow \mu X$ Monte Carlo events. These events were put through a complete GEANT detector simulation, Level 1 and Level 2 trigger simulators, full reconstruction, and offline cuts. As shown in Figure 1, the overall efficiency is 26% for $p_T^\mu > 5$ GeV and $|\eta| < 1$. For muons in $1 < |\eta| < 1.7$, it is 18%.

3.3. Results and Discussion

The inclusive muon cross section for $|\eta| < 1$ and $1 < |\eta| < 1.7$ is shown in Figures 2(a) and 2(b) respectively. The point to point systematic error on the cross section measurement are shown as error bars. The main sources of systematic error are error on the luminosity measurement (12%) and the cosmic ray plus albedo backgrounds of $\approx$ 10% for $|\eta| < 1$ and $\approx$ 20% for $1 < |\eta| < 1.7$. There is an additional overall uncertainty of 30% due to, as yet poorly understood detector efficiencies. The data has been compared to (NLO) ISAJET Monte Carlo predictions. Figures 2(a) and 2(b) show separately the predicted contribution to the cross section from b$\rightarrow \mu X$, c$\rightarrow \mu X$, and π or K decays, as well as their summed contribution.

The shape of the p_T^μ spectrum is in good agreement with expectation. Although no jet was required either in the trigger or the analysis, it was found that nearly 70% of the events have jets associated with them, suggesting that most of the events are indeed from b decays as expected. Work is in progress to decrease the systematic errors and to extract the $b\bar{b}$ cross section.

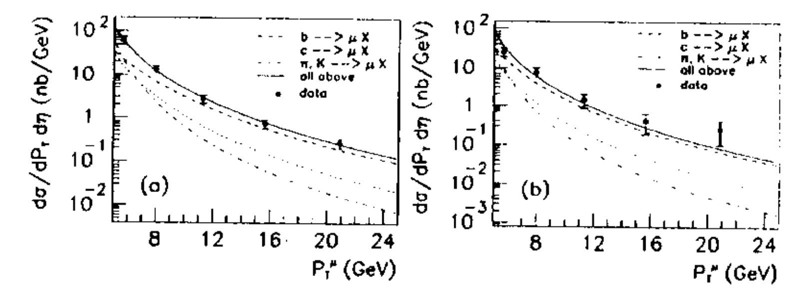

Figure 2: Inclusive muon cross sections for: (a) $|\eta| < 1$; (b) $1 < |\eta| < 1.7$.

4. INCLUSIVE J/ψ CROSS SECTION

4.1. Event Selection

For the J/ψ study it was required that the event have two muons at both Level 1 and Level 2 trigger with $p_T^\mu > 3$ GeV at Level 2.

4.2. Data Analysis

In the offline analysis two good quality muons were required in the fiducial volume $|\eta| < 0.8$ with a dimuon transverse momentum $p_T^{\mu\mu} > 8$ GeV. In addition both muons were required to be consistent with reconstructed vertex position and to have a calorimeter energy deposition consistent with a minimum ionizing particle and not back to back in η and ϕ ($\Delta\theta <$ 170° and $\Delta\phi <$ 160°).

4.3. Results and Discussion

Figures 3(a) and 3(b) respectively show the dimuon mass spectrum for non-isolated and isolated muons for unlike and like sign muon pairs for an integrated luminosity of 7 pb^{-1}. Isolation is defined to be a muon pair with no jet (with jet cone size $\Delta R = \sqrt{\Delta\eta^2 + \Delta\phi^2} = 0.7$ and $E_T^{jet} >$ 8 GeV) within ΔR =0.7 of the either of the muons. If one or both of the muons are within a jet, it is defined to be a non-isolated muon pair. Unlike sign muons clearly show a J/ψ peak for both the samples. The Upsilon (Υ) peak is also evident in the unlike sign isolated dimuon pairs but not in the non-isolated pairs. The like sign muon spectrum displays no resonant structure.

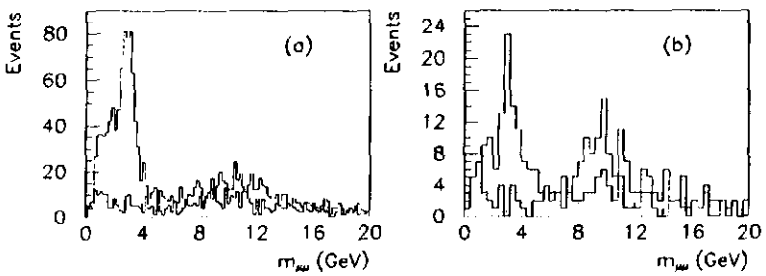

Figure 3: Unlike-sign (unshaded) and like sign (shaded) invariant mass for: (*a*) non-isolated and (*b*) isolated dimuons.

The J/ψ mass distribution for both isolated and non-isolated muons was fitted with a Gaussian signal plus a polynomial background to match the tail of distribution well beyond the J/ψ peak region. The estimated number of J/ψ events is 138$\pm$15 from 3.5 $pb^{-1}$of data. The acceptance times efficiency for J/ψ was evaluated using ISAJET Monte Carlo events, passed through a complete Geant detector simulation, Level 1 and Level 2 trigger simulators, full reconstruction and offline cuts. The overall efficiency as a function of p_T of the J/ψ is shown in Figure 4(a). The bands show the present systematic uncertainty in the efficiency measurement. Figure 4(b) shows the inclusive J/ψ cross section. The experimental results are compared to (NLO) ISAJET Monte Carlo predictions for J/ψ production from direct charmonium production (CPM), bbar production (BPM) and the sum of two processes [1,4]. The data points are shown with statistical errors only and lie significantly above the ISAJET predictions. Further study of the data is in progress and the present overall normalization uncertainty is $\approx$ 100% (See Fig 4(a)).

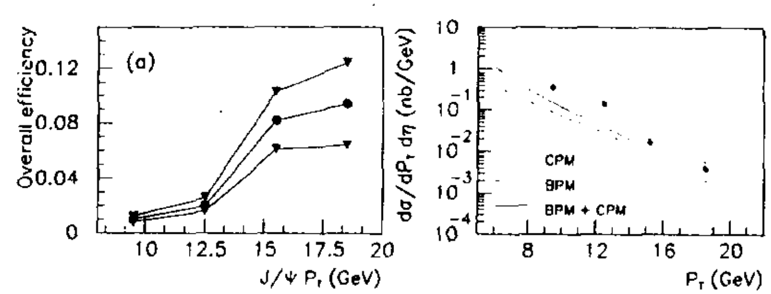

Figure 4: (*a*) Overall efficiency for J/ψ; (*b*) Inclusive J/ψcross section.

5. CONCLUSIONS

The DØ experiment has just completed its first run and has accumulated nearly 15 $pb^{-1}$of data. Using a limited data set we have measured the inclusive muon and the inclusive J/ψ cross-sections. The preliminary results are in agreement with the expectation of the Monte Carlo models. However, at present the error analysis is at primitive stage and further work is required to analyze the full data set and complete the error analysis before we can calculate the $b\bar{b}$ cross section.

6. ACKNOWLEDGEMENTS

We will like to thank the technical staff of Fermilab and other collaborating institutions for their support. Funding has been provided by the U.S. Department of Energy, the U.S. National Science Foundation, the CNPQ in Brazil, the Colciencias in Columbia, the Commissariat a L' Energie in France, the State Committee for Atomic Energy in Russia and the Department of Energy in India.

7. REFERENCES

1. P. Nason, S. Dawson and R. K. Ellis, *Nucl. Phys.* **B303** (1988) 607; **B327** (1989) 49. W. Beenaker, H. Kuijf, W. L. van Neervan and J. Smith, *Phys. Rev.* **D40** (1989) 54. W. Beenaker, W. L. van Neervan, R. Meng, G. Schuler and J. Smith, *Nucl. Phys.* **B351** (1991) 507.
2. S. Abachi *et al.*, "The DØ Detector", submitted to NIM in Phys. Research A.
3. K. Hikasa et al., Review of Particle Properties, Particle Data Group *Phys. Rev.* **D45** (1992) III.84.
4. E. W. N. Glover, A. D. Martin and W. J. Stirling, *Z. Phys.* **C38** (1988) 473; C. Peterson et al., *Phys. Rev.* **D27** (1983) 105.

B_s Mixing

Leaders:

X. Lou
Indiana University

D. Ritchie
Fermi National Accelerator Laboratory

List of Participants

T. Alexopoulas
University of Wisconsin

M. Arenton
University of Virginia

T. Burnett
University of Washington

M. Cummings
University of Hawaii

V. Golovatyuk
University of Virginia

K. Johns
University of Arizona

R. Kowalewski
CERN

R. Lipton
Fermi National Accelerator Laboratory

X. Lou
Indiana University/CERN

D. Ritchie
Fermi National Accelerator Laboratory

J. Skarha
Johns Hopkins University

Q. Wang
Rockefeller University

B. Wicklund
Argonne National Laboratory

Other B Physics—B_s Mixing

REPORT OF THE MIXING SUB-GROUP*
OF THE δ WORKING GROUP (OTHER B PHYSICS)

DAVID J. RITCHIE
Fermi National Accelerator Laboratory[†]*, P. O. Box 500*
Batavia, Illinois 60510-0500, USA

and

JOHN E. SKARHA
Department of Physics and Astronomy
The Johns Hopkins University
Baltimore, Maryland 21218, USA

and

ANDRZEJ ZIEMINSKI
Department of Physics
Indiana University
Bloomington, Indiana 47405, USA

1. INTRODUCTION

1.1 Motivation

With the mixing parameter x defined as $\Delta m/\Gamma$ for neutral B mesons, the ratio of the mixing parameters for the B_d and B_s mesons is given by:

$$x_d/x_s = |V_{td}/V_{ts}|^2 \,(m_{B_d}/m_{B_s})\,(\tau_{B_d}/\tau_{B_s})\left(f^2_{B_d}B_d/f^2_{B_s}B_s\right). \tag{1}$$

The value of x_d is known to good precision[1] ($x_d = 0.665 \pm 0.088$), and the ratio of theoretical form factors $\left(f^2_{B_d}B_d/f^2_{B_s}B_s\right)$ should be calculated to 10% - 20% accuracy within next couple of years[2]. Therefore, a measurement of x_s can provide a precise measurement of the $|V_{td}/V_{ts}|$ ratio. This information, coupled with the measurements of $|V_{ub}|$ and $|V_{cb}|$ from CLEO[3], enables an independent determination of the CKM unitarity triangle through a measurement of its sides, rather than angles. Present estimates for quantities entering Eq. (1), predict a value of x_s within a range[4] of 10 to 30 within the Standard Model.

---

*The Mixing Sub-Group consisted of Theo Alexopoulas (University of Wisconsin at Madision), Mike Arenton (University of Virginia), Toby Burnett (University of Washington), Mary Ann Cummings (University of Hawaii), Slava Golovatyuk (University of Virginia), Ken Johns (University of Arizona), Robert Kowalewski (CERN), Ron Lipton (Fermilab), Xinchou Lou (CERN), David Ritchie (Fermilab), John Skarha (Johns Hopkins University), Qingfang Wang (Rockefeller University), Barry Wicklund (Argonne National Laboratory), and Andrzei Zieminski (Indiana University).

[†]Operated by Universities Research Association Inc. under contract with the United States Department of Energy - Contract No. DE-AC02-76CH03000.

1.2 *Principles for evaluating* B_s *Mixing Proposals*

The Mixing Subgroup reviewed aspects of the B_s mixing measurements, including:

- theoretical uncertainties[†]
- CDF[1] and D0 prospects and proposed upgrades
- Super Fixed Target (SFT) prospects at the SSC[5]
- x_s reach of current e^+e^- experiments[6] operating at the Z^0.

The LEP results and prospects are discussed in the companion paper by X. Lou. The available statistics limit the x_s reach of the e^+e^- experiments to values less than 10. Only hadronic experiments have a reasonable chance to extend the x_s determination range up to 20. Therefore the rest of this summary is concerned with the hadronic experiments only.

A methodology for comparing various B_s mixing experiments, developed by the group, is presented in the companion paper by T. Burnett[7]. The large expected value of x_s (> 10) requires an excellent time resolution to observe B_s oscillations. Therefore only exclusive, fully reconstructed B_s decay modes are suitable. We found the decay modes $B_s \to D_s 3\pi$ and $B_s \to D_s \pi$ with only charged particles in the final state to be the most attractive for the B_s mixing determination at large values of x_s. They have a relatively large combined branching ratio[1] ($4.2 * 10^{-4}$), allow self tagging at $t > 0$, and have additional kinematic constraints to help improve the background rejection.

The number of events required to determine x_s was estimated using two methods. A first estimate (termed 'the BCD method') used a formula, taken from one of the BCD proposals[8], based on a requirement of 25 events in the 8th quarter of oscillations. A second estimate (termed 'the maximum likelihood method', or ML) required the σ for the x_s measurement as computed by the maximum likelihood method to be less than 0.20. In the case of perfect time resolution and a dilution factor of 1, this corresponds to at least 25 events observed. Monte Carlo simulations[7] indicate that in 90% of the cases the ML method would obtain a correct value of x_s with a σ_x of 0.20.

The formulas used by the BCD and ML methods for the required number of detected events ($= \varepsilon N_{\rm prod}$, where $N_{\rm prod}$ is the number of produced events and ε is the efficiency for detecting them) were:

$$N_{\rm det}^{\rm BCD}(x_s) = \frac{50 x_s}{\pi D^2} \cdot \exp\left[\frac{4\pi}{x_s} + ({x_s}^2 - 1)\frac{\sigma_t^2}{2}\right], \tag{2}$$

$$N_{\rm det}^{\rm ML} = \frac{1}{D^2 d_{time}^2 \sigma^2}, \tag{3}$$

or, for the choice of σ_x made above,

$$N_{\rm det}^{\rm ML} = \frac{25}{D^2 d_{time}^2}, \tag{4}$$

where D represents the total dilution factor excluding the effective dilution factor d_{time} due to time resolution[7]. Monte Carlo simulations indicate that the number of events given by the ML method should be sufficient for a first measurement of x_s, whereas the BCD method gives the number of events required for a precision measurement.

1.3 *Comparison Table Contents*

See Table I for a summary of our investigations for the individual experiments. The organization of Table I is described as follows:

- Rows 1 through 9 describe assumptions concerning expected luminosity, the $B\overline{B}$ cross section, selected B_s decay modes, and $t = 0$ tagging.
- Rows 10 through 13 give the assumed efficiencies for geometrical acceptance, off-line reconstruction, triggering, and tagging for $t > 0$. The numbers were determined by Monte Carlo studies done previously[9,10].
- Row 14, the number of B_s's reconstructed, is obtained from the number of B_s produced in 10^7 seconds (Row 6) multiplied by the branching ratio (Row 8) and the overall efficiency (Row 21).
- Rows 15 and 16 describe the expected proper time resolution as determined by Monte Carlo studies.
- Rows 17 through 20 give various dilution factors. d_{mix} represents an inherent mistagging at $t = 0$ due to mixing of some of the b-quark hadrons recoiling against the B_s. It is averaged over expected fractions of b-quark hadrons. d_{tag} represents mistagging at $t = 0$ due to experimental misidentification of the tagging lepton, d_{bg} represents background in the reconstructed B_s mass spectrum, and d_{time} represents the effective dilution due to finite time resolution[7]. d_{time} is a function of the expected x_s value. We quote numbers for $x_s = 5$, 10 and 20.
- Rows 21 and 22 give the total efficiency (= the product of the individual efficiencies) and the product of the dilution factors.
- Rows 23 and 24 give the numbers of events required to measure x_s, as determined by the two methods. They should be compared against the number of reconstructed B_s per nominal year (10^7 seconds), given in row 14.
- Row 26 gives the maximum x_s and is determined from the proper time uncertainty alone using the formula[1] $x_s^{max} = (\pi/2)(\tau/\sigma_t)$.

3. CONCLUSIONS

The tables indicate that the several experiments proposing to measure x_s should be able to go to an x_s of at least 20 based on time resolution alone. The SFT experiment, with its excellent proper time resolution due to the precise measurement of the long B decay length with a silicon vertex detector, has the best x_s reach. However, studies remain to be done to determine whether or not there are sufficient statistics to measure large x_s.

In approximately a year's running with the Main Injector at full luminosity, upgraded CDF and D0 detectors should be able to accumulate enough events to determine $x_s \leq 20$. Thus, B_s mixing measurements are feasible by the end of this century and hadronic collider

†The Mixing Sub-Group would like to acknowledge the contributions of David London and Andreas Kronfeld with regard to discussions concerning the theoretical uncertainties.

experiments have a clear advantage with their large $B\overline{B}$ cross section. Many of the Monte Carlo inputs used in this summary should be verified by CDF during the forthcoming run in 1994. This will lead to an improved understanding of the statistics required and ultimate x_s reach of hadron collider experiments.

5. REFERENCES

1. John E. Skarha and A. Barry Wicklund, "Prospects for Measuring B$_s$ Mixing at CDF", these proceedings.
2. A. Kronfeld, private communication.
3. M. Artuso, invited talk, this workshop.
4. A. Ali and D. London, DESY Report No. DESY-93-022.
5. M. Arenton, private communication.
6. See separate contributions from X. Lou and C. Baltay in these proceedings.
7. T. H. Burnett, "Methodology for Comparison of B-Mixing Experiments", this proceedings.
8. K. T. McDonald, "Maximum-Likelihood Analysis of CP-Violating Asymmetries," Princeton/HEP/92-04. See also BCD Collaboration, Expression of Interest for A Bottom Collider Detector at the SSC, May 25, 1990, p. 14-16.
9. "CDF SVX II Upgrade Proposal", CDF Note No. **1922** (1993)
10. R. Lipton, D0 Note No. **1905**.

Table I - Comparison of proposed B$_s$ Mixing Measurement Prospects at Hadron Accelerators

1	Experiment:	CDF - Mode 1	CDF - Mode 2 (C)	CDF - Mode 3 (C)	D0	SFT
2	Energy E$_{cm}$ (TeV)	1.8	1.8	1.8	1.8	0.193
3	Luminosity L (10^{33} cm^{-2}s^{-1})	0.1	0.1	0.1	0.1	0.02 (D)
4	Cross section $\sigma_{b\bar{b}}$ (μb)	100	100	100	100	2 (E)
5	B$_s^0$ fraction	0.15	0.15	0.15	0.15	0.15
6	N_{prod} / 10^7 s	$3.0 * 10^{10}$	$3.0 * 10^{10}$	$3.0 * 10^{10}$	$3.0 * 10^{10}$	$1.2 * 10^8$
7	Mode to tag B$_s^0$	B$_s \to$ D$_s 3\pi$, D$_s\pi$	B$_s \to$ *lepton* D$_s$	B$_s \to$ *lepton* ϕ	B$_s \to$ D$_s 3\pi$, D$_s\pi$	B$_s \to$ D$_s 3\pi$
8	B$_s^0$ branching ratio	$(4.2 \pm 0.7) * 10^{-4}$	$(3.8 \pm 0.5) * 10^{-3}$	$(8.9 \pm 2.0) * 10^{-3}$	$(4.2 \pm 0.7) * 10^{-4}$	$2.5 * 10^{-4}$
9	B (t=0) tag	e, μ	e, μ	e, μ	μ^+, μ^-	lepton
10	ε_{geom}	0.7	0.7	0.7	0.5	0.57
11	ε_{reco} (A)	$0.30 * \varepsilon_1^{rec}$	$0.37 * \varepsilon_2^{rec}$	$0.41 * \varepsilon_3^{rec}$	0.27	0.48
12	ε_{trig}	$1.63 * 10^{-3}$	$1.63 * 10^{-3}$	$1.63 * 10^{-3}$	$5.00 * 10^{-3}$	$0.8 * 10^{-2}$
13	ε_{tag}	1.0 (F)	0.039	0.039	0.6	1.0 (F)
14	Number of B$_s^0$ reconstructed	$4313 * \varepsilon_1^{rec}$	$1877 * \varepsilon_2^{rec}$	$4871 * \varepsilon_3^{rec}$	5103	66
15	a ($\sigma_t = a \oplus bt$) (G)	0.08	0.11	0.13	0.08	0.025
16	b ($\sigma_t = a \oplus bt$) (G)	0.036	0.10	0.15	0.0	0.0
17	d_{mix}	0.66	0.66	0.66	0.65	0.76
18	d_{tag}	0.80	0.80	0.80	0.6	0.90
19	d_{bg} (B)	–	–	–	–	–
20	d_{time} (x_s = 5/10/20)	0.88/0.69/0.26	0.45/0.16/0.02	0.31/0.085/0.0082	0.88/0.69/0.26	1.0/1.0/1.0
21	Total efficiency ε	$0.34 * 10^{-3} * \varepsilon_1^{rec}$	$0.0165 * 10^{-3} * \varepsilon_2^{rec}$	$0.0182 * 10^{-3} * \varepsilon_3^{rec}$	$0.41 * 10^{-3}$	$2.2 * 10^{-2}$
22	$d_{mix} d_{tag} d_{bg} d_{time}$ (x_s = 5/10/20)	0.46/0.36/0.14	0.24/0.084/0.011	0.16/0.044/0.004	0.34/0.27/0.10	0.68/0.68/0.68
23	N$_{B_s}$ req. for $x_s = 10$ (BCD)	2755	5989	14101	5046	1233
24	N$_{B_s}$ req. (x_s = 5/10/20) (ML)	116/188/1.3K	442/3.5K/224K	933/12.4K/1.3M	212/345/2.4K	53/53/53
25	σ_x for N$_{B_s}$ (ML)	0.20	0.20	0.20	0.20	0.20
26	Maximum x_s	20	11	8	20	63

Notes: (A) $\varepsilon_{1,2,3}^{rec}$ are event reconstruction efficiencies to be determined using the data. (B): Background estimates to be determined from the data; d_{bg} taken as 1.0. (C): Estimates are for single lepton data; up to x2 signal available from dilepton data. (D) 10^7 interactions per second. (E): $A^{0.27}$ enhancement for Silcon target. (F): ε_{tag} is included in ε_{trig}. (G) t measured in units of proper time.

Prospects for Measuring B_s Mixing at CDF

John E. Skarha
Department of Physics and Astronomy
The Johns Hopkins University
Baltimore, Maryland 21218, USA

and

A. Barry Wicklund
Division of High Energy Physics
Argonne National Laboratory
Argonne, Illinois 60439, USA

1. INTRODUCTION

1.1 *CDF B Physics Potential*

The original design of the Collider Detector at Fermilab (CDF)[1] was optimized for high p_T physics measurements associated with W and Z boson, top quark, and QCD jet production. This choice resulted in an emphasis on the central pseudorapidity region ($|\eta| < 1.0$) for detector coverage. Thus, CDF has excellent tracking ($\Delta p_T/p_T = 0.0066 \oplus 0.0014 p_T$), good calorimetry, and a suitable muon system in the central region. Even with this limited coverage, the large $\bar{p}p \to bX$ cross section of nearly 100 μbarns for $|\eta| < 1.0$ has allowed the CDF experiment to make many B physics measurements[2]. In addition, with the successful operation of the CDF silicon vertex detector (SVX)[3], the capability for making time-dependent B_s mixing measurements becomes a reality. Upgrade plans, which include extending the tracking and lepton identification into the forward region and the implementation of a high-rate DAQ system, make a time-dependent B_s mixing measurement an attractive goal during the anticipated high-luminosity Main Injector collider runs. We discuss here the feasibility and potential of making a B_s mixing measurement based on extrapolations of the current CDF detector performance using colliding beam data and the expected upgrade plans.

1.2 *Physics Motivation*

The physics motivation for measuring the B_s mixing parameter X_s has been discussed many times[4]. First, it allows an independent measurement of the CKM matrix element V_{ts}, which is expected to be equal in magnitude to V_{cb}. Equation (1) gives the standard expression for X_s (there is a similar expression for X_d), in which top quark exchange in the box diagrams is assumed to be dominant:

$$X_s \equiv \frac{(\Delta M)_{B_s}}{\Gamma} = \tau_{B_s} \frac{G_F^2}{6\pi^2} M_W^2 M_{B_s} (f_{B_s}^2 B_{B_s}) \eta_{B_s} y_t f_2(y_t) \mid V_{ts}^* V_{tb} \mid^2, \tag{1}$$

where τ_{B_s} and M_{B_s} are the lifetime and mass of the B_s meson, B_{B_s} and f_{B_s} are the B_s bag parameter and decay constant, η_{B_s} is a QCD correction factor and $y_t f_2(y_t)$ depends on the top quark mass. We see here the dependence on the B_s mass and lifetime; the former has been measured recently in the $B_s \to J/\psi\phi$ decay mode at CDF[5], and the latter is expected to come from the same channel in the near future.

A measurement of the ratio of X_s to X_d allows cancellation of the top quark mass dependence and reduced dependence on the bag parameter-decay constants. This results in an improved measurement of V_{td}, as shown in Equation (2):

$$\frac{X_s}{X_d} \propto \frac{f_{B_s}^2 B_{B_s} \mid V_{ts} \mid^2}{f_{B_d}^2 B_{B_d} \mid V_{td} \mid^2}. \tag{2}$$

V_{td} of course contains the phase of the CKM matrix, which is thought to be the source of CP-violation in the Standard Model. Calculation of the ratio $f_{B_s}^2 B_{B_s}/f_{B_d}^2 B_{B_d}$ is believed to be more reliable and have less error than determining $f_{B_s}^2 B_{B_s}$ or $f_{B_d}^2 B_{B_d}$ alone[6]. Finally, the value of X_s is necessary for asymmetry measurements related to the unitary triangle angle γ in the B_s decay modes.

Standard model prediction of X_s places it in the range $10 - 30$ for a top mass less than 200 GeV[7]. These large values of X_s correspond to rather rapid oscillations of the B_s meson flavor and provide an experimental challenge to measure time-dependent B_s mixing. This is in contrast to the X_d measurements performed by ARGUS[8] and CLEO[9] which result in combined average[10] $X_d = 0.665 \pm 0.088$.

2. EXPERIMENTAL APPROACH

2.1 *Precursor Measurements*

We see the CDF approach to measuring B_s mixing as a "walk before you run" strategy. Although the current priority for CDF is the study of high P_t phenomena, steady progress has been achieved in the identification of B decays and in the use of the silicon detector and lepton-identification tools. CDF has already made a measurement of time-integrated B^0 mixing[11]. This will be improved on in the data sample taken in Run 1A (~ 20 pb^{-1}) and in the soon to be acquired Run 1B data (an additional 60 pb^{-1} or more is expected on tape).

Run 1A data may also allow a time-integrated B_s mixing measurement through lepton-D_s, lepton charge correlation. Such a measurement would have little X_s reach but might shed some light on the $b \to B_s$ and $b \to B_d$ fractions at CDF when combined with the time-integrated B^0 measurement. Another possibility in the present Run 1A data is a time-dependent B_d mixing measurement using lepton-secondary vertex, lepton correlations. In this case, no clear charm signal is identified (to maintain statistics), but the lepton associated secondary vertex position is plotted for same and opposite sign lepton pairs. Since the B_d oscillation is so slow, rather poor resolution in the decay time may still yield a time-dependent measurement of X_d . The LEP experiments have already demonstrated time-dependent B_d mixing in lepton-associated charm modes[12].

2.2 *General Considerations*

The general method for any mixing measurement requires determining the flavor of a neutral B meson (B_d or B_s) at production and decay. The B meson flavor is usually determined through the associated lepton from B semileptonic decay. The lepton from the other B gives the flavor of the first B at production, and the lepton from the B itself gives its flavor at decay. There is, of course, dilution of the lepton tag due to B_d, B_s oscillations, charm cascade decays, and fake leptons. The effects of dilution on the B_s mixing measurement are discussed elsewhere[13]. Other tagging methods include the charge sign tagging from associated strange particle ($K^{\pm}$) production in the $b \to c \to s$ cascade, charge counting of tracks associated with the B decay vertex, and resonant or non-resonant tagging of the first generation hadron produced in the $b \to B$ hadronization[14].

The time dependent oscillation of neutral B meson is given by the following mixing probabilities:

$$Prob(B \to \overline{B}) = \frac{1}{2}e^{-t/\tau}(1 - cos(Xt/\tau)), \tag{3}$$

$$Prob(B \to B) = \frac{1}{2}e^{-t/\tau}(1 + cos(Xt/\tau)), \tag{4}$$

where X is the mixing parameter. So, given a set of events which are tagged as either $B \to \overline{B}$ or $B \to B$ events, the distribution of these events should follow the exponentially-damped cosine dependence given above. The specific cosine dependence can be isolated by taking the difference of mixing probability equations and dividing by the sum:

$$\frac{Prob(B \to B) - Prob(B \to \overline{B})}{Prob(B \to B) + Prob(B \to \overline{B})} = cos(Xt/\tau). \tag{5}$$

The ability to resolve the cosine oscillations for a given mixing parameter X depends on the proper time resolution σ_t/τ. The decay time $t = L/\beta\gamma c = Lm/pc$ depends on the decay length, momentum, and mass. This relation also holds in the transverse plane, which is more suitable for solenoid geometry central collider detectors like CDF, so that $t = L_T m/p_T c$. The proper time resolution σ_t/τ is then given by:

$$\frac{\sigma_t}{\tau} = \sqrt{(\frac{\Delta L_T}{L_{0T}})^2 + (\frac{t}{\tau}\frac{\Delta p_T}{p_T})^2}, \tag{6}$$

where $L_{0T} = p_T c\tau/m$. The proper time resolution σ_t/τ thus depends on the transverse decay length resolution of the B vertex and the B momentum resolution. For a detector like CDF, with a transverse decay length resolution of ~ 50 microns and $\Delta p_T/p_T \sim 0.2\% p_T$, the proper time resolution is dominated by the transverse decay length resolution for fully reconstructed B_s decays and is dominated by the B_s momentum resolution for partially reconstructed decays.

The maximum X_s reach for a given proper time resolution can be derived rather simply from the cosine dependence[15]. If the product of $X_s\sigma_t/\tau$ is greater than $\pi/2$, then there will be smearing between the positive and negative amplitudes of the cosine and the cosine dependence will be washed out. This constraint thus sets the maximum X_s reach for a given proper time resolution:

$$X_s^{max} = \frac{\pi}{2}\frac{\tau}{\sigma_t}. \tag{7}$$

So, for example, the maximum X_s reach for $\sigma_t/\tau = 0.10$ is ~ 16. Different B_s decay modes have different proper time resolutions and X_s sensitivities depending on whether the decay is fully or partially reconstructed. Purely hadronic B_s decays such as $B_s \to D_s\pi$, which are so far less easily identified in $\bar{p}p$ collisions, offer the best proper time resolution and thus the largest range of probing for X_s . Unfortunately, the clean $B_s \to J/\psi\phi$ signature offers no help for measuring B_s mixing since the flavor of the B_s at decay cannot be determined from the final state particles. As mentioned above, this mode will however eventually yield a precision measurement of the B_s lifetime, which will be needed for a B_s mixing analysis. For the present CDF tracking chamber and vertex detector, the proper time resolution for fully reconstructed B_s decays is ~ 0.08, allowing X_s to be measured up to 20 before resolution effects significantly smear out the oscillations. The addition of an inner layer of silicon pixels to improve the decay length resolution is a possible way to extend the X_s reach.

In Table 1, we list the product branching ratios for exclusive B_s mixing decay modes. We consider here only the $B_s \to D_s\pi\pi\pi$ and $B_s \to D_s\pi$ decays. For the decay branching ratios, we used the $s \to d$ interchanged $B_d \to D\pi\pi\pi$ and $B_d \to D\pi$ Particle Data Group[16] (PDG) values. These B_s decay modes have the advantage of containing a D_s, which can be cleanly identified in its $\phi\pi$ (already seen at CDF[17]) or K^*K final states. Neither of these B_s decays has been reconstructed yet at CDF, but several purely hadronic B_s decays have been seen at LEP[12]. Run 1A or Run 1B data at CDF should yield several of these events. Of course, in order to obtain large samples of these exclusive B_s events on tape, the single lepton threshold (on the lepton trigger from the other B) will have to be lowered and the detector coverage improved, or these purely hadronic decays will have to be triggered directly with a secondary vertex trigger. CDF is now planning a secondary vertex trigger for the Run II collider run and beyond[18]. Initially this trigger will select on high impact parameter tracks and look for $B^0 \to \pi^+\pi^-$ decays. Improvements to this trigger should allow online triggering of separated secondary vertices Summing up the two B_s decay modes with the 3 D_s final states, we find a combined product branching ratio of 4.2x10^{-4}.

Table 1: Branching Ratios for Exclusive B_s Mixing Modes.

Decay Mode	Branching Ratio	Comment
$D_s \to \phi\pi$	$(2.8 \pm 0.5)\%$	PDG, 1992
$D_s \to \phi\pi\pi\pi$	$(1.2 \pm 0.4)\%$	PDG, 1992
$D_s \to K^*K$	$(2.6 \pm 0.5)\%$	PDG, 1992
$\phi \to KK$	$(49.1 \pm 0.8)\%$	PDG, 1992
$K^* \to K\pi$	$(67.0 \pm 0.0)\%$	PDG, 1992
$B_s \to D_s\pi\pi\pi$	(8.0 ± 2.5)x10^{-3}	from B_d mode, PDG, 1992
$B_s \to D_s\pi$	(3.2 ± 0.7)x10^{-3}	from B_d mode, PDG, 1992
$B_s \to D_s\pi\pi\pi, D_s \to \phi\pi, \phi \to KK$	(1.1 ± 0.4)x10^{-4}	product branching ratio
$B_s \to D_s\pi\pi\pi, D_s \to \phi\pi\pi\pi, \phi \to KK$	(4.7 ± 2.2)x10^{-5}	product branching ratio
$B_s \to D_s\pi\pi\pi, D_s \to K^*K, K^* \to K\pi$	(1.4 ± 0.5)x10^{-4}	product branching ratio
$B_s \to D_s\pi, D_s \to \phi\pi, \phi \to KK$	(4.4 ± 1.2)x10^{-5}	product branching ratio
$B_s \to D_s\pi, D_s \to \phi\pi\pi\pi, \phi \to KK$	(1.9 ± 0.8)x10^{-5}	product branching ratio
$B_s \to D_s\pi, D_s \to K^*K, K^* \to K\pi$	(5.6 ± 1.6)x10^{-5}	product branching ratio
$B_s \to D_s\pi\pi\pi, D_s \to$ 3 modes	(3.0 ± 0.7)x10^{-4}	sum of 3 modes
$B_s \to D_s\pi, D_s \to$ 3 modes	(1.2 ± 0.2)x10^{-4}	sum of 3 modes
$B_s \to$ 2 modes, $D_s \to$ 3 modes	(4.2 ± 0.7)x10^{-4}	sum of 6 modes

Table 2 lists the product branching ratios for inclusive B_s mixing modes. Here, the semileptonic decay of the B_s is required, and then the reconstruction of the D_s or ϕ is necessary to tag the presence of a B_s decay. There are, of course, backgrounds from the decays of other B hadrons to a D_s or ϕ. Due to the missing neutrino or lack of a reconstructed D_s, the B_s is only partially reconstructed, and the X_s reach is limited due to the uncertainty on the B_s momentum. These exclusive decay modes can be examined in either single lepton or dilepton triggered samples. In the single lepton case, the flavor of the B_s at production has to be provided by some tagging method, while in the dilepton sample the lepton from the other B is conveniently triggered on and provides the flavor tag.

Table 2: Branching Ratios for Inclusive B_s Mixing Modes.

Decay Mode	Branching Ratio	Comment
$D_s \to \phi\pi$	$(2.8 \pm 0.5)\%$	PDG, 1992
$D_s \to \phi\pi\pi\pi$	$(1.2 \pm 0.4)\%$	PDG, 1992
$D_s \to \phi\pi\pi^0$	$(6.7 \pm 3.3)\%$	PDG, 1992
$D_s \to \phi\rho$	$(5.2 \pm 1.6)\%$	PDG, 1992
$D_s \to \phi l\nu$	$(1.4 \pm 0.5)\%$	PDG, 1992
$D_s \to \phi X$	$(17.3 \pm 3.8)\%$	PDG, 1992
$B_s \to D_s l\nu$	$(10.5 \pm 0.5)\%$	B mode e,μ ave., PDG, 1992
$B_s \to D_s l\nu, D_s \to \phi\pi, \phi \to KK$	(1.4 ± 0.3)x10^{-3}	product branching ratio
$B_s \to D_s l\nu, D_s \to \phi\pi\pi\pi, \phi \to KK$	(6.2 ± 2.1)x10^{-4}	product branching ratio
$B_s \to D_s l\nu, D_s \to K^*K, K^* \to K\pi$	(1.8 ± 0.4)x10^{-3}	product branching ratio
$B_s \to D_s l\nu, D_s \to$ 3 modes	(3.8 ± 0.5)x10^{-3}	sum of 3 modes
$B_s \to D_s l\nu, D_s \to$ 2 phi modes	(2.0 ± 0.4)x10^{-3}	sum of 2 modes
$B_s \to D_s l\nu, D_s \to \phi X, \phi \to KK$	(8.9 ± 2.0)x10^{-3}	product branching ratio

2.3 *Expected Rates*

We now consider the expected Run 1A, Run 1B, Run 1A+1B combined and Run II+ (1000 pb^{-1}) data samples obtained at CDF relevant for B_s mixing studies. In each case the listed numbers correspond to the data samples after applying lepton identification and fiducial cuts. We assume no drastic changes or improvements to the present Run 1A trigger, which had single electron and muon triggers for $p_T(l) > 6$ GeV/c (prescaled) and $p_T(l) > 9$ GeV/c (independent from the 6 GeV/c trigger and not prescaled) and dimuon ($p_T(\mu) >\sim 2.5$ GeV/c), $e-\mu$ ($E_T(e) > 5$ GeV, $p_T(\mu) > 3$ GeV/c), and dielectron ($E_T(e) > 5$ GeV) triggers. This is *rather conservative* given the large increase in data samples possible by improving the DAQ system and lowering the trigger p_T thresholds. For all of the following numbers, we have required that secondary vertex information be available (50% efficiency for Run 1A and 1B, 100% efficiency for Run II+) for the partially reconstructed B_d and B_s decays and the reconstructed D_s, D_0 and ϕ decays; for each of the latter we assume a reconstruction efficiency of 40%. However, we have not included a vertex separation efficiency. For the dilepton samples, the number of reconstructed D_0 and ϕ events is based an observed rate of ~ 5/pb^{-1} in the dimuon sample[19]. This extrapolates to $\sim 100/20$pb^{-1} in the dimuon sample, 16/20pb^{-1} in the $e-\mu$ sample and 3/20pb^{-1} in the dielectron sample, all before requiring secondary vertex information. Because of large uncertainties in the identification and reconstruction efficiencies, we have not included here estimates for reconstruction of purely hadronic B_s decays[20].

Table 3 lists the expected (after full analysis) single lepton and dilepton data samples after fiducial and lepton id cuts for the Run 1A data. For the partially reconstructed B_d and B_s decays in the single lepton sample, we have included a low p_T lepton (e,central μ) tagging efficiency[21] (including the semileptonic branching ratio) of 1.8%. A tagging efficiency of a few percent is not unexpected given the soft p_T and broad rapidity distributions of B mesons and the present CDF detector coverage.

For Run 1B, we have assumed a x2 increase in the number of recorded $p_T > 6$ GeV/c electron events due to an improvement in the single electron trigger[22]. We have also assumed an increase in the low p_T lepton (e,μ) tagging efficiency from 1.8% $\to$ 2.5% due to improved understanding of the larger angle muon system.

Table 3: Run 1A CDF Single Lepton and Dilepton Data Samples.

Decay Mode	$P_T(l) > 6$	$P_T(l) > 9$	Combined
$B \to e\nu DX$	100,000	200,000	300,000
$B \to \mu\nu DX$	100,000	50,000	150,000
$B \to l\nu DX$	200,000	250,000	450,000
$B \to l\nu DX; B \to lX$	3,600	4,500	8,100
$B \to l\nu D^0 X, D^0 \to K\pi; B \to lX$	4	5	10
$B_s \to l\nu D_s X, D_s \to \phi\pi, \phi \to KK; B \to lX$	1	2	3
$B_s \to l\nu D_s X, D_s \to 3$ modes; $B \to lX$	4	5	9
$B_s \to l\nu D_s X, D_s \to \phi X, \phi \to KK; B \to lX$	9	11	20

Decay Mode	$\mu\mu$	$e\mu$	ee	Combined
$B \to l\nu X; B \to l\nu X$	40,000	6,600	1,340	47,940
$B \to l\nu X; B \to l\nu D^0 X, D^0 \to K\pi$ events	50	8	2	60
$B \to l\nu X; B \to l\nu X, \phi \to KK$ events	50	8	2	60

Including these improvements combined with the expected x3 increase in the luminosity for Run 1B, there is a significant increase in the number of tagged partially reconstructed B_d and B_s decays (Table 4), and lower limits on the value of X_s might be determined in both the single and dilepton samples.

Table 4: Run 1B CDF Single Lepton and Dilepton Data Samples.

Decay Mode	$P_T(l) > 6$	$P_T(l) > 9$	Combined
$B \to e\nu DX$	600,000	600,000	1,200,000
$B \to \mu\nu DX$	300,000	150,000	450,000
$B \to l\nu DX$	900,000	750,000	1,650,000
$B \to l\nu DX; B \to lX$	22,500	18,750	41,250
$B \to l\nu D^0 X, D^0 \to K\pi; B \to lX$	27	23	50
$B_s \to l\nu D_s X, D_s \to \phi\pi, \phi \to KK; B \to lX$	9	8	17
$B_s \to l\nu D_s X, D_s \to 3$ modes; $B \to lX$	25	21	45
$B_s \to l\nu D_s X, D_s \to \phi X, \phi \to KK; B \to lX$	56	47	103

Decay Mode	$\mu\mu$	$e\mu$	ee	Combined
$B \to l\nu X; B \to l\nu X$	120,000	19,800	4,020	143,820
$B \to l\nu X; B \to l\nu D^0 X, D^0 \to K\pi$ events	150	24	6	180
$B \to l\nu X; B \to l\nu X, \phi \to KK$ events	150	24	6	180

For completeness, we have combined the Run 1A and Run 1B expected rates in Table 5. We assume here that the increased 2.5% low p_T lepton tagging efficiency can be applied to the entire single lepton sample. Again, observable signals of tagged B_d and B_s decays should be seen. This data should receive thorough analysis by the time Run II data taking begins, and all of the lessons learned from reconstructing B_d and B_s decays should be available immediately on the Run II sample.

Table 6 lists the projected Run II+ (1 fb^{-1} data sample), assuming no major changes to the present single lepton and dilepton trigger, but including improvements to the detector and tagging efficiencies. These improvements include a doubling of the secondary vertex detection coverage, resulting in nearly 100% acceptance and increase in the lepton (e, μ) coverage for tagging, not triggering, out to $|\eta| < 2$. This results in an increase in the low p_T lepton tagging efficiency from 2.5% to 3.9%.

Table 5: CDF Run 1A+1B Combined Single Lepton and Dilepton Data Samples.

Decay Mode	$P_T(l) > 6$	$P_T(l) > 9$	Combined
$B \to e\nu DX$	700,000	800,000	1,500,000
$B \to \mu\nu DX$	400,000	200,000	600,000
$B \to l\nu DX$	1,100,000	1,000,000	2,100,000
$B \to l\nu DX; B \to lX$	27,500	25,000	52,500
$B \to l\nu D^0 X, D^0 \to K\pi; B \to lX$	33	30	63
$B_s \to l\nu D_s X, D_s \to \phi\pi, \phi \to KK; B \to lX$	11	10	22
$B_s \to l\nu D_s X, D_s \to 3$ modes; $B \to lX$	30	28	58
$B_s \to l\nu D_s X, D_s \to \phi X, \phi \to KK; B \to lX$	69	63	131

Decay Mode	$\mu\mu$	$e\mu$	ee	Combined
$B \to l\nu X; B \to l\nu X$	160,000	26,400	5,360	191,760
$B \to l\nu X; B \to l\nu D^0 X, D^0 \to K\pi$ events	200	32	8	240
$B \to l\nu X; B \to l\nu X, \phi \to KK$ events	200	32	8	240

The secondary vertex detection improvement to the CDF detector should be ready for the start of Run II, but the lepton coverage upgrade is likely to come later in the Run II+ running. Nevertheless, we assume these modifications in our rate estimates, which really correspond to CDF operating with an increased B physics priority. Of course, now the rates are very large and an X_s measurement in the partially reconstructed B_s decay modes, with an X_s reach up to possibly 10, is likely. A measurement of X_s in fully reconstructed B_s decay modes is also possible and this is discussed elsewhere[20].

Table 6: CDF Run II+ (1000 pb^{-1}) Single Lepton and Dilepton Data Samples.

Decay Mode	$P_T(l) > 6$	$P_T(l) > 9$	Combined
$B \to e\nu DX$	8,750,000	10,000,000	18,750,000
$B \to \mu\nu DX$	5,000,000	2,500,000	7,500,000
$B \to l\nu DX$	13,750,000	12,500,000	26,250,000
$B \to l\nu DX; B \to lX$	536,250	487,500	1,023,750
$B \to l\nu D^0 X, D^0 \to K\pi; B \to lX$	1287	1170	2457
$B_s \to l\nu D_s X, D_s \to \phi\pi, \phi \to KK; B \to lX$	440	400	839
$B_s \to l\nu D_s X, D_s \to 3$ modes; $B \to lX$	1180	1073	2252
$B_s \to l\nu D_s X, D_s \to \phi X, \phi \to KK; B \to lX$	2681	2438	5119

Decay Mode	$\mu\mu$	$e\mu$	ee	Combined
$B \to l\nu X; B \to l\nu X$	2,000,000	330,000	67,000	2,397,000
$B \to l\nu X; B \to l\nu D^0 X, D^0 \to K\pi$ events	5000	800	200	6000
$B \to l\nu X; B \to l\nu X, \phi \to KK$ events	5000	800	200	6000

3. CONCLUSION

Based on a preliminary analysis of the Run 1A data sample, we have made estimates for the expected number of partially reconstructed B_d and B_s events at CDF for Runs 1A, 1B and II+ (1 fb^{-1}). These estimates are based on an extrapolation from the present Run 1A sample and assume *no major changes* to the B physics triggers and modest improvements to the present detector. From these estimates, we expect observable B_d and B_s time-dependent mixing signals in the Run 1B data and measurements of X_s (up to ~ 10) in the Run II+ sample using partially reconstructed modes. Fully reconstructed B_s decays in the $B_s \to D_s\pi$ and $B_s \to D_s\pi\pi\pi$ should be seen in Run 1B, and a precision measurement of the B_s lifetime in the $B_s \to J/\psi\phi$ mode is expected. Measurements of X_s up to 20 in fully reconstructed B_s decays using the Run II+ data sample are also conceivable[23].

7. REFERENCES

1. F. Abe et al. (CDF Collaboration), *Nucl. Instrum. Methods Phys. Res., Sect. A* **271** (1988) 387.
2. See for example: F. Abe et al. (CDF Collaboration), *Phys. Rev. Lett.* **71** (1993) 500, and references therein.
3. B. Barnett et al., *Nucl. Instrum. Methods Phys. Res., Sect. A* **315** (1992) 125; F. Bedeschi et al., *Fermilab Report No.* FERMILAB-CONF-92/263-E.
4. A. Ali and D. London, *DESY Report Nos.* DESY-92-075 and DESY-93-022; J. L. Rosner, *J. Phys. G* **18** (1992) 1575.
5. F. Abe et al. (CDF Collaboration), *Phys. Rev. Lett.* **71** (1993) 1685.
6. See Ref. [4] above, also the talk by A. Kronfeld at this workshop.
7. A. Ali and D. London, *DESY Report No.* DESY-93-022.
8. H. Albrecht et al. (ARGUS collaboration), *Z. Phys. C* **55** (1992) 357.
9. M. Artuso et al. (CLEO collaboration), *Phys. Rev. Lett.* **71** (1993) 1680.
10. Weighted average of the CLEO and ARGUS measurements to determine $\overline{\chi_d}$ and then X_d . The CLEO tagging method measurement was used.
11. F. Abe et al. (CDF Collaboration), *Phys. Rev. Lett.* **67** (1991) 3351.
12. See, for example, the talk by R. Kowalewski at this workshop.
13. See the contribution to this workshop by T. Burnett.
14. See, for example, the talks by C. Hill, M. Gronau, and T. LeCompte at this workshop.
15. N. Lockyer et al. *Proposal for a B-Physics Experiment at TEV I: The μBCD* (1990) 21.
16. K. Hikasa et al. (Particle Data Group), *Phys. Rev. D* **45** (1992) 1.
17. See, for example, the talk by J. Mueller at this workshop.
18. See G. Punzi et. al. contribution to this workshop.
19. L. Song, private communication.
20. See the workshop δ group summary for details.
21. C. Campagnari, private communication.
22. See K. Byrum contribution to this workshop.
23. CDF SVX II Upgrade Proposal, *CDF Note No.* **1922** (1993).

METHODOLOGY FOR COMPARISON OF B-MIXING EXPERIMENTS

T. H. BURNETT
Physics Department, FM-15, University of Washington
Seattle, WA 98195, USA

1. INTRODUCTION

An objective of this workshop was to provide a basis for comparison of the capabilities of different experiments, identifying the components entering into the comparison. A suggested framework was provided by the organizers in the form of a table that allows one to see the computations leading to the three primary elements in the determination of the resolution to be expected in the measurment of an asymmetry. These are: (1) N, the number of produced events; (2) ϵ, the total efficiency for detecting these events, such that ϵN is the number of events to be analyzed for the effect; and (3) $D \leq 1$, the total *dilution factor* reflecting a reduction of the effect to be expected due to the presence of background or mistagging. The effective number of events is further reduced to $\epsilon N D^2$.

In B_s mixing, we wish to measure the quantity $x_s = \Delta M/\Gamma$. An experiment observes two distributions, according to whether the charge conjugations of the B_s at production and decay are the same or different:

$$\frac{dn_{\pm}}{dt} = \frac{\epsilon N}{2} e^{-t}[1 \pm D \cos x_s t] \tag{1}$$

with the $\pm$ corresponding to same/different. (We express t in units of the B_s decay time.) Thus the experimental challenge is to assign the appropriate sign to each presumed B_s decay, and measure its proper time at the time of decay. Figure 1 is a cartoon that emphasizes the four measurements thus required for each event. As shown, a $b\bar{b}$ pair is created, the b hadronizes by picking up an $\bar{s}$-quark to form a $\bar{B}_s$, which may decay as either a B_s or a $\bar{B}_s$. An experiment must tag the charge conjugation of the B_s at creation, usually by identifying the recoil B; identify the nature of the B_s at decay; measure the distance between the two vertices; and measure the momentum of the B_s in order to determine the proper time.

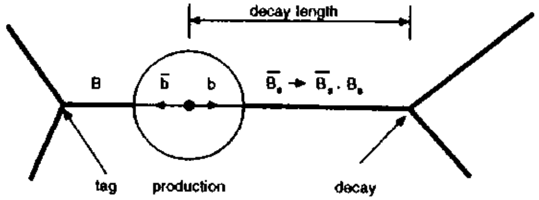

Figure 1. Diagram showing the basic process and quantities to measure to dete

1.1 The tag

The "tag" is the technique used to identify the state of the B_s at produc is most often done by detecting a lepton, presumably from the semi-leptonic deca meson or baryon that was pair produced with the B_s. This has an inherent ineffi to the 20% branching fraction for leptonic decays. Worse is the dilution effects and mixing of the tagging B. Other techniques are

- A leading charged K. The idea is to determine whether the B_s started out or $\bar{s}$ quark by finding a meson, particularly a $K^{\pm}$, containing the *other* s qua apparently feasable at LEP or SLC, where each b quark forms a jet, multiṗ low, and one has particle ID.
- Jet charge at an e^+e^- machine: At LEP or SLC most of the time one sees tw jet opposite the one containing the B_s was initiated by a b-quark, the charg can be used as a tag. This charge can be measured indirectly by a weighted the observed charges of the hadrons.
- Forward-backward assymetry in polarized e^+e^- collisions: Uniquely at SL(larized beams, the angle of the B_s with respect to the incoming electron is dilution factor varies from 0 at 90 degrees to $0.93P$, where $P \approx 0.65$ is the pc at 0 degrees.

1.2 The Decay

Three items about the B_s must be determined when it decays: (1) Its ider $\bar{B}_s$; (2) the position of its decay vertex; and (3) its momentum. The last two are order to reconstruct the proper time of decay. The proposed techniques are:

- Inclusive leptonic decay: the sign of the lepton satisfies (1) with the usual fraction efficiency penalty, Requirement (2) means that at least one other the decay be found. Because of the missing neutrino, full reconstruction is n(resulting in an inherent resolution for the momentum of $\approx 15\%$.
- Exclusive leptonic decay: modes are $\ell\nu\phi$ and $\ell\nu D_s$.
- Full reconstruction: modes proposed for this are πD_s and $3\pi D_s$.

2. HOW MANY EVENTS?

Let us delve into the realm of small statistics to try to answer a deceptively simple question: given a set of events distributed according to Eq.(1) with perfect time resolution, how many are needed to measure x_s? A simple criterion is that the oscillatory term in Eq. (1) be clearly seen. This implies determining that the coefficient of this term is different from zero by, say 5σ. Assuming $D = 0.4$, and using $\sigma = 1/D\sqrt{\epsilon N}$, we find $\epsilon N > 150$. A far more severe restriction is that presented in the BCD proposal[1]. It is that the eighth quarter cycle of the mixing oscillations contain 25 events, and has the form

$$N_{\text{min}}(x_s) = \frac{50x_s}{\pi D^2} \cdot \exp\left[\frac{4\pi}{x_s} + (x_s{}^2 - 1)\frac{\sigma_t^2}{2}\right] \tag{2}$$

This depends on x_s: values at $x_s = 5, 10, 20$ for $\sigma_t = 0$ are 6500, 3700, and 3900, respectively. This is rather more that the 150 events estimated above. The difference is that our original criterion was to definitely establish the *presence* of the oscillatory term, while it is also necessary to have a proper measurement of its *frequency*, i.e. x_s. To study this, we created a simulation of experiments, each with N events distributed according to Eq. (1), then checked to see if the likelihood function allowed a fit that was consistent with the input x_s. With 150 events, the fit is satisfactory 90% of the time, for x_s in the range 5-20, giving a result consistent with the expected error of 0.2. It is remarkable that fluctuations in the distribution can result in misleading likelihood functions. Performing the same analysis for 600-event experiments, with an expected error of 0.1, we find unsatisfactory fits only 1% of the time. This suggests that if the magnitude of the oscillatory term is 10 σ, that a satisfactory measurement of x_s can be made 99% of the time.

2. TIME RESOLUTION

A very important consideration in measuring x_s is the resolution for time measurement. Roughly, if the resolution in t is σ_t, one can measure x_s only if the value is less than $1/\sigma_t$. In this section we make this statement more quantitative.

The *expected* resolution in x_s, if determined using maximum likelihood, in the limit of large numbers, is:

$$\frac{1}{\sigma^2} = \epsilon D^2 N \int_{t_{\text{min}}}^{t_{\text{max}}} \frac{f_0(t) f'(t)^2}{f_0(t)^2 - D^2 f_x(t)^2} dt \tag{3}$$

where $f_0(t) = e^{-t}$, $f_x(t) = e^{-t}\cos x_s t$, and $f'(t) = te^{-t}\sin x_s t$. Note that for $D = 1$, $t_{\text{max}} = \infty$, the integral is simply $\int_0^\infty e^{-t}t^2 dt = 2$, (the case derived by McDonald[1]) while for $D < 1$, with the same limits, it becomes approximately 1. The maximum of the integrand in this case is at $t = 2$, indicating that the maximum information is at two mean lives.

When the resolution in t is finite, one simply smears the functions f_0, f_x, and f', and evaluates the integral. This must be done numerically.

In the spirit of presenting experimental factors in terms of efficiencies and dilution factors, we note that the square root of the integral in Eq. (3) is in effect a dilution factor. Thus we define the *time dilution factor* by

$$d_t{}^2 = \int_{t_{\text{min}}}^{t_{\text{max}}} \frac{\tilde{f}_0(t) \tilde{f}'(t)^2}{\tilde{f}_0(t)^2 - D^2 \tilde{f}_x(t)^2} dt \tag{4}$$

where $\tilde{f}_0$ represents the function obtained from f_0 by time smearing:

$$\tilde{f}_0(t) = \int_0^\infty \frac{f_0(t')}{\sqrt{2\pi}\sigma(t')} \exp\left[-\frac{1}{2}\left(\frac{t-t'}{\sigma(t')}\right)^2\right] dt' \tag{5}$$

where the time measurement resolution function we use is parametrized by $\sigma(t) = a \oplus bt$. Finally, we present a table, showing values of d_t calculated for various values of a and b, corresponding to various proposals, and for $x_s = 5, 10, 20$.

Table 1. Time dilution factors.

a	b	d_t		
		$x_s = 5$	10	20
0	0.15	0.35	0.135	0.025
0.11	0.10	0.45	0.16	0.017
0.13	0.15	0.31	0.085	8.2×10^{-3}
0.08	0	0.88	0.69	0.27

It should be stressed that the above were calcluated with $t_{\rm min} = 0$, which assumes that the decay can be detected without separation of vertices. For inclusive or semi-inclusive muon detection, this is unrealistic. The effect is to reduce the reach in x_s when $\sigma_t > 0$, again certainly the case with muons.

4. REFERENCES

1. H. Castro, *et al.* "A Bottom Collider Detector for the Fermilab Tevatron: a Letter of Intent for the BCD", RX-1230, Oct 1988.
2. K.T. McDonald, "Maximum-Likelihood Analysis of CP-Viloating Asymmetries", Princeton/HEP/92-04.

OBSERVABILITY OF MIXING IN PARTIALLY RECONSTRUCTED B_d AND B_s AT THE SFT

T.J. Lawry, S. Conetti, G. Corti, B. Cox, E.C. Dukes,
A.P. McManus, K. Nelson, I. Tzamouranis
Physics Dept., U. of Virginia, McCormick Rd.
Charlottesville, Va., 22901 USA

1. INTRODUCTION

Observation of mixing ($B_d \rightarrow \bar{B}_d$ and $B_s \rightarrow \bar{B}_s$) is of great physical interest. Mixing is also experimentally challenging since it requires that the beauty particle be detected, that its particle-antiparticle nature be tagged both at production and decay, and that its lifetime in the rest frame be measured with high resolution. We propose to study mixing at the SSC Fixed Target experiment[1] (SFT). In one year of running 1.6×10^{10} $B\bar{B}$ events[2] will be produced. The branching ratio $B \rightarrow lX$, where l is a charged lepton, is 21% (for the average of B_d and B_u), we assume B_s is the same. Assuming $B_u/B_d/B_s$ fractions 0.38/0.38/0.14, we get 2.0×10^8 $B_u \rightarrow lX, B_d \rightarrow lX$ events, and 7.5×10^7 $B_u \rightarrow lX, B_s \rightarrow lX$ events. Our trigger efficiency for double semi-leptonic B events[3] is 51%. We can afford to cut very hard on the data.

Because of the high vertex resolution and long flight paths of the B, the distance the B travels in the lab is well measured[4] ($L/\sigma L \approx 380$). The difficulty is to reconstruct the Lorentz $\Gamma = E_B/M_B$ since much of the energy of the B is in undetected neutral particles. We define the M_B^{vis} and E_B^{vis} to be the the invariant mass and energy of all charged daughters of the B which fall inside the spectrometer angular acceptance of 2-75 mrad. We find that $\Gamma^{vis} = E_B^{vis}/M_B^{vis}$ gives a useful estimate of the true Γ since much of the effect of missing neutrals cancels in the ratio.

2. PYTHIA SIMULATIONS

Figure 1 shows the PYTHIA simulations of M_B^{vis}/M_B (solid), and E_B^{vis}/E_B (dashed) for $B_d \rightarrow lX$ decays. Figure 2 shows Γ^{vis}/Γ with (dashed) and without (solid) a $M_B^{vis} > 4\ GeV/c^2$ mass cut. B_s decays are similar.

Figure 3 shows the lifetime distributions t^{vis}/τ computed from Γ^{vis} and the measured length of the B flight path, for $B_d \rightarrow B_d$ (solid) and $B_s \rightarrow B_s$ (dashed) decays. The experimental statistics will be about 300 times greater than that shown in Figure 3. The B_d mixing parameter is 0.72, the B_s mixing parameter is 15. We require $M_B^{vis} > 4\ GeV/c^2$ to reduce the error in the lifetime and remove background. The smooth curve is the lifetime distribution that would be measured by a perfect detector. Since it is difficult to distinguish B_d and B_s experimentally, the measured distribution would be the sum of the two histograms in Figure 3. The lifetime distributions for tagged $B_d \to \bar{B}_d$ (dashed) and $B_s \to \bar{B}_s$ (solid) are shown in Figure 4.

We can greatly reduce the statistical fluctuations shown in Figures 3 and 4 by weighting B_s, B_d decays by their probability to decay at different times. The main source of experimental error in lifetime is the error in Γ^{vis} which is due to the angular acceptance of the spectrometer. Since the distance traveled by the average B is 9 cm, the error in the lifetime is uncorrelated with the lifetime, except for very shortlived decays where vertex resolution becomes important[4]. We take the 1925 B_s, and 6858 B_d decays passing all cuts in the Monte Carlo and decay them 100 times using the true lifetime distribution in the rest frame $\exp(-t/\tau)(1 \pm \cos(xt/\tau))$ where $x = 0.72$ for B_d and 15 for B_s. For each of the 100 decays we take $t^{vis} = (\Gamma^{vis}/\Gamma)t$. In other words we take the dashed curve of Figure 3 and oversample it 100 times. Figure 5 shows the result for the sum of $B_d \to \bar{B}_d$ and $B_s \to \bar{B}_s$. The smooth curve is a simple fit to the "data", it gives $x_d = 0.72 \pm 0.05$ and $x_s = 15.4 \pm 0.22$. Since the B_s and B_d decays dominate at short and long lifetimes respectively, it is easy to extract the mixing parameters.

3. SAMPLE SIZE

The trigger efficiency for double semi-leptonic B events is 51%. From PYTHIA, 3.74% of B_d pass the 4 GeV/c^2 mass cut, as do 5.19% of the B_s. We also require that the B_u have $M > 2$ GeV/c^2 (54.1% pass this cut). The acceptance for $B_u B_d$ events is 1.03% (2.0×10^6 events) and the $B_u B_s$ events have 1.43% acceptance (1.1×10^6 events).

We conclude that mixing can be studied at the SFT with B mesons whose decays are not fully reconstructed, allowing very high statistics studies to be done.

4. REFERENCES

1. B. Cox et al. "The SFT: A Super Fixed Target Beauty Experiment at the SSC," these proceedings.
2. Ibid., Section 4.
3. Ibid., Table 14.
4. Ibid., Table 4 and following.

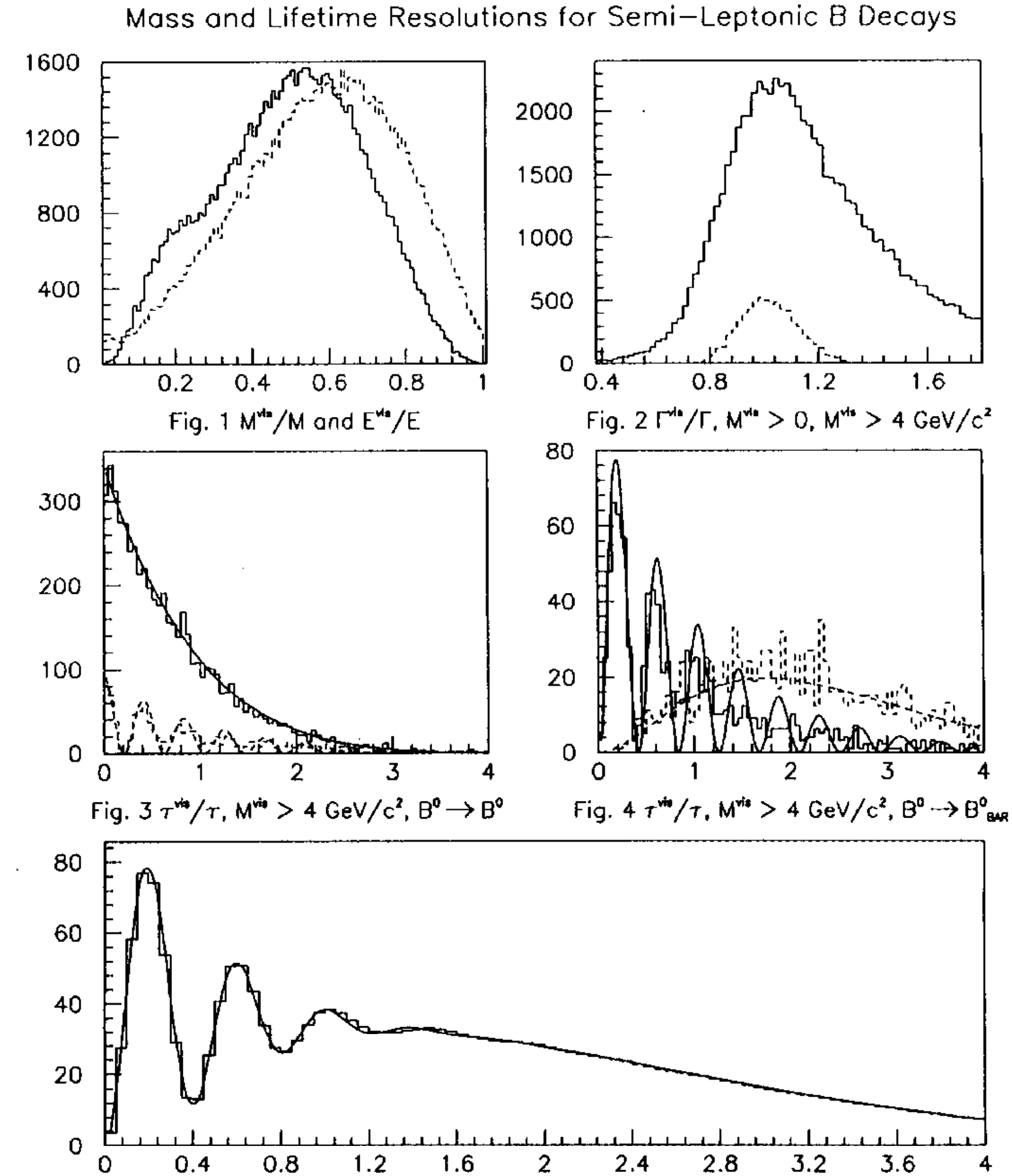

Fig. 1 M^{vis}/M and E^{vis}/E

Fig. 2 Γ^{vis}/Γ, $M^{vis} > 0$, $M^{vis} > 4$ GeV/c^2

Fig. 3 τ^{vis}/τ, $M^{vis} > 4$ GeV/c^2, $B^0 \to B^0$

Fig. 4 τ^{vis}/τ, $M^{vis} > 4$ GeV/c^2, $B^0 \to B^0_{BAR}$

Fig. 5 As Fig. 4, Oversampled, Fit for X_d, X_s

Prospects for $B_s^0\overline{B_s^0}$ Oscillation Measurement at LEP

XinChou Lou
Dept. of Physics, Indiana University
Bloomington, Indiana 47408, USA
and
PPE Division, CERN
Geneva, Switzerland

1 Introduction

The measurements of $B_d^0\overline{B_d^0}$ mixing [1] have provided direct constraint on the CKM matrix element $|V_{td}|$. Similarly, it is generally expected that a measurement of $B_s^0\overline{B_s^0}$ mixing will put strict constraint on $|V_{ts}|$ [2] and the CKM unitary triangles. However data on average neutral B meson mixing at high energy e^+e^- and hadron colliders indicate a rapid $B_s^0\overline{B_s^0}$ oscillation. Therefore with knowledge of the time integrated $B_s^0\overline{B_s^0}$ mixing alone it is not sufficient to extract $|V_{ts}|$. The time dependent $B_s^0\overline{B_s^0}$ mixing must be directly measured.

Direct observations of the decays of the B_s meson, the measurements of its lifetime and mass have been recently reported [3, 4, 5, 6, 7]. At LEP the B_s meson can be effectively tagged via its semileptonic decays. The electric charge of a primary lepton tells if the decaying b meson is a B_s^0 or $\overline{B_s^0}$. Various techniques that identify the b quark flavour at B_s^0 production time (t=0) are being developed. The installations of silicon microvertex detectors at all the four LEP experiments allow for precise determination of the B_s^0 decay vertex and subsequently the reconstruction of the B_s^0 decay proper time. All these make it possible for the LEP experiments to study the $B_s^0\overline{B_s^0}$ oscillation in the near future.

The following sections describe the methods of B_s tagging at LEP, the techniques of b flavour (t=0) identification and the reconstruction of B_s^0 decay proper time. Finally a Monte Carlo study is presented on the sensitivity of the x_s measurement at LEP assuming a total of $4\cdot10^6$ hadronic Z^0 events will be collected per LEP detector at the end of LEP1.

2 Tagging the B_s^0 Meson at LEP

At LEP only a handful of exclusive B_s decays have been reconstructed [4, 7]. It is apparent that the exclusive Bs events will be statistically limited for a $B_s^0\overline{B_s^0}$ mixing measurement. The semileptonic B_s^0 decays $B_s^0 \to D_s^- \ell^+ X$ have been detected in numbers much larger than those of the exclusive B_s^0 events. A typical signal-to-noise of 2:1 is seen in the LEP data in these channels. Furthermore the presence of the s quark in the B_s^0 meson should result in abundant ϕ meson production in its decays. A preliminary study in OPAL* shows that about 70% of the $\phi\ell^{\pm}$ pairs detected in Z^0 decays are the decay products of the B_s^0. The background $\phi\ell^{\pm}$ events arise predominantly from fragmentation ϕ's combining with a primary lepton from b hadron decays. The $\phi\ell^{\pm}$ reconstructed in OPAL appears to have a typical signal-to-noise of 1.6:1.

Other B_s^0 tagging methods are also under consideration at LEP. The inclusive D_s^- events, for example, would provide a larger B_s^0 sample with a typical B_s^0 purity of 50% [4]. However the process $W^+ \rightarrow \bar{s}c$, which results in a D_s^+ in b hadron decays, competes with the spectator diagram $B_s^0 \rightarrow D_s^- X$. Therefore the electric charge of the D_s meson does not invariably give the b flavour of the decaying B_s^0. Moreover the proper time resolution for the D_s tagged events is expected to be considerably worse than that of the semileptonic B_s^0 events. Nevertheless the D_s decays seems to be a promising B_s^0 tagging method if the above two problems can be overcome.

Table 1. Branching Ratios Used [1].

Decay Process	Branching Ratios
$B_s^0 \rightarrow D_s^- \ell^+ X^{(1)}$	$\sim$0.22
$D_s^- \rightarrow \phi\pi^-, \phi \rightarrow K^+K^-$	$(1.39 \pm 0.35) \cdot 10^{-2}$
$D_s^- \rightarrow K^{0*}K^-, K^{0*} \rightarrow K^+\pi^-$	$(1.73 \pm 0.33) \cdot 10^{-2}$
$D_s^- \rightarrow \phi X^{(1)}$	$\sim$0.30
$\phi \rightarrow K^+K^-$	0.491 ± 0.008
$B_s^0 \rightarrow D_s^- \ell^+ X, D_s^- \rightarrow \phi\pi^-, K^{0*}K^-$	$(6.9 \pm 1.1) \cdot 10^{-3}$
$B_s^0 \rightarrow \phi\ell^+ X, \phi \rightarrow K^+K^-$	$\sim 3.2 \cdot 10^{-2}$

(1) Measurements do not exist; assumed values. ℓ = e + μ where applicable.

Based on a simulation of the OPAL detector, the detection efficiencies for the visible final states are found to be 0.09 for $B_s^0 \rightarrow D_s^- \ell^+ X$ and $D_s^- \rightarrow K^-K^-\pi^-$, and 0.10 for $B_s^0 \rightarrow \phi\ell^+ X$ and $\phi \rightarrow K^+K^-$. Using the branching ratios listed in Table 1. a sample of $\sim$130 $B_s^0 \rightarrow D_s^- \ell^+ X$ and $\sim$660 $\phi\ell^{\pm}$ events are expected to be reconstructed from $4 \cdot 10^6$ hadronic Z^0 decays.

3 Identification of b Flavour of the B_s^0 at t=0

Three techniques, which have been investigated at LEP, will be described in this section. They are *opposite jet lepton tag*, the *fragmentation charged kaon tag* and the *jet charge method.*

The b hadron and anti-b hadron produced in Z^0 decays are well separated topologically due to large mass of the Z^0. Having reconstructed a B_s^0, the jet opposite to the B_s^0 containing jet is very likely to be associated with an anti-b hadron. The charges of prompt leptons (e, μ), characterised by their large momentum and large momentum component transverse to the jet, provide information on the b flavour (t=0) of the reconstructed B_s^0 meson. Experimentally the correctness of this tag is diluted by fake leptons and a 12% average b hadron mixing found in Z^0 decays[8]. Monte Carlo simulations show that typically a tagging efficiency of 4-5% with 75% correctness can be achieved using the opposite jet lepton tag.

During the hadronisation process of the $\bar{b}$ quark, a s quark must be produced in order to form a B_s^0 meson. The $\bar{s}$ quark, which is also produced in pair with the s quark, would form a strange meson. The electric charge of this kaon (if charged) or of the charged kaon produced in the decays of this strange meson should be the same as that of the $\bar{b}$ quark. The fragmentation kaon tag is based on the identification of these charged kaons in the B_s^0 events. By relying on the dE/dx measurements in the OPAL experiment at LEP, a Monte Carlo study shows that this method can identify about 20% of the reconstructed semileptonic B_s^0 decays for which either the D_s^+ or a ϕ have been fully reconstructed. The corresponding correctness of this tag is about 75%.

The jet charge is defined as [9]

$$Q_{jet} = \frac{1}{E_{beam}^{\kappa}} \cdot \sum_{i=1}^{n} q_i \cdot (p_i)^{\kappa} \qquad (1)$$

where E_{beam} is the beam energy, q_i and p_i are the charge and momentum of track i, and κ is a weighting factor. The sum runs over all charged tracks associated to the same jet, except for those from B_s^0 decays. The value of κ is chosen to be 0 for tracks in the B_s^0 containing jet, and 1 for tracks in the non-B_s^0 jets. This choice of κ enhances the correlation between the jet charge and the b flavour of the decaying b hadron opposite to the B_s^0 jet, with which an average mixing of only 12% is found. Meanwhile the jet charge of the B_s^0 jet, which is actually the sum of the charge of fragmentation tracks since the B_s^0 is neutral, anti-correlates with the b flavour (t=0) of the B_s^0. The following criteria is used in OPAL

$$|Q_{jet}(B_s) - 10 \cdot Q_{jet}(opp)| > 1.0 \qquad (2)$$

where $Q_{jet}(B_s)$ and $Q_{jet}(opp)$ are the jet charges of the B_s^0 jet and of the most energetic non-B_s^0 jet, respectively. This criteria combines the jet charge information from both the B_s^0 jet and the jet containing the other b hadron to maximise the b flavour (t=0) identification power. About 70% of the B_s^0 events pass this criteria. The corresponding correctness of the b flavour (t=0) identification is found to be 75%, with little dependence on the jet finding algorithm and the $B_s^0\bar{B}_s^0$ mixing parameter.

4 Proper Time Reconstruction

The B_s^0 decay proper time, t_p, can be expressed as

$$t_p = dl/(c\beta\gamma) \qquad (3)$$

*The main cuts are: p_k >2 GeV, p^{ℓ} >3 GeV, p_T^{ℓ} > 1 GeV and 2.0< $M(\phi\ell)$ <5.0 GeV. $K^{\pm}$ are selected with the dE/dx measurements in the OPAL jet chamber.

where dl is the 3-d decay length of the B_s^0, $\beta\gamma$ is the Lorentz boost of the B_s^0. We need to measure dl and $\beta\gamma$ in order to reconstruct t_p. The 2-d decay length of B_s^0 can be measured in the plane transverse to the beam direction by all the LEP detectors with the high precision silicon microvertex detector. This 2-d decay length can be converted into dl by using the direction cosines of the reconstructed B_s^0. By requiring the 2-d decay length error to be less than 1 mm, an average 250 μm error on the decay length can be achieved. The estimation of γ has been demonstrated in ref. [5] by OPAL, by paramtrising γ as a function of the momentum and the invariant mass of the $D_s^+\ell^-$ pair. The typical uncertainties range from 15.7% at low momentum and low mass region to 6.4% at high momentum and high mass region, resulting an average boost error of 12%.

The uncertainty on t_p arise from dl and γ

$$\sigma_t^2 = \left(\frac{t_p\sigma_{dl}}{dl}\right)^2 + \left(\frac{t_p\sigma_\gamma}{\gamma}\right)^2 \tag{4}$$

where σ_t, σ_{dl} and σ_γ are the r.m.s errors on the proper time, B_s^0 decay length and the boost, respectively. Depending on the track quality and kinematic cuts applied, an average σ_t/t of 16% to 20% can be achieved at LEP.

5 Sensitivity of the x_s Measurement

In Table 2. quantities relevant to the $B_s^0\overline{B_s^0}$ mixing measurement at LEP are summarised. Notably the b flavour (t=0) mistag probability is typically 25%; and most B_s^0 events selected can be used for the oscillation measurement.

In order to understand the sensitivity of a x_s measurement at LEP1, simple Monte Carlo simulations were performed, assuming 700 B_s^0, $\overline{B_s^0}$ decays are reconstructed with an overall signal-to-noise ratio of 1.1:1. The b flavour (t=0) mistag is taken to be 0.25. The smearing due to B_s^0 decay length error, $\frac{t_p\sigma_{dl}}{dl}$, is assumed to be 0.10, and the proper time uncertainty from the boost estimate is parametrized as $0.14\cdot t_p$. The proper time is smeared as described by eq. (4).

In Figures 1.a-b the generated proper time and the reconstructed proper time of oscillated B_s^0 events are shown. Figure 1.c is shown with a b flavour (t=0) mistag of 0.25. Finally in Figure 1.d the background, for which a 'proper time' of 1.3 ps is assumed, is included. A fit to Figure 1.d yields x_s=3.9±0.3, compared with the generated value x_s=4.0.

In Table 3. the results of the Monte Carlo simulation are summarised. For a given x_s value (up to x_s=10) a total of 30 simulations were carried out, each with a fit to a different 700 B_s^0, $\overline{B_s^0}$ decay sample. The mean x_s fitted, x_s^{fit}, and the mean variance, $< |x_s^{fit} - < x_s^{fit} > | >$, were calculated based on 30 fits to the proper time distributions equivalent to Figure 1.d for each generated x_s.

Table 2. $B_s^0\overline{B_s^0}$ Oscillation Measurement at LEP

Experiment	OPAL at LEP
C. M. energy (TeV)	0.09 (M_z)
Assumed luminosity ($cm^{-2}s^{-1}$)	$1.3\cdot10^{31}$
Assumed $\sigma_{b\bar{b}}$	maximum 6.5(1) nb
Assumed B_s^0 fraction (per b quark)	0.12
Flavour (decay time) tag	$B_s^0 \to D_s^-\ell^+X$, $B_s^0 \to \phi\ell^+X$
Flavour (t=0) tag	lepton charge, fragmentation $K^\pm$, jet charge
B.R. of B_s^0 modes	$\sim(6.9\pm1.1)\cdot10^{-3}$, $\sim3.2\cdot10^{-2}$
B_s^0 reconstruction efficiency	0.09, 0.10
Number of B_s^0 reconstructed	130 $D_s^-\ell^+$, 660 $\phi\ell^\pm$
B_s^0 signal-to-noise ratio	2:1, 1.6:1
Efficiency of flavor (t=0) tag	0.05, 0.20 , 0.70
Overall mistag (t=0) probability	25%, 25%, 25%
$t_p\cdot\sigma_{dl}/dl$	~10 - 15 %
$\sigma_{(\beta\gamma)}/(\beta\gamma)$	~12 -15 %

(1) Value at the Z^0 peak. In LEP operation the actual corss-section is lower due to energy scan.

Table 3. x_s Sensitivity at LEP

x_s generated	$< x_s^{fit} >$	$< \|x_s^{fit} - < x_s^{fit} > \| >$	Comments
1.0	0.95	0.10	all good fits
2.0	2.13	0.14	all good fits
3.0	3.14	0.23	all good fits
4.0	4.00	0.33	all good fits
5.0	4.97	0.33	all good fits
6.0	5.85	0.30	all good fits
7.0	6.97	0.42	all good fits
8.0	8.16	0.72	all good fits
9.0	8.81	0.54	~10% fits unstable
10.0	10.35	0.80	~20% fits unstable

The $B_s^0\overline{B_s^0}$ oscillation can be reliably measured for 8.0< x_s, as shown in Table 3. The 8.0< x_s < 10 region should be measurable by combining results from all four LEP experiments to eliminate bad fits. A set of larger decay length error and boost estimation error* have also been used in the Monte Carlo study, resulting in a slightly worse sensitivity on x_s.

6 Summary

The possibility of measuring $B_s^0\overline{B_s^0}$ oscillation at LEP is investigated in this paper. Various techniques of B_s^0 tagging and b flavour (t=0) identification have been developed by the LEP

*Assuming $\frac{t_p\sigma_{dl}}{dl}$=0.12 and $\frac{\sigma_\gamma}{\gamma}$=0.15.

experiments. The successful comissioning of high precision silicon microvertex detectors at LEP allow for precise determination of the B_s^0 decay vertex. With the estimate of the B_s^0 boost, it is possible to search for $B_s^0\overline{B_s^0}$ oscillation directly in Z^0 decays. Assuming that $4 \cdot 10^6$ Z^0 events will be collected per LEP detector by the end of LEP1, the 8.0< x_s region can be explored. With significant improvements in the B_s^0 decay proper time measurement, LEP experiments potentially can measure x_s upto 10. However beyond x_s=10 it will be very difficulty for LEP to extract x_s based on semileptonic B_s^0 events. The exclusive B_s^0 decay sample, which will be statistically limited due to small decay branching ratios, is unlikely to offer a better solution in the $x_s > 10$ region.

References

[1] Particle Data Group, K. Hikasa *et al.*, Phys. Rev. **D 45** (1992) 1.

[2] See for example:
P. J. Franzini, Phys. Rep. **173** (1989) 1; and
A. Ali, in Proceedings of the XXVI International Conf. on High Energy Physics, August 6-12, 1993, Dallas, USA.

[3] ALEPH Collab., D. Buskulic *et al.*, CERN-PPE/92-73, submitted to Phys. Lett.;
DELPHI Collab., P. Abreu *et al.*, CERN-PPE/92-104, submitted to Phys. Lett.

[4] OPAL Collab., P. D. Acton *et al.*, Phys. Lett. **B 295** (1992) 357.

[5] OPAL Collab., P. D. Acton *et al.*, Phys. Lett. **B 312** (1993) 501.

[6] See talk by V. Scarpine, in *Heavy Flavours*, Sept. 3-7, 1993, Pavia, Italy.

[7] See summary talk by M. Cattneo, in *Heavy Flavours*, Sept. 3-7, 1993, Pavia, Italy.

[8] See summary talk by F. Ligabue in *Heavy Flavours*, Sept. 3-7, 1993, Pavia, Italy.

[9] S. Tarem, private communication.

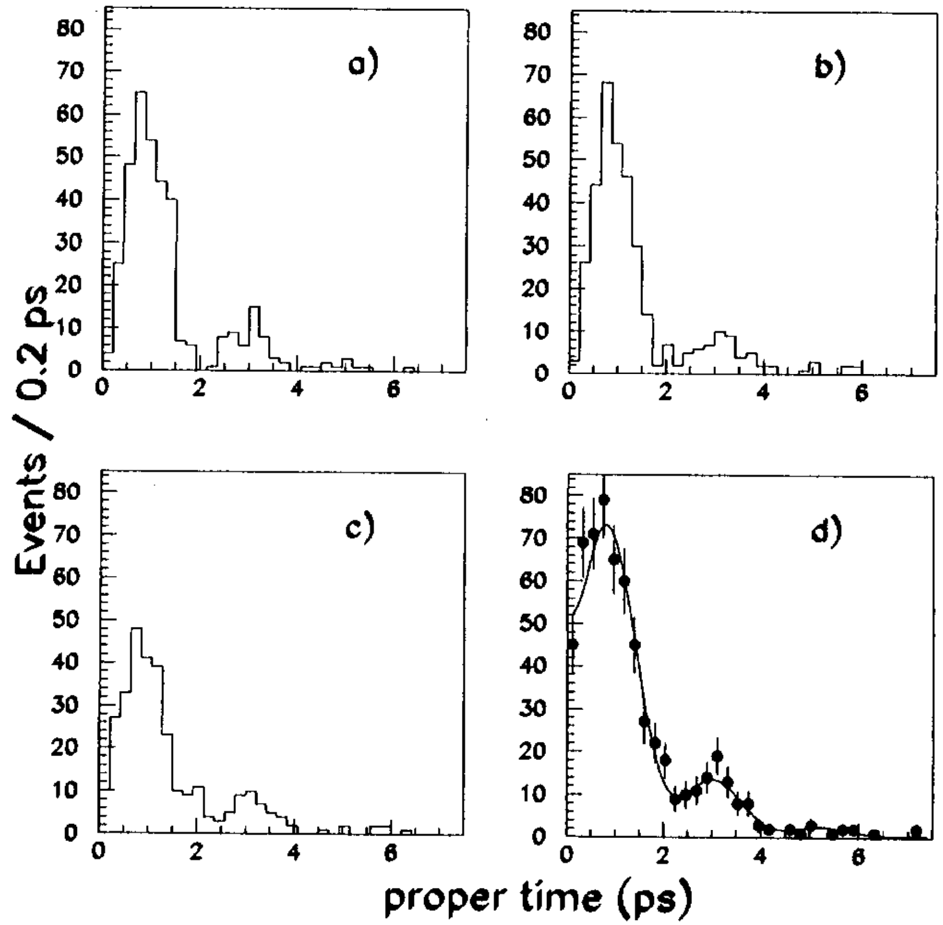

Figure 1: The B_s proper time distributions of oscillated B_s^0 events:
a) where proper times are the true, generated time values;
b) where the proper time has been smeared;
c) after a b flavour (t=0) mistag of 25% has been added to b);
d) after a signal-to-noise of 1.1:1 has been taken into account.
A B_s^0 lifetime of 1.3 ps has been used in the simulation. The 'proper time' of the background has been assumed to follow a smeared lifetime distribution of τ=1.3 ps. The generated x_s value is 4.0. The x_s fitted is 3.9±0.3 (stat. only).

$B-\overline{B}$ MIXING IN SLD

C.BALTAY
Representing the SLD Collaboration

Physics Department, Yale University,
Box 6666, 554 Gibbs Laboratory,
New Haven, CT 06511, USA

The mixing of B^0 and $\overline{B^0}$ is one of the most important topics in B physics because the mixing occurs through second order weak box diagrams involving t to d and t to s quark transitions. The mixing parameters are thus sensitive to the CKM matrix elements V_{td} and V_{ts} which are presently difficult to access experimentally in other ways.

Mixing in the B_d^0 system has been observed in the ARGUS, CLEO and UA1 detectors. They measured the mixing integrated over time

$$\chi_d = \frac{mixed}{mixed + unmixed} = (\frac{1}{2})\frac{x_d^2}{1+(x_d)^2}, \tag{1}$$

and obtained a value of $x_d \sim 0.7$ where x_d is defined as Δ/Γ in the B_d^0 system. Since V_{ts} is expected to be larger than V_{td}, we expect the mixing to be substantially larger in the B_s^0 system. In this case, $\chi_s \to \frac{1}{2}$ and a time integrated mixing measurement is not very sensitive to x_s. It is thus imperative to measure the time dependence of B_s^0 mixing which is proportional to $\cos(x_s t)$ and is thus sensitive to x_s in the expected range of values. At this time there is a preliminary measurement from ALEPH of the time dependence of B_d^0 mixing, but there are no measurements of the time dependence of B_s^0 mixing. Such a measurement is one of the aims of an extended SLD program.

To observe $B^0 - \overline{B^0}$ mixing one has to establish the $B/\overline{B}$ character of the meson both at production and at the decay point. The usual technique used so far has been to look for a high P_t lepton to tag both of the B mesons produced in each event. In this method the lepton efficiency, which is of the order of 5%, comes in squared, and a prohibitively large sample of B_s^0 would be required for a precision measurement.

The availability of highly polarized electrons from SLC allows SLD to use a much more efficient method in which the large forward-backward asymmetry for $e^+e^- \to b + \bar{b}$, which can be written as

$$A_{FB}^{b\bar{b}} = \frac{(B^0 forward) - (\overline{B^0} forward)}{(B^0 forward) + (\overline{B^0} forward)}, \tag{2}$$

is used to tag the $B/\overline{B}$ character of each B_s^0 at production in a statistical way. For incident electrons with 70% polarization the polarization improved asymmetry is

$$\tilde{A}_{FB}^{b\bar{b}} \simeq 50\%, \tag{3}$$

Thus the forward going meson has a 75% probability of being a B^0 rather than a $\overline{B^0}$, (if the detector had full angular acceptance).

There are several methods to tag the B at the decay point. In the detailed study carried out for this paper we have used a high P_t lepton tag. The high P_t lepton (electron or muon) selects the $b\bar{b}$ events from a background of lighter quarks, and the sign of the lepton establishes the $B^0/\overline{B^0}$ character at decay. The B branching ratio into leptons times the lepton detection efficiency times the probability of passing the $P_t \geq 1GeV$ cut gives a net lepton tag efficiency of around 6% (this efficiency includes the angular acceptance of the upgraded vertex detector planned for SLD).

The B^0 decay point can be reconstructed by intersecting the high P_t lepton with the B jet axis. An improvement in the B^0 decay length precision can be obtained by reconstructing the D produced in the B decay by finding the D decay vertex with at least two outgoing charged tracks. The high quality vertex detection capability of SLD is crucial for this purpose. Our simulations indicate that the efficiency of reconstructing a reliable B decay length with the upgraded vertex detector is about 50%. The resolution in the B decay length is about $150\mu m$, with substantial tails.

To calculate the proper B^0 decay time from the measured decay length we need to know the B^0 momentum. Since we are using B's tagged by a high P_t e or μ, there is some momentum carried off by invisible $\nu's$. We thus estimate the B^0 momentum by using energy conservation in the overall $e^+e^- \to B + \overline{B} + x$ process, the thrust axis, and a correction in each hemisphere for the charged and neutral eneryg tracks coming from the primary vertex. The resolution obtained for the B^0 momentum is around 10%, but with substantial non-Gaussian tails.

To estimate the total number of B decays we use the measured branching ratio

$$\frac{Z \to b\bar{b}}{Z \to hadrons} = 22\% \tag{4}$$

Thus in a sample of 10^6 hadronic Z decays we expect 220,000 $b\bar{b}$ pairs or 440,000 b or $\bar{b}$ (with our method of using the A_{FB} to tag B's, each b or $\bar{b}$ provides a separate independent measurement). We make the usually accepted assumption that $b\bar{b}$ pairs produce baryons, $B^{\pm}$, B_d^0, and B_s^0 with relative frequencies of 9%, 38%, 38%, and 15%, respectively. We then use the event selection efficiencies discussed above to arrive at the expected data sample of B decays, as shown in Table VIII.

Table VIII

Numbers of Tagged B decays in a 10^6 Z sample.

	Fract.	No. Produced	Lepton Tagged		Lifetime Measured	
			VXD2	VXD3	VXD2	VXD3
B baryons	9%	40,000	2,000	2,400	500	1,200
$B^{\pm}$	38%	167,000	8,400	10,000	2,150	5,000
B_d^0	38%	167,000	8,400	10,000	2,150	5,000
B_s^0	15%	66,000	3,300	4,000	900	2,000
Totals	100%	440,000	22,000	26,400	5,700	13,200

The method of analysis using this data sample is to plot the forward backward asymmetry using the $B^0/\overline{B^0}$ character of the B's at decay time versus the proper decay time. This A_{FB} will oscillate with a $cos(x_s t)$ dependence (for example at the decay time when all B^0 have oscillated to $\overline{B^0}$, the measured A_{FB} will have the opposite sign from the A_{FB} at production). We can thus measure x_s by fitting the frequency of oscillation of A_{FB}.

In the present simulation we did not attempt to separate the B_s from the other b hadrons shown in Table VIII but have fitted A_{FB} versus proper time for the combined sample. This works because A_{FB} will not oscillate for the baryons or the charged $B^{\pm}$, and B_s^0 is expected to oscillate at a much higher frequency than B_d^0.

A detailed Monte Carlo simulation of this data sample, using $x_d = 0.7$ and taking $x_s = 7.0$, is shown in Figure 1. The higher frequency B_s^0 oscillation is clearly apparent over the lower frequency B_d^0 oscillation and the constant $B^{\pm}$ and baryon background. The χ^2 fit versus x_s is shown for this sample in Figure 2, with a clear minimum near $x_s = 7$. We have simulated 1000 experiments with 10^6 Z's each, and plot the x_s obtained in each experiment (i.e. the x_s with the minimum χ^2) in Figure 3. We see that we can expect a measurement of x_s with a precision of better than 10% with such a data sample.

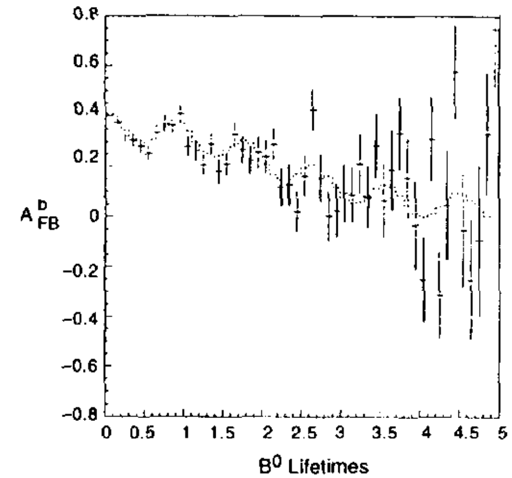

Figure 1. Monte Carlo simulation of A_{FB} vs. the B proper decay time τ_B for the combined data sample described in Table 1.

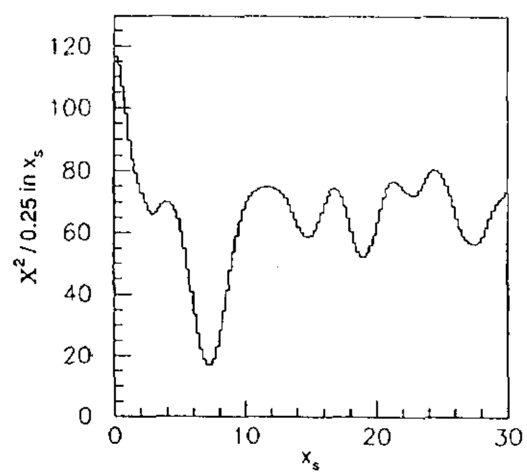

Figure 2. χ^2 fit vs. x_s for the data sample in Figure 1.

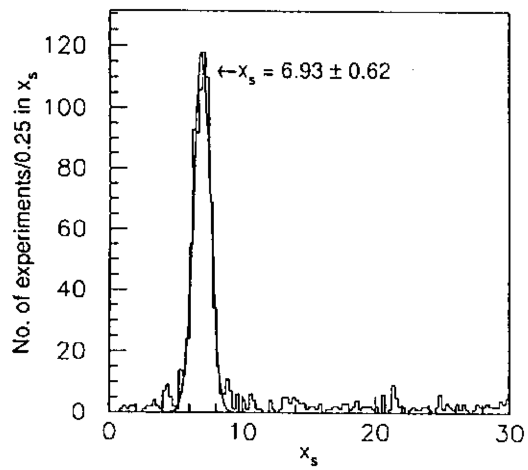

Figure 3. Best fit for x_s in a simulation of 1000 experiments with 10^6 Z's each.

A more efficient way to utilize the data is to do a maximum likelihood analysis. The probability of each event is evaluated, with its particular value of B^0 direction ($cos\theta$), proper lifetime with its error, , electron beam polarization, and sign of charge of the high p_t lepton. The best value of x_s is the one for which the likelihood of getting the entire event sample is a maximum. The significance of the result is taken to be the number of standard deviations by which the B_s^0 fraction for the fit with the best value of x_s differs from no B_s^0 at all. The results of such an analysis is shown in Figure 4 with different values of x_s as input to the Monte Carlo.

As x_s gets larger, it becomes more difficult to resolve the higher frequency oscillations with our resolution in the proper decay time. The estimated significance of resolving the B_s^0 oscillations as a function of x_s are shown in Figure 4. We see from this figure that SLD should be able to make a significant measurement up to for an interesting range of $x_s \sim 15$.

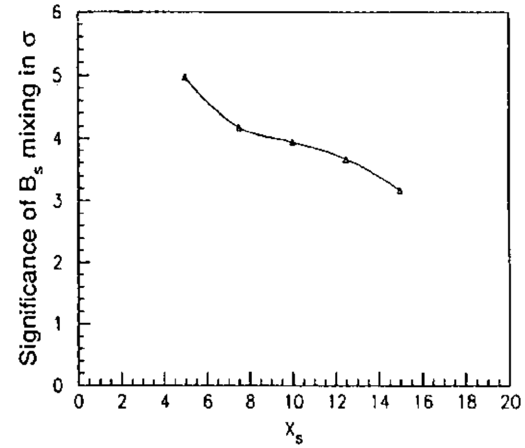

Figure 4. The significance of resolving the B_s^0 oscillations for different values of x_s, with the proposed improved vertex detector.

The importance of $B^0 - \overline{B^0}$ mixing, comes from the sensitivity to certain CKM matrix elements which are difficult to access by other measurements at this time. The mixing is believed to proceed via second order weak box diagrams as show in Figure 5.

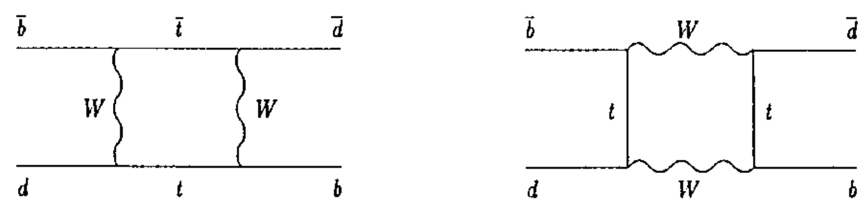

Figure 5. The box diagrams relevant in $B^0 - \overline{B^0}$ mixing.

The mixing parameter x for B_d^0 and B_s^0 mixing can be written as

$$x_{d,s} \equiv (\frac{\Delta m}{\Gamma})_{d,s} = \frac{G_F^2}{6\pi^2}|V_{tb}V_{td,s}|^2 m_t^2 m_B \tau_B B f_B^2 F^2 \eta, \qquad (5)$$

where Δm is the $B_1 - B_2$ mass difference (in analogy with the neutral K system), B is the so called Bag Model Constant, f_B is the weak decay constant, and F^2 and η are QCD correction factors, and the other symbols have their usual meanings.

We believe that a precise measurement of the ratio of the B_s to B_d mixing parameters has a good probability of fully determining the CKM unitarity triangle. The unitarity triangle can be written as

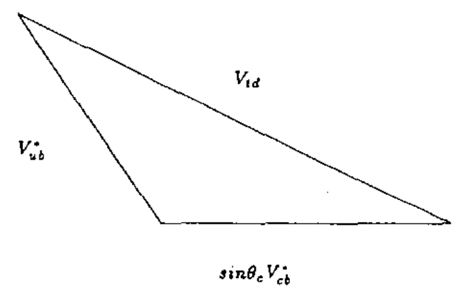

B_d^0 mixing is sensitive to V_{td} (see Equation 5). However, the precision in this measurement of V_{td} is limited to about 40% because of the uncertainty in the theoretical knowledge of the Bf_B^2 factors in Equation 5 relating V_{td} to X_s. The lack of knowledge of the top mass, which comes in squared in Equation 5, makes things even worse. Thus even a very precise measurement of B_d^0 mixing will not define the unitarity triangle very well.

To see how to use the measurement of B_s^0 mixing to learn about the unitarity triangle*, we rewrite the triangle by dividing all three sides by V_{cb} (which can be taken to be real by convention). In addition, we make use of the observation that $V_{cb} = V_{ts}$ to an accuracy of better than a few percent to write $V_{td}/V_{cb} = V_{td}/V_{ts}$. The triangle thus becomes

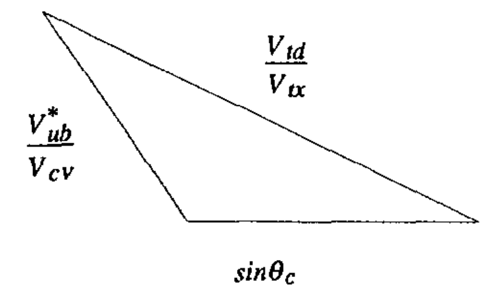

The lower side, the sine of the Cabibbo angle, is very well known. We expect that $\frac{V_{ub}}{V_{cb}}$ will be known to an accuracy of $\sim 15\%$ or better from measurements of ratios of B decays to u and c quarks at CLEO.

The ratio $\frac{V_{td}}{V_{ts}}$ can be obtained from the ratio of B_d^0 to B_s^0 mixing parameters. From Equation 5 we see that

$$\frac{x_d}{x_s} = (\frac{V_{td}}{V_{ts}})^2 \times R \qquad (6)$$

where R is the ratio of the other factors

$$R = (\frac{M_{Bd}}{M_{B_s}})(\frac{\tau_{Bd}}{\tau_{B_s}})(\frac{B_d f_{Bd}^2}{B_s f_{B_s}^2}) \qquad (7)$$

While the individual quantities $B_{d,s}$, $f_{d,s}$ are not very well known, their ratio can be estimated to an accuracy of about 10%. We should thus be able to measure the $\frac{V_{td}}{V_{ts}}$ ratio with an accuracy of 10%. Since a knowledge of the length of the three sides of a triangle fully determine the triangle, such a measurement would

* We thank J.D. Bjorken for an interesting discussion on this point.

dramatically improve our knowledge of the unitarity triangle, as illustrated in Figure 6. A nonvanishing area of this triangle leads to CP violating effects. Thus a determination of the triangle will give a measure of the size of CP violations in

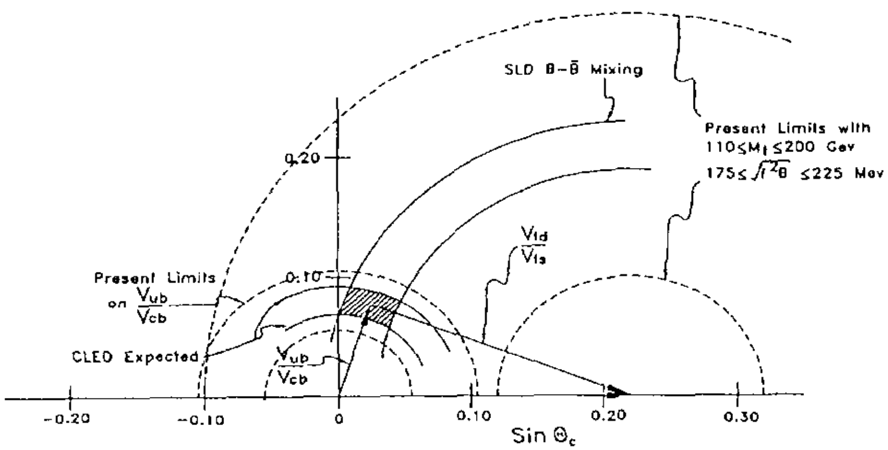

Figure 6. Determination of the CKM matrix Unitarity triangle with a 10% measurement of ratio of the B_s to B_d mixing parameters.

MEASUREMENT OF $B^\circ - \bar{B}^\circ$MIXING USING DIMUONS AT DØ

KEN JOHNS
Physics Department, University of Arizona
Tucson, AZ 85721

1. INTRODUCTION

During the 1992-1993 collider run at the Fermilab Tevatron, the DØ detector was commissioned and collected 16.1 pb^{-1} of data which focused on high p_T physics such as top searches and electroweak measurements. The B physics accessible in the first run of DØ includes single, dimuon, and J/ψ production cross section measurements over a wide range of rapidity and the measurement of the combined $B^\circ - \bar{B}^\circ$ mixing probability χ.

Mixing between B° and its anti-particle can occur in the Standard Model via well-known box diagrams. The time averaged mixing probability χ is given in terms of the mixing parameter x as

$$\chi = \frac{P(B^\circ \to \bar{B}^\circ)}{P(B^\circ \to B^\circ) + P(B^\circ \to \bar{B}^\circ)} \approx \frac{x^2}{2+2x^2}, \tag{1}$$

where x is the mass difference of the mass eigenstates divided by their average decay width. Note if $\tau_{decay} >> \tau_{mix}$ then $x >> 1$ and $\chi \to 1/2$.

The mixing parameters x_d and x_s are of interest because they can be written in terms of parameters of the Standard Model

$$x_q = \frac{G_F^2}{6\pi^2} f_{Bq}^2 B_{Bq} m_{Bq} \tau_{Bq} m_t^2 \frac{A(z)}{z} \eta_q^{QCD} |V_{tq} V_{tb}^*|^2, \tag{2}$$

for q = d or s quark and where $f_{Bq}^2 B_{Bq}$ is a calculable constant and $z = \frac{m_t^2}{m_W^2}$. In particular, x_d and x_s depend on the CKM matrix elements V_{td} and V_{ts}. An accurate measurement of χ (or χ_s) can be used to set a lower limit on x_s and thus help constrain elements of the CKM matrix.

For the semileptonic decay of B mesons into muons, the combined mixing probability χ is defined as

$$\chi = \frac{BR(b \to B^0 \to \bar{B}^0 \to \mu^+)}{BR(b \to \mu^\pm)}, \tag{3}$$

which is an average over both B_d° and B_s° mesons which can mix as well as charged B mesons which can not. The b or $\bar{b}$ can be tagged by the sign of the muon from the semi-leptonic decay of the B.

The semileptonic decay of a $B^\circ\bar{B}^\circ$ pair into muons (direct decay) will give rise to unlike sign dimuons. Flavor mixing of a B° or $\bar{B}^\circ$ will result in like sign dimuons. Like sign dimuons can also be produced by secondary decays in which one muon comes from the decay $b \to \mu$ while the other comes from the decay $b \to c \to \mu$. In the presence of mixing the

Process	Type	Like Sign	Unlike Sign
P1	$b \to \mu^-, \bar{b} \to \mu^+$	$2\chi(1-\chi)$	$(1-\chi)^2+\chi^2$
P2	$b \to \mu^-, \bar{b} \to \bar{c} \to \mu^-$	$(1-\chi)^2+\chi^2$	$2\chi(1-\chi)$
P3	$b \to c \to \mu^+, \bar{b} \to \bar{c} \to \mu^-$	$2\chi(1-\chi)$	$(1-\chi)^2+\chi^2$
P4	$b \to c\mu^-, c \to \mu^+$	0%	100%
P5	$c \to \mu^+, \bar{c} \to \mu^-$	0%	100%
P6	Drell-Yan, J/ψ, Υ	0%	100%
P7	decay background	50%	50%

Table 1: Fraction of like and unlike sign dimuons from contributing processes

fraction of like and unlike sign dimuons for various processes producing dimuons is given in Table 1.

Experimentally, one measures the ratio R of like to unlike sign dimuons. The data analysis for the measurement of R is discussed in Section 3. In order to extract χ from R it is necessary to model the relative contributions of all processes contributing to dimuon production (see Table 1). Our Monte Carlo modeling of these processes is described in Section 4. Once the relative fractions of the contributing processes are known, χ can be extracted from R as the solution to a quadratic equation.

2. THE DØ DETECTOR

The DØ detector consists of inner tracking and transition radiation detectors, a uranium-liquid argon calorimeter, and an extensive muon detection system. Details of the DØ detector and its performance are given in reference [1]. This measurement emphasizes muon detection thus a few relevent highlights of the muon system are included here.

The muon system consists of 5 iron toroids plus 3 layers of 10cm wide proportional drift tubes. A small angle muon system consisting of 3cm wide proportional tubes extends the η coverage of the muon system to $|\eta| < 3.3$. The signed momentum of the muon is measured by its bend in the toroid and multiple scattering thus limits the momentum resolution to be $\geq 18\%$. The thickness of the calorimeter plus iron is 14-18 λ. This implies a very small punchthrough probability (10^{-4}) and also permits good muon identification within a jet.

Each drift cell in the muon system provides a latch bit indicating whether or not it was hit for each beam crossing. The Level 1 muon trigger is a hardware trigger which uses these bits to look for muon hits in 60cm wide roads and requires at least 2 hits per layer in 2 or 3 layers, depending upon the detector geometry. The Level 2 muon trigger is a software trigger which uses code similar to that used in offline muon reconstruction. For this analysis the trigger requirement was two Level 1 muons and two good quality muon tracks from Level 2 with $p_T^{\mu} > 3$ GeV.

3. DATA ANALYSIS

The data set used in this preliminary analysis corresponds to an integrated luminosity of 8.4 pb^{-1}. Offline cuts for the mixing analysis include:

Two or three high quality muon tracks in $|\eta| < 1.1$;
1 GeV energy deposition in the associated calorimeter cell plus its nearest neighbors;
$\int B \cdot dl$ for each muon > 0.5 GeV;
$\Delta\phi < 160°$ (cosmic ray rejection);
$m_{\mu\mu} > 6$ GeV (removes J/ψ's);
$2 < p_T^{\mu} < 25$ GeV (ensures proper sign determination).

In addition, each event is required to have at least one associated jet where an associated jet is defined as a jet with $E_T^{jet} > 8$ GeV within $\Delta R = \sqrt{\Delta\eta^2 + \Delta\phi^2} = 0.8$ of the muon. Further, all muons having associated jets in the event must satisfy $p_T^{rel} > 1.2$ GeV where p_T^{rel} is the transverse momentum of the muon relative to the jet axis. These cuts serve to enhance the fraction of dimuons coming directly from $b\bar{b}$ decay.

Using these cuts we find a total of 116 like sign and 234 unlike sign dimuon events. The ratio of like to unlike sign events does not change significantly if we relax the associated jet requirement and ask only that at least one jet be found anywhere in the event or if we relax the jet requirement entirely and impose additional cosmic ray rejection cuts. The fraction of cosmic rays in these events is estimated to be $\approx 15\%$ based on visual scan of a subset of the sample. Correcting for cosmic ray background we find the ratio of like to unlike-sign dimuons to be

$$R = \frac{like}{unlike} = 0.51 \pm 0.06(stat) \pm 0.02(sys), \tag{4}$$

where the systematic error reflects the uncertainties associated with our estimated fraction of cosmic rays.

1 Monte Carlo Simulation

To determine the relative fraction of the processes listed in Table 1, we use the ISAJET Monte Carlo event generator combined with a fast detector simulator. A sample of 10000 dimuon events from $b\bar{b}$ and $c\bar{c}$ processes were generated using the ISAJET Monte Carlo which includes next-to-leading order contributions. The events were next passed through a fast DØ simulator which employs parameterizations of the DØ detector response to hadrons and leptons as well as the Level 1 and Level 2 trigger efficiencies. The offline cuts described above were then applied and the relative fractions of contributing processes of surviving events are shown in Table 2.

Process	Type	Fraction
P1	$b \to \mu^-, \bar{b} \to \mu^+$	0.66 ± 0.15
P2	$b \to \mu^-, \bar{b} \to \bar{c} \to \mu^-$	0.15 ± 0.06
P3	$b \to c \to \mu^+, \bar{b} \to \bar{c} \to \mu^-$	0.09 ± 0.04
P4-P6	$b \to c\mu^- + c \to \mu^+$, $c\bar{c}$, J/ψ, Υ	0.02 ± 0.02
P7	decay background	0.08 ± 0.04

Table 2: Fraction of contributing processes to dimuon events

The accuracy of the fast simulation model was checked by processing 5000 dimuon ISAJET events through the full GEANT detector simulation, complete trigger and reconstruction packages, and offline cuts. Similar fractions are observed within statistical errors to those in Table 2.

4. RESULTS AND CONCLUSIONS

Assuming the relative fractions of contributing processes given in Table 2 and using the measured value of R from equation (4) we find the (time averaged) combined mixing parameter χ to be

$$\chi = 0.14 \pm 0.03(stat) \pm 0.06(sys) \qquad (Preliminary), \tag{5}$$

where the systematic error is dominated by the uncertainties in our estimation of the fractions of contributing processes. This error was determined by allowing the fractions of contributing processes to vary within 3σ and comparing the extracted values of χ with our stated result. Our preliminary value of χ is in good agreement with earlier results from CDF and LEP [2][3][4] [5][6][7].

In progress are improvements to this measurement including analysis of dimuon data from the full eta coverage ($|\eta| < 3.3$) of the DØ detector and reduced systematic errors through increased Monte Carlo statistics and the use of alternative techniques in estimating the fractions of contributing processes. With reduced statistical and systematic errors a lower limit on x_s can be determined. For Run 1b of DØ beginning in January, 1994, an order of magnitude increase in collected dimuon events is expected.

The real measurement of interest is x_s. A direct measurement of x_s must await run 2 of DØ when a solenoid and high resolution tracking system (scintillating fibers and silicon) will be added. Here x_s can be measured from the proper time distribution of B_s°decays using for example $B_s^\circ \rightarrow D_s\pi\pi\pi$ and $D_s \rightarrow \phi\pi$ with a muon tag on the opposite side. Estimates indicate an x_s reach of 15-20 could achieved with this method.

5. ACKNOWLEDGEMENTS

The DØ collaboration consists of the following institutuions: Universidad de los Andes (Colombia), University of Arizona, Brookhaven National Laboratory, Brown University, University of California,Riverside, Centro Brasiliero de Pesquisas Fisicas (Brazil), CINVESTAV (Mexico), Columbia University, Delhi University (India), Fermilab, Florida State University, University of Hawaii, University of Illinois, Chicago, Indiana University, Iowa State University, Korea University (Korea), Lawrence Berkeley Laboratory, University of Maryland, University of Michigan, Michigan State University, Moscow State University (Russia), New York University, Northeastern University, Northern Illinois University, Northwestern University, University of Notre Dame, Panjab University (India), Institute for High Energy Physics (Russia), Purdue University, Rice University, University of Rochester, CEN Saclay (France), State University of New York,Stony Brook, SSC Laboratory, Tata Institute of Fundamental Research (India), University of Texas, Arlington, and Texas A&M University.

References

[1] S. Abachi et al., "The DØ Detector", submitted to NIM.

[2] C. Albajar et al., Phys. Lett. **B262** (1991) 171.

[3] F. Abe et al., Phys. Rev. Lett. **67** (1991) 3351.

[4] B. Adeva et al., Phys. Lett. **B288** (1992) 395.

[5] D. Decamp et al.,Phys. Lett. **B258** (1991) 236.

[6] P. Acton et al., Phys. Lett. **B276** (1992) 379.

[7] P. Abreu et al., Phys. Lett. **B301** (1993) 145.

B Decays

Leaders:

B. Reay
Ohio State University

B. Grinstein
Superconducting Super Collider Laboratory

B. Grinstein
Superconducting Super Collider Laboratory

N. W. Reay
Ohio State University

B_C SPECTROSCOPY AND PENTAQUARKS

K. Byrum
Argonne National Laboratory

N. Denisenko
Fermi National Accelerator Laboratory

J. Izen
University of Texas at Dallas

H. Lipkin
Weizmann Institute of Science

R. Lipton
Fermi National Accelerator Laboratory

S. Meshkov
Superconducting Super Collider Laboratory

N. W. Reay
Ohio State University

LEPTONIC AND SEMILEPTONIC DECAYS

J. Amundson
University of Chicago

C. Dib
Universidad Técnica Federico Santa María

G. Hou
National Taiwan University

V. Jain
Vanderbilt University

K. Kinoshita
Virginia Polytechnic Institute

A. Kronfeld
Fermi National Accelerator Laboratory

P. LeBrun
Fermi National Accelerator Laboratory

R. Oakes
Northwestern University

J. Taron
Ohio State University

RARE DECAYS

D. Cline
University of California (Los Angeles)

B. Grinstein
Superconducting Super Collider Laboratory

G. Hou
National Taiwan University

H. Lipkin
Weizmann Institute of Science

J. Park
University of California (Los Angeles)

A. Schwartz
Princeton University

J. Soares
Carnegie Mellon University

Semileptonic and leptonic decays of B hadrons

K. KINOSHITA,[a] J. AMUNDSON,[b] C. DIB,[c] G.W.S. HOU,[d] V. JAIN,[e]
A. KRONFELD,[f] P. LEBRUN,[f] R. J. OAKES[g] AND J. TARON[h]

[a] *Virginia Polytechnic Institute and State University, Blacksburg, Virginia 24061-0435 USA*
[b] *University of Chicago, Chicago, Illinois USA*
[c] *Universidad Tecnica Federico Santa Maria, Valparaiso, Chile*
[d] *National Taiwan University, Taipei, Taiwan, ROC*
[e] *Vanderbilt University, Nashville, Tennessee, USA*
[f] *Fermilab, Batavia, Illinois, USA*
[g] *Northwestern University, Evanston, Illinois, USA 60208*
[h] *Ohio State University, Columbus, Ohio, USA*

1. INTRODUCTION

Exclusive semileptonic and leptonic decays of B mesons are affected far less than hadronic decays by uncertainties due to strong interactions of quarks. As such, they are the modes of choice for measurement of the CKM matrix elements V_{cb} and V_{ub}. Nonetheless, past calculations of the decay widths have relied on phenomenological models such as the non-relativistic quark model and QCD sum rules to describe the behavior of the b and spectator quarks. The reliance on models can be lessened or eliminated by using heavy-quark symmetry arguments and/or lattice QCD. Both have made sufficient progress in recent years to kindle hope for smaller theoretical uncertainties in future determinations of CKM matrix elements. This optimism must be tempered by the experimental realities, as this comparison with theory will require the measurement of helicity-dependent form factors as a function of q^2.

Interest is currently focused mainly on those decays for which prospects appear to be good, both for exerimental measurement and theoretical certainty. We first list the modes and discuss the theoretical motivations. We then consider the prospects for experimental measurement of these modes, making projections five years into the future (1998).

2. THEORETICAL PROSPECTS

From a theoretical standpoint, (semi)leptonic decays may be organized as follows, where "D" refers to D_u, D_d, or D_s mesons:

1. Leptonic modes ($\tau\bar{\nu}$, $\mu\bar{\nu}$)
2. Three-body $b \to c$ modes ($\{D/D^*/D^{**}/\Lambda_c\}l\bar{\nu}$)
3. Four-body $b \to c$ modes ($\{D/D^*\}\{\pi/K\}l\bar{\nu}$)
4. Three-body $b \to u$ modes ($\{\pi/\rho/\eta/\omega/N\}l\bar{\nu}$)
5. $b \to u$ modes for the study of ρ–ω interference ($\pi\pi l\bar{\nu}$)

The width of purely leptonic decays of B_q ($q = u, c$) is proportional to $|V_{qb}|^2 f_{B_q}^2$, where f_{B_q} is the decay constant, and $|V_{qb}|$ is the CKM matrix element of interest. The tauonic mode suffers least from helicity suppression. These and the three-body tauonic modes are also of interest, because they are sensitive to some proposed extensions of the standard model. For example,[1] charged Higgs boson effects may enhance $B \to \tau\bar{\nu}$, $\mu\bar{\nu}$ above standard model expectations of order 10^{-4} and 4×10^{-7}, respectively. The ratio $BR(B \to \mu\bar{\nu})/BR(B \to \tau\bar{\nu}) \simeq 0.0045$ would remain unchanged. Conversely, the interference effect with charged current contributions may be destructive, and rates of purely leptonic modes may well be much below standard model expectations.

The bulk of the interest is in measurements of semileptonic decays to determine $|V_{cb}|$ and $|V_{ub}|$. This analysis requires theoretical calculations of form factors, which depend on $y = v \cdot v'$, where $v^{(\prime)}$ is the velocity of the initial (final) state meson. Below we briefly discuss theoretical prospects for obtaining the form factors. We discuss $|V_{cb}|$ and $|V_{ub}|$ separately, because the theoretical issues differ somewhat for the two cases. For more details see the contributions of Grinstein for HQET and Kronfeld for lattice QCD in these Proceedings.

2.1 Decays involving V_{cb}

Heavy-quark symmetry normalizes the form factors for heavy-to-heavy transitions such as $B \to D^{(*)} l\nu$ and $\Lambda_b \to \Lambda_c l\nu$ at zero recoil $y = 1$ in the infinite mass limit. Heavy-quark effective theory (HQET) classifies the $1/m^n$ corrections. For a generic form factor $f(y)$

$$f(1) = 1 + c_1 \frac{\bar{\Lambda}}{m_c} + c_2 \frac{\bar{\Lambda}^2}{m_c^2} + \ldots, \tag{1}$$

where $\bar{\Lambda} = m_D - m_c$ and the c's are coefficients of order unity which are independent of m_c or have at most a logarithmic dependence on m_c. HQET does not, however, predict these coefficients. In the special case $B \to D^* l\nu$, symmetry considerations show that c_1 vanishes.[2] This means that normalization at the point of zero recoil for this decay is known up to corrections that are of order $\bar{\Lambda}^2/m_c^2$. This allows for model-independent measurement of V_{cb} with small theoretical errors.

Estimating the size of the corrections is important for determining the theoretical uncertainty on the determination of V_{cb}. For this, one must turn to models or lattice QCD. Until now calculations have been performed with QCD sum rules, relativistic quark models and non-relativistic quark models. The first goal of the models is to predict the constant $\bar{\Lambda}$. Calculations in QCD sum rules estimate $\bar{\Lambda} = 500 \pm 100$ MeV,[3] while the non-relativistic quark model indicates that $\bar{\Lambda}$ should just be the constituent mass of the light quark, *i.e.*, $\bar{\Lambda} = m_{u,d} \simeq 300$ MeV.[4] The relation $\bar{\Lambda} = m_D - m_c$ means that the value of $\bar{\Lambda}$ affects both the numerator and the denominator in the expression $\bar{\Lambda}^2/m_c^2$. The difference in the estimated size of the theoretical uncertainty on $|V_{cb}|$ from $B \to D^* l\nu$ is therefore around 4%.

More theoretical work is being done to further understand these corrections. Although heavy-quark effective theory is a valuable tool, more experience is needed before one will know whether the $1/m$ expansion is quantitatively reliable for charm. Measurements of the decays $B \to Dl\nu$, $B_s \to D_s^{(*)} l\nu$ and $\Lambda_b \to \Lambda_c l\nu$ will be needed to carry out these tests.

Lattice QCD can also be used to calculate the form factors directly. The lattice calculations are most reliable for y near 1, the same the kinematic point as in HQET. The limitations of the lattice are time and computer power, and it is unlikely that direct calculations will soon improve on the 4% uncertainty expected from applying HQET. In the next 5 years, the matrix element for $B \to D^* l\nu$ at the endpoint should be calculable to ~5–10%. On the other hand, a lattice calculation of $\bar{\Lambda}$ can probably be done more reliably than in the models. Lattice QCD can also be used at $y > 1$ and provide a valuable cross-check with the experimental y dependence.

2.2 Decays involving V_{ub}

As mentioned above, the leptonic decay of the B can yield V_{ub}, given f_B. Because of the low helicity-suppressed rate, however, semileptonic decays are more feasible. In particular, at $y \approx 1$ the decay $B \to \rho l\nu$ is especially promising, because only one factor survives and the phase-space suppression is less than for $B \to \pi l\nu$.

To date, determinations of $|V_{ub}|$ have used inclusive semileptonic decays. There are calculations based on perturbative QCD that predict inclusive $b \to ul\nu$ rates[5], and different quark models that predict exclusive transitions (and their sum), including the full lepton spectrum.[6] Unfortunately, these calculations disagree mainly at the endpoint, which is precisely where measurements are free of background from $b \to c$ transitions. Hence, the models are contradictory in the kinematic region where the experiment is feasible. To avoid the reliance on models one must study exclusive semileptonic decays and use HQET and or lattice QCD.

Semileptonic form factors for $B \to \{\pi, \rho\}$ cannot be pinned down with heavy-quark symmetry, because the final state hadron consists only of light quarks. One can, however, use heavy-quark symmetry to relate B and D decays into the same light hadron. Including α_s corrections from short-distance QCD and $1/m$ corrections from HQET one finds

$$\frac{A_1^{B\to\rho}(1)}{A_1^{D\to\rho}(1)} = 1 + c_l \log \frac{m_b^2}{m_c^2} + c_1(\mu) \left(\frac{1}{m_c} - \frac{1}{m_b} \right) + \ldots. \tag{2}$$

In a constituent quark model, one finds numerically:[7]

$$\frac{A_1^{B\to\rho}(1)}{A_1^{D\to\rho}(1)} \simeq 1.15 \pm 0.01 \pm 0.04, \tag{3}$$

where the first uncertainty is proper of the model parameters and the second is due to the uncertainty in m_c. One consequently finds for the differential rates at $y = 1$:

$$\left. \frac{d\Gamma(B \to \rho l\nu)/dy}{d\Gamma(D \to \rho l\nu)/dy} \right|_{y=1} \approx 22. \left| \frac{V_{ub}}{V_{cd}} \right|^2 \times (1 \pm 0.07). \tag{4}$$

Although this ratio is predicted at the 7% level, it will be difficult to measure numerator and denominator experimentally, since both rates have vanishing phase space at $y = 1$. An extrapolation to points $y > 1$ will be necessary, but the extending the calculations to those points would be less reliable.

Lattice QCD calculations can calculate the form factors for $B \to \rho l \nu$ and $B \to \pi l \nu$ directly. Although no calculations of B decay form factors have yet been carried out, experience from the light hadron spectrum, the B decay constant, and K and D form factors suggests than a combined error of $\sim$ 15% will be attainable in a year or so. Within five years, the uncertainties may be as small as 5–10%. As with the HQET, the calculations are most reliable at the endpoint $y = 1$, with some deterioration for $y > 1$. As with our estimates for $B \to D^{(*)} l \nu$ form factors, these estimates do not include estimates of the error from the quenched approximation. It is still somewhat of an open question, how well the quenched approximation performs as a phenomenology. Nevertheless, this piece of B physics is the one most likely to profit from lattice QCD.

3. EXPERIMENTAL CONSIDERATIONS

For our five-year projections, we consider existing facilities of three types, e^+e^- symmetric colliders at the $\Upsilon(4S)$ (CESR), e^+e^- colliders at higher energies (LEP) and $p\bar{p}$ colliders at high energy (Tevatron). SSC is beyond this time scale, but it is reasonable to assume that the FNAL environment is most applicable; the number of b events collected by a generic detector after one year of running at the SSC is estimated to be two orders of magnitude higher than the projected number for FNAL. Other possibilities not considered are e^+e^- collisions just above B_s or Λ_b threshold and high energy fixed target facilities. The three facilities considered differ greatly in nearly all of the many factors which determine the accuracy of each measurement: numbers of events, event selection efficiencies, and types and quantities of expected background. We discuss first the many general considerations which were used as input to our evaluation and then the specific results used to make our projections. Some of the projected estimates depend on Monte Carlo simulations for crucial detector components which are not yet built.

The number of events produced is determined by the cross section and integrated luminosity. The number remaining after all triggering and analysis requirements depends on other factors, such as event particle multiplicities, the presence of other b-hadron decays which can enter signals, and energy and angular distributions of b-hadrons. In $p\bar{p}$ collisions the distribution peaked at small angles, so that a large fraction of produced b-hadrons fall outside the acceptance of the existing detectors. We consider only the portion which has been observed at CDF, which is estimated to be ~20% of the total. The five-year projections of integrated luminosity, numbers of b-hadrons produced within detector acceptances, and estimated mean and transverse momenta of those b-hadrons are given in Table I.

Table 1. Projected integrated luminosity (1998), numbers of b-hadrons produced within detector acceptances, and mean and transverse momenta for the three facilities considered.

Facility	$\int L dt$	N_{B_d}	N_{B_u}	N_{B_s}	N_{Λ_b}	N_{B_c}	$\langle p_B \rangle$, $\langle p_B^T \rangle$(GeV/c)
CESR	20 fb^{-1}	2×10^7	2×10^7	0	0	0	0.3, 0.3
LEP	100 pb^{-1}	8×10^5	8×10^5	2×10^5	2×10^5	8×10^2	35, 25
FNAL	1 fb^{-1}	8×10^9	8×10^9	2×10^9	2×10^9	8×10^6	10-15, 10-15

Detection efficiencies will also vary by mode, depending on the types and number of particles required for reconstruction. It is assumed that the detectors used will be those currently in place at the three facilities, with some upgrades. For LEP and FNAL we assume capabilities for high resolution vertex reconstruction, projected in the plane perpendicular to the beam ("2-d") for LEP and in three dimensions ("3-d") for FNAL (the detector assumed for FNAL is not yet in place, although a "2-d" silicon-based detector ran successfully during the last collider run). It is assumed that detection of π^0 at momenta below 1 GeV/c is possible only at CESR and that none of the detectors will have hadron identification for momenta above 1 GeV/c.

Backgrounds to signals can originate from random combinations of particles or from nonrandom sources. The rate of random accidental candidates depends on event particle multiplicity. Because the presence of a neutrino among the decay products introduces a fairly large intrinsic uncertainty in energy-momentum, the resolution of the detector does not in general define the background, *unless* missing energy and momentum measurements are sufficient to further define the neutrino. Such "neutrino detection" is now used for some measurements at CESR and at LEP; at ALEPH, the resolution on visible energy is ~3 GeV and is crucial to a search for inclusive $B \to \tau$ decays. More often, reduction of random background is accomplished through kinematic and vertex requirements. At CESR the B is nearly at rest, so that the neutrino's energy and momentum may be deduced from those of the detected daughters of the semileptonic decay. Requiring that the neutrino mass implied by these be near zero is very effective in suppressing background. At higher energies, the b-hadrons appear in jets and usually carry a large fraction of the jet energy. Requiring candidates to have a high energy and be associated with a jet are then effective discriminators against random background. Another characteristic of b-hadrons at higher energies is their finite decay length, which is measurable with silicon strip detectors. Requiring that a candidate's reconstructed vertex be separated from the event origin favors tracks which are all associated with a single decay and is very effective in reducing the multiplicity of random tracks. Both LEP and FNAL projections rely heavily on precise vertex measurements to reduce backgrounds.

A major consideration for all cases is that of nonrandom backgrounds, where b-hadron decays other than the one under investigation appear in the signal. This type of background is difficult to reduce and may dominate the event sample. An example is the decay $B_u \to D^0 l^- \bar{\nu}$, which is difficult to distinguish from the more abundant $B \to D^* l^- \bar{\nu}$ ($D^* \to D^0 \pi$) where the π is not detected; consequently, a large subtraction of the latter's contribution is required. An advantage of studying $\Upsilon(4S)$ decays is that B_u and B_d are produced with no B_s and Λ_b. To balance this, vertex reconstruction capability in higher energy machines may enable significant reduction of backgrounds from modes with one or more additional daughters by rejecting those candidates with additional tracks consistent with originating at its vertex.

Another potentially important tool, particularly for distinguishing feeddown from higher B states, is particle identification. In the facilities considered here, such a capacity will probably not be implemented in the next few years. This question was therefore not studied in detail here.

4. EXPERIMENTAL PROJECTIONS

4.1 Leptonic decays and decays with τ

Pure leptonic and semitauonic decays are difficult to measure because of large missing energies. Both are also relatively rare, the semitauonic due to reduced phase space and the leptonic due to helicity suppression.

Searches for $B_u \to \tau\nu$ and $B_u \to \mu\nu$ at CLEO have thus far yielded no positive results. The 90% confidence upper limits on branching fractions from 0.9 fb^{-1} of data are 0.013 and 2.0×10^{-5}.[8] The Standard Model predictions are 10^{-4} and 4×10^{-7}, respectively. The branching fractions which may be probed with additional data depends somewhat on the level of backgrounds which are found – tighter cuts may be necessary. With 20 fb^{-1} of integrated luminosity, we estimate sensitivities of $\sim 10^{-3}$ and $\sim 10^{-5}$, respectively. A feasibility study at ALEPH[9] yields a preliminary conclusion that it is possible with the projected luminosity to probe the leptonic decays $B \to \tau\overline{\nu}, \mu\overline{\nu}$ to branching fractions of 10^{-4}. This should allow the full range of possible enhancements from charged Higgs boson effects to be explored.

At LEP a search for decays $B \to \tau X$ finds[10] a branching fraction $(2.76 \pm 0.47 \pm 0.43) \times 10^{-2}$. This value is in agreement with the Standard Model and rules out enhancements predicted by some extended models. It is worth emphasizing, however, that charged Higgs boson effects are more enhanced in purely leptonic decays than is possible in semileptonic decays. Although the inclusive $B \to \tau X$ result is fully consistent with standard model expectations, it does not exclude the possibility of enhancements[1] in $B \to \tau\overline{\nu}$ and $B \to \mu\overline{\nu}$.

4.2 Semileptonic decays with V_{cb}

The decay $\overline{B}_{u,d} \to D^* l^- \overline{\nu}$ is the only mode to date to have been used to measure $|V_{cb}|$ via HQET and is likely to continue its dominant role. The result from 1.65 fb^{-1} of data from CLEO 1.5, ARGUS and CLEO II is $|V_{cb}| = 0.038 \pm 0.003 \pm 0.004$,[11] where the first error is statistical and the second systematic, mainly due to the uncertainty in the B lifetime. A simple extrapolation to 20 fb^{-1} of data would give statistical errors around ± 0.0007. The limiting uncertainty will undoubtedly be systematic, however, mainly from the measurement of the B lifetime. The error here will probably improve by at most a factor of 2 in the next few years, so that the overall error of ± 0.006 may be reduced to ± 0.002.

At LEP, D^*-lepton correlations and vertex requirements have yielded a signal/background of around five for the decay $\overline{B}_d \to D^{*+} l^- \overline{\nu}$.[12] The signal quality is similar for other charmed three-body decays. The projected yield is ~ 750 decays $\overline{B}_d \to D^{*+} l^- \overline{\nu}$, and although this does not appear competitive with CESR, the vertexing capability will enable rejection of such backgrounds as $\overline{B}_d \to D^{**} l^- \overline{\nu}$ and $\overline{B}_d \to D^{*+} \pi l^- \overline{\nu}$, as well as studies of these modes and of $B \to D l^- \overline{\nu}$. These are important for establishing the relative rates to the different channels, for testing the theory, and for reducing systematic uncertainties. For B_s and Λ_b three-body decays the LEP sample will be an important contribution, with ~ 50 and ~ 150 events, respectively. The 150 events $\Lambda_b \to \Lambda_c l^- \overline{\nu}$ should give statistical errors on $|V_{cb}|$ which are roughly equivalent to those from current measurements with $B \to D^* l^- \overline{\nu}$, around ± 0.006. We note, however, that the absolute normalization of the width may have larger systematic uncertainties, as the production rate of baryons is difficult to establish.

Although at the $p\overline{p}$ collider the fragmentation is softer and background is much higher, Monte Carlo studies indicate that with 3-d vertexing it is possible to achieve a signal/background for the $D^* l^- \overline{\nu}$ mode which is of the same order as that achieved at LEP with 2-d vertexing.[13] With the projected luminosities of Table I, the yield would be about twice that at LEP.

Other interesting measurements involve four-body modes calculated via HQET and chiral perturbation theory,[14] such as $\overline{B}_d \to D^{*+} \pi l^- \overline{\nu}$. These are the backgrounds to $\overline{B}_d \to D^{*+} l^- \overline{\nu}$ described above, and it appears that they may be measured quite cleanly at LEP.

4.3 Semileptonic decays with V_{ub}

The inclusive $b \to u$ semileptonic rate of B_u/B_d mesons has been measured with 0.9 fb^{-1} of data at CESR and gives a value for $|V_{ub}|/|V_{cb}|$ of 0.075 ± 0.008, with theoretical range ± 0.02.[15] Measurement of exclusive modes is necessary to reduce the theoretical uncertainties. A search for decays $B^- \to V^0 l^- \overline{\nu}$ where V^0 is either ρ^0 or ω^0 yields a net 2σ excess of candidates.[16] If this is interpreted as a signal, it corresponds to a branching fraction of 1×10^{-4} and is consistent with the inclusive measurement. If we project from this to 20 fb^{-1} of data, the statistical error will be 8 – 25% on the branching fraction and 4 – 13% on $|V_{ub}|$. With such a large data sample, it may be possible to perform the first measurements of form factors.

The projected luminosity at LEP is insufficient for $b \to u$ measurements. Although no studies are yet available of projections at the Tevatron, it seems unlikely, given the higher backgrounds and results from studies of the charm modes, that there will be a great advantage relative to LEP.

5. CONCLUSIONS

Although semileptonic and leptonic decays are favored for measurement of CKM elements due to their minimal theoretical uncertainty, measurements of $|V_{cb}|$ and $|V_{ub}|$ are currently limited by uncertainties of the theory. Because of new developments with HQET and lattice gauge theories, this situation is likely to change in the next few years, with both theoretical and experimental uncertainties reduced significantly. The new focus is on the semileptonic partial width at points near q^2_{max}.

The modes involving V_{cb} which are of highest theoretical interest are the vector meson decays ($B \to D^* l\nu$) and baryon decays ($\Lambda_b \to \Lambda_c l\nu$). The present experimental uncertainty on $|V_{cb}|$ is around 20%. We expect that in five years the best statistical errors on $|V_{cb}|$ will be better than 2%, from measurements of the decay $B \to D^* l\overline{\nu}$ at CESR, but that systematic errors will undoubtedly be larger, around 7%; the expected theoretical uncertainty is 4%. LEP and/or the Tevatron may be able to provide important supplementary information on this mode, as they will have better access to the crucial region near q^2_{max} and better rejection of backgrounds from modes with higher multiplicity. This would serve to reduce the systematic uncertainties. Λ_b measurements will probably be done at LEP, possibly at the Tevatron, but systematic uncertainties may be problematic.

Tests of theories which combine HQET and chiral perturbation theory to describe four-body modes appear to be possible at LEP.

The $b \to u$ modes are more difficult, both theoretically and experimentally. The leptonic decays $\tau\nu$, $\mu\nu$ are most clean, from the theoretical standpoint. Taking full advantage of vertexing and missing energy measurements, it appears that LEP will be sensitive to the Standard Model prediction for $\tau\nu$, at a level of 10^{-4}. Experimentally, the semileptonic modes will be more precisely measured, and any progress will probably be made at CESR. We project from inclusive measurements and indications from searches for exclusive decays that statistical errors on $|V_{ub}|$ will be $5 - 15\%$ within five years. The first measurements of form factors may be possible with such a data sample, and these may be necessary to reduce systematic errors. Present theoretical uncertainties are $\sim 25\%$. Reduction of these to $< 10\%$ may be possible in the next five years.

6. ACKNOWLEDGEMENTS

We thank V. Sharma and P. Sphicas for sharing the results of their studies with us.

7. REFERENCES

1. W. S. Hou, NTUTH-92-21, *Phys. Rev.* **D**, in press.
2. M.E. Luke, *Phys. Lett.* **B252** (1990) 447; M. Neubert, *Phys. Lett.* **B264** (1991) 455.
3. M. Neubert, *Phys. Rev.* **D47** (1993) 4063.
4. J.F. Amundson, Univ. of Chicago preprint EFI-93-39.
5. G. Altarelli, N. Cabibbo, G. Corbo, L. Maiani, and G. Martinelli, *Nucl. Phys.* **B208** (1982) 365.
6. N. Isgur, D. Scora, B. Grinstein, and M.B. Wise, *Phys. Rev.* **D39** (1989) 799; M. Wirbel, B. Stech, and M. Bauer, *Z. Phys.* **C29** (1985) 637.
7. C.O. Dib and F. Vera, *Phys. Rev.* **D47** (1993) 3938.
8. D. Cinabro, in *"The Fermilab Meeting DPF92,"* C. Albright, P. Kasper, R. Raja and J. Yoh, eds. (World Scientific, Singapore) p. 843 (1992).
9. V. Sharma, private communication.
10. D. Buskulic et al., *Phys. Lett.* **B298**, 479 (1993); A. Putzer in *Proceedings of the 5th International Symposium on Heavy Flavour Physics*, Montreal, Canada, July 1993.
11. M. Artuso, talk this workshop.
12. D. Buskulic et al., *Phys. Lett.* **B307**, 194 (1993); F. V. Weber, in *"The Fermilab Meeting DPF92,"* C. Albright, P. Kasper, R. Raja and J. Yoh, eds. (World Scientific, Singapore) p. 571 (1992).
13. P. Sphicas, private communication.
14. H. Y. Cheng et al., Cornell preprint CLNS 93/1204 (1993).
15. J. Bartelt et al., CLEO 93-15, submitted to Phys. Rev.
16. A. Bean et al., *Phys. Rev. Lett.* **70**, 2681 (1993).

AN OVERVIEW OF B RARE DECAYS

YOSEF NIR

Department of Nuclear Physics, Weizmann Institute of Science
Rehovot 76100, Israel

for the δ B rare decays subgroup

The very large number of bottom hadrons to be produced in future high energy hadron colliders would provide a golden opportunity for a detailed study of B physics. Naturally, most interest lies in rare processes that are sensitive to New Physics, namely CP violating asymmetries⋆ and Flavor Changing Neutral Current decays. We have set to ourselves the following goals:

- Review B physics capabilities at existing accelerator facilities, *i.e.* CLEO, LEP, SLC and Tevatron, by the year 2000;
- Identify generic channels that can probe new physics;
- Single out specific channels that seem especially promising for hadron colliders;
- Make a "back of the envelope" estimate of possible number of detected events, hardware required and possible background.

We emphasize, however, that a detailed Monte Carlo program is needed to provide more definitive answers: we have mainly tried to point out channels that justify such a detailed study.

⋆ We have not studied CP asymmetries that would measure the angles α, β and γ of the unitarity triangle – those have been investigated by other working groups in this workshop.

1. B PHYSICS EXPERIMENTS

The CLEO experiment is an e^+e^- machine running at the $\Upsilon(4S)$ resonance. At present, it has 4×10^6 B-mesons. The number will rise to 2×10^7 at phase II of the experiment and 6×10^7 at phase III. The hadrons produced are exclusively B_d and B_u mesons (about 50% each). The production is coherent. There is no B vertex information. D vertex information will be available at the later phase. The experiment has reasonable $K-\pi$ separation. The produced B-mesons are essentially at rest, and the resulting events isotropic.

The LEP experiment is an e^+e^- machine operating at the Z resonance. It will have 4×10^6 hadronic events at each of its four detectors: with $\Gamma_{b\bar{b}}/\Gamma_{\rm had} \sim 0.22$, this means about 2×10^6 bottom hadrons. The bottom hadrons consist of an incoherent mix of B_u, B_d, B_s, B_c and bottom baryons. The vertex ability is limited to $\gamma \gtrsim 5-6$. Of the four detectors, only DELPHI has $K-\pi$ separation. The B-jets are high momentum and thus well defined.

The SLC experiment is an e^+e^- machine operating at the Z resonance. It will have (at best) 10^6 hadronic events, and thus 4×10^5 bottom hadrons. The bottom hadrons consist of an incoherent mix of B_u, B_d, B_s, B_c and bottom baryons. The vertex ability is good. It has good $K-\pi$ separation. The B-jets are high momentum and thus well defined.

The Tevatron experiment is a $p\bar{p}$ collider running at a CMS energy of 2 TeV. At present, it has 10^{10} bottom hadrons in acceptance region. By the year 2000 it will have about 10^{11} bottom hadrons in the collider mode. The bottom hadrons consist of an incoherent mix of B_u, B_d, B_s, B_c and bottom baryons. It has vertex ability. It has no $K-\pi$ separation. The B-jets are high momentum and thus well defined.

We now turn to the potential capability of the SSC/LHC.

In **the collider mode with a 4π detector**, the cross section for bottom production is about 1% of the total cross section. Thus we expect about 2×10^6 B's/sec or 2×10^{13} B's/year. In the central region we expect 5×10^{12} B's/year. The bottom hadrons consist of an incoherent mix of B_u, B_d, B_s, B_c and bottom baryons. The machine should be capable of vertex tagging. It would have no $K-\pi$ separation.

In **the collider mode with a forward detector**, and assuming $\mathcal{L} \approx 10^{32}$ cm^{-2} sec^{-1}, we expect about 5×10^{11} B's/year. Other features are as for the 4π detector, except that the forward detector would have $K-\pi$ separation.

In **the fixed target mode**, we expect 10^7 interactions/sec, which would yield 2×10^{10} B's/year. The special features are good acceptance, good vertex definition and $K-\pi$ separation.

Finally, we present some figures of merit for different detectors.

Table 1. Detectors.

	CDF III	SDC	BCD	HERA	SFT
Int. rate (MHz)	5	100	10	40	10
$b\bar{b}$/event	10^{-3}	10^{-2}	10^{-2}	10^{-6}	1.6×10^{-4}
Product I (MHz)	5×10^{-3}	1	10^{-1}	4×10^{-5}	1.6×10^{-3}

2. THEORY OF RARE PROCESSES

We chose to concentrate our study in three directions:

(*i*) CP asymmetries in neutral B decays into final CP eigenstates that are predicted to be (close to) zero in the Standard Model. We call these "clean zeros".

(*ii*) Rare decays with two final charged leptons.

(*iii*) CP asymmetries in charged B-mesons and baryons.

We now briefly discuss the Standard Model predictions for, as well as the prospects of New Physics in each of these three classes.

Clean Zeros in the CP asymmetries are predicted within the Standard Model for three classes of B_s decays. More precisely, some of these asymmetries measure $\sin 2\beta'$ [1] where

$$\beta' \equiv \arg\left[-\frac{V_{cs}V_{cb}^*}{V_{ts}V_{tb}^*}\right]. \tag{01}$$

The angle β' is thus an angle in the unitarity triangle formed by products of elements from the second and third columns. The constraints on the length of the sides of this triangle imply

$$|\sin 2\beta'| \leq 0.05 \left(\frac{|V_{ub}/V_{cb}|}{0.1}\right)|\sin\gamma|. \tag{02}$$

These three classes of asymmetries are given in Table 2.

Table 2. CP asymmetries in B_s decays.

Final State	Quark Sub-Process	BR (est.)	SM Prediction
$\psi\phi$	$\bar{b}\to\bar{c}c\bar{s}$	10^{-3}	$-\sin 2\beta'$
ψK_S	$\bar{b}\to\bar{c}c\bar{d}$	2×10^{-5}	$-\sin 2\beta'$
$\phi\phi$	$\bar{b}\to\bar{s}s\bar{s}$	10^{-5}	0

The prediction for the $\bar{b}\to\bar{s}s\bar{s}$ processes is based on the assumption that penguin diagrams with virtual u and c quarks are equal, up to the different CKM combinations. In reality, this is likely to be violated by a few percent.

The predictions for CP asymmetries in B_s decays are sensitive to New Physics (for a detailed discussion and a guide to the literature, see [2]) with

(*i*) Significant new contributions to FCNC;

(*ii*) New sources for CP violation.

Examples for extensions of the SM where large deviations from the SM predictions are possible are

a. Non-minimal SUSY models, where squark-gluino box diagrams may contribute significantly to $B_s-\bar{B}_s$ mixing with new phases in the quark-squark-gluino mixing matrix;

b. Multi scalar models without Natural Flavor Conservation, where scalar-mediated tree diagrams contribute to $B_s-\bar{B}_s$ mixing with new phases in the flavor changing Yukawa couplings;

c. Models with $SU(2)$-singlet down-like quarks, where Z-mediated tree diagrams contribute to $B_s-\bar{B}_s$ mixing with new phases in the fermionic Z couplings;

d. Fourth quark generation, where box diagrams with t' may contribute significantly to $B_s-\bar{B}_s$ mixing with new phases in the 4×4 quark mixing matrix.

In these models, the asymmetries in Table 2 may be large or even maximal, instead of the zero asymmetry predicted by the Standard Model.

Thus, it is not only interesting to check whether hadron colliders can measure the few percent asymmetries allowed by the Standard Model. Instead, we are interested in whether large asymmetries, of order 0.3, can be discovered in future hadron colliders.

Rare decays with two final charged leptons proceed, within the Standard Model, via electroweak penguin diagrams and box diagrams. In addition, there are important long-distance contributions to $B\to X\mu^+\mu^-$ which make it difficult to give an exact prediction.

Inclusive modes, with Standard Model predicted short-distance rates of

$$
\begin{aligned}
BR(B \to X_s\mu^+\mu^-)_{SD} &= (3.5-14.0)\times 10^{-6}, \\
BR(B \to X_d\mu^+\mu^-)_{SD} &= (1.5-6.0)\times 10^{-7},
\end{aligned} \tag{03}
$$

are very difficult to measure in hadron colliders. Instead, we focus on various exclusive modes. Our estimate for the Standard Model predictions for these modes is (for Standard Model branching ratio calculations, see *e.g.* [3] for $b \to s\mu\mu$, [4] for $B_s \to \tau\tau$ and [5] for $B_s \to \mu\mu$):

$$
\begin{aligned}
BR(B \to K\mu^+\mu^-) &\sim 10^{-6}, \\
BR(B \to \pi\mu^+\mu^-) &\sim 5\times 10^{-8}, \\
BR(B_s \to \tau^+\tau^-) &\sim 4\times 10^{-7}, \\
BR(B_s \to \mu^+\mu^-) &\sim 2\times 10^{-9}.
\end{aligned} \tag{04}
$$

The precise branching ratios depend on the mass of the top quark.

Examples of extensions of the Standard Model that could significantly affect these predictions are (for a detailed discussion and a guide to the literature, see [6]):

a. SUSY and multi-scalar models. The extra charged scalars contribute through penguin and box diagrams with the Standard Model W-boson replaced by charged scalars. The extra neutral scalars contribute through penguin diagrams with the Standard Model Z-boson replaced by neutral scalars;

b. Models with extra $SU(2)$-singlet down-like quarks, where Z-mediated tree diagrams contribute;

c. Multi-scalar models with no Natural Flavor Conservation, where scalar-mediated tree diagrams contribute;

d. Fourth generation quarks contribute through box diagrams with virtual t';

e. Anomalous WWZ couplings affect the electroweak penguin diagrams;

f. Extended Technicolor models predict flavor changing Z couplings and four-fermi operators that affect the decays;

g. Leptoquarks may mediate the decays at tree level.

Thus, new physics may significantly enhance the rate. However, the experimental bound from UA1 [7],

$$
BR(B \to X\mu^+\mu^-) \le 5\times 10^{-5}, \tag{05}
$$

makes it unlikely that the enhancement is by more than one order of magnitude (except, maybe, the mode with final tau-leptons).

The question that we pose here is, then, whether hadron colliders can measure decay rates that are at the Standard Model level or, at most, ten times higher.

Direct CP Violation may be observed in the decays of charged B-mesons or bottom baryons. We focus on decays dominated by (strong or electromagnetic) penguin diagrams. Theoretically, the asymmetries are difficult to calculate because of large hadronic uncertainties (see *e.g.* [8]). In Table 3 we list examples of modes that might exhibit CP asymmetries:

Table 3. Direct CP violation in bottom hadrons decays.

Mode	Quark Sub-Process	BR (est.)	a_{CP} (SM)
$B^- \to K^-\phi$	$b \to s\bar{s}s$	10^{-5}	0.005
$B^- \to K^-K^{*0}$	$b \to d\bar{s}s$	5×10^{-7}	0.05
$\bar{B} \to \bar{K}^*\gamma$	$b \to s\gamma$	10^{-5}	0.005
$\bar{B}_s \to K^*\gamma$	$b \to d\gamma$	10^{-6}	0.05
$\Xi_b^0 \to \Lambda\phi$	$b \to d\bar{s}s$	10^{-5}	0.05
$\Xi_b^0 \to \Lambda\psi$	$b \to d\bar{c}c$	5×10^{-5}	0.01

We emphasize that the calculation of the Standard Model predictions for the asymmetries $a_{CP}(\mathrm{SM})$, might be wrong by a factor of a few in either direction.

There is very little theoretical study of the possible effects of New Physics on these asymmetries. However, it is likely that interesting effects arise in extensions of the Standard Model where there are new significant contributions to these decays. Two examples would be:

a. Models with $SU(2)$-singlet down-like quarks, where these decays get contributions from Z-mediated tree diagrams;

b. Fourth quark generation, where penguin diagrams with t' contribute.

The question that we ask here is, then, whether asymmetries of order 10–20% (which can still be accommodated within the Standard Model) or higher (signalling new physics) can be detected.

3. CLEAN ZEROS

For most measurements of CP asymmetries in B_s decays, it is important to have the following two features:

(*i*) A good mass resolution that would allow $B_s - B_d$ separation. This is required because the same final hadronic state would correspond to *different* CP asymmetries in B_s and B_d decays.

(*ii*) A good length/momentum resolution. One needs to make a time dependent measurement, so that the required resolution depends on the yet-unknown mass difference in the B_s system, x_s ($x_s = 2\pi$ corresponds to 1 oscillation/lifetime). For example, if the resolution is $\Delta\tau \approx 0.1$ (no p dependence) and if to have a measurement of the asymmetry we need to resolve 1/4 oscillation, then the measurement is possible only if $x_s \lesssim 15$.

Below we evaluate the feasibility of these measurements with the SFT spectrometer in the fixed target mode of the SSC. We take the number of B_s's produced to be 3.4×10^9/year.

The decay $B_s \to \psi\phi$ can be detected through $\psi \to \mu^+\mu^-$ or e^+e^- and $\phi \to K^+K^-$. The properties of the SFT spectrometer that we assume are:

a. Acceptance for $\mu\mu + KK + \mu = 0.3$;

b. ϵ_{trig} for 2 muons with $P_t \geq 1\ GeV = 0.8$;

c. ϵ_{tag} with e, μ and $K = 0.8$;

d. ϵ_{vert} (2 vertices $\Longrightarrow (0.7)^2) = 0.5$;

e. $\epsilon_{\mathrm{rec}} = (0.95)^4 = 0.8$.

Thus, $\epsilon_{\mathrm{tot}}(\mathrm{SFT}) = 0.08$, giving about 15000 events/year. This may allow a measurement of the asymmetry at the level of a few percent.

For this mode, $B_s - B_d$ separation is not important, because it is highly suppressed in B_d decays. To suppress background, we propose: (*i*) minimum bias requirement of 2μ with $P_t \geq 1\ GeV$ and $P \geq 20\ GeV$ suppresses background like 10^{-5} (simulation was done); (*ii*) mass reconstruction of ψ with $\sigma_M = 10\ MeV$.

The decay $B_s \to \psi K_S$ can be detected through $\psi \to \mu^+\mu^-$ or e^+e^- and $K_S \to \pi^+\pi^-$. As for the previous mode, we estimate $\epsilon_{\mathrm{tot}}(\mathrm{SFT}) = 0.08$, giving about 400 events/year. This may allow a measurement of the asymmetry at the level of 10% or so. For this mode, $B_s - B_d$ separation is crucial, because most events would come from B_d with an asymmetry of $\sin 2\beta$.

The decay $B_s \to \phi\phi$ can be detected when both $\phi \to K^+K^-$. The properties of the SFT spectrometer that we assume are:

a. Acceptance for K^+K^-, K^+K^- + other $\mu = 0.3$;

b. ϵ_{trig} for the other (e,μ) with $P \geq 20\ GeV$, $P_t \geq 1.5\ GeV = 0.1$;

c. $\epsilon_{\pi/K} = 0.8$, $\epsilon_{\mathrm{vert}} = 0.5$, $\epsilon_{\mathrm{rec}} = 0.7$.

Thus, $\epsilon_{\mathrm{tot}}(\mathrm{SFT}) = 0.08$, giving about 60 events/year. This may allow a measurement of the asymmetry at the level of 20% or so. For this mode, $B_s - B_d$ is not important because it is highly suppressed in B_d decays. However, as the final state is $K^+K^-K^+K^-$, one needs to trigger on the other B. To suppress background, we propose: (i) minimum bias requirement of μ with $P_t \geq 1.5\ GeV$ rejects background like 6×10^{-3}; (ii) mass reconstruction of ϕ and mass of B_s with $\sigma_M = 13\ MeV$ can dramatically suppress background (but simulation is needed).

4. FCNC DECAYS

(i) $B^\pm \to K^\pm \mu^+\mu^-$.

We consider the collider mode with a 4π detector. The trigger is 2μ or $2e$ and some P_T cut, so that the triggering efficiency is $\epsilon_{\rm trig} \sim 0.1$. The reconstruction efficiency is ~ 0.8 for each of the final particles, so that $\epsilon_{\rm rec} \sim (0.8)^3 \sim 0.5$. We estimate the vertex efficiency at $\epsilon_{\rm vert} \sim 0.8$. The total efficiency is then

$$\epsilon_{\rm tot} = \epsilon_{\rm trig} \times \epsilon_{\rm rec} \times \epsilon_{\rm vert} \approx 4 \times 10^{-2}. \qquad (06)$$

At the Tevatron, with 10^{11} B's, of which 3×10^{10} are $B^\pm$, the Standard Model branching ratio of $\sim 10^{-6}$ leads to

$$N_{\rm evts} \sim \epsilon_{\rm tot} \times BR(B^\pm \to K^\pm\mu^+\mu^-) \times N_{B^\pm} \sim 1200. \qquad (07)$$

The question of background is very important here. The dominant background is likely to come from $B \to D\mu\nu$, with the subsequent $D \to K\mu\nu$. The branching ratios are approximately 0.1 and 0.03, respectively, so that the overall branching ratio is approximately 3×10^{-3}. We envisage the following handles to suppress this background:

a. Kinematic fit to $K\mu\mu$ ($E_{\nu_1} \sim E_{\nu_2} \sim 0$) would suppress the background by $\sim 10^{-2}$.

b. $B - D$ vertex separation would suppress the background by $\sim 10^{-1}$.

c. Requiring $M(K\mu) \neq M(D)$ would suppress the background by $\sim 10^{-1}$.

Altogether, the background may be suppressed to the level of 3×10^{-7}. We conclude then the the decay $B^\pm \to K^\pm\mu^+\mu^-$ can probably be measured at the Standard Model level of 10^{-6}.

(ii) $B^\pm \to \pi^\pm\mu^+\mu^-$.

The crucial point about observing this mode is that we need to have π/K separation for $B^\pm$. This would probably require forward detector. We estimate $\epsilon_{\pi/K} \sim 0.1$. This adds to the factor 20 suppression in the branching ratio, compared to the K-mode:

$$N_{\rm evts} \sim \epsilon_{\rm tot} \times BR(B^\pm \to \pi^\pm\mu^+\mu^-) \times N_{B^\pm} \times \epsilon_{\pi/K} \sim 6. \qquad (08)$$

We conclude that sensitivity to the Standard Model rate is unlikely to be achieved.

We note, however, that $B^0 \to \pi^0\mu^+\mu^-$ might have better prospects of being measured. No π/K separation is needed, but the large number of photons may pose a problem. We estimate that $N_{\rm evts}$ may be 3–5 times larger than in the charged mode: $N_{\rm evts} \sim 20 - 30$ for the Standard Model rate.

We expect the main background to come (similarly to the final kaon case) from $B \to D\mu\nu$ and the subsequent $D \to \pi\mu\nu$ (with branching ratio $\sim 3 \times 10^{-3}$). Using the same cuts as in the final kaon mode, the background can be suppressed to below signal.

(iii) $B_s \to \tau^+\tau^-$.

We considered the possibility to detect the τ-lepton through either its leptonic decay or its decay to three charged pions. First, we studied the $\tau\tau \to e\mu+\nu$'s case. The advantage is that this mode is self triggering. We estimate the efficiency in detecting the $\mu^\pm e^\mp$ with a P_T cut to be $\epsilon \sim 0.1$. Thus, we expect at the Tevatron

$$N_{\rm evts} \sim \epsilon_{\rm tot} \times BR(B_s \to \tau^+\tau^-) \times N_{B_s} \times BR(\tau^+\tau^- \to \mu^\pm e^\mp X) \sim 24. \qquad (09)$$

However, we find that background constitutes a major problem. The dominant background comes from $B_s \to D_s\tau\nu$ (with branching ratio $\sim 3 \times 10^{-3}$) and the subsequent $D_s \to \tau\nu$ (with branching ratio $\sim 10^{-2}$). There are not many handles over this background, as its topology is similar to the signal. With the estimated branching ratio of 3×10^{-5}, we find it hard to see how it can be pushed below 10^{-6}, still above the Standard Model branching ratio for $B_s \to \tau^+\tau^-$.

Second, we study the $\tau \to 3\pi\ X\nu$ modes. The dominant background comes from $B_s \to D_s\tau\nu$, and the subsequent $\tau \to 3\pi\ X\nu$ and $D_s \to 3$ prong (about 20%, mainly $K\bar{K}\pi$). A rough estimate gives $\frac{\text{background}}{\text{signal}} \sim 150$. We see two ways to suppress this background: (a) K identification, which would require K/π separation, and (b) use $B_s \to \tau^+\tau^-$ kinematics. There are 3 vertices and, therefore, 12 constraints. There are also 12 unknown parameters (3 for the momentum of each of the two neutrinos, 3 for the momenta of B_s, τ^+ and τ^-, and 3 for $\{x, y, z\}$ of the B_s decay). One can then make a 0-C fit which may give some handles. This would be hard, and a detailed Monte Carlo is needed to evaluate the feasibility of this method.

(iv) $B_s \to \mu^+\mu^-$.

The Standard Model branching ratio is tiny, of order 2×10^{-9}. For this mode (unlike the τ-mode), we expect the number of events to be the limiting factor and not the background. With good $\delta m_{\mu\mu}$ determination, one could use $m_{\mu\mu} = m_B$ and vertexing to eliminate background. To estimate the number of events, we take a 4π detector in the SSC, with $\sim 8 \times 10^{11}$ B_s's/year, and assume trigger efficiency of $\epsilon_{\text{trig}} \sim 0.01$:

$$N_{\text{evts}} \sim \epsilon_{\text{trig}} \times BR(B_s \to \mu^+\mu^-) \times N_{B_s} \sim 16. \tag{010}$$

This is hard, but the situation might be better with a forward detector.

5. DIRECT CP VIOLATION

We have studied CP asymmetries in various $B^{\pm}$, Λ_b and Ξ_b decays. Typically, the Standard Model predicts asymmetries of order a few percent (with relatively large uncertainties). These modes are self-tagging. They would probably require an independent trigger. K/π separation would be helpful (it may be useful to consider K trigger). For the baryonic modes, we need to normalize to standard modes in $p-p$ collisions. The best mode is probably $\Lambda_b \to \Lambda\psi$, with $\lambda \to p\pi^-$ and $\psi \to \ell^+\ell^-$ ($BR \sim 4 \times 10^{-5}$).

(i) $b \to s\gamma$.

For a detailed discussion of CP asymmetries in this mode, see ref. [9]. CLEO has measured the exclusive mode [10]: $BR(B \to K^*\gamma) = (4.5 \pm 1.5 \pm 0.9) \times 10^{-5}$. The eventual expectations for measurement of the inclusive branching ratio (dominated by background) are an upper bound of 1.2×10^{-4}, if no signal is observed, and a 10% accuracy measurement, if signal is observed at the Standard Model rate, $BR(B \to X_s\gamma) = (3-5) \times 10^{-4}$.

Can hadron machines be competitive? A Monte Carlo study of this mode has been carried out at UCLA [11]. An energy resolution of $\frac{10\%}{\sqrt{E}}$ and an angular resolution of 1 mrd for γ's are assumed. The signal is extracted by applying π^0 and η mass cuts. For the region $P_T \geq 3.6\ GeV$ the background is completely suppressed but the signal is still statistically significant.

(ii) $B^- \to K^-(K^+K^-)_\phi$; $B^- \to K^-(K^+\pi^-)_{K^{*0}}$.

We study the CP asymmetries in the $B^- \to K^-\phi$, $\phi \to K^+K^-$ mode ($BR \sim 10^{-5}$, $a_{CP} \sim 0.005$), and in the $B^- \to K^-K^{*0}$, $K^{*0} \to K^+\pi^-$ mode ($BR \sim 5 \times 10^{-7}$, $a_{CP} \sim 0.05$).

To estimate the efficiency, we use the following SFT numbers:

$$\begin{aligned}\epsilon_{\text{tot}} \sim& \text{accept.} \times \epsilon_{\text{trig}} \times \epsilon_{\text{vert}} \times \epsilon_{\text{rec}} \times \epsilon_{K/\pi} \\ \sim& 0.3 \times 0.2 \times (0.7)^3 \times (0.95)^3 \times (0.9)^3 \sim 0.02.\end{aligned} \tag{011}$$

The total number of events is then

$$\begin{aligned}N_{\text{evts}}((K^-K^+)_\phi K^-) \sim& \epsilon_{\text{tot}} \times BR(B^- \to \phi K^-) \times N_{B^-} \times BR(\phi \to K^-K^+) \\ \sim& 1000.\end{aligned} \tag{012}$$

Similarly,

$$N_{\text{evts}}((K^-\pi^+)_{K^{*0}}K^-) \sim 50. \tag{013}$$

However, K/π separation is critical. For $B^- \to \phi K^-$, there is background from $B^- \to \phi\pi^-$ (with opposite a_{CP}!), and we need a factor of 10 rejection. For $B^- \to K^{*0}K^-$, there is background from $B^- \to \bar{K}^{*0}\pi^-$, and we need a factor of 400 rejection.

(*iii*) Bottom Baryon Decays.

For a detailed discussion of CP asymmetries in baryon decays, see ref. [12]. The modes $\Lambda_b \to pK^-$ and $\Lambda_b \to \Lambda\rho^0$ have branching ratios of order 10^{-5} and CP asymmetries of order a few percent. To estimate the number of events, we take the fraction of bottom baryons to be 0.1 of the bottom hadrons, $\epsilon_{\text{trig}} \sim 10^{-3}$, $\epsilon_{\text{rec}} \sim 0.5$ and $\epsilon_{\text{vert}} \sim 0.5$. The number of events, as fraction of total b's, is then

$$\frac{N_{\text{evts}}}{b-\text{hadrons}} \sim \epsilon_{\text{tot}} \times BR(\Lambda_b \to pK^-) \times (N_{\Lambda_b}/N_b) \sim 2.5 \times 10^{-10}, \tag{014}$$

so that at the SDC we expect 1250 events.

Suppression of background can be achieved by

a. Secondary vertex,

b. Kinematics ($\Delta m \approx 25\ MeV$),

c. Particle ID (in some detectors).

This would make this measurement essentially background-free.

For $\Lambda_b \to (p\pi^-)_\Lambda(K^+\pi^-)_{K^{*0}}$, we estimate the number of events, as fraction of total b's:

$$\frac{N_{\text{evts}}}{b-\text{hadrons}} \sim \epsilon_{\text{tot}} \times BR(\Lambda_b \to \Lambda K^{*0}) \times BR(\Lambda \to p\pi) \times BR(K^{*0} \to K^+\pi^-) \\ \times (N_{\Lambda_b}/N_b) \sim 10^{-10}, \tag{015}$$

so that we expect about 500 events in the SDC. This mode is probably relatively background free.

For $\Xi_b^0 \to (p\pi^-)_\Lambda(K^+K^-)_\phi$, we estimate the number of events, as fraction of total b's:

$$\frac{N_{\text{evts}}}{b-\text{hadrons}} \sim \epsilon_{\text{tot}} \times BR(\Xi_b \to \Lambda\phi) \times BR(\Lambda \to p\pi) \times BR(\phi \to K^+K^-) \\ \times (N_{\Xi_b}/N_b) \sim 10^{-11}, \tag{016}$$

(where we estimate $\Xi_b^0/\Lambda_b \sim 0.1$) so that we expect about 50 events in the SDC.

For $\Xi_b^0 \to (p\pi^-)_\Lambda(\mu^+\mu^-)_\psi$, we estimate the number of events, as fraction of total b's:

$$\frac{N_{\text{evts}}}{b-\text{hadrons}} \sim \epsilon_{\text{tot}} \times BR(\Xi_b \to \Lambda\psi) \times BR(\Lambda \to p\pi) \times BR(\psi \to \mu^+\mu^-) \\ \times (N_{\Xi_b}/N_b) \sim 7 \times 10^{-9}. \tag{017}$$

We need to add a factor to account for self triggering (by two muons and some P_T cut). We estimate this extra factor to be 0.1%, reducing the above estimate to 7×10^{-12}. We then expect 35 events for the SDC.

An *optical trigger* would help with these modes.

6. CONCLUSIONS

Hadron colliders are capable of investigating aspects of B physics where high statistics is a necessity and background is easily rejected. Among the "clean zeros" in CP asymmetries in B_s decays, the $B_s \to \psi\phi$ mode seems promising for hadron colliders. Among flavor changing decays with two final charged leptons, the $B \to K\mu^+\mu^-$ mode seems to be experimentally most feasible. For the observation of direct CP violation, the $B^- \to \phi K^-$ and $\Lambda_b \to pK^-$ modes seem promising. A detailed Monte Carlo investigation of these and other modes is well worth performing.

7. REFERENCES

1. Y. Nir, in the *Proc. of the Twentieth SLAC Summer Institute on Particle Physics, July 1992*, ed. L. Vassilian (1992).
2. Y. Nir, these proceedings.
3. B. Grinstein, M.J. Savage and M.B. Wise, Nucl. Phys. B319 (1989) 271; A. Ali, T. Mannel and T. Morozumi, Phys. Lett. B273 (1991) 505.
4. W. Skiba and J. Kalinowski, IFT-25-92 (1992).
5. M. Savage, Phys. Lett. B266 (1991) 135.
6. D. London, these proceedings.
7. C. Albajar *et al.* (UA1 Collaboration), Phys. Lett. B262 (1991) 163.
8. J.M. Gerard and W.S. Hou, Phys. Lett. B253 (1991) 478; Phys. Rev. D43 (1991) 2909; L. Wolfenstein, Phys. Rev. D43 (1991) 151; H. Simma, G. Eilam and D. Wyler, Nucl. Phys. B352 (1991) 367.
9. J.M. Soares, Nucl. Phys. B367 (1991) 575.
10. R. Ammar *et al.* (CLEO Collaboration), Phys. Rev. Lett. 71 (1993) 674.
11. D.B. Cline *et al.*, UCLA-APH0070-6/93 (1993).
12. I. Dunietz, Z. Phys. C56 (1992) 129.

A STUDY OF SOME RARE SELF-TAGGING B DECAYS

A. J. SCHWARTZ
Physics Department, Princeton University
Princeton, New Jersey 08544

1. INTRODUCTION

To observe a manifest violation of CP symmetry in the B system requires observing a difference in total or differential rate between decays of B's and $\overline{B}$'s. The necessity of knowing the initial-state flavor requires, for non-flavor-specific decays such as ψK_S, identifying the b-flavored meson or baryon which was produced in association with the B of interest. Such 'opposite-side' tagging has been extensively studied[1,2] and usually results in a significant loss in acceptance. An alternative method[3] is to study decay channels which by virtue of charge, strangeness or other additive quantum numbers unambiguously identifies the b or $\bar{b}$ nature of the decaying B. For example, observing a final state of D^0K^- indicates B^- decay, while $\overline{D^0}K^+$ indicates B^+ decay. Thus to observe CP violation in an experiment producing equal numbers of B^+'s and B^-'s, one compares the number of observed D^0K^- decays to the number of observed $\overline{D}^0K^+$ decays. A difference in yields indicates a difference in decay rates.

A partial list of self-tagging decay modes of current theoretical interest is given in Table 1, along with the branching ratio and CP asymmetry expected from Standard Model physics.[3,4] The decay mode $B^0_d \rightarrow K^{0*}\overline{K}^{0*}$ can probably not be self-tagged but is included for completeness. CP violation arises within the Standard Model from the interference of two or more amplitudes with different weak phases ϕ_1 and ϕ_2. Because weak phases change sign under CP conjugation, the interference term which arises upon squaring the sum of the amplitudes is proportional to $\cos(\phi_1-\phi_2)$ for B decay and $\cos(\phi_2-\phi_1)$ for $\overline{B}$ decay. Because of the evenness of the cosine function, to observe a physical effect requires an additional phase which does not change sign under CP, e.g. a strong phase; the interference term is then $\cos(\phi_1-\phi_2+\Delta\delta)$ for B's and $\cos(\phi_2-\phi_1+\Delta\delta)$ for $\overline{B}$'s, where $\Delta\delta \equiv \delta_2-\delta_1$ is the difference in strong phases. If the strong phases for some reason are equal, $\Delta\delta=0$ and no difference in decay rates will be seen.

The first two modes listed in Table 1 have a CP asymmetry resulting from the interference of two tree-level Cabibbo-suppressed amplitudes. The latter eight modes result from penguin graphs which have interference arising from different quark flavors propagating within the internal loop; the dispersive amplitude resulting from off-shell flavors interferes with the absorptive amplitude arising from on-shell flavors. In this table and throughout this paper, charge-conjugate modes are assumed. The list is limited to those modes with the greatest potential for experimental observation, i.e. two-body decays with all charged daughters in the final-state. For modes producing neutral kaons, only K^{0*} and $\overline{K^{0*}}$ final states are considered as the secondary vertex arising from the $K^* \to K^{\pm}\pi^{\mp}$ decay is considered essential for rejecting background at the requisite level. Finally, only the first six modes are pursued here, as these alone can produce two or more charged K's in the final state when $D^0_1 \to K^+K^-$, $\phi \to K^+K^-$, or $K^{0*} \to K^+\pi^-$. These K's can potentially be used to trigger a fixed-target experiment, and such a trigger is studied here. Both the acceptance and rate of the trigger are considered, and the number of events which an experiment using such a trigger could observe by the end of the 1990's is estimated.

Table 1. Self-tagging B decay modes with all charged daughters. The estimated branching ratios and CP asymmetries are from references 3 and 4. Charge-conjugate modes are assumed.

Quark subprocess	Decay mode	Branching ratio	CP asymmetry
$b \to uW^-$, $W^- \to \bar{u}d$	$B^- \to D^0_1 K^-$	$\sim 10^{-4}$	$\sim 10\%$
$b \to cW^-$, $W^- \to \bar{u}s$	$B^0_d \to D^0_1 K^{0*}$		
$b \to s s\bar{s}$	$B^0_d \to \phi K^{0*}$	$\sim 10^{-5}$	$\sim 0.5\%$
	$B^- \to \phi K^-$		
$b \to d s\bar{s}$	$B^0_d \to K^{0*}\overline{K}^{0*}$	$\sim 10^{-6}$	$\sim 10\%$
	$B^- \to K^{0*}K^-$		
$b \to s u\bar{u}$	$B^0_d \to K^+\pi^-$	$\sim 10^{-5}$	few percent
	$B^- \to K^-\rho^0$		
$b \to d u\bar{u}$	$B^0_s \to K^-\pi^+$	$\sim 10^{-6}$	$\sim 10\%$
	$B^- \to \pi^-\rho^0$		

2. EXPERIMENTAL METHOD

The two or more charged K's produced by the first six modes of Table 1 can be tagged by threshold Čerenkov counters. The main difficulty in using such counters as a trigger is preventing the trigger from being saturated by pions from the primary interaction. To accomplish this one chooses a counter with a K threshold high enough such that a large fraction of accepted K's *do not* cause it to fire; the $\int B\,dl$ of the spectrometer magnet and position of the counter are then adjusted such that most pions below *their* threshold are not accepted. For example, a counter filled with N_2 has Čerenkov thresholds of $p_{\rm thresh}(\pi) = 5.7$ GeV/c and $p_{\rm thresh}(K) = 20.2$ GeV/c. For a magnet giving a p_T impulse of 530 MeV/c, kaons below threshold are bent by $> 1.5°$ while pions below threshold are bent by $> 5.3°$. A Čerenkov counter located 20 m downstream of the magnet covering $|x| < 1.86$ m is thus hit by kaons below threshold but missed by π's (the magnet bends in the horizontal plane). A kaon with momentum 5.7–20.2 GeV/c can thus be identified with a well-segmented scintillator firing in anti-coincidence with a Čerenkov mirror located immediately behind (Figure 1). This simple picture neglects the intrinsic p_T, or more specifically p_x, of the π or K and also assumes that the π or K enters the magnetic field at $x \sim 0$. The latter condition can be imposed by positioning the production target as close to the upstream end of the magnet as possible and (if necessary) placing tracking stations within the magnetic field. The intrinsic p_x which a track must have to be accepted is to first approximation limited to an interval $\Delta p_x = \pm p_z \tan\theta$ around the negative of the p_x impulse of the magnetic field, where θ is the half-angle subtended by the Čerenkov counter. If the angle subtended is small, then pions with low momentum must have values of p_x near $-p_x^{\rm magnet}$ to be accepted. If such larger-p_x tracks can be rejected, e.g. by a strategically-placed collimator, then only a fraction of π's below threshold would be accepted by the Čerenkov counter.

Figure 2 shows data from FNAL hadroproduction experiment 791, in which a 500 GeV/c π^- beam is incident on Pt and C target foils. The experimental layout is shown in Figure 3. The total $\int B\,dl$ of the spectrometer magnets correspond to a p_T impulse of 530 MeV/c, which is why this value was used above. Figure 2a shows the x position of tracks at a z position 20 m downstream of the center of the magnets plotted versus track momentum. There is an abundance of low momentum tracks (nominally pions) within the region $|x| < 1.86$ m. Figure 2b shows the same data but with a cut $|x| < 4$ cm made at the upstream end of the first magnet. This cut restricts tracks to enter the magnetic field at $x \sim 0$, and because the production target is located 2 m further upstream also restricts p_x to have magnitude $\lesssim 200$ MeV/c. The plot shows that low-momentum tracks are significantly reduced from the central x region. Figure 2c shows the projection in momentum of tracks with $|x| < 1.86$ m from Figures 2a and 2b. The difference between the solid and dashed histograms shows that the cut $|x| < 4$ cm effectively eliminates pions below threshold (5.7 GeV/c); using an N_2 Čerenkov counter covering $|x| < 1.86$ m to trigger should thus yield a $K^{\pm}$ sample with little pion contamination.

3. ACCEPTANCE

To optimize the acceptance of such a trigger one requires that the momentum interval between π and K thresholds for a particular Čerenkov gas be well-matched to the momentum spectrum of kaons of interest which are incident on the counter. Table 2 lists the π and K thresholds for three different gases spanning a range of indices of refraction. The fourth and fifth columns list the angles through which tracks at these momenta would bend, and the sixth and seventh columns list the z position from the center of the magnet and the horizontal coverage respectively of a Čerenkov counter which would accept K's below threshold but reject π's below threshold. The table assumes that the magnet gives a p_T impulse of 530 MeV/c, that particles enter the magnet near $x = 0$, and that the initial p_x of tracks is small. The z positions of 10, 20, and 40 m (from center of magnet) are chosen to give a Δx sufficient for good mirror segmentation but also give a kaon survival fraction of $> 80\%$. The transverse dimensions of Table 2 are checked against data in Figures 2f and 2i to confirm that such apertures accept few tracks with $p < p_{\rm thresh}(\pi)$. For the He counter, the cut $|x| < 4$ cm at the upstream end of the first magnet reduces the number of tracks below threshold by a factor 5.6 (Figure 2i); an upstream cut of $|x| < 3$ cm reduces such tracks by a factor 10.2.

To find the acceptances of such counters, we generate event samples of the six di-kaon decay modes of Table 1 with the LUND Monte Carlo. We also generate a sample of $B^- \to D^0K^-$ decays where $D^0 \to K^-\pi^+$; the rate of this decay along with the rate of $B^{\pm} \to D^0_1 K^{\pm}$ (plus charge-conjugate modes) can be used to extract the CKM angle γ even if a CP asymmetry is *not* manifest.[3] For the B modes studied only the secondary decays

$D_1^0 \to K^+K^-$, $D^0 \to K^-\pi^+$, $\phi \to K^+K^-$, and $K^{0*} \to K^+\pi^-$ are considered.

Table 2. Čerenkov momentum thresholds, bending angles corresponding to such thresholds, and z position and horizontal coverage of counters which would accept K's below threshold but reject π's. The magnetic field gives a p_x impulse of 530 GeV/c and the initial p_x of tracks is assumed small.

Counter gas	p_{thresh} (π)	p_{thresh} (K)	θ_π	θ_K	z (m) from center of magnet	$\lvert x\rvert < w$ (m) horizontal coverage
Freon 12	3.0	10.6	10°	2.9°	10	1.77
N_2	5.7	20.2	5.3°	1.5°	20	1.86
Helium	16.7	59.0	1.8°	0.51°	40	1.27

The standard E791 event generator is used in which quarks and gluons are scattered and fragmented via PYTHIA 5.6 and JETSET 7.3.[5] The fraction of events in which at least two kaons are accepted by a particular combination of counters from Table 2 is calculated and tabulated in Table 3. The acceptances include the fact that some decay modes have more than two kaons in the final state, and thus more than one combination of kaons can satisfy the trigger. The acceptances also include the probability that the kaons live long enough to reach $z = 10$, 20, or 40 m and that their x-positions at these z values are within the horizontal aperture of the relevant Čerenkov counter (see Table 2). This last requirement reduces the acceptance significantly, but to enlarge the solid angle of a counter would probably saturate the trigger with pions below threshold. All tracks are required to have $|x| < 4$ cm at the upstream end of the first magnet. This reduces the acceptance by a factor of 2 - 3, but the restriction is also probably needed to prevent soft pions from saturating the trigger.

Table 3. The acceptance of the trigger for different combinations of Čerenkov counters from Table 2. Only secondary decays $D_1^0 \to K^+K^-$, $D^0 \to K^-\pi^+$, $\phi \to K^+K^-$, and $K^{0*} \to K^+\pi^-$ are considered. The acceptances include the probability that the K's live long enough to reach the counters, that they fall within the counter apertures, and that they have $|x| < 4$ cm at the upstream end of the first magnet.

Decay Mode	Acceptance for different combinations of counters						
	Freon 12 only	N_2 only	Helium only	Freon 12 N_2	Freon 12 Helium	Helium N_2	All 3 counters
$B^- \to D_1^0K^-$	0.0000	0.0022	0.0298	0.0026	0.0360	0.0452	0.0486
$B_d^0 \to D_1^0K^{0*}$	0.0000	0.0014	0.0360	0.0024	0.0432	0.0564	0.0620
$B^- \to D^0K^-$	0.0000	0.0004	0.0094	0.0004	0.0100	0.0116	0.0120
$B_d^0 \to \phi K^{0*}$	0.0002	0.0082	0.0778	0.0092	0.0790	0.0966	0.0978
$B^- \to \phi K^-$	0.0010	0.0110	0.0600	0.0120	0.0610	0.0814	0.0824
$B_d^0 \to K^{0*}\overline{K}^{0*}$	0.0000	0.0000	0.0100	0.0000	0.0102	0.0120	0.0122
$B^- \to K^{0*}K^-$	0.0000	0.0002	0.0072	0.0002	0.0076	0.0090	0.0092

Table 3 shows that using an N_2 counter covering $|x| < 1.86$ m at 20 m and an He counter covering $|x| < 1.27$ m at 40 m gives acceptances for several modes of 5 - 10%. The acceptance when using all three counters together is only slightly higher. The acceptance is smallest for modes which rely on the K^- daughter of a B being detected, as the large Q of the decay provides the daughter K^- with large p_T, making it easy to miss the counters if the decay plane is not close to vertical. Finally, leaving a hole in the counters for the beam to pass through results in a negligible loss in acceptance.

4. TRIGGER RATE

To estimate the trigger rate we again study E791 data. Assuming the rate from soft pions is eliminated or significantly reduced, the trigger may be dominated by events with two kaons in the relevant momentum ranges coming from the primary interaction. The rate of this occuring is calculated from data as follows. In E791, the light yields from two Čerenkov counters (Figure 3) are used to compute a normalized likelihood for a track to satisfy a particular mass hypothesis, given its measured momentum. For each counter the Poisson probability $\mu^N e^{-\mu}/N!$ is calculated, where N is the number of photoelectrons observed and μ is the number expected for $m = m_\pi$, m_K, etc. The relative likelihood for a mass hypothesis is taken as the product of the two Poisson probabilities for that hypothesis multiplied by the *apriori* likelihood of the particle being an $e/\mu/\pi/K$ or p. The *apriori* likelihoods are just those which one would assign to a track if no Čerenkov information existed. These likelihoods are measured from a separate study of particle fluxes and for E791 have nominal $e/\mu/\pi/K/p$ values of 0.02/0.01/0.12/0.81/0.04 respectively. The relative likelihoods are then normalized as:

$$\mathcal{L}_i = \frac{A_i \times P_i^{up} \times P_i^{down}}{\sum_i (A_i \times P_i^{up} \times P_i^{down})} \tag{1}$$

where P_i^{up} is the Poisson probability for the upstream Čerenkov counter, P_i^{down} is the Poisson probability for the downstream counter, the A_i are the *apriori* likelihoods, and the summation i runs over species e, μ, π, K and p. For more details the reader is referred to reference 6. The normalized kaon likelihood for a sample of tracks which would be accepted by either the N_2 or He counters of Table 2 is shown in Figure 4. The *apriori* likelihood of a track being a kaon is 0.12, and the large peak at this value reflects the large number of tracks which had a light yield such that the Čerenkov counters could not discriminate among π, K, or p. The peak at 0.75 represents tracks which are K-p indefinite.

For an individual event, the probability that there is at least one kaon in the event which would trigger a particular combination of Čerenkov counters from Table 2 is:

$$1 - \prod_j (1 - \mathcal{L}_K)_j \tag{2}$$

where j runs over all tracks accepted by the counters, i.e. tracks having momenta in one of the relevant ranges and projecting within the corresponding aperture. For consistency with the acceptance calculation of the previous section, all tracks are required to have $|x| < 4$ cm at the upstream end of the first magnet. The probability (2) is calculated event-by-event for each of seven counter combinations, and the average probability for 5000 minimum bias events is found. The calculation is then repeated using a more restricted sample: those events which already have a kaon present ($\mathcal{L} > 0.5$ for an accepted track). The kaon candidate itself is excluded from the second probability calculation. The probability for an event to have two kaons accepted by a particular counter combination is then the average probability for an event to have at least one kaon accepted multiplied by the average probability for an event to have a second kaon accepted given that it already has at least one accepted. This 'di-kaon' probability is multiplied by the fraction of interactions which satisfy the minimum bias trigger (0.45) to arrive at a di-kaon trigger fraction. The resultant trigger fractions for the seven combinations of counters are listed in Table 4. For an He counter at $z = 40$ m and an N_2 counter at $z = 20$ m, the trigger fraction is 0.57%. Whether this rate can be tolerated at the first trigger level depends on beam intensity, the through-put of higher-level triggers, and ultimately the tape-writing speed.

Table 4. The fraction of interactions which trigger the detector for different combinations of Čerenkov counters from Table 2. The rejection of the trigger is the reciprocal of the listed values.

Trigger fraction for different combinations of counters						
Freon 12 only	N_2 only	Helium only	Freon 12 N_2	Freon 12 Helium	Helium N_2	All 3 counters
0.00033	0.0019	0.00084	0.0032	0.0026	0.0057	0.0082

5. FINAL SENSITIVITY

The overall detection efficiency for the six modes of interest is the (geometric acceptance) $\times$ (secondary branching ratios) $\times$ (reconstruction efficiency). Taking the geometric acceptances from the He + N_2 column of Table 3 and assuming the reconstruction efficiency to be a nominal 0.70, one arrives at the values listed in the second column of Table 5. Multiplying these efficiencies by the expected B branching ratios and the number of B's produced in a given running period gives the number of rare decays observed.

The number of B's which can potentially be produced in a fixed-target experiment at FNAL is estimated from the data of FNAL E789, which searched for the decay $B \to \psi X$, $\psi \to \mu^+\mu^-$. This experiment took B data for two months with a relatively high intensity beam (5×10^{10} protons per spill) and has identified 24 $B \to \psi X$ candidates in 50% of their data.[7] With a geometric acceptance of 0.006 and a vertex efficiency of 0.25, this event yield implies that they produced 4.8×10^7 B's (taking $B(B \to \psi X) = 0.0112$ and $B(\psi \to \mu^+\mu^-) = 0.0597$[8]). It is estimated that this experiment could handle $10\times$ greater beam intensity (limited by rates in the silicon vertexer),[9] and running at such an intensity for three 4-month periods would gain a factor of 60 in statistics. The experiment could thus produce 2.9×10^9 B's by the latter half of the 1990's. Multiplying half of this number (assuming charged and neutral B's each comprise half the sample) by the overall efficiencies of Table 5 gives the projected event samples listed in the fourth column. For comparison, the numbers of events one must reconstruct in order to observe a CP asymmetry at the 3σ statistical level are listed in the fifth column. Comparing the two columns shows that the experiment could not establish CP violation in B decays unless the CP asymmetries or branching ratios were larger than expected. The experiment could measure the rates of these rare processes, which may be very worthwhile, and it may be able to measure $\sin\gamma$, depending on the value of γ and the difference in strong phase shifts between $B^- \to D^0K^-$ and $B^- \to \overline{D}^0K^-$; this last issue is addressed in reference 10.

Table 5. The total detection efficiency (see text), the expected branching ratio, the number of reconstructed events in 2.9×10^9 B decays, and the number of events needed to see a CP asymmetry at the 3σ statistical level. Only secondary decays $D_1^0 \to K^+K^-$, $D^0 \to K^-\pi^+$, $\phi \to K^+K^-$, and $K^{0*} \to K^+\pi^-$ are considered.

Decay mode	Total efficiency	Expected B.R.	# of events observed in 2.9×10^9 B decays	# of events needed for 3σ asymmetry
$B^- \to D_1^0K^-$	1.3×10^{-4}	$\sim 10^{-4}$	19	450
$B_d^0 \to D_1^0K^{0*}$	1.1×10^{-4}	$\sim 10^{-4}$	16	450
$B^- \to D^0K^-$	3.0×10^{-4}	$\sim 10^{-4}$	43	–
$B_d^0 \to \phi K^{0*}$	2.2×10^{-2}	$\sim 10^{-5}$	320	1.8×10^5
$B^- \to \phi K^-$	2.8×10^{-2}	$\sim 10^{-5}$	410	1.8×10^5
$B_d^0 \to K^{0*}\overline{K}^{0*}$	3.7×10^{-3}	$\sim 10^{-6}$	5.5	450
$B^- \to K^{0*}K^-$	4.2×10^{-3}	$\sim 10^{-6}$	6.1	450

In closing, three issues which this study did not address should be mentioned: that of background rejection, normalization, and running a silicon vertexer in a high intensity proton beam. The background rejection of the experiment is expected to be very good, as all decays of interest have at least one secondary vertex, at least one 2-body mass constraint, and at least two charged kaons. The $B^0 \to D_1^0K^{0*}$ mode, which has two secondary vertices, three charged kaons, and a higher 10^{-4} branching ratio, may be especially clean.

The issue of normalization arises because B^+'s and B^-'s or B^0's and $\overline{B}^0$'s are not necessarily produced in equal numbers in pp collisions, and one cannot simply compare yields of ϕK^- events and ϕK^+ events, for instance. Instead one must normalize the yields to some more copious but self-tagging and reconstructable mode such as $B^- \to \psi K^-$ or $B^0 \to \psi K^{0*}$. This will probably require another trigger stream, such as a dimuon stream.

The question of running a silicon vertexer efficiently in a high intensity beam is an open issue which may be solved by de-focusing the beam at the target/vertexer station such that the radiation dose is distributed over a larger area of silicon.[11] It may also be desirable to reduce occupancy in the detector by using pixel-based CCD's[12] rather than more conventional silicon strips.

6. ACKNOWLEDGEMENTS

I thank the workshop organizers Jeff Appel and Vera Luth for providing a pleasant and productive research environment, the E791 collaboration for providing use of its Monte Carlo program, and Lucien Cremaldi and Shekhar Mishra for useful discussions.

7. REFERENCES

1. *The Physics Program of a High-Luminosity Asymmetric B Factory at SLAC*, SLAC-353 (1989).
2. *CESR B Factory: Physics Rationale for a B-Factory*, CLNS 91-1043 (1991).
3. M. Gronau and D. Wyler, *Phys. Lett.* **265B** (1991) 172.
   I. Dunietz, *Phys. Lett.* **270B** (1991) 75.
   M. Gronau and D. London, *Phys. Lett.* **253B** (1991) 483.

4. J.-M. Gérard and W.-S. Hou, *Phys. Lett.* **253B** (1991) 478.

J.-M. Gérard and W.-S. Hou, *Phys. Rev.* **D43** (1991) 2909.

5. T. Sjöstrand, CERN-TH.6488/92 (1992).

6. D. Bartlett *et al.*, *Nucl. Instr. Meth.* **A260** (1987) 55.

7. C. Shekhar Mishra, *B Results from Fixed-Target Experiments at Fermilab*, talk presented at the Workshop on *B* Physics at Hadron Accelerators, Snowmass, CO, 1993.

8. K. Hikasa *et al.* (Particle Data Group), Phys. Rev. D45 (1992).

9. C. Shekhar Mishra, private communication.

10. S. Stone, *Possible Ways of Observing CP Violation at a Symmetric e^+e^- B Factory*, HEPSY 92-2 (1992).

11. *FNAL proposal 867*, B. Cox, spokesman.

12. C. J. S. Damerell *et al.*, *Proceedings of the XXVI International Conference on High Energy Physics: Dallas, TX 1992*, James R. Sanford, editor (American Institute of Physics, New York, 1993).

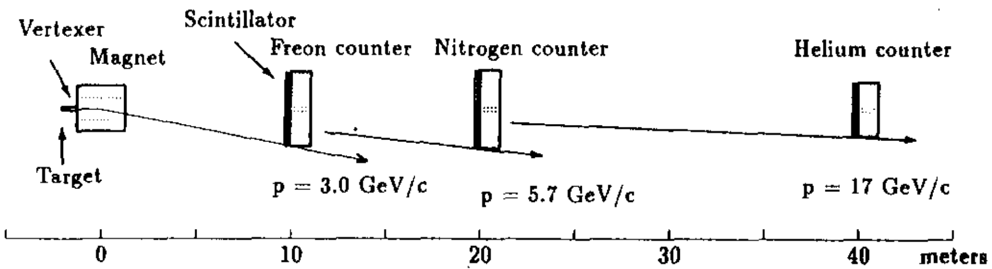

Figure 1. Plan view of detector for triggering on $B \to K^{\pm}K^{\pm}X$ decays.

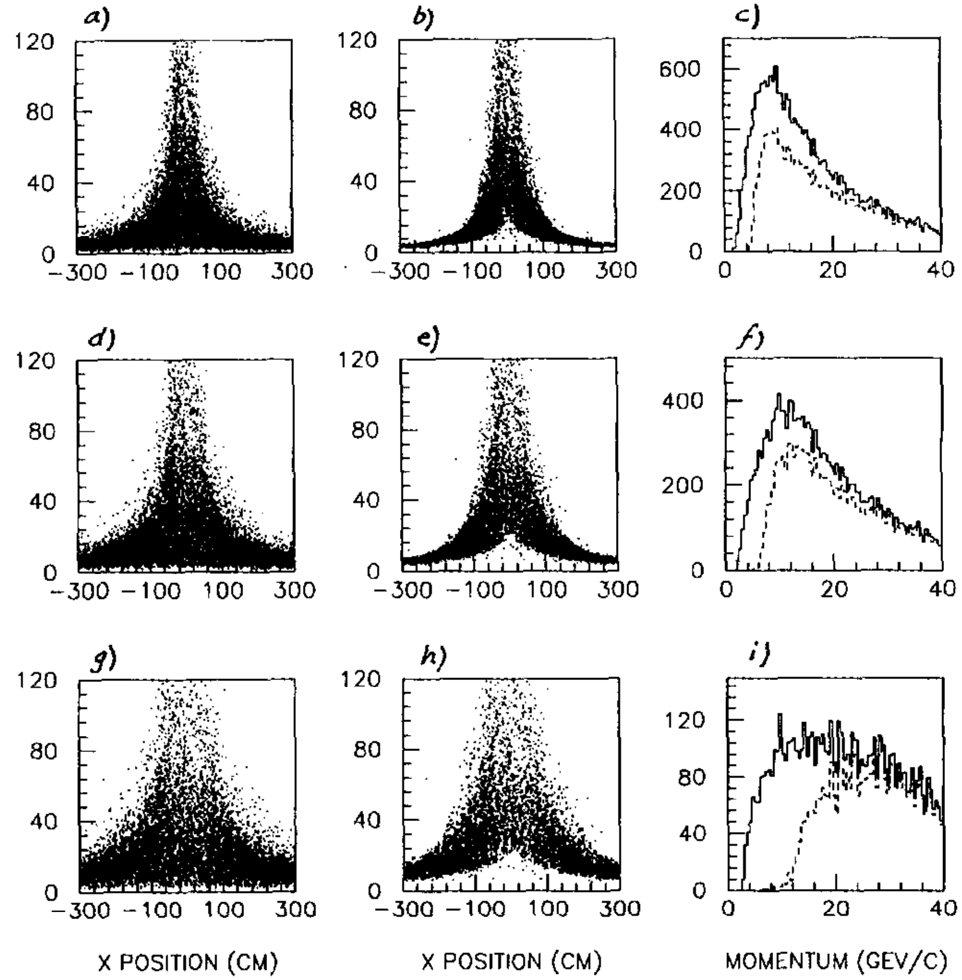

Figure 2. Data from FNAL hadroproduction experiment 791. *a)* The x position of tracks 20 m downstream of the center of the magnets plotted versus track momentum (GeV/c). *b)* Same as *a* except the tracks are required to have $|x| < 4$ cm at the upstream end of the first magnet. *c)* Momentum projection of *a* (solid) and *b* (dashed). Only tracks with $|x| < 1.86$ m are plotted. *d)* – *f)* Same as *a* – *c* except that $z = 10$ m and the aperture cut is $|x| < 1.77$ m. *g)* – *i)* Same as *a* – *c* except that $z = 40$ m and the aperture cut is $|x| < 1.27$ m.

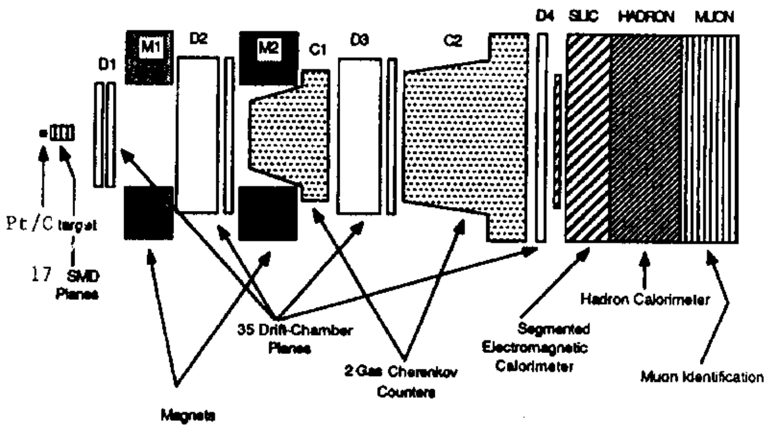

Figure 3. Plan view of the detector used for FNAL experiment 791.

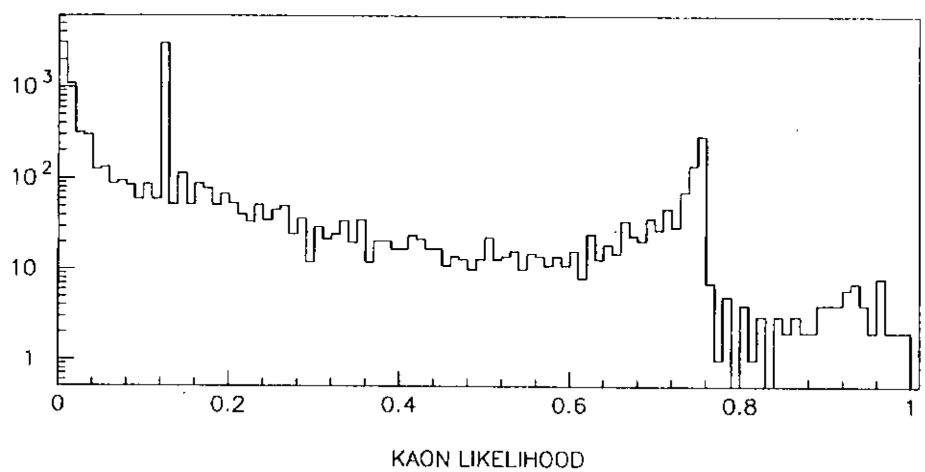

Figure 4. The kaon likelihood (see text) for E791 tracks which would be accepted by the N_2 or He Čerenkov counters of Table 2. All tracks are required to have $|x| < 4$ cm at the upstream end of the first magnet.

CP VIOLATION OUTSIDE THE STANDARD MODEL PHENOMENOLOGY FOR PEDESTRIANS

HARRY J. LIPKIN

Department of Nuclear Physics, Weizmann Institute of Science
Rehovot 76100, Israel

and

Raymond and Beverly Sackler Faculty of Exact Sciences
School of Physics and Astronomy, Tel Aviv University, Tel Aviv, Israel

and

High Energy Physics Division, Argonne National Laboratory
Argonne, IL 60439-4815, USA

1. INTRODUCTION - TWO WAYS TO SEE CP VIOLATION

Before 1964 the two kaon flavor eigenstates K^o and $\bar{K}^o$ carrying strangeness ± 1 were believed to be CP - conjugate and mixed by a CP-conserving weak interaction into mass eigenstates $|K_S\rangle$ and $|K_L\rangle$ which were also CP eigenstates with opposite eigenvalues. Very different lifetimes arise ($\tau_S = 9\times 10^{-11}$ sec; $\tau_L = 5\times 10^{-8}$sec) because the dominant 2π decay mode with largest phase space is allowed by CP only for K_S. $K_L \rightarrow 2\pi$ was a transition between CP-eigenstates with opposite eigenvalues and therefore forbidden.

So far the only experimental evidence for CP violation is the 1964 discovery[1] of $K_L \rightarrow 2\pi$ where the two mass eigenstates produced by neutral meson mixing both decay into the same CP eigenstate. This result is described by two parameters,

$$\eta_{+-} \equiv \frac{\langle\pi^+\pi^-|T|K_L\rangle}{\langle\pi^+\pi^-|T|K_S\rangle} \equiv \epsilon + \epsilon'; \quad \eta_{oo} \equiv \frac{\langle\pi^o\pi^o|T|K_L\rangle}{\langle\pi^o\pi^o|T|K_S\rangle} \equiv \epsilon - 2\epsilon' \tag{1.1}$$

Today $\epsilon \approx$ its 1964 value, ϵ' data are still inconclusive and there is no new evidence for CP violation. One might expect to observe similar phenomena in other systems and also direct CP violation as charge asymmetries between decays of charge conjugate hadrons $H^\pm \rightarrow f^\pm$. Why is it so hard to find CP violation? How can B Physics help? Does CP lead beyond the standard model? We now present a pedestrian symmetry approach which exhibits the difficulties and future possibilities of these two types of CP-violation experiments, neutral meson mixing and direct charge asymmetry: what may work, what doesn't work and why.

2. CHARGE ASYMMETRIES -DIFFICULTIES AND POSSIBILITIES

2.1 *How CPT complicates detection of CP Violation*

Can decays of K^+ and K^- be different? For decays to charge conjugate final states $|f^\pm\rangle$ described by the Fermi Golden Rule, CPT and hermiticity show there is no asymmetry,

$$W_{K^\pm\rightarrow f^\pm} \approx (2\pi/\hbar)|\left\langle f^\pm\right| H_{wk}\left|K^\pm\right\rangle|^2\rho(E_f) \tag{2.1}$$

$$\frac{|\langle f^-|H_{wk}|K^-\rangle|}{|\langle f^+|H_{wk}|K^+\rangle|} = \frac{CPT|\langle f^-|H_{wk}|K^-\rangle|}{|\langle K^+|H_{wk}^\dagger|f^+\rangle^*|} = \frac{|\langle K^+|H_{wk}|f^+\rangle|}{|\langle K^+|H_{wk}|f^+\rangle^*|} = 1 \tag{2.2a}$$

CPT also requires equal total widths of K^+ and K^-. Since s-wave elastic $\pi^\pm\pi^o$ scatterings go into one another under CPT, $\sigma_{el,s}(\pi^+\pi^o) = \sigma_{el,s}(\pi^-\pi^o)$ is a very narrow Breit-Wigner resonance at the kaon mass with the same width for both charge states,

$$\Gamma_{tot}(K^+) = \Gamma_{tot}(K^-) \tag{2.2b}$$

Thus the following conditions are necessary for observation of charge-asymmetric decays:

1. Golden rule breaks down. This is exact first order perturbation theory and can only break down where higher order contributions are important. Second-order weak contributions are negligible; thus higher order strong contributions are needed.
2. Conspiracy of several decay modes. Total widths must be equal. Any asymmetry in the partial widths of a pair of conjugate modes must be compensated by opposite asymmetries in other modes.

For kaons all charge asymmetry effects should be small. All principal decays lead to approximate strong S-matrix eigenstates and the golden rule should be good. S-wave $\pi^\pm\pi^o$ is an exact eigenstate of strong S since no inelastic channels are open. The 3π final states are dominated by I=1 s-wave and thus all nearly proportional to the same strong-S eigenstate. The I=3 component is $\Delta I = 5/2$ and doubly suppressed by $\Delta I = 1/2$.

2.2 Beating CPT for Charge Asymmetries in B Physics

Can decays of B^+ and B^- be different? Here many more channels are open, different decay modes can conspire to give the same total width and final state rescattering can beat the Fermi golden rule via higher order transitions in strong interactions; e.g.

$$B^- \to \bar{K}^o\pi^- \to K^-\pi^o; \qquad B^+ \to K^o\pi^+ \to K^+\pi^o \tag{2.3}$$

$$\frac{W_{B^+\to K^+\pi^o}}{W_{B^-\to K^-\pi^o}} = \frac{|S_{el}M(K^+\pi^o) + S_{cex}M(K^o\pi^+)|^2}{|S_{el}M(K^-\pi^o) + S_{cex}M(\bar{K}^o\pi^-)|^2} \tag{2.4}$$

where $M(f^\pm) \equiv \langle f^\pm|H_{wk}|B^\pm\rangle$ and S_{el} and S_{cex} denote strong elastic and charge exchange scattering. This has no simple counterpart in the kaon system. Here both $(K\pi)$ isospin eigenstates $I = 1/2$ and $I = 3/2$ are $\Delta I = 1$ and equally allowed.

A CP-violating asymmetry can arise in a toy model with only $B \to K\pi$ decays. The isospin eigenstates $(K\pi)_I$ are exact strong-S eigenstates. However, asymmetries can occur when final states are not strong eigenstates; e.g. $K^\pm\pi^o$, Thus for I=1/2 and 3/2,

$$|A\{(B^+ \to (K\pi)_I\}| = |A\{B^- \to (\bar{K}\pi)_I\}| \tag{2.5}$$

$$\Gamma_{tot}(B^+) = \sum_I \Gamma\{B^+ \to (K\pi)_I\} = \Gamma_{tot}(B^-) = \sum_I \Gamma\{B^- \to (\bar{K}\pi)_I\} \tag{2.6}$$

$$A\{B^\pm \to f^\pm\} = \sum_I C_I^f |A\{B^\pm \to (K\pi)_I\}| \cdot e^{\pm iW_I} e^{iS_I} \tag{2.7}$$

where C_I^f denotes isospin Clebsch-Gordan coefficients. Every isospin amplitude is written as the product of its magnitude, and weak and strong phase factors e^{-iW_I} and e^{iS_I}. The weak CP-violating phase reverses sign under charge conjugation; the strong CP-conserving phase remains unchanged. Then I=3/2 - 1/2 interference can produce charge asymmetry,

$$|A\{B^+ \to K^+\pi^o\}|^2 - |A\{B^- \to K^-\pi^o\}|^2 = -4C_{\frac{1}{2}}^f C_{\frac{3}{2}}^f |A_{\frac{1}{2}}A_{\frac{3}{2}}| \sin(W_{\frac{1}{2}} - W_{\frac{3}{2}}) \sin(S_{\frac{1}{2}} - S_{\frac{3}{2}}) \tag{2.8a}$$

$$|A\{B^+ \to K^o\pi^+\}|^2 - |A\{B^- \to \bar{K}^o\pi^-\}|^2 = 4C_{\frac{1}{2}}^f C_{\frac{3}{2}}^f |A_{\frac{1}{2}}A_{\frac{3}{2}}| \sin(W_{\frac{1}{2}} - W_{\frac{3}{2}}) \sin(S_{\frac{1}{2}} - S_{\frac{3}{2}}) \tag{2.8b}$$

The asymmetries are seen to be equal and opposite for the two charge states, cancel in the total rates as expected from CPT and vanish unless *both* $W_{\frac{1}{2}} \neq W_{\frac{3}{2}}$ *and* $S_{\frac{1}{2}} \neq S_{\frac{3}{2}}$. The vanishing of the asymmetry when $S_{\frac{3}{2}} = S_{\frac{1}{2}}$ is simply interpreted in view of eq. (2.4) since $S_{\frac{3}{2}} = S_{\frac{1}{2}}$ implies no charge exchange, $S_{cex} = 0$. Thus the condition for observing an asymmetry is that at least two amplitudes arising from different strong eigenstates must contribute, and that they must have both different strong phases and different weak phases.

2.3 Charge Asymmetry in Standard Model - Trees and Penguins in $B \to K\pi$ Decays

In the standard model two diagrams with different weak phases contribute to $B \to K\pi$ decays via two different strong eigenstates and can produce a CP asymmetry[2,3]. The tree diagram gives only $K^\pm\pi^o$; the penguin only I=1/2 $K\pi$.

$$B^+(\bar{b}u) \to_{(tree)} \to \bar{u} + W^+ + u \to \bar{u} + u + \bar{s} + u \to K^+ + \pi^o \tag{2.9a}$$

$$B^-(b\bar{u}) \to_{(tree)} \to u + W^- + \bar{u} \to u + \bar{u} + s + \bar{u} \to K^- + \pi^o \tag{2.9b}$$

$$B^+(\bar{b}u) \to_{(penguin)} \to \bar{t} + W^+ + u \to \bar{s} + u \to (K\pi)_{I=1/2} \tag{2.10a}$$

$$B^-(b\bar{u}) \to_{(penguin)} \to t + W^- + \bar{u} \to s + \bar{u} \to (\bar{K}\pi)_{I=1/2} \tag{2.10b}$$

So far no penguin contributions have been unambiguously identified and all model calculations should be taken with a grain of salt. The tree has two suppressed weak vertices, $b \to u$ and $s \to u$; the penguin has no such suppression and may be strong enough to compete with the tree and produce tree-penguin interference and CP violation.

Detection of $B^\pm \to K_S\pi^\pm$, forbidden in the simple tree diagram without final state interactions, would indicate either penguin or tree with final state interactions. Comparison with the $K^\pm\pi^o$ modes can check relative tree-penguin strengths. The two CP-violating ratios $\frac{|A\{B^+\to K^o\pi^+\}|^2 - |A\{B^-\to \bar{K}^o\pi^-\}|^2}{|A\{B^+\to K^o\pi^+\}|^2 + |A\{B^-\to \bar{K}^o\pi^-\}|^2}$ and $\frac{|A\{B^+\to K^+\pi^o\}|^2 - |A\{B^-\to K^-\pi^o\}|^2}{|A\{B^+\to K^+\pi^o\}|^2 + |A\{B^-\to K^-\pi^o\}|^2}$ can test CP violation over a wide range of relative penguin and tree contributions. Their numerators are equal, but the denominator for the tree-allowed $K^\pm\pi^o$ may be much larger if the penguin is relatvely small.

3. SYMMETRY ANALYSIS OF NEUTRAL MESON $M^O - \bar{M}^O$ MIXING

3.1 A Quasispin Description of Neutral Meson Mixing

We describe neutral meson mixing by a quasispin SU(2) picture with the two flavor eigenstates of the meson system, denoted by M and $\bar{M}$ defined as eigenstates of σ_z with "spin up" and "spin down" respectively[4,5,6,7],

$$\sigma_z|M^o\rangle = |M^o\rangle; \quad \sigma_z|\bar{M}^o\rangle = -|\bar{M}^o\rangle \tag{3.1}$$

Strong and electromagnetic interactions conserve quasispin. Weak interactions break quasispin. If CPT is conserved the mass eigenstates M_S and M_L are equal mixtures of M° and $\bar{M}^\circ$. We can then choose phases and the direction of the quasispin x axis to make

$$|M_L\rangle = (1/\sqrt{2})(|M^\circ\rangle + |\bar{M}^\circ\rangle); \quad \sigma_x |M_L\rangle = |M_L\rangle; \quad \langle M_L|\sigma_z|M_L\rangle = \langle M_L|\sigma_y|M_L\rangle = 0 \quad (3.2)$$

If CP is conserved, M_S and M_L are eigenstates of both CP and σ_x. If CP is violated, M_S and M_L are not necessarily orthogonal and both can decay into the same CP eigenstate $|f\rangle$. However, an orthonormal basis of linear combinations of the two mass eigenstates can always be constructed to forbid a given decay mode $|f\rangle$ for one of the basis states,

$$\langle f|T\left|M_\nu^f\right\rangle = 0; \qquad \left\langle M_\mu^f\middle|M_\nu^f\right\rangle = 0 \qquad (3.3)$$

This can be seen explicitly in the kaon case by using eqs. (1.1)

$$|K_\nu^{oo}\rangle \equiv |K_L\rangle - \eta_{oo}|K_S\rangle; \quad \langle\pi^\circ\pi^\circ|T|K_\nu^{oo}\rangle = 0 \qquad (3.4a)$$

$$\left|K_\nu^\pm\right\rangle \equiv |K_L\rangle - \eta_{+-}|K_S\rangle; \quad \left\langle\pi^+\pi^-\middle|T\middle|K_\nu^\pm\right\rangle = 0; \quad \langle\pi^\circ\pi^\circ|T\left|K_\nu^\pm\right\rangle = -3\epsilon'\langle\pi^\circ\pi^\circ|T|K_S\rangle \qquad (3.4b)$$

The parameter ϵ' expresses the difference between the states $|K_\nu^\pm\rangle$ and $|K_\nu^{oo}\rangle$. A $|K_\nu^\pm\rangle$ beam should not decay to $\pi^+\pi^-$, while the decay $K_\nu^\pm \to \pi^\circ\pi^\circ$ is proportional to ϵ' and could be used in a null experiment to determine ϵ'.

The basis (3.3) determines a direction in quasispin space. If M_ν^f and M_μ^f are equal mixtures of M° and $\bar{M}^\circ$, which often occurs when $|f\rangle$ is a CP eigenstate,

$$\left|M_\nu^f\right\rangle = (1/\sqrt{2})(e^{i\theta_f}|M^\circ\rangle + e^{-i\theta_f/2}\left|\bar{M}^\circ\right\rangle) = e^{i\sigma_z\theta_f/2}|M_L\rangle; \quad \left\langle M_\nu^f\middle|\sigma_z\middle|M_\nu^f\right\rangle = 0 \qquad (3.5a)$$

$$\left|M_\mu^f\right\rangle = (1/\sqrt{2})(e^{i\theta_f}|M^\circ\rangle - e^{-i\theta_f/2}\left|\bar{M}^\circ\right\rangle) = -ie^{i\sigma_z(\theta_f+\pi)/2}|M_L\rangle; \quad \left\langle M_\mu^f\middle|\sigma_z\middle|M_\mu^f\right\rangle = 0 \qquad (3.5b)$$

Then the state M_ν^f defines an axis in the $x-y$ plane at an angle θ_f away from the x axis. The values of θ_f for two different CP eigenstates are directly to the CP-violation parameters ϵ and ϵ' in the kaon case. If they are the same for two eigenstates, like $\pi^+\pi^-$ and $\pi^\circ\pi^\circ$, $\epsilon' = 0$. If CP is conserved, $\theta_f = 0$ when f is a CP-eigenstate.

The EPR effect provides a means for creating beams of particles in the state $\left|M_\nu^f\right\rangle$ defined by eq. (3.3). The decay of the odd-parity ϕ vector meson at rest into an odd-parity state of two neutral kaons with momenta $\vec{k}$ and $-\vec{k}$ can be described both in the $(K^\circ;\bar{K}^\circ)$ and $(K_\mu^\pm;K_\nu^\pm)$ bases.

$$\phi \to K^\circ(\vec{k})\bar{K}^\circ(-\vec{k}) - K^\circ(-\vec{k})\bar{K}^\circ(\vec{k}) = K_\nu^\pm(\vec{k})K_\mu^\pm(-\vec{k}) - K_\mu^\pm(-\vec{k})K_\nu^\pm(\vec{k}) \qquad (3.6)$$

If a decay $K_\mu^\pm \to \pi^+\pi^-$ is detected at $-\vec{k}$, the wave function collapses to make $K_\nu^\pm$ beam at $\vec{k}$. This proposal[8], called "An experiment for the future" in 1968 is now being implemented at ϕ factories.

A similar approach to the B system, using the basis (3.3) and the odd-parity $\Upsilon(4S)$ as the B analog of the ϕ gives

$$\Upsilon(4S) \to B^\circ(\vec{k})\bar{B}^\circ(-\vec{k}) - B^\circ(-\vec{k})\bar{B}^\circ(\vec{k}) = B_\nu^f(\vec{k})B_\mu^f(-\vec{k}) - B_\mu^f(-\vec{k})B_\nu^f(\vec{k}) \qquad (3.7)$$

The EPR effect is in common use in $\Upsilon(4S)$ B decay experiments[9,7], noting that detecting a $B_\mu^f \to f$ at $-\vec{k}$ produces a B_ν^f beam at $\vec{k}$.

3.2 Quasispin Symmetry Breaking by Mass and Lifetime Differences

The lifetime difference is determined by phase space and independent of the standard model. The mass difference is determined by dynamical effects depending upon standard model. Lifetime symmetry breaking is dominant in the kaon system where a pure K_L state can be produced simply by waiting. Mass breaking is dominant in heavy quark mesons and can be described as a "magnetic field" in quasispin space.

In the B system where the lifetime difference is negligible we denote the mass eigenstates as B_L (light) and B_H (heavy), rather than long and short, The states B_L and B_H are orthogonal and eqs. (3.2) and (3.5) can be rewritten

$$|B_L\rangle = (1/\sqrt{2})(|B^\circ\rangle + \left|\bar{B}^\circ\right\rangle); \quad \sigma_x|B_L\rangle = |B_L\rangle; \quad \langle B_L|\sigma_z|B_L\rangle = \langle B_L|\sigma_y|B_L\rangle = 0 \quad (3.8a)$$

$$|B_H\rangle = (1/\sqrt{2})(|B^\circ\rangle - \left|\bar{B}^\circ\right\rangle); \quad \sigma_x|B_H\rangle = -|B_H\rangle; \quad \langle B_H|\sigma_z|B_H\rangle = \langle B_H|\sigma_y|B_H\rangle = 0 \quad (3.8b)$$

$$\left|B_\nu^f\right\rangle = (1/\sqrt{2})(e^{i\theta_f}|B^\circ\rangle + e^{-i\theta_f/2}\left|\bar{B}^\circ\right\rangle) = e^{i\sigma_z\theta_f/2}|B_L\rangle; \quad \left\langle B_\nu^f\middle|\sigma_z\middle|B_\nu^f\right\rangle = 0 \qquad (3.9a)$$

$$\left|B_\mu^f\right\rangle = (1/\sqrt{2})(e^{i\theta_f}|B^\circ\rangle - e^{-i\theta_f/2}\left|\bar{B}^\circ\right\rangle) = e^{i\sigma_z\theta_f/2}|B_H\rangle; \quad \left\langle B_\mu^f\middle|\sigma_z\middle|B_\mu^f\right\rangle = 0 \qquad (3.9b)$$

A geometrical picture of the quasispin space is shown in Fig. 1

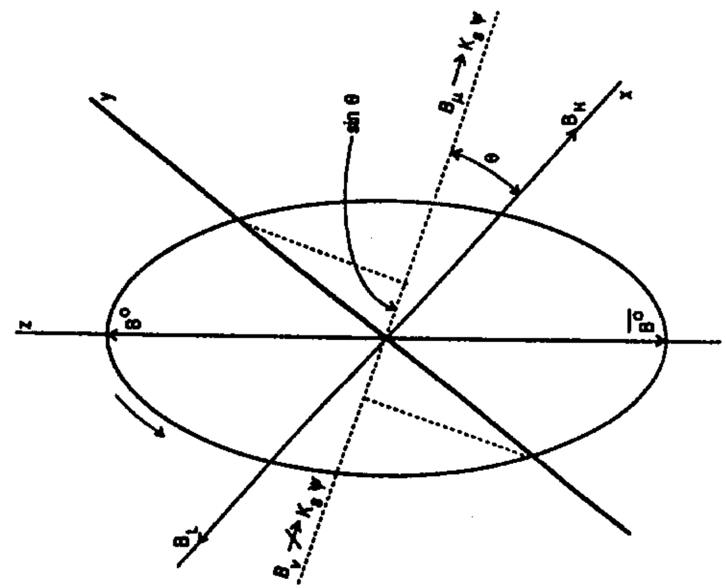

Figure 1. Geometrical representation of quasispin space

The time development of a general neutral B meson state is given by the product of a common exponential decay for all states and a quasispin precession in the magnetic field. Thus for a meson which is in the state $|B(0)\rangle$ at time $t = 0$

$$|B(t)\rangle = e^{-\frac{\Gamma}{2}t}e^{-i\omega\sigma_x(t/2)}|B(0)\rangle = e^{-\frac{\Gamma}{2}t}\cdot\{\cos(\frac{\omega t}{2}) - i\sigma_x\sin(\frac{\omega t}{2})\}|B(0)\rangle \qquad (3.10)$$

where Γ is the decay width and ω the mass difference between the two eigenstates.

3.3 Experiments as Quasispin Polarization Measurements

Many experiments can be described as polarization measurements in some direction in quasispin space at time t of a beam polarized at $t = 0$. A neutral B produced at time $t = 0$ in a hadronic experiment together with another B can be tagged as B or $\bar{B}$ by observing the decay of the other B. In many experiments the decay of the tagged B is observed to decay at time t and the quantity of physical interest is the difference between the decay rates into a given final state f for B's tagged as B or $\bar{B}$. This is proportional to the expression:

$$N(B^o \to f) - N(\bar{B}^o \to f) = |\left\langle B^f_\mu \right| e^{-i\omega\sigma_x(t/2)} |B^o\rangle|^2 - |\left\langle B^f_\mu \right| e^{-i\omega\sigma_x(t/2)} \left|\bar{B}^o\right\rangle|^2 \qquad (3.11a)$$

$$N(B^o \to f) - N(\bar{B}^o \to f) = \left\langle B^f_\mu \right| e^{-i\omega\sigma_x(t/2)}\sigma_z e^{i\omega\sigma_x(t/2)} \left| B^f_\mu \right\rangle = \left\langle B^f_\mu \right| \sigma_z e^{i\omega\sigma_x t} \left| B^f_\mu \right\rangle =$$

$$= \left\langle B^f_\mu \right| \sigma_z \cos(\omega t) + i\sigma_z\sigma_x \sin(\omega t) \left| B^f_\mu \right\rangle = \left\langle B^f_\mu \right| \sigma_z \left| B^f_\mu \right\rangle \cos(\omega t) - \left\langle B^f_\mu \right| \sigma_y \left| B^f_\mu \right\rangle \sin(\omega t) \qquad (3.11b)$$

where we have used quasispin algebra in the basis $(B^f_\mu; B^f_\nu)$ defined by eq.(3.3).

For the case where the state $\left| B^f_\mu \right\rangle$ is $|B^o\rangle$ we obtain

$$N(B^o \to B^o) - N(\bar{B}^o \to B^o) = \cos(\omega t) \qquad (3.12)$$

This is just the well known $B^o - \bar{B}^o$ mixing independent of all CP violation, described here as a quasispin polarization measurement in the z direction at time t of a beam polarized in the z direction at $t = 0$.

If $\left| B^f_\mu \right\rangle$ is an equal mixture of B^o and $\bar{B}^o$ eq. (3.9b) gives

$$N(B^o \to f) - N(\bar{B}^o \to f) = -\langle B_H | e^{-i\sigma_z\theta_f/2}\sigma_y e^{i\sigma_z\theta_f/2} |B_H\rangle \sin(\omega t) = -\sin(\omega t)\sin\theta_f \qquad (3.13)$$

The same approach can be applied to an experiment in which a B is tagged in some state $\left| B^f_\nu \right\rangle$ and its decay is observed after a time t in a mode allowed only for B or allowed only for $\bar{B}$; e.g. leptonic modes. The difference between the probabilities of decay into B or $\bar{B}$ allowed modes; e.g. a lepton asymmetry, is just given by the quasispin polarization in the z direction of the tagged state.

$$|\langle B^o | e^{-i\omega\sigma_x(t/2)} \left| B^f_\nu \right\rangle|^2 - |\left\langle \bar{B}^o \right| e^{-i\omega\sigma_x(t/2)} \left| B^f_\nu \right\rangle|^2 = \left\langle B^f_\nu \right| e^{i\omega\sigma_x(t/2)}\sigma_z e^{-i\omega\sigma_x(t/2)} \left| B^f_\nu \right\rangle$$

$$= \left\langle B^f_\nu \right| \sigma_z \left| B^f_\nu \right\rangle \cos(\omega t) + \left\langle B^f_\nu \right| \sigma_y \left| B^f_\nu \right\rangle \sin(\omega t) \qquad (3.14a)$$

A common example of such an experiment is the $\Upsilon(4S)$ decay, (3.7), where one B decays into a CP eigenstate like $K_S\psi$ and the other into a leptonic mode[9]. In the basis $(B_\mu; B_\nu)$ where $(K_S\psi|T|B_\nu\rangle = 0$ the second B is tagged to be in the state $|B_\nu\rangle$ (3.9a) at the time that the $K_S\psi$ decay of the other B is observed, and

$$|\langle B^o | e^{-i\omega\sigma_x(t/2)} \left| B^f_\nu \right\rangle|^2 - |\left\langle \bar{B}^o \right| e^{-i\omega\sigma_x(t/2)} \left| B^f_\nu \right\rangle|^2 = -\sin(\omega t)\sin\theta_f \qquad (3.14b)$$

In the same experiment, the case where leptonic decay occurs *before* the $K_S\psi$ decay the observed lepton asymmetry is given by eq. (3.13) but with opposite sign, since observing a B^o decay tags the other as $\bar{B}^o$ and vice versa. Thus combining eqs. (3.13) and (3.14b) shows that the lepton asymmetry observed at time t_1 when a $K_S\psi$ decay is observed at a later time $t_2 = t_1 + t$ is equal and opposite to that observed at time $t_2 = t_1 + t$ when a $K_S\psi$ decay is observed at an earlier time t_1. Thus the CP-violating lepton asymmetry cancels out if the results are integrated over time. Since time measurements are difficult in the rest frame of the $\Upsilon(4S)$ where the two B mesons move very slowly "asymmetric B factories" have been proposed to produce the $\Upsilon(4S)$ in flight so that the B mesons traverese a measurable distance before decay. This cancellation is also shown by another quasispin algebra identity[6],

$$|\langle B_\mu | e^{-i\omega\sigma_x(t/2)} |B^o\rangle| = |\langle B_\mu | e^{-i\omega\sigma_x(t/2)}\sigma_z |B^o\rangle| = |\langle B_\mu | \sigma_z e^{i\omega\sigma_x(t/2)} |B^o\rangle| =$$

$$= |\langle B_\nu | e^{i\omega\sigma_x(t/2)} |B^o\rangle| = |\langle B^o | e^{-i\omega\sigma_x(t/2)} |B_\nu\rangle^*| \qquad (3.15)$$

The probability that a meson created as a B^o at time t_1 will be observed as a B_μ at time t_2 equals the probability that a meson created as a B_ν at time t_1 will be observed as a B^o at time t_2. Thus

$$P\{B^o(t_1) \to B_\mu(t_2)\} = P\{B_\nu(t_1) \to B^o(t_2)\} \qquad (3.16)$$

$$P\{\Upsilon(4S) \to \bar{B}^o(t_1)B_\mu(t_2)\} = P\{\Upsilon(4S) \to \bar{B}^o(t_1)B^o(t_1)\} \cdot P\{B^o(t_1) \to B_\mu(t_2)\} \qquad (3.17a)$$

$$P\{\Upsilon(4S) \to B_\mu(t_1)B^o(t_2)\} = P\{\Upsilon(4S) \to B_\mu(t_1)B_\nu(t_1)\} \cdot P\{B_\nu(t_1) \to B^o(t_2)\} \qquad (3.17b)$$

$$P\{\Upsilon(4S) \to \bar{B}^o(t_1)B_\mu(t_2)\} = P\{\Upsilon(4S) \to B_\mu(t_1)B^o(t_2)\} \qquad (3.18)$$

4. HOW B AND K PHYSICS DIFFER - GOOD AND BAD NEWS

No Dominant B Decay Mode
- No Lifetime Difference
- Mass Eigenstates Not Separated by Waiting

Many B Decay Modes
- Rich Data - Small Branching Ratios $\approx 1\%$
- Final State Rescattering - Beats Golden Rule
- Conspiracies Beat CPT Restrictions

$B^o - \bar{B}^o$ Oscillations During Decay
- Time Dependence Confuses Measurements
- CP Violation Observable in Mixing Phases

All Dominant Hadronic B decays involve 3 Generations
- CP violation Observable in B Decays in Direct Diagrams $b \to c\bar{u}d$
- CP Violation in c and s decays only via diagrams with virtual t and b quarks

5. CONCLUSION - THE LIPKIN APPROACH TO CP

In 1956, after a 100% parity violation[10] was found in a difficult experiment, a much simpler experiment[11] showed that beta rays were polarized, proving parity violation. Anyone who had started our experiment[11] at the same time as Ambler et al[10] would have obtained results first and discovered parity violation. But the community had been brainwashed by the theorists who insisted that parity violation violated the "standard model" of that time. They only considered sensitive experiments where a negative result could shoot down this crazy theory, not a simple experiment that could only detect a 100% effect.

Moral for CP : Don't be brainwashed by the standard model. It might even fail to explain CP and lead to new physics beyond. This would not challenge its validity in all other areas. Keep it in mind but try to use a more general approach. Data inadequate for testing standard model CP predictions will be available long before adequate data. These preliminary data can supply information useful for planning subsequent experiments. There may also be unexpected large effects. Look for easy experiments that even Lipkin can do - even if theorists say no. Any indication of CP violation in B physics would be a great breakthrough.

Among questions that can be investigated with early data and be useful for future plans are: Is there CP violation in B physics? What is the ball park of CP violation? What are the branching ratios for physically interesting final states like CP eigenstates? Are there additional CP eigenstates not yet observed that can be useful; e.g. (a) States containing η_c and other charmonium states. (b) States like ψK^* where different partial waves have different CP eigensvalues - perhaps one partial wave is dominant. (c) States like $K_S\psi' \to K_S\pi^+\pi^- X$ where the particle X is not observed but can be identified by missing mass kinematics. How can one estimate penguin contributions?

6. ACKNOWLEDGEMENTS

We thank the Institute for Nuclear Theory at the University of Washington for its hospitality and the Department of Energy for partial support during the completion of this work. Work also supported in part by the U.S. Department of Energy, Division of High Energy Physics, Contract W-31-109-ENG-38.

7. REFERENCES

1. J.H. Christensen et al., *Phys. Rev. Lett.* **13** (1964) 138.
2. Yosef Nir and Helen Quinn *Phys. Rev. Lett.* **67** (1991) 541
3. Harry J. Lipkin, Yosef Nir, Helen R. Quinn and Arthur E. Snyder, *Phys. Rev.* **D44** (1991) 1715
4. T. D. Lee and C. S. Wu, *Ann. Rev. Nuc. Sci.* **16** *(1966) 511*
5. Harry J. Lipkin, Argonne preprint ANL-HEP-PR-88-66 Submitted to Nuclear Physics B (1988)
6. Harry J. Lipkin, *Phys. Lett.* **B219** *(1989) 474*
7. Harry J. Lipkin, In: "Developments in General Relativity, Astrophysics and Quantum Mechanics", A Jubilee Volume in Honour of Nathan Rosen, Jerusalem, Edited by F.Cooperstock, L.P. Horwitz and J. Rosen, Annals of the Israel Physical Society, 9 (1990) p. 315
8. Harry J. Lipkin, *Phys. Rev.* **176** (1968) 1715.
9. I. I. Bigi and A. I Sanda, Nuc. Phys. **B281**, 41 (1987).
10. E. Ambler et al., *Phys. Rev.* **105** (1957) 1413.
11. A. de-Shalit et al., *Phys. Rev.* **107** (1957) 1459.

The Search for Flavor Changing Neutral Currents in Rare B Decays

David B. Cline
University of California Los Angeles, Department of Physics
405 Hilgard Avenue, Los Angeles, CA 90024-1547

UCLA-PPH0054-6/93

Abstract

The search for tree level FCNC with heavy flavors is sensitive to physics beyond the standard model. We discuss three types of FCNC experiments, (i) Precise study of $b \to s + \gamma$, (ii) Search for $B_s^\circ \to \tau^+\tau^-$, and (iii) $B \to \mu^+\mu^- X$. We also comment on the UA1 limit for $B \to \mu\bar{\mu}X$.

(1) Introduction

Even before the discovery of weak interaction processes that occur without the change of charge in 1973 the issue of the existence of process that also change the Flavor of the quarks was raised. Indeed the early absence of these processes helped the Rise of the Standard Model of Elementary Particles. Recently a large number of new possibilities have been raised concerning these effects, it is now believed that the experimental observation could be a key indicator of Physics beyond the standard model.

As the evidence for the standard model's correctness grows it is important to look for processes that will be particularly sensitive to physics beyond the standard model. We note that even though ~ 3 million Z°'s have been collected, there is still no evidence for loop corrections. Thus it is important to look for processes that are either completely due to a loop (i) or that should be very small in the standard model, (ii) and (iii). An example of these processes that are studied here are:

(i) $B \to X_s + \gamma$
(ii) $B_s^\circ, d \to \tau^+\tau^-$
(iii) $B \to \mu^+\mu^- X$

Historically, the search for FCNC has been a key component in the rise of the standard model, as illustrated in Table 1[1]. The search for Flavor Changing Neutral Currents (FCNC) was carried out with strange particles mainly in the period 1963-1970[2]. The first definitive search for Neutral Currents that change the Flavor was undertaken by the author and his colleagues using the Lawrence Berkeley Laboratory Kaon Beam. In the mid seventies the absence of FCNC prompted the concept of "Natural Flavor Conservation" for the Neutral Currents[3]. The GIM model was also partially invented to explain these results[4]. This has come to be a key development in the "Rise of the Standard Model" and strongly limits the types of quarks that exist in nature. This is an example of how null experiments can strongly influence the direction of a field of science. In Figure 1 we trace some of the early and more recent experimental search for FCNC processes[5]. The impact of the null search for FCNC in the standard model is powerful, as is illustrated in Table 1[6].

We sketch the current status of the FCNC amplitude limits in Figure 1. There have been several recent estimates of the expected branching ratios for Rare B decays. We quote the recent report from A. Ali (reported at the Santa Monica Meeting on "30 Years of Weak Neutral Currents", February 1993) and it is reproduced in Table 2[1,8,9]. A more complete analysis of FCNC decays that comes from a B Physics study at this Snowmass meeting is given in Table 3[7]. We now turn to the individual decay and missing processes indicated above and attempt to justify the numbers reported in Table 2. These three processes represent a wide range of processes that are either 3rd Family, 2nd Family, or 3rd $\rightarrow$ 2nd transitions. Figure 2 shows some Feynman diagrams that would give rare FCNC B decays and would imply new physics beyond the standard model[8,9].

There are potentially two types of elementary processes that can give rise to a FCNC reaction

(i) Through Quark Processes

(ii) Through Higgs Boson Processes

In the early seventies a model put forward by Glashow, Illiopoulous and Maiani (GIM) explained why process (i) should be strongly suppressed provided a fourth quark existed (charm)[4]. In 1974 this quark was discovered in the J/Ψ experiments at Brookhaven National Laboratory and at the Stanford Linear Accelerator Center. Later a concept called "Natural Flavor Conservation" NFC was advocated by Glashow and Weinberg to forbid process (ii). It has not been questioned until very recently. If NFC fails, a whole world of new elementary particle physics processes become possible albeit it at a rather small rate. Recently L. Hall at UCB and Steve Weinberg (UT Austin) have advocated that NCF could fail[10]!

In the past few years another concept has gained ground in Elementary Particle Physics, namely the Supersymmetric Theory. This theory indicates that nature is symmetric at very high energy, where for every particle we now know there will be a super pardner, with different properties. Again this theory also provides for FCNC processes.

Thus we see that two leading theories indicate the existence of FCNC, other theories do as well, in fact FCNC detection maybe the most important experimental task ahead for Elementary Particle Physics. We now turn to the current and possible future search and study of FCNC processes at accelerators and colliders around the world.

We consider two type of detectors and hadron collisions in this report

(I) <u>High Luminosity Multi TeV Collider and a Solenoid Detector</u>. We take as an example the Compact Muon Solenoid Detector to be constructed at the CERN LHC, and assume that the LHC operates at the luminosity of 10^{33}cm^{-2}sec^{-1} that will produce 10^{13}B$\bar{\text{B}}$ pairs per year. Special trigger for the rare B decays discussed here would be employed. Our group is a member of this detector collaboration.

(II) <u>An Advanced Fixed Target Experiment at Either Fermilab or SSC</u>. We consider the proposal experiments 865 and 867 at FNAL as well as the Super Fixed Target Detector proposal for the SSC. At FNAL an effective sample of $\sim 10^{-8}$ $\bar{B}B$ pairs can be obtained where as at the SSC the number would be about 10^{10} (with SFT). Special triggers for the B decays discussed here would be employed. Our group is a member of E771, P867 and the SFT proposal to the SSC.

(III) <u>Remarks on the Significance of the Limit $B \rightarrow \mu\bar{\mu}X$ from UA1[11]</u>.

This limit is an example of the power of these type of experiments the limit is 5 x 10^{-5} to 90% CL. It was carried out by the UCLA component of UA1 under my guidance. Figure 3 shows the region of the decay phase space that was used for the search. With this limit we can safely state that the size of direct FCNC contributions can't be more than an order of magnitude larger than the Standard Model. However, this may not provide a strong constraint for processes like $B \rightarrow \tau\bar{\tau}$ that are for pure 3rd Family transistors!

(2) Rare B Decays

(i) <u>Sensitive Study of $B \rightarrow X_s\gamma$ at a Fixed Target Experiment[12]</u>

The decay mode $b \rightarrow s + \gamma$ is of great theoretical interest, and could provide constraint on SUSY the charge Higgs sector and other possible deviation from the standard model! The work reported here has been carried out by a UCLA group (D. Cline, J. Park and J. Rhoades).

Simulation studies are being conducted of the photons from the inclusive decay $b \rightarrow s\gamma$ using the Monte Carlo program PYTHIA to generate b events. Since $b \rightarrow s\gamma$

decays are not implemented in PYTHIA, we treat the decay as a two body decay, assuming that the s and spectator quarks hadronise into a state with a mean mass halfway between the K^* and the K_4^*. This generates a mass distribution with FWHM equal to the $K_4^* - K^*$ mass difference. The shape is a Gaussian, truncated at the low end at the mass of the K^* and at the high end at the mass of the B.

We assume an energy resolution of $\frac{10\%}{\sqrt{E}}$, an angular resolution of 1 m rad for γ's, and (since the calorimetric photon measurement will dominate the resolution) a perfect momentum resolution for hadrons.

The transverse momentum distributions for γ's from B events have been obtained. The B background includes all γ's; the signal includes only those γ's originating from the b quark. The $b \to s\gamma$ photons are broadly peaked in the transverse momentum, with a mean of 2.3 GeV and rms width of 0.8 GeV, while the photons from B background events had a mean P_t of 0.2 GeV, and the distribution fell off somewhat more slowly than exponential. The p_t spectrum of γ's from 1,000 non-B events was also obtained to permit background subtraction. The transverse momentum of the photons had a mean p_t of 0.17 GeV and dropped off at a p_t of 2.5 GeV.

Figure 4 shows the p_t distributions of γ's from 250,000 B background events superimposed with 1,000 B signal events after the π° mass range cut of $0 \leq m_{\gamma\gamma} \leq 0.2$ GeV is applied and with the mass cut $0 \leq m_{\gamma\gamma} \leq 0.2$ GeV and with $\eta \to \gamma\gamma$ suppression. For the region $p_t \geq 3.6$ GeV the background is completely suppressed, but the signal is statistically significant. The signal retention is 6.34%.

Table 4 shows the numbers of γ's from 1,000 $B \to X_s\gamma$ events and from 250,000 B background events as functions of the minimum p_t cut. The threshold p_t of 3.6 GeV is not sensitive to an E_γ cut. It is clear from the analysis that a dedicated $B \to X_s\gamma$ measurement could be carried out at a hadron fixed target or even possible colliding beam machine, assuming a wide band trigger (like the optical trigger) is used.

(ii) Search for $B_s^\circ \to \tau^+\tau^-$ and Other Rare B Decays

(a) $B \to \mu^+\mu^- X_s$

We follow the UA1 results which indicate that, in the mass range of 3.8 to 4.4 GeV, a signal may be detected[11]. For a branching ratio of $\sim 5\text{x}10^{-6}$ we would expect that (10^{10}) $B\bar{B}$ production would be required to obtain a signal or ~ 10 events above background. Since the signal is background limited, it will require a careful study of the background and a detailed subtractor. This may be possible with the CDF or $D_\circ$ detectors at FNAL over the next few years. This would be very difficult for fixed target experiments at FNAL or even e^+e^- B factories to detect. At the LHC or SSC it should be rather straight forward. Some theoretical estimates for this process can be found in the references.

(b) $B \to \mu^+\mu^-$

This decay represents a process that is likely to provide an excellent signal, if the detector has adequate mass resolution, but will be severely rate limited if the branching fraction is $\sim 2\text{x}10^{-9}$, as expected in the standard model[11]. Again, using the detection efficiency obtained in the UA1[11] experiment for this decay mode of ~ 4 percent and a branching fraction of $\sim 10^{-9}$ and a 10 events signal, we estimate that a sample of 10^{11} $B\bar{B}$ events will be required to clearly detect this signal. Of course, models beyond the standard model could enhance this branching fraction by a factor of ~ 10, but not much more since we know that $B \to \mu^+\mu^-$ is within a factor of 10 of the standard model prediction. Thus, an interesting search could be carried out when $\sim 10^{10}$ $B\bar{B}$ events have been produced.

(c) $B \to \tau + \bar{\tau}$ (Reference 9)

This process has only 3rd family particles and may be sensitive to new types of theories that are beyond the standard model. It also presents perhaps the greatest challenge for detection of any FCNC B decay since the experimental signature is so complex and the branching ratio so small, even in beyond the standard model estimates. The estimated branching ratio in the standard model is $3.8x10^{-7}$. There are estimates for the branching ratio in some models that can go to $\sim 10^{-4}$. In addition, this process is not constrained directly by the UA1 limits on $B \to \mu^+\mu^- X$ and thus, any sensible search and limit is likely to be interesting. The method of detection and backgrounds for this process are discussed in Ref. [7]. We summarize these results here. For the branching ratio $\sim 10^{-5}$, there seems to be little background, but at $\sim 10^{-6}$ the process

$$B_s^\circ \to D_s + \tau + \bar{\nu}_\tau$$
$$\hookrightarrow \bar{\tau} + \nu_\tau$$

will likely become an important source of background[7].

We have suggested some kinematic tricks to reduce this background in the Snowmass working group. A Monte Carlo study similar to that for $B \to X + \gamma$ is being started at UCLA. Table 3 lists some of the possible rates for the various processes discussed here from the Snowmass workshop.

(3) Sensitivity of the FCNC to New Physics

There are several classes of models that may have FCNC processes. We list them in a generic sense.

1. Supersymmetric Theory
2. Technicolor

3. Multiple Scalars

4. 4th Family

We believe that these four classes of theories covers most of the reports in the literature. However, it could be that the discovery of FCNC processes may be unpredicted by any extant theory and could lead to the correct theory.

There is general belief that FCNC must exist in almost all models that go beyond the standard model, since the concept of Flavor Conservation is ad hoc and the Higgs sector is more complex than that assumed by the standard model[13]. In Figure 2 we show some of the diagrams that give FCNC processes from some of the theories. Clearly, the search for FCNC in B decays is of great importance.

(4) Novel Triggers for Beauty Selection

The production of $\bar{B}B$ pairs at hadronic machines is very large. As a rule of thumb here are the kinds of rates expected per year for various machines:

a) Fixed Target at FNAL $\sim 10^8$ $\bar{\mathrm{B}}$B/year

b) Colliding Beams at FNAL $\sim 10^9 - 10^{10}$ $\bar{\mathrm{B}}$B/year

c) Dedicated Fixed Target Experiment at the LHC or SSC $\sim 10^{10}$ $\bar{\mathrm{B}}$B/year

d) LHC or SSC Collider $\sim 10^{12} - 10^{13}$ $\bar{\mathrm{B}}$B/year

As a rule of thumb (from the UA1 experiment) the overall detection efficiency for rare processes is unlikely to exceed $\sim 10^{-2}$ [11]. Thus, in order to detect all the various decays discussed in Section 3, we will need the full range of B production, up to the Super Colliders.

The major issue in using these very large $\bar{B}B$ rates is the event trigger selection. The total hadronic event production per year will vary from $10^{12} - 10^{15}$. These events must be sorted through somehow to extract the $(10^{-5} - 10^{-3})$ fraction of $\bar{B}B$ events and then to find the rare events a factor of $10^{-4} - 10^{-9}$ is required. This is obviously an extremely difficult undertaking.

The key to the use of the large $\bar{B}B$ rates is the event trigger. We will discuss two concepts for event triggers that we believe hold promise for the FCNC studies and describe two extremes:

1. Trigger $J/\Psi \to \mu^+\mu^-$ events to tag a $\bar{B}B$ event. This is currently being used in the E771 experiment at FNAL. In principle this could give a trigger with an efficiency of $\sim 10^{-3}$.

2. Trigger on the impact parameter displacement of charged tracks from the $B/\bar{B}$ decay using a fast Cherenkov light signal (optical trigger). Future use of a new type of photo detector (VLPC) may be important for this technique.

There are other concepts, like the detection of an impact parameter using a nearby silicon tracking array, and the expected different track multiplicity for events with $\bar{B}B$, and the total events, that we will not discuss.

(5) Conclusions

We have illustrated in this brief report the importance of a dedicated search for FCNC rare B decays at present and future hadronic machines. We also showed that the small branching factors for these processes very likely require their study at hadron machines. In order for this to be accomplished, novel trigger techniques will be required. The optical trigger is one such clever idea. The continuing search for FCNC processes is of great importance. In Table 5 we list some of the models that can be tested by these rare decay modes.

I wish to thank the Rare B - FCNC group at Snowmass for helpful discussions.

(6) References

1) Proceedings of the International Symposium on 30 Years of Neutral Currents: from Weak Neutral Currents to the (W)/Z and Beyond, to be published by the American Institute of Physics, editors D. Cline and A.K. Mann.

2) D. Cline, The Search for Weak Neutral Currents, Proc. of Ecol Int. Hecg Novi (1967), and Thesis at Univ. of Wisconsin (1965); U. Camerini, et. al., Phys. Rev. Lett 13 318 (1964); J. Klems, et.al., Phys. Rev. Lett. 24 1086 (1070); U. Camerini, et.al., Phys. Rev. Lett 23 1086 (1969); Report on the SLAC meeting on the Rise of the Standard Model, to be published (1992).

3) S. Glashow and S. Weinberg, Phys. Rev. D15 (1977) 1968; E.A. Paschos, Phys. Rev. D15 (1977) 1966.

4) S. Glashow, J. Illiopoulous and L. Maiani, Phys. Rev. D2 1285 (1970).

5) D. Cline, The Continuing Search for Flavor Changing Weak Neutral Currents, Cmnts. in Part. Phys. (1987); D. Cline, The Search for Rare B Decays and B - B° Mixing, Pub. in Proc. of Third Topical Seminar on Heavy Flavors, San Miniato, Italy (1991), and Proc. of the meeting on Rare B and K Decays and Novel Flavor Factories, AIP Book, July 1992.

6) S. Glashow, Nucl. Phys. 22 579 (1961); S. Weinberg, Phys. Rev. Lett. 19 1264 (1967); A. Salam, Proc. 8th Nobel Symposium, Aspenasgarden, 1968, editor N. Svartholm, Published by Almqvist and Wisell, Stockholm, 1968, p. 367.

7) D. Cline, unpublished

8) See Reference 1, Report of M. Ito for the rare K decay situation.

9) See Reference 1, Report of A. Ali for rare B decays predictions.

10) L. Hall and S. Weinberg, LBL Preprint (1993).

11) C. Albajar, et.al., (UA1 Collaboration); Phys. Lett. B262 (1991) 163; K.M. Ankoviak, Ph.D. Thesis, University of California, Los Angeles, 1991.

12) D. Cline, J. Park, J. Rhoades and M. Atac, UCLA Report.

13) See for example and other references P.J. O'Donnell, M. Sutherland and H.K.K. Tung, Phys. Rev. D46 (1992) 4091.

TABLE 1

Impact of FCNC Search on the Rise of the Standard Model

PROCESS	PERIOD	IMPLICATION
$s \not\to d$	$\sim$ 1963	FCNC Absent at first level of
$(K^+ \to \pi^+ \nu\bar{\nu})$	$\sim$ 1970	Weak Interaction [GIM Mechanism]
$s \not\to$ Loop $\not\to d$	$\sim$ 1960-74	New Quark in Loop, $m_q \sim 2$ GeV
$K^\circ - \bar{K}^\circ$,		
$K_S - K_L$ mixing		(Charm)
$s \not\to d$	$\sim$ 1970's	Natural Flavor Conservation for NC
$c \not\to u$		implies that only Q = 1/3, Q = 2/3 quarks
etc.		exist in doublets in nature
$b \not\to d$	$\sim$ 1980's	Necessary existence of
$b \not\to s, B^\circ - \bar{B}^\circ$		(massive) t quark
STRONG LIMITS ON		
$s \not\to d$	$\sim$ 1990's	Limits on supersymmetric interactions
$b \not\to d$		and other exotics
$\nu_e \not\to \nu_\mu$		
$K \to \mu e$		

TABLE 2

Estimates of the branching fractions for FCNC B-decays in the Standard Model for $m_t = 150\,\mathrm{GeV}$ and $f_B = 200\,\mathrm{MeV}$. Note that the CKM-suppressed decays, given in row 3 and 4, depend on $|V_{td}|$, and the numbers correspond to $|V_{td}| = 0.007$. Experimental upper limits are also listed.

B FLAVOR CHANGING NEUTRAL CURRENTS (A. Ali)[20] ($m_t = 150\,\mathrm{GeV}$, $f_B = 200\,\mathrm{MeV}$, $\mu = m_b$)		
DECAY MODES	Br	EXP. UPPER LIMITS (90% C.L.)
$(B_d,\ B_u) \to X_S\gamma$	4.0×10^{-4}	8.4×10^{-4} [CLEO] *(a)*
$(B_d,\ B_u) \to K^*\gamma$	$(4.0 - 7.0) \times 10^{-5}$	0.92×10^{-4} [CLEO] *(a)*
$(B_d,\ B_u) \to X_d\gamma$	$(0.5 - 3.0) \times 10^{-5}$	-
$(B_d,\ B_u) \to \rho + \gamma$	$(1.0 - 3.0) \times 10^{-6}$	-
$(B_d,\ B_u) \to X_S e^+e^-$	1.2×10^{-5}	-
$(B_d,\ B_u) \to X_S \mu^+\mu^-$	6.7×10^{-6}	5.0×10^{-5} [UA1] *(b)*
$(B_d,\ B_u) \to K e^+e^-$	4.4×10^{-7}	5.0×10^{-5} [PDG] *(c)*
$(B_d,\ B_u) \to K \mu^+\mu^-$	4.4×10^{-7}	1.5×10^{-4} [PDG] *(c)*
$(B_d,\ B_u) \to K^* e^+e^-$	3.7×10^{-6}	-
$(B_d,\ B_u) \to K^* \mu^+\mu^-$	2.3×10^{-6}	2.3×10^{-5} [UA1] *(b)*
$(B_d,\ B_u) \to X_S \mu\bar{\mu}$	6.6×10^{-5}	-
$(B_d,\ B_u) \to K \nu\bar{\nu}$	5.2×10^{-6}	-
$(B_d,\ B_u) \to K^* \nu\bar{\nu}$	2.0×10^{-5}	-
$B_S \to \gamma\gamma$	2.0×10^{-8}	-
$B_S \to \tau^+\tau^-$	3.5×10^{-7}	-
$B_S \to \mu^+\mu^-$	7.5×10^{-9}	-
$B_S \to e^+e^-$	4.0×10^{-14}	-

(a) E.H. Thorndike (CLEO Collab.), Contr. #531, LP-HEP 91 Conf., Geneva, Switz.
(b) C. Albajar, et al., (UA1), Phys.Lett. B262 145 (1991).
(c) K. Hikasa, et al., (Particle Data Group), Phys.Rev. D45 1 (1992).

TABLE 3

Future Search for Rare B FCNC Decays

MODE	BR ON STD. MODEL	POSSIBLE NO. EVENTS COLLECTED PER YEAR OF OPERATION	B SOURCE AND PROPOSED DETECTOR	REMARKS ON BACK-GROUND
$B^\pm \to K^+\mu^+\mu^-$ e^+e^-	$\sim 10^{-6}$	~5000	pp Collider (LHC)/CMS $P_{\perp B} > 10\,\mathrm{GeV}/c$	$B \to D\mu\nu$ $\hookrightarrow K\mu\nu$ $-[S/B] > 1$
$B^\circ \to \pi^\circ e^+e^-$ $\mu^+\mu^+$	5×10^{-8}	~100	Fixed Target LHB or SFT at SSC	$B \to D\mu\nu$ $\hookrightarrow \pi^\circ\mu\nu$ $S/B > 1$
$B_s^\circ \to \tau\bar{\tau}$	3×10^{-7}	30 - 180 But Back- ground at 10^{-6} Level!	Fixed Target or Collider (LHC) (CMS)	Serious Back- ground in $B_S \to D_S\bar{\tau}\nu$ $\hookrightarrow \pi\bar{\nu}$
$B_s^\circ \to \mu^+\mu^-$	2×10^{-9}	$\gtrsim 20$	Collider (High L) LHC/CMS	$S/B \gg 1$
$B^\circ \to \phi\tau\bar{\tau}$	$\sim 10^{-7}$	~ 30	Collider (High L) LHC/CMS	$B \to \phi D_S\bar{\tau}\nu$ $\hookrightarrow \tau\bar{\nu}$ $S/B > 1$

TABLE 4. **Numbers of γ's from 1,000 $B \to X_s\gamma$ events and from 250,000 B Background Events as Functions of the Minimum p_t Cut, with the Mass Cut $0 \leq m_{\gamma\gamma} \leq 0.2$ GeV and with $\eta \to \gamma\gamma$ Suppression.**

p_t (GeV/c)	No. of γ's from 1K Signal	No. of γ's from 250K Background	Normalized Background using BR of $4\text{x}10^{-4}$	(Signal/Bkg)
2.8	127	22 ± 4.69	220 ± 46.9	0.58
3.0	101	$14^{+4.1}_{-3.4}$	140^{+41}_{-34}	0.72
3.2	72	$7^{+3}_{-2.35}$	$70^{+30.}_{-23.5}$	1.028
3.4	56	$3^{+2.15}_{-1.45}$	$30^{+21.5}_{-14.5}$	1.33
3.6	46	$0^{+1.15}_{-0.}$	$0^{+11.5}_{-0.}$	
3.8	34	$0^{+1.15}_{-0.}$	$0^{+11.5}_{-0.}$	
4.0	26	$0^{+1.15}_{-0.}$	$0^{+11.5}_{-0.}$	
4.2	19	$0^{+1.15}_{-0.}$	$0^{+11.5}_{-0.}$	
4.4	15	$0^{+1.15}_{-0.}$	$0^{+11.5}_{-0.}$	
4.6	10	$0^{+1.15}_{-0.}$	$0^{+11.5}_{-0.}$	
4.8	6	$0^{+1.15}_{-0.}$	$0^{+11.5}_{-0.}$	

TABLE 5

Impact on the Existence of New Families of Particles
an the Search and Observation of FCNC

FCNC Process	Theory	Present Result	Future Prospsect
$B \to \mu^+\mu^- X_s$	Technicolor; New Scalar Particles (Hall/Weinberg)	Limit 5×10^{-5} from UA1 Experiment at CERN	Observation or Limit to 5×10^{-6} at FNAL
$B \to X_s + \gamma$	Super Symmetry; Technicolor; 4th Family of Elementary Particles	Current Limit of 5×10^{-4} (Cornell)	Observation of a Similar Reaction $B \to K^*\gamma$ - Study in Progress at UCLA to Observe at High Rate
$B \to \tau\bar{\tau}$ (3rd Family to 3rd Family)	New Scalars; SUSY; Technicolor 4th Family	No Current Search	Crucial for all Theories Study of Detection in Progress at UCLA

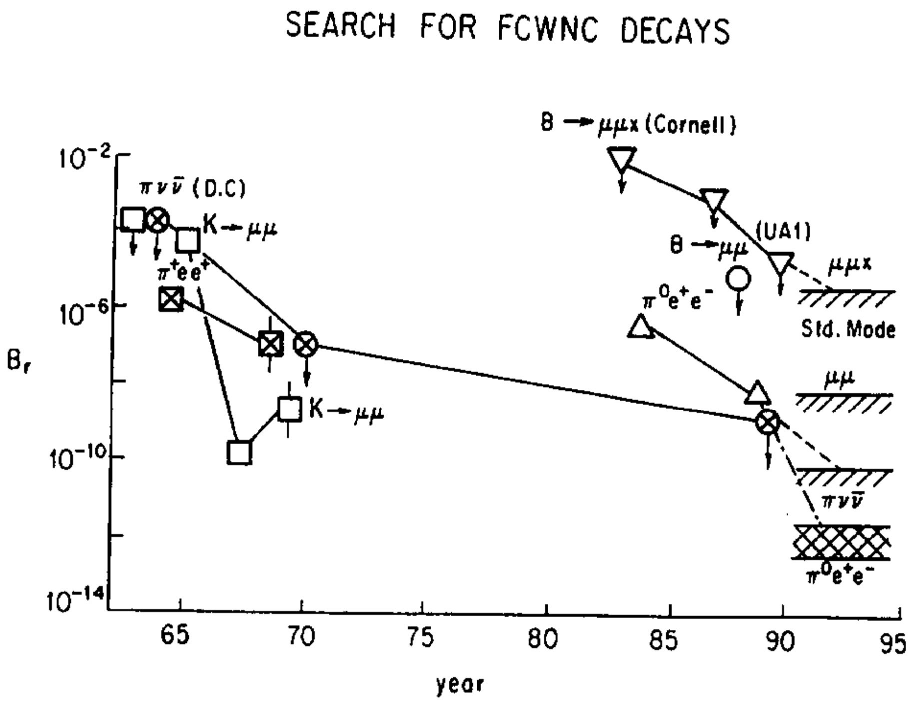

Figure 1. A plot of the limits on FCNC - Rare K, B and Charm decays as a function of time (from reference 5).

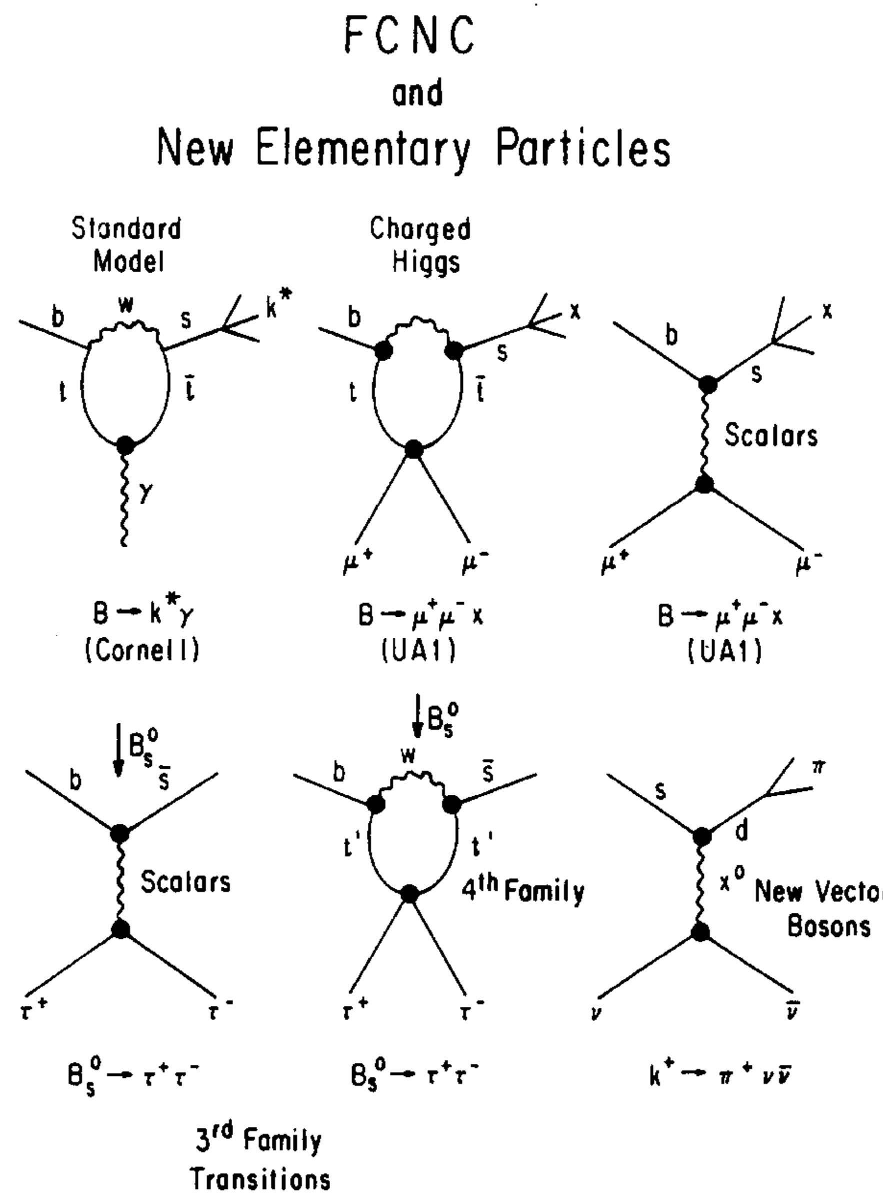

Figure 2. Some examples of Feynman diagrams for FCNC - Rare B and K decays that arise through new physics (beyond the standard model) [reference 5].

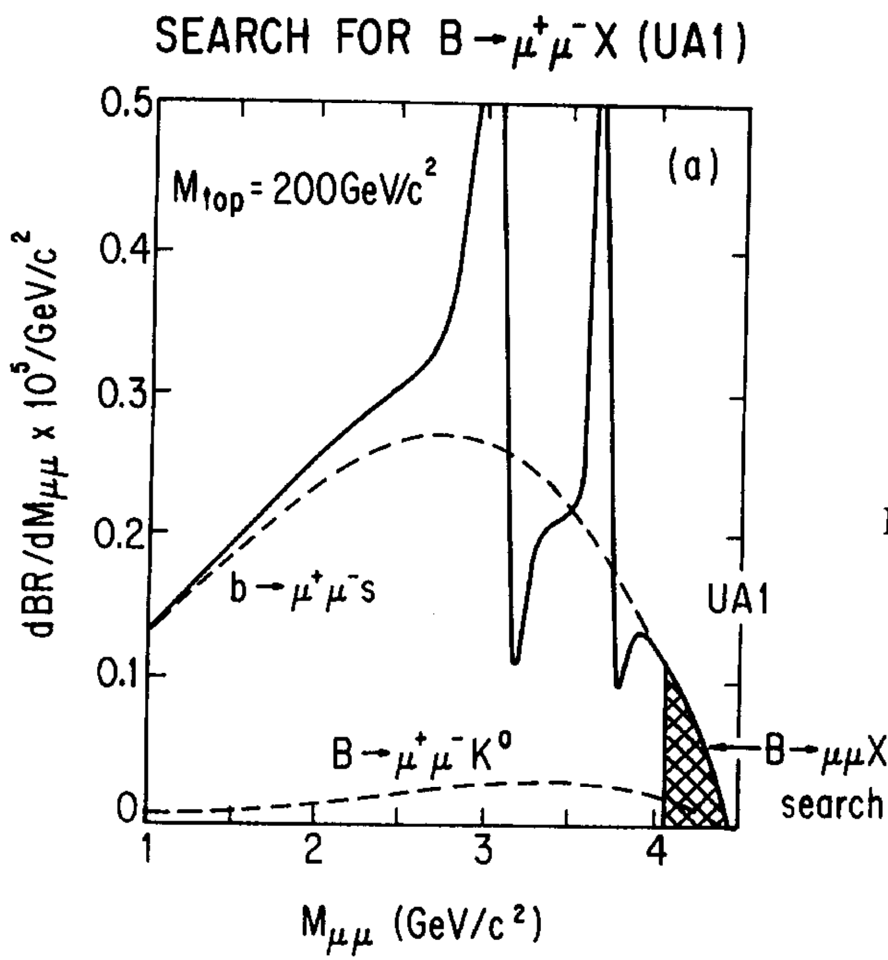

Figure 3. The $M_{\mu\bar{\mu}}$ $B \to \mu\bar{\mu}X$ decay spectrum and the region used by the UA1 group (the UCLA component) to search for this decay mode.

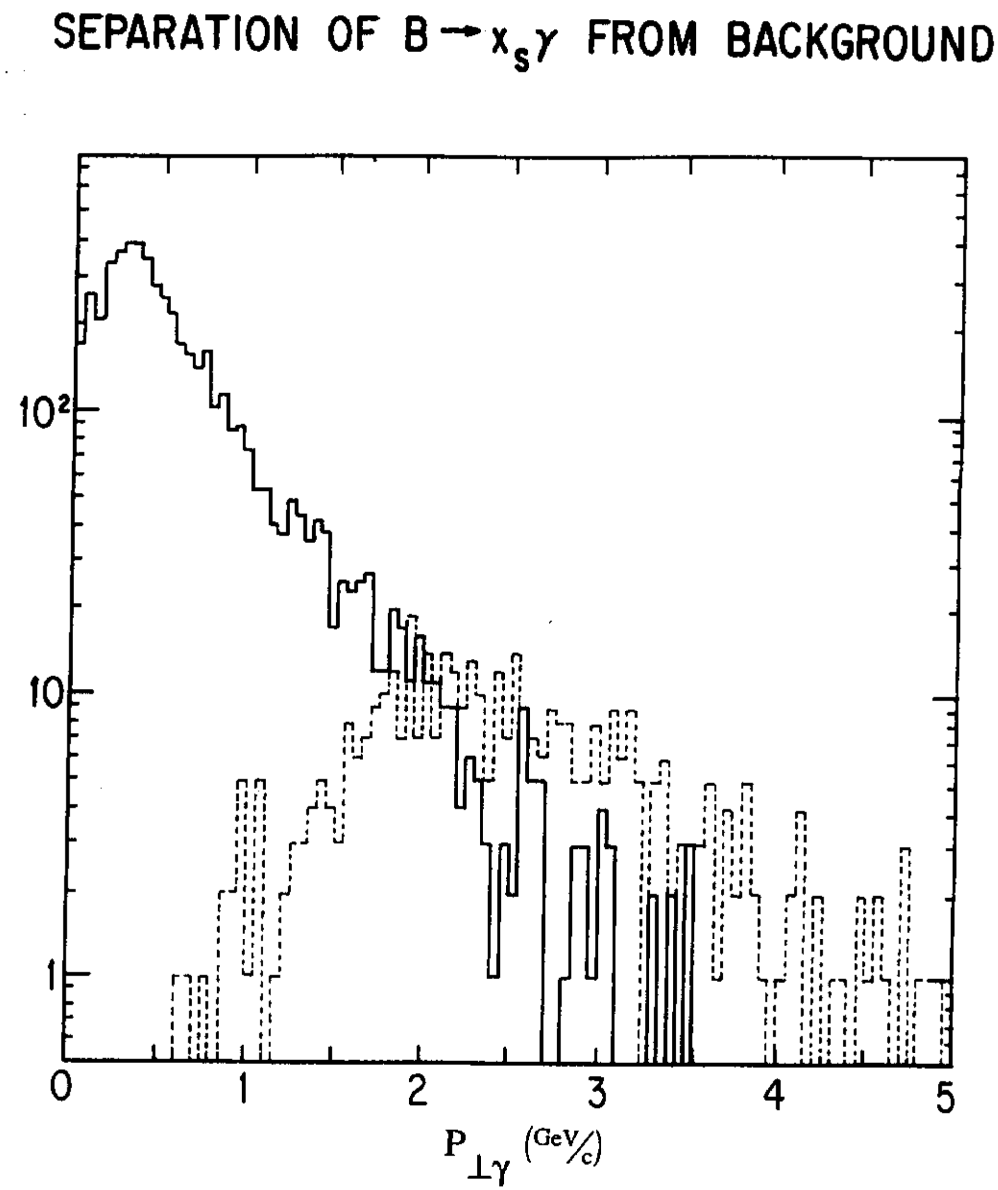

Figure 4. The p_t distributions of γ's from 250,000 B background events superimposed with 1,000 B signal events after the π^0 mass range cut of $0 \le m_{\gamma\gamma} \le 0.2$ Gev is applied with $\eta \to \gamma\gamma$ suppression. For the region $p_t \ge 3.6$ GeV the background is completely suppressed, but the signal is statistically significant.

SIMULATION STUDY OF B→$X_s\gamma$

D. CLINE, J. PARK, J. RHOADES and M. ATAC
Department of Physics and Astronomy
University of California at Los Angeles
405 Hilgard Avenue, Los Angeles, California 90024, USA

1. INTRODUCTION

A comprehensive study of charm and beauty decays is proposed in P867 as an extension of Fermilab experiment E771. Most of the decay modes studied for the proposal rely on the detection of a high p_t muon or high mass dimuon pair in the spectrometer. The addition of a Ring Imaging Cerenkov Counter, which is under consideration, would increase the number of decay modes accessible. No major upgrades are planned for the electromagnetic detector, but it may be possible to use the existing calorimeter to detect photons from rare beauty decays.

As part of the ongoing simulation for P867, we have studied the decay $b \rightarrow s\gamma$. We expect several $\times\ 10^4$ such events to be produced, with about 10^3 satisfying the acceptance and trigger. The main problem in detecting the signal is that there is a very significant photon background. Our simulations suggest that with good electromagnetic calorimetry and by optimizing cuts, adequate background suppression will be possible, and the signal will be detectable.

2. $b \rightarrow s\gamma$ SIMULATION

Simulation studies are being conducted of the photons from the inclusive decay $b \rightarrow s\gamma$ using the Monte Carlo program PYTHIA to generate B events. Since $b \rightarrow s\gamma$ decays are not implemented in PYTHIA, we treat the decay as a two body decay, assuming that the s and spectator quarks hadronise into a state with a mean mass halfway between the K^* and the K_4^*. This generates a mass distribution with FWHM equal to the K_4^* - K^* mass difference. The shape is a Gaussian, truncated at the low end at the mass of the K^* and at the high end at the mass of the B.

We assume an energy resolution of $\frac{10\%}{\sqrt{E}}$, an angular resolution of 1 mrad for γ's, and (since the calorimetric photon measurement will dominate the resolution) a perfect momentum resolution for hadrons.

The transverse momentum distributions for γ's from B events have been obtained. The B background includes all γ's; the signal includes only those γ's originating from the b quark. Figure 1 shows the p_t spectrum of γ's from 10,000 B background events. Figure 2 shows the p_t spectrum of γ's from 1,000 $b \rightarrow s\gamma$ events. The $b \rightarrow s\gamma$ photons were broadly peaked in the transverse momentum, with a mean of 2.3 GeV and rms width of 0.8 GeV, while the photons from B background events had a mean p_t of 0.2 GeV, and the distribution fell off somewhat more slowly than exponential. The p_t spectrum of γ's from 1,000 non-B events was also obtained to permit background subtraction (Figure 3). The transverse momentum of the photons had a mean p_t of 0.17 GeV and a maximum p_t of 2.5 GeV.

According to Ali[1] the standard model prediction for the branching ratio of $b \to s\gamma$ is $(2\sim5)\times10^{-4}$. Assuming a branching ratio of 4×10^{-4}, there should be 20 signal events corresponding to the 50,000 background events we generated. Since even at the peak of the signal p_t the background exceeds the signal by 2 orders of magnitude, we have investigated several cuts to see whether we can extract the signal from the background.

In order to suppress γ's from π^0, we exclude from the analysis all γ's which are consistent (within the calorimeter resolution) with combining with any other γ in the event to form a π^0. Various $\gamma\gamma$ mass-range cuts are examined. If the mass range $0 \leq m_{\gamma\gamma} \leq 0.2$ GeV is excluded, the signal to background ratio is improved by a factor of 142, with a signal retention of 55%. Figure 4 shows the invariant mass distribution of $\gamma\gamma$ pairs from background B events. The upper and lower mass limits of the π^0 mass range cut are indicated. The distribution peaks at the π^0 mass, with a π^0 mass resolution (σ) of 7.1 MeV. Table 1 summarizes the π^0 mass resolution as a function of photon energy resolution in the calorimeter.

Table 1. π^0 Mass Resolution

Energy Resolution at 1 Gev in rms (%)	π^0 Mass Resolution (Mev/c^2)
5	4.62
7	5.75
10	7.09
15	9.36

After the π^0 mass range cut of $0 \leq m_{\gamma\gamma} \leq 0.2$ GeV is applied, the background γ's from π^0 are entirely eliminated. This leaves high-p_t γ's from B or D to η decays, which may be overrepresented in PYTHIA, as evidenced by the apparent lack of such background in CLEO data.

Figure 5 shows the p_t distributions of γ's from 250,000 B background events superimposed on 1,000 B signal events after the π^0 mass range cut of $0 \leq m_{\gamma\gamma} \leq 0.2$ GeV is applied. There are about 20 γ's from signal events with $p_t \geq 3.5$GeV, and these are all from η decays. Figure 6 shows the p_t spectrum of γ's from 250,000 B background events superimposed on 1,000 B signal events, with the mass cut $0 \leq m_{\gamma\gamma} \leq 0.2$ GeV and with $\eta \to \gamma\gamma$ suppression. For the region $p_t \geq 3.6$ GeV the background is completely suppressed, but the signal is statistically significant. The signal retention is 6.34%.

Table 2 shows the numbers of γ's from 1,000 $B \to X_s\gamma$ events and from 250,000 B background events as functions of the minimum p_t cut. The threshold p_t of 3.6 GeV is not sensitive to an E_γ cut. This is shown in Table 3, which includes an additional cut of $E_\gamma \geq$ 70 GeV.

Figure 7 shows the invariant mass distribution of γ pairs which survived the π^0 mass range cut described above. It peaks at the η mass with η mass resolution (σ) of 74.5 MeV.

Table 2. Signal to Background Ratio with no E_γ Cut

p_t Cut (GeV/c)	No. of γ's from 1K Signal	No. of γ's from 250K Background	Normalised Background using BR of 4×10^{-4}	(Signal/Bkg) -
2.8	127	22 ± 5	220 ± 47	0.58
3.0	101	14^{+4}_{-3}	140^{+41}_{-34}	0.72
3.2	72	7^{+3}_{-2}	70^{+30}_{-24}	1.03
3.4	56	3^{+2}_{-1}	30^{+22}_{-15}	1.33
3.6	46	0^{+1}_{-0}	0^{+12}_{-0}	-
3.8	34	0^{+1}_{-0}	0^{+12}_{-0}	-
4.0	26	0^{+1}_{-0}	0^{+12}_{-0}	-
4.2	19	0^{+1}_{-0}	0^{+12}_{-0}	-
4.4	15	0^{+1}_{-0}	0^{+12}_{-0}	-
4.6	10	0^{+1}_{-0}	0^{+12}_{-0}	-
4.8	6	0^{+1}_{-0}	0^{+12}_{-0}	-

Table 3. Signal to Background Ratio with $E_\gamma \geq 70$ GeV.

p_t Cut (GeV/c)	No. of γ's from 1K Signal	No. of γ's from 250K Background	Normalised Background using BR of 4×10^{-4}	(Signal/Bkg) -
2.8	71	10^{+4}_{-3}	100^{+35}_{-29}	0.71
3.0	60	6^{+3}_{-2}	60^{+28}_{-22}	1.00
3.2	46	3^{+2}_{-1}	30^{+22}_{-15}	1.53
3.4	40	3^{+2}_{-1}	30^{+22}_{-15}	1.33
3.6	33	0^{+1}_{-0}	0^{+12}_{-0}	-
3.8	24	0^{+1}_{-0}	0^{+12}_{-0}	-
4.0	18	0^{+1}_{-0}	0^{+12}_{-0}	-
4.2	15	0^{+1}_{-0}	0^{+12}_{-0}	-
4.4	14	0^{+1}_{-0}	0^{+12}_{-0}	-
4.6	9	0^{+1}_{-0}	0^{+12}_{-0}	-
4.8	5	0^{+1}_{-0}	0^{+12}_{-0}	-

3. FURTHER STUDIES

Preliminary studies are also being conducted of the exclusive decay mode $B \to K^*\gamma$. First, all $K\pi$ combinations are formed, and events in which the invariant mass is outside the range of the K^* (0.7 GeV to 1.1 GeV) are vetoed. Then we select $K\pi$ pairs consistent with the K^* mass, and form all combinations of these K* candidates and γ's which survived the π^0 mass cut. The following additional cuts are then applied: an invariant mass cut on K^*-γ; a cut on the opening angle of the K^*-γ; and a primary vertex cut on the K^*-γ.

Further studies are needed using the GEANT simulation of the proposed P867 detector.

4. CONCLUSION

Simulation studies have been conducted of the photons from the inclusive decay $b \to s\gamma$ using the Monte Carlo program PYTHIA to generate B events. An energy resolution of $\frac{10\%}{\sqrt{E}}$ and an angular resolution of 1 mrad for γ's are assumed. The signal is extracted by applying π^0 and η mass cuts. For the region $p_t \geq 3.6$ GeV the background is completely suppressed but the signal is still statistically significant. The results show that B's may be observed from this decay.

5. ACKNOWLEDGEMENTS

We wish to thank Prof. D. Kaplan for many helpful discussions.

6. REFERENCES

1. A. Ali, T.Ohl and T. Mannel, *Phys. Lett.* **B 298** (1993) 195.

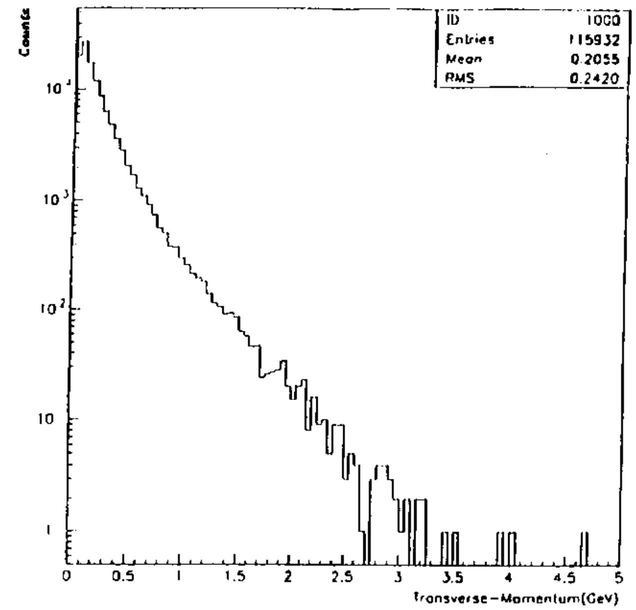

Figure 1: The p_t spectrum of γ's from 10,000 B background events.

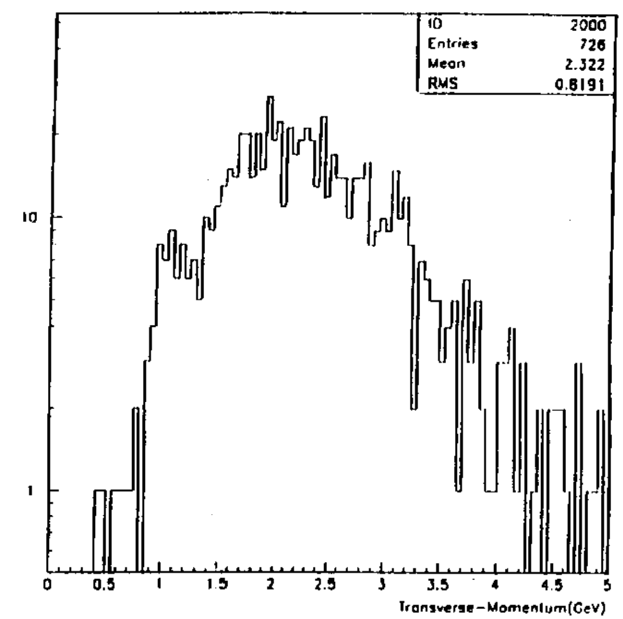

Figure 2: The p_t spectrum of γ's from 1,000 $b \to s\gamma$ events.

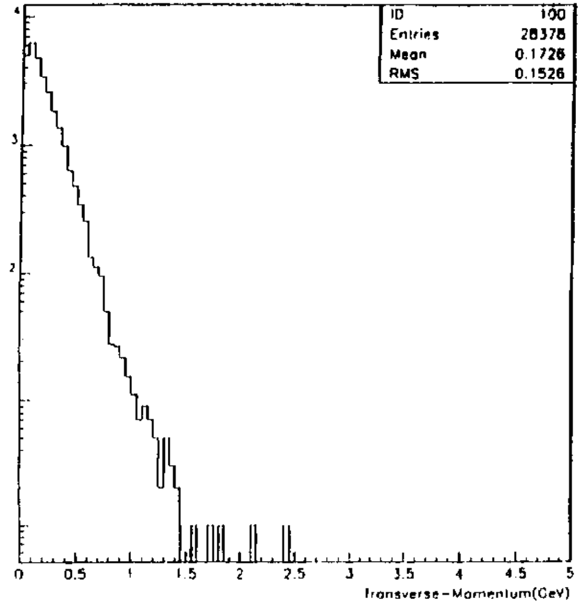

Figure 3: The p_t distributions for γ's from 1,000 minimum bias events.

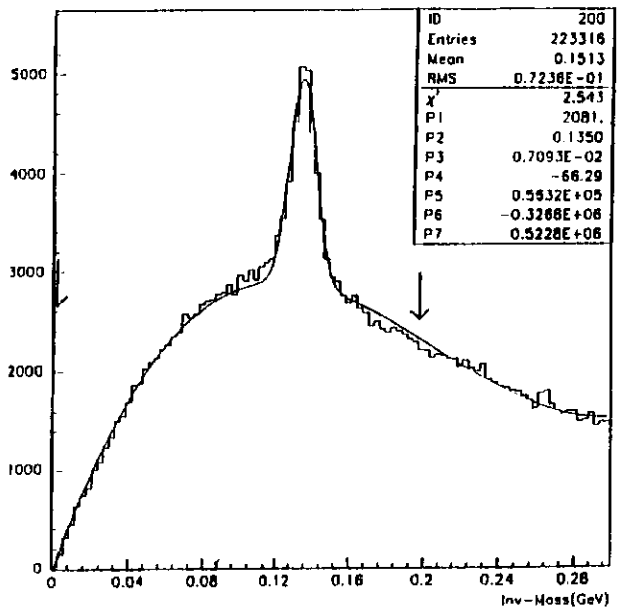

Figure 4: The invariant mass distribution of $\gamma\gamma$ pairs from background B events. The upper and lower mass limits of the π^0 mass cut are marked.

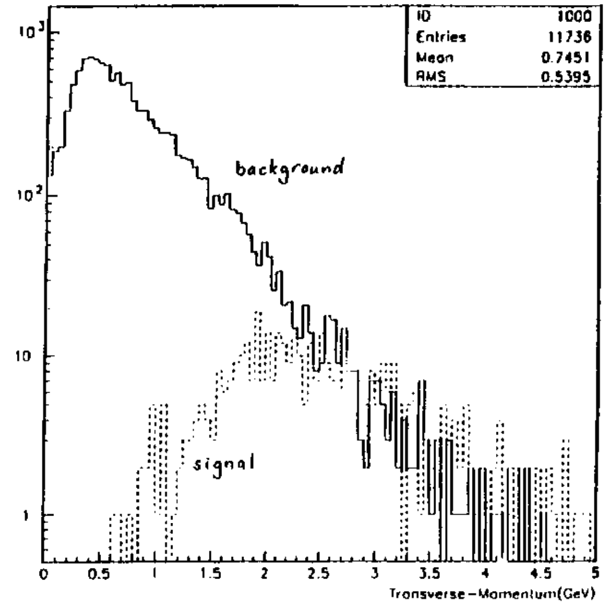

Figure 5: The p_t distributions of γ's from B background events and B signal events.

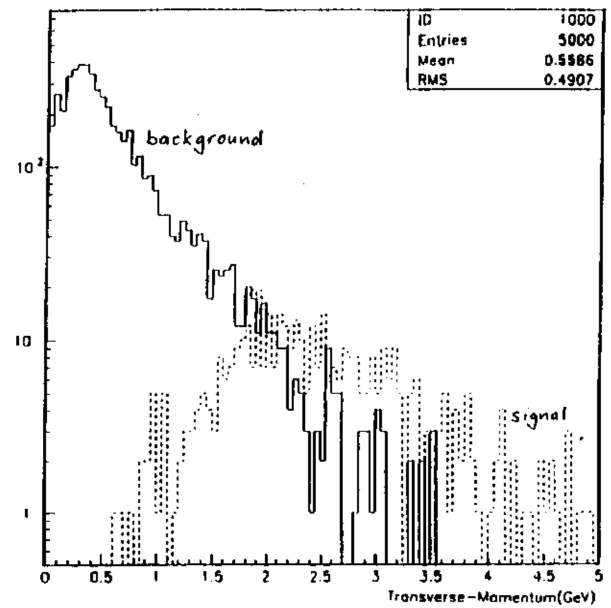

Figure 6: The p_t distributions of γ's from B background events and B signal events, with $\eta \to \gamma\gamma$ suppression.

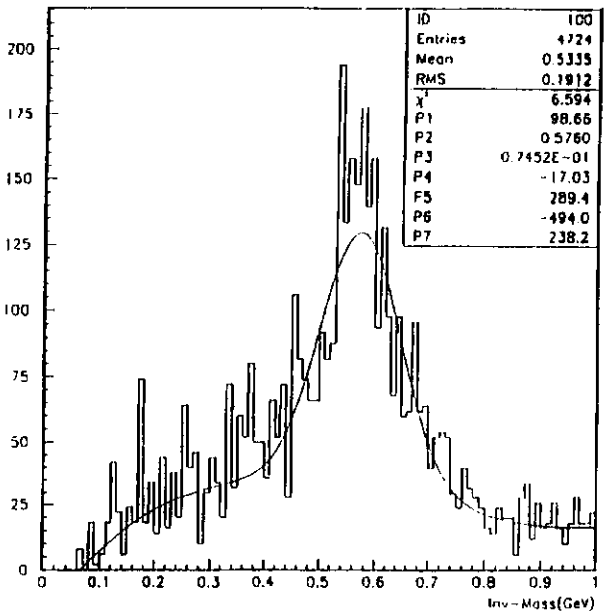

Figure 7: The invariant mass distribution of $\gamma\gamma$ pairs which survive the π^0 mass cut.

Other Spectroscopy

Leader:

J. Rosen
Northwestern University

List of Participants

J. Marques
Northwestern University

J. Rosen
Northwestern University

L. Spiegel
Fermi National Accelerator Laboratory

HEAVY FLAVOR SPECTROSCOPY

J. Rosen and J. Marques
Northwestern University, Evanston, IL 60208, USA

and

L. Spiegel
Fermilab, Batavia, IL 60510, USA

1. INTRODUCTION

As a useful by-product of the unfolding searches for mixing and CP-violation effects in the beauty sector there will accrue very large data samples for the study of heavy flavor spectroscopy. Interest in this field may be provisionally divided into two general classes:

I Hidden flavor states, i.e. $c\bar{c}$ and $b\bar{b}$ onium states.

II Open flavor states
 a) The D, D_s, B, B_s, and B_c meson systems
 b) Charm and beauty flavored baryons

In this brief note we emphasize that there are many missing (undiscovered) states in both categories—states which are not readily produced exclusively due to quantum number preferences or states which are not readily observed inclusively due to experimentally difficult decay channels. As recorded luminosities increase it may be possible to fill in some of the holes in the present listings of heavy flavor states. Of particular interest to us would be the identification of heavy flavor mesons which are not easily explained in terms of a $q\bar{q}$ paradigm but rather may be evidence for **hadro-molecular** states.

At Snowmass 1993 the topic of self-tagging schemes in B meson production was very much in vogue. Whether or not excited B-meson flavor-tagging will prove to be competitive with traditional methods based on the partner $\bar{B}$ decay remains to be seen. We suggest however that the richness of the excited B-system may undermine the efficacy of self-tagging schemes.

2. HEAVY FLAVOR ONIUM STATES

Figure 1, the bottomonium spectrum, illustrates several salient features of heavy flavor onium spectroscopy. The observed states, shown in solid lines, consist of six $^3S_1$ and six $^3P_{J=0,1,2}$ states. Conspicuous in their absence are D-wave states, singlet P-wave states, and the $^1S_0$'s. Potential model predictions for some of these states are shown in dashed lines. The reasons for this pattern are well known: much of the world's sample of beauty particles (hidden and open) comes from e^+e^- machines where the $b\bar{b}$ pair has the quantum numbers of the virtual annihilation photon, 1^{--}. Triplet P-wave states are subsequently populated through radiative decays of higher-lying $^3S_1$ states. On the other hand, inclusive production at hadron colliders might lead to a more democratic population of quantum levels. The problem then becomes one of identifying transitions to the ground state through small and experimentally difficult decay modes.

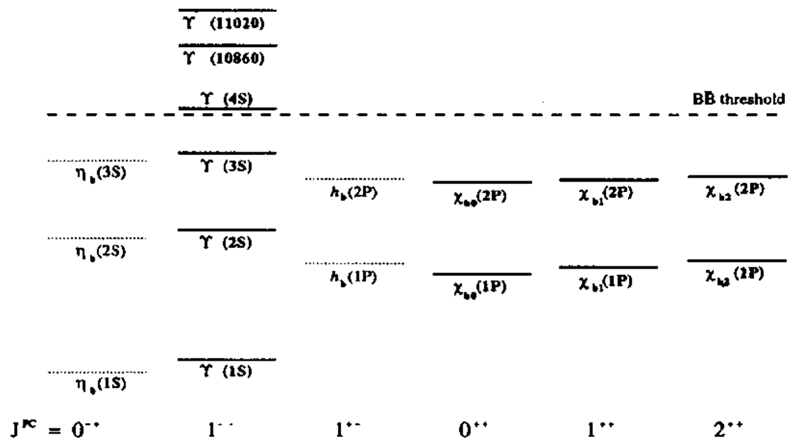

Figure 1. The bottomonium spectrum.

The charmonium spectrum is somewhat better represented in terms of observed states. In contrast to bottomonium there is an established $^1S_0$ (η_c) and there is the recent discovery of the singlet 1^1P_1 (h_c) in a hadro-formation experiment[1]. As anticipated, the observed mass of the h_c is very close to the spin-weighted centroid of the triplet P-wave family. The h_c has also been seen inclusively, again solely in the $J/\psi\pi^0$ decay mode, albeit with lower statistical accuracy[2]. One interesting feature of this decay mode ($J/\psi\pi^0$) is that it violates isospin conservation. This mode also suggests investigating $\Upsilon\pi^0$ final states as a possible signature for the bottomonium $^1P_1$'s.

Generally the spacings between charmonium and bottomonium states are reasonably well described by potential models. Also, independent of the choice of model there appears to be a general scaling in level spacings with quark mass. Thus on the whole potential model predictions should serve as useful guides to undiscovered states.

3. EXCITED HEAVY FLAVOR STATES

A summary of the present understanding of the quark-model assignments for open flavor mesons can be found in the Particle Data Group review[3]. As in the hidden flavor spectra, many slots remain to be experimentally filled. We draw particular attention to the first excited kaon, the $K_1(1270)$ ($J^P = 1^+$). The largest decay branching ratio for this state is into $K\rho$ (42±6%), which can be contrasted with the decay into $K^*(892)\pi$ (16±5%). Why the $K\rho$ mode is so dominant is not readily understood within the quark-antiquark constituent picture. Intriguingly, the central mass of the $K_1(1270)$ is very close to the sum of the central mass of the broad ρ (770) and the K (500 MeV). Also, we note that 1270 MeV is substantially lower than the centroid of the natural triplet system around 1400 MeV. The PDG listing suggests a mixing between the states at 1270 and 1400 but an interesting alternative is to think of the 1270 state as a hadro-molecular system, that is, a four-quark, L=0, isodoublet system with equivalent descriptions:

$$(\bar{s}u\ d\bar{d}) \quad \Leftrightarrow \quad K^0\rho^+ \quad \text{or} \quad K^+(\omega^0+\rho^0)/\sqrt{2} \qquad (1)$$

$$(\bar{s}d\ u\bar{u}) \quad \Leftrightarrow \quad K^+\rho^- \quad \text{or} \quad K^0(\omega^0-\rho^0)/\sqrt{2} \qquad (2)$$

The appearance of $K\rho$ and $K\omega$ modes is very natural in this picture: within the hadro-molecular system the bound ρ (or ω) decays leading to the observed final states.

The concept of non-standard meson and baryon states is not new—a multi-quark explanation has been proposed for the $f_0(975)$ and $a_0(980)$[4], for example. The study of heavy resonances which appear to exist at the boundary between QCD and nuclear physics may shed some light on the nature of the confinement process.

Within the quark model the ground state neutral B mesons consist of a $\bar{b}d$ (B^0) or a $\bar{b}s$ (B^0_s). To date only one excited state, the B^*, has been observed. The mass of this 1^- (quark model assignment) state is 5324.6±2.1 MeV. As this state is relatively narrow and much less than a pion mass above the B meson ground states, decays to the ground state take place radiatively. Unfortunately the signature photon energy is too low for presently configured collider spectrometers.

Figure 2 outlines the relationship between the ground states and first excited P-wave states for the K, D, and B systems. The horizontal bars about the central mass values are not uncertainties but rather represent single line widths (±1Γ). None of the excited beauty meson P-waves have yet been seen; the prediction that they lie some 450 MeV above the S-wave states reflects the first order domination of the mass of the light quarks in the splittings (which go as the reciprocal of the reduced mass). At the 1993 Snowmass conference the results[5] of more detailed calculations for masses of the 1^3P_1 and 1^3P_2 excited D_s, B, and B_s mesons were presented. Figure 2 also shows the $K_1(1270)$ state, discussed above, and where analogs of this hadro-molecular-interpreted state would lie in the charm and beauty systems.

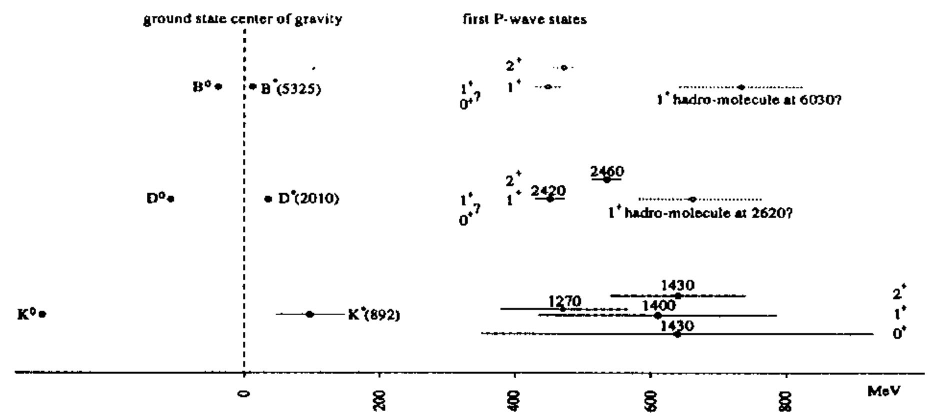

Figure 2. S-wave and P-wave Heavy Flavor States

Whether or not there is a significant cross section for these excited states, relative to the ground states, is an open question. Presumably a high statistics charm hadro-production experiment such as FNAL E-791 could address the question of resonance production in the D sector. Results from e^+e^- machines and photoproduction experiments may not necessarily be indicative of hadro-production trends.

Excited beauty mesons will tumble down to the lowest lying ground states (either B or B_s) through a combination of radiative transitions and strong decays. As such they will appear to come from the primary interaction vertex. Due to parity conservation the 1^3P_1 state cannot decay directly by pion emission to the B ground state but can go through the B^*. Single pion emission of the 1^3P_2 (and presumably broader 1^3P_0) is allowed. One variant of self-tagging would involve identifying a charged pion whose direction vector is close to the neutral B vector and whose $\pi^{\pm}B^0$ invariant mass is close to the 1^3P_2. We note however a couple reasons why this type of resonance self-tagging may be difficult:

1. Although the production of P-wave states may be large, only a restricted number of decays—those with a charged pion and neutral B meson in the final state—are relevant. For example, given equal initial populations of the 1^3P_2 ($B^{**+}, B^{**0}, \bar{B}^{**0}, B^{**-}$), only one-third of the strong decays will lead to the desired final state.

2. Contributions from dipion decays such as $B^{**0} \rightarrow \pi^+\pi^- B^0$ where one of the pions is soft and missed and the other appears to resonate with the B^0 with consequent flavor dilution. A hadro-molecular state (BV, $V=\rho,\omega$) would fall in this category.

It would appear that flavor self-tagging will not work for B_s^0 since the $\bar{b}s$ system has zero isospin and consequently no transitions involving single charged pions. If any or all of the P-wave states lie below the m_B+m_K threshold, those states will decay by E1 γ emission. Above this threshold B_s^0 excited states will fall apart into B+K (or B+Kπ) and consequently short circuit the B_s^0. This is directly analogous to the more familiar situation in charmonium where transitions to low lying states are effectively quenched above the open charm thresholds, $2m_D$ and $m_D+m_{D^*}$.

We conclude by observing that there is a rich field of spectroscopy to be mined. Not only is it interesting in its own right, but it can clarify outstanding issues in light quark spectroscopy as well as serve as a technical basis for symmetry studies such as CP violation.

4. ACKNOWLEDGMENTS

We wish to thank the U.S. Department of Energy for supporting our participation in the 1993 Snowmass Workshop on B Physics at Hadron Accelerators and the Workshop organizers for facilitating an enlightening and productive environment.

5. REFERENCES

1. T.A. Armstrong et al. *Phys. Rev. Lett.* 69 (1992) 2337.

2. L. Antoniazzi et al. FERMILAB-Pub-92/265-E (1993). Submitted to *Phys. Rev. D.*

3. Particle Data Group, *Phys. Rev.* **D45** (1992). The table referred to in on page III.69.

4. R.J. Jaffe, *Phys. Rev.* **D15**, (1977) 267

5. From a working session talk (*Properties of Excited B Mesons*) presented by C. Quigg at the Snowmass 1993 B-Physics Workshop. These results will soon exist in pre-print form: E. Eichten, C. Hill, and C. Quigg, FERMILAB—Pub-93/255—T.

B_c

CHRIS QUIGG
Fermi National Accelerator Laboratory
Batavia, Illinois 60510 USA

1. MOTIVATION

Mesons with beauty and charm hold a special fascination for the theorist. A bound state of two heavy quarks, B_c admits reliable calculations of both spectroscopy and decay. A rich spectrum of extremely narrow $c\bar{b}$ states awaits discovery. The deep binding of the heavy quarks has a pronounced influence upon the B_c lifetime and the pattern of weak decays. The decays of B_c may open new ways of measuring the Kobayashi-Maskawa matrix element V_{cb}.

These are timely issues because the first observation of B_c is imminent. More than 10^9 b quarks are produced in a year's run of the Tevatron Collider. They materialize not only as B_u and B_d, but also as B_s, b-baryons, and still rarer birds. CDF has successfully operated a silicon vertex detector in the Tevatron environment, and has shown that subtle spectroscopy of the χ_c states is possible in a hadron collider. The $\psi\pi$ decay mode offers a reasonable tag for discovery and subsequent study of the B_c. For all these reasons, Estia Eichten and I are filling in a portrait of the B_c and its excited states.[1] In this talk, I will summarize what we have learned.[2]

2. THE B_c SPECTRUM

The $c\bar{b}$ quarkonium system occupies a region of space already probed by the ψ and Υ families, so the Schrödinger equation will provide a reliable description of the bound-state spectrum. Calculating the B_c mass is straightforward: (i) Choose a quarkonium potential with c- and b-quark masses determined from ψ and Υ; (ii) Compute the 1S center of gravity; (iii) Add the hyperfine splitting,

$$M(B_c) = M(1S) - \tfrac{3}{4}\Delta M; \quad M(B_c^*) = M(1S) + \tfrac{1}{4}\Delta M \ ,$$

where $\Delta M = \alpha_s|\Psi(0)|^2/m_b m_c$. After surveying a variety of potentials that provide good descriptions of the ψ and Υ spectra, we estimate that $M(B_c) = 6256 \pm 20$ MeV/c^2, and that $M(B_c^*) - M(B_c) \approx 72$ MeV/c^2.

We have used standard methods to calculate the entire spectrum, including fine-structure and hyperfine-structure splitting, in the Buchmüller-Tye potential.[3] Figure 1 shows that approximately fifteen narrow states will lie below the BD flavor threshold.

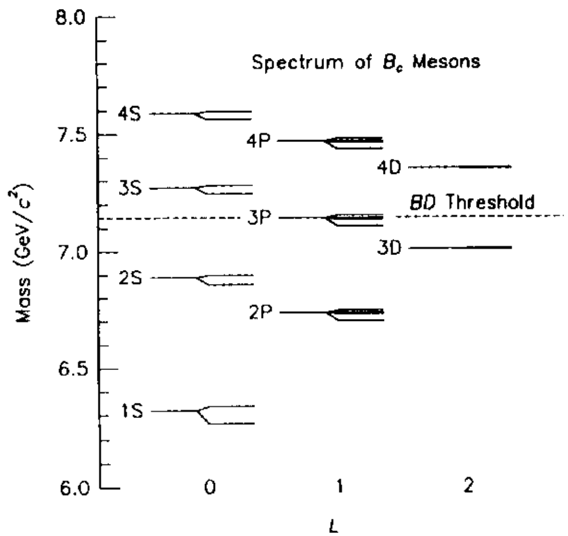

Figure 1. The spectrum of $c\bar{b}$ states.

3. TRANSITIONS WITHIN THE B_c SPECTRUM

The $c\bar{b}$ system is the true hadronic analog of the hydrogen atom because, in contrast to $c\bar{c}$ or $b\bar{b}$, its constituents cannot annihilate into gluons. All the excited $c\bar{b}$ states below flavor threshold decay by electromagnetic or hadronic transitions that cascade to the ground-state B_c, which decays weakly. Only for the 2S levels do hadronic decays ($\rightarrow 1S + \pi\pi$) dominate over the electromagnetic transitions. All the $c\bar{b}$ levels are extraordinarily narrow, with total widths ranging between 21 and 173 keV.

We believe that, in time, it will be possible to map out part of the $c\bar{b}$ spectrum by detecting γ or $\pi\pi$ in coincidence with weak decays of B_c. That would be a wonderful triumph of experimental technique and an opportunity to test our understanding of the force between quarks.

4. THE LIFETIME OF B_c

Weak decays of B_c proceed through the decay of either heavy quark or by $c\bar{b}$ annihilation into a virtual W^+. To estimate the semi-inclusive decay rates of the c and $\bar{b}$ quarks, we modify the spectator picture to take account of the deep binding of the heavy quarks. The influence of confinement has been overlooked in previous work on B_c decays, in which c and $\bar{b}$ have been regarded as free. It has a decisive effect on the systematics of B_c decays.

For the (Cabibbo-Kobayashi-Maskawa–suppressed) decays of the $\bar{b}$ antiquark, the binding of the $\bar{b}$ to c reduces the $\bar{b} \rightarrow \bar{c}$ decay rate by about 40 percent compared with the decay rate of a free $\bar{b}$ antiquark, to $\Gamma(B_c \rightarrow \bar{b}s + W^*) = 3.9 \times 10^{11}\ \mathrm{s}^{-1}$.

For the (CKM-favored) decays of the c quark, binding suppresses the $c \rightarrow s$ transition by a factor of 4.8 compared to the decay rate of an isolated c quark. This compensates for the favorable quark mixing ($|V_{cs}| \gg |V_{cb}|$) and makes the $c \rightarrow s$ decay, at $\Gamma(B_c \rightarrow \bar{b}s + W^*) = 0.7 \times 10^{11}\ \mathrm{s}^{-1}$, less important than $\bar{b} \rightarrow \bar{c}$.

Table 1. Partial decay rates and branching fractions for semi-inclusive B_c decays.

Channel	Partial Width ($10^{10}\ \mathrm{s}^{-1}$)	Branching Fraction (%)
$(c\bar{c})e\nu_e$	6.90	10
$(c\bar{c})\mu\nu_\mu$	6.86	10
$(c\bar{c})\tau\nu_\tau$	1.33	2
$(c\bar{c})u\bar{d}$	18.79	27
$(c\bar{c})c\bar{s}$	5.56	8
$(s\bar{b})e\nu_e$	2.91	4
$(s\bar{b})\mu\nu_\mu$	2.67	4
$(s\bar{b})u\bar{d}$	1.57	2
$\tau\nu_\tau$	6.70	10
$c\bar{s}$	15.77	23
Total	69.06	

The compact size of the $c\bar{b}$ system means that the pseudoscalar decay constant f_{B_c} will be large, so that annihilation decays into massive final states are also prominent. We adopt the value $f_{B_c} = 500$ MeV, suggested by quarkonium calculations, to estimate decay rates. Decays into light products are helicity-suppressed, but decays into $c\bar{s}$ and $\tau^+\nu_\tau$ proceed with significant rates, so that $\Gamma(B_c \rightarrow W^*) = 2.2 \times 10^{11}\ \mathrm{s}^{-1}$.

The decay rates computed using constituent-quark masses for the decay products of the virtual W-boson are collected in Table 1. Adding up the decay rates presented there, we arrive at a total rate that corresponds to a lifetime $\tau(B_c) = 1.44$ ps. Annihilations account for 33% of the total rate, c-decays for 11%, and $\bar{b}$-decays for 56%. Using current-quark masses instead of constituent-quark masses for the decay products of the virtual W^*, we find $\tau(B_c) = 1.28$ ps. In this case, c-decays increase to 19% at the expense of annihilations. We adopt 1.35 ± 0.15 ps as our best *semi-inclusive* estimate for the B_c lifetime. The uncertainty reflects the broad range of experimentally allowed values of $|V_{cb}|$, as well as limitations of the modified spectator approximation that we shall bring to light at once.

To the extent that f_{B_c} is known—and we estimate that the uncertainty from potential model calculations is no more than 20% today—a measurement of the annihilation decay rate constitutes an independent determination of $|V_{cb}|$. It is worth thinking about how such measurements would be made, and normalized.

5. EXCLUSIVE DECAYS

Only a small number of final states are available for the decay of the charmed quark in B_c. Among the Cabibbo-favored decays, the list

$$B_c \rightarrow \pi \begin{Bmatrix} B_s \\ B_s^* \\ B_s^{**} \\ B_u K \end{Bmatrix};\quad K \begin{Bmatrix} B_u \\ B_u^* \\ B_u \pi \end{Bmatrix};\quad \rho \begin{Bmatrix} B_s \\ B_s^* \end{Bmatrix};\quad K^* \begin{Bmatrix} B_u \\ B_u^* \end{Bmatrix}$$

is nearly exhaustive. We can use a combination of heavy-quark methods[4] and the nonrelativistic wave functions to calculate the exclusive rates for these decays. We have found the semi-inclusive decay rate $c \rightarrow s + W^+$ calculated in the spectator model to be significantly inaccurate for transitions like $B_c \rightarrow \rho B_s^{(*)}$ that lie very close to the kinematical limit. This is because inclusive-exclusive duality is not local, but represents an averaging over a "typical hadronic" scale of energies. When the allowed phase space for decay is concentrated near threshold, semi-inclusive methods cannot be trusted. We estimate the exclusive decay rates $\Gamma(B_c \to B_s\pi) \approx \Gamma(B_c \to B_s\rho) \approx 10 \times 10^{10}\ \mathrm{s}^{-1}$, far larger than the semi-inclusive estimate for $B_c \to (s\bar{b})u\bar{d}$ that should include them. A similar conflict would arise in calculations of the tau decay rates, if the tau mass were around 1 GeV/c^2. Increasing the exclusive decays of the charmed quark will decrease $\tau(B_c)$ to perhaps 1.1 to 1.2 ps.

For the $\bar{b} \to \bar{c}$ transitions, the kinematical situation is favorable for trustworthy calculations of exclusive decay rates. The $\bar{c}$ moves with a velocity close to that of the spectator c, so it is a good approximation to treat the wave functions of the B_c initial state and the $c\bar{c}$ final state nonrelativistically. The rates for the semileptonic decays to ψ, ψ', χ_c, and η_c, as well as the lepton spectra in the rest frame of the decaying B_c, can then be calculated in terms of a quantum-mechanical overlap integral.

With an adventurous spirit, it takes just a little imagination to consider B_c decays as a source of tagged B_s for the study of B_s-$\overline{B}_s$ mixing and CP violation in the B_s system. The decay

$$\begin{array}{ccc} B_c^+ & \to & B_s^{(*)}\ell^+\nu \ , \\ (c\bar{b}) & & (\bar{b}s) \end{array}$$

which occurs with a branching fraction about four percent for either electrons or muons, identifies the flavor of B_s at the time of its production. An ℓ^+ signals the decay $c \to s$, yielding $\bar{b}s = B_s$, while an ℓ^- tags $b\bar{s} = \overline{B}_s$. The subsequent decay of the B_s into $D_s\ell\nu$ or D^-K^+, etc. constitutes a second flavor measurement at the time of decay. Event rates at the SSC and LHC, or at the Tevatron with the Main Injector, may make this a practical technique, particularly if displaced-vertex triggering becomes a reality.

6. PRODUCTION AT THE TEVATRON

Just how rare will B_c be in high-energy collisions? A number of estimates, most recently a perturbative calculation of the rate at which energetic b quarks fragment into B_c and B_c^*, suggest that B_c should be produced at about 10^{-3} of the b rate in the Tevatron collider.[5] We would therefore expect about 10^6 B_c to be produced in the next collider run at Fermilab. Similar estimates suggest that a few hundred B_c should be produced per million hadronic events at LEP.

Promising signatures for the discovery of B_c include

$$B_c \to \psi\pi, \quad \psi \hookrightarrow e^+e^- \text{ or } \mu^+\mu^- \ ,$$

for which we estimate a branching fraction of 0.4% times 6.3%, or 2.5×10^{-4}, and

$$B_c \to \psi\ell\nu, \quad \psi \hookrightarrow e^+e^- \text{ or } \mu^+\mu^- \ ,$$

for which we estimate 1.5% times 6.3%, or 9.4×10^{-4}. The semi-inclusive branching fraction for $B_c \to \psi$ + anything will be around 10%. The ψa_1 mode may also be detected with good efficiency. Decay modes that involve two short tracks may also be appealing targets. The $D_s^*\psi$ ($\approx 5\%$) and $B_s\pi$ modes are of special interest.

7. SUMMARY

Mesons with beauty and charm are an interesting theoretical laboratory that should soon become accessible to experiment. We can predict the properties of $c\bar{b}$ states with confidence. In particular, we expect the mass of the ground-state B_c to lie close to 6256 MeV/c^2. More than a dozen narrow states lie below flavor threshold. They cascade to the ground state by making electromagnetic or hadronic transitions within the $c\bar{b}$ spectrum. The excited states are extraordinarily narrow. They may be observable in γ or $\pi\pi$ coincidences with B_c.

Weak decays of B_c are affected by the strong binding of the $\bar{b}$ and c constituents. Our estimates of the semi-inclusive decay rates lead to a lifetime $\tau(B_c) \approx 1.35 \pm 0.15$ ps that is appreciably longer than the guess $\tau(B_c) \approx (1/\tau_b + 1/\tau_c)^{-1} \approx 0.71$ to 0.88 ps, which neglects binding. The semi-inclusive analysis understates the importance of B_s + light hadron modes. Our best lifetime estimate is 1.1 to 1.2 ps.

Finally, while B_c is an exotic—indeed, undiscovered—state today, it may have important practical applications in the future. The decay $B_c \to B_s\ell\nu$ may provide a clean and efficient flavor tag for B_s.

8. ACKNOWLEDGEMENT

This work was performed at the Fermi National Accelerator Laboratory, which is operated by Universities Research Association, Inc., under contract DE-AC02-76CHO3000 with the U.S. Department of Energy.

9. REFERENCES

1. Estia J. Eichten and Chris Quigg, in preparation. This paper includes complete references to earlier work.
2. For earlier work on B_c, see for example, D. Du and Zi Wang, *Phys. Rev. D* **39**, 1342 (1989); S. S. Gershteĭn, A. K. Likhoded, and S. R. Slabopitskiĭ, *Int. J. Mod. Phys. A* **6**, 2309 (1991); M. Lusignoli and M. Masetti, *Z. Phys. C* **51**, 549 (1991); Chao-Hsi Chang and Yu-Qi Chen, *Phys. Lett.* **B284**, 127 (1992).
3. W. Buchmüller and S.-H. H. Tye, *Phys. Rev. D* **24**, 132 (1981).
4. For a closely related application, see Elizabeth Jenkins, Michael Luke, Aneesh V. Manohar, and Martin J. Savage *Nucl. Phys.* **B390**, 463 (1993).
5. Eric Braaten, Kingman Cheung, and Tzu-Chiang Yuan, Northwestern preprint NUHEP-TH-93-6 (unpublished).

B^{**} PROPERTIES

CHRIS QUIGG
Fermi National Accelerator Laboratory
Batavia, Illinois 60510 USA

1. INTRODUCTION

If significant numbers of B mesons are produced through one or more narrow excited $(\bar{b}q)$ states, the strong decay $B^{**\pm} \to B^{(*)0}\pi^{\pm}$ will tag the neutral meson as $(\bar{b}d)$ or $(b\bar{d})$, respectively. This might be dramatically more efficient than using the pair-produced partner of the B as a flavor tag, and could advance the search for the expected large CP-violating asymmetry in (B^0 or $\bar{B}^0$) $\to J/\psi K_S$ decay. B^{**}-tagging might also resolve kinematical ambiguities in semileptonic decays of charged and neutral B mesons by choosing between two solutions for the momentum of the undetected neutrino.[1]

Estia Eichten, Chris Hill, and I have used heavy-quark symmetry to estimate the masses, widths, and branching fractions of orbitally excited B, D_s, and B_s states from the properties of corresponding K and D levels.[2] Our analysis show that one requirement for the utility of B^{**}-tagging—narrow resonances—is likely to be met by the B_2^* and B_1. Experiment will have to rule on the strength of these lines and the ratio of signal to background.

For our purposes, the essential idea of the heavy-quark limit is that the spin $\vec{s}_Q$ of the heavy quark and the total (spin + orbital) angular momentum $\vec{j}_q = \vec{s}_q + \vec{L}$ of the light degrees of freedom are separately conserved.[3] Each energy level in the excitation spectrum of $(Q\bar{q})$ mesons is composed of a degenerate pair of states characterized by j_q and total spin $\vec{J} = \vec{j}_q + \vec{s}_Q$, i.e., by $J = j_q \pm \frac{1}{2}$. The ground-state pseudoscalar and vector mesons, which are degenerate in the heavy-quark limit, correspond to $j_q = \frac{1}{2}$, with $J = 0$ and 1. Orbital excitations lead to two distinct doublets associated with $j_q = L \pm \frac{1}{2}$.

2. MASSES

The leading corrections to the spectrum prescribed by heavy-quark symmetry are inversely proportional to the heavy-quark mass. We may write the mass of a heavy-light meson as

$$M(n\mathrm{L}_J(j_q)) = M(1\mathrm{S}) + E(n\mathrm{L}(j_q)) + \frac{C(n\mathrm{L}_J(j_q))}{m_Q}\,, \tag{1}$$

where n is the principal quantum number and $M(1\mathrm{S}) = [3M(1\mathrm{S}_1) + M(1\mathrm{S}_0)]/4$ is the mass of the ground state. The excitation energy $E(n\mathrm{L}(j_q))$ has a weak dependence on the heavy-quark mass that we have evaluated in a potential model.[4]

We focus upon the $j_q = \frac{3}{2}$ states observed as narrow $D\pi$ or $D^*\pi$ resonances because their counterparts in other heavy-light systems should also be narrow. Our overall strategy is to use the observed properties of the K and D mesons to predict the properties of the orbitally excited B, D_s, and B_s mesons.

There is no ambiguity about the $2^+(\frac{3}{2})$ levels $K_2^*(1429)$ and $D_2^*(2459)$. We identify $D_1(2424)$ as a $j_q = \frac{3}{2}$ level because it is narrow, as predicted by heavy-quark symmetry. Following Ito et al.,[5] we identify $K_1(1270)$ as the $1^+(\frac{3}{2})$ level, because that assignment gives a consistent picture of masses and widths. For a given value of the charmed-quark mass, a fit to the strange and charmed resonances leads to predictions for other heavy-light masses. Our expectations are summarized in Table 1. The prediction for the 1^+ D_s meson lies 34 MeV below $D_{s1}(2536)$; that discrepancy is a measure of the limitations of our method.

3. DECAY WIDTHS

The decay of an excited heavy-light meson H to a heavy-light meson H' and a light hadron h is governed by heavy-quark symmetry. The two-body decay rate for an ℓ-wave transition may be written as

$$\Gamma(H \to H'h) = C^2 p^{2\ell+1} F \exp(-p^2/\kappa^2), \tag{2}$$

where p is the three-momentum of the decay products in the rest frame of H, C is a normalized 6-j symbol, and F sets the strength of each independent decay amplitude. Once F is determined from the charmed or strange mesons, this dynamical quantity may be used to predict related decays, including those of orbitally excited B mesons. We determine the overall strength of the decay and the momentum scale κ of the form factor by fitting to existing data. We assume that κ is typical of hadronic processes ($\approx$ 1 GeV) and that it varies little with decay angular momentum ℓ.

The decays $2P(\frac{3}{2}) \to 1S(\frac{1}{2}) + \pi$ are governed by a single $\ell = 2$ amplitude. To evaluate the transition strength F, we fix $\Gamma(D_2^* \to D\pi) + \Gamma(D_2^* \to D^*\pi) = 25$ MeV, as suggested by recent experiments.[6] This determines all the pionic transitions between the $2P(\frac{3}{2})$ and $1S(\frac{1}{2})$ multiplets. The results are shown in Table 1, where we indicate the variation of the predicted rates as the momentum scale κ ranges from 0.8 to 1.2 GeV. The strengths of K and (negligible) η transitions are determined by $SU(3)$. The predictions agree well with what is known about the $L = 1$ D and D_s states.

Increasing the D_{s1} and D_{s2}^* masses by 34 MeV to match the observations of D_{s1} increases each of the partial widths for those states by 1 or 2 MeV. The narrow width observed for D_{s1} is close to the prediction from heavy-quark symmetry. This suggests that mixing of the narrow $2P(\frac{3}{2})$ level with the broader $2P(\frac{1}{2})$ state is insignificant. This pattern should hold for B and B_s as well.

Our estimates for the ρ transitions are also shown in Table 1. The dependence on the momentum scale κ in the form factor is much more pronounced than for the pseudoscalar transitions because of the wide variation in momentum over the ρ peak.

The results collected in Table 1 show that both the B_2^* and the B_1 states should be narrow (20 to 40 MeV), with large branching fractions to a ground-state B or B^* plus a pion. These states should also have significant two-pion transitions that we have modeled by the low-mass tail of the ρ resonance. The strange states, B_{s2}^* and B_{s1}, are very narrow ($\Gamma \lesssim 10$ MeV); their dominant decays are by kaon emission to the ground-state B and B^*.

Table 1. Masses and decay rates of the $2P(\frac{3}{2})$ heavy-light mesons.

	Width (MeV)			
Transition	Calculated	PDG 1992	CLEO 1993	E687 1993
$D_2^*(2459) \to D^*\pi$	9			
$D_2^*(2459) \to D\pi$	16			
$D_2^*(2459) \to D\rho$	5 to 13			
$D_2^*(2459) \to$ all	30 to 38	19 ± 7	28^{+8+6}_{-7-6}	$24 \pm 7 \pm 5$
$D_1(2424) \to D^*\pi$	11 to 13			
$D_1(2424) \to D\rho$	8 to 11			
$D_1(2424) \to$ all	19 to 23	20^{+9}_{-5}	20^{+6+3}_{-5-3}	$15 \pm 8 \pm 5$
$D_{s2}^*(2537) \to D^*K$	2 to 4			
$D_{s2}^*(2537) \to DK$	6 to 7			
$D_{s2}^*(2537) \to$ all	8 to 11			
$D_{s1}(2502) \to D^*K$	3 to 6	< 4.6	< 2.3	< 3.2
$B_2^*(5767) \to B^*\pi$	11			
$B_2^*(5767) \to B\pi$	10			
$B_2^*(5767) \to B^*\rho$	13 to 29			
$B_2^*(5767) \to B\rho$	4 to 13			
$B_2^*(5767) \to$ all	38 to 63			
$B_1(5755) \to B^*\pi$	14			
$B_1(5755) \to B^*\rho$	11 to 33			
$B_1(5755) \to B\rho$	6 to 8			
$B_1(5755) \to$ all	31 to 55			
$B_{s2}^*(5846) \to B^*K$	2 to 4			
$B_{s2}^*(5846) \to BK$	1 to 3			
$B_{s2}^*(5846) \to$ all	3 to 7			
$B_{s1}(5834) \to B^*K$	1 to 3			

4. ACKNOWLEDGEMENTS

This work was performed at the Fermi National Accelerator Laboratory, which is operated by Universities Research Association, Inc., under contract DE-AC02-76CHO3000 with the U.S. Department of Energy.

5. REFERENCES

1. C. T. Hill, Fermilab-Conf-93-256/T and These Proceedings.
2. Estia J. Eichten, Christopher T. Hill, and Chris Quigg, Fermilab-Pub-93/255-T.
3. N. Isgur and M. B. Wise, *Phys. Lett. B* **232**, 113 (1989). For a review, see M. Neubert, SLAC-PUB-6263, *Phys. Rep.* (to be published).
4. W. Buchmüller and S.-H. H. Tye, *Phys. Rev. D* **24**, 132 (1981).
5. T. Ito, T. Morii, and M. Tanimoto, *Prog. Theor. Phys.* **90**, 213 (1993).
6. P.L. Frabetti et al. (E687 Collaboration), Fermilab-Pub-93/249-E; G. Crawford et al. (CLEO Collaboration), contribution no. 282 to the XVI International Symposium on Lepton and Photon Interactions; Particle Data Group, *Phys. Rev. D* **45**, S1 (1992).

List of Participants

A. Abashian
Virginia Polytechnic Institute

G. Apollinary
Rockefeller University/
Fermi National Accelerator Laboratory

K. Bazizi
University of California

R. Carrigan, Jr.
Department of Energy/
Fermi National Accelerator Laboratory

L. Cremaldi
University of Mississippi

I. Dunietz
Fermi National Accelerator Laboratory

A. Erwin
University of Wisconsin

R. Frey
University of Oregon

L. Garren
Fermi National Accelerator Laboratory

S. Geer
Fermi National Accelerator Laboratory

M. Halling
Cornell University/
Fermi National Accelerator Laboratory

V. Kubarowski
Superconducting Super Collider Laboratory

E. Ma
University of California (Riverside)

L. Markosky
University of Arizona/
Fermi National Accelerator Laboratory

B. Newberger
University of Texas at Austin

M. Schmidt
Yale University

T. Sen
Superconducting Super Collider Laboratory

M. Sheaff
University of Wisconsin

D. Silverman
University of California (Irvine)

L. Song
Fermi National Accelerator Laboratory

R. Stefanski
Fermi National Accelerator Laboratory

J. Wilcox
Northeastern University

H. Yamamoto
California Institute of Technology

E. Yao
University of Michigan

Theory of Heavy Flavors

Convenors:

B. Grinstein
Superconducting Super Collider Laboratory

J. Smith
State University of New York at Stony Brook

List of Participants

J. Amundson
University of Chicago

U. Baur
Florida State University

C. Dib
Universidad Técnica Federico Santa María

I. Dunietz
Fermi National Accelerator Laboratory

M. Gronau
Technion—Israel Insitute of Technology

G. Hou
National Taiwan University

B. Kayser
National Science Foundation

A. Kronfeld
Fermi National Accelerator Laboratory

E. Levin
Fermi National Accelerator Laboratory

H. Lipkin
Weizmann Institute of Science

D. London
University of Montreal

E. Ma
University of California (Riverside)

R. Meng
Argonne National Laboratory

Y. Nir
Weizmann Institute of Science

R. Oakes
Northwestern University

C. Quigg
Fermi National Accelerator Laboratory

S. Riemersma
Southern Methodist University

D. Silverman
University of California (Irvine)

J. Soares
Carnegie Mellon University

J. Taron
Ohio State University

W. Tung
Michigan State University

NEW PHASES IN CP VIOLATING B DECAY ASYMMETRIES FROM MIXING TO SINGLET DOWN QUARKS

DENNIS SILVERMAN AND WOON-SENG CHOONG
Department of Physics, University of California, Irvine
Irvine, CA 92715, USA

1. INTRODUCTION

Groups such as E_6 with extra $SU(2)_L$ singlet down quarks give rise to flavor changing neutral currents (FCNC) through the mixing of four or more down quarks[1,2,3,4]. These FCNC with Z^0 mediated exchange may contribute part of $B_d^0 - \bar{B}_d^0$ mixing and of $B_s^0 - \bar{B}_s^0$ mixing, giving a range of non-zero values for the fourth quark's mixing parameters. If these are a large contributor to the $B_d - \bar{B}_d$ mixing, they introduce three new angles and two new phases into the CP violating B decay asymmetries. The size of the contribution of the FCNC amplitude U_{db} as one side of the unitarity quadrangle is less than 0.05 of the unit base at the 1-σ level, but we find that it can contribute as large an amount to $B_d - \bar{B}_d$ mixing as does the standard model. We find that the new phases can appear in this mixing as well as in $B_s - \bar{B}_s$ mixing, and give total phases completely different from that of the standard model in CP violating B decay asymmetries.

FCNC experiments put limits on these new mixing angles that constrain the possibility of new physics accounting for $B_d^0 - \bar{B}_d^0$ and $B_s^0 - \bar{B}_s^0$ mixing. Here we analyze jointly all constraints on a 4×4 mixing matrix obtained by assuming only one of the $SU(2)_L$ singlet down quarks mixes appreciably. We use[5] the experiments used on the 3×3 CKM sub-matrix elements[6] which include those on the six matrix elements $V_{ud}, V_{cd}, V_{us}, V_{cs}, V_{ub}, V_{cb}$ of the u and c quark rows, and, in the neutral K system, include $|\epsilon|$, $K_L \to \mu\mu$ (for which there are two experiments), and also $B_d - \bar{B}_d$ mixing. For studying FCNC, we add the $B \to \mu\mu X$ bound (which constrains $b \to d$ and $b \to s$), Δm_K (which constrains $s \to d$ along with the other K experiments), and $Z^0 \to b\bar{b}$ (which directly constrains the V_{4b} quark mixing element). We analyze all of these together using a joint χ^2 for fitting all of the 13 experiments in the nine parameter angle space of the 4×4 mixing matrix. We include both the standard model and FCNC contributions through effective Hamiltonians. We then make a maximum likelihood plot for the phase difference of the combined amplitude for $B_d - \bar{B}_d$ mixing minus the standard model phase, versus the phase of the standard model amplitude alone, which show that almost any phase can occur through new physics to be observed in CP violating B_d^0 decay asymmetries. Similar conclusions follow for $B_s - \bar{B}_s$ mixing, only with a smaller allowed region of new phases. From the bound on the mixing elements, the new singlet down quark might have a mass above the 500 GeV range.

2. FLAVOR CHANGING NEUTRAL CURRENTS FROM MIXING

We use the 4×4 matrix V which diagonalizes the initial down quarks (d^0_{iL}) to the mass eigenstates (d_{jL}) by $d^0_{iL} = V_{ij}d_{jL}$. The combination of the diagonal matrix in the up quarks and the matrix V give the charged current interactions[1,2,3,4]. Here the 3×4 submatrix of V couples the three up quarks to the four down quarks. The 3×3 submatrix of V for $i,j = 1,2,3$ takes the role of the CKM matrix for mixing the standard model quarks, but it is not unitary by itself. The flavor changing neutral currents between the j'th and i'th down quarks have amplitudes $-U_{ij} \equiv V^*_{4i}V_{4j}$

The diagonal weak isovector neutral current couplings are reduced in strength by $(1 - |V_{4i}|^2)$. FCNC experiments will bound the three amplitudes U_{ds}, U_{sb}, and U_{bd} which contain three new mixing angles and three phases.

3. FCNC EFFECTIVE HAMILTONIAN

The FCNC tree processes with Z^0 exchange would contribute at the same time as the second order weak neutral current flavor changing processes in the standard model. At the FCNC tree level of a four Fermion effective Hamiltonian, for quarks coupling to muon pairs, the FCNC couple to a virtual Z^0 created in the neutral current annihilation channel. In the four quark effective Hamiltonian, the FCNC contribute through tree level Z^0 exchange as well, and both annihilation and exchange graphs contribute the same. We can then add the FCNC Z^0 exchange terms to the standard model second order weak four Fermion effective Hamiltonian H_{eff}, as computed by Inami and Lim[7], and carry them along in all treatments of H_{eff} applied to various neutral current processes.

4. $B_d - \bar{B}_d$ MIXING

Mixing may occur by the $b - \bar{d}$ quarks in a $\bar{B}_d$ annihilating to a virtual Z through a FCNC with amplitude U_{db} , and the Z then creating $\bar{b} - d$ quarks through another FCNC, again with amplitude U_{db}, which then becomes a B_d meson.

For $B_d - \bar{B}_d$ mixing the four quark $b - d$ coupling, gives[5]

$$x_d = \frac{2G_F}{3\sqrt{2}} B_B f_B^2 m_B \eta_B \tau_B \left|(U_{std})^2 + (U_{db})^2\right| \tag{1}$$

where

$$U^2_{std} \equiv \frac{\alpha}{4\pi \sin^2\theta_W} y_t f_2(y_t)(V^*_{td}V_{tb})^2, \tag{2}$$

and $x_d = \Delta m_{B_d}/\Gamma_{B_d} = \tau_{B_d}\Delta m_{B_d} = \tau_{B_d}2|M_{12}|$.

The CP violating decay asymmetries rely on a relative phase between the $B^0_d - \bar{B}^0_d$ mixing and the b quark decay amplitudes into final states of definite CP. Since we have found that Z mediated FCNC processes may contribute significantly to $B^0_d - \bar{B}^0_d$ mixing, the phases of U_{db} would be important. To leading order in $s_{34}, s_{24}e^{-i\delta_{24}}$, and $s_{14}e^{-i\delta_{14}}$ we have

$$U_{db} = -s_{34}(s_{34}V^*_{td} + s_{14}e^{-i\delta_{14}} - s_{24}e^{-i\delta_{24}}s_{12}). \tag{3}$$

We note that the first term has the same phase as in the standard model where the box diagram with the t quark dominates the mixing. This requires a numerical analysis to find how much the other terms contribute.

5. LARGE NEW PHASES APPEAR IN CP VIOLATING B DECAY ASYMMETRIES

In maximum likelihood correlation plots, we use for axes two output quantities which are dependent on the angles, such as $|U_{db}|$ and $|U_{std}|$, and for each possible bin with given values for these, we search through the nine dimensional angular data set and put in that bin the minimum χ^2 that gives the coordinates in the bin. We then draw contours at several χ^2 in this plane to present the results. We find that $|U_{db}|$ can go from zero up to as large as the magnitude of $|U_{std}|$ at a similar confidence level, with the same true for $B_s - \bar{B}_s$ mixing.

We define the phases of the complete $B_d - \bar{B}_d$ amplitude, ϕ_{tot}, the standard model amplitude, $\phi_{std} = 2\beta$, and their difference, ϕ_{diff} by

$$\phi_{tot} = \arg(U^2_{std} + U^2_{db}), \tag{4}$$
$$\phi_{std} = \arg(U^2_{std}) = \arg((V^*_{td}V_{tb})^2) = 2\beta, \tag{5}$$
$$\phi_{diff} = \phi_{tot} - \phi_{std}. \tag{6}$$

¿From the maximum likelihood plot with ϕ_{diff} on the y-axis and $\phi_{std} = 2\beta$ on the x-axis for $m_t = 150$ GeV we find that the phase difference between the total amplitude including FCNC and the standard model amplitude can range up to $\pm 180°$ for $B_d - \bar{B}_d$ mixing. The phase of $B_d - \bar{B}_d$ mixing enters into the CP violating B decay asymmetries, such as in $B^0_d \to J/\psi K_S$. From the analogous plot for $B_s - \bar{B}_s$ mixing, using analogous phases ϕ_{tot-sb}, $\phi_{std-sb} = \arg((V^*_{ts}V_{tb})^2) = 2\beta_s$, and $\phi_{diff-sb}$, the phase difference ranges over $\pm 10°$ at 1-σ and $\pm 25°$ at 2-σ. $\beta_s = \arg(V^*_{ts}V_{tb})$ is the small angle from the $b - s$ unitarity quadrangle which occurs in $b \to c\bar{c}s$ decays as $B_s \to \psi\phi$. ϕ_{std-sb} runs from $-5°$ to $3°$ at 1-σ due to the quadrangle allowing negative β_s.

6. CORRECTIONS TO CKM UNITARITY TRIANGLES AND NEXT DOWN QUARK MASS

The unitarity of the 4×4 mixing matrix requires orthogonality of the different rows. Instead of the three terms in the CKM orthogonality relation, which give a triangle in the complex plane, we now have four terms which give a quadrangle. The fourth side in the $b - d$ quadrangle is $U_{db} = V^*_{ud}V_{ub} + V^*_{cd}V_{cb} + V^*_{td}V_{tb}$. This is bounded at 1-$\sigma$ by $|U_{db}/(V^*_{cd}V_{cb})| \leq 0.05$, which is at a barely detectable size.

To estimate the new D quark mass, we use a Fritzsch ansatz relation between down quark mass ratios and mixing angles $\theta^2_{34} \simeq m_b/m_D$. The $|V_{4b}|$ mixing matrix element has the limit $|V_{4b}| \simeq \theta_{34} \leq 0.1$. This gives a lower bound for m_D of $m_D \geq 100 \times m_b = 500$ GeV.

7. REFERENCES

1. M. Shin, M. Bander, and D. Silverman, *Phys. Lett.* **B219**, (1989) 381.
2. Y. Nir and D. Silverman, *Nucl. Phys.* **B345**, (1990) 301.
3. Y. Nir and D. Silverman, *Phys. Rev.* **D42**, (1990) 1477.
4. D. Silverman, *Phys. Rev.* **D45**, (1992) 1800.
5. W.-S. Choong and D. Silverman, U.C. Irvine Report 93-14.
6. W.-S. Choong and D. Silverman, U.C. Irvine Report 92-36.
7. T. Inami and C. S. Lim, *Prog. Theor. Phys.* **65**, (1981) 297.

CHIRAL LAGRANGIANS, SOFT-MESON LIMITS AND EFFECTIVE LAGRANGIANS

Robert J. Oakes
Department of Physics and Astronomy, Northwestern University
Evanston, IL 60208, U.S.A.

ABSTRACT

The distinguishing features of the Chiral Lagrangian, Soft-Meson limit, and Effective Lagrangian methods for estimating matrix elements are summarized.

Estimating the ratio of matrix elements $\langle\psi K|H_w|B\rangle/\langle\psi\pi|H_w|B\rangle$ arose during this workshop in connection with Dunietz's talk on CP nonconservation. The various methods discussed were chiral perturbation theory, soft-meson limits and effective Lagrangians. Hopefully, the following remarks will be helpful in clarifying these approaches and their relation to each other.

– Chiral Lagrangians, with some form of symmetry breaking, provide a systematic approach to calculating the corrections to the chiral symmetry limit, including the nonanalytic log terms. The symmetry breaking includes, at least, the masses. The physical decay constants and form factors are themselves given by a perturbation expansion, the leading term being the chiral symmetry limit.

– The chiral symmetry limit not only requires the masses to vanish, but the coupling constants must also assume their symmetric values; a point that must be taken into account in comparing the chiral perturbation calculations with the soft-meson limit.

– The soft meson limit provides the value of an amplitude at a point outside the physical region. The extrapolation can not be expected to be smooth unless rapidly varying contributions, such as poles and angular momentum factors, are explicitly taken into account. The corrections are of the order of $(m/f)^2$ where f is the meson decay constant and, in general, are unknown.

– In the effective Lagrangian approach all possible couplings of the fields describing the particles relevant to the energy regime are included explicitly. The parameters, masses and coupling constants, can be determined from some existing set of data and predictions for other phenomena can then be made. Alternatively, various approximations; e.g., vector meson dominance, can be incorporated to constrain the parameters. Essentially, one is simply using the effective Lagrangian to relate two different sets of data in this approach.

Consequently, it is equally valid to approximate Dunietz's matrix element ratio $\langle\psi K|H_w|B\rangle/\langle\psi\pi|H_w|B\rangle$ by either 1 or f_π/f_K; the corrections in both cases being the order of $(m_\pi/f_\pi)^2$ and $(m_K/f_K)^2$, the same as the difference between the two approximations. In the chiral Lagrangian approach perturbation theory provides a systematic way to calculate these corrections to the chiral symmetric limit, however, without any estimate of the size of the neglected higher order contributions.

This work was supported in part by the U.S. Department of Energy, Division of High Energy Physics, under Grant DE-FG02-91-ER40684.

PCAC relation for $D^* \to D$ axial form factors

Claudio O. Dib
Universidad Federico Santa María, Valparaíso, Chile
and
Josep Taron
The Ohio State University, Columbus, OH, U.S.A.

The spin-flavour symmetry among hadrons containing one heavy quark (b, c) and the chiral symmetry $SU(3)_L \times SU(3)_R$ associated with the light quarks (u, d, s), spontaneously broken down to $SU(3)_V$, can be invoked simultaneously to provide relations among matrix elements involving such heavy hadrons and soft Goldstone bosons (π, K, η). This treatment has recently been formulated under the form of an effective theory which incorporates the heavy quark and chiral symmetries at the same time [1, 2, 3, 4]. The effective lagrangian consists of an infinite number of terms, with an increasing number of derivatives, each of which is an expansion in inverse powers of the heavy quark masses. The coefficients of the different terms can not be fixed by symmetry arguments alone, and will be fitted from experiment.

To lowest order in both chiral and $1/m_Q$ expansions, the interaction lagrangian contains a term of the form (see [5]):

$$-\frac{2g}{f_\pi}\left(\partial^\nu M_{ba} D_a^\dagger D^*_{b\,\nu} + \text{h.c.}\right), \tag{1}$$

where M is the 3×3 Goldstone boson matrix, and D_a and $D^*_{a\,\nu}$ (a= u,d,s) stand for the $SU(3)_V$ triplet pseudoscalar and vector fields, respectively. The constant g is nothing but the effective coupling of $D^* D\pi$, which is a dimensionless quantity of order unity and can be fitted from $\Gamma(D^* \to D\pi)$.

The object of this note is to clarify a discussion brought up by E. Levin about relations of coupling constants in the effective lagrangian. The relation derived below is the analog of the Goldberger-Treiman relation for nucleons [6], for the case of the form factors of the matrix element

$$\langle D(p')|A^\mu|D^*(p,\epsilon)\rangle = g_1(q^2)\epsilon^\mu + g_2(q^2)(\epsilon\cdot q)(p+p')^\mu + g_3(q^2)(\epsilon\cdot q)q^\mu, \tag{2}$$

where $q = p - p'$, and A^μ is the axial current of the chiral symmetry, which is conserved in the chiral limit (*i.e.* $m_\pi \to 0$). Thus

$$\langle D(p')|\partial_\mu A^\mu|D^*(p,\epsilon)\rangle = (\epsilon\cdot q)\left[\, g_1(q^2) + g_2(q^2)(m^2_{D^*} - m^2_D) + g_3(q^2)q^2 \,\right]$$

$$= \mathcal{O}(m_\pi^2) \to 0. \tag{3}$$

Taking q^2 close to zero, the form factor $g_3(q^2)$ is dominated by the pion pole at $q^2 = 0$. Then, for $q^2 \to 0$ it follows that:

$$g_1(q^2) + g_2(q^2)(m_{D^*}^2 - m_D^2) + \mathrm{Res}\ g_3(q^2)\Big|_{q^2=0} = 0. \tag{4}$$

The matrix element (2) is dominated at $q^2 \to 0$ by the diagram:

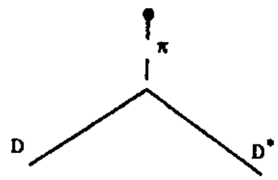

where

$$\langle 0|A^\mu|\pi(q)\rangle = i f_\pi q^\mu =$$ 

and the $D^* D\pi$ vertex is $g_{D^*D\pi}\ (\epsilon \cdot q)$; $g_{D^*D\pi}$ corresponds to g in the effective lagrangian (1). One then finds

$$\mathrm{Res}\ g_3(q^2)\Big|_{q^2=0} = -\ f_\pi\ \ g_{D^*D\pi}. \tag{5}$$

In the infinite c-quark mass limit, the pseudoscalar meson D and the vector meson D^* become degenerate in mass, and the relation (4) reads:

$$g_1(0) = f_\pi\ \ g_{D^*D\pi}. \tag{6}$$

It is easy to verify that the leading terms of the lagrangian in Ref. [5] satisfy this relation for $q^\mu \to 0$. Indeed, the hadronized A^μ current reads

$$A_\mu^A = -2g\left(D_a^\dagger D_b^* \ +\ \mathrm{h.c.}\right) T_{ba}^A \ +\ \mathcal{O}(q_\mu), \tag{7}$$

which verifies Eq. (6).

Notice that relation (4) is valid for finite mass values of the heavy mesons, and the mass difference $m_{D^*} - m_D$ does not originate from chiral symmetry breaking but from hyperfine splitting, which is of order $\mathcal{O}(1/m_Q)$.

We benefited from helpful conversations with J. Amundson and E. Levin. This work was supported in part by Fondecyt, Chile, grant No. 92-0806, and in part by U.S.A. grant DE-FG02-91-ER40690.

References

[1] M.B. Wise, Phys. Rev. D45, 2188 (1992).

[2] G. Burdman and J. Donoghue, Phys. Lett. B280, 287 (1992).

[3] J.L. Goity, Phys. Rev. D46, 3929 (1992).

[4] T.M. Yan *et al.*, Phys. Rev. D46, 1148 (1992).

[5] M.B. Wise, Caltech preprint CALT-68-1860, 1993, unpublished.

[6] M.L. Goldberger and S.D. Treiman, Phys. Rev. 110, 1178 (1958).

PROBING THE $WW\gamma$ VERTEX IN RADIATIVE b-QUARK DECAYS

U. BAUR
Physics Department, Florida State University,
Tallahassee, FL 32306, USA

Abstract

The recent CLEO results on on radiative b-quark decays are used to derive constraints on anomalous $WW\gamma$ couplings. These constraints are compared with expectations from $p\bar{p} \to e^{\pm}\not{p}_T\gamma + X$ at the Tevatron. The usefulness of exclusive radiative B meson decay channels in probing the $WW\gamma$ vertex is largely limited by present theoretical uncertainties in the calculation of hadronic matrix elements.

One of the major goals of future experiments at the Tevatron is to probe the structure of the $WW\gamma$ vertex in $W\gamma$ and W^+W^- production. Such direct tests of three vector boson vertices through tree level processes have to be contrasted with indirect tests which involve one-loop processes. Whereas bounds derived from tree level processes are essentially model independent, limits on anomalous $WW\gamma$ couplings extracted from processes which are sensitive to three vector boson couplings only at the one-loop level usually do depend on specific assumptions [1]. The dependence on model specific assumptions is most pronounced in quantities where anomalous couplings lead to divergencies, *e.g.* the S, T and U parameters.

Some one-loop processes, such as $b \to s\gamma$, yield finite answers due to the GIM mechanism. Recently, the CLEO Collaboration reported [2] the observation of the decay $B \to K^*\gamma$ with a branching fraction of $B(B \to K^*\gamma) = (4.5 \pm 1.5 \pm 0.9) \cdot 10^{-5}$. In the following we analyze the implications of this measurement on the anomalous $WW\gamma$ couplings, $\Delta\kappa$ and λ, and compare the result with expectations from future experiments at the Tevatron.

Our calculations are based on the results obtained in Ref. [3] for the inclusive radiative decay $b \to s\gamma$ for arbitrary anomalous couplings $\Delta\kappa$ and λ. Apart from non-standard contributions to the $WW\gamma$ vertex we assume the Standard Model to be valid. QCD corrections are incorporated following Ref. [4]. To estimate the branching fraction of the exclusive decay mode $B \to K^*\gamma$ we use the approach of Ref. [5]. In this model, $B(B \to K^*\gamma)$ is estimated by integrating the invariant mass distribution of the hadrons recoiling against the photon from the $m_K + m_\pi$ threshold up to $\mathcal{O}(1\text{ GeV})$, assuming that this range is completely saturated by the K^* resonance. The upper integration limit,

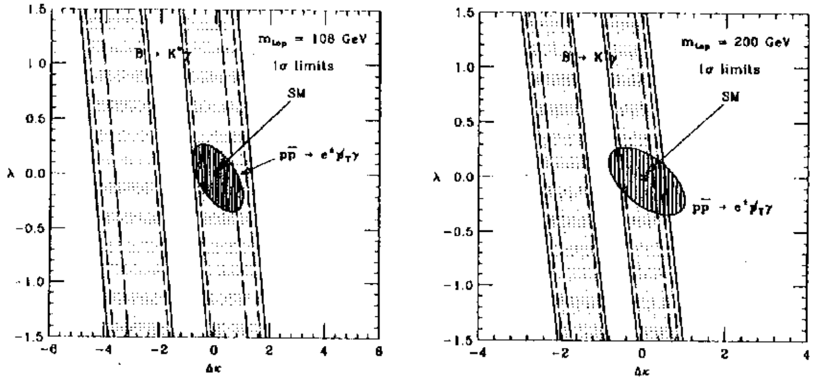

Figure 1: Allowed regions in the $\Delta\kappa - \lambda$ plane for $m_{top} = 108$ GeV and $m_{top} = 200$ GeV. The region allowed by present $B \to K^*\gamma$ data is indicated by the shaded bands. The short-dashed lines outline the limits from $B \to K^*\gamma$ expected from CDF with an integrated luminosity of 100 pb^{-1}. The long-dashed lines show the bounds from the CLEO upper limit on the branching ratio for the inclusive decay $b \to s\gamma$. The hatched area, finally, displays the allowed region in the $\Delta\kappa - \lambda$ plane which is expected to result from $p\bar{p} \to e^{\pm}\not{p}_T\gamma + X$ at the Tevatron with $\int \mathcal{L}dt = 100$ pb^{-1}.

however, is only loosely defined. Together with uncertainties in the B meson wave function, this results in rather large uncertainties in the estimated $B \to K^*\gamma$ branching ratio. For the present lower experimental limit on the top quark mass [6], $m_{top} = 108$ GeV, we find $B(B \to K^*\gamma) = (2-9)\cdot 10^{-5}$. For $m_{top} = 200$ GeV, we obtain $B(B \to K^*\gamma) = (3-12)\cdot 10^{-5}$. These ranges are consistent with the branching ratios obtained in other models [7].

The resulting constraints on $\Delta\kappa$ and λ depend explicitly on m_{top}, and are shown in Fig. 1. In order to obtain 1σ limits from $B \to K^*\gamma$, we have added the statistical and systematic errors in the branching ratio linearly. Despite the large uncertainties in the calculation of the $B \to K^*\gamma$ decay rate, the CLEO measurement excludes large regions of the $\Delta\kappa - \lambda$ plane. At the 1σ level, only two rather narrow bands remain allowed. The width of these bands depends quite strongly on m_{top}. The region between the two bands is not excluded with a very high significance; it still allowed at the 2σ level.

The CLEO collaboration recently also presented a new upper 95% CL limit on the branching ratio of the inclusive decay $b \to s\gamma$ [8] of $B(b \to s\gamma) < 5.4 \cdot 10^{-4}$, derived from the inclusive photon energy spectrum in B decays. The $b \to s\gamma$ decay rate is much more accurately predicted theoretically than that of the exclusive channel $B \to K^*\gamma$. The region in the $\Delta\kappa - \lambda$ plane which is consistent with the CLEO limit on $b \to s\gamma$ is the one between the two long-dashed lines in Fig. 1. The bounds obtained from inclusive radiative b decays reduce the region allowed by $B \to K^*\gamma$ somewhat. Similar results have also been obtained in Ref. [9].

The current measurement of the $B \to K^*\gamma$ branching fraction is based on 13 signal events [2]. A much larger event sample is possible in the near future from CLEO and, with a special photon trigger [10], also from CDF. If this trigger were implemented, up to 100 $B \to K^*\gamma$ events are expected in the 1993-94 run. Assuming that the central value of the branching ratio does not change, and systematic errors coincide with those of Ref. [2], the anticipated improvement is shown in Fig. 1 by the short-dashed lines. Since theoretical uncertainties dominate, the resulting bounds are only slightly better than those obtained with the present data. A substantial improvement in the calculation of $B(B \to K^*\gamma)$, however, may result from a lattice computation of the hadronic matrix element in the near future. The CDF photon trigger may also allow the observation of radiative B_s decays in the channel $B_s \to \phi\gamma$ [10]. The number of events expected is similar to the rate foreseen for $B \to K^*\gamma$. So far, no theoretical calculation of the $B_s \to \phi\gamma$ branching ratio has been performed.

To contrast the bounds on $\Delta\kappa$ and λ from radiative B decays with those from diboson production, we have also included the 1σ limits expected from $p\bar{p} \to W^{\pm}\gamma + X \to e^{\pm}\not{p}_T\gamma + X$ with 100 pb^{-1} [11] in Fig. 1. $W\gamma$ production is expected to yield much stronger bounds for λ while $B \to K^*\gamma$ tends to give better limits for $\Delta\kappa$. The two processes thus complement each other.

In conclusion, we have shown that present CLEO data on radiative b decays yield valuable information on anomalous $WW\gamma$ couplings. Future improvements of limits extracted from exclusive B (and B_s) decays depend mostly on the ability to obtain more accurate estimates of the hadronic B decay matrix elements. Combined with limits expected from $p\bar{p} \to W\gamma$, $\Delta\kappa$ and λ can be highly constrained in the near future.

ACKNOWLEDGEMENTS

I would like to thank A. Kronfeld, T. LeCompte, R. Springer and J. Thaler for useful discussions. This research was supported by the U.S. Department of Energy under Contract No. DE-FG05-87ER40319.

REFERENCES

1. K. Hagiwara *et al.*, MAD/PH/737 preprint (March 1993); C. P. Burgess *et al.*, McGill-93/14 preprint (June 1993).
2. R. Ammar *et al.* (CLEO Collaboration), CLNS-93-1212 preprint (May 1993), to appear in *Phys. Rev. Lett.*
3. S. Chia, *Phys. Lett.* **240B** 465 (1990); K. Numata, *Z. Phys.* **C52** 691 (1991); K. Peterson, *Phys. Lett.* **282B** 207 (1992).
4. B. Grinstein, R. Springer and M. B. Wise, *Phys. Lett.* **202B** 138 (1988).
5. A. Ali and C. Greub, *Phys. Lett.* **259B** 182 (1991).
6. N. Shaw, talk given at the *Workshop on Physics at Current Accelerators and the Supercollider*, Argonne Nat. Lab. June 2 – 5, 1993.
7. see *e.g.* A. Ali, DESY 92-058 preprint (April 1992) and references therein.
8. E. Thorndike, talk given at the *1993 APS Meeting*, Washington, D.C., April, 1993.
9. T. Rizzo, ANL-HEP-PR-93-19 preprint (April 1993).
10. T. LeCompte and J. Mueller, private communication.
11. U. Baur, T. Han, and J. Ohnemus, FSU-HEP-930519 preprint (May 1993).

PARTON MODEL (MÖSSBAUER) SUM RULES FOR $b \to c$ DECAYS

HARRY J. LIPKIN
Department of Nuclear Physics, Weizmann Institute of Science
Rehovot 76100, Israel

and

School of Physics and Astronomy
Raymond and Beverly Sackler Faculty of Exact Sciences
Tel Aviv University, Tel Aviv, Israel

The parton model is a starting point or zero-order approximation in many treatments. We follow an approach previously used for the Mössbauer effect and show how parton model sum rules derived for certain moments of the lepton energy spectrum in $b \to c$ semileptonic decays remain valid even when binding effects are included. The parton model appears as a "semiclassical" model whose results for certain averages also hold (correspondence principle) in quantum mechanics. Algebraic techniques developed for the Mössbauer effect exploit simple features of the commutator between the weak current operator and the bound state Hamiltonian to find the appropriate sum rules and show the validity of the parton model in the classical limit, $\hbar \to 0$, where all commutators vanish.

We assume that bound states of one heavy quark and other degrees of freedom are described by a Hamiltonian depending upon the heavy quark flavour only via its mass. The dynamics of the other degrees of freedom, including the interactions between them and the heavy quark, are described by a flavour-independent operator ΔH, which depends on the co-ordinate $\vec{X}$ of the heavy quark and on the other degrees of freedom, denoted by ξ_ν, but is independent of the heavy quark momentum $\vec{P}$. Thus $[\Delta H, \vec{X}] = 0$, but $[\Delta H, \vec{P}] \neq 0$ and we can write the Hamiltonians H_b and H_c for systems containing a single b or c quark

$$H_b = H(\vec{P}, m_b, \vec{X}, \xi_\nu) = \sqrt{m_b^2 + \vec{P}^2} + \Delta H \tag{1a}$$

$$H_c = H(\vec{P}, m_c, \vec{X}, \xi_\nu) = \sqrt{m_c^2 + \vec{P}^2} + \Delta H \tag{1b}$$

These assumptions hold in a number of conventionally used models, and in particular in the nonrelativistic constituent quark potential models with various potentials. Spin effects are neglected; they are taken into account in a more detailed treatment[1].

The hadronic transition in semileptonic $b \to c$ decays is described by the matrix element $\langle f_c | J(\vec{q}) | i_b \rangle$ of the fourier component carrying three-momentum $(\vec{q})$ of the flavor-changing weak current between an initial state $|i_b\rangle$ containing one and only one valence b quark and a final state $|f_c\rangle$ containing one and only one valence c quark. We assume that $J(\vec{q})$ depends only on the position of the heavy quark and not on the other degrees of freedom. Thus

$$[J(\vec{q}), \Delta H] = 0 \tag{1c}$$

$$R(\vec{q}) = H[(\vec{P}+\vec{q}), m_c, \vec{X}, \xi_\nu] - H[(\vec{P}), m_c, \vec{X}, \xi_\nu] = \sqrt{(\vec{P}+\vec{q})^2 + m_c^2} - \sqrt{\vec{P}^2 + m_c^2} \approx \frac{q^2}{2m_c} \quad (6c)$$

$$I_{bc} = \delta m + H[\vec{P}, m_c, \vec{X}, \xi_\nu] - H[\vec{P}, m_b, \vec{X}, \xi_\nu] \approx \vec{P}^2 \cdot \frac{\delta m}{2m_c m_b} \quad (6d)$$

are respectively the heavy quark mass difference, the free recoil energy and the "isomer" or "isotope" shift.

The sum rules can also be expressed in terms of the energy E_W carried by the W; i.e. by the leptons,

$$\langle E_W(\vec{q})\rangle \equiv \sum_{|f_c\rangle} E_W |\langle f_c| J(\vec{q}) |i_b\rangle|^2 = M_i - \langle [E_c(\vec{q})]\rangle = \delta m - \langle i_b| R(\vec{q}) + I_{bc} |i_b\rangle$$

$$\approx \delta m - \frac{q^2}{2m_c} - \langle i_b| \vec{P}^2 |i_b\rangle \cdot \frac{\delta m}{2m_c m_b} \quad (7a)$$

$$\langle [E_W(\vec{q})]^2\rangle - \langle [E_W(\vec{q})]\rangle^2 = \langle i_b| \{R(\vec{q}) + I_{bc}\}^2 |i_b\rangle - \langle i_b| \{R(\vec{q}) + I_{bc}\} |i_b\rangle^2 \approx$$

$$\approx \frac{\langle i_b| \vec{P}^2 |i_b\rangle \cdot q^2}{3m_c^2} + \frac{(\delta m)^2}{4m_c^2 m_b^2} \cdot (\langle i_b| P^4 |i_b\rangle - \langle i_b| P^2 |i_b\rangle^2) \quad (7b)$$

The sum rule can also be used to obtain an upper bound for the strength of the transition to a given final state $|f_m\rangle$ with energy E_m. Replacing all energies except E_m in the sum rule with the lowest possible energy E_g gives the inequality

$$E_m |\langle f_m| J(\vec{q}) |i_b\rangle|^2 + E_g(1 - |\langle f_m| J(\vec{q}) |i_b\rangle|^2) \leq \langle [E_c(\vec{q})]\rangle = M_i + R(\vec{q}) + I_{bc} - \delta m$$

$$\approx M_i + \frac{q^2}{2m_c} + \langle i_b| \vec{P}^2 |i_b\rangle \cdot \frac{\delta m}{2m_c m_b} - \delta m \quad (8a)$$

Where $E_g = M_D + \frac{q^2}{2M_D}$ is the energy of the lowest available state of the charmed system. Then

$$|\langle f_m| J(\vec{q}) |i_b\rangle|^2) \leq \frac{\langle [E_c(\vec{q})]\rangle - E_g}{E_m - E_g} \approx \frac{1}{E_m - E_g} \cdot \left(\frac{q^2}{2M_D m_c} \cdot [M_D - m_c] + \epsilon\right) \quad (8b)$$

where

$$\epsilon = [M_i - m_b] - [M_D - m_c] + \langle i_b| \vec{P}^2 |i_b\rangle \cdot \frac{\delta m}{2m_c m_b} = \langle i_b| H_c - H_b |i_b\rangle + M_i - M_D \quad (8c)$$

Note that the matrix element $\langle i_b| H_c |i_b\rangle$ is just an approximate value for M_D calculated by taking the expectation value of H_c with $|i_b\rangle$ as a trial wave function. It is thus exact to first order in the perturbation $H_c - H_b$ which is first order in the reciprocal mass difference $\frac{m_b - m_c}{m_b m_c}$. Thus ϵ is second order in $1/m_c$.

Thus the probability of excitation by an energy $E_m - E_g$ is bounded by the ratio to this energy of the small energy $\frac{q^2}{2M_D m_c} \cdot [M_D - m_c]$ which goes to zero as $q^2 \to 0$ with a small correction ϵ which vanishes in the heavy quark symmetry limit.

This treatment can be extended to include spin and relativistic effects. However it can be expected to be already particularly good in the low-recoil domain of small q^2 where the bound (8) places serious limits on the probability of high excitations; i.e. on low lepton energies.

REFERENCES

1. Harry J. Lipkin *Phys. Lett.* **B308** (1993) 105.

B MESON DECAY CONSTANTS

Robert J. Oakes
Department of Physics and Astronomy, Northwestern University
Evanston, IL 60208, U.S.A.

ABSTRACT

The ratio of B meson decay constants F_{B_s}/F_{B_d} is shown to be very close to unity if the chiral symmetry of the Lagrangian is broken only by quark masses and the light quark flavor SU(3) is a good symmetry of the states.

The decay constants for the B mesons have been of interest during this workshop for both experimental and theoretical reasons: F_B determines the $B \to \tau\nu$ rate and there are recent results for the ratio F_{B_s}/F_{B_d} from lattice calculations.[1] The ratio F_{B_s}/F_{B_d} can be shown to necessarily be quite close to unity if the chiral symmetry of the Lagrangian is broken only by quark mass terms and SU(3) flavor symmetry among the light quarks is used.

We assume the energy density is of the form $H(x) = H_0(x) + H_1(x)$ where H_0 is SU(6) x SU(6) symmetric. H_1 contains the quark mass terms, which break SU(6) x SU(6), and transform like the $(6,\bar{6})+(\bar{6},6)$ representation.[2]

The B decay constants F_B are defined covariantly and therefore

$$\langle 0|\partial^\mu A_\mu^{(B)}|B\rangle = M_B{}^2 F_B \tag{1}$$

The divergences of the axial currents are given by the commutators of the axial changes with H_1:

$$\partial^\mu A_\mu{}^{(B)}(x) = -i\left[Q_5{}^{(B)}, H_1(x)\right] \tag{2}$$

These can easily be calculated since $H_1(x)$ is simply the quark mass terms which have definite transformation properties under chiral SU(6) x SU(6); viz. $(6,\bar{6})+(\bar{6},6)$. One readily finds

$$M_{B_s}{}^2 F_{B_s} = (m_b + m_s)\langle 0|\bar{b}\gamma_5 s|B_s\rangle \tag{3}$$

and

$$M_{B_d}{}^2 F_{B_d} = (m_b + m_d)\langle 0|\bar{b}\gamma_5 d|B_d\rangle \tag{4}$$

Since B_u, B_d, and B_s belong to an SU(3) triplet the matrix elements in Eqs. (3) and (4) are expected to be nearly equal. We emphasize that the operators are SU(3) triplets by definition, so this approximation depends only on the absence of any mixing of other states in the vacuum and B meson states, which is expected to be negligible since there are no nearby states that can mix.

With this approximation Eqs. (3) and (4) give the ratio

$$F_{B_s}/F_{B_d} = (M_{B_d}/M_{B_s})^2 (m_b + m_s)/(m_b + m_d) \tag{5}$$

For the mesons we take the values[3] $M_{B_d} = 5279$ MeV / c^2 and[4] $M_{B_s} = 5383$ MeV / c^2 and for the (current) quark masses we shall use[5] $m_b = 5$ GeV / c^2, $m_s = 150$ MeV / c^2, and $m_d = 10$ MeV / c^2. From Eq. (5) we then obtain the value $F_{B_s} / F_{B_d} = 0.99$, with a small uncertainty coming from the errors in the values of the masses used. For comparison, recent lattice calculations[1] find $F_{B_s} / F_{B_d} = 1.1$ with an error of about 5%.

The main point is that F_{B_s} / F_{B_d} must be quite close to unity if the chiral symmetry of the Lagrangian is broken only by quark masses and light quark SU(3) flavor symmetry is a good approximation for the state vectors.

Of course, one also expects F_{B_u} / F_{B_d} to be very close to unity since only flavor SU(2) symmetry is involved. On the other hand, the ratio F_{B_c} / F_{B_s} should differ substantially from unity. Although

$$F_{B_c} / F_{B_s} = (M_{B_s} / M_{B_c})^2 (m_b + m_c) / (m_b + m_s) \langle 0 | \bar{b}\gamma_5 c | B_c \rangle / \langle 0 | \bar{b}\gamma_5 s | B_s \rangle \tag{6}$$

there is not a good symmetry relating the B_c and B_s states and the matrix elements are, therefore, expected to be quite different. Indeed, potential model estimates[6] indicate $F_{B_c} / F_{B_s} \sim 2$ to 3, as one might expect, since B_c is a "heavy-heavy" meson and B_s is a "heavy-light" system.

Obviously, these same arguments can be applied to the D mesons, as well as possible T mesons, but this workshop concerns B physics.

It is a pleasure to thank the organizers for making this workshop both pleasant and productive. This work was supported by the U.S. Department of Energy, Division of High Energy Physics, under Grant DE-FG02-91-ER40684

REFERENCES

1. C. Bernard, J. Labrednz, and A. Soni, Preprint UW/PT-93-06 (June, 1993).
2. This is the straightforward generalization to six quarks of SU(3) x SU(3) symmetry breaking. M. Gell-Mann, R. Renner, and R.J. Oakes, Phys. Rev. 175, 2195 (1968).
3. Particle Data Group, Phys. Rev. D45, Part 2, (1992).
4. D. Mueller (CDF Collaboration), these proceedings.
5. These values of the current quark masses should not be taken too literally, as they come from different determinations, but are in the ranges given in ref. 3.
6. E. Eichten and C. Quigg, Fermilab preprint and these proceedings

Charged Particle Tracking and Vertexing

Convenors:

R. Johnson
University of California -Santa Cruz

M. Purohit
Princeton University

A. Weidemann
University of Tennessee

List of Participants

COLLIDER FORWARD

L. Garren
Fermi National Accelerator Laboratory

K. Gounder
University of Mississippi

R. Harr
Yale University

J. Izen
University of Texas at Dallas

N. W. Reay
Ohio State University

L. Spiegel
Fermi National Accelerator Laboratory

COLLIDER CENTRAL

M. T. Cheng
Academia Sinica Taiwan/
Fermi National Accelerator Laboratory

D. Coupal
Superconducting Super Collider Laboratory

E. Engels
University of Pittsburgh

R. Frey
University of Oregon

A. Jawahery
University of Maryland

H. Jöstlein
Fermi National Accelerator Laboratory

J. Hylen
Fermi National Accelerator Laboratory

X. Lou
Indiana University/CERN

S. Mishra
Fermi National Accelerator Laboratory

A. Sill
Texas Tech University/
Fermi National Accelerator Laboratory

J. Skarha
Johns Hopkins University

F. Snider
Johns Hopkins University

J. Spalding
Fermi National Accelerator Laboratory

J. Warchol
University of Notre Dame

J. Wilcox
Northeastern University

D. Wu
Prairie View A&M University

FIXED TARGET

J. Chen
Colorado State University

S. Golovatyuk
University of Virginia

M. Halling
Cornell University/
Fermi National Accelerator Laboratory

A. McManus
University of Virginia

W. Toki
Colorado State University

I. Tzamouranis
University of Virginia

M. Walter
DESY—Institut für
Hochenergiephysik Zeuthen

NEW TECHNOLOGIES

D. Cords
Stanford Linear Accelerator Center

D. Crosetto
Superconducting Super Collider Laboratory

G. Punzi
Scuola Normale Superiore/INFN Pisa

W. Selove
University of Pennsylvania

TRACKING AND VERTEXING FOR B PHYSICS AT HADRON ACCELERATORS

Robert Johnson
Institute for Particle Physics, University of California at Santa Cruz
Santa Cruz, CA 95064

and

Milind Purohit
Department of Physics, Princeton University
Princeton, NJ 08544

and

Achim W. Weidemann†
Department of Physics and Astronomy, University of Tennessee
Knoxville, TN 37996-1200

1. INTRODUCTION

In this note, we report on some of the activities of the Tracking and Vertexing Working Group of this Workshop.

Track and vertex finding is essential to exploit the high production rate of B-mesons at hadron accelerators, both for triggering and analysis. Here, we review the tracking and vertex-finding systems of some of the major existing and proposed collider and fixed-target experiments at existing and future hadron accelerators, with a view towards their usefulness for B-physics. The capabilities of both general-purpose detectors and those of dedicated B-physics experiments are considered.

2. OVERVIEW OF GENERAL COLLIDER EXPERIMENT CAPABILITIES

In this section, we consider the tracking systems of some major generic collider experiments. Subsequent sections compare their performance for flavor tagging and B_s mixing. Depending on the center-of-mass energy the B decay products are spread over $\pm$ 2-3 units of pseudorapidity η at the Tevatron, $\pm$4-5 units of η at LHC, and $\pm$ 7 units of η at the SSC[1]. Hence, the angular coverage of a tracking/vertexing system is important; a large and continuous acceptance in η is required to detect B decays at the large rate required. For effective b-quark tagging, the tracking/vertexing system must resolve track impact parameters at the level of tens of microns, so as to allow tagging of B decays by their displaced vertices. A good momentum resolution is required to allow, for example, reconstructing the B mass from $B \to \pi^+\pi^-$ decays, or the J/ψ mass in $B \to J/\psi K \to \mu^+\mu^- K$. Thus, good impact parameter resolution and reasonable momentum resolution over as wide a range of η as possible are needed for B physics.

† Mail Address: SLAC, MS 94, P.O.B.4349, Stanford, CA 94309

The existing detectors mainly use drift chambers for tracking, but have upgrades considered or installed with Silicon systems. The different SSC/LHC proposals all have Silicon strip systems, complemented with straw tubes or gas microstrip detectors at larger distances from the interaction point. As an example, the SDC tracking design is described in a contribution to these proceedings.[2]

In the following figures, we show a schematic representation of a quarter section of the tracking system and resolutions of various track parameters (p_T, Impact parameter, phi, z, tan(θ) as function of η) for various collider detector options, prepared by Alan Sill using a parametrization of detector properties.

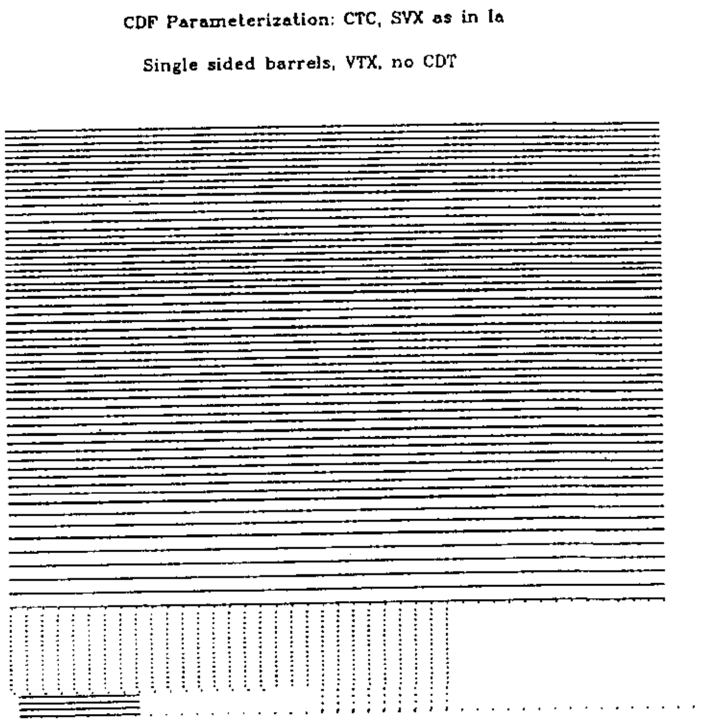

Figure 1. Schematic of quarter cross-section of CDF Ia.

Figure 1. shows CDF as configured in run Ia, with 4 layers of single-sided Silicon vertex detector (SVX) barrels surrounding the beam pipe. The 84 layers of a Central Tracking Chamber (CTC) are immersed in a 1.4 Tesla B-field. For CDF SVX upgrade II, the Silicon barrels are to be extended in z and made double-sided. Finally, for upgrade III, shown in Figure 2., a Silicon disk tracking system with 7 layers on each side is added.

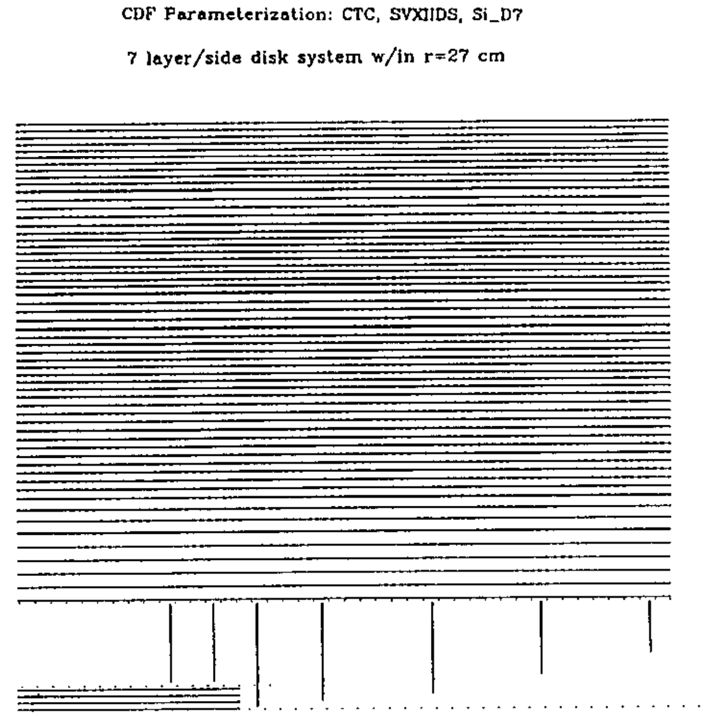

Figure 2. Schematic of quarter cross-section of CDF III.

The following figures 3. and 4. show the tracking resolutions for the two cases of CDF Ia and III. Notice how the 2-d impact parameter resolution improves to about 12 μm out to $\eta \approx 3$. Fig. 5 shows the $B \to \pi\pi$ mass resolution for this configuration, being close to 0.3% for $|\eta| \leq 1$.

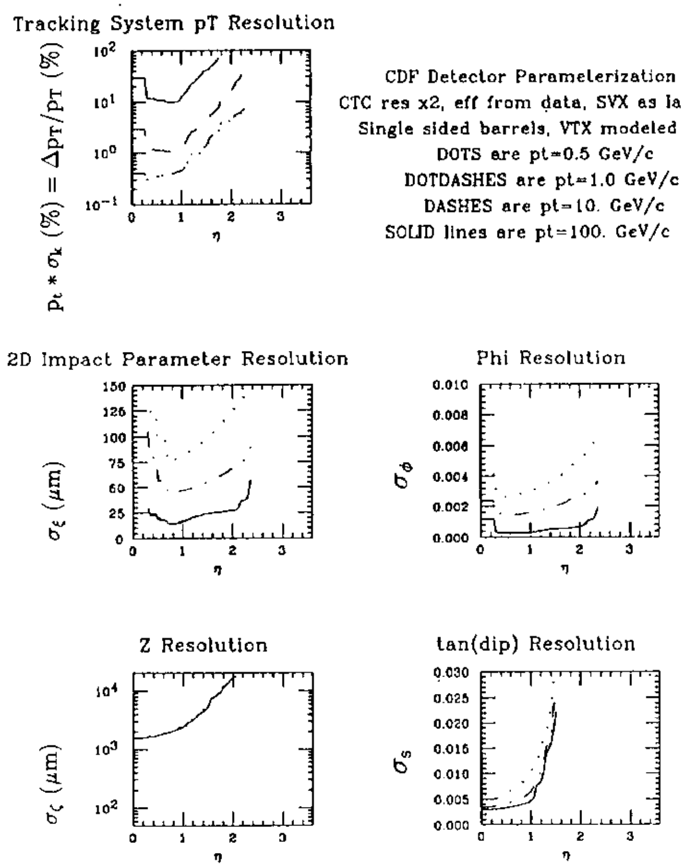

Figure 3. Tracking resolutions for CDF Ia.

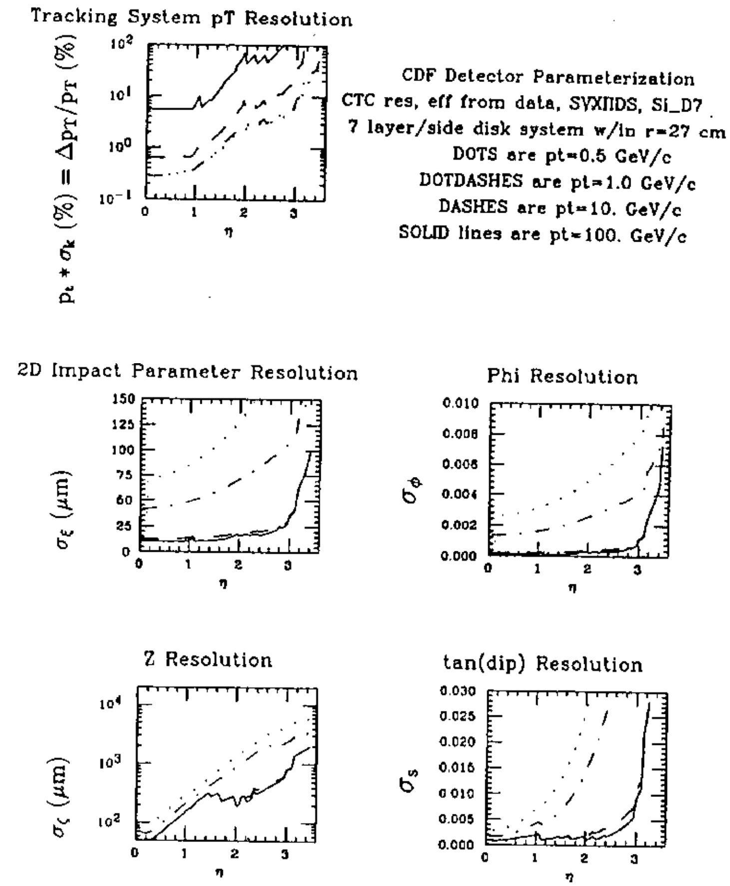

Figure 4. Tracking resolutions for CDF III.

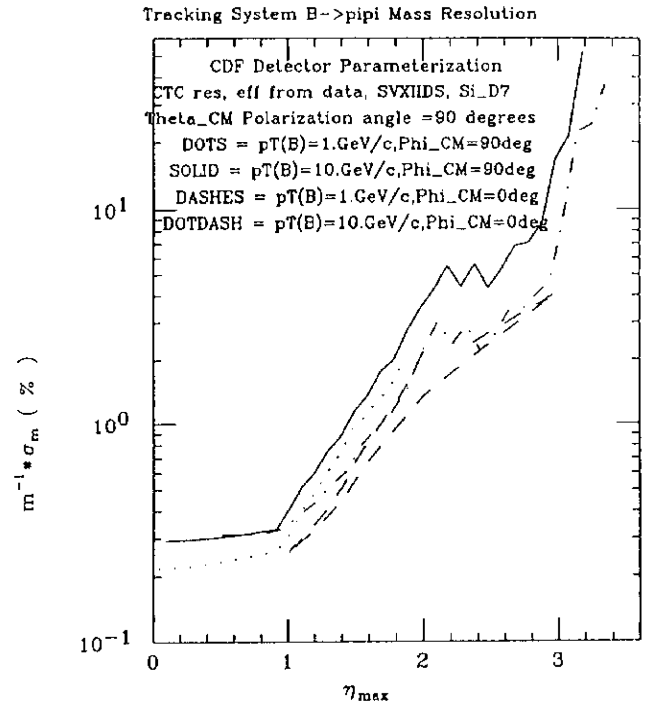

Figure 5. $B \to \pi\pi$ mass resolution for CDF III.

The D0 detector is also improving its tracking capability (see Figures 6-8) by replacing its inner detector with Silicon strips arranged in barrels, disks, and with four concentric superlayers of scintillating fibres. The CDF upgrade has more material at high η, thus more multiple scattering. If D0 would install double-sided barrel detectors, their impact parameter resolution would improve. The smaller tracking volume for D0 leads to poorer momentum and mass resolution compared to CDF.

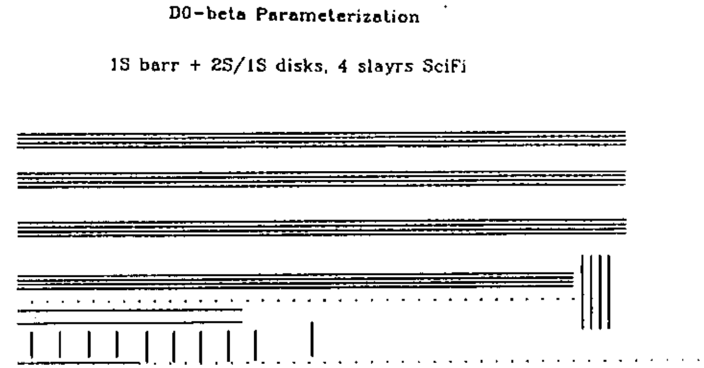

Figure 6. Schematic of quarter cross-section of the D0 upgrade.

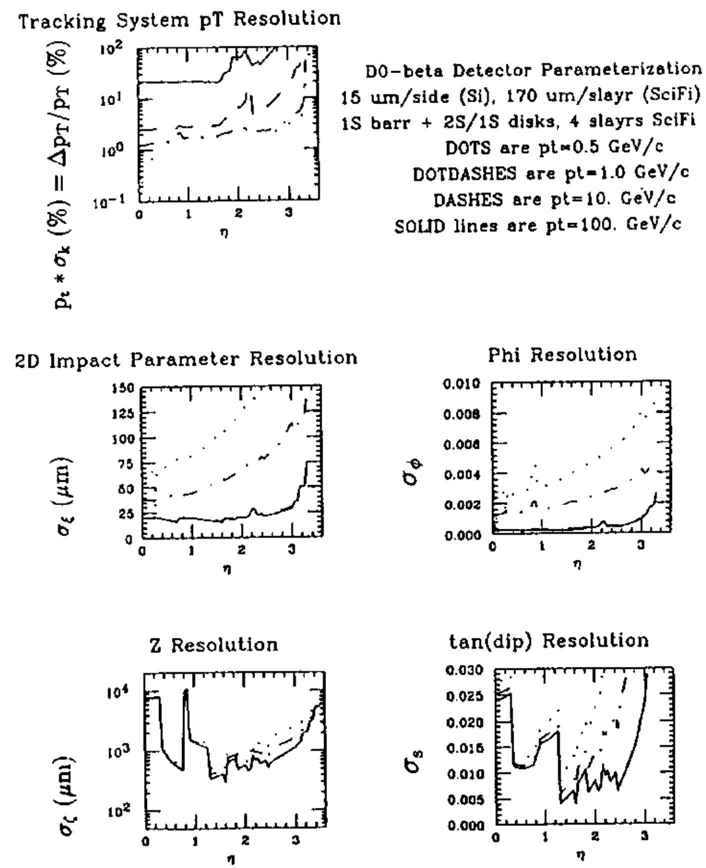

Figure 7. Tracking resolutions for D0 Upgrade.

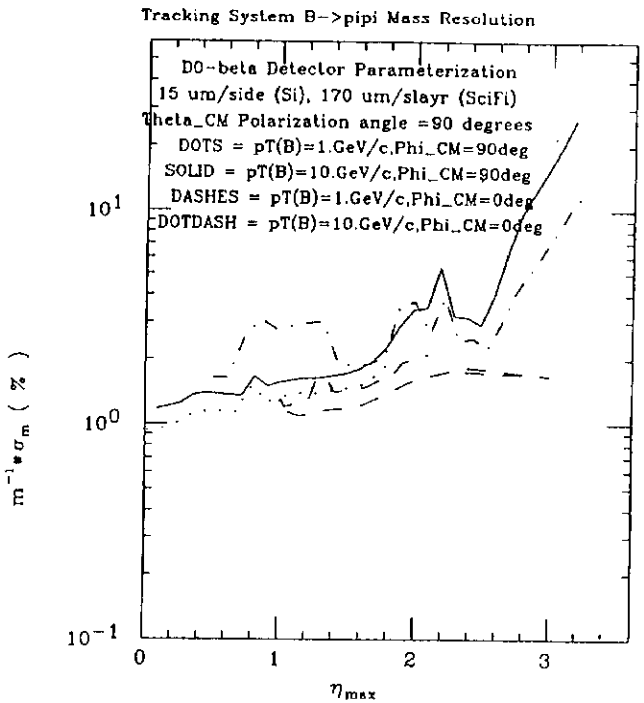

Figure 8. $B \to \pi\pi$ mass resolution for the D0 upgrade.

Next we show these figures for the major SSC detector proposals. Figures 9–11 illustrate the SDC detector at SSC.

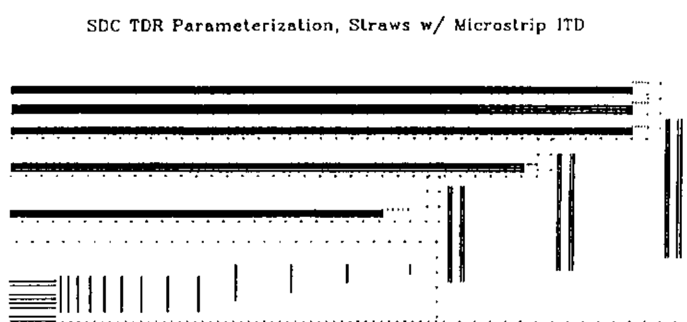

Figure 9. Schematic of quarter cross-section of SDC tracking.

Notice that the scale is different; SDC is much larger and longer than CDF. SDC has a larger η coverage, but accepts the same fraction of the B cross-section as CDF.

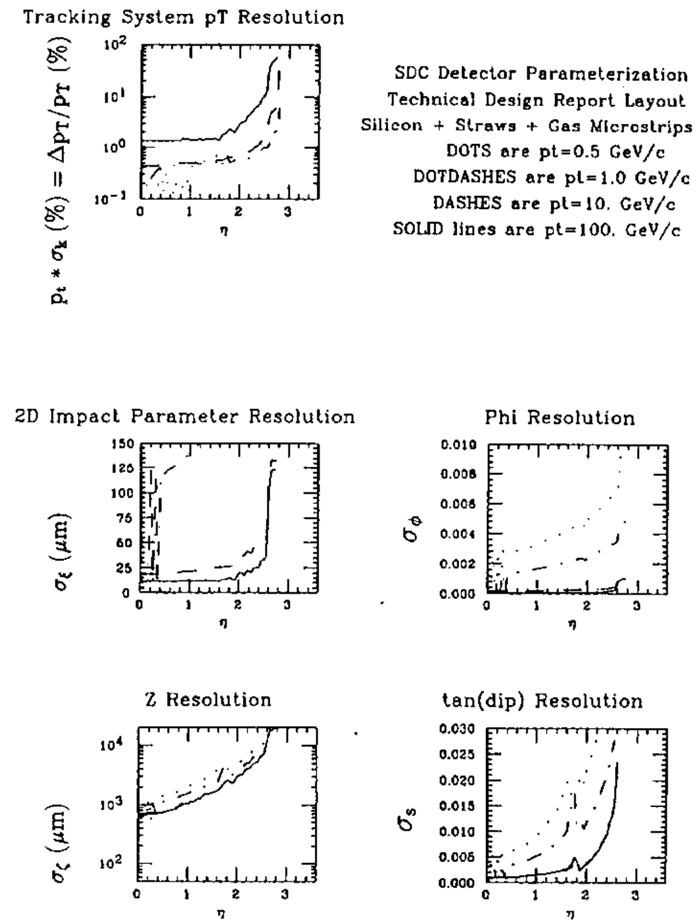

Figure 10. Tracking resolutions for SDC

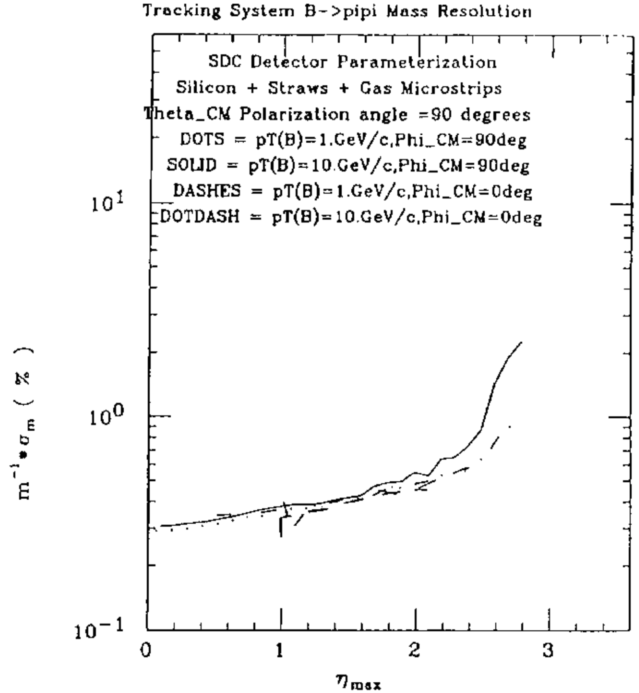

Figure 11. $B \to \pi\pi$ mass resolution for SDC.

The mass resolution is comparable to CDF's; however that of SDC extends to larger η.

The GEM Central Tracker consists of Silicon microstrips arranged in barrels (6 layers, double-sided) and disks, and eight layers of interpolating pad chambers, covering the region $|\eta| \leq 2.5$, all in a solenoid with a 0.8 T B-field. See Figures 12–14.

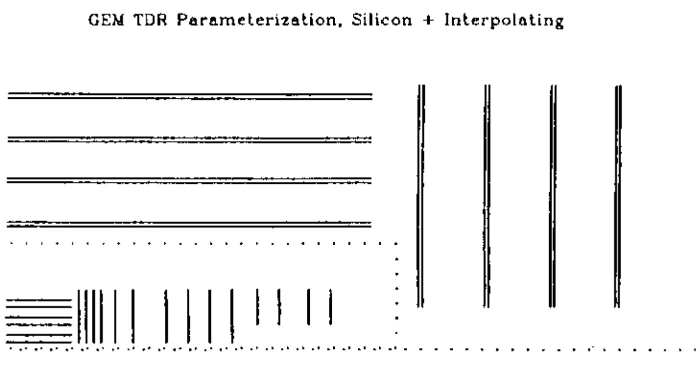

Figure 12. Schematic of quarter cross-section of GEM tracking.

Again, note a factor ~ 2 scale change, GEM is only about half as large as SDC.

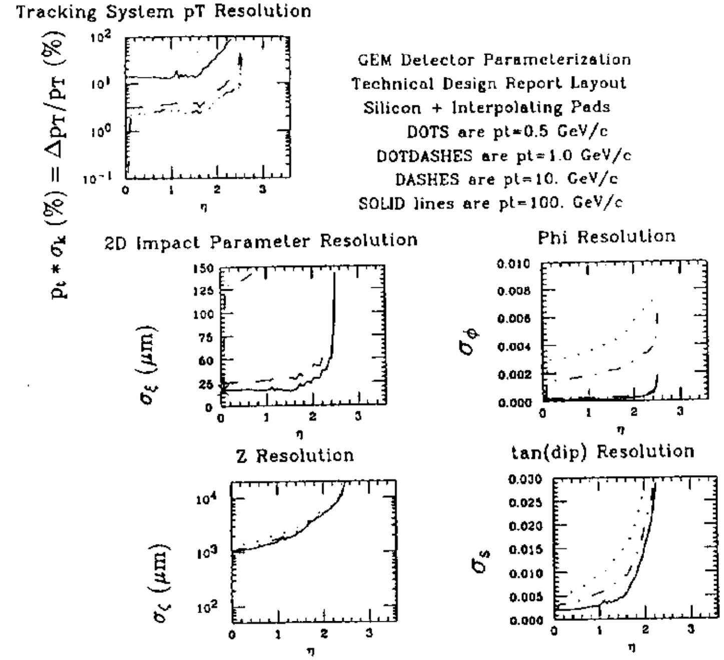

Figure 13. Tracking resolutions for GEM.

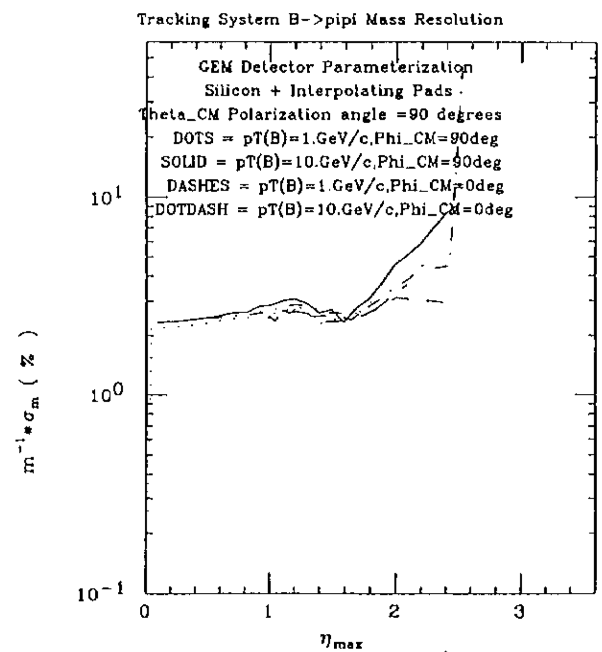

Figure 14. $B \to \pi\pi$ mass resolution for GEM.

The mass resolution of CDF and SDC is better than that of D0 and GEM.

The CMS central tracking system consists of 4 layers of Silicon microstrips and two times four layers of microstrip gas chambers. The $J/\psi \rightarrow \mu\mu$ mass resolution is 26 MeV.

The ATLAS proposal forsees a Silicon Tracker with a layer of pixel detectors followed by two of Silicon strips, covering $|\eta| \leq 1.5$.

The capabilities of the detector proposals specialized for B-physics, BCD and COBEX, have been described in detail elsewhere. (See Ref. 2 for references.) Their particular emphasis is the forward tracking coverage, which will be considered in Section 5.

3. COMPARISONS OF TRACKING PERFORMANCE

We compared the tracking system for various detectors considering the parmeters important for flavor tagging, B_s mixing and $B \rightarrow J/\psi K_s$ decays, as examples.

The following items are of relevance for flavor tagging:

- Good acceptance for the lepton tag in η, as B and $\overline{B}$ are emitted with large $\Delta\eta$.
- Low p_T of B tracks requires low p_T thresholds (<0.5 GeV).
- The multi-prong B final states with typically 4-5 tracks necessitate rather good tracking efficiency (>98%/track) for reconstruction of the Bs.
- Good mass and vertex resolution (< 40μm vertex resolution, $\sim$ 25 MeV mass resolution) needed to avoid combinatorics from non-associated B tracks. Three-dimensional vertex reconstruction is helpful to reject other backgrounds.
- An impact parameter or secondary vertex trigger is needed for hadronic B decays.
- Good momentum resolution is needed over a large η region to determine the charge sign of tagging lepton or other particle.

We list these tracking parameters for the Tevatron experiments and SSC proposals in Table 1 on the following page. Table 2 lists the some quantities relevant for studies of B_s mixing, and Table 3 those for studies of $B \rightarrow \Psi K_s$.

The decay length resolutions for all detectors are in the 40-60μm range. The maximum reach for X_s, the frequency of B_s oscillations multiplied with the lifetime, is 20-25. There are differences between the detectors in impact parameter resolution and ψ mass resolution shown in Table 3.

Table 1. Tracking Performance for Flavor Tagging

	CDF	D0	BCD	SDC	GEM
Tracking Efficiency	98%	99%	99%	98%	98%
Tracking Acceptance	$\|\eta\| <2.5$	$\|\eta\| <3.2$	$\|\eta\| <4$	$\|\eta\| <2.5$	$\|\eta\| <2.5$
Decay Length Res.(μm)	40	50	40	40	60
Typ. Vertex Res.cut(μm)	100	$\sim$ 100	$\sim$ 100	$\sim$ 100	$\sim$ 100
p_T Resolution ($\eta = 0$)	$.001p_T$+0.004	$0.0008p_T$+0.015	$0.00017p_z$ + 0.003	$0.00016p_T$+0.003	$0.0012p_T$+ 0.035
p_T Resolution ($\eta = \eta_{max}$)	$.04p_T$+0.01	$0.0025p_T$+0.03	$0.00003p_z$ + 0.003	$0.0003p_T$+0.003	$0.0025p_T$+ 0.035
J/ψ mass Resolution (MeV)	20	50	18	13	80
Ch. Track $p_T^{min}(\eta = 0)$ (GeV/c)	0.2	0.17	0.1	0.5	0.5
Ch. Track $p_T^{min}(\eta = \eta_{max})$ (GeV/c)	0.5	0.5	0.5	1	1
Ch. Track $p_T^{max}(\eta = \eta_{max})$ (GeV/c)	10	10	N/A	N/A	N/A
Lepton $p_T^{min}(\eta = 0)$ (GeV/c)	2	3.5	1 (e), 2 (μ)	10	10
Lepton $p_T^{min}(\eta = \eta_{max})$ (GeV/c)	2	5	1 (e), 2 (μ)	10	10
Lepton $p_T^{max}(\eta = \eta_{max})$ (GeV/c)	10 (e), 50(μ)	240 (μ)	N/A	N/A	N/A
Trigger p_T Resolution	0.02 at p_T =2GeV	N/A	N/A	N/A	N/A
Trigger Vertex Resolution	40μm	N/A	N/A	N/A	N/A
3D vs. 2D Comb. Rejection	2.5	N/A	~2.5	~2.5	~2.5

Table 2. Tracking Performance for B_s Mixing

	CDF	D0	BCD	SDC	GEM
Decay Length Res.(μm)	40	50	40	40	60
Typ. Vertex Res.cut(μm)	100	~ 100	~ 100	~ 100	~ 100
p_T Resolution ($\eta = 0$)	$.001p_T$+0.004	$0.0008p_T$+0.015	$0.00017p_x + 0.003$	$0.00016p_T$+0.003	$0.0012p_T$+ 0.035
p_T Resolution ($\eta = \eta_{max}$)	$.04p_T$+0.01	$0.0025p_T$+0.03	$0.00003p_x + 0.003$	$0.0003p_T$+0.003	$0.0025p_T$+ 0.035
Proper Time Resolution	0.08 .	0.08	0.06	<0.08	<0.08
Maximum X_s Reach	20	20	25	> 20	> 20
Tracking Acceptance	$\|\eta\|$ <2.5	$\|\eta\|$ <3.2	$\|\eta\|$ <4	$\|\eta\|$ <2.5	$\|\eta\|$ <2.5
Ch. Track $p_T^{min}(\eta = 0)$ (GeV/c)	0.2	0.17	0.1	0.5	0.5
Ch. Track $p_T^{min}(\eta = \eta_{max})$ (GeV/c)	0.5	0.5	0.5	1	1
Ch. Track $p_T^{max}(\eta = \eta_{max})$ (GeV/c)	10	10	N/A	N/A	N/A
Lepton $p_T^{min}(\eta = 0)$ (GeV/c)	2	3.5	1 (e), 2 (μ)	10	10
Lepton $p_T^{min}(\eta = \eta_{max}$) (GeV/c)	2	5	1 (e), 2 (μ)	10	10
Lepton $p_T^{max}(\eta = \eta_{MAX}$) (GeV/c)	10 (e), 50(μ)	240 (μ)	N/A	N/A	N/A
$p_T^{min} for B_s$ (GeV/c)	8	6	3	12	12
Lepton Trigger Acceptance	64%	44%	>50%	>50%	>50%
B_s Acceptance	70%	50%	>50%	>50%	>50%

Table 3. Tracking Performance for $B \to \psi K_s$

	CDF Run III	D0 Run III	SDC	GEM	BCD	ATLAS	CMS
Accelerator Parameters							
$\sqrt{s}$	2 TeV		40 TeV			14,16 TeV	
Luminosity	10^{31-32}		10^{32-33}		10^{32}	10^{33}	
Beam σ_x	30 μm		5 μm			20 μm	
Beam σ_y	30 μm		5 μm			20 μm	
Beam σ_z	25 cm		5 cm			3 cm	
Crossing frequency	132 or 396 ns		16 ns			25 ns	
Trigger							
Trigger Mode	2 leptons		1,2, or 3 leptons			tag $\mu, p > 6$ GeV	hfill
μ η-Acceptance	$\|\eta\|$ <1	$\|\eta\|$ <3.6	$\|\eta\|$ <2.5	$\|\eta\|$ <2.5	$\|\eta\|$ <4	$\|\eta\|$ <1.6	$\|\eta\|$ <2.4
μ p_T^{min} (GeV/c)	2	3.5	10	10	2	5	4
electron η-Acceptance	$\|\eta\|$ <1	$\|\eta\|$ <4	$\|\eta\|$ <2.5	$\|\eta\|$ <2.5	$\|\eta\|$ <4	$\|\eta\|$ <2.5	N/A
e p_T^{min} (GeV/c)	6?	6 ?	10	10	1	2	N/A
Trigger Vertex Resolution	45μm	N/A	N/A	N/A	N/A	N/A	N/A

Table 3. continued (Tracking Performance for $B \to \psi K_s$)

	CDF Run III	D0 Run III	SDC	GEM	BCD	ATLAS	CMS
Track Reconstruction							
η-Acceptance	$\lvert\eta\rvert < 2.5$	$\lvert\eta\rvert < 3.2$	$\lvert\eta\rvert < 2.5$	$\lvert\eta\rvert < 2.5$	$\lvert\eta\rvert < 5$	$\lvert\eta\rvert < 2.5$	$\lvert\eta\rvert < 2.4$
Azimutal Acceptance	100%	100%	100%	100%	loss to field	100%	100%
Efficiency	98%	99%	98%	98%	99%	95%	95%
p_T Resolution, $\eta = 0$	$0.0006p_T$	$.0008p_T+.015$	$.00016p_T+.003$	$.0012p_T+.035$	$.00017p_z+.003$	$0.0005p_T$	$0.0001p_T$
Multiple Scatt. Limit	0.003	0.01	0.003	0.035	0.003	0.01	0.003
p_T Resolution, $\eta = 2$	$0.008p_T$	$.0025p_T+.03$	$.0003p_T+.003$	$.0025p_T+.035$	$.00003p_z+.003$	$0.0006p_T$	$0.00006p_T$
Multiple Scatt. Limit	0.02	0.02	0.003	0.035	0.003	0.02	0.003
p_T^{min} (GeV/c)	0.2	0.167	0.5	0.3	0.1	0.5*	0.4
$r-\phi$ Impact Param. Resolution	10μm	20μm	14μm	25μm	7-10μm	27μm	45μm
z Impact Param. Resolution	27 μm	300 μm	0.1-1 mm	1 mm	10 μm		0.15-1 mm^z
$\psi - K_s$ Reconstruction							
ψ Mass Resolution (MeV)	10	50	13	75-150	18	37	26
K_s Efficiency	35%	45%	Order of 60%		order 50%	35%	35%
$\psi - K_s$ Mass Resolution (MeV)	18*	20*			order 20	50†	6.5
2-d Decay Length Resolution	40 μm	50 μm	40μm	60 μm	40 μm	0.2-0.4 mm	40-100 μm
3-d Vertex Detection?	90° stereo		sm. angle stereo†	stereo strips	60 μm	pixel+stereo	2mm?
Notes:	Run III Upgrade *ψ mass constraint	Run III Upgrade *ψ mass constraint	† or pixel option	Resoln. 2x worse at 10^{34}	based on $\pi\pi$ dipole field	† w/o mass constr. * 1 GeV cut for π from K_s	^{z} Decay in/out-side Si

4. FORWARD TRACKING/VERTEXING AT HADRON COLLIDERS

Two specialized experiments have been proposed especially for B-physics at hadron colliders, distinguished by large coverage in pseudorapidity, namely BCD and COBEX.

BCD has a Silicon vertex detector, and a straw tube tracking system; COBEX is distinguished by having its Silicon detector in 'Roman Pots' inside the beampipe vacuum.

In Table 4. below, we give some of the parameters of their tracking and vertexing system.

Table 4. Tracking/Vertexing Parameters for Forward Collider Detectors

	COBEX	BCD Forward
E_{CMS}	16,40 TeV	40 TeV
Luminosity	10^{32}	10^{32}
η_{min}	1.2	1.2*
η_{max}	6.0	5.5
θ_{min}	5 mrad	8 mrad
θ_{max}	600 mrad	580 mrad
$r_{Beampipe}$	none	1 cm
$r_{Silicon}$	4-6mm	~ 1.25cm
$\delta p/p$ (GeV)		0.001p
$B^0 \to J/\psi K_s^0$ mass res.	8.7 MeV	
$B^0 \to \pi^+\pi^-$ mass res.	21.7 MeV	20 MeV
Impact Par. Res. p=∞		6 μm
σ_z of primary	200 μm	100-200 μm
σ_z of secondary	150 μm	μm
single μ trigger p_T	1.2 GeV	1-1.5 GeV
L/σ cut for $B^0 \to \pi^+\pi^-$		15 MeV
L cut for $B^0 \to J/\psi K_s^0$	0.5 mm	

* Notice that BCD also has central coverage.

A more detailed comparison between the two approaches – Silicon vertex detector inside *vs.* outside the beampipe – is given in Ref. 3. It also concludes that there is little difference in the resulting quantities of interest for B physics.

A forward BCD detector has the potential to be upgraded to include also the central rapidity region (though there might be an awkward region near 45°).

A few questions remain open in forward B tracking.

For example, how often does radiation damage require replacement of Silicon detectors? For a Silicon detector a distance of r cm from the beam with a luminosity of $\mathcal{L}cm^{-2}s^{-1}$, the radiation dose per 'year' of 10^7 sec is

$$2.7Mrad(\frac{1cm}{r})^2(\frac{\mathcal{L}}{10^{32}});$$

thus for BCD Silicon, at r = 1.25 cm, the dose is 1.7 Mrad/year; for COBEX at r = 0.5cm, 10.8 Mrad/year. Does that mean that one has to replace the Silicon elements closest to the beam every 3 months? Also, which dose will strips and pixel detectors suffer without losing functionality?

While for pixels occupancy presents no problems, is the same true for microstrips?

Are large superconducting quadrupole magnets feasible, with the fields needed for the advertised momentum resolution?

How can one make a trigger for $B^0 \to \pi^+\pi^-$?

Can central detectors do as well as a forward detector on particle identification? In other respects, it seems that from a tracking perspective there is no compelling evidence that a forward B collider experiment is better than a *dedicated* central collider (not SDC or GEM). Cost might decide this issue.

5. BACKGROUNDS

From fixed target experiments we know that charm signals suffer from large backgrounds. These backgrounds arise due to combinatorics in charm events, due to combinatorics in non-charm events and due to combining pieces of charm and even strange decays with other tracks to give a kinematically viable candidate. It is only to be expected that these backgrounds be as large or larger in beauty events at the SSC due to the higher multiplicity. However, the better signal to background could improve matters. Therefore, a preliminary study was done, using 5000 events each, of minimum bias, charm and beauty events to study backgrounds to $\pi^+\pi^-$ decays.

In the study, only the BCD and COBEX detectors were compared. The detectors were idealized in a simple Monte Carlo which incorporated multiple scattering and intrinsic resolutions. Firstly, it was found that there is not much difference between the two in terms of resolutions. Secondly, fake vertices in the B mass region were counted as a function of the vertex separation.

From 5000 event samples, one finds that in the region of large vertex separation (signal efficiency over 80%) no minimum bias events survive in either detector, only one charm event survives (in the COBEX detector) and two generic $b\bar{b}$ survived in the BCD simulation and about six in the COBEX simulation. These numbers are to be compared to about 120 signal events which survive.

Clearly, there will be significant backgrounds from generic $b\bar{b}$ events. Whether the charm and minimum bias backgrounds are meaningful needs to be resolved with further study.

6. TRACKING PERFORMANCE FOR FIXED-TARGET EXPERIMENTS

Fixed target events either use an extracted beam impinging on an instrumented target such as SFT and LHB, or use a gas jet or thin wire introduced into the circulating beam as target and have the detectors surround the beampipe, such as GAJET and HERA-B. The large Lorentz boost of all particles produced leads to very large decay lengths for B mesons in the lab frame, 9.5 cm for the 20 TeV proton beam of the SSC, 300 times the vertex resolution. However, this advantage is offset by the small angles between the emerging tracks, leading to high occupancies in the tracking detectors immediately downstream from the decay. On the other hand, it becomes affordable to add more layers of tracking detectors covering the smaller solid angle in the forward direction only (rather than having to cover 4π at a collider detector).

The SFT target consists of a combination of Silicon planes and Beryllium foils. Tracking efficiencies are better than 95% for single tracks, 90% for 2 tracks; resolutions are of the order of a few μm. The $B^0 \to \pi^+\pi^-$ mass resolution is about 12MeV. More detail is given in a contribution to the workshop[4].

Another contribution[6] shows that an active target has no advantage over one with separate target foils followed by detector planes, due to the high occupancy in the planes immediately following an interaction.

HERA-B uses 15 planes (perpendicular to the beam) of double-sided Silicon strip detectors arranged with increasing distance along the beam axis to provide uniform coverage in η.

In the following Table 5 we compare some parameters of the SFT and HERA-B detectors.

Table 5. Tracking/Vertexing Parameters for SFT and HERA-B

	SFT	HERA-B
Av.B Decay Length	9 cm	7 mm
Impact Par. Res.(r)	8μm	20-30 μm
σ_r of primary	4 μm	$16 \pm 5\mu$m
σ_z of primary	60 μm	$350 \pm 14\mu$m
$\sigma p/p$	0.0029	0.0001p
$\sigma p_T/p_T$	0.0045	0.0001p
J/ψ Mass Res.	7.6 MeV	85MeV
B Mass Res.	21.7 MeV	

Notice that HERA-B also plans for a RICH counter system which will provide Kaon identification for Kaon energies of 8-80 GeV.

7. NOVEL IDEAS FOR VERTEX TRIGGERING

Clearly an ideal trigger for B decays would recognize the existence of secondary vertices displaced from the primary one. In the past the long time required to read out a drift chamber or pixel devices, as well as the difficulty of finding vertices in an environment of numerous multiple-scattering-smeared tracks in the vertex region prevented the realization of such a trigger.

However, the improvement in vertex detectors and fast track finding techniques with specialized processors might soon make such a trigger possible.

A Silicon Vertex Tracker trigger processor[7] has been proposed to be built for the CDF run II; it uses data from the Silicon vertex detector and the central drift chamber to reconstruct tracks in two dimensions fast enough for use at trigger level 2 ($\sim 10\mu$s).

New specialized computer architectures, such as that of the proposed '3D-Flow' massively parallel array processor system[8] together with fast pixel devices[8,9] located close to the interaction point might make a level 1 B trigger based on displaced secondary vertices a reality.

8. CONCLUSIONS

As regards the usefulness multi-purpose detectors for B physics, all of them have sufficient capability to do some measurements, with perhaps CDF and SDC being at a slight advantage compared with D0 and GEM.

For the specialized collider detectors, BCD and COBEX are comparable in vertex and mass resolution in the forward region, and in backgrounds.

An advantage of fixed-target experiments is the larger decay length; it is however offset by the small angles between the decay products. Fixed-target experiments also offer good mass resolution and possibly Kaon identification, at a smaller cost than a 4π detector.

Finally, we note the promising work in pixel detectors and fast trigger devices which is in progress.

9. ACKNOWLEDGEMENTS

We thank the organizers for smooth organization of a successful workshop, and the workshop participants and working group members for interesting presentations, discussions and contributions. We thank our respective funding agencies for support.

10. REFERENCES

1. A. Sill, Tracking System Considerations for B-Physics Detectors at Hadron Colliders, Contribution to the 4th Workshop, B-Physics at Hadron Colliders, Fermilab, November 16-17, 1992.
2. D. P. Coupal, SDC Tracking Capabilities for B Physics, Contribution to this workshop.
3. R. F. Harr, P .E. Karchin, C. J. Kennedy, Comparison of Forward Collider Detectors for B Physics, Contribution to this workshop.
4. A. P. McManus, S. Conetti, G. Corti, B. Cox, E. C. Dukes, T. Lawry, K. Nelson, I. Tzamouranis, Tracking Considerations for Fixed Target B Experiments at SSC and LHC, Contribution to this workshop.
5. E. C. Dukes, On the Configuration of an Active Target for a Fixed-Target B Experiment at SSC Energies, Contribution to this workshop.
6. P. Lebrun, A Realistic Study on a Forward Geometry Collider Spectrometer: Performance of a Typical Fixed Target Spectrometer at the Tevatron collider, Contribution to this workshop.
7. G. Punzi, Contribution to this workshop (Trigger/DAQ Section).
8. D. Crosetto, Contribution to this workshop (Trigger/DAQ Section).
9. W. Selove, Impact Parameter trigger and Vertex Detector for Forward Collider, Contribution to this workshop (Trigger/DAQ Section).
10. D.Cords, S. Shapiro, Contribution to this workshop (Trigger/DAQ Section).

SDC TRACKING CAPABILITIES FOR B PHYSICS

DAVID P. COUPAL

*Superconducting Super Collider Laboratory,**
2550 Beckleymeade Avenue, Dallas, TX 75237

1. INTRODUCTION

The $b\bar{b}$ production cross section is estimated[1] to be 1 mb at $\sqrt{s} = 40\ TeV$, implying 10^{12} produced $b\bar{b}$ pairs at an SSC luminosity of $10^{32} cm^{-2} sec^{-1}$ ($0.1 \times$ design). SDC has the potential to exploit this high rate to explore a number of B physics topics, in particular, CP-violation in the neutral B meson. This note describes the SDC particle tracking design (Section 2) and its predicted performance parameters relevant to B physics (Section 3).

2. DESIGN

The SDC central tracking design[2] is shown in Fig. 2.1. At the innermost radius is the vacuum beampipe, currently taken as 4 cm radius and 1 mm thick Beryllium. To date, this design has not been optimized with B physics in mind, which would drive it towards a thinner smaller-radius design.

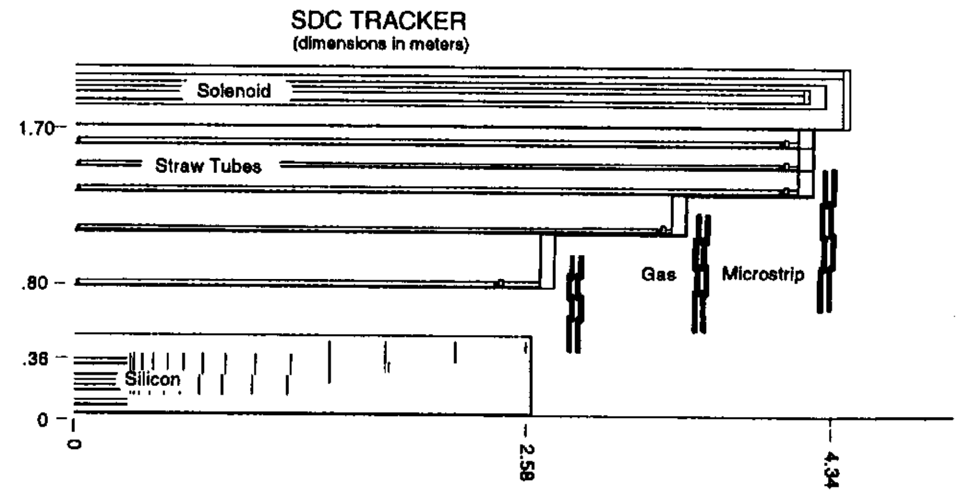

Figure 2.1: The SDC tracking detector.

* Operated by the Universities Research Association, Inc., for the U.S. Department of Energy under Contract No. DE-AC35-89ER40486.

Outside the beampipe, a silicon system made up of barrels and forward disks provides the bulk of the pattern recognition and vertexing capabilities. Outside the silicon, in the region $|\eta| < 1.8$, a 5-superlayer straw tube tracker provides momentum resolution for high p_t tracks and level-1 triggering. For $|\eta| > 1.8$, the same functions are provided by a gas microstrip detector with 3 superlayers. The components are situated inside a 2 Tesla superconducting solenoid with a 1.7 m inner radius.

The silicon detector consists of 8 barrels of double-sided silicon, one side with axial strips and the other with strips at a 10 mrad stereo angle. The inner barrel layer is at a radius of 9 cm from the beamline and the outer layer is at 36 cm. There are 13 layers of double-sided forward disks on each end of the barrel. Strip pitch is 50 microns for the barrel detectors and 32-58 microns for the wedge-shaped disk detectors. The resolution per barrel superlayer is predicted to be 17 microns, including an estimate of mis-alignment contributions.

A pixel option being considered by SDC would replace the inner 2 barrel silicon layers with 2 pixel barrel layers at radii of 6 and 8 cm and possibly 2 small disks at both ends of the barrel. The pixel size is 50 microns in $r - \phi$ and 250 microns in z. Charge sharing across pixels should improve the resolution to significantly better than $(pixel\ size)/\sqrt{12}$.

The straw tube tracker has 5 superlayers, each containing 8 straw layers for axial superlayers (1, 3 and 5) and 6 straw layers for the 10 mrad stereo superlayers (2 and 4). The per tube resolution is estimated to be roughly 120 microns and the superlayer resolution (including estimates of mis-alignment contributions) is predicted to be 85 microns.

The gas microstrip detector covers the region $|\eta| > 1.8$ with 3 superlayers, each consisting of 2 layers of radial strips and 2 stereo layers at ± 100 mrad. The strip pitch is 200-450 microns, with a predicted resolution per superlayer of 60-100 microns.

3. PERFORMANCE

The resolution of various track parameters are shown in Fig. 3.1 as a function of η. The pixel option makes a small improvement in impact pararmeter resolution due to its smaller radius but significantly improves the resolution in the z component of the track extrapolation to the beamline (z0) from $\sim$ 1mm to $\sim 100\mu m$. These track resolutions translate into invariant mass resolutions shown in Fig. 3.2 for the J/ψ mass in the decay $B \rightarrow J/\psi K \rightarrow \mu^+\mu^- K$ and the B meson mass in the decay $B \rightarrow \pi^+\pi^-$. There is a minimum p_t cut of 4 GeV/c for muons and 2 GeV/c for pions. These results come from a GEANT simulation of the SDC tracking detector. The reconstructed mass resolutions in Fig. 3.2 are not vertex-constrained, which will improve the resolution slightly.

As is clear in Fig. 3.1, the p_t range of interest in B physics (2-20 GeV/c) suggests that multiple scattering will affect vertexing capabilities. To look at SDC vertexing performance we consider at a decay mode of particular interest for CP violation, namely $B_d^0 \rightarrow \pi^+\pi^-$. This B decay mode was generated using ISAJET and input to a GEANT simulation of the SDC tracker and a track and vertex reconstruction algorithm. We then form the vertex chi-square (χ_V^2) between the secondary vertex reconstructed with the $\pi^+\pi^-$ and the primary vertex, assumed in this study to be known to infinite precision. This assumption is reasonable at the SSC since the 5 by 5 μm transverse size of the beam is small compared to the mean tranverse displacement of the secondary B decay vertex ($\sim 2mm$). B_d^0 that travel some distance before decaying will have a large χ_V^2. Fig. 3.3 shows the integral of the normalized χ_V^2 distribution for $B \rightarrow \pi^+\pi^-$ and for pairs of charged pions from minimum bias. This plot then gives the acceptance as a function of the minimum cut on χ_V^2. One can cut at large values of χ_V^2 (100-200) to suppress the background while retaining reasonable acceptance for $B_d^0 \rightarrow \pi^+\pi^-$ (0.3-0.4). The minimum bias cross section is, of course, much larger than the signal. An evaluation of the background is beyond the scope of this study, requiring a detailed simulation that includes non-gaussian effects such as track mis-reconstruction and additional cuts to suppress $\pi^+\pi^-$ backgrounds.

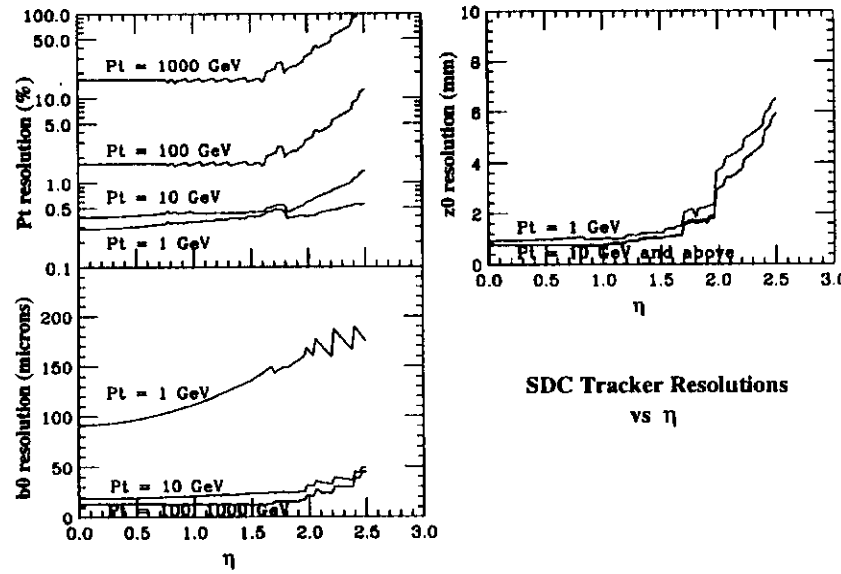

Figure 3.1: SDC single track resolutions versus pseudo-rapidity (η). Shown are resolutions for p_t and track impact parameter (b0) and z position (z0) at distance of closest approach to beamline.

4. CONCLUSIONS

The SDC design of its central tracker is well-suited for doing B physics. A number of design options exist to further enhance these capabilities, namely replacing the inner silicon layers with pixels and/or moving the inner layers closer to the interaction region with a smaller-radius thinner beam pipe. Further studies of the SDC potential for B physics are in progress.

5. REFERENCES

1. E.L. Berger and R. Meng, Phys. Rev. D46, 169 (1992).
2. SDC Technical Design Report, SSCL-SR-1215 (1992).

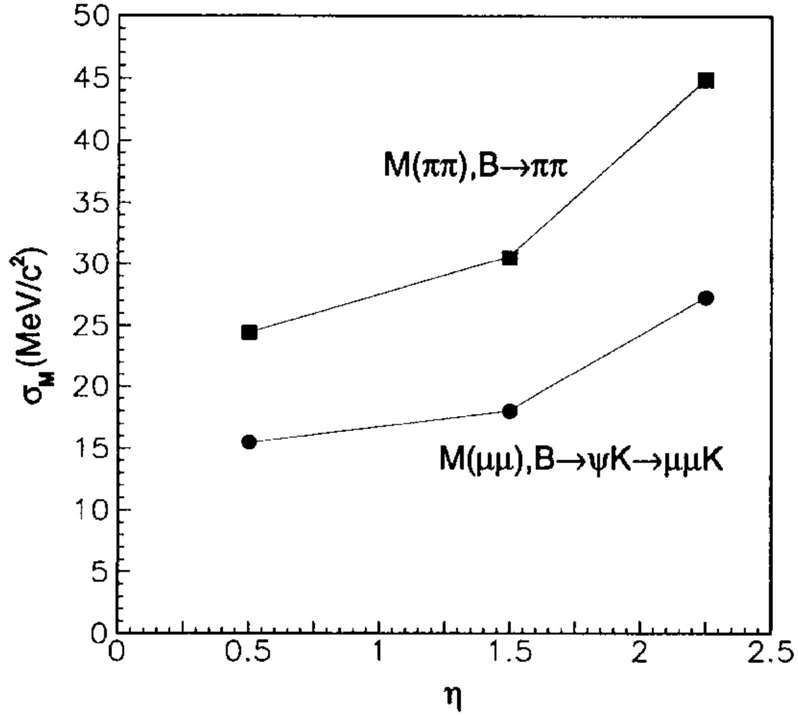

Figure 3.2: SDC resolution in the reconstructed J/ψ mass for $B \to J/\psi K \to \mu^+\mu^- K$ and the reconstructed B mass for $B \to \pi^+\pi^-$ versus pseudo-rapidity (η). The tracks are required to have a minimum p_t of 4 GeV/c for muons and 2 GeV/c for pions.

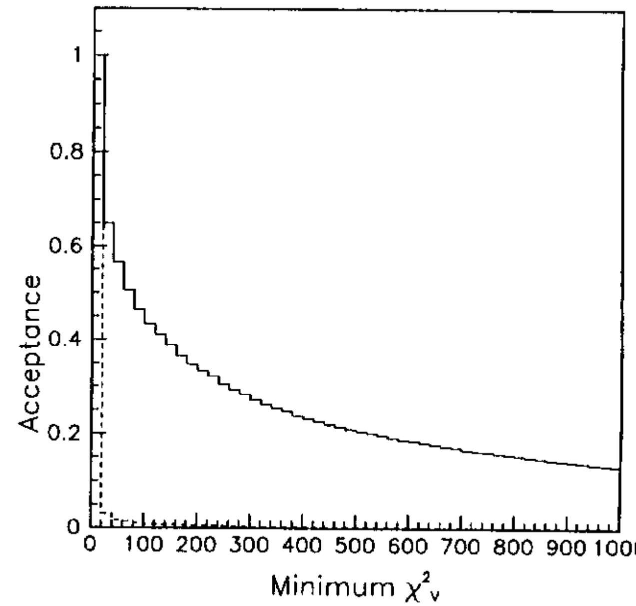

Figure 3.3: Acceptance versus minimum vertex chi-square for $B \to \pi^+\pi^-$ (solid) and pairs of charged pions from minimum bias events (dashed).

Comparison of Forward Collider Vertex Detectors for B Physics at Hadron Accelerators

Robert F. Harr, Paul E. Karchin and Christopher J. Kennedy
Physics Department, Yale University
New Haven, CT 06511, USA

1. INTRODUCTION

Two silicon vertex detector designs have been proposed for a forward collider B physics experiment at the SSC: in one the silicon system is put outside the beampipe (like in the forward part of the proposed BCD detector[1]); and in the other the silicon system is put inside the beampipe, close to the circulating beams, with the use of "roman pots" (as in the COBEX proposal[2]). In what follows these will be referred to as the inside and outside designs. The two designs are significantly different in their construction and impact on the rest of the experiment. We would like to understand how the designs compare for doing B physics and what are the factors that most greatly influence the results.

Two measurements relying on the vertex detector and of particular importance for B physics are the reconstructed vertex position and B mass. We have analyzed the resolution achievable in these 2 quantities for "models" of the two forward collider vertex detector designs. The design parameters – beampipe radius and thickness, silicon position and resolution, etc. – have been varied about their nominal values to observe their effect on these resolutions.

We find very little difference between the two designs; both give nearly the same decay length error, impact parameter error, and reconstructed B mass error, for a large range of geometrical parameters. The design parameter having the most significant impact on the errors of B decay vertices is found to be the point resolution of the silicon detectors.

2. METHODOLOGY

2.1 The Vertex Error Calculation

General equations for track and vertex reconstruction can be derived using the technique of least squares[3]. With the least squares technique, the error on the result can be calculated if one knows the errors on the measurements, independent of the measurements and the calculation of the result itself. Neglecting the primary vertex error, we can calculate the *expected* covariance matrix for a reconstructed vertex from estimates of the point measurement errors and multiple scattering errors for the desired detector configuration.

The result is an equation for the vertex covariance matrix in terms of the momentum vectors of the decay products and the position of the vertex. We will get distributions of the resulting errors if we integrate the equation over a random distribution of momentum vectors and vertex positions for a particular decay mode. We have generated these distributions using PYTHIA[4] version 5.6 for $B_d^0 \to \pi^+\pi^-$ and $B_d^0 \to \psi K_s^0$ at the SSC.

We use a simple model of each detector to calculate the expected covariance matrix of each track to be used in reconstructing the decay vertex. To simplify the calculations, the model has no magnetic field in the region of the vertex detector. The covariance matrices are calculated with the Kalman filtering equations[5], starting with the last measurement in the vertex detector and working inward to the secondary vertex. It is assumed that any tracking detector beyond the vertex detector would have worse resolution than the vertex detector and would contribute negligibly to the vertex covariance. Without the aid of any other detector, a track must intersect at least 2 silicon planes in order to be measured and used in reconstructing a vertex.

With the track covariance matrices calculated, only an estimate of the momentum resolution of the detector is needed to calculate the error on the reconstructed B_d^0 mass. We will assume that the momentum is measured in a downstream detector with a dipole magnet and use the parameterization:

$$\sigma_{p_z} = k \mid p_z \mid \sqrt{p_z^2 + p_0^2} \tag{1}$$

where k is a constant, p_z is the component of the momentum along the beam, and p_0 is the momentum below which multiple scattering dominates.

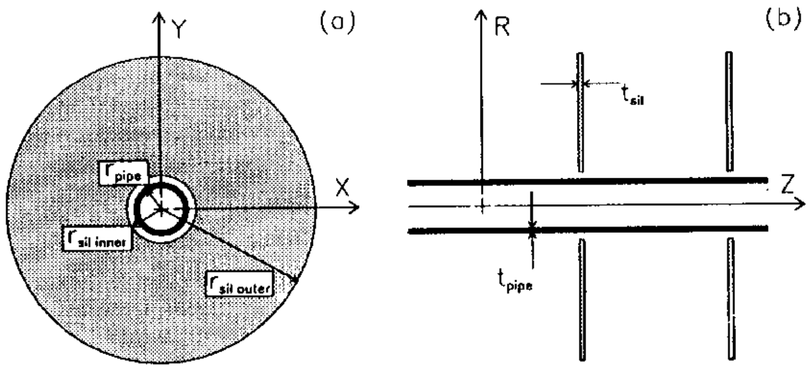

Figure 1: The outside the beampipe design showing the beampipe (dark shading) and the first 2 silicon discs (light shading). (a) is a view down the beam axis and (b) is a cross section in a plane containing the beam axis. The design is azimuthally symmetric. R is a radius in the x-y projection.

2.2 The Detector Designs

Several points are common between the two designs. Both detectors are assumed to reconstruct and identify tracks with momenta > 0.5 GeV/c and to cover not more than

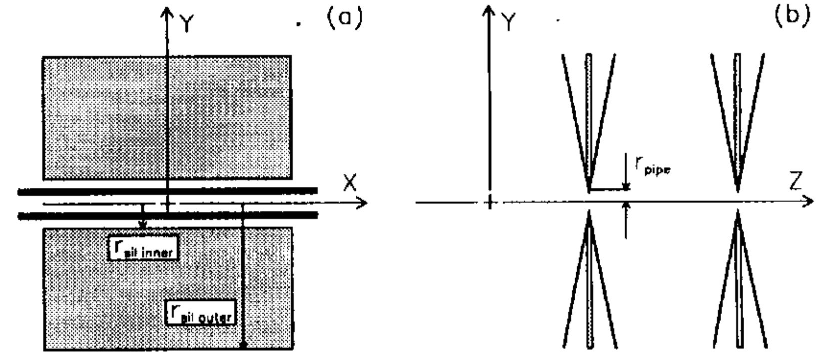

Figure 2: The inside the beampipe design showing the RF shield (dark shading) and the first 2 silicon planes (light shading). (a) is a cross section taken at the position of one of the silicon planes and perpendicular to the beam and (b) is a cross section in the y-z plane. The parameters t_{sil} and t_{pipe} have not been drawn in this figure for clarity but should be obvious from the figure of the outside the beampipe design.

$1 < \eta < 6$ (recall that tracks must intersect at least 2 silicon planes to be measured). The silicon detectors are assumed to be 300 μm thick and measure both x and y coordinates with a resolution of σ_{pt}. (*e.g.* pixel or double sided strip detectors). There are n_{sil} detector planes at positions z_{sil}^i. (The z axis coincides with the beam, with $z = 0$ at the primary vertex; the y axis is in the vertical direction; and the x axis is in the horizontal direction.) Two spacing schemes are used: "linear" spacing, where the distance between successive planes is constant; and "rapidity" spacing, where the distance between succeeding planes is a constant multiple of the preceding distance.

For the outside design (Fig. 1) the beampipe is a beryllium cylinder of radius r_{pipe} and thickness t_{pipe}. The silicon detectors are considered as discs covering the radii from $r_{sil\ inner}$ to $r_{sil\ outer}$.

For the inside design (Fig. 2) the silicon is a pair of rectangular wafers positioned at $\pm r_{sil\ inner}$ from the beam in the y direction. Each rectangular wafer is of size ($r_{sil\ outer} - r_{sil\ inner}$) in the y direction and twice that in the x direction. The silicon is separated from the beam by a beryllium RF shield with the triangular shape shown in Fig. 2. The inner edge of the RF shield is at $\pm r_{pipe}$ from the beam in the y direction and has a thickness of t_{pipe}.

3. RESULTS

In Table 1 we list the parameters for our "nominal" vertex detector designs. They correspond roughly to what appears in Refs. 1 and 2.

The last two parameters, k and p_0, are independent of the vertex detector design. They are needed to calculate the momentum resolution, which in turn is used to calculate the error on the reconstructed B_d^0 mass. Their nominal values are chosen for demonstration purposes and don't necessarily reflect the values proposed by the experimenters.

Table 1: "Nominal" design parameters for the inside and outside designs. See section 2.2 in the text and Figs. 1 and 2 for their definitions.

item		inside design	outside design
r_{pipe}	(mm)	4.0	10.0
t_{pipe}	(mm)	0.2	0.4
$r_{sil\ inner}$	(mm)	5.0	12.5
$r_{sil\ outer}$	(mm)	55.0	112.5
t_{sil}	(mm)	0.3	0.3
σ_{pt}	(μm)	5	5
n_{sil}		8	6
z_{sil}	(mm)	20., 60., 100., 140., 180., 220., 260., 280.	15., 30., 60., 120., 240., 480.
k	(GeV)$^{-1}$	0.0001	0.0001
p_0	(GeV)	10.0	10.0

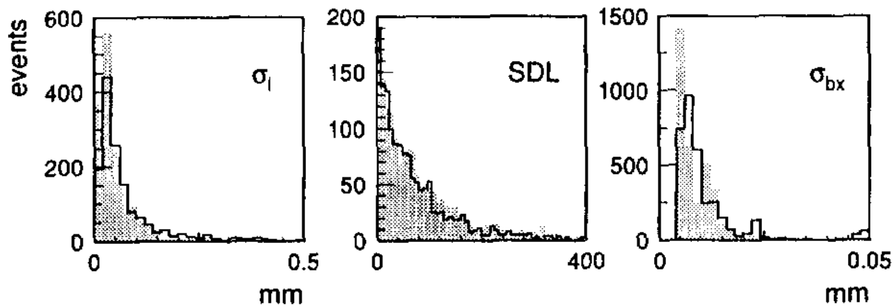

Figure 3: The distributions of σ_l, SDL, and σ_{bx}, the x component of the impact parameter errors, for the pions in $B_d^0 \to \pi^+\pi^-$ decays. The shaded (line) histogram is for the nominal outside (inside) design.

3.1 *Vertex Resolution*

Using a sample of 10000 B_d^0 events where the B_d^0 is forced to decay to $\pi^+\pi^-$,[6] we get the distributions of decay length errors (σ_l), decay length divided by its error (SDL= l/σ_l), and impact parameter errors (σ_b) shown in Fig. 3. The nominal outside design achieves 25% smaller errors than the nominal inside design, due primarily to the "rapidity" versus the "linear" plane spacing. This is shown in Fig. 4 where we compare the nominal outside design to an inside design with "rapidity" spacing. The two designs are now very close in vertex resolution and it is quite good. Taking $c\tau$ (= 300μm for a B meson) as the average impact parameter of B decay tracks, these designs achieve impact parameter resolutions at least 10 times smaller. Taken another way, the average SDL is greater than 80.

The optimal plane spacing is not investigated here. Instead, we use the "rapidity" spacing for both designs from now on.

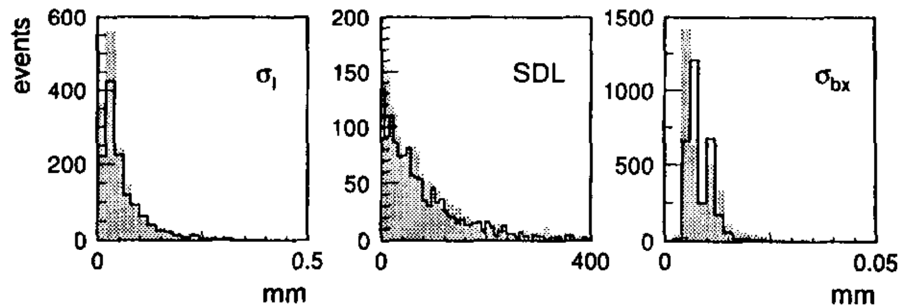

Figure 4: Like Fig. 3 but with "rapidity" detector spacing for both designs. There is a $\sim$ 10% acceptance loss for the inside design due to the gap in y.

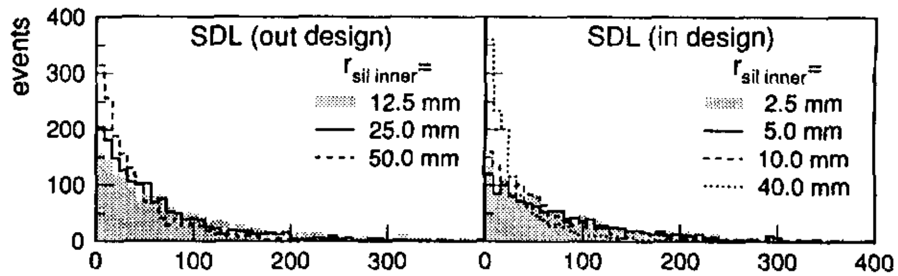

Figure 5: Effect of varying $r_{sil\ inner}$ on SDL.

We varied the silicon radius, beampipe/RF shield radius, beampipe/RF shield thickness, the point resolution, etc. to investigate their relative importance to the resolutions. Figs. 5 and 6 show the results when $r_{sil\ inner}$ and σ_{pt} are varied. (The acceptance is kept constant by scaling $r_{sil\ outer}$ and z_{sil} in proportion to $r_{sil\ inner}$.) A summary of the results is presented in Table 2. There is a strong dependance on σ_{pt}, a much weaker dependance on $r_{sil\ inner}$, and almost no dependance on t_{pipe}. Doubling σ_{pt} from 5 μm to 10 μm changes SDL more than moving the silicon 1 cm further from the beam or quadrupling the thickness of the beampipe/RF shield. If σ_{pt} = 20 μm, the fraction of events with SDL< 20 increases from $\sim$ 20% to $\sim$ 50%.

The dominance of the point resolution in the vertex errors is due in large part to the rather high momenta and transverse momenta of the pions in the accepted $B_d^0 \to \pi^+\pi^-$ decays. Although good vertex resolution is not required to find $B_d^0 \to \psi K_s^0$ decays where $\psi \to \mu^+\mu^-$, we expect worse resolution in reconstructing the ψ vertex since the muons have lower momenta and transverse momenta (see Fig. 7). The distributions for σ_l, SDL, and σ_b are plotted in Fig. 8. The effect is about the same as increasing σ_{pt} to 8 or 10 μm for $B_d^0 \to \pi^+\pi^-$. The results for $B_d^0 \to \psi K_s^0$ are included in Table 2 for comparison with $B_d^0 \to \pi^+\pi^-$. The two detector designs still perform similarly. With lower particle momenta,

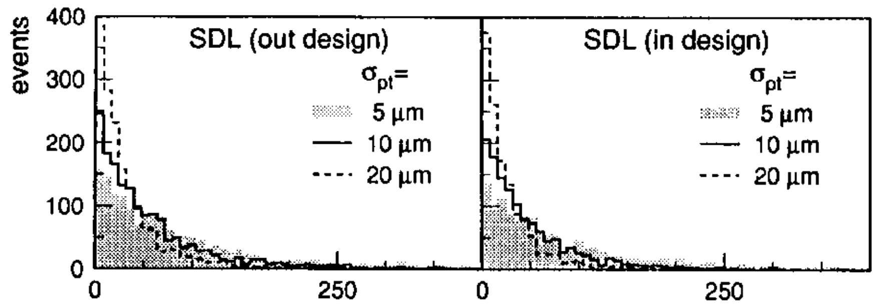

Figure 6: Effect of varying σ_{pt} on SDL.

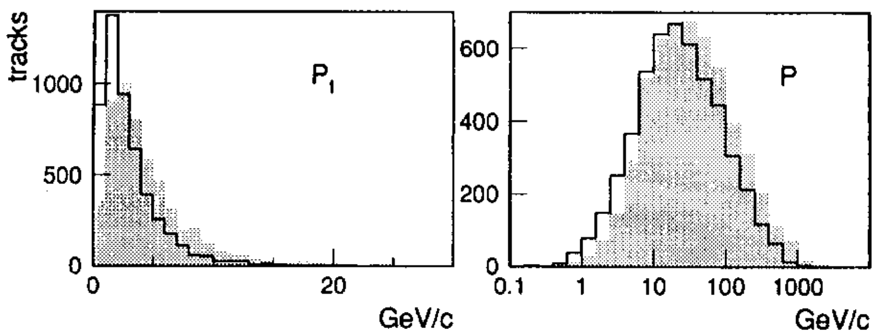

Figure 7: The P_t and P distributions for $B_d^0 \to \pi^+\pi^-$ (shaded histogram) and $B_d^0 \to \psi K_s^0$ with $\psi \to \mu^+\mu^-$ (solid line) at the SSC.

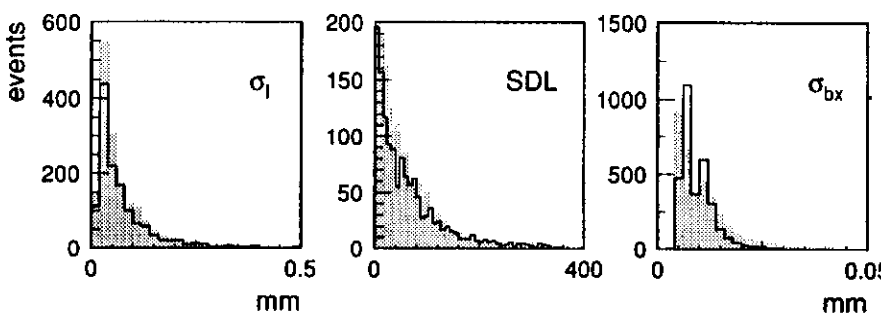

Figure 8: Resolutions for reconstructing the $\psi \to \mu^+\mu^-$ decay from $B_d^0 \to \psi K_s^0$ decays. The shaded histogram (solid line) is for the outside (inside) design. The same design parameters are used here as in generating Fig. 4.

Table 2: The average value of SDL for varied parameter values. "Nominal" and superscript "nom" refer to the nominal parameter values listed in Table 1.

parameter changes	inside design $B_d^0 \to \pi^+\pi^-$	inside design $B_d^0 \to \psi K_s^0$	outside design $B_d^0 \to \pi^+\pi^-$	outside design $B_d^0 \to \psi K_s^0$
nominal	81	65	82	58
$1/2 \times r_{sil\ inner}^{nom}$	84	73	96	78
$2 \times r_{sil\ inner}^{nom}$	69	49	64	42
$4 \times r_{sil\ inner}^{nom}$	50	33	43	25
$1/2 \times t_{pipe}^{nom}$	82	66	84	61
$2 \times t_{pipe}^{nom}$	79	62	78	54
$\sigma_{pt} = 10\,\mu m$	50	41	57	43
$\sigma_{pt} = 15\,\mu m$	36	30	42	33
$\sigma_{pt} = 20\,\mu m$	27	23	32	27

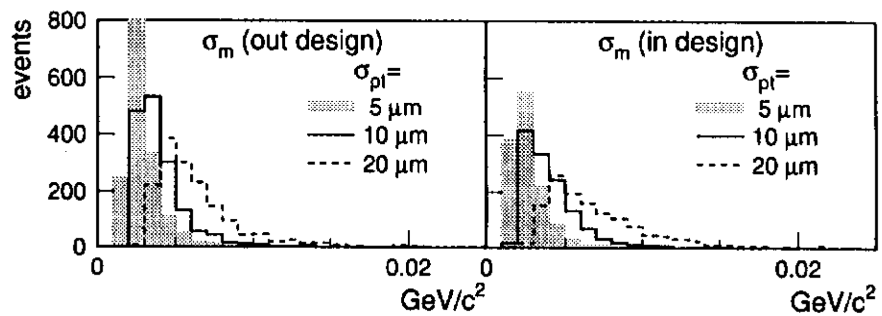

Figure 9: Effect of varying σ_{pt} on the B mass resolution.

σ_{pt}, while still important, is no longer the only dominant factor in determining the vertex resolution.

3.2 Mass Resolution

Calculating the error on the reconstructed mass serves two purposes: we get an estimate of the lower bound on the error coming from the reconstruction of the opening angle in the vertex detector and we get an estimate of the momentum resolution that must be achieved if one wants to distinguish a B_d^0 from a B_s^0 on the basis of the reconstructed mass. The B_d^0-B_s^0 mass difference is approximately 100 MeV[7]; a mass resolution significantly smaller than this is desirable.

In Fig. 9 we plot the contribution to the B_d^0 mass error from the opening angle error, for the same point resolutions as in Fig. 7. Changes in this plot will have a reduced effect when added in quadrature with the contribution due to the momentum measurement error

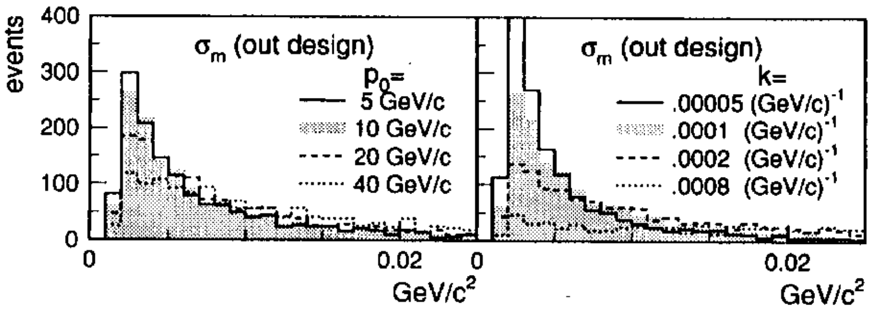

Figure 10: Effect of varying p_0 and k on the B mass resolution for the outside design. Results for the inside design are similar.

to get the total B_d^0 mass error. The total is displayed in Fig. 10 for nominal geometry parameters and varied momentum resolution parameters.

Both designs can achieve mass resolutions in the range 10-20 MeV. The mass resolution is less sensitive to changes in the vertex detector parameters than the spatial resolution but otherwise follows the same general trends.

4. CONCLUSIONS

Despite our initial prejudice that a vertex detector positioned closer to the beam would be superior for reconstructing B decays, we find that there is very little difference as long as the inner radius is less than $\sim 2\,$cm. For $B_d^0 \to \pi^+\pi^-$ both proposed designs perform well. Both vertex detectors are capable of reducing combinatoric backgrounds while keeping a substantial fraction of the signal with tight vertex requirements. With a good magnetic spectrometer, both can well reconstruct the B_d^0 mass.

Due to a lack of other constraints, $B_d^0 \to \pi^+\pi^-$ seems to be the decay with the greatest demands on vertex resolution. We looked at the $\psi \to \mu^+\mu^-$ vertex from $B_d^0 \to \psi K_s^0$ decays as an example of reconstructing a vertex with lower p and p_t decay products. At these lower momenta, the two designs still perform comparably.

The most important parameter for determining the vertex resolution is the silicon detector point resolution. A $\sigma_{pt} = 5\,\mu$m is difficult to achieve in practice, requiring:

- a silicon readout pitch of $50\,\mu$m or less,
- good signal to noise (but limits the detector lifetime in a high radiation environment),
- tracks at near to normal incidence to the detector (silicon resolution degrades with increasing angle of incidence),
- pulse height information for interpolation between pixels or strips, and
- alignment of the vertex detector to a few microns.

In particular, access to pulse height information could put a severe limit on the readout speed of the vertex detector and limit the data taking rate.

If, for a particular detector design, the point resolution is larger than $5\,\mu$m then there is even less to gain in resolution by moving the silicon detectors closer to the beam. Of course, angular coverage versus channel count and cost may be the dominant issue in such a design.

In order to obtain B_d^0-B_s^0 mass separation at 3σ, the momentum resolution should be better than $\sigma_p/p = 0.001\,p$ (for p in GeV/c) in the large p limit. An effective lower limit on the momentum resolution depends on the silicon point resolution. For $\sigma_{pt} = 10\,\mu$m this lower limit is about $\sigma_p/p = 0.0001\,p$. A moderate ($\sim 10\,$GeV/c) scattering term in the momentum resolution doesn't seem to cause any problems.

5. ACKNOWLEDGEMENTS

The authors gratefully acknowledge support by the Texas National Research Laboratory Commission's Research and Development Program and by the United States Department of Energy. R.H. thanks the Texas National Research Laboratory Commission for support under the SSC Fellowship program.

6. REFERENCES

1. *Expression of Interest for a Bottom Collider Detector at the SSC,* May 1990.
   K.T. McDonald, *Beampipes for Forward Collider Detectors,* August 1992.
2. S. Erhan, *et al,* Nucl. Instr. and Meth. **A333**(1993)101.
   J. Ellet *et al,* NIM **A317**(1992)28-46.
   A. Brandt, *et al, Study of Beauty Physics at the SPS-Collider with Real-Time Use of Silicon Microvertex Information,* CERN-SPSC/88-33, January 1989 (P238 proposal).
3. R.L. Gluckstern, Nucl. Instr. and Meth. **24** (1963) 381.
   H. Eichinger and M. Regler, *Review of Track-Fitting Methods in Counter Experiments,* yellow report CERN 81-06, June 1981.
   Paul Avery, Applied Fitting Theory I-III, CBX 87-38-40, August 1987.
4. T. Sjöstrand and M. Bengtsson, Comp. Phys. Comm. **43** (1987) 367.
   H.U. Bengtsson and T.Sjöstrand, Comp. Phys. Comm. **46** (1987) 43.
5. R. Früwirth, Nucl. Instr. and Meth. **A262** (1987) 444.
6. More details on the event generation can be found in *Comparison of Forward and Central Collider Detectors for Beauty Physics,* C. Kennedy, R. Harr and P. Karchin, these proceedings.
7. Particle Data Group, Phys. Rev. **D45** (1992).

Tracking Considerations for Fixed Target B Experiments at SSC and LHC

A.P. McManus, S. Conetti, G. Corti, B. Cox, E.C. Dukes,
T. Lawry, K. Nelson, I. Tzamouranis
Physics Department, University of Virginia, McCormick Rd.
Charlottesville, Va 22901, USA

1. INTRODUCTION

Fixed target beauty (B) experiments proposed at the SSC or LHC come in two basic types. Extracted beam experiments use a bent crystal of silicon or some other method to extract a beam of protons parasitically from the circulating beam as the collider experiments are taking data. The two chief extracted beam experiments are the LHB[1] collaboration at the LHC and the SFT[2] collaboration at the SSC. The second type of fixed target experiment places the detector around the circulating beam using a gas jet or thin wire(s) as a target. The (GAJET[3]) experiment proposed at CERN for LHC and the Hera-B[4] experiment at DESY are of this type.

2. GENERAL COMMENTS ON FIXED TARGET TRACKING

The basic difference affecting design between fixed target experiments and collider experiments is the large Lorenz boost that all decay products are given in fixed target experiments. Because of this, all fixed target experiments are long (50-100 meters) and cover a small solid angle ($\theta \sim 100$ mrad) unlike the typical collider experiment which attempts to cover a 4π solid angle and on average has much lower momentum decay products. The basic layout of a fixed target B experiment[5] is as follows: the target (internal/external) is followed by a silicon microvertex detector, wire chambers, one or two dipole magnet(s), additional wire chambers, and a calorimeter followed by a muon detector. There is a hadron ID system placed before or after the magnet(s).

All fixed target experiments have better primary vertex resolution than collider experiments either because the target is small (internal target or external target) or because the vertex detector is very close to the target (external target). The large Lorenz boost gives very long decay paths for B particles in the lab frame with an average B decay length of 16mm for an 800 GeV proton beam or 95mm for a 20 TeV proton beam. Hence the ratio of decay length to vertex resolution is $l/\sigma \geq 300$ for SSC fixed target experiments.

3. OCCUPANCY CONSIDERATIONS

The occupancy of a strip or wire is defined to be the probability that the strip or wire will fire in an average event. It is generally believed that efficient tracking is not possible with occupancies greater than 10%. Let θ be the angle a track makes with the beam direction. Fixed target interactions with beam energies of many TeV produce large numbers of charged tracks at small θ. The need for low occupancy is an important detector constraint for fixed target experiments.

In Figure 1 we show the PYTHIA simulation of the occupancy versus θ for strips which subtend 10^{-5} radians in $B-\bar{B}$ events with beam energy of 20 TeV ($\sqrt{s}=193$ GeV). At θ of 2-3 mrad the occupancy is about 1% and rises to 10% for strips which subtend 10^{-4} radians. A strip of 25 micron width subtends 10^{-5} radians if it is 2.5 meters from the primary interaction. If a gas tracking chamber is placed 10 meters from the primary interaction and has wire spacings of 1 mm, then each wire subtends 10^{-4} radians. Therefor 2 or 3 mrad is the practical lower θ limit for tracking with gas chambers.

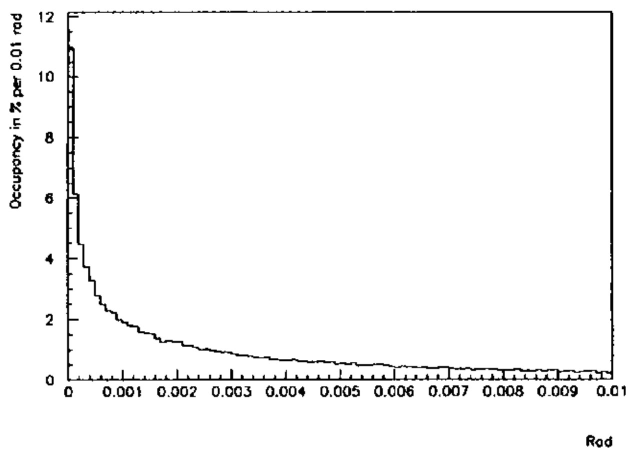

Figure 1: Occupancy of a fixed target experiment at SSC energies as a function of angle.

Silicon microstrip detectors can have occupancies below 10% even at $\theta=0$ provided they are at least several meters from the primary interaction. However the radiation dose at a collider[5] with luminosity of 10^{32} is $2.7\times10^{6}/d^{2}$ rad per year, where d is the distance from the beam in cm. So the silicon must be at least 1 cm from the beam which forces $\theta>1$ mrad even for detectors 10 meters from the primary interaction. For extracted beam fixed target experiments[2], the silicon may extend down to $\theta=0$.

4. ACTIVE TARGET CONSIDERATIONS

An active target provides topological information which supplements the kinematic information from the rest of the detector. Requiring all tracks to come from the same vertex greatly reduces combinatoric background when reconstructing B decays. Mis-tags from D decays can be corrected if the B to D decay chain is recognized. The charge of a B_u is the best possible tag. Measuring the charge of the B_u is very difficult without the topological information from the active target.

The SFT active target was studied using a Pythia event generator coupled to GEANT (with simulated delta rays, multiple scattering, secondary interactions and Coulomb scattering) and the SFT silicon tracking program. The primary and secondary vertex resolutions and impact parameter resolutions are listed in Table 1. The tracking efficiency for finding a single track was found to be 95 %.

Table 1. Vertex resolutions and impact parameter resolutions.

	σ_x	σ_r	σ_z
Primary vertex*	8 μm	8 μm	58 μm
Primary vertex(using beam track)*	3 μm	4 μm	58 μm
Secondary vertex (typical B)	6 μm	8 μm	300 μm
Secondary vertex ($B\to\pi\pi$)	4 μm	6 μm	250 μm
Impact parameter (lepton)		8 μm	
Two track distance of closest approach	3 μm	4 μm	

* assuming 200 μm active target foils

To evaluate the ability of the active target to distinguish charged from neutral B tracks, the distance of the B vertex to the nearest other charged track was calculated and the resulting histogram is shown in Figure 2. The median of the distribution is 100 μm which means that for one half of all B events the B vertex is separated by at least 3 strips (25 μm pitch) from the nearest charged track in at least one view.

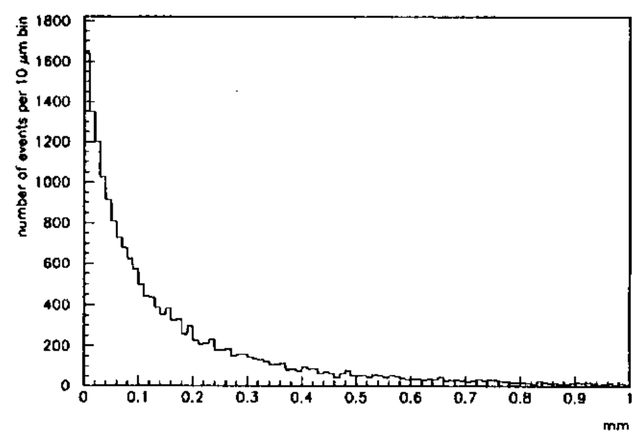

Figure 2: Distance of closest approach for any charged track to the B decay vertex.

5. MAGNETIC SPECTROMETERS AND TRACKING

5.1 *Performance Considerations*

All of the B Physics studies which are planned require very good tracking efficiencies and resolutions at high rates ($10^7 \rightarrow 10^8$ interactions per second) both in the silicon microvertex detector and the spectrometer proper. Special attention has been given to providing for adequate redundancy in the SFT spectrometer[6] to assure the requisite level of performance. The SFT Spectrometer is a two magnet system where the magnets are operated with opposite and equal P_t kicks of magnitude 1.2 GeV/c each. The tracking information is provided by a silicon microvertex detector composed of a live target and tracker planes, followed by sets of pad chambers and wire chambers placed before, between, and after the two analysis magnets. The silicon microvertex detector is optimized for high precision off-line tracking for the B and charm decays and provides hit information to the vertex trigger. The pad chambers provide fast input to the tracking trigger. The tracking chambers upstream of the analysis magnets are positioned to detect the K^0 and Λ decays. Various characteristics of the SFT spectrometer tracking components are summarized in Table 2.

Table 2. SFT spectrometer tracking components.

Tracking Device	Characteristics
Si live target	90 planes - 15 per view (x,y,u,v,u',v') 200 μm double sided
Si tracker	30 planes - 5 per view (x,y,u,v,u',v') 200 μm double sided
Front spectrometer	30 planes - 10 per view (x,u,v) wire chambers/ straw tubes 3 planes of pad chambers
middle spectrometer	30 planes - 10 per view (x,u,v) straw tubes 2 planes of pad chambers
rear spectrometer	54 planes - 18 per view (x,u,v) straw tubes 3 planes of pad chambers

In order to minimize multiple scattering and maximize resolutions, all spaces between chambers, including the volume inside of the magnets have been filled with He bags. In addition, the silicon microstrip detector will be operated in a He gas environment.

5.2 *Momentum and Mass Resolutions*

The momentum and mass resolutions of the SFT spectrometer have been studied using a tracking simulation and they are given in Table 3. The tracks used in the extraction of the resolution of the SFT configuration have been generated using Monte Carlos of; a) Random momentum distributions within geometric acceptance b) Pythia generated two-body final states of:

$$J/\psi \rightarrow \mu\mu \tag{1}$$

$$B \rightarrow \pi\pi, K\pi, KK \tag{2}$$

These tracks have been propagated through the SFT spectrometer while taking into account chamber resolutions and multiple scattering. Chamber efficiencies are assumed to be 90% throughout the spectrometer. Fitted tracks have been produced using a reconstruction program and were compared to the input tracks in order to evaluate reconstruction efficiency and obtain track and mass resolutions.

The global track momentum resolution as a function of momentum is

$$\sigma_P/P = .0009 + .00000841 * P \tag{3}$$

for the SFT spectrometer.

Table 3. SFT momentum resolution and mass resolution.

	σ_{P_t}/P_t	σ_P/P	σ_M (MeV)
$J/\psi \rightarrow \mu\mu$	0.0039	0.0025	7.6
$B \rightarrow \pi^+\pi^-$	0.0045	0.0029	13.0

The excellent mass resolution shown in Table 3 assumes that the mass of the tracked particle is known. Figure 3 shows the mass spectrum for five decay modes: $B_d^0 \rightarrow \pi\pi$, $B_d^0 \rightarrow K\pi$, $B_s^0 \rightarrow K^+K^-$, $B_s^0 \rightarrow K\pi$ and $B_s^0 \rightarrow \pi\pi$ where one or both of the kaons have been assigned a pion mass. Since these modes may well have comparable branching ratios, the need for particle identification is clear.

Figure 4 depicts the SFT mass resolution for all of the above modes, with particle identification provided by a RICH and a TRD. The hadron identification efficiencies and rejections used can be found within these proceedings[7] in the hadron identification section.

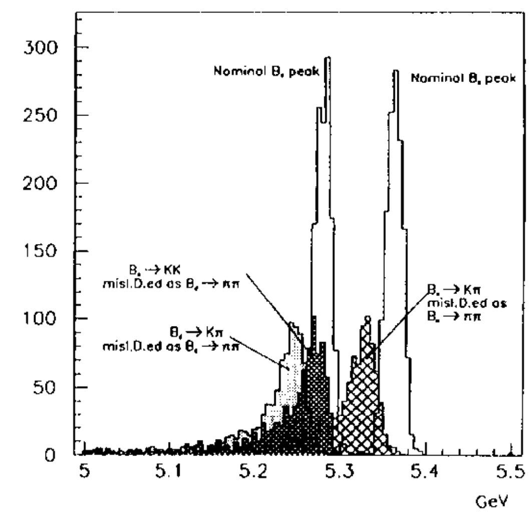

Figure 3: Mass spectra for B_d and B_s modes without particle identification.

6. CONCLUSIONS

Extracted beam fixed target experiments provide the excellent mass resolution and particle identification efficiency needed for B physics. Active targets enhance the ability of the detector to reconstruct complex decay modes. Coulomb scattering in the silicon of the active target does not prevent the detector from achieving high mass resolution. While internal target experiments would have similar mass resolutions, momentum resolutions and particle ID efficiencies, they cannot use an active target and the beam pipe would not allow them to detect the smallest angle tracks.

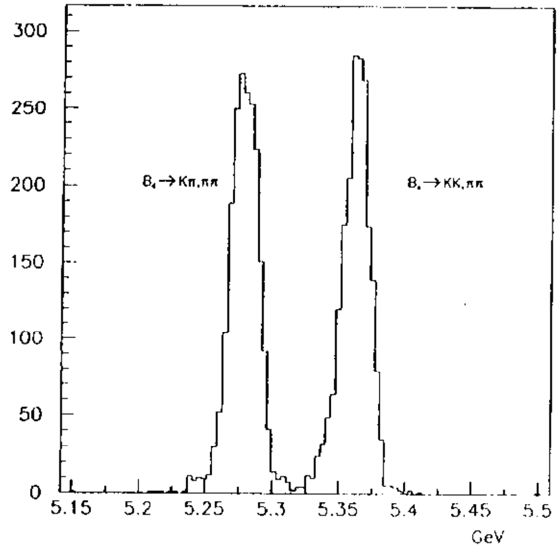

Figure 4: Mass spectra for B_d and B_s modes with particle identification.

7. REFERENCES

1. G. Carboni *et al*, LHB Collaboration, INFN PI/AE91/04, (1991).
2. B. Cox *et al*, EOI-14, SSC Laboratory (1990).
3. Y. Lemoigne, GAJET Collaboration, Nucl. Instr. Meth. **A333** (1993).
4. W. Schmidt-Parzefall *et al*, An Experiment to Study CP Violation Using an Internal Target at the HERA Proton Ring, Letter of intent, DESY-PRC 92/04 (1992)
5. Workshop on B Physics at Hadron Accelerators, Summary Talks
6. B. Cox *et al*, The SFT a Super Fixed Target Beauty Facility at the SSC, Proceedings of the Workshop on B physics, Snowmass, July 1993.
7. K.S. Nelson *et al*, Hadron Identification in a Fixed Target experiment at the SSC, Proceedings of the Workshop on B physics, Snowmass, July 1993.

ON THE CONFIGURATION OF AN ACTIVE TARGET FOR A FIXED-TARGET B EXPERIMENT AT SSC ENERGIES

E.C. DUKES
Physics Department, University of Virginia
Charlottesville, VA 22901, USA

1. INTRODUCTION

The optimal configuration of target and silicon microvertex detector for fixed-target B experiments has yet to be determined. For fixed-target charm experiments the usual setup consists of a series of inert target foils — typically a few millimeters thick and separated by a few centimeters — immediately followed by a silicon microvertex detector. Because of the larger boost at the SSC, the efficacy of using active target foils — tightly packed silicon microstrip detectors — has been considered by at least one group: the SFT collaboration [1]. It is hoped that with an active target the tracks of charged B's themselves can be measured, improving charged B reconstruction efficiencies.

We examine two issues concerning silicon active targets for fixed-target experiments at the SSC: 1) the effect on the acceptance of the requirement that the B decay vertices occur outside of the target foils, and 2) the ability of an active target to directly track charged B's.

2. THE NEED FOR ISOLATED B DECAY VERTICES

Is there a need for requiring that B decays vertices be isolated from the target foils? The lesson from fixed-target charm experiments is ambiguous: some experiments cut out decay vertices occurring in the target material, others do not.

First consider the process $B_d \to \pi^+\pi^-$. The combinatoric background from the large pion production cross section is enormous. With $\sigma_{b\bar{b}}/\sigma_T \approx 1 \times 10^{-4}$ and $\mathrm{BR}(B_d \to \pi^+\pi^-) \approx 1.0 \times 10^{-5}$ the signal to noise (before any cuts) is less than 10^{-9}! The background is reduced by cuts on: mass, transverse momentum, vertex-χ^2, closest-distance-of-approach, and vertex-separation. It is not yet clear whether these cuts can sufficiently reduce the backgrounds to allow a clean measurement of a CP asymmetry [2]. A more difficult source of background comes from $\pi^+\pi^-$ pairs produced in secondary interactions in the target foils — a source of pions comparable in number to that from primary interactions. Monte Carlo studies indicate that this background is not a problem at the analysis level [3]. At the trigger level this background may be much harder to reduce to a tractable level. If a secondary vertex trigger is needed, it may be necessary to require that the secondary vertices be isolated from the target foils.

The situation with the $B_d \to J/\psi K_s$ mode is more favorable. Nevertheless, although this is the cleanest mode accessible experimentally, there is a large background of directly produced J/ψ's. This yield can be estimated using the parameterization of Lyons [4] for the J/ψ cross section:

$$\sigma(pN \to J/\psi X) \approx 1700 \exp(-17 m_\psi/\sqrt{s})\ nb,$$

where m_ψ is the J/ψ mass. In fixed-target at the SSC, $\sqrt{s} = 194$ GeV and $\sigma_\psi = 1.3\ \mu$b, which is roughly equal to the $b\bar{b}$ production cross section of 1.5 μb [5]. Hence the ratio of directly produced J/ψ's to B decay J/ψ's is:

$$\frac{N(direct\ J/\psi)}{N(B \to J/\psi X)} = \frac{\sigma_\psi(194\ GeV)}{\sigma_{b\bar{b}}(194\ GeV)} \frac{1}{2 \times BR(B \to J/\psi X)},$$

$$= 42,$$

using a branching ratio of 1.02% for $B_d \to J/\psi X$ [6]. The extra factor of two in the denominator accounts for the fact that two B hadrons are produced. The ratio of directly produced to $B_d \to J/\psi K_s$ decay J/ψ's is 2100:1 (using a branching ratio of 0.051% for $B_d \to J/\psi K_s$ [7] and a fragmentation probability of 0.4 for B_d). At the analysis level this background can be easily reduced to zero by mass and vertex cuts. At the trigger level it may not be necessary to cut out directly produced J/ψ's: the production rate of directly produced J/ψ's is approximately 830 per second of which only 12% decay into lepton pairs to give a rate of 100 Hz which is within the bandwidth of, for example, the SFT data acquisition system [8]. (We have used a luminosity of $\mathcal{L} = 2.26 \times 10^{31} cm^{-2} s^{-1}$, which corresponds to an event rate of 10^7 per second for a silicon target.) We conclude that directly produced J/ψ's are probably not a background requiring B decay vertices which are separated from the primary interaction vertex.

A potentially more insidious background is J/ψ's from secondary interactions in the target. The topology of such events would look like $B \to J/\psi X$ decays. An estimate of the production rate of J/ψ's from this source requires knowledge of the mean momentum of stable secondaries and their number. The average momentum of stable hadrons from 20 TeV fixed-target Pythia minimum bias events is about 400 GeV ($\sqrt{s} = 27$ GeV) and the average number is about 20. The J/ψ cross section at this energy, using the Lyons parameterization, is $\sigma_\psi(27\ \mathrm{GeV}) = 0.25\ \mu$b. The ratio of secondarily produced J/ψ's from this source to those from B decays is:

$$\frac{N(secondary\ J/\psi)}{N(B \to J/\psi X)} = \frac{\sigma_\psi(27\ GeV)}{\sigma_{b\bar{b}}(194\ GeV)} \left\{\frac{\sigma_T(194\ GeV) A^{0.72} \mathcal{L} \rho l N_{av}}{A^{1.0} \mathcal{L}}\right\} \frac{10}{2 \times BR(B \to J/\psi X)},$$

$$= 3,$$

where $\sigma_T(194\ GeV)$ is the total cross section (40 mb), ρ is the target density of silicon (2.33 g/cm^3), l is the target length (1.8 cm), and N_{av} is Avagadro's number. The length we have used is that of the 4% λ_I SFT active target. The factor of 10 represents the fact that an average of 20 stable secondaries see on average half the length of the target. The ratio of secondarily produced J/ψ's to those produced in $B_d \to J/\psi K_s$ decays is a factor of 50 greater or 150:1. This background is eliminated at the analysis level by the B mass cut. At the trigger level, the production rate of secondarily produced J/ψ's is approximately 60 per second giving a dilepton trigger rate of 4 Hz.

We conclude that the requirement that the B decay vertices lie outside of the target foils may be necessary to reduce the backgrounds to $B \to \pi^+\pi^-$ at the trigger level. Monte Carlo studies indicate that it isn't a problem at the analysis level, although we remind the reader that such studies invariably underestimate sources of backgrounds. The backgrounds due to secondary interactions are probably not a problem for the spectacular $B_d \to J/\psi K_s$ signature, either at the trigger or analysis levels. For physics with partially reconstructed B's, such as semileptonic decays, the backgrounds are larger, particularly for decay modes with many final states, and the requirement that the B decay vertex lie outside of the target foils seems essential.

3. ACCEPTANCE LOSSES IN A MULTI-FOIL TARGET

If one assumes that B decay vertices must be required to lie outside of the target foils, then care must be taken to space the foils enough apart so that the fraction of decays in the foils is small. In this section we estimate the fraction of events lost by this requirement and attempt to find the optimal number of foils as a function of target length.

In order to find the number of B decays occurring in the material of a multifoil target, the B lifetime distribution needs to be determined. This was done using Pythia to simulate 20 TeV fixed-target $b\bar{b}$ production, B fragmentation and decay. The B lifetime used was 1.31 ps. The B decay vertex distribution along the incident beam direction was fit to a double exponential, giving a chi-squared of 1.2 (Fig. 1). To find the fraction of decays taking place in the target foils, uniform $b\bar{b}$ production throughout the entire target was assumed and the double exponential fit was used as the decay vertex distribution.

The fraction of B's decaying in a target with the same number of foils (90) and thickness (1.8 cm) as the SFT target, is shown in Fig. 2 as a function of the target length. Here, by target thickness, we mean the total length of silicon material in the target and by target length we mean the total length of the target, including the space between the foils. Two cases are shown in Fig. 2: one in which only decays occurring in target foils are counted; the other in which decays occurring in the target foils as well as in a region of 1 mm length on either side of the foils are counted. We call this additional distance the added exclusion length in the following discussion. It is needed because of the resolution error in the decay vertex. With an estimated secondary vertex resolution of $\sigma_z = 300\ \mu m$ [9] (in the longitudinal or boost direction) the added exclusion length of 1 mm corresponds to roughly $3\sigma_z$. We see from Fig. 2 that the fraction of B decays occurring in the target is quite large with the 1 mm added exclusion length. Lengthening the target decreases the loss, but at the cost of decreasing the acceptance or increasing the area of the downstream silicon microstrips.

The fraction of B decays inside target foils is a strong function of the added exclusion length. This is shown in Fig. 3 which gives the fraction decaying in the target as a function of the added exclusion length for a 18 cm long target: the length of the SFT target. At the trigger level a larger than $3\sigma_z$ exclusion length may be needed. If that is the case then to keep the fraction decaying in the target small, either a very long target or a smaller number of foils is needed.

To find the optimal target configuration, the number of foils that minimizes the fraction of B decays occurring in the target material was determined as a function of target length (always keeping the target thickness at 1.8 cm). With perfect vertex resolution (no added exclusion length) the optimal number of foils would be as many as possible. However, with an added exclusion length — and we use 1 mm again — a finite number of foils gives the smallest loss. The result is plotted in Fig. 4 as a function of the target length. For a target of the SFT length (18 cm), five foils give the smallest fraction of B decays occurring in the target material: 14.3%.

A comparison of the SFT target with the ideal target (both with an added 1 mm exclusion length) is shown as a function of target length in Fig. 5. The solid line shows the 90 foil SFT target and the dashed line shows the fraction lost with the optimal number of foils (at each target length).

4. OBSERVING CHARGED B TRACKS

The ability to see a charged B track requires that the B traverse a sufficient number of silicon planes and that it be sufficiently separated from other charged secondaries. The median B decay length at 20 TeV fixed-target energies is approximately 3 cm. Hence the B lifetime is enough to enable it to pass through a sufficient number of silicon planes if they are closely packed. Is the B track sufficiently separated from the other charged particles to allow it to be tracked? We start with a back-of-the-envelope estimate. The average charged particle multiplicity for $b\bar{b}$ events is 30, of which half are in the forward hemisphere in the center-of-mass. A massless particle at 90° in the center of mass is boosted to a polar angle of $\theta = 1/\gamma$ or about 10 mrad in the laboratory frame. Hence about 15 charged particles occupy a 10 mrad cone, giving an occupancy of roughly 1 charged particle per mrad.

To get a more quantitative estimate of the occupancy, the angle between the charged B and its closest charged partner was determined. Only those charged particles which pass by the decay vertex of the B were considered. The angular separation is shown in Fig. 6. The mean angle is 2.5 mrad and the median angle is 1.5 mrad; consistent with the back-of-the-envelope estimate. On average, the B needs to travel a distance of 2 cm before it is separated by 1 strip from the closest charged partner in a silicon microstrip detector with 25 μm pitch.

The silicon strip occupancy near the charged B's was determined by finding the transverse separation between the B and its charged partners at 1 cm z intervals, starting at the production point. This was only done for charged B's with lifetimes greater than 4 cm. The results for distances of 1 cm and 4 cm from the production point are shown in Figs. 7 and 8. The occupancy in 25×25 μm^2 cells, as well as the x and y projections are shown. The occupancy of silicon strips adjacent to the B is very high: over 100% at 1 cm from the production point and approximately 100% at 4 cm from the production point. It falls off rather slowly with 8% occupancy 20 strips (0.5 mm) away from the B (at 4 cm from the production point). Even B's at polar angles greater than 5 mrad (the median B production angle) and decay lengths greater than 4 cm — about 11% of the total number — are accompanied by large occupancies, as is shown in Figs. 9 and 10. At 4 cm from the production point the occupancy is on the order of 30% in the strips nearest to the B track.

Silicon pixel devices would reduce the occupancy. The smallest cell size imaginable is 25×25 μm^2. The number of such channels needed with an active target the size the SFT proposes to use — 10×10 cm^2 — would be 16 million per foil! Even with pixels the occupancies adjacent to the B are discouragingly high: at 4 cm from the production point it is approximately 10% for all B's and 2% for those produced at angles greater than 5 mrad.

We caution the reader that the events used in this analysis are from a Pythia simulation and come from pp rather than pSi interactions. The multiplicities in pSi interactions are much greater [10]. Hence the occupancies estimated here are a lower limit.

5. CONCLUSIONS

We have examined two issues concerning multi-foil active silicon microstrip targets for fixed-target B experiments at SSC energies: the acceptance loss due to the requirement that the B decay vertices lie outside of the target foils, and the ability of the target to separate charged B tracks from other charged tracks in the event.

We conclude, at least with respect to these two considerations, that the target foils should be separated by at least several centimeters, and that most charged B's cannot be tracked with any active target configuration due to the high occupancies in planes immediately following the interaction point. Even pixel devices with a cell size of 25×25 μm^2 have too large an occupancy if placed closely enough together to allow the average B to traverse enough planes to conceivably be tracked.

In light of these results, it appears that an active target has no advantages over a separate target foil followed by tracker configuration. The latter configuration has some clear advantages. These include: more flexibility in the choice of target material and interaction length, target foil and silicon plane spacings that can be separately optimized (with perhaps several cm target spacing and several mm tracker spacing), and less channels for equivalent tracking efficiency.

6. REFERENCES

1. "An Expression of Interest in a Super Fixed Target Facility (SFT) at the Superconducting Super Collider", SSC-EOI0014.
2. O.R. Long et al., "Monte Carlo Simulations of $B_d^o \rightarrow \pi^+\pi^-$ from p-p Interactions at $\sqrt{s} = 40$ TeV", Princeton/HEP/92-07, August 13, 1992.
3. T. Lawry, in these proceedings.
4. L. Lyons, *Prog. Nucl. Part. Phys.* **7** (1981) 169.
5. E. Berger and R. Meng, *Phys. Rev.* **D46** (1992) 169.
6. K. Berkelman and S.L. Stone, *Annu. Rev. Nucl. Part. Sci.* **41** (1991) 1.
7. A. Bean et al., (CLEOII), "Decay Rates and Polarization in Inclusive and Exclusive $B \rightarrow \psi$ Decays", unpublished.
8. See the summary of the Trigger and Data Acquisition Group in these proceedings.
9. A. McManus, these proceedings.
10. M.J. Tannenbaum, *Inter. Jour. of Mod. Phys.* **A4** (1989) 3377.

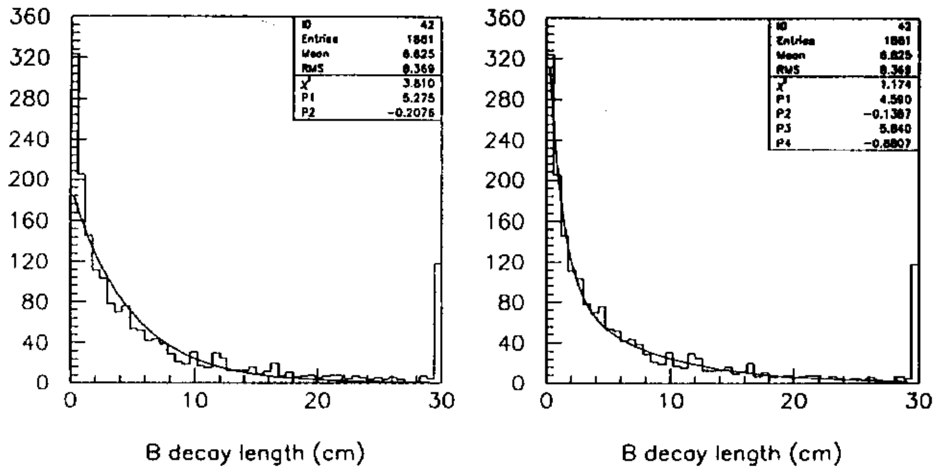

Figure 1: Decay distribution of uncut 20 TeV B's. The left-hand plot is fit to a simple exponential whereas the right-hand plot is fit to a double exponential.

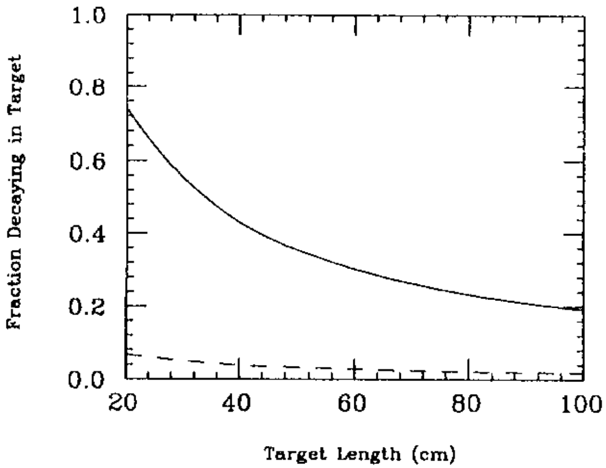

Figure 2: The fraction of B decay vertices occurring in the target foils of a 90 foil, 1.8 cm thick target, as a function of the target length. Two cases are plotted: one in which only decays occurring in the foils are tabulated (dashed line); the other where decays occurring in the foils as well as in an additional 1 mm on both sides of the foil are tabulated (solid line).

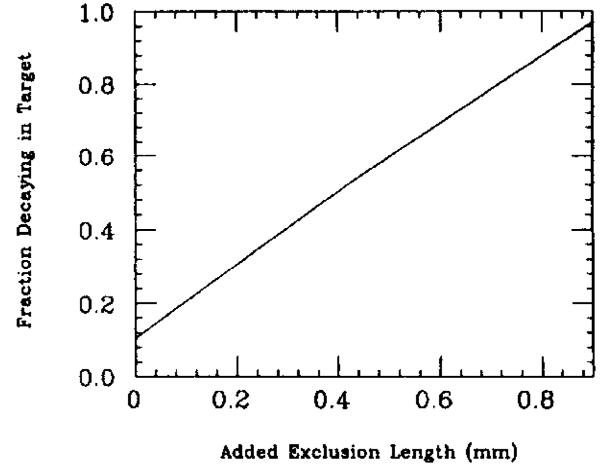

Figure 3: The fraction of B decay vertices occurring in the target foils of a 90 foil, 18 cm long, 1.8 cm thick target, as a function of the exclusion length added to both sides of each foil.

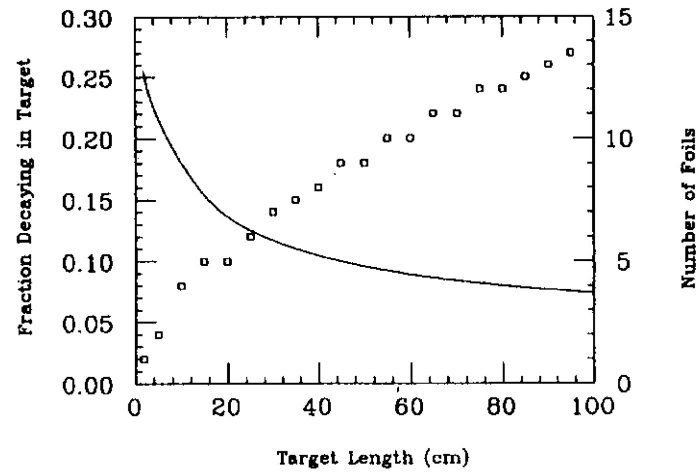

Figure 4: The minimal fraction of B decays occurring in the target foils of a 1.8 cm thick target, as a function of the target length (solid line). A 1 mm exclusion length has been added to both sides of each foil to account for vertex resolution. The right axis gives the corresponding number of target foils (square points).

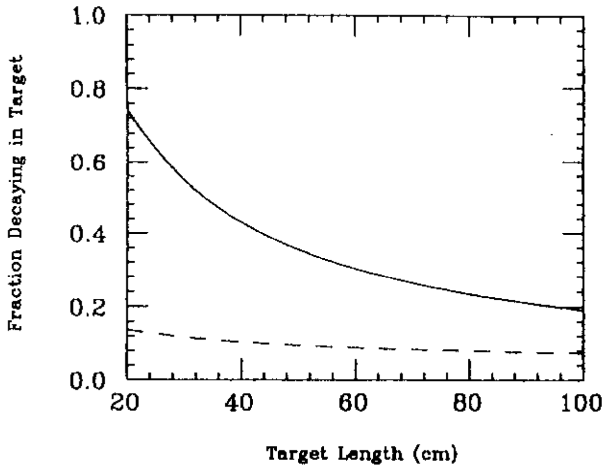

Figure 5: The fraction of B decays occurring in the target foils of a 90 foil target (solid curve) and a target where the number of foils has been optimized to minimize the number of decays occurring in the target (dashed curve), as a function of the target length for a 1.8 cm thick target. A 1 mm exclusion length on both sides of each foil has been added.

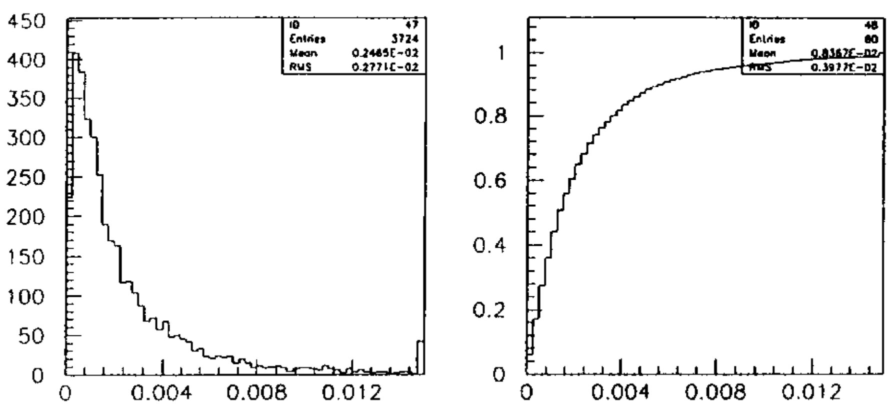

Figure 6: The left plot is a histogram of the angle between the B and its closest charged partner. The right plot shows the integral distribution. Units are radians.

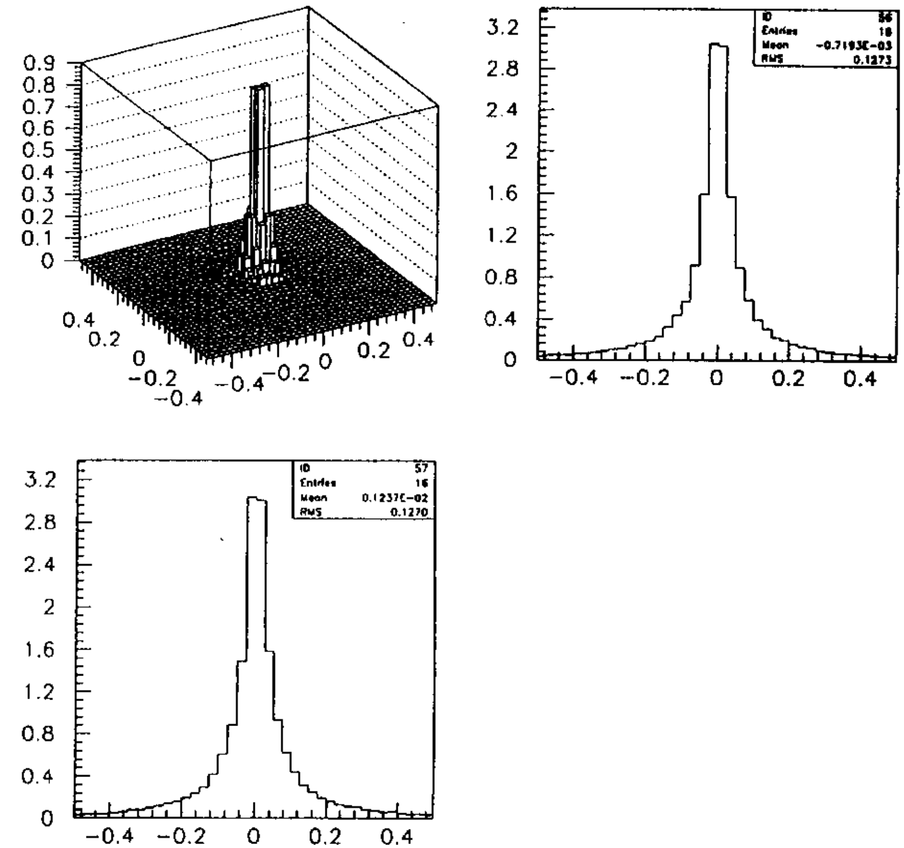

Figure 7: Top left: the occupancy of $25 \times 25\ \mu m^2$ cells adjacent to the B track at 1 cm from the production vertex, for B's with decay lengths greater than 4 cm. The upper right-hand plot shows the x projection and the lower left-hand plot shows the y projection. Units are millimeters.

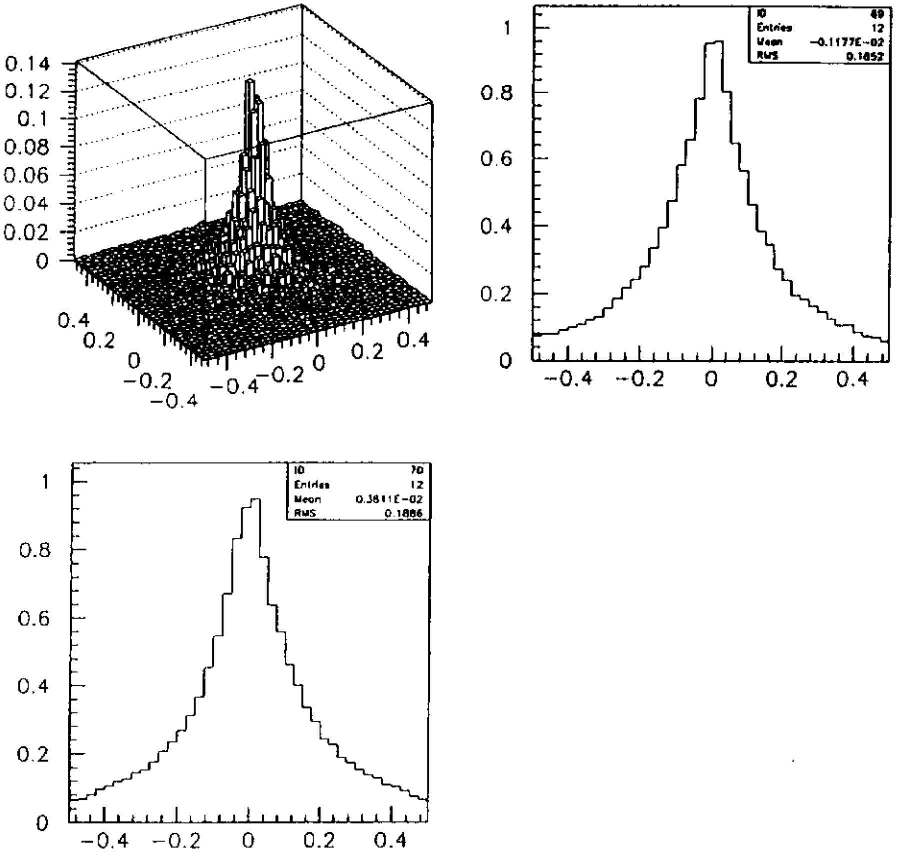

Figure 8: Top left: the occupancy of $25 \times 25\ \mu\mathrm{m}^2$ cells adjacent to the B track at 4 cm from the production vertex, for B's with decay lengths greater than 4 cm. The upper right-hand plot shows the x projection and the lower left-hand plot shows the y projection. Units are millimeters.

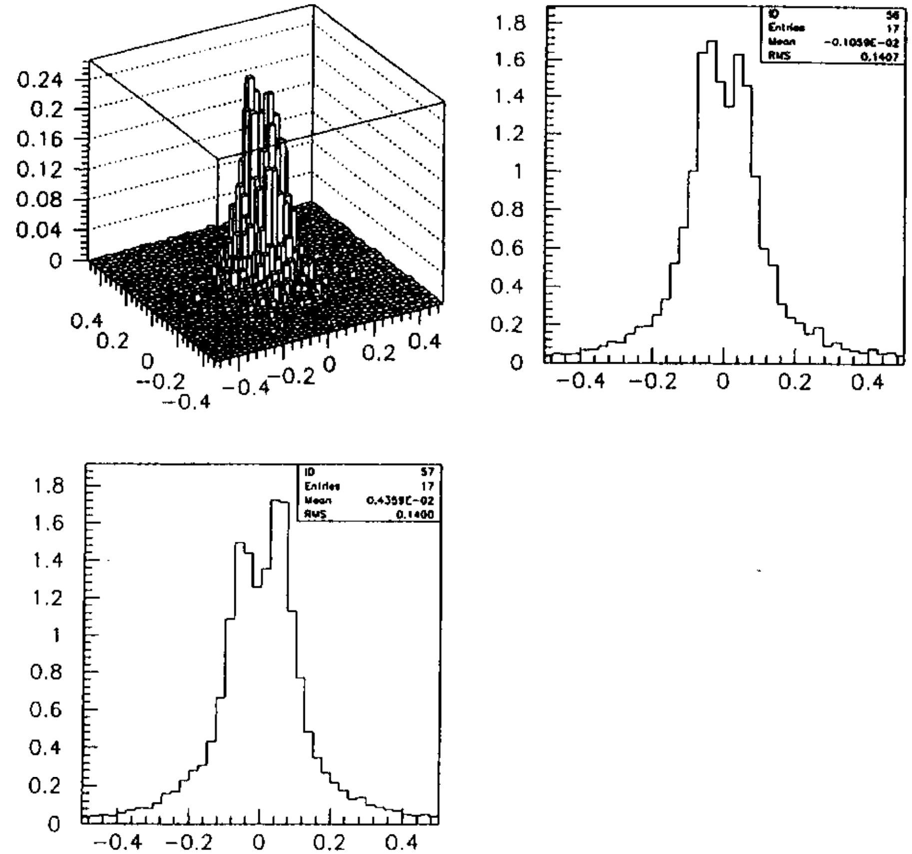

Figure 9: Top left: the occupancy of $25 \times 25\ \mu\mathrm{m}^2$ cells adjacent to the B track at 1 cm from the production vertex, for B's with decay lengths greater than 4 cm and polar angles greater than 5 mrad. The upper right-hand plot shows the x projection and the lower left-hand plot shows the y projection. Units are millimeters.

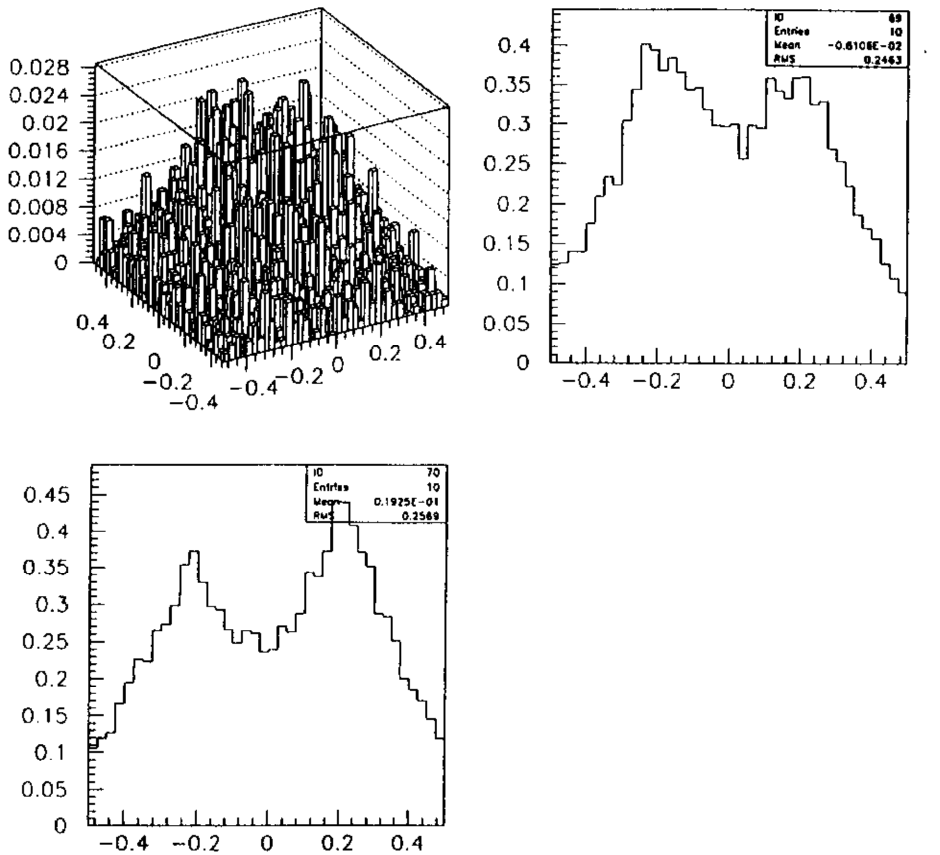

Figure 10: Top left: the occupancy of $25 \times 25\ \mu m^2$ cells adjacent to the B track at 4 cm from the production vertex, for B's with decay lengths greater than 4 cm and polar angles greater than 5 mrad. The upper right-hand plot shows the x projection and the lower left-hand plot shows the y projection. Units are millimeters.

A realistic study on a Forward Geometry Collider Spectrometer: Performance of a typical fixed target spectrometer at the Tevatron Collider

Paul Lebrun
Fermi National Accelerator Laboratory, Batavia, Illinois 60510

Abstract

The performance of a forward heavy quark experiment at the collider can be estimated in a very realistic way, by simply carrying an existing fixed target spectrometer (E687) to the Tevatron Collider, changing only the beam/target configuration while keeping all reconstruction cuts identical to those used in reconstructing real charmed particles collected during the last fixed target run. Based on the golden - and typical - decay mode $D \rightarrow K\pi\pi$, it is found that the overall charm acceptance $\times$ efficiency is $\approx 3\%$, the 5-body B decay $B \rightarrow D\pi\pi$ being about .6%. Such an experiment compares very favorably to E-831 and has real potential to study in great detail doubly suppressed Cabbibo decays and to observe $D^0 - \bar{D}^0$ mixing. In addition, this exercise allows us to perform a rough but effective reality check on similar design (e.g. COBEX).

1. MOTIVATION AND METHOD

Two large central detectors at the Tevatron collider are currently in operation. While they clearly have been designed to study large mass objects (electroweak boson, top quark), they have significantly contributed to our knowledge of B physics. This success has been anticipated, as numerous proposals to build a dedicated Heavy Quark collider detector have been written in the last 5 years[1].

While these proposals are mainly addressing B physics and CP violation in particular, little attention has been paid to the Charm sector, where interesting physics remains to be done, such as an in depth study of doubly Cabbibo suppressed decays and $D^0 - \bar{D}^0$ mixing. Ultimately, CP violation will also have to be studied in Charm, to strengthen our understanding of this peculiar phenomena. Currently, the global assumption is that Charm Physics should be done at fixed target energies, where multiplicities are small and rates are acceptable, and B physics should probably be done more productively at the collider. But, as current generation fixed target spectrometers must be upgraded to take more rate and as a very fast trigger is still hard to achieve, it might make sense to consider the Tevatron as a Charm factory, where the Charm to non-Charm cross section ratio is expected to be much higher than at Fixed Target. At the Tevatron, Charm is produced mainly via gluon-gluon interaction, and, without P_t cuts, should probably be considered as a non-perturbative phenomena, where QCD-based models become somewhat unreliable. Let us simply state that PYTHIA predicts a total Charm cross section of about 3.4 mbarns. In other words, the probability to emit a $c-\bar{c}$ pair through soft ($P_t \leq 4.0$ GeV/c) gluon emission is about 7 % per event. In any event, this probab ility is higher at the collider than at a fixed target photoproduction experiment, such as E687, where only 1 to 1.5 % of the hadronic events contain Charm.

As a ± 3 to 4 unit of rapidity coverage is rather costly to achieve at the collider, our community is currently debating which kinematic region to cover (or start covering !). In order to establish reality checks on acceptance calculations, Joel Butler proposed a *gedanken experiment*: by simply carrying the known E687 spectrometer[2] to the collider, one can do a realistic calculation of what the sensitivity for Charm (and possibly Beauty) at the collider would be. Rather than generating a top-down design for a new experiment, the idea here is to use existing knowledge - a Monte-Carlo benchmarked against existing data. The event generator will be modified to take into account obvious change in kinematics and keeping the experimental Monte-Carlo (with the exception of the target region), data reconstruction and final analysis cuts *as in E687*. Once the acceptance and efficiency issues are understood, assuming realistic cross section estimates and achievable luminosities, one can compare the relative merits of a next generation fixed target and Collider heavy quark experiment.

2. DESCRIPTION OF THE ADAPTION OF THE E687 MONTE-CARLO

A somewhat complete simulation of the E687 spectrometer has been implemented using the GEANT3 package. While Calorimetry tuning has been done using GEANT3, a more flexible Monte-Carlo featuring fast and robust charged particle tracking has been written and is referred to as ROGUE. Within ROGUE, the default event generator is currently based on the LUND/PYTHIA[3] package. Photoproduction as well as hadroproduction can be studied using this package, using the same underlying hypothesis on parton dynamics - namely perturbative QCD.

Default PYTHIA parameters were used, no P_t or η biases were applied. In order to reduce possible systematic uncertainties in the simulation, a few modifications had to be made to the interface between LUND/PYTHIA and ROGUE:

1. The primary photon generator has been turned off, the PYTHIA beam and energy set for the current Tevatron collider ($P-\bar{P}$, 1.8 TeV). The overall efficiency of the recoil electron shower counter trigger (RESH) in the last E687 run was around 50 %, it is assumed that at the collider a minimum biased trigger can do better than that...

2. As ROGUE is responsible for decaying the Charmed or B particles, PYTHIA has been instructed to keep unstable particles alive. As ROGUE is set to decay only a single $c-\bar{c}$ or $b-\bar{b}$ pair, other 'spectator' heavy quarks produced in a jet were ignored. Events containing particles that ROGUE has no knowledge of - such as on mass shell electroweak bosons - were rejected. Since these multiple heavy quark events or high P_t phenomena are characterised by small cross sections this cut does not affect the answer. (Typically, less than 1% of the events were rejected).

3. Charged Multiplicity limit : The E687 Monte-Carlo and reconstruction programs have evidently been tuned for the multiplicity encountered in typical fixed target experiments. It is believed that ROGUE/PASS1 can handle multiplicities around 30 with 'decent' efficiency. The multiplicity is expected to be somewhat higher at the collider. In order to speed up the program, this limit has been implemented in two phases: first, one selects 'spectator' particles in a cone of $\pm 250 mrad$ around the Z axis (one cone, as we are simulating a single arm spectrometer at the Collider), second, up to 30 of these particles are traced through the spectrometer. In addition, in order to take into account the loss of acceptance at high rapidity due to the beam pipe mechanical constraint, tracks must have an opening angle greater than 1 mrad. It has been verified - at least for Charm - that imposing a limit of 30 charged tracks per event does not bias the sample.

It has been assumed that the entire E687 spectrometer can be carried *as is* to the collider, with the exception of the Beryllium target. The extent of the beam crossing along the Z direction is assumed to 4 cm., as the geometrical acceptance of the Microstrip system has been tuned for a 4 cm Beryllium target. No provision for the beam pipes or other accelerator equipment has been made. Counter and chamber efficiencies, background noise in the PWC system are taken into account in the ROGUE simulation package and have not been modified in any fashion. Most important, the reconstruction and analysis cuts have not been touched.

3. CRUDE GEOMETRICAL ACCEPTANCE CONSIDERATIONS.

At the Tevatron collider, Charmed particles are expected to be produced over roughly ± 3 units of rapidity, with an average transverse momentum of 1.7 GeV/c. Once again, as we are concerned with a forward geometry, single arm for now, one can start by making a cut on the polar angle, θ, of these tracks :

$$0.001 \leq \theta \leq 0.25$$

This cut corresponds to a window in pseudo rapidity of $\eta \geq 2$. Since production drops quickly beyond $\eta \approx 3$, one has roughly one unit to 1.5 units of rapidity coverage for Charm, corresponding to a single D acceptance of roughly 29 %. Only a few tracking elements of the E687 spectrometer do actually cover 250 mrad; this is therefore an upper limit to the acceptance. As two charmed particles are produced in the collision, the probability to observe one of them is twice that. Efficiencies quoted on table 1. correspond to accepting a single D decaying into a specific mode, the other D decaying without any particular bias.

Because the production for B's is slightly more central, and since the D meson produced in B decays carries less momentum than the promptly produced D's, the coverage for generic 5-body B decay is expected to be smaller than for generic, prompt Charm. (See Table 1 and 2). The absolute systematic error on these acceptance numbers is of the order of $\pm 5\%$. These uncertainties are due to an incomplete determination of the E687 spectrometer geometry and production model characteristics.

4. EFFICIENCY FOR 3-BODY DECAY MODE OF THE D MESON

Events with a D^+ (Charged conjugate assumed) were selected from a sample of prompt charm and, in a subsequent run, from $B \rightarrow \pi\pi D^+$. In both cases, the D^+ meson decays into $K^-\pi^+\pi^+$. The other charmed (or B) particle in the event was traced in the Monte-Carlo, but no attempt to reconstruct the final state was made.

All generated events containing a Charm pair were submitted to the trigger simulation and the PASS1 reconstruction. Tables 1 and 2 summarizes the effective acceptance, including reconstruction efficiencies, at various stages of the calculation, starting with the trigger.

1. The First Level Trigger (Master Gate) requires evidence for at least two charged particles in the spectrometer. This can occur in either of two ways: two or more particles in the inner part of the spectrometer as signified by at least two sets of hits in the $H \times V$ hodoscope (characterised by a rough angular aperture of 29 by 54 mrad.) , or only one track in the $H \times V$ hodoscope and one track in the outer hodoscope. (characterised by a maximum angular aperture of 130 by 135 mrad.)

2. The Multiplicity trigger is the first component of the second level trigger and consists of requiring - in addition to the Master Gate - two (Low Multiplicity) or three (High Multiplicity) confirming hits in the P0 and P1 systems outside the pair region (covering about a few mrad or less in the X direction). These chambers are located at 4 m. and 6.4 m. downstream of the interaction region and are approximately 76 cm by 127 cm.

3. The Hadronic trigger is the second component of the second level trigger and consists of requiring roughly more than ≈ 50 (Low) to ≈ 70 GeV (High) in the hadrometer covering roughly 30 mrad by 45 mrad. Because of the finite resolution of this hadrometer (consisting of Iron plates and Iarocci gas counters). This cut is a bit fuzzy, the efficiency as function of incident hadronic energy has been measured and is shown in ref. [2]

4. For events satisfying the first and second level triggers, the single charged tracking acceptance and reconstruction efficiency have been measured for the Kaon and pion from the D decay.

5. In addition to trigger and track reconstruction, one has to require Cerenkov particle identification for the Kaon track. A loose criteria was chosen, as one simply requires that the particle be identified as 'heavy', (e. g., at least one Cerenkov cell off in the correct momentum range - in E687 jargon, ISTATP = 4, 7, 12).

6. In addition to Kaon identification and reconstruction, one now requires that the two other prongs from the D decay are accepted and reconstructed in the Microstrip and PWC system.

7. One now ignore the Monte-Carlo GOD's block information and proceeds with the Charm selection code (in the E687 jargon, the EZDEE filter). In this analysis, one requires a good second vertex significantly detached from a good 'primary' vertex consisting of the D^+ and at least one other charged track. The detachment criteria was $L/L_{\sigma L} > 7.0$ At this point, for the real E687 spectrometer, the signal to noise (as defined as the height of peak at the D mass over the background) is about one to one. Thus, these D's are considered useful for physics investigation leading to the final analysis.

8. One now proceeds with the final analysis cuts. As the signal to noise requirement depends on the physics one has to do, these are negotiable. For the purpose of this study, let us limit ourself to the cuts used in a typical Dalitz analysis of $D^+ \to K^-\pi^+\pi^+$. Using the following cuts, in the Fixed Target Photoproduction E687, it has been showed that the signal to noise is better than 15/1 :

   - Target fiducial cuts in Z.
   - $L/L_{\sigma L} > 15.0$
   - The confidence level associated to the χ^2 of the vertex fit be greater than 0.05
   - $ISO1$ cut at 0.01 [1]
   - $ISO2$ cut at 0.0025 [2]

While the collider implementation clearly takes an original loss due to geometrical acceptance, it is worth noting that the vertexing is not more difficult at the collider, despite of the fact that many tracks do have low momentum. This is partly because the charged track multiplicity at the primary vertex - ignoring the D tracks, which are inferred and not directly measured by the Microstrip detector - is only of the order of 1 in photoproduction, while it is more substantial at the collider, allowing for a better determination of the pr imary vertex location. The average L/σ_L are 29. for E687 and 32. at the co llider.

Note also that the mass resolution at the collider is a bit worse at the collider. The mass resolution at the D for E687 is about 10 to 13 MeV/c^2 for E687 and at the collider is of the order of 19 MeV/c^2. This is due to the increase of the number of wide angle tracks at the collider. Such tracks have to be reconstructed at the edge of the acceptance, where magnetic corrections as well as multiple scattering effects are a bit tricky to handle. Most importantly, although the relative momentum resolution increases as the track momentum increases (due to larger magnetic deflections), the error on the opening angle at the decay or production vertex increases substantially, leading to an overall increases of the error on the invariant mass. Fortunately, this degradation is small and manageable. Possible improvements could probably be achieved by working harder on magnetic field corrections. In addition, one will have to be more careful on the amount of material in such spectrometer, as multiple scattering degrades the overall spectrometer performance faster in a Collider setting than in the Fixed Target case.

A similar calculation can be done for a typical all-charged B decay, e.g., $B^- \to D^+\pi^-\pi^-; D^+ \to K^-\pi^+\pi^+$. The abbreviated result is shown on Table 2 and demonstrates clearly that, as expected, the E687 spectrometer performs significantly better for Charm than for Beauty. As E687 has not yet shown a B signal corresponding to this decay mode, the final analysis cuts are uncertain[3]. The number on the last section of Table 2 refers to the D analysis cuts discussed above, and corresponds to the D acceptance, not the full B final state. Assuming that the efficiency on the B vertex selection is 100 %, one can deduce an acceptance of 0.6 % for B at the collider, while the corresponding number for Charm at the collider is 3.1 %.

5. BACKGROUND STUDIES

In addition to luminosity and acceptance issues, a crucial factor is obviously the signal to noise. While the background in the F.T. photoproduction case has been clearly identified and measured accurately, the background level at the collider is a bit speculative. In the following study, one has assumed that the individual performance of each system (PWC, Microstrip, Cerenkov counters..) is as good at the collider as it currently is at the fixed target laboratory.

[1]Isolation cut type 1 refers to the probability that one of the daughter track from the D points back to the primary

[2]Isolation cut type 2 refers to the probability that a spectator or a primary track points back to the D vertex

[3]Assuming that the gluon-fusion model prediction is correct, during the last fixed target run, about 13,000 B's were produced, 2.5 decaying into this particular mode. Taking into account the acceptance, the chance of observing one event in this decay mode is dim !

Table 1. Comparison of Acceptance and Reconstruction Efficiency for Charm

Acceptance stage	Acc. (%) Photoproduction, Fixed Target	$P-P$, Collider
Crude Kinematics	-	-
D^+ within 250 mrad.	99.	29.
Triggering	-	-
Master Gate	86.	73.
Multiplicity (Low)	64.5	57.
Multiplicity (High)	61.	53.4
Hadronic, Low threshold	94.	81.6
Hadronic, High Threshold	89.	74.
Level I- II Trigger	55.	46.4
PASS1 Reconstruction	-	-
Kaon reconstructed	47.	13.
Kaon rec. and identified	40.	8.
$K\pi\pi$ recon. and ident.	29.	4.4
Charm Analysis Cuts	-	-
EZDEE Charm selection	$17.2 \pm .05$	$3.1 \pm .2$
High Purity Vertex cuts	$7.8 \pm .3$	$1.4 \pm .1$

Table 2. Comparison of Acceptance and Reconstruction Efficiency for Beauty.

Acceptance stage	Acc. (%) Photoproduction, Fixed Target	$P-P$, Collider
PASS1 Reconstruction	-	-
Kaon reconstructed	6.	15.
Kaon rec. and identified	5.0	6.3
$K\pi\pi$ recon. and ident.	3.3	2.4
$\pi\pi K\pi\pi$ recon., identif.	1.9	0.9
Charm Analysis Cuts	-	-
EZDEE Charm selection	$2.5 \pm .2$	1.5 ± 0.1
Final Vertex cuts	$1.3 \pm .1$	0.64 ± 0.08

5.1 *Fixed Target, Photoproduction*

It has been shown that, for most if not all of the Charmed final states E687 has analysed, the dominant background is due to Charm itself, e.g. other topologies or final states contribute to the background under the fully reconstructed final state of interest[4]. If one considers carefully the background in a mass region where this Charmed background is minimum, but relevant. For golden decay mode of the D, this corresponds to a region characterised by $M_D \approx 1.940$ GeV. One can show that the next background source to deal with is due to hadronic reinteraction in the Beryllium target. This is after the events have been cleaned out of multiple incident photons. Typical signal to noise ratios (measured at the peak of the Gaussian mass bump) $R = d(N_{signal}))/d(M)/d(N_{background}))/d(M)$ are about 20 to 1 using th e high purity vertex cuts.

5.2 *Collider.*

At the collider, the widely believed presumption is that the charged multiplicity at the primary vertex is too high, masking the secondary decays. In fact, this higher multiplicity is a benefit, even with a rather modest (by current collider standards) 12-plane SVX detector. In order to show that this detector can handle collider backgrounds, two distinct Monte-Carlo runs have been analysed using the cuts described in the previous section.

In the first run, one has considered $c-\bar{c}$ pairs, where charmed mesons are let free to decay following the dominant modes specified in the blue book. Using identical vertex cuts, the signal to noise is approximately 15 to 1, or be tter. Note that the cuts used have not been optimised for the collider. In the second run, 100,000 minimum bias events - where Charmed or B particles have been removed - were generated and subjected to the same analysis. Very few false secondary vertices were accepted in the signal region. Although more statistics is needed, probably along with cuts more appropriate to the collider kinematics, this calculation shows that minimum biased events at the collider are less of a problem than anticipated.

Hadronic reinteractions in the target, or embedded pairs due to photon conversion are unique to the fixed target photoproduction experiment, and do not exist at the collider. Note that multiple interactions at the collider can easily be distinguished from secondary vertices, by either momentum balanced cuts (assuming that we have a two arm spectrometer), or by requiring that the secondary vertices be transversely detached from the beam crossing region. Thus, it is anticipated that, using current (or older!) technology, the background at the collider will be less of a problem than at fixed target.

6. OUTLOOK

About 6.6 million charm pairs have been produced at the E687 Beryllium target during the last fixed target run. Calling this a 10^7 seconds year of running, this gives roughly a measured production rate of 1/sec, out of which $\approx 1\%$ decay into an all-charged final state that can be reconstructed, identified and triggered upon. If the charm cross section at the Tevatron collider is about one milibarn, at an achievable luminosity of 10^{31}, the production rate is 10,000/sec. This study shows that, using the same spectrometer, the acceptance and efficiency at the collider is only a factor 5 smaller than the one at Fixed Target. In addition, the ratio of the Charm cross section to the total cross section is most likely higher at the collider than it is at fixed target. This means triggering is relatively easier at the collider. Finally, the background is expected to be as manageable - if not more - at the collider than it is at fixed target, due to the absence of target and favorable cross section ratios .

Prior to consider a serious proposal for such a spectrometer a few closing remarks are appropriate:

- The E687 SVX detector design will of course not work at the collider, where nothing can be placed within at least 2mm of the beam during collision and at $\approx 1cm/$ during shot setup and scraping. In addition, the luminous region covers at least 30 cm., not 4 cm. But this problem has already been addressed in various proposals.
- As one of the physics goal is charm mixing or doubly Cabbibo suppressed decays, whether it is at the collider or at fixed target, the dominant background for these processes is due to Cabbibo allowed decays. The only way to reduce this background is not to work on tracking or vertexing, but to strengthen the Cerenkov identification. This probably means Ring Imaging technology. Once again, recent progress has been achieved, albeit at a non negligible cost. This also will also reduce the length of the spectrometer and make the collider implementation easier.
- As previously mentioned, multiple scattering and/or interactions of prompt particles in the spectrometer materials must be minimized. More R&D is probably required for the front end of such a spectrometer.

7. ACKNOWLEDGEMENTS

I wish to acknowledge the crucial input from the E687 collaboration, and, in particular, from Joel Butler for having stress the relevance of a benchmarked Monte-Carlo and reconstruction package. I also had very useful discussions with Lynn Garren and, while at Snowmass, with members of the tracking group.

8. REFERENCES

1. See for instance the list compiled by Jeff Appel and Vera Luth for the B-Physics workshop, June 1993 at Snowmass
2. P. L. Frabetti *et al.*, Nucl. Instr. and Meth. in Phys. Res., sect. A **320**, 519 (1992).
3. Pythia 5.6 and Jetset 7.3 Physics and Manual, Torbjorn Sjostrand, CERN-TH 6488/92
4. P. Lebrun, *What is the Charm background made of ?* E687 memo, May 1993.

e and γ Detection

Convenors:

E.C. Dukes
University of Virginia/
Superconducting Super Collider Laboratory

H. Paar
University of California -San Diego

List of Participants

K. Byrum
Argonne National Laboratory

L. Camilleri
CERN

N. Denisenko
Fermi National Accelerator Laboratory

P. Eerola
CERN

P. Limon
Fermi National Accelerator Laboratory

J. Marques
Northwestern University

C. Park
Fermi National Accelerator Laboratory

A. Peryshkin
Fermi National Accelerator Laboratory

B. Wicklund
Argonne National Laboratory

SUMMARY OF THE ELECTRON ID GROUP

E.C. Dukes
University of Virginia,
Charlottesville, VA 22901, USA

1. INTRODUCTION

Lepton identification is extremely important for any B physics experiment attempting to measure CP violation. The reasons are obvious: 1) single lepton triggers operate on 44% of *all* $b\bar{b}$ pairs; 2) lepton triggers are the only triggers (outside of secondary vertex triggers) that are feasible for a variety of important B decay modes: for example, $B^\circ \to D^+D^-$, $B^\circ \to J/\psi K_s$, and $B_s \to K_s\gamma$; and 3) events triggered with leptons are already tagged. Although having both electron and muon systems adds to the cost and complexity of the detector, there are several reasons why both electron and muon triggers and detectors should be used.

- Yields for CP modes in any foreseen B experiment are low and provide little extra margin of safety, particularly if the CP asymmetries are on the low end of the theoretical predictions. Having an electron as well as a muon trigger gives at least a factor of two gain in yield as well as increased tagging efficiency.

- For a fixed target experiment and a forward collider detector, the forward region is inhabited by leptons with very large momenta. Magnetic spectrometers have a momentum resolution which degrades with increasing momentum whereas calorimeters have a resolution which improves with increasing momentum. In addition, muons with very high energies lose a considerable amount of energy in dense matter due to radiation [2], further worsening the energy resolution.

- In theory, an electron trigger can have an arbitrarily small transverse momentum threshold whereas the muon threshold — for a central collider detector — has a hard lower limit determined essentially by the rather large amount of material ("iron cutoff") the muon must traverse to be unambiguously identified as a muon. Although for CDF and D0 this theoretical limit is rather soft: 1.5 GeV and 3.0 GeV respectively, for the collider detectors planned for the SSC and LHC it is much higher: 6.0 GeV and 10.0 GeV respectively for Atlas and SDC.

- Finally, redundancy is important. Recent experience with large collider detectors has shown that the muon and electron detectors do not always perform equally well.

Most dedicated experiments which propose to search for CP violation in the B system have not given electron identification the same consideration as muon identification. One reason for this is the prevailing opinion that electron identification will be difficult, particularly at the trigger level, due to the presence of large backgrounds. Although the backgrounds to B decay electrons are larger than those to muons, they are not overwhelming and can be eliminated. An example of how well one can identify electromagnetic final states in the presence of large backgrounds is given in the paper by Marques and Rosen showing that charmonium states can be resolved in the presence of a background a million times larger [3].

The electron identification group (whose participants are listed in [1]) focused its efforts on learning what state-of-the-art *collider* detectors are doing in electron identification. To this end we entertained several talks each from the CDF and D0 collaborations at Fermilab, as well as several talks from proposed SSC and LHC experiments. (See papers by Byrum, Denisenko and Peryshkin in these proceedings). Each talk was followed by lively discussion. We also attempted to understand what the backgrounds to electron identification will be at the new higher energy hadron colliders — the SSC and LHC — our prejudice being that only these machines will have the energy and luminosity needed to see CP violation in the B system. None of the approved experiments at the SSC or LHC is optimized for B physics. Hence we focused on dedicated forward collider and fixed target detectors. We report here mainly on these latter studies.

2. ELECTRON MOMENTUM FROM B SEMILEPTONIC DECAYS

To get an idea of the momenta of interest we have plotted in Fig. 1 the average electron momentum at SSC fixed target ($\sqrt{s} = 194$ GeV) and collider energies ($\sqrt{s} = 40$ TeV). Note the large momenta at small angles: in fixed-target mode the average electron momentum is approximately 500 GeV at 3 mrad, the smallest SFT angle [4], and in collider mode it is approximately 200 GeV at a pseudorapidity of 5.5 (8 mrad), slightly larger than the smallest COBEX angle [5]. Muons at these momenta are difficult to measure well. The dynamic range is rather large: 25 GeV to 1,000 GeV in fixed target mode and 5 GeV to 200 GeV in collider mode.

The transverse momentum of leptons from B semileptonic decays is shown in Fig. 2 for fixed target and collider modes at the SSC. Shown is the fraction of $B \to e^{\pm}X$ events that survive a given cut on the electron transverse momentum. The B's are not produced with large transverse momenta and hence, for yields needed to measure CP asymmetries, fairly soft transverse momentum cuts need to be made.

3. TOOLS OF ELECTRON IDENTIFICATION

The tools of electron identification are many. They are listed below in Table 1 along with a rough estimate of their useful momentum range. There is not space here, nor did we attempt in this session, to review the performance of the various methods of electron identification. Further information can be found in references [6]-[8] as well as in the literature. Some very general criteria for any electron detector can be given. It must be fast enough to function in interaction rates of 10^7 s^{-1} and up. It must also be relatively radiation

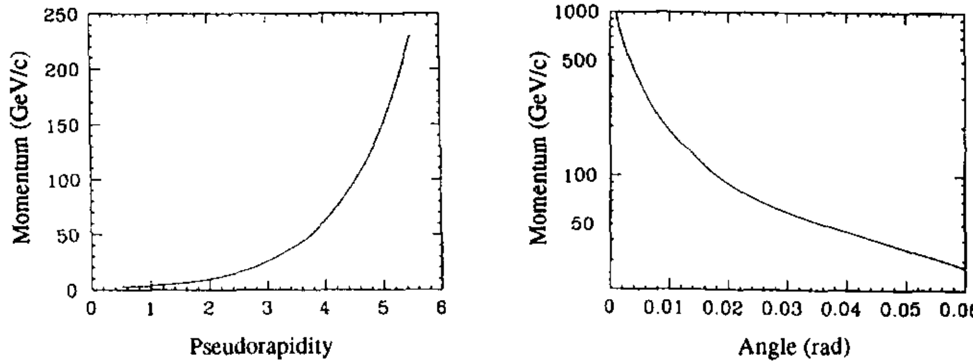

Figure 1: The average momentum of electrons from B semileptonic decays at the SSC as a function of angle for the fixed-target mode ($\sqrt{s} = 194$ GeV) and as a function of pseudorapidity for the collider mode ($\sqrt{s} = 40$ TeV).

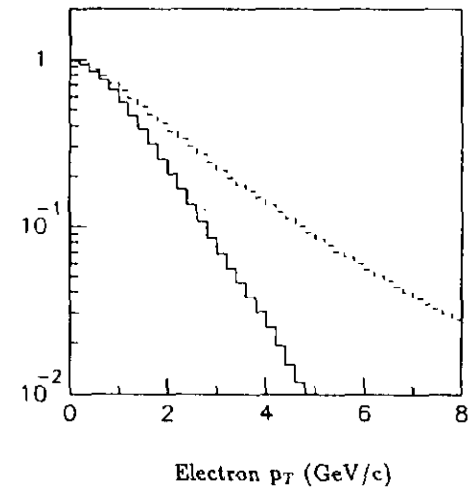

Figure 2: Fraction of semileptonic B decays surviving an electron transverse momentum threshold at $\sqrt{s} = 194$ GeV (solid curve) and $\sqrt{s} = 40$ TeV (dashed curve).

hard, particularly in the forward regions. Finally, the electron detector must work well at the trigger as well as the analysis level. This last requirement is the most severe — the interaction rate must be reduced by a factor of about 1,000 at the first trigger level [9].

Table 1: Tools of electron identification.

Method	Momentum (GeV)
Calorimetry	
Electromagnetic	1–1,000
Hadronic	3–1,000
Tracking	1–1,000
E/P	1–300
TRD	1–100
Cerenkov	
Threshold	1–60
Rich	1–60
dE/dx	<5
Time-of-flight	<1
Synchrotron Radiation	50–1,000

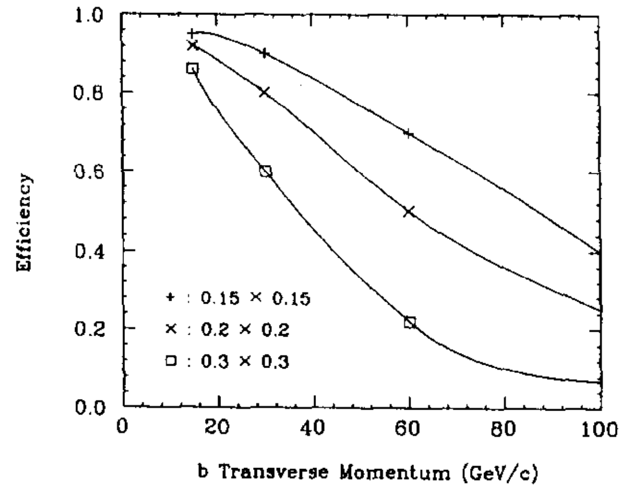

Figure 3: The efficiency for $B \rightarrow e^{\pm}X$ decays as a function of the transverse momentum of the b quark and for three different $\Delta\eta \times \Delta\phi$ cell sizes for the SDC detector (Had/EM < 0.04).

3.1 *Calorimetry*

By far the most useful tool is electromagnetic and hadronic calorimetry. This is particularly true at the trigger level where there is much experience with calorimeter triggers. Electromagnetic calorimetry alone can provide factors of approximately 100 in hadron rejection with good electron efficiency based on longitudinal and lateral shower shape differences. (See, for example, ref. [10].) Good calorimeter segmentation, preshower, or shower maximum detectors, are needed to get good hadron rejection factors. Another order of magnitude or so in rejection can be obtained using E/P cuts. Such cuts, however, are difficult to make at the trigger level. Rejection factors are extremely detector dependent as well as momentum dependent.

Hadronic calorimetry in conjunction with electromagnetic calorimetry provides even higher rejection factors while retaining good electron efficiency. Present collider detectors — CDF and D0, for example — use cuts on the fraction of energy in the hadronic calorimeter to that in the electromagnetic calorimeter (Had/EM cuts) to select electron candidates. Care must be taken, however, that the signal $B \rightarrow e^{\pm}X$ not be rejected with such cuts, for example, when electrons occur in jets.

In the central region ($y \approx 0$) Had/EM cuts are not deadly to B's except those with large transverse momentum. Figure 3, from an SDC simulation by Barry Wicklund [12], shows the efficiency for semileptonic B decays in SDC as a function of the b-quark transverse momentum for three different $\Delta\eta \times \Delta\phi$ cell sizes and for Had/EM < 0.04. The efficiency is quite high at all but the highest transverse momenta and is highest for the smallest cell sizes. The hadronic cell size cannot be made arbitrarily small without greatly reducing the hadronic rejection factor. With the smallest cell size shown in Fig. 3 (0.15 × 0.15) one is still safe. At SSC energies the average angular separation between a B semileptonic decay electron and the nearest hadron is approximately 200 mrad at $|y| < 1$. This corresponds to a distance of 35 cm at 1.75 m, the radius at which the SDC calorimeter starts. The SDC hadronic cell size (0.1 × 0.1) corresponds to 17.5 cm^2. A hadronic shower will deposit most of its energy within this cell size [11].

In the forward region of a collider detector, or in a fixed target experiment, the problem of hadrons overlapping electrons is much worse. Although the size of the calorimeter needed for a given rapidity coverage is reduced by $\Delta y \simeq \Delta\theta/\sin\theta$ in the forward region of a collider detector, this savings comes at a price. At very forward rapidities — a rapidity of 5.5, for example — the average angle between the electron from B semileptonic decays and the nearest hadron is only 4 mrad. This corresponds to 8 cm at 20 m, a typical distance of a forward collider calorimeter from the interaction point. Unlike the case at $y = 0$, this separation is smaller than hadronic shower sizes for even the most compact calorimeters and hence Had/EM cuts cannot be used for forward rapidities. The same is true for the forward region of a fixed target experiment.

3.2 *Other Techniques*

Other techniques of electron identification are not nearly as useful as calorimetry, particularly for central collider detectors. Time-of-flight cannot be used at energies over a few hundred MeV for flight paths of the order of a meter. Ionization measurements (dE/dx) have been successfully used in e^+e^- collider detectors, such as the TPC and OPAL [13], to discriminate between various particle species, including electrons and pions. Recently

CDF has also had a measure of success in separating electrons and pions in their central tracking chamber. The requirements for good dE/dx measurements, however, are in general inconsistent with the requirements of a high-rate B experiment. Nor can dE/dx be used effectively at the trigger level.

Ring imaging Cerenkov detectors (RICH) also cannot be used effectively at the trigger level. They suffer from the added disadvantage of being too large for central collider detectors, except when liquid or solid radiators are used. There are, however, no suitable liquid radiators for $e\pi$ separation in the momentum range of interest. In addition, RICH detectors are essentially the only means of kaon identification and it is difficult to find radiators optimized for $K\pi$ separation as well as for $e\pi$ separation.

Transition radiation detectors (TRD) have been used successfully for electron identification [14]. Like RICH's, they are not very effective at the trigger level, although E715 at Fermilab managed to get a pion rejection of 40 at the trigger level [15] (and a factor of 1,600 rejection at the analysis level, with an electron efficiency of 99.5%). TRD's have been used in collider detectors — UA2 and D0 — but they have not been terribly successful. The reason for this is lack of space. It is extremely difficult to get high rejection factors with short TRD's. The E715 TRD is 360 cm long whereas the UA2 and D0 TRD's are only 21.5 cm and 31.5 cm long respectively. Despite this, Atlas is planning on employing TRD tracking detector which should give a pion rejection from 10 to 1,000 (for an electron efficiency of 0.90) depending on the rapidity. This rejection is luminosity dependent, dropping off by about an order of magnitude in going from 1×10^{33} to $2 \times 10^{34}\mathrm{cm}^{-2}\mathrm{s}^{-1}$.

4. BACKGROUNDS AT THE SSC TO A SINGLE ELECTRON TRIGGER

To achieve a 50% efficiency for $B \to e^{\pm}X$ decays, thresholds of 1.2 GeV and 1.8 GeV are respectively needed for fixed target and collider experiments at the SSC. Because the collider cross section is a factor of 1,000 greater than the fixed target cross section, the collider electron trigger threshold can be raised higher to get an equivalent number of B events. The geometric acceptance of fixed target experiments, however, is larger than collider experiments — forward or central — and so one cannot push the collider p_T threshold too high and still achieve equivalent B rates.

There are (at least) six types of backgrounds to electrons that must be eliminated at the trigger level as well as analysis level. They are listed in Table 2 along with the tools that can be used to eliminate them. The rates of each of these backgrounds is detector dependent, but an idea of their relative magnitudes, as a function of the transverse momentum threshold, is given in Fig. 4 for fixed target and collider experiments at the SSC. The equivalent minimum bias trigger rate for each of the backgrounds, assuming that a 50% trigger efficiency is desired for $B \to e^{\pm}X$ decays, is given in Table 3, as well as the needed rejection factor to get a factor of 10^4 reduction in the rate.

4.1 *Conversion Electrons*

The top left figure shows the rate (per minimum bias event) of $\gamma \to e^+e^-$ conversions assuming a 10% conversion probability. Pythia minimum bias events were generated to make this plot and the electron (or positron) with the highest p_T was taken. The rate is 1×10^{-4} in fixed target mode and 1×10^{-2} in collider mode. Note that the average gamma multiplicity

Table 2: Backgrounds to electron identification.

Background	Tools	Comments
$\gamma \to e^{\pm}$ conversions	Tracking	Upstream conversions difficult at trigger level.
Dalitz decays	Tracking	Impact parameter cut needed.
Gammas	Tracking, TRD	Fairly easy at trigger level.
Gamma charged hadron overlap.	Tracking and shower shape, E/P, TRD, Had/EM	2^{nd} and 3^{rd} level.
Charged hadrons	Shower shape, E/P, Had/EM	Easy at level 1.
$D \to e^{\pm}X$	p_T cut	Not a problem.

Table 3: Rough estimate of background rejection rates needed to reduce the minimum bias trigger rate by 10^4 in fixed target and collider modes at the SSC, while retaining 50% of the B events.

	Fixed Target		Collider	
$B \to e^{\pm}X$ efficiency	0.5		0.5	
p_T threshold	1.2 GeV		1.8 GeV	
	Rate	Rejection	Rate	Rejection
$\gamma \to e^+e^-$ (10%)	1×10^{-4}	.1	1×10^{-2}	100
γ	1×10^{-2}	100	2×10^{-1}	2,000
γ hadron overlap	8×10^{-4}	8	5×10^{-2}	500
$\pi^{\pm}K^{\pm}$	8×10^{-2}	800	5×10^{-1}	5,000
D $\to$ eX	1×10^{-5}	1	3×10^{-3}	30

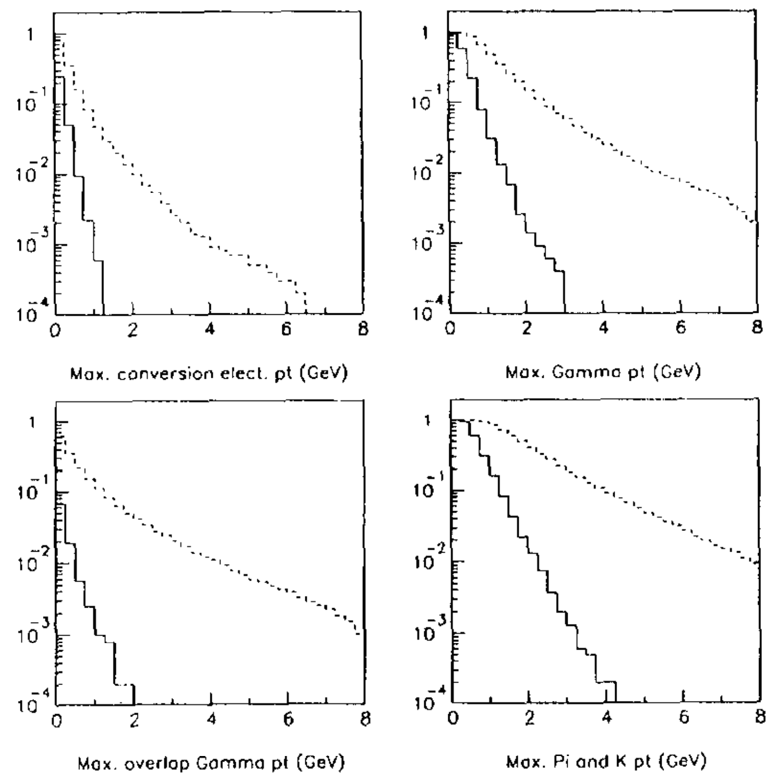

Figure 4: Rate per minimum bias event of various backgrounds to a $B \to e^{\pm}X$ trigger as a function of the transverse momentum threshold and for fixed target, $\sqrt{s} = 194$ GeV, (solid curve) and collider, $\sqrt{s} = 40$ TeV, (dashed curve) energies. Top left: the $\gamma \to e^+e^-$ rate (with 10% conversion probability). Top right: the γ rate. Bottom left: γ charged hadron overlap rate. Bottom right: charged pion and kaon rate.

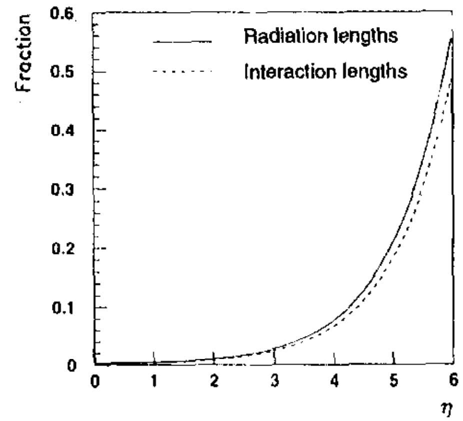

Figure 5: Material a particle traverses in a 1 mm thick Be beam pipe as a function of pseudorapidity. The solid curve gives the amount in radiation lengths and the dashed curve gives the amount in interaction lengths.

in a "typical" SSC forward collider experiment (1.5 < y < 5.5) is 28 out of a total of 104 gammas and for a "typical" fixed target experiment ($5 < \theta < 75$ mrad) is 8 out of a total 21 gammas. The 10% conversion probability used to make Fig. 4 may be an underestimate. For example, although the 4% λ_I silicon active target of the SFT proposal is 21% of a radiation length (gammas see on average half this length), there is approximately another 5% of a radiation length of material in the spectrometer. For forward collider detectors the radiation length is less than 10% at small rapidities, but it increases rapidly with increasing rapidity due to the beam pipe, until at $\eta = 5$ is over 20% for a 1 mm thick Be beampipe (see Fig. 5). Reducing the problem with novel beam pipe designs has been discussed in several references [16]–[17], but it appears that these is no satisfactory solution to the problem.

Conversion electrons can only be eliminated by tracking. Hence they are difficult to get rid of at the first trigger level. If the conversion occurs early enough it is almost impossible to eliminate at any trigger level, if not the analysis level. Fortunately, conversion electrons tend to have small transverse momenta because the gammas come almost exclusively from pizero decays and hence on average only have half the transverse momentum of the pizero, and because in the conversion, on average, the electron or positron only has half the transverse momentum of the gamma. They are not the major background for either fixed target or collider modes.

4.2 *Gammas*

The top right-hand plot in Fig. 4 shows the minimum bias gamma rate as a function of the gamma p_T threshold (again, for fixed target and collider modes at the SSC). Gammas that don't convert are easy to eliminate using either a track stub shower matching requirement or a TRD requirement. To reduce the rate by 10^1 a reduction of roughly 100 is needed in fixed target mode and 2,000 in collider mode. The latter may be somewhat difficult to achieve.

4.3 Gamma Charged Hadron Overlap

The rate, shown in the bottom left-hand plot of Fig. 4 is for stable charged hadrons which lie within a $\Delta y \times \Delta\phi = 0.1 \times 4^\circ$ of a gamma, a rather generous overlap except for the most forward regions. There are many tools available to eliminate this background: track shower matching, E/P cuts, Had/EM cuts, as well as TRD cuts. It does not appear to be a problem.

4.4 Charged Hadrons

The rate of charged pions and kaons is shown in the bottom right-hand plot of Fig. 4. It is the largest background, but the easiest to eliminate. A large part of the rate is reduced by the fact that most electromagnetic calorimeters are relatively hadron blind and hence only see a fraction of the hadronic p_T. Shower shape, E/P and Had/Em cuts can reduce the rate further to the desired level.

5. CONCLUSIONS

It appears that single electron triggers with high efficiency for $B \to e^{\pm}X$ decays are possible, both for fixed target and collider detectors at SSC (and LHC) energies. Backgrounds, *for a given B efficiency*, are smaller in fixed target experiments, but this advantage is offset by the need for higher efficiencies due to the much smaller cross section at fixed target energies. The additional space that fixed target and forward collider detectors have over central collider detectors makes more electron identification tools available. This advantage is somewhat offset by the problems in the very forward region for a fixed target and forward collider detector. For example, Had/EM cuts cannot be used in the forward region, and E/P cuts lose their power. Electromagnetic calorimetry will undoubtedly be the major tool of electron identification — and perhaps will suffice alone — but only with improvements over calorimeters in exisiting collider experiments: including better momentum resolution, granularity and preshower detectors.

The major challenge is getting enough electron identification at level 1 to get the minimum bias trigger rate down by the factor of 1,000 or so that is needed. If this can be done — and it will require some tracking at level 1 — then trigger thresholds for electrons in central collider detectors can be set lower than the "iron threshold" of typical muon systems. Further reductions to get to the tape writing bandwidth can be obtained easily at levels 2 and 3.

6. ACKNOWLEDGEMENTS

We thank the organizers of the workshop for their efforts in preparing this successful meeting, and the members of the electron identification group for many stimulating discussions. This work is supported in part by the US Department of Energy.

7. REFERENCES

1. Participants of the electron identification group included: K. Byrum, L. Camilleri, D. Coupal, N. Denisenko, E. Dukes (convener), P. Eerola, J. Giomataris, P. Limon, J. Marques, H. Paar (convener), C. Park, A. Peryshkin, J. Rosen and B. Wicklund.
2. W. Lohmann, R. Kopp, and R. Voss, "Energy Loss of Muons in the Energy Range 1–10,000 GeV," CERN Report 85-03 (1985).
3. J. Marques and J. Rosen, these proceedings.
4. The SFT Expression of Interest, SSC-EOI0014, May 1990.
5. S. Erhan, M. Medinnis, P.E. Schlein and J.G. Zweizig, Nucl. Instr. and Meth. **A333** (1993) 101.
6. G. Brandenburg et al., *Identification of Electrons at the SSC*, Proceedings of the 1986 Summer Study on the Physics of the Superconducting Supercollider, June 23–July 11, 1986, (ed. by R. Donaldson and J. Marx), p. 420.
7. G.B. Yodh et al., *Electron Identification*, Proceedings of the 1984 Summer Study on the Design and Utilization of the Superconducting Super Collider, June 23-July 13, 1984, Snowmass, Colorado, Ed. R. Donaldson and J.G. Morfin, p. 523.
8. *Report of the Working Group on Muon, Electron and Hadron Identification*, Report of the Task Force on Detector Research and Development for the Superconducting Super Collider, SSC-SR-1021, June 1986, p. 159.
9. See the summary paper on Electronics, DAQ and Computing, these proceedings.
10. Y. Fukui et al., e/π Separation in the CDF End Plug EM and Hadronic Calorimeters, *Identification of Electrons at the SSC*, Proceedings of the 1986 Summer Study on the Physics of the Superconducting Supercollider, June 23–July 11, 1986, (ed. by R. Donaldson and J. Marx), p. 417.
F. Berger et al., Nucl. Instr. and Meth. **A321** (1992) 152.
D. Acosta et al., Nucl. Instr. and Meth. **A302** (1991) 36.
Engleman et al., Nucl. Instr. and Meth. **A216** (1983) 45.
11. D. Acosta et al., Nucl. Instr. and Meth. **A316** (1992) 184.
12. B. Wicklund, *B-jet Tagging Using Electrons at SDC*, SDC91-00051.
13. M. Hauschild et al., Nucl. Inst. and Meth. **A314** (1992) 74.
14. B. Dolgoshein, Nucl. Instr. and Meth. **A326** (1993) 434.
15. A. Denisov et al., preprint Fermilab-Conf-84/134E (1984).
16. K.T. McDonald, *Beampipes for Forward Collider Detectors*, Princeton/HEP/92-0, August 7, 1992.
17. J.D. Bjorken, *Beampipe Geometries for FAD*.

IMPROVEMENT IN THE CDF L2 ELECTRON TRIGGER USING THE CENTRAL SHOWER MAX DETECTOR

Karen L. Byrum
High Energy Physics, Argonne National Laboratory,
9700 South Cass Ave., Argonne, Illinois 60439 USA

1. INTRODUCTION

As part of a trigger upgrade for CDF run 1b, new electronics will bring the central shower max detector (CES) into the "level-2" trigger algorithm. This upgrade will allow the trigger to select electrons within a finer segmentation in the $r-\phi$ view. This will be achieved by requiring a pulse height in the shower max detector be associated with a projected track from the central fast tracker to within 2 degrees. In CDF run 1a, the track was only required to point to the same 15 degree wedge as the electron electromagnetic cluster. This tighter matching will decrease the "level-2" electron cross section by about a factor 2, while maintaining the electron purity.

2. THE CDF TRIGGER

The CDF trigger employs a "level-3" processor farm, which does offline reconstruction to select highly enriched event samples for physics analysis. The input to this farm is provided by the "level-1" and "level-2" triggers, which use fast analogue signals from the calorimeter and raw TDC information from the central tracker and muon chambers, to define electron, muon, jet and missing E_t trigger objects. To match the bandwidth of the hardware Event Builder and the level-3 farm, the level-2 accept rate is constrained to be less than around 35 Hz, or 3000 nb at a luminosity of 10^{31} cm^{-2}s^{-1}. The CDF single electron trigger, with a 9 GeV threshold, has a "level-2" accept rate of 500 nb , or about 18% of the total bandwidth. The actual electron purity is around 7% or 30 nb after "level-3" and offline processing [1].

2.1 The Level-1 Trigger

The CDF calorimeter cells are 0.1 (η) by 0.25 (radians) for both the electromagnetic and hadronic calorimeters. In the central region of $|\eta| < 1.$, there are a total of 20 η by 24 ϕ towers. The CDF "level-1" electron trigger requires one trigger cluster with $E_t > 6$GeV where a trigger cluster is defined to be 0.2 η by 0.25 (radians).

2.2 *The Level-2 Electron Trigger*

The "level-2" electron trigger matches a stiff track to an electromagnetic cluster. The electromagnetic cluster is defined to be a cluster which:

1. Satisfied $Had/Em < 12.5\%$ where the hadronic energy is the energy in the hadronic trigger towers underneath the EM towers in the cluster;
2. Was found by the EM cluster-finder, *i.e.* there were trigger towers with $E_t > 9$ GeV in the seed tower and $E_t > 7$GeV in the shoulder tower or $E_t > 6$ GeV in the seed tower and $E_t > 5$ GeV in the shoulder tower.

A stiff track was defined as a track found by the central fast tracker with $P_t > 9.2$ GeV/c for the $E_t > 9$ GeV electron trigger or $P_t > 6$ GeV/c for the $E_t > 6$ GeV electron trigger. A "level-2" electron trigger required the track point to the same ϕ wedge as the electromagnetic cluster. The new trigger upgrade requirement would require the stiff track extrapolate to a CES wire cluster above a threshold where the CES cluster would be in the same hemisphere (east or west) as the EM cluster and the ϕ match would be within approximately 2 degrees.

3. THE TRIGGER UPGRADE

The upgraded "level-2" trigger electronics would consist of both upgraded front end rabbit electronics boards [2] called XCES plus surface mounted fastbus electronics boards called CERES. The XCES cards will cluster the CES wires into groups of 4. A CES module is a rectangular chamber of dimensions 48 cm x 115 cm which contains 32 wires approximately 1.45 cm apart in the $r-\phi$ view. Each group of 32 wires is read out by a single Rabbit electronics card. In addition, cathode strip pads (not used by XCES) separate the CES module into 5 cells in the $r-\theta$ view. The XCES cards perform analog sums of the 4 clustered wires and generate a differential TTL high if this sum is above an adjustable threshold.

In the CDF geometry each 15 degree wedge contains 2 halves, one half-wedge for each hemisphere. Each half-wedge consists of two CES modules, separated at approximately $z = 121$ cm and located at a radius of 184 cm from the $p-\bar{p}$ interaction point. The XCES signals from the two modules in each hemisphere are then OR'ed together to provide 8 bits of information per half wedge.

The CERES board will receive the XCES signals along with the track information from the central fast tracker to determine if a "level-2" accept should be issued for each event.

4. ELECTRON LEVEL-2 TRIGGER RATES

The "level-2" trigger rates in CDF as a function of the calorimeter E_t threshold are shown in Figure 1. The top curve shows the baseline CDF trigger used in the 1992 run with a track P_t threshold set at either 9.2 GeV or 6.0 GeV for the two E_t thresholds. The bottom curves show the same rates with an additional strip chamber pulse height requirement, where the 2100 value is greater than 97% efficient for selecting electrons with $E_t > 7$ GeV and the 3500 value is greater than 85% efficient. The electron level-2 rates are listed in Table 1. Assuming the same electron "level-2" bandwidth of 500 nb will be available for run 1b, with

	σ(L2) (nb)	σ(Purity) (nb)	$\sigma(b \to eX)$ (nb)
$E_t > 9$ No XCES	500	30	10
$E_t > 9$ XCES	250	30	10

Table 1: CDF Level-2 Electron Cross Sections

a 100% XCES efficiency, the number of $B \to eX$ per pb^{-1} can be doubled by lowering the E_t threshold at "level-2".

5. TEST RESULTS FROM RUN 1A

During the last month of the 1992 run 1a, two XCES cards were implemented on one wedge of the CES detector. These signals were received by the CERES board which itself operated in a parasitic mode within the working "level-2" trigger. Figure 2 shows the efficiency of the XCES cards for XCES DAC = 60. This DAC setting corresponds roughly to an electron of $E_t = 5$ GeV or to an 85% efficiency of detecting electrons with E_t threshold of $E_t > 7$ and a P_t track of $P_t > 6$ GeV/c.

6. REFERENCES

1. J.W. Dawson, *et.al.* in *Digital Electronics for the Inclusion of Shower Max and Preshower Wire Data in the CDF Second-Level Trigger*, CDF-2069 (1993).
2. G. Drake, *et.al.*, in CDF Front End Electronics: The RABBIT System. Nuclear Instruments and Methods in Physics Research, A269 (1988) 68-81.

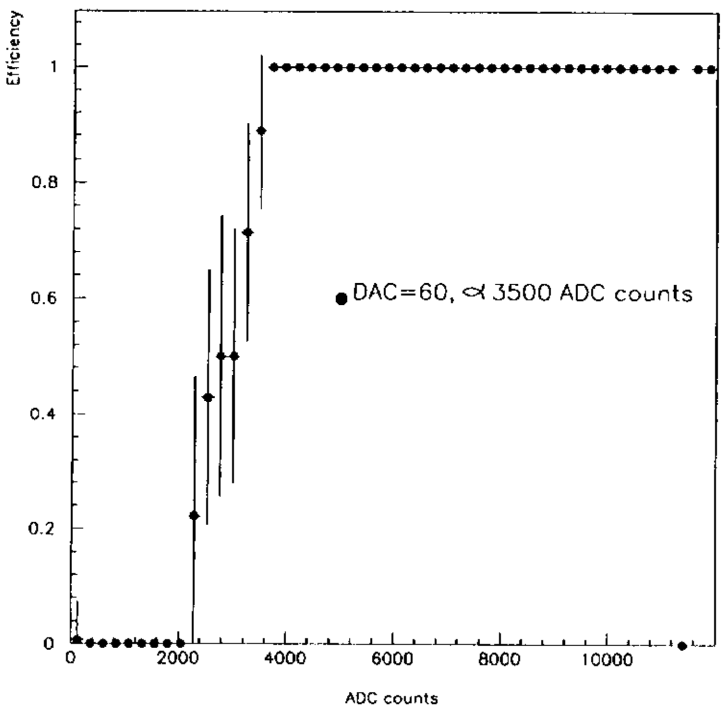

Figure 1. The "level-2" trigger rates as a function of the calorimeter E_t threshold.

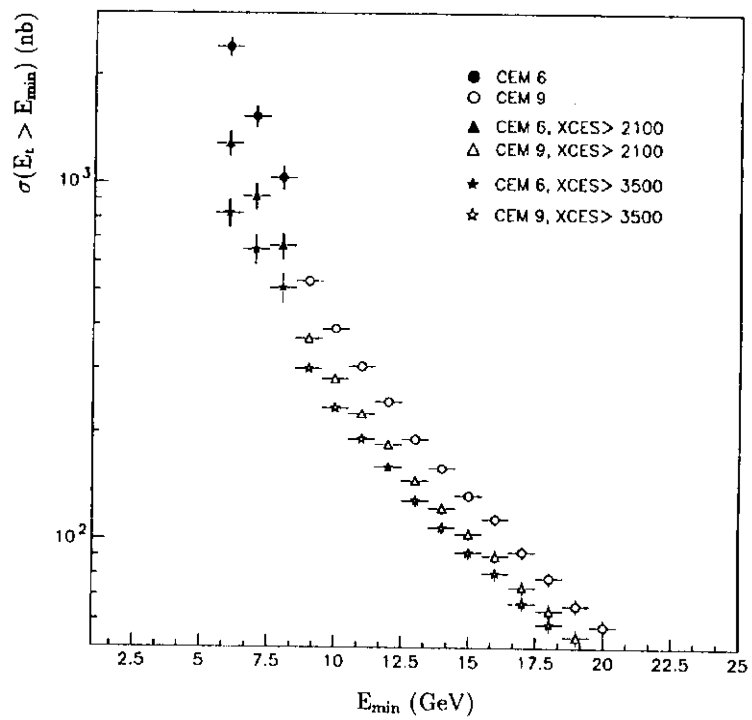

Figure 2. The efficiency of a typical XCES electronic card.

ELECTRON IDENTIFICATION IN THE D0 DETECTOR

NINA DENISENKO
Fermi National Laboratory
P.O.Box 500, Batavia, Illinois 60510

for the D0 collaboration

ABSTRACT

We present the characteristics of the D0 detector together with the methods applied to identify electrons. The electron identification technique uses calorimeter information together with data from the central tracking detectors. The fine longitudinal and transverse segmentation of the D0 calorimeter enables us to achieve very good pion rejection for electrons above 20 GeV. The D0 calorimeter also provides excellent linearity of response for electrons above 10 GeV. Here we present recent results of studies of energy response for electrons with energy down to 2 GeV and discuss necessary extensions of electron identification algorithms for B-physics studies.

1. INTRODUCTION

The D0 experiment has just completed its first collider run. The physics goals of this run included mostly the high p_t physics: top, electroweak, QCD, new particle searches and B-physics. It was demonstrated that the design aims of D0, excellent calorimetry, good energy resolution for electrons, photons and jets, high efficiency for events of interest were achieved. In addition to that during the first D0 collider run the opportunities to expand the physics menu to low p_t physics were studied. Because of the plans to increase the luminosity of the Fermilab Collider by 1995/96 up to several units of 10^{31} cm^{-2} sec^{-1} and to drop the bunch spacing to 400 ns (it is 3.5 μs now) it is planned to upgrade the central tracking system of the D0 detector in order to meet new demands. At the same time the upgraded tracking system will allow D0 to extend its measurement capabilities towards lower p_t B-physics such as mixing and CP violation in electron channels which makes it necessary to extend the existing electron ID technique to low energies.

Below we present characteristics of the D0 detector systems used for the electron identification. We also discuss trigger efficiencies, offline algorithms and results of simulation studies for electron identification for the upgraded D0 detector.

2. THE D0 DETECTOR

The D0 detector consists of three major systems: the calorimeters, the central tracking system and the muon system.

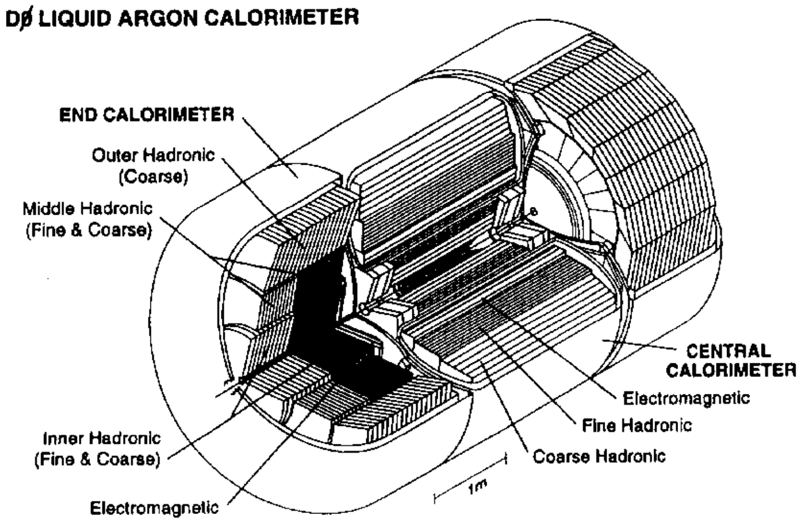

Figure 1. Cutaway view of the D0 calorimeters.

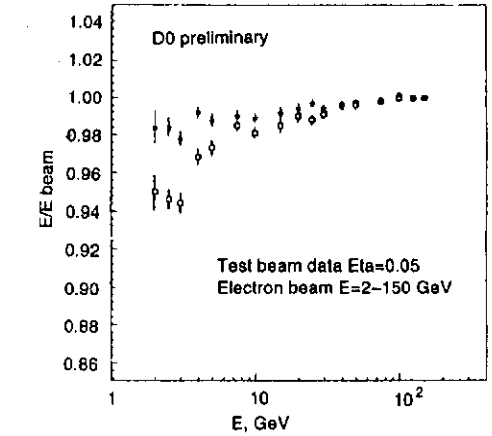

Figure 2. Energy reconstructed in the CC calorimeter normalized to the nominal test beam energy for electrons 2 - 150 GeV for two sets of sampling weights [5].

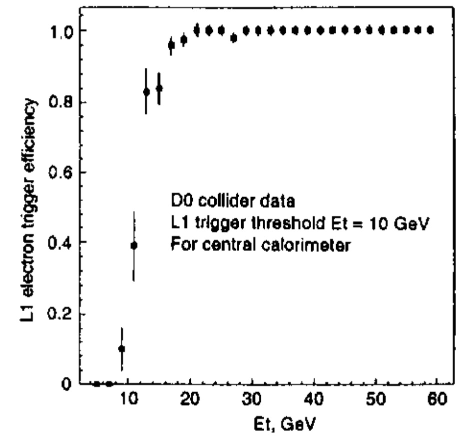

Figure 3. Efficiency of the Level1 electron triggers vs E_t of electrons.

The D0 calorimeters are uranium-liquid argon sampling calorimeters. There are three calorimeters of roughly equal size: a central calorimeter (CC) and two end calorimeters (EC). The cutaway view of the D0 calorimeters is shown in Fig. 1. The end calorimeters each have a ring of 16 outer hadronic modules; inside this is a ring of 16 middle hadronic modules and at the center is a single large inner hadronic module (ECIH). In front of the ECIH is a finely segmented electromagnetic calorimeter (ECEM). The central calorimeter consists a ring of Coarse Hadronic calorimetry, inside of which are the fine hadronic modules followed by the electromagnetic calorimeter (CCEM). The technical details of the calorimeter design can be found in [1,2].

The calorimeters provide full azimuthal ϕ coverage, where ϕ is the angle in the plane perpendicular to the beam. The central calorimeter covers the pseudorapidity region $|\eta| < 1.2$ and the end calorimeters cover $|\eta| > 1.4$ down to the beam pipe ($|\eta| \approx 4.2$). All electromagnetic calorimeter modules are longitudinally segmented into four layers. For the ECEM the longitudinal layers are respectively 0.3, 2.6, 7.9 and 9.3 radiation lengths thick. For the CCEM they are 2, 2 , 7 and 10 radiation lengths thick. Transverse segmentation of the calorimeter modules is provided by readout of the calorimeter cells as pseudo-projective towers of size 0.1×0.1 in η and ϕ space. The third longitudinal EM layer typically contains 65% of the electron shower energy and its transverse segmentation is made finer (0.05×0.05). The semiprojective tower geometry for EM modules lines up with fine hadronic modules behind them. The calorimeter modules were tested during several fixed target runs at Fermilab.

The EC calorimeter response to electrons with energies from 10 to 150 GeV was studied in the 1990 run [1]. In 1991 the measurements were done for the Cental calorimeter with electrons in an energy range from 2 to 150 GeV [3,4]. Using this data the energy resolution and linearity of the calorimeters were extracted. For both EC and CC the electromagnetic sampling resolution was roughly 15 $\%/\sqrt{E}$ with a constant term of 0.5%. The hadronic sampling resolution was found to be 50 $\%/\sqrt{E}$ with a constant term of 4%. The linearity of the calorimeter response is shown in Fig. 2. For electrons above 15 GeV it is linear within 0.3 %. For low energies a little loss in the response is seen. For electrons with an energy of 2.5 GeV the deviation from linearity is about 50 MeV [5].

The central tracking system consists of a vertex drift chamber (VTX), a transition radiation detector, a central drift chamber (CDC) and forward drift chambers (FDC). To identify electrons a track reconstructed in these chambers should match an electromagnetic cluster found in one of the D0 calorimeters. The position resolution of the central calorimeter extracted for test beam electrons is approximately $\delta\, dr = 3$ mm and $\delta\, dz = 3$ mm for high momentum electrons. While the position resolution of tracking chambers is much better, and for the CDC, for example, it is $\delta\, d\phi = 1$ mrad and $\delta\, d\theta = 10$ mrad.

3. TRIGGERS

The D0 trigger system for electrons consists of two levels of hardware triggers and one level of software triggers. Level0 selects a valid beam-beam crossing based on a scintillator coincidence. The Level1 triggers are used to find electron and jets candidates based on calorimeter information. The calorimeter processor covers $|\eta| < 4.$ in trigger towers of $d\eta = 0.2$ by $d\phi = \pi/32$. Level 1 electron candidates are formed based on EM energy in trigger towers exceeding one of several thresholds. 32 hardware triggers are defined as a logical combination of many hardware conditions. During the collider run seven D0 triggers included electrons.

The software filtering of events (Level 2 trigger) is performed on one of the 50 VAX 4000/60 nodes where the FORTRAN filtering code was running. For each hardware trigger bit there is a set of "filter tools". Software filter tools refine the hardware trigger decision using the full detector information. Filter tools exist for jets, muons, electrons, photons, missing E_t, scalar E_t and narrow jets. The electron and photon filtering tools make cuts on longitudinal shape (energy fractions in the four EM layers and in the first hadronic layer) and on the transverse shower shape using the 0.05×0.05 segmentation of the third EM layer. Many electron filters require the electron to be isolated in the calorimeter. In addition, track matching can be done for the electrons and that is the only difference between electrons and photons on that level. The Level 2 electron trigger with no track match and with a threshold of 20 GeV has a rejection factor of 25. A factor of 2 - 4 results from the track match requirement for $|\eta| < 1.2$ [6].

Both the hardware and software trigger performance are well reproduced by Monte Carlo simulations. The efficiency of the Level 1 triggers for isolated electrons vs E_t is shown in Fig.3 . It is seen that for electrons with $E_t > 20$ GeV the efficiency of Level 1 is always better than 98%. The efficiency of the Level2 tools for W and Z electrons are better than 98%.

The first D0 collider run was devoted to high p_t physics and all electron triggers had high energy thresholds in Level1 ($E \geq 7GeV$) and in Level2 ($E \geq 12$ GeV). However, some attempts have been made to reduce the trigger threshold down to 2.5 Gev to select $\Upsilon \rightarrow e^+ + e^-$ and $J/\psi \rightarrow e^+ + e^-$ [7] decays and to study the D0 capabilities of doing B-physics with electrons. Two triggers were tested. The first trigger was used to collect a sample of events with two electrons and an associated "jet". That trigger required the presence of two trigger towers with EM energy exceeding 2.5 GeV, while the energy deposit in the hadronic layers had to be smaller than 1 GeV and required a jet with $p_t > 2.5$ GeV. The other trigger did not require a jet and was prescaled by a factor of 3. The Level1 rates for those triggers were measured at a luminosity of $2.8 \times 10^{30}\ cm^{-2}\ sec^{-1}$ as 60 Hz and 90 Hz respectively. This means that with certain modifications such triggers can be included in the D0 trigger list. The Level2 tools apply shape cuts and isolation cuts which were tuned on isolated electrons from test beam data down to 5 GeV. In addition to them several filters with loose isolation cuts were introduced to record non-isolated electrons. At the moment intensive Monte Carlo and off-line studies are being conducted to analyse the obtained data and estimate rejection factors and efficiencies.

4. OFF-LINE ALGORITHMS

The off-line electron ID technique is based on the fact that the shape of the electromagnetic and hadronic showers can be used to differentiate between electrons (photons) and hadrons. Electrons deposit almost all their energy in the EM section of the calorimeter, while hadrons deposit significant amounts of energy in the hadronic layers. The cut on the fraction of the energy in the EM calorimeter ($f_{EM} > 90\%$) has an efficiency of greater than 99% for the test beam electrons with energy 10 - 150 GeV.

To improve the discrimination against hadrons both the longitudinal and the transverse shower shape should be taken into account. That may be done using an H-matrix technique [1,8,9]. For a "training" sample of Monte Carlo generated electron showers using the mean energy $\langle E_i \rangle$ deposited in a calorimeter cell i one can define the correlation coefficient C_{ij} as

$$C_{ij} = \langle (E_i - \langle E_i \rangle) (E_j - \langle E_j \rangle) \rangle .$$

The covariance H-matrix then is:

$$H_{ij} = C_{ij}^{-1}.$$

For each event an effective χ^2 is calculated from:

$$\chi^2 = \sum_{i,j} (E_i - \langle E_i \rangle) H_{ij} (E_j - \langle E_j \rangle).$$

The D0 calorimeter has finer transverse segmentation in the third EM layer. In addition to the fraction of shower energy in the first EM layer (EM1), the fraction of shower energy in the second EM layer (EM2) and in the fourth EM layer (EM4) we included in the H matrix definition the fraction of shower energy in each cell of a 6×6 array centered on the hottest tower in the third EM layer. To include the energy and impact parameter dependence into the matrix the logarithm of the total energy and the position of the event vertex were added as parameters. This gives us a 41 dimensional matrix. To simulate the electron shower we used GEANT 3.14 and a detailed representation of the calorimeter geometry. We have verified the excellent agreement of the MC with the calorimeter response and then trained the H-matrix for each of the 37 different detector η towers. Using this H-matrix for the collider events we are able to calculate a χ^2 and place a cut to separate EM and Hadronic showers.

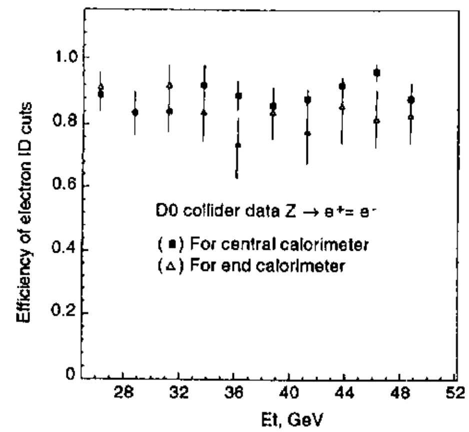

Figure 4. Efficiency of the standard D0 electron ID cuts for $Z \rightarrow e^+ + e^-$ events.

The electron identification is done in three steps. First of all electron candidates are identified as nearest neighbor clusters of the EM and the first hadronic layer calorimeter cells. Then the fraction of the energy deposited in EM layers is calculated for the cells forming the cluster. For the clusters which pass the cut on the fraction of EM energy we calculate the H-matrix χ^2 and find a track matched with the position in the calorimeter. We define the position of the shower centroid using a weighted center of gravity method [10]. In Fig.4 the efficiency of the standard electron ID cuts [11] is shown for $Z \rightarrow e^+ + e^-$. It is seen that the efficiency is about 80% with no systematic dependence on the electron E_t.

5. ELECTRON/PION DISCRIMINATION

To obtain the best discrimination against hadrons and to provide high electron finding efficiency the H-matrix χ^2 cuts were carefully selected. The H-matrix was applied to test beam electrons and the χ^2 cut was chosen to have 95% efficiency. Then the pion rejection factor was determined by applying the same cuts to single pion test beam data. The rejection factors are shown in Fig. 5 as a function of pion momentum for the case of cutting $HAD/EM < 0.02$ ($f_{EM} > 98\%$), and for the case of a cut on $HAD/EM < 0.04$ ($f_{EM} > 96\%$) followed by the H-matrix χ^2 cut. It is seen that the rejection factor is 900-3000 for particles with momentum 50 - 150 GeV/c.

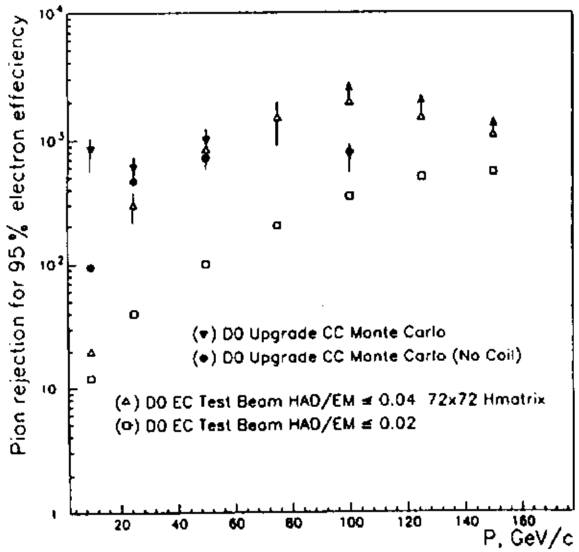

Figure 5. Pion/electron rejection factor vs pion momentum.

For energies below 20 GeV the situation becomes worse and the rejection factor does not exceed 10. As it was shown in [12], for the fully upgraded D0 detector it is possible using a modified H-matrix to obtain larger pion rejection factors for energies below 50 GeV. After the full upgrade the current D0 tracking system will be replaced by a combination of silicon microstrip barrel and disk detectors along with a full scintillating fiber tracker. These detectors will be located inside a superconducting solenoid, with a preshower detector located just outside the magnet. For the electron ID studies an H-matrix was generated using additional information from the preshower detector and the position of the interaction vertices. Using the Monte Carlo generated H-matrix plus the E/p cut and calorimeter/preshower position matching, electron/pion rejection factors were calculated. In Fig.5 solid points and triangles represent these calculations. It can be seen that the predicted rejection factor is more than 500 for all energies starting from 10 GeV. The main improvement observed in pion rejection at low energy is due to the E/p cut.

6. MODIFICATION OF ELECTRON ID FOR B-PHYSICS

The electron ID techniques discussed above were created for isolated high energy electrons. For B-physics studies where low energy electrons are often accompanied by hadrons the efficiency of electron finding dropped down to 30% [12] after applying the cuts tuned for isolated particles. This makes especially important the optimization of isolation criteria for both Level 2 triggers and off-line algorithms. It also means that transverse shower development parameters included in the H-matrix should be much more carefully selected assuming the possible presence of hadrons near electrons. One of the solutions here may be using the H-matrix with only longitudinal shower development parameters, loose isolation cuts together with tight track matching requirements. Using the obtained data and MC generated events the electron ID algorithms for low-energy non-isolated electrons are now being tested. These studies should be performed together with necessary trigger simulations before the coming collider run (1b) when we hope to include electron triggers for B-events.

7. REFERENCES

1. S. Abachi et al., *Nucl. Instr. Meth.* **A324**(1993)53.
2. H. Aihara et al., to be published in *Nucl. Instr. and Meth. A.*
3. P. Bhat, *Proceedings of the American Physical Society Division of Particles and Fields Conference, Fermilab*, Nov, 1992.
4. K. De, *Proceedings of the XXVI International Conference on High Energy Physics*, Aug, 1992, Dallas, Texas.
5. N. Denisenko, *Internal D0 Note 1852*, Aug, 1993.
6. J. Linnemann, *Proceedings of the American Physical Society Division of Particles and Fields Conference, Fermilab*, Nov, 1992.
7. M. Tartaglia, *Internal D0 Note 1723*, May, 1993.
8. R. Engelmann et al., *Nucl. Instr. Meth.* **216**(1983)45.
9. M. Narain, *Proceedings of the American Physical Society Division of Particles and Fields Conference, Fermilab*, Nov, 1992.
10. T.C. Awes et al., *Nucl. Instr. Meth.* **A311**(1992)130.
11. U. Heintz, M. Narain, *Internal D0 Note 1814*, Jul, 1993.
12. S.Abachi et al., *Internal D0 Note 1733*, May, 1993.

IDENTIFYING B-JETS WITH ELECTRONS

Alexander PERYSHKIN
FERMILAB, P.O.Box 500 Batavia, IL 60510
(for the DØ Collaboration*)

ABSTRACT

A possibility of detecting electrons from b-quark decays with the D0 detector is considered in this note. The efficiency and a purity estimations based on a Monte Carlo studies are presented as well.

1. Introduction

B-jet identification is important for b-physics studies at proton colliders and is also useful in suppressing QCD background in top searches. This paper reports the results of an investigation of the efficiency and background of identifying b-jets by detecting and reconstructing electrons from the semi-leptonic decay of b-quarks.

The energy of an electron from b-quark decay in the b-quark rest frame is limited to half the b-quark mass, about 2.5 GeV. In the lab frame the energy of a b-quark may be boosted to several hundred GeV, but the transverse momentum of the electron relative to the jet does not change. This means that an electron from a b-quark decay is always close to the b-jet from which it came. As seen in Fig.1 the average distance in $\eta - \phi$ space between an electron from the b-quark decay and the nearest b-jet is about 0.2. This is smaller than average jet cone size. Therefore the overlap of the hadron and electron showers is significant. This overlap makes electron detection rather difficult.

The main causes of background to the sample of electrons from b-quark decays are shower fluctuations of charged hadrons, the overlap of charged tracks and π^0 showers and the conversion of photons from π^0 decays. The most important features of the D0 detector [1] which help to suppress this background are the fine longitudinal and transverse segmentation of its calorimeter, and the good spatial resolution and dE/dX measurement capability of the central tracking system.

This paper reports the efficiency for suppressing backgrounds using shower shape and track-cluster matching. Monte Carlo generated events are used to deter-

*See, [1] for a full list of the DØ Collaboration institutions.

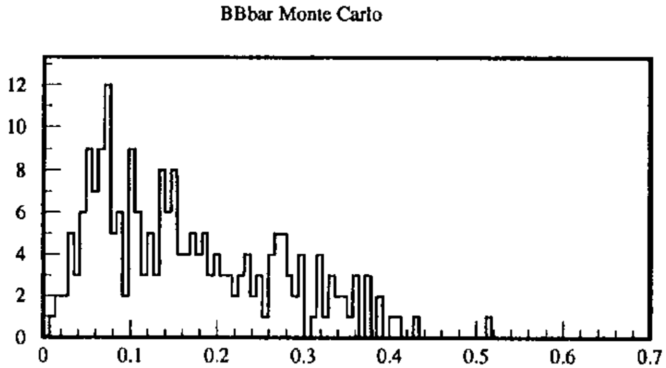

Figure 1: Distance in $\eta - \phi$ space between electrons and the jets which contained the b-quark.

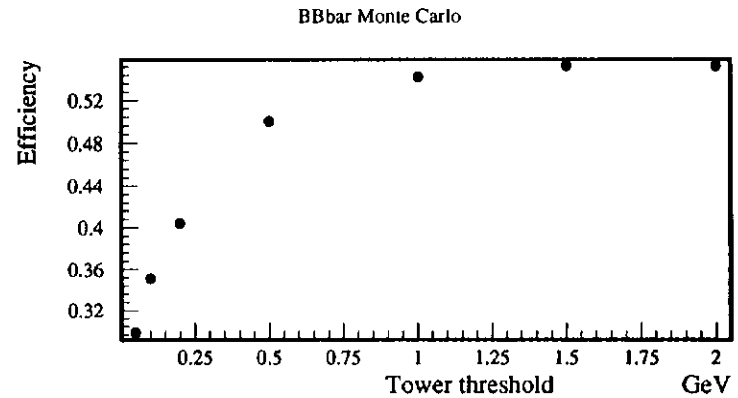

Figure 2: Efficiency of the true electron identifying dependence on the neighboring tower's threshold.

mine the identification efficiency and background rejection power.

2. Event analysis

The present analysis was performed on 400 $b\bar{b}$ and 400 $t\bar{t}$ Monte Carlo events. Events were generated by ISAJET and a full detector simulation was done using GEANT. For every event one of the b-quarks was forced to decay to an electron with $E_t^e > 2$ GeV. This analysis assumes that an EM cluster found near the MC electron ($\Delta R < 0.06$) is a true electron. EM clusters outside this region are considered to be fake electrons.

Efficiency of an electron detection is the ratio of the number of identified true electrons to the number of all ISAJET generated electrons from B decay with $E_t^e > 2$ GeV. Purity of an electron sample is defined as the ratio of the number of EM clusters corresponding to true electrons to the number of all EM clusters that were found.

In this analysis the clustering algorithm was optimized so as to increase the probability of identifying electrons near jets. Fig. 2 shows the electrons identifying efficiency dependence on the neighboring tower's minimum energy. The efficiency was measured after two major cuts. They are the EM fraction greater than 0.9 ($\mathrm{FH1}/E_{total} < 0.1$) and portion of the cluster energy outside the central tower less than 0.6 of whole cluster energy. Optimizing of the neighboring tower's threshold yielded an increase in efficiency by almost a factor of 2 and the purity also improved. With optimization of the cuts the b tagging efficiency reaches about 56% out of a possible 68%.

In order to find parameters that provide maximum background rejection a number of functions related to EM shower shape and cluster to track distance were examined. They are listed in the Table 1. The first part of Table 1 includes combinations of the layer energies, number of cells and the energy in various sizes of cones in η, ϕ space. The second part of the Table 1 summarizes purity when cuts based on moments in η, ϕ and radial (longitudinal) directions are used.

The standard definition of moments was used:

$$M^n = \sum_{i=1}^{N} E_i x_i^n$$

where M^n is the n-th power moment, N is the number of cells in the EM cluster, E_i is the i-th cell's energy and x_i is the i-th cell's location in the η, ϕ or radial direction. Moments may be centralized by replacing x_i by $x_i - \bar{x}$ and normalized by dividing by M^0. In this note only normalized moments were used. All moments of power 2 or more were centralized.

Figures 3 and 4 show first and second longitudinal moments for MC events: an isolated electron, an e^- near a jet and for a jet that contains a fake electron, i.e. an EM shower fluctuation in a jet.

Events were pre-selected by requiring that each EM cluster has $E_t > 3$ GeV. The purity after the pre-selection cut was 25%. The purity of the MC sample was examined for the cuts listed in Table 1. Each cut was applied until 10% of the MC events were rejected. For the remaining 90% of the events the purity is given in the last column of the Table 1. The cuts which tend to improve the purity of the sample are the track cluster distance cut and longitudinal shower size cut (RMS or longitudinal moment 2).

Parameter	min	max	purity
E_{total} (GeV)	4.	40.	.26
$(EM1+EM2+EM3)/E_{total}$	0.65		.34
$EM4/E_{total}$		0.22	.31
$FH1/E_{total}$		0.1	.36
N_{cells}		35	.30
E outside central tower/EM		0.5	.29
E in .4 cone/EM	0.99	2.3	.28
E in .2 cone/EM	0.8	1.3	.29
(E in .4 cone–E in .2 cone)/EM		1.2	.26
Longitudinal H-matrix χ^2		100.	.39
track cluster distance (cm)		8.	.40
ϕ 2nd moment (radian)		0.32	.34
ϕ 3rd moment (radian)		0.3	.26
η 2nd moment		0.25	.36
η 3rd moment		0.1	.31
Longitudinal 1st moment (X_0)		12.	.34
Longitudinal 2nd moment (X_0)		100.	.37
Longitudinal 3rd moment (X_0)	-100.	2500.	.29

Table 1: List of shower shape and track parameters. Minimum and maximum cut values correspond to point where efficiency change by 0.9 after applying that single cut.

Results obtained using several combinations of the most powerful parameters are presented in the Table 2. The combination of several shower shape cuts and a track–to–cluster distance cut yields an efficiency of 34% and a purity 81% for $b\bar{b}$ and the same efficiency and 71% purity for $t\bar{t}$ events.

3. Conclusion

This cluster finding algorithm optimization improves the efficiency of identifying electrons from b-quark decays to greater than 50% and improves the purity of the electron sample. At this stage of the analysis a combination of cuts was found which is capable of tagging 23% of the top to lepton+jets decays. For this estimation was used 25% value of the branching ratio for decay of any b-jets from $t\bar{t}$ event to electron with $E_t^e > 2$ GeV. The main advantage of electron b-jet tagging for isolating top is the method's ability to reduce, by a factor of 2, the W+4jets background.

Further development of this analysis could involve use of an H-matrix constructed from a set of the more powerfully discriminating functions we have discussed. This may increase electron detection efficiency while maintaining the rejection power we have demonstrated.

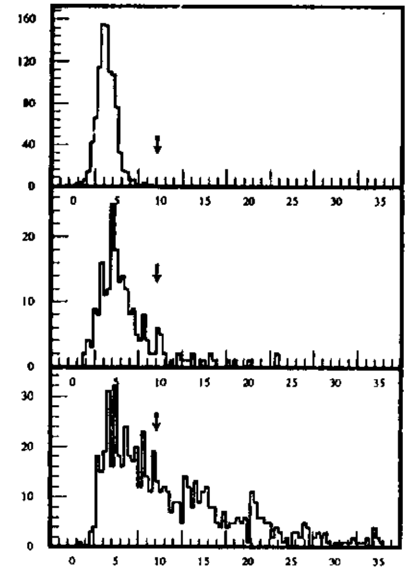

Figure 3: First normalized longitudinal moment for: an isolated electron, e^- near jet and a fake electron. The abscissa is in radiation lengths.

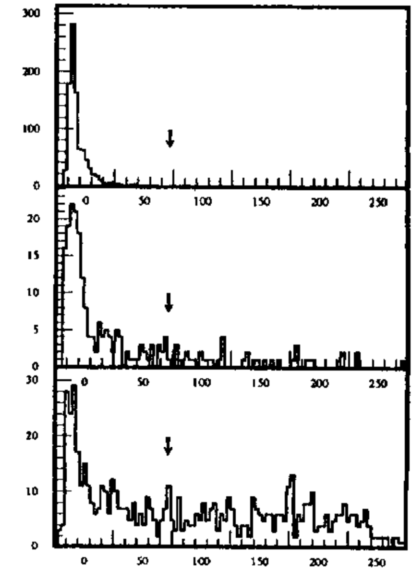

Figure 4: MC results for the second longitudinal moment for: an isolated electron, e^- near jet and a fake electron. An arrow shows the cut value corresponding a 90% efficiency for the true e^- near jet.

It is a pleasure to thank J.Qian and R.Raja for many fruitful discussions and assistance.

References

1. S. Abachi et al., *Submitted to Nucl. Inst. and Methods in Phys. Res.* and *preprint Fermilab-Pub-93/179 (July 1993)*.;

Universidad de los Andes, Bogota Colombia; University of Arizona; Brookhaven National Laboratory; Brown University; University of California, Riverside; LAFEX, Centro Brasiliero de Pesquisas Fisicas, Rio de Janeiro, Brasil; CINVESTAV, Mexico City, Mexico; Columbia University; Fermi National Accelerator Laboratory; University of Florida; Florida State University; University of Hawaii; University of Illinois, Chicago; Indiana University; Iowa State University; Lawrence Berkeley Laboratory; University of Maryland; University of Michigan; Michigan State University; Moscow State University, Russia; New York University; Northeastern University; Northern Illinois University; Northwestern University; University of Notre Dame; University of Panjab, Chandigarh, India; Institute for High Energy Physics, Protvino, Russia; Purdue University; Rice University; University of Rochester;

name of combination	parameter name	min	max	eff.	purity
HMTR	Longitudinal H-matrix		20.	.58	.46
TCD	track cluster distance		4.	.75	.51
CLUSTER					
	ϕ moment 2		.32		
	η moment 2		.25		
	Longitudinal moment 1		12.		
	Longitudinal moment 2		100.		
				.79	.53
CLUSTER*TCD				.49	.73
CLUSTER*TCD*HMTR				.34	.81

Table 2: Efficiency and purity providing by combinations of the most effective cuts for $b\bar{b}$ Monte Carlo events.

DAPNIA-CE Saclay, France; State University of the New York - Stony Brook; Superconducting Supercollider Laboratory; Tata Institute of Fundamental Research, Bombay India; University of Texas - Arlington; Texas A&M University; ZRL, Bristol Rhode Island.

ELECTROMAGNETIC SHOWER SPECTROSCOPY IN A HIGH RATE HADRONIC INTERACTION ENVIRONMENT; FERMILAB EXPERIMENT E760 PERFORMANCE

JOSE L. MARQUES AND JEROME ROSEN
Department of Physics and Astronomy
Northwestern University, Evanston, Illinois 60208, U.S.A.

1. INTRODUCTION

As far as electro-magnetic shower spectroscopy is concerned, the emphasis of the 1993 Snowmass B-physics Workshop has been colored by the nature and operating performance of existing hadronic colliders (principally CDF and D0). It is important to note that these detectors are (1) primarily concerned with detection in central rapidity, (2) very coarsely sectorized, (3) primarily designed for $W^{\pm}, Z^{0}$, and top decays, and (4) deeply concerned with hermeticty (i.e. preservation of the transverse energy balance for neutrino purposes). These design considerations do not reflect those of B physics. For example, hermeticty is irrelevant to B spectroscopy per se.

A fine grained shower calorimeter is capable of (1) excellent electron-hadron separation which is essential for measurements of semi-electronic decays of B's and D's down to moderately low $p_{\perp}$, (2) good γ, π^{0}, η, η', $\omega \rightarrow \pi^{0}\gamma$, and $K^{0}_{s} \rightarrow \pi^{0}\pi^{0}$ reconstruction.

E760 is an experiment devoted to the study of resonant charmonium production initiated by proton-antiproton annihilations. It features a fully towered shower calorimeter with 1280 elements, 66% of 4π coverage, and operates at interaction rates of 1Mhz. The interactions between the circulating $\bar{p}$ beam and the hydrogen gas jet target are asymmetric with a consequent γ_{cm} factor of 1.5-2.0.

What relevance does this experiment have with respect to proposed hadronic B physics studies?

We invite the reader to look at the E760 experiment from the following quixotic vantage point. Pseudo-B^{0} particles are created in the mass range 3-4 GeV (with a 0.25 MeV/c^2 center of mass resolution!). We study all neutral decay modes with as many as 7 separate γ showers <u>or</u> final states characterized by $\bar{p}p \rightarrow \psi + X \rightarrow e^{+}e^{-} + X$. Our pseudo-$B^{0}$'s are pristine, isolated, and have no overlay of "debris" from an overlapping $\bar{B}^{0}$ or from the primary vertex. Nevertheless, E760's performance is so strong (background rejection approaching 10^{9}!) that we think that some overlay of combinatorial background would not completely diminish an inclusive B^{0} shower spectrometer extrapolated from the E760 design.

We turn now to a short description of E760 and its operating performance. In section 3 we will return to the consideration of how this performance projects into the design of future hadro-production B spectrometers.

2. E760

Experiment E760 operates in the Fermilab Antiproton Accumulator and is described in earlier publications[1]. E760 and its approved successor E835, study the annihilation of stochastically cooled antiprotons with protons from an internal hydrogen gas jet target. Since $\bar{p}p$ annihilations can reach all combinations of J^{PC} through 2 or 3 intermediate gluon annihilation, E760 has the capability of directly forming all the charmonium resonances. The main thrust of E760 is to study all the low lying (below the open charm threshold) charmonium resonances produced by the exclusive reaction:

$$\bar{p}p \rightarrow 2(3)g \rightarrow \bar{c}c \rightarrow \text{electromagnetic final states.} \tag{1}$$

E760 obtains precision measurements of charmonium resonance parameters from excitation profiles, which are obtained by stepping the beam momentum to perform energy scans across the various resonances. The precision of this method relies heavily on knowledge of the initial state energy. The mean $\bar{p}$ momentum can be determined[2] to better than one part in 10^{-4} while the Accumulator's stochastic cooling system ensures that the beam momentum spread is small (typically $\sigma_{beam} \approx 250$ keV/c in the center of mass).

The total interaction cross section for $\bar{p}p$ at the charmonium formation energies is about 30 mb while the charmonium cross sections of interest range from tens of nb to tens of pb. The E760 detector must therefore be extremely selective in order to reject the enormous hadronic background.

2.1 The E760 Detector

The E760 detector (see figure 1) is a non-magnetic, large acceptance spectrometer with cylindrical symmetry about the beam axis. The central barrel has full azimuthal acceptance and polar acceptance from 12° to 70°, while the forward end-cap extends polar acceptance down to 2°. The detector has been optimized for detection of high-mass electromagnetic final states while still conforming to the extremely limited space available inside the Accumulator tunnel.

The central detector is built out of a series of concentric cylindrical layers that begin at the Accumulator vacuum pipe. There are two sets of scintillator hodoscopes, H1 and H2 with 8-fold and 32-fold azimuthal segmentation respectively. The central tracking is divided into three inner and one outer chamber. The first inner chamber is made of two sets of straw drift tubes. These aluminized mylar tubes are instrumented with a charge-division readout to give a polar as well as an azimuthal coordinate. Beyond the straw tubes is radial projection chamber (RPC) and a separate multiwire proportional chamber (MWPC). The RPC provides up to 16 ionization measurements along charged tracks, while the MWPC with its transverse pad readout provides a another measurement of the polar coordinate. The outer tracking chamber is a barrel of limited streamer tubes (LST) with two layers and a planar multiwire proportional chamber in the forward direction with acceptance down to 12°. Between the inner and outer tracking elements is a threshold Čerenkov counter with

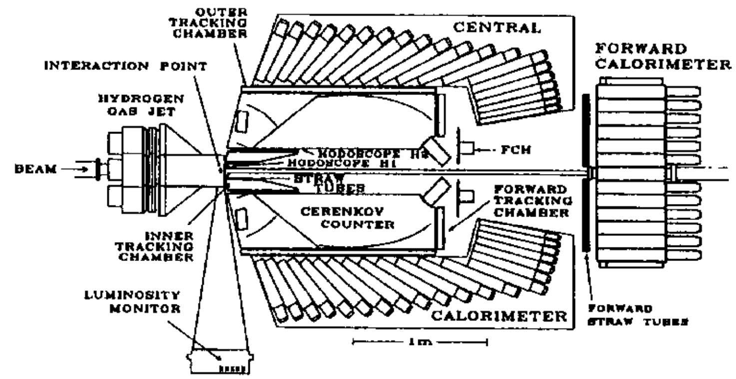

Figure 1: The E760 detector.

the same 8-fold azimuthal segmentation as H1 and a 2-fold polar segmentation. The forward segment ($15° < \theta < 38°$) of the Čerenkov contains CO_2 at 1 atm while the backward segment ($38° < \theta < 65°$) contains Freon13 at 1 atm. The outermost component of the central detector is a lead glass electromagnetic Central Calorimeter (CCAL)[3] built out of 1280 towers that point to the interaction region. The calorimeter is segmented into 20 "rings" in the polar coordinate and 64 "wedges" in the azimuth.

The forward end-cap is instrumented with a scintillator hodoscope (FCH) that has 8-fold azimuthal segmentation. This is followed by three planes of straw tubes and a fine sampling lead/scintillator Forward Calorimeter (FCAL). The Forward Calorimeter is made up of 144 towers that are individually read out through wavelength-shifter bars.

The luminosity monitor is a 1 cm x 5 cm surface barrier silicon detector mounted 1.5 m from the interaction region. It detects recoil protons that are elastically scattered at 86.5° from the beam direction. The luminosity is determined by normalizing the number of recoil counts to the known elastic scattering cross section,

$$\mathcal{L} = N_{elastic}/[\frac{d\sigma}{d\Omega}d\Omega] \tag{2}$$

where $d\Omega$ is the solid angle subtended by the silicon detector. The error in the measurement of the absolute luminosity is due the error in the fit to the measured $\bar{p}p$ total cross section and in the uncertainty in the detector solid angle $d\Omega$. The overall error in the measured luminosity is estimated to be ±4%.

2.2 Trigger and Event Selection

E760 employs three basic triggers: a high $p_\perp$ charged trigger, a high $p_\perp$ neutral trigger, and a neutral total energy trigger.

The two high $p_\perp$ triggers were designed to select high mass objects decaying into either $\gamma\gamma$ or e^+e^- in reactions like:

$$\bar{p}p \rightarrow \bar{c}c \rightarrow \gamma\gamma$$

$$\bar{p}p \rightarrow \bar{c}c(J^{PC} = 1^{--}) \rightarrow e^+e^- \qquad (3)$$
$$\bar{p}p \rightarrow \bar{c}c \rightarrow \bar{c}c(J^{PC} = 1^{--}) + X \rightarrow e^+e^- + X$$

where X is γ, π^0, or $\pi\pi$. At the fast trigger level central calorimeter inputs are used to impose mass and coplanarity constraints[4]. For the neutral final state the scintillator hodoscopes (H1 and FCH) are used to veto charged particles. For the charged final states H1, H2, and the Čerenkov are used to tag the electrons. The charged $p_\perp$ trigger is sufficiently effective (< 10 Hz rate to tape) to be easily accommodated within the data aquisition bandwidth. The neutral $p_\perp$ trigger requires further processing in the online processors. The processors identified hits in the CCAL, compute the invariant masses of all the photon pairs, and the total energy deposited in the calorimeters. Only neutral $p_\perp$ events with $M_{\gamma\gamma} > 2.0$ GeV/c^2 are recorded on tape (~30 Hz). The $p_\perp$ triggers are effective for selecting $\bar{c}c$ resonances with high efficiency (typically 85%).

In order to look at multi-body neutral final states, a total energy trigger was implemented. The total energy trigger is designed to select those events in which most of the available energy is deposited in the central calorimeter. The basic requirement of the total energy trigger is that 90% of the available energy be deposited in the central calorimeter. The total energy requirement is imposed at both the first level trigger and in the online processors. The rate to tape from the total energy trigger is typically 70 Hz.

The selection of events is described in detail in previous publications so we will only outline our general procedure here. Events that pass the low level cuts are kinematically fitted to the specific event topology in question. For final states containing electrons we require that the at least one electron be tagged by the Čerenkov. As we will see in the next section, this simple set of selection criteria is capable of extracting very small signals from the hadronic background.

2.3 Some Results

In this section we present a couple examples of the extreme sensitivity of the E760 detector in the face of an enormous hadronic background.

As an example of the results achieved in the detection of final states that contain electrons, figure 2(a) shows the invariant mass $m_{e^+e^-}$ for events collected at the ψ' formation energy. The large peak at lower mass arises from the inclusive decays $\bar{p}p \rightarrow \psi' \rightarrow \psi + X \rightarrow e^+e^- + X$ while the small peak at higher mass is due to the exclusive decay $\psi' \rightarrow e^+ + e^-$. The shaded area represents the residual background estimated by normalizing to equal luminosity events collected outside the ψ' resonance region. Figure 2(b) shows the invariant mass distribution for data taken during the scan of the $^1P_1$ (h$_c$). A comparison of figures 2(a) and 2(b) shows clear evidence for events of the type $\bar{p}p \rightarrow \psi + X \rightarrow e^+e^- + X$ in figure 2(b) at a level 100 times smaller than in figure 2(a).

The cross hatched events in figure 2(b) are those events that unambiguously fit the reaction $\bar{p}p \rightarrow \psi + \gamma \rightarrow (e^+e^-) + \gamma$. These events could not come from the decay of the singlet P since such a decay would violate C-parity conservation. However, when the width of the nearby χ_1 and χ_2 resonances (which decay to $\psi + \gamma$) along with the beam energy distribution are taken into account, the observed cross section is fully accounted for. The two vertically striped events in figure 2(b) fit the exclusive reaction $\bar{p}p \rightarrow (e^+e^-)$ and can be attributed to the continuum. In fact E760 has measured this cross section at $s = 8.9$, 12.4, and 13.0 GeV^2 and has been able to extract a measurement of the timelike electromagnetic

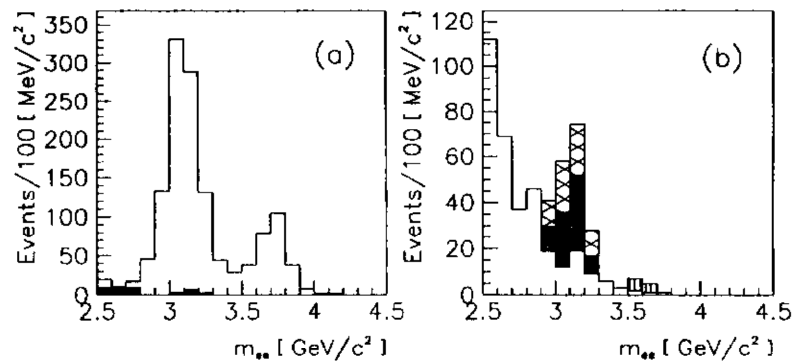

Figure 2: Distribution of events vs $m_{e^+e^-}$ (a) taken at the ψ'($\int L \approx 1$pb^{-1}) (b) taken near the spin weighted center of gravity of the $^3P_{0,1,2}$ ($\int L \approx 16$pb^{-1}).

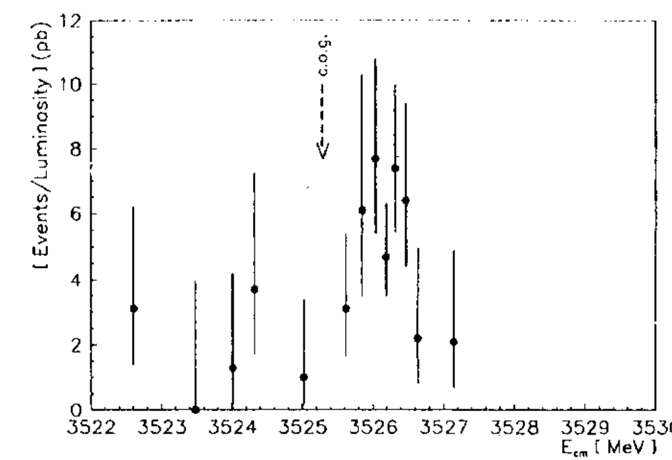

Figure 3: $^1P_1$ excitation curve, where the number of events per integrated luminosity are plotted vs center of mass energy in 150 keV bins.

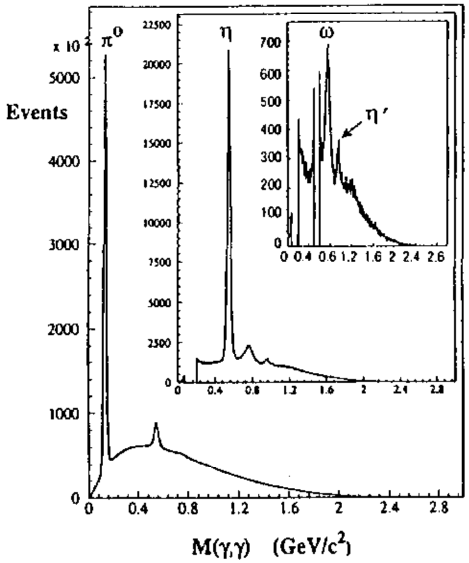

Figure 4: $\gamma\gamma$ invariant mass plot from a sample of $\bar{p}p \to 6\gamma$ events.

proton form factors[5]. The events in figure 2(b) that are shaded in black fit the exclusive reaction $\bar{p}p \to \psi + \pi^o \to (e^+e^-) + (\gamma\gamma)$ and are plotted in figure 3. The data in figure 3 are binned into 150 keV bins and clearly show the excitation curve for the ${}^1P_1$ resonance atop a ~2 pb continuum background cross section[6]. It is worth noting that the probability that the structure in figure 3 arose from a statistical fluctuation is less than 1 in 400.

As a second example of the kind of fine calorimetry that can be done in $\bar{p}p$ annihilations we now consider some all neutral final states. The E760 calorimeter is capable of reconstructing the entire range of mesons that decay into two photons, from the π^o to the χ_{c2}. Figure 4 shows the two photon invariant mass plot for a sample of $\bar{p}p \to 6\gamma$. The π^o is clearly reconstructed. In the first inset to figure 4, the π^o has been suppressed and the η is the prominent feature. Finally in the second inset both the π^o and the η have been suppressed, and one can clearly see the ω and even the $\eta\prime$. This fine calorimetry is extremely important for the rejection of background when looking for charmonium resonances that decay into two photons since the dominant sources of backgrounds are $\bar{p}p \to \pi^o\pi^o$ and $\bar{p}p \to \pi^o\gamma$. Figure 5 shows E760's preliminary results for its scan of the η_c resonance. The solid line in figure 5 shows the fit to the resonance plus background, the dashed line represents the predicted background level from a study of the observed $\bar{p}p \to \pi^o\pi^o$ and $\bar{p}p \to \pi^o\gamma$ cross sections.

3. Comments on Electromagnetic Calorimetry for B-physics

In the last section (2.3), we have provided a smattering of spectroscopic data from E760. As noted in section 1, the shower spectrometer is fully towered and fine grained (1280 cells). Shower clusters from 20 MeV to 3 GeV are processed and used. The π^o detection efficiency is in the range (90-99)%. Consequently, when the interest is in isolating primary γ's (e.g.

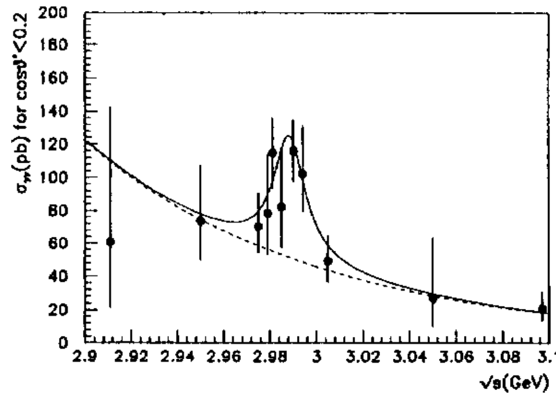

Figure 5: The η_c excitation curve observed as $\bar{p}p \to \gamma\gamma$. The solid line shows the fit to the resonance plus background, the dashed line represents the predicted background level from a study of the observed $\bar{p}p \to \pi^o\pi^o$ and $\bar{p}p \to \pi^o\gamma$ cross sections. This result is **preliminary**.

$\eta_c, \eta_c' \to \gamma+\gamma$) or transition γ's (e.g. $\chi_c \to \psi+\gamma$, $h_c \to \eta_c+\gamma$) π^os are rejected by substantial factors.

The calorimeter cell sizes are a fairly small multiple of a Moliére radius. Consequently, the shower clusters provide both energy ($\sigma_{energy} = 6.0\%/\sqrt{E[GeV]} + 1.4\%$) and shower position ($\sigma_{position} = 9$ mm) information. We eschewed coarse shower blocks which would have required an active counter system.

Of course a hadronic B-physics experiment will be manifestly committed to inclusive studies with fewer fit constraints and additional combinatorial background. Nevertheless, we believe that E760 quality results can be achieved if a fine grained shower system is deployed. At least 10^3 cells per unit rapidity is advisable. A powerful B experiment should aspire to detection efficiency equal to or exceeding 3 units of rapidity.

A few general words about angular coverage are in order. A central collider system providing optimized coverage over pseudo rapidity $|\eta| \le 1$ ($40° < \theta < 140°$) encompasses 76% of the total 4π solid angle coverage. Shower detectors are generally deployed inside a solenoidal magnet or outside the coils. A forward detector operating at $\eta \ge 2$ ($\theta < 15.4°$) encompassing only 3.5% of 4π is a somewhat simpler proposition. It is basically a 2 dimensional planar detector. The region $1 < \eta < 2$ is a transition region which awkwardly sits between a cylindrical geometry and a planar one. This region is extremely difficult to accommodate into a realistic detector.

The best of all worlds would be an asymmetric collider which would boost the peak $b\bar{b}$ production cross section into a forward regime. As an illustration, let's consider 2 TeV protons colliding with 10 GeV protons. This scenario would provide an $E_{cm} \approx 280$ GeV which would yield a pleasant production cross section[†] of about 5-10 μb. In this case

[†]We prefer to project $\sigma_{b\bar{b}}$ from the known $\sigma_{c\bar{c}}$ using scaling:
$\sigma_{b\bar{b}}(E_{cm} = 120 \text{ GeV}) \approx \left(\frac{m_c^2}{m_b^2}\right) \sigma_{c\bar{c}}(E_{cm} = 40 \text{ GeV}) \approx (0.1)(30\ \mu b) = 3\ \mu b$.
By extrapolation $\sigma_{b\bar{b}}(E_{cm} = 280 \text{ GeV}) \approx (5-10)\ \mu b$.

the center of mass frame will be boosted to $\gamma_{cm} \approx 7$ which shifts the peak production cross section to $\eta = 2.6$. In this region one could deploy a finely segmented planar electromagnetic calorimeter with only modest cost of effort.

Shower detector design cannot be considered in isolation from other detector considerations which compete for money and space. To discuss consideration of microvetex tracking, RICH systems, and the like would pull us far afield. Suffice it to say here, that our considered prejudice for the ideal B-experiment is in favor of a forward spectrometer featuring a fine grained electromagnetic shower detector.

A final consideration worthy of comment is triggering. E760 employed calorimetric triggering exclusively at both levels 1 and 2. Admittedly, we exploited the constraints afforded to us by the exclusive nature of the channels we studied. Nevertheless, we believe that hard wired triggering for $e^{\pm}$ produced showers can facilitate ψ (or Υ) $\rightarrow e^+e^-$ triggering and possibly semi-electronic decays with appropriate $p_\perp$ cuts. Electron triggering can compete effectively with muonic triggering if carefully and cleverly executed. The off-line capabilities are enormous. For example, CP violation design studies often discuss the $B^0 \rightarrow \psi$ (or ψ')K_s^0 decay channel. Why not include $B^0 \rightarrow \chi_c K_s^0$; $\chi_c \rightarrow \psi\gamma$ or even $B^0 \rightarrow h_c K_s^0$; $h_c \rightarrow \psi\pi^0$? There are other CP eigenstates as well, e.g. $B^0 \rightarrow \psi K^*(890)$; $K^*(890) \rightarrow K_s^0\pi^0$.

Elsewhere in these proceedings[7], we have discussed a variety of spectroscopic possibilities short of CP violation in the B, D, B_s... systems that are worthy of study. Rich systems of excited energy levels are awaiting discovery and study.

4. Acknowledgements

We wish to thank the U.S. Department of Energy for supporting our participation in the 1993 Snowmass Workshop on B physics at Hadron Accelerators. We also wish to thank the Workshop organizers and the many support personnel from both Fermilab and SSCL for making such an enlightening and productive environment possible. Lastly we thank the many members of the E760 collaboration whose hard work has contributed to this presentation.

5. References

1. T.A. Armstrong et al., Nucl. Phys. **B373**, 35

2. T.A. Armstrong et al., Phys. Rev. **D47**, 772

3. Bartoszek et al., Nucl. Instr. and Meth. **A301** 47

4. R. Ray et al., Nucl. Instr. and Meth. **A307** 254

5. T.A. Armstrong et al., Phys. Rev. Lett. **70**, 1212

6. T.A. Armstrong et al., Phys. Rev. Lett. **69**, 2337

7. J.R. Rosen, J.L. Marques, and L. Speigel, *Heavy Flavor Spectroscopy*, Delta working group, Snowmass Workshop on B Physics at Hadron Accelerators, 1993

Muon Detection

Convenors:

D. Hedin
Northern Illinois University

N. Stanton
Ohio State University

List of Participants

A. Abashian
Virginia Polytechnic Institute

G. Álvarez
Indiana University

B. Choudhary
University of California (Riverside)

G. Corti
University of Virginia

M. Cummings
University of Hawaii

R. Demina
Northwestern University

V. Glebov
Superconducting Super Collider Laboratory

P. Karchin
Yale University

V. Kubarowski
Superconducting Super Collider Laboratory

T. Lawry
University of Virginia

T. LeCompte
University of Illinois at Urbana-Champaign/
Fermi National Accelerator Laboratory

L. Markosky
University of Arizona/
Fermi National Accelerator Laboratory

M. Mohammadi
State University of New York at Stony Brook

N. Neumeister
Institut für Hochenergiephysik
d. Österreichische

V. Papadimitriou
Fermi National Accelerator Laboratory

D. Wagoner
Prairie View A&M University

A. Zieminski
Indiana University

D. Zieminska
Indiana University

SUMMARY
MUON DETECTION WORKING GROUP

NOEL R. STANTON[1]
Physics Department, Kansas State University
Manhattan, KS 66506 USA

1. INTRODUCTION

1.1 The Muon Working Group

The areas of concentration of the Muon Working Group[2] reflected its composition: about half of the group was interested primarily in extending the capability of existing general purpose colliders (CDF, D0). Smaller numbers of people were interested in B physics with general purpose colliders at the SSC and LHC, with SSC fixed target experiments, and with dedicated forward colliders.

1.2 Why Muons?

Good muon tagging, and possibly also muon triggering, is essential for studying CP violation in $B_i \to J/\psi X$, $J/\psi \to \mu^+\mu^-$; as a flavor tag, with the semimuonic decay $B \to \mu^+ X$ or $\overline{B} \to \mu^- X$ tagging the flavor of the partner; for studying the physics of the semimuonic B decays themselves; and for looking for really rare decays like $B \to \mu^+\mu^-$.

1.3 How to Identify Muons

Some simple ideas involved in muon identification are illustrated in Fig. 1. If particles traverse an absorber of thickness x, the probability for a hadron to pass through without interacting is $\exp(-x/\lambda)$, where λ is the collision length. The thicker the absorber, the better the hadron rejection, as long as the muon is energetic enough to get through the absorber. Note however that for a central detector, where $p \approx p_T$, the typical p_T's useful for B physics (~ 2 GeV/c) do not permit very thick absorbers[3].

Just detecting a particle on the other side of an absorber is usually insufficient for good muon identification. The detected particle could be a low-energy survivor of a hadron interaction (punch through); or it could be a real muon, but not the track of interest (mismatch); or, it could have come from another source entirely, having avoided passing through the absorber. Ideally, the position, direction, arrival time, and momentum of the exiting particle should match those expected from the entering one. However, such desirable redundancy must be balanced against detector size and cost.

Even if the particle entering the absorber is unambiguously identified as a muon, it might

[1]Co-convener D.A. Hedin.

[2]The following presentations were given: Vaia Papadimitriou, 'CDF Muon Upgrades'; Tom LeCompte, 'CDF Problems and Cures'; Ken Johns, 'D0 Muon Triggers'; Dave Hedin, 'D0 Muons, Central Region'; Vladimir Glebov, 'D0 Muons, Forward Region'; Norbert Neumeister, 'Muons in CMS'; Patty McBride, 'Muons in SDC'; Gloria Corti, 'Muons in E771 and SFT'; Al Abashian, 'Resistive Plate Chambers'; Mohammad Mohammadi, 'GEM Muon System'; Valery Kubarovsky, 'SDC Muon System'.

[3]For iron, $\lambda \approx 0.11$ m, and 1 GeV of energy loss occurs in about 1.2 m.

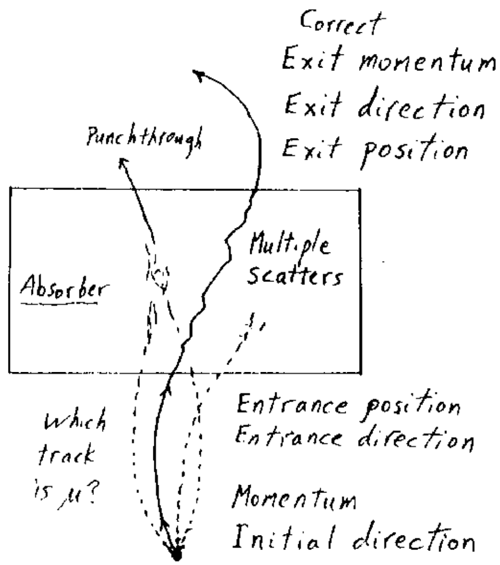

Figure 1. How to identify muons.

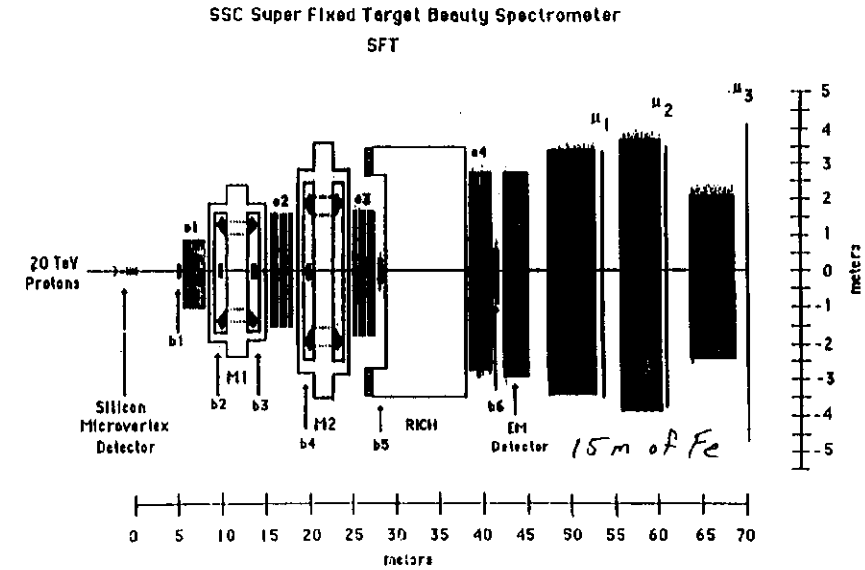

Figure 2. Layout of the proposed SFT spectrometer.

be a pion or kaon which decayed in flight before it could interact in the absorber. Compact detectors, in which the flight distance from production point to absorber is small, have an advantage in reducing false muon ID from this source.

2. FIXED TARGET B EXPERIMENTS

The chief disadvantage of fixed target experiments for high-statistics B physics is the reduced production cross section at lower $\sqrt{s}$. However, there are also some distinct advantages which compensate at least partially for this handicap at SSC or LHC energies.

1. It is easy to get good geometrical acceptance, ~ 0.8 for $B \to \mu X$, ~ 0.6 for $B \to J/\psi X$, with $J/\psi \to \mu^+\mu^-$.
2. Because of the large Lorentz boost, there is little loss in $B \to \mu X$ efficiency for thick absorbers; 10-20 GeV of energy loss is no problem.
3. B's are 'high p_T' physics for $\sqrt{s}$ typical of fixed target experiments, and this can be used to great advantage in hardware triggers or offline selection. An extreme example: Fermilab E653, in a 600 GeV/c π^- beam with an offline muon p_T cut of 1.5 GeV/c, achieved a factor of 50,000 in background rejection.
4. Muon p_T triggers are not hard, and dimuon mass triggers are possible.

An example of one such experiment, the SFT (Super Fixed Target) detector proposed for a 20 TeV proton beam at the SSC, is shown in Fig. 2. It has a muon p_T trigger, and 15 m of iron absorber.

An important advantage of fixed target experiments over central colliders for B physics is the fact that p and p_T are not the same; one gets two background rejection factors, not one. The average muon momentum $\hat{p}_\mu$ in $B \to \mu X$ is >> $\hat{p}_\mu$ for centrally produced π, K decays to muons, and in addition $\hat{p}_{T\mu}$ in $B \to \mu X$ is >> $\hat{p}_{T\mu}$ for μ' s from such π's and K's. The expected discrimination for SFT is illustrated in Fig. 3. Requiring $p_\mu > 20$ GeV/c is already worth a factor of 10 in π, K rejection, and a modest p_T cut of 1.5 GeV/c gives a total rejection of $\times 1000$ against π, K and $\times 40$ against charm.

Some parameters of SFT and of the proposed LHB detector at LHC are compared in Table 1.

For fixed target experiments, muon ID and muon-based triggers are relatively easy and quite powerful. However, because of the small $B\bar{B}$ cross section it is not clear that FT experiments can afford to use only muons from $B \to J/\psi X$ for CP studies, or only muons from $B \to lX$ for tagging; the corresponding electron channels are also needed for statistics. Unfortunately, these electron channels appear to be a good deal more difficult than the muon ones.

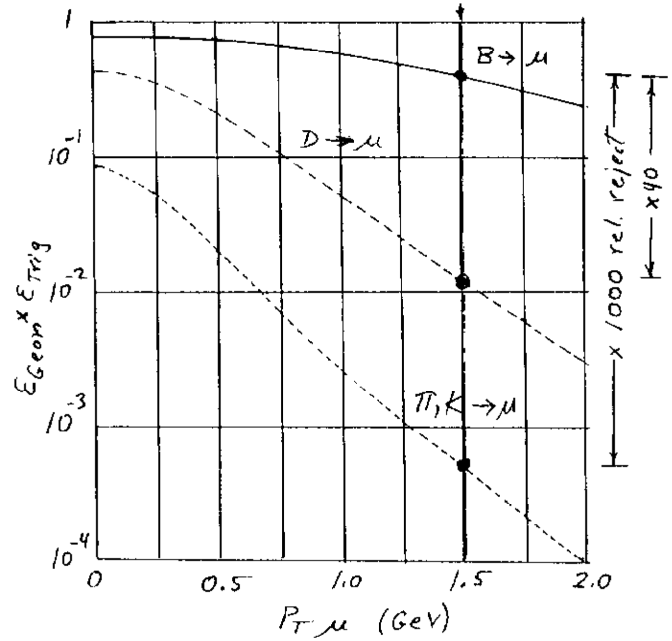

Figure 3. Product of geometrical and trigger efficiencies for B's in SFT, and for background muons from π, K decays and charm, as a function of the minimum allowed $p_{T\mu}$. A momentum cut of $p_\mu > 20$ GeV/c has already been imposed.

Table 1. Some parameters of SFT and LHB.

	Single μ		Dimuon
Parameter	SFT	LHB	SFT
Muon coverage	2 - 75 mr	< 100 mr	2 - 75 mr
π, K decay distance	40 m	30 m	40 m
Absorber thickness	15 m	6 m	15 m
Minimum p_μ (GeV/c)	20 GeV/c	10 GeV/c	20 GeV/c
Minimum $p_{T\mu}$	1.5 GeV/c	1.2 GeV/c	1.0, 0.5 GeV/c
Muon geom. effic. $\epsilon_{g\mu}$	0.82	?	0.68
Muon trigger effic. $\epsilon_{T\mu}$	0.45×BR	?	0.95
$\epsilon_{g\mu} \cdot \epsilon_{T\mu}$	0.37×BR	0.45×BR	0.65
π, K rejection	$\sim$ 2000	> 100	?
$c\bar{c}$ rejection	$\sim$ 100	?	?
Tagging effic. $\epsilon_{\mu Tag}$	—	—	0.8×BR

3. FORWARD COLLIDERS

One such proposed forward collider experiment, COBEX at LHC[4], is sketched schematically in Fig. 4. Of necessity, the beam pipe passes through the muon range filter, which cannot be as thick as those for SSC and LHC fixed target experiments. Forward collider experiments lie between the kinematic regimes of fixed target and central colliders: p_μ and $p_{T\mu}$ are still separately effective in reducing backgrounds, but less so than for fixed target. The COBEX proponents require an additional impact parameter requirement to get sufficiently low trigger rate; this costs an additional factor of about 0.13 for reconstruction efficiency.

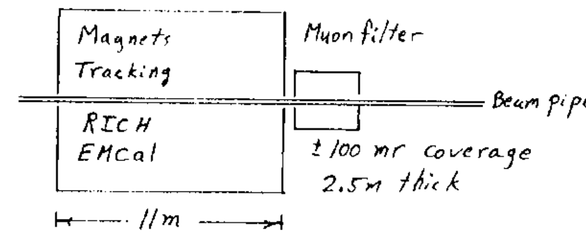

Figure 4. Cartoon of the proposed COBEX detector at LHC.

4. UPGRADED CENTRAL COLLIDERS: CDF AND D0

Upgraded existing central colliders are certainly proving grounds for future B experiments. It is also interesting to know how well they could compete with dedicated B experiments when the upgrades are complete.

4.1 CDF

The CDF muon system and the upgrades planned for it are discussed in detail in the paper by T. LeCompte and V. Papadimitriou. Muon detection in the central region (pseudorapidity$|\eta| < 0.8$) is shown schematically in Fig. 5, and the evolution of the detector is illustrated in Fig. 6. For the muon system, these consist of increasing the absorber thickness (Central Muon Upgrade) and η coverage (Central Muon Extension) in the central region, and moving the forward muon system closer to increase angular coverage and decrease the potential π, K decay path. There will also be upgrades to the CDF rate capability and to the silicon tracking.

Difficulty was encountered with the Central Muon Extension during the last CDF run with backsplash from the beam pipe and forward calorimeter. This backsplash bypassed the absorber and produced an unacceptably large trigger rate. The cure was a beam pipe of lower mass, and tighter timing of the muon scintillators.

[4]There was unfortunately no COBEX expertise available, so that the forward collider option is less fully developed than the others in this report.

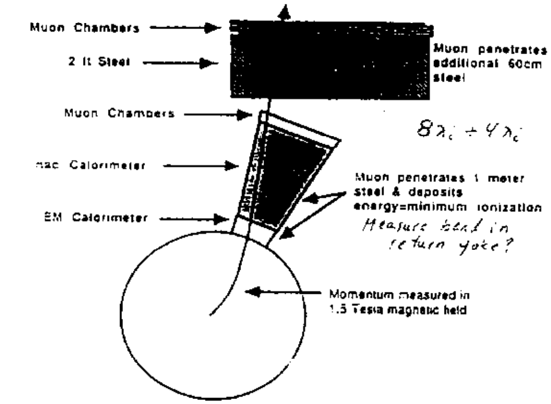

Figure 5. Sketch of CDF muon detection in the central region.

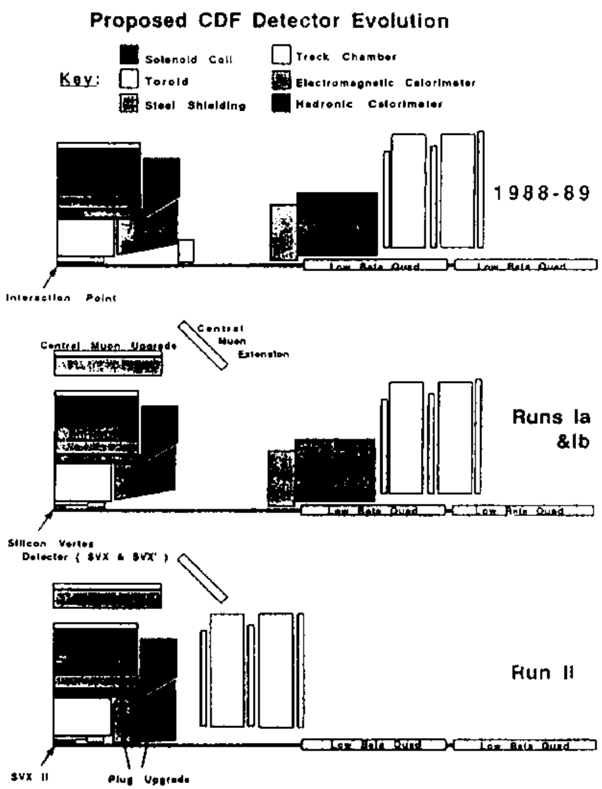

Figure 6. Evolution of CDF.

Table 2. Comparison of CDF and D0 parameters for $B \to \mu X$.

Parameter	CDF Run Ia (now)	CDF Run III (M.I.)	CDF B physics takeover	D0 Run III (M.I.)
$\lvert\eta\rvert$ for muons	< 0.55	< 1.0	< 2.8	< 3.4
π, K decay dist.	1.5 m	1.5 m	1.5 m	0.7 m
Filter thickness	12λ	8-12λ	8-12λ	10-18λ
Min. $p_{T\mu}$ (GeV/c)	~ 7.5	6.0 3.0+IP ?	5.0? 3.0+IP ?	4.0
Geom. effic. $\epsilon_{g\mu}$ (η, ϕ)	0.10	0.25	0.50	0.60
Trig. effic. $\epsilon_{T\mu}$	0.01×BR	0.025×BR	0.025×BR	0.027×BR
$\epsilon_{g\mu} \cdot \epsilon_{T\mu}$	0.001×BR	0.006×BR	0.012×BR	0.016×BR
Punchthru (online) fraction (offline)	0.20 < 0.05	0.20 < 0.05	0.20 < 0.05	
π, K decay fraction	0.50	0.25	0.35	< 0.05 tot
$c\bar{c}$ BG after cuts	< 0.15	—	—	0.10
$B \to \mu X$ per year	0.5M	150M	300M	~ 400M

Table 3. Comparison of CDF and D0 parameters for $B \to J/\psi X$, with $J/\psi \to \mu^+\mu^-$, plus a muon away-side tag.

Parameter	CDF Run Ia (now)	CDF Run III (M.I.)	CDF B physics takeover	D0 Run III (M.I.)
$\lvert\eta\rvert$ for muons	< 0.55	< 1.0	< 2.8	< 3.4
π, K decay dist.	1.5 m	1.5 m	1.5 m	0.7 m
Filter thickness	12λ	8-12λ	8-12λ	10-18λ
Min. $p_{T\mu}$ (GeV/c)	3.0, 1.5	2.0	1.5	3.0
Geom. effic. $\epsilon_{g\mu}$ (η, ϕ)	0.25	0.35	0.42	0.75
Trig. effic. $\epsilon_{T\mu}$	0.014	0.014	0.03 ?	0.12
$\epsilon_{g\mu} \cdot \epsilon_{T\mu}$	0.0035	0.005	0.012	0.09
Away-side μ tag ϵ_{tag}	0.1×BR	0.4×BR	0.5×BR	0.53×BR
$\epsilon_{g\mu} \cdot \epsilon_{T\mu} \cdot \epsilon_{tag}$	3.5×10^{-4}×BR	2×10^{-3}×BR	6×10^{-3}×BR	5×10^{-2}×BR

5. GENERAL-PURPOSE COLLIDERS AT LHC AND SSC

Distributions in p_T and η for muons from B decay at LHC energy are shown in Fig. 9. B's are very much low-p_T physics, with the peak of the muon p_T distribution at about 1.5 GeV/c.

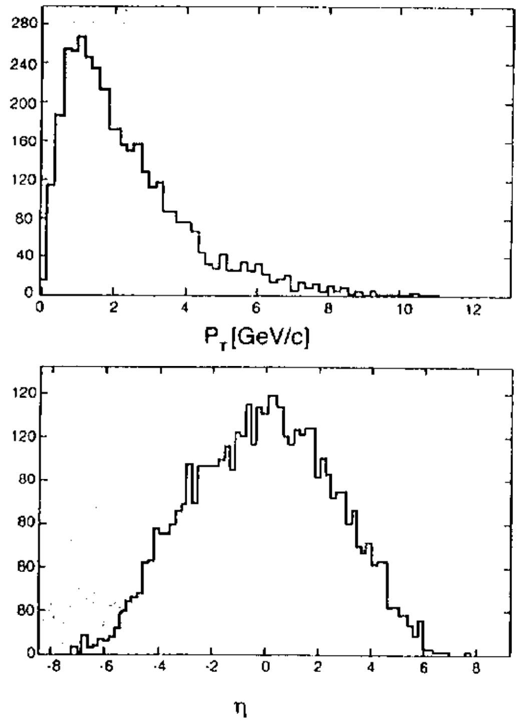

Figure 9. Expected distributions in p_T and η for muons from B decay at LHC energy.

5.1 SDC and GEM at SSC

B physics has not had high priority in planning for GEM and SDC, and thinking about how to use low-luminosity ($\sim 10^{33}$) initial running for B physics is just beginning. As with central colliders at lower energy, an important issue is how to trigger at an acceptable rate on muons of relatively low p_T. The results of one such study for SDC by D.P. Coupal is reproduced in Fig. 10. Coupal limited his study to b quarks produced with $p_T > 10$ GeV/c; this leaves an estimated 250μb out of a total SSC $b\bar{b}$ cross section of 1-3 mb. For this preselection, Fig. 10 shows the relative acceptance for 1μ, 2μ, and 3μ triggers as a function of p_T for $B \to J/\psi K_s^0$, $J/\psi \to \mu^+\mu^-$, tagged by $\overline{B} \to \mu^- X$. Tracks with $p_T < 5$ GeV/c will barely penetrate the SDC calorimeter and toroid. The acceptance for triggering on three muons with $p_T > 5$ GeV/c is about the same as that for one muon with $p_T > 20$ GeV/c, about 2% of that for no p_T requirement.

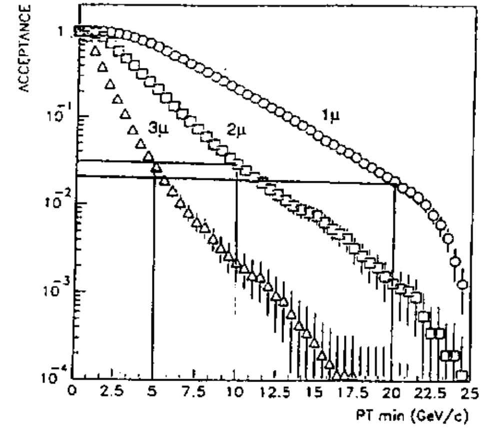

Figure 10. Relative acceptance in SDC for $|\eta| < 2.5$ for 1μ, 2μ, and 3μ triggers, as a function of p_T, from $B \to J/\psi K_s^0$, $J/\psi \to \mu^+\mu^-$, tagged by $\overline{B} \to \mu^- X$.

The muon trigger concept of GEM is illustrated in Fig. 11; muons are tracked in a magnetic field in air after they emerge from the calorimeter. GEM will be able to trigger on single muons or dimuons with $p_T > 10$ GeV/c and $|\eta| < 2.5$, and to tag B jets with muons with $p_T > 15$ GeV/c.

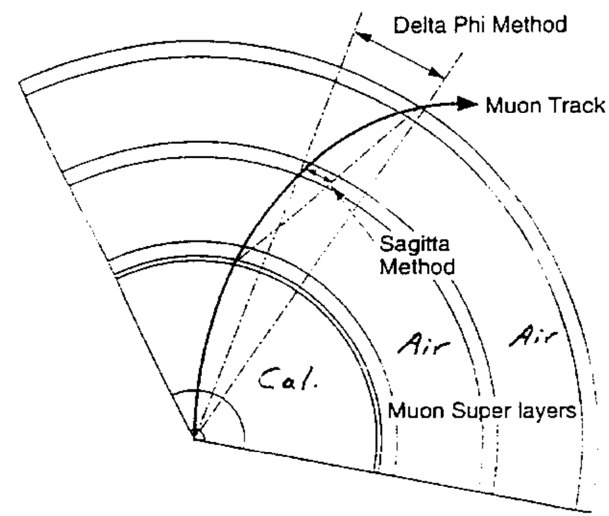

Figure 11. Level 1 muon trigger concept for GEM.

5.2 CMS at LHC

The Compact Muon Spectrometer (CMS) proposed for LHC (Fig. 12) is optimized for muon identification. As shown in Fig. 13, the detector has considerable redundancy, including multiple momentum measurements, and tight ϕ coverage with no gaps for $|\eta| < 2.5$. The CMS proponents have done substantial planning for doing B physics in the early running (luminosity $\sim 10^{33}$), and have carefully studied resolution, backgrounds, and calibration of the dilution factor. They will be able to do trimuons with $p_T < 4$ GeV/c or dimuons with $p_T < 5$ GeV/c with a 100 Hz trigger rate at that luminosity, and then turn up the p_T threshold as luminosity increases. For the trimuon option and an integrated luminosity of 10^4 pb^{-1}, CMS can obtain about 5.6×10^6 events per year of $B \to J/\psi K^0_s$, $J/\psi \to \mu^+\mu^-$ with an away-side muon tag, giving errors on $\sin(2\beta)$ of 0.06 to 0.09.

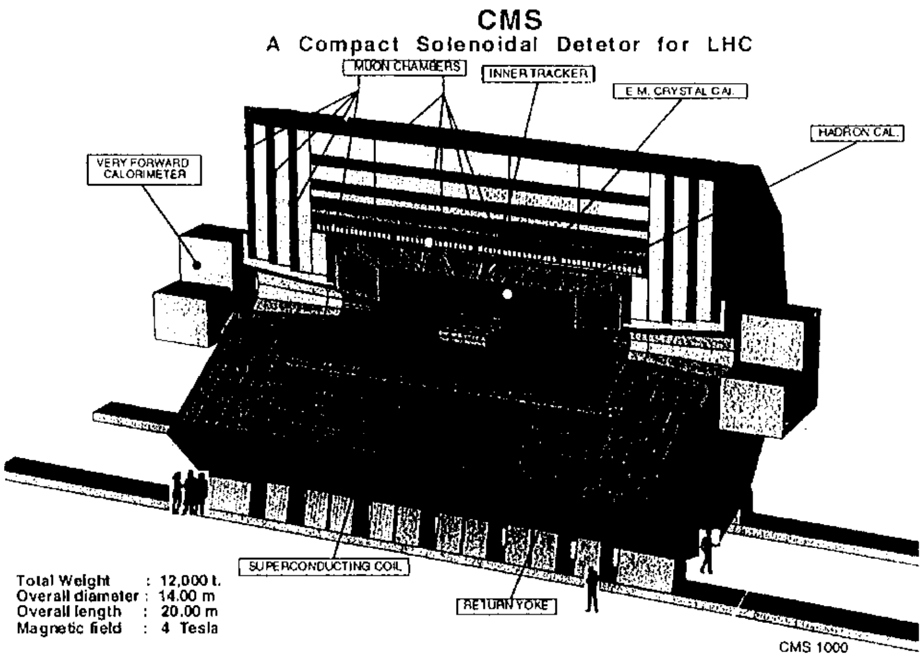

Figure 12. The proposed CMS detector for LHC.

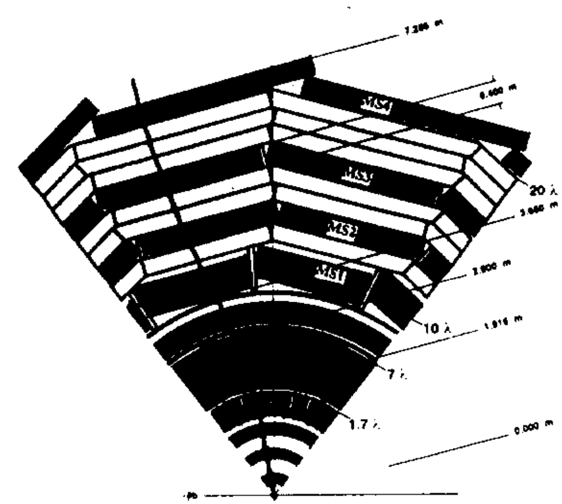

4 Stations MS1 - MS4

Redundancy

ϕ Acceptance

3 independent momentum measurements

in air (before absorber), after coil, after return yoke

very good coverage for low-p_T muons

MS1+ MS2 ≈ 100%

Per Station:

40 cm space

10-16 measuring planes

→ track vector in r-ϕ space

position accuracy: ~ 100 μm

direction: ~ 1 mrad

Figure 13. Muon detection in CMS.

MUON IDENTIFICATION AND TRIGGERING AT DØ

MARY ANNE C. CUMMINGS
Department of Physics and Astronomy, University of Hawaii
Honolulu, HI 96896

DAVID HEDIN
Physics Department, Northern Illinois University
DeKalb, IL 60115

KEN JOHNS
Physics Department, University of Arizona
Tucson, AZ 85721

1. INTRODUCTION

The DØ detector is a large, general-purpose detector designed to take full advantage of the 2 TeV energy of the Fermilab collider. The design of the experiment emphasizes accurate identification, complete angular acceptance, and precise measurement of the decay products of W and Z bosons: charged leptons (both electrons and muons), quarks and gluons, which emerge as collimated jets of particles, and noninteracting particles, such as neutrinos. The primary physics goals of DØ include searching for new phenomena, such as the top quark or particles outside the Standard Model, and high-precision studies of the W and Z bosons. In addition, the excellent muon identification allows the study of b quark production and decay.

The DØ detector is shown in Figure 1. It consists of three major hardware systems: calorimetry, muon detection, and central tracking, which together allow fairly complete characterization of most proton-antiproton collision events. The central tracking system consists of four drift-chamber systems (vertex, central, and two end systems) and transition radiation detectors for electron identification. Surrounding the central tracking system are three uranium/liquid-argon calorimeters. The uranium is a dense medium, allowing containment of high energy hadron showers in a relatively short depth, as well as equal response to electrons and hadrons, while the liquid-argon ionization medium gives ease of calibration, stability, radiation hardness, and the ability to build in fine segmentation in all three coordinates. The energy resolution due to sampling fluctuations alone is $\frac{\sigma}{E} \approx \frac{16\%}{\sqrt{E}}$ for electrons and $\approx \frac{49\%}{\sqrt{E}}$ for charged pions. Finally, surrounding the calorimeters is the muon system described in more detail below.

2. DØ MUON SYSTEM

The muon system consists of 5 iron toroids plus 3 layers of proportional drift tubes (see Figure 2). The muon toroids are used to measure the signed muon momentum and absorb all remnant portions of hadron showers. The central toroid is 1.09 m thick while the ends are each 1.52 m thick. The toroids are operated with an average field of 1.9 T. The momentum resolution is dominated by multiple scattering with a typical value of 20%. The combined calorimeter plus toroid thickness varies from about 14 λ in the central region to 19 λ in the end regions. This thickness reduces the hadronic punchthrough by a factor of 10^{-4} below prompt sources of muons and allows good muon identification within a jet.

Three layers of drift chambers, one between the calorimeter and toroid and two outside the toroid, are used to measure muon trajectories. The wide-angle muon system consists of 164 chambers, using 10 cm cells, which cover the angular region greater than about 10 degrees. These chambers combine drift time measurement with time division and vernier pads to obtain 3D points. The innermost layer has four measurement planes while the outer two have three each so that most muons are measured with ten 3D points. In the small-angle (SAMUS) region between 5 and 20 degrees, six modules of 3.0 cm drift cells are used with each module having six planes in an XX,YY,UU configuration. The smaller cell size is needed in this region to reduce cell occupancy and to sharpen the p_T^μ threshold of the trigger. Figure 3 gives the muon geometric acceptance as a function of η for different layer requirements. Gaps in the central region coverage are due to support and service structures.

Muon identification utilizes information from the muon system itself, the central tracking, and the calorimeter. The primary backgrounds in the central region are from cosmic rays, which are out of time with the beam crossing and do not intercept the primary vertex, and hadron-induced spray (often uncorrelated chamber hits) which produces poorly fit tracks which also tend to miss the vertex. Good tracks in the muon chambers are defined by using appropriate track quality cuts (for example, on the χ^2 of the fit and the number of hits on the track) and that there are no muon chambers along the track without hits. The hit density is largest at small angles and our multi-layer chamber coverage is also best in this region (with some muons hitting 24 wire chamber planes).

The DØ calorimeter is sensitive to minimum ionizing energy depositions, and the presence of such energy along the muon track helps to eliminate non-muon backgrounds. Muon chamber tracks are also matched with the central detector tracks. In addition to properly projecting to the muon chamber hits, the matched central track can be required to have a good fit and small impact parameter. This aids in eliminating non-muon and cosmic ray backgrounds, and can also tag π/K decays. Finally, timing information in the central tracking and muon chambers can also be used to remove cosmic ray muons.

3. DØ MUON TRIGGER SYSTEM

The goal of the DØ trigger system is to reduce the roughly 250 kHz interaction rate to 2 Hz of good physics events to be written to *8mm* tape. There are three stages to the DØ muon trigger. The first two (Level 1 and 1.5) use hardware logic to make trigger decisions in about 3.5 and 20 μs respectively. Also used at Level 1 is a hardware jet trigger which uses energy sums in $\Delta\phi = \Delta\eta = 0.2$ calorimeter trigger towers to identify jets. At Level 2, muon reconstruction and jet finding software is used on a VAX model 4000-60 processor farm. The Level 2 trigger is a subset of the offline reconstruction software and is designed to take about 100 - 400 ms per event. The total trigger rate (all triggers) out of Level 1 is about 350 Hz. The Level 1.5 muon trigger reduces this rate to about 100 Hz which is sent into Level 2. Level 2 outputs 2 Hz of events to tape. The Level 1 and Level 1.5 muon hardware triggers are described in detail below.

A block diagram of the muon trigger system is shown in Figure 4. The basic information provided by the wide- and small- angle muon chambers to the muon trigger system is a single latch bit for each of the approximately 15,000 drift cells of the muon system. This bit information gives the bend coordinate of hit drift cells with a granularity of 10 cm in WAMUS ($|\eta| < 1.7$) and 3 cm in SAMUS ($2.4 < |\eta| < 3.3$). Together with the analog time and charge signals, these bits are transmitted to the MCH and received by 200 Module Address Cards (MAC's) which reside in 24 VME data crates using custom backplanes. Each muon data crate has a 68020 microprocessor used for downloading data, in-situ electronics testing, and event building. The MAC cards and subsequent level 1 and level 1.5 muon trigger electronics are kept physically distinct for the 5 separate η regions of the muon detector (CF, EF-North, EF-South, SAMUS-North, and SAMUS-South).

The MAC cards receive the latch bits, perform zero suppression for data acquisition, and generate bit patterns corresponding to hit centroids for input to the level 1 and level 1.5 muon trigger electronics. Centroid is defined here as the most likely half-cell (5 cm in WAMUS and 1.5 cm in SAMUS) traversed by a track projected to the midplane of an A, B, or C layer muon chamber. Centroid PAL logic is programmed using pairs of drift cells and can find the correct centroid even in the presence of geometrical inefficiencies or delta rays. The MAC cards transmit a bit pattern corresponding to a logical OR of the centroids to the level 1 muon trigger (called the CCT or Coarse Centroid Trigger). In WAMUS (SAMUS) this OR is performed on a group of 3 (4) centroids. The MAC cards also produce a a full list of centroids to be sent to the level 1.5 muon trigger (called the OTC or Octant Trigger Card).

The WAMUS CCT cards receive the OR'd bit pattern from the MAC cards and OR them again (OR-by-4) into hodoscopic patterns of 6 cell width (60 cm). Each CCT can accept inputs from up to 13 MAC cards. In the CF region this corresponds to inputs from 3 A layer MAC's, 5 B layer MAC's, and 5 C layer MAC's. The resultant bit patterns of B and C layer MAC's are input to two PAL's which jointly produce a 12 bit output pattern corresponding to A layer bits for 12 possible roads. This "predicted" A layer bit pattern is then compared with the actual 12 bit A layer pattern to determine good level 1 trigger muons.

Other η regions such as SAMUS-N and -S and overlap regions in which muon tracks begin in SAMUS chambers and continue into sections of the WAMUS chambers use CCT cards for level 1 triggering as well. For example, in the SAMUS region, CCT's are first used to find spacepoint triplets in each of the A, B, and C layers using spatial coincidences of X, Y and U plane bit patterns from from SAMUS MAC's. Bits from good X-Y-U triplets in each of the three layers are next used to search separately for X, Y, and U roads of 12 cm width. Finally, bits from found X, Y, and U roads are used to find triple coincidences corresponding to good A layer spacepoints which are taken as good level 1 trigger muons in this region.

The output of all CCT's for a given η region is sent to a second CCT-like card which performs counting of muons in that region. Two bits of muon multiplicity for each of the η regions is sent to the Trigger Monitor Card (TRGMON) described below. CCT decisions are available within the 3.5us inter-bunch crossing time. The results from individual CCT cards are latched and readout using the CCT LATCH card which resides in the OTC VME crates.

After a trigger framework decision of any level 1 muon trigger, the MAC full centroid lists are strobed into the OTC cards for level 1.5 decision making. Triggers requiring the muon level 1.5 trigger delay sending digitizing orders until the level 1.5 trigger with its sharper transverse momentum threshold can confirm good level 1 muon triggers. Each OTC accepts inputs from 3 layers of MAC's. The mapping of MAC's to OTC's follows that for CCT's except that centroids from a given layer are transmitted serially and not in parallel as the bit patterns for the CCT's are. The OTC compares all combinations of A, B, and C centroids to determine if they correspond to tracks above a threshold transverse momentum (typically 3 - 7 GeV/c). The address space for each combination exceeds the physical limits of available fast SRAM's so instead each combination of A, B, and C centroids is used to generate 2 addresses to 2 SRAMS's containing combinations which correspond to tracks exceeding a given transverse momentum threshold. A good trigger requires a "1" from both memories. A 4 x 4 array of these SRAM's allows the lookups for the 16 combinations of 1 A centroid, 4 B centroids, and 4 C centroids to be carried out in parallel.

For each good trigger combination further processing is done by using the latched input centroids as address inputs for a second set of memories. These memories produce 2 24 bit trigger words which are user defined and output to FIFO's for read out by the OTCMGR described below. Presently these trigger words are simply the centroids for good triggers however this information is also available for further processing both on the OTCMGR and at level 2. Processing times for the level 1.5 trigger in WAMUS regions are typically less than 2 us.

The SAMUS OTC trigger faces a large combinatoric problem due to the large flux of beam jet related particles near the beam. In the SAMUS region, three types of OTC's are used to first find separately X and Y A-B-C layer roads and good X-Y-U spacepoint triplets in the B layer of SAMUS. Centroids from these three OTC's are sent to a second level of OTC's which link the B layer centroids from X and Y roads with the B layer centroids of good X-Y-Y spacepoint triplets. Combined processing times for both stages of SAMUS OTC's can exceed 100 us however each OTC contains a programmable long timeout which aborts trigger processing in the case of very long processing times.

After each OTC's processing is complete, its output FIFO is read by the OTCMGR (OTC manager) card. The OTCMGR collects, processes, and buffers the trigger words from all defined OTC's in a given OTC crate. A status word for each defined OTC is read out as well. A new version of the OTCMGR uses the centroid information contained in the trigger words to apply a second transverse momentum threshold to the event. This allows the level 1.5 muon trigger the flexibility of 2 different transverse momentum thresholds. The OTCMGR for each η region processes all the trigger words for that region and sends to the TRGMON 3 user defined bits of transverse momentum, multiplicity, and/or geographic information. Upon receipt of good level 1 or level 1.5 trigger from the framework all trigger words in the OTCMGR are read out by the VME Buffer/Driver (VBD) in each OTC crate.

The TRGMON (Trigger Monitor) card receives from each η region two bits of level 1 muon multiplicity and three bits of level 1.5 information The TRGMON resides in a separate VME crate called the muon supervisor crate along with several TIMER cards which control timing signals sent to the MAC crates. These level 1 and level 1.5 η region bits are mapped into 16 level 1 and 16 level 1.5 physics bits (e.g. 2 muons anywhere in $|\eta| < 3.3$) via downloadable RAM on the TRGMON. It is these 16 level 1 and level 1.5 bits which are sent to the AND-OR network of the trigger framework along with trigger information from other detector systems to determine whether any of the programmed 32 specific level 1 physics triggers have fired.

In the $|\eta| < 1.0$ region, the Level 1 muon trigger efficiency (excluding geometrical effects) shows a plateau at 90% for $p_T^\mu > 8$ GeV and is half that value at $p_T^\mu = 4$ GeV. The Level 1.5 muon trigger efficiency in that region shows a plateau at 85% for $p_T^\mu > 12$ GeV and is half that value at $p_T^\mu = 7$ GeV.

Level 1 Trigger	Level 1 σ	Level 2 Trigger	Level 2 σ
MUON(1,Y1)	50 μb	1 $p_T^\mu > 3$ GeV in Y1	1.5 μb
MUON(1,Y2)	65 μb	1 $p_T^\mu > 3$ GeV in Y2	7.0 μb
MUON(1,Y4)	600 μb	1 $p_T^\mu > 3$ GeV in Y4	10.0 μb
MUON(2,Y2)	3.5 μb	2 $p_T^\mu > 3$ GeV in Y2	0.08 μb
MUON(1,Y2) JET(1,3)	3.0 μb	1 $p_T^\mu > 3$ GeV in Y2, $E_T^{jet} > 10$ GeV	0.25 μb
MUON(2,Y4) JET(1,3)	5.0 μb	2 $p_T^\mu > 3$ GeV in Y4, $E_T^{jet} > 10$ GeV	0.005 μb

Table 1: B Triggers for DØ run 1a. MUON (n,Ym) is defined as n muons in η region Ym. Region Y1 is $|\eta| < 1.0$, Y2 is $|\eta| < 1.7$, and Y4 is $|\eta| < 3.3$. JET(n,m) is defined as n jet trigger towers > m GeV

4. B TRIGGERS AT DØ

On DØ , B's are identified by their semileptonic decay into muons. Thus triggers for b physics are dominantly muon triggers. The b physics triggers used in the first run of DØ are listed in Table 1 along with the measured rates out of Level 1 and Level 2. The rates of single muon triggers without any jet trigger requirement are too high to be run without large prescales. Data for these triggers were collected with special single muon trigger runs at times of lower Tevatron luminosity.

Improvements in b triggering for run 1b of DØ include installation of new scintillator on the top of DØ (for improved cosmic ray muon rejection at Level 2 and possibly Level 1), use of Level 1.5 with lower p_T^μ thresholds (giving increased rejection), a large tile jet trigger (larger ($\Delta\eta = 0.8$ x $\Delta\phi = 1.6$) trigger towers will give increased rejection from sharper E_T^{jet} efficiency curves), and improved Level 2 muon identification algorithms.

5. ACKNOWLEDGEMENTS

The DØ collaboration consists of the following institutuions: Universidad de los Andes (Colombia), University of Arizona, Brookhaven National Laboratory, Brown University, University of California,Riverside, Centro Brasiliero de Pesquisas Fisicas (Brazil), CINVESTAV (Mexico), Columbia University, Delhi University (India), Fermilab, Florida State University,

University of Hawaii, University of Illinois, Chicago, Indiana University, Iowa State University, Korea University (Korea), Lawrence Berkeley Laboratory, University of Maryland, University of Michigan, Michigan State University, Moscow State University (Russia), New York University, Northeastern University, Northern Illinois University, Northwestern University, University of Notre Dame, Panjab University (India), Institute for High Energy Physics (Russia), Purdue University, Rice University, University of Rochester, CEN Saclay (France), State University of New York, Stony Brook, SSC Laboratory, Tata Institute of Fundamental Research (India), University of Texas, Arlington, and Texas A&M University.

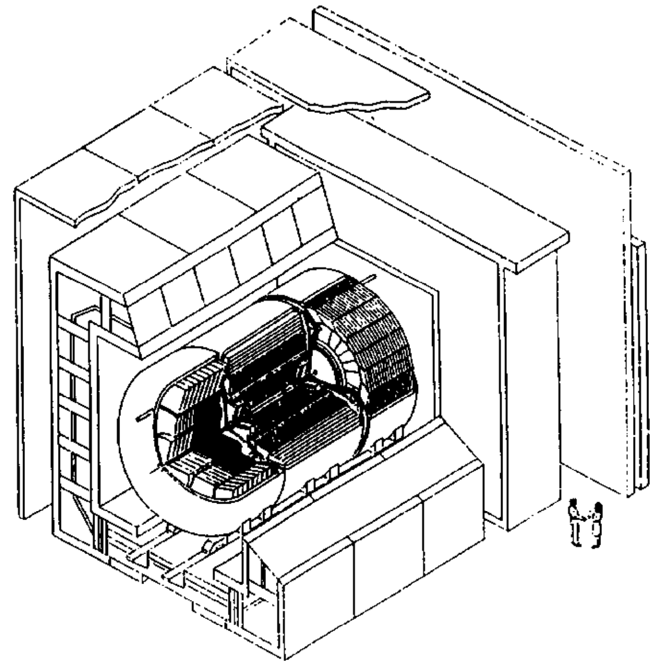

Figure 1: The DØ detector.

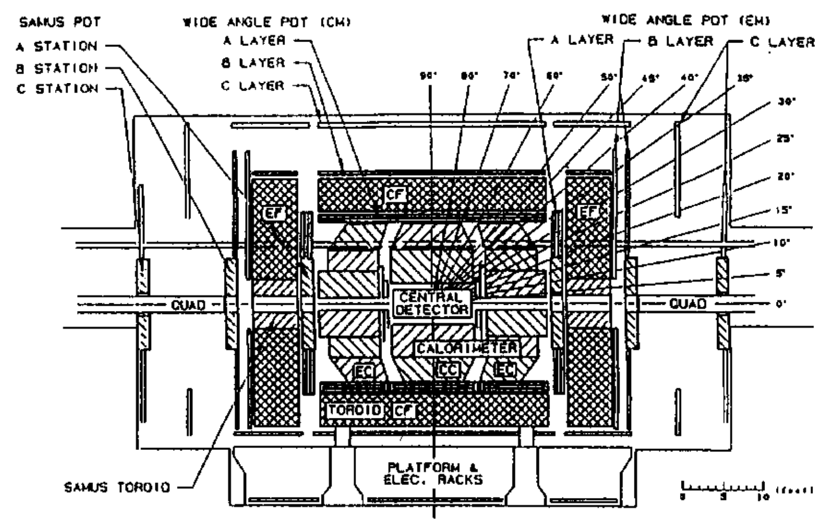

Figure 2: The DØ muon system.

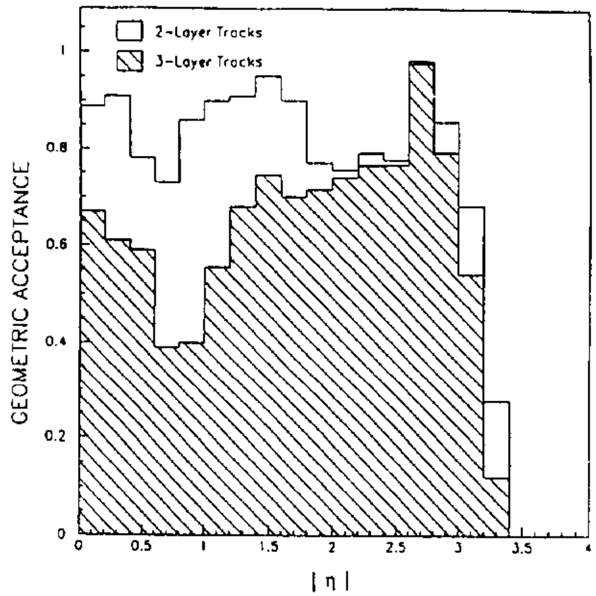

Figure 3: Geometrical acceptance of the DØ muon system.

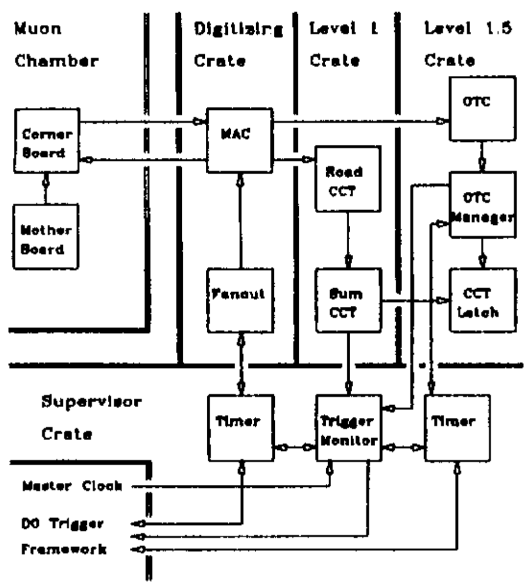

Figure 4: Block diagram of the DØ muon trigger system

THE CDF MUON SYSTEM

Thomas J. LeCompte
University of Illinois at Urbana-Champaign
and
Vaia Papadimitriou
Fermi National Accelerator Laboratory

We describe the characteristics of the CDF muon system and our experience with it. We explain how the trigger works and how we identify muons offline. We also describe the future upgrades of the system and our trigger plans for Run IB and beyond.

1. Description of the CDF Muon System

The CDF muon system consists of four subsystems: The Central MUon chambers (CMU), the Forward MUon chambers (FMU), the Central Muon uPgrade chambers (CMP), and the Central Muon eXtension chambers (CMX). The first two subsystems were parts of the detector from the 1987 collider run. The last two were added only in 1992, for Run IA (See Figure 1 Top. Figure 1 Bottom shows the detector in the Run II configuration).

CMU:

The CMU system is located around the outside of the central hadron calorimeter at a radial distance of 3.47 m from the beam axis. It is segmented in ϕ into 12.6° wedges which fit into the top of each 15° central calorimeter wedge. This leaves a gap in the central muon coverage of 2.4° between each wedge. Each muon wedge is further segmented in ϕ into three modules of 4.2° each. Each of the three modules consists of four layers of four rectangular drift cells. A stainless steel resistive 50 μm sense wire is located at the center of each cell. The chambers measure four points along the trajectory with an accuracy of 250 μm per point in the ϕ direction. Charge division gives an accuracy of σ =1.2 mm per point in the z direction. The chambers cover the angular region $56° < \theta < 124°$ or $|\eta| < 0.63$. In this region their average coverage is 84% due to the ϕ gaps between the wedges and the boundary between the central arches at $\theta = 90°$. Because there is an average of only 5.4 pion interaction lengths between the CMU chambers and the event vertex, about 1 in 220 hadrons traverses the calorimeter without interacting, thereby causing the hadron to be misidentified as a muon. Another limitation of the detector is its restricted θ coverage.

FMU:

The CDF forward muon system consists of two muon spectrometers measuring muon momentum and position for polar angles 3°-16° (forward) and 164°-177° (backward). This system consists of a pair of magnetized iron toroids instrumented with three sets of drift chambers and two planes of scintillation trigger counters. We have an average of 17 pion interaction lengths in FMU and therefore there is no pion punch-through background. The main source of background in FMU is decays of pions and kaons in the space between the interaction point and the detector.

CMP:

The CMP consists of an additional 60 cm of steel absorber behind the current central muon system, followed by a second set of muon chambers. The return yoke of the CDF solenoid already provides the necessary steel at the top and bottom of the central detector so that it is only necessary to add more steel on the two sides, where two movable steel walls were installed. The CMP chambers have single wire drift cells. Four chamber layers are required, with one pair of chambers half-cell staggered relative to the other pair. CMP has a pseudorapidity coverage of $|\eta| \leq 0.57$ and has an average ϕ coverage of about 80%, so that the fraction of CMU also covered by CMP is 72%. It reduces the punch-through rate by a factor of ~ 10 (see Figure 2) which allows us to lower the p_T thresholds without the trigger rates becoming unmanageable, and also to identify muons within jets which is especially important for bottom and top physics.

CMX:

CMX consists of "pinwheels" of drift cells around each end of the detector. It extends the θ coverage by covering the region $.62 < |\eta| < 1.0$. In the region $-45^o < \phi < 225^o$ the cells lie on a conical surface to maximize the acceptance. In the region $225^o < \phi < 315^o$ the cells have been assembled in a flat pinwheel-like structure to minimize the space occupied. Because of the angle at which particles traverse the calorimeter, the amount of steel is larger here than in CMU and no new steel is added. We have 8 layers of drift cells between 2 layers of scintillator which provide three-dimensional tracking. The scintillators (CSX) provide the timing of the muon track. The cell dimensions are 1" x 6" x 72" and we have a single wire per cell. The resolution is 250 μm (1 cm) perpendicular to (along) the wire. Forty-eight cells are glued into a module covering 15^o in ϕ. Two arches with 8 modules each were installed on each side of the detector for Run IA. CMX covers currently 2/3 of ϕ; 30^o at the top of the detector have no coverage due to interference with the main ring shielding and the cryogenics. 90^o in the bottom were not instrumented either. We have an increase of approximately 25 % in the dimuon sample due to the dimuons that have one muon in the CMX.

3. Today: Run IA Triggers

CDF uses a three tiered trigger system. Level 1 (L1) has an input rate of 300 kHz, to match the 3.5 μs crossing time. Level 2 (L2) has an maximum input rate of approximately 2.5 kHz, and an output rate of about 20 Hz. Level 3 is a farm of computers that runs a slightly streamlined version of the offline reconstruction code, and can write about 6 Hz to tape.

At Level 1, we require either a single muon with a p_T above a high threshold, or two muons with p_T's above a lower threshold. For the central region, the high threshold is approximately 6 GeV, and for the extension it is 10 GeV. The low threshold is 3 GeV everywhere. Because the p_T is measured by the slope of the track in the muon chambers, with a lever arm of only a few centimeters, this measurement is cruder than measuring the transverse momentum in the central tracking chamber; the turn-ons are therefore rather soft. In addition, if the muon is in a CMU chamber that is not in a CMP ϕ gap, there must also be a CMP hit for the muon to pass the high p_T threshold. Low p_T muons do not have this CMP requirement. The total Level 1 muon cross section is about 110 μb.

By Level 2, CTC tracking information in the $r-\phi$ plane is available from the CFT, or Central Fast Tracker. A track with $p_T > 9.2$ GeV is required to match within 5 degrees of the muon stub for a single muon trigger, and a track with $p_T > 3$ GeV is required to match within 15 degrees of one of the two muon stubs for a dimuon trigger. (The 15 degree requirement is there because there is not enough hardware to implement the 5 degree match on both sets of triggers.)

This dimuon trigger has two changes relative to the 1988-1989 run trigger, changes designed to increase the number of J/ψ's written to tape per unit luminosity. One change was to lower the trigger threshold at Level 2: in the 1988-89 run we required both muons to have $p_T > 3$ GeV/c; that requirement has been relaxed to requiring at least one muon to have $p_T > 3$ GeV/c. Figure 3 shows the substantial increase in J/ψ yield from this change. In the 1988-89 run we also required that the two muons be separated from each other by at least one full muon wedge. In Run IA, the separation requirement was reduced to a singe muon chamber This change increased the acceptance by approximately a factor of ~ 2 at high p_T's, for a combined trigger efficiency increase for J/ψ's of approximately a factor of five. Figure 4 shows the dimuon trigger efficiency plotted against muon p_T for the Level 1 trigger; Figure 5 shows the same thing for the Level 2 trigger.

3. Experience with the CMX system

Making the CMX system work was not trivial. The CMX allocated trigger cross section for Run IA was 64 μb for Level1 and 78 nb for Level2. In May 1992, though, we had 4000 μb at L1 and L2 was significantly above the allocated cross section as well. The excess of triggers was not associated with the main ring, since the triggers were azimuthally symmetric. The excess was not due to pion punch-through that we had not anticipated, since the triggers did not pile up at cracks in the calorimeter. It was not some kind of strange beam loss either, since we did not observe any kind of east/west (proton/antiproton) asymmetry. These convinced us that the triggers were coming from the $\bar{p}p$ interaction. One clue in the understanding of the problem was that there was no calorimeter energy associated with the triggers. This led us to think that the triggers might possibly be coming from interactions of low-angle particles in the beam pipe or in the forward calorimeter. In addition, these particles appeared to have extremely low momentum, and rates in the front and back sections of the CMX showed indications that a substantial fraction of these particles were ranging out in the chamber material. The secondary-interaction or "spray" hypothesis was further supported by the fact that there was much more activity in the inner surface of the endplug calorimeter in Run IA than there was in the 1988-89 collider run. If there was a spray of particles from the beampipe into the plug calorimeter, it could also affect the rates of CMX. Monte Carlo studies were performed which were successful in predicting the observed trigger rates. In August 1992 we were convinced that the problem was due to particles interacting in the beam pipe and in the forward calorimeter. The available solutions were: a) to change the beam pipe; b)since a particle coming from the beam pipe or the forward calorimeter is delayed by roughly ten or twenty nanoseconds respectively relative to particles coming from the interaction point, we could apply a tight time gate to the scintillator coincidence; c)request that the muon has fired the Hadron Calorimeter TDCs.

In February 1993 we replaced the old, 69 mil thick stainless steel beam pipe by a thin one which was 30 mils of Aluminum and the trigger rates were reduced by factors of 2-3. The addition of a tight time gate at the scintillators and the Hadron Calorimeter TDC requirement made finally the L1 trigger rates manageable in March of 1993.

4. Offline muon reconstruction

Although we identify muons at L1 by requiring a muon track, and at L2 by requiring that this muon track matches to a Central Tracking Chamber (CTC) track, we have to apply tighter cuts offline in order to reject background. We first request that there is less than 3-4 σ difference in position between each muon chamber track and its associated, extrapolated CTC track, in both $r\phi$ and z views where σ is the calculated uncertainty due to multiple scattering, energy loss, and measurement uncertainties. One can make similar requirements for the slope. We have not used slope cuts till now but we may do in the future. (The remaining difficulty arises from the effect of δ rays in the muon chambers causing a mismeasurement of the slope) These cuts have efficiencies greater than 98% while they reduce the background by a factor of approximately five. Depending on the analysis, we also perform isolation cuts by looking at the energy in a cone around the muons and other energy related quantities or we request that the muon has CMP confirmation. It is seldom easy to understand the efficiency of the calorimetric cuts and therefore they are usually avoided.

5. 1993: Run IB

In Run IB, the delivered luminosity is expected to double, and the trigger bandwidth at Level 2 and Level 3 will also (approximately) double. This means that the cross-section at Level 1 will have to be reduced by approximately a factor of two. To do this, we are adding the additional requirement that the hadron calorimeter TDCs show energy deposition within 30 ns of the interaction. A muon deposits approximately 1 GeV of energy in the central or endwall hadronic calorimeter, which provides sufficient light at the phototube to measure the time. This information is used offline to reject cosmic rays; the plan is to use it online as well, to reject all out of time backgrounds: cosmic rays, forward calorimeter albedo, spray from the beampipe, main ring-induced particles, etc. Additionally, the CSX scintillators on the CMX will also be required to be in time, to within a few nanoseconds, further reducing the out of time background. Applying these timing cuts reduces the cross-section by more than a factor of two, so we are using the additional available bandwidth to implement a so-called "η gap" trigger. Muons which are in the ϕ region covered by the CMP, but not the η region (rejected by the IA trigger) will be accepted at Level 1 if there is hadron TDC confirmation in the η region not covered by the CMP.

At Level 2, the total cross-section is approximately the same. However, the cross-sections of several triggers, including the single muon and dimuon triggers, is increasing with luminosity. To fight this, a number of changes will be made. First, the Level 2 CFT (Central Fast Tracker) thresholds will be made different for muons with and without CMP confirmation. CMU-only and CMX muons will have a 12 GeV threshold; these triggers are intended for electroweak and top physics. The CMU-CMP muons, however, will have their threshold *lowered* to 7 or 8 GeV. The rationale is to trade low purity muon triggers for higher purity triggers, thus decreasing the overall trigger rate and increasing the number of $B \to \mu + X$ events simultaneously.

For dimuons, more drastic steps must be taken. The current trigger, which requires only one of the two muons to have a CFT track with $p_T > 3$ GeV has a cross-section that grows considerably with luminosity. Many of these events have one real muon of $p_T > 3$ GeV, and one junk stub. Requiring a track to point to both muon stubs is expected to solve the cross-section growth problem. Unfortunately, requiring both legs to pass the $p_T > 3$ GeV threshold (the current CFT lower limit) removes 80% of the J/ψ's. To solve this, the CFT is being modified so that the lowest p_T threshold is 2 GeV. This 2-2 trigger should have approximately the same J/ψ rate as the Run IA 3-0 trigger. J/ψ's that pass this trigger will have decays even more symmetric than those that pass the 3-0 trigger; this may have implications for J/ψ polarization physics. It is also possible that we will be able to make a tighter track-stub matching cut (5 degrees instead of 15) in Run IB.

Level 3 will remain essentially unchanged. The p_T thresholds will be changed to reflect the new Level 2 thresholds, and it is possible that the tracking will be restricted to the region of ϕ that caused the trigger - e.g. on J/ψ triggers, the away side jet won't be tracked.

6. 1996: Run II and beyond

In Run I the FMU chambers were located $\sim$ 10 m away from the interaction point. For Run II FMU will move closer to the interaction point ($\sim$ 5 m away) to increase the polar angle coverage for muons, as well as to reduce the decay in flight background by reducing the decay length. This will create some triggering problems though; the FMU chambers were built to form roads with the planes of chamber cells which point at a vertex 10 m and not 5 m away. The trigger roads can be rewired to work under the new conditions but at the cost of not having a sharp p_T threshold. We plan to use scintillator signals from the upgraded plug calorimeter as a L1 trigger. We may also be able to use the FMU scintillator signals but probably the occupancy will be too high at Run II and beyond. There are also thoughts of using timing information from the plug calorimeters at L1, if there is timing information available,

In the central region, hardware upgrades that had been started for Run I will be completed for Run II. In particular, the bottom portion of the central muon extension will be installed, and the ϕ gaps in the CMP will be filled. In addition, the CMU will be operated in proportional mode rather than streamer mode.

Also in Run II, the beam bunch spacing will decrease from 3.5 μs to 396 ns, in preparation for the 192 ns crossing time in the Main Injector era. The maximum drift time in the CMU chambers is about 700 ns, and the maximum drift time the CMP chambers is about 2 μs. So, establishing the correct t_0 becomes the critical new feature of the Run II trigger.

The CMP chambers will be surrounded by scintillators, called the "CSP" detector, for Central muon Scintillator uPgrade. (Slightly fewer than half the counters have been installed in the CDF collision hall to test the system in Run IB.)

These will be able to give a t_0 for high p_T muons. However, for B physics, we would prefer not to rely on the CMP/CSP for t_0 information, because of the more restrictive momentum requirement it imposes on muons from J/ψ decays. Two alternative sources of t_0 information have been identified: calorimeter TDCs and the planned new hardware tracker.

The proposed "XFT" (eXtremely Fast Tracker) hardware tracker will provide a set of tracks and estimates of their transverse momentum for each crossing. A dimuon trigger could be implemented by requiring two low p_T CMU stubs, and two XFT tracks of $p_T >\sim 1.5$ GeV matching to these stubs. The crossing with the two XFT tracks is taken to be the crossing of the dimuon event, and the time of that crossing is the t_0 of the interaction.

If difficulties arise in doing this, the alternative plan is to use TDCs on the hadron calorimeter outputs. This is more than sufficient to identify which 132 ns crossing caused the trigger.

Unlike Run I, the bandwidth is not really a limiting factor. The rates from the $B \to \pi^+\pi^-$ trigger overwhelm everything else. Planned thresholds are 1.5 GeV on each leg for dimuon triggers, 6 GeV for single muon triggers in the upgrade region (3 GeV if the muon has a large impact parameter as measured by the Level 2 vertex tracker), and 9 GeV for muons without CMP confirmation: again, for W, Z and top physics.

7. Summary

The CDF muon system, originally designed for electroweak and top physics, is capable of triggering on $B \to \mu + X$ and $B \to J/\psi + X$ decays. Since the 1989-1989 run, we have increased coverage with the addition of the CMX, purity with the addition of the CMP, and yields by lowering trigger thresholds. A rich program of investigating the physics of b's is already underway. The CDF strategy for the future is to continue increasing the coverage and triggering efficiency.

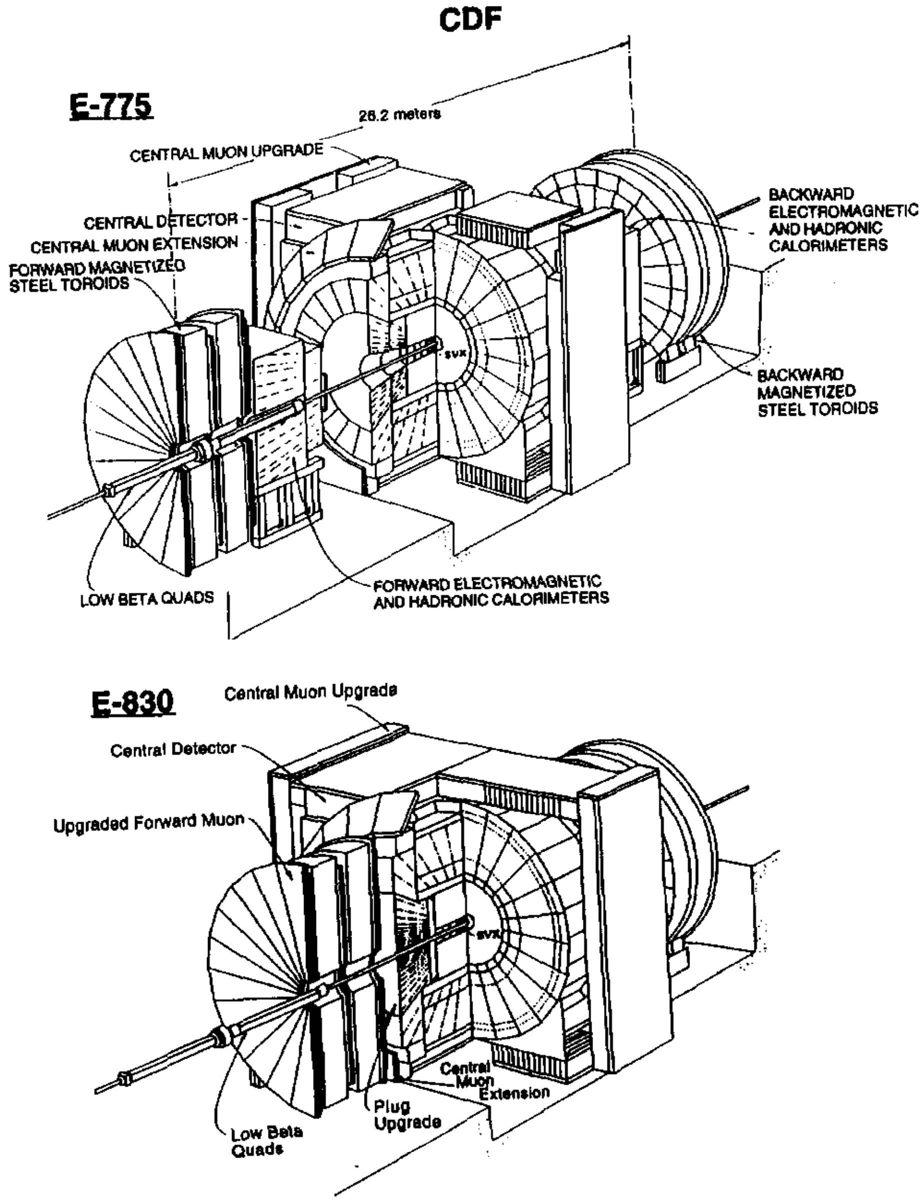

Figure 1.

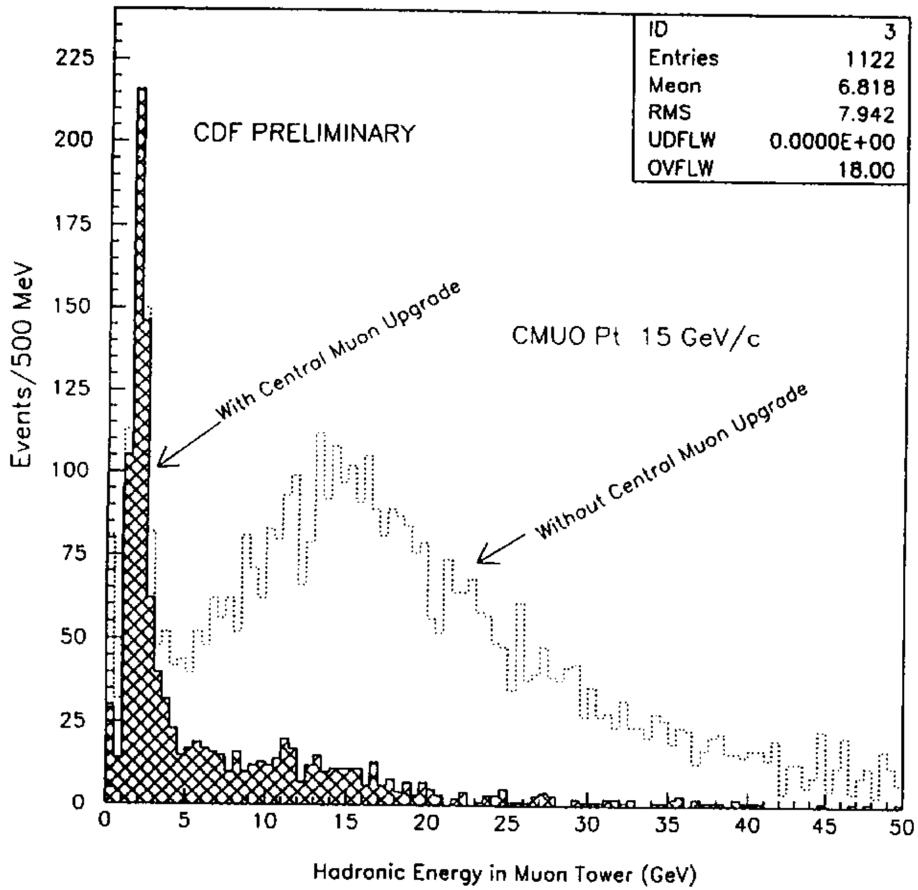

Figure 2

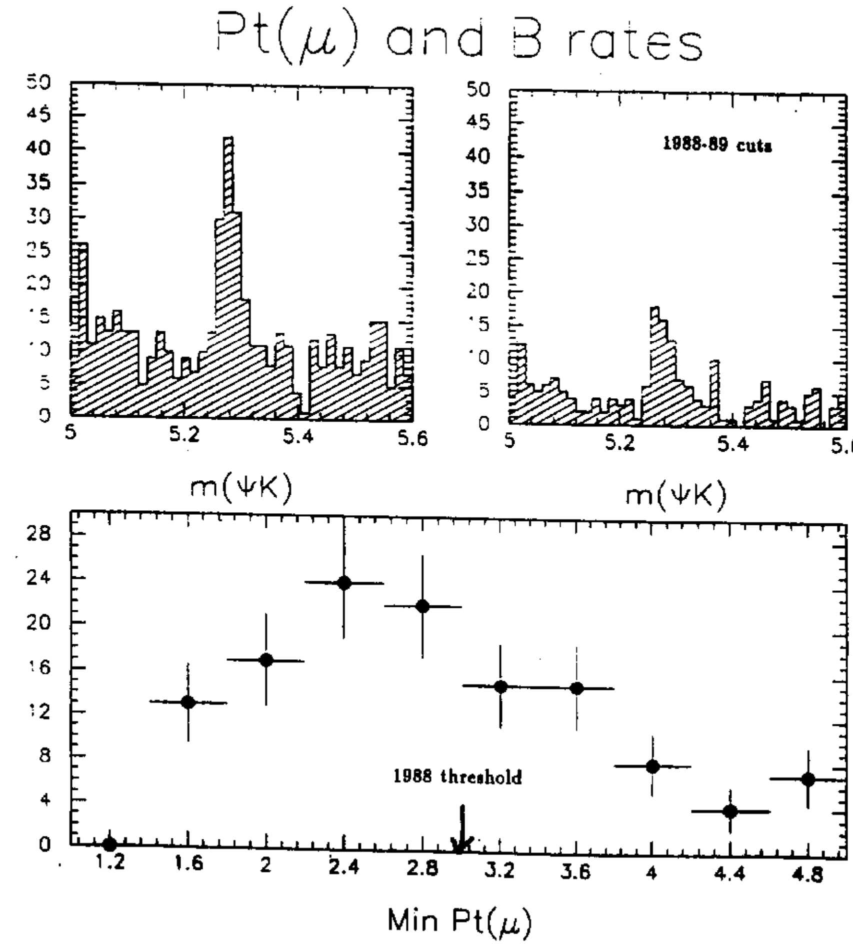

Figure 3

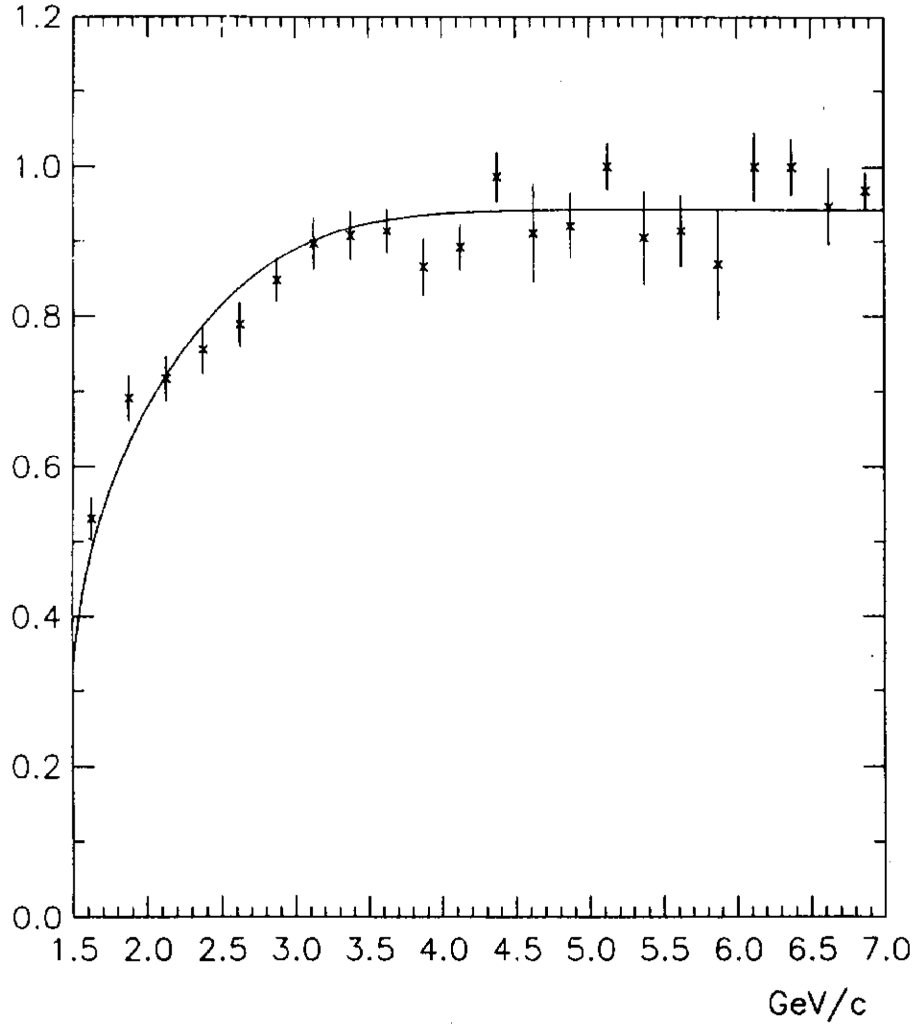

Figure 4

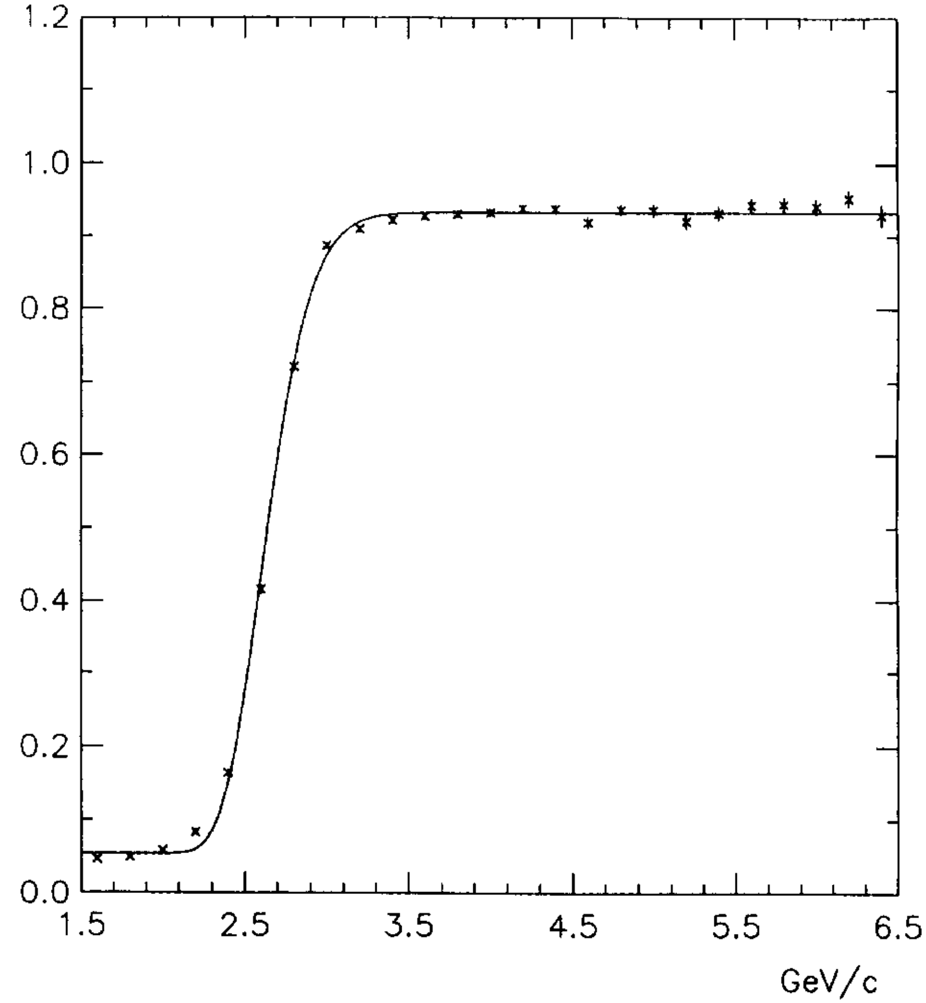

Figure 5

Hadron ID

Convenors:

K. Nelson
University of Virginia

M. Sheaff
University of Wisconsin-Madison

List of Participants

R. Aleksan
CEN Saclay

T. Alexopoulas
University of Wisconsin

M. Artuso
Syracuse University

B. Cox
University of Virginia

F. DeJongh
Fermi National Accelerator Laboratory

Y. Giomataris
Lausanne University

V. Jain
Vanderbilt University

C. Kennedy
Yale University

R. Kephart
Fermi National Accelerator Laboratory

K. Kinoshita
Virginia Polytechnic Institute

S. Kwan
Fermi National Accelerator Laboratory

J. Lewis
Fermi National Accelerator Laboratory

X. Lou
Indiana University/CERN

Y. Mukhin
Syracuse University

P. Schuler
Superconducting Super Collider Laboratory

H. Yamamoto
California Institute of Technology

SUMMARY OF THE HADRON ID GROUP

K. Nelson[1] and M. Sheaff[2], Co-convenors

Roy Aleksan[3], Theodoros Alexopoulos[2], Marina Artuso[4], Brad Cox[1]
Fritz DeJongh[5], Joannis Giomataris[6], Vivek Jain[7], Chris Kennedy[8]
Bob Kephart[5], Kay Kinoshita[9], Simon Kwan[5], Jonathan Lewis[5]
Xinchou Lou[10], Yuri Mukhin[4], Peter Schuler[11], Hitoshi Yamamoto[9]

1. INTRODUCTION

The members of the Hadron ID Working Group represented a wide spectrum of experimental environments and detector expertise. On most afternoons, two or three speakers presented results from detectors used for particle identification. The majority of the presentations were reports on the performance of detectors used in current generation experiments, but some detailed the results of more speculative work being performed in the framework of detector research and development for expected future experiments or upgrades to existing experiments. One session was held jointly with the Electron ID Working Group because the talks on Transition Radiation Detectors[1] and the Hadron Blind Detector[2] were of interest to both groups.

One of the more noteworthy features of this working group was the large representation and contribution from members of the CLEO collaboration, despite the fact that this workshop was organized to discuss B physics at hadron accelerators. The present CLEO experiment utilizes dE/dx and time-of-flight (TOF) detectors for particle identification. Three standard deviation pion/kaon separation is achieved by the former up to $\sim$.7 GeV/c and the latter up to .9 GeV/c. Members of the group are carrying out an aggressive research program to develop techniques for extending the hadron ID capability to at least the 2.5 GeV/c needed for the symmetric collider program and even beyond this to the 4 GeV/c

[1]University of Virginia
[2]University of Wisconsin
[3]CE Saclay, France
[4]Syracuse University
[5]Fermilab
[6]University of Lausanne, Switzerland
[7]Vanderbilt University
[8]Yale University
[9]Harvard University
[10]Indiana University
[11]SSClab

required for the proposed asymmetric machine of the future[3,4]. In order to provide space for the hadron ID upgrade, it will be necessary to improve the capabilities of the tracking system to attain the same resolutions as previously achieved but in 20 cm less radial space.

Since no hadron ID is currently contemplated for the central collider experiments approved for either the LHC or SSC, our discussions focused only on central collider experiments at the Fermilab Tevatron. However, since the luminosity of these machines is likely to be somewhat below design at turn-on and since the large cross section for B production at such high energies allows for a very rich program of B physics at lower luminosity ($\sim 10^{32}\ cm^{-2} sec^{-1}$), we hope that the detector groups will at least consider ways in which they might include this capability. It is difficult to retrofit detectors with subsystems for hadron ID once built[5]. This was evident in the presentations made by members of the CDF group[6,7]. A modification to the amplifier-shaper-discriminator cards in the CDF central tracking chamber allows pion/kaon separation at low momentum by measurement of dE/dx. However, at least for some analyses, the momentum range covered is not very well matched to the tracks to be identified once all selection cuts on candidates are made. This is likely to be true for the proposed TOF upgrade as well. A Ring Imaging Cerenkov Counter (RICH) would be a better match but there is not enough space outside of the central tracking chamber for a RICH, so that the central tracking chamber would have to be replaced in order to add one.

The proposed forward collider and fixed target experiments at any of the three laboratories do include hadron ID detectors. However, because the very small cross section for B's in fixed target at the Tevatron precludes measurements of CP violation in B decays in that experimental environment, we limited our discussions of fixed target experiments to those proposed for the LHC or SSC only.

2. DO WE NEED HADRON ID IN ORDER TO MEASURE CP VIOLATION IN B DECAYS?

The need for hadron ID in future B experiments is dependent on the specific measurements to be performed and must be established on that basis. Once the case is made, it is necessary to determine whether there are viable techniques which can provide the required discrimination in the various experimental environments proposed for the measurements.

Hadron ID is useful for the purpose of augmenting the lepton tags of the "other" B in measurements of CP violation which require tagging of the other side B. While it is not absolutely essential that hadron ID play a role here since the lepton tags are reasonably efficient and can even be used in the event triggers, estimates of the relative contribution of K tags vary from a factor of three[8] to a factor of five[9] depending on the momentum range (i.e., the experimental environment) and the cuts assumed. Thus, including the kaon tags can considerably reduce the experiment running time needed to reach the desired accuracy in such measurements. Most of the decay modes that have been proposed as good candidates for CP violation studies do require this type of tagging, e.g., the decays of neutral B's to CP eigenstates where both B^o (or B^o_s) and $\bar{B}^o$ (or $\bar{B}^o_s$) decay to the same final state. Examples of decays of this type are $B^o_d \to \pi^+\pi^-$, the most often mentioned candidate for measurement of the angle α, and the decay usually identified as the prime candidate to be the "discovery" channel, $B^o_d \to J/\psi K_s$. (See reference 10 for a discussion of these and other channels in which CP violation phases can be measured.)

A possible method for flavor tagging of B decays has recently been suggested[11], which may prove to be even more effective than the other side tags. In analogy to the D system, where D^{**} production accounts for some 20 to 30% of the D's produced in the e^+e^- continuum, it is postulated that a sizeable fraction of B's may result from the production of B^{**} resonances. If this is indeed the case, the mass difference of the B^{**} and the B coupled with the batchelor pion (or kaon) sign will identify the B as a B^o or $\bar{B}^o$. It is also possible that fragmentation effects alone will lead to a correlation in the sign of the nearest hadron and the flavor of the B for low-mass B-π (or K) pairs. Particle ID will play an important role if these ideas prove fruitful. The sign of the accompanying hadron will identify the B as a B^o or $\bar{B}^o$. The flavor of the accompanying hadron (π or K) will identify the B as B_d or B_s.

Hadron ID (coupled with good tracking resolution) allows the separation of B decay channels of interest from backgrounds due to the reflections of B decays with similar topologies. The example usually cited is $B^o_d \to \pi^+\pi^-$, for which both $B^o_d \to K\pi$ and $B^o_s \to K\pi$ are expected to be backgrounds when the B is misreconstructed by assigning the pion mass to the kaon in the decay. The results of a detailed Monte Carlo study indicate that the large combinatoric background to $B^o_d \to \pi^+\pi^-$ can be eliminated by cuts on vertex separation, on the p_t of the tracks, and on the distance of closest approach of the reconstructed B to the primary vertex[12]. Thus, the reflections of the other B decays modes mentioned above are expected to form the major backgrounds to this decay.

3. WHAT ARE THE DETECTORS OF CHOICE FOR HADRON ID IN THE PROPOSED EXPERIMENTAL ENVIRONMENTS?

Although the p_t distributions of B decay products are peaked at very low values, so that, e.g., approximately half of the lepton daughters from direct B decays have p_t below 1 GeV/c[13], the momenta of the B decay secondaries vary widely over the full kinematic range of proposed future B detectors. This can be seen in Figure 1, which is reproduced from the Bottom Collider Detector (BCD) Proposal[13]. The top three plots show the integrated momentum specta of B decay products for a representative set of ten non-leptonic decays modes with relatively low multiplicity in, from left to right, the central, intermediate, and forward regions of the detector. The bottom three are the same distributions for the decay $B^o \to K^+\pi^-$, chosen for the plot since it is the decay that yields the highest momentum kaons. Since detectors for hadron ID discriminate on the basis of p and not p_t, the demands placed on these detectors are very different depending on the kinematic region covered. Techniques need to be found which allow the separation of pions from kaons at from below 1 GeV/c to approximately 4 GeV/c in the central region, as well as methods which work in the range of tens of GeV/c in the intermediate region and up to hundreds of GeV/c in the forward region.

Particle identification techniques discussed for use at low momenta, i.e., in the central and intermediate regions, were dE/dx, TOF, and RICH counters. As shown in Figure 2, the combination of dE/dx and TOF can be expected to provide at least 2σ separation between pions and kaons up to almost 5 GeV/c assuming the expected performance of the CDF central tracker when used for dE/dx[6]. (Note that the curves are shown versus p_t for $\eta = 0$, where p is p_t.) The time resolution needed for a TOF detector that would actually fill in the dE/dx crossover region with pion/kaon separation having 2σ accuracy is somewhat beyond what is possible with current technology. However, time resolution of 110 ps has been achieved in counters tested for use as TOF detectors[14]. The OPAL dE/dx discrimination is somewhat better than that in the CDF detector and even extends all the way out to 20 GeV/c[15]. This is accomplished by using a pressurized chamber and instrumenting a large number of planes, both of which serve to increase the ionization statistics. The discrimination achieved is shown in Figure 3. For comparison, the expected discrimination of a RICH counter proposed as a CLEO upgrade[4,6] is shown in Figure 4. The RICH uses a liquid radiator, C_5F_{12}, which has a low threshold, $\gamma_t \sim 1.5$, and thus "turns on" for pions at just above 200 MeV/c and for kaons at about 750 MeV/c. The maximum momentum versus dip angle at which 4σ separation can be realized in this detector is shown in the figure. To demonstrate that the discrimination shown extends to high enough momentum, the maximum kaon momentum for $B \to K\pi$ decays versus dip angle is also shown. See Reference 16 for a comparison of the dE/dx, TOF and RICH techniques including also threshold Cerenkov counters. The figures of merit for the different detectors are discussed in this reference, which is one of the submissions to this section of the proceedings.

The RICH detector was the clear choice of the group for the hadron ID detector of the future. Several of the participants are actively involved in research and development on this technique, The large number of both liquid and gaseous radiators available for use allow for a wide option of n values, where n is the index of refraction, and thus a large range in γ_t. The combination of both kinds of radiator in a single detector is possible, so that discrimination of hadron species can be achieved over a large range in momentum. The conventional techniques for detection and readout, a detection volume filled with photosensitive gas which acts as a time projection chamber, is suitable for e^+e^- machines but not for hadron machines. Thus, most of the research and development projects involve studies of "fast" cathodes with a thin layer of CsI adsorbed on the surface for detection of the Cerenkov photons. TMAE is sometimes also added. While the results of the tests are not yet consistent from laboratory to laboratory, the bottom line is that, even for the results showing the lowest quantum efficiency, enough photoelectrons are emitted to make this a viable technique[17]. Further research should improve the performance substantially. Discrimination using RICH counters does not extend to momenta much higher than 200 GeV/c. At higher momenta than this, and thus for the most forward region of the forward collider or fixed target experiments, it is planned to augment the RICH system with TRD's. The expected discrimination as a function of momentum for the forward RICH can be found in References 18 and 19, and that for TRD's in References 1, 19, and 20.

One further point that came out in the discussions of the CDF detector[6] was the fact that dE/dx in the silicon planes allows particle ID at very low momentum. This is shown in Figure 5b) and is to be compared to the same plot for the central tracker shown in Figure 5a). Since the very low momentum tracks are not seen in the central tracker, the silicon planes provide the only particle ID for those. The combination of the two detectors together gives better discrimination than would either one alone above the crossover region. Since dE/dx information comes along, not really "for free", but at the price of including analog readout on tracking detectors, we would urge the proponents of future detectors to consider this option in making their plans. Analog readout also allows for better tracking resolution in some cases, which could provide further motivation.

4. ACKNOWLEDGEMENTS

The authors would like to thank Chris Kennedy for his zeal in providing the huge stack of plots made using Isajet simulations to the group at their request.

5. REFERENCES

[1] M. Sheaff, "Use of Transition Radiation Detectors for B Tagging/Triggering in Collider or Fixed Target Experiments", talk given at this workshop, published in these proceedings.

[2] J. Giomataris, "The Hadron Blind Detector", talk given at this workshop.

[3] K. Kinoshita, "Some Novel Ideas in Particle ID Detectors", talk given at this workshop.

[4] M. Artuso, "Proposed Fast Ring Imaging Cerenkov Detector for CLEO Upgrade", talk given at this workshop.

[5] K. Nelson, "Summary of Hadron ID Working Group", talk given at this workshop.

[6] J. Lewis, "Experience with dE/dx in the Central Tracking Chamber at CDF", talk given at this workshop. Figure 4 was shown by this speaker and also by the speaker in Reference 4, above.

[7] R. Kephart and F. deJongh, "Proposal to Include a Time-of-Flight Detector in CDF", talk followed by a discussion presented at this workshop.

[8] S. Erhan, M. Medinnis, P. E. Schlein, and J. G. Zweizig, "COBEX. a Dedicated Collider B Experiment", NIM **A233** (1993) 101.

[9] H. Castro et al. (The BCD Collaboration), "Addendum to the Proposal for a B-Physics Experiment at TeV I: The μBCD", submitted to the Fermilab PAC on January 7, 1991.

[10] K. T. McDonald, "Six Ways to Measure CP-Violating Phases in B Decays", Princeton/HEP/92-09.

[11] M. Gronau, A. Nippe, and J. Rosner, "Method for Flavor Tagging in Neutral B Meson Decays", Phys. Rev. **D47**, (1993) 1988. See also, M. Gronau and J. Rosner, "Framework for Identification of Neutral B Mesons", TECHNION-PH-93-31, EFI 93-43, submitted for publication in Phys. Rev. Letters.

[12] O. R. Long et al., "Monte Carlo Simulations of $B_d^o \to \pi^+\pi^-$ from p-p Interactions at $\sqrt{40}$ TeV", UPR/216E, Princeton/HEP/92-07, SSCL/PP/139.

[13] H. Castro et al., "Proposal for a B-Physics Experiment at TEV I, The μBCD", proposal submitted to the Fermilab Physics Advisory Panel on October 8, 1990.

[14] R. T. Giles, F. M. Pipkin, and J. P. Wolinski, "Tests of Conventional and Microchannel Plate Photomultipliers as Components of a Scintillation Time-of-Flight System", NIM **A252** (1986) 41.

[15] Xinchou Lou, talk given at this workshop. Figure 5 is reproduced from M. Hauschild et al., " Particle Identification with the OPAL Jet Chamber", NIM **A314** (1992) 74.

[16] S. Kwan, "Comparison of Particle Identication Methods", published in these proceedings.

[17] S. Kwan, "Fast CsI-doped Cathodes - Recent Results", talk followed by a discussion at this workshop. See D.F. Anderson, S. Kwan, and V. Peskov, "CsI and Some New Photocathodes", talk presented at the *First Workshop on RICH Detectors*, Bari, italy, June 2-5, 1993, FERMILAB-Conf-93/128, to be published in the proceedings in a future issue of NIM A.

[18] M. Artuso and Y. Mukhin, "Fast Ring Imaging Detectors for Forward B Collider Experiments", published in these proceedings.

[19] K. S. Nelson, "Hadron Identification in a Fixed Target Experiment at the SSC", published in these proceedings.

[20] L. Camilleri, "Design Choices and Issues for Fixed Target B Experiments", plenary talk given at this workshop, to be published in the proceedings.

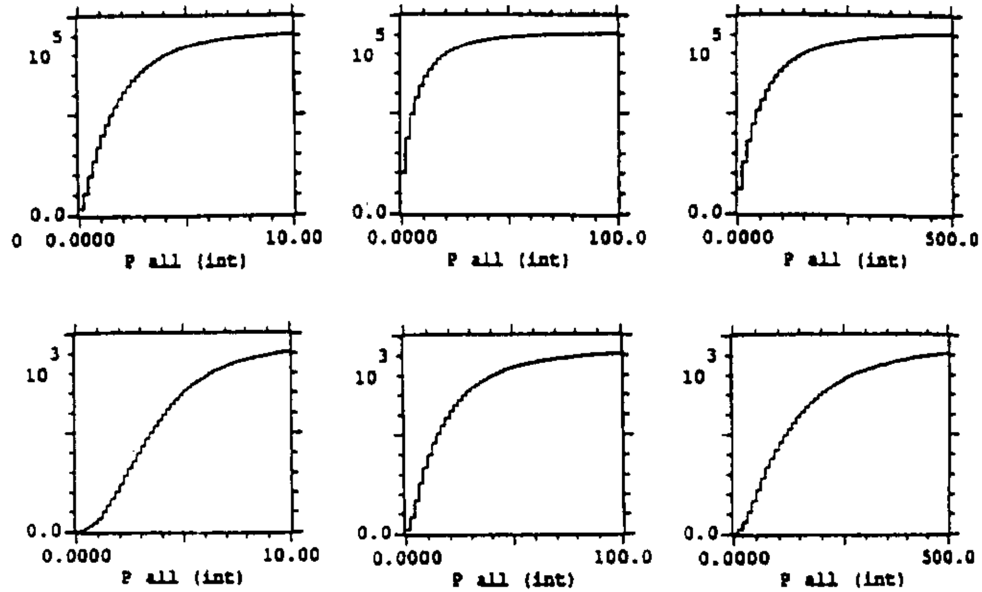

Figure 1. The integral momentum spectra of B-decay products in the Central, Intermediate, and Forward detectors, according to an ISAJET simulation of the proposed Bottom Collider Detector experiment (Reference 13). The upper three plots average over the ten different decay modes listed in Table 5 of Ref. 13. The lower three plots are for the mode $B^0 \rightarrow K^+\pi^-$, which has the stiffest momentum spectrum of any nonleptonic decay.

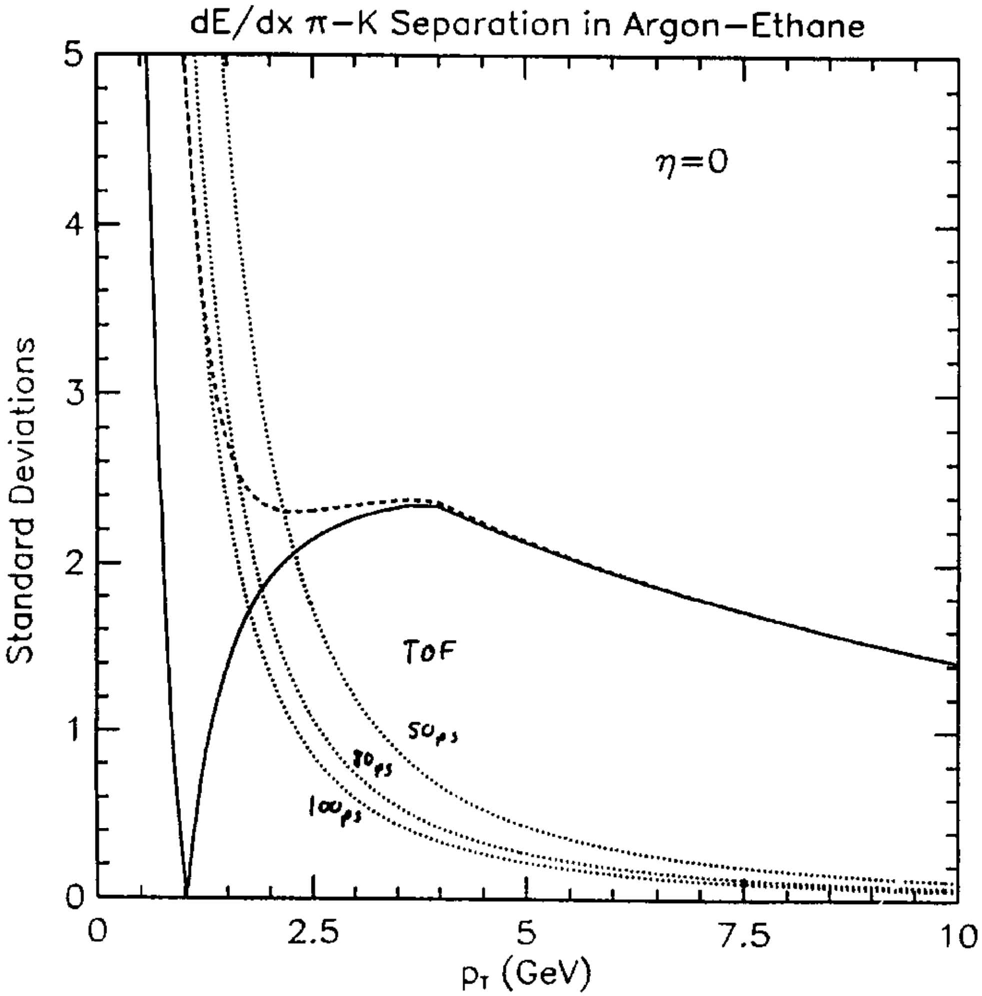

Figure 2. Expected K/π separation in number of standard deviations versus momentum at η=0 for dE/dx and Time-of-flight detectors in CDF.

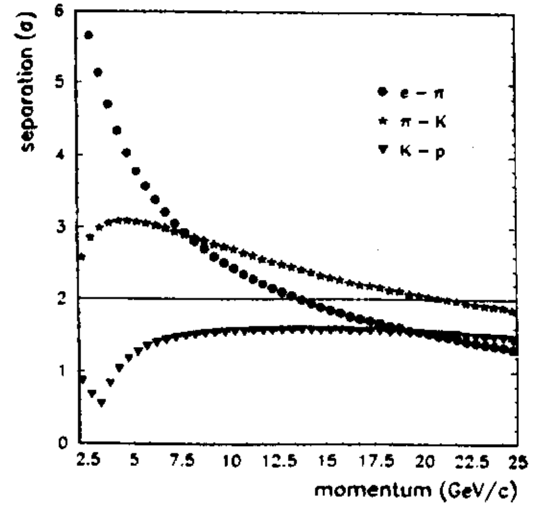

Figure 3. Particle separation in number of standard deviations versus momentum using dE/dx in the OPAL jet chamber.

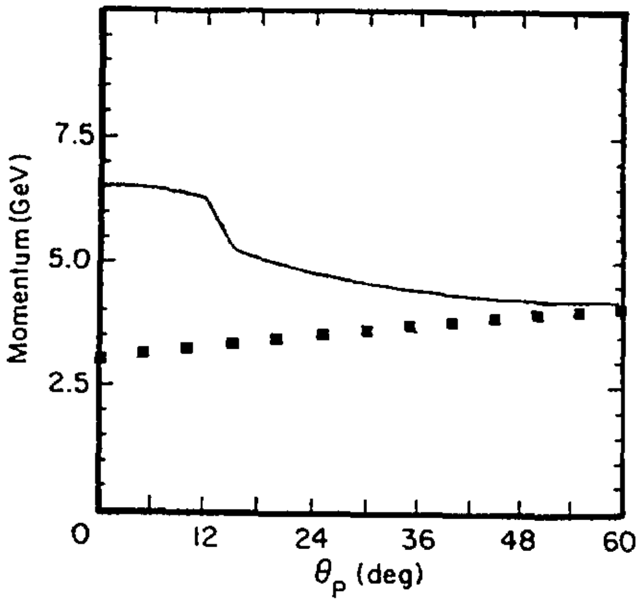

Figure 4. Expected performance of a Fast RICH proposed for a CLEO upgrade as a function of momentum and dip angle. The solid line shows the 4σ separation contour versus the two variables. The RICH systen assumed has a liquid C_5F_{12} radiator, 5mm x 5mm pixel size, and cylindrical focusing geometry. The squares indicate the maximum momentum versus dip angle for K's from $B^o \to K^+\pi^-$ decays.

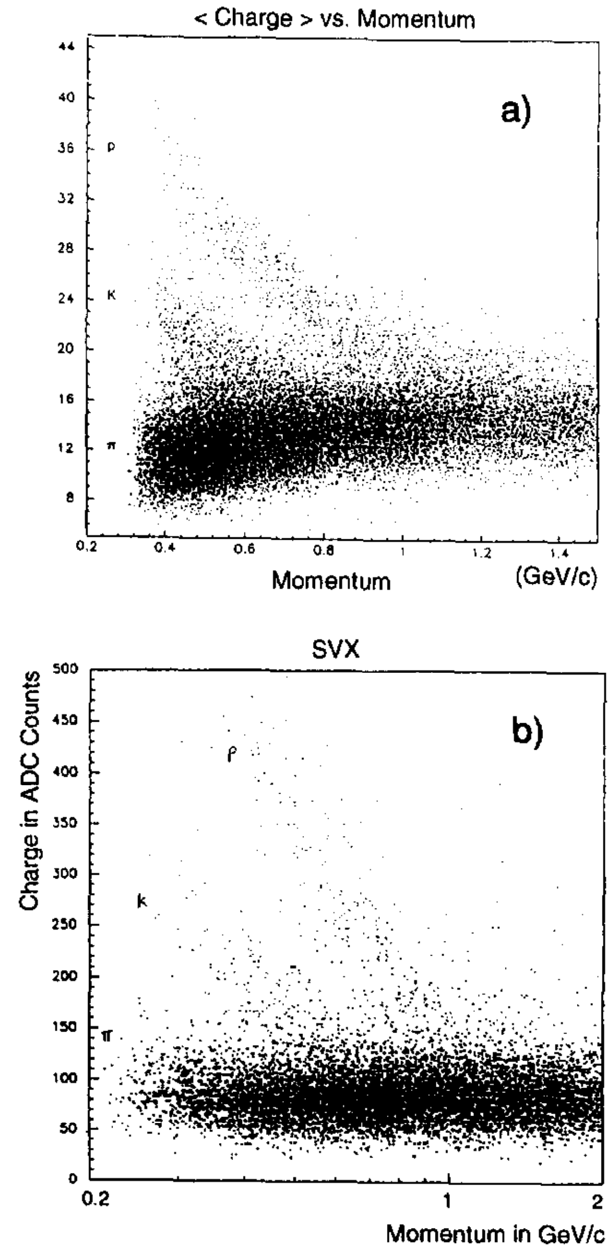

Figure 5. Charge versus momentum for the central tracker, a), and the silicon vertex detector, b), in CDF. What is shown in a) is the average charge and in b), the minimum charge.

Comparison of Particle Identification Methods

S. Kwan
Fermi National Accelerator Laboratory
P.O. Box 500, Batavia, Illinois 60510

1. Introduction

There are four primary methods for hadron identification which can be applied in a B experiment: (1) Time of flight (TOF); (2) ionization loss (dE/dx); (3) Cherenkov radiation, including Ring Imaging Cherenkov counters (RICH), threshold counters and various novel ideas such as the internally reflected Cherenkov imaging counters (DIRC)[1] and the Hadron Blind Detector[2] and (4) transition radiation[3]. No single device is able to cover the wide range of momentum of hadrons from the central collider geometry to the fixed target configuration at the SSC/LHC. Both the TOF and the dE/dx are useful only at low momentum and their use has been restricted to central collider geometry in hadron machines or e^+e^- machines. Even there, a combination of the two methods or with Cherenkov counters is required to give the whole range of momentum coverage. On the other hand, a RICH can be useful at central or forward collider experiments and fixed target experiments as well as e^+e^- experiments (e.g. DELPHI, SLD) including B-factories. For the high momentum domain in the fixed target experiments for the SSC/LHC, a TRD is needed to cover the momentum range from 200 GeV/c up to 500 GeV/c. The physics of the various processes are covered in the excellent review article [5]. Here we will briefly compare the performance of a Cherenkov threshold system, RICH and TOF.

2. Threshold Cherenkov Counter

The performance of any Cherenkov system can be described by N_0, a figure of merit which is given by:

$$N_0 = (370\ \mathrm{eV}^{-1}\ \mathrm{cm}^{-1})\ \varepsilon\ \Delta E \qquad (1)$$

where ε is the average over the whole acceptance bandwidth (ΔE in the photon energy domain) of the detector efficiencies including the quantum efficiency of the photon detector, transmission of the system and mirror reflection.

Threshold Cherenkov counters are widely used in fixed target experiments because of their large phase space acceptance and simplicity in operation. The threshold of a Cherenkov counter is given by:

$$\gamma_t \ \beta_t = \frac{1}{\sqrt{n^2-1}} \tag{2}$$

where n is the refractive index of the Cherenkov radiating medium. The quantity $\gamma\beta = |p|/m$ (c=1) is useful in comparing different particle identification techniques since both TOF and dE/dx also scale with this variable. For threshold Cherenkov counters, for two particles of unequal masses m_1 and m_2, the range in momentum over which particles will be separated is : $\Delta p = \gamma_t\beta\ (m_1-m_2)$. Though such a counter does not cover as wide a range of momentum as a RICH, it can be combined with other techniques or used in a multi-counters system. As an example, we take the two large multicellular threshold Cherenkov systems C1 and C2 in the Fermilab Tagged Photon Spectrometer which has been used successfully in a series of charm experiments E691/E769/E791. C1 which has 28 cells, is filled with nitrogen at STP(index of refraction, n=1.0003089) and C2 which has 32 cells is filled with a mixture of nitrogen and helium (80% He, n=1.0000901 at STP). By careful attention to the details of the light collection, a typical N_0 of 70 cm^{-1} for C1 and 123 cm^{-1} for C2 was obtained corresponding to a mean number of detected photoelectrons N (where $N= N_0 L \sin^2\theta$, L being the length of the radiator) of 15 in each cell of C1 and C2 per each isolated high momentum track. Even though N seemed to be large, ΔE was also large (about 5.3 eV) and the actual detection efficiencies attained were only 3.1% and 6% respectively. The resolution of these counters is given by:

$$\frac{\sigma_\beta}{\beta} = \frac{\tan^2\theta}{(2\sqrt{N})} \tag{3}$$

which when evaluated for C1 and C2 in the above example would give values of $7.7.10^{-5}$ and $2.3\ .10^{-5}$ respectively.

3. RICH

The resolution of a RICH detector is given by:

$$\frac{\sigma_\beta}{\beta} = \tan\theta \frac{\sigma_\theta}{\sqrt{N}} \tag{4}$$

where σ_θ is the total angular error per detected photon. Comparison of the equations (3) and (4) shows that the resolution of a RICH detector is better than that of a threshold counter by a factor of $\tan\theta/(2\sigma_\theta)$ which could be as much as 250 for the least chromatic radiators like He or Ne. This difference is due to the fact that a RICH counter directly measures θ whereas in threshold counters it is only inferred from the value of N. Eq. (4) could be rewritten as:

$$\frac{\sigma_\beta}{\beta} = \frac{n\beta \sin\theta\sigma_\theta}{\sqrt{N}} = \frac{n\beta\ \sigma_\theta}{\sqrt{(N_0 L)}} = K_r \tag{5}$$

which could be defined as the quality factor for a RICH detector. The particle identification capability of a RICH detector can be expressed in the number of standard deviations n_σ to differentiate a particle of mass m_1 from a particle of mass m_2. Identification with n_σ standard deviations may be attained at momentum:

$$p = \sqrt{\left(\frac{m_1^2-m_2^2}{2K_r n_\sigma}\right)} \tag{6}$$

For a 1.4 m long radiator of CF_4 gas (1 bar and 293°K, γ_t=31.8) with detector parameters (photon energy=6.5 eV, ΔE=1 eV and N_0=75 cm^{-1})[6], the RICH β resolution $=1.6.10^{-6}$ which is about a factor of 125 better than an equivalent threshold counter with γ_t=31.8. Three σ separation between π/K is in principle possible up to 153 GeV/c for this RICH whereas the equivalent threshold counter can do π/k separation only from 5 to 17 GeV/c.

4. TOF

A TOF counter measures the flight time $t = L/\beta$ (c=1) a particle would take to traverse a flight path L. For two particles of unequal mass m_1 and m_2 but of equal momentum p, the flight time difference over L is given by:

$$(t_1 - t_2) = \frac{L}{2}\left(\frac{m_1^2 - m_2^2}{p^2}\right) \tag{7}$$

This time difference is small, e.g. with a 1 m long flight path, the time difference between a 1 GeV/c pion and kaon is only 380ps. Also, one can see that the time difference decreases as p^2. Using TOF measurements, the particles will be separable when:

$$\gamma\beta \leq \sqrt{\frac{L}{2(t_1 - t_2)}} \tag{8}$$

Given the present technological limit in time resolution, the maximum permissible flight path and by systematic errors for large TOF systems, this method of particle identification is useful from about 800 MeV to about 2 GeV/c in which it fills the so called "crossover" regions in the dE/dx measurements.

The β resolution for a TOF system is given by:

$$\frac{\sigma_\beta}{\beta} = \frac{\sigma_\tau}{L} \qquad (9)$$

where σ_τ is the time resolution. To get to the same β resolution as the RICH quoted above, one needs a time resolution of 7.5 fs! It is obvious that a TOF device cannot compete with gaseous RICH in the high γ domain($\gamma > 20$) so a comparison in the low γ domain would be more appropriate. Here one has to use liquid or solid Cherenkov radiators. A proximity focusing liquid RICH counter would give a β resolution of $1.2.10^{-3}$ [6] which still corresponds to a time resolution of 4 ps over a distance L =1 m.

5. Discussion

Of course, in comparing the different techniques, there are other things to be considered apart from the performance of the detectors. For example, dE/dx is usually available in gaseous tracking chambers in collider experiments. Other factors such as (1) technical difficulty and the necessary R&D involved; (2) construction and operation costs; (3) manpower needed; (4) triggering possibilities; (5) detector mass and space available; (6) stability and ease of operation and (7) inherent limits to the performance such as decays in flight, interactions in the material of the system or backgrounds have to be considered and weighed carefully before a decison is made to choose a particular technology.

6. References

1. B. Ratcliff, SLAC-PUB-6047, 1993.
2. Y. Giomataris and G. Charpak , NIM A310(1991) 589.
3. M. Sheaff, this workshop.
4. D. Bartlett et. al., NIM A260 (1987) 55.
5.W.W. Allison and P. Wright, *The Physics of Charged Particle Identification*, in Experimental Techniques in High Energy Physics, ed. T. Ferbel, Addison-Wesley, 1987.
6 J. Seguinot and T. Ypsilantis, CERN-LAA/PI/91-004.

USE OF TRANSITION RADIATION DETECTORS (TRD's) FOR B TAGGING/TRIGGERING IN FUTURE COLLIDER OR FIXED TARGET EXPERIMENTS*,**

M. Sheaff
Physics Department
University of Wisconsin
Madison, Wisconsin, 53706

1. INTRODUCTION

Transition Radiation Detectors (TRD's) have been used successfully for particle identification in high energy physics experiments over approximately the last ten years. They have been utilized in a variety of experimental environments, including the Intersecting Storage Rings at CERN[1], hadron collider experiments at the CERN Sp$\bar{p}$S and at the Fermilab Tevatron[2], and an internal gas jet target experiment at the Sp$\bar{p}$S[3] as well as fixed target experiments at both laboratories[4,5,6,7,8]. The primary application has been electron identification[1,2,3,4,5,6], but, more recently, they have been used to identify hadrons as well, including both primary beam particles[7] and secondaries in the very forward region of a multiparticle spectrometer[8]. These versatile detectors show great promise for use in the identification of B decay products in future heavy quark experiments at hadron accelerators. While their anticipated role in the central or moderately forward region of the collider would be to identify electrons, in fixed target or in the very forward collider region, they would be expected instead to discriminate among hadron species. This is because the total TR energy radiated is proportional to the Lorentz factor, γ, of the charged particle. Thus, a TRD which "turns on" for electrons between 1 and 2 GeV demonstrates the same response to pions only when they reach an energy of 250-500 GeV.

This is demonstrated in Figure 1, which shows the expected average number of TR photons radiated and detected per module of the E769/791 TRD[7] for electrons, pions, kaons, and protons incident as a function of particle energy. The numbers shown have been calculated using the simulation package developed for modeling this detector[9], which was found to reliably predict the actual detector performance. The measured efficiency for the x-ray capture signal to be above the 4 keV threshold set on the electronic readout circuit, which was 83%, has been included in the numbers shown. Comparisons to the results of Reference 4 indicate that saturation is not modeled correctly in the simulations, so it has

*Talk presented at the "Workshop on B Physics at Hadron Accelerators", Snowmass, Colorado, June 21 - July 2, 1993

**Work supported under NSF PHY-86-15287 and PHY-89-01274, and DOE DE-AC02-76-ER00881-Task D and DE-AC02-76-CHO-3000.

been put in by hand at the gamma value corresponding to that for pions at an energy of 500 GeV. This seems prudent, since no experimental data are available from the E769/791 detector at higher pion energies than this. Tests run during E791 indicated that saturation does not occur below this value, although this is somewhat above the saturation energy for pions of 430 GeV predicted using the method discussed in Reference 10. (Note the author's comments on the reliability of this estimate, however.)

Because it has been shown to model the E769/791 TRD well at both 250 GeV and 500 GeV, the TRD simulation package will be used in what follows to estimate the discrimination possible using TRD's for particle identification in the various regimes detailed above. The projections will include the actual detector properties, including readout by means of a latch. (See the note included in Reference 9.) Thus, the summed hit probabilities for the two-plane detector assemblies assumed in the simulations in Section 3 will be somewhat below those indicated on the curves shown on Figure 1. The dashed line on the plot shows the drop in response for the pions due to the use of a latch for readout. The crosses, which show the measured response at 250 GeV and 500 GeV, are to be compared to this. An enhanced performance, closer to the solid curve, could be achieved by instead recording all electronically separable clusters using a pipelined readout as is proposed for SSC experiments[11]. In all the simulations, a 10% background per plane has been assumed from ionization loss alone, which is consistent with the background measured in this detector during the E769 run.

First, a few remarks about Transition Radiation for those not familiar with the technique. Like Cerenkov Radiation, TR is a relativistic effect. It is the radiation that is emitted when a relativistic charged particle crosses the interface between two media with different plasma frequencies (or, equivalently, different dielectric constants). It is a bulk property of matter, i.e., there is a minimum thickness of material that the particle must traverse, commonly called the "formation zone", below which radiation will not occur at the interfaces. Since the total energy radiated at each such interface depends linearly on the fine structure constant, $\alpha = 1/137$, radiators must be constructed from many thin foils (~100-200) in order to build a practical detector[10]. The E769/791 detector is an example of a typical, practical TRD.

2. DESCRIPTION OF THE E769/791 TRD

The E769/791 TRD was made from 24 identical modules, one of which is shown schematically in Figure 2. Each contains a radiator made from 200 12.7 μm polypropylene (CH_2) foils stacked alternately with nylon net spacers, which are 180 μm thick. The nylon net was cut away in the region of the beam since it was found to attenuate the TR x-rays by a factor of approximately 2. The radiator volume was flushed with helium during the E769 run but was run with air during the E791 tests, since the difference is not significant. The radiator is followed by a two-plane proportional chamber with single cell depth .635 cm, and active area 76 mm wide by 65 mm high. The 64 sense wires (anodes) are spaced at 1 mm and all are oriented horizontally since the chambers were not used to measure position. The wires are 10.2 μm gold-plated tungsten and the cathodes are 12.7 μm mylar with 140 Å of aluminum sputtered onto both sides. The chamber gas used was xenon bubbled through methylal at 0°C, which results in a mixture that is approximately 90% xenon. There is a .3175 cm buffer volume filled with nitrogen in front and in back of the two-plane chamber. The gas volumes were maintained at equal pressure to keep the chamber gains uniform across the planes.

Because it is comprised of many layers, each with a relatively small number of foils in the radiator stack followed by two chamber planes that are shallow in depth, this detector is an example of a "fine-sampling TRD[12,13]. This means that at most one x-ray is likely to be captured per plane, which is the reason that the latch readout, although not optimum, sufficed. Also, because of the short integration time of the electronics circuits used, which shaped the pulses from the very localized ionization of an Fe_{55} source to 26 ns full width at half maximum, this TRD discriminates using the technique of "cluster counting" [13,14]. This has been shown to give better separation between species than the method of total charge collection.

While the total length of the detector as built was 2.79 m, an equivalent detector could be built in approximately 1.52 m by eliminating all wasted space. The total amount of material in the detector was 8.7% of an interaction length and 16.9% of a radiation length including two .3175 cm scintillation counters used for gating. It would be difficult to reach the 90% efficiency for pions coupled with a factor of 30 in background rejection (in this case protons, since the kaons were separately tagged by means of a Differential Isochronous Self-Focusing Cerenkov counter [DISC][15]) that was achieved with this detector with much less material than this. The method by which the pion sample was selected is illustrated in Figure 3, which shows the distribution of TRD planes hit per event for all events in which the beam particle was not tagged by the DISC as a kaon from a typical E769 data run. As shown by the curves in the figure, the proton and pion peaks were each fit with a double binomial on a run-by-run basis. A plane count cut was chosen such that 90% of the integrated pion distribution lay above it. Then, the background above this cut was calculated using the proton curve. The technique was verified using plane count distributions made for the protons and pions separately during special runs in which the DISC pressure was set to tag them. Further details about the E769/791 detector are contained in Reference 7.

3. USE OF TRD's TO IDENTIFY HADRONS IN FIXED TARGET OR FORWARD COLLIDER

Figure 4 shows the expected spectrum for pions from the decay $B \rightarrow \pi\pi$ in GaJet, an internal gas jet target experiment proposed for the CERN Large Hadron Collider (LHC)[16]. As shown by the arrows on the figure, the spectrum extends to very high momenta, $\geq$200 GeV, above which the planned Ring Imaging Cerenkov Counter (RICH) will no longer be able to cleanly separate pions from kaons. Thus, the experiment plans to use a TRD to reduce the $B \rightarrow K\pi$ background to the mode of interest in the momentum range indicated on the figure. The proposed TRD is made from xenon-filled straw tube detectors 4 mm in diameter and spaced on 8 mm centers. Tubes are staggered from one row to the next. As shown in Figure 5, each straw tube layer follows a foil layer made from 12 15 μm CH_2 foils with $\sim$ 320 μm gaps. The total depth of the 100 module detector is 80 cm and it contains approximately 10% of a radiation length of material. The threshold for x-ray clusters is set to 5 keV, which is well above the peak of the minimum ionizing background pulses, which is at 1.8 keV.

Figure 6 shows the results of simulations of this detector. The number of hits above the TR threshold expected per track for pions and for kaons at 150, 200, 300, 400, and 500 GeV is shown in the plots to the left. The kaon suppression factor as a function of the energy of the hadron is shown in the plot on the right. A factor of ten in suppression is expected between 150 and 460 GeV.

As in GaJet, the Super Fixed Target Beauty Experiment (SFT) at the Superconducting Supercollider (SSC) plans to use the combination of a RICH and a TRD for the identification of hadron secondaries resulting from the decays of B hadrons[17]. Figure 7 displays the distributions in the number of hits above the 4 keV threshold expected per track for protons (dotted line), kaons (dot-dash line), and pions (solid line) traversing a detector with 24 radiator-chamber modules identical in construction to the E769/791 detector. The curves shown are for particle energies of 200, 400, 600, 800, and 1000 GeV, respectively. Discrimination is needed to higher secondary energies than for GaJet because of the higher energy of the primary beam at the SSC. The rejection for kaons or protons versus efficiency for pions is somewhat better for this detector than for the one proposed by GaJet. However, this is at the price of about 50% more material in the detector.

4. USE OF TRD's TO IDENTIFY ELECTRONS IN THE CENTRAL AND MODERATELY FORWARD COLLIDER

Since electrons radiate TR and hadrons do not over a two order of magnitude range in momentum, the momentum window over which it is possible to discriminate electrons from hadrons is large. A TRD can be designed to saturate at just below 2 GeV for electrons, so that above that value, the efficiency for electrons is constant. In the same detector, since the effect goes as γ, pions do not radiate appreciable TR until they are at energies near that same value of γ, in the range of hundreds of GeV. When used in combination with an electromagnetic calorimeter, the two can provide a background rejection of $\sim 10^{-4}$ with good selection efficiency for electrons.

Figure 8, which is reproduced from the Micro-Bottom Collider Detector (μBCD) proposal submitted to Fermilab[18], shows the inclusive lepton p_t spectra from a) direct B decays and c) daughter D decays and and also the integrated spectra, labeled b) and d). Figure 8 b) shows that even for the harder direct decays one-half of the integrated lepton spectrum lies below 1 GeV/c in p_t. Since p_t equals p at 90°, the requirement for good electron identification, even for the purpose of tagging the "other" B in an event, extends down to a momentum at least as low as this. Figure 9 shows the expected hit distributions for electrons (solid line) and pions (dotted line) at 0.5, 1.0, 1.5, and 2.0 GeV/c in a possible future TRD appropriate for use in the central region of a hadron collder. The simulations were carried out assuming 24 modules, each with a radiator made from 50 12.7 μm foils followed by a single-plane xenon-filled detector .635 cm in depth. The results indicate that a TRD could be built with total depth less than half a meter which is capable of discriminating electrons from pions at as low a momentum as 1 GeV/c.

Not only can TRD's be used offline to discriminate between electrons and hadrons, but they should also make it possible to trigger on electrons online at the first trigger level providing the cell sizes are small and the drift time in the gas and the electronics can be made fast enough. Since they are constructed using narrowly spaced wire chambers, TRD's are also capable of identifying electrons inside jets, which makes them well suited for identifying b and c jets. And, they can simultaneously be used as high resolution tracking detectors and for particle identification by splitting the wire signals and subjecting them to multiple thresholds[19]. The down side of TRD's is that they represent a significant amount of material, especially in radiation lengths.

5. ACKNOWLEDGMENTS

The assistance of Timothy Meyer, a Fermilab summer student who is an undergraduate at Johns Hopkins University, with the simulations and the plots is gratefully acknowledged.

6. REFERENCES

[1] J. Cobb et al., "Transition Radiators for Electron Identification at the CERN ISR", NIM 140 (1977) 413.

[2] R. Ansari and B. Merkel, "Transition Radiation Detectors for Hadron Colliders" ,talk given by B. Merkel at the "Symposium on Particle Identification at High Luminosity Hadron Colliders", Fermilab, April 5-7, 1989, published in the proceedings of the symposium edited by Treva Gourlay and Jorge Morfin, p. 359.

[3] A. Vacchi, "Large-Area Transition Radiation Detectors for Electron Identification in the UA6 Experiment at the CERN $p\bar{p}$ Collider", NIM A252 (1986) 498.

[4] A. V. Kulikov et al.,"Performance of the E715 Transition Radiation Detector", talk given at the First Annual Meeting (New Series) of the Division of Particles and Fields of the American Physical Society, Santa Fe, New Mexico, Oct 31 - Nov 3, 1984. Published in the proceedings edited by T. Goldman and Michael Martin Nieto, World Scientific Publishing Co. Pte. Ltd.

[5] G. Barr et al., "The NA31 Transition Radiation Detector", IEEE Transactions on Nuclear Science 36 (1989) 66.

[6] M. Clemen (representing the Helios collaboration), "The Helios Transition Radiation Detector", talk given at the "Symposium on Particle Identification at High Luminosity Hadron Colliders", Fermilab, April 5-7, 1989, published in the proceedings of the symposium edited by Treva Gourlay and Jorge Morfin, p. 339.

[7] "Use of a Transition Radiation Detector in a Beam of High Energy Hadrons", D. Errede et al., NIM **A309** (1991) 386.

[8] M. Baake et al., "A Transition Radiation Detector for Kaon/Pion Separation", NIM A281 (1989) 325.

[9] The simulation package has two parts. The first is a calculation of the average number of TR photons as a function of energy produced by the radiators including detection in the xenon chamber planes. See L. C. Myrianthopoulos et al., "Status Report on the University of Maryland Transition Radiation System for Beam Particle Identification", University of Maryland, MdDP-TR-80-106, May 1980, unpublished, for details. Since the Monte Carlo part of that program was appropriate for the total charge method as opposed to "cluster counting", the method used in the E769/791 TRD, the part of the package that generates the detector hits was written by our group. The simulations take into account the fact that signals were simply latched and not scaled, so that two clusters seen in the same chamber plane would be recorded as one.

[10] X. Artru et al., "Practical theory of the multilayered transition radiation detector", Phys. Rev. D12 (1975) 1289, discusses these and other properties of Transition Radiation. See p. 1297 for a discussion of saturation.

[11] R. Van Berg, "BCD Tracking Electronics",talk given at the Workshop on B Physics in p-p Collisions at the SSC, June 6-8, 1989.

[12] B. Dolgoshein, "Transition Radiation Detectors and Particle Identification", NIM A252 (1986) 137.

[13] T. Ludlam et al.,"Particle Identification by Electron Cluster Detection of Transition Radiation Photons", NIM 180 (1981) 413.

[14] C. Fabjan et al., "Practical Prototype of a Cluster-Counting Transition Radiation Detector", NIM 185 (1981) 119.

[15] M. Benot et al., "Cerenkov Counters for Particle Identification at High Energies", NIM 105 (1972) 431.

[16] L. Camilleri, "Design Choices and Issues for Fixed Target B Experiments", talk given at this workshop.

[17] K. Nelson, "Hadron Identification in a Fixed Target Experiment at the SSC", these proceedings.

[18] H. Castro et al., "Proposal for a B-Physics Experiment at TEV I, The μBCD", proposal submitted to the Fermilab Physics Advisory Panel on October 8, 1990.

[19] J. T. Shank et al., "Test-beam Performance of a Tracking TRD Prototype", NIM A309 (1991) 377.

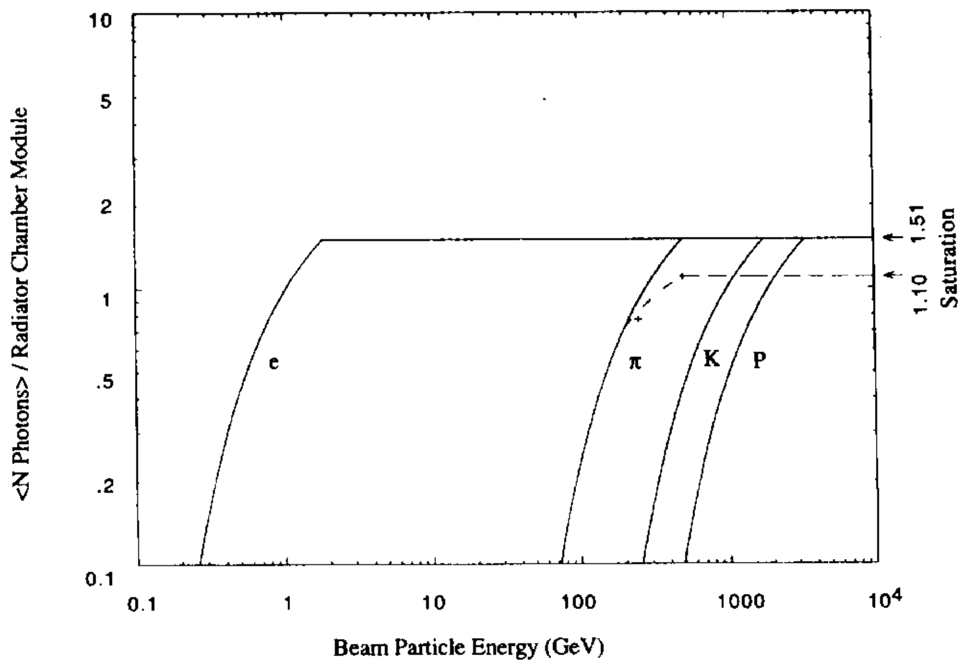

Figure 1. Expected average number of photons detected above the 4 keV threshold in each module of the E769/791 TRD for electrons, pions, kaons, or protons incident as a function of particle energy. The dashed line shows the degradation in performance due to readout by means of a latch. The crosses indicate the measured performance of the detector at 250 and 500 GeV.

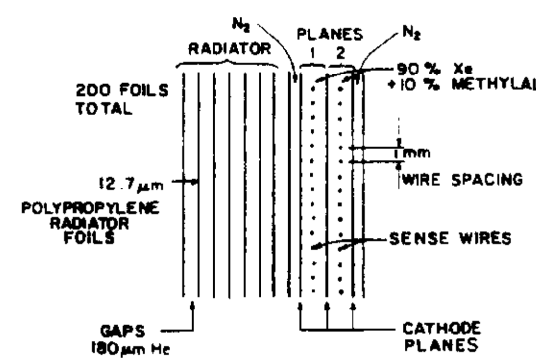

Figure 2. Schematic of one module of the E769/791 TRD in elevation view. The beam is incident from the left in the figure.

K. GABATHULER.

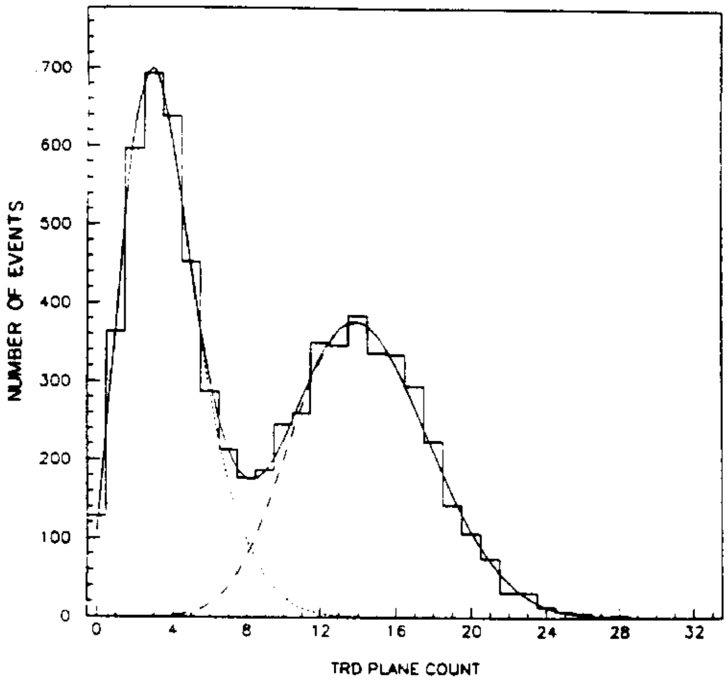

Figure 3. TRD plane count distributions for all event triggers on a typical E769 data tape for which the incident beam particle was not tagged as a kaon by the DISC Cerenkov counter. The peak to the left contains protons and the one to the right, pions. The results of the double binomial fits to each of the two peaks are indicated by the curves on the plot.

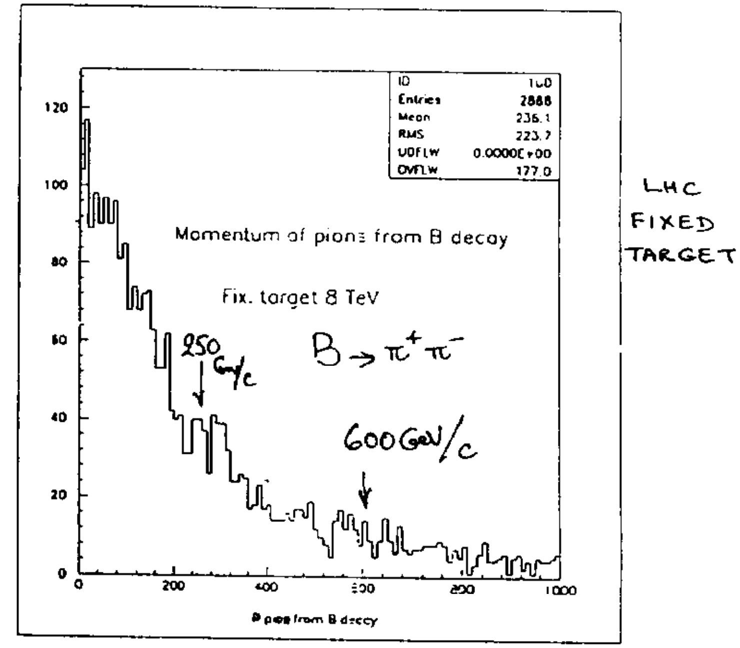

Figure 4. Expected spectrum for pions from the decay $B \to \pi\pi$ in GaJet, an internal gas jet target experiment proposed for the LHC.

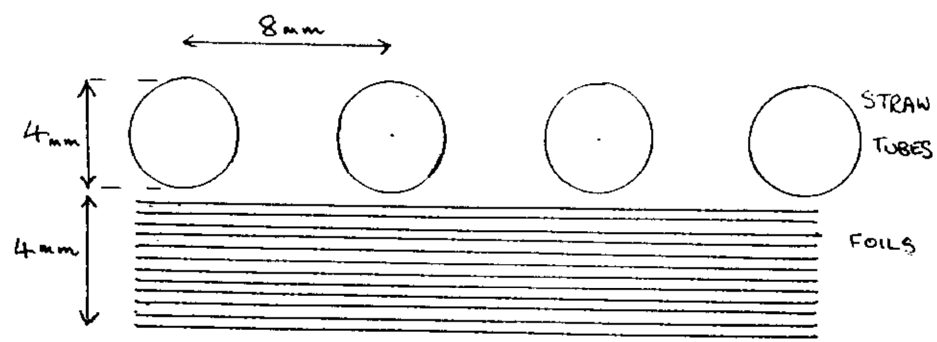

Figure 5. Schematic of proposed GaJet TRD. Particles are incident from below in the figure.

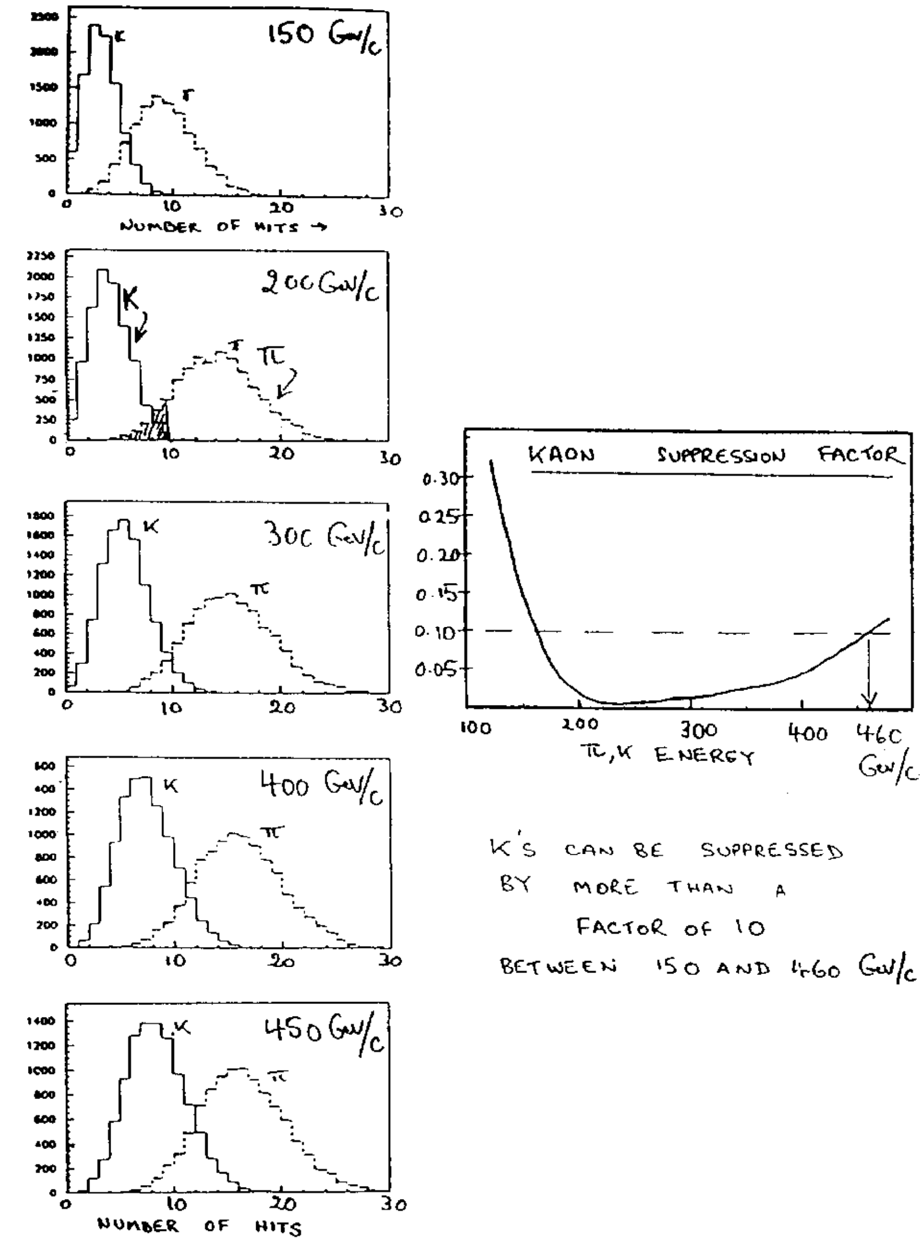

Figure 6. Plots to the left show the results of simulations of the distributions in hit straws for the proposed GaJet TRD for kaons and pions at 150, 200, 300, 400, and 450 GeV. The plot to the right shows that a kaon suppression factor of 10 is expected between 150 and 460 GeV.

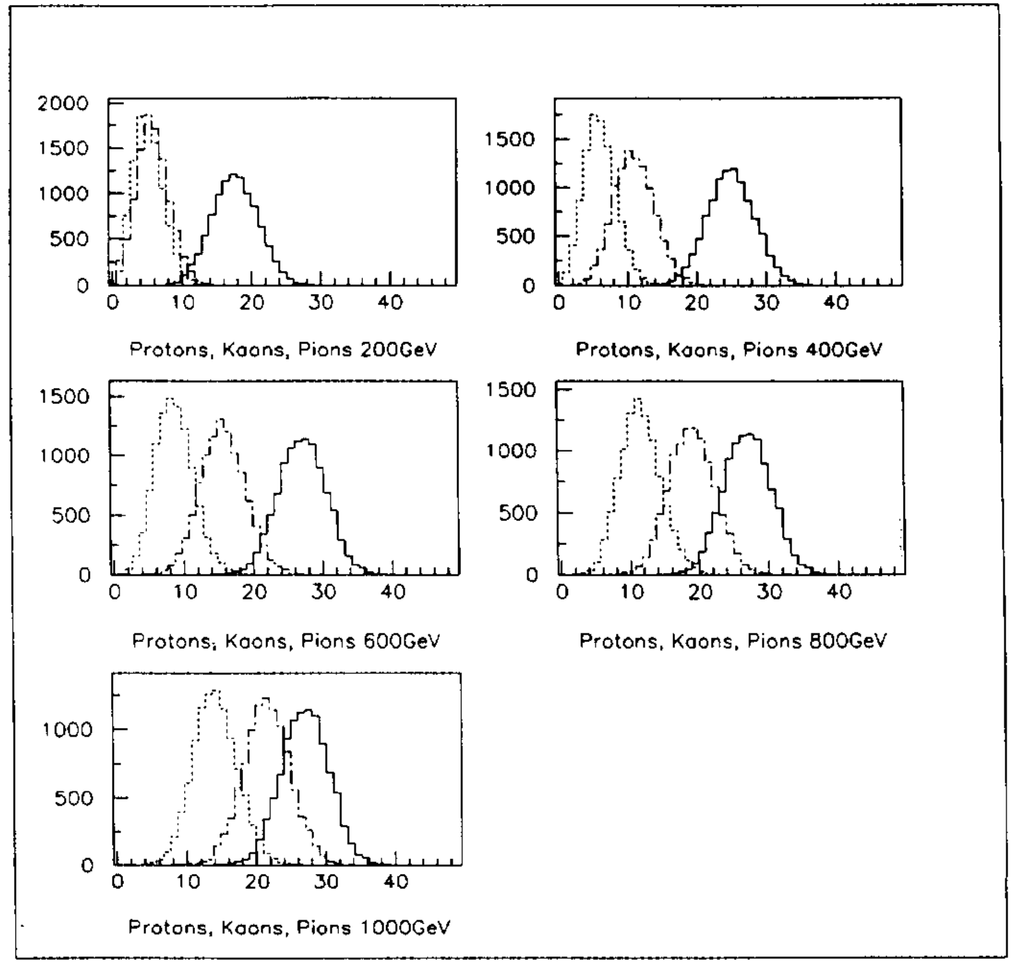

Figure 7. Expected hit distributions above the threshold for TR per track for protons (dotted line), kaons (dot-dash line), and pions (solid line) at 200, 400, 600, 800, and 1000 GeV. The simulations assume a TRD identical in construction to the E769/791 detector. Saturation for pions at 500 GeV/c results in poorer K/pi separation at higher momenta.

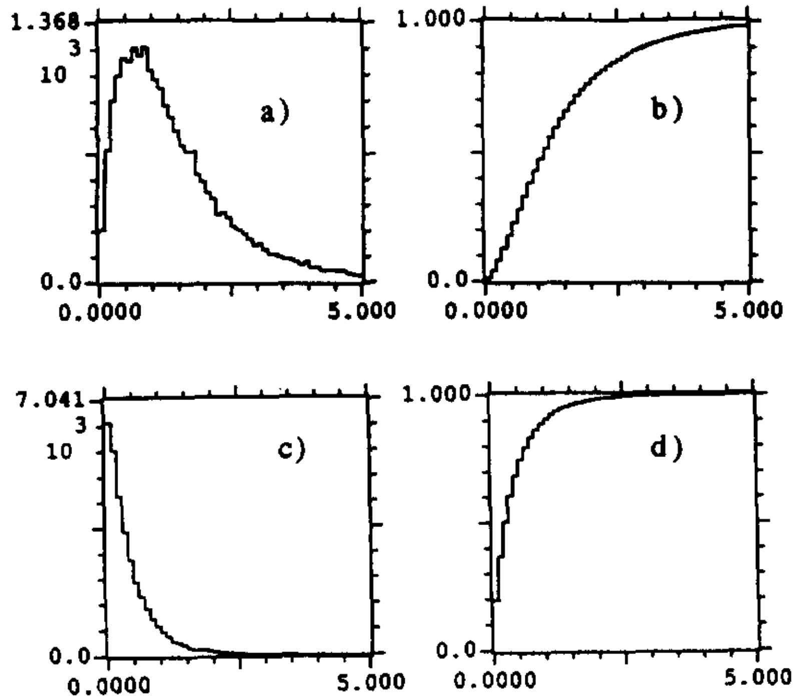

Figure 8. Expected inclusive lepton spectra from B decays according to simulations made for the μBCD proposal to Fermilab (Reference 18). a) The p_t spectrum for single leptons from B$\rightarrow l^{\pm}$X. b) The integral of the spectrum shown in a). c) The p_t spectrum for leptons from B$\rightarrow$D X, with D$\rightarrow l^{\pm}$Y. d) The integral of the spectrum shown in c).

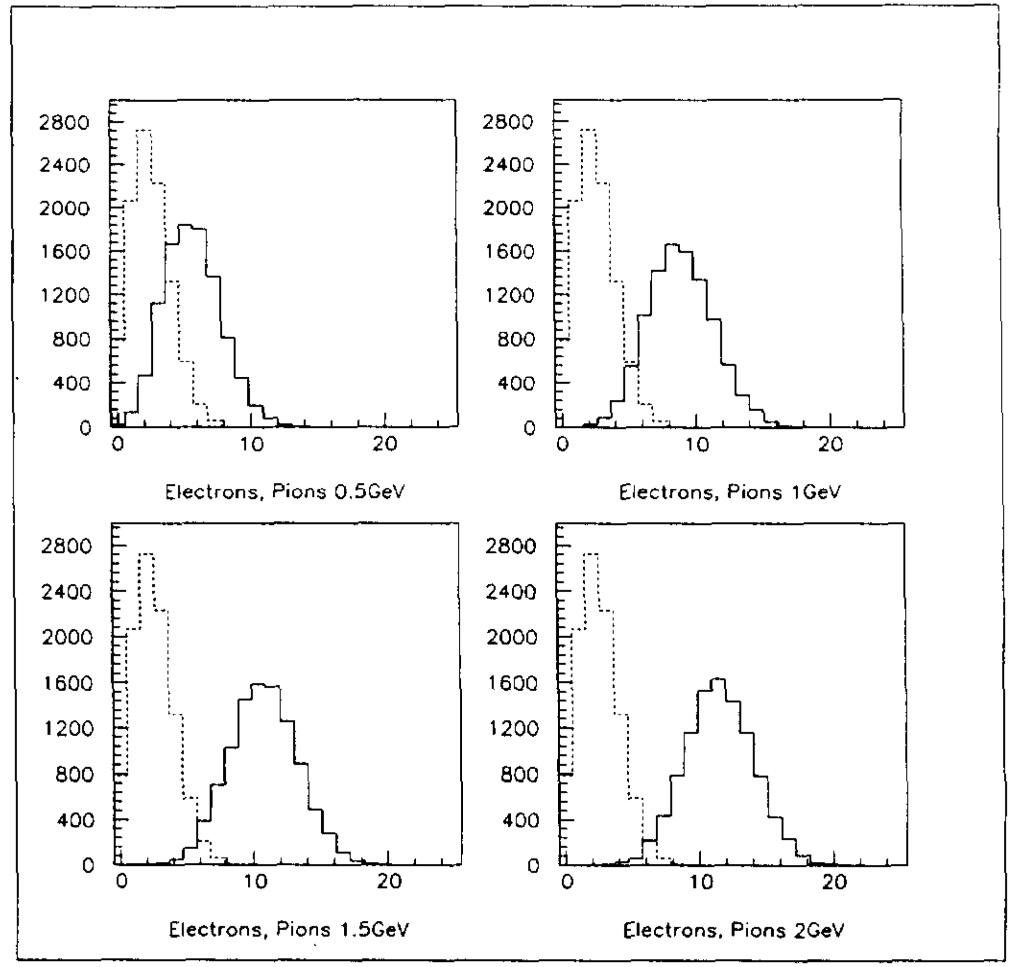

Figure 9. Expected hit distributions for electrons (solid line) and pions (dotted line) at 0.5, 1.0, 1.5, and 2.0 GeV in a "fine-sampling" TRD built from 24 modules, each with a radiator composed of 50 12.7 μm CH_2 foils followed by a single-plane xenon-filled MWPC with cell depth .635 cm.

FAST RING IMAGING DETECTORS FOR FORWARD B COLLIDER EXPERIMENTS

Marina Artuso and Yurii Mukhin
Department of Physics, Syracuse University, Syracuse, NY 13244, USA

1. INTRODUCTION

A good hadron identification system is a crucial element in an experiment designed to measure CP violation asymmetries in B decays. In particular the reactions $B \to \pi^+\pi^-$ and $B \to K^\pm\pi^\mp$ need to be disentangled with high accuracy. Note that the kinematics of the reactions $B \to \pi^+\pi^-$ and $B \to K^\pm\pi^\mp$ are so similar that conventional particle identification approaches have no chance to provide adequate separation between these two decay channels.

An experiment designed to detect B's produced in the forward direction in a hadron collider has the advantage of having enough longitudinal space to allow the insertion of a fast Ring Imaging Cherenkov (RICH) detector, which should suit both the particle identification needs and the processing speed required at SSC. In order to set the scale for the momentum coverage needed, simulation studies have indicated that most particles coming from B decays at SSC have a momentum smaller or roughly equal to 100 GeV.[1] In the next section the performance expected for a typical fast RICH detector suitable for this application is discussed.

The fast RICH detector considered in the present study can be located downstream the tracking system. We show that a single gaseous fast RICH can accomplish the physics goals, namely that the lowest momentum at which the particle species need to be unambiguously identified is of the order of a few GeV, corresponding to the threshold of the most common gas radiators.

2. A FAST RICH FOR A SSC FORWARD COLLIDER EXPERIMENT

Figure 1 shows the schematic detector configuration assumed: the fast RICH system occupies a region between 4.5 and 7.5 meters downstream the interaction region. The distance of 4.5 m is assumed to leave enough space for the tracking system. This distance is not critical for our conclusion and we can easily adapt our system to a greater longitudinal separation from the interaction point. The detector length is determined by the requirement of maintaining a minimum of approximately 10 photoelectrons within the whole angular coverage. This requirement is vital to ease the pattern recognition problem with the high occupancy expected in hadron collider environments.

Figure 2 shows the geometry of the detector studied and the relevant coordinates. This system consists of a gaseous radiator enclosed in a vessel which has a spherical mirror at its outer side along the beam line and a flat quartz entrance window. The gas chosen in the present study is CF_4: among the gaseous fluorocarbons is the one having the lowest chromatic dispersion. Other fluorocarbons, like C_2F_6, are characterized by similar performance. The momentum thresholds for producing Cherenkov radiation are 4.4 GeV, 15.8 GeV, 30.0 GeV and 0.016 GeV for π's, K's, p and e's respectively.

Near the entrance window there is a gaseous photosensitive detector with pad readout. The photosensitive element needs to match the bandwidth of the radiator and the quartz window(s). Solid state photodetectors, namely CsI (with or without adsorbed TMAE) constitute the most attractive choice. We have assumed an average quantum efficiency of 28% in the bandwidth between 6 and 7 eV. This is likely to be a reasonable efficiency for CsI vacuum deposited photocathodes with adsorbed TMAE.[2,3] We are aware that there are reports from our groups of a lower quantum efficiency,[4,5] and we hope that the many groups presently investigating these photocathodes will make progress in understanding the factors affecting their performance. In particular, the effect of the polarization and the incident angle of the radiation is presently poorly known but crucial to understand the performance of these photocathodes in conjunction with Cherenkov radiation, which is polarized and focused at a characteristic angle. The mirror reflectivity is assumed to be 80%. For the present study, the chamber efficiency is taken to be 100%.

It has been assumed that the detector is very close to the inner surface of the gaseous radiator, in order to maximize the radiator active volume and therefore the number of photoelectrons. The mirror radius is chosen in order to optimize the image focusing on the detector surface, or, in other words, to minimize the sensitivity to the location of the emission point along the charged particle trajectory, z_e, which is unknown. It is well known that spherical mirrors focus the image on a spherical surface with radius $r_m/2$. For small apertures a flat surface at a distance $r_m/2$ from the mirror has equivalent properties.

3. PERFORMANCE OF THE PROPOSED FAST RICH

The number of photoelectrons can be predicted from relationship:

$$N_{pe} = \frac{\alpha}{\hbar c} < \epsilon > \Delta E \tag{1}$$

where α is the fine structure, constant, $\hbar$ is Planck constant, c is the speed of light and the average efficiency $<\epsilon>$ is the average over the detector bandwidth, ΔE, of the product of the quantum efficiency Q, the overall transmission coefficient T of the elements along the path of the Cherenkov photons and the average mirror reflectivity R. Figure 3 shows the expected number of photoelectrons for a mirror radius of 6 m, corresponding to the optimal focusing discussed before.

The resolution expected for the reconstructed Cherenkov angle is calculated with an analytical method detailed below. The coordinates of the photoelectrons at the pad surface of the detector can be related to the Cherenkov photon angular coordinates θ and ϕ, which are respectively the polar and azimuthal angle with respect to the direction of the charged particle. These two constraints define θ and ϕ as implicit functions of the other variables which enter in the transport equations:

$$F(x,y,z,\theta,\phi,\theta_p,\phi_p,z_e,E_{ph}) = x - f(\theta,\phi,\theta_p,\phi_p,z_e,E_{ph}) \tag{2}$$

$$G(x,y,z,\theta,\phi,\theta_p,\phi_p,z_e,E_{ph}) = y - g(\theta,\phi,\theta_p,\phi_p,z_e,E_{ph}) \tag{3}$$

where θ_p is the charged particle dip angle (measured with respect to the normal to the detector surface) and ϕ_p is the charged particle azimuthal angle, z_e is the coordinate of the emission point along the charged particle path and E_{ph} is the photon energy. From these relationships we can calculate the derivatives $\partial\theta/\partial v_i$, where v_i identifies each variable which appear in the above equations:

$$\frac{\partial\theta}{\partial v_i} = -\left[\frac{\partial F,G)/\partial(v_i,\phi)}{\partial(F,G)/\partial(\theta,\phi)}\right] \tag{4}$$

The expected error in the reconstructed Cherenkov angle can be calculated as:

$$\sigma_\theta(\phi)^2 = \Sigma_i \left[\frac{\partial\theta}{\partial v_i}\right]^2 \sigma_{v_i}^2 \tag{5}$$

The relative importance of the different contributions to the error in the Cherenkov angle changes depending upon the charged particle angle θ_p.[6] The uncertainty associated with the emission point along the particle trajectory z_e, which is the dominant source of error in proximity focusing systems, is negligible in this case if we choose the mirror radius such as the detector is close to its focusing surface (in this case a sphere with separation $r_m/2$ from the mirror). The chromatic error, due to the uncertainty in the photon energy within the system bandwidth, is quite small due to the low dispersion of the gas radiator. Some additional chromatic aberration produced by the refraction in the quartz window has been taken into account. In the present study a pixel size of 1×1 mm^2 has been assumed. This corresponds either to the actual pad segmentation in the detector or to an effective size achieved via analog or digital centroid method.[7] This fine segmentation is dictated by the small chromatic error characterizing gas radiators. A larger pixel size would be the dominant error in the reconstructed Cherenkov angle in a properly focused system, namely with the detector as close as possible to the focal surface of the mirror.

Photons are generated at equal intervals in the angle ϕ, which determines the photon location in the Cherenkov cone and the resolutions calculated at each angle $\sigma_\theta(\phi)$ are weighted by the corresponding transmission coefficient $T(\phi)$:

$$<\sigma_\theta> = \sqrt{\int T(\phi)d\phi / \int T(\phi)d\phi/\sigma_\theta^2} \tag{6}$$

Figure 4 shows the results for a mirror radius of 6 meters, which represents the optimum focusing condition.

Finally, Figure 5 summarizes the momentum at which a 4 σ $K-\pi$, $p-K$ and $\pi-e$. It can be seen that for small incident angles ($\theta_p \approx 8°$) a 4σ π-K separation is achieved up to 250 GeV. The degradation associated with the particle incident angle is due to the lower number of photo-electrons in the assumed radiator geometry and to a diminished focusing effect due to the non optimal mirror-radiator distance at the edges. The design of the optimum detector geometry for maximum separation power over the whole angular acceptance of the B spectrometer can be optimized only when the tracking scheme is defined, and the angular spread of the particle downstream the analyzing magnet is defined. In a recent study[1] an angular aperture of 10° is assumed, over which our proposed detector would achieve nearly optimal separation power. An alternative scheme[8] has been proposed: it has similar geometry for an angular range between 0 and 5.7° and an upstream fast RICH covering the region between 5.7° and 34.4° located before the momentum analyzing magnet. In addition, it involves a liquid radiator in both sectors. This solution improves the performance and ease of construction of the hadron identification system at the expense of some valuable tracking volume.

In conclusion, our study shows that a fast RICH system based on a gas radiator and solid state CsI photocathode has a great potential to meet the challenge of providing adequate hadron identification in the momentum range relevant for a forward B spectrometer. An optimization of the focusing scheme for the required angular acceptance can be achieved once the parameters for the corresponding tracking system are defined.

4. ACKNOWLEDGEMENTS

We would like to thank Tom Ypsilantis who helped us getting started in the FAST RICH detection technique and Sheldon Stone and Raymond Mountain which were a constant source of lively discussions.

5. REFERENCES

1. M. Botlo et al., *SSC Preprint SSCL-538* (1992).

2. J. Seguinot et al., *Nucl. Inst. Meth.* **A297** (1990) 133.

3. D. Anderson et al., *Nucl. Inst. Meth.* **A323** (1992) 626.

4. V. Dagendorf et al., *Nucl. Inst. Meth.* **A308** (1991) 519.

5. G. Charpak, *CERN Preprint CERN PPE/92-220* (1992).

6. J. Seguinot and T. Ypsilantis, *CERN Preprint CERN-LAA/PI/91-004* (1991).

7. R. Arnold et al., *Nucl. Inst. Meth.* **A314** (1992) 465.

8. A. Brandt et al., *Proposal P238 for SPS-Collider* (1990).

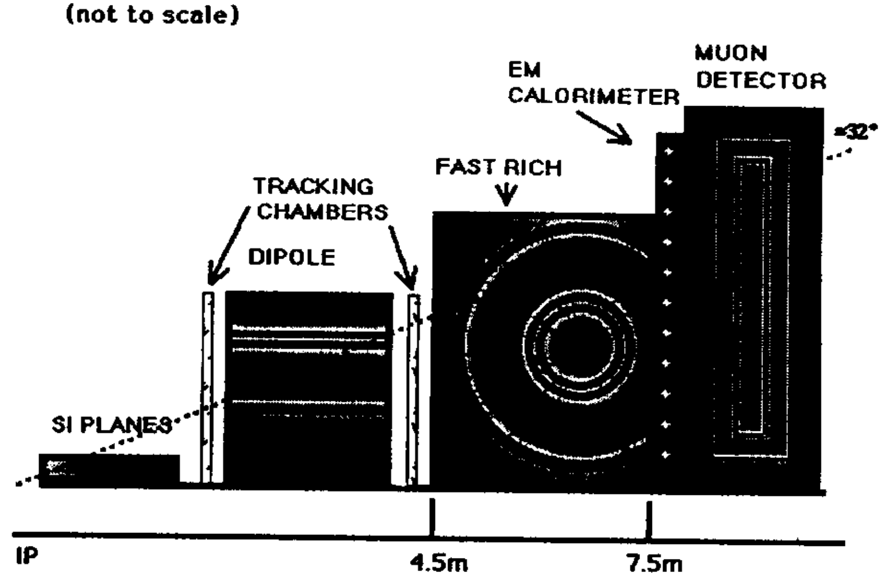

Figure 1: Schematic view of the forward collider detector.

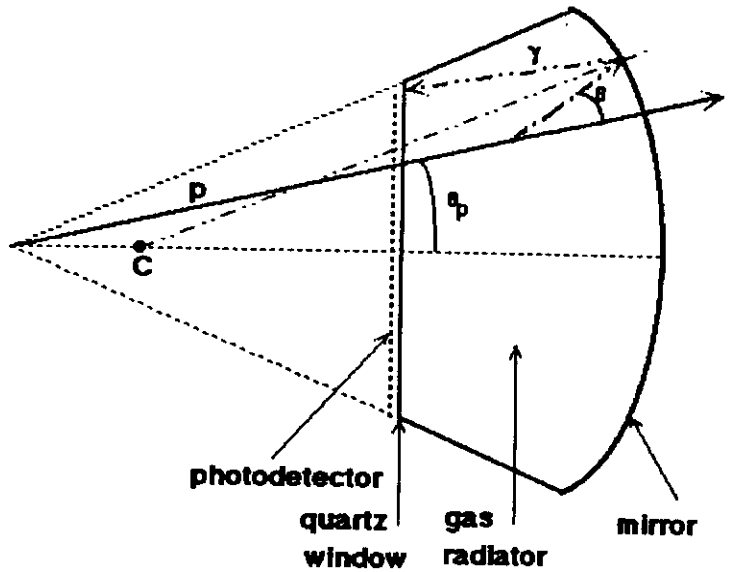

Figure 2: Schematic view of the Forward Collider Fast RICH Detector.

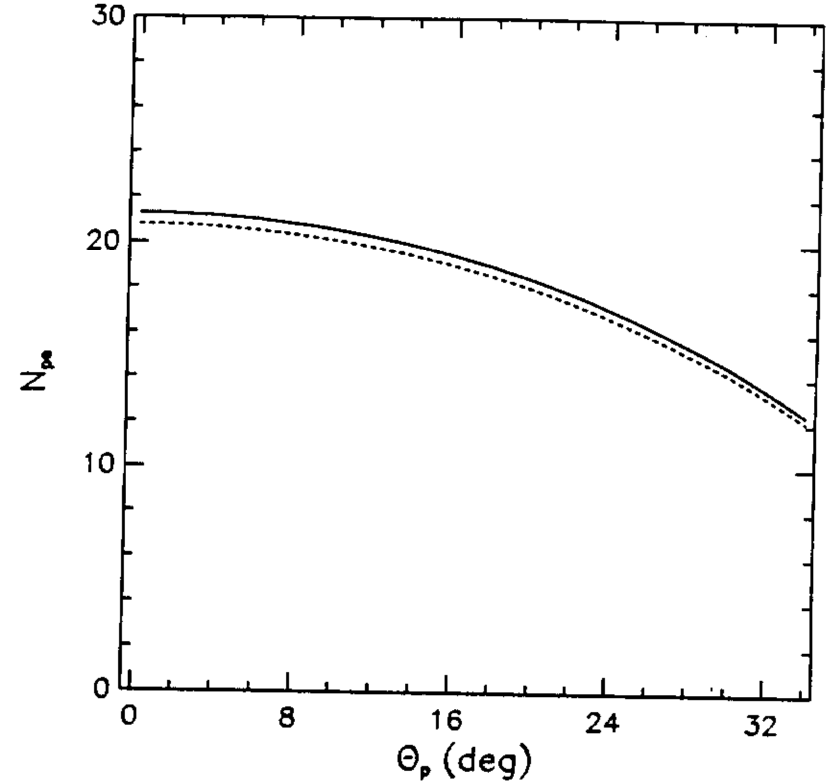

Figure 3: Expected number of photoelectrons

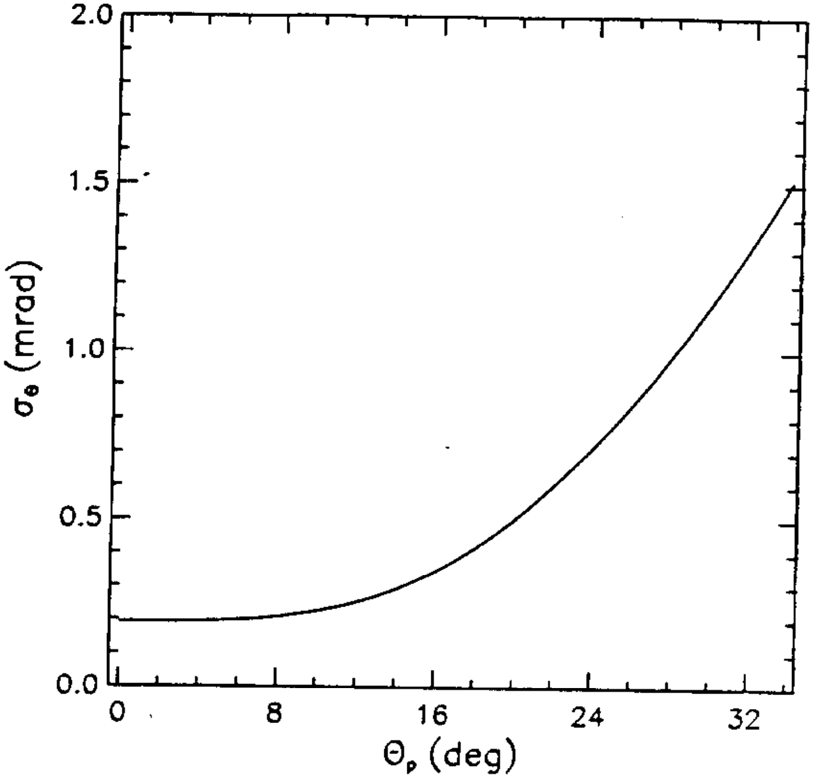

Figure 4: Weighted error in the Cherenkov angle as a function of the charged particle dip angle θ_p

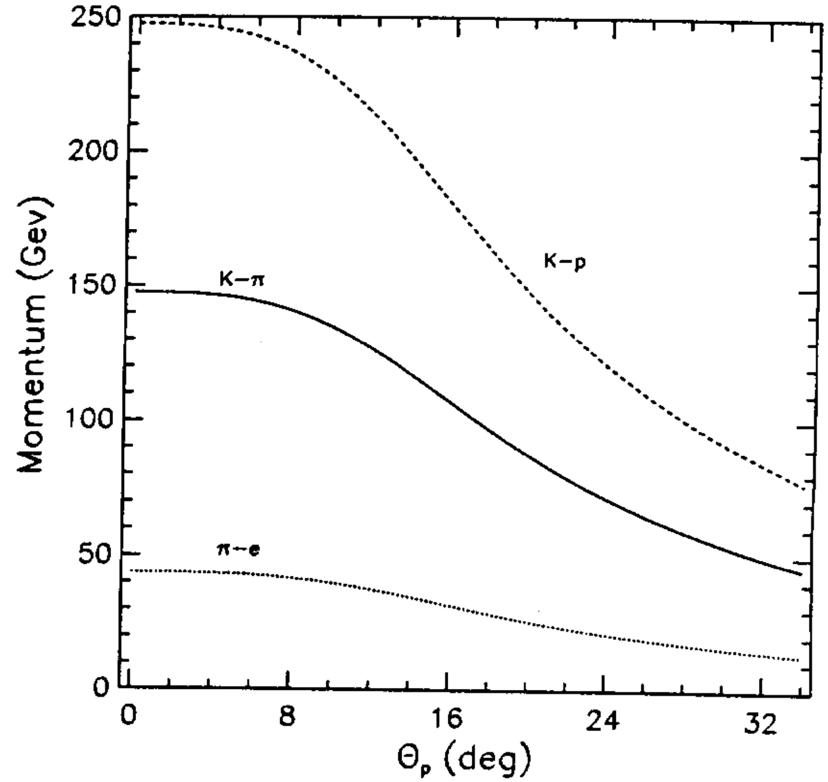

Figure 5: 4 σ particle separations: solid line corresponds to $K-\pi$ separation, dashed line corresponds to $K-p$ separation, dotted line to $e-\pi$ separation.

HADRON IDENTIFICATION IN A FIXED TARGET EXPERIMENT AT THE SSC

K.S. Nelson and B. Cox
High Energy Physics Laboratory, Univ. of Virginia
Charlottesville, Va. 22903

1. INTRODUCTION

This article will present the design criteria and expected performance of a hadron identification system in a fixed target experiment at the SSC. The proposed SFT spectrometer[1] will be used as a model for the discussion.

2. KINEMATIC RANGE FOR PHYSICS GOALS

Two primary uses of hadron identification in a B physics experiment are flavor tagging and the rejection of background due to particle reflections in the reconstruction of exclusive decay modes. In the first case it will be seen that use of kaons can increase substantially the number of events which can be tagged. In the latter case, decays in which particles are mis-identified can form a background to a desired decay mode.

2.1 Tagging

To be specific consider the example of tagging the $t = 0$ flavor of the the CP mode $B \rightarrow J/\psi K_S$ by the decay of the other B hadron in the event. It is assumed that the CP state itself triggers the apparatus, e.g. through the di-muon decay of the ψ.

PYTHIA is used to generate fixed target $p-p$ collisions at $\sqrt{s} = 193\,\mathrm{GeV}$. The acceptance is taken to be $2mr\,(3mr) < \theta < 75mr$ in polar angle for muons (hadrons). In addition all particles are required to have $E > 20\,\mathrm{GeV}$ to minimize multiple scattering in the active silicon target and to allow muons to penetrate the hadron shield. Out of 40,000 generated events approximately 9,000 $B_d \rightarrow J\psi K_S$ decays satisfy these cuts. Figure 1 shows the energy spectra of $\pi/K/p$ daughters of the other B hadron, which have a transverse impact parameter $b_{xy} > 20\mu m$. The relative particle ratios shown in figure 2 are important for the determination of cuts to discriminate among the particle types (sec. 3.2).

The gain in statistical power by using Kaon tags compared to muon tags is demonstrated in figure 3. The probabilty that the charge of a muon or kaon correctly identifies the flavor (b or $\bar{b}$) of its parent is shown in figure 3a as a function of P_T. Here an assignment of "correct" assumes that the muon occurs in a $b \rightarrow c$ transition and the kaon occurs at the end of a $b \to c \to s$ cascade. When more than one muon or kaon is available as a tag then the one having the highest P_T is chosen. From figure 3a one sees that the fraction of correct [2] muon tags increases with P_T up until about 1 GeV/c while the fraction of correct kaon tags appears to be nearly independent of P_T. The fraction of events for which a tag particle is available is shown in figure 3b as a function of the P_T cut. Integration over all P_T indicates that there is approximately 3 times as many potential kaon tags as muon tags. However after P_T cuts of 1 GeV/c for muons and 0.3 GeV/c for kaons are made, approximately 5 times as many kaon tags survive as compared to muons.

2.2 *Reconstruction of Exclusive Modes*

Hadron ID may not always be necessary in cases where intermediate mass constraints are available although it may be crucial in reducing, as yet, unanticipated backgrounds. In contrast simpler, *e.g.* two-body, decay modes may require hadron ID to reject so-called "reflected" decays. Perhaps the most demanding example is the separation of a desired CP mode $B_d \to \pi\pi$ from $B_d \to \pi K$. The momentum resolution of a fixed target spectrometer may not be sufficient to distinquish between these two modes on reconstructed mass alone. Figure 4 shows the π/K energy spectra assuming equal branching fractions to these two modes. The distributions appear remarkably similar in shape with $\pi/K \sim 3$.

3. THE FIXED TARGET HADRON ID SYSTEM

The identification of hadrons in the momentum ranges indicated in figures 2 and 4 can be achieved in a combined system composed of a RICH and a TRD. A simplified layout of the proposed SFT experiment is shown in figure 5. For reasons of clarity only the components relevant to particle identification are displayed.

3.1 *Detector Description*

The Čerenkov radiator gas is chosen to be Neon which implies a pion threshold of $\sim 12\,\mathrm{GeV/c}$ and a maximum Čerenkov angle of $\theta_c = 11.6\,mrad$. Assuming a conservative value for the figure-of-merit $N_o = 50/cm$, a $16m$ long radiator would yield

$$\langle N_{ph} \rangle = N_o L \sin^2 \theta_C \sim 11$$

detected photons for an infinite momentum ring. As illustrated in figure 5b Čerenkov photons are focussed by segmented mirrors onto photon detectors located outside of the experimental aperture. The expected error $\Delta\theta_{Opt}$ in measured Čerenkov angle θ_C due to the off-axis imaging is estimated from [3] to be less than 1% of θ_C. The chromatic error[4]

$$\Delta\theta_{Chr} = \frac{dn}{dE_{ph}} \frac{1}{n \tan\theta_C} \Delta E_{ph}$$

depends on the photon energy bandwidth ΔE_{ph} of the detector and is $\sim 100\mu rad$ for the broadest bandwidth detector considered; a UV enhanced photomultiplier tube. The final source of error is the finite position resoution due to pixel size s,

$$\Delta\theta_{Pos} = \frac{s}{\sqrt{12}f} \quad \text{, where}$$

the focal length $f = 16m$ and the pixel size is taken to be in the range $0.5cm < s < 1.0cm$. The lower end of this range could be achieved in a solid photocathode wire chamber[5] while the upper end could be satisfied by exisiting small diameter phototubes[6]. Using these sources of error figure 6 shows the separation significance of π and K rings as a function of momentum P.

As the ability of the RICH to discriminate between π and K rings falls below 4σ in the range of 175 – 200 GeV/c a TRD is used to extend the particle ID capability of the SFT experiment up to $\sim 500\,\mathrm{GeV/c}$.

The design and simulation of the detector is taken to be similar to the Fermilab E769 TRD[7]. There are 24 modules in depth, each composed of either a stack of radiator foils or a foam radiator followed by a double layer of Zenon filled PWCs. This detector and its simulation are described in more detail in another contribution to these proceedings[8].

3.2 *Detector Performance*

In the simplest case particle detection efficiency and rejection of background are inter-related by the choice of cut on the physical signal from a detector. In the abscence of a specific requirement on either efficiency or background, figure 7 illustrates a method for establishing an experimental cut for separating pions from kaons in the TRD.

Figure 7 shows the distribution of the number of TRD planes firing for pions and kaons at 200 GeV/c, using the simulation in [8]. In this sample the π/K ratio is taken to be 3, as might be expected for particles stemming from a secondary vertex. The cut is chosen at the intersection of these two distributions. The kaon detection efficiency and the pion contamination within the "kaon-identified" sample is obtained from the cumulative distributions evaluated at the cut value. The results are plotted in figures 8a and b for $\pi/K = 3$ and 10 and $200\,\mathrm{GeV/c} < \mathrm{P} < 1000\,\mathrm{GeV/c}$. In [8] it is noted that the "practical" pion TR yield may well saturate for $P = 500\,\mathrm{GeV/c}$. The calculation is repeated in figure 10 with this limiting behavior.

A similar calculation is done for the RICH to obtain the curves of figure 9. The drop in efficiency below 50 GeV/c is due to the requirement of at least three photons being detected. In these calculations a pixel size of $s = 1\,cm$ is assumed.

Referring to figures 8 and 9, if one requires a kaon efficiency > 90% and a pion contamination < 10% then the combination of both detectors permit a momentum range of $50\,\mathrm{GeV/c} < P < 700\,\mathrm{GeV/c}$ for an assumed particle ratio $\pi/K = 3$. A less favorable particle ratio of $\pi/K = 10$ would restrict the momentum range to $50\,\mathrm{GeV/c} < P < 500\,\mathrm{GeV/c}$. The lower momentum cut of 50 GeV/c is necessary if one requires a "postive kaon id" of a particle in order to distinquish it from other non-radiating particles such as protons.

4. CONCLUSIONS

Using the two simple examples of flavor tagging and reconstruction above, adequate hadron identification in a fixed target experiment at the SSC is feasible using a combination of a RICH and a TRD. The large momentum range associated with fixed target kinematics can be covered by detectors built with exisiting technologies.

5. REFERENCES

1. SSC EOI-14 *An Expression of Interest in a Super Fixed Target Beauty Facility at the SSC* May, 1990.
2. At this P_T the incorrect muon tags are due primarily to decays of a daughter D meson. Of course if sufficient vertex resolution is available these may be avoided by detecting the tertiary vertex.
3. T. Ypsilantis, *Cerenkov Ring Imaging*, Physica Scripta **23** (1981) 371-376
4. T. Ypsilantis, *Particle Identification at Hadron Colliders*, in Proccedings of the Symposium on Particle Identification at High Luminosity Colliders, Fermilab, April 1989.
5. N.S. Lockyer, et al., *Observation of Cerenkov Rings Using a Low-Pressure Parallel-Plate Chamber and a Solid Cesium-Iodide Photocathode*, Nucl. Instr. and Meth. **332** (1993) 142.
6. Model FEU-68, MELZ, Moscow, Russian Federation.
7. D. Errede et al., *Use of A Transition Radiation Detector in a Beam of High Energy Hadrons*, Nucl. Instr. and Meth. **309** (1991) 386.
8. M. Sheaff, *Use of Transistion Radiation Detectors (TRD's) for B Tagging/Triggering in Future Collider or Fixed Target Experiments*, these proceedings.

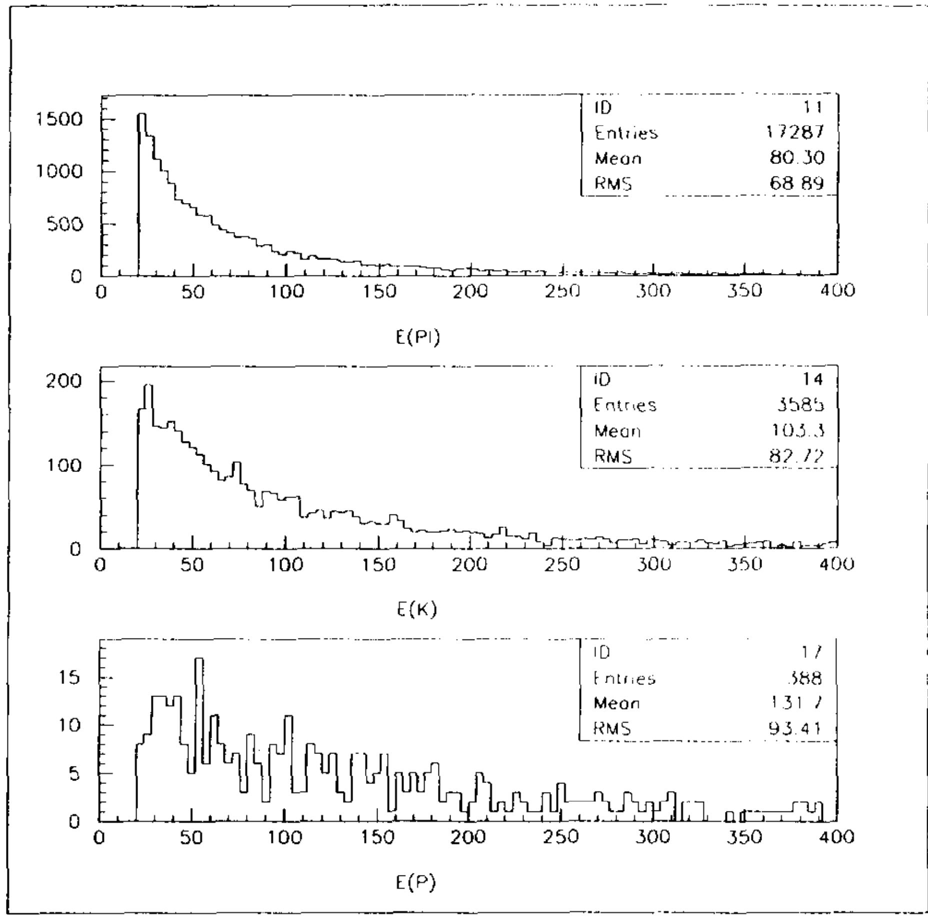

Figure 1: Laboratory energy distributions of π, K and p from the decay of the "other" B hadron in events triggered by $B_d \to \psi K_S$.

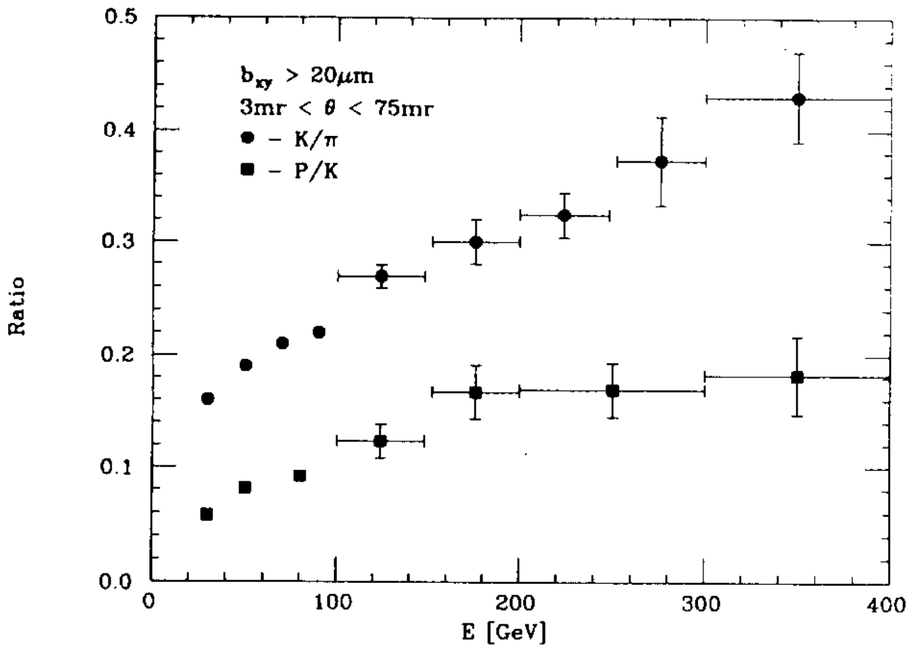

Figure 2: Ratio of particles in the decay of the "other" B hadron.

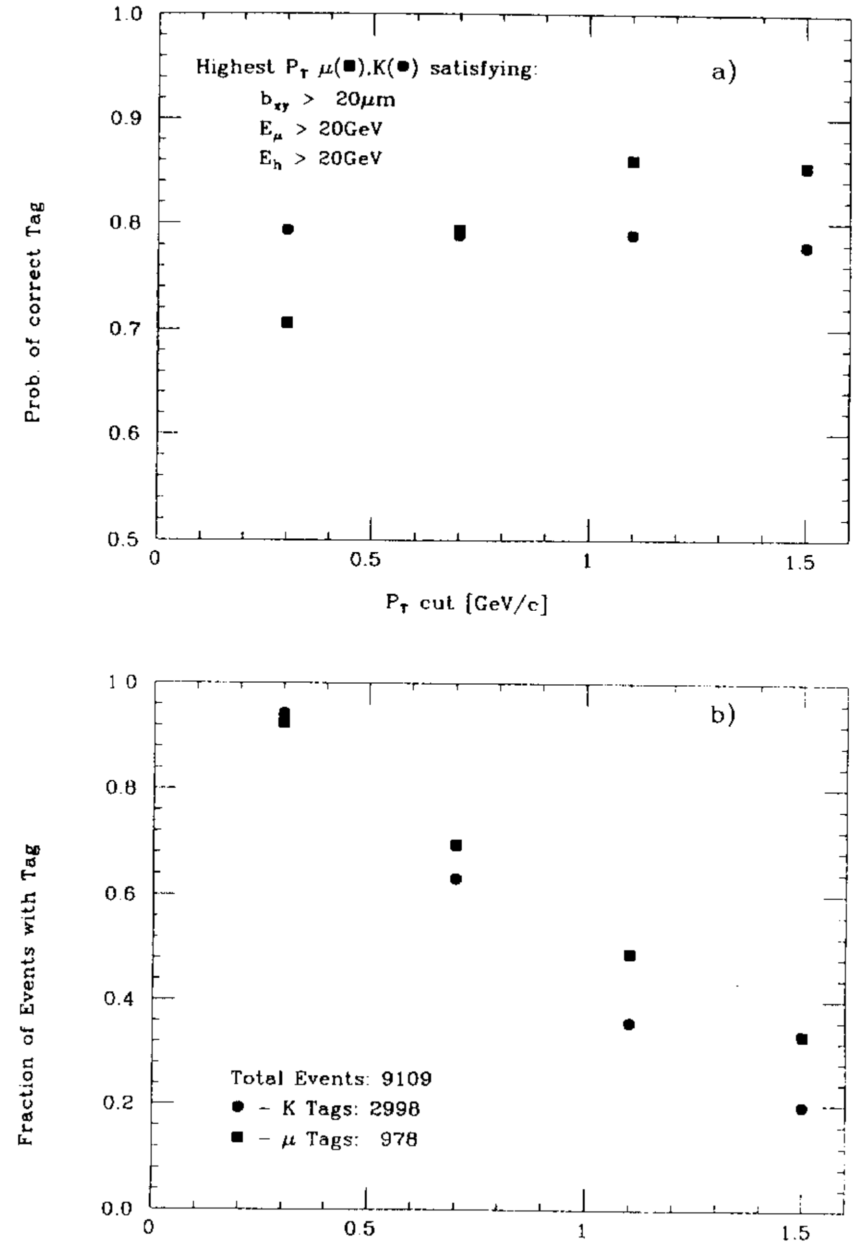

Figure 3: (a) The probability that the tagging particle provides the correct flavor, b or $\bar{b}$, of its parent hadron and b) the relative fraction of events for which there is a tagging particle.

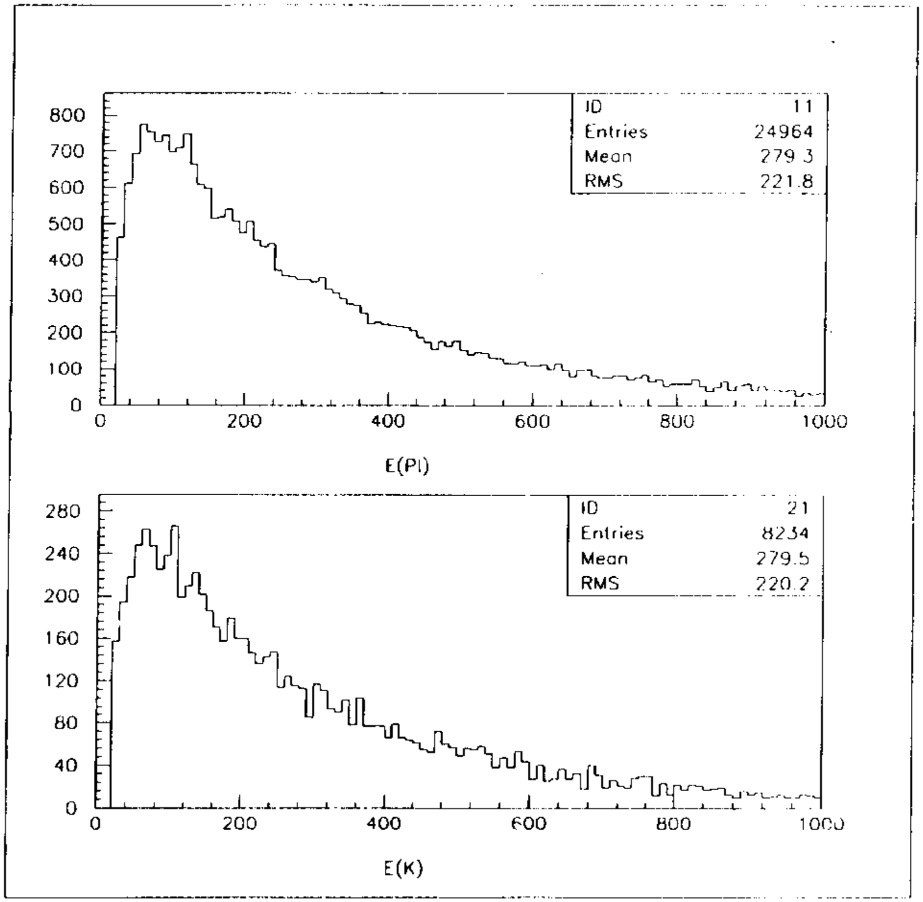

Figure 4: Laboratory energy distributions of pions and kaons within the acceptance and from $B_d \to \pi\pi$ and $B_d \to K\pi$.

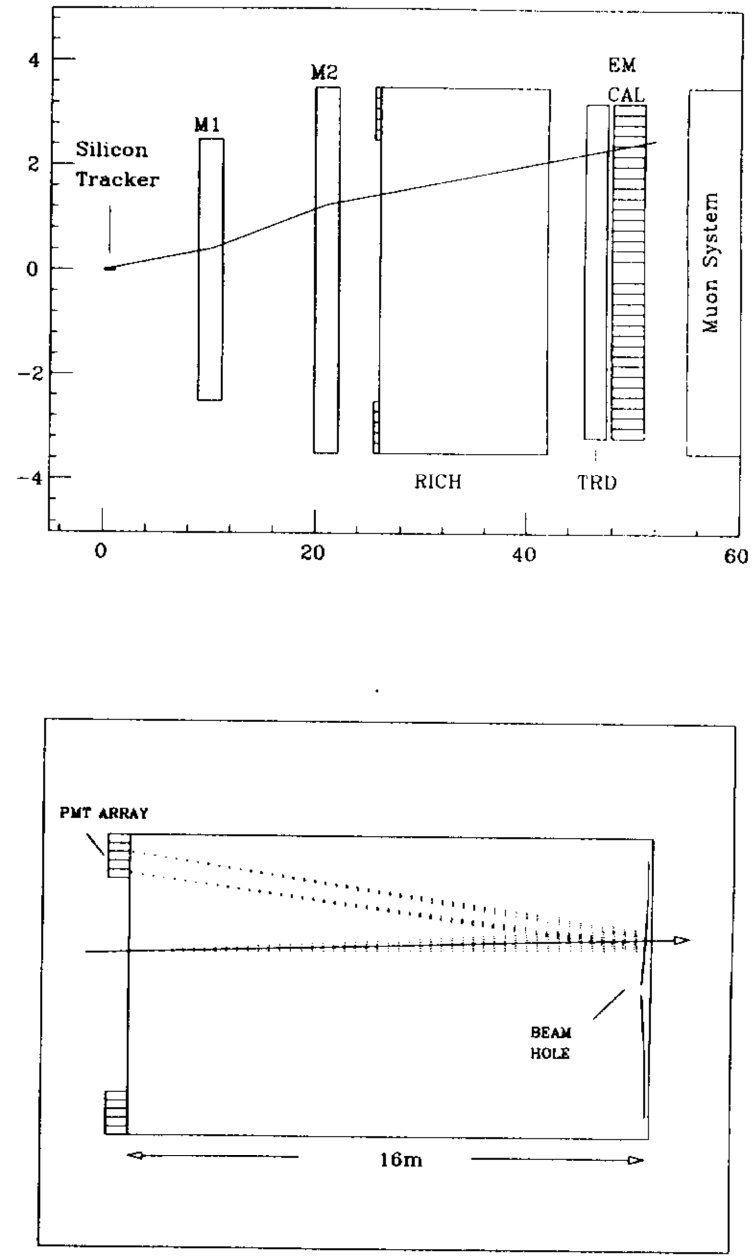

Figure 5: Plan view of the proposed SFT experiment with blow-up of the RICH. Also indicated are the trajectories of a particle and its radiated Čerenkov photons.

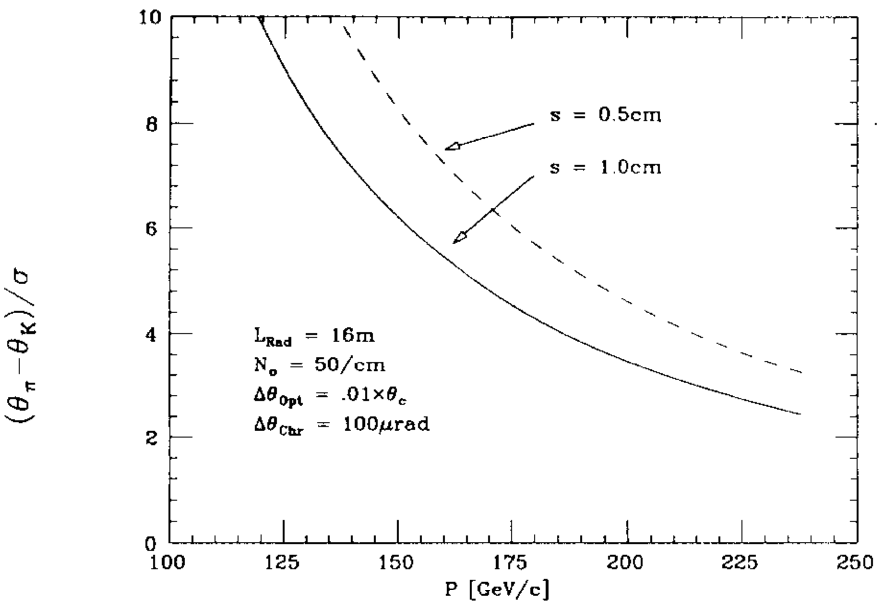

Figure 6: The number of standard deviations separating pion and kaon Čerenkov rings.

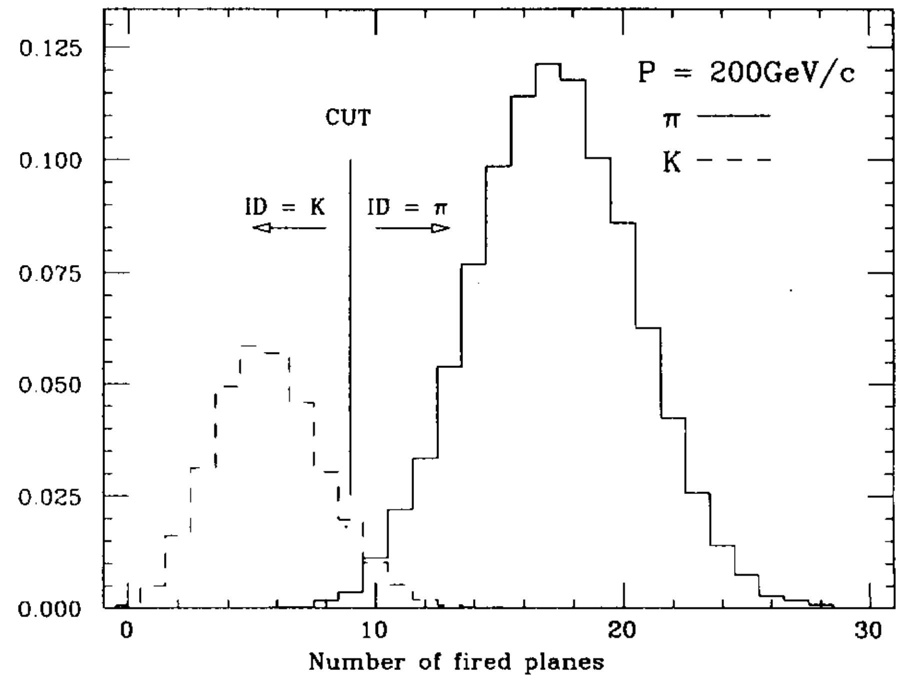

Figure 7: Number of TRD planes firing for pions and kaons. The ratio of particles is taken to be $\pi/K = 3$. The point of intersection of the two distributions is used as the cut separating kaons from pions.

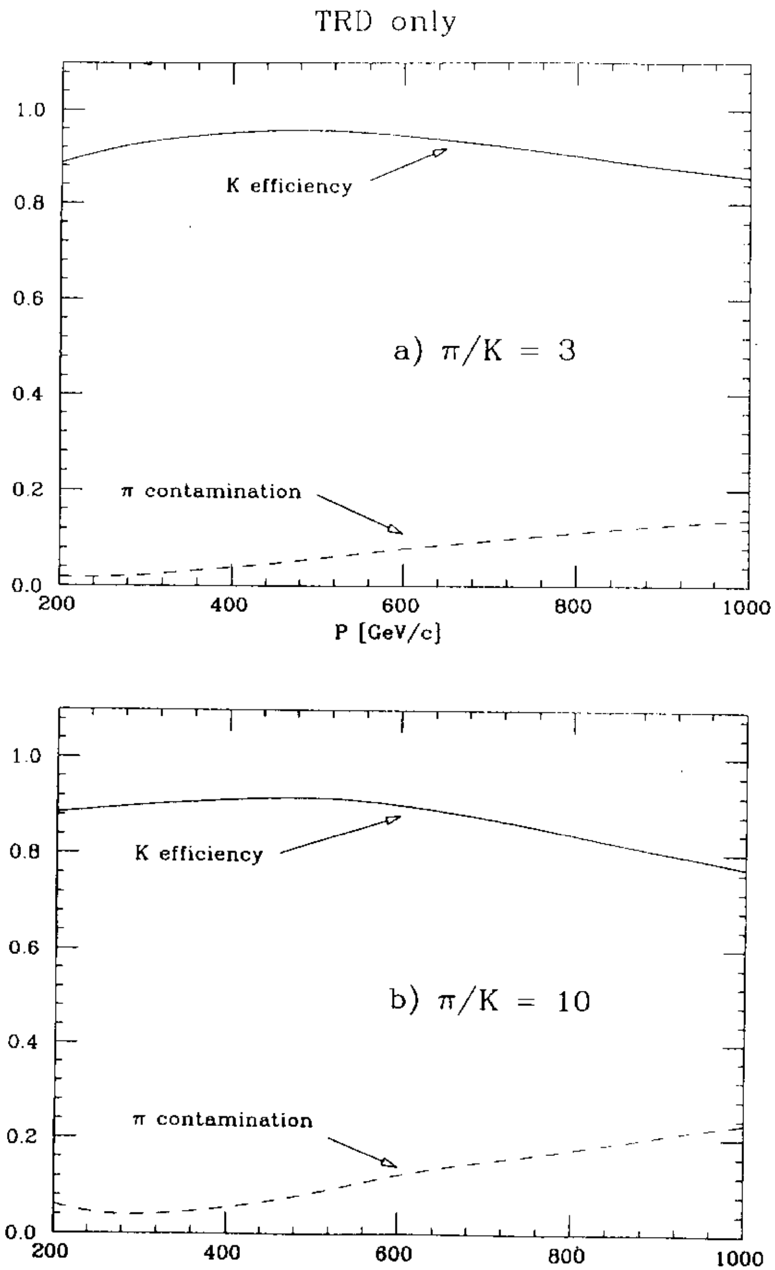

Figure 8: The efficiency for identifying kaons using the TRD and the fraction of the identified kaon sample which is actually pions, for two values of assumed π/K ratios.

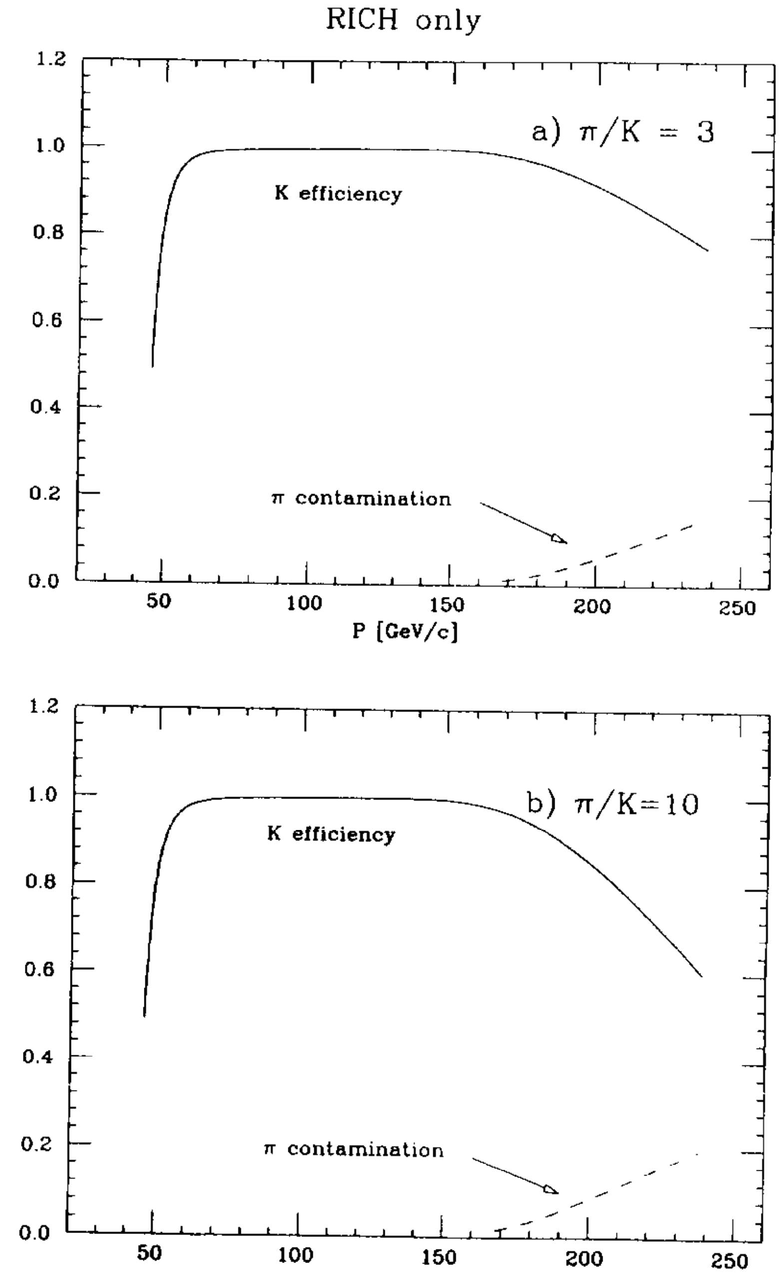

Figure 9: Same as figure 8 except only the RICH is used. The properties of the RICH are those specified in the text; $L = 16\,cm$, $\gamma_{thr} = 86$, $N_o = 50/cm$ and $s = 1\,cm$.

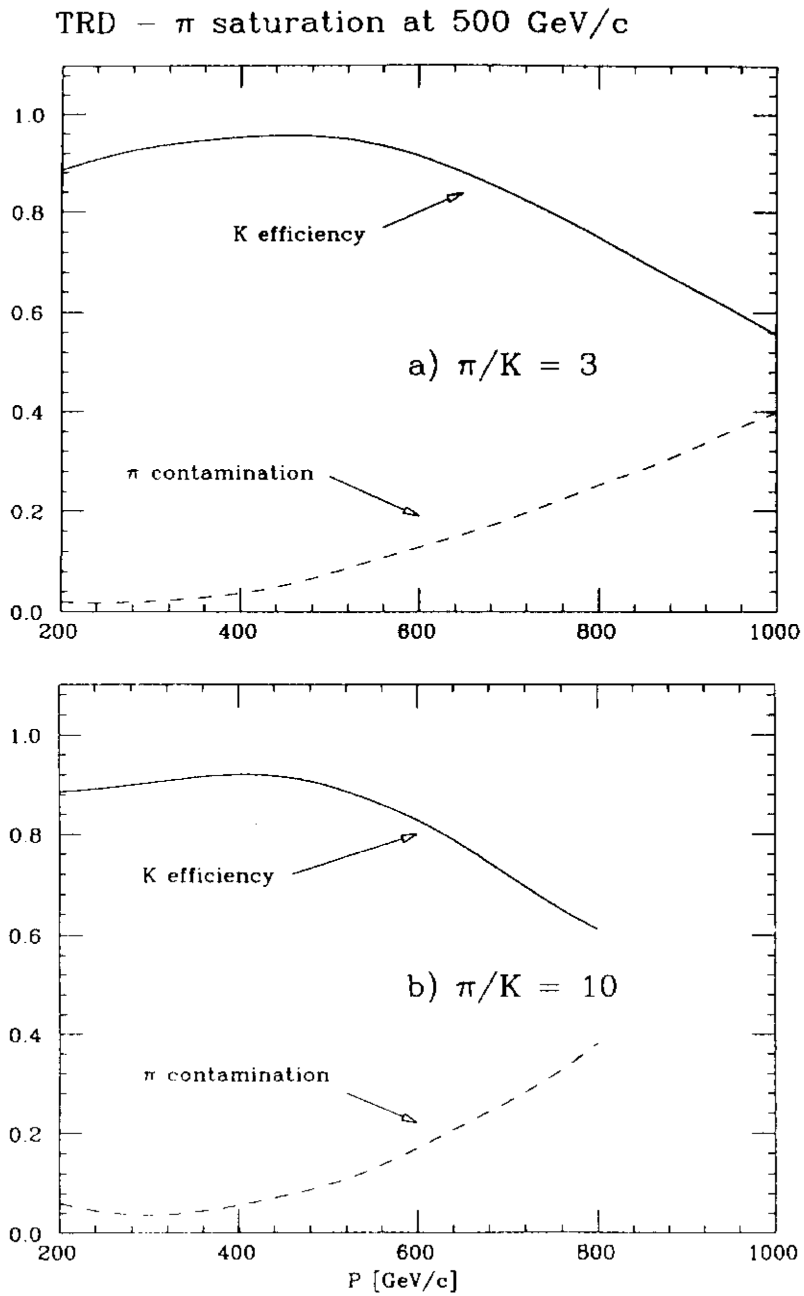

Figure 10: Same as figure 8 except that the pion TR yield is forced to saturate at its 500 GeV/c value.

Experience with dE/dx at CDF

J.D. Lewis
Fermi National Accelerator Laboratory
Batavia, IL 60510

Prior the the 1992-93 Tevatron collider run, the CDF Central Tracking Chamber[1] (CTC) was instrumented to measure charge deposition in addition to drift times for the outer 54 of its 84 sense wire layers in order to measure specific ionization (dE/dx). The Amplifier-Shaper-Discriminator (ASD) cards were modified to include charge integration. The amplifier output is discharged at a constant rate, converting the integrator pulse height to the width of the discriminated pulse. LeCroy 1879 TDC's measure both the arrival time and the width of a pulse. A typical pulse width from a minimum ionizing particle is 12 counts or 24 ns. However, the limited resolution does not present a problem because primary ionization statistics yield an expected single pulse resolution of 40%.[2]

Because the integration time of the circuit is short, the measured pulse height (*i.e.* the pulse width) is sensitive to the shape of the sense wire pulse and is not a linear function of the input charge for pulses that are only a few times larger than the average for minimum ionizing particles. A number of hit selection criteria and corrections are required. To limit the effect of field non-uniformities on the charge collection, hits used for dE/dx must be in a region where the drift field is uniform, greater than 4 mm from either the sense wire plane or the cathode wire plane. A hit isolation cut, using only hits that are more than 40 ns from the nearest hit on the same sense wire, reduces the effect of charge deposited by other tracks on measurement of hits on a track of interest. Calibrations have been made for run-by-run variations in gas gain caused by changes in atmospheric pressure, temperature and gas mixture. The pulse shape is highly dependent on the angle the track makes with the drift direction and with the wire. Currently correction functions to account for this effect are being developed. Calibrations for wire-by-wire variations in gain are also under study. The actual dE/dx measurement is formed from the the mean of the lowest 50% of corrected hit widths.

Because the p_T spectrum of B's is soft, the topology of minimum-bias events is similar to B events, so they can be used to study the performance of dE/dx for B physics. Typical tracks in minimum-bias events have 30 hits available for dE/dx measurement after hit selection. Using only the run-by-run corrections, we achieve a dE/dx resolution better than 15%. This resolution provides over one standard deviation separation between electrons and pions at 5 GeV and can be useful in identifying soft electrons for tagging B flavor. Figure 2 shows dE/dx measurements for kinematically identified electrons and pions in the momentum range 1-3 GeV. The outlook for dE/dx in CDF is that correction functions will be complete before analysis of data from Tevatron Run 1B begins. For Run 2, new preamplifiers will be required for the CTC so that it will be possible to run at lower gain. This will also require new ASD boards, allowing the opportunity to include charge integration in the design from the start and providing linear response over a much wider range of pulse heights and shapes. The plan is continue to use the same charge-to-width conversion scheme. In the distant future, one might envision adding a time-of-flight system to CDF at the radius of the solenoid. Figure 2 shows K-π separation as a function of momentum for tracks at normal incidence with dE/dx measurement with the same number of hits but realizing the theoretical resolution[2] and with time-of-flight measurement with 100 ps resolution.

REFERENCES

1. F. Bedeschi, *et al.*, *Nucl. Instrum. and Meth.*, **A268**, 50 (1988).
2. W.W.M. Allison and J.H. Cobb, *Ann. Rev. Nucl. Part. Sci.*, **30**, 253 (1980).

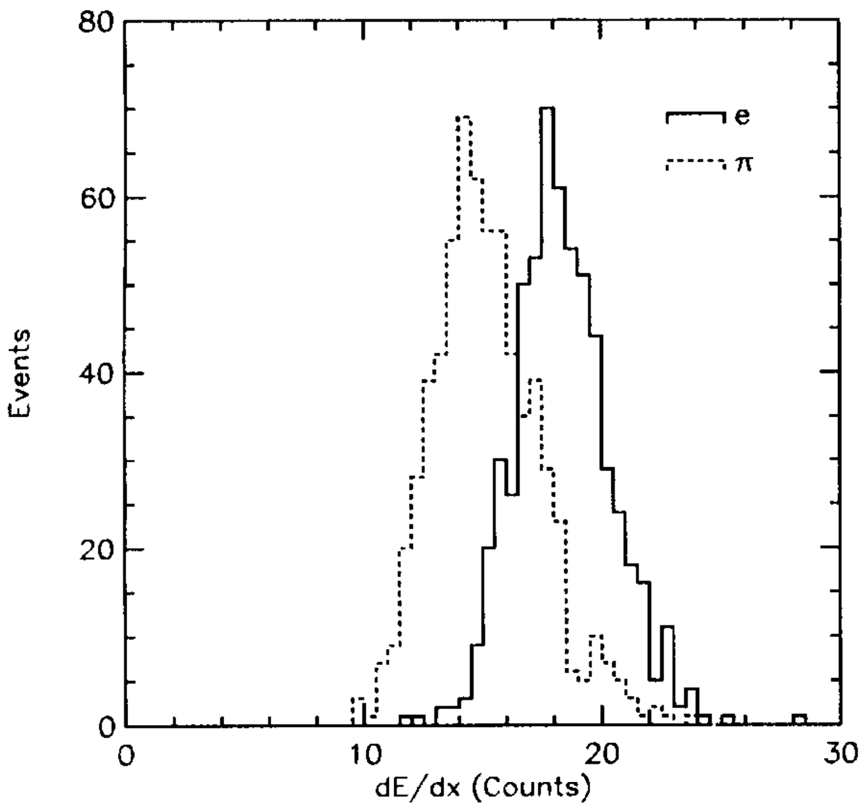

Figure 1: Truncated mean dE/dx values for kinematically identified electrons and pions measured in TDC counts for tracks with momentum in the range 1-3 GeV.

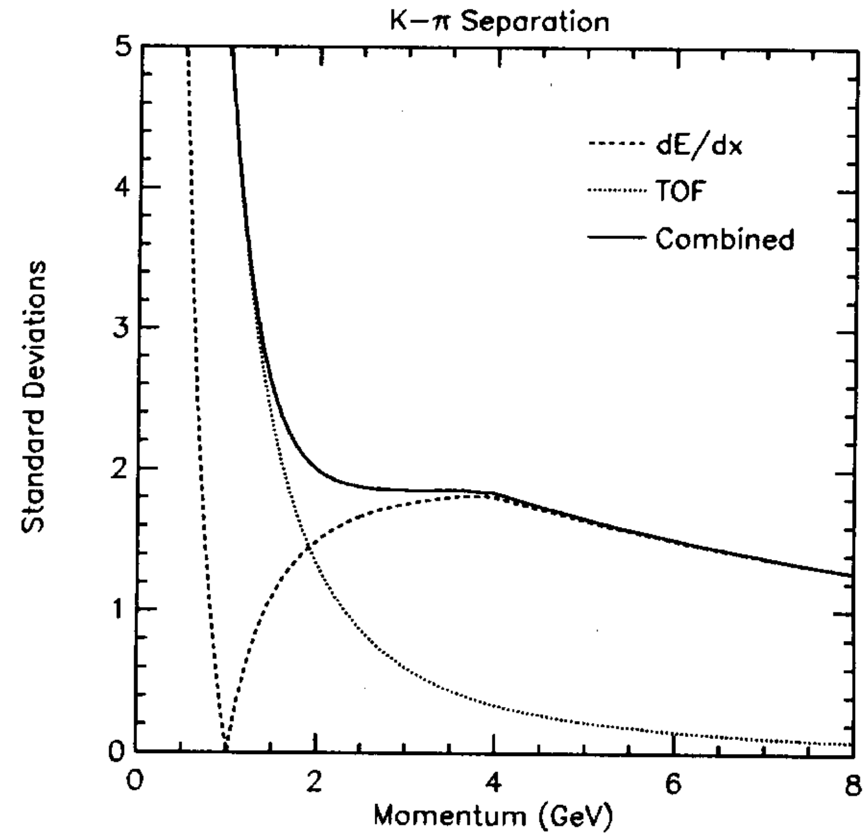

Figure 2: Separation between pions and kaons as a function of momentum for tracks at normal incidence with a dE/dx system like the current CTC but realizing the theoretical resolution and a 100 ps time-of-flight resolution. Dashed line is the effect of combining the two measurements.

Electronics, DAQ, and Computing

Convenors:

J. Dorenbosch
Superconducting Super Collider Laboratory

S. Geer
Fermi National Accelerator Laboratory

List of Participants

G. Abrams
Lawrence Berkeley Laboratory

M. Arenton
University of Virginia

E. Blucher
University of Chicago

S. Conetti
University of Virginia

D. Cords
Stanford Linear Accelerator Center

D. Crosetto
Superconducting Super Collider Laboratory

A. Erwin
University of Wisconsin

M. Halling
Cornell University/
Fermi National Accelerator Laboratory

E. Hartouni
University of Massachusetts

W. Hofmann
Max-Planck-Institut für Kernphysik

C. James
Fermi National Accelerator Laboratory

K. Johns
University of Arizona

M. Johnson
Fermi National Accelerator Laboratory

J. Lewis
Fermi National Accelerator Laboratory

S. Loucatos
CEN Saclay

S. Mani
University of California (Davis)

D. Ritchie
Fermi National Accelerator Laboratory

W. Selove
University of Pennsylvania

P. Shepard
University of Pittsburgh

J. Slaughter
Yale University

P. Sphicas
Massachusetts Institute of Technology

D. Summers
University of Mississippi

P. Wilson
University of Chicago

S. Wojcicki
Superconducting Super Collider Laboratory

Electronics, Trigger, Data Acquisition, and Computing Working Group on Future B Physics Experiments

S. Geer
Fermi National Accelerator Laboratory, Batavia, Illinois 60637, USA

INTRODUCTION

Electronics, trigger, data acquisition, and computing: this is a very broad list of topics. Nevertheless in a modern particle physics experiment we think in terms of a data pipeline in which the front end electronics, the trigger and data acquisition, and the offline reconstruction are linked together. In designing any piece of this pipeline it is necessary to understand the bigger picture of the data flow, data rates and volume, and the input rate, output rate, and latencies for each part of the pipeline. All of this needs to be developed with a clear understanding of the requirements imposed by the physics goals of the experiment; the signal efficiencies, background rates, and the amount of recorded information that needs to be propagated through the pipeline to select and analyse the events of interest. Any assessment of the strengths, weaknesses, and feasibility of any given data pipeline scheme needs to be tempered with a few words of caution:

i) The electronics and computing technology used in high data volume pipelines is evolving rapidly. This introduces uncertainty in our estimates of the capabilities of technologies that will be used in a few years time. Factors of two in rate capability at each stage of the pipeline are well within the uncertainties of the future B physics pipelines discussed in these proceedings .. perhaps factors of ten uncertainty are not out of line for some of the more aggressive extrapolations.

ii) The design of a data pipeline is an iterative process. The iteration is both between the physics goals of the experiment and the technical feasibility of meeting those goals, and also between the various pieces of the data pipeline: for example the capability of the offline computing to reconstruct the dataset in a reasonable amount of time can and will have an impact on the triggering goals of the experiment. An assessment of a future pipeline becomes part of the iterative procedure .. we would expect that weaknesses that might be apparent in the comparisons of the various pipelines described in these proceedings will likely be addressed as the designs evolve.

iii) The physics goals which underlie the design of future B physics data pipelines are themselves in the process of being understood in more detail. It may be that our perception of which B physics approach will be the most rewarding will change in the coming years.

GOALS AND ACHIEVEMENTS

Given the above, in a single workshop we cannot expect to be able to make definitive choices between the various experimental approaches that are being proposed. However, we were fortunate to have the active participation of 26 people in the group, representing a broad collective expertise with greatly varying backgrounds and experience. This enabled us to:

(a) Compile a list of currently proposed parameters for the data pipelines of a great variety of proposed future B physics experiments at hadron machines. The results of this endeavor are presented in the paper by Sergio Conetti et al: "Comparison of Trigger and Data Acquisition Parameters for Future B Physics Experiments". The tables contain information as given by the proponents of the various approaches. Many of the numbers were questioned as we compiled them, and some of the numbers were subsequently revised by the proponents as a result of discussions and the collective learning process that occurs in a workshop. Nevertheless the tabulated numbers do not represent a consensus about the feasibility of the various approaches. However the similarities and differences between the experiments are instructive.

(b) Look at a number of technical developments that are being proposed or considered for use in future B physics data pipelines and gain a sense of the direction things are moving in. There were quite a number of presentations in the working group sessions on new technologies. The various contributions have been edited by Jean Slaughter, and her contribution in these proceedings summarizes this material. The quantity and quality of the R&D discussed is certainly encouraging. As a part of our activities on new technologies there was a subgroup run by Marvin Jonson on trigger processors, and a mini-workshop organized by Paul Shepard on deadtimelless front-end electronics. Reports from both of these activities appear in the proceedings.

I would like to conclude with some of the things which impressed me as the working group sessions progressed. Firstly, the technology required to meet the demanding high data volume needs of the next round of B physics experiments appears to be available, now or within a couple of years. This seems to be the case for both fixed target and collider B physics experiments. Secondly, although there are many differences between the various data pipelines that are being proposed, there are also striking similarities. All experiments have a multi-level trigger scheme (most have levels 1, 2, and 3) where the final level consists of a computing farm that can run offline-type code and reduce the data volume by a factor of a few. Finally, the ability to reconstruct large data volumes offline in a reasonably short time, and making large data volumes available to many physicist for analysis, imposes severe constraints on the foreseen data pipelines, and a significant uncertainty in evaluating the various approaches proposed.

COMPARISON OF TRIGGER AND DATA ACQUISITION PARAMETERS FOR FUTURE B PHYSICS EXPERIMENTS

S. Conetti
Univ. of Virginia, Charlottesville, VA 22901, USA

S. Geer
Fermi National Accelerator Laboratory, Batavia, Illinois 60637, USA

1. INTRODUCTION

The main task of the Trigger and Data Acquisition Working Group was to collect the global parameters of the Trigger/DA schemes envisaged by various approaches to future hadronic B physics, and to perform a zeroth order comparison of the overall performances. A few general comments are in order before presenting the detailed tables:

1- The numbers are presented as provided to the working group by representatives of the various collaborations. Due to the limited time, no in depth attempt was made to verify the validity of the quoted performance figures, nor to examine the technical implications and feasibility of any given scheme.

2- The level of reliability for the performance figures reported in the tables covers a wide range, due to the large variation in the procedures followed to derive the actual numbers. In order of decreasing reliability, sources of estimates were:

- extrapolations from data
- full detector and trigger simulation (with or without support from data)
- event generation (e.g. Pythia) plus smearing to simulate detector response
- educated guess
- performance goal, rather than actual projection

3- The exchange of ideas and information among workers with different backgrounds and experience was very constructive. As a result of the discussion some pre-conceptions were removed, triggering schemes and ideas were sharpened and the overall picture of triggering on B's in a high rate environment became clearer.

2. PERFORMANCE TABLES

The condensed picture of all the data that became available at the workshop is presented in Table 1. In spite of the large quantity of numbers appearing in the table, an even cursory examination of it allows us to identify some common trends and to make some general comments.

Starting from the top, the first well recognized fact is that all detectors, including the ones like SDC, GEM and ATLAS which were not designed having B physics in mind, are capable of addressing B -> J/ψ channels, by triggering on di-muons and possibly di-electrons. Even so, there are large differences in efficiency for the B-> J/ψ channels when going from collider to fixed target environments. These differences are due to the increased discriminating power of a lepton p_T cut in the fixed target mode because the transverse momenta characteristics of B decay products, typically around one or two GeV/c, are large compared to minimum bias interactions at fixed target energies, while the same is not true for collider energies. On the other hand, the B cross-sections are much larger at collider energies.

While everyone appears to be capable of developing a viable J/ψ trigger, the situation changes drastically for the other channels of interest (following the workshop's theme, one representative reaction for each of the unitarity angles, plus a generic b trigger addressing "all other B physics", were included in Table 1). As shown in the Table, only a few of the dedicated B detectors present capabilities for non-J/ψ modes or for an inclusive B trigger (it should be noted that, for the purpose of this document, CDF III and D0 III are being considered as dedicated B detectors since they represent the best effort of the collaborations to upgrade their detectors in order to address B physics). It is interesting to examine the similarities in the approaches of different detectors to the trigger sequence: effectively every setup plans for a Level 1 trigger based upon lepton and/or hadron p_T, with a notable difference for GAJET that proposes the intriguing idea of impact parameter optical trigger. At Level 2, all the entries, with the exception of the high p_T non B-specific detectors, include the implementation of a multiple vertex and/or impact parameter trigger. All detectors also envisage a last level of selection performed in a Level 3 Processor Farm, although it should be noted that the Level 3 rejection factors reported in the Table are generally derived from the two sources of lowest reliability (i.e. educated guesses or simply design goals). Some special remark should also be made about the BCD approach. The BCD basic strategy is to require a 10^2 suppression at Level 1, no Level 2 and a further factor of 100 at Level 3. By their own admission, the BCD performance parameters provided by the proponents are design goals rather than simulation results. Moreover the realism of the goals - a 10^2 rejection at Level 1 with a modest 1 GeV/c p_T cut or a Level 3 accepting 10^6 events (= 500 Gbytes) per second - has been questioned. On the other side one should recognize the soundness of the basic philosophy of the BCD approach, stating that since B production at the SSC in collider mode represents 1% of the total cross-section it is wise to develop a trigger that is as loose as possible at the lower levels while trying to defer the selection to when the events can be fully analyzed.

Going back to the table entries, the brief descriptions of trigger choices also contain the rules for developing a generic B trigger; the two main approaches are:

1- presence of one (or more) high p_T lepton (possibly reinforced by a high p_T hadron) plus some sort of vertex/impact parameter trigger.

2- presence of several (two or more) high p_T hadrons, again combined with an indication of secondary vertices activity. The values of p_T threshold can be optimized to get the best acceptance for, e.g., the B -> ππ decay mode.

It is obvious that both of these approaches can be developed and run in parallel and in fact they end up providing similar acceptances for an inclusive B trigger, since the loss due to the semi-leptonic Branching Ratio in the first approach is offset by the need to impose higher p_T thresholds when a lepton is not present.

A few words about rates: rather than comparing luminosities, possibly a misleading quantity when comparing beam beam collisions with beam impinging on a heavy target, a better indication of how hard the detectors (and front end electronics) need to work is given by the list of Interaction Rates and Input Rates to Level 1. An Interaction Rate larger than the corresponding L1 Input Rate indicates a regime of more than one interaction per crossing (or per beam bucket on target), the ratio between the two giving the average number of interactions per crossing.

A more detailed discussion and comparison of the different strategies and their hardware implementations would be quite interesting, but goes far beyond the scope of the present document. It is worthwhile, nevertheless, to get a feeling for the relative complexity of the hardware by looking at the product, either at Level 1 or 2, of the Input Rate by the Latency. We have indicated in bold characters the cases where such a product exceeds 100% system occupancy, forcing therefore the need for pipelined and/or parallel processing, a fairly straightforward requirement at Level 1, but typically a rather complicated (and/or costly) proposition at Level 2. A few more comments can be made about some general features.

Concerning the performance requested from Level 1, one notices a very wide spread of values, ranging from a reduction of minimum bias of a factor 7 for COBEX up to 6000 for SDC and GEM. Much less spread is observed at Level 2 (ranging from 10 to 100), and even less at Level 3, where all detectors settle for rejections between 5 and 10 (with the exception of BCD). Combining all levels together, all detectors end up achieving global rejections contained in the relatively narrow range of 10^4 to 10^5, except for ATLAS ($4\ 10^5$) and COBEX, which envisages a global rejection of 10^3. This rather modest rejection, obviously chosen to minimize the loss of B events (first rule of triggering: there is no free lunch, any attempt to reject background will also entail a loss of signal), does not come without technical complications since it requires that data be logged at the rather ambitious rate of 300 Mbytes/sec (3 times higher than SDC but still lower than BCD).

Another important issue is whether the performances required by the various detectors represent a major jump with respect to what is being done routinely today. For this purpose we have collected (Table 2) the parameters relative to the best representatives of today's hadronic B physics: CDF, the most fertile producer of B hadro-production results to-date, and two examples of fixed target experiments, FNAL E771/P867, heavily based upon B-specific triggers, and E791, more of a charm than a B experiment, relying on the technique of an open trigger. The comparison between today and tomorrow is contained in Table 3, showing the growth of the most critical parameters going from CDF I to CDF III and from E771 to the SFT. While one can observe expected growths of fairly large factors in most entries, all of the extrapolations are rather reasonable, especially when the requirements of the B experiments are compared to the SSC high p_T detectors. The increase in the trigger efficiency for B->J/ψ modes needs some commenting; for CDF, a factor of 10 increase is achieved by increasing the acceptance of the microvertex detector and lowering the lepton trigger p_T threshold, while in the fixed target mode most of the gain comes from the increase in geometric acceptance typical of the SSC vs Tevatron environment for equal solid angle coverage. The Table shows how both Level 2 and 3 triggers will need to work at a much higher level of performance, which is nevertheless quite compatible even with today's technology. Finally, the projected increase in logging rates and data set volume ends up being within a factor of four of what has already been achieved by E791 (see Table 2).

3. FINAL COMPARISONS AND CONCLUSIONS

The major purpose of any triggering scheme is to maximize the number of signal events recorded on tape, while minimizing the background. From the information contained in Table 1 we have extracted and compiled the rates of B production vs. the rate at which B events are expected to be logged onto tape. Table 4 shows how, in spite of the large differences in B production rates, spanning over three orders of magnitude (or more than four if HERA-B is included) the logging rates for B events are contained within one order of magnitude (or two including HERA-B). This is a consequence of the by now well recognized effect of the larger acceptance and better triggerability of fixed target detectors, which start up with a disadvantage in terms of B cross-section

In conclusion, we have seen that dedicated B detectors are able to address at the trigger level the whole spectrum of B decays, as opposed to just collecting B->J/ψ events and that the appropriate trigger strategy is a combination of high p_T leptons, high p_T hadrons and vertex/impact parameter triggers. The performance required of the trigger/DA systems appears to be, with some possible exceptions, well within today's technology , or at most a mild extrapolation of it. Dedicated detectors should be able to log inclusive B events at the rate of up to a few hundred per second, or for rare decays of the type e.g. B-> $\pi\pi$, of a few tens per hour.

4. ACKNOWLEDGMENTS

The gathering of the material here contained and the format of presentation were the result of the effort of several members of the Trigger and DAQ Working Group. A particularly important role was played by J. Dorenbosch , M. Halling and S. Loucatos.

5. REFERENCES

The sources of information exploited to fill the summary tables were the following:

CDF : F. De Jongh, T. LeCompte, P. Wilson, FNAL
D0 : R. Lipton, FNAL
SDC : J. Dorenbosch, SSCL
GEM : J. Dorenbosch, SSCL
BCD : K. MacDonald, Princeton University
COBEX : NIM A 333, 101, 1993
HERA-B : W. Hofmann and T. Lohse, Heidelberg Univ.
SFT: S. Conetti, University of Virginia
GAJET : S. Loucatos, Saclay
ATLAS : P. Eerola, CERN
LHB : F. Ferroni, Rome and S. Loucatos, Saclay
E771/P867: S. Conetti, University of Virginia
E791: M. Halling, FNAL and D. Summers, University of Mississippi

Table 1: TRIGGER, DATA ACQUISITION, AND COMPUTING SUMMARY FOR FUTURE EXPERIMENTS

	CDF III	D0 III	SDC	GEM	BCD FULL	COBEX-LHC	HERA-B	SFT	GAJET	ATLAS	LHB
Trigger Eff: ψK_S	2.5%† ee,μμ	8% μμ	0.1% ee,μμ	0.1% ee,μμ	14% ee,μμ?	12% μμ	40-50% ee,μμ	56% ee,μμ	24% ee,μμ	?	32% ee, μμ or μ
$\pi\pi$	>4%	?	?	?	>2%	0.75%	?	45%	24%	0.3%	62% ?
$D_S K^-$	2%	?	?	?	>2%	?	?	40%	13%	?	?
Inclusive b	>0.5%	1.6%	?	?	>2%	?	?	≥20%	?	?	?
Luminosity	10^{32}	10^{32}	10^{33}	10^{33}	10^{32}	10^{32}	4.10^{33}	10^{33}	2.10^{33}	10^{33}	10^{33}
Int. Rate (MHz)	5	5	100	100	10	7	40	10	70	60	10
bbar per interaction	10^{-3}	10^{-3}	10^{-2}	10^{-2}	10^{-2}	7.10^{-3}	10^{-6}	$1.6.10^{-4}$	3.10^{-5}	10^{-2}	10^{-4}
Million Det. Channels	0.6	1	4 ?	?	2	0.6	0.5	0.65	1	10	1.2
L1	Pt had e,μ	μ 2μ	Pt had e,μ	Pt had e,μ	Pt e μ vertx	μ	2 lept mass	Pt had e,μ	Optl Pt Imp Si	Pt μ	SumEt Pt had e,μ
Latency (μs)	4	?	4	2	2	?	10	1	0.02(1)	2	0.2
Input (MHz)	2.5	2.5	60	60	10	7	10	10	40	40	10
Output (KHz)	100	10	10-100	10-100	N.A.	1000	10	50	400	100	100
L2	imp lept id mass photon	μ vertx	lept-id mass	lept-id mass	N.A.	μ Pt imp	lept id trk imp	vertx	Pt imp vertx ?	Trk Pt œ μμ	Pt 2 had imp
Latency (μs)	20	?	10-50	2.10^5	N.A.	?	1000?	10	10-20?	1000?	20
Output (KHz)	<1	0.5	1	1	100	30	1	5	3	1	5
L3 FARM (MIPS)	$< 10^5$	?	?	2.10^5	10^6	?	10^4	?	?	?	10^5
Output (Hz)	< 100	< 100	100	100	1000	5000	100	1000	300	<100	<500
OFFLINE Evnt Size (Kb)	< 220	190	1000	400	500	60	50	20	50	200	50
Raw Data-Set Size /yr (Tb)	< 220	< 190	1000	400	5000	3000	50	200	150	200 ?	250
CPU (MIPS)	< 70K	?	100K	400K?	2.10^6	?	10K	20K	?	?	10K
Rec. Data-Set Size/yr (Tb)	< 320	?	2000	200	5000	?	< 50	?	?	?	?

† 4% for μμ if CDF can trigger μμ up to $\eta = 3$.

Table 2: TRIGGER, DATA ACQUISITION, AND COMPUTING SUMMARY FOR EXISTING EXPERIMENTS

	CDF Ia	E771/P867	E791
b - modes and Trigger Efficiencies	ψK_S (0.3%; ψ -> μμ.) B -> ψX (1%; ψ -> μμ) B -> Xlν (0.05%)	B -> ψX (6% / 16%; ψ -> μμ) B -> μX (4.5% / 13%)	ccbar (40%)
Interaction Rate (KHz)	300	3000 / 5000	40
bbar per interaction	10^{-3}	10^{-6}	10^{-6}
Detector Channels	80K	50K	24K
L0	N.A.	interaction in target	interaction
Input Rate (KHz)	N.A.	53000	530000
Output Rate (KHz)	300	3000 / 5000	40
L1	2μ, Pt >1.5 lept Pt >6	2μ, 1μ, Pt >0.8	Loose Et
Latency (ms)	3.5	0.6	
Output Rate (KHz)	2	N.N./1.5	20
L2	μ Trk match Pt	N.A. / vertex	N.A.
Latency (ms)	20	5	N.A.
Input Rate (KHz)	2	N.A. / 1.5	N.A.
L3 FARM	1000 MIPS	N.A.	N.A.
Input Rate (Hz)	15	N.A.	N.A.
Output Rate (Hz)	3	500 / 150	10 000
OFFLINE Event Size (Kb)	100	5	2.5
Raw Data-Set Size / year	1.5 Tb	1 month run	50 Tb
Raw Data-Set Size - Total	1.5 Tb	1 Tb	50 Tb
CPU Required (MIPS)	1100	1500 / 1500	10 000
Reconstrtd DataSet Size/yr	2.7 Tb	?	16 Tb

Table 3: Comparison of Present and Future Experiments

	CDF I -> CDF III	E771 -> SFT
Interaction rate (MHz)	.3 -> 5	3 -> 10
Channel count	$8x10^4$ -> $6x10^5$	$5x10^4$ -> $6x10^5$
J/psi trigger eff. (including geom. accept.)	0.3 % -> 2.5 (8) %	10 % -> 60 %
Level 2 Input (Hz)	$2x10^3$ -> 10^5	$1.5x10^3$ -> $5x10^4$
Level 3 Input (Hz)	15 -> 1000	0 -> 5000
Data set/year (Tbytes)	1.5 -> 200	10 -> 200

Table 4: Comparison of Event Rates

	bb / Sec Produced	EVENTS TO TAPE/SECOND				
		TOTAL(*)	B INCL.	ψK_S	$\pi\pi$	$D_S K$
CDF	$5x10^3$	<100	>25	$1.2x10^{-3}$ (3.8)	$1.6x10^{-3}$	$0.6x10^{-3}$
D0	$5x10^3$	<100	–	$3.8x10^{-3}$	–	–
SDC	10^6	100	–	$1.9x10^{-2}$	–	–
GEM	10^6	100	–	$1.9x10^{-2}$	–	–
BCD	10^5	1000	>2000(**)	$2.7x10^{-1}$	$1.6x10^{-2}$	$1.2x10^{-2}$
COBEX	$5x10^4$	5000	–	$5.8x10^{-2}$	$3x10^{-3}$	-
HERA-B	40	100	–	$4.1x10^{-4}$	–	–
SFT	$1.6x10^3$	1000	320	$1.9x10^{-2}$	$5.8x10^{-3}$	$3.8x10^{-3}$
GAJET	$2.1x10^3$	300	–	$1.0x10^{-2}$	$4.0x10^{-3}$	$1.6x10^{-3}$
ATLAS	$6x10^5$	<100	–	–	$2.0x10^{-2}$	-
LHB	10^3	<1000	–	$0.7x10^{-2}$	$5.0x10^{-3}$	-

(*) Signal + Background
(**) Note: the BCD figures are reported as given by the proponents. Obviously the B logging rate displayed here will have to be reduced in order to allow for the unknown rate due to irreducible backgrounds from minimum bias and

TRIGGERING AT THE SFT

S.Conetti, M. Arenton, G. Corti, B. Cox, C. Dukes
T. Lawry , I. Tzamouranis
High Energy Physics Laboratory, U. of Virginia
Charlottesville, VA 22901
A.Erwin
Physics Department, University of Wisconsin
Madison, WI 53706

1. INTRODUCTION

One essential feature of a fixed target B experiment, when compared to collider detectors, is the much better performance achievable at the trigger level in terms of background rejection for a given signal retention. To a large extent this is due to the fact that, in the fixed target environment, transverse momenta carried by products of B decay are larger than those typical of minimum bias interactions. This is illustrated in detail in fig. 1: fig 1a shows the integral distribution of the maximum P_T for π and K (i.e. the fraction of minimum bias events with at least one charged pion or kaon passing a transverse momentum cut) for the fixed target vs. the collider environment. One can see that a cut of, e.g., 2 GeV/c reduces the fixed target rate by two orders of magnitude, while only affecting the collider rate by a factor of 2. In contrast, fig. 1b gives the integral P_T distribution typical of B decay products (more specifically the P_T of the muon from inclusive $B \to \mu$ decays); the distribution falls gently in the range of interest, so that one can achieve reasonable acceptances for P_T cuts in the 1-2 GeV/c range. In view of this, the SFT trigger strategy is strongly based upon the transverse momentum characteristics of the events, requiring, at the first level, suitable combinations of P_T cuts on leptons and hadrons; in the following, we will discuss separately the muon, electron and hadron triggers, and then show how they can be combined to achieve the required global performance. Next, we will discuss how the unique properties of the SFT live target allow the implementation of a multiplicity jump, multi-vertex trigger, providing a further level of rejection at higher levels of triggering.

2. MUON TRIGGER

The muon trigger hardware consists of 3 or more planes of Resistive Pad Chambers (RPC) behind 20 GeV of shielding, combined with a set of pad chambers located before the shielding[1]. A muon P_T cut of 1.5 GeV/c is imposed by using Programmable Logic Gate Arrays to accept only those pad chamber coincidences which are consistent with the P_T cut: in such a configuration, the information from the RPC muon detectors is only used to identify the region in space where a muon was detected, while the pad chambers in front of the shield determine P_T with good resolution. The angular acceptance of the trigger is 2-75 mrad. From PYTHIA simulations the trigger acceptance is 37%, so acceptance times the branching ratio to muons gives an acceptance of 8% of the $B-\bar{B}$ cross section. The acceptance of 8% includes only events where the muon comes directly from the B. If one includes muons from the decay chain $B \to DX, D \to \mu X'$ the acceptance rises to 8.8%.

The geometric acceptance times branching ratio for the $c-\bar{c}$ cross section is 0.18%. From Table I the charm trigger rate is comparable to the trigger rate for beauty.

The main source of unwanted triggers comes from $\pi, K \to \mu\nu$ decays in flight. Assuming a distance of 50 meters from the target to the start of the hadron shielding, PYTHIA simulations predict a trigger rate from decay of pions and kaons of 1 trigger per 2270 minimum bias events. From Table I, the total muon trigger rate is 4.4 khz, assuming 10^7 interactions per second. When accounting for the finite P_T resolution intrinsic to the envisaged triggering hardware, our simulations show a rate increase of about 50%.

Table I. High P_T Muon Trigger.			
Process	Cross Section μ barns	Acceptance	Relative Rate
$B-\bar{B}$	3.75	8.0%	1.0
$c-\bar{c}$	75-300	0.18%	0.45-1.8
Inelastic	32,000	0.044%	46.9

Note that both the $B-\bar{B}$ and $c-\bar{c}$ cross sections include an A enhancement of 2.5 since the target is assumed to be Silicon (A=28.1). The lower limit on the $c-\bar{c}$ cross section is the measured value from current fixed target experiments, the upper limit assumes the cross section scales linearly with $\sqrt{s}$.

3. ELECTRON TRIGGER

At first glance, implementation of an electron trigger appears to be much more problematic than a muon trigger, since in minimum bias interactions muons will be present only in the case of π, K in flight decay, while practically every event, in addition to a large number of photons, will also contain e^+e^- pairs due to photon conversions in the target or in the detector elements. Even so, a more detailed analysis shows that, since the electrons and positrons are the product of the cascade chain $\pi^0 \to \gamma\gamma \to e^+e^-$, their typical momenta and transverse momenta are rather small when compared with electrons from B decay.

The hardware of the electron trigger consists of an Electromagnetic Calorimeter (EC) with active pre-radiator, a Transition Radiation Detector (TRD) and the same pad chambers as for the muon trigger. Similarly to the muon strategy, Calorimeter and TRD are used to signal the likely presence of an electron in a given region of space, while the pad chambers confirm the presence of a candidate track consistent with the electron location and measure its P_T. For electrons we require $P_T > 1.5\ GeV/c$ and $E_e > 20\ GeV/c^2$. The acceptance of the trigger is 2-75 mrad. The acceptances and branching ratios for B events are the same for electrons and muons.

One source of unwanted triggers is photon conversion to e^+e^- in the silicon target. The photons from an average event pass through half the target plus the downstream silicon tracking planes, which gives a photon conversion probability of 11.7%. When imposing the E and P_T cuts mentioned above, PYTHIA simulations predict a trigger rate from photon conversions of 1 trigger per 2780 minimum bias events.

A second source of unwanted triggers is hadron-electron confusion. With the conservative assumption that the combination of EC and TRD provides an online hadron rejection factor of 100, then PYTHIA simulations predict a trigger rate from e/π confusion of 1 trigger per 1430 minimum bias events. A third source of unwanted triggers is accidental overlap of photons and charged hadrons in the electromagnetic calorimeter. This rate is small compared to the other backgrounds. Assuming 10^7 interactions per second, the electron trigger rate is 1.5 khz, from photon conversions and 6.8 khz from e/π confusion. Again this rate will increase by about 50% due to the finite P_T resolution.

Table II. High P_T Electron Trigger.			
Process	Cross Section μ barns	Acceptance	Relative Rate
$B-\bar{B}$	3.75	8.0%	1.0
$C-\bar{C}$	75-300	0.18%	0.45-1.8
Inelastic $\gamma \to e^+e^-$	32,000	0.015%	16.0
Inelastic e/π confusion	32,000	0.068%	72.5
Inelastic γ/hadron overlap	32,000	0.077%	82.1

4. HADRON TRIGGER AND FIRST LEVEL STRATEGY

The fast information from the pad chambers, besides participating in the definition of the lepton triggers, can also be exploited to produce a high P_T multi-hadron trigger. While the main motivation for such a trigger is to go after decays of the type $B \to \pi^+\pi^-$, it will also increase the collected sample of generic inclusive B's. According to our simulations, a reasonable choice of P_T thresholds for the $B \to \pi^+\pi^-$ decay is an asymmetric P_T cut on two hadrons , with thresholds set at 3.0 and 1.0 GeV/c respectively. Such a condition, which will retain 45% of the $B \to \pi^+\pi^-$ events where both π's are within the spectrometer's acceptance, will also accept 8% of the generic B decays, while rejecting miminum bias events at the rate of 10^{-3}. The information relative to the presence of high P_T hadrons can also be combined with the lepton triggers, to provide additional rejection with negligible loss of B signal.

In summary, we are envisaging to recognize, at Level 1, the presence of high P_T leptons and hadrons, in order to form several independent trigger conditions, viz. a generic muon-hadron or electron-hadron trigger, a J/ψ- oriented di-muon and di-electron trigger, and a di-hadron trigger aimed mainly at $B \to \pi^+\pi^-$ decays but also capable of recording inclusive B decays with reasonable efficiency. Table III shows the summary of P_T thresholds for the various conditions and their overall effect on minimum bias and charm events. From Table III it then appears that the combination of all trigger conditions would provide an overall Level 1 rejection of about 3 x 10^{-3}. As mentioned earlier, finite P_T resolution would increase the actual rate to 5 x 10^{-3}.

Table III. Summary of First Level Trigger.			
Trigger Type	P_T Thresholds	Min bias Suppression	Charm Suppression
$\mu^+\mu^-$	1.0, 0.5	8.4×10^{-5}	2.1×10^{-6}
e^+e^-	1.0, 0.5	7.6×10^{-4}	8.8×10^{-7}
μ hadron	1.5, 1.0	2.5×10^{-4}	2.7×10^{-7}
e hadron	1.5, 1.0	9.7×10^{-4}	2.7×10^{-7}
hadron hadron	3.0, 1.0	1.0×10^{-3}	6.6×10^{-5}
Total suppression	3.1×10^{-3}		

5. SECOND AND THIRD LEVEL TRIGGER

In addition to the P_T spectrum of the secondaries, another distinctive feature of B events to be exploited at trigger level is the presence of multiple vertices (two B and two charm decay vertices for the typical B event). At the SFT we are envisaging to develop a multi-vertex trigger, based upon the principle of multiplicity jumps, to provide a further level of selection. Multiplicity jump triggers have been investigated rather extensively[2,3] and are known to be affected by fluctuations, especially when the number of multiplicity measurements available is limited. At the SFT, the separation between vertices is of the order of several centimeters, and the active target configuration allows to perform several measurements of each multiplicity state. In this context, the silicon-based scheme of ref. 3 appears to be particularly appropriate for the SFT configuration, since the analogue multiplicity measurements could be provided by the same elements that are used for tracking. Another advantage of the pulse height scheme of ref. 3 is that it might allow in principle, to recognize and discard fake secondary vertices due to secondary interactions, characterized by a larger energy deposition in the foils at the interaction point, followed by a decrease in measured pulse height when the nuclear break-up products are ranged out. Given the non-trivial aspects of multi-vertex recognition, it is expected that it will be performed with the help of a fast processor (or possibly a neural network), and consequently it will operate as a second level trigger. Alternative schemes of multi-vertex recognition, based upon a system of Associative Memories[4] comparing tracks reconstructed in the upstream vs. downstream sections of the vertex detector is also being considered. In any case, it appears that multi-vertex recognition will provide the extra level of mild rejection which is required of the second level trigger. A final selection step will be executed by a micro-processor farm which will have access to the complete event record.

The overall trigger performance figures, summarized in Table IV, have been shown [5] to be very competitive when compared with other options for studying B physics at hadron machines.

Table IV. Summary of Trigger Performance.						
Trigger Level	Input Rate	Output Rate	B acceptance			
			$J/\psi K_s^0$	$\pi\pi$	D,K	Inclusive B
Level 1	10^7	5×10^4	.65	.53	.47	.24
Level 2	5×10^4	5×10^3	.9	.9	.9	.9
Level 3	5×10^3	10^3	.95	.95	.95	.95
Global	10^7	10^3	.56	.45	.38	.21

6. REFERENCES

1) B. Cox et al., The SFT, a Super Fixed Target Beauty Experiment at the SSC, these proceedings.
2) M. Halling, presentation at the Snowmass Trigger and DAQ Working Group. See also M. Halling et al., NIM A 333, 324 (1993)
3) T. Alexopoulos and A. Erwin, A Multiplicity Jump Trigger Using Silicon Planes, these proceedings.
4) S. Conetti, Associative Memory ASIC's for Trigger Systems, First Annual Conference on Electronics for Future Colliders, LeCroy Corp., Chestnut Ridge, NY, May '91.
5) S. Conetti and S. Geer, Comparison of Trigger and Data Acquisition Parameters for Future B Physics Experiments, these proceedings.

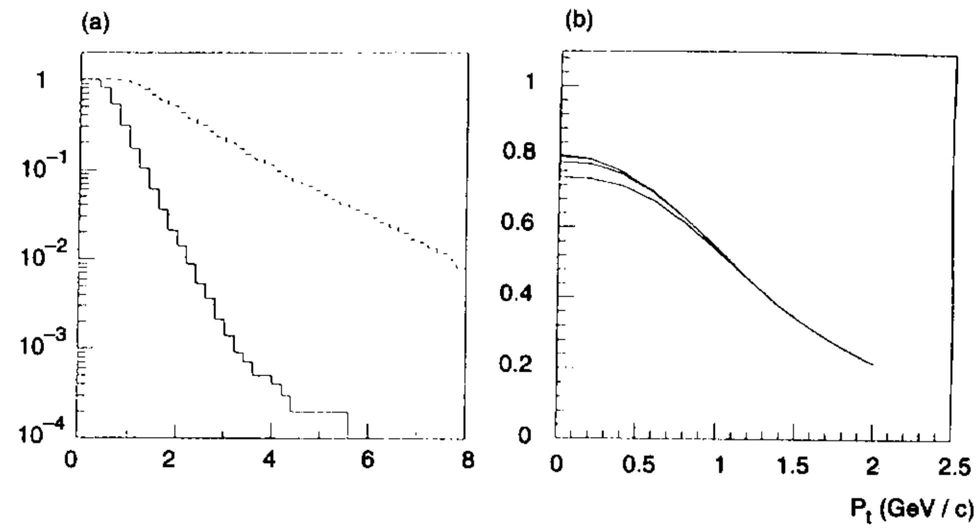

Fig. 1: Integral P_T distributions for minimum bias and B events. 1a: fraction of minimum bias events with at least one π or K with P_T larger than threshold. The solid curve is for $\sqrt{s}$=194 GeV and the dashed curve for $\sqrt{s}$= 40 TeV. 1b: fraction of $B \to \mu$ decays with p_t^μ greater than threshold for $\sqrt{s}$ =194 GeV. The four curves correspond to μ momentum cuts of 5,10,15,20 GeV/c respectively.

COBEX TRIGGER AND DATA ACQUISITION PARAMETERS*

E.P. Hartouni
Department of Physics and Astronomy, University of Massachusetts
Amherst, MA 01003, USA

1. INTRODUCTION

COBEX (COlliding Beauty Experiment) is an open geometry forward spectrometer dedicated to exploring B-physics and designed to run at a hadron collider. Its principle design features allow it to exploit the expected large forward hadro-production rate of B-mesons. COBEX will be capable of providing large data samples of reconstructed, exclusive B-meson decays with good measurements of the decay proper lifetimes, mass and initially produced flavors (*i.e.* tagging). The details of the physics scope, measurement techniques and apparatus plan for COBEX can be found in References [1] through [4].

This talk will limit itself to a description of the triggering and data acquisition parameters required by COBEX to achieve its physics goals.

2. OUTLINE

The talk will proceed by first discussing some of the COBEX characteristics relevant to specific B-meson decay modes important to the measurement of CP-violation and flavor mixing. Next comes a description of the trigger options followed by the implementing trigger architecture. The final section will present the expected rates of events based on Monte Carlo simulation of the particular decay modes.

3. COBEX PHYSICS GOALS

COBEX has been proposed as a B-physics experiment capable of achieving a measurement of CP-violation in B-meson decay. It also has the potential to measure B_s mixing. Both topics benefit from the ability to tag $e^{\pm}$, $\mu^{\pm}$ and $K^{\pm}$, to reconstruct the B-meson decay vertex accurately and to measure the decay children momenta well. The open geometry spectrometer must also have good multiparticle detection efficiency. These features would provide COBEX the possibility of studying other aspects of B-physics. Examples of possible observations and measurements include among others: B-meson decay modes, lifetimes, masses and production mechanisms. Such a general purpose detector would also be capable of searching for additional *b*-hadrons, *e.g.* B_c, Λ_b etc. Finally, COBEX may be able to exploit the relatively large $c\bar{c}$ cross sections and obtain very large samples of charm particle decays.

The most ambitious goals of COBEX concern the measurement of CP-violation, and thus most of the following estimates[3] are based on decay modes for which unambiguous observations can be made. COBEX has been studied for a number of collider situations. The TEVATRON option is considered here.

* Supported by US National Science Foundation Grant PHY90-14879

4. TRIGGER OPTIONS

The fundamental trigger philosophy of COBEX is to select with the broadest possible criteria those events which have the highest probability of containing a b-hadron decay. These events are selected in four steps: 1) the data acquisition system is **gated** on the beam crossing, 2) a **level 0** trigger determines if a $p\bar{p}$ interaction occurred at the time of the crossing, 3) the silicon detector data is reconstructed online and in real time to provide a **level 1** trigger indicating that the event is inconsistent with having a single vertex (referred to as the "topology" trigger) *or* it is determined that an event with at least one μ having a transverse momentum of greater than 1.2 GeV/c is contained in the event (referred to as the "muon" trigger), and 4) the event is fully reconstructed by a processor farm and if selected (this is a **level 2** trigger) is recorded on tape.

5. TRIGGER AND DATA ACQUISITION ARCHITECTURE

The COBEX trigger and data acquisition system consists of three decision levels. An initiating event *gate* occurs for every beam crossing at the interaction region. The **level 0** decision, an "interaction pre-trigger", determines the existence of a $p\bar{p}$ interaction. This determination requires information from a set of scintillation counters and fast pulse logic. The data acquisition system resets if the level 0 trigger determines that no interaction occurred. Absence of the level 0 reset results in the digitization and readout of the data into FIFO buffers. These buffers are controlled so that the **level 1** triggers can either pass the event on for further processing or reject the event. The FIFOs are deep enough to buffer the data flow in the digital pipeline against fluctuations in event size and computation time. This reduces the readout dead time due to such fluctuations.

Two data streams, the Silicon Strip Detector and Muon Detector, provide information to a Data Driven Processor (DDP) which reconstructs the event and provides trigger information for level 1. The Silicon Strip Detector allows a DDP to reconstruct track trajectories and determine a primary interaction vertex for each x- and y- view. A χ^2 is formed from the distance of closest approach of the tracks. This proceedure is iterated and the two tracks with the largest χ^2 are excluded from the calculation. The final χ^2 forms the basis of the "topology" trigger. An event with small χ^2 has a high probability of being consistent with containing a single vertex (the interaction vertex).

The Muon Detector data are used to reconstruct the μ momenta. The momentum magnitude provides the information for the "muon μ" trigger. Both the "topology" trigger and the "muon" trigger can be combined in the DDP to decide on the disposition of the event.

Assuming that the level 1 trigger "passes" the event, all of the data flows into a micro-processor farm. At this stage the events are fully reconstructed, and hence, all information required to form a standard "DST" strip are available. This event filter happens as a **level 2** trigger. Events passing at this level are written to tape. The exact triggers applied at level 2 will depend on actual experimental conditions. The level 2 processor "farm" will be made large enough to accommodate the event flow from level 1, to tape.

6. TRIGGER AND DATA ACQUISITION RATES

The following rates are calculated for the assumptions presented in Tables 1 and 2, which represent the running conditions at the Fermilab TEVATRON. The events used in this study were generated using PYTHIA. Details can be found in the P845 Proposal[2]. Table 1 has the calculations relevant to the "CP-reach" of COBEX for both the "topology" and "muon" triggers for two B-meson decays. The bottom line entry quantifies the error in the determination of the CP-violating parameter sin $(2\phi_i)$, related to the difference of the decay proper life time distributions for events with B^0 and $\bar{B}^0$ tagged. It should be noted that the numbers for $B \to \pi^+\pi^-$ numbers do not include the effect of background under the $\pi^+\pi^-$ invariant mass distribution. The effect of these backgrounds are currently under study.

The Table 2 calculations do not include the increased trigger rates due to the inclusion of a "muon" trigger. However, the bandwidth into the level 2 farm can be increased by increasing the number of nodes in the farm or by increasing the speed of each node. The relatively small event sizes result from zero-suppression and "sparsification" algorithms placed early in the readout pathways. Triggering and data acquisition strategies for B-physics experiments have been recently reviewed[4].

7. ACKNOWLEDGMENTS

Peter Schlein, Mike Medinnis, Samin Erhan and John Zweizig of COBEX have graciously provided the answers to questions I had during the preparations for this talk. Many of the numbers have been reworked by me for the TEVATRON setup. Thus errors, if and where they occur, are my fault entirely. I would also like to thank Mike Kreisler for reading and commenting on this talk.

8. REFERENCES

1. A.Brandt et al., *P238 Proposal to CERN*, CERN-SPSC/88-33 (1989); CERN-SPSC/89-43; CERN-SPSC/89-55.
2. J.Ellett et al., *P845 Proposal to Fermilab* (1991).
3. S.Erhan et al., Nucl. Instr. and Meth. **A333** (1993) 101.
4. J.Zweizig et al., Nucl. Instr. and Meth. **A333** (1993) 223.

Table 1. Comparison of yield estimates and error on sin $(2\phi_i)$ for a 200 pb^{-1} run of COBEX at the TEVATRON[3].

Decay Mode	$B \to \pi^+\pi^-$		$B \to J/\psi K_s^0$	
Trigger	Topology	Muon	Topology	Muon
Peak luminosity (10^{32} cm^{-2} s^{-1})	1.0	1.0	1.0	1.0
$\sigma_{b\bar{b}}(\mu barns)$	75	75	75	75
Full branching ratio	1×10^{-5}	1×10^{-5}	2.8×10^{-5}	1.4×10^{-5}
Geometric acceptance (600 mrad)	0.15	0.15	0.20	0.32
Trigger efficiency	0.20	0.013	0.20	0.12
Reconstruction efficiency	0.37	0.14	0.33	0.12
Tagging efficiency	0.36	0.76	0.36	0.37
$0.56D^2$	0.09	0.19	0.09	0.09
Events in $2\times10^7 s$	480	25	1200	360
$\delta[\sin(2\phi_i)]$ *for* $200pb^{-1}$	0.15	0.45	0.096	0.18

Table 2. COBEX data rates at the TEVATRON[2].

Luminosity	10^{32} cm^{-2} s^{-1}	
Total inelastic σ	$60\text{x}10^{-27}$ cm^2	
Int. Rate	6 MHz	
$b\bar{b}$/interact	1.25x10-3	
Numbers of detector channels	527600	
Level 0	Scintillator	
Input	2.53 MHz	maximum beam crossing rate
Level 1	Topology	
Latency time	3.8 µs	
Input rate	.6MHz	Maximum readout rate
Output rate	6.7 KHz	
Level 2	µP Farm	for full event reconst.
Latency	1000 µs	each processor
Output rate	36Hz	$c\bar{c}$ and $b\bar{b}$ only
MIPS	$34\text{x}10^3$	=670x50 MIPS
event size	60 K Bytes	
recorded data set	3 G Bytes	

Part 2 of the Summary for the Electronics, DAQ, and Computing Working Group: Technological Developments

A.J. Slaughter
Physics Department, Yale University,
New Haven, CT 06511, USA

1. Introduction

The attraction of hadron machines as B factories is the copious production of B particles. However, the interesting physics lies in specific rare final states. The challenge is selecting and recording the interesting ones. Part 1 of the summary for this working group, "Comparison of Trigger and Data Acquisition Parameters for Future B Physics Experiments" summarizes and compares the different proposals. In parallel with this activity, the working group also looked at a number of the technological developments being proposed to meet the trigger and DAQ requirements.

The presenations covered a wide variety of topics, which are grouped into three categories: 1) front-end electronics, 2) Level 0 fast triggers, and 3) trigger and vertex processors. The group did not discuss on-line farms or offline data storage and computing due to lack of time.

2. Front-end Electronics

Pixels would be ideal for use in high resolution vertex detectors, but the problem has been the readout. Steve Shapiro reported on recent work to develop a data push architecture for an array of pixels. The new design features allow the detection of the particle itself to initiate the readout cycle, sending the address of the hit in terms of the rows and columns within the array, the time of arrival, and the pulse height onto a data line for use in the trigger and in the data acquisition system. The details of his presentation can be found in reference 1.

Paul Shepard organized a mini-workshop on deadtimeless read-out for silicon vertex detectors. The goal of the workshop was very specific: how to modify the design of the SVXII for deadtimeless operation by allowing simultaneous read and write to the pipeline. The conclusions are summarized in a contributed paper to this session.

3. Level 0 Fast Triggers

Compared to a colliding beam experiment at the same accelerator, fixed target experiments suffer a large penalty in cross section. One advantage of the fixed target option may be very fast level 0 triggers. There were four presentations on ideas for such triggers.

3.1 *Optical impact parameter trigger*

The original idea for this trigger came from Charpak, Giomataris, and Lederman[2]. A hemispherical shell with the appropriate index of refraction is centered on a point target. Cerenkov light produced in the shell by tracks originating at the target escapes. Light from tracks with a finite impact parameter is internally reflected and eventually exits the edges of the shell where it is detected in a phototube. The contribution by Y. Giomatsris and S. Loucatos explains the idea, gives the results of an experimental test, and discusses some of the limitations and possible improvements. This trigger is being studied in conjunction with the Gas-Jet proposal at LHC and P865, a fixed target proposal at FNAL.

3.2 *Optical sum(Pt) trigger*

B decay particles have, on average, higher transverse momenta than tracks in minimum bias events. A conceptual design for a variation on the previous trigger to exploit this difference was presented by Y. Giomataris. The target is placed upstream of a toroidal magnet and the spherical shell is downstream. The geometry is such that the apparent impact parameter due to the bending in the toroidal field is inversely proportiaonal to the transverse momentum of the particle. Therefore the cut on the internally reflected light in the shell becomes a cut on the sum of the transverse momenta of the event. Obviously, the central conductor of a toroidal magnet presents problems, but a design using a dipole magnet may be possible.

3.2 *Multiplicity jump triggers*

There were two talks on multiplicity jump triggers. These triggers detect the difference in the number of tracks before and after a B decay. Previous attempts to do this in charm experiments have had limited success, due to nuclear fragments, Landau fluctuations and problems with online calibration, electronic noise, and stability of the gains of a large number of microstrip amplifiers. M. Halling reported[3] on an experimental test of a design that detected and compared the Cerenkov light from two separated quartz plates downstream of a target. They found a resolution of 2.7 MIPS over a range of multiplicities from 5 to 20 tracks and measured an average multiplicity jump of 2 for a sample of K_s° decays.

As described in a contribution to these proceedings, A. Erwin has looked at ways to use the large number of silicon planes in a B experiment to make a multiplicity jump trigger.

4. Track and Vertex Processors

All the B experiments discussed at this workshop expect to use some kind of trigger in which tracks are found and the presence (or absence) of a secondary vertex deduced. There were talks on a proposed CDF trigger upgrade for Run II, the data driven processor for CODEX, and an conceptual detector/trigger design by W. Selove. The later two are described in contributions to these proceedings.

The proposed trigger upgrades to CDF are in the context a change of the DAQ architecture that was described in a talk by P. Sphicas[4].

P. Wilson discussed the XFT(Extremely Fast Tracker). The information from the central drift chamber tracker (CTC) would be used to find tracks at Level 1. The algorithm is based on the unique CTC geometry. The requirements and performance goals as given in his talk are:

1. Pipelined to find tracks within 2 microseconds for level 1 decision
2. Decision every 132 ns
3. $\delta p_t/p_t \leq 1.8\% p_t$
4. $\delta\phi/\phi \cong 9$ mrad
5. $\epsilon_{track} \cong 98\%$

The tracks can then be used for low pt inclusive lepton triggers and a possible hadronic B trigger in which the mass is reconstructed.

Giovanni Punzi described the SVT or Silicon Vertex Tracker. The processor uses seed tracks from the XFT and hits from the silicon vertex detector to do precision tracking at the trigger level. The goal is an impact parameter resolution on the order of 30 microns and decision time of less than 10 microseconds so that the trigger can be used at level 2. The algorithm does pattern recognition via an associative memory. The pattern of hits in the silicon acts as an address into memory which contains a set of possible roads. Once pattern recognition is done the hits are passed to a DSP processor farm for fitting. A final processor tags secondary tracks by evaluating the impact paramter in the transverse plane with respect to the beam.

After listening to the presentations on the various experimental proposals and plans for trigger processors, a subgroup tried to draw some general conclusions on DAQ and trigger architecture. The discussion is summarized in a contribution to these proceedings by M. Johnson.

6. Conclusions

It was very clear from this workshop that the trigger is a central element of the experimental design for a dedicated B detector. It drives the DAQ architecture and strongly influence detector configuration. The encouraging note was that solutions are emerging as fast, essentially deadtimeless digization of the data at the front-ends becomes a reality.

7. REFERENCES

1. S. Shapiro et al., *Progress on the Design of a Data Push Architecture for an Array of Optimized Time Tagging Pixels*, SLAC-PUB-6249.
2. M. Halling and S. Kwan, *Nucl Instr. and Meth.* **A333** (1993) 324.
3. G. Charpak et al., *Nucl Instr. and Meth.* **A306** (1991) 439.
4. P. Sphicas, *Proceedings of the 1992 IEEE Nuclear Science Symposium and Medical Imaging Conference* October 1992, Orlando, Florida.

REPORT OF THE SUBGROUP ON DEADTIMELESS FRONT-END ELECTRONICS

P. F. SHEPARD
Department of Physics and Astronomy
University of Pittsburgh, Pittsburgh, PA 15260

The subgroup on deadtimeless front-end electronics and data acquisition systems met for two days on June 28-29. Presentations were made by the following individuals.

R. Yarema	Deadtimeless Silicon Readout Electronics
E. Nygard	RD20 Front-end Electronics Development
S. Kleinfelder	SVX-II and Beyond
M. Johnson	Silicon Readout Systems
E. Nygard	Possible DAQ solutions for Tracking Detectors at the LHC
S. Mani	Pixel Detectors with Data Driven Readout

This report summarizes some of the material presented at these discussions. It concentrates on the need for and technical obstacles to the development of high rate deadtimeless front-end electronics for silicon vertex trackers.

The large yield of $b\bar{b}$ events at hadron colliders indicate the desirability of level 1 trigger rates of order 50-100 kHz. In order to eliminate undesirable deadtime the required front-end electronics needs to be fully pipelined and capable of supporting subsequent trigger levels without incurring any deadtime. In these discussions it has been assumed that the level 1 latency time is of order 2-4 μs. For example, the planned level 1 latency for CDF in the main injector era is 32 beam crossings at 132 ns between crossings or 4.2 μs.

Shown in Fig. 1 is a simplified schematic of one channel of the preamplifier and analog pipeline section of the present SVX II readout chip design for CDF and D0. The length of the pipeline is 32 cells. The preamplifier attains approximately deadtimeless operation by only resetting during the relatively long gaps between groups of beam in the collider.

However, the pipeline is not deadtimeless because it has only a single port and is not capable of simultaneous read and write operations. During the digitization, sparsification and readout of the data into level 2, the clocking of the storage capacitors is stopped, the switch to the preamplifier section is opened and the switch to the digitization/readout section is closed. In the digitization configuration the pipeline is incapable of accepting data from subsequent beam crossings until the digitization process is finished, a process which takes 7-9 μs per event. For a level 1 accept rate of

50 kHz this results in a deadtime of 35-45 %. The reason for accepting this limitation in the first place is that it avoids the complication of having simultaneous analog and digital operations with the possible adverse effect on the analog operation due to substrate and bond wire couplings.

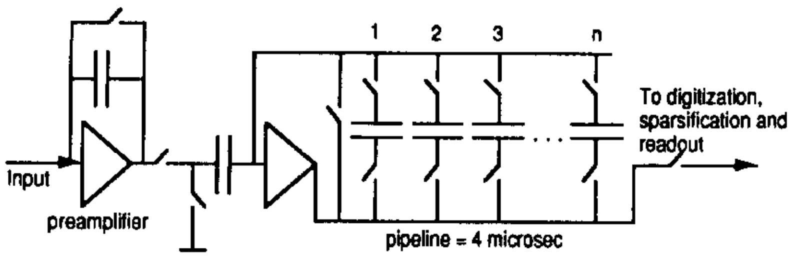

Figure 1. One channel of the SVX II preamplifier and analog pipeline section.

It is possible to overcome this deadtime limitation by constructing a dual port analog pipeline, i.e. one which is capable of simultaneous read and write operations. Research on dual port pipelines for silicon strip detector applications is being pursued aggressively by both the RD2 and RD20 projects at CERN. E. Nygard reported on RD20 developments. Shown in Fig. 2 is a simplified schematic of the dual port pipeline being developed by RD20. The RD2 design is similar.[1]

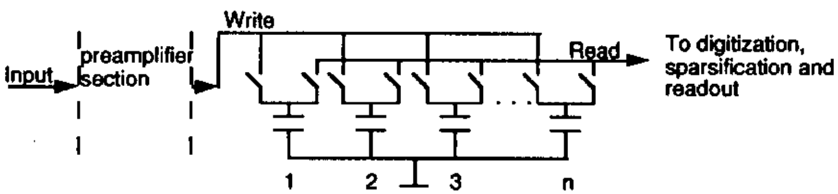

Figure 2. Schematic of one cell of the RD20 analog pipeline under development at CERN.

The RD20 design has simultaneous read and write capability, associative skip logic and level 1 buffering. A pipeline with 160 storage cells and 128 channels per chip is planned. A 32 channel version has been implemented in a rad soft design. Work to implement the design in a rad hard Harris process is in progress. With simultaneous read and write capability it is possible to continue to write into the pipeline each beam crossing while a different cell or cells are being read for digitization in response to a level 1 trigger. Extra cells are provided to buffer the statistical fluctuations in the level 1 trigger and skip logic is needed so that cells waiting for processing after a level 1 accept are not overwritten.

It is possible to extend the SVX II analog pipeline design to a dual port version. This is shown in Fig. 3. This can be accomplished by the addition of a second set of switches to each storage capacitor and a second read amplifier in addition to the write amplifier already present. Not shown is the additional pointer and skip logic required.

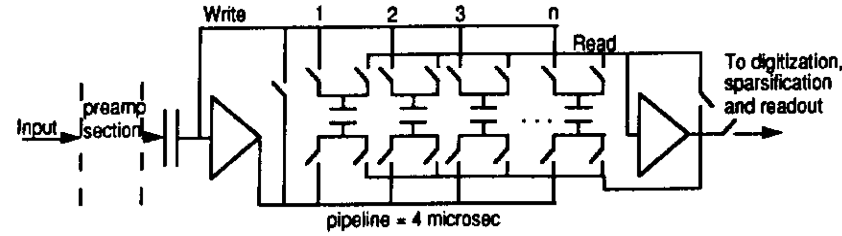

Figure 3. Possible modification of the SVX II pipeline to a dual port pipeline.

The necessary addressing logic for a dual port pipeline has been developed at LBL for the analog pipelining of calorimeter signals for the SSC and could be adapted for use here, possibly in a more simplified form.[2] The additional pipeline cells for buffering, the new read amplifier, additional busses and skip logic can be expected to increase the physical length of the pipeline across the chip by a factor of about 1.5.[3] This could force the readout chip to be divided into two chips, one containing the preamplifier and analog pipeline and the other the digitization and readout logic. Finding a rad hard two poly process would be of considerable benefit in reducing the size of the pipeline. It has already been learned from the SVX II single port design that cross talk can be a serious problem and considerable care is required in layout to avoid it. Crosstalk can be removed and area for capacitors maximized using a mirrored layout technique.[4]

A more critical issue is not the pipeline design, but possible noise coupling in a chip which has simultaneous data acquisition and readout. In this situation the sensitive front-end amplifier is active while digitization and readout is occurring with a high speed clock. This can introduce noise through bond wire and substrate coupling. Bond wire coupling issues was studied using the SVXC chip and a solution to this source of noise coupling exists using differential lines, reduced logic level swings and/or layout techniques.[5] Substrate coupling is probably the most difficult problem to solve. Operation of various digital elements, particularly large drivers, affects the substrate and thus analog circuits on the same chip. Possible solutions to this problem include isolation techniques, silicon on insulator (SOI) fabrication processes and finally the use of separate chips for the analog and digital circuits. Work to study the effect of isolation techniques on the substrate coupling problem are in progress.[6]

REFERENCES

1. *Nucl. Instr. and Methods in Phys. Res.*, A326 (1993) 100-111.
2. S. Kleinfelder, Comments at the meeting.
3. R. Yarema, Comments at the meeting.
4. *Ibid.*
5. *Ibid.*
6. *Ibid.*

AN IMPACT-PARAMETER OPTICAL DISCRIMINATOR FOR B DECAYS

Y. GIOMATARIS
Lausanne University, Switzerland

and

S. LOUCATOS
SPP-DAPNIA, CE-Saclay
91191 Gif-sur-Yvette Cedex, France

1. INTRODUCTION

At future hadron machines (LHC, SSC) the b-production cross-section in fixed-target experiments is sufficiently large to allow observation of CP-violation in the $B\overline{B}$ system. Provided that the size of the target is small, the precise knowledge of the primary vertex, is a strong advantage over collider experiments. At the LHC, a luminosity of 2×10^{33} cm^{-2} s^{-1} in a small interaction region can be achieved using a thin jet target [1]. The ratio of $\sigma_{b\bar{b}}$ to σ_{tot} is 10^{-5}, the bunch crossing rate is expected to be 40 MHz and the interaction rate 70 MHz. The time between two interactions (25 ns) requires pipe-line architecture of a silicon microvertex trigger. A fast first-level selection of the events can reduce the input rate into a Si trigger and hence the depth of the pipe-line. The optical discriminator, described hereafter, is a possible solution. The idea is to use the Čerenkov light emitted by charged particles crossing a spherical crystal shell and retain those having a sizeable impact parameter with respect to the centre of the sphere where the target is located [2].

2. THE PRINCIPLE OF THE OPTICAL DISCRIMINATOR

The principle of the Optical Discriminator (OD) is illustrated in Fig. 1. The radiator is a thin crystal with a refractive index n_1, shaped as a shell limited by two concentric spheres and surrounded by a medium of refractive index n_2. To avoid the detection of relativistic particles coming from the target, i.e. with $b = 0$, it is shown in [3] that the refraction indices have to satisfy the condition: $n_1^2 - n_2^2 = 1 - \epsilon$ with ϵ small and positive. When a single crystal is used in air or vacuum, $n_2 = 1$, and n_1 has to be close to, but lower than, $\sqrt{2}$. The choice of ϵ will determine the minimum impact parameter $b_{\min}$ which will be the threshold of the device. In order to obtain a good sensitivity to very small impact parameters, but avoid background from minimum bias tracks coming from the optical centre, the minimum impact parameter b_{min}must be small but greater than some lower limit.

Chromatic dispersion has also to be taken into account: n, ϵ and $b_{\min}$ are λ-dependent. This chromaticity has to be minimized. Unfortunately, such a quasi-achromatic behaviour cannot be obtained with a single medium ($n_1 \simeq \sqrt{2}$ and $n_2 = 1$): $b_{\min}$ varies with the wavelength (chromatic aberration). However, if the crystal is constructed with a core of a high index material (n_1) and a cladding of an appropriate lower index material (n_2), the

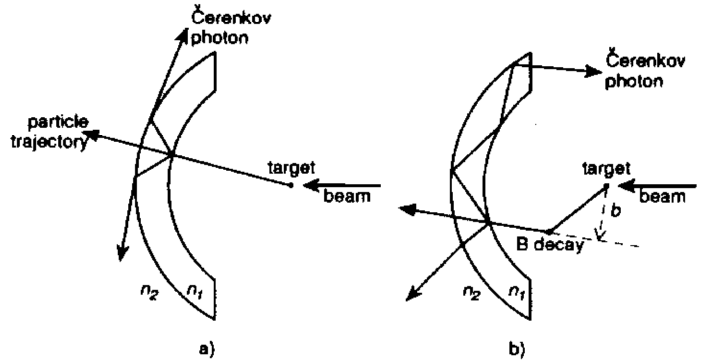

Figure 1: The principle of the optical discriminator: a particle with zero impact parameter (a) produces Čerenkov light refracted through the surface of the crystal, whereas for a particle with a non-zero impact parameter, (b) part of the Čerenkov light is internally reflected and trapped.

wavelength dispersion of the core material may be balanced by the dispersion of the cladding material giving an achromatic pair.

The principle of the detector was tested at FNAL [4] and at CERN [3].

3. EXPERIMENTAL TEST RESULTS

We summarize here the results obtained at the CERN PS test beam with 8 GeV/c momentum pions. The simplest case, that of a single medium, was chosen: a LiF crystal, whose refractive index is close to, but does not exceed, $\sqrt{2}$ for wavelengths above 270 nm. The emitted light was guided by an ellipsoidal mirror to a photomultiplier.

The distribution of the signal amplitude is shown in Fig. 2. The background due to the scintillation of the air inside the vessel during the passage of the particles has been measured and is subtracted. The agreement with a detailed simulation is good and the behaviour of the device well understood. The fall at large impact parameters is due to the cut-off imposed by a 40 mm diaphragm in front of the photomultiplier. Rejection of large impact parameters can thus be achieved by adjusting the diameter of the diaphragm in front of the PM. This is a useful property of the OD, as closing the window will reduce the background due to delta rays and nuclear interactions. If optical fibres are used, instead of a mirror for light readout, the same pleasant feature is encountered, owing to the optical fibre aperture.

At zero impact parameter the observed signal is not zero. This is due to two kinds of sources: i) Processes that take place in the crystal and may still be present in future B experiments and which are the inherent background (delta rays and nuclear interactions in the crystal and propagation of unwanted photons) and ii) Effects associated only with our test-beam measurement and the set-up excluding the crystal. The observed value of (0.04 ± 0.02) p.e. has to be considered as a first estimate of the crystal-induced inherent background.

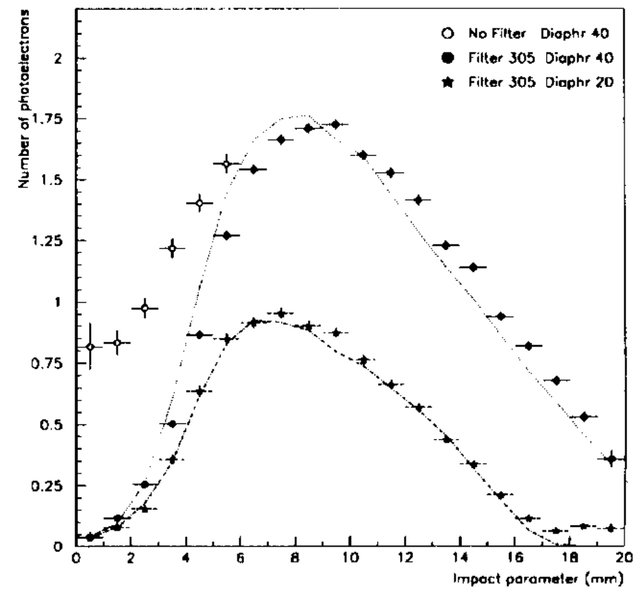

Figure 2: Amplitude of the signal as a function of the impact parameter with and without filter and with two different diaphragms. Data (points) and Monte Carlo (lines).

Studies are being pursued for a more precise determination. The contamination caused by the inherent background to B-meson search, will depend on the threshold imposed on the signal. Simulation studies are under way and show that contamination can be suppressed by coincidence techniques.

4. PERSPECTIVES

The experimental results obtained are in agreement with expectations and demonstrate the ability of the OD to reject small impact parameters. However, the presently obtained threshold is too high and its rise too smooth for a direct application as a B-event selector.

A program of technical development of the device has started, to obtain a high efficiency in B-meson pairs and a strong rejection factor against unwanted minimum bias events [5]. Solutions under study are: achromatic pairs, replacing the air or vacuum surrounding the crystal by a liquid or a gas under pressure, using the reflection threshold condition on the inner surface of the crystal instead of on the outer one, etc. A further improvement of the signal at small impact parameters can be obtained by splitting the total thickness of the device into seven such 2-layer elements (fig. 3).

Figure 4 shows efficiencies for $B_d \to \pi^+\pi^-$ and minimum bias events expected for a 6-

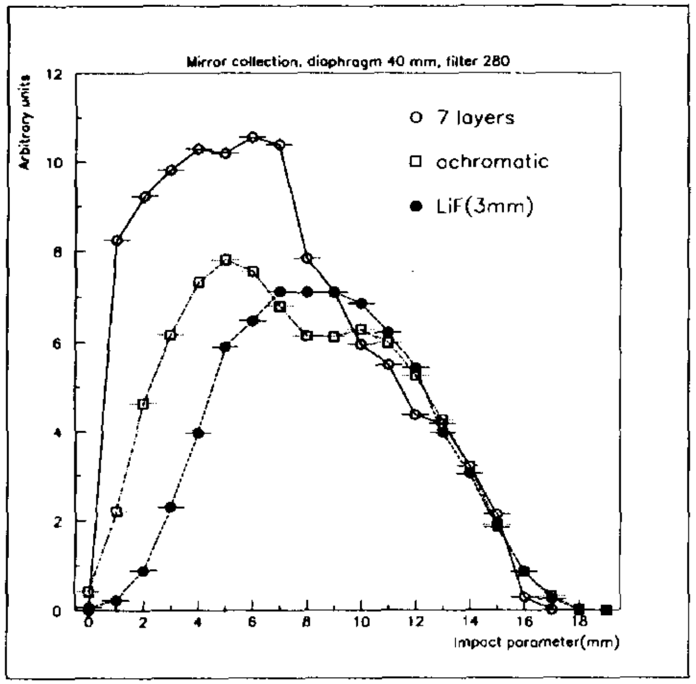

Figure 3: Comparison of expected signals for different crystal configurations, as a function of the impact parameter. For a 3 mm LiF crystal, an achromatic crystal and a 7 layer one.

layer sapphire-liquid assembly. A reduction factor of 10 should be achieved with a threshold at 8 p.e. The efficiency for $B_d \to \pi^+\pi^-$ events is around 60%. A similar efficiency is expected for $B_d \to J/\psi K_s$ decays.

Another way to improve the efficiency is to increase the quantum yield of the photodetector. A new development concerning visible-light photon counters (VLPCs) seems to be promising, as quantum efficiency is optimum (80%) in the range from 400 to 800 nm [6]. Rejection may be improved by using the information of the direction of the emitted light, with a segmented, VLPC detector. A test of an OD with VLPC read-out is in preparation.

The optical discriminator device is part of the proposed detectors for the Gajet experiment at the LHC [1] and P865 at the Tevatron [7].

5. REFERENCES

1. T. Nakada, 'A Study of CP Violation in B-meson Decays Using a Gas Jet at LHC', Expression of Interest at the General Meeting on LHC Physics and Detectors, Evian-les-Bains, 1992.

   Y. Lemoigne, 'A CP Violation Gas Jet Experiment at the CERN LHC', UNK B-factory workshop, Liblice castle, Tcheque Republic, 18-22 January 1993.

   L. Camilleri, these proceedings.

   S. Loucatos, these proceedings.
2. G. Charpak, Y. Giomataris and L. Lederman, Nucl. Instrum. Methods **A306** (1991) 439.
3. G. Charpak et al., Nucl. Instrum. Methods **A332** (1993) 91.
4. D.M. Kaplan et al., Nucl. Instrum. Methods **A330** (1993) 33.
5. G. Charpak et al., CERN/DRDC/P30, 1991 and Addendum, CERN/DRDC/92-53, 1992 (RD30).
6. M. Atac et al., Nucl. Instrum. Methods **A314** (1992) 56.
7. L. D. Isenhower et al., FNAL proposal P865 April 1993.

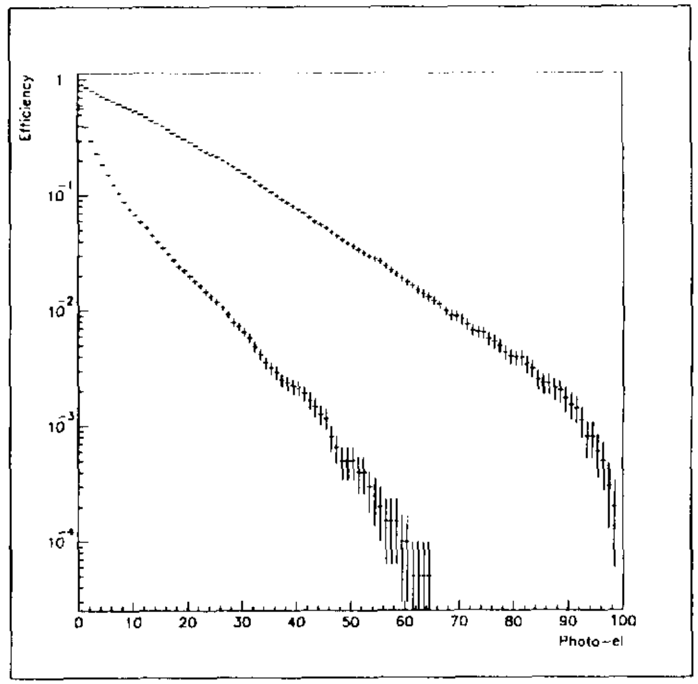

Figure 4: Efficiencies versus number of photoelectrons for $B_d \to \pi^+\pi^-$ (upper curve) and minimum bias (lower curve) events.

THE P_t SELECTION OF B EVENTS WITH THE OPTICAL DISCRIMINATOR

Y. GIOMATARIS
Lausanne University, Switzerland

J. DERRÉ
SPP-DAPNIA, CE-Saclay, France

1. INTRODUCTION

We propose a very fast (few ns) trigger using an optical discriminator for B-meson selection in proton-proton collision experiments. With only few read-out channels, the device can perform a fast trigger on the global P_t of the event and it is insensitive to low P_t particles ($P_t \leq 1$GeV). We discuss possible applications of this device for collider or fixed-target experiments at LHC, at the highest luminosity operation. Simulations show very promising results : in the fixed-target (collider) mode we expect a rejection factor of 100 (10) on minimum bias events, with 45% of efficiency on the B's, independent of their decay mode. We also discuss applications of this device in present detector designs.

To select B events in a fixed target experiment, an impact parameter optical discriminator has been proposed [1]. By trapping the Čerenkov light in a thin crystal, events with tracks having a significant impact parameter can be selected in a few ns. Extensive tests in a particle beam have demonstrated the feasibility of this trigger device [2,3]. A limitation of the Optical Trigger is the need for a very small interaction region (100 μm) which limits its application to the fixed-target mode or to colliders having a small interaction diamond, like the asymmetric tilted collider [4,5]. In addition, in order to obtain a good rejection factor for minimum bias event and good efficiency for $b\bar{b}$ events, the device must be sensitive to very small impact parameters; the result is a low number of photoelectrons for B-meson events. A research and development program has started in order to improve the output signal [6]. Based on the same principle, but taking another approach, we propose to trigger on events with charged tracks having a small impact parameter behind a magnet. As all the light of the Čerenkov cone is collected, the number of the photoelectrons is now confortable and good efficiency for B-meson pairs can be obtained.

2. P_t CUT PRINCIPLE

The transverse momentum, P_t, of charged tracks from B events is higher than those from the minimum bias ones. So an efficient selection of B events consists in selecting the charged tracks with a P_t higher than 1-2 GeV/c. This is quite a low value and it is often hard to obtain with a threshold applied on the signal of a calorimeter. In most of the collider experiments the lowest typical applied P_t threshold is higher than 5-8 GeV/c. It results in an unacceptable large inefficiency and the goal is to lower those thresholds.

Our idea is to tranform the P_t threshold into an impact parameter threshold. A magnet, placed on the path of the tracks gives to each of them a kick $d\theta$, θ being the diffusion angle :

$$d\theta = 0.3 \int Bdl \times \frac{\theta}{P_t} \tag{1}$$

Such a kick is equivalent to an impact parameter, b, with respect to the target.

If the magnet is a toroid with the same axis as the beam, $\int Bdl \times \theta$ is a constant, since the magnetic field is maximum around the beam axis and falls inversely proportional to the distance of the axis. So a P_t cut is translated into an impact parameter cut. Figure 1 shows a schematic view of an experimental set-up with a toroidal magnet forward spectrometer along the beam axis of a fixed-target or a collider experiment. The magnet is axially symmetric as well as all the major elements of the spectrometer.

The spherical crystal, placed behind the magnet, is centered on the target. Its edge is a strip on the surface of a cone having its top at the center of the sphere. In this way the outgoing light from a particle with small impact parameter focusses to the optical center. On the contrary, most of the light emmitted from a particle with a significant impact parameter is either trapped in the crystal or goes out without pointing to the center.

Thus, the collection of the light which focusses to the center of the sphere is a selection of tracks with small kick, i.e. high P_t.

3. SIMULATION

B's and Minimum Bias events have been generated by Pythia in two cases: in a fixed target (FT) experiment, and in collider mode at LHC (8 TeV per proton beam). In the FT case, the crystal has an acceptance of 300mrd, while in the collider it has 600mrd with a hole of 10mrd along the beam. The Čerenkov light created by the charged particles through the crystal has been simulated and followed up to the exit face by Monte Carlo. The light collection is done by quartz fibers placed along the exit cone pointing to the center of the crystal. The numerical acceptance of the fibers gives a natural cut on the outgoing light angle. The collected light is converted in electrons by a very fast photodetector e.g. a photomultiplier.

The kick of tracks has been simulated in a toroidal magnet giving 3.3 Tm near to its axis, along the beam. This means that $d\theta$ is equal to $10mrd$ divided by P_t(GeV/c) times the sign of the particle charge. As the crystal is behind the magnet, it is quite far from the primary vertex (a few meters). So the size of the interaction region has a negligible effect on the impact parameters generated by the magnet.

As shown in Figure 2, it is clear that the impact parameter b is strongly correlated with the angle of the light into the fiber.

The fibers, with an numerical acceptance of about 100 mrd, accept all the light from particles with small b, but only a small part from high b. The results on the efficiency versus the threshold (in photoelectrons) are given in Figure 3., respectively for B's and Minimum Bias events.

¿From the previous figures, we can deduce the variation of the reduction factor of the minimum bias events with respect to the efficiency of the B's, which is shown in Figure 4.

In a fixed target experiment at LHC, a rejection of 100 can be obtained with 45% efficiency on B's. In collider mode, we get only a rejection of 10 with the same efficiency on B's (with one spectrometer arm). But this rejection factor corresponds to the same minimum bias rate, because in the collider mode only 1/10 of the luminosity of the FT mode is needed.

The main difficulty of this scheme is the implementation of toroid coils near the beam.

4. CONCLUSION

The selection of B's by an optical P_t discriminator is very promising and gives higher efficiency in the fixed-target mode. It is a very fast, global trigger, independent of the decay mode. It is a way to improve the efficiency for B-meson pair selection in existing collider experiments suffering of important losses caused by trigger limitations. It can be used for future Beauty investigations in very high luminosity proton collisions. The effect of a deterioration of the obtained rejection due to gamma conversions in the crystal needs further studies. The implementation of a toroidal magnet in such an experiment is also an open question.

5. REFERENCES

1. G. Charpak, L. M. Lederman, and Y. Giomataris, Nucl. Instrum. Methods **A306**, 439 (1991).
2. G. Charpak *et al.*, Nucl. Instrum. Methods **A332** (1993) 91.
3. Y. Giomataris and S. Loucatos, "The Optical Discriminator", these proceedings.
4. Y. Giomataris et al., Proc. 26th Int. Conf. on High Energy Physics, Dallas, 1992, Vol. 2, p. 1738.
5. Y. Giomataris, CERN/PPE/93-142, submitted to the Workshop on heavy quark at fixed target, Frascati, may 31st-June 2nd, 1993
6. G.Charpak et al., "Study of an optical trigger to be used for beauty search in fixed target mode at the LHC" CERN/DRDC/P30 20th August 1991, approved as RD30.

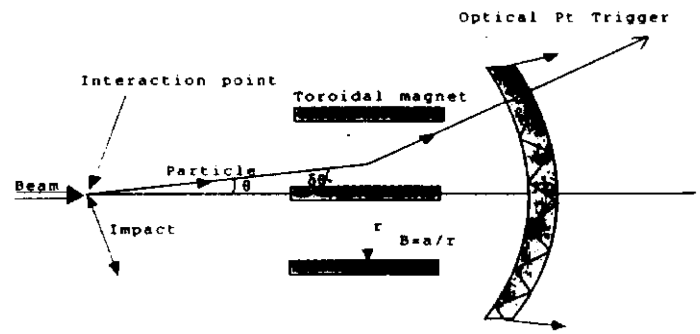

Fig. 1: Scheme of a forward spectrometer with a toroidal magnet.
The crystal is located downstream of the magnet (schematic).

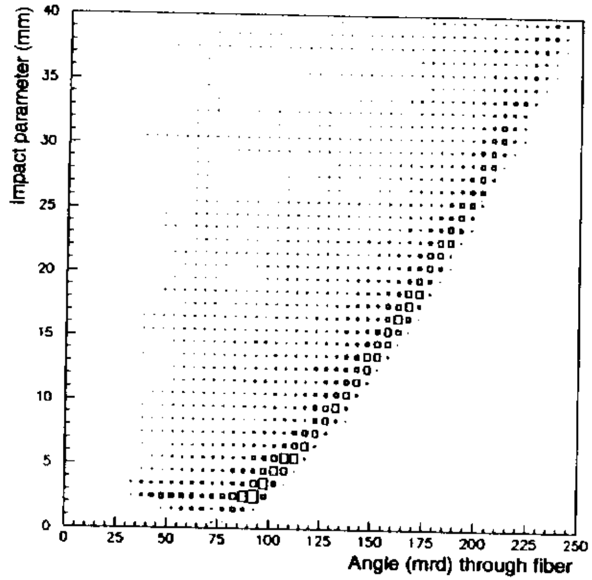

Fig. 2: Correlation of the impact parameter with the angle of the light going into the fibers.

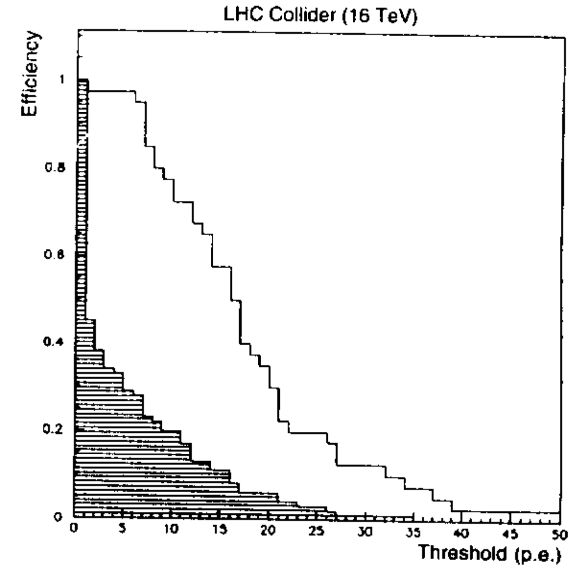

Fig. 3b: Efficiency versus threshold (number of p.e.) for B (white) and Minimum bias (hatched) events, at the LHC and in the collider mode

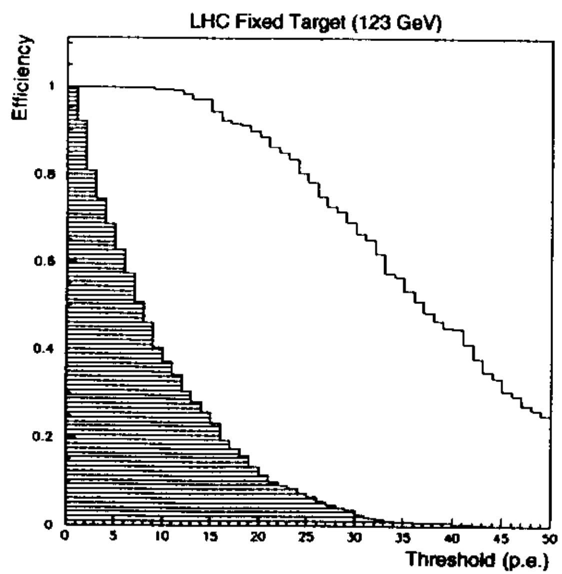

Fig. 3a: Efficiency versus threshold (number of p.e.) for B (white) and Minimum bias (hatched) events, in case of a fixed target experiment

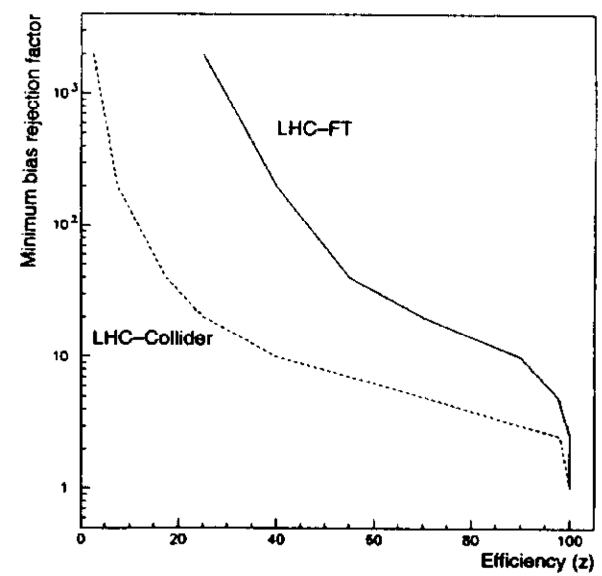

Fig. 4: Minimum bias rejection factor versus efficiency for LHC-FT and LHC-Collider (one-arm spectrometer).

A Multiplicity Jump Trigger Using Silicon Planes

T. Alexopoulos and A. R. Erwin
University of Wisconsin
Madison, WI 537706

Since silicon tracking planes are already present in a B decay experiment, it is an attractive idea to use these as part of a multiplicity jump detector. Two average B decays would produce a multiplicity jump of around 10 in the final state. Such a trigger has been tried for a fixed target Charm experiment with disappointing success.[1] The failure was attributed to the difficulty in adequately controlling the gains of a large number of microstrip amplifiers.

One could limit the number of amplifiers needing adjustment by collecting all the charge from a silicon wafer with a single amplifier on the backside of each microstrip detector as shown schematically in Fig. 1. An efficient system for monitoring and calibrating with single beam tracks should be employed frequently during the run.

Input noise does not appear to be a problem for planes as thin as 300 μm. Using a $2.8 \times 2.8\ cm^2$ Hamamatsu plane into a single Fermilab QPA02 amplifier, we obtain 16 mV signals from minimum ionizing particles in the presence of about 5 mV rms noise. Thinner detectors would imply more capacitance and thus more noise and smaller signals.

The Landau tail on the high energy side of the energy loss distribution suggests some difficulty. Fig. 2 shows energy loss distributions for 5 GeV/c pions in a 300 μm plane and several multiplicity jumps of 6. For about 30 secondary particles there is an obvious inefficiency for distinguishing larger statistical fluctuations from a real jump of 6. This problem can be mitigated by working only with plane-pairs and accepting the smaller multiplicity of the pair. See the diminished tail in inset of Fig. 2. For large numbers of planes (such as 90 in the SFT proposal), one can employ more complex algorithms.

The most difficult problem for the silicon detectors comes from the proton spallation products of the heavy nuclear target. The behavior of the spallation protons is essentially independent of beam energy and particle type and well described by a simple computer model.[2]

If silicon wafers are the only target material, then about 45% of the collisions will not have a significant spallation proton (i.e. one which ranges through more than one 300 μm thick wafer). See Fig. 3. If one arranges for most of the target material to be Be, then about 57% of the collisions will not contain a significant spallation proton. For about half of the events a simple multiplicity jump can be used correctly to pass judgement on B production candidates selected by other components of the trigger (e.g. dimuon identification).

The greatest difficulty arises when the target is constructed entirely of active 300 μm wafers. A stopping, normally incident proton can produce a 30X to 40X minimum pulse in the stopping wafer. (See Fig. 4.) If the amplifier does not saturate, it produces a multiplicity jump of 6 to 14 when compared with the preceding wafer. All earlier multiplicity jumps are 5 or less. The simplest procedure would be to reject all events in which any wafer has more than 30X minimum energy deposited in it. This unfortunately would reject about half of the legitimate B events.

The algorithm that used plane-pairs to reduce the Landau tail would also eliminate observation of the large multiplicity jump at the stopping wafer, since that jump involves only one pair of planes. (See Fig. 4.) If one chooses to use passive Be as target material between Si wafers, then the large multiplicity jump of a stopping proton can be vetoed by the large multiplicity decrease in the following plane.

If the pulse heights from the active wafers are immediately digitized by flash ADC's, the simple digital logic for jump detection can be programmed into Xilinx logic arrays. Decisions can probably be made fast enough to participate in a level one trigger.

REFERENCES

1. P. Weilhammer, Proc. of the workshop on *New Solid State Devices for High Energy Physics*, LBL-22778 and CERN EP/86-54 (1985).
2. K. Braune, et al., *Z. Phys.* **C13** (1982) 191.

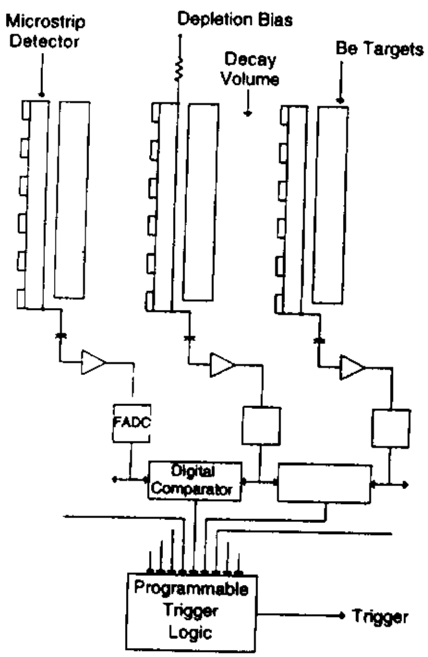

Fig. 1 Portion of a possible multiplicity jump trigger.

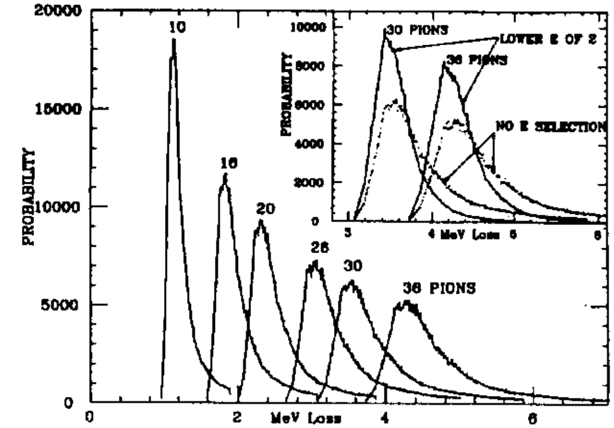

Fig. 2 Some energy loss distributions in 300 μm Si wafers.

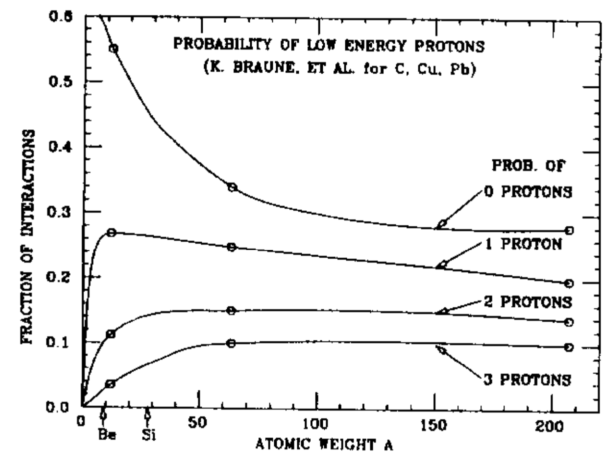

Fig. 3 Fraction of collisions with slow protons vs. atomic weight.

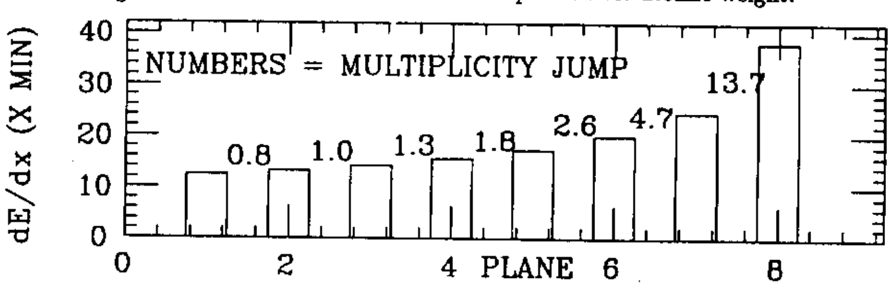

Fig. 4 dE/dx of a stopping proton in 300 μm Si planes expressed as multiples of minimum ionization. Numbers give multiplicity jump between planes.

IMPACT PARAMETER TRIGGER and VERTEX DETECTOR FOR FORWARD COLLIDER

W. SELOVE
Physics Department, University of Pennsylvania
Philadelphia, PA 19104

Abstract

In a forward collider design, Coulomb scattering produces an unavoidable smearing of the vertex region by low-p_t tracks. A detector and triggering design is described which aims at differentiating B events from mimimum bias events with high efficiency, in spite of this smearing, by measuring momentum and p_t of all tracks in real time, and triggering only when an event shows a number of high-p_t tracks with substantial impact parameters. Triggering efficiency an order of magnitude larger than for a lepton trigger can be anticipated. Detector planes are located within 4 millimeters of the beam line; a replaceable-vertex-region design provides for rapid replacement of radiation damaged closest elements at time intervals of a few months.

1. INTRODUCTION

Many of the most important objectives of the study of B hadrons require the level of statistics which can only be obtained at the large hadron colliders. The available production rates are particularly attractive for machines of the SSC and LHC type. The design of detectors for suitable experiments has attracted a very large amount of effort. Some of the earliest detailed designs were developed by N. Lockyer, K. McDonald, and collaborators.[1] These early designs emphasized good coverage of the central region, where most B mesons are produced in a symmetric hadron collider. Schlein and collaborators have developed a different design, focused on the use of those B mesons (and baryons) which are produced into a "forward" cone, typically one covering angles from 5 or 10 mrad to 600 mrad from the beam line.[2,3] Such a design has the advantage of promising to collect of order 1/3 of the B's which could be collected with an extended-central-region detector, while costing only a fraction as much as such a central detector, a most important advantage when the costs involved are in the tens of millions of dollars for the forward design and in the hundreds of millions for the central design.

Two critical components of a dedicated B experiment are the vertex detector and the trigger system. For a forward collider, it is important to minimize the extrapolation distance, from detector planes to vertex region, by locating the forward detector planes close to the beam – within a few millimeters if possible. Early work on this problem was done by the CDF group.[4] Schlein and collaborators have built and operated a silicon strip detector array, with planes very close to the beam, and have thus shown the important result that such close operation appears practical. Their vertex detector system is designed to provide a B trigger in a hadron collider experiment.[5]

In a B experiment for the SSC, one wishes to make use of the maximum possible production rate for B mesons. Recent designs for such an experiment have taken a luminosity of 10^{32} as the desirable rate to design for. At this luminosity, interactions would occur at 10^7 per second, and B meson pairs would be produced at 10^5 per second. It is a challenging problem to design a trigger, and a vertex detector, which at these rates (a) could operate rapidly enough to provide a Level-1 trigger, (b) could give a large rejection factor against "ordinary" events without being fooled by apparent secondary vertices when none are in fact present, and (c) could at the same time have a very high efficiency for true B events. In this report I describe a vertex detector and trigger system which is a forward-collider design, as is Schlein's, but which has a number of new elements and features which promise to provide very substantially improved performance. (See Section 3.) With regard to radiation damage, the report also describes a new approach providing for operation to 5 or 10 Mrad, and presents a proposal for meeting the problem of occasional replacement of damaged regions of the detector planes.

2. OBJECTIVES

At a luminosity of 10^{32} at the SSC, the interaction rate will be 10 MHz and the B-production rate 0.1 MHz. While it may not be practical to think of recording all B events, at this rate, it is desirable to have a Level-1 trigger which has at the same time very high efficiency for B events and very good rejection for minimum bias events.

In a forward collider design, Coulomb scattering in the first detector plane encountered produces an unavoidable smearing of the vertex region, with impact parameters varying inversely with the p_t of forward tracks - actually, inversely with the "y-component" of the p_t . The smearing tends to interfere both with any Level-1 trigger which seeks to detect the presence of secondary decay vertices and with any further determination, e.g. in a later triggering level, of the presence of multiple vertices or of candidates for some particular rare type of decay.

If the p_t of each individual track can be determined in real time, a triggering system can be employed which in a Level-1 trigger ignores the lowest-p_t tracks. This approach would provide, in principle, maximum rejection of minimum-bias events while retaining maximum sensitivity and efficiency for B events, which tend to have a number of high-p_t tracks with substantial impact parameters. Such an approach is similar in principle to determining the chi-square value with which the event satisfies a single-vertex hypothesis, but does not require an actual chi-square calculation.

3. MAJOR DESIGN FEATURES

Figure 1 shows the proposed layout of the silicon vertex detector, and Figure 2 shows the proposed magnetic field arrangement. The design shown in Fig. 1 assumes that the length of the actual interaction region is only a few centimeters, as would be the case at the SSC. There is a series of forward planes, close to the beam line as in Schlein's design. The spacing of most of those planes is uniform in pseudorapidity, as suggested by McDonald.[6] In the central region there is also a set of barrel cylinders, covering about 2 units of pseudorapidity.

The purpose of the barrel system is to make possible a very precise determination of the longitudinal coordinate of the primary vertex, using central-region tracks. This coordinate is needed for the real-time tracking; and it is also needed for distinguishing those cases in which more than one primary interaction occur at once.

The magnet layout shown in Fig. 2 uses three dipoles. One is located at the interaction region. It has two functions. One: it allows quite accurate momentum determination of tracks at larger angles, so that the downstream magnet system does not have to have an extremely large aperture. Two: with only a modest strength, of order 0.1 GeV/c p_t kick in 30 cm, particle momenta and p_t values can be determined at high speed, for almost all tracks produced in an interaction. Real-time p_t determination is the primary tool for making a high-efficiency impact-parameter trigger.

The second and third dipoles are part of a conventional spectrometer system.

The silicon planes in the vertex detector will be pixel planes. This is necessary in order to obtain high speed tracking. Pixel planes with data-driven readout, with fairly high speed readout, have been developed by S. Shapiro and collaborators.[7]

Finally, an outline of a system for real time tracking has been reported to this Workshop by D. Crosetto and me. The basic scheme is described in section 7 below. The system uses a massively parallel very high speed processor with 3-dimensional interconnections, developed by Crosetto. That system, and its application to the real-time tracking problem, is described in a report by Crosetto.[8]

4. RADIATION DAMAGE

In order to distinguish heavy-quark events from others, by an impact parameter trigger, the vertex smearing due to Coulomb scattering must be minimized. It has long been known, and particularly emphasized recently by McDonald, that for the smaller angle part of a forward collider detector the transverse smearing due to Coulomb scattering is inversely proportional to the transverse momentum of a track. In fact this smearing depends not just on p_t but on the "y" component of p_t , i.e. on p_y . (y is the vertical axis, and is the direction in which a gap is left in the detector planes in Schlein's design.) Thus tracks of low p_y will give the worst smearing of impact parameter when extrapolated back to the vertex region.

The smearing is proportional not only to $1/p_y$ but also to the distance R from the beam line at which a track first encounters a silicon detector. To obtain efficient separation of heavy-quark events from minimum bias events it is advantageous to bring the silicon planes close to the beam line - to within a few millimeters if possible.

At such close distances, and at high luminosity, radiation damage is a limiting consideration. Recent detailed studies of radiation damage effects on silicon detectors lead me to the conclusion that individual detector wafers can be satisfactorily operated, with today's materials, at up to 5 Mrad or so. (See Appendix A.) At the SSC, and at a luminosity of 10^{32}, and if the closest part of the detector planes is 4 millimeters from the beam line, the radiation dose in the very closest part of the detector wafers will be about 1.5 Mrad per month. Thus one should plan to replace the closest part of the wafers at intervals of perhaps 3 months. Alternatively, one might operate with full sensitivity at 4 mm for 3 months, and then with loss of sensitivity in the very closest part of the planes for an additional 3 or 4 months; at that time, full sensitivity will still remain beyond a radius of 6 mm.

If the vertex detector planes are composed of quadrant sections, as in Schlein's P238 run at CERN,[5] one can plan to use a design which permits replacing only the most severely damaged part of each plane, at intervals. If, for example, in each quadrant the closest 1 square cm of each plane is built as a separately replaceable unit, then at intervals of 3 to 6 months only a few percent of the total silicon area has to be replaced. A possible arrangement for a replaceable vertex region section of the detector is described in Appendix B.

5. VERTEX SMEARING IN A FIXED-TARGET EXPERIMENT

In an ideal tracking detector, sequences of hits delineate unambiguous and error-free tracks, the tracks can be extrapolated with no errors, and they define perfectly the vertices which are the sources of the tracks. Figure 3 shows an example of the hits and tracks found in a sample double-vertex event in experiment E771, a fixed-target B experiment at Fermilab. The two vertices are about 6 mm apart. The detector planes in this view start 3 cm downstream of the vertices. Tracks from the secondary vertex are shown with long dashes. The track with short dashes is a track whose slope matches closely the slope of a triggering high-p_t muon found in the spectrometer downstream of the vertex detector.

In this experiment, the target region contained a number of target "foils", each 2 mm thick, with 4 mm gaps between them. The vertical lines in Fig. 4 at z coordinates of -37 mm, -31, -25, etc, up to -7 mm, show the locations of the front faces of these foils. In this event, the triggering high-p_t muon came from the decay of a high-p_t pion produced at the primary vertex. The secondary vertex is located in the following target foil, and appears to be a secondary interaction in the target material.

The tracks shown in Figure 3 were found by a multi-stage tracking program, which first finds an apparent primary vertex, then looks for tracks which intersect in a tight bundle near that vertex, identifies hits from such tracks and removes them from the hit bank, and then searches for additional tracks using the remaining hits. This procedure is quite effective in finding multiple-vertex events, in this experiment.

However, if there are two vertices within a short distance from each other, say within 2 or 3 mm, it is very difficult to recognize that there are multiple vertices. The nature of the difficulty is emphasized in Figure 4, which shows the tracks found in the first stage of the tracking program, when a primary vertex is being sought. These "original" tracks show extensive smearing of the vertex region, due to two principal kinds of effects. 1) Even for tracks which use relatively well-isolated hits, extrapolation errors back to the vertex region, caused by measurement uncertainties (finite strip widths) and by Coulomb scattering, cause smearing. 2) In angular regions where several planes have high occupancy, multiple false tracks are found by the tracking program.

6. VERTEX SMEARING IN A FORWARD-COLLIDER EXPERIMENT

Figure 5 shows a Monte-Carlo (Pythia) minimum-bias event, for the Tevatron. The tracks drawn correspond to the 26 charged particles produced in the "forward cone" (positive p_z), within 600 mrad of the beam. Five of these tracks, numbers 10 through 14, go down the beam hole and do not reach the vertex detector planes.

Figure 6 shows what happens to the 21 tracks which do hit the vertex detector planes, when Coulomb scattering in the first detector plane hit is taken into account in a crude way. The vertex region is quite smeared; 3 of the tracks extrapolate back with apparent impact parameters larger than 90 microns rms, and 2 more with values above 35 microns rms, just from Coulomb scattering in the first plane hit.

If at the first detector plane which is hit the distance from the beam line is y_1, and if the y-component of transverse momentum is p_y, and if the detector thickness is 300 microns, then the rms displacement in impact parameter, due to the scattering in that plane, is

$$b = \frac{0.8\ y_1}{p_y}\ \mu m\,, \qquad \text{where } b \text{ is in microns when } y_1 \text{ is in mm and } p_y \text{ is in GeV/c}.$$

For a detector array like that in Figure 1, and with R, the y-distance from beam line to first strip, equal to 4 mm, y_1 will be about 5 mm, and b is approximately $(4/p_y)$ in microns. Thus a p_y value of 0.10 GeV/c gives a b of 40 microns rms. The tracks in Fig. 6 which show displacements larger than 40 microns thus have p_y values of about 0.05 GeV/c; and the fact is that in 21 tracks, at the Tevatron, several have p_y values this small.

B decays typically produce several tracks each with p_y greater than 0.5 GeV/c. If p_y can be measured at trigger level, for every track, then a promising trigger for B candidates can be made by requiring the presence of several high-p_y tracks with substantial impact parameters, say above 50 or 75 microns. With Coulomb scattering held to about 10 microns rms, and with measurement error held similarly, such a high-p_t impact-parameter trigger offers the possibility of giving high rejection of minimum bias events while retaining maximum sensitivity and efficiency for B events.

7. ON-LINE P_T MEASUREMENT

Figure 7 illustrates the basic scheme for on-line measurement of momentum and transverse momentum. A primary vertex is located at z_0, and detector planes at z_1, z_2, etc. The detector planes are pixel planes, with a position resolution better than 5 microns rms in one direction. We take the case that the resolution in x is 5 microns and in y is 10 microns. (Shapiro has found a resolution better than 5 microns in the "narrow" dimension direction of the pixel planes he has tested. To obtain also good resolution in the other direction, it will be necessary to use an additional plane at each station; this could be either a pixel or a short-strip plane.)

The z coordinate of the primary vertex is determined to within 100 microns, using tracks through the barrel part of the vertex detector. With a very small beam cross section, the primary vertex is then well defined in 3 dimensions. Consider a track, curving in y, which then gives hits at (y_1, z_1), (y_2, z_2), etc. From the points (y_0, z_0) and (y_1, z_1) we calculate a slope for the chord, and the extrapolated straight-line expected hit position at z_2. The calculation, as explained further in the report by Crosetto, is made in about 100 nsec. Note that since the planes are pixel planes, this extrapolation is carried out in both x and y, and note that in x the trajectory is indeed a straight line.

The plane at z_2 is searched, in the vicinity of the straight-line extrapolation, for a matching hit. In x, the non-bend plane, the matching hit should be found within one resolution width, which means within less than about 20 microns for momentum above 1 GeV/c and for plane spacing about 2 cm. When a matching x hit is found at z_2, the y interval in the vicinity of the straight line extrapolation is searched. For tracks of momentum 1.0 GeV/c, in a magnetic field of 1.0 Tesla, and with planes at z separations of 2 cm, the magnetically produced deviation of the actual hit from a straight line fit, from one chord to the next, will be 120 microns. For a more extreme case, with a momentum again of 1 GeV/c but at a small angle in y, 50 mrad, the first hits would be at z = 12, 17, and 25 cm, and the deviations from straight line fits would be about 500 microns.

The region which must be searched, particularly in x, is quite small, and it appears likely that tracks from the primary vertex can be recognized, and their momentum and p_t values measured very rapidly, to sufficient accuracy for a Level-1 trigger. For tracks from a heavy quark decay vertex, with the decay vertex within 1.0 millimeter transversely from the beam, the proposed search and tracking procedure appears likely to also work well. Much more detailed study will be needed to make a critical evaluation of the efficiency, and of possible problems from background processes.

8. RATES

At the SSC and at 10^{32} luminosity, and taking the B-Bar production cross section to be about 10^{-27}cm^2, 100,000 B pairs will be produced per second. Single B's into a forward detector of half-angle 30 degrees, with all fragments contained, or one less than all, will be about 20,000 per second. In a "standard year", of 10^7 running seconds, the number of single B's into the detector will thus be about 2×10^{11}. And the number which will also have a tagging particle contained, from the other B, will be about 5×10^{10}.

This is about 3 orders of magnitude larger than the the annual rate of B-Bbar pairs expected for present designs of electron-positron B factories. It is this very high production rate, into the detector, which offers the promise of greater sensitivity for an SSC B experiment than for e+/e- B factories. To capitalize on this capability, however, will require a triggering system which can pick out some 10^4 events/sec with a high-p_t secondary vertex, out of 10^7 interactions/sec. It should also be noted that along with the 10^4 B events/sec which one would like to examinine with higher level triggers, there will be a larger number of charm events, perhaps nearly an order of magnitude larger. This large yield of charm events also offers the possibility of new significant studies of very weak processes.

One is thus led to the view that for a Level-1 heavy-quark trigger for an SSC experiment it is desirable to reject "ordinary" events by a factor of up to 100, but not more than 100, while retaining highest possible efficiency for secondary-vertex events. Further trigger levels will probably be required before events are delivered to the recording system — even if a rejection factor of 100 can be achieved, 10^5 events per second, or of order 1 gigabyte per second, would still remain to be dealt with.

The objective, then, for the Level-1 trigger being proposed, is to reduce the event rate by a factor of 100, while retaining high efficiency for heavy-quark events with distinguishable decay vertices.

9. SUMMARY

This report describes an approach to a secondary-vertex type trigger, for Level-1 use in a B experiment at the SSC. The scheme uses a configuration of vertex detector, magnets, and pixel planes, which together with a massive interconnected parallel processor, of the Crosetto type, can provide on-line tracking with momentum information. The p_t information gives a major improvement in the clarity of the vertex region, and makes possible the use of impact-parameter measurements on high-p_t tracks to provide a means for efficiently selecting B events. The objective is to reject ordinary events by a factor of up to 100, while accepting a major fraction of the 10^4 tagged B's, and of the still larger number of charmed mesons, which would be collected per second in the detector at a luminosity of 10^{32}.

As compared with a high-p_t muon trigger, which is a possible alternate trigger for a high-luminosity B experiment, the high-p_t impact-parameter trigger offers an order of magnitude higher efficiency for collecting B events. The real-time tracking provides, in addition, detailed momentum vector information for use in higher level triggers.

10. ACKNOWLEDGEMENTS

I have benefited greatly from the work of many others who have studied and devised designs for B experiments at high energy hadron accelerators. I am particularly indebted to Peter Schlein and his associates, who first stimulated my thinking on forward collider designs. Special thanks also to Kirk McDonald and Nigel Lockyer for many enlightening discussions. Finally, the work of Dario Crosetto and of Steve Shapiro and associates, described in their reports to the Workshop, has been indispensable in the development of a scheme for measuring track momenta rapidly enough for use in a Level-1 trigger. The p_t information on individual tracks is of critical importance in making an efficient impact-parameter trigger.

11. REFERENCES

1. See for example "Expression of Interest EOI-0008", submitted to the SSC Laboratory, 1990.
2. S. Erhan, M. Medinnis, P. Schlein, and J. Zweizig, CERN-PPE/91-10 (1991).
3. S. Erhan et al. {COBEX Collaboration}, "COBEX, a Dedicated Collider B Experiment", *Nucl. Inst. and Meth.* **A333** (1993) 101, and previous references contained therein.
4. G. Apollinari et al., *Nucl. Instr. and Meth.* **A252** (1986) 467; and S. White, private communication.
5. "Development and Test of a Large Silicon Strip System for a Hadron Collider Beauty Trigger", J. Ellett et al., *Nucl. Instr. and Meth.* **A317** (1993) 28.
6. K. T. McDonald, "Vertex Detectors for B Physics at the SSC", SSC Physics Symposium, Madison Wisconsin, March 1993, and reports to the Workshop.
7. S. Shapiro, D. Cords, and S. Mani, "Pipeline Readout of an Array of Time Tagging Pixels ....", SLAC-PUB-5916, Sept. 1992, and reports to the Workshop.
8. D. Crosetto, report to the Workshop.
9. A detailed account of this effect in the E771 detectors, and its interpretation, is given in a paper by A. Boden, L. Fortney, V. Golovatyuk, W. Kowald, J. Lys, A. McManus, T. Murphy, W. Selove, and R. P. Smith, submitted to Nucl. Instr. and Methods.

APPENDIX A. RADIATION TOLERANCE

Radiation damage effects in silicon detectors have been studied for a number of years. Initial indications were that for high energy protons an integrated fluence up to 10^{14} protons/cm^2 could be tolerated without causing appreciable loss of pulse height. This corresponds to approximately 3 Mrad, neglecting the effects of secondary particles produced in interactions in the silicon.

Recently, in experiment E771, it has been found that by the time 1 Mrad was reached, the silicon strip detectors showed substantial loss of pulse height, and that by 2 Mrad the detectors were virtually dead in the region where the beam particles had passed through.

The loss of signal in the beam region of the E771 detectors has now been understood to occur because of effects related to the formation of p-type impurities under irradiation. The problem basically resulted from the fact that the bias voltage was not sufficiently high to keep the detectors fully depleted at the fluence levels reached. With increasing fluence the density of p-type impurities increases, and finally the bulk material becomes dominantly p-type. The voltage required for full depletion then increases with further fluence, reaching approximately 200 volts at 2 Mrad. Moreover, the electric field gradient in the depleted part of the detector reverses sign, after type inversion, and the electric field becomes relatively strong at the "n-side", dropping to a minimum at the p-side. The result is that if the applied bias voltage is insufficient to give full depletion, and if the point of type inversion has been passed, then an undepleted layer exists near the p-side, the electric field is very weak in the depleted material near that undepleted layer, and the current into the p strips drops very rapidly with further increasing fluence. The E771 detectors reached this condition starting around 1 Mrad, where the voltage required for full depletion had increased to roughly equal the bias voltage which was used, 100 volts.[9] It has been known for some time that if one has double-sided silicon strip detectors, then the strips on the n side continue to function after type inversion, even if the bias voltage, V_{bias}, is less than the voltage V_{depl} needed for full depletion. The pulse height will decrease under this condition, but not extremely rapidly; the charge collected from a minimum ionizing particle traversing the detector will be smaller than that obtained with full depletion, by approximately the ratio of the depleted thickness to the full detector thickness, so by the square root of V_{bias}/V_{depl}. Thus even if the bias voltage is only 1/4 of V_{depl}, for example, the collected charge, on the n strips, will still be approximately half of the asymptotic fully-depleted value.

It is thus clear that if one reads out with n-type strips, rather than with p-type strips, then a 300 micron thick detector operated at 100 volts will still give useful signals, approximately half of the asymptotic pulse height even at 4 Mrad or so. It is possible to go even further. If one uses detector readout elements of small area — pixels, or short strips — the signal-to-noise ratio is much improved compared to longer strips. One can then use thinner detectors, so that the voltage required for full depletion is smaller. Useful operation is then possible at still greater fluence values. Thus for example planes of 150 microns thickness can be expected to require only 75 volts for full depletion at 3 Mrad, not 300 volts; and at 12 Mrad should still give half of the asymptotic pulse height. For a forward collider design, where Coulomb scattering in the detector planes produces a large amount of vertex smearing, the use of thinner planes than those used in conventional strip detectors provides the further attractive result of reduced Coulomb scattering.

It is from these considerations that I come to the conclusion that silicon detector wafers, with readout elements of small area as proposed in this report, can be satisfactorily operated up to 5 Mrad or more.†

APPENDIX B. REPLACEABLE VERTEX-REGION SECTION

With silicon planes coming within a few millimeters of the beam line, radiation damage can be expected to require replacement of the closest parts of the planes at intervals shorter than a year. Figure 8 shows a proposed layout of a replaceable beam section in the vertex-detector region. Gate valves are used, to allow rapid pumpdown after replacement. In the forward region the gate valve forms the last part of a muon wall. With a detector having only one arm, a gate valve can also be installed freely in the backward region.

† I am indebted to T. Ohsugi, T. Kondo, and H. J. Ziock, for very helpful discussions; and to L. Fortney for many extremely useful discussions and for relentlessly pursuing the study of the E771 results and their interpretation.

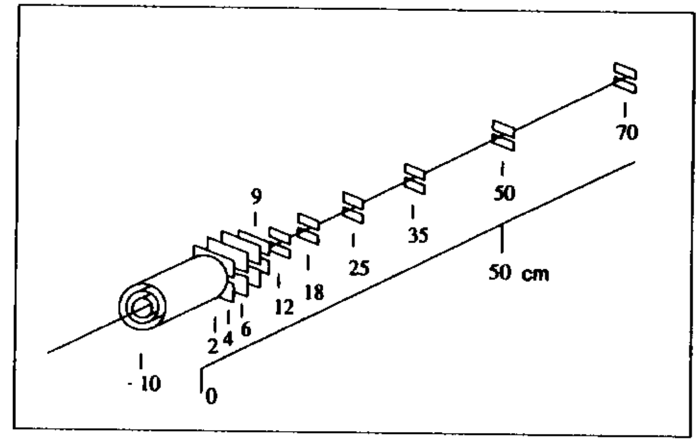

Fig. 1 Vertex Detector

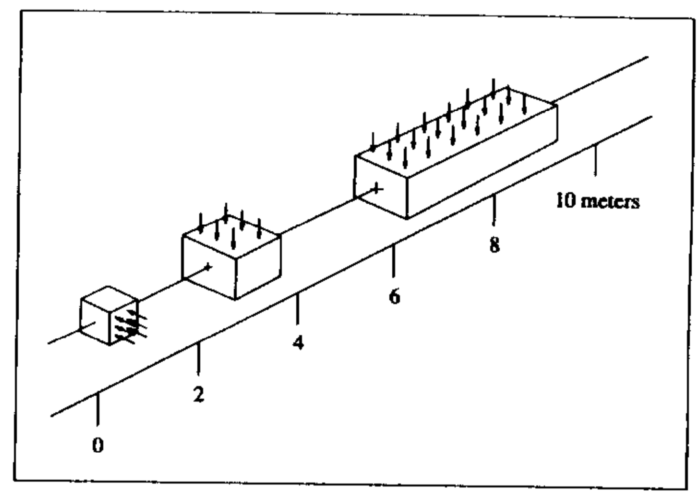

Fig. 2 Magnet arrangement

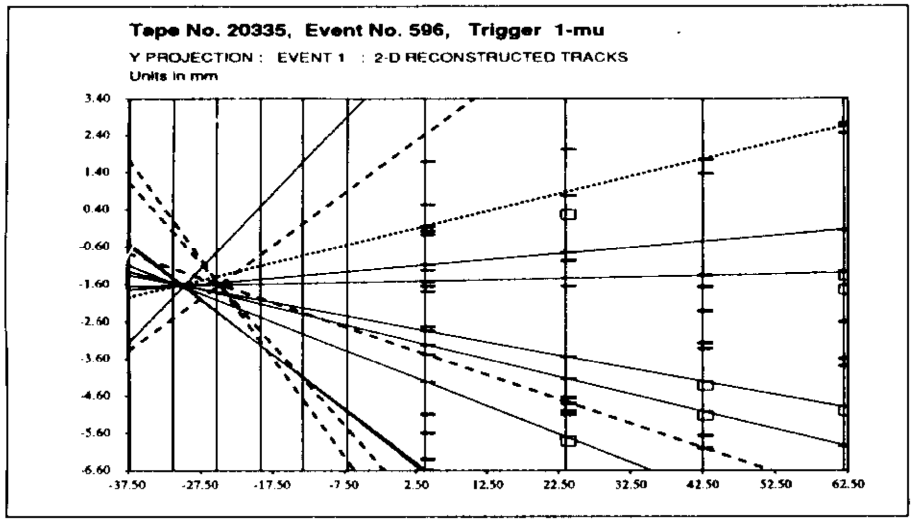

Fig. 3 Double-vertex event. Primary and secondary tracks

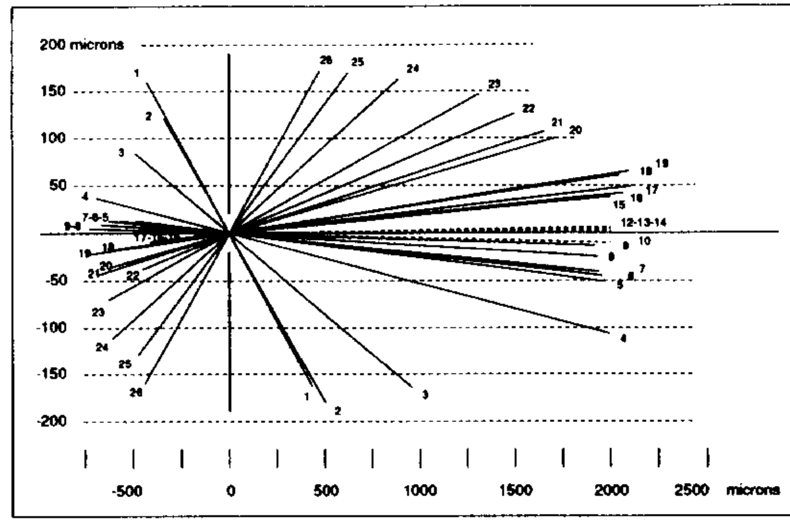

Fig. 5 Minimum-bias event. Unscattered tracks

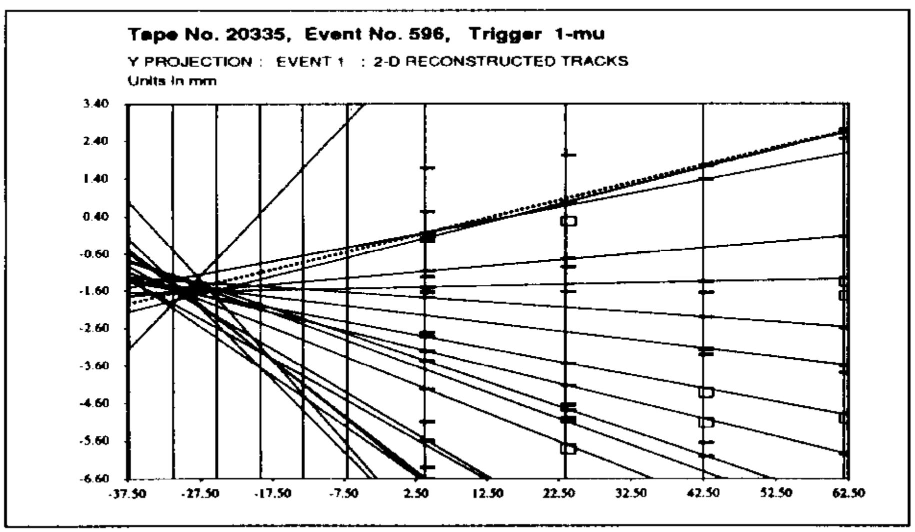

Fig. 4 Double-vertex event. Original tracks

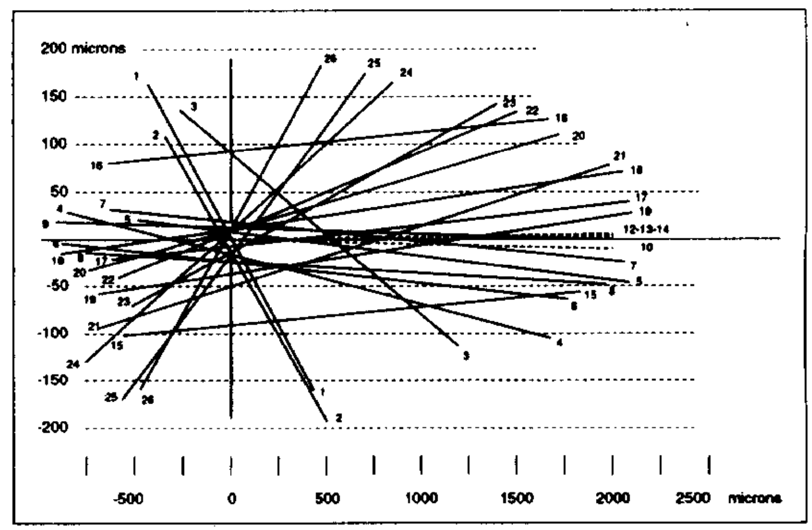

Fig. 6 Scattered tracks

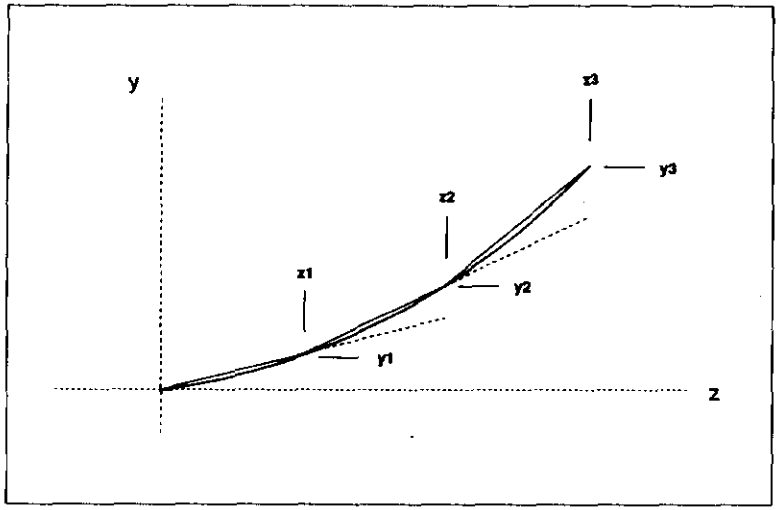

Fig. 7 Trajectory for momentum determination

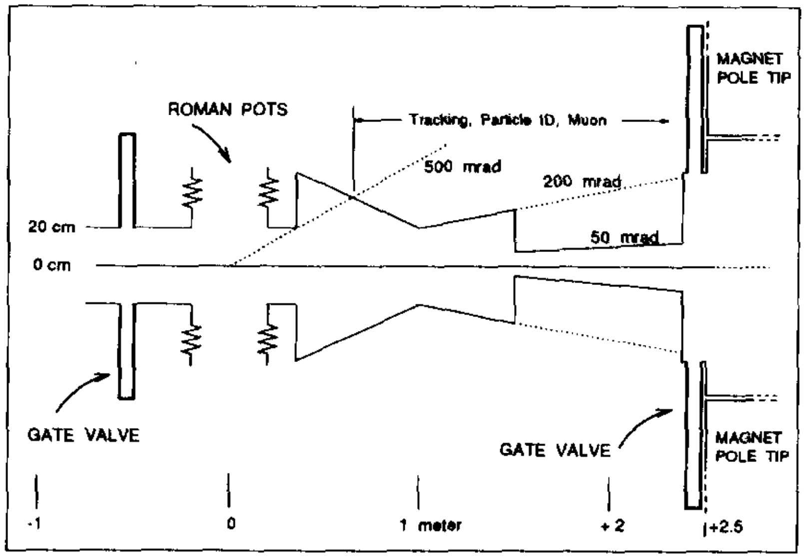

Fig. 8 Replaceable vertex beam section

REAL-TIME TRACKING WITH A 3D-FLOW PROCESSOR ARRAY*

D. Crosetto

Superconducting Super Collider Laboratory+
2550 Beckleymeade Ave.
Dallas, TX 75237

Abstract

The problem of real-time track-finding has been performed to date with CAM (Content Addressable Memories) or with fast coincidence logic, because the processing scheme was thought to have much slower performance. Advances in technology together with a new architectural approach make it feasible to also explore the computing technique for real-time track finding thus giving the advantages of implementing algorithms that can find more parameters such as calculate the sagitta, curvature, pt, etc. with respect to the CAM approach. The report describes real-time track finding using new computing approach technique based on the 3D-Flow array processor system. This system consists of a fixed interconnection architecture scheme, allowing flexible algorithm implementation on a scalable platform. The 3D-Flow parallel processing system for track finding is scalable in size and performance by either increasing the number of processors, or increasing the speed or else the number of pipelined stages. The present article describes the conceptual idea and the design stage of the project.

1. INTRODUCTION

In order to have better rejection at the Level-1 trigger, based on the calculation of additional parameters with respect to CAM, a 3D-Flow parallel processing system approach has been investigated.

A competitive solution in performance to the CAM approach is derived by using not only a parallel-processing solution, but also a processor with a special architecture presently not available on the market. These features are contained in the 3D-Flow processor and consist of high-speed communication ports (a large number of them to allow fast communication in six directions), and standard arithmetic operation as in regular processors. In addition, the processor also perform some special instructions to more efficiently execute high energy physics algorithms, FIFOs at the input port, to derandomize the processor clock with an external device clock (at the detector), and data-driven types of operations. Highlights of the proposed scheme are depicted in Section 3.2.

2. 3D-FLOW PROCESSOR

The 3D-Flow processor, Figure 1(a) and 1(b), is a programmable, data stream pipelined device that allows fast data movements in six directions with digital signal-processing capability. The design of the processor has been completed, and 225 hours of consultancy from industry have checked the feasibility of the 3D-Flow idea. A total of 6000 lines of VHDL code, describing the behavior of the single units and their interconnection, allows one to simulate algorithms and check the timing of all signals in the circuit. A table format of Microsoft Excel sets the input/output conditions at the external pins of the processor at each state. Other formats are used to download data-memory values into the processor. Program memory, thresholds and counter values have also been provided.[1, 2]

The 3D-Flow operates on a data-driven principle. Program execution is controlled by the presence of the data at five ports (North, East, West, South, and Top) according to the instructions being executed. A clock synchronizes the operation of the cells (a prototype will be made at 60 MHz). With the same hardware one can build low-cost, programmable, Level-1 triggers for a small and low-event-rate, or high-performance, programmable Level-1 triggers capable of executing more complex algorithms.

---

*Presented at the Workshop on B Physics at Hadron Accelerators, June 2, 1993, Snowmass, Colorado.
+Operated by the Universities Research Association, Inc., for the U.S. Department of Energy under Contract No. DE-AC35-89ER40486.

At each input port of the 3D-Flow processor there is a FIFO that de randomizes the data from the calorimeter to the processor array. North, East, West, and South ports are 12-bit parallel bidirectional on separate lines for input and output, while the Top port is 12-bit parallel input only, and the Bottom port is 12-bit parallel output only. North, East, West, and South ports are used to exchange data between adjacent processors belonging to the same 3D-Flow array (stage).

Top and bottom ports are used to route input data and output results between stages under program control. Each 3D-Flow cell consists of a Multiply Accumulate unit (MAC); arithmetic logic units (ALUs); comparator units; encoder units; a register file; an interface to the Universal Asynchronous Receiver and Transmitter (UART), used to preload programs and to debug and monitor during their execution; data-memory to be used also as a look-up table to linearize the compressed signal, to remove pedestals, and to apply calibration constants; and a program storage surrounded by a system of three-ring buses. At each clock, a three-ring bus system allows input data from a maximum of two ports and output to a maximum of five ports. During the same cycle, results from the internal units (ALU, *etc.*) may be sent through the internal ring bus to a maximum of five ports. The architecture of the 3D-Flow Processor cell is shown in Figure 1(a), the input/output in Figure 1(b).

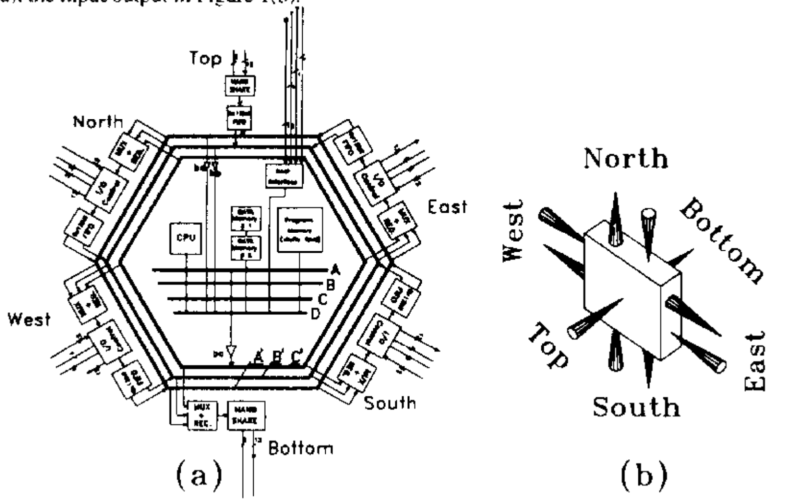

Figure 1. 3D-Flow Processor.

3. REAL-TIME TRACK FINDING AND REJECTION

3.1 Lookup-tables versus computing techniques

Real-time tracking techniques, used to date in experiments are of the look-up table type. The look-up table technique has a very fast response, but it requires a large amount of memory and is limited to recognizing only tracks that have been prerecorded into the memory.

Another technique, not used very much to date, is the computing technique that offers the advantage of implementing algorithms rather then just relying on a coincidence. One reason that it has not been used is its much lower performance with respect to look-up tables.

The following approach of real-time tracking, with the 3D-Flow parallel-processing system offers a fast and programmable response that may solve the problem in some real-time tracking applications.

Figure 2 depicts how information from different sub-detectors is sent into the 3D-Flow parallel-processing system.

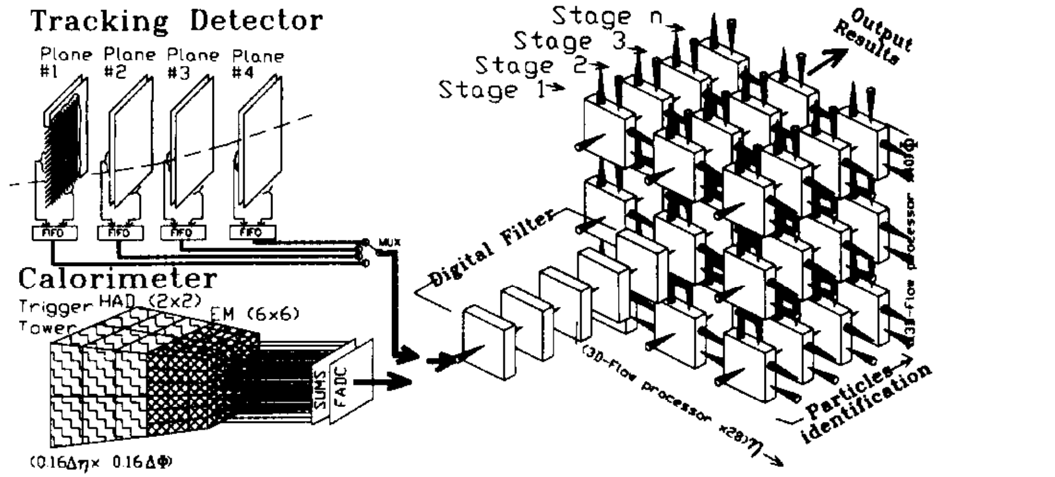

Figure 2. 3D-Flow system receiving data from different sub-detectors.

In the track-finding application, a number of 3D-Flow processors are used for each "plane." Depending on the complexity of the algorithm and the number of tracks expected in a given area, the user decides the most convenient price/performance segmentation of the "plane" in smaller areas, each of which sends the information to a 3D-Flow processor.

As an illustrative example, Figure 3 shows the mapping of the strip (wire) signals to a 3D-Flow processor array, while Figure 4 shows the mapping of the signals from a subset of a tracking detector into a 3D-flow processor. Thus, if we have a "plane" (consisting of several subplanes "x", "y", "u", "v") of 512 wires or strips and we know *a priori* from Monte Carlo simulation that the number of expected tracks is not greater than 10, then a convenient segmentation would be a 11×11 3D-Flow processor array for each "plane," such that each one receives as input a small fraction of information of the entire plane (*e.g.*, 48 wires or strips of each subplane).

We assume that an approximate vertex point has been located in a first step of the Level-1 tracking program.[3] For each detector plane there is a 2-dimensional 3D-Flow processor array; for successive detector planes there are successive arrays (or stages).

Each 3D-Flow processor takes the x and y coordinates from a hit on the first plane and computes the predicted coordinates on the next plane by a straight-line extrapolation. If curved tracks are expected in one or two dimensions, the processor in the next array should look for a hit in a wider region of interest. In the next plane, and in the corresponding small area, the 3D-Flow processor checks whether the predicted x and y coordinates lie in its region of operation. If so, the processor should find a hit which may come close to a straight-line predicted value (or deviates by a relatively small amount if a curvature is expected). The processor calculates, for this track, the new slopes (in x and y), the sagitta, the momentum (P), and the transverse momentum. The results of the calculation are passed on to the 3D-Flow processor that will operate on the corresponding area element in the next plane.

If the calculation to see whether the predicted x, y coordinate pair lies in the operating region of the individual 3D-Flow processor shows that it does not, the processor then forwards the received quantities to the adjacent 3D-Flow processor in the same array (or stage). The processor that finds that the predicted coordinates match its operating area then checks for continuity of the track in that plane by searching for a hit in its region. If the hit is found, the processor calculates the momentum, etc., and the result is forwarded to the next processor array (or stage), and so on.

3.2 Tracking Detector Versus 3D-Flow Processor Array

The tracking detector versus the 3D-Flow processor array is shown in Figures 3 and 4.

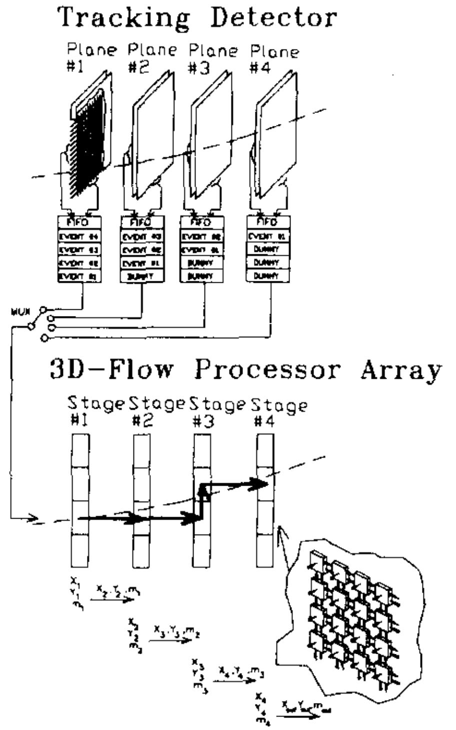

Figure 3. Tracking detector versus 3D-Flow processor array.

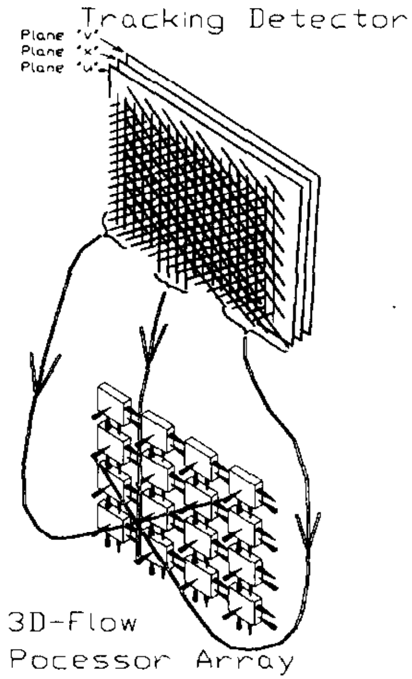

Figure 4. Mapping of signals from a subset of a tracking detector into a 3D-Flow processor.

The signal from the wires of the central plane is sent to the input of all 3D-Flow processors of the second column, as are the signals from the wires of the other planes to the other processors as shown in Figure 4.

3.3 Timing and Synchronization

Depending on the amount of computing required to calculate the unknown parameters and the number of hits per plane, the user selects an appropriate segmentation of the plane and associates it to a 3D-Flow processor array. Note that the high communication speed of the 3D-Flow processor allows the exchange of data between adjacent areas, thus allowing a system with no boundary limitation.

In Table 1 the four columns represent the activity of the processors in the four arrays (or stages); the rows indicate (from top to bottom) the timing sequence; the activity at each timing sequence for the arrays is indicated in the corresponding row.

Since each processor has the capability to simultaneously move data and perform calculations, two columns have been reserved for each processor array in order to indicate these activities. For example, row "zero" indicates that data event #1, from detector plane #1, is moved to processor stage (or array) #1; and row "one" indicates that the received data of event #1, from plane #1, is processed in the processor stage (or array) #1, at the same time that the processor is receiving the data of event #2 from plane #1, and so on for row "three," *etc.* Following this sequence, by row "eight" the results of event #1 are ready for output. At this time, the pipe is full, and all the processors are performing the two operations of moving and computing on data from different events.

Table 1. Timing of "data moving" and "data processing" on each 3D-Flow stage. Results are moved in sequence after computing.

Time	Detector Plane #1 = 3D-Flow array # 1		Detector Plane # 2 = 3D-Flow array # 2		Detector Plane # 3 = 3D-Flow array # 3		Detector Plane # 4 = 3D-Flow array # 4	
	3D-Flow Processing	3D-Flow Data mover	3D-Flow Processing	3D-Flow Data mover	3D-Flow Processing	3D-Flow Data mover	3D-Flow Processing	3D-Flow Data mover
0		in EV1-PL1-ST1						
1	Computing EV1-PL1	in EV2-PL1-ST1		in EV1-PL2-ST2				
2		Res EV1 to ST2						
3	Computing EV2-PL1	in EV3-PL1-ST1	Computing EV1-PL2	in EV2-PL2-ST2		in EV1-PL3-ST3		
4		Res EV2 to ST2		Res EV1 to ST3				
5	Computing EV3-PL1	in EV4-PL1-ST1	Computing EV2-PL2	in EV3-PL2-ST2	Computing EV1-PL3	in EV2-PL3-ST3		in EV1-PL4-ST4
6		Res EV3 to ST2		Res EV2 to ST3		Res EV1 to ST4		
7	Computing EV4-PL1	in EV5-PL1-ST1	Computing EV3-PL2	in EV4-PL2-ST2	Computing EV2-PL3	in EV3-PL3-ST3	Computing EV1-PL4	in EV2-PL4-ST4
8		Res EV4 to ST2		Res EV3 to ST3		Res EV2 to ST4		Res EV1 to Out

4.0 CONCLUSIONS

The 3D-Flow system provides an alternative to real-time finding lookup-table technique with a relative fast track finding computing technique. The advantages among the two techniques is the less amount of memory required by the computing technique, thus lower cost. Additionally, it allows calculation of more parameters, *e.g.* sagitta, pt, *etc.* in order to achieve better rejection.

ACKNOWLEDGMENTS

I would like to acknowledge W. Selove and T. Pal for the fruitful discussions.

REFERENCES

1 D. Crosetto, "3D-Flow processor for a programmable Level-1 trigger," Nuclear Science Symposium (NSS), Medical Imaging Conference (MIC), Orlando, Florida, October 26-31,1992.

2 D. Crosetto, "Digital Programmable Level-1 Trigger with 3D-Flow Assembly," SSCL-PP-445, August, 1993. *Submitted to Nuclear Instruments and Methods in Physics Research.*

3. W. Selove, "Impact Parameter Trigger and Vertex Detector for Forward Collider," Univ of Pa. Report UPR-222E, Aug. 31, 1993. Submitted to Proceedings of the Workshop on B Physics at Hadron Accelerators, Snowmass Colorado, June 1993.

DATA DRIVEN PROCESSOR "VERTEX TRIGGER" FOR B EXPERIMENTS

E.P. Hartouni
Department of Physics and Astronomy, University of Massachusetts
Amherst, MA 01003, USA

1. INTRODUCTION

Data Driven Processors (DDP's) are specialized computation engines configured to solve specific numerical problems, such as vertex reconstruction. The architecture of the DDP which is the subject of this talk was designed and implemented by W. Sippach and B.C. Knapp at Nevis Lab. in the early 1980's[1]. This particular implementation allows multiple parallel streams of data to provide input to a heterogeneous collection of simple operators whose interconnection form an algorithm. The *local* data flow control allows this device to execute many algorithmic steps in parallel and many events concurrently. The DDP so configured can execute algorithms extremely quickly provided that care is taken in the layout of the algorithm. I/O rates of several hundred megabytes/second are routinely achieved thus making DDP's attractive candidates for complex online calculations.

This talk originates from a series of discussions which became CERN RD-21[5]. The original question was: "can a DDP reconstruct tracks in a Silicon Vertex Detector, find events with a separated vertex and do it *fast enough* to be used as an online trigger?" Restating this inquiry as three questions and describing the answers to the questions will be the subject of this talk. The three specific questions are:

(1) Can an algorithm be found which reconstructs tracks in a planar geometry and no magnetic field;
(2) Can separated vertices be recognized in some way;
(3) Can the algorithm be implemented in the Nevis-UMass DDP and execute in 10-20 μs?

The answer to these questions is "yes".

2. OUTLINE

The discussion begins with a description of the Silicon Vertex Detector geometry relevant to vertex reconstruction. The next section consists of a statement of the algorithm developed for vertex reconstruction in the SVD. A comparison of the simulated data with data from CERN P-238[2] verifies that the calculation correctly predicts vertices. A short section describes the DDP implementation, relevant architecture and execution time. Finally the expected trigger efficiency based on Monte Carlo is presented.

3. SILICON VERTEX DETECTOR

The algorithm will depend on the detector's geometry, channel configuration, spatial resolution, channel occupancy, noise and event type (especially minimum bias). The specification of the algorithm benefited greatly from the existence of data from CERN P-238 which utilized a 43000 channel SVD system. This SVD consisted of 4 quadrants each $(4.5\ \text{cm})^2$ in area. Each quadrant had 6 planes of x-view and 6 planes of y-view. The strip pitch was 50 μm and strip width 25 μm. The entire detector was centered on the SPS beamline with the planes perpendicular to the beam. This test run demonstrated that the transverse and longitudinal vertex positions (x, y, z) can be determined to 25, 25 and 20 μm.

The test also demonstrated the feasibility of operating an SVD close to the beam of the SPS, and the viability of forward open geometry spectrometers such as proposed by the COBEX collaboration.

4. VERTEX RECONSTRUCTION ALGORITHM

The algorithm was developed by generating minimum bias and B-meson events using a PYTHIA-GEANT simulation. The results of the simulations were checked against the data from P-238 to insure some degree of veracity. The "data" from the physics/detector simulation was then submitted to a DDP emulator which performed the algorithm in Table 1 in an exact software model of the DDP.

Table 1. Vertex reconstruction algorithm

executed in parallel for each detector segment	Find Points	calculate the geometric centers of the strip clusters
	Find Tracks	using *points* from three planes, loop over *points* in first and third plane and predict the second plane's *point* within 25 μm (note that narrow road eliminates tracks which scatter in Silicon, accidental tracks, etc.).
	Reject Duplicates	loop over list of *tracks* comparing slopes and intercepts, eliminate those track duplicates farthest from beam.
executed for all track candidates	Calculate Primary Vertex	calculate the z-position of intersection with beam line for the list of *tracks*.
	Track Elimination	eliminate *tracks* with 1mm or more projected impact parameter (events with more than 10 such *tracks* are rejected).
iterate these steps 2 times	Calculate χ^2	Use *track* slope and intercepts to calculate an event χ^2 at primary vertex.
	Eliminate *Track*	eliminate *track* with worst χ^2.
	Calculate final χ^2	

The calculation can be organized so that the "typical" event reconstruction time might be less than the "full" event reconstruction time. This is achieved by organizing the algorithm to reject events which cannot possibly pass the final cuts, e.g. the *strip* multiplicity is too small, the *point* multiplicity is too small, the *track* multiplicity is too small, etc. Many events can be eliminated on only a partial computation.

The final decision made by the algorithm must decide if all the tracks come from a common vertex. This decision used the final χ^2 from the reconstruction calculation. Typical vertex distributions from P-238 fit Gaussians in x- and y-views with σ = 100 and 84 μm. This was consistent with a 30 μm measurement resolution and a 76 μm beam width in the y-views. Similar resolutions could be obtained online providing a potentially powerful separated vertex trigger.

5. IMPLEMENTATION OF THE DDP

The algorithm described in the preceding section will be partially constructed and operated during CERN RD-21. The basic outline of the implementation has been described in other references[3]. Although the particular hardware implementation in ECL is ten years old the DDP returns large computation time advantages over standard commercially available systems. "Modernization" of the hardware is possible, as are new architectures[6]. There are plans underway at UMass to pursue some of these possibilities.

The performance of the processor in terms of computation speed breaks into two parts: calculation latency and computation time. The latency is defined here as the time for the result to emerge from the bottom of the pipeline. In the case that the result *is* the trigger decision, this time is also the "computation time". However, results may be available *before* the full computation has completed. Thus the time to the first result is the pipeline latency, the time to the last result is the computation time. Offline studies of the RD-21 DDP demonstrate that an entire event requires of order 10^4 clock cycles for the event to pass through the DDP. At 50ns per clock cycle this would require 500 μs. However, this is the latency of the DDP. The computation time is proportional to the product of the number of strips in first and third planes. A number of events can be pipelined in the DDP, reducing the time between output by the number of events in the pipeline. Further increases in computation speed can be achieved by taking full advantage of the parallelism available in the DDP architecture. In this SVD geometry the x- and y-views of each quadrant of detectors could have separate line finder hardware. This would result in an eight fold increase in the most computationally intensive stage. These details are presented here to provide a glimpse at some of the issues which need to be resolved at the implementation stage of the DDP design.

6. TRIGGER EFFICIENCY

Details of the trigger studies have been presented elsewhere[3]. Many of the specific results of these studies depend on the exact properties of the events and the detectors. Monte Carlo results have been checked with data when ever possible, e.g. the P-238 data were used to check the PYTHIA-GEANT simulations.

Figure 1 shows the efficiency of the separated vertex trigger for $B_s \to D_s^* \pi^+ \pi^+ \pi^-$ and $B_d \to J/\psi K_s^0$ as functions of the χ^2 cut in the DDP algorithm. This study indicates that the minimum bias event backgrounds could be suppressed by 1/100 for a χ^2 cut of 30 while the B-meson decay modes would be reduced by 1/4 to 1/2.

The practical aspects of such triggers is being studied by RD-21 at CERN in a "fixed target" mode, i.e. using a target foil behind which the SVD is positioned. This test will help verify the simulation study results and provide valuable experience in interfacing the DDP to the SVD readout electronics.

7. ACKNOWLEDGMENTS

Many people participated in the design of this particular DDP algorithm from initial ideas through detailed offline simulation to the assembling of hardware. I would like to acknowledge the very capable work of Jamie Ellett, Mike Medinnis, Samim Ehran, John Zweizig, and Bruce Knapp. Peter Schlein initiated the original questions, and has provided the impetus to continue the RD-21 work. Mike Kreisler oversaw the production of boards, and has acted as a sounding board for this talk.

8. REFERENCES

1. B.C.Knapp and W. Sippach IEEE Trans. on Nucl. Sci. **27** (1980) 578
   E.P.Hartouni et al., IEEE Trans. on Nucl. Sci. **36** (1989) 1480
   B.C.Knapp Nucl. Instr. and Meth. **A289** (1990) 561
2. A.Brandt et al., *P238 Proposal to CERN*, CERN-SPSC/88-33; CERN-SPSC/89-43; CERN-SPSC/89-55
3. J.Ellett et al., *P845 Proposal to Fermilab* (1991)
4. S.Erhan et al., Nucl. Instr. and Meth. **A333** (1993) 101
5. J.Ellett et al., *R&D for Collider Beauty Physics at the LHC*, CERN/DRDC 91-18, DRDC/P28
6. D.Crosetto Nucl. Instr. and Meth. **A311** (1992) 49
   D.Crosetto and L.Love, *Fully Pipelined and Programmable Level 1 Trigger*, SSCL-576 (1992)

Figure 1. Trigger efficiency of the seperated vertex trigger algorithm used in the DDP as a function of the χ^2 cut for COBEX at the TEVATRON.

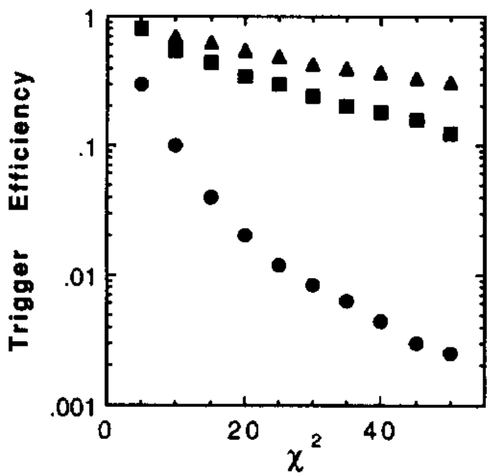

REPORT OF THE TRIGGER PROCESSOR SUBGROUP

M. JOHNSON
Fermi National Accelerator Laboratory
Batavia, IL 60510 USA

This is a summary report of a small group of people who met one afternoon to discuss trigger processors. The members of the group were A. Erwin, E. Hartouni, M. Johnson, J. Lewes, W. Selove, P. Shepard, D. Summers and P. Wilson.

The trigger processor group spent much of its time discussing new architecture's for high rate experiments. There was an attempt to differentiate between data driven architectures and the more conventional systems where triggers are divided into a series of levels. This was not too successful because most people felt that there were elements of the data driven architecture in almost all trigger systems -- particularly at the front end. There are, however, broad divisions that are present in almost every trigger system. These are listed in table 1.

Table I. Definition of the trigger levels.

Level 1	This is the section of the trigger that is truly dead timeless. The data is pipelined with enough buffers so that no crossing (event in fixed target) is lost. A trigger decision is generated at every crossing (but delayed by the length of the pipeline).
Level 3	Processor farm with one complete event per processor.
Level 2	Everything in between.

We also agreed that the development of complex, high rate experiments will force several changes in trigger architectures. At high rates, even small amounts of dead time per trigger are important. Since the level 1 system is dead timeless, more complex decisions will be moved to level 1. An example of this trend was given by Peter Wilson. He described the Xtra Fast Tracker (XFT) for CDF. This device uses data from the Central Tracking Chamber to form track segments at level 1 time (about 2 μs.) This data is used both for level 1 decisions and as input to level 2 processors such as the silicon vertex detector. W. Selove and D. Crosetto described a proposed system for a pixel detector that would take hits from a pixel detector and from tracks at level 1. Each group of pixels is connected to a processor and every processor is connected to its neighbors over one of six paths (faces of a cube). Processors are stacked in depth to form a pipeline. At every crossing the results from one stage are transferred to the next stage in the pipeline until the computation is completed.

The level 2 is a catchall for everything between the dead timeless level 1 and the microprocessor farm. It varies from very simple calculations in a small fixed target experiment to multi element event fitting in a large collider experiment. Dead time is very important at this level since the calculations often take tens of microseconds. Pipelining can still be used but usually only the smaller, fixed target experiments can use it. E. Hartouni described a system for E690 that did not have distinct level 1, 2 and 3 structure and was fully pipelined. There were enough stages in the pipeline so that dead time did not occur until the entire data stream was blocked. Their event size was only 1 KB so the large number of registers was not prohibitively expensive. There were several independent pipelines in the system so their event rejection scheme is more complicated than one with distinct levels. Their system had several points in the pipeline where an event would hold until the other pipelines caught up. Reject signals would intercept events at these points and discard them.

When pipelining is impossible, the dead time can be substantially reduced by buffering the data from level 1. This does not eliminate dead time but it can substantially reduce it. Events from level 1 arrive with a poisson distribution. Level 2 processing time is usually variable and it typically follows an exponential distribution. Assuming that there is only one queue (never really true), there is a simple formula from queuing theory that gives the probability that all buffers are full (the system is dead).

$$a = \frac{(1 - r)r^n}{1 - r^{n+1}}$$

Here, a is the probability that all the buffers are full, n is the number of buffers and r is the ration of input rate to output rate. a and r must be less than 1. One can use this formula to find the input rate for a specific dead time as a function of the number of buffers. Fig. 1 is a plot of the ratio of the input rate for n buffers to the single buffer case as a function of the number of buffers for 10% dead time. It shows that with 8 buffers, one can get about 9 times the input rate compared to a single buffer for a 10% dead time.

An important issue in any trigger system is event synchronization. This is usually not a problem for level 1 since an event leaves the pipeline at the same time. It is also not a problem for level 3 because an entire event is in a single processor. Level 2 can become a problem if it uses multiple buffers and multiple data streams and processors. Since different level 2 processors proceed at different rates, one does not easily know where the event is in a given data stream. One data stream may have a given event in the input queue, another will have the event in the output queue and a third may be processing the event. There is the further option of aborting all other processors on an event accept in one processor or letting all processors proceed to completion before accepting the event.

There are two ways of handling these multiple streams. One way is to lock all the processors together so that no processor can proceed to the next event until the current event is finished. We will refer to this as the locked processor scheme. The second one is to let the faster processors proceed on to the next event as soon as they have finished the current one. For the case where all processors must run to completion before accepting an event, there is no gain in letting one processor to get ahead of another. The throughput rate is determined by the slowest element so one should use the locked processor mode. For the case where a fast processor can go ahead, there is a gain that depends on the reject rate for the fast processor. For large reject rates, almost all events must also be processed by the slow processor so it again dominates the throughput rate. There is a small gain as the reject rate declines because the effective rate into the slow processor is reduced by the ratio of the accept rate to the total rate for the faster processor. This assumes that the faster processor eventually gets at least one event ahead of the slow one so that accepted events are not processed at all by the slow processor. This gain is quite slow, however, so it usually is not worth the complexity that this adds to the system.

Highly selective trigger systems are crucial to experiments to measure very rare processes such as CP violation in the B system. The rapid development of comercial high speed digital signal processors and application specific integrated circuits hold great promise for delivering these systems. However, these technologies are very sophisticated so successful designs will require good understanding their capabilities by physicists.

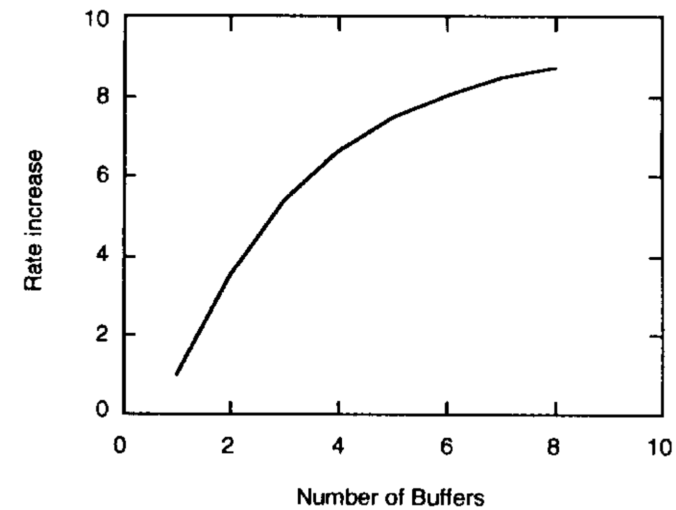

Figure 1. Rate increase compared to 1 buffer as a function of the number of buffers for 10% dead time. This assumes a Poisson input distribution and a single stage queue.

Machine Detector Interface

Convenors:

V. Bharadwaj
Fermi National Accelerator Laboratory

S. White
Brookhaven National Laboratory

List of Participants

J. Bjorken
Stanford Linear Accelerator Center

G. Bourianoff
Superconducting Super Collider Laboratory

L. Camilleri
CERN

R. Carrigan, Jr.
Department of Energy/
Fermi National Accelerator Laboratory

W. Chou
Superconducting Super Collider Laboratory

J. Cooper
Fermi National Accelerator Laboratory

Y. Giomataris
Lausanne University

G.P. Goderre
Fermi National Accelerator Laboratory

J. Holt
Fermi National Accelerator Laboratory

D. Johnson
Superconducting Super Collider Laboratory

T. Lohse
Max-Planck-Institut für Kernphysik

K. McDonald
Princeton University

T. Murphy
Fermi National Accelerator Laboratory

B. Newberger
University of Texas at Austin

T. Pal
Superconducting Super Collider Laboratory

D. Ritson
SLAC/Superconducting Super Collider Laboratory

T. Sen
Superconducting Super Collider Laboratory

M. Syphers
Superconducting Super Collider Laboratory

SUMMARY OF THE MACHINE DETECTOR INTERFACE WORKING GROUP

S. WHITE
Brookhaven National Laboratory
Upton, NY 11973, USA

and

V. BHARADWAJ
Fermi National Accelerator Laboratory, P.O. Box 500, Batavia,
Il 60510, USA

1. INTRODUCTION

The Machine Detector Interface working group met to consider the accelerator and beamline issues as they impact the various B physics experimental options. The options may be divided into fixed target type and colliding beam type experiments. The fixed target experiments use both extracted beams and internal targets in storage rings. For the colliding option, apart from using existing and planned accelerators (e.g., Tevatron and SSC) the working group spent some time looking at the concept of asymetric hadron colliders. The latter may offer some kinematical advantages and their novel nature make them look advantageous.

2. MACHINE DETECTOR INTERFACE PAPERS

The papers for this working group may be divided into three parts. The first four papers explore the fixed target options, the next three the colliding options. The last six papers are individual contributions of interesting ideas that may be useful in the design of accelerators and experiments. The papers are entitled

Fixed and Internal Target Options: Parameters and Impact

Test of an Internal Wire Target at the HERA Proton Ring

Extraction from TeV-Range Accelerators using Bent Crystal Channeling

Synopsis of a Design of a Crystal Extraction Facility in the SSC East Utility Straight

Design of the SSC Medium-Beta Interaction Regions

Summary of the Snowmass Working Group on Machine Detector Interface

Asymmetric Collider

Experimental Modification of SSC Interaction Region

Radiation Environment and Shielding at the SSC

Fixed-Target Particle Fluxes and Radiation Levels at SSC Energies

Longitudinal Wakefield Focusing: An Unconventional Approach to Reduce the Bunch Length in Tevatron

Obtaining Slow Beam Spills at the SSC Collider

Ultra Thin Beam Pipes for Internal Target B Experiments

Point-Like Internal Targets for B Experiments

3. COMMENTS ON VARIOUS EXPERIMENTAL APPROACHES

Experimental approaches to future b-physics experiments differ widely. Proposals for future experiments discussed at this workshop aim to use center of mass energies from $\sqrt{s} =$ 40 GeV (HERA-B) up to the $\sqrt{s} = 40$ TeV at the energy of the SSC (COBEX,BCD,SDC...). Although the B production fraction improves by three orders of magnitude over this energy range, lower energy, fixed target approaches have been advocated for a number of reasons.

On one hand it is argued that in lower energy collisions B mesons are more easily identified because the physics background has lower multiplicity and mean p_t. On the other hand, many arguments relate to the machine detector interface which was the subject of our working group. For example, because of the importance of measuring the secondary vertex position in these experiments, the accelerator beampipe plays a special role --particularly in the forward direction. Collider proposals have chosen either to place their microvertex detectors outside the beamtube (in which case the radial location of the first tracking layer is limited to ≥ 1 cm by machine requirements at injection energy) or inside the beampipe with a "Roman Pot" mechanism to move them close to the beam after stable conditions are achieved. Fixed target experiments using extracted beams do away with the troublesome beampipe.

Similarly, fixed target approaches may simplify the task of triggering on secondary vertices since the length of the interaction region is typically 10–30 cm in pp colliders while it can be made arbitrarily short with a foil or wire target. Another argument for the fixed target approach relates to the boost of the b-decay secondary particles which may be better tracked and identified in a forward detector geometry. If there is indeed a tradeoff between optimum boost and center of mass energy it may well be that the most favorable conditions for b experiments would exist at an asymmetric hadron collider.

FIXED AND INTERNAL TARGET OPTIONS: PARAMETERS AND IMPACT

C. T. MURPHY
Fermilab, Box 500, Batavia, Illinois 60510, USA

The accelerator and experimental parameters of the various fixed target and internal target B-physics proposals have been collected and compared in Table 1 below. The Hera-B experiment targets protons on fine wires in the halo of the circulating beam; it is discussed in detail in the article following by Thomas Lohse. The GAJET experiment targets protons on a hydrogen gas jet in the circulating beam of LHC; it is discussed by L. Camilleri elsewhere in these proceedings. The LHB crystal experiment extracts protons from LHC using a bent crystal and makes B's in a solid target external to the machine. The SFT (Super Fixed Target) experiment does the same thing at the SSC. It is discussed in an article elsewhere in these proceedings. The extraction scheme for the SSC is discussed in the article following by Dukes, Murphy, and Parker, and a test of this scheme which has begun at the Tevatron is discussed in the article by Carrigan, Murphy, and Newberger. In the final article of this section, D. Ritson discusses a scheme for creating large step sizes of halo beam onto a crystal or wire target by perturbations of transverse phase space.

Table 1. Parameters of several experiments.

Parameters	Hera-B Wire	'GAJET' H_2 jet	'LHB' x-tal	'SFT' SSC x-tal
$\sqrt{s}$ (GeV)	43	115	115	193
$\sigma_{b\bar{b}}$ (μb)	.008-.02	.6-1.0	.6-1.0	2.0
$b\bar{b}$ produced/sec	25-60	1270-2120	600-1000	1600
inelastic interaction rate (Mhz)	30	70	10	10
bunch spacing (ns)	96	25	25	17
interactions/bunch	3	2	0.25	0.2
target material	Cu	H_2	Cu	Si
target length (mm)	0.3	2	7.5	18
beam $\sigma_{x,y}$ (μm)	700x50	10x10		500x500

In Table I, the cross section per nucleon for $b\bar{b}$ pairs produced by protons is given in line two. The lower number is the cross section recommended by J. Smith at this workshop; the higher number is the one used by the proposers of the experiments. To obtain the number of events produced per second, an A-dependence of A^1 for the $b\bar{b}$ cross section has been assumed. The bunch spacing and interactions/bunch refer to an RF bunch.

Although the GAJET experiment promises a large yield, it has a handicap of having two inelastic interactions per RF bunch. The Hera-B experiment also has three interactions per bunch, but they will usually be in different wires which are spacially quite separate from each other (there are 8 wires). While the yield of the Hera-B experiment is low, it is the only proposal discussed here for an accelerator which already exists, and thus has a large head-start on the other experiments.

TEST OF AN INTERNAL WIRE TARGET AT THE HERA PROTON RING

THOMAS LOHSE
MPI für Kernphysik
Heidelberg, 69029, Germany

1. INTRODUCTION

Shortly after the HERA machine started its luminosity operation a working group was formed to study the possibility of exploiting the HERA proton beam for a high statistics B experiment able to discover CP violation in the B system. The effort resulted in two detailed reports [1,2] submitted to the DESY PRC.

HERA has four interaction points, two of which are occupied by the two large experiments H1 and ZEUS, and one which is planned to be used by the HERMES experiment. The fourth interaction zone is currently available and suited to house a dedicated B detector. In principle, HERA has two independent rings and one could investigate the possibility of proton proton collisions (with asymmetric energies). Since this would, however, interfere with the routine e-p operation, we concentrated on the fixed target option in which protons from the beam halo interact with massive internal targets, e.g., thin wires grouped around the beam center at distances of about 4 r.m.s. beam sizes.

In the fixed target mode, the center of mass energy is only slightly above 40 GeV. This is quite close to the $b\bar{b}$-threshold and thus the B cross-section is tiny; about 10 to 20 nb are expected theoretically. The charm cross section– a dangerous background– is three orders of magnitude larger and the total inelastic cross section dominates by 6 orders of magnitude. In order to get a precision of 0.05 in $\sin(2\beta)$, one thus has to produce a huge number, 10^{15}, of inelastic events, requiring 5 snowmass-years of data taking at interaction rates of about 30 MHz. These rates are in principle achievable at the HERA proton ring: With a nominal $2 \cdot 10^{13}$ protons stored and lifetimes around 50 to 100 hours, natural beam losses correspond to 50–100 MHz. We have to require, however, that the internal target is very efficient and able to absorb around 50% of all halo protons (which are about to leave the machine anyhow).

Since the feasibility of an internal target is of primary importance, beam tests were set up at the HERA proton ring. The main results of the 1992 tests are summarized in the following.

2. EXPERIMENTAL SET-UP

The choice for the target location, 118 m upstream of the center of the HERA west hall, was dictated by practical necessities like finding a beam pipe section void of other machine elements. Relevant parameters for optics, beam and target are summarized in Table 1. The optics are quite different from that for the proposed final target arrangement; most significantly the relatively large horizontal β-function of 93 m exceeds the maximal value of 50 m assumed for a B experiment. In addition, other (position independent) parameters, the total current in the machine, the machine aperture, and the number of target wires, were smaller than in the design in reference[1].

Table 1: Parameters of the target wire and the proton beam at the test location 118 m upstream of the HERA west hall.

Proton Beam:		
Beta function	$\beta_x = 96$ m	$\beta_z = 27$ m
Alpha	$\alpha_x = -1.68$	$\alpha_z = 1.10$
Emittance	$\epsilon_x = 9 \cdot 10^{-9}$ rad m	$\epsilon_z = 9 \cdot 10^{-9}$ rad m
Spatial dispersion	$d_x = 0.82$ m	$d_z = 0$
Angular dispersion	$d_{x'} = 24$ mrad	$d_{z'} = 0$
Beam size (r.m.s)	$\sigma_x = 0.9$ mm	$\sigma_z = 0.5$ mm
Number of bunches	10 (with 96 ns spacing)	
Typical current	1.6 mA ($= 2 \cdot 10^{11}$ protons)	
Target Wire:		
Material	Copper	
Diameter	100 μm	
Interaction length	151 mm	
Radiation length	14.3 mm	

The target was mounted vertically on a movable fork. It consisted of a 100 μm thick copper wire, followed by a second spare wire and finally a 100 μm thick copper foil. Since the first wire was not damaged during the tests, the back-up targets were never used. The fork was driven by a stepping motor (normally used for collimators) with a step size of 3 μm. It was directly controlled via the collimator control panel from the HERA control room. The target area was very close to the main proton collimators. These beam scrapers were situated about 6 m downstream of the target. Secondary collimators existed 214 m and 259 m downstream of the main collimators.

Fig. 1 shows the whole experimental set-up. Downstream of the target (T) and a beam pipe section of increased diameter (200 mm), telescopes were placed above, below and at both sides of the beam pipe. Each of the four telescopes consisted of two plastic scintillators, a smaller one (S1, 40 × 40 mm^2) positioned at 1.4 m from the target, and a larger one (S2, 80 × 80 mm^2) at 1.8 m, followed by a scintillator-lead shower counter (Sh) of the same active area and a depth of 18 radiation lengths. After the first measurement, the upper telescope was dismantled and its two scintillators were placed 0.3 m upstream of the target as "VETO" counters (V1, V2). This rearrangement allowed us to determine to what extent the telescopes were triggered by beam related background and not by interactions in the target.

During the whole running period HERA was filled by a short train of 10 consecutive bunches (with a bunch spacing of $\approx$ 96 ns). The arrival times at the test experiment were derived from a close-by beam pick-up. Only the bunch-crossing (BX) signal of the leading bunch was allowed to trigger the telescopes. This rules out any pile-up from preceding

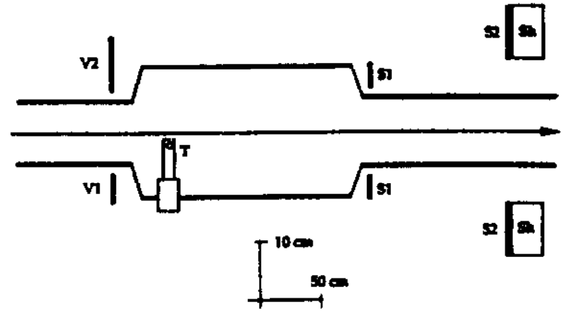

Figure 1: Sketch of the experimental set-up. S1, S2: scintillators; Sh: shower counters; V1, V2: scintillators used as VETO counters; T: target.

bunches. Data on the background detected by Si-pin-diodes in the vicinity of the collimators and from ZEUS (scintillators C5, proton-gated) and H1 (veto wall) were continuously displayed in the control room and were partly available off-line.

In total we performed 7 experiments with the wire close to the beam, corresponding to a total of 22 hours of data taking. In particular, the wire was several times systematically moved towards the beam in small steps, while HERA was operated in normal luminosity mode. In these situations, where the test experiment was running in a purely parasitic mode, the main collimators were positioned at about 5 r.m.s. beam widths from the nominal proton beam position and were not moved. In two occasions during the power saving hours in November, when only protons had been stored in the machine, the collimators could be opened with the wire already positioned in the beam halo.

The beam lifetimes were typically around 100 h when the target was retracted. Without e-p collisions, the lifetime was probably much larger, but no measurement beyond 100 h was available. The presence of the target reduced the lifetime to typically 30–50 h, either with or without e-p collisions, and no distinct differences between these two situations were observed.

The data presented here were taken from those running periods where the conditions were rather stable, i.e., neither jumps in the beam position nor violent beam losses in either the proton or the electron beam occured.

3. INTERACTION RATES IN WIRE SCANS

In the parasitic experiments, the wire was carefully moved towards the beam in small steps of 30 μm. An example is shown in Fig. 2a, which displays the horizontal wire position as a function of time. At time 2000 s a first increase of the trigger rate (Fig. 2b) was observed. Simultaneously the percentage of triggers with the VETO counters fired (Fig. 2c) dropped from 90% to 35%, demonstrating that this increase in the trigger rate was not due to beam background (which could have possibly been created by the disturbance by the wire). The obvious interpretation is that at this time the wire just moved out of the shadow of the collimator and started to scrape away protons from the beam halo.

In the following hours the wire was moved another 14 times towards the beam, as can be seen in Fig. 2. After each step, the coincidence rate first increased sharply, accompanied by a corresponding drop in beam lifetime. Within minutes, the rate then gradually settled

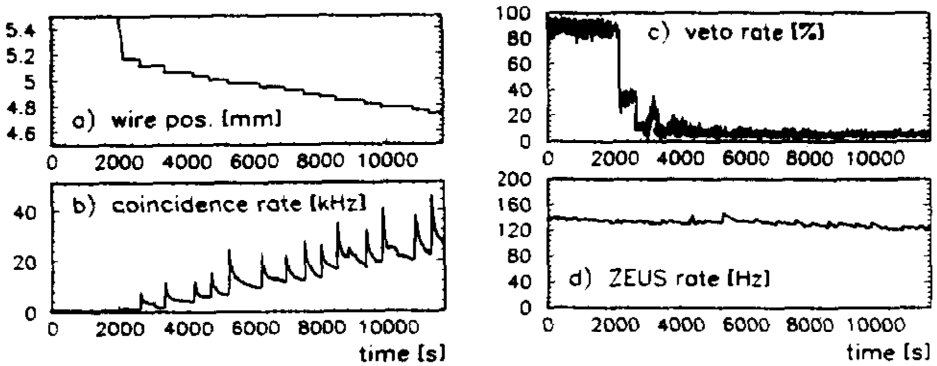

Figure 2: Wire scan information versus time: a) Horizontal wire position; b) ORed coincidence rate using three scintillator telescopes; c) percentage of triggers with VETO counters fired; d) background rate measured by the proton gated ZEUS scintillator C5.

to a new equilibrium and the beam lifetime recovered[1]. The equilibrium rate increased steadily while the wire was moved in, showing its increasing efficiency in scraping protons with increasing distance from the collimator shadow. The percentage of triggers with VETO counters firing dropped to 5% after the first few wire moves and stayed at this level for the rest of the experiment.

The transient after a wire step can be semi-quantitatively understood. The wire cleans up the halo with betatron-amplitudes beyond the wire position and the beam profile is slowly re-adjusting to the new boundary condition given by the wire. The shape of the rate dependence after a wire step is identical to that observed on the pin-diodes after a collimator is moved in. The only quantitative difference is the transient time which is about a factor of 5 longer for the wire than for the collimator. This is no surprise since the wire is acting like a semi-transparent scraper and particles with amplitudes beyond the wire position thus have a finite lifetime.

During the whole operation the data taking of the other HERA experiments was not disturbed. Fig. 2d shows the ZEUS background rate, which stayed constant throughout the run and was only little affected by the wire movements.

4. EVENT TOPOLOGY

It was shown in the last section that the rate of VETO events drops quickly to about 5% of the total trigger rate when the wire moves in and then stays at this level independently of the total interaction rate. There are two possible origins of this 5% remnant:

- The wire disturbs the beam and thus produces beam background events, the rate of which scales exactly with the interaction rate.
- In the real inelastic interactions in the wire, a significant number of tracks are emitted backwards, so that a VETO counter is hit in roughly 5% of the cases.

The following analysis shows that the second effect is most probably the dominating one.

Fig. 3 shows the time spectra of VETO hits in events where one (hatched histograms) or both (open histograms) VETO counters fired. When the wire is totally retracted, the

[1]We checked in a dedicated experiment, in which the wire stayed in one position for about 30 minutes, that the rate really reaches an equilibrium.

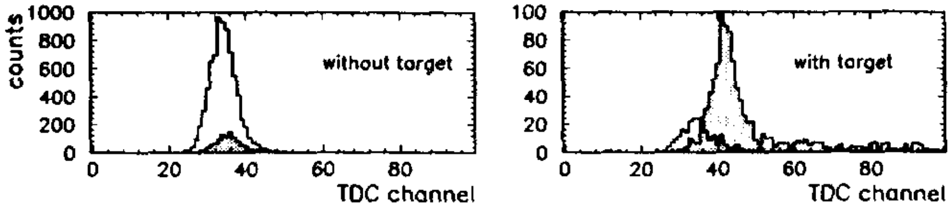

Figure 3: Time spectra of events, where one (hatched histograms) or both (open histograms) VETO counters had fired. One TDC channel corresponds to 0.6 ns. The spectra are shown for the wire retracted or fully moved in.

background events set both VETO counters at once in almost all cases. When the target is moved in, however, $\approx 80\%$ of the events set only one counter, showing the presence of a new low multiplicity component in the counters. In addition, in these events where only one VETO counter is set, the VETO signal is delayed by ≈ 3 ns with respect to the beam background. This could be due to slow particles coming from the target; it takes the beam 1 ns to arrive at the wire target, and secondary particles near the velocity of light would reach the VETO counters 1 ns after the interaction of a halo proton in the wire, i.e., after a total delay of 2 ns.

In a more quantitative analysis[2] of the rates of single and double VETO hits we could extract the fraction of background events triggering the detector. The measurements indicate that the wire does not increase the background but cleans up the beam (at least locally), such that the background rate is reduced by a factor 2 to 3.

The interpretation of the VETO signals requires the existence of slow particles moving into the backwards hemisphere. The origin of these particles is not obvious, since a proton interaction with a nucleus in the wire produces secondary particles strongly boosted in the forward direction. Simulations based on the FRITIOF[3] generator and a GEANT detector simulation in fact predict that less than 1% of the interactions should produce a particle hitting a VETO counter.

One possible explanation is the production of nuclear fragments, not included in the event generator. These fragments are protons with kinetic energies below a few hundred MeV, observed by several experiments in hadronic interactions over a wide range of center of mass energies[4]. At the smallest kinetic energies (below 25 MeV) these fragments are produced isotropically. With increasing energies they acquire a slight forward boost. The multiplicity produced in interactions with nuclear targets is a strong function of the mass number of the target nucleus. Heavy target materials, like the copper wire used in our test experiment, therefore have a certain disadvantage as compared to lighter targets, since the slow moving fragments can produce considerable radiation damage to detector elements.

An independent hint for the existence of extra particles not properly described by the FRITIOF generator is obtained from the analysis of the event topology in the forward hemisphere. It is observed that the trigger telescopes are more strongly correlated, i.e. fire more often simultaneously, than expected from Monte Carlo events. The events are thus more crowded than expected. This effect is not yet quantitatively understood.

5. TARGET EFFICIENCY

The interaction rates measured in the test run (10 to 100 kHz) are small as compared to the requirements for a B experiment (10 to 50 MHz). The main reason is the fact that the machine is still running with a small fraction of the final design current. A quantity

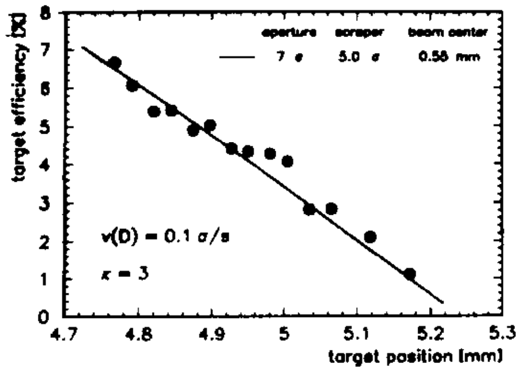

Figure 4: Target efficiency obtained from the observed coincidence rate as function of the target position (relative to an arbitrary zero-point near the assumed center of the beam pipe). Also shown is the efficiency predicted by tracking simulations.

which is more useful than the absolute interaction rate is therefore the target efficiency, i.e., the fraction of protons interacting in the wire as compared to the total number of protons leaving the machine. Target efficiencies of 50% are sufficient to reach the desired interaction rate for design proton currents and design lifetimes of the proton beam[1].

The target efficiency, ϵ_T, can be computed using the number of protons, N_p, stored in the machine, the lifetime τ_p of the proton beam, and the measured interaction rate on the wire, R^{wire}:

$$\epsilon_T = \frac{1}{\epsilon_{acc}} \cdot \frac{\tau_p}{N_p} \cdot R^{wire} \quad . \tag{1}$$

Here, ϵ_{acc} is the acceptance of the trigger telescopes, which has to be estimated by Monte Carlo simulation. For the test set-up we find $\epsilon_{acc} = 43\%$ based on the FRITIOF generator and the GEANT detector simulation.

The coincidence count rates of Fig. 2, always taken ten minutes after the last wire movement, were converted to target efficiencies, shown in Fig. 4 as function of the target position (relative to the assumed center of the beam pipe). At about 5.24 mm the wire leaves the shadow of the collimators and the target efficiency starts to become non-zero. At 4.7 mm (i.e., about half a r.m.s. beam width further in) the efficiency reaches 6 to 7%.

A single particle tracking simulation[1] was used to predict the target efficiency for the single wire target of the test experiment. The prediction is indicated in Fig. 4. It is in good agreement with the measurements. We used estimates for the actual machine parameters, in particular a tight collimator setting at 5 σ. We also varied assumptions on the drift speed of halo particles as well as assumptions on coupling and absolute beam position. The predicted target efficiency was found to be rather insensitive to these parameters.

The target efficiency in the test experiment was limited by the large β-function and the tight aperture. In a control experiment with only protons in the machine (and experiments switched off) we opened the collimators and reached interaction rates of 100 kHz, corresponding to 15% target efficiency. The aperture was in this case still limited by an unidentified obstacle in the proton ring around 5.5 σ (horizontally).

6. SUMMARY

The first phase of test experiments using internal wire targets has led to a proof of principle of the technology, together with rather detailed understanding of the mechanisms relevant for the interaction of wire targets and beam halo. The main results are:

- Interactions of halo protons with the wire have been observed with rates up to 100 kHz.
- The wire does not produce large beam background; it reduces the beam lifetime to typically 40 to 50 h.
- Tracking simulations are able to quantitatively predict the observed interaction rates. Extrapolating to design parameters, the models predict rates sufficient for a major B experiment at HERA.
- Transients of rates observed directly after a wire movement resemble those expected for a semi-transparent scraper.

Nonetheless, a number of problems remain. The most serious ones are the unexpected event topology, suggesting that the events are more crowded than expected, and the time structure of VETO signals, suggesting the existence of a component of more or less isotropically produced slow particles. These problems will be attacked by a more sophisticated target and detector, which have been installed for the 1993 run. We are confident that these tests will give the final proof of the feasibility of a halo target for the planned B experiment.

7. REFERENCES

1. H. Albrecht et al., *An Experiment to Study CP Violation in the B System Using an Internal Target at the HERA Proton Ring*, Letter of Intent, **DESY-PRC 92/04** (1992).
2. H. Albrecht et al., *An Experiment to Study CP Violation in the B System Using an Internal Target at the HERA Proton Ring*, Progress Report, **DESY-PRC 93/04** (1993).
3. B. Andersson, G. Gustafson and Hong Pi, **LU-TP-92-20** (1992).
4. A. Abduzhamilov et al., *Z. Phys.* **C40** (1988) 1, *Z. Phys.* **C40** (1988) 223;
   J.A. Gaidos et al., *Phys. Rev. Lett.* **42** (1979) 82;
   J.E. Finn et al., *Phys. Rev. Lett.* **49** (1982) 1321;
   A.S. Hirsch et al., *Phys. Rev.* **C29** (1984) 508.

EXTRACTION FROM TEV-RANGE ACCELERATORS USING BENT CRYSTAL CHANNELING

R. A. CARRIGAN, JR., G. JACKSON, and C. T. MURPHY
Fermilab, Batavia, Illinois 60510, USA

and

B. NEWBERGER
University of Texas, Austin, Texas 78712, USA

Abstract

Plans and first results from Fermilab Experiment 853 are presented. E853 is an experiment to test the feasibility and efficiency of extracting a low-intensity beam from the halo of the Tevatron using channeling in a bent silicon crystal. The motivation of the experiment is to apply crystal extraction to trans-TeV accelerators like the SSC. Channeling developments related to crystal extraction and some early results from accelerator studies at the Tevatron are presented.

1. INTRODUCTION

The possibility of beam extraction from accelerators using bent crystals has been discussed since Tsyganov first proposed bent crystal channeling [1]. Protons have already been extracted using bent crystals at Dubna [2], Serpukhov [3], and the SPS at CERN [4]. The idea of extracting halo beam from the SSC with a bent crystal was first seriously discussed by C. R. Sun [5]. Further considerations of the idea [6,7,8] led to a proposal [9] that the SSC (Superconducting Super Collider) East Campus footprint be modified to make this possibility feasible at a later time. The possibility of an SSC facility led to a proposal for an experimental feasibility study of this extraction method in the Fermilab Tevatron, a superconducting accelerator very similar to the SSC. This experiment (E853) has now been approved for 72 hours of dedicated study time during the Fermilab Collider Run in 1994. Some of the accelerator tests connected with the experiment have already been carried out.

The experiment and the associated channeling studies have several goals. For channeling the crystal must be able to be aligned to the beam quickly, crystal quality must be satisfactory, and the crystal must be able to survive the radiation damage due to the proton beam. One goal of the accelerator experiment is to extract one million 900 GeV/c protons/s with 10^{12} protons circulating. Other goals are to show that the luminosity lifetime is not seriously shortened and that no intolerable backgrounds are created at the Tevatron collider experiments. In addition, the relationship between the RF (radio frequency) modulation amplitude used for extraction and the extraction efficiency will be determined.

2. SSC EXTRACTION

The idea of extracting the natural halo of the circulating SSC beam to make low-intensity beams has intrigued people for the last decade. Since this halo will eventually be absorbed on "scraper" collimators, why not put it to better use? The current proposal is to install a copy of the abort insert planned for the SSC West Utility Straight Section in the unused East Utility Straight Section, but with a bent crystal replacing the abort kicker magnets. Details of the SSC extraction concept are given in the next paper of these proceedings and in Ref. 10.

3. THE TEVATRON EXPERIMENT

E-853 is taking place in the C0 straight section of the Tevatron, the normal location of the proton abort line. The abort line consists of a three-bend magnetic dogleg that provides a 4 mrad horizontal kick so the abort line can clear the magnets at the downstream end of the long straight section. The middle bend in the dogleg consists of a series of Lambertson magnets. During collider runs, the abort line is not used at 900 GeV, so one of the kicker magnets has been replaced by a bent crystal. Further details are given in Ref. 11.

Two issues raised at this workshop were the effects of environmental noise on the beam stability and the possibility of accidently moving the entire circulating beam onto the crystal because of a large instability too rapid to trigger the beam abort promptly. The latter is judged to be impossible in either the SSC or the Tevatron, but further quantitative study is needed on both issues.

4. CHANNELING CONSIDERATIONS

Recent studies [12] indicate that for the crystal used for SSC extraction the number of type A dislocation loops should be kept small and that linear dislocations densities must be less than 1/cm^2. The silicon crystal to be used for Tevatron extraction has been selected to be dislocation-free (less than 1 dislocation/cm^2). A suitable sample was found by observing the line width in double x-ray scattering and by using film decoration techniques[13]. The 40 mm long crystal is 10 mm wide and 3 mm thick so that it is substantially thicker than the vertical beam diameter (σ_y=0.32 mm). With the use of x-ray scattering the crystal has been oriented so that the curved surface contains a (110) plane that will be parallel to the accelerator beam at the upstream end of the crystal. The techniques used for this crystal analysis are described in more detail in other publications [13].

The alignment and flatness of the vertical surface facing the circulating beam (the effective septum face) are critical factors. The 640 μrad bend angle of the crystal must be controlled to 120 μrad, half the acceptance angle of the extraction channel. These issues are also discussed in Ref. 11.

An analysis [14] of the effect of the crystal bender on the crystal lattice was carried out with the finite element program ANSYS to simulate the stresses and deformation in the crystal while being squeezed in the holder. It was found that due to the finite stiffness of the aluminum benders and the flap-back of the bent crystal, a design bend for the aluminum bender of 0.96 mrad was required to get an actual full bending angle of 0.64 mrad in the crystal. Along the surface of the crystal facing the beam, the variation of this bend angle was negligible at the entrance and exit of the crystal due to the silicon overhang beyond the lengths of the aluminum pieces. The force required to accomplish this bend is less than 5 kg with a maximum stress in the crystal of less than 10^7 pascals.

The possibility of radiation damage of the crystal has been investigated. In a study at BNL[15] at high fluence we have found measurable radiation-induced dechanneling produced at a fluence of $4*10^{20}$ protons/cm^2. While this is of some concern at the beam intensities expected for the SSC, particularly for radiation-induced dislocations[12], it is not significant for the lower beam intensities and short runs planned for the Tevatron tests. Heating effects of the beam losses on the crystal have also been calculated and are negligible at the Tevatron.

5. CRYSTAL IMPACT EFFICIENCY

The challenge is that there is inadequate natural halo, in either the SSC or the Tevatron, to obtain extracted intensities high enough to be interesting for experiments. Halo must be generated by perturbations of either the transverse or longitudinal phase space in a manner which does not appreciably decrease the collider luminosity. As a result, the usual method of resonant extraction in the horizontal plane is not permitted. For that reason, techniques have been investigated that create off-momentum halo in longitudinal phase space using RF voltage modulations and thereby continuously populate the region of phase space near the crystal. The crystal is placed at a point of high dispersion so that the off-momentum particles are at large x at the crystal.

In this approach particles which are already in the tail of the momentum distribution are rapidly excited to larger momenta so as to achieve large step sizes, without affecting very much the core of the momentum distribution. The most promising technique of populating the halo (the CERN [16] approach is along the same line) is by generating amplitude-dependent diffusion rates in either the longitudinal (SSC and Tevatron) or transverse (LHC and SPS) planes. By generating a signal which has a small effect at low amplitudes but generates large particle diffusion rates at greater oscillation amplitudes, luminosity lifetime can be preserved while creating a steady state population of particles which feed into the crystal. These are observed in Monte Carlo simulations to strike well into the crystal (greater than 1 μm) with the betatron motion aiding the penetration. This avoids surface irregularities and crystal edge misalignments and maximizes the extraction efficiency. This diffusion rate profile is generated by taking advantage of phase space non-linearities which create amplitude-dependent particle tunes. Since each particle reacts only to RF signals at their local resonant frequencies, frequency-dependent signal power densities cause amplitude dependent diffusion rates. Though in most cases simply-shaped random RF noise is utilized, more complicated waveforms have also been investigated as a mechanism to improve the mean penetration depth into the crystal [17].

A diffusion model [18] has been developed for crystal extraction using RF noise-induced halo growth based on a diffusion equation. This has some similarities to the diffusion in transverse energy approach used for analyzing crystal dechanneling. Monte Carlo simulations (1000 particles) have also been used to track diffusing particles through a million turns of the SSC lattice. The diffusion results (which are less computationally intensive) and the simulation program agree. The simulation shows that there are viable scenarios to provide halos without disturbing the core of the beam.

We are also investigating a second approach to increasing the penetration depth into the crystal by adding another thin, aligned crystal to spread the beam with channeling oscillations. This could increase the penetration into the bent crystal substantially and relax the radiation load on the crystal. Another idea being explored is the use of a simple thin multiple-scattering target to achieve the same effect [19].

6. EARLY RESULTS RELATED TO TeV-RANGE EXTRACTION

During the recent Tevatron collider run, an unbent crystal was placed at the planned location of the bent crystal but to the outside of the ring. This was used to study whether halo beam scattered by the crystal created intolerable backgrounds at either of the two collider experiments [20]. Several sets of measurements were performed. The effect of RF noise on the beam in the absence of collimation was studied during a store at 900 GeV. Collimation effects were also observed with conventional collimators and the silicon crystal at the proposed bent crystal location.

For the diffusion studies two levels of external random noise were applied to the RF system. With an rms external voltage of 500 mV, corresponding to an rms RF gradient fluctuation of 5 KV/turn, it was found that the longitudinal density narrowed while there were many more particles at large amplitude. Once the equilibrium shape of the longitudinal bunch distribution was established, an exponential particle loss rate appeared. With 5 KV/turn noise, the relative proton loss rate corresponded to a beam lifetime loss constant of 12 minutes. With a reduced noise level of 50 mV (an RF voltage jitter of 500 V rms) the loss rate time constant was 17 hours, so that a factor of 10 reduction in noise amplitude was responsible for a 100-fold loss rate reduction. The nominal intensity time constant for Tevatron Collider protons varies from 40 to 120 hours.

To estimate the impact of a bent crystal on the CDF (Collider Detector at Fermilab) detector a horizontal collimator was placed next to the beam at A0, one-third around the ring from C0. The collimator was brought in until losses were observed on it. The rms RF amplitude noise level was set at 500 V/turn. Even though this noise level induced a loss rate ten times that which is desired for crystal extraction, the maximum proton background rate measured in the CDF detector was 5 KHz. Depending on the luminosity, a background rate below the 5-10 KHz range is considered acceptable at the CDF detector.

In order to assure that the measurements made with the collimator were meaningful for crystal extraction calculations, an unbent silicon crystal was installed on the radial outside of the accelerator beam, so that it could not intercept DC beam. (DC beam consists of those particles which have diffused out of the RF bucket and are spiraling radially inward due to synchrotron radiation losses.) On the other hand, particles with large betatron amplitudes could strike the silicon crystal as their momentum error increased. With the crystal as the primary aperture and the same diffusion conditions as above (10 times that planned for extraction), it was found that the CDF loss increased from approximately 2 KHz to 10-15 KHz.

Based on these studies, the effects of crystal extraction should have little or no deleterious effects on a collider experiment and it should be possible to perform parasitic studies of crystal extraction during a collider run.

A group at CERN is currently carrying out a similar experiment [4,16] in the SPS, operating at 120 GeV. Their method of inducing diffusion is to introduce white noise on a horizontal damper (electrostatic plates capable of deflecting the beam a few tens of μrad). To date, they report extracting beam with an efficiency of about 9%. Their studies indicate that it is important to consider multi-turn extraction, since a particle first incident on the crystal with an angle greater than the critical angle will be multiply-scattered by the crystal to a different point in phase space and often will reenter the crystal on a later betatron oscillation with a smaller angle.

7. ACKNOWLEDGEMENTS

We would like to acknowledge the support of the SSC Laboratory for the equipment for this experiment. This work was supported in part by the US Department of Energy under contracts DE-AC35-89-ER-40486 and DE-AC02-76CH0300. One of us (BSN) would like to acknowledge support by the Texas National Laboratory Commission under Grant RGFY 93-321.

8. REFERENCES

1. E. N. Tsyganov, Fermilab TM-682 (1976).
2. V. V. Avdeichikov et al., JINR 1-84, Dubna (1984). English translation: Fermilab FN-429 (1986).
3. See, for example, A. A. Asseev, M. Bavizhev, E. A. Ludmirsky, V. A. Maisheev, and Yu. S. Fedotov, *Nucl. Instr. and Meth.* **A309** (1991) 1.
4. H. Akbari et. al., *Phys. Lett.* **B313** (1993) 491.
5. C. R. Sun, R. A. Carrigan, Jr., T. E. Toohig, and D. Neuffer, in *Proceedings of the Summer Study on the Design and Utilization of the SSC (Snowmass)*, eds. R. Donaldson and J. Morfin (APS, New York, 1984), p. 483.
6. M. Harrison and T. Toohig, in *Proceedings of the 1986 Summer Study on the Physics of the SSC (Snowmass)*, eds. R. Donaldson and J. Marx (APS, New York, 1986), p. 534.
7. A. S. Vodopyanov et al., "Slow Extraction of 20 TeV Accelerated Beam out of SSC Using a Bent Crystal", preprint of the Joint Institute for Nuclear Research, Dubna (1987).
8. B. Cox et. al., in *Proceedings of the Summer Study on High Energy Phsyics in the 1990's (Snowmass)*, ed. S. Jenson (World Scientific, New Jersey, 1988), p. 538.
9. C. T. Murphy and R. Stefanski, SSCL-428 (1989).
10. B. Parker, C. Dukes, and C. T. Murphy, SSCL-643 (1993).
11. C. T. Murphy, in *The Fermilab Meeting: DPF 92* (Proceedings of the 7th Meeting of the APS Division of Particles and Fields), ed. Carl H. Albright (World Scientific, Sinapore, 1993), p. 1615.
12. V. M. Biryukov, M. D. Bavizhev, and E. N. Tsyganov, SSCL-N-777 (1991).
13. V. V. Baublis et al., *Nucl. Instr. and Meth.*, to be published (1993).
14. Z. Tang, Fermilab TM-1827 (1993).
15. S. Baker et al., *Nucl. Instr. and Meth.*, to be published (1993).
16. S. Weisz, et al., "Proton Extraction from the CERN SPS by a Bent Crystal", *Proc. 1993 Part. Acc. Conf.* (Washington, DC 1993).
17. W. Gabella, J. Rosenzweig, R. Kick, and S. Peggs, "RF Voltage Modulation at Discrete Frequencies, with Applications to Crystal Channeling Extraction", *Proc. 1993 Part. Acc. Conf.* (Washington D.C. 1993). Fermilab TM-1783.
18. B. S. Newberger, H. J. Shih, and J. A. Ellison, *Nucl. Instr. and Meth.* **A235** (1993) 9. B. S. Newberger, H. J. Shih, and J. A. Ellison, *Phys. Rev. Lett.* **71** (1993) 356.
19. A. Asseev et. al., *Nucl. Instr. and Meth.* **A324** (1993) 31.
20. G. Jackson, "Results from Beam Diffusion and Collimation Measurements in Preparation for Fermilab Tevatron Crystal Extraction", *Proc. 1993 Part. Acc. Conf.* (Washington D.C. 1993).

SYNOPSIS OF A DESIGN OF A CRYSTAL EXTRACTION FACILTIY IN THE SSC EAST UTILITY STRAIGHT

E.C. DUKES
Dept. of Physics, University of Virginia
Charlottesville, VA 22901, USA

C.T. MURPHY
Fermilab, Box 500, Batavia, IL 60510, USA

B. PARKER
SSC Laboratory, Dallas, TX 75237, USA

1. INTRODUCTION

The option of extracting a small faction of the circulating 20 TeV SSC beam has been discussed for some time (see previous article in this volume). The potential uses of such a beam would be many, but in particular, the opportunities of doing B physics are very appealing and have led to an Expression of Interest (EOI-14) which discusses extracting approximately 10^8 protons/sec from the halo of the circulating beam using a bent silicon crystal [1]. From the beginning the SSC has recognized the exciting physics potential of an extracted beam, and the SSC footprint includes a stratified fee land area and a buried beam zone access area for the muon vector from an extracted beam hall [2].

In this memo we consider the implementation of a crystal extraction system in the east utility straight of the SSC. We show that an extraction system can be added with only minor alterations to the collider: the addition of a three-magnet dogleg (identical to that designed for the west utility straight); the addition of two dipole strings; and the addition of a 160 meter long alcove to mate the extracted beam line microtunnel to the collider tunnel. The present scheme to allow for momentum scraping in the east utility straight is not affected. The design of the alcove is similar to that of the two alcoves needed for the scraper shielding in the east utility straight. As is the case with the scraper alcoves, excavating the alcove before the tunnel is finished is cost effective and would alleviate much of the disruption and added cost involved in adding an alcove to the finished tunnel at a later date. The full details of this scheme are found in an SSCL Report [3].

2. SHORT DESCRIPTION OF EXTRACTION SYSTEM

The east utility straight is 1350 meters long. Details of the utility straights, including magnet and spool piece specifications, are given in reference [4]. Changes to the lattice to make the dispersion large in the east utility straight, thus making momentum scraping possible, are still in progress. The dispersion needed for momentum scraping is consistent with that needed for crystal extraction. Momentum scraping will be done with a system of scrapers and collimators situated in a warm dogleg. The extraction scheme proposed here is consistent with the present ideas for momentum scraping, although the dogleg angle required for extraction is slightly larger in order to allow the extracted beam to completely miss the spool pieces and cryostats of downstream magnets.

The extraction line is shown in schematic form in Fig. 1. The circulating beam is bent toward the outside of the ring by a dipole magnet. Immediately after the dipole a silicon crystal bends a small fraction of the beam halo in the vertical direction. The channeled particles enter the field-free region of a Lambertson magnet string and continue on down the utility straight. Near the end of the dogleg a warm dipole string steers the beam into an alcove situated at the end of the east utility straight. A string of standard collider dipole magnets at the alcove bends the extracted beam further away from the utility straight and into a microtunnel of 18 inch diameter and 150 meter length. Another microtunnel of 48 inch diameter follows, connecting to a 15 foot diameter shaft. After the two microtunnels the beam is far enough away from the collider tunnel to allow for shafts and large diameter tunnels to be excavated without compromising the integrity of the collider tunnel.

3. MAGNET LAYOUT FOR THE EXTRACTION SYSTEM

The dogleg portion of the extracted beam is a direct copy of the dogleg used for the beam abort in the West utility straight (with a few elements such as the abort painters and blowup quadrapoles removed). The lower beam (which is going north) is bent 1.266 mrad towards the outside of the tunnel (away from the center of the ring) by a 13 meter BSM dipole magnet. After the BSM magnet a two meter insert houses the crystal and goniometer which is moved horizontally into the halo of the circulating beam. The crystal is slightly bent in the vertical direction to give a bend of 160 μrad upward to channeled protons. The channeled protons enter the field free region of a 144 meter long Lambertson string and continue on past the magnets at the end of the dogleg.

The positions of the scrapers and collimators in the east utility straight are consistent with the addition of the Lambertson and closed orbit dipole magnets. Omitted from Fig. 1 is the shielding required for the momentum scrapers and the position of the alcoves to accommodate the shielding. They are positioned at approximately 150 ± 15 meters from the center of the straight and are 25 meters long.

The extracted beam goes through the magnet supports of the three magnets at the end of the dogleg. If the tunnel wall is at its nominal value, or further out from the theoretical tunnel center, then a magnet support identical to that being designed for the west utility straight, where the beam abort also goes through magnet supports, can be used. Otherwise, a special magnet support will be needed for the three magnets at the end of the dogleg.

A trim magnet (ED1) is needed for fine pointing the beam to the alcove. There is about 30 meters of free space between the last collimator and the magnet string at the end of the dogleg. The ED1 magnet string is placed in this location. A bend of 0.308 mrad is needed to get the beam to the proper position at the start of the alcove. This would require a field of 20.54 Tm or 5 standard TUD warm dipoles with a 17.5 meter slot length. They fit comfortably in the allowed space.

4. ALCOVE DESIGN

The alcove starts just after the QU4 quadrapole magnet at 1160 meters from the start of the East utility straight and is 160 meters in length. The alcove depth is 3 feet for the first 120 meters and 4 feet for the remaining 40 meters.

The alcove has been positioned to begin just after the QU4 dipole and end just before the end of the east utility straight. By situating the alcove at the end of the straight, advantage is taken of the sharp turn the circulating beam takes in the DS region, separating the extracted beam line tunnel and collider tunnels apart as rapidly as possible. This minimizes the length of microtunnel needed to transport the beam to the first shaft (which is required to be at least one shaft diameter from the collider tunnel).

A sharp bend is needed in order both to get the beam deep enough into the alcove to allow a microtunnel to be bored, and to increase the angular separation of the extracted beam from the collider tunnel. The bend (ED2) is done by 5 standard 15 meter collider dipoles with a total bend angle of 7.6 mrad. The ED2 string is situated between QU4 and QF and hence the cryo and power from the lower ring can be used. Special spool pieces transferring the cryo and power need be designed. After the ED2 magnet string is a quadrapole magnet, EQ1, which is identical to QU1 (8.825 meter slot length) and which allows the size of the beam at the experimental target to be controlled.

5. THE EXTRACTED BEAM TUNNEL

The use of microtunnels allows a modest sized alcove to be used to mate the collider tunnel with the extracted beam line. The minimum diameter microtunnel that can be bored for a reasonable distance is approximately 18" in diameter. This size microtunnel would be 150 meters in length and would be followed by a microtunnel of 48" diameter and 200 meter length. (An 18" diameter tunnel cannot be bored for the full 350 meter length without the possibility of large deviations from the nominal line.) After 350 meters the beam line is far enough away (approximately 8 meters) from the collider tunnel to allow a small hall to be excavated without affecting the integrity of the collider tunnel. The hall would be $15 \times 15 \times 40$ ft^3, which is an adequate size for the tunneling machine and associated machinery. A shaft to the surface would be at this hall.

The position of the experimental hall shown in Fig. 1 is essentially the same as that proposed by Murphy and Stefanski [5]. The beam line would be microtunnel with occasional shafts for access to trim magnets, pumps and other equipment. Detailed design of the beam line is yet to be worked out. In order to avoid the muon vectors coming from IR5 (GEM) and IR8 (SDC) the experimental hall is located 2,000 meters from the end of the east utility straight. At this point the hall is about 560 feet from the collider tunnel, well within the fee simple land acquired by the SSC. There is no water above the experimental hall preventing a shaft from reaching the surface.

6. COST ESTIMATE

A preliminary cost estimate has been performed by Gunter Matthes of PBMK [6]. This estimate includes overhead and design and construction management fees. The alcove is estimated to cost about $1.0M, and the microtunnels, shaft, and first access chamber are about $1.6M. These estimates are very conservative and undoubtedly overstate the true cost. In particular, the estimates of the microtunnel costs are little better than rough guesses at $775 and $550 per linear foot respectively for 48" and 24" diameter tunnels (no estimate for an 18" diameter tunnel was possible). These should be compared to the costs of $1,000 and $600 per linear foot respectively for the lined and unlined collider tunnels!

Matthes' estimate of the time needed to complete the excavation of the alcove is 4 months. Note that the tunnel is in Taylor Marl, which greatly adds to the alcove cost. The time needed to excavate the shaft, chamber, and microtunnel is estimated to be 3, 1, and 2.5 months respectively.

These estimates assume that the alcove would be excavated before the tunnel is finished, that is, after only the liner and perhaps floor have been added to the excavated tunnel. Excavating the alcove after the tunnel is finished would be far more expensive and could disrupt the collider construction timetable. At this time it is not known when the east utility straight tunnel will be finished.

We have no cost estimate for the tunnel to the experimental area or the experimental hall itself. Nor have we made estimates of the cost of the magnetic elements as it is impossible at this time to get reliable figures.

7. ACKNOWLEDGEMENTS

The authors would like to thank N. Mokhov, J. Shively, R. Smellie, and T. Toohig for suggestions and discussions.

8. REFERENCES

1. The SFT Collaboration, *An Expression of Interest in a Super Fixed Target Beauty Facility at the SSC*, EOI-14, submitted to the SSC PAC, 25 May 1990.
2. L. Coulson, R. Crawley, H. Edwards, D. Getz, M. Gilchriese, R. Schwitters, P. Shelley, R. Stefanski, and T. Toohig, "Footprint Characterization Document", SSCL-SR-1041 (Rev. 1), June 1992.
3. B. Parker, C. Dukes, and C. T. Murphy, SSCL-643, October 1993.
4. "Collider Accelerator Utility Sections", Specification No. E10-000073, Issue Date: 3/8/93, Revision: Draft E.
5. C.T. Murphy and R. Stefanski, "Modification to Footprint to Accommodate an External Fixed-Target Hall", SSCL-428, September 1989.
6. Gunter Matthes, private communication.

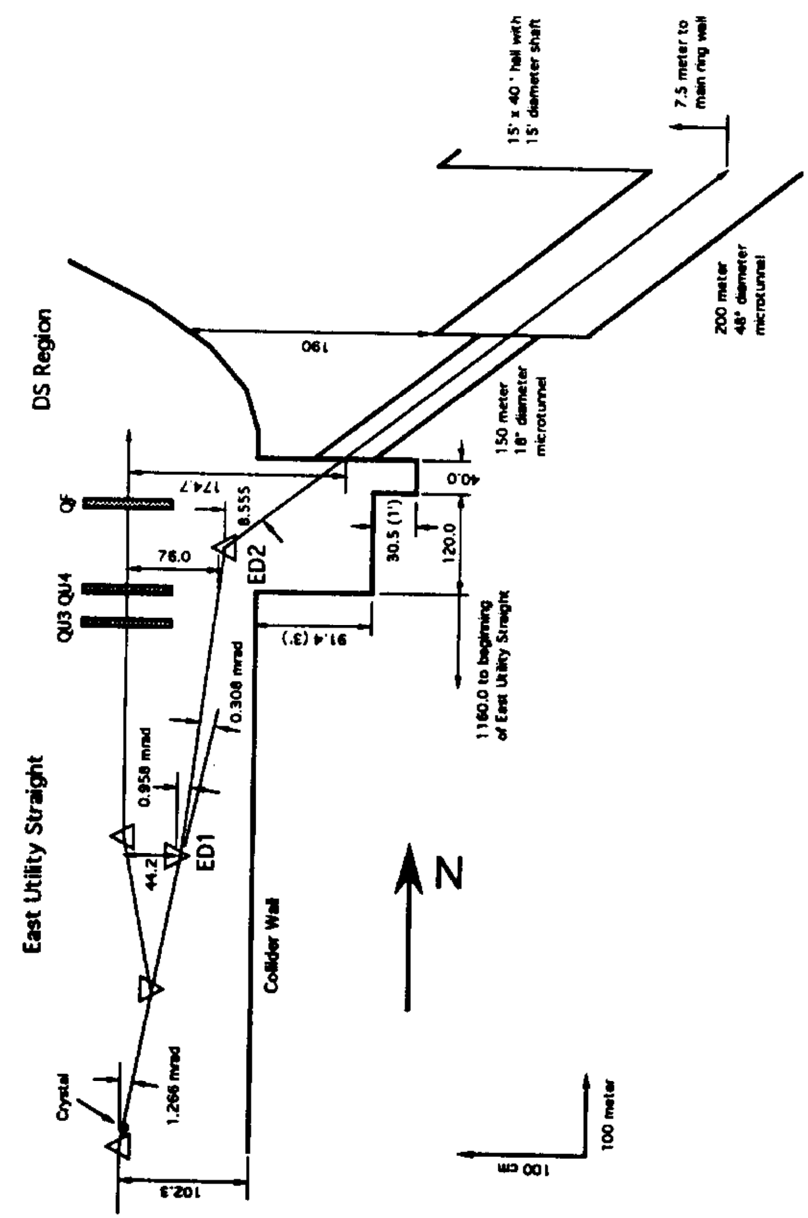

Fig. 1: Plan view of the extraction line for the east utility straight showing the alcove and the microtunnel out to the first shaft. The positions of the magnetic elements are given in meters from the beginning of the east utility straight. Units along the beam direction are in meters whereas units transverse to the beam direction are in centimeters.

DESIGN OF THE SSC MEDIUM-BETA INTERACTION REGIONS

YURI M. NOSOCHKOV
Superconducting Super Collider Laboratory *
2550 Beckleymeade Avenue, Dallas, TX 75237, USA

1. INTRODUCTION

In the SSC design[1] the 87.12 km long collider lattice consists of two 35.28 km identical arcs located on the North and South sides of the machine and two 8.28 km clusters placed on the West and on the East. Each cluster contains two Interaction Regions (IRs), the Utility section and the interconnect sections between them. According to present plans the goal for the optics in the East IRs is to provide for a high value of the luminosity and, hence, for a low β^* at the Interaction Point (IP). The West IRs are aimed at providing for a large space for detector which can be achieved at the cost of higher value of the β^* and lower luminosity.

The optics of each IR are based on the same optical configuration which gives an opportunity to use mostly identical quadrupoles and dipoles in four IRs. Trivial modification of the central region in this basic configuration allows for a wide range of values for detector free space from $L^* = 20$ m to $L^* = 90$ m, suitable for the experiments in both clusters. L^* denotes here the distance between the IP and the nearest magnetic element of the machine. In this paper we briefly review the current design of the so-called medium-β IR optics with a large free space for detector of $L^* = 90$ m, which could be used in the West cluster.

2. IR CONFIGURATION

Figure 1 shows a vertical schematic view of a complete IR.[2] The total IR length is 1890m. The first beam goes along its beam line from the top left side on the picture to the bottom right, while the second beam starts at the top right and proceeds to the bottom left side. The vertical dipoles straddle the beam lines, the focusing quadrupoles are shown above the lines and the defocusing quadrupoles below. The optics are antisymmetric with respect to the IP, which means a mirror symmetrical magnet locations, but opposite magnetic fields on the left and right sides of the IR.

Each half IR is composed of three modules: the final focus triplet, the $M = -I$ section and the tuning section. Besides the quadrupoles there are vertical dipoles placed in two steps, which bring the beams into collision. The final focus triplet quadrupoles and adjacent splitting dipoles located in the center of the IR are common to both rings. The beams share the same beam pipe inside these magnets. The triplets focus the beams to extremely small sizes at the IP and, therefore, these magnets are quite strong (i.e., long). In the above

*Operated by the Universities Research Association Inc., for the U.S. Department of Energy, under contract DE-AC35-89ER40486

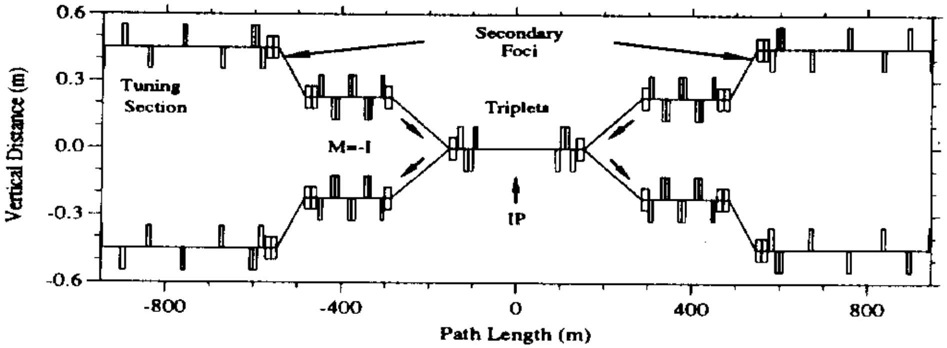

Figure 1: Vertical view of the IR. $L^* = 90$ m.

figure the triplet focusing polarities are shown for the first beam, and they are opposite for the second beam. The $M = -I$ section is a module of 8 quadrupoles providing the negative identity transfer matrix across this section. It is used to compensate for the vertical dispersion generated by the adjacent pairs of dipoles and it is located in the 45 cm vertical separation region which requires a 2-in-1 magnet design. The rest of the quadrupoles in the IR form the tuning section located in the region of standard 90 cm vertical distance between the rings. There are 6 families of the tuning quadrupoles in this section which have independent power supplies and provide a variable β^* at the IP.

It is an important design feature that the triplet gradients are not touched during the β-squeeze which allows a possibility for doing this procedure independently in two rings. Secondly, no additional magnetic errors are introduced in the triplets during the β-squeeze. Another optical feature is the inclusion of a secondary focus symmetrically on each side of the IR, a point at which the IP is imaged. This image can be used basically as a means of doing beam diagnostics at the IP.

3. OPTICAL PROPERTIES

In the present design with $L^* = 90$ m, the gradients of the tuning quadrupoles can be set to provide a minimum β^* of 1.95 m. This corresponds to a β_{peak} in the triplets of 9 km which is about the maximum value allowing a region of a good field quality for the beam in the 5 cm bore quadrupoles used in the IR. Theoretically, even lower value of β^* could be achieved with larger bore triplets. The lattice functions in the IR corresponding to $\beta^* = 1.95$ m are shown in Figure 2. This configuration provides a high luminosity and can be used at collision conditions. At injection energy, however, much lower β_{peak} value and, hence, higher β^* are required because of the larger beam emittance. The optimum solution for injection conditions is when the β^* is 40 m and the β_{peak} is reduced to less than 600 m.

A smooth transition between the two optical configurations is achieved by varying the gradients of the six quadrupoles in the tuning section. The variation of gradients during the β squeeze is shown in Figure 3. The above change of the gradients keeps the transfer matrix across the IR constant, thus not affecting the rest of the machine. It is planned that at normal operation conditions the β-squeeze will take place in each magnetic cycle shortly after the top energy is reached. Because of significantly slower change of the tuning gradients

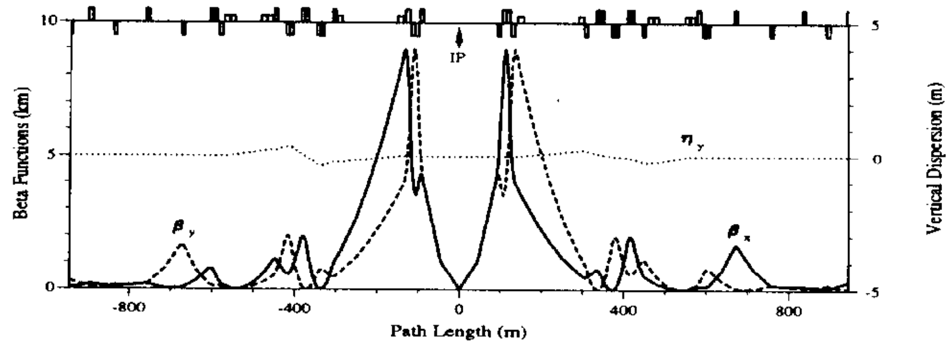

Figure 2: Lattice functions in the IR at collision. $L^* = 90$ m, $\beta^* = 1.95$ m.

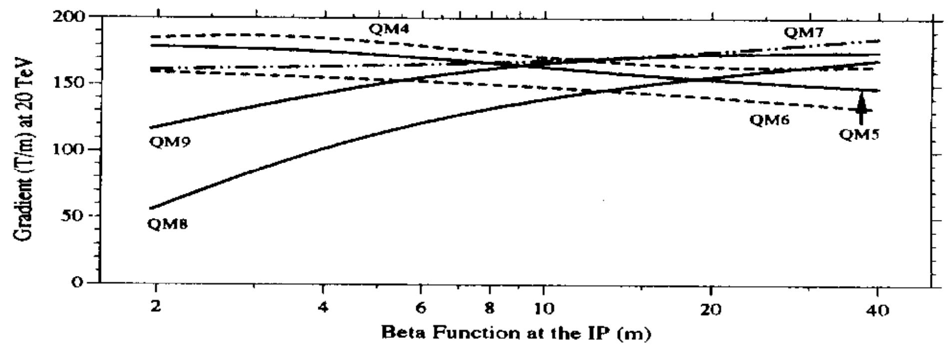

Figure 3: Tuning gradients. $L^* = 90$ m.

as a function of β^* at the beginning of the β-squeeze than at its end, an exponential change of the β^* with time will be applied. The approximate duration expected for the β-squeeze is about 100 seconds, which is consistent with technical requirements for a variation of the current with time in the quadrupole power supplies.

4. GENERAL PARAMETERS

Table 1 presents general SSC beam parameters and their comparison for the low-β and medium-β IRs. In the case of medium-β IR the parameters are presented for collision and injection values of β^*. Due to large proton energy in the SSC, the synchrotron radiation from the beam becomes so large that it causes a significant reduction of the beam emittance during store time and therefore an increase of the average luminosity.[3]

5. ALTERNATIVE IR CONFIGURATION

The current design of the IR optics provides for a wide range of the available space for

Parameter	Low-β IR, $L^* = 20.5$ m $\beta^* = 0.5$ m	Medium-β IR, $L^* = 90$ m $\beta^* = 2$ m / $\beta^* = 40$ m
Beam energy (TeV)	2×20	2×20
Initial luminosity ($cm^{-2}s^{-1}$)	10^{33}	$3 \cdot 10^{32}$ / $1.5 \cdot 10^{31}$
Average luminosity ($cm^{-2}s^{-1}$)	$1.4 \cdot 10^{33}$	$4.2 \cdot 10^{32}$ / $2.1 \cdot 10^{31}$
Interaction rate (s^{-1}) for $\Sigma = 80$ mb	$1.1 \cdot 10^{8}$	$3.4 \cdot 10^{7}$ / $1.7 \cdot 10^{6}$
Interactions per crossing	2.1	0.6 / 0.03
Store time (hrs)	24	24
Fill time (min)	72	72
Number of bunches per beam	15840	15840
Number of protons per bunch	$8.1 \cdot 10^{9}$	$8.1 \cdot 10^{9}$
Number of protons per beam	$1.3 \cdot 10^{14}$	$1.3 \cdot 10^{14}$
Initial rms beam size at IP (μm)	5	10 / 45
Bunch length (cm)	6	6
Bunch spacing (ns)	16.7	16.7
Typical crossing angle (μrad)	135	100
RF frequency (MHz)	360	360
Abort gap (μs)	4.93	4.93
Space for detector (m)	± 20.5	± 90
Number of IRs	2	2
Hall size (m^3)	$100 \times 30 \times 60$	TBD

Table 1: General SSC parameters for low-β and medium-β IRs.

detector from ± 20 m to ± 90 m around IP. A further increase of this space would require a modification of the baseline design. An example of such alternative optics is shown on Figure 4. It is almost the baseline configuration, except there are no 2-in-1 regions with $M = -I$ sections in this design. Hence, additional space is available between the final focus triplets and also outside them. The main problem in this design is a compensation of the vertical dispersion generated by the IR dipoles. The strengths of additional skew quadrupoles required to correct for this dispersion become unreasonably large at low and medium values of β^*. A possibility for such optics could be a high-β IR configuration.[4]

6. COLLIMATORS IN THE IR

Figure 5 shows locations of the collimators labeled CIR1, CIR2,..., etc. in one IR.[5] The scheme does not show all the magnets in the IR except those located next to collimators. The nearest to the IP collimators CIR01, CIR02 have fixed 25 mm diameter aperture to protect the 50 mm bore triplet quadrupoles. All the other collimators have movable jaws positioned at 16σ distance from the beam at injection energy and at 20σ at collision conditions.

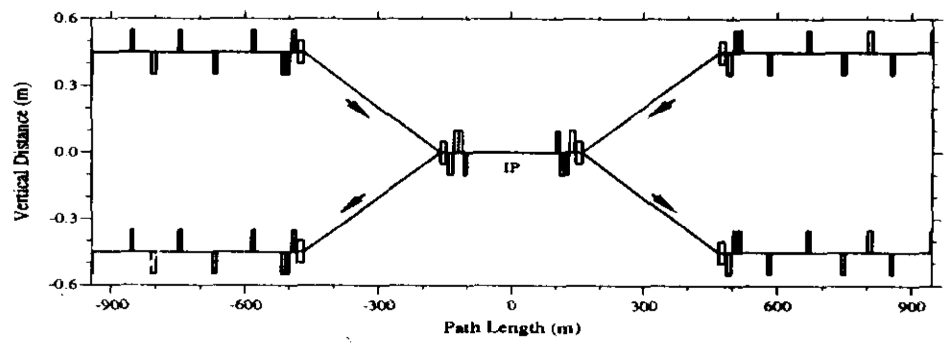

Figure 4: Alternative IR Design. $L^* = 100$ m.

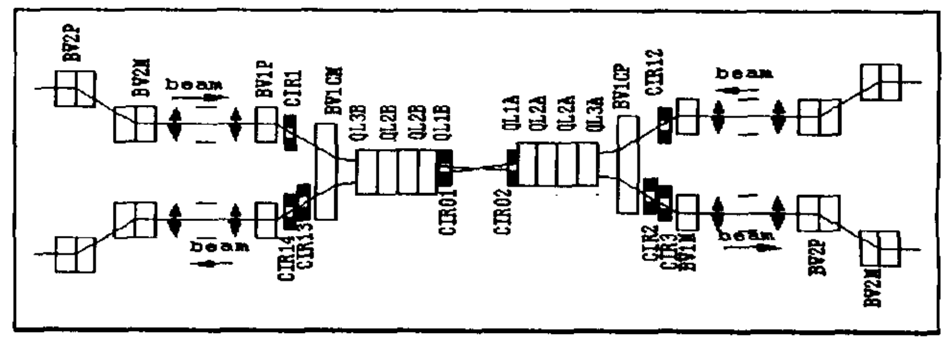

Figure 5: Collimators in the IR.

7. REFERENCES

1. J.R. Sanford, D.M. Mathews, Eds., *Site-Specific Conceptual Design*, SSCL Document SSCL-SR-1056 (1990).
2. Y. Nosochkov et al., "Current Design of the SSC Interaction Regions," *Proceedings of the Part. Acc. Conf.*, Washington, May 1993.
3. W. Chou et al., "Emittance and Luminosity Evolution during Collisions in the SSC Collider," *Proceedings of the Part. Acc. Conf.*, Washington, May 1993.
4. D.M. Ritson, private communication.
5. A. Drozhdin, private communication.

SUMMARY OF THE SNOWMASS WORKING GROUP ON MACHINE-DETECTOR INTERFACE

V. BHARADWAJ, P. COLESTOCK, J. COOPER, G. GODERRE, J. HOLT
Fermi National Accelerator Laboratory
P. O. Box 500, Batavia, Il. 60510

1. MACHINE DETECTOR INTERFACE CONSIDERATIONS

From the detector point of view, what experimenters need is an outline of the EXPECTED machine parameters tempered with some indication of the POSSIBLE machine parameters. Given guidance from accelerator physicists on the machine, experimenters may get the germ of an idea of how to exploit a particular machine property. Similarly, given some indication of what is important to the experimenters, accelerator physicists may have ideas of how to modify the machine appropriately. We discuss below a list of machine parameters as viewed by experimentalists.

1.1. Luminosity

From the discussions in the other working groups at this workshop it is apparent that no planned experiment anticipates a wealth of data -- typical experiments are looking at B-physics in exclusive channels with small branching ratios. For example, to measure the CP Asymmetry angle beta, we hope to use the decay B --> $J/\psi + K^0_S$. The B branching ratio for this decay is only 4×10^{-4}. Then in addition the J/ψ--> 2μ or 2 electrons branching ratio is only 0.06, the K^0_S --> π–π branching ratio is 0.68, the typical detector rapidity and P_t efficiencies are small, and the B must be tagged by seeing a lepton from the other B in the event. The typical overall efficiencies are of the order of 10^{-9}. Therefore the experimenter's demand for B-physics is for the largest possible integrated luminosity in the shortest possible time, i.e. for higher and higher luminosities.

1.2. Number of Bunches / Bunch Spacing

This parameter coupled with the luminosity gives the number of interactions per crossing seen by a detector. Here there are not many quantitative studies (in fact we are aware of no specific study on B-physics), but the gut feeling is that fewer interactions per crossing is better, since the detector information is then less confused. In high transverse momentum (P_t) physics (e.g. W, Z, top,...) these extra interactions are not expected to be a major headache since the extra particles in the event from the extra interactions are from minimum bias events and have typical Pts less than a few GeV compared to the phenomena being investigated. This confusion factor is likely to be more important for "soft" B-physics (decay products of 5 GeV object produced with low Pt) than it is for high Pt physics at the same accelerator.

Given a trigger on a rare event, the average number of extra interactions is the same as the number of interactions per crossing. Recall that the probability of n interactions per crossing is given by Poisson statistics, so the distributions have very long tails. The average number of interactions per crossing is only part of the story, and the number of triggered events with more than 3 extra interactions in the crossing can be large. See Table 1 for an example at the Tevatron at a luminosity of 10^{32}.

Table 1. Interactions of the Tevatron at luminosity 10^{32}

Bunch spacing (nsec)	number of bunches	average number of extra interactions	% with > or = 3 extra	% with > or = 6 extra	% with > or = 10 extra
3	6	15.4	100 %	99 %	90 %
396	36	1.8	25 %	1 %	-----
132	99	0.6	2 %	-----	-----

The bunch structure also has severe implications for the detector electronic read-out systems. It is worth noting that both CDF and DO at the Tevatron are attempting to build electronics in all systems capable of 132 nsec between crossings as part of the round of detector upgrades leading to Tevatron Collider Run II with 396 nsec spacing. The object is to build all this electronics once and avoid the need of another expensive upgrade later. It is important to understand the Tevatron bunch scenario for 132 nsec as these electronics designs are being frozen within the next year. For example, the required existence of an abort gap between some bunches may provide an opportunity for the experimenters in their design. How long are these abort gaps ? How many are seen at an interaction region ? Similar questions and answers should have an effect on B-detectors at the SSC.

1.3. Beam Energy

In our thoughts this is fixed at the SSC, but historically has been variable over a small range (546 GeV to 900 GeV, perhaps eventually even slightly higher) at the Tevatron. B cross sections rise with energy and larger statistical samples are always better -- this is one clear advantage of the SSC. It has been pointed out at this workshop that the theory prediction of the B cross section from CERN p-pbar to the Tevatron does not match the results reported by CDF. If the Tevatron could be operated with high luminosity at a lower energy, we could learn information vitally important to all the planned experiments at higher energy colliders.

1.4. Luminosity Lifetime

Experiments must cope with PEAK luminosities while the final physics results depend on the INTEGRATED luminosity. By setting a trigger threshold on some parameter, the experimenter triggers the detector on a fixed cross section and therefore the trigger rate is directly proportional to luminosity. As the luminosity decreases, the experimenters usually retaliate by lowering the parameter threshold so as to keep the trigger rate near the peak capability of the detector. However, the greatest INTEGRATED luminosity comes from the short periods at the highest luminosity, so the final experimental statistics on a given process are strongly coupled to the peak luminosity. Any effort which smooths the peak to valley ratio of luminosity is welcome.

1.5 . β^*/ Longitudinal Emittance

These two parameters couple to give the length of the luminous region. At the Tevatron the region is very long (sigma of order 30 cm) and this complicates the experimental design of the silicon vertex detectors now at the heart of most collider detector b-physics strategies. For example the CDF SVXII is now designed as a 1.02 meter-long barrel to cover the rapidity range of η <1.0, while a device only 0.22 meters long would be required if the Tevatron were a longitudinal point source. At an estimated silicon barrel cost approaching 40 K$ per centimeter of length, this extended source problem translates directly into a lot of cash. Could changes in the RF or a small crossing angle help this situation without too much compromise in the luminosity ? Again, at the Tevatron, these devices are being designed now for Collider Run II and beyond, so feedback on the machine possibilities will be far more timely now than five years from now. The silicon detectors under design all have conceptual upgrade paths, so information on possible changes in the luminous region for far future collider runs is also useful.

1.6. Transverse Emittance

Experiments (e.g., CDF's SVT) now envision fast secondary vertex triggers based on silicon vertex detector information. The idea is to look for charged tracks with a large impact parameter when extrapolated to the transverse beam position, as expected if the track actually comes from a secondary vertex. Therefore these trigger devices depend on a small and stable transverse beam size. What are the expected (and possible) machine parameters ? Note that the presence of extra interactions in an event can confuse these triggers -- for example if you wished to make a secondary vertex cut at 100 microns with such a trigger and the tranverse beam size were already of order 100 microns, the trigger would select multiple interactions and not b-decays. Similarly, if the transverse beam spot moved by 100 microns between collider stores or during a single store, the trigger could be confused unless this transverse position information were available in real time. On the other hand if the experimenters assume a 50 micron beam size but 10 microns is possible, this can make a huge difference in the trigger design and performance. Clearly this is an area where the experimentalists and accelerator physicists must be on the same wavelength all the time.

2. SUMMARY OF TEVATRON PERFORMANCE - PAST, PRESENT AND PROJECTIONS

In this section we give a summary of Tevatron Collider performance, focussing on the recent Collider Run as it relates to the potential for future B-physics experiments at Fermilab. We consider the overall performance characteristics, and present specific issues concerning intensity limitations, lifetimes and beam stability.

2.1. Performance summary of the 1992-93 Tevatron Collider Run

The recently completed Collider Run has seen the successful implementation of separated orbits and simultaneous operation of two interaction regions. As a result of these and other improvements, the peak luminosity achieved was over a factor of four greater than previous levels and the average delivered luminosity exceeded 1 pb^{-1} / week. A plot of the integrated luminosity over the run, as compared to the previous run, is shown in Fig. 1

There was a steady increase in the initial luminosity, and in the integrated luminosity per store during the early phases of the run, which can largely be attributed to increases in the extracted number of pbars which achieved collision. The inital luminosity was observed to be essentially proportional to the number of available pbars, as shown in Fig. 2. In this figure, two different operating modes are depicted: the nominal $\beta^* = 0.5$ m and the $\beta^* = 0.25$ m, corresponding to two alternate low-beta insertion lattices in use.

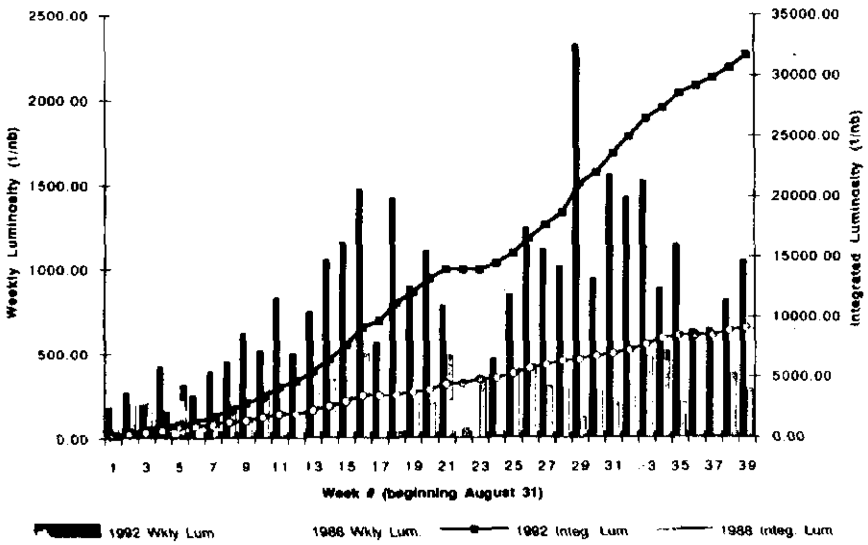

Figure 1. Integrated Collider luminosity for the 88-89 and 92-93 runs.

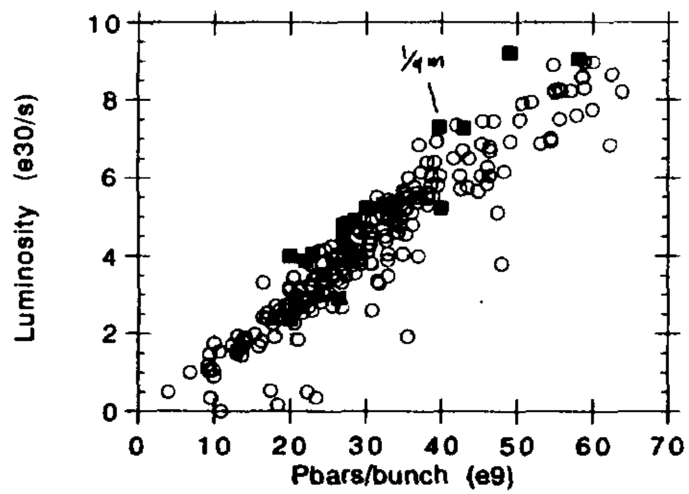

Figure 2. Initial luminosity as a function of pbars achieved at collision. Two operating modes are shown: the open circles are at $\beta^* = 0.5$ m and the solids are at $\beta^* = 0.25$ m.

Under typical operating conditions, initial luminosities in the range of 6-8 x 10^{30} cm^{-2} sec^{-1} were achieved accompanied by luminosity lifetimes in the range of 15 hrs, as shown in Fig. 3. The lifetimes were seen to be due primarily to emittance growth which, in turn, is believed to be caused by low-level power supply noise. Fig. 3 indicates that the lifetime is largely independent of luminosity, although there may be a slight degradation at lower β^* due to the fact that less time was spent finding and maintaining an optimal operating point under these conditions. The corresponding particle lifetimes are shown in Fig. 4, which shows the time evolution of protons and pbars during the course of three successive stores.

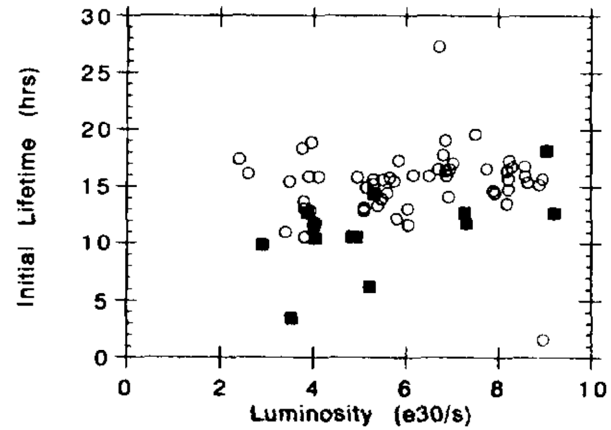

Figure 3. Initial luminosity lifetime as a function of the initial luminosity. The open circles correspond to $\beta^* = 0.5$ m and the solids correspond to $\beta^* = 0.25$ m.

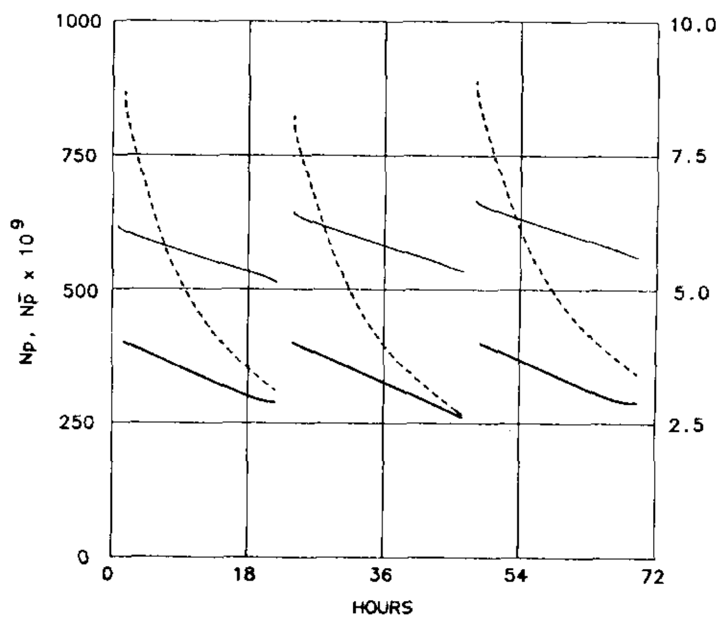

Figure 4. Time evolution of three successive Collider stores for particle intensities (protons, light solid, p-bars, heavy solid) and the measured luminosity (dashed). The dominant factor in the luminosity lifetime is due to emittance growth at the rate of 0.3 π / hr.

2.2 *Operational Issues*

In addition to the usual issues related to hardware reliability, there were a number of operational issues which affected the stability of the beam. The primary issue affecting operation was due to periodic drifts in the Tevatron orbit, and hence in the Tevatron operating point as a result of the nonlinear fields in the device, believed to be due primarily to the nonlinearities in the low beta quadrupoles. The position of the interaction region was observed to drift by as much as 200 microns over the course of several stores, accompanied by tune changes and, in some cases, changes in the particle lifetimes. Although not possible during this run, it is believed that such orbital changes can be controlled in future operation.

2.3 *Projected Tevatron Operation*

The operation of the Tevatron Collider follows three stages in the coming years, as shown in Table 1. The first of these stages, labelled 1B, involves the commissioning of a new, higher-energy Linac, accompanied by an expected gain of a factor of three in integrated luminosity. In Phase II, the number of bunches will be increased to 36 X 36, giving rise to an expected increase in luminosity of an additional 30%. Finally, in the Main Injector era, the integrated luminosity is expected to reach 20 pb^{-1}/wk.

Another mode of operation has been considered in which the bunch number is increased to 99 X 99. In order for such a mode of operation to be feasible, it is necessary to develop fast rise-time kickers. This option will be explored more fully in the following section.

2.4 *Tevatron Bunch Loading*

Presently the Tevatron collider operates with six proton and six pbar bunches spaced evenly around the ring (3500 nsec spacing). The bunches are loaded one at a time starting with the protons. Each bunch consists of eleven buckets coalesced into one which is done in the Main Ring. As the intensity per bunch increases, the number of interactions per crossing as seen by the experiments increases to an unacceptable level. Therefore in a future collider run, the Tevatron will switch to thirty-six bunch operation. How these bunches are loaded is constrained by a number of factors.

1. There must be a gap in the bunch train for the abort kickers to rise to their nominal voltage.

2. Both experiments (B0 and D0) must receive the same luminosity.

3. To use the present coalescing system, the bunches must be spaced no less than twenty-one buckets (396 nsec) apart.

4. No bunch-"air" collisions.

The constraints dictate a three-fold symmetry of three groups of twelve bunches spaced at twenty-one buckets within the group. Figure 5 shows this configuration at a particular moment in time. The abort gap is 2600 nsec which is smaller than the present gap of 3500 nsec. Development on shortening the rise time of the abort kicker is underway.

As with the present loading scheme, the protons would be loaded first. Twelve batches would be coalesced into twelve bunches spaced at 376 nsec. They would be injected into the Tevatron as a group. Three injections would fill the Tevatron. The present injection kickers are adequate for this purpose. The pbars however, are loaded in a different way. The pbar source will be modified extract four batches of pbars. These would then be coalesced in the Main Ring and injected into the Tevatron. This requires an injection kicker with a rise time of at least 376 nsec and a flattop time of at least 1224 nsec. A kicker meeting these requirements is under development.

For ninety-nine bunch operation in the Main Injector era and assuming two experiments, the injection kicker timing requirements become very stringent. The bunches would be grouped in three groups of thirty-three each with a bunch spacing of 131 nsec. Injection kickers would have to be developed with this rise time. Also there would have to be modifications to the Main Injector coalescing system as well as RF modifications to the pbar source. The protons could be loaded in batches of thirty-three but the pbars would be loaded twelve at a time.

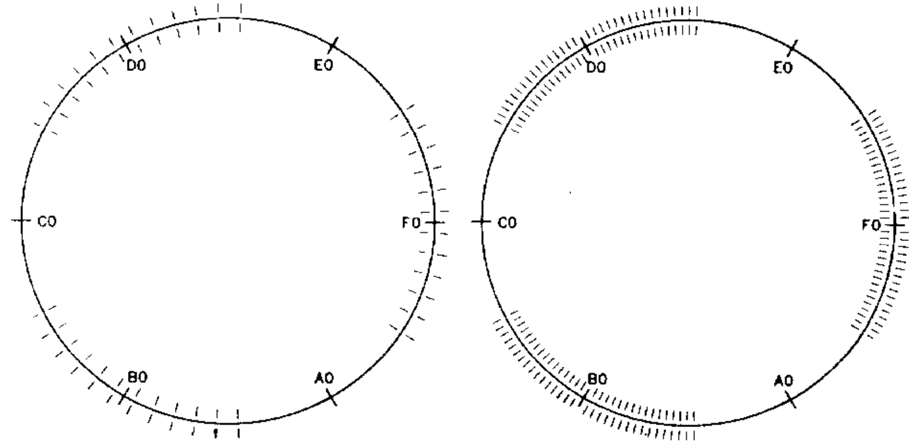

Figure 5 (a). Loading scheme for the 36 X 36 mode of operation. The bunches are arranged with three-fold symmetry and an abort gap sufficient to permit clean removal of the beam. (b) Loading scheme for 99 X 99.

2.5 *Other Projected Improvements - Bunched-beam Cooling*

A proposed scheme for improving the integrated luminosity is the use of stochastic cooling of the bunched-beam in the Tevatron. The process by which this is done is similar to that routinely carried out in anti-proton storage rings, but with the additional complication that the feedback signal must be carefully separated from the large coherent signals associated with the bunched beam. This project is now in development at Fermilab and if successful can significantly increase the integrated luminosity of a given store. The effect of a cooling time on the order of 20 hrs. can lead to a 50% increase in integrated luminosity, as shown in Fig. 6

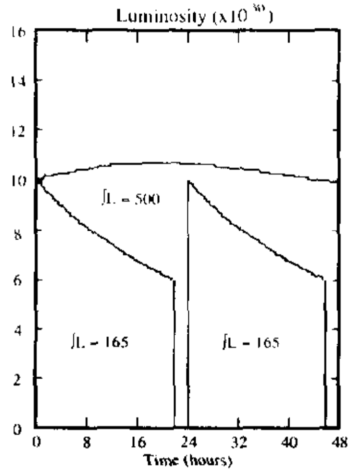

Figure 6. Simulation of Bunched-beam cooling. An increase in integrated luminosity of approximately 50% is realized with a 20 hr. cooling time

2.6 Bunch Shortening

In an effort to permit shorter bunches in the Tevatron, an investigation was undertaken to determine viable means of controlling bunch length. One scheme proposed was that of raising the rf frequency. However, upon further study it was determined that a much simpler method was to raise the rf voltage. The bunch length scaling with voltage is shown in Fig. 7. The associated scaling of the momentum spread is shown in Fig. 8.

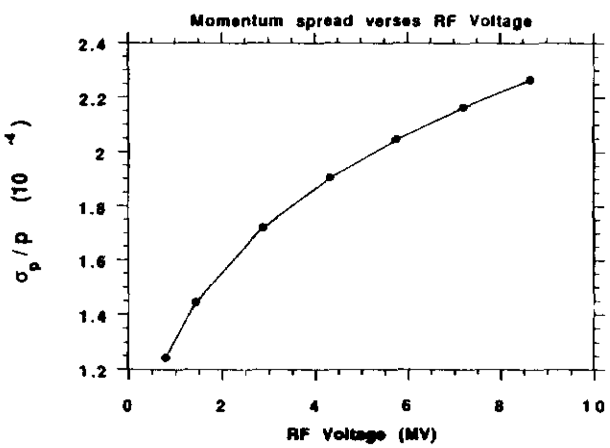

Figure 7. Bunch length scaling with rf voltage

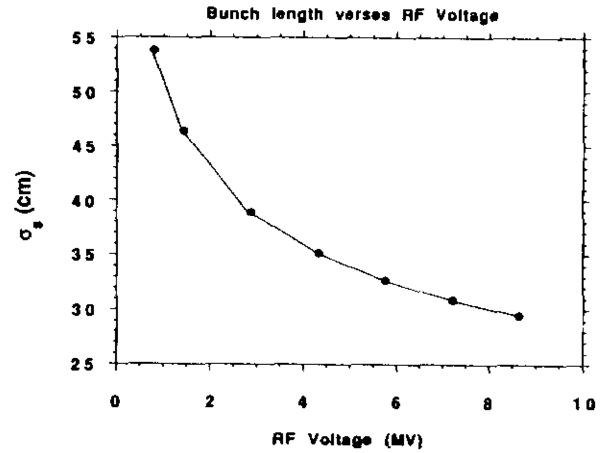

Figure 8. Momentum spread scaling with rf voltage

It should be noted that it is assumed that the Tevatron is well below instability thresholds such that the shorter bunch lengths do not present a stability problem for the Collider.

ASYMMETRIC COLLIDER

V. BHARADWAJ, P. COLESTOCK, G. GODERRE,
D. JOHNSON, P. MARTIN, AND J. HOLT
Fermi National Accelerator Laboratory
P.O. Box 500, Batavia, Il. 60510

and

D. KAPLAN
Northern Illinois University
DeKalb, Il.

1. INTRODUCTION

The study of *CP* violation in beauty decay is one of the key challenges facing high energy physics [1]. Much work [2] has not yielded a definitive answer how this study might best be performed. However, one clear conclusion is that new accelerator facilities are needed. Proposals include experiments at asymmetric electron-position colliders [3] and in fixed-target and collider modes at LHC [4] and SSC [5]. Fixed-target and collider experiments at existing accelerators, while they might succeed in a first observation of the effect, will not be adequate to study it thoroughly.

Giomataris [6] has emphasized the potential of a new approach to the study of beauty *CP* violation: the asymmetric proton collider. Such a collider might be realized by the construction of a small storage ring intersecting an existing or soon-to-exist large synchrotron, or by arranging collisions between a large synchrotron and its injector. An experiment at such a collider can combine the advantages of fixed-target-like spectrometer geometry, facilitating triggering, particle identification and the instrumentation of a large acceptance, while the increased $\sqrt{s}$ can provide a factor > 100 increase in beauty-production cross section compared to Tevatron or HERA fixed-target. Beams crossing at a non-zero angle can provide a small interaction region, permitting a first-level decay-vertex trigger to be implemented [7]. To achieve large $\sqrt{s}$ with a large Lorentz boost and high luminosity, the most favorable venue is the high-energy booster (HEB) at the SSC Laboratory, though the CERN SPS and Fermilab Tevatron are also worth considering.

We next comment on these issues in somewhat more detail:

1. The cross section for beauty production in hadron collisions is a rapidly increasing function of energy at currently available energies [8]. Thus a modest increase in $\sqrt{s}$ can provide a large increase in beauty production rate.

2. A Lorentz-boost γ confines the beauty decay products, distributed ≈ isotropically in the center of mass, to a cone of typical half-angle $\tan^{-1}(1/\gamma)$. Thus less detector area is needed with boosted events, and a spectrometer of given cost can have higher beauty detection probability. An additional effect is that much of the increase in beauty cross section at very high $\sqrt{s}$ consists of events produced in the extreme foreward or backward direction , which typically go down the beam pipe undetected. These are exemplified by comparing the (expensive) CDF detector, with beauty geometrical acceptance < 10% for typical decay modes, with the (more modest) fixed-target detectors of Fermilab Proposal 865 [9] and the HERA-B proposal [10], whose acceptances for typical decay modes are > 50%.

3. At the values of $\sqrt{s}$ (~a few hundred GeV) we are considering, beauty events are distinguished by substantially higher transverse momenta than are typical of "minimum-bias" background events, and this distinction can be used in the trigger to reject the background. At ultra-high energy (e.g. Tevatron or SSC collider), the mass of the b quark becomes negligible with respect to the available center-of-mass energy, so that beauty production becomes kinematically similar to the background.

4. The ability to trigger on the beauty decay vertex is crucial to carrying out a sensitive study of beauty decay in a wide variety of modes. Thus (for example) CDF intends to implement a fast vertex trigger for Tevatron Run II, and the optical impact-parameter trigger features prominently in the LHC fixed-target "GAJET" proposal. Other triggering schemes provide inadequate sensitivity, for example the high-p_t dilepton triggers currently in use by CDF have efficiency < 1% for the ~ 1% of beauty decays to J/ψ, and the high-p_t single-muon trigger used by the Fermilab fixed-target experiment E771 is < 50% efficient for the ~ 10% of beauty decays to muons. Tests of the optical impact parameter trigger are in progress at CERN; it appears likely that background rejection factors ~ 10-100 can be achieved with beauty efficiency > 50%, largely independent of decay mode.

5. Hadron identification is key in a beauty experiment, for example it makes possible kaon-tagging of the initial beauty quantum number [10], and it improves the signal/background ratio for the kaon-rich final states of the copious beauty to charm decay cascade. The higher momenta of Lorentz-boosted beauty decay products and the fixed target-like spectrometer layout facilitate effective hadron identification using threshold or ring-imaging gas Cherenkov counters.

We estimate [6] that given the good acceptance and trigger efficiency possible in an asymmetric-collider experiment, ~ 10^{10} produced beauty events per year should permit a detailed study of beauty *CP* violation, as well as other topics of interest such as B_s mixing and flavor-changing neutral-current decays [9, 11]. This calls for luminosity in the range ~ 10^{32} - 10^{33} cm^{-2} sec^{-1}; the exact value needed depends on $\sqrt{s}$ and the still imperfectly known beauty cross section, as well as how much running time is made available per year. We have begun studies to understand the limits to luminosity in asymmetric configurations with various crossing angles.

2. SCALING LAWS FOR THE ASYMMETRIC COLLIDER USING THE TEVATRON

One option explored at this workshop was the possibility of an asymmetric collider using the Tevatron and a new machine whose energy and size are to be specified.

The following conclusions were reached in these discussions:

1. space charge forces are the dominant limit to intensity in the low energy ring; these may be mitigated, to some degree, by the use of flat beams;

2. beam-beam forces, and the associated tune shift in the high energy beam, are the primary limits to intensity (and emittance) in the high energy machine; an assumption was made to limit the fraction of the total beam-beam tune shift due to the new interaction region to approximately one third of the now acceptable level; this will reduce the detector luminosities by about 1/3;

3. geometric constraints most likely will preclude the use of common quadrupoles for the low energy and high energy rings in the interaction region; thus large-angle, or even 90° crossing is preferred.

Based on these considerations, a simple scaling law for the asymmetric collider could be obtained. In the low energy machine, the acceptable space charge tune shift is of order unity, and in terms of machine parameters is given by

$$\Delta\nu_{sc}=\frac{\tilde{N}_L r_o (1-\beta_L^2)\beta_{yL} g_L}{4\pi\beta_L\gamma_L(1+a_L)\sigma_{yL}^2}$$

where g_L is the fraction of particles intersecting the high energy ring, a_L is the ratio of the horizontal to vertical beam sizes, r_o is the classical proton radius, β_{yL} is the vertical beta function, N_L is the number of particles in the ring, s_{yL} is the vertical beam size and γ_L and β_L are the usual relativistic factors. For a flat bunched beam in the high energy ring intersecting a DC beam in the low energy ring at right angles, the following approximate expression for the luminosity can be given

$$L=\frac{N_H N_L g_L f_o}{4\pi\sigma_{yL}\sigma_{yH}}$$

The beam sizes in the respective rings are forced to be equal and are given by

$$\sigma_{yL}=\sqrt{\frac{\varepsilon_{NL}}{6\pi\gamma_L}}=\sigma_{yH}$$

where a_L and a_H are the aspect ratios of the respective beams. Using the space charge limit above, the maximum luminosity can be expressed in the following form

$$L_{sc}<\frac{\beta_L\gamma_L^{5/2}\varepsilon_L^{1/2}N_H f_o a_H(1+a_L)}{2\sqrt{6}\pi^{3/2}R_L r_o\beta_{yL}^{1/2}}\Sigma$$

where Σ is the maximum allowable tune shift, taken here to be 0.1. Now it is further noted that there is a maximum allowable field strength in present-day magnets at about 6T with a minimum bend radius of about 8 m. This means that R_L is actually a function of energy above about 14 GeV. Anticipating this limit, the final form of the space charge limit is in the following form, using Tevatron parameters:

$$L_{sc}<6.5\times10^{29}\,\frac{\gamma_L^{3/2}a_H(1+a_L)}{\beta_{yL}^{1/2}}\ \mathrm{cm^{-2}sec^{-1}}$$

We now invoke the limit due to the beam-beam forces exerted by the low energy ring on the high energy ring, given by

$$\Delta\nu_{BB}=\frac{\tilde{N}_L r_o (1+\beta_L^2)\beta_{yL} g_L}{4\pi\beta_L\gamma_L(1+a_L)\sigma_{yL}^2}$$

In a similar fashion we have the limit due to the beam-beam tune shift as

$$L_{B\text{-}B}<2.0\times10^{29}\,\frac{\gamma_L(1+a_L)}{\beta_{yL}}\ \mathrm{cm^{-2}sec^{-1}}$$

In the above we have made the assumption that the maximum allowable tune shift due to beam-beam effects is about one-third of the present allowable tune shift in the Collider. This causes a reduction of the Collider luminosity of about 1/3. If we now further assume that the minimum beta function in the Tevatron is on the order of a few meters with an emittance of 20π (present conditions, see below), then the dominant limit on the luminosity becomes the beam-beam limit.

The results are plotted in Fig. 1 against the necessary luminosity as governed by the bb cross-section. This shows that a possible solution can be found at a value of $\gamma_L = 100$. If an aspect ratio of 10:1 can be achieved in the high energy ring in the interaction region, then $\gamma_L = 100$ with $\beta_L = 4$ m and $\beta_H = 2$ m. Such a situation is viable provided a new low-β region can be installed.

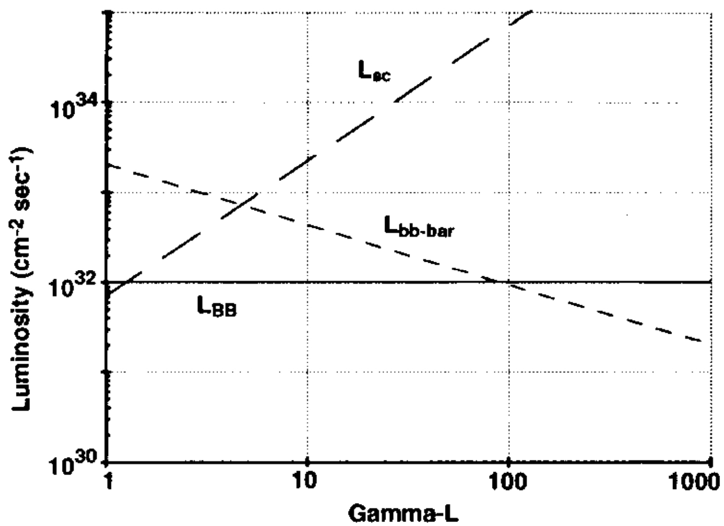

Fig. 1 Luminosity limits due to space charge and beam-beam forces plotted versus the required luminosity for b-b-bar events. Beam-beam limits dominate requiring $g_L > 100$ for sufficient luminosity.

REFERENCES

[1] See for example F. J. Gilman, "B Physics," in *Proceedings of the Workshop on High Sensitivity Beauty Physics at Fermilab*, A. J. Slaughter, N. Lockyer, and M. Schmidt, eds., Fermilab, November 11-14, 1987.

[2] See for example the proceedings of the workshops *B Physics at Proton Accelerators* and *B Physics at Hadron Accelerators* at SSC Laboratory, June 29-30, 1992, August 13-14, 1992, September 25-26, 1992, at Fermilab, November 16-17, 1992, and at Snowmass, CO, June 21-July 2, 1993.

[3] "CESR-B: Conceptual Design for a B-Factory Based on CESR," June 1993; "PEP-II, An Asymmetric B Factory: Conceptual Design Report," SLAC-418, June 1993.

[4] Measurement of CP-Violation in B-decays using an LHC extracted beam: an Expression of Interest," G. Carboni, spokesperson;"An experiment to study CP violation in B decays using an internal gas jet at LHC," L. Camilleri, spokesperson.

[5] H. Castro *et al.*, "Expression of Interest for a Bottom Collider Detector at the SSC," N. S. Lockyer, spokesperson, SSCL-SR-1163, May 1990.

[6] Y. Giomataris, "Comments on the Future of *B* Physics in Hadron Machines," Lausanne preprint IPNL 92-4 (1992), and "Perspectives on an Asymmetric Proton Collider with Small Crossing Angle for *B* Physics," presented at *Heavy Quarks at Fixed Target*, Laboratori Nazionali di Frascati, Frascati, Italy, May 31-June 2, 1993.

[7] G. Charpak, L. M. Lederman, and Y. Giomataris, Nucl. Instr. & Meth. A306 (1991) 439; D.M. Kaplan *et. al.*, Nucl. Instr. & Meth. **A330** (1993) 33; G. Charpak *et al.*, Nucl. Instr. & Meth. **A332** (1993) 91.

[8] E.L. Berger, "Heavy Flavor Production," *in Proceedings of the Advanced Research Workshop on QCD Hard Hadronic Processes*, St. Croix, Virgin Islands, Oct 8-13, 1987.

[9] L.D. Isenhower *et al.*, "P865: Revised Letter of Intent for a High-Sensitivity Study of Charm and Beauty Decays," D. M. Kaplan, spokesperson, April 2, 1993.

[10] H. Albrecht et al., "An Experiment to Study CP Violation in the B System Using an Internal Target at the HERA Proton Ring," Letter of Intent to DESY, W. Hofmann and W. Schmidt Parzefall, spokespersons, October 1992.

[11] Flavor-changing neutral-current beauty decays have been treated theoretically by A. Ali and C. Greub, Z. Phys. C49, 431 (1991), Phys. Lett. 259B, 182 (1991), and "Rare Decays B ~ Xd+gamma in the Standard Model," DESY preprint 92-048, March 1992;
A. Ali, T. Ohl, and T. Manuel, Phys. Lett. 298B, 195 (1993).

EXPERIMENTAL MODIFICATION OF SSC INTERACTION REGION

D. E. JOHNSON
Superconducting Super Collider Laboratory*
2550 Beckleymeade Avenue
Dallas, Texas 75237, USA

1. INTRODUCTION

The SSC Collider design has four interaction regions. Two of these regions are configured for high-luminosity collisions and have been previously described in detail. The other two regions are, as yet, uncommitted. Early Collider designs called for two medium-luminosity regions, and lattice designs very similar to those for the high-luminosity regions were developed.[1] An updated medium-beta design was recently developed.[2] Questions have been raised by experimental proponents as to the possibility of inserting analyzing magnets into the lattice design. This paper examines the interference of experimental magnets with the basic machine lattice.

2. LATTICE DESIGN

A layout of one-half of the Medium-beta IR design along with its lattice functions is shown in Figure 1.

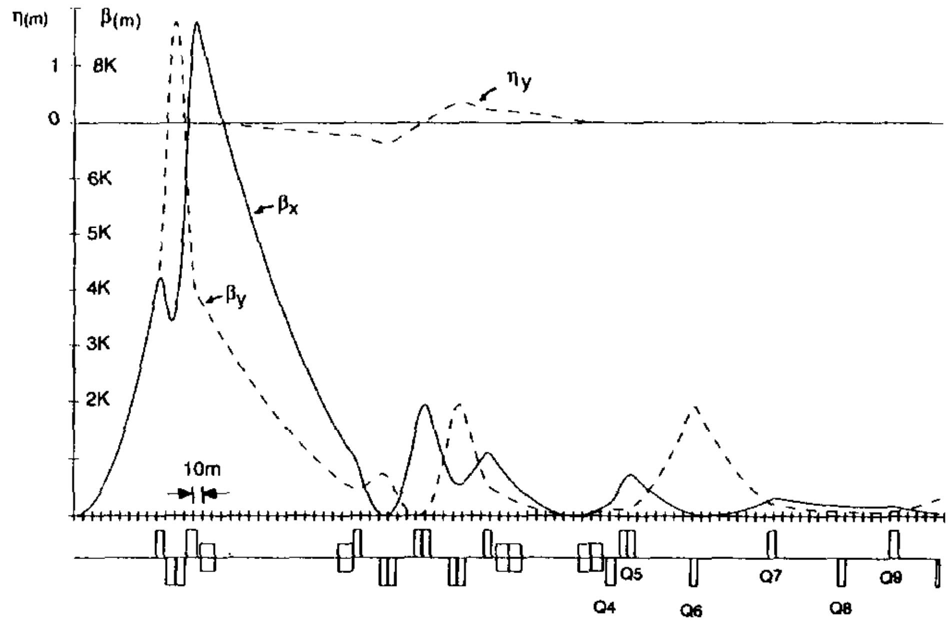

Figure 1. Layout of Medium-beta Interaction Region

The beta-squeeze is accomplished by adjusting the quadrupoles Q4 – Q9 on either side of the interaction point through a relatively small, continuous tuning range. This tuning is done after the beams have been accelerated to 20 TeV. As the beta function at the IP is reduced, the chromaticity produced by the IR quadrupoles increases dramatically. This increase must be continuously tracked by the correction sextupoles. Concurrent with the beta squeeze, the two beams are brought into collision with a set of trim dipoles on either side of the IP. The timing details of beta squeezing and crossing control will be determined experimentally in the future. Thus, the ability to control in detail the beam's behavior throughout the interaction region will exist as part of the basic lattice. This ability may be used to provide for analyzing magnets as well as for its primary purpose.

Many of the proposals for experiments in a medium-luminosity region desire to have a variety of magnets in or around the beamline. These magnets include dipoles, quadrupoles, sextupoles, toroids, and solenoids. All of the requests which have been examined can be accommodated with slight modifications to the basic IR design. These modifications consist mainly of a small retuning of the interaction quadrupoles, and, in some cases, the introduction of compensating magnets. The effect of the experimental magnets on the very stiff Collider beams is almost negligible, and can be easily controlled. An example of such compensation is presented below.

The Full Acceptance Detector proposal is currently considering analyzing magnets such as the ones listed in Table 1.[3]

Table 1. FAD Magnet Request.

Distance From IR (m)	Magnet Type	p_T Kick at Coil GeV/c	Aperture Radius (m)
3.0	Quad	0.8	1.5
6.5	Quad	0.8	0.75
16.5	Sextupole	0.8	0.75
38.0	Sextupole	0.8	0.75
70.0	Dipole	1.1	0.75

The FAD magnets can be accommodated into the SSC IR design in the following manner. The quadrupoles are inserted with opposite signs and their effects are removed with a vary slight retuning of the beta-squeezing quadrupoles. The dipole is compensated with the addition of two other trim dipoles, forming a simple orbit three bump. This could also be compensated by some complication on the crossing-angle system, if desired. The sextupoles are globally tuned out through the existing chromaticity sextupoles. Their effect on the beam adds nothing to the existing sextupole requirements.

Figure 2 shows the lattice functions for the fully compensated experimental region and Table 2 lists the tuning quadrupole gradients at 20 TeV for the original IR design and for the compensated design. The compensation adjustment is far smaller than that required to produce the beta squeeze and will not cause any increase in the system. Some increased complexity will be added due to the need to track the effects of the analyzing magnets along with all of the other IR systems, but the increase is small, and easily tolerable.

Table 2. IR Tuning Gradients for $\beta^* = 2$m

Quad	Standard (T/m)	Compensating (T/m)
Q4	-184.2866	-186.0234
Q5	177.9441	178.4417
Q6	-158.9960	-158.3286
Q7	161.3788	161.6200
Q8	-52.5808	-54.3169
Q9	115.8781	115.7887

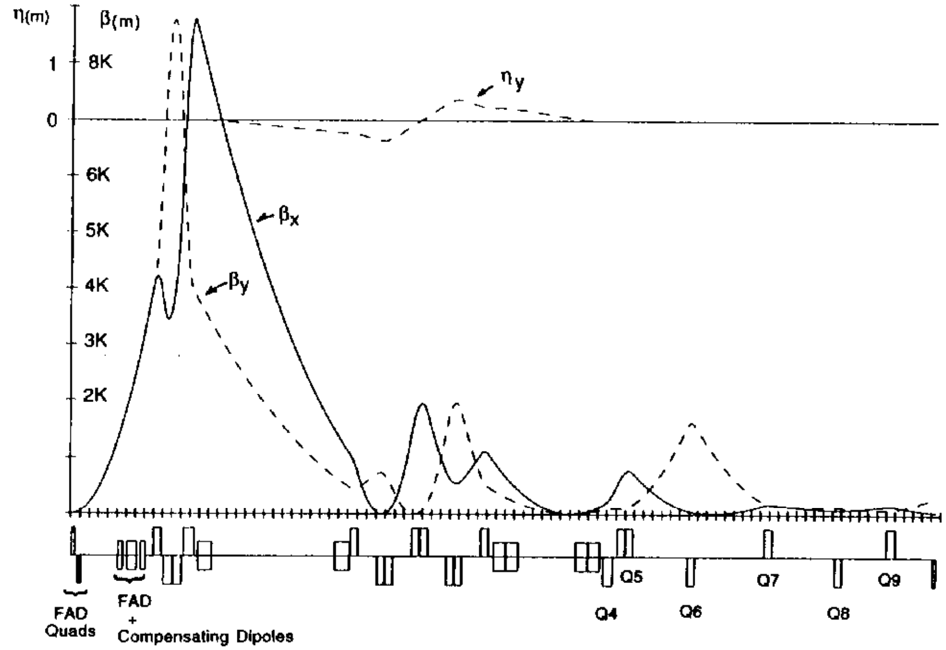

Figure 2. Medium-beta Interaction Region with compensated experimental magnets.

References

1. *Site-Specific Conceptual Design*, **SSCL–SR–1056** (1990), p. 55.
2. Y. Nosochov, report these proceedings.
3. B.J. Bjorken, private communication.

★ Operated by Universities Research Association, Inc., for the U.S. Department of Energy under Contrct No. DE-AC35-89ER40486.

RADIATION ENVIRONMENT AND SHIELDING AT THE SSC

Milind V. Diwan
26 June 1993
Physics Research Division, SSC Laboratory, Dallas, Texas.

INTRODUCTION

Much higher radiation levels are expected at the SSC compared to all previous colliders because of the increased center of mass energy (40 TeV) and the increased luminosity (10^{33}cm^{-2}s^{-1} for a general purpose high $P_{\perp}$ detector, and 10^{32}cm^{-2}s^{-1} for the proposed B detectors). We have performed a comprehensive study of the radiation environment for the proposed GEM detector[1] at the SSC. As a result of this study, we have developed a shielding scenario that will ensure that the detector will operate with its design performance for at least 10 years at the standard luminosity of 10^{33}cm^{-2}s^{-1}. We define a standard SSC year (SSCY) as 10^7 s.

The main concerns of our study have been:

- The charged particle, neutron, and photon fluxes, and the hit rates generated in the inner tracker and the muon spectrometer.
- The radiation doses delivered, especially to the inner tracker layers, the endcap and forward calorimeter components, and the beam line components within and near the experiment.
- Radioactivation of the inner and forward parts of the detector and the beam line, and levels of radioisotopes generated in the experimental hall.

While much of our study was specific to the detector geometry proposed for the GEM experiment, many of the results are applicable to other SSC experiments. In particular, the general considerations of energy loss in the collision hall presented in Section 2 should be applicable to the proposed B-physics experiments. In Section 3, we present some results specific to GEM, and we draw conclusions specific to proposed B-physics detector geometries such as BCD[2-3] .

ENERGY DEPOSITION

There are three major sources of radiation: local beam loss in the collider tunnels; interactions of the 20 TeV proton beams with the residual gas in the beam pipe; and particle production at the interaction point. The contributions of each of these sources to the total particle fluence and the deposited energy will depend on the luminosity. At the standard SSC

---

1 "GEM Technical Design Report," presented by the GEM Collaboration, SSC-SR-1219, April 30, 1993.
2 "Bottom Collider Detector," SSC-EOI0008, May 25, 1990.
3 "Comparison of BCD and COBEX strategies for B Physics at Hadron Colliders," K.T. McDonald, Princeton-HEP-92-11.

luminosity of $10^{33}cm^{-2}s^{-1}$ the radiation levels will be dominated by the particle production at the interaction point.

Beam loss in the walls of the beam pipe occurs simultaneously around the accelerator. The beam size is large in the final focus quadrupoles near the interaction points (IP), so the beam loss is particularly severe in these regions. Using the MARS12 code system[4-5], we have estimated neutron and charged particle fluxes due to this beam loss by making simulations of proton orbits around the accelerator and of the hadronic cascades due to the lost protons. For the interaction region geometry anticipated for GEM, we find that the contribution from this source is negligible. We expect the same conclusion to hold for the B detector, unless there are dramatic changes in the low beta quadrupole magnets.

The particle fluxes due to interactions of 20 TeV beam protons with atoms of the residual gas (beam gas interactions) in the evacuated beam pipe was computed using the MARS12 code system. The calculation assumed a pressure of 10^{-8} torr of nitrogen in the warm regions of the beam pipe (which extends up to the low beta quadrupoles located 35 m from the interaction point). A density of 4.0×10^8 N_2 molecules/cm^3 was assumed for the cold regions of the beam pipe inside the magnets. The cross section of 20 TeV protons (50 mb/nucleon) is such that this density corresponds to a loss of 1.7×10^{11} protons/m/SSCY from the two rings in the 100-m-long experimental hall. We used the value of 2×10^{11} protons/m/SSCY, which includes a small contribution from protons whose orbits are disturbed by the other interaction regions.[6] The details of the calculation are shown in Reference 1. Beam gas interactions as far as 60 meters away from the interaction point contribute to the particle fluences in the central cavity of the detector. The secondaries from the interactions are directed towards the interaction point. They further interact in the forward edges of the calorimeters producing a shower of particles near the beam line in the central cavity. For GEM, we have estimated that at the standard SSC luminosity ($10^{33}cm^{-2}s^{-1}$) the contribution to low energy neutron flux due to beam gas interactions is less than 3% everywhere in the detector. The contribution to the charged hadron flux at a radius of 10 cm from the interaction point is about 6%. The beam gas hadron flux is distributed approximately flatly in radius (R) in the central cavity, but the charged hadron flux from p-p collisions falls as $1/R^2$.

At the nominal B detector luminosity of $10^{32}cm^{-2}s^{-1}$ the contribution from beam gas interactions near the beam line will become significant, since the machine current, 1.3×10^{14} protons/ring, is expected to remain the same. The exact numbers will depend on the geometry of the forward elements. The number of beam gas interactions may be reduced by demanding a vacuum better than 10^{-8} torr, but this may not be practical for a B-physics detector because of the lack of space for pumps in the forward regions.

4 I. Baishev, A. Druzhdin, and N. Mokhov, SSC-306, 1991.

5 N. Mokhov, "MARS12 code system," Presentation in the Simulating Accelerator Radiation Environments Workshop, Santa Fe, New Mexico, Jan. 1993, to be published. Also see N. Mokhov, MARS10 Code Manual, FERMILAB-FN-509, 1989.

6 N. Mokhov, Collider ARC PDRR, May 26-27, 1993.

Now we examine the contribution from p-p collisions at the interaction point. We used the event generator DTUJET[7] to estimate the energy deposited in the detector and in the nearby beam line elements by 40 TeV p-p interactions. Figure 1 shows the fraction of the total energy from the interaction point emitted as a function of pseudorapidity.

DTUJET produces a pseudorapidity (η) plateau of 7.5 charged particles per unit pseudorapidity (for $-5 < \eta < 5$) and mean transverse momentum of 0.6 GeV in agreement with extrapolation of data from lower energies. There is no data in the far forward regions ($|\eta| > 6.0$); therefore, we assign an error of a factor 2 to the distribution of total radiated energy. For a detector covering $|\eta| < 6$, we see that roughly 5% of the energy is deposited in $3 < |\eta| < 6$ and more than 90% of the energy escapes the detector. At least part of this energy must be intercepted in a thick collimator placed in front of the low beta quadrupoles. This reduces the heat load on the cryogenic magnets and the radiation damage to the coil insulation. For GEM, we have chosen a 3 m (16.7 interaction lengths) deep iron collimator with a 25 mm diameter inner aperture placed 32 m from the interaction point. For a lower luminosity B detector the inner diameter of the collimator can be larger. Unfortunately, the errors on these calculations are such that it is conservative to assume that we need a collimator with the smallest possible inner aperture.

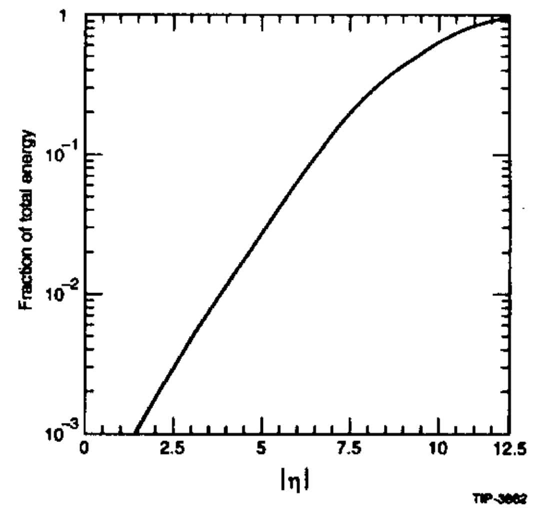

Figure 1. Fraction of the total energy from the interaction point emitted as a function of pseudorapidity.

7 J. Ranft, et al., in "Multiparticle Dynamics," Seewinkel, Austria, 1986. J. Ranft, Presentation in the Simulating Accelerator Radiation Environments Workshop, Sante Fe, New Mexico, Jan. 1993, to be published. See also J. Ranft, et al., UL-92-7 and UL-HEP-93-01, Leipzig, Germany. We have used the February 1, 1993 version of DTUJET.

The amount of energy lost from the collider at the interaction point (4.0×10^9 TeV/s and 4.0×10^8 TeV/s for lower luminosity) is greater than the beam loss in the accelerator magnets near the interaction point (approximately 4.0×10^7 TeV/s) or the beam loss in the residual gas of the vacuum pipe (4.0×10^7 TeV/s). The energy intercepted by the forward calorimeters (5%) is less than the energy into to the collimators (about 30%). Due to the proximity of sensitive detectors to the forward calorimeters, both the collimator and the forward calorimeter regions will be the dominant sources of background neutron and photon fluxes. For a lower luminosity detector beam gas interactions contribute a large fraction of the background near the beampipe.

SHIELDING CONSIDERATIONS

In this section, we briefly describe the shielding designed for the GEM detector and draw some conclusions for the proposed B-physics experiments. Figure 2 shows the detector and shielding configuration for GEM. The detector can be divided in three parts for shielding consideration: the central tracker cavity, the calorimeter covering $|\eta| < 5.8$, and the muon system.

The Central Tracker Cavity

The main concerns in this region of the detector are random hit rates due to albedo neutrons and photons and the total radiation dose to the sensitive detector elements such as the silicon tracker. An earlier SSC Laboratory Central Design Group report, SSC-SR-1033[8], addressed the radiation environment in the central detector cavity. The albedo neutron and photon fluxes in the central cavity are affected by the volume of the cavity, the composition of the electromagnetic calorimeter, and by the shielding material placed in front of the calorimeter. The neutron flux scales as $1/R^2$, where R is the characteristic dimension of the central cavity. Furthermore, the flux is proportional to (1+A), where A is the mean number of reflections that a neutron experiences before being absorbed. For the GEM detector, we plan to place borated polyethylene on the surfaces of the calorimeter to reduce the flux of albedo neutrons by fast absorption. With this shielding in place, we calculate the average flux of neutrons of all energies to be about 4×10^{12} n/cm²/SSCY. The average flux of photons above 100 keV will be about 6×10^{12}/cm²/SSCY. These calculations were performed using the LAHET-MCNP code system.[9] The single rates in the central cavity are dominated by the charged particles from the interaction point. The lifetime of the innermost silicon strip detector, placed 10 cm from the interaction point, is also dominated by the

[8] D.E. Groom, "Radiation Levels in the SSC Interaction Regions," SSC-SR-1033, June 10, 1988.
[9] "User Guide to LCS: the LAHET Code System," Richard E. Prael and Henry Lichtenstein, Los Alamos National Laboratory, LA-UR-89-3014, Sep. 1989. "MCNP: A General Monte Carlo Code for Neutron and Photon Transport," Judith F. Briesmeister, LA-7396-M Rev. 2, Sep. 1986. "Radiation Calculations using LAHET/MCNP/CINDER90," Proceedings of the II International Conference on Calorimetry in High Energy Physics, Corpus Christi, LA-UR-89-3014, Oct. 1992.

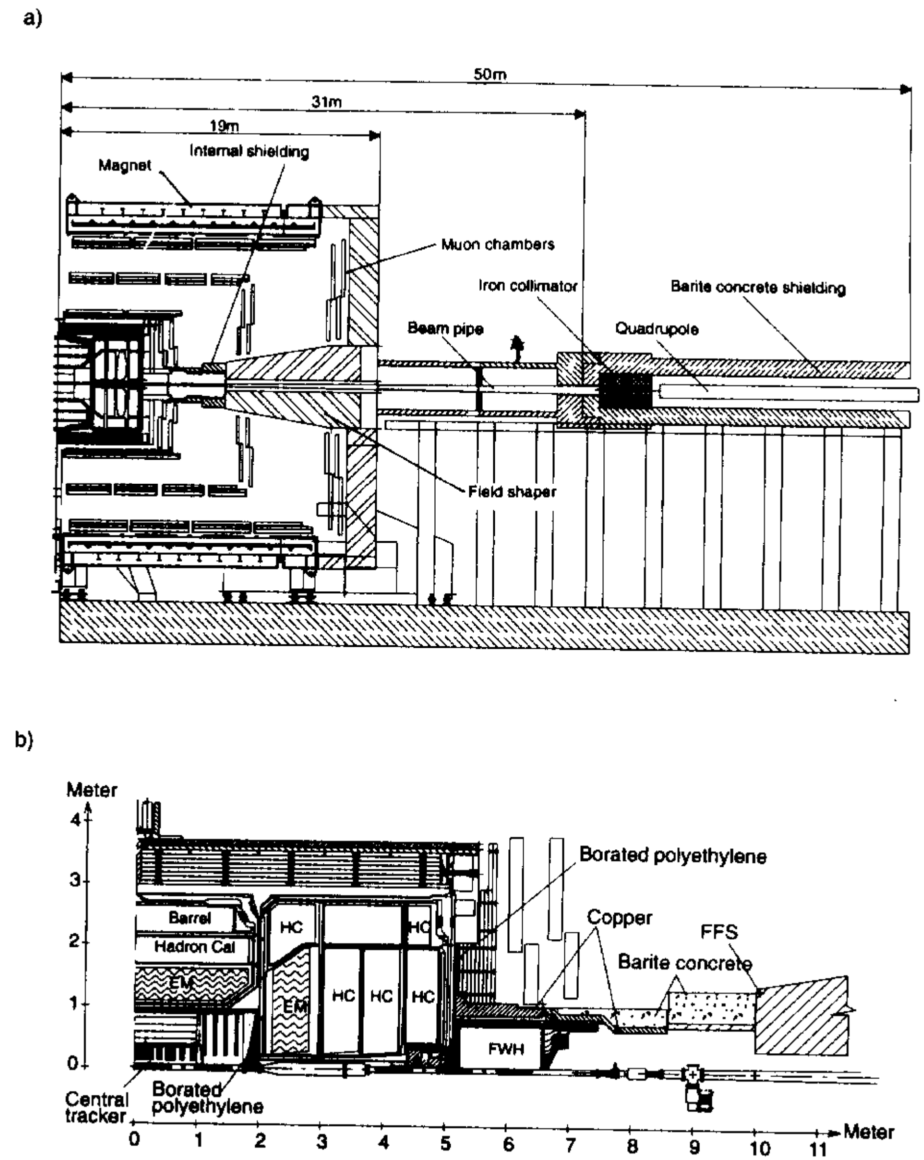

Figure 2. Detector and shielding configuration designed for GEM. a) Elevation view of half of the detector and shielding around the collimator and the quadrupole. b) Details of the shielding near the GEM calorimeter.

radiation dose due to the charged particles. The dose at standard luminosity to a detector placed R cm from the beam line is 50 Mrad/$(R/cm)^2$/SSCY. We expect the silicon to survive about 10 years at standard luminosity ($10^{33}cm^{-2}s^{-1}$).

For the B-physics detectors, the luminosity will be lower ($10^{32}cm^{-2}s^{-1}$), the tracking volume will be larger than a general purpose detector like GEM. Also, for some B detector designs a more open geometry is contemplated. All of the above differences will lower the neutron and photon albedo fluxes to about $10^{11}/cm^2$/SSCY. The lower luminosity should allow operation of silicon detectors as close as 1 cm to the interaction point. Other systems such as RICH detectors, time of flight counters are also needed for the B detector. Hit rates and damage to these systems need to be accessed.

Calorimeters

The main concern for these systems is the radiation dose in the forward calorimeters. The maximum dose at the inner corners of the forward calorimeter is dominated by electromagnetic showers. The hadronic dose is distributed over a much larger volume that the electromagnetic dose as expected from the ratio of interaction length to radiation length. For GEM, we have chosen to place the forward calorimeter close, 4.5 m, from the interaction point. This choice has resulted in a compact design with no gaps through which neutrons can escape and cause random hits in the muon system. The maximum doses at standard luminosity to forward calorimeters expected in GEM are 400 Mrad/SSCY at the inner edge with 10 Mrad/SSCY of hadronic dose distributed uniformly in the $3 < |\eta| < 5.8$ region. For the lower luminosity B detector, the forward systems will probably be farther away from the interaction point with corresponding decrease in the maximum dose.

Muon System

We have spent considerable effort in reducing random hits due to neutrons and photons in the muon chambers. The largest sources of neutrons in the detector are the collimator and the forward calorimeters. The muon chambers are approximately 10 times more sensitive to photons than to neutrons. Most of the photons in the muon system, however, are produced by interactions of neutrons. Therefore, we have concentrated on removing neutrons as close to their sources (the collimator and the forward calorimeter) as possible. We have accomplished our goal by hermetically sealing the entire beam line. The thick calorimeter serves as a shield in the central region; the concrete and the field shaper shield the beam pipe, the collimator, and the quadrupoles. We have computed the neutron and photon fluxes using the GEANT-CALOR[10,11,12] and the LAHET-MCNP code systems. The computations were performed with and without the shielding shown in Figure 2. The fluxes without the shielding are in the range of 10^{11} - 10^{12} neutrons/cm^2/SSCY at standard luminosity through the muon system. The photon flux is about 30% of the neutron flux. The shielding shown in Figure 2 reduces these fluxes by about two orders of magnitude.

As explained in Section 2, the lower luminosity at the B detector will reduce the contribution to particle fluxes in the muon system due to p-p interaction by a factor of 10, but the contribution due to beam gas interactions will remain the same. Therefore, one should expect a reduction of only about a factor 5 or a flux of few times 10^{11} neutrons/cm^2/SSCY in the muon system without shielding. The exact distribution will depend on the choice of detector geometry and the size of the hall. It is likely that the muon system will produce the trigger for the B detector. The trigger requirements, along with the muon chamber technology and the granularity, will determine the amount of shielding necessary. The experience from designing GEM suggests that a closed geometry is preferable to open geometries, which might be easier to construct. Thick concrete shielding around the beam line up to the tunnel entrance will probably be needed.

After a choice of the B detector geometry, calculations with one of the above mentioned code systems should be performed to assess the background rates and shielding.

The radiation task force for GEM consisted of the following individuals: Gerry Chapman, Joe Coyne, Milind Diwan, Yuri Efremenko, Yuri Fisyak, Vladimir Gavrilov, David Lee, Mike Marx, Roger McNeil, Nikolai Mokhov, Brent Moore, Kate Morgan, Vasiliy Morgunov, John Rutherfoord, Laurie Waters, Bill Wilson, and Craig Wuest.

I thank Linda Fowler for typesetting this paper on such short notice.

10 "CALOR: A Monte Carlo Program Package for the Design and Analysis of Calorimeter Systems," T.A. Gabriel, J.D. Amburgey, B.L. Bishop, ORNL/TM-5619, Apr. 1977. "User's Guide for the FLUNEV Code," J.M. Zazula, Desy-internal-rep D3-90-66, Jan. 1990. "FLUKA and KASPRO Hadronic Cascade Codes," J. Ranft, Erice 1978, Proceedings, Computer Techniques in Radiation Transport and Dosimetry.

11 Y. Fisyak, K. McFarlane, L. Roberts, GEM-TN-92-162, 1992.

12 C. Zeitnitz, T.A. Gabriel, "The GEANT-CALOR Interface," III Conference for Calorimetry in High Energy Physics, Proceedings (to be published), Corpus Christi 1992. C. Zeitnitz, T.A. Gabriel, "The GEANT-CALOR Interface," International Conference on Monte Carlo Simulation in High Energy and Nuclear Physics, Proceedings (to be published), Tallahassee, 1993. See also J.O. Johnson, T.A. Gabriel, "Development and Evaluation of a Monte Carlo Code system for analysis of Ionization Chamber Responses," ORNL/TM-10196, July 1987.

FIXED-TARGET PARTICLE FLUXES AND RADIATION LEVELS AT SSC ENERGIES

EDMOND C. DUKES
Physics Department, University of Virginia
Charlottesville, VA 22901, USA

1. INTRODUCTION

We calculate the charged particle fluxes and radiation doses from minimum ionizing particles (MIP), electromagnetic showers, and hadronic showers, in a fixed-target experiment at the SSC. We follow the work of Groom [1], essentially boosting his results into the laboratory frame.

The radiation in dense matter, such as a calorimeter, is produced by several sources: electromagnetic showers, hadronic showers, and minimum ionizing particles. We do not consider other sources of radiation such as beam halo, A dependent effects, and low energy neutrons from secondary sources. Nor do we consider the effects of magnetic fields. Low energy neutrons have been shown to be an important source of radiation for collider experiments at the SSC [2]. In fixed-target experiments, where the spectrometer is more open and where most detector elements are far away from secondary particle dumps, these sources are not as important. They are also very much detector and experimental hall dependent. Hence the results presented here are only a lower limit of the estimated radiation dose.

2. PARTICLE RATES

We need to know the number and momenta of particles of each type (hadron and photon) impacting a particular area:

$$\frac{d^2N}{d\Omega dp}. \tag{1}$$

We start with the invariant cross section

$$E\frac{d^3\sigma}{dp^3} = f(\vec{p}, s), \tag{2}$$

and work our way back to Eq. 1. In general, the invariant cross section is a function of the particle momentum $\vec{p}$ and the center-of-mass energy s. We may rewrite it as a function of rapidity y and transverse momentum p_t:

$$\frac{d^2\sigma}{\pi dy dp_t^2} = f(p_t, y, s). \tag{3}$$

The invariant cross section is well described at small to average values of transverse momentum by the factored form:

$$f(p_t,y,s) = g(p_t,s)\,h(y,s) = A(y)e^{-p_t/B}, \tag{4}$$

where both A and B are weak functions of s. This functional form greatly underestimates the large transverse momentum behavior of the cross section where a power law is more appropriate. However, the probability of a particle having a large transverse momentum is tiny and as such does not affect these results. It is more convenient to deal with a distribution differential in p_t rather than p_t^2:

$$\frac{d^2N}{dy\,dp_t} = \frac{1}{B^2}H(y)p_t e^{-p_t/B}. \tag{5}$$

This equation has been normalized such that after integration over all transverse momenta:

$$\frac{dN}{dy} = H(y). \tag{6}$$

H(y) is the rapidity distribution. Multiplying Eq. 5 by p_t and integrating over all transverse momentum gives $2H(y)B$. $2B$ then is the mean transverse momentum.

In our subsequent discussions we will use pseudorapidity η and and rapidity interchangeably. The pseudorapidity of a particle is defined to be $\eta = -\ln\tan(\theta/2)$ and is approximately equal to the rapidity when *both* $p > m$ and $p_t > m$ are true. (For example, a 100 MeV pion at 10 mrad has $y = 4.8$ and $\eta = 5.3$.) The particles we are concerned with are charged and neutral pions with an average transverse momentum of 0.350 GeV/c, so the above approximation is a good one for most transverse momenta.

The center-of-mass rapidity that a typical fixed-target spectrometer sees lies approximately between −2 and +1 (3.5 mrad to 72 mrad) as is shown in Fig. 1. This interval lies on the flat part of the rapidity plateau. The $\sqrt{s}$ dependence of the height of the rapidity plateau is well described by the form

$$\frac{dN}{d\eta}\Big|_{\eta=0} = 0.01 + 0.22\ln s. \tag{7}$$

At $\sqrt{s} = 193.7$ GeV, $H(0) = 2.3$.

In our subsequent discussion it will prove to be more convenient to use the polar angle θ rather than the pseudorapidity η. Using the fact that

$$2\pi\sin^2\theta\frac{d}{d\Omega} = \frac{d}{d\eta}, \tag{8}$$

Eq. 5 becomes

$$\frac{d^2N}{d\Omega\,dp_t} = \frac{H}{2\pi B^2\sin^2\theta}\,p_t\,e^{-p_t/B}, \tag{9}$$

and the number of particles incident on an area da is, using the fact that $d\Omega = da/r^2$,

$$\frac{d^2N}{da\,dp_t} = \frac{H}{2\pi B^2}\frac{1}{(r\sin\theta)^2}\,p_t\,e^{-p_t/B}. \tag{10}$$

3. NUMBER OF PARTICLES

Integrating Eq. 9 over all transverse momenta gives the number of particles impacting a unit solid angle $d\Omega$:

$$\frac{dN}{d\Omega} = \frac{H}{2\pi\sin^2\theta}. \tag{11}$$

The number of particles impacting an area da is

$$\frac{dN}{da} = \frac{H}{2\pi r^2\sin^2\theta} = \frac{H}{2\pi r_\perp^2}, \tag{12}$$

where $r_\perp^2$ is the radial distance of da from the beam line. Plugging the numbers in for the height of the pseudorapidity plateau gives the number of charged particles per unit area per interaction:

$$\frac{dN}{da} = \frac{0.37}{r_\perp^2}\ \text{charged particles/area interaction.} \tag{13}$$

This is plotted in Fig. 2.

Assuming these charged particles are all minimum ionizing particles, we can convert Eq. 13 into radiation units (energy/mass). For polystyrene a minimum ionizing particle deposits $dE/dx = 1.95$ MeV/g/cm^2, and since 1 Gy (100 Rad) = 6.24×10^9 MeV/g (or 1 Gy = 3.2×10^9 MIP/cm^2) then 1 MIP/cm^2 = 3.125×10^{-10} Gy. Hence

$$D_{\rm MIP} = \frac{1.2\times10^{-10}}{r_\perp^2}\ \text{Gy/interaction}, \tag{14}$$

where $D_{\rm MIP}$ is the radiation dose and $r_\perp$ is in cm. This is plotted in Fig. 3.

4. DOSE FROM ELECTROMAGNETIC AND HADRONIC SHOWERS

The flux of charged particles from the primary interaction given by Eq. 9 is composed largely of charged and neutral pions, the charged component being twice the neutral. The flux of gammas is essentially the charged particle flux since most come from the decay of pizeros. However, their average transverse momentum is half that of the charged pions.

All of the gammas will shower in a dense material, depositing far more radiation than a minimum ionizing particle. The charged hadrons (pions) will shower as well. The electromagnetic energy is deposited nonuniformly with most of it coming at the shower maximum. The hadronic energy is deposited much more uniformly and over a much larger volume.

It has been shown [1] that the maximum radiation dose deposited by either an incident gamma or a hadron of momentum p can be parameterized by

$$\text{Dose} = \frac{dD}{df} = Ap^\alpha\ \text{Gy/incident particle/cm}^2, \tag{15}$$

where f is the flux of particles per unit area (dN/da), A is a constant and α is a number between 0 and 1. For an electromagnetic shower $A = 3.2\times10^{-9}$ and $\alpha = 0.93$ where p is given in GeV/c [3]. The dose is not a strong function of material. To find the total dose we need fold Eq. 10 with Eq. 15 and integrate over all transverse momenta. We have (using $p = p_t/\sin\theta$):

$$D = \frac{A}{2\pi B^2}H\int_0^\infty \frac{p_t^{\alpha+1}}{(r\sin\theta)^2\sin^\alpha\theta}e^{-p_t/B}dp_t \tag{16}$$

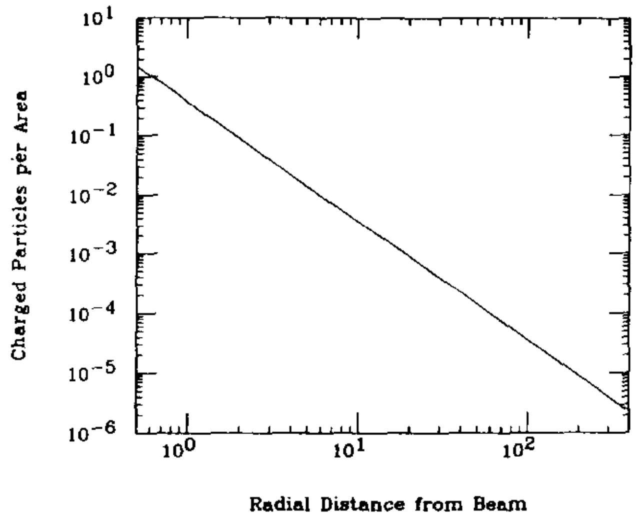

Fig. 2. The number of charged particles per unit area per interaction as a function of the radial distance from the beam.

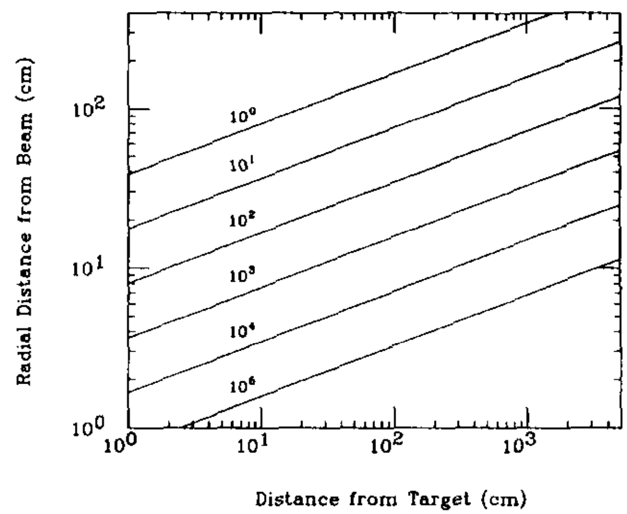

Fig. 4. The maximum electromagnetic radiation dose in a dense material per interaction as a function of the distance from the target and the radial distance from the beam. The dose is given in units of 10^{-14} Gy.

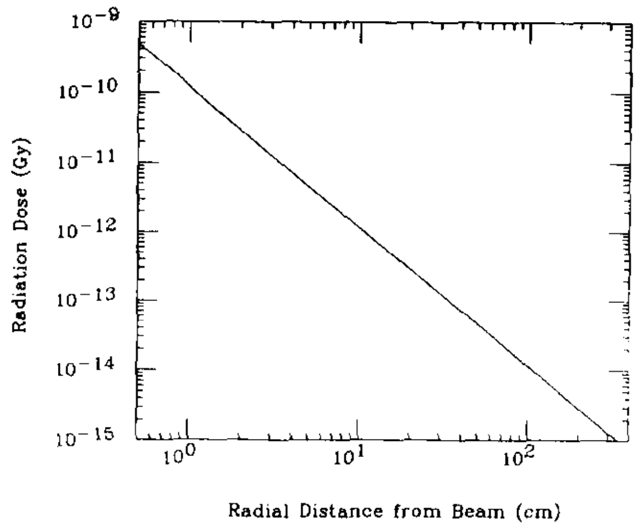

Fig. 3. The radiation dose in polystyrene per interaction due to minimum ionizing particles as a function of the radial distance from the beam.

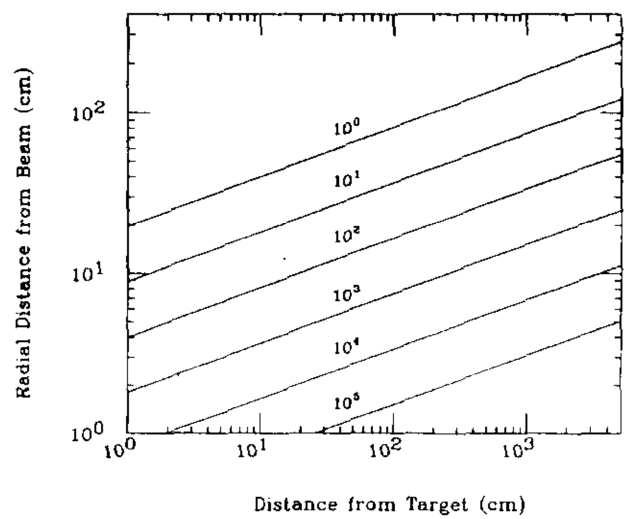

Fig. 5. The hadronic radiation dose in a dense material per interaction as a function of the distance from the target and the radial distance from the beam line. The dose is given in units of 10^{-14} Gy.

and

$$D = \frac{A}{2\pi} H \frac{B^\alpha}{(r\sin\theta)^2\sin^\alpha\theta}\int_0^\infty x^{\alpha+1}e^{-x}dx \qquad (x = p_t/B) \tag{17}$$

$$= \frac{A}{2\pi} H \frac{B^\alpha}{(r\sin\theta)^2\sin^\alpha\theta}\Gamma(\alpha+2). \tag{18}$$

$\Gamma(\alpha+2)$ is the Gamma function.

Groom has shown that the exponential form for the transverse momentum distribution can be replaced by the average momentum. Following his lead, we replace the momentum spectrum $(1/B^2)p_t e^{-p_t/B}$ in Eq. 16 by $\delta(p_t - \bar{p}_t)$,

$$D = \frac{A}{2\pi} H \int_0^\infty \frac{p_t^\alpha}{(r\sin\theta)^2\sin^\alpha\theta}\delta(p-\bar{p})dp, \tag{19}$$

where $\bar{p}_t = 2B$. Integrating over transverse momentum gives:

$$D = \frac{A}{2\pi} H \frac{(2B)^\alpha}{(r\sin\theta)^2\sin^\alpha\theta}. \tag{20}$$

The difference between Eq. 20 and Eq. 18 is $\Gamma(\alpha+2)$ vs 2^α, or with $\alpha = 0.93$, 1.91 vs 1.88, which is less than 2%. Since the difference is small we continue using Eq. 20 only. The maximum dose rate from electromagnetic showers using Eq. 20 is

$$D_{em} = \frac{A}{2\pi} H \left(\frac{2B}{\sin\theta}\right)^\alpha \frac{1}{r^2\sin^2\theta}\ \text{Gy/interaction}. \tag{21}$$

Using the values given above for $H(0)$, A, and α, and $2B = \bar{p}_t = 0.350/2$ GeV/c gives

$$D_{em} = 4.4\times 10^{-10}\frac{1}{r_\perp^2\sin^{0.93}\theta}\text{Gy/interaction}, \tag{22}$$

where $r_\perp$ is in cm. The result is plotted in Fig. 4.

To do the same for hadronic showers is to repeat the above discussion using different values for A (3.8×10^{-10} Gy), α (0.89), and $2B$ (0.350). The *maximum* dose is about 9 times less than the dose caused by a gamma of the same energy (@ 10 GeV). The reason is the more uniform distribution of energy in a hadronic shower. The maximum energy deposition occurs at about one interaction in depth. Plugging the numbers in gives:

$$D_{had} = 0.55\times 10^{-10}\frac{1}{r_\perp^2\sin^{0.89}\theta}\text{Gy/interaction}, \tag{23}$$

where $r_\perp$ is in cm. This result is plotted in Fig. 5.

5. REFERENCES

1. D. E. Groom, Ed., *Radiation Levels in the SSC Interaction Regions*, SSC-SR-1033, (1988).
2. T. Pal, these proceedings.
3. D. E. Groom et al., SSCL-285, (1990). This is an erratum to SSC-SR-1033. In particular the maximum electromagnetic dose in that memo was found to have been overestimated by a factor of three.

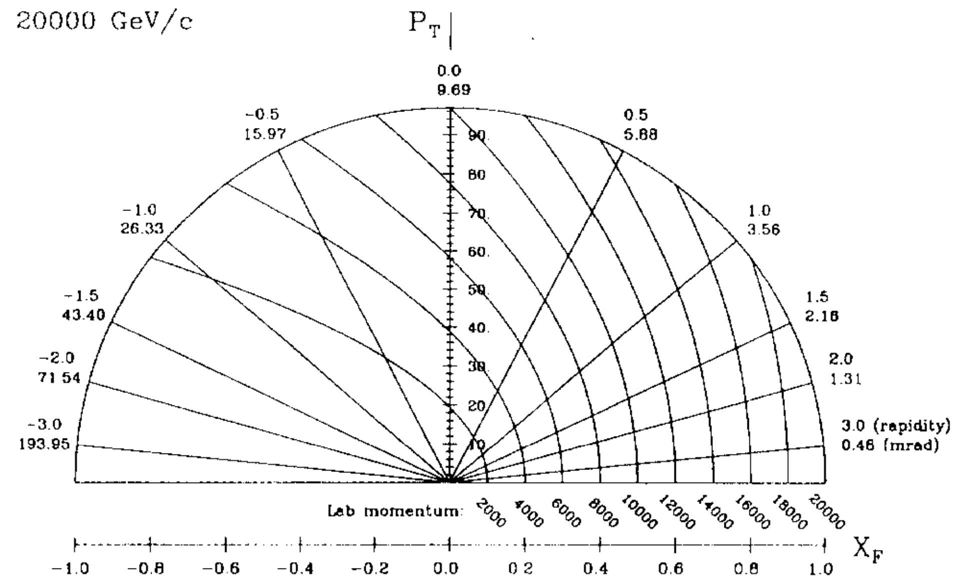

Fig. 1. The relation between center-of-mass pseudorapidity and laboratory angle at fixed-target energies at the SSC. The horizontal axis is the fractional momentum in the beam direction. The vertical axis is the transverse momentum. Lines radiating from the origin are in 0.5 pseudorapidity increments. The equivalent laboratory angles (in mrad) are given.

LONGITUDINAL WAKEFIELD FOCUSING: AN UNCONVENTIONAL APPROACH TO REDUCE THE BUNCH LENGTH IN TEVATRON

A. GERASIMOV
Fermi National Accelerator Laboratory, P.O. Box 500, Batavia, IL 60510, USA*

Achieving a shorter bunch length in Tevatron would provide a better information on the primary vertex and will allow the collider experiments to use shorter vertex detector.[1] It would also allow an increase of luminosity by a further reduction of the β-functions at the interaction point. The conventional path to this goal by using higher RF voltages or increasing the number of RF cavities appears however prohibitively expensive.[2] I propose here an alternative solution of "wakefield focusing" building on the ideas of Alexei Burov[3-5] for electron storage rings.

The physics of the wakefield focusing can be explained as follows: the rear particles in the bunch are affected by the front particle wakefields, but not vice versa. Therefore, for the flat (step-function) wakefield the rear particles will be stronger decelerated by the wakefields than the front ones. For the energies above transition, the longitudinal "mass" is negative, and the reduction in energy incurs the reduction in the revolution period. Subsequently, above transition the rear particles will tend to "catch up" with the front ones, so that the wakefields will provide an extra focusing and the bunch length is reduced. Below transition, the effect of the wakefield is opposite and the bunch length is increased. It is assumed that the wakefields decay within one revolution period, so that the corresponding impedance is the broadband one.

An approximately capacitive structure was proposed in Reference 5 in the form of a dielectric channel. It would not however be feasible for much longer proton bunches. I propose another type of structure for creating the capacitive impedance: a narrow flat-flanked gap in the conducting pipe. A row of such gaps produces an additive effect and allows to achieve the high wakefields.

In Figure 1, electric field pattern is shown at the moment after the bunch passed the gap is presented. The simulation was done with the use of the wakefield-calculation code TBCI.[6] This code allows to simulate only the closed cavities, so I added a large cavity on the outside of the gap. In the narrowband scheme, the cavity is actually the necessary element of the scheme.

*Operated by the Universities Research Association, Inc. under contract with the U.S. Dept. of Energy.

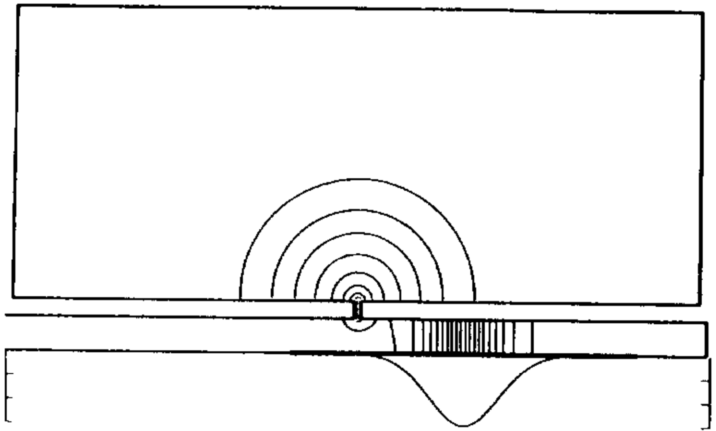

Figure 1. Electric field lines for the gap-cavity system.

The wakefield function $W(s)$, is presented in Figure 2. Horizontal scale of the graph is in meter units. One can see that after reaching a maximum at distances $\sim 2\sigma$ behind the peak of the bunch density, the wake function decreases only slightly and stay nearly constant for about 70 cm

For the purpose of focusing with the broadband impedances, the wakefield has to stay nearly constant (after reaching its maximum) for a few sigmas of the bunch distribution.[3,4] In the new scheme with narrowband-type of wake that I propose, there is no need to have the wakefield that stays constant for more than 2σ. For the Tevatron bunch with $\sigma \approx 30$ cm, this condition is still not well satisfied as the wakefield decreases noticeably after reaching the maximum. The reason for that is the leaking of the charge to the outer surface of the pipe as mentioned above.

In order to have the maximum possible wakefield focusing in the broadband scheme, one needs to achieve the total wakefield potential W_{max} that equals the maximum RF potential V_{RF}. For Tevatron, where $V_{RF} \sim 1$ MV and bunch intensities are about $N_p \sim 1.2 \cdot 10^{11}$ (particles per bunch), one can estimate the necessary gap capacitance $C = \frac{r\Delta}{h}$ (with r for the inner pipe radius, Δ the thickness of the wall and h the gap length) as $C \approx .14 \cdot 10^{-3}$ (m). It was assumed here that the gap satisfies the "flat capacitor" restrictions $h \ll \Delta$ as well as the condition $\Delta \ll r$. That small capacitance creates the problem since it means the short discharge time.

To solve it, I propose the usage of the ferromagnetic filling of the outside cavity. The basic idea in our case is that the high permeability of the filling on the outer side of the gap (which is not filled) will drastically increase the surface inductance of the outer surface. One can expect that the time constant of the leakage to the outer surface will increase as $\tau' \sim \tau\sqrt{\epsilon\mu}$.

The other aspect of the advantage of the ferromagnetic filling is that the speed of light in the outside cavity will be reduced by a factor of $\sqrt{\epsilon\mu} \sim 50$. this means that if there are many gaps in a row and they are separated by a distance $a = 2$–4 cm, the total wakefield will be purely additive with respect to the individual gap wakefields up to the distances $s \sim a\sqrt{\epsilon\mu} \sim 100$–$200$ cm. This is more than the bunch length in Tevatron and is sufficient for the purpose of the wakefield focusing with narrowband impedance.

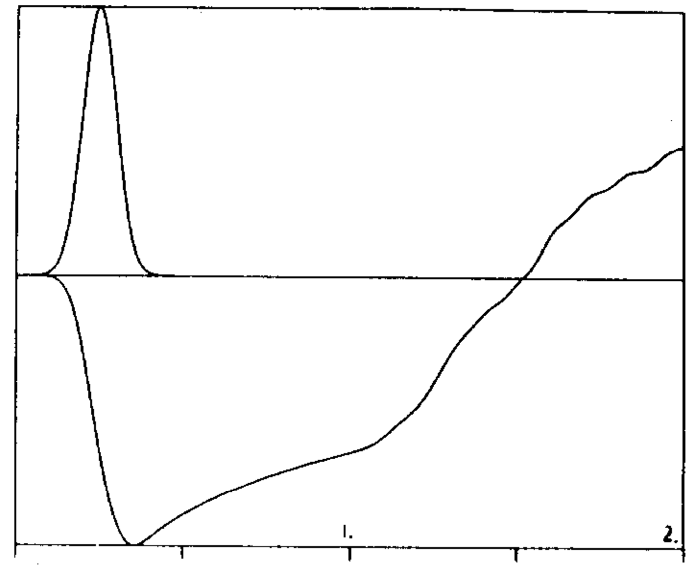

Figure 2. Wakefield function $W(s)$ for the case of Figure 1.

Overall outlay of the structure can be as follows: Packages of gaps with thin conducting inserts are alternating with beam pipe section of about 2–5 cm long. The outside of the pipe is coated with ferrite. Let's assume 5 cm pipe section will be required. The length of the package should be increased to as much as the discharge time limitation allows, but increasing it much above 10 cm would not gain much. Assume therefore the length of the package $h = 10$ cm. In order to minimize the capacitance $C = r\Delta/h$, the smallest possible radius of the pipe should be taken. For Tevatron, with certain effort one could probably achieve about $r = 2.5$ cm. The width Δ cannot be reduced to much less the r, but can probably be made as small as $\Delta = 1$ cm. This corresponds to the capacitance of the package $C = \frac{r\Delta}{h} = 0.25 \cdot 10^{-2}$ (m). It would take then about 100 packages and a total length of about 15 m (including the space between packages) to achieve the bunch length reduction by a factor of 2. The package of rows should be divided into several separate structures each with its own cavity.

Numerical simulation of bunch compression by the adiabatic increase of the wakefield was carried out by implementing the single-turn mappings for each particle that included both the RF field and the wakefield effects.

The wakefield intensity parameter ϵ, that is the ratio of the maximum RF voltage to the maximum wakefield voltage, is slowly increased from 0. to ϵ_{max} over the time period much longer than the synchrotron period $1/\omega_s$. Results are presented in Figure 3, where the center-of-mass displacement $a = \langle x \rangle$ and size σ of the bunch are shown as a function of time (measured in turns).

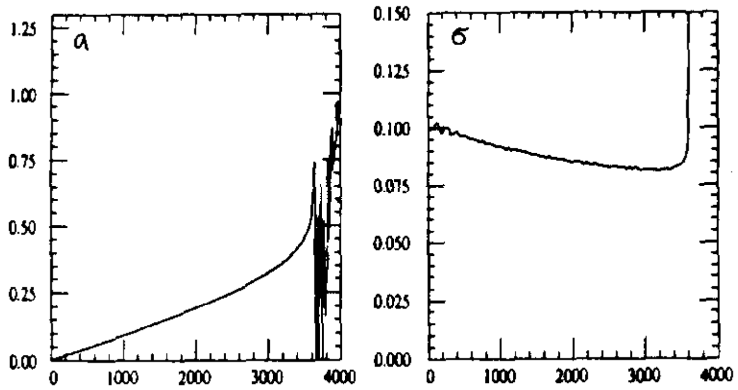

Figure 3a, b. Time dependence of (a) bunch displacement a, and (b) half bunch length σ for initial $\sigma_0 = 0.1$, $\omega_s = 0.1$ and $\epsilon_{max} = 2.1$. Time units are in turns.

One important feature of this graph is that there is a sudden increase in σ and oscillations of a that start when displacement a reaches the value close to 0.5. The reason for that is quite simple: when the wakefields are stronger than RF voltage, the beam is getting decelerated on each turn (so it will be lost very fast).

One can see indeed that the adiabatic compression is working but the relative reduction of the bunch length for the value of σ is quite small. One natural way to remove the energy balance limitation is to think up a way to "recycle" the energy of the wakefields and return it back to the beam. For the structures with the cavity as in Figure 1 this comes about quite naturally when the quality factor Q will be high. The energy loss can be made arbitrarily small by achieving high Q if the resonant frequency of the cavity ω_r is tuned not close to any of the revolution frequency multiples. The total wakefield force now has the contributions from the previous turns.

One example of the simulation results of the adiabatic bunch compression with the high-Q wakefields (narrowband impedance) is presented in Figure 4. The parameters that specify the broadband component are $\omega_r/\omega_0 = 514.5$, $Q = 10290$ (which corresponds to the decay of the wakefield in 20 turns) and main RF harmonic number $h = 1028$.

In Figures 4a, b one can see that the bunch is focused to a significantly smaller size while the displacement of its center-of-mass is kept at a fairly low value. The latter is the indication of the low parasitic loss (small deceleration). This is also the reason why in this regime one can raise ϵ to so high value $\epsilon_{max} = 6.2$ without losing the stationary phase regime as in the broadband case.

A more detailed report on this work is to appear shortly as a Fermilab preprint. Many Fermilab people contributed to this work by sharing their expertise and giving useful advice. I am particularly thankful to Fady Harfoush for the help with TBCI calculations and to David Wildman of discussions of RF cavity properties.

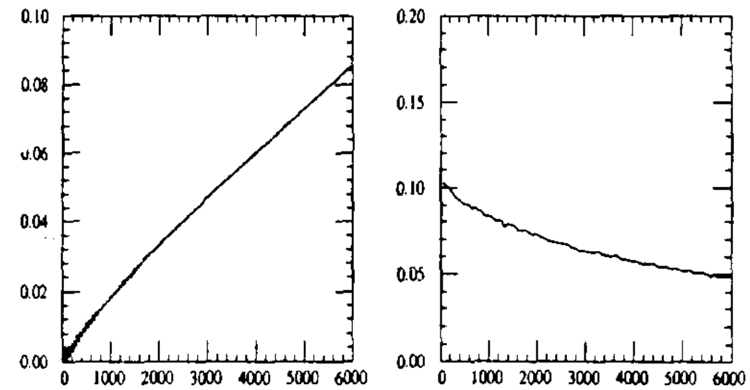

Figure 4a, b. Time dependence of (a) bunch displacement a, and (b) half bunch length σ for $\sigma_0 = 0.1$, $\omega_s = 0.1$ and $\epsilon_{max} = 6.2$. Time units are in turns.

REFERENCES

1. P. Martin, Fermilab bunch length reduction, presentation at 4-th FNAL/SSCL Workshop on B Physics at Hadron Accelerators, November 16–17, 1992 (unpublished).
2. Machine-Detector Interface Working Group Report, Workshop on B Physics at Hadron Colliders, Snowmass, June 21–July 2.
3. A. Burov, Part. Accel. 28 (1990) 47.
4. A. Burov, Bunch lengthening, self-focusing and splitting. Int. J. Mod. Phys. A (Proc. Suppl.) 2B (1993) 1148.
5. A. Burov, A.N. Novokhatski, Wake potentials of dielectric canal, ibid, p. 537, The device for bunch self-focusing, INP Preprint 90-28.
6. T. Weiland, DESY 82-015, DESY-M-83-02 and NIM 213 (983), NIM 215 (1983).

OBTAINING SLOW BEAM SPILLS AT THE SSC COLLIDER

D. Ritson
Stanford Linear Accelerator Center
Stanford, CA 94309

1. INTRODUCTION

There is substantial interest in providing slow-spill external proton beams in parallel with "interaction running" at the 20 TeV SSC collider. The proposal is to cause a flux of particles to impinge on a target consisting of a bent crystal extraction channel.[1] Additionally, a slow spill onto a conventional internal target could be used as a source of secondary beams for physics or test purposes and might also be used for B-physics as proposed for HERA. The "natural" beam loss rates from elastic and diffractive beam gas scattering and IP collisions are not sufficient to provide suitably intense external proton beams. The presently favored scheme for providing sufficient spill intensity is to increase the emittance of the beam via rf noise excitation of the longitudinal synchrotron oscillations.[1]

To prevent loss of luminosity, the rf excitation is non-linear and preferentially blows up the halo of the beam. The "target" is to be located at a region of high dispersion forcing particles at the edge of the momentum space onto the target.

T. Lohse[12] in this workshop has described a proposed internal target to be used at HERA that will not employ rf excitation but will use the finite loss rates observed at the HERA machine.[12] The Hera losses are caused by a variety of sources in addition to beam gas scattering or IP interactions. These sources include machine imperfections, improperly centered IP collisions, tune modulation, poor chromaticity correction, beam-beam interactions etc. Initially, the beam lifetime at HERA was too short to obtain satisfactory integrated luminosities. Subsequently, through careful attention to detail, the beam lifetime was increased to > 20 hours. Even with these changes, present loss rates provide the required intensity onto an internal target. The Tevatron and SPS proton anti-proton colliders have had similar experiences with their investigations of loss rates and also find that beam lifetimes may be substantially shorter than expected solely from beam gas and IP interactions. This paper proposes deliberately introducing controlled errors like moving the betatron tune gradually closer to the edge of the operating diamond to provide the desired beam loss rates.

Qualitatively such errors move the edge of the chaotic region or dynamic aperture of the beam closer to the beam, effectively "scraping off" halo particles. The particles, once out of the dynamic aperture, diffuse into increasingly chaotic regions of the aperture until they impinge on an appropriately positioned internal target.

We discuss mechanisms available to shorten beam lifetimes, corresponding rates of diffusion out through the aperture, and target entry step distributions.

2. LOSS MECHANISMS

A satisfactory loss mechanism should satisfy the following criteria:

1. The perturbation should be simply and precisely controllable.
2. The perturbation should not cause accumulation of the beam into stable island regions.
3. Ideally, the perturbation of choice should be simple to implement and economic.

We believe the approach most likely to satisfy all the above criteria is to use tune shifts that move the beam closer to the high order controlling resonances in the vicinity of the operating tune point, perhaps to be used in combination with errors in chromatic correction. Other approaches could involve the introduction of positive chromaticity into the lattice or the excitation of a high multipole magnetic element in the lattice. An overview of the physics and operational experiences of such approaches can be found in a number of publications.[2,3]

2.1 Effects of tune shifts.

Early studies at the SPS collider explored beam losses as a function of operating point.[4] These studies dramatically illustrated that moving the operating point close to resonances as high as tenth order strongly decreased the lifetimes of the beams while in collision mode. Subsequent simulations and operational work with hadron colliders confirm these observations.[3] The loss mechanism is not straightforward and appears to involve the generation of chaotic phenomena.

At the SSC, the bunch spacing is very small (5 metres), and this small spacing will basically determine the parameters of the interaction configuration. The "short-range" beam-beam forces come from the central collisions at the IP, and the counter-circulating beam is the source of "long-range" beam-beam forces at a large number of satellite collision points before the beams are bent apart into their separate rings. To minimize the long-range effects, the beams are to be crossed at the IPs with the largest crossing angles that are consistent with other physical constraints. Even then, the long-range tune shifts are comparable in magnitude to the beam-beam tune shift at the central collision point.

Figure 1 shows a figure taken from an SSC report by J. Irwin[13] showing the effects of high order resonances in combination with the long range beam-beam interactions in the tune plane in the vicinity of a typical operating point close to 0.26 in tune. Resonances up to eleventh order are included. Superimposed on the tune plane is the beam footprint calculated by Tennyson[5] with the tune as a function of both vertical and horizontal amplitude.[6] The most notable feature of the footprint is the "wings" in the tune space at large betatron amplitudes. These wings are the direct result of the strong long-range tune shifts encountered as particles pass close to the countercirculating bunches at large amplitudes.

Small changes in the operating point can move the high amplitude wings, but not the main core of the beam, to the boundaries of the tune space set by high order resonance lines and cause particles in the wings to become unstable. With increasing amplitude, such unstable particles move even closer to the countercirculating bunches and encounter increasingly strong non-linear forces that further destabilize their motion.

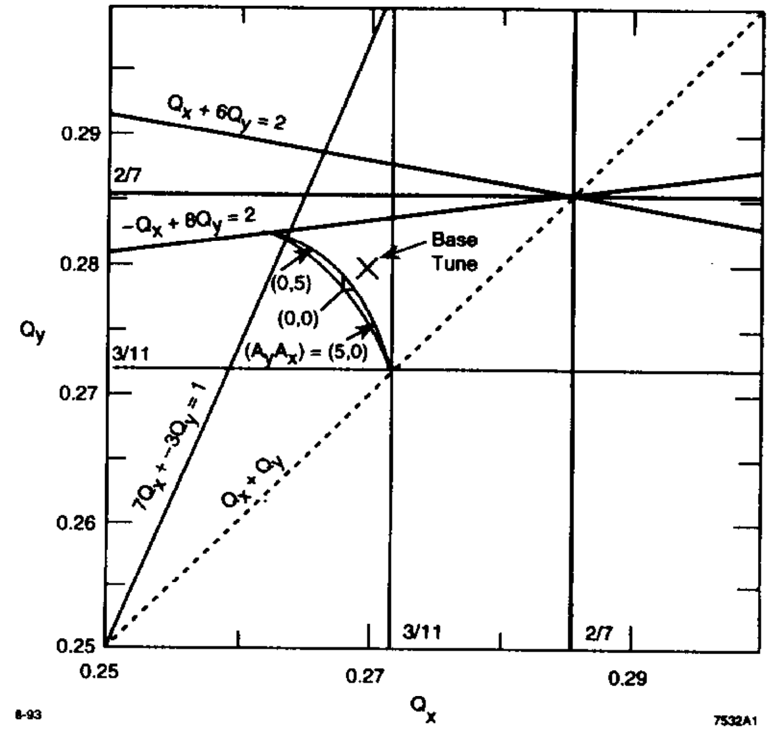

Figure 1. Tune space around the expected operating point at 0.26. Resonances are shown up to tenth order. The $Q_x = Q_y$ first order coupling resonance is shown as a dotted line.

A controlled movement of the SSC operating point should successively remove high amplitude particles and result in a required beam loss rate without at the same time affecting the central beam phase space and the luminosities.

2.2 Chromaticity Effects on beam life-time.

The same local and global SSC correctors designed to remove chromaticity can also of course be used to introduce non-zero first or second order chromaticity. Non-zero lattice chromaticity causes particles to modulate their tune in synchronism with their off momentum component at the synchrotron frequency while undergoing synchronous motion. Thus a machine with finite chromaticity is tune modulated at the synchronous frequency. Tune modulation gives sidebands to resonance lines that enhance the effects of these resonances, and if overlap with other resonances occurs, chaotic regions in phase space may be created. This has been investigated extensively both by simulation and experiment.[2]

Chromaticity errors alone in an SSC crossing configuration, although destabilizing the beams, could possibly result in trapping particles in stable "islands" in phase space. It might well prove advantageous to use chromaticity errors in combination with shifts in the operating tune to avoid island formation.

2.3 The use of strong non-linear multipole field errors.

The long-term dynamic aperture of a machine is decreased by the presence of high multipole magnetic field errors.[7] This has long been suggested as a means to provide "massless scrapers."[10] However, locating non-linear magnetic elements at the high beta points in the IR triplets is ruled out because they would simultaneously destabilize both the beam and the countercirculating beam. At other locations in the lattice, beta values are substantially smaller, and through simulation we find that very strong elements would be required. This is because the long-range forces present from the countercirculating beam at $\sim 10\sigma$ are very strong sources of non-linearity, and a significant modification of loss rates requires the introduction of commensurate-strength non-linearities. This does not exclude this option but does make it substantially less attractive.

3. DIFFUSION RATES AND ENTRY STEP DISTRIBUTIONS

Typically targets would be located 5–10 σ out from the beam orbit and $1-2\sigma$ in from the primary beam scraper. At such a location, rf noise excitation causes slow changes in beam size and entry steps of a few microns.[1] In terms of an effective diffusion velocity at the target, this corresponds to a few microns beam movement over a synchronous period, a velocity commensurate with or less than that expected from orbit movements caused by seismic or cultural noise.[8] Maintaining a uniform spill rate is likely to require stabilization of the orbit at the target by a feedback system sensing instantaneous spill rates. This is feasible but adds complexity.

Reference 11 discusses the use of a "spreader" target to increase the step size into the primary SSC collimator. We have investigated using a spreader target in combination with rf noise excitation and find that a 0.5-radiation-length tungsten spreader target positioned 30 microns in from the edge of the main target will increase step sizes by an order of magnitude. However, the effective diffusion velocity into the spreader target, in conjunction with orbit instability, sets the spill modulation. Therefore the spill pattern is unchanged by the addition of a spreader target.

For mechanisms that modify the dynamic aperture, the target is located beyond the edge of the long term dynamic aperture. We have simulated outward diffusion of particles at the target location with such mechanisms. Figs. 2 a and b show histograms of entry steps at nominal SSC interaction conditions with horizontal and vertical tunes set to 0.42 for targets located at 7 and 10σ from the beam respectively. The entry steps are now tens of σs in magnitude and correspond to effective diffusion velocities at the target of tens of microns over a few revolution periods. The effective velocities now substantially exceed the velocities of orbit movements expected from seismic or cultural disturbances. Therefore, obtaining a uniform spill does not require stabilization of the orbit at the target position.

With the small target entry steps that result from rf noise excitation, the crystal must be positioned with a horizontal beam offset for vertical bend.[9] In this configuration, there is substantial loss of efficiency if vertical entry angles exceed 1 microradian. For extraction of off-momentum particles (rf noise excitation), this is not a problem because the rms of

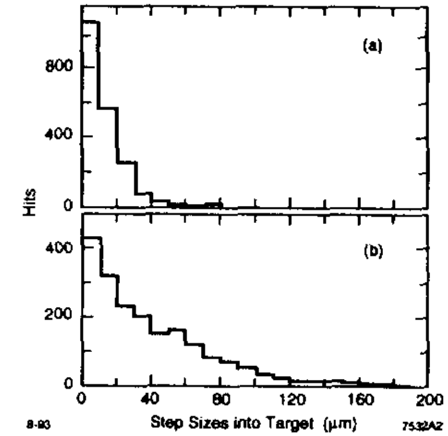

Figure 2. (a) and (b), derived from simulation, show histograms of the entry steps into targets located 7 and 10σ away from the central orbit, respectively. The conditions are for nominal SSC beam intensities, emittances and crossing angles, and for fractional tunes of 0.42 in horizontal and vertical.

the nominal vertical angular divergence is 0.3 microradians. For our suggested mechanisms that extract particles at large betatron amplitude, there could be problems with a target positioned in this way. In the presence of substantial cross-coupling, vertical entry angles could well exceed 1 microradian. However, with the now substantially larger entry steps into the crystal, the machining tolerances to be expected for the surfaces of the crystal permit good channeling efficiency for crystals positioned with a vertical beam offset for a vertical bend. In this configuration the channeling efficiency is naturally insensitive to horizontal beam divergence, and in the vertical plane particles enter the crystal only at extremes of their betatron orbit motion with directions closely parallel to the beam axis and therefore effectively with small vertical beam divergence. Thus the 1.0 microradian constraint on vertical entry angle does not cause substantial losses in chanelling efficiency.

4. WIRE INTERNAL TARGETS

HERA proposes to use a thin, high-A internal target for B-Physics. The high A provides an enhanced relative cross-section for B-production.[24] For SSC energies we have verified the HERA result that for a high Z target to be efficient, it should be located in a relatively low β region. This precludes its use in a SSC utility straight. However the use of carbon targets in a utility straight would give quite acceptable efficiencies, and locating a high Z target at the SSC close to secondary IP focii would be satisfactory.

5. CONCLUSIONS

In additon to rf noise excitation, other methods should be able to provide slow controlled beam spills onto SSC targets. The most convenient and easily controlled of such methods is to move operating tunes so as to keep the large amplitude beam halo on an edge of the "operating diamond." This positions the dynamic aperture to cause short lifetimes before loss for large amplitude particles. The target is naturally located for nominal SSC operation outside the edge of the dynamic aperture, where effective diffusion velocities are large. This ensures that spill intensities remain uniform and are minimally modulated by orbit movements from cultural and seismic disturbances.

We believe that both rf noise emittance growth and movement of the edge of the dynamic aperture are likely to satisfactorily provide controlled beam loss and that a final choice of choice of method may be determined by operational experience at current accelerators or with the SSC.

REFERENCES

1. B.S.Newberger, H.J. Shi and J.A. Ellison, NIM, A325 (1993) 9–15.
2. cf for instance X. Altuna et al.,Corpus Christi 1991, Proceedings, 355.
3. cf for instance S. Saritepe et al, Frontiers of Particle Beams: Intensity Limitations, Proceedings, Hilton Head Island, 1990.
4. AIP Conference Proc. No 127, p. 244, 1983.
5. J.L.Tennyson, SSC–155, 1988.
6. D.Ritson, SLAC-TN-91-009,1991.
7. cf for example Garavglia, Kauffman, Stiening and Ritson, SSCL–268 1990.
8. cf for example G.E. Fischer, P.L. Morton (SLAC), SLAC–PUB–3870, 1986.
9. B.Newberger, presentation at this workshop.
10. A.W. Chao, M. Month, BNL–19080,Jun 1974.
11. R.Soundranayagam et al, Particle Accel.Conf: IEEE 1991:625-627.
12. Tests of Internal wire targets at HERA, this workshop.
13. J.Irwin, SSC–233, 1989.

ULTRA THIN BEAM PIPES FOR INTERNAL TARGET B EXPERIMENTS

HANS JÖSTLEIN
Fermi National Accelerator Laboratory
MS 122, P.O. Box 500, Batavia, Illinois 60540

Experiments looking for particles from B-decays at colliders, especially at large eta, find that the material presented by typical beam pipe walls (0.5 mm Be) present a significant mass, causing multiple scattering.

Under external pressure conditions, wall thickness is needed to resist deformation of the pipe. The pipe is unstable if the energy released by the reduction of internal volume exceeds the energy stored in the deformed pipe wall material. Both energies are proportional to the cube of the deformation. The deformation mode depends on pipe length between stabilizers, and can range from oval (basic mode) to high order "ripple type" modes.

Very low mass pipes can be designed by combining a thin wall pipe with periodic ring type stiffeners.

This design can be made compatible with the very low outgassing requirements by using a two step process. The thin pipe "sleeve" is made by brazing a thin Be sheet into a cylinder, and by brazing on appropriate ends. This sleeve can be vacuum baked and tested at reduced differential pressure, but not be fully evacuated.

After the sleeve has been leak checked and vacuum baked, the external stiffening rings are attached using adhesives.

We are currently developing such structures in the Fermilab Physics Department.

POINT-LIKE INTERNAL TARGETS FOR B EXPERIMENTS

HANS JÖSTLEIN
Fermi National Accelerator Laboratory
MS 122, P.O. Box 500, Batavia, Illinois 60540

Fixed target geometries are being studied for B experiments. Some use internal targets in colliders, e.g. the proposal for HERA.

Their current proposal uses very thin stretched wires (see Figure 1). The wires are brought into the beam halo when the beam is stabilized. Their measurements have confirmed that sufficient luminosity and stability can be obtained without impairing collider performance for concurrent other experiments.

Fixed target geometries lead to high laboratory momenta of the secondary particles, resulting in large vertex displacements. Wires constrain the primary vertex in the two dimensions transverse to the wire. The third dimension is constrained only by the beam spot size. It appears desirable to use a point like target, if possible, to constrain the event vertex in three dimensions.

Another concern is the possible instantaneous luminosity fluctuations. Successive bunches in the collider may exhibit different widths, or undergo collective motion and lead to fluctuations on a fast time scale, leading to pile-up problems in the detector. This is a well known problem when splitting small amounts of beam from the fringes. The fluctuations get better the closer one gets to the core of the main beam.

It appears technically feasible to answer both concerns with the following target design, as seen in Figure 2.

The target consists of an extremely thin wall, short, tubular section, as shown in the sketch. The wall would be a few microns thick, the tube diameter about 30 microns, and the length a millimeter or so. This target could be made by vapor depositing diamond on a carrier wire of 30 microns diameter, and then etching away the support wire from one end. The resulting structure is a wire, with the thin tubular section extending from one end. The wire would be driven into the beam until satisfactory luminosity is achieved. Diamond has a very high thermal conductivity and working temperature. The support wire could be Tungsten or other high temperature material. Chemical vapor deposition of diamond is now commercially available, e.g. for tool coating, at reasonable cost.

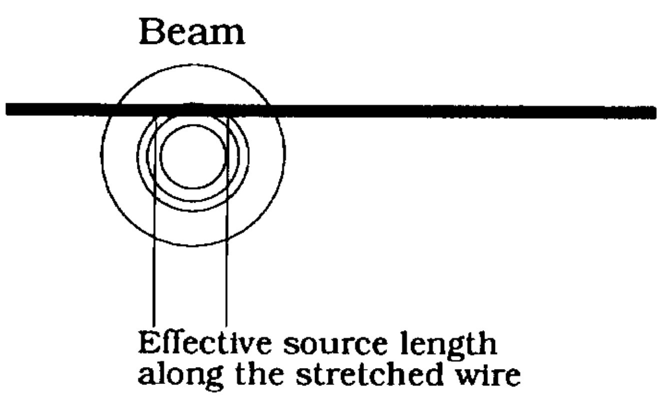

Figure 1. Stretched wire solution (HERA proposal)

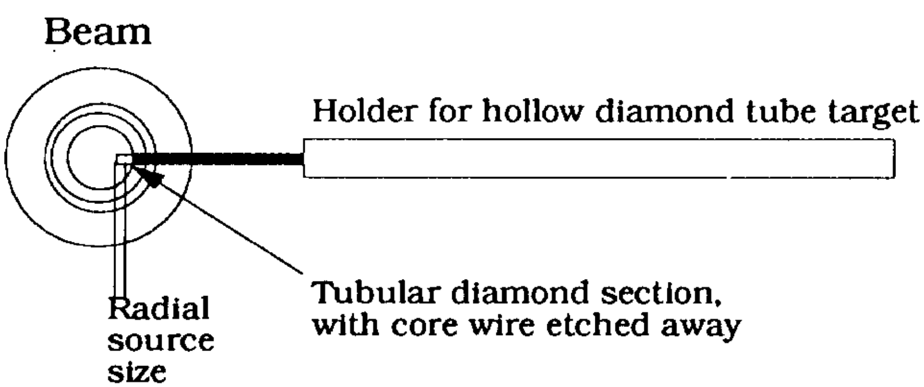

Figure 2. Tubular diamond "point target"solution

Other Contributed Papers

MEASUREMENTS OF THE $B^0\bar{B}^0$ CP ASYMMETRY

VERA LÜTH
Superconducting Super Collider Laboratory
2550 Beckleymeade Avenue
Dallas, Texas 75237-3946, United States

A figure of merit for a measurement of CP violation is the error on the intrinsic asymmetry A_{CP}. The observed asymmetry A_{obs} will always be smaller than A_{CP} due to a number of effects that dilute the measurement. If we define

$$A_{obs} = \mathrm{D} \cdot A_{CP},$$

where D represents the product of all dilution factors, then the error on A_{CP} is given by[1]

$$\delta A_{CP} = \frac{1}{D}\sqrt{\frac{1-A_{obs}^2}{N_{obs}}} = \frac{1}{D\sqrt{N_{obs}}} = \frac{1}{D\sqrt{\varepsilon\, Br\, N_{prod}}}.$$

In other words, N_{prod}, the number of produced B^0 or $\bar{B}^0$ needed to obtain a given error on δA_{CP} is given by

$$N_{prod} = \frac{1}{\delta^2 A_{CP}} \cdot \frac{1}{D^2 \cdot \varepsilon\, Br}.$$

Thus, to determine the figure of merit for a particular decay mode one must determine the number of reconstructed events N_{obs} and calculate the corresponding dilution factor D. N_{obs} depends on the luminosity and production cross section, on the branching ratio of the B^0 or $\bar{B}^0$ into the specific final state under study, Br, and on ε, the reconstruction efficiency for both the combination of the signal CP state and any tagging signal. The production rate N_{prod}, the dilution factor D, and the efficiency ε, differ substantially in magnitude as a function of energy and detector layout. The detection efficiency and dilution factor can both be written as a product of several factors that can be estimated for a particular experiment. These factors depend critically on the decay mode under study, the tagging method, the detector configuration, and more generally on the production process, backgrounds, and detector performance. Furthermore, our present knowledge of these quantities varies largely, as well our ability to ultimately measure the dilution factor which relates the experimentally observed asymmetry to the true CP asymmetry.

B^0 AND $\bar{B}^0$ PRODUCTION RATE.

The number of produced $B^0 / \bar{B}^0$ per year is given by the following relation,

$$N_{prod} = \int L dt \cdot \sigma_{b\bar{b}} \cdot 2 f_0$$

where

$\int L dt$ represents the luminosity integrated over $10^7 s$,

$\sigma_{b\bar{b}}$ is the cross section for $b\bar{b}$ production, and

f_0 is the fraction of neutral $B^0_{d,s}$ mesons produced per b or $\bar{b}$.

Predictions for hadro-production cross-sections exist, though the inclusive $b\bar{b}$ production measured at the Tevatron, over a limited acceptance, is substantially larger than theoretically predicted. The fraction of B_d^0 mesons is assumed to be of the order of 0.38 in high energy hadro-production. The production cross sections for various experiments are listed in Table I.

Table I: Cross sections for $b\bar{b}$ production in pp interactions.

	c.m. Energy (GeV)	Cross section cm^2
HERA proton beam	40	$2\cdot10^{-32}$
Tevatron F.T.	63	$4\cdot10^{-32}$
LHC FT	123	$1\cdot10^{-30}$
SSC FT	195	$2\cdot10^{-30}$
Tevatron Collider	1800	$5\cdot10^{-29}$
LHC Collider	14,000	$3\cdot10^{-28}$
SSC Collider	40,000	$1\cdot10^{-27}$

B^0 BRANCHING RATIOS

Only a few of the branching ratios to CP eigenenstates have been measured. Most of them are derived following the assumption of BSW. The values to be used in this workshop are listed in Table II.

Table II: B^0 Branching Ratios

Final State	Branching Ratio
ψK_s	$4\cdot10^{-4}$
ψK^{*0}	$1.5\cdot10^{-4}$
$\psi' K_s$	$4\cdot10^{-4}$
D^+D^-	$6\cdot10^{-4}$
$\pi^+\pi^-$	$2\cdot10^{-5}$
$\rho^\pm\pi^\mp$	$6\cdot10^{-5}$
$a^\pm\pi^\mp$	$6\cdot10^{-5}$

EFFICIENCIES.

The total detection efficiency, excluding the generally poorly known branching ratio for the decay to the CP eigenstate under study, can be conveniently factored as

$$\varepsilon = \varepsilon_{dec}\cdot\varepsilon_{trig}\cdot\varepsilon_{CP}\cdot\varepsilon_{tag}$$

with the following definitions:

ε_{dec} is the branching ratio for the specific final state that is observable for the decay to a CP eigenstate.

ε_{trig} is the efficiency to trigger on the event.

ε_{CP} is the efficiency to detect and fully reconstruct a specific CP eigenstate, and

ε_{tag} is the efficiency for obtaining a B flavor tag in the $b\bar{b}$ event with the detected specific final state.

Obviously, ε depends on the detailed layout and performance of the assumed detectors, including the effects of background. The factorization of ε is useful to obtain insight into the performance of an experiment, though the specific values for the factored efficiencies will be correlated (e.g., other factors depend on the trigger).

DILUTION FACTORS

The dilution of the measured asymmetry can be attributed to three principal sources,

$$D = d_{mix}\cdot d_{tag}\cdot d_{bg}$$

with the following definitions:

d_{mix} accounts for the mixing of the neutral B meson prior to its decay;

$d_{tag} = 1-2w$ results from the fraction w of decays that are incorrectly tagged; and

$d_{bg} = \sqrt{S/S+B}$ results from the presence of background in the observed sample of $N_{obs} = S+B$ decays.

Both d_{tag} and d_{bg} depend strongly on the CP decay mode under study and the tagging method, thus they are very closely linked to the respective detection efficiencies.

Dilution Due To Evolution With Time. At a hadron machine, the b and $\bar{b}$ evolve incoherently and hadronize nearly independently. The rate for a single neutral B meson decaying to a CP eigenstate is

$$R(B^0\to f_{CP})\propto e^{-\Gamma t}\{1+sin2\phi_{CP}sin(x\Gamma t)\}$$

or

$$R(\overline{B}^0\to f_{CP})\propto e^{-\Gamma t}\{1-sin2\phi_{CP}sin(x\Gamma t)\}.$$

Due to mixing of the neutral B mesons, the observed asymmetry is

$$A_{obs}(t) = D' sin\ x\Gamma t\ sin2\ \phi_{cp}$$

where $D' = d_{tag}\cdot d_{bg}$. The asymmetry $A_{obs}(t)$ is zero for $t=0$ and rises to a maximum at $t=\pi/2x\Gamma$, resulting in an overall dilution of the measurement. Still, the asymmetry integrated over all decay time does not vanish and in principle no measurement of the decay time is required. In this case, the dilution due to the mixing is $d_{mix} = x/1+x^2)$, resulting in a value $d_{mix} = 0.47\ (0.14)$ for $x = 0.7(7.0)$. If on the other hand, the decay times are measured, the time dependence of the asymmetry can be fit, resulting in a dilution of

$$d_{mix}{}^2 = \frac{1+4x^2+2x\ sin2x\ \Gamma t_o - cos\ 2x\Gamma t_o}{2(1+4x^2)}.$$

Here t_0 is the lifetime cut, applied to reject background. For t_0=0, one obtains $d_{mix} = \sqrt{2x^2 / 1 + 4x^2}$ resulting in $d_{mix} \approx 0.58\ (0.50)$ for $x = 0.7\ (7.0)$.

Of course, a cut in the decay times ($t_0 > 0$) will also affect the detection efficiency and thereby the statistical error on the asymmetry measurement. Furthermore, the resolution of the decay time measurement will impact on the fit and thereby d_{mix}. For large x, the time dependent fit will result in $d_{mix} \to 0.5$ while the time integrated measurement will result in a very small dilution factor. More importantly, the observation of the time dependence of the asymmetry will provide the very important verification of the origin of the asymmetry and will significantly enhance the credibility of the measurement.

Dilution Due To Tagging Errors. The flavor of the B^0 or $\overline{B}^0$ can be tagged by the decay of the second B particle, either through its semi-leptonic decay or through the flavor of a decay charm particle, most readily by the charge of the secondary kaon. A fraction of B decays will be incorrectly tagged either because the tagging B mixes into the wrong flavor or because the tagging lepton does not originate from the decay of the B, but instead from the cascade decay of a charmed meson (resulting in the wrong sign). In addition, lepton and kaon signals may originate either from particles not associated with the B decay or cascade decay, or can be due to accidental or other background sources. Prompt muon signals can be faked by backgrounds such as π and K decay or hadronic punch through (resulting in a wrong sign tag 50% of the time). In general, as one improves the purity of the tagging sample by stricter selection criteria the corresponding efficiencies decrease.

As an example, we give results from a study performed by Natalie Roe of the D0 group.[2] It is assumed that b quarks hadronize as B_d, B_u, B_s, and Λ_b in the ratio $f_u : f_d : f_s : f_\Lambda = 0.38 : 0.38 : 0.14 : 0.10$. If we denote the fraction of tags due to semi-leptonic decay from a mixed B decay, due to cascade decays of charm, from pion or kaon decay and hadron punch through as F_B, F_C, F_D, and F_P, respectively, then the wrong-sign tagging fraction is given by

$$w = \alpha \cdot F_B + (1 - \alpha) \cdot F_C + \frac{(F_D + F_P)}{2}.$$

The relative signal and background contributions to the lepton tag vary strongly as a function of the cut on transverse momentum. For instance, Monte Carlo studies for the upgraded D0 detector indicate that the optimum ratio of the signal and background contribution is obtained for a cut at $p_t = 2\,GeV/c$, resulting in $F_B = 0.80$, $F_C = 0.17$, $F_D = 0.03$ and $F_P = 0.0$. The fraction of tagging B's which mixes to give a wrong-sign tag is given by $\alpha = f_s / 2 + x_d^2 / 2(1 + x_d^2) \cdot f_d = 0.14$. It is assumed that the B_s mesons are fully mixed ($x_s \geq 5$). The term $(1 - \alpha)\ F_C$ takes into account that cascade leptons have the correct sign if the B meson mixes before it decays. The D0 Monte Carlo simulation results in $w = 0.27$ and $d_{tag} = 0.44$ with a cut at $p_t = 2\,GeV/c$ on the muon transverse momentum. It is assumed that the backgrounds due to punch through and pion and kaon decay are charged symmetric and that the rates of B^0 and $\overline{B}^0$ production are equal over the whole detector. Both of these assumptions need to be experimentally verified, especially in the case of pp as opposed to $\bar{p}p$ collisions..

Dilution Due To Background. The presence of background in the sample of reconstructed CP decays dilutes the measured asymmetry by a factor $S/S + B$. However, the number of observed decays, N_{obs}, increases as $(S + B)/S$ so that the effect of the background is $d_{bg} = \sqrt{S/S + B}$, even if the background is charge symmetric.

The level of background remains an open experimental question for most decay modes. The CDF group reported a ratio of $S / S + B \approx 0.5$ for the observed sample of $J/\psi K^{\pm}$ decays. A constraint on the K_S mass plus the requirement of a lepton tag and additional cuts on the decay vertex are sure to improve this ratio substantially, though at a significant loss in efficiency. On the other hand, lowering the p_t requirements for the multi-lepton trigger and less stringent cuts on the track reconstruction may increase the level of background. This is an area where more study and actual experimental data are necessary to improve our understanding of the potential for B physics at hadron accelerators.

SUMMARY TABLE

To provide a basis for a comparison of different experiments, Table III gives a list of the above parameters that determine a figure of merit for the measurement of CP violation for a given decay mode in a given detector model. The data in the table represent the expectations for an e^+e^- B Factory like those presently under study at Cornell, KEK, and SLAC. It is hoped that as a result of this workshop similar data will become available for all the proposed experiments under study, for a variety of decay modes related to different angles in the unitarity triangle.

---

[1] See also: D. Hitlin, F. Porter, N. Roe, J. Dorfan, V. Lüth, A. Snyder, Babar Note #81, SLAC (1992).

[2] N. Roe, DO Note #1122 (1991).

Table III: Measurement of CP Asymmetry: Angle b

Experiment	PEP B FACTORY
Energy E_{cm} (TeV)	0.010
Luminosity $L(10^{33} cm^{-2} s^{-1})$	3.0
Cross section $\sigma_{b\bar{b}}(\mu b)$	0.0012
Cross section $\sigma_{tot}(mb)$	0.005
B^0 fraction, f_0	0.5
$N_{prod} / 10^7 s$	$3.6 \cdot 10^7$
$\mathrm{Br}(J/\psi K_s)$	$4 \cdot 10^{-4}$
CP final state	$l^+ l^- \pi^+ \pi^-$
B flavor tag	$l^\pm, K^\pm$
ε_{det}	0.14
ε_{trig}	0.98
ε_{CP}	0.57
ε_{tag}	0.45
d_{mix}	$0.47 \rightarrow 0.57$
d_{tag}	0.84
d_{bg}	1.00
Total efficiency ε	$3.6 \cdot 10^{-2}$
Total dilution D	$0.40 \rightarrow 0.48$
Figure of Merit, $1/D^2\varepsilon$	$5.6 \rightarrow 3.8 \cdot 10^{-3}$
N_{prod} for $\delta A_{CP} = 0.1$	$4.4 \leftarrow 3.0 \cdot 10^7$
Time for measurement $(10^7 s)$	$1.24 \leftarrow 0.84$

Dilution Measurements for CP Violation in B Decay

A. Fridman*
CERN, Geneva, Switzerland

Abstract

The dilution effect appearing in the search for CP violation in the $B_d^0, \bar{B}_d^0$ decay is discussed. We consider pN collisions at large c.m. energy (LHC and SSC projects). A measurement of the dilution parameter is proposed by considering $B^{\pm}, B_d^0, \bar{B}_d^0$ decaying into channels where CP violation is not present.

1 - Introduction

The dilution effect was often discussed in the search for CP violation effects in $B_d^0, \bar{B}_d^0$ decaying into a self-conjugated state[1-3], F ($F = \bar{F}$). The mixing phenomena $B_d^0 \leftrightarrow \bar{B}_d^0$ allows the search for CP violation with the requirement of tagging the associated beauty hadron produced in the event where the F state has been observed. The dilution effect is due to the misidentification of this associated beauty hadron. In the following we discuss methods for measuring the dilution effect occuring in pp experiments. Note that this measurement would allow one to estimate the real value (or its upper limit) of the parameter describing the CP violation of the $B_d^0, \bar{B}_d^0$ decay (see below).

Let us consider that tagging will be given by the charge of the lepton in the semileptonic decay of the associated beauty hadron, namely $B, \bar{N}_b \rightarrow l^+X$ and $\bar{B}, N_b \rightarrow l^-X$ (X meaning anything). Here $N_b \equiv bqq$ ($\bar{N}_b \equiv \bar{b}\bar{q}\bar{q}$) represents a beauty baryon. The CP violation could then be detected by comparing the number (N_-) of l^-FX and (N_+) l^+FX events obtained in a given experiment. Thus CP violation in the B_d^0 decay will lead to a non-zero value of the asymmetry parameter[4]

$$A = \frac{N_- - N_+}{N_- + N_+} .$$

In hadron hadron collisions several types of beauty hadron pairs can be produced. With events where there is only one pair of beauty hadron in the final state, we

* LPNHE, Université de Paris VI et VII

obtain the following calculation of the asymmetry parameter[3-5]:

$$A = -\left[\frac{nx_d}{1+x_d^2}(p_\pm + p_N) + \frac{n(x_s+x_d)}{(1+x_s^2)(1+x_d^2)}\, p_s + \frac{nx_d}{(1+x_d^2)^2}\, p_d\right] \tag{1}$$

The CP violation effect is described by the parameter[4,6] $n \equiv \sin 2\phi$. The quantities $p_\pm$, p_d, p_s and p_N are the production rates in $pp \to b\bar{b}X$ interactions of the $B^\pm$, B_d^0 (or $\bar{B}_d^0$), B_s^0 (or $\bar{B}_s^0$) and N_b (or $\bar{N}_b$), respectively, taken here as:

$$p_\pm : p_d : p_s : p_N = 0.38 : 0.38 : 0.14 : 0.10\ . \tag{2}$$

The mixing of the $B_{d,s}^0$ meson is given by the $x_{d,s}$ parameters, related to the mixing by[4] (assuming that there is no CP violation in the $B_{d,s}^0 \leftrightarrow \bar{B}_{d,s}^0$ process),

$$\alpha_{d,s} \equiv \frac{B_{d,s}^0 \to \bar{B}_{d,s}^0}{B_{d,s}^0 \to \bar{B}_{d,s}^0 + B_{d,s}^0 \to B_{d,s}^0} = \frac{1}{2}\,\frac{x_{d,s}^2}{1+x_{d,s}^2}\ , \tag{3}$$

$$\beta_{d,s} \equiv \frac{B_{d,s}^0 \to B_{d,s}^0}{B_{d,s}^0 \to \bar{B}_{d,s}^0 + B_{d,s}^0 \to B_{d,s}^0} = 1 - \alpha_{d,s}\ . \tag{4}$$

Formula (1) is obtained by assuming that there is no CP violation in the decay amplitudes[3-5] and that their moduli are equal for the decays of the various pairs of beauty hadrons[7]. Apart from this approximation, formula (1) takes into account all the mixing processes exactly. Note that $|A|$ is smaller than the value obtained by tagging only charged B mesons[3]. In this latter case we would have

$$A_\pm = -\frac{nx_d}{(1+x_d^2)}\ , \tag{5}$$

giving $|A_\pm| \simeq |0.47 \sin 2\phi|$ with[8] $x_d = 0.72$. Using for the general case, formula (1) and (2), $x_s = 8$, the asymmetry parameter becomes $|A| = |0.36 \sin 2\phi|$. This expression is not very sensitive to x_s, since by taking $x_s = 10$, $|A|$ varies by less than 2 %.

Let us denote by $N(b\bar{b})$ $[N_\pm(b\bar{b})]$ the number of $pp \to b\bar{b}X$ events needed to detect $\sin 2\phi$ with a given number of standard deviations in the case of formula (1) [formula (5)]. Using then the expression $N_t = s^2(1/A'^2 - 1)$, relating the total number of events N_t necessary to observe an asymmetry parameter A' with s standard deviations, we obtain

$$\frac{N_\pm(b\bar{b})}{N(b\bar{b})} \simeq 1.5\,\frac{1 - 0.22\sin^2 2\phi}{1 - 0.13\sin^2 2\phi}\ .$$

We thus see that by using the general case [formula (1)], we need less $pp \to b\bar{b}X$ events than in the case of using $A_\pm$ despite the fact that $|A| < |A_\pm|$ (and even if the $B^\pm$ detection efficiency were to be 100 %). Note that this last unequality is often considered as a component of the dilution effect due to mixing, although it is the mixing process that allows here searching for CP violation in $B_d^0, \bar{B}_d^0$ decays.

2 - Dilution effects

The asymmmetry parameter A given by equation (1) will decrease because of the mistagging of the $l^\pm$ due to

A) the cascade process, $b \to c \to l^+$ ($\bar{b} \to \bar{c} \to l^-$) where the l has the opposite charge of the $b \to l^-$ ($\bar{b} \to l^+$) decay,

B) the l's coming from other decaying particles (K, π, for example),

C) the punchthrough in the detector (charge of the leptons identified wrongly).

Mistagging of $e^\pm$ and $\mu^\pm$ will certainly be different for cases B and C as they depend essentially on the detector used in a given experiment. Note also that these cases contribute equally to the misidentification of l^+ and l^- in the final state.

Let us now define the mistagging parameter of the leptons. Assuming that the correct (wrong) number of events is represented by $N_\pm^c$ ($N_\pm^w$), one has

$$A_m = \frac{N_+^c + N_+^w - N_-^c - N_-^w}{N_t} \tag{6}$$

where A_m denotes the measured A value (the subscript m will denote hereafter a measured quantity). Here N_t is the total number of (true and wrong) tagged events, whereas the sign indicates the charge of the lepton. The real A value and the fraction of wrong tagging (w) are defined by

$$A = \frac{N_+^c - N_-^c}{N_+^c + N_-^c} = \frac{N_-^w - N_+^w}{N_+^w + N_-^w}\ , \tag{7a}$$

$$w = \frac{N_+^w + N_-^w}{N_t} = 1 - \frac{N_+^c + N_-^c}{N_t} . \tag{7b}$$

One obtains then $A_m = A(1-2w)$, where A is given by formula (1). Let us now suggest how to measure w in order to estimate A as well as the number of events required to observe an eventual asymmetry with a given number of standard deviations.

3 - The measurement of w

In order to estimate w, we consider $B^\pm \to f^\pm$, $B_d^0 \to f$ and $\bar{B}_d^0 \to \bar{f}$ decay channels where CP violation should not occur ($f \neq \bar{f}$, see Ref. 9). Then the measurement in an experiment of the number of events having these kinds of decays [$N_m(f^\pm)$, $N_m(f)$ and $N_m(\bar{f})$] would allow one to estimate the expected number of events having the final states $f^\pm, f$ or $\bar{f}$ in addition to the tagging lepton [$N(l^\pm f^\mp)$, $N(l^- f)$ and $N(l^+ \bar{f})$]. A difference between the $N(lf)$ estimates and the observed number of events [$N_m(lf)$] will allow one to estimate the dilution parameter w for the cases A to C.

a) The $B^\pm \to f^\pm$ decay

Let us first consider the $B^+ \to f^+$ decays. The events having $l^- f^+ X$ in the final state will be produced by the following beauty hadron pairs appearing at the production time ($t = 0$):

1a) B^+B^-,

2a) $B^+\bar{B}_d^0$,

3a) $B^+\bar{B}_s^0$,

4a) B^+N_b .

Then the relations between the expected number of $l^- f^+ X$ events [$N(l^- f^+)$] and the observed ones [$N_m(f^+)$] will be given by

$$\frac{N(l^- f^+)}{N_m(f^+)} = BR(b \to l^- X) \times [p_\pm + p_d\, \beta_d + p_s\, \beta_s + p_N] , \tag{8}$$

where we assume that the semileptonic branching ratio, $BR(b \to l^- X)$, is nearly identical for the four cases[10]. Note that $\beta_{d,s}$ [formula (4)] is introduced as $\bar{B}_{d,s}^0 \to B_{d,s}^0$ does not contribute to the $l^- f^+ X$ final state. With equation (2) and $x_s = 8$, one find that $N(l^- f^+)/N_m(f^+) \sim 0.87 \times BR(b \to lX)$.

The measured number of events $N_m(l^- f^+)$ thus allows to obtain

$$w \simeq \frac{N(l^- f^+) - N_m(l^- f^+)}{N(l^- f^+)} \tag{9}$$

[see formula (7b)]. The same type of evaluation could also be obtained with the $l^+ f^- X$ final state. In fact, a larger statistic could be obtained by taking the $B^+ \to f^+$ and $B^- \to f^-$ decays, yielding

$$w \simeq \frac{N(l^- f^+) + N(l^+ f^-) - N_m(l^- f^+) - N_m(l^+ f^-)}{N(l^- f^+) + N(l^+ f^-)} . \tag{10}$$

b) The $B_d^0 \to f$ process

Here we have to take into account the coherence of the mixing processes when a pair of neutral beauty mesons is produced. As an example, let us consider the $l^- f X$ final state. The following pairs of beauty hadrons (produced at $t = 0$) can contribute to the production, namely

1b) $B^- B_d^0$,

2b) $\bar{B}_s^0 B_d^0$ and $B_s^0 \bar{B}_d^0$ (coherent mixture),

3b) $\bar{B}_d^0 B_d^0$,

4b) $N_b B_d^0$.

For these cases the production rates (P_{ix}) can be calculated with the wave functions describing the decay processes[4,6] without CP violation effects, and leading to

$$\begin{aligned}
P_{1b} &\propto BR(B \to lX)\; p_\pm p_d , \\
P_{2b} &\propto Br(B \to lX) \left[1 + \frac{1 - x_d x_s}{(1+x_d^2)\,(1+x_s^2)}\right] \frac{p_s p_d}{2} , \\
P_{3b} &\propto BR(B \to lX) \left[1 + \frac{1}{(1+x_d^2)^2}\right] \frac{p_d^2}{2} , \\
P_{4b} &\propto BR(B \to lX)\; p_N p_d .
\end{aligned}$$

Similarly to the previous case, we obtain

$$\frac{N(l^- f)}{N_m(f)} = BR(b \to l^- X) \Bigg[\left(1 + \frac{1 - x_d x_s}{(1+x_s^2)(1+x_d^2)}\right) \frac{p_s}{2} + \left(1 + \frac{1}{(1+x_d^2)^2}\right) \frac{p_d}{2} + p_\pm + p_N \Bigg] , \tag{11}$$

assuming again that the decay amplitudes are identical in the four cases. This gives a ratio of $N(l^- f)/N_m(f) \sim 0.82 \times BR(b \to l^- X)$ with the same assumptions as above. By measuring the $N_m(f)$ and $N_m(\bar{f})$ as well as $N_m(l^- f)$ and $N_m(l^+ \bar{f})$ one gets a formula similar to (10) but where $f^+ \to f$ and $f^- \to \bar{f}$.

4 - Discussion and conclusions

Previous works[2,3] have shown that large values of w might be due to the cascade processes. In pp interactions at large c.m. energy, kinematical cuts have to be chosen in order to decrease w without reducing the number of events too much[11]. These cuts will, of course, depend on the c.m. energy and the detector used for the experiment.

The absence of CP violation in $B^\pm \to f^\pm$ decay occurs when there is only one graph that contributes to the decay[4,6]. For instance, the $B^\pm \to J/\psi K^\pm$ process could be used (see Fig. 1). These channels could be studied easily as the search for CP violation in the $B_d^0, \bar{B}_d^0 \to J/\psi K_s^0$ decays (with $J/\psi \to l^+ l^-$) has been proposed in all the intentions for pp experiments at the LHC or SSC projects[12]. The triggering method for these reactions could certainly be useful for the identification of the $B^\pm \to J/\psi K^\pm$ channels. However, in the collider experiments no particle identification of $K^\pm$ and $\pi^\pm$ is expected. This might somewhat complicate the detection of the $B^\pm \to J/\psi K^\pm$ channels (large background). The $B_d^0 \to J/\psi K^{*0}$ and $\bar{B}_d^0 \to J/\psi \bar{K}^{*0}$ decays (case b in section 3) could be identified more easily because of the K^{*0} and $\bar{K}^{*0}$ decays. The decay of K^{*0} and $\bar{K}^{*0}$ need to have charged K in their final states in order to identify the B_d^0 or $\bar{B}_d^0$ mesons. One could, for instance, consider the $K^{*0} \to K^+\pi^-$ and $\bar{K}^{*0} \to K^-\pi^+$ decays.

Let us also note that a charged K due to the cascade process (Fig. 1b) $b \to c \to K^-$ ($\bar{b} \to \bar{c} \to K^+$) will have the same charge as the lepton appearing in the $b \to l^-$ ($\bar{b} \to l^+$). If one could detect $B \to l^+ K^+ X$ or $\bar{B} \to l^- K^- X$ (where the K is due to the c or $\bar{c}$ decay) for the tagging process, one would have events where the lepton does not arise from the cascade process. Moreover, if the inclusive $B, \bar{B} \to l^\pm K^\pm X$ branching ratio was really known, it would be possible to use the method described in Section 3 in order to evaluate the dilution part that would not be due to the cascade process.

From the present discussion, it appears that the measurement of the quoted channels in a given experiment will be important in order to measure the $w \neq 0$ value due to the dilution effects. Then kinematical cuts could be investigated in order to decrease w without reducing the sample of events too much. Finally, the knowledge of w allows one to estimate A as well as the number of events needed to measure $A_m = A(1 - 2w)$ with a given number of standard deviations.

Acknowledgement

It is a pleasure to thank I.I. Bigi, D. Froidevaux and N. Neumeister for useful discussions. We also thank W-D. Schlatter for useful comments.

References

1) M. Botlo et al., Further Comments about B-physics in pp Interactions, Report SSCL-538 (1992).
2) The Physics Program of a High-Luminosity Assymmetric B Factory at SLAC, SLAC-353 (1989);
Natalie Roe, LBL Reports and D0 notes, 1022 (1990) and 1122 (1991).
3) M. Cannalire and A. Fridman, Nuovo Cimento 106A (1993) 251.
4) I.I. Bigi and A.I. Sanda, Nucl. Phys. B281, 41 (1987).
5) M. Chaichian and A. Fridman, Phys. Lett. B298 (1993) 218.
6) See also the lecture notes, A. Fridman, Mixing and CP Violation in the B-System, CERN-EP/88-123 (1988).
7) Strictly speaking, the amplitudes T_{1-4} for the l^+F state, for example, are not equal as one has $T_1 = \langle l^+X|B^+\rangle\langle F|\bar{B}_d^0\rangle$, $T_2 = \langle l^+X|B_S^0\rangle\langle F|\bar{B}_d^0\rangle$, $T_3 = \langle l^+X|B_d^0\rangle\langle F|\bar{B}_d^0\rangle$ and $T_4 = \langle l^+X|\bar{N}_b\rangle\langle F|\bar{B}_d^0\rangle$ (see Ref. 3). In the spectator model all the semileptonic parts of T_1 to T_3 are equal. For $\bar{N}_b \to l^+X$ we use the same amplitude, although the N_b lifetime is expected to be shorter than those of the mesons. Note that we also consider that $|T_j| = |\bar{T}_j|$ (see Refs. 3 and 4).
8) ARGUS Collab., H. Albrecht et al., Phys. Lett. B192 (1987) 245.
9) Clearly we assume here that $B_d^0 \to f \to X'$ and $\bar{B}_d^0 \to \bar{f} \to X''$ lead to final states where $X' \neq X''$.
10) This is also an approximation since the total width (or lifetime) of the N_b decay is expected to be different from those of the B mesons.
11) In $e^+e^- \to \Upsilon(4S) \to B\bar{B}$ the decrease of the cascade process is made with lepton momentum cuts since the B mesons have practically no momentum in the laboratory system. The situation is more complicated in pp interactions, where the B momentum is usually not known.
12) The LHC letters of intent: The compact Muon Solenoid (CMS), CERN/LHCC 92-3 (1992), General-Purpose pp Experiment at the Large Hadron Collider at CERN (ATLAS), CERN/LHCC 92-4 (1992) as well as the SSC expressions of interests. See also the letter of intent: An Experiment to Study CP Violation in the B System Using an Internal Target at the HERA Proton Ring, DESY-PRC 92/04 (1992).

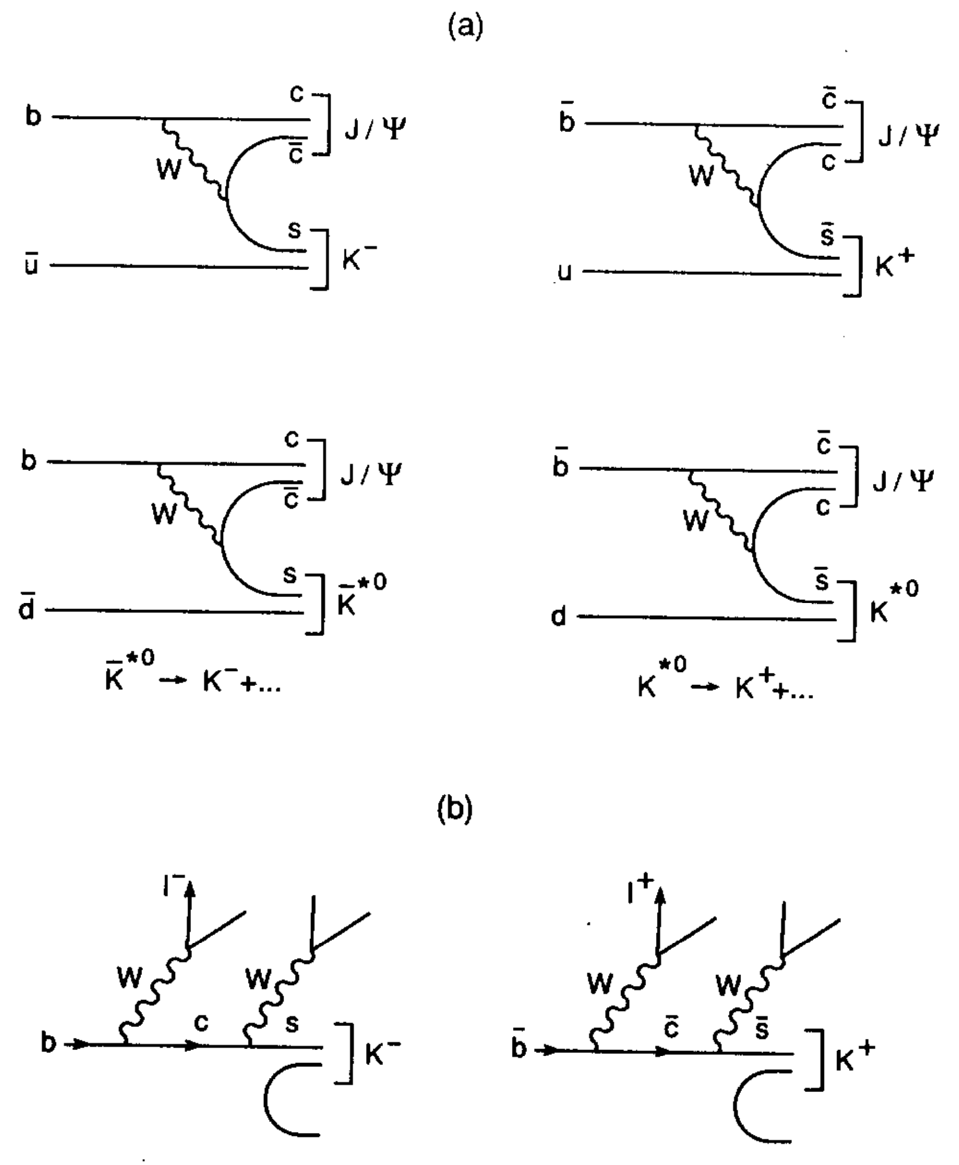

Fig. 1 - a) Diagrams contributing to the $B^\pm \rightarrow J/\psi K^\pm$, $\bar{B}_d^0 \rightarrow J/\psi \bar{K}^{*0}$ and $B_d^0 \rightarrow J/\psi K^{*0}$ decays. b) The quark decays leading to the $\bar{B} \rightarrow l^- K^- X$ and $B \rightarrow l^+ K^+ X$ processes.

FLAVOR IDENTIFICATION OF NEUTRAL B MESONS USING CORRELATED PIONS

MICHAEL GRONAU
Department of Physics, Technion - Israel Institute of Technology
Technion City, 32000 Haifa, Israel

and

JONATHAN L. ROSNER
Enrico Fermi Institute and Department of Physics
University of Chicago, Chicago, Illinois 60637

1. INTRODUCTION

The identification of the flavor of neutral B mesons at a given time is a crucial element in measurements of CP asymmetries in neutral B decays.[1] In a $e^+e^- \to \Upsilon(4S)$ B-factory[2] the flavor of $B^0(\overline{B}^0)$ is determined unambiguously by observing a charged lepton from the decay of the other neutral B. The two neutral B mesons form a *coherent* $C(B^0\overline{B}^0) = -1$ pair and the charge of the lepton serves to "tag" the flavor of the other B at the time of semileptonic decay. Since the CP asymmetry is odd in the time-difference of the two decays, asymmetric storage rings are needed for an asymmetry measurement.

In high energy e^+e^- collisions and in hadronic reactions[3] a conventional method of determining the flavor of neutral B mesons is again to use as a "tag" the lepton from a semileptonic decay of an associated b hadron. In this case the flavor is misidentified part of the time as a result of $B^0 - \overline{B}^0$ mixing. The probability of misidentification depends on the relative production rates of B^0_d, B^0_s , B^+ and b baryons, which can only be crudely estimated.

An alternative method of flavor identification was recently suggested,[4] which avoids having to observe the decay of the associated b-hadron. This method uses a correlation between the flavor of decaying neutral B mesons and the charge of pions produced nearby in phase space. Here we wish to expand upon this method.[5]

In Section 2 we present two arguments which support a $B - \pi$ correlation, based on "B^{**}" resonances and on b quark jet fragmentation, and estimate the expected magnitude of this correlation. Flavor tagging is based on a statistical correlation and involves a dilution factor. In Section 3 we describe the manner in which this factor enters the general time-dependence of neutral B decays. We study decays to flavor eigenstates, to CP eigenstates and to other interesting states from which CKM phases can be determined. Section 4 discusses "B^{**}" resonance decays, stressing the importance of corresponding studies using charmed mesons. We conclude in Section 5.

In this discussion we will assume that at high energies produced B^0 and $\overline{B}^0$ are always incoherent with respect to one another. This commonly accepted hypothesis, which is usually assumed in any high energy tagging method, should eventually be tested experimentally. A more general study, which also allows a partially coherent admixture of B^0 and $\overline{B}^0$, is beyond the scope of this presentation. It can be found elsewhere.[5,6]

2. THE $B - \pi$ CORRELATION

One argument for a correlation between the flavor of a neutral B and the charge of a nearby pion is based on the existence of positive-parity "B^{**}" resonances, with $J^P = 0^+,\ 1^+,\ 2^+$. The idea stems from a method which has been used to identify neutral D mesons through the decays of charged D^* resonances.[7] The $D^{*\pm}$ resonance, with spin-parity $J^P = 1^-$, lies just above the $D\pi$ decay threshold, giving rise to a charactersitic soft pion. The corresponding 1^- B^* lies only about 46 MeV above the B, so that $B^* \to B\pi$ is forbidden. However, there are positive-parity resonances, with $J^P = 0^+,\ 1^+,\ 2^+$, and masses below about 5.8 GeV/c^2 which are expected to couple to $B\pi$ and/or $B^*\pi$. This mass value can be extrapolated from the corresponding known positive-parity charmed resonance masses. Details are given in Section 4. When a B^{**} resonance decays to $B\pi$ and/or $B^*\pi$ mesons a π^+ will accompany a B_d^0 and not a $\overline{B}_d^0$. The relative production rate of B^{**} is unknown at present. D^{**} production accounts for about 20% of all D mesons produced in the e^+e^- continuum and in charm photoproduction.[8] It is not unreasonable to assume a similar production rate for B^{**} in e^+e^- and in hadronic collisions.

The second argument is that in b-quark fragmentation the leading pion carries information about the flavor of the neutral B (B^*). This is illustrated in Fig. 1, which demonstrates that a nearby π^+ is more likely to accompany a B_d^0 than a $\overline{B}_d^0$. This effect was recently calculated for LEP energies[9] using a soft fragmentation version of JETSET 7.3. It was found that the correlation factor $[N(B^0\pi^+) - N(B^0\pi^-)]/[N(B^0\pi^+) + N(B^0\pi^-)]$, for pions with the lowest $M(B\pi)$ value in each event, increases from a value of 0.17 at $M(B\pi) = 5.5$ GeV/c^2 to the value of 0.27 at 5.8 GeV/c^2, and stays constant up to 6.2 GeV/c^2, where very small rates are expected. Adding B^{**} production at a level of 20% may lead to a correlation factor as large as 40% or so at LEP energies. The correlation may be less pronounced at the Tevatron, where the b and $\bar{b}$ jets are less strongly separated. An important experimental question is how to maximize this correlation in a given experiment, using varying kinematical constraints on the $B - \pi$ system, such as the range of invariant mass or the relative angle/rapidity of the two particles.

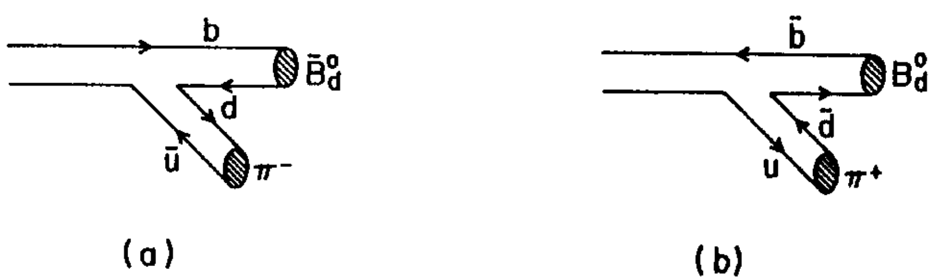

Figure 1: b ($\bar{b}$) fragmentation into $\overline{B}_d^0$ (B_d^0) and a charged pion.

3. TIME-DEPENDENT RATES AND ASYMMETRIES

3.1 Decays to States of Specific Flavor

Consider low-mass $B - \pi$ combinations, and denote[4] the relative production rates of "right-sign" combinations by $N(B^0\pi^+) = P_1$ and that of "wrong-sign" combinations by $N(B^0\pi^-) = P_2$. In general one expects $P_1 > P_2$. For simplicity we will only discuss charge-symmetric production processes, such as in e^+e^- and $\bar{p}p$ collisions, where one has $N(B^0\pi^+) = N(\overline{B}^0\pi^-)$, $N(B^0\pi^-) = N(\overline{B}^0\pi^+)$. Let us imagine that a neutral B decays to a state of identifiable flavor, for instance $B_d^0 \to J/\psi\ K^{*0}$, or $\overline{B}_d^0 \to J/\psi\ \overline{K}^{*0}$, where the flavor of the neutral K^* is identified by $K^{*0} \to K^+\pi^-$ or $\overline{K}^{*0} \to K^-\pi^+$.

The produced neutral B mesons oscillate between a B^0 and a $\overline{B}^0$ state with a frequency given by the mass-difference of the two mass-eigenstates, $\Delta m \equiv m_H - m_L$. We assume that the produced B^0 and $\overline{B}^0$ are incoherent with respect to one another. At proper time t the relative numbers of "right-sign" combinations ($B^0\pi^+$ or $\overline{B}^0\pi^-$), $R(t)$, and the numbers of "wrong-sign" combinations ($B^0\pi^-$ or $\overline{B}^0\pi^+$), $W(t)$, are then given by

$$R(t) = e^{-\Gamma t}[P_1 \cos^2(\frac{\Delta m t}{2}) + P_2 \sin^2(\frac{\Delta m t}{2})] , \tag{1}$$

$$W(t) = e^{-\Gamma t}[P_1 \sin^2(\frac{\Delta m t}{2}) + P_2 \cos^2(\frac{\Delta m t}{2})] . \tag{2}$$

The decay widths of B_H and B_L are both assumed equal to Γ. The time-dependent asymmetry is

$$\frac{R(t) - W(t)}{R(t) + W(t)} = \frac{P_1 - P_2}{P_1 + P_2} \cos(\Delta m t) , \tag{3}$$

and the corresponding time-integrated asymmetry is

$$\frac{\int [R(t) - W(t)] dt}{\int [R(t) + W(t)] dt} = \frac{P_1 - P_2}{P_1 + P_2} \frac{1}{1 + (\Delta m/\Gamma)^2} . \tag{4}$$

The time-dependent correlation of Eq. (3) has a characteristic $\cos(\Delta m t)$ behavior. Its coefficient gives the tagging dilution factor $(P_1 - P_2)/(P_1 + P_2)$, which measures the $B - \pi$ correlation at the production.

An alternative way to measure $(P_1 - P_2)/(P_1 + P_2)$ by using charged B mesons instead of neutral ones exists when the production process is isospin-independent. This is the case in e^+e^- annihilation. On the other hand, in $\bar{p}p$ collisions, while this may follow from $\bar{p}p$ annihilation into gluons, there exisit also other mechanisms[6] which lead to non-isoscalar final states. If isoscalar production holds, then the dilution factor can be obtained by forming right-sign and wrong-sign combinations of charged pions with charged B mesons in the same low-mass range as with neutral B mesons:

$$\frac{P_1 - P_2}{P_1 + P_2} = \frac{N(B^+\pi^-) - N(B^+\pi^+)}{N(B^+\pi^-) + N(B^+\pi^+)} . \tag{5}$$

Isoscalar production may be checked by comparing Eq. (5) with Eqs. (3) and (4).

3.2 Decays to CP Eigenstates

Consider B decays to a CP eigenstate, such as $B_d^0 \to J/\psi\ K_S$, and take $B-\pi$ combinations in the same low mass-range as in the specific flavor decays. $B^0-\overline{B}^0$ oscillations lead to time-dependent rates. One now defines a time-dependent asymmetry in terms of the charge of the pion produced along with the neutral B:

$$\mathrm{Asym.}(J/\psi\ K_S,\pi;t) \equiv \frac{N(J/\psi\ K_S,\pi^+;t) - N(J/\psi\ K_S,\pi^-;t)}{N(J/\psi\ K_S,\pi^+;t) + N(J/\psi\ K_S,\pi^-;t)} . \tag{6}$$

We find

$$\mathrm{Asym.}(J/\psi\ K_S,\pi;t) = -(\frac{P_1-P_2}{P_1+P_2})\sin 2\beta \sin(\Delta m t) , \tag{7}$$

where β is one of the angles of the CKM unitarity triangle.[1] Similarly, the time-integrated asymmetry is

$$\mathrm{Asym.}(J/\psi\ K_S,\pi) = -(\frac{P_1-P_2}{P_1+P_2})(\frac{(\Delta m/\Gamma)}{1+(\Delta m/\Gamma)^2})\sin 2\beta . \tag{8}$$

That is, the usual asymmetry is diluted by the tagging dilution factor $(P_1-P_2)/(P_1+P_2)$. The procedure is to first measure this factor in the flavor asymmetry of Eqs. (3) and (4) and then determine the angle β from the CP asymmetries.

3.3 Decays to Non-CP Eigenstates

Angles of the unitarity triangle can also be determined from neutral B decays to states f which are not CP eigenstates.[1] This is feasible when both a B^0 and a $\overline{B}^0$ can decay to a final state f which appears in only one partial wave, provided that a single weak CKM phase dominates each of the corresponding decay amplitudes. Two interesting examples are $B_d^0 \to \rho^-\pi^+$, for which one must neglect the penguin amplitude, and $B_s^0 \to D_s^- K^+$, where a single amplitude is known to contribute in the standard model. Here we will show how the dilution factor enters this method.

The time-dependent rates for states which start as B^0 or $\overline{B}^0$ at $t=0$ and decay at proper time t to the state f or its CP-conjugate $\bar{f}$ are given in Ref. 1. The corresponding time-dependent rates for states f or $\bar{f}$ in conjunction with pions of positive or negative charges are given by:

$$\begin{aligned}\Gamma_{f\pi^\pm}(t) &= (1/2)e^{-\Gamma t}\{|A|^2+|\bar{A}|^2 \pm [P_1-P_2][(|A|^2-|\bar{A}|^2)\cos(\Delta m t) \\ &\quad +2|A\bar{A}|\sin(\Delta\delta+2\phi_M+\Delta\phi_D)\sin(\Delta m t)]\} , \\ \Gamma_{\bar{f}\pi^\pm}(t) &= (1/2)e^{-\Gamma t}\{|A|^2+|\bar{A}|^2 \mp [P_1-P_2][(|A|^2-|\bar{A}|^2)\cos(\Delta m t) \\ &\quad +2|A\bar{A}|\sin(\Delta\delta-2\phi_M-\Delta\phi_D)\sin(\Delta m t)]\} ,\end{aligned} \tag{9}$$

where we have taken $P_1+P_2=1$. $|A|$ and $|\bar{A}|$ are the magnitudes of the decay amplitudes of B^0 and $\overline{B}^0$ to f, $\Delta\delta$ and $\Delta\phi_D$ are the strong and weak phase-differences between these amplitudes, and ϕ_M gives the phase of $B^0-\overline{B}^0$ mixing ($\phi_M=\beta$, 0 for B_d^0, B_s^0, respectively).

These four rates depend on four unknown quantities, $|A|$, $|\bar{A}|$, $\sin(\Delta\delta+2\phi_M+\Delta\phi_D)$ and $\sin(\Delta\delta-2\phi_M-\Delta\phi_D)$. Measurement of the rates allows a determination of the weak CKM phase $2\phi_M+\Delta\phi_D$. In the two cases $B_d^0\to\rho^-\pi^+$ and $B_s^0\to D_s^-K^+$ this phase obtains the values 2α and γ, respectively. The dilution of the two oscillating terms ($\cos(\Delta m t)$ and $\sin(\Delta m t)$) will affect the statistical power of the analysis.

4. MASSES AND DECAY DISTRIBUTIONS OF "B^{**}" RESONANCES

4.1 Positive-Parity D Mesons

The bound states of a charmed quark c with a light anti-quark $\bar{q}$ in an $L=1$ system have been discussed in many places, including Refs. 10–12. The understanding of such resonances will help in anticipating the properties of the corresponding mesons involving b quarks.

The fine structure of the $L=1$ $c\bar{q}$ system is dominated by whether the sum $\mathbf{L}+\mathbf{S_q}\equiv\mathbf{j}$ corresponds to $j=1/2$ or $3/2$. The states with $j=1/2$ and their expected decay modes are:

$$J^P_{2j} = 0^+_1 : \ \to (D\pi)_{\ell=0} , \tag{10}$$

$$J^P_{2j} = 1^+_1 : \ \to (D^*\pi)_{\ell=0} , \tag{11}$$

Neither of these states has been observed yet. The states with $j=3/2$ are expected to be:

$$J^P_{2j} = 1^+_3 : \ \to (D^*\pi)_{\ell=2} , \tag{12}$$

$$J^P_{2j} = 2^+_3 : \ \to (D\pi)_{\ell=2}, (D^*\pi)_{\ell=2} . \tag{13}$$

The states in these two pairs of equations are expected to be split by an interaction whose strength depends on one inverse power of the heavy quark mass.

Candidates for the 1^+_3 and 2^+_3 states exist:[8]

$$D^*(2420) \to D^*\pi , \tag{14}$$

$$D^*(2460) \to D\pi,\ D^*\pi . \tag{15}$$

The identification of the 2^+_3 state is unique just on the basis of decay modes. The identification of the 1^+_3 state is supported by the small mass splitting between the states and by the Dalitz plot distribution in the $D\pi\pi$ final state. This distribution is consistent with the production of an $\ell=2$ $D^*\pi$ final state.[8]

Adjusting the predictions of Ref. 10 to make the 1^+_3 and 2^+_3 states correspond to the observed ones, one then expects the 0^+_1 and 1^+_1 states to show up around 2.34 and 2.35 GeV/c^2, respectively. Other predictions for these states have been summarized in Ref. 11. A recent interesting suggestion[13] is that these particles could be the parity doublets of the 0^- D and 1^- D^* mesons, split from them by chiral symmetry breaking.

The failure to observe the 0^+_1 and 1^+_1 states up to now has usually been ascribed to their ability to decay via S-waves, and thus to be extremely broad. It is important, nonetheless, to see if such states can be identified, perhaps by comparison with exotic channels. Thus, for instance, to search for the 0^+_1 state one might compare π^+D^0 (non-exotic) and π^-D^0 (exotic) channels, while to search for the 1^+_1 state one might compare π^-D^{*+} (non-exotic) and π^+D^{*+} (exotic) channels.

One also expects $0_1^+, 1_1^+, 1_3^+$ and 2_3^+ *strange* charmed mesons, about 100 MeV above the corresponding nonstrange ones. (This is about the observed splitting between the D_s^+ and the D^+, and between the D_s^{*+} and the D^{*+}.) A candidate for the 1_3^+ strange state has been seen:[14]

$$D_s^*(2536) \to D^*\overline{K} \quad , \tag{16}$$

The absence of a $D\overline{K}$ mode suggests that this is not the 2_3^+ state.

4.2 Extrapolation to Positive-Parity B Mesons

A detailed study of the spectroscopy of $L = 1$ $b\bar{q}$ mesons has recently been performed in Ref. 15. Some earlier treatments are contained in Ref. 16. Here we comment on those features which can be obtained primarily from extrapolating the known or expected properties of the $L = 1$ $c\bar{q}$ mesons.

The fine-structure splitting between the states 1_3^+ and 2_3^+ scales as $1/m_Q$, where Q is the heavy quark. Thus, we expect the corresponding $b\bar{q}$ states to be split by $m_c/m_b \simeq 1/3$ times the splitting in the charm system, or about 13 MeV. Now, the spin-weighted average of the charmed 1_3^+ and 2_3^+ masses is about 2445 MeV/c^2, which lies about 470 MeV/c^2 above the spin-weighted average of the D and D^* masses. Thus, if the dynamics of the $c\bar{q}$ and $b\bar{q}$ systems are similar, we expect the spin-weighted average of nonstrange 1_3^+ and 2_3^+ $b\bar{q}$ states to lie about 470 MeV/c^2 above $[3M(B^*) + M(B)]/4 \simeq 5313$ MeV/c^2, or at 5783 MeV/c^2. (Taking account of the slightly greater binding energy of the $b\bar{q}$ system, the authors of Ref. 15 find this value to be 20 MeV/c^2 lower.)

The $(1_3^+,\ 2_3^+)$ states should then lie at (5775, 5788) MeV/c^2 (or (5755, 5767) MeV/c^2 in the estimate of Ref. 15). The $(0_1^+,\ 1_1^+)$ states should lie about 100 MeV lower. For the corresponding strange states, one should add about 100 MeV. (This appears to be true in comparing the B^0 with the recently observed B_s^0,[17] and in comparing nonstrange and strange $J^P = 1^+$ charmed mesons.) We summarize these expectations in Table I. The $\ell = 0$ decays [except for $b\bar{s}(0_1^+) \to \overline{B}K$, which has very little energy release] should correspond to very broad resonances, while the $\ell = 2$ decay widths should be tens of MeV or less (as in the $D^*(2420)$ and $D^*(2460)$ cases). Detailed estimates have been made in Ref. 15.

Table I. Expected properties of $L = 1$ $b\bar{q}$ states.

	$\bar{q} = \bar{u}$ or $\bar{d}$		$\bar{q} = \bar{s}$	
J^P_{2j}	Mass (GeV/c^2)	Decay mode(s)	Mass (GeV/c^2)	Decay mode(s)
0_1^+	5.68	$(\overline{B}\pi)_{\ell=0}$	5.78	$(\overline{B}K)_{\ell=0}, \overline{B}_s^*\gamma$
1_1^+	5.68	$(\overline{B}^*\pi)_{\ell=0}$	5.78	$\overline{B}_s\gamma,\ \overline{B}_s^*\gamma$
1_3^+	5.78	$(\overline{B}^*\pi)_{\ell=2}$	5.88	$(\overline{B}^*K)_{\ell=2}$
2_3^+	5.79	$(\overline{B}\pi)_{\ell=2}, (\overline{B}^*\pi)_{\ell=2}$	5.89	$(\overline{B}K)_{\ell=2},\ (\overline{B}^*K)_{\ell=2}$

4.3 The 2S States

Tagging using an associated kaon may be a promising method for identifying strange B mesons.[5,18] In order to make use of methods for tagging $D_s^+ = c\bar{s}$ or $\overline{B}_s^0 = b\bar{s}$ using an associated kaon, one must study $K^-D_s^+$ or $K^-\overline{B}_s^0$ combinations above threshold: 2.46 or 5.87 GeV/c^2, respectively. The 2_3^+ $c\bar{u}$ state, $D^*(2460)$, should be just barely able to decay to $K^-D_s^+$. The $K^-\overline{B}_s^0$ threshold is above any of the nonstrange resonances in Table I. If a resonance is to be responsible for $K^-\overline{B}_s^0$ or $K^-\overline{B}_s^{*0}$ correlations, the lowest candidate will be a $2S$ state.

The spin-weighted averages of $2S$ $c\bar{c}$ and $b\bar{b}$ states probably lie about 0.6 GeV/c^2 above the corresponding $1S$ states. The spacing between $1S$ and $2S$ states of one light quark and one heavy quark is probably slightly greater than this.[19] In Ref. 15 the $2S - 1S$ spacings are found in a QCD-motivated potential of the Buchmüller-Tye[20] type to be about (740, 720, 680, 660) MeV/c^2 for $(D,\ B,\ D_s,\ B_s)$ states. At any rate, the decay modes $\overline{B}_s^0K^-$ and $\overline{B}_s^{*0}K^-$ appear to be allowed for the $J^P = 1^-$ $2S$ $b\bar{u}$ state.

Making use of the estimates of Ref. 15 for nonstrange states but just adding 100 MeV/c^2 for strange states, we expect the $2S$ $c\bar{q}$ and $b\bar{q}$ levels to have the approximate masses shown in Table II. If the strange states really have smaller $2S - 1S$ spacings than the nonstrange ones, as predicted in Ref. 15, one should subtract about 60 MeV/c^2 from the estimates in the second column of Table II. Here we have assumed the same hyperfine splittings as in the $1S$ cases. The hyperfine splitting in a nonrelativistic model should be proportional to $|\Psi(0)|^2$, where $\Psi(\mathbf{r})$ is the Schrödinger wave function. For a system of reduced mass μ bound in a linearly rising potential $V(r) = ar$, $|\Psi(0)|^2 = (\mu/4\pi)\ \langle dV/dr\rangle = (\mu a/4\pi)$ independently of principal quantum numbers. There is some reason to suspect that this is an appropriate limit for a light quark bound to a heavy one.

Table II. Estimated masses and sample decay modes of $2S$ $c\bar{q}$ and $b\bar{q}$ levels.

	$q = \bar{u}$ or $\bar{d}$		$q = \bar{s}$	
J^P	Mass (GeV/c^2)	Decay mode(s)	Mass (GeV/c^2)	Decay mode(s)
$c\bar{q}$ (0^-)	2.68	$D^*\pi,\ D_s^*\overline{K}$	2.78	D^*K
$c\bar{q}$ (1^-)	2.82	$D^{(*)}\pi,\ D_s^{(*)}\overline{K}$	2.92	$D^{(*)}K$
$b\bar{q}$ (0^-)	6.00	$\overline{B}^*\pi,\ \overline{B}_s^*\overline{K}$	6.10	$\overline{B}^*K$
$b\bar{q}$ (1^-)	6.05	$\overline{B}^{(*)}\pi,\ \overline{B}_s^{(*)}\overline{K}$	6.15	$\overline{B}^{(*)}K$

The results of Tables I and II suggest that $\overline{B}_s^{(*)}\overline{K}$ correlations may be similar to $D_s^{(*)}\overline{K}$ correlations, which should be easier to study. One possible exception is that the $D(2460)$ should be just barely to decay to $D_s^+K^-$, while the corresponding $J^P = 2^+$ resonance in the B system is expected to be too light to decay to $\overline{B}_sK^-$.

1. *Effect of loss of photon in $B^* \to B\gamma$.* The D^* can decay to $D\pi$ or $D\gamma$, but the B^* is only able to decay to $B\gamma$. The energy of this photon is so low (about 46 MeV) that its detection is unlikely in most experiments. (See, however, Ref. 21.) Even if the photon is missed in the decay $B^{**} \to B^*\pi \to B\gamma\pi$, the effective mass of the $B\pi$ system is shifted down from the true B^{**} mass, but not broadened appreciably.

To see this, let p_π, p_B and p_γ be the momenta of the pion, B, and photon in the B^* rest frame. Let θ_γ be the angle between the photon and the pion in this frame. We have $|\vec{p}_\gamma| = E_\gamma = 46$ MeV $= |\vec{p}_B|$, while for $M(B^{**}) = 5.79$ GeV (the value we predict for the 2_3^+ state), one has $p_\pi = 464$ MeV. A bit of arithmetic leads to

$$M_{B\pi} \simeq M_{B^{**}} - E_\gamma + \frac{E_\gamma p_\pi}{M_{B^{**}}} \cos\theta_\gamma \quad , \tag{17}$$

or, for $M(B^{**}) = 5.79$ GeV, $M(B\pi) \simeq M(B^{**}) - [46 - 3.8(\cos\theta_\gamma)]$ MeV/c^2. The predicted mass differences between the $B\pi$ system and the B are then:

$$M(B\pi) - M(B) = \begin{cases} (448 + 4\cos\theta_\gamma)\ \mathrm{MeV}/c^2 & (1_3^+) \\ (461 + 4\cos\theta_\gamma)\ \mathrm{MeV}/c^2 & (2_3^+) \end{cases} \tag{18}$$

where in both cases a photon from $B^* \to B\gamma$ has been missed. Its loss causes negligible broadening of the resonances. The resonance masses are about 20 MeV/c^2 lower in the estimates of Ref. 15. The decay of the 2_3^+ state to $B\pi$ leads to a peak with

$$M(B\pi) - M(B) \simeq 500\ \mathrm{MeV}/c^2 \tag{19}$$

The relative strengths of the peaks in 1_3^+ and 2_3^+ decay are 3:2 as shown in Refs. 11 and 12.

2. *Dalitz plot analysis of $D^{**} \to D^*\pi_1$, $D^* \to D\pi_2$.* Let us define θ to be the angle between the two pions in the D^* rest frame. We recall some results already quoted in Ref. 11 for the distribution in θ (equivalent to a Dalitz plot variable). When a spin-2 D^{**} decays to $D^*\pi$, it does so via a D-wave, and the decay probability $W(\theta)$, normalized in such a way that

$$\frac{1}{2}\int_{-1}^{1} d(\cos\theta) W(\theta) = 1 \quad , \tag{20}$$

is $W(\theta) = (3/2)\sin^2\theta$. When a spin-1 D^{**} decays to $D^*\pi$, it can do so either by an S-wave (as expected for the 1_1^+ state) or a D-wave (as expected for the 1_3^+ state). The corresponding distributions are

$$W(\theta) = \begin{cases} 1 & (S\ \text{wave}) \ , \\ (1 + 3\cos^2\theta)/2 & (D\ \text{wave}) \ . \end{cases} \tag{21}$$

It appears that the decay $D(2420) \to D^*\pi$ is compatible with the distribution for D wave. This supports the identification of the $D(2420)$ as the 1_3^+ state. The $D(2460)$ indeed appears to have $J^P = 2^+$.[8]

When and if another resonance decaying to $D^*\pi$ is discovered, we predict that the distribution will be isotropic in θ as expected for the 1_1^+ state.

3. *Dalitz plot analysis of $B^{**} \to B^*\pi \to B\gamma\pi$.* The Dalitz plot distribution given by the θ_γ dependence can be measured if one can detect the photon.[21] Normalizing distributions $W(\theta_\gamma)$ as above, we find for a spin-2 B^{**} decaying to $B^*\pi$, with $B^* \to \gamma B$, that $W(\theta_\gamma) = 3(1 + \cos^2\theta_\gamma)/4$. This function is peaked at $\theta_\gamma = 0$ and π. The corresponding distributions for a spin-1 B^{**} decaying to $B^*\pi$ in a state of angular momentum ℓ are $W(\theta_\gamma) = 1$ for $\ell = 0$ and $W(\theta_\gamma) = (2 + 3\sin^2\theta_\gamma)/4$ for $\ell = 2$. This last function is peaked at $\theta_\gamma = \pi/2$.

4. *Distributions for polarized D^{**} and B^{**}.* Dalitz plot distributions similar to that of $D^{**} \to D^*\pi_1$, $D^* \to D\pi_2$ cannot be measured for B^{**} decays since the decay $B^* \to B\pi$ is kinematically forbidden. However, if D^{**} or B^{**} resonances are produced with any polarization, their decays to $D^{(*)}\pi$ or $B^{(*)}\pi$ may produce pions with a non-isotropic distribution with regard to the polarization axis. This point has recently been emphasized in Ref. 22.

Let us imagine that a spin-J resonance R (standing for D^{**} or B^{**}) is produced along some axis $\hat{n}$. By parity invariance one expects the same probability for helicity λ and $-\lambda$ with respect to $\hat{n}$, but, aside from this, populations associated with different helicities can differ. This, in turn, can lead to non-trivial distributions in the angle θ_1 between the momentum of the pion π_1 to which the resonance R decays and the direction $\hat{n}$. Labelling these relative decay probabilties by $W_{|\lambda|}(\theta_1)$, where

$$\frac{1}{2}\int_{-1}^{1} d(\cos\theta_1) W_{|\lambda|}(\theta_1) = 1 \quad , \quad W_0(\theta_1) + 2\sum_{|\lambda|>0}^{J} W_{|\lambda|}(\theta_1) = 2J + 1 \quad , \tag{22}$$

we have (for $P \equiv D$ or B, $V \equiv D^*$ or B^*):

$\underline{R(2^+) \to P\pi}$

$$W_0(\theta_1) = (5/4)(3\cos^2\theta_1 - 1)^2 \ , \quad W_1(\theta_1) = (15/2)\sin^2\theta_1\cos^2\theta_1 \ , \quad W_2(\theta_1) = (15/8)\sin^4\theta_1 \ , \tag{23}$$

$\underline{R(1^+) \to (V\pi)_{\ell=0}}$

$$W_0(\theta_1) = W_1(\theta_1) = 1 \quad , \tag{24}$$

$\underline{R(1^+) \to (V\pi)_{\ell=2}}$

$$W_0(\theta_1) = (3/4)(1 + 3\cos^2\theta_1) \quad , \quad W_1(\theta_1) = (3/4)(1 + [3/2]\sin^2\theta_1) \quad , \tag{25}$$

$\underline{R(2^+) \to V\pi}$

$$W_0(\theta_1) = (15/2)\sin^2\theta_1\cos^2\theta_1 \quad , \quad W_1(\theta_1) = (5/4)(1 - 3\cos^2\theta_1 + 4\cos^4\theta_1) \quad , \quad W_2(\theta_1) = (5/4)(1 - \cos^4\theta_1) \quad . \tag{26}$$

Of course, for $R(0^+) \to P\pi$ there is no θ_1 dependence.

The above distributions are relevant to any attempt to select pion-D or pion-B correlations by means of angular rather than effective-mass cuts. If different values of $|\lambda|$ are populated differently, such angular cuts can either enhance or degrade a signal which was due originally to a specific resonance or band of resonances.

5. CONCLUSION

We have discussed the possibility of identifying neutral B mesons using hadrons produced nearby in phase space. The simplest example is the expected correlation between a B_d^0 and a π^+, which we expect to be stronger (with relative probability P_1) than that between a $\bar{B}_d^0$ and a π^- (with relative probabilty $P_2 < P_1$). The correlation is expected to be most pronounced for low effective masses or small rapidity differences. It can exist as a result of resonances in the $B\pi$ system, but can also be due simply to the fragmentation of a $\bar{b}$ quark. We gave some estimates of the correlation factor $(P_1 - P_2)/(P_1 + P_2)$.

The proposed tagging method is based on a statistical correlation. We have noted that time-dependent asymmetries, in neutral B decays to flavor-eigenstates, to CP-eigenstates and to other states from which CKM phases can be obtained, are diluted by the correlation factor $(P_1 - P_2)/(P_1 + P_2)$. As guidance for studies of this correlation one may look at the corresponding correlations involving D mesons. We have treated several issues regarding resonances, discussing some properties of the positive-parity charmed mesons and their extrapolation to B mesons, expected masses of $2S$ states, and the angular distributions in decays.

6. ACKNOWLEDGEMENTS

We are grateful to J. Butler, E. Eichten, H. Frisch, G. Gustafson, C. Hill, B. Kayser, T. LeCompte, H. Lipkin, C. Quigg, A. I. Sanda, V. Sharma, M. Shochet, S. Stone, and A. Yagil for helpful discussions, and to D. G. Cassel and H. Tye for extending the hospitality of the Newman Laboratory of Nuclear Science, Cornell University, during part of this investigation. Part of this study was performed at the Aspen Center of Physics and at the Snowmass Workshop on B Physics at Hadron Accelerators. This work was supported in part by the United States – Israel Binational Science Foundation under Research Grant Agreement 90 – 00483/2, by the Fund for Promotion of Research at the Technion, and by the U. S. Department of Energy under Grant No. DE FG02 90ER–40560.

7. REFERENCES

1. M. Gronau, TECHNION-PH-93-36, presented at this workshop.
2. *The Physics Program of a High-Luminosity Asymmetric B-Factory at SLAC*, ed. D. Hitlin, SLAC-PUB-353 (1989) and SLAC-PUB-373 (1991); *Physics Rationale for a B-Factory*, K. Lingel *et al.*, CLNS 91-1043 (1991); *Physics and Detector at KEK Asymmetric B Factory*, K. Abe *et al.*, KEK Report 92-3 (1992).
3. See e.g. *B Physics at Hadron Accelerators, Proceedings of a workshop at Fermilab*, Nov., 1992, ed. J. A. Appel (Fermilab, Batavia, Il, 1992); *Beauty 93, Proceedings of the First International Workshop on B Physics at Hadron Machines*, Liblice Castle, Melnik, Czech Republic, Jan. 18 -22, 1993, ed. P. E. Schlein, *Nucl. Instrum. Meth.* **331** (1993) No. 1.
4. M. Gronau, A. Nippe and J. L. Rosner, *Phys. Rev.* **D47** (1993) 1988.
5. M. Gronau and J. L. Rosner, TECHNION-PH-93-32, EFI 93-41 (September 1993), to be published in *Phys. Rev.* **D**.
6. M. Gronau and J. L. Rosner, EFI 93-43, TECHNION-PH-93-31 (August 1993), submitted to *Phys. Rev. Lett.*
7. S. Stone, in *Heavy Flavors*, ed. A. J. Buras and M. Lindner, (World Scientific, Singapore, 1992).
8. ARGUS Collaboration, H. Albrecht *et al.*, *Phys. Lett* **B221** (1989) 422; **B231** (1989) 208; **B232** (1989) 398; Fermilab E691 Collaboration, J. C. Anjos *et al.*, *Phys. Rev. Lett.* **62** (1989) 1717; CLEO Collaboration, P. Avery *et al.*, *Phys. Rev.* **D41** (1990) 774; *Phys. Lett.* **B303** (1993) 377; Fermilab E687 Collaboration, P. L. Frabetti *et al.*, FERMILAB-Pub-93/249-E (1993).
9. G. Gustafson and J. Hakkinen, work in preparation. We thank G. Gustafson for informing us about these results prior to their publication.
10. A. De Rújula, H. Georgi, and S. L. Glashow, *Phys. Rev. Lett.* **37** (1976) 785(C).
11. J. L. Rosner, *Comments on Nucl. Part. Phys.* **16** (1986) 109.
12. N. Isgur and M. B. Wise, *Phys. Rev. Lett.* **66** (1991) 1130; Ming Lu, M. B. Wise, and N. Isgur, *Phys. Rev.* **D45** (1992) 1553.
13. W. A. Bardeen and C. T. Hill, Fermilab-Pub-93/059-T and SSCL-PP-243, to be published in *Phys. Rev.* **D**.
14. ARGUS Collaboration, H. Albrecht *et al.*, *Phys. Lett.* **B230** (1989) 162; **B297** (1992) 425; CLEO Collaboration, J. Alexander *et al.*, *Phys. Lett.* **B303** (1993) 377.
15. E. J. Eichten, C. T. Hill, and C. Quigg, Fermilab report no. FERMILAB-Pub-93/255-T, submitted to *Phys. Rev. Letters*; C. T. Hill, Fermilab report no. FERMILAB-Pub-93/256-T, presented at this workshop; C. Quigg, Fermilab report no. FERMILAB-Conf-93/257-T, presented at this workshop.
16. See, in particular, Refs. 12–14 of Ref. 11.
17. ALEPH Collaboration, preprint 93-97, 1993; CDF Collaboration, F. Abe *et al.*, *Phys. Rev. Lett.* **71** (1993) 1685.
18. A. Ali and F. Barreiro, *Zeit. Phys.* **C30** (1986) 635.
19. A. Martin, *Phys. Lett.* **100B** (1981) 511; W. Kwong, C. Quigg, and J. L. Rosner, *Ann. Rev. Nucl. Part. Sci.* **37** (1987) 325.
20. W. Buchmüller and S.-H. H. Tye, *Phys. Rev.* **D24** (1981) 132.
21. L3 Collaboration, paper No. 227 contributed to *the XVI International Symposium on Lepton-Photon Interactions*, Cornell University, Ithaca, NY, Aug. 10-15, 1993.
22. A. F. Falk and M. E. Peskin, SLAC report SLAC-PUB-6311, August, 1993.

Comparison of Forward and Central Collider Detectors for Beauty Physics

Christopher J. Kennedy, Robert F. Harr, Paul E. Karchin
Physics Department, Yale University
New Haven, Connecticut 06511

ABSTRACT

A comparison of geometry, tracking, and muon triggering indicates that a central detector has a higher efficiency than a forward detector of equal psuedo rapidity coverage at both Tevatron and SSC energies. The difference at the Tevatron is considerable, about a factor of four. At the SSC, however, the difference is about a factor of two, so other considerations such as vertexing, particle ID, or cost may make a large forward detector an attractive option.

1. INTRODUCTION

There have been many proposals to study B-physics at hadron colliders, both at SSC and Fermilab energies. Attempts to compare these proposals are often complicated by differences in specific detector systems, most of which are currently unbuilt and untested. Considering the intricacies of the problems with specific detector systems, we have carried out this analysis in an attempt to understand the most general issues involved in these experiments, independent of their specific subsystems.

We analyzed potential experiments at the Fermilab Tevatron (TEV), center of mass energy of 1.8 TeV, and the Superconducting Super Collider (SSC) center of mass energy of 40 TeV. For each of these two energy ranges we looked at three detector geometries: a central detector with a pseudo-rapidity (η) coverage of -2 to 2, a big forward detector with an η coverage of 1.5 to 5.5, and a small forward detector in the range of 1.5 to 3.5 units of η. These η ranges were chosen because at the SSC both SDC[1] and GEM[2] cover approximately -2 to 2. The big forward detector was chosen to match the η coverage of the central detector, four units of pseudo- rapidity, with a minimum η of 1.5. This value was chosen since it is sufficiently forward to make it practical to build. The small forward detector's η range was chosen to determine the effect on acceptance of restricting the coverage, presumably to save money.

We looked at two specific decays:

$$
\begin{aligned}
B_d^0 &\rightarrow \psi + K_s^0, \psi \rightarrow \mu^+ + \mu \ , K_s^0 \rightarrow \pi^+ + \pi^- \\
B_d^0 &\rightarrow \pi^+ + \pi^-
\end{aligned}
\quad (1)
$$

These two decays were selected for a variety of reasons. They are both important decays in determining CP violation in the B sector and therefore will be of great interest in any B-physics experiment. Additionally, the comparisons in efficiency between two and four body decay states is of interest. Also of interest is the efficiency of a muon trigger for muonic final states, with the muons coming from the ψ decay, and a non-muonic final state, where the source of non-background muons is the other B particle in the event. This comparison is important both for using the muon as a trigger and to use it as a tag of the B.

This study was done utilizing PYTHIA 5.6[3] and JETSET 7.3[4]. The initial interaction at the SSC energy was two 20 TeV protons colliding with each other. The interaction at the TEV energy was one 0.9 TeV proton colliding with a 0.9 TeV anti-proton. Decays of pions and kaons were allowed in a cylindrical region of radius 1.7 m, approximately corresponding to the calorimeter radius for both CDF and SDC, and a length of 10m, consistent with the expected distance from vertex to calorimeter in a forward detector. Events were selected where the $\bar{b}$ quark forms a B^0 meson. The B^0 meson was forced to decay into the desired final state. In the case of B^0 to ψK_s, the ψ was forced to decay to two muons and the K_s was forced to decay into two charged pions. The b quark was allowed to hadronize and was decayed according to PYTHIA, which implies no Cabibbo suppressed B decays. $B - \overline{B}$ mixing was not turned on in PYTHIA for this study. For each of the conditions that we studied, 10,000 events were generated. Ten thousand events were also generated for the minimum bias study. When generating the minimum bias background, events containing b quarks were eliminated. We did not consider the effects of multiple interactions within one beam crossing.

2. GEOMETRIC ACCEPTANCE AND TRACKING

The first area of investigation is the efficiency of the two modes in the various experimental configurations and energies. We first required that all daughter particles fell within the given η range ($\eta_{min} < \eta < \eta_{max}$). Next we required that all of the particles were "trackable". This was approximated by imposing a 0.5 GeV/c minimum momentum requirement on all of the daughter particles ($P > 0.5\ GeV/c$). This requirement had almost no effect on the efficiency in the forward detectors and a realtively small effect on the $B^0 \rightarrow \pi\pi$ decay in any configuration. It did cause a considerable reduction in efficiency for the B^0 to ψK_s decay in the central detector. A muon tag was imposed next. This muon tag required that the second B in the event decayed into a state containing a muon and that the the muon was also in the specified η range($\eta_{min} < \eta_{tag} < \eta_{max}$). This muon tag immediately caused a factor of 10 reduction due to the branching ratio of B to μ X. Finally, the 0.5 GeV/c momentum requirement was placed on the tagging muon to insure the ability to track the muon ($P_{tag} > 0.5 GeV/c$). Results are presented in Table 1.

Table 1. Efficiency in % for a big central detector, a big forward detector, and a small forward detector. The efficiencies do not incude the branching fractions for $\psi \rightarrow \pi^+\pi^-$ and $K_s \rightarrow \mu^+\mu^-$ (Analysis selection criteria are cumulative.)

Selection Criterion	ψK_s SSC	ψK_s TEV	$\pi\pi$ SSC	$\pi\pi$ TEV
$-2 < \eta < 2$	32	42	38	49
$P > 0.5$ GeV/c	23	29	38	49
$-2 < \eta_{tag} < 2$	1.7	2.6	2.8	3.7
$P_{tag} > 0.5$ GeV/c	1.6	2.4	2.7	3.6
$1.5 < \eta < 5.5$	17	13	20	16
$P > 0.5$ GeV/c	17	13	20	16
$1.5 < \eta_{tag} < 5.5$	1.5	0.9	1.2	0.95
$P_{tag} > 0.5$ GeV/c	1.5	0.9	1.2	0.95
$1.5 < \eta < 3.5$	7.4	6.5	10	11
$P > 0.5$ GeV/c	7.3	6.5	10	11
$1.5 < \eta_{tag} < 3.5$	0.4	0.29	0.38	0.57
$P_{tag} > 0.5$ GeV/c	0.4	0.29	0.38	0.57

The big forward detector has relatively smaller efficiencies than the central detector at both TEV and SSC energies. This is primarily due to the particle distribution at the respective energies. Figure 1 shows the number of daughter particles as a function of pseudo-rapidity for both decays and both energies (Fig. 1a and 1b). The distribution in η for the TEV energies is much more populated near zero than the distribution for SSC energies and falls quickly between three and four. The distribution for SSC energies cuts off more slowly and still has an appreciable particle density up to about an η of 5. We were aware that the QCD calculation of the angular distribution of b quarks, by Berger and Meng[5], does not exactly match the PYTHIA distributions[6]. We investigated the effect of these discrepancies by weighting the PYTHIA distribution to match their QCD predictions. We found that the corrections were at or below 20%. Since these corrections are small compared to differences between geometries they were ignored.

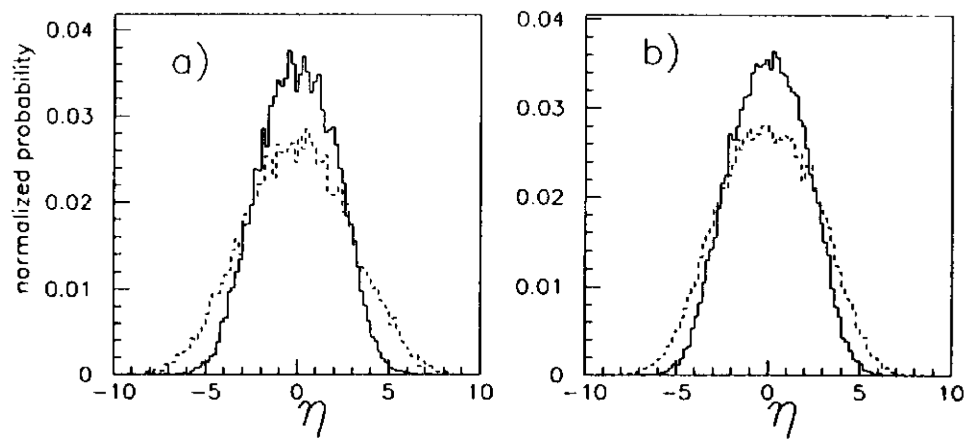

Figure 1. Normalised daughter particle distribution in eta. (The area under each plot is one.) For a) $B \rightarrow \psi K_s$ and b) $B \rightarrow \pi\pi$, for TeV (solid line) and SSC (dashed line) energies.

3. MUON TRIGGER

The efficiency of the single muon trigger was examined as a function of both momentum (P) and transverse momentum (P_t). We also were interested in the percentage of minimum bias events which were rejected as a function of cuts on muon P and P_t. Log plots 2a and 2b show that the efficiency of minimum bias events drops quickly for both increasing P and P_t. The efficiencies of both tagged and untagged B events, although starting at a lower value due to efficiency, decrease much less rapidly than the minimum bias background. Since the general behavior of efficiencies as a function of P and P_t are so similar in terms of what the efficiency of the signal is for a given background reduction, seen in all of the samples, only the efficiency plots versus P_t will be presented. The efficiencies as a function of P_t for all three detector configurations are presented in figures 3,4, and 5. For the B^0 to ψK_s signal, the efficiencies of the untagged samples allow us to consider the possibility of other tagging schemes such as looking for the kaon from the decay chain of the other B in the event or the pion from a B^{**} decay. These tagging schemes were not examined here since their efficiencies are very dependent on the specific particle ID systems of the detector and thus beyond the scope of this invesigation. For the B^0 to $\pi\pi$ samples only the tagged efficiencies are presented. In addition the minimum muon P_t for a minimum bias reduction of 100 and the efficiencies related to this P_t cut for signal are presented below (Table 2).

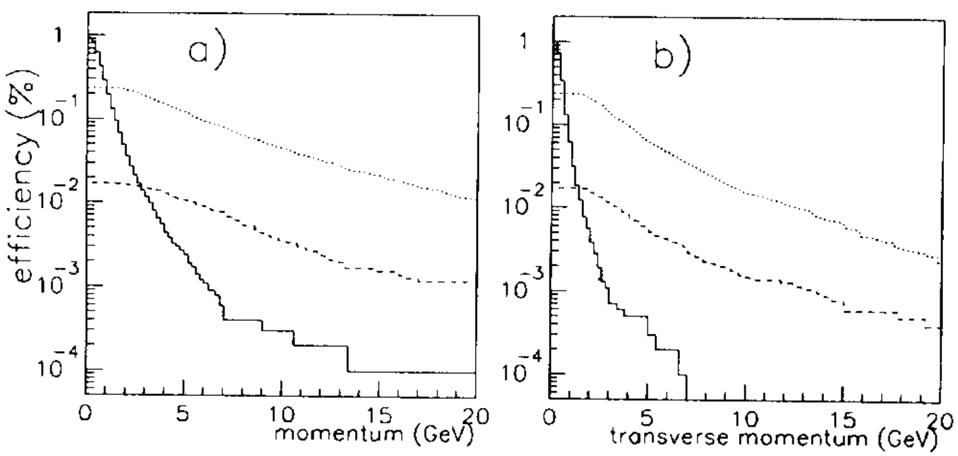

Figure 2. Comparison of efficiencies of a minimum muon a) momentum and b) transverse momentum on minimum bias events (solid line), untagged $B \to \psi K_s$ (dotted line) and tagged $B \to \psi K_s$ for a central detector at SSC energies.

Table 2. Efficiencies in %. Transverse momentum cuts on the trigger muon are explained in the text.

η range	P_t Cut (GeV/c)	ψK_s notag	ψK_s tag	$\pi\pi$ tag
-2 < η < 2 SSC	1.50	22.8	1.61	1.84
-2 < η < 2 TeV	1.0	28.3	2.44	2.78
1.5 < η <5.5 SSC	1.0	16.8	1.45	0.96
1.5 < η < 5.5 TeV	0.75	12.9	0.91	0.77
1.5 < η < 3.5 SSC	1.0	7.39	0.43	0.34
1.5 < η < 3.5 TeV	0.75	6.45	0.29	0.47

4. CONCLUSIONS

As we can see from Table 2 there seems to be a fairly strong advantage in efficiency for the central region especially in comparison to the small forward region. This is most pronounced at the Tevatron. The tagged $\pi\pi$ decay in the central detector has a total efficiency of 2.8% but only .77% for the big forward detector, down by a factor of almost 4. The efficieny for the small forward detector is down by almost a factor of 6. Although there is a factor of two difference in efficiency between the central and big forward detectors at SSC energies, other factors, such as cost or space constraints preclude us from eliminating this option at the SSC. The forward detector geometry allows the possibility of having a second arm in the opposite direction to increase efficiency. It must be remembered that all of these results will be affected by other factors, including vertexing, particle identification and actual η coverage. At present no hadron collider detectors have the ability to fully trigger, identify and reconstruct B events over any of the η ranges discussed in this analysis.

5. ACKNOWLEDGEMENTS

The authors gratefully acknowledge the support of the Texas National Research Laboratory Commission and the Unived States Department of Energy.

REFERENCES

1. SDC Technical Design Report, SDC Publication, SDC-92-201, 1992.
2. GEM Technical Design Report, SSC Publication, SSCL-SR-1219, 1993.
3. H. Bengstsson and T. Sjostrand, Comp. Phys. Comm. **46** (1987) 43.
4. T. Sjostrand and M. Bengtsson, Comp. Phys. Comm. **43** (1987) 367 .
5. E. L. Berger and R. Meng, *Phys. Rev.* **D46** (1992) 169.
6. R. F. Harr and P. E. Karchin, *SSC preprint* (1992).

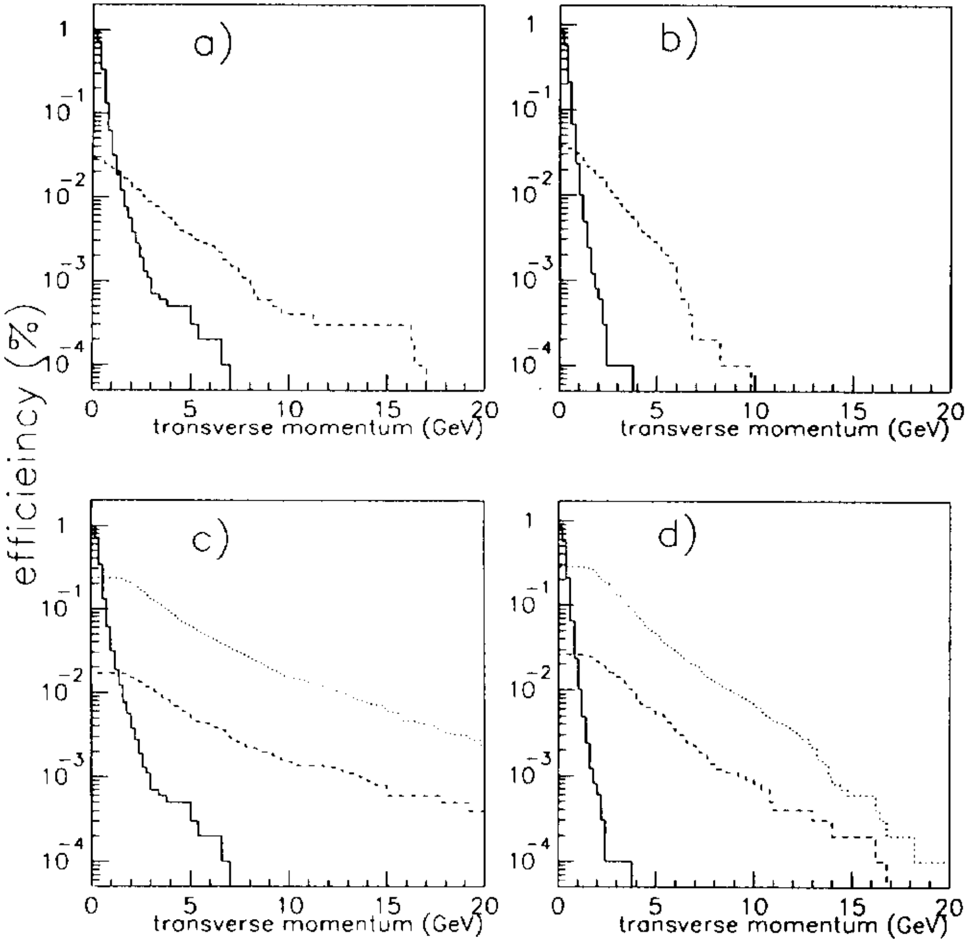

Figure 3. Efficiency as a function of transverse momentum cut in the central region $-2 < \eta < 2$ for: a) $B \to \pi\pi$ at SSC energies, b) $B \to \pi\pi$ at TeV energies, c) $B \to \psi K_s$ at SSC energies and d) $B \to \psi K_s$ at TeV energies for minimum bias (solid line), tagged decays (dashed line), and untagged decays (dotted line, only ψK_s decay).

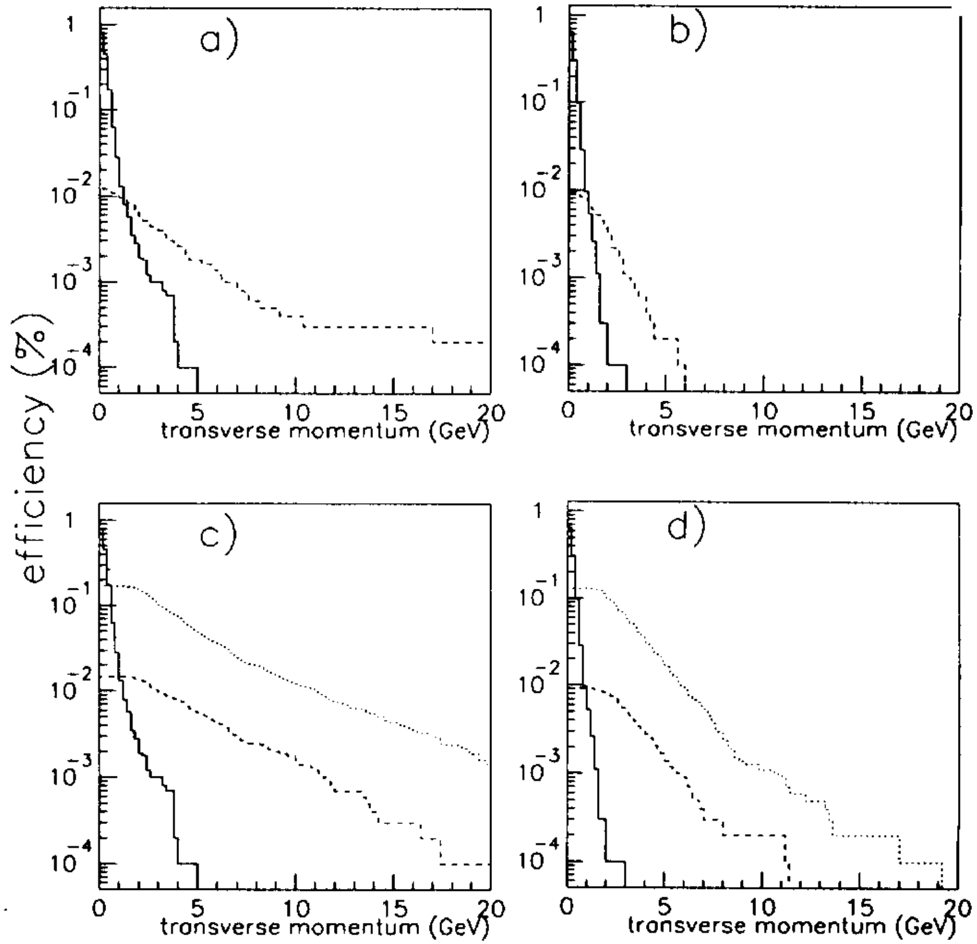

Figure 4. Efficiency as a function of transverse momentum cut in the big forward region $1.5 < \eta < 5.5$ for: a) $B \to \pi\pi$ at SSC energies, b) $B \to \pi\pi$ at TeV energies, c) $B \to \psi K_s$ at SSC energies and d) $B \to \psi K_s$ at TeV energies for minimum bias (solid line), tagged decays (dashed line), and untagged decays (dotted line, only ψK_s decay).

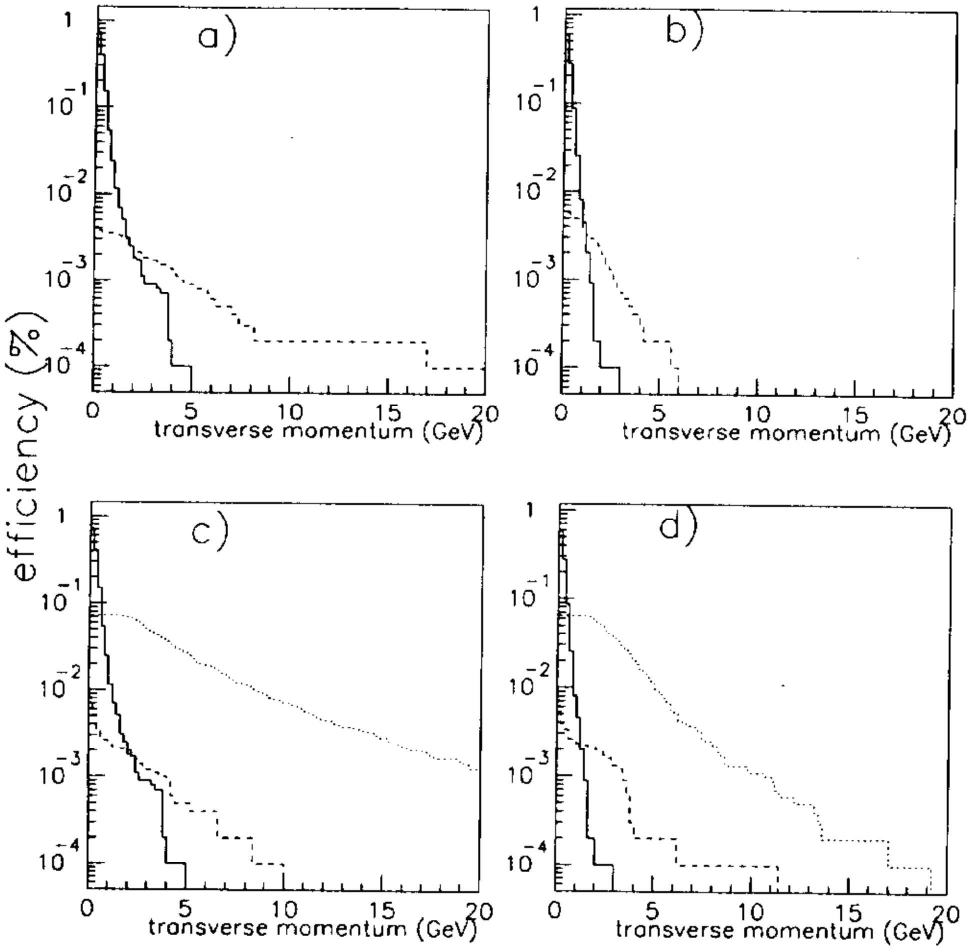

Figure 5. Efficiency as a function of transverse momentum cut in the small forward region $1.5 < \eta < 3.5$ for: a) $B \to \pi\pi$ at SSC energies, b) $B \to \pi\pi$ at TeV energies, c) $B \to \psi K_s$ at SSC energies and d) $B \to \psi K_s$ at TeV energies for minimum bias (solid line), tagged decays (dashed line), and untagged decays (dotted line, only ψK_s decay).

THE SFT

A SUPER FIXED TARGET BEAUTY EXPERIMENT AT THE SSC

B. Cox[2], T. Alexopoulos[3], M. Arenton[2], S. Conetti[2], G. Corti[2], C. Dukes[2], A. Erwin[3], V. Golovatyuk[2], T. Lawry[2], A. McManus[2], C.T. Murphy[1], K. Nelson,[2] L. Spiegel[1], I.Tzamouranis[2]

(1) Fermi National Accelerator Laboratory, P.O. Box 500, Batavia, IL 60510
(2) University of Virginia, Charlottesville, Virginia 22901
(3) University of Wisconsin, Madison, WI 53706

Abstract

The observation and precision measurement of CP violation asymmetries and the phase of the CKM matrix is a major objective of B experiments at the SSC. The yields of reconstructed and tagged B decays and the various factors which minimize the dilution factors make measurements of CP asymmetries in the fixed target option known as the SFT more than competitive with much more expensive hadron collider experiments and significantly better than asymmetric e^+e^- B factories. Moreover, the superior time resolution possible in the SFT configuration allows a precision in the measurements of mixing and time dependent CP violation effects in B_s decays that is possible with no other option. We present estimates of the sensitivity and precision of measurement of the CKM matrix element phases possible with the SFT option for various B decay modes.

1. Introduction

The SFT[1] "external" fixed target experimental configuration has several technical advantages in the measurement of CP violating asymmetries compared to e^+e^- or hadron collider experiments and is more economical to implement. Some of these technical advantages generated by the Lorentz boost and are common to both internal (gas jet)[2] and external target (extracted beam/live target) fixed target B options[1,3] although the two types of fixed target B experiments differ considerably in their implementation. However, the use of a live target in which the full interaction and subsequent decay vertices can be observed directly is possible only in the "external" fixed target option. As will be shown, the live target coupled with the other technical advantages of the fixed target experiment are more than enough to offset the larger B cross sections available at collider energies.

The higher momentum of B hadrons and the resulting longer B decay lengths and higher momentum of the B decay products result in lower multiple scattering and much better ratios of vertex resolution to decay length in the SFT ($<L/\sigma_L>$ for B decays $\approx$ 380!) than in collider options. This makes possible very good time resolution measurements of the CP asymmetries in both B^0_d and B^0_s decay distributions, minimizing "dilution" effects due to mixing and minimum decay length criteria. The very good time resolution also makes possible measurements using the rapidly oscillating B^0_s and allows use of more complex analysis procedures using decays into CP non conjugate final states where analysis of the time distributions are essential. Indeed, it is possible given the kinematics of the very high momentum B decays to observe B^0 oscillations and even to extract B^0_d and B^0_s mixing parameters from partially reconstructed B decays[4]. The superior ratio of decay length to resolution of fixed target experiments also significantly decreases the dilution effects due to mistagging by allowing association of the tagging particle with a given secondary or tertiary vertex. Moreover, the relatively low multiplicity of the SSC fixed target events together with the better vertex resolution and longer decay lengths leads to better vertex recognition and reconstruction efficiencies for both the tagging and CP B decays. The overall result of these effects is to make possible more precise measurements of the angles of the unitarity triangle.

Finally, the fact that a fixed target spectrometer need cover only a relatively small solid angle compared to a forward collider experiment, let alone a 4π hadron or e^+e^- experiment, leads to undeniable economies in detector construction. A qualitative summary of the relative merits of collider versus fixed target (either internal or external target) are summarized in Table 1. The factors in favor of SFT are designated by a +. Asterisks indicate items that are advantages or disadvantages peculiar to the external (extracted beam/live target) option in distinction to the internal target option. Table 2 compares a few collider and fixed target B production parameters. In Table 2, we have taken 10^7 interactions per second as a limit for high rate B physics fixed target or collider detector (0.18 interactions per bucket at the SSC) to avoid the problem of multiple high multiplicity events per bucket. The heavy target enhancement of the pN B production and total cross sections is taken to be $A^{0.28}$ for the fixed target experiment.

Table 1
Advantages of Fixed Target Vs. Hadron Collider B Physic Options

Cross Sections	-
Difficult Extraction*	-
Higher Acceptance	+
External Experimental Area*	+/-
No Beam Pipe*	+
Higher Momentum Secondaries	+/-
Lower Track Multiplicity	+
Active Target*	+
Higher Reconstruction Efficiencies	+
Vertexing Efficiencies/Resolutions*	+
Track Resolutions	+
Radiation Damage*	+
Triggering Efficiency/Flexibility	+
Time Resolution	+
Smaller Detectors/Lower Cost	+

Table 2
B Production Parameters for the SSC Fixed Target Compared to SSC Collider

	SSC Collider	SSC Fixed Target (SFT)
Interaction Rate	10^7 Int./sec	10^7 Int./sec
σ_T (pN or pSi)	100 mb	356 mb
σ_{BB} (pN or pSi)	1000μb	56μb
σ_{BB}/σ_T	1/100	1/6300
Event Charged Multiplicity	"few" hundred	$\approx$ 20
$\langle p_B \rangle$	43 GeV/c	445 GeV/c
$\langle p_{lepton} \rangle$	36 GeV/c	280 GeV/c
Median B Decay Length	3 mm	42 mm
Mean B Decay Length	13 mm	95 mm

2. The SFT Spectrometer

The SFT spectrometer shown Fig. 1 is a two magnet open geometry forward spectrometer. The SFT spectrometer provides angular coverage from approximately 2 to 75 mrad for muons and electrons by means of a five layer Resistive Plate Counter (RPC) muon detector and a scintillating fiber EM calorimeter. Particle ID for π,K and protons is provided over the same angular range by a RICH counter/transition radiation detector (TRD) combination [5] for momenta between 50 and 700 GeV/c with kaon efficiency greater than 90% and pion contamination less than 10%. The EM calorimeter coupled with the TRD provides electron ID. Straw tube and silicon microstrip planes provide charged particle trajectory measurements both upstream and downstream of the analysis magnets. The specification and parameters of the SFT spectrometer are described more fully in EOI-14[1] than possible is here. If particle ID is not necessary for a particular track, then charged particle reconstruction can be performed using silicon microstrip detectors at angles less than 2 mrad with respect to the beam.

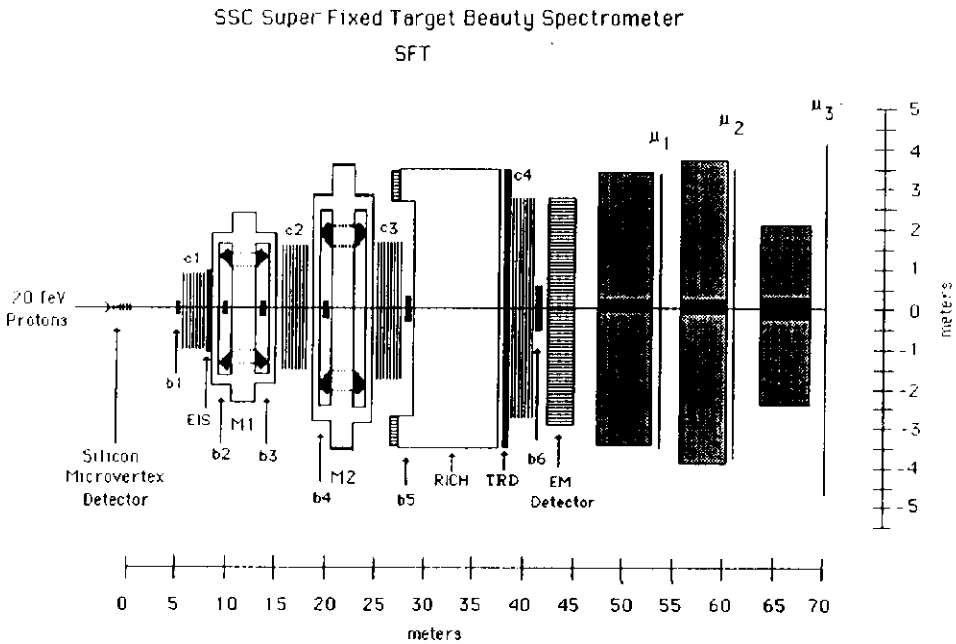

Fig. 1
SFT Spectrometer

While space does not permit a detailed description of all detectors, the acceptances and the momentum, spatial, and time resolutions have been estimated for this spectrometer using GEANT simulations which incorporate experience obtained in the Fermilab fixed target program[6]. We have estimated[7] the various vertex resolutions given in Table 3 for the SFT silicon microvertex detector/live target arrangement based on a detailed track reconstruction in a hit level Monte Carlo of $B^0_d \to \pi^+\pi^-$ decays in 20 TeV fixed target interactions in the silicon live target, including multiple scattering, charge sharing, delta rays, strip widths, secondary interactions, etc.

Table 3
SFT Silicon MVXD Vertex Resolutions

	σ_x	σ_r	σ_z
Primary Vertex	6 μm	8 μm	58 μm
Primary Vertex (using beam tracks)	3 μm	4 μm	58 μm
Secondary Vertex (Ntracks≥2, all momenta)	6 μm	8 μm	300 μm
Secondary Vertex (Ntracks=2, p≥20 GeV/c)*	4 μm	6 μm	250 μm
Lepton Impact Parameter	-	8 μm	-
Two track Distance of Closest Approach	3 μm	4 μm	-

Table 4 gives the average z separations of B decays in the SFT as compared with the z resolutions for the various vertex quantities.

Table 4
SFT Primary, Secondary and Tertiary Vertex Separations and Resolutions

	Average z Separations	σ_z separation Resolution
Primary - B vertex	90 mm	0.25 mm
B vertex - $D^{\pm}$ vertex	75 mm	0.35 mm
B vertex - D^0 vertex	40 mm	0.35 mm
B vertex - $D^{\pm}_s$ vertex	40 mm	0.35 mm

As can be seen, the separation of primary and secondary vertices is very much larger than the resolutions that can be attained in the SFT live target resulting in $\tau(B)/\sigma_\tau \approx 70$ or even more impressive,

$$\langle\text{Decay length}\rangle/\sigma_L \approx 380$$

With this sort of ratio of decay length to vertex resolution, the $15\sigma_z$ cut set as a standard to insure adequate separation of primary and secondary vertices is not serious at all for the fixed target option in distinction to the collider configuration where it causes significant loss of B decays. These excellent vertex resolutions also result in

$$\sigma_\tau \approx 0.018 \text{ ps}$$

a time resolution achievable in no other option.

The tracking system of the SFT, optimized in several ways, combined with the two magnet system operated with equal and opposite 1.5 GeV/c p_t kicks, results in a momentum resolution of

$$\sigma_p/p = .0009 + 0.00000841 \cdot p$$

The two body mass resolutions of the spectrometer corresponding to these tracking resolutions are given in Table 5 for the $J/\Psi \to \mu\mu$ and $B^0_d \to \pi^+\pi^-$. These resolutions are important to minimize backgrounds and the dilutions in the CP asymmetries that result from them.

Table 5
SFT Spectrometer Track Momentum and Two Body Mass Resolutions

	σ_{p_t}/p_t	σ_p/p	σ_M (Mev/c^2)
$J/\Psi \to \mu^+\mu^-$	0.0039	0.0025	7.6
$B^0 \to \pi^+\pi^-$	0.0045	0.0029	13.0

Finally, because of the large number of tracking planes, the efficiency for single track and two track vertex reconstruction are ≥95% and ≥90% respectively. These resolutions and efficiencies when combined with the expected efficiencies for K/π/p/e/μ identification possible with the RICH/TRD/EM Calorimeter/RPC μ detector system of the SFT result in the estimates of Table 6 for the mistagging and overall efficiencies for the tagging μ,e or K particles used to determine the particle or antiparticle nature of the other B in the event.

Table 6
Mistags/Efficiencies

Tags	Mistags			Efficiencies				
	Vertex Assoc.	Detectr Ineff.	Total Mistag	Vertex Assoc.	Vertex Sep.	Particle ID	Track Rec.	Total
$B \to \mu^\pm$	<0.025	<0.010	≤0.035	0.95	0.95	0.99	0.95	0.85
$B \to e^\pm$	<0.025	≈0.05	<0.075	0.95	0.95	0.95	0.95	0.82
$B \to K^\pm$	<0.025	≈0.10	≤0.125	0.95	0.95	0.90	0.95	0.77

3. The Measurement of the Angles of the Unitarity Triangle

As is well known, the unitarity of the CKM matrix[8] can be expressed in six independent relationships[9], one of which is

$$V_{ud}V^*_{ub}+V_{cd}V^*_{cb}+V_{td}V^*_{tb}=0 \qquad (1)$$

This relationship can be expressed as a triangle in the complex plane, the angles of which are the phases of the CKM matrix elements in the Wolfenstein approximation[10]. Following Aleskan et al[11], for finite resolution, time dependent measurements of B decays into CP eigenstates (referred to as Class I decays hereafter) or "almost" CP eigenstates or eigenstates at the quark level (referred to as Class II decays), the error in sin(2ϕ) is given by

$$\delta(\sin 2\phi) \equiv \frac{1}{d_{tag}} \bullet \frac{1}{d_{CP}} \bullet \frac{1}{d_\rho} \bullet \frac{1}{d_{Bkg}} \bullet \frac{1}{d_{mistag}} \bullet \frac{1}{d_{res}} \bullet \frac{1}{\sqrt{N_{recon}}} \qquad (2)$$

where ϕ is one of the angles of the unitarity triangle and N_{recon} is the sum of the reconstructed and tagged B^0 and $\bar{B}^0$ decays in the selected mode for which a measurement of CP asymmetries is being analyzed. Use of other types of decay modes for determination of the CKM matrix phases is also possible. For example, measurements of four (or six) amplitudes for B decays of the Class III form

$$\begin{array}{lll} B \to \bar{D}^0 + X & \bar{B} \to \bar{D}^0 + \bar{X} & \\ B \to D^0 + X & \bar{B} \to D^0 + \bar{X} & X \neq \bar{X} \\ B \to D^0{}_1 + X & \bar{B} \to D^0{}_1 + \bar{X} & \end{array}$$

can and will be used for determination of the angles, particularly "γ". Here the quotation marks indicate that the angle "γ" is the angle gamma of the unitarity triangle defined by equation (1) above only in the Wolfenstein approximation[12]. For the precision of measurement anticipated for the SFT and other options at the SSC, the differences between "γ" and γ will be significant. For brevity, the method of analysis[13] of Class III decays will not be discussed in detail here but is referred to in the contributions to this workshop of the fixed target γ working group[14].

The various "dilution" factors in the error are

$$d_{tag} = \text{dilution of } B_{tag} \text{ mixing } = \left[p_\pm + p_\Lambda\right] + \frac{p_s \bullet x_s}{\left[1+x_s^2\right]} + \frac{p_d \bullet x_d}{\left[1+x_{d,s}^2\right]}$$

where $p_\pm, p_d, p_s, p_\Lambda$ are the hadronization fractions for $B_u^\pm$, B_d^0, B_s^0, Λ_b

d_{CP} = dilution due to CP decay statistics

$$= e^{-\tau_{cut}} \bullet \left[1 + \frac{2x_{d,s}\sin 2x_{d,s}\tau_{cut} - \cos 2x_{d,s}\tau_{cut}}{1+4x_{d,s}^2}\right] \xrightarrow[\tau_{cut} \Rightarrow 0]{} \sqrt{\frac{2x_{d,s}^2}{1+4x_{d,s}^2}}$$

d_ρ = dilution due to deviation of final state from a CP eigenstate

$$= \frac{2\rho}{1+\rho^2} \xrightarrow[f \Rightarrow CP\ eigenstate]{} 1$$

$$d_{bkg} = \text{dilution due to background} = \sqrt{\frac{S}{S+B}}$$

$$d_{mistag} = \text{dilution due to mistagging } = (1-2w)$$

$$d_{res} = \text{dilution due to time resolution} = e^{-\sigma_t^2 x^2/2}$$

A few things can be immediately noted about the error, δsin2ϕ and the various dilution factors. δsin2ϕ is inversely proportional to the square root of the number of reconstructed, tagged events and inversely proportional to the dilution factor. If a choice is to be made, it is better to give up statistics in a particular decay channel in order to improve its dilution factor. Since all terms are positive in the expression for d_{tag}, this dilution factor is minimized if all possible species of the other B are used for tagging. However, it should be cautioned that the doubly damaging dilution d_{mistag} due to mistagging may be less bothersome if a particular B species is selected for the tagging B. The mistagging can arise from several sources

1. b->c->μ,e decay: This source of mistags is minimized by p_t cuts on leptons and can be eliminated completely if the complete event topology including all secondary and tertiary vertices is reconstructed. In fact, mistags can be identified and changed to proper tags if the leptons and K's can be assigned to the proper vertices. A capability for complete vertex topology is a strength of the SFT live target experimental configuration.

2. π,K->μ,e decays: This source is minimized by association of the lepton with the primary vertex. It is also minimized in the trigger sample by p_t cuts on lepton imposed by the trigger.

3. Punchthrough of hadrons through the muon shield: This is not a serious problem for the SFT fixed target muon detector since, as shown below, the shield can be very thick because of the high momentum of the Lorentz boosted fixed target muons from B decay.

4. γ->e conversions This source is minimized by p_t and momentum cuts on e^+e^- pair since the conversion electrons from the π^0 decay photons are relatively low in energy. This will be quantitatively discussed in the triggering section below.

We have attempted to estimate the dilution factors for the various combinations of B^0_d and B^0_s decays even though important information about the various modes (such as hadronization factors, backgrounds, values of physics parameters such as ρ, x_s, etc.) are poorly known or completely unknown at this time. We describe below the assumptions we have made in the estimation of the dilution factors.

We have used hadronization factors $p_\pm/p_d/p_s/p_\Lambda$ = 0.38 / 0.38 / 0.14 / 0.10 and mixing parameters x_d=0.7 and x_s=10 to calculate $1/d_{tag}$=1.49. We have used the same mixing parameters and a $15\sigma_z \approx 3.75$mm minimum path length criterion (leading to a $\tau_{cut} = 15\sigma_z/L_{decay}$ of 0.039 for the SFT silicon vertex detector) to calculate $1/d_{CP} \approx 1.77$ and 1.40 for B^0_d and B^0_s respectively. Since $\sigma_\tau \approx \sigma_z/L_{decay}$ = 0.0026, the effect time resolution results in $1/d_{res} \approx 1$ even for B^0_s decays for the SFT. The minimum time cut and the effect of the finite time resolution are much more serious for the collider configurations (especially the central collider configuration) since the ratio of resolution to path length is much poorer than for the fixed target configuration. In particular, measurements of B^0_s time distributions are very difficult in collider experiments. Next, since little is known about ρ for the non CP eigenstate modes, we have again followed the lead of Aleksan et al[11] and assumed a value of 1/2 for the ratio of the rates for $\bar{B}^0$->f to B^0->f for the non CP eigenstate modes. This results in $1/d_\rho$=1.03 for such modes as compared to 1 for the decays into true CP eigenstates. Finally, while the backgrounds considered so far for the various modes have been negligible, this work is still in progress. Table 7 below indicates the various backgrounds under study. Each of these types of backgrounds must be studied mode by mode.

Table 7
Backgrounds Under Study

Background	Estimate	Comment
Secondary Interactions[15]	negligible	Special to the SFT Most serious for B->$\pi\pi$
B decays of Same[7,16] Topology	In process	Example: B->$\pi\pi$ vs. B->Kπ Particle ID required Minimized by good mass resolution
B decays of Different Topology	In process	Loss or gain of a track Complete reconstruction of B decays minimizes this background
Backgrounds due to accidental vertices	negligible	Good track and vertex resolution compared to decay lengths minimizes this background

We have made what seems to us a conservative assumption that a minimum signal to background ratio of 5/1 can be achieved for most modes. This assumption leads to $1/d_{bkg}$ = 1.12.

Collecting all of these factors together, we show in Table 8 below estimates of the individual and overall dilution factors appropriate to Class I and II decays of neutral B's that we are considering.

Table 8
Dilution Factors

B_{CP}	B_{tag}	$1/d_{tag}$	$1/d_{CP}$	$1/d_\rho$	$1/d_{bkg}$	$1/d_{mistag}$	$1/d_{res}$	$1/d_{total}$
B^0_d	$\mu^\pm$ $e^\pm$ $K^\pm$	1.49	1.77	1.0,1.03	1.12	1.075 1.18 1.33	≈ 1	3.17,3.27 3.48,3.59 3.93,4.05
B^0_s	$\mu^\pm$ $e^\pm$ $K^\pm$	1.49	1.40	1.0,1.03	1.12	1.075 1.18 1.33	1.001	2.51,2.59 2.76,2.84 3.11,3.20

These dilution factors are used in what follows to weight properly the various CP decays that are tagged using the three possible tagging methods listed in Table 8.

3. Yields of Beauty Decays in the SFT

The final number necessary for the estimates of the error in the determination of sin2ϕ is the number of reconstructed and tagged events, N_{recon}.

$$N_{recon} = N_B \cdot f_B \cdot BR_{CP} \cdot BR_{tag} \cdot A_{accep} \cdot \varepsilon$$
$$\varepsilon = \varepsilon_{CP} \cdot \varepsilon_{tag} \cdot \varepsilon_{trig}$$

N_B ≡ Number of B's produced per year of operation in the SFT
BR_{CP} ≡ Composite Branching ratio for the CP decay
BR_{tag} ≡ Composite Branching ratio for the tag decay
f_B ≡ Hadronization ratio for specific CP and tagging B configuration
Accp ≡ Composite acceptance for the B_{CP}, B_{tag} and trigger particles.
ε_{CP} ≡ Composite detector and reconstruction efficiencies for CP B decay
ε_{tag} ≡ Composite detector and reconstruction efficiency for tagging B decay
ε_{trig} ≡ Composite detector efficiency for trigger

In the following sections, we will evaluate Nrecon for specific modes.

The cross section for pp-> $B\bar{B}$ production as a function of $\sqrt{s}$ has been calculated to third order by Nason, Dawson and Ellis[17]. These calculations have been further refined by Berger and Ming[18]. Based on these calculations, a B hadroproduction cross sections for pN interactions of 2 μb and 0.5 to 1μb at SSC and LHC fixed target energies respectively are expected. In addition, to estimate the production of B's by protons on silicon for the SFT live target, an A dependence of $A^{1.0}$ has been assumed resulting in a pSi cross section of 56 μb for B production at 193 GeV. To estimate the number of the various B species, the hadronization fractions $p_{\pm}/p_d/p_s/p_\Lambda$ = 0.38 / 0.38 / 0.14 / 0.10 have been used.

Using a total inelastic cross section of 32 mb for pN interactions at 193 GeV and an atomic number dependence of $A^{0.72}$, the total cross section for pSi interactions at 193 Gev/c at the SFT is calculated to be 352 mb. This leads to the expectation of one $B\bar{B}$ pair for every 6300 interactions in pSi interactions at 193 GeV (compared to ≈1/100 at $\sqrt{s}$=40 TeV, a factor of 60). Using the crystal extracted beam with intensity 2.5×10^8 protons/second producing 10^7 interactions per second in the SFT live target region 4.0% of an interaction length) operated for 10^7 seconds, 10^{14} interaction will be produced in one year of operation. The average number of interactions per beam bucket (16 ns spacing) will be 0.1 to 0.2 at this intensity. As a result, we expect cleaner interactions compared to other options such as gas jet and wire experiments which plan for 2 to 4 interactions per bucket. The $B\bar{B}$ production together with the hadronization fractions given above results in the expected yields of the various B species per year in the SFT given Table 9 below:

Table 9
Production per Year (10^7 sec) of B Pairs in SFT

B Pair Cross Section for pN	2 μb
B Pair Production Cross Section for pSi	56 μb
Number of B Pairs	1.6×10^{10}
Number of $B^{\pm}_u$	1.2×10^{10}
Number of B^0_d	1.2×10^{10}
Number of B^0_s	4.5×10^9
Number of B^0_c	3.2×10^7
Number of Λ_b	3.2×10^9

Given these species of B's, the numbers of interesting B decays which are useful for triggering, tagging or CP studies themselves can be estimated. Table 10 tabulates the production per year in the SFT of these decays. Table 10 also includes yields of combinations of CP and lepton/kaon tagging or lepton triggering using the other B decays where tagging is needed

Table 10
Production per Year of Interesting B Decays in the SFT

∠	Class	B_{CP}	Tag	BR*	#/year	Trig	Requirements
		B->$l^{\pm}$	-	0.21	6.7×10^9		
		B->$K^{\pm}$	-	0.85	2.7×10^{10}		
α	I	B^0_d->$\pi^+\pi^-$	B->$l^{\pm}$	2.1×10^{-6}	2.5×10^4	$l^{\pm}$	Time/Tag
		B^0_d->$\pi^+\pi^-$	B->$K^{\pm}$	8.5×10^{-6}	1.0×10^5	h^+h^-	
	II	B^0_d->$a^+\pi^-$	B->$l^{\pm}$	7.9×10^{-7}	1.0×10^4	$l^{\pm}$	Time/Tag
		B^0_d->$a^+\pi^-$	B->$K^{\pm}$	3.2×10^{-6}	3.8×10^4	h^+h^-	
		$\bar{B}^0_d$->$a^-\pi^+$	B->$l^{\pm}$	3.2×10^{-6}	3.8×10^4	$l^{\pm}$	
		$\bar{B}^0_d$->$a^-\pi^+$	B->$K^{\pm}$	1.3×10^{-5}	1.5×10^5	h^+h^-	
β	I	B^0_d->$J/\Psi K^0_s$	B->$l^{\pm}$	5.7×10^{-6}	6.8×10^4	l^+l^-	Time/Tag
		B^0_d->$J/\Psi K^0_s$	B->$K^{\pm}$	2.3×10^{-5}	2.8×10^5	l^+l^-	
	I	B^0_d->D^+D^-	B->$l^{\pm}$	2.3×10^{-6}	2.8×10^4	$l^{\pm}$	Time/Tag
	I	B^0_d->$D^{*+}D^{*-}$	B->$l^{\pm}$	2.7×10^{-5}	3.3×10^5	$l^{\pm}$	Time/Tag
"γ"	I	B^0_s->ρK^0_s	B->$l^{\pm}$	1.1×10^{-7}	5.0×10^2	$l^{\pm}$	Time/Tag
	I	B^0_s->$D^+_s D^-_s$	B->$l^{\pm}$	1.4×10^{-5}	6.4×10^4	$l^{\pm}$	Time/Tag
	II	B^0_s->$D^+_s K^-$	B->$l^{\pm}$	3.2×10^{-6}	1.4×10^4	$l^{\pm}$	Time/Tag
		$\bar{B}^0_s$->$D^+_s K^-$	B->$l^{\pm}$	2.3×10^{-6}	1.0×10^4	$l^{\pm}$	
	III	B^0_d->$\bar{D}^0 K^{0*}$	self	2.7×10^{-5}	3.2×10^5	$l^{\pm}$	
		B^0_d->$D^0 K^{0*}$		2.7×10^{-6}	3.2×10^4		
		B^0_d->$D^0_1 K^{0*}$		0.6×10^{-6}	0.6×10^3		
	III	B^+->$\bar{D}^0 K^+$	self	5.5×10^{-6}	3.8×10^5	$l^{\pm}$	
		B^+->$D^0 K^+$		5.5×10^{-7}	5.1×10^3		
		B^+->$D^0_1 K^+$		1.2×10^{-7}	1.4×10^3		
	I	B^0_d->$\Psi\rho^0$	B->$l^{\pm}$	1.2×10^{-6}	5.4×10^3	l^+l^-	Time/Tag
		B^0_d->$\Psi\rho^0$	B->$K^{\pm}$	5.2×10^{-6}	2.3×10^4	l^+l^-	
	I	B^0_s->$\Psi\phi$	B->$l^{\pm}$	2.6×10^{-5}	1.2×10^5	l^+l^-	Time/Tag
		B^0_s->$\Psi\phi$	B->$K^{\pm}$	1.0×10^{-4}	4.7×10^5	l^+l^-	

The branching ratios of Table 10 are composite branching ratios for the required B decay configuration. They include branching ratios for all secondary decays such as K^0_s->ππ, J/Ψ-->μμ, φ->K^+K^- required to produce an experimentally detectable final state. The composite branching ratio also contains the branching ratios for the tagging and trigger decays of the "other" B where required. For B->D decay composite branching ratios of Table 10, we have used only the experimentally accessible D modes into all charged decay products given in Table 11 in our determination of the yields of B decays suitable for CP violation measurements. These all charged decays result in 2, 3, 4 or 5 charged particles in the final state in a variety of topologies (one prong, two prong and three prong vertices in one or two vertex topologies with the incoming neutral or charged B sometimes observed in the SFT live target). The geometric acceptances of each of the modes in Table 10 that have a $D^{\pm}$ or D^0 in the final state have been determined from a Monte Carlo which includes the 3 and 5 body final states or the 2 and 4 body for the charged D's and neutral D mesons respectively, properly weighted with the BR's for the individual channels. In the final yield calculations, the tracking, particle ID and vertexing efficiencies for the D's are also included using the weighted average of the product of these factors for the various modes taking into account the various vertex topologies of the modes.

Table 11
Major All Charged $D^{\pm}_d$, D^0, D^0_{CP}, $D^{\pm}_s$ Decay Modes

D Meson	Mode	BR	Total
$D^{\pm}_d$	$K^{\pm}\pi^+\pi^-$	9.6×10^{-2}	10.5×10^{-2}
	$K^{\pm}\pi^+\pi^-\pi^+\pi^-$	6.1×10^{-3}	
	$\pi^+\pi^-\pi^{\pm}$	2.8×10^{-3}	
$D^{\pm}_s$	$K^+K^-\pi^{\pm}$	3.9×10^{-2}	6.7×10^{-2}
	$\pi^+\pi^-\pi^{\pm}$	1.2×10^{-2}	
	$K^+K^-\pi^+\pi^-\pi^{\pm}$	1.4×10^{-2}	
	$\pi^{\pm}\pi^+\pi^-\pi^+\pi^-$	0.2×10^{-2}	
	$K^{\pm}\pi^+\pi^-$	1.4×10^{-3}	
D^0_d	$K^-\pi^+$	3.7×10^{-2}	12.8×10^{-2}
	$K^-\pi^+\pi^-\pi^+$	7.5×10^{-2}	
	K^+K^-	4.1×10^{-3}	
	$K^+K^-\pi^+\pi^-$	2.4×10^{-3}	
	$\pi^+\pi^-$	1.6×10^{-3}	
	$\pi^+\pi^-\pi^+\pi^-$	7.5×10^{-3}	
	$\pi^+\pi^-\pi^+\pi^-\pi^+\pi^-$	4.0×10^{-4}	
D^0_{CP}	$\pi^+\pi^-$	1.6×10^{-3}	5.6×10^{-3}
	K^+K^-	4.1×10^{-3}	

The SFT Trigger Strategy

We must determine how much of the B production tabulated in Table 10 remains in the triggered event sample written to tape. The flexible three level triggering strategy adopted for the SFT detector[19] is based on detection of high p_t leptons and hadrons. To reduce the Level I 10^7 interaction/sec rate to a level sufficient for a second level trigger ($\approx 10^4$ /sec), we plan to adopt a strategy similar to the one successfully employed for muon triggers in Fermilab Experiment E771 to both hadrons and leptons in the SFT. The SFT triggers will impose at level I both p_t and momentum requirements on hadrons and leptons within the angular range 2 mrad to 75 mrad as given below:

• opposite charge dilepton trigger
max. p_t lepton >1.0 GeV/c, min. p_t lepton>0.5 GeV/c
p_{lepton} >20 GeV/c

• opposite charge dihadron trigger
max. p_t >3.0 GeV/c, min. p_t >1.0 GeV/c

• lepton -hadron trigger
p_t lepton >1.5 GeV/c, p_t hadron >1.0 GeV/c
p_{lepton} >20 GeV/c

This ensemble of triggers allows us to trigger on semileptonic and kaon decays from tagging B decays or on the various CP decay topologies of interest (B^0_d->$\pi^+\pi^-$, B^0_d->$J/\Psi K^0_s$, $B^{\pm}$->$D^0K^{\pm}$, B^0_s->D^0K^{*0}, etc.).

Level I

The Level I p_t requirement is imposed by forming coincidences of collections of pads in several planes of pad chambers which encompass all possible trajectories of tracks above a given p_t threshold. The lepton ID for the high p_t μ or e are imposed on this tracking trigger at Level I by requiring an additional coincidence to be satisfied by a signal from the region of the muon detector or electromagnetic calorimeter which is pointed at by the high p_t charged particle trajectory formed by the pad coincidences. In the case of the RICH/TRD, as discussed below, the requirement of the particle ID is imposed at Level II because of the additional complications of extracting information from the RICH. Any particle not receiving a e or μ ID at level I is considered to be a hadron. The minimum momentum requirement for muons is imposed by the thickness of the muon detector. The minimum momentum requirement for the $e^{\pm}$ is set by imposing a threshold on the electromagnetic detector elements indicated by the high p_t track trajectory. This trigger, which can be implemented with Programmable Logic Array chips, will require approximately 150 ns to form, similar to the high p_t muon trigger of E771[20]. A latency period of approximately 1 μsec will be required to collect all signals necessary for this trigger from the spectrometer.

The dielectron, dimuon, dihadron and hadron lepton triggers have inefficiencies due to the various detector components required to form them. Intrinsic to each of these triggers is the tracking trigger formed using the pad chamber signals. In order to minimize pad chamber inefficiencies, five planes of pad chambers will be used and each plane signal will be formed from the OR of signals from a double gas gap. To form the pad coincidence which defines the track, any three out of five will be required. This should effectively eliminate inefficiencies at this stage of the tracking trigger. We expect to achieve better than 98% efficiency for each track pair with this system.

A second component of the inefficiency will be present due to inefficiency in track ID for the electron and the muon. We will identify the muon using Resistive Plate Chambers (RPC's) similar to those used in E771. Requiring any three of five chambers to define a muon, we expect to achieve efficiencies better than 99% per muon. The situation with electrons may be worse since the electron is tagged by a coincidence of the TRD and the EM calorimeter. To be conservative, we assume this can be formed with greater than 95% efficiency per electron or 90% per electron pair. Overall, we estimate the detector efficiencies for the single electron, single muon, dihadron, dielectron, dimuon, electron hadron and muon hadron triggers to be 95%, 99%, 98%, 90%, 98%, 94% and 98% respectively.

The major contributions to the muon and electron trigger rates are due to π,K semimuonic decays, hadron punch through and charm meson decay in the case of the muon trigger. The main backgrounds to the electron trigger are the overlap of charged hadrons and photons, e/π misidentification, and photon conversions in the target. For e/π misidentification, we make the conservative assumptions that the EM calorimeter gives an online pion rejection of a factor of ten and the TRD adds a second factor of ten.

The major contributors to the dihadron trigger rates are direct production of charged hadrons in the primary interaction and charm meson decays into charged kaons. The p_t cut eliminates much of the π,K->μ decay triggers for the muon trigger and a substantial fraction of the π^0->$\gamma\gamma$->e^+e^- conversion triggers for the electrons. The μ,e triggers due to punch through hadrons in the case of the muon trigger and conversion electrons from π^0 photons in the case of the electron trigger are further reduced by the 20 GeV/c minimum momentum cut on the electron and muon candidates in Level I

The SFT trigger rate has been estimated using PYTHIA simulations for minimum bias and charm production. The retention of B signals for the modes of interest have also been estimated using PYTHIA. The trigger rates for each Level I trigger are summarized in Tables 12.

Table 12
Level I Interaction Rate Suppressions of Trigger Backgrounds

Trigger Type (p_t max, p_t min)	Level I π,K->μ,e Suppression	Level I γ Backround Suppression	Level I Charm->μ,e Suppression
High P_t $\mu^\pm$ (1.5)	4.4×10^{-4}	-	2.1×10^{-5}
High P_t $e^\pm$ (1.5)	-	1.6×10^{-3}	2.1×10^{-5}
e^+e^- (1.0,0.5)	-	7.6×10^{-4}	8.8×10^{-7}
$\mu^+\mu^-$ (1.0,0.5)	8.4×10^{-5}	-	2.1×10^{-6}
h^+h^- (3.0,1.0)	1.0×10^{-3}	-	6.6×10^{-5}
μ-hadron (1.5,1.0)	2.5×10^{-4}	-	2.7×10^{-7}
e-hadron (1.5,1.0)	-	9.7×10^{-4}	2.7×10^{-7}
Total Suppression		3.1×10^{-3}	

We estimate that we can achieve at Level I an overall suppression of 5×10^{-3} taking into account the finite p_t resolution for p_t cuts required by the various triggers. This would result in 50 KHz of triggers passed on to Level II for further filtering.

For those events triggered on decay products from the B_{CP} decays themselves, both lepton and kaon tagging using the other B decay are possible. For those events in which the other B decay provides the trigger, only the given decay product (high p_t lepton or kaon) is normally available for tagging purposes. This will be further discussed in the tagging section.

SFT Level II

As discussed above, the various level I SFT triggers result in a composite Level I trigger rate of approximately 50KHz. An additional level of triggering is required to reduce the trigger rate to the goal of <10^4 events per second feeding Level III. This additional global trigger rejection of a factor of ≥5 for all modes can be provided by a relatively loose requirement for presence of secondary vertices in the silicon detector.

The Level II trigger is based on use of associative memories for fast tracking in the silicon detector. Associative memories are inverse memories that can be programmed with all possible valid track trajectories. When hit information from the silicon detector is provided to the associative memories, the data patterns are compared with the stored configurations. Providing there are matches between data hit patterns and valid track possibilities, the associative memories return the location of the correspondence which can be used as an index for track slopes and intercepts. Once tracks are reconstructed in this manner, a post associative memory processor will process the tracks, evaluating a function of the impact parameters which indicates the likelihood of the presence of secondary vertices in the event. Using this algorithm, Monte Carlos estimates indicate that the required factor of ten suppression of trigger rate can be achieved with a B retention of 90%. Thus, we expect a trigger rate of 5000 triggers/second surviving Level II.

SFT Level III

Level III of the SFT data acquisition system is provided by an online farm of relatively modest proportions, not markedly larger than those already in operation or proposed for the Fermilab fixed target program. We expect to be able to easily achieve a reduction of a factor of five for events selected for offline analysis by this farm. Finally, we estimate that composite SFT trigger and data acquisition system would have less that 10% dead time and pass approximately 1000 20 KByte events/second to storage at 10^7 interactions per second. Therefore, a relatively modest data storage capacity is required for the SFT (<20 MBytes/second).

B Signal Retention

Level I, II, and III of the data acquisition system necessarily result in loss of B signal in the various decay modes. We have investigated the signal loss using PYTHIA and simulations of the SFT detector. Preliminary results for acceptances and trigger efficiencies and the trigger level retention factors are given in Table 13 for both CP decay products and the tagging particles if required.

Table 13

Level I Signal Retention for B_{CP} and "Other" Tagging B Decays

B Decay Topology	Accp. charged tracks	Eff_{trig} Level I	Eff_{trig} Level II	Overall Fraction A*Trig	Trigger/ Threshold GeV/c
B->$\mu^{\pm}$	0.82	0.45•0.99	0.90	0.33	High P_t μ (1.5)
B->$e^{\pm}$	0.82	0.45•0.95	0.90	0.31	High P_t e (1.5)
B^0_d->$\pi^+\pi^-$ • B->$l^{\pm}$,$K^{\pm}$	0.55, 0.50	0.57•0.98	0.90	0.28,0.26	h^+h^- (3.0,1)
B^0_d->$\pi^+\pi^-$ • B->$l^{\pm}$	0.74	0.45•0.96	0.90	0.29	μ/e•$h^{\pm}$ (1.5,1)
B^0_d->$a^+\pi^-$ • B->$l^{\pm}$	0.72	0.44•0.96	0.90	0.27	μ/e•$h^{\pm}$ (1.5,1)
B^0_d->J/ΨK^0_s•B->$l^{\pm}$,$K^{\pm}$	0.30, 0.25	0.91•0.97	0.90	0.23,0.21	l^+l^- (1,.5)
B^0_d->D^+D^- • B->$l^{\pm}$	0.53	0.42•.96	0.90	0.19	μ/e•$h^{\pm}$ (1.5,1)
B^0_d->$D^{*+}D^{*-}$• B->$l^{\pm}$	0.53	0.42•.96	0.90	0.19	μ/e•$h^{\pm}$ (1.5,1)
B^0_s->ρK^0_s • B->$l^{\pm}$	0.28	0.45•0.96	0.90	0.11	μ/e•$h^{\pm}$ (1.5,1)
B^0_s->$D^+_sD^-_s$• B->$l^{\pm}$	0.53	0.42•0.96	0.90	0.20	μ/e•$h^{\pm}$ (1.5,1)
B^0_s->$D^+_sK^-$ • B->$l^{\pm}$	0.55	0.42•0.96	0.90	0.21	μ/e•$h^{\pm}$ (1.5,1)
B^+->D^0K^+ • B->$l^{\pm}$	0.55	0.42•0.96	0.90	0.21	μ/e•$h^{\pm}$ (1.5,1)
B^0_d->J/$\Psi\rho$ •B->$l^{\pm}$,$K^{\pm}$	0.56,0.51	0.91•0.97	0.90	0.44,0.40	l^+l^- (1,0.5)
B^0_d->J/$\Psi\phi$ •B->$l^{\pm}$,$K^{\pm}$	0.60,0.55	0.91•0.97	0.90	0.48,0.44	l^+l^- (1,0.5)

The acceptance factors in Table 13 include all the charged decay products of the B_{CP} and $B_{trig/tag}$. For some triggers, both lepton and kaon tagging are used. In these cases the first number in the acceptance column is for lepton tagging and the second number for kaon tagging. The second factor in the Eff_{trig} is the efficiency due to detector inefficiencies. If the lepton from the other B decay provides the trigger, then pions from the B decays are not required to have Θ>2mrad.

Yields of Reconstructed/Tagged Events

All the acceptance and efficiency factors contributing to the yield of reconstructed and tagged events in the SFT are collected and the expected numbers of events in potentially interesting modes have been summarized in Table 14 below. All branching ratios for the various interesting B decay configurations have been included in the estimates of the numbers of B_{CP} decays produced per year in the SFT. The estimates include the branching ratios for the tagging and triggering particles as well as for the CP decay and the decays of secondary D's, K^0_S, ϕ, etc..

The acceptances listed in Table 14 are the overall acceptances for every component of the B event that must be reconstructed in order for the event to be useful in the extraction of a particular angle of the unitarity triangle. For example, for B decays where triggering or tagging is required, the acceptance of the triggering or tagging particle are included in the acceptance.

The efficiency estimates in Table 14 include estimates of ε_{trig}, ε_{tag} and ε_{CP}. ε_{trig}, the trigger efficiency, includes both the effect of trigger settings such as minimum p_t and p of the triggering tracks as well as the estimated efficiency of the detector components which generate the trigger. In addition, the trigger efficiency includes a factor of 0.9 to account for a live time goal of 90%. ε_{tag} is the efficiency for tagging the event. This quantity does not contain branching ratios or acceptances but reflects only the efficiency with which the process of tagging the event can be accomplished. This process requires several steps which vary from mode to mode but generally includes some particle ID for the tagging particle, the reconstruction efficiency for the tagging particles, the vertex association efficiency among other factors. Similarly, the ε_{CP} factor contains no branching ratios or acceptances. It only reflects the efficiency with the charged decay products of the BCP decay can be reconstructed and form a vertex distinguishable from other vertices in the event. The product of the three efficiency factors is the efficiency for triggering on, reconstructing and tagging a particular B_{CP}•B_{tag} event topology for events where the necessary decay products of both B's are in the acceptance of the spectrometer. N_{recon}, the penultimate entry in Table 14, is the total number of accepted, triggered, tagged and reconstructed B events of each given topology which are available for use in either time independent or dependent extraction of the angles α, β and γ of the unitarity triangle.

Finally, the various event samples which are tagged with both a lepton or a kaon must be corrected for overlaps between the two kinds of tags. The sum of the two tagged samples is greater than the actual number of K or lepton tagged events because of the events which contain both a lepton and a K from the decay of the other B. Kaons are present in 85% and leptons in 21% of the B decays. If we make the assumption that the tags completely overlap, then every B->l decay will also have a kaon tag if we ignoring losses of either K's or leptons due to inefficiencies. With this assumption, we can have no more than the number of kaon tagged events as the total number of tagged decays and the lepton tag does little except corroborate the kaon tag. The opposite assumption would be that they are maximally uncorrelated would lead to 100% of the events tagged by one or the other with a 6% overlap. We adopt the average position that there is a 15% overlap. Therefore, a total of 85% +6% =91% of the sum of the kaon and lepton tag samples will have one or the other or both types of tags.

In addition, a correction must be made, in the case of the event topologies such as B->$\pi\pi$ which are collected by two different triggers to account for events which satisfy both single lepton and dihadron triggers. If we assume the overlap between the two triggers is maximal then every dihadron trigger which has a lepton tag would also produce a lepton trigger and these triggers must be subtracted from the dihadron trigger sample to reduce the overlap. While, not every lepton tag produces a trigger, a conservative approach yielding an upper limit on the overlap would be to assume that the lepton tags and the lepton trigger overlap completely. Therefore, we take the number of dihadron triggers corrected as described above for overlaps in lepton and hadron tags as a lower limit on the number of independent B^0_d->$\pi^+\pi^-$ events accumulated by both triggers. As indicated in Table 13, the only example treated in this paper of a specific B decay accumulated by multiple triggers is the B->$\pi\pi$ decays. Since an attempt will be made to accumulate all different modes with as many different triggers as possible, we will have to address the issue of trigger overlaps more completely in future work.

The number of events corrected for tag and/or trigger overlap is given in the column labeled Ncorr in Table 14.

Table 14
Summary of Reconstructed/Tagged B Yields in the SFT Per Year

B (CP • tag • trig)	Prod.	Accp	ε_{trig}	ε_{tag}	ε_{CP}	N_{recon}	N_{corr}
$B \to \mu^\pm$	3.4×10^9	0.82	0.40	0.89	-	9.9×10^8	
$B \to e^\pm$	3.3×10^9	0.82	0.40	0.82	-	8.9×0^8	-
$B \to K^\pm$	2.7×10^{10}	0.82	-	0.77	-	1.7×10^{10}	
$B^0_d \to \pi^+\pi^-$ • $B \to l^\pm$ (tag)	2.5×10^4	0.55	0.50	0.85	0.73	4,300	
$B^0_d \to \pi^+\pi^-$ • $B \to K^\pm$(tag)	1.0×10^5	0.50	0.50	0.77	0.73	14,100	16,700
$B^0_d \to \pi^+\pi^-$ • $B \to l^\pm$(trig/tag)	2.5×10^4	0.74	0.39	0.85	0.73	4,500	
$B^0_d \to a^+\pi^-$ • $B \to l^\pm$(trig/tag)	1.0×10^4	0.72	0.38	0.85	0.60	1,400	1,400
$\bar{B}^0_d \to a^-\pi^+$ • $B \to l^\pm$(trig/tag)	3.8×10^4	0.72	0.38	0.85	0.60	5,300	5,300
$B^0_d \to J/\Psi K^0_S$ • $B \to l^\pm$(tag)	6.8×10^4	0.30	0.79	0.85	0.66	9,000	34,000
$B^0_d \to J/\Psi K^0_S$ • $B \to K^\pm$(tag)	2.8×10^5	0.25	0.79	0.77	0.66	28,100	
$B^0_d \to D^+D^-$ • $B \to l^\pm$(trig/tag)	2.8×10^4	0.53	0.36	0.85	0.35	1,600	1,600
$B^0_d \to D^{*+}D^{*-}$ • $B \to l^\pm$(trig/tag)	3.3×10^5	0.53	0.36	0.85	0.38	20,300	20,300
$B^0_s \to \rho K^0_S$ • $B \to l^\pm$(trig/tag)	5.0×10^2	0.28	0.41	0.85	0.60	30	30
$B^0_s \to D^+_s D^-_s$ • $B \to l^\pm$(trig/tag)	6.4×10^4	0.53	0.36	0.85	0.35	3,600	3,600
$B^0_s \to D^+_s K^-$ • $B \to l^\pm$(trig/tag)	1.4×10^4	0.55	0.36	0.85	0.40	940	940
$\bar{B}^0_s \to D^+_s K^-$ • $B \to l^\pm$(trig/tag)	1.0×10^4	0.55	0.36	0.85	0.40	670	670
$B^0_d \to \bar{D}^0_d K^{0*}$ • $B \to l^\pm$(trig/tag)	3.2×10^5	0.45	0.36	0.85	0.38	16,700	16,700
$B^0_d \to D^0 K^{0*}$ • $B \to l^\pm$(trig/tag)	3.2×10^4	0.45	0.36	0.85	0.38	1,670	1,670
$B^0_d \to D^0_1 K^{0*}$ • $B \to l^\pm$(trig/tag)	0.6×10^3	0.45	0.36	0.85	0.42	35	35
$B^+ \to \bar{D}^0_d K^+$ • $B \to l^\pm$(trig)	3.8×10^5	0.55	0.36	0.85	0.42	26,900	26,900
$B^+ \to D^0 K^+$ • $B \to l^\pm$(trig)	5.1×10^3	0.55	0.36	0.85	0.42	360	360
$B^+ \to D^0_1 K^+$ • $B \to l^\pm$(trig)	1.4×10^3	0.55	0.36	0.85	0.47	110	110
$B^0_d \to \Psi\rho^0$ • $B \to l^\pm$(tag)	5.4×10^3	0.56	0.79	0.85	0.60	1,200	5,000
$B^0_d \to \Psi\rho^0$ • $B \to K^\pm$(tag)	2.3×10^4	0.51	0.79	0.77	0.60	4,300	
$B^0_s \to \Psi\phi$ • $B \to l^\pm$(tag)	1.2×10^5	0.60	0.79	0.85	0.54	26,000	101,000
$B^0_s \to \Psi\phi$ • $B \to K^\pm$(tag)	4.7×10^5	0.55	0.79	0.77	0.54	85,000	

4. Estimated Errors in α, β and 'γ' per year of SFT Operation

Collecting all the factors which contribute to the error in ϕ as given in equation (2), we have made estimates of the errors in α, β and 'γ' per year of SFT operation using several B-> CP eigenstate modes. We point out that additional information and measurements of these angles can be obtained using Class II and Class III decays (as well as other B decay types not discussed in this paper. These errors are preliminary and incorporate only a portion of the CP•tag topologies that can be used for measurements of CP violation in B decays in fixed target experiments. Therefore, they should be considered as upper limits on the errors that can be achieved in the determination of each angle. The results are given in Table 15 below.

Table 15
Expected Errors in α, β and 'γ' per Year of SFT Operation
From Time Dependent Measurements of B_{CP}-> CP Eigenstates

∠	B (CP • tag • trig)	Prod.	Accp	ε_{tot}	N_{recon}	$1/d_{tot}$*	$\delta\sin2\phi$	$\delta\phi$
	$B^0_d \to \pi^+\pi^-$ • $B \to l^\pm$ (tag)	2.5×10^4	0.55	0.31				
α	$B^0_d \to \pi^+\pi^-$•$B \to K^\pm$(tag)	1.0×10^5	0.50	0.28	16,700	3.71	0.030	0.9°
	$B^0_d \to \pi^+\pi^-$•$B \to l^\pm$(trig/tag)	2.5×10^4	0.74	0.24				
	$B^0_d \to J/\Psi K^0_S$•$B \to l^\pm$(tag)	6.8×10^4	0.30	0.44	34,000	3.80	0.021	0.6°
β	$B^0_d \to J/\Psi K^0_S$•$B \to K^\pm$(tag)	2.8×10^5	0.25	0.40				
	$B^0_d \to D^+D^-$•$B \to l^\pm$(trig/tag)	2.8×10^4	0.53	0.11	1,600	3.33	0.097	2.8°
	$B^0_d \to D^{*+}D^{*-}$•$B \to l^\pm$(trig/tag)	3.3×10^5	0.53	0.12	20,300	3.33	0.026	0.7°
	$B^0_s \to \rho K^0_S$•$B \to l^\pm$(trig/tag)	5.0×10^2	0.28	0.21	30	2.64	0.242	7.0°
	$B^0_s \to D^+_s D^-_s$•B>$l^\pm$(trigtag)	6.4×10^4	0.53	0.11	3,600	2.64	0.050	1.4°
'γ'	$B^0_d \to \Psi\rho^0$•$B \to l^\pm$(tag)	5.4×10^3	0.56	0.40	5,000	3.00	0.045	1.3°
	$B^0_d \to \Psi\rho^0$•$B \to K^\pm$(tag)	2.3×10^4	0.50	0.37				
	$B^0_s \to \Psi\phi$•$B \to l^\pm$(tag)	1.2×10^5	0.60	0.36	101,000	3.00	0.010	0.3°
	$B^0_s \to \Psi\phi$•$B \to K^\pm$(tag)	4.7×10^5	0.55	0.33				

*Weighted by the proportion of the μ, e and K tags

5. Summary

The SFT facility is more than competative with e^+e^- and collider configurations for precision measurements of CP violation and determination of the phases of the CKM matrix. Based on the \$43.5M cost estimate of EOI-14[1] and the \$117M and >\$200M estimates for a forward collider[21] and e^+e^- options[22] respectively, the fixed target option appears to be the most economical method of performing measurements of CP violation.

6. References

[1] B. Cox et al, EOI-14, SSC Laboratory (May, 1990).
[2] Y.Lemoigne, GAJET Collaboration, Nucl. Instr. Meth. **A333**, 13(1993)
[3] G. Carboni et al, LHB Collaboration, INFN PI/AE91/04, (1991)
[4] T. Lawry et al., "Observability of Mixing in Partially Reconstructed Bd and Bs at the SFT", these proceedings.
[5] K. Nelson and B. Cox, "Hadron Identification in a Fixed Target Experiment at the SSC", these proceedings.
[6] Fermilab Experiment E771, Fermilab Proposal P771, (1986).
[7] A.P. McManus et al., "Tracking Considerations for Fixed Target Experiments at the SSC and the LHC", these proceedings.
[8] M. Kobayashi and T.Maskawa, Prog. Theor. Phys. 49, 652(1973).
[9] I. Bigi, UND-HEP-92-BIG01, (1992).
[10] L. Wolfenstein, Phys. Rev. Lett. 51, 1945(1983).
[11] R. Aleksan, I.Dunietz, B. Kayser and F. Le Diberder, Nuclear Physics B361, 141(1991).
[12] B. Kayser, "What Do Gamma Modes Measure", presentation at the 1993 Snowmass Workshop on B Physics.
[13] M. Gronau and D. Wyler, Phys. Lett. **B265**, 172(1991).
[14] B. Cox et al., "Measurement of the Angle Gamma in the SSC Fixed Target Experiment, the SFT", these proceedings.
[15] T. Lawry et al., "Backgrounds to $B^0 \to \pi^+\pi^-$ from Secondary Interactions in a Silicon Microvertex Detector at the SFT ", these proceedings.
[16] T. Lawry et al., "Measuring the Angle β in $B^0_d \to D^*\bar{D}^*$ Decays at the SFT", these proceedings.
[17] P.Nason, S. Dawson and R.K. Ellis, Nucl. Phys. B303, 607(1988).
[18] E.L. Berger and R. Ming, ANL-HEP-PR-92-11, (1992).
[19] S. Conetti, "Triggering at the SFT", these proceedings.
[20] S.N. Zhang et al, A High Pt Muon Trigger Processor, IEEE Transactions on Nuclear Science, **NS39**, No. 4, 814(1992).
[21] K. Foley et al., "Experiments, Detectors and Experimental Areas for the Super Collider", eds. R. Donaldson and M.G.D. Gilchriese, 701(1987).
[22] A Feasibility Study for Asymmetric B Factory Based on PEP, SLAC-353.

Conference Program

Schedule for Monday, June 21

9:00	Welcome
9:15	CP Violation in the Standard Model *M. Gronau, Technion*
10:45	B Decays in the Standard Model and Beyond *D. London, University of Montreal*
11:45	B Hadroproduction *J. Smith, State University of New York-Stonybrook*
2:00	B Decay Rates—Measurement and Predictions *H. Yamamoto, Harvard University*
3:00	Design Choices and Issues for Collider Experiments *J. Spalding, Fermi National Accelerator Laboratory*
4:30	Design Choices and Issues for Fixed Target B Experiments *L. Camilleri, CERN*

Schedule for Tuesday, June 22

9:00	Introduction to Morning Group Sessions *Convenors*
10:30	Breakup into Individual Morning Working Groups
2:00	Introduction to Afternoon Group Sessions *Convenors*
4:00	Breakup into Individual Afternoon Working Groups
5:30	Adjourn

Schedule for Wednesday, June 23

11:15 B Physics Measurements at CDF
J. Mueller, Rutgers University

12:00 B Physics Measurements at D0
M.A. Cummings, University of Hawaii

2:00 Extracting α, β and γ from $B \to J/\Psi$ Decays
I. Dunietz, Fermi National Accelerator Laboratory

Schedule for Thursday, June 24

11:15 Measurement of Semileptonic Decays of B Mesons
M. Artuso, Syracuse University

11:45 Measurement of Semileptonic Decays of Charm Particles
J. Cumalat, University of Colorado

2:00 Heavy Quark Effective Theory
B. Grinstein, Superconducting Super Collider Laboratory

Schedule for Friday, June 25

11:30 Measurements of B Mixing, Lifetimes, etc. at LEP
R. Kowalewski, CERN

2:00 Outlook on Future B Physics at the Tevatron Collider
C. Hill, Fermi National Accelerator Laboratory

Schedule for Saturday, June 26

8:30 Working Group Discussions $\alpha - \delta$

- B Production Cross Sections — *J. Smith et al.*
- B** Tagging — *M. Gronau*
- Machine Parameters — *V. Bharadwaj*

10:30 Working Groups α–δ

2:00 Working Groups A–G

4:00 Working Groups A–G

5:30 Adjourn

Schedule for Monday, June 28

11:30 Background Levels and Effects on Detectors
T. Pal, Superconducting Super Collider Laboratory

2:00 Capabilities of e^+e^- B Factories
Y. Sakai, KEK

Schedule for Tuesday, June 29

WORKING GROUP SESSIONS—NO PLENARY TALKS

Schedule for Wednesday, June 30

11:30 Charm and Beauty Measurements at Fixed Target
S. Mishra, Fermi National Accelerator Laboratory

2:00 What Can We Expect from Lattice Gauge Theory?
A. Kronfeld, Fermi National Accelerator Laboratory

2:30 Where Can New Physics Show Up in B Physics
Y. Nir, Weizmann Institute

Schedule for Thursday, July 1

SUMMARY TALKS

8:30	General Announcements
8:45	A: Theory of Heavy Flavors
9:45	G: Machine Detector Interface
11:00	F: Electronics, DAQ, and Computing
11:45	B: Tracking and Vertexing
14:00	D: Muon Detection
14:35	C: e and γ Detection
15:10	E: Hadron ID
16:15	δ: Other B Physics
17:30	Adjourn

Schedule for Friday, July 2

SUMMARY TALKS

8:30	γ: Measurement of Angle γ
9:30	α: Measurement of Angle α
11:00	β: Measurement of Angle β
12:00	Workshop Conclusions
12:30	Adjourn


EXIT


CALIFORNIA


EXIT


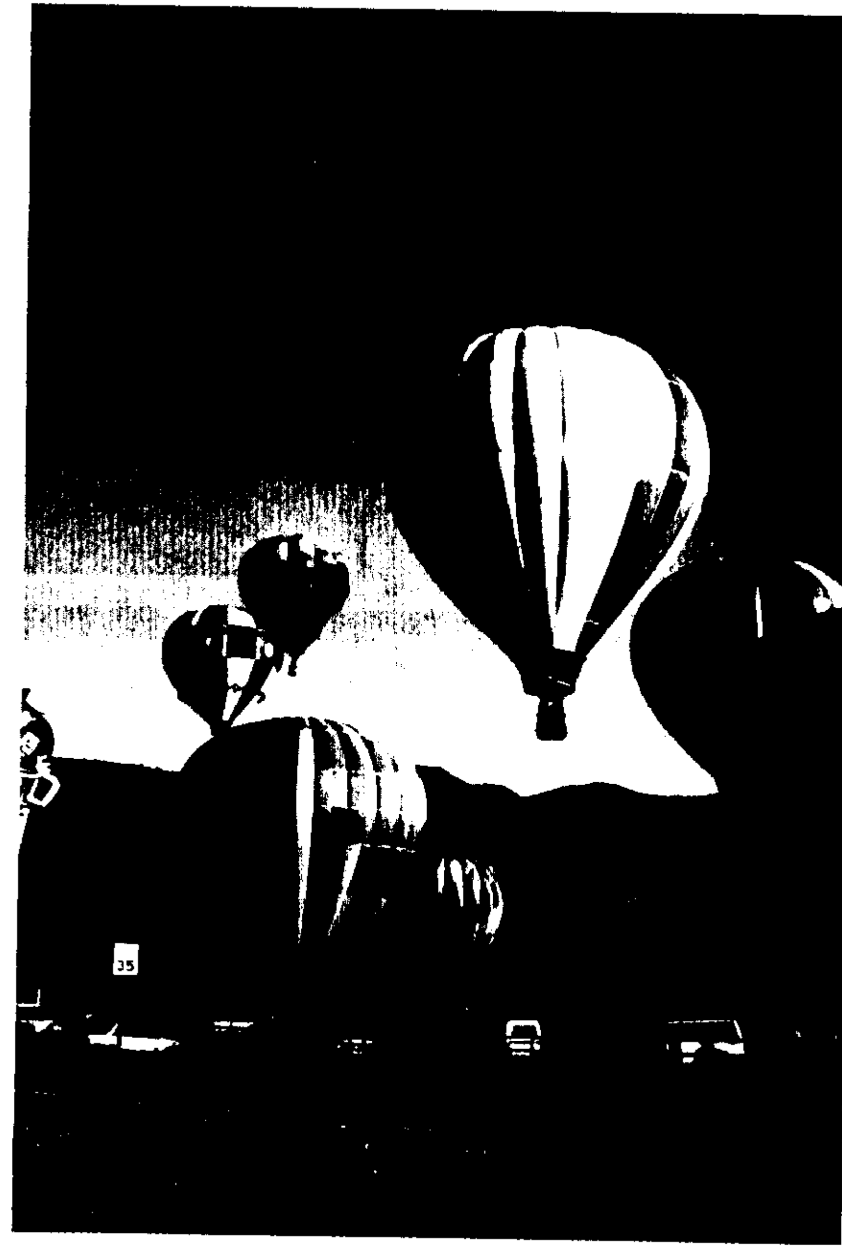

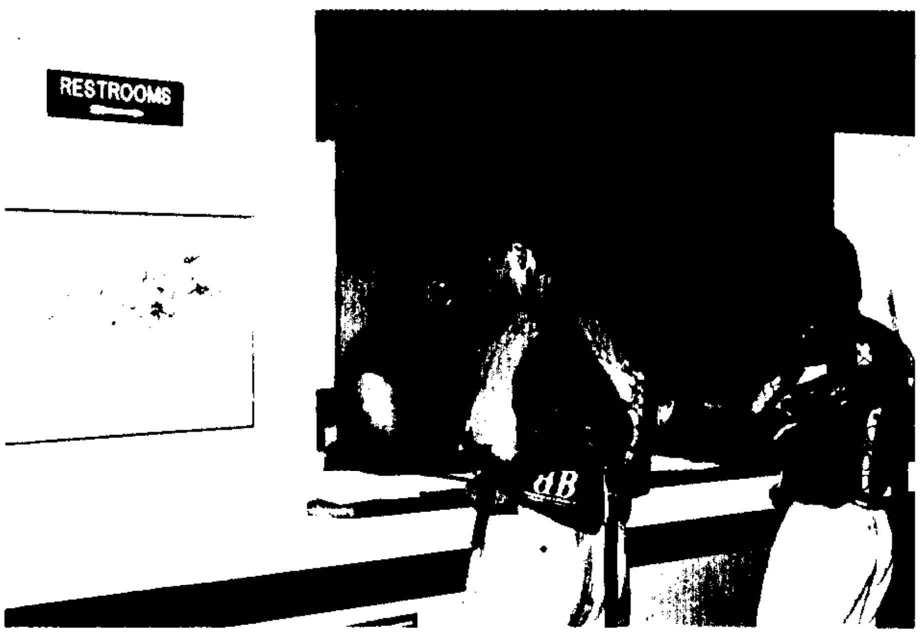
RESTROOMS


SHAKLEE










List of Attendees

List of Attendees

A. Abashian
Virginia Tech

G. Abrams
Lawrence Berkeley Laboratory

R. Aleksan
CEN Saclay

T. Alexopoulos
University of Wisconsin

G. Álvarez
Indiana University

J. Amundson
University of Chicago

G. Apollinary
Rockefeller University/
Fermi National Accelerator Laboratory

J. Appel
Fermi National Accelerator Laboratory

M. Arenton
University of Virginia

M. Artuso
Syracuse University

P. Avery
University of Florida

F. Azfar
University of Pennsylvania

U. Baur
Florida State University

V. Bharadwaj
Fermi National Accelerator Laboratory

F. Bird
Superconducting Super Collider Laboratory

J. Bjorken
Stanford Linear Accelerator Center

E. Blucher
University of Chicago

G. Bourianoff
Superconducting Super Collider Laboratory

C. Brown
Fermi National Accelerator Laboratory

T. Burnett
University of Washington

J. Butler
Fermi National Accelerator Laboratory

K. Byrum
Argonne National Laboratory

L. Camilleri
CERN

C. Campagnari
Fermi National Accelerator Laboratory

R. Carrigan, Jr.
Department of Energy/
Fermi National Accelerator Laboratory

J. Chen
Colorado State University

M. Cheng
Academia Sinica Taiwan/
Fermi National Accelerator Laboratory

W. Chou
Superconducting Super Collider Laboratory

B. Choudhary
University of California (Riverside)

D. Christian
Fermi National Accelerator Laboratory

D. Cline
University of California (Los Angeles)

P. Colestock
Fermi National Accelerator Laboratory

S. Conetti
University of Virginia

J. Cooper
Fermi National Accelerator Laboratory

D. Cords
Stanford Linear Accelerator Center

G. Corti
University of Virginia

D. Coupal
Superconducting Super Collider Laboratory

B. Cox
University of Virginia

L. Cremaldi
University of Mississippi

D. Crosetto
Superconducting Super Collider Laboratory

M. Cummings
University of Hawaii

J. Cunningham
Brandeis University

F. DeJongh
Fermi National Accelerator Laboratory

R. Demina
Northwestern University

N. Denisenko
Fermi National Accelerator Laboratory

C. Dib
Universidad Técnica Federico Santa María

J. Dorenbosch
Superconducting Super Collider Laboratory

E. Dukes
University of Virginia

I. Dunietz
Fermi National Accelerator Laboratory

P. Eerola
CERN

E. Engels
University of Pittsburgh

A. Erwin
University of Wisconsin

H. Frisch
University of Chicago

R. Frey
University of Oregon

L. Garren
Fermi National Accelerator Laboratory

S. Geer
Fermi National Accelerator Laboratory

F. Gilman
Superconducting Super Collider Laboratory

Y. Giomataris
CERN-PPE

V. Glebov
Superconducting Super Collider Laboratory

G. Goderre
Fermi National Accelerator Laboratory

V. Golovatyuk
University of Virginia

J. Gonzalez-A
University of Pennsylvania

K. Gounder
University of Mississippi

B. Grinstein
Superconducting Super Collider Laboratory

M. Gronau
Technion—Israel Institute of Technology

M. Halling
Cornell University/
Fermi National Accelerator Laboratory

R. Harr
Yale University

E. Hartouni
University of Massachusetts

J. Hassard
Imperial College

D. Hedin
Northern Illinois University

J. Heinrich
University of Pennsylvania

W. Hofmann
Max-Planck-Institut für Kernphysik

J. Holt
Fermi National Accelerator Laboratory

G. Hou
National Taiwan University

J. Hylen
Fermi National Accelerator Laboratory

J. Izen
University of Texas at Dallas

V. Jain
Vanderbilt University

C. James
Fermi National Accelerator Laboratory

H. Jawahery
University of Maryland

K. Johns
University of Arizona

M. Johnson
Fermi National Accelerator Laboratory

H. Jöstlein
Fermi National Accelerator Laboratory

D. Judd
Prairie View A&M University

D. Kaplan
Northern Illinois University

P. Karchin
Yale University

B. Kayser
National Science Foundation

C. Kennedy
Yale University

R. Kephart
Fermi National Accelerator Laboratory

K. Kinoshita
Virginia Polytechnic Institute

S. Kleinfelder
Lawrence Berkeley Laboratory

R. Kowalewski
CERN

M. Kreisler
University of Massachusetts

J. Kroll
Fermi National Accelerator Laboratory

S. Kwan
Fermi National Accelerator Laboratory

T. Lawry
University of Virginia

P. Lebrun
Fermi National Accelerator Laboratory

T. LeCompte
University of Illinois at Urbana-Champaign

E. Levin
Fermi National Accelerator Laboratory

J. Lewis
Fermi National Accelerator Laboratory

P. Limon
Fermi National Accelerator Laboratory

H. Lipkin
Weizmann Institute of Science

R. Lipton
Fermi National Accelerator Laboratory

N. Lockyer
University of Pennsylvania

T. Lohse
Max-Planck-Instit für Kernphysik

D. London
University of Montreal

X. Lou
Indiana University/CERN

S. Loucatos
CEN Saclay

K. Luk
Lawrence Berkeley Laboratory

V. Lüth
Superconducting Super Collider Laboratory

E. Ma
University of California (Riverside)

S. Mani
University of California (Davis)

L. Markosky
University of Arizona/
Fermi National Accelerator Laboratory

J. Marques
Northwestern University

P. McBride
Superconducting Super Collider Laboratory

K. McDonald
Princeton University

A. McManus
University of Virginia

H. Melanson
Fermi National Accelerator Laboratory

R. Meng
Argonne National Laboratory

S. Meshkov
Superconducting Super Collider Laboratory

C. Mishra
Fermi National Accelerator Laboratory

M. Mohammadi
State University of New York at Stony Brook

J. Mueller
Rutgers University

Y. Mukhin
Syracuse University

C. Murphy
Fermi National Accelerator Laboratory

K. Nelson
University of Virginia

N. Neumeister
Institut für Hochenergiephysik
d. Österreichische

B. Newberger
University of Texas at Austin

Y. Nir
Weizmann Institute

Y. Nosochkov
Superconducting Super Collider Laboratory

R. Oakes
Northwestern University

H. Paar
University of California, San Diego

K. Paick
Prairie View A&M University

T. Pal
Superconducting Super Collider Laboratory

V. Papadimitriou
Fermi National Accelerator Laboratory

J. Park
University of California (Los Angeles)

C. Park
Fermi National Accelerator Laboratory

J. Peoples
Fermi National Accelerator Laboratory

A. Peryshkin
Fermi National Accelerator Laboratory

G. Punzi
Scuola Normale Superiore/INFN Pisa

M. Purohit
Princeton University

B. Reay
Ohio State University

S. Riemersma
Southern Methodist University

D. Ritchie
Fermi National Accelerator Laboratory

D. Ritson
Stanford Linear Accelerator Center/
Superconducting Super Collider Laboratory

J. Rosen
Northwestern University

E. Rosenberg
Iowa State University

P. Schlein
University of California (Los Angeles)

M. Schmidt
Yale University

W. Schmidt-Parzefall
University of Hamburg

P. Schuler
Superconducting Super Collider Laboratory

A. Schwartz
Princeton University

W. Selove
University of Pennsylvania

T. Sen
Superconducting Super Collider Laboratory

S. Shapiro
Stanford Linear Accelerator Center

V. Sharma
CERN

M. Sheaff
University of Wisconsin

P. Shepard
University of Pittsburgh

A. Sill
Texas Tech University/
Fermi National Accelerator Laboratory

D. Silverman
University of California (Irvine)

J. Skarha
John Hopkins University

J. Slaughter
Fermi National Accelerator Laboratory

J. Smith
State University of New York at Stony Brook

F. Snider
Johns Hopkins University

J. Soares
Carnegie Mellon University

L. Song
Fermi National Accelerator Laboratory

J. Spalding
Fermi National Accelerator Laboratory

P. Sphicas
Massachusetts Institute of Technology

L. Spiegel
Fermi National Accelerator Laboratory

N. Stanton
Kansas State University

R. Stefanski
Fermi National Accelerator Laboratory

D. Summers
University of Mississippi

M. Syphers
Superconducting Super Collider Laboratory

R. Tanaka
Superconducting Super Collider Laboratory

J. Taron
Ohio State University

W. Toki
Colorado State University

W. Tung
Michigan State University

I. Tzamouranis
University of Virginia

A. Wagner
DESY

D. Wagoner
Prairie View A&M University

M. Walter
DESY

Q. Wang
Rockefeller University

A. Weidemann
University of Tennessee

S. White
Brookhaven National Laboratory

A. Wicklund
Argonne National Laboratory

J. Wilcox
Northeastern University

P. Wilson
Enrico Fermi Institute, University of Chicago

S. Wojcicki
Superconducting Super Collider Laboratory

D. Wu
Prairie View A&M University

A. Yagil
Fermi National Accelerator Laboratory

H. Yamamoto
Harvard University

H. Yamamoto
California Institute of Technology

D. Zieminska
Indiana University

A. Zieminski
Indiana University

Author Index

AUTHOR INDEX

Aleksan, R. 291, 299, 551
Alexopoulos, T. 551, 615, 713
Amundson, J. 389
Arenton, M. 595, 713
Artuso, M. 97, 551, 569
Atac, M. 427
Avery, P. 313
Azfar, F. 229

Baltay, C. 377
Baur, U. 455
Berger, E. L. 339
Bharadwaj, V. 637, 657, 663
Bird, F. 323
Blucher, E. 309
Burnett, T. H. 367
Byrum, K. L. 511

Camilleri, L. 53
Carrigan, Jr., R. A. 645
Choong, W.-S. 449
Choudhary, B. C. 351
Cline, D. B. 417, 427
Colestock, P. 657, 663
Conetti, S. 259, 371, 485
..........................589, 595, 713
Cooper, J. 657
Cords, D. 313
Corti, G. 259, 319, 371
..........................485, 595, 713
Coupal, D. P. 267, 475

Cox, B. 209, 319, 371, 485
......................551, 575, 595, 713
Crosetto, D. 625
Cummings, M. C. 73, 537
Cunningham, J. 309

δ B Rare Decays Subgroup 395
D0 Collaboration 351, 515, 519
DeJongh, F. 243, 551
Denisenko, N. 515
Derré, J. 611
Dib, C. O. 389, 453
Diwan, M. V. 669
Donati, S. 227
Dukes, E. C. 209, 231, 371
.....................485, 489, 505, 595
..........................649, 673, 713
Dunietz, I. 83

Eerola, P. 237, 271
Ellis, N. 237, 271
Erwin, A. 319, 595, 615, 713

Fridman, A. 695
Froidevaux, D. 237, 271

Gadomski, S. 237
Gagliardi, G. 227
Garren, L. 313
Geer, S. 587, 589
Gerasimov, A. 677

Giomataris, J. 551
Giomataris, Y. 607, 611
Goderre, G. 657, 663
Golovatyuk, V. 713
Gonzalez-A, J. 285
Gounder, K. 233
Grinstein, B. 109
Gronau, M. 1, 701

Harr, R. F. 313, 479, 707
Hartouni, E. P. 599, 629
Hassard, J. F. 247, 279, 281
Hedin, D. 537
Heinrich, J. 229
Hill, C. T. 127
Holt, J. 657, 663
Hou, G. W. S. 389

Jackson, G. 645
Jain, V. 389, 551
Jawahery, A. 199
Johns, K. 383, 537
Johnson, D. 663
Johnson, D. E. 667
Johnson, M. 633
Johnson, R. 463
Jöstlein, H. 685, 687

Kaplan, D. 663
Karchin, P. E. 313, 479, 707
Kayser, B. 251, 291, 299

Kennedy, C. J. 313, 479, 551, 707
Kephart, B. 551
Kinoshita, K. 389, 551
Kowalewski, R. V. 121
Kroll, J. 309
Kronfeld, A. S. 175, 389
Kwan, S. 213, 551, 557

Lawry, T. J. 209, 231, 259, 371
.........................485, 595, 713
Lebrun, P. 389, 497
LeCompte, T. J. 543
Lewis, J. D. 217, 551, 583
Lipkin, H. J. 411, 457
Lipton, R. 221
Lohse, T. 255, 641
London, D. 11, 199, 299
Long, O. 229
Lou, X. 373, 551
Loucatos, S. 607
Luk, K. B. 199, 213
Lüth, V. 691

Margetides, S. 279, 281
Marques, J. L. 435, 523
Martin, P. 663
McManus, A. P. 209, 231
.........................371, 485, 713
Meng, R. 333, 339
Mishra, C. S. 163, 221
Mueller, J. A. 63, 217
Mukhin, Y. 551, 569
Murphy, C. T. 639, 645, 649, 713

Nelson, K. S. 319, 371, 485
.........................551, 575, 713
Neumeister, N. 275
Newberger, B. 645
Nir, Y. 185, 395
Nosochkov, Y. M. 653

Oakes, R. J. 389, 451, 459

Pal, T. 139
Papadimitriou, V. 343, 543
Park, J. 427
Parker, B. 649
Peryshkin, A. 519
Punzi, G. 227
Purohit, M. 463

Quigg, C. 439, 443

Rhoades, J. 427
Riemersma, S. 333
Ritchie, D. J. 357
Ritson, D. 681
Rosen, J. 435, 523
Rosner, J. L. 701

Sakai, Y. 151
Schuler, P. 551
Schwartz, A. J. 405
Selove, W. 617
Sheaff, M. 551, 561
Shepard, P. F. 605
Silverman, D. 449
Skarha, J. E. 357, 361
Slaughter, A. J. 603
SLD Collaboration 377
Smith, J. 19
Snider, F. D. 309
Spalding, J. 45, 217
Sphicas, P. 291, 309
Spiegel, L. 435, 713
Stanton, N. R. 531

Taron, J. 389, 453
Toki, W. 247
Tung, W. K. 19
Tzamouranis, I. 371, 485, 595, 713

Weidemann, A. W. 463
Weinzierl, S. 271
White, S. 637
Wicklund, A. B. 361
Wilson, P. 217

Yamamoto, H. 29, 263, 551

Zieminski, A. 331, 357